VISCOELASTIC PROPERTIES OF POLYMERS

John D. Ferry

Professor of Chemistry
University of Wisconsin

THIRD EDITION

JOHN WILEY & SONS
New York • Chichester • Brisbane • Toronto • Singapore

Copyright © 1980 by John Wiley & Sons, Inc.

All rights reserved. Published simultaneously in Canada.

Reproduction or translation of any part of this work beyond that permitted by Sections 107 or 108 of the 1976 United States Copyright Act without the permission of the copyright owner is unlawful. Requests for permission or further information should be addressed to the Permissions Department, John Wiley & Sons, Inc.

Library of Congress Cataloging in Publication Data:

Ferry, John D

Viscoelastic properties of polymers.

Includes bibliographies and indexes.

1. Polymers and polymerization.
2. Viscoelasticity. I. Title.

TA455.P58F4 1980 620.1'9204232 79-28666

ISBN 0-471-04894-1

Printed in the United States of America

10 9 8

To Barbara

Viscoelastic Properties of Polymers

Preface

The extensive development of the subject of this book between the first edition in 1961 and the second edition in 1970 has progressed unabated in the past decade and is reflected in a further expansion of references and authors cited in this third edition. Even so, the present edition inevitably represents a smaller proportion of the total literature than did those preceding.

The chapters remain the same as in the second edition. As before, the emphasis is still on linear viscoelasticity of amorphous polymers. Although the phenomena of nonlinear viscoelasticity are given more attention, this subject and the properties of crystalline and glassy polymers are treated somewhat superficially and the reader is referred to other treatises and reviews, with the admonition that current developments may lead to a clearer understanding within a few years.

There have been a few minor changes in symbols, and the notation conforms to the recommendations of the Society of Rheology published in 1976. Numerical values are still given mostly in cgs units, but the equivalent values in SI units are frequently added.

As before, I am grateful to my present and former students and associates at the University of Wisconsin for their generous contributions to this edition in the form of general perspective and specific advice. Their researches cited here were supported in part by the agencies named in the preface to the first edition and also by the National Institutes of Health and the NATO Research Grants Programme.

Efforts to prevent this revision from being too far out of date on the day of publication have been greatly facilitated by unpublished data and other information generously made available by Professors D. J. Plazek, W. W. Graessley, R. B. Bird, A. J. Kovacs, J. L. Schrag, C. W. Macosko, N. W. Tschoegl, and G. C. Berry, and by Drs. M. Doi, O. Kramer, C. R. Taylor, and D. S. Pearson. Different portions of the manuscript were read by Professors R. B. Bird, N. W. Tschoegl, D. J. Plazek, J. L. Schrag, W. W. Graessley, J. J. Aklonis, A. S. Lodge, and A. Peterlin; and Drs. R. A. Dickie, D. J. Massa, and T. L. Smith. I am greatly indebted to them for their valuable advice. The manuscript was painstakingly typed by Miss Paulette A. Schlomann.

JOHN D. FERRY

Madison, Wisconsin
March 1980

Preface to the First Edition

It is interesting to observe the evolution of science in microcosm by following the development of a highly specialized fragment of it, especially one which cuts across several conventional fields, such as the subject of this book. The familiar pattern of alternation between experimental and theoretical advances is apparent. Underlying each advance is a conceptual scheme which is an arbitrary and subjective choice of one investigator or school; in this conceptual abstraction, attention is focused on certain aspects of observed behavior that are believed to be particularly important or useful to describe, and other aspects are ignored. The conceptual scheme leads to a set of characteristic physical quantities which can be defined, measured, and correlated by theoretical relationships.

Naturally, in the spontaneous development of the subject, alternative conceptual schemes arise, each with its favored definitions, parameters, and terminology. Sometimes the languages are readily translatable, in other cases with extreme difficulty. In the course of time, a majority of the scientific community may adopt one scheme, and for a while a degree of order prevails.

The subject of the viscoelasticity of polymers has not quite reached this last stage of development, but it has matured to the point where some kind of summarizing treatment seems desirable. The phenomenological theory of linear viscoelasticity is essentially complete. The molecular origin of some aspects of the viscoelastic behavior peculiar to polymers is semi-quantitatively understood, as are their dependences on temperature, molecular weight, concentration, and other variables. Moreover, the relationships are well enough understood to permit rule-of-thumb predictions of behavior in practical situations to a far greater extent, I believe, than has been exploited up to now. Other aspects such as the effects of molecular weight distribution and the properties of highly cross-linked, glassy, and crystalline polymers are very poorly understood, but the direction which further experimental and theoretical developments should take is fairly clear.

This book was written with several objectives in view. First, I have tried to assemble the working information needed by investigators in the field for making measurements and interpreting data—information which has hitherto been scattered in dozens of separate publications. A uniform notation has been used, most

of it in accordance with the recommendations of the Society of Rheology. Second, the exposition is I hope straightforward enough so that new investigators, of whom there are many in industrial laboratories encountering the phenomena of polymer viscoelasticity without any previous experience, can use it to familiarize themselves with the subject. Third, certain needs for further theoretical and experimental advances are pointed out. Finally, a few examples of practical applications are given in the hope that these will stimulate a much wider use of approximate interconversions of viscoelastic functions, and reduced variables describing effects of temperature, pressure, and concentration, to predict viscoelastic behavior and correlate it with other properties under a wide variety of conditions.

I owe a profound debt to my former students and associates who, over the years, have participated in studies of the viscoelastic properties of polymers at the University of Wisconsin, and whose collective experience has contributed greatly to writing this book. The work cited from our own laboratory was supported by the Research Committee of the Graduate School of the University of Wisconsin; the Ordnance Corps, Department of the Army; National Science Foundation; Office of Naval Research; Allegany Ballistics Laboratory; and Union Carbide Chemicals Company.

In addition to the many citations of published investigations from other laboratories, unpublished data and theoretical calculations were generously made available by the late Professor E. Jenckel and by Drs. A. Kovacs, J. Lamb, R. S. Marvin, A. R. Payne, and K. Ninomiya.

Most of the manuscript was written during tenure of a National Science Foundation Senior Postdoctoral Fellowship at the University of Brussels in 1959. I am deeply indebted to Professor L. de Brouckère for the kind hospitality of the Laboratoire de Chimie Analytique et Minérale at the University, and to European Research Associates for the use of library facilities. Different chapters were read by Professor Edwin R. Fitzgerald of Pennsylvania State University and by Drs. Robert F. Landel, Thor L. Smith, Robert S. Marvin, Kazuhiko Ninomiya, Donald J. Plazek, Malcolm L. Williams, and André J. Kovacs; I am grateful for their constructive criticism. The proof of the entire book was painstakingly read by Professor Fitzgerald and Dr. Plazek.

JOHN D. FERRY

December, 1960

Contents

1. The Nature of Viscoelastic Behavior **1**

A. Introduction, 1

B. Strain, Stress, and Linear Constitutive Equations for Simple Shear, 3

1. Equations of Change, 4
2. Infinitesimal Strain Tensor, 4
3. Stress Tensor, 5
4. Constitutive Equation for Linear Viscoelasticity in Simple Shear, 6

C. Description of Linear Time-Dependent Experiments in Shear, 8

1. Stress Relaxation after Sudden Strain, 8
2. Stress Relaxation after Cessation of Steady Shear Flow, 9
3. Stress Growth after Initiation of a Constant Shear Rate, 9
4. Creep after Sudden Stress, 10
5. Other Types of Transient Experiments, 10
6. Periodic or Dynamic Experiments, 11
7. Correlation of Experimental Data to Provide Information over Wide Ranges of Time Scale, 14

D. Mechanical Model Analogies of Linear Viscoelastic Behavior, 15

E. The Boltzmann Superposition Principle; Elastic Recovery, 17

F. Linear Stress-Strain Relations for Other Types of Deformation, 20

1. Bulk Compression or Dilatation, 21
2. Simple Extension, 22
3. One-Dimensional Extension in Infinite Medium (Bulk Longitudinal Deformation), 25
4. Inhomogeneous Deformations, 25

G. Finite Strains and Large Strain Rates, 26

1. Normal Stress Differences, 27
2. Non-Newtonian Flow, 29
3. Other Time-Dependent Phenomena, 29

Supplement 1: Summary of Moduli and Compliances, 29

Supplement 2: Complex Notation for Dynamic (Sinusoidal) Stress-Strain Relations, 30

2. Illustrations of Viscoelastic Behavior of Polymeric Systems **33**

A. Linear Viscoelastic Behavior in Shear or Simple Extension, 33

1. Description of the Polymers Chosen for Illustration, 34
2. The Creep Compliance, 37
3. The Stress Relaxation Modulus, 40
4. The Storage Modulus, 41
5. The Loss Modulus, 42
6. The Dynamic Viscosity, 43
7. The Storage Compliance, 44
8. The Loss Compliance, 45
9. The Loss Tangent, 46

B. Linear Viscoelastic Behavior in Bulk (Voluminal) Deformation, 48

C. Nonlinear Viscoelastic Phenomena in Shear, 49

1. Normal Stress Differences, 49
2. Non-Newtonian Flow, 51
3. Stress Relaxation after Large Sudden Strains, 52
4. Stress Relaxation after Cessation of Steady-State Non-Newtonian Flow, 52

D. Conclusions, 54

3. Exact Interrelations among the Viscoelastic Functions **56**

A. Mechanical Model Analogies, 57

1. The Maxwell Element, 57
2. The Voigt Element, 58
3. Discrete Viscoelastic Spectra, 58

B. The Relaxation and Retardation Spectra, 60

1. The Relaxation Spectrum, 60

2. The Retardation Spectrum, 61
3. Interrelations between the Spectra, 63

C. Calculation of Viscoelastic Functions and Constants from the Spectra, 64

D. Calculation of Relaxation and Retardation Spectra from Experimentally Determined Viscoelastic Functions, 67

E. Calculation of One Experimentally Observable Viscoelastic Function from Another, 68

1. Interrelation of the Two Transient Functions, 68
2. Interrelation of a Transient with the Corresponding Dynamic Functions, 68
3. Interrelations between the Components of a Complex Dynamic Function, 69
4. Evaluation of Viscoelastic Constants, 70

F. Calculation of More Complicated Experimental Functions, 71

1. Deformation at Constant Rate of Strain, 71
2. Deformation at Constant Rate of Stress Loading, 72
3. Stress Relaxation after Cessation of Steady-State Flow, 73
4. Creep Recovery or Elastic Recoil, 73
5. Recovery after Partial Stress Relaxation, 74

G. Comments on the Phenomenological Theory of Linear Viscoelasticity, 74

H. Relations from Nonlinear Constitutive Equations, 76

Approximate Interrelations among the Linear Viscoelastic Functions **80**

A. Calculation of Spectra from Experimental Functions, 81

1. Relaxation Spectrum from Relaxation Modulus, 81
2. Retardation Spectrum from Creep Compliance, 82
3. Relaxation Spectrum from Storage Modulus, 83
4. Retardation Spectrum from Storage Compliance, 84
5. Relaxation Spectrum from Loss Modulus, 85
6. Retardation Spectrum from Loss Compliance, 86
7. Criteria of Applicability of Various Approximations, 86

B. Interrelations between the Spectra, 87

1. One Spectrum and Transient Known, 87
2. One Spectrum and Dynamic Data Known, 88
3. One Spectrum Known with Constant Logarithmic Slope, 88

C. Calculation of Viscoelastic Functions from the Spectra, 88

D. Calculation of One Experimentally Observable Viscoelastic Function from Another, 89

1. Interrelation of the Two Transient Functions, 89
2. Interrelation of a Transient with the Corresponding Dynamic Functions, 90
3. Interrelation between the Components of a Complex Dynamic Function, 92
4. Criteria of Applicability, 92

E. Calculation of Spectra from More Complicated Experimental Functions, 92

F. Table of Correction Factors, 94

5. Experimental Methods for Viscoelastic Liquids 99

A. Creep, 99

1. Rotation between Coaxial Cylinders, 99
2. Torsion between Parallel Plates or Cone and Plate, 101
3. Calculation of η_0 and J_e^0 from Creep Measurements in the Terminal Zone, 103
4. Nonlinear Creep and Non-Newtonian Viscosity, 104

B. Shear Stress Relaxation and Stress Growth, 104

C. Normal Stress Measurements, 105

1. Measurements of Total Thrust, 106
2. Measurements of Pressure Gradients, 106
3. Measurements Involving Hole Pressures, 107

D. Dynamic (Oscillatory) Measurements without Sample Inertia Effects ("Gap Loading"), 107

1. Direct Measurements of Sinusoidally Varying Stress and Strain, 108
2. Measurements Involving the Mechanical Impedance of a Moving Element, 110
3. Transducer Measurements by Electrical Impedance, 114

E. Dynamic (Oscillatory) Measurements of Characteristic Impedance ("Surface Loading"), 116

F. Shear Wave Propagation, 121

G. Dynamic Measurements on Liquids in Solid Matrices, 124

H. Measurement of Dynamic Viscoelastic Functions by Eccentric Steady Flow Instruments, 124

I. Isothermal and Adiabatic Measurements, 125

1. Difference between Adiabatic and Isothermal Moduli for Perfect Elastic Materials, 125
2. Critical Frequencies for Isothermal-Adiabatic Transitions, 126
3. Time-Dependent Effects Associated with Heat Flow, 126

6. Experimental Methods for Soft Viscoelastic Solids and Liquids of High Viscosity 130

A. Creep, 132

B. Stress Relaxation, 133

C. Dynamic Measurements without Sample Inertia Effects, 135

1. Direct Measurements of Sinusoidally Varying Stress and Strain, 135
2. Transducer Measurements by Electrical Impedance, 136
3. Compound Resonance Devices with Forced Oscillations, 139
4. Compound Resonance Devices with Free Oscillations, 142

D. Wave Propagation, 144

E. Methods with Other Features, 148

1. Simple Extension at Constant Strain Rate, 148
2. Impact Measurements, 149
3. Sinusoidal Deformations with Large Amplitudes, 149
4. Combined Static and Dynamic Measurements, 150
5. Dynamic Mechanical Measurements Combined with Other Physical Properties, 150

7. Experimental Methods for Hard Viscoelastic Solids 154

A. Creep and Stress Relaxation, 156

B. Direct Measurements of Sinusoidally Varying Stress and Strain, 157

C. Resonance Vibrations, 158

D. Compound Resonance Vibration Devices, 160

E. Wave Propagation, 161

F. Methods Adapted to Fibers, 161

1. Creep and Stress Relaxation, 162
2. Dynamic Measurements, 163

8. Experimental Methods for Bulk Measurements **168**

A. Bulk Transient Measurements 168

B. Bulk Dynamic Measurements, 169

1. Homogeneous Deformation with Direct Measurement of Pressure, 169
2. Homogeneous Deformation by Longitudinal Waves in a Confining Liquid, 170
3. Longitudinal Bulk Wave Propagation, 171

9. Dilute Solutions: Molecular Theory and Comparison with Experiments **177**

A. Rigid Solute Molecules, 179

1. Elongated Rodlike Models, 179
2. Other Rigid Models, 182
3. Jointed Bead-Rod Model, Three Beads, 183

B. Linear Flexible Random Coils: The Bead-Spring Model, 183

1. The Bead-Spring Model with No Hydrodynamic Interaction among Beads, 185
2. The Bead-Spring Model with Dominant Hydrodynamic Interaction, 191
3. Partial Hydrodynamic Interaction, 192
4. Non-Θ-Solvents, 193
5. Comparisons of Characteristic Parameters for Bead-Spring Model Theories, 194
6. Comparison of Theory for Linear Molecules with Experiment, 194
7. Effect of Molecular Weight Distribution, 198
8. Branched Flexible Random Coils, 200

C. Partially Flexible Elongated Molecules, 204

1. Helical Macromolecules, 205
2. Polyelectrolytes, 207

D. Behavior at Finite Concentrations, 209

1. Effects of Domain Overlap, 209
2. Onset of Entanglement Coupling, 212
3. Rigid Rodlike Macromolecules, 213

E. Behavior at High Frequencies and in High-Viscosity Solvents, 214

F. Non-Newtonian Flow, 219

G. Practical Aspects of Viscoelasticity of Dilute Solutions, 219

10. Molecular Theory for Undiluted Amorphous Polymers and Concentrated Solutions; Networks and Entanglements 224

A. Undiluted Polymers of Low Molecular Weight, 224

1. Modified Rouse Theory, 225
2. Closed Form of Rouse Theory: Ladder Networks, 228
3. Effect of Molecular Weight Distribution, 229
4. Effect of Branching, 232

B. Cross-Linked Networks, 233

1. Idealized Network with Fixed Cross-Links, 234
2. Network with Mobile Cross-Links, 237
3. Network with Random Distribution of Strand Lengths, 239
4. Role of Network Defects, 240

C. Uncross-Linked Polymers of High Molecular Weight, 241

1. The Nature of Entanglement Coupling, 241
2. Behavior in the Transition Zone, 247
3. Behavior in the Terminal Zone, 247
4. Transient Network Models for Viscoelastic Properties in the Terminal Zone, 252
5. Practical Aspects of Behavior in the Terminal Zone, 253
6. Behavior in the Plateau Zone, 254

D. Behavior in and near the Glassy Zone, 254

1. Limiting Behavior at High Frequencies, 255
2. Persistence of Relaxation and Retardation Spectra into the Glassy Zone, 256

E. Nonlinear Behavior in Uncross-Linked Polymers of High Molecular Weight, 257

1. Apparent Viscosity in Non-Newtonian Flow, 257
2. Steady-State Compliance and Normal Stress Differences, 259
3. Other Manifestations of Nonlinear Behavior, 259

11. Dependence of Viscoelastic Behavior on Temperature and Pressure 264

A. Origin of the Method of Reduced Variables, 266

1. Deduction from the Dilute-Solution Theories for Flexible Random Coils, 266
2. Deduction from Theory for Undiluted Polymers, 267
3. Empirical Development of the Use of Reduced Variables, 270
4. Reduced Variables for Undiluted Polymers in Terms of Steady-Flow Viscosity, 271
5. Reduced Variables Applied to Polymers of High Molecular Weight, 271
6. Application of Reduced Variables near the Glassy Zone of Time or Frequency, 272

B. Procedure and Criteria for Applicability of the Method of Reduced Variables, 273

C. The WLF Equation and the Relation of Temperature Dependence of Relaxation Times to Free Volume, 280

1. The Glass Transition and Free Volume, 280
2. Relation of Molecular Mobility to Free Volume, 285
3. The WLF Equation, 287
4. Modification of the WLF Equation with an Energy Term, 289

D. Free-Volume Interpretation of the Dependence of Relaxation Times on Pressure and Other Variables, 291

1. Pressure Dependence of Relaxation Times, 291
2. Interrelation of Effects of Temperature and Pressure on Relaxation Times, 294
3. Changes in Relaxation Times during Isothermal Contraction near the Glass Transition, 298
4. Effects of Molecular Weight and Other Variables on Free Volume and Relaxation Times, 298

E. Reduced Variables and Free-Volume Parameters from Other Than Viscoelastic Measurements, 301

1. Dielectric Dispersion, 301
2. Nuclear Magnetic Resonance Relaxation, 302
3. Diffusion of Small Molecules in Polymers, 303

F. Examples of More Limited Applicability of the Method of Reduced Variables, 304

1. Glassy and Highly Crystalline Polymers, 304
2. Multiple Viscoelastic Mechanisms with Different Temperature Dependences, 305
3. Changes in Internal Structure due to Crystallinity, 312

G. Treatment of Data at Fixed Frequency or Time and Varying Temperature, 312

H. Application of Reduced Variables to Bulk and Nonlinear Viscoelastic Properties, 314

1. Bulk (Volume) Viscoelasticity, 314
2. Normal Stresses, 314
3. Non-Newtonian Viscosity, 315
4. Ultimate Properties and Other Practical Aspects of Behavior, 315

12. The Transition Zone from Rubberlike to Glasslike Behavior **321**

A. The Location of the Transition Zone on the Time or Frequency Scale, 322

B. The Monomeric Friction Coefficient, 328

1. Comparisons at Constant Temperature, 329
2. Relation of Friction Coefficient to Free Volume in the Methacrylate Series, 333
3. Comparisons at Corresponding Temperatures, 335
4. Estimation of ζ_0 from the Steady-Flow Viscosity, 337
5. Correlation of ζ_0 with Data from Diffusion of Small Foreign Molecules, 338
6. Relation of ζ_0 to the Onset of the Transition Zone, 342

C. Shapes of the Spectra and Viscoelastic Function in the Transition Zone, 343

1. Relaxation Spectra Reduced to Corresponding States, 343
2. Relation of the Shape of H to Those of Other Viscoelastic Functions, 346
3. Behavior of Copolymers and Polymer Mixtures, 348
4. Behavior of Filled Systems, 356

D. The Transition Zone in Polymers of Low Molecular Weight, 359

13. The Plateau and Terminal Zones in Uncross-Linked Polymers **366**

A. Manifestations of Entanglement Networks, 366

1. Maxima in the Loss Compliance and Retardation Spectrum, 366
2. Storage Modulus and Loss Tangent, 368
3. Relaxation and Retardation Spectra, 369

B. Estimations of Entanglement Spacings, 372

1. Integration of Retardation Spectrum or Loss Compliance, 372

2. Other Methods for Estimating M_e, 376
3. The Critical Molecular Weight M_c from Viscosity or Viscoelastic Time Scale, 377
4. The Critical Molecular Weight M_c' from Steady-State Compliance, 378

C. Behavior in the Terminal Zone, 379

1. Viscosity at Vanishing Shear Rate, 379
2. Dependence of Non-Newtonian Shear Viscosity on Shear Rate, 380
3. Terminal Relaxation Time and Steady-State Compliance, 382
4. Effects of Branching, 385
5. Effects of Molecular Weight Distribution, 387

D. Behavior in the Plateau Zone, 391

1. Width of Plateau Zone on Time Scale, 392
2. Andrade Creep, 392
3. Effects of Molecular Weight Distribution, 393

E. Nonlinear Behavior in Uniaxial Extension, 395

1. Stress Relaxation, 396
2. Uniaxial Extension at Constant Strain Rate, 398
3. Creep and Creep Recovery, 400

14. Cross-Linked Polymers and Composite Systems **404**

A. Effects of Cross-Linking in the Transition Zone, 404

B. Effects of Cross-Linking in the Plateau and Terminal Zones, 407

1. Maxima in the Loss Compliance and Retardation Spectrum, 407
2. Additivity of Contributions of Cross-Links and Trapped Entanglements to the Equilibrium Modulus, 408
3. Changes in the Retardation Spectrum during Early Stages of Cross-Linking, 411
4. Approach to Elastic Equilibrium in Lightly Cross-Linked Systems, 414
5. Slow Relaxation Mechanisms and the Plateau Modulus G_N, 417
6. Relaxation of Unattached Macromolecules in Networks, 419
7. Densely Cross-Linked Polymers, 420

C. Nonlinear Behavior in Cross-Linked Polymers, 420

1. Nonlinear Behavior at Equilibrium, 420
2. Stress Relaxation and Creep, 422
3. Stress-Strain Behavior at Constant Rate of Deformation, 423
4. Small Dynamic Strains Superimposed on Large Static Strains, 424

5. Oscillating Deformations with Large Amplitudes, 424

D. Time-Dependent Mechanical Phenomena due to Chemical Changes, 425

E. Effects of Rigid-Particle Fillers, 426

1. Equilibrium Elastic Properties, 426
2. Viscoelastic Properties, 429

F. Behavior of Blends of Incompatible Polymers, 431

15. The Glassy State **437**

A. Amorphous Solids and Supercooled Liquids of Low Molecular Weight, 438

B. Polymers in the Glassy Zone, 443

1. Viscoelastic Functions at Constant Temperature, 444
2. Isochronal or Quasi-Isochronal Viscoelastic Measurements, 448
3. Local Molecular Motions, 449

C. Nonlinear Behavior of Glassy Polymers, 452

1. Stress and Strain Dependence of Viscoelastic Properties, 452
2. Anisotropic Systems, 453

16. Crystalline Polymers **457**

A. Viscoelastic Functions at Constant Temperature, 458

1. Oriented Single-Crystal Mats, 458
2. Highly Crystalline Polymers from Melts, 460
3. Polymers with Low Degree of Crystallinity, 464

B. Isochronal Viscoelastic Measurements, 465

1. Oriented Single-Crystal Mats, 466
2. High Crystalline Polymers from Melts or Cast from Solvents, 467
3. Polymers with Low Degree of Crystallinity, 469

C. Relation of Viscoelasticity to Molecular Motions, 472

1. Motions within the Crystal Lattice, 472
2. Motions outside the Lattice, 473

D. Resonance Dispersion, 473

E. Nonlinear Viscoelastic Behavior, 475

F. Effects of Orientation and Drawing, 477

17. Concentrated Solutions, Plasticized Polymers, and Gels **486**

A. The Transition Zone, 487

1. The Temperature Dependence of Relaxation and Retardation Times, 487
2. Concentration Dependence of the Monomeric Friction Coefficient, 489
3. Shapes of the Viscoelastic Functions, 498
4. Isochronal or Quasi-Isochronal Viscoelastic Measurements, 499
5. Reduced Variables for Concentration Dependence, 500

B. The Plateau Zone, 501

1. Manifestations of Changes in Entanglement Spacing with Concentration, 501
2. Reduced Variables for Concentration Dependence, 506
3. Elongated Rigid or Semirigid Macromolecules, 507

C. Linear Viscoelastic Behavior in the Terminal Zone, 509

1. Viscosity at Vanishing Shear Rate, 509
2. Terminal Relaxation Time and Steady-State Compliance, 511
3. Effects of Branching and Molecular Weight Distribution, 515

D. Nonlinear Viscoelastic Behavior in the Terminal Zone, 515

1. Dependence of Non-Newtonian Shear Viscosity on Shear Rate, 516
2. Creep and Creep Recovery, 518
3. Normal Stress Differences, 520
4. Stress Relaxation after Large Sudden Strains, 520
5. Stress Growth and Relaxation following Initiation and Cessation of a Constant Shear Rate, 523
6. Combined Oscillatory and Steady-State Shear, 527
7. Nonlinear Constitutive Equations, 528

E. Gels Cross-Linked in Solution, 529

1. Pseudo-Equilibrium Mechanical Properties, 531
2. Viscoelastic Properties in the Transition Zone, 534
3. Viscoelastic Properties in the Plateau Zone, 537
4. Behavior at Very Long Times, 537

F. Gels Swollen after Cross-Linking, 539

G. Gels of Semirigid Macromolecules, 540

18. Viscoelastic Behavior in Bulk (Volume) Deformation **545**

A. Volume Creep, 545

1. Criteria of Linearity and Relation of Nonlinearity to Free Volume, 547
2. Experimental Measurements, 550

B. Isothermal Volume Change after Temperature Jump, 550

1. Kinetics of Volume Changes, 551
2. Effects of Isothermal Volume Changes on Shear and Elongational Relaxation Processes, 554

C. Dynamic Properties in Bulk Compression, 558

D. Bulk Longitudinal Viscoelastic Behavior, 562

1. Dilute Polymer Solutions, 563
2. Undiluted Polymers and Concentrated Solutions, 564

19. Applications to Practical Problems **570**

A. Viscoelastic Behavior under More Complicated Time Patterns, 571

1. Tensile Stress Relaxation following Deformation at Constant Strain Rate, 571
2. Energy Stored, Energy Dissipated, and Work of Deformation in Transient Loading, 571
3. Energy Stored and Dissipated in Periodic (Sinusoidal) Loading, 572
4. Cycling Deformations at Constant Strain Rate, 572
5. Rebound of Rigid Spheres from Viscoelastic Surfaces, 574
6. Rolling Friction on a Viscoelastic Surface, 574

B. Miscellaneous Applications of Viscoelastic Properties, 575

1. Generation of Heat in Rapid Oscillating Deformations, 575
2. Vibration Damping and Noise Abatement, 576
3. Sliding Friction, 577
4. Tack and Adhesion, 578
5. Abrasion, 579
6. Processability, 579
7. Technological Characteristics of Cross-Linked Rubbers, 579
8. Tire Flatspotting, 580
9. Lubrication, 580

C. Numerical Examples of Approximate Predictions of Viscoelastic Behavior, 580

1. Minimum in Loss Tangent for Uncross-Linked Polymers, 581
2. Onset of Transition Zone on Frequency Scale, 581
3. Terminal Relaxation Time (Low Molecular Weight) and Its Dependence on Temperature and Pressure, 581
4. Terminal Relaxation Time (High Molecular Weight), 582
5. Effect of Plasticizer on Mechanical Loss, 582
6. Terminal Relaxation Time in Dilute Solution, 582

D. Ultimate Mechanical Properties, 583

1. Rupture above the Glass Transition Temperature, 583
2. Rupture below the Glass Transition Temperature, 587

Appendix A. List of Symbols **591**

Appendix B. Applicability of Various Dynamic Methods for Viscoelastic Measurements **599**

Appendix C. Form Factors and Maximum Stresses and Strains for Various Deformation Geometries **602**

Appendix D. Examples of Numerical Data for Dynamic and Relaxation Moduli and Creep Compliance **604**

Appendix E. Theoretical Viscoelastic Functions Reduced in Dimensionless Form **610**

Author Index **617**

Subject Index **633**

CHAPTER 1

The Nature of Viscoelastic Behavior

A. INTRODUCTION

The classical theory of elasticity deals with mechanical properties of elastic solids, for which, in accordance with Hooke's law, stress is always directly proportional to strain in small deformations but independent of the rate of strain. The classical theory of hydrodynamics deals with properties of viscous liquids, for which, in accordance with Newton's law, the stress is always directly proportional to rate of strain but independent of the strain itself. These categories are idealizations, however; although the behavior of many solids approaches Hooke's law for infinitesimal strains, and that of many liquids approaches Newton's law for infinitesimal rates of strain, under other conditions deviations are observed. Two types of deviations may be distinguished.

First, when *finite* strains are imposed on solids (especially those soft enough to be deformed substantially without breaking), the stress-strain relations are much more complicated (non-Hookean deformation); similarly, in steady flow with *finite* strain rates, many fluids (especially polymeric solutions and undiluted uncrosslinked polymers) exhibit marked deviations from Newton's law (non-Newtonian flow). The dividing line between "infinitesimal" and "finite" depends, of course, on the level of precision under consideration, and it varies greatly from one material to another.

Second, even if both strain and rate of strain are infinitesimal, a system may exhibit behavior which combines liquidlike and solidlike characteristics. For example, a body which is not quite solid does not maintain a constant deformation under constant stress but goes on slowly deforming with time, or creeps. When such a body is constrained at constant deformation, the stress required to hold it diminishes gradually, or relaxes. On the other hand, a body which is not quite liquid may, while flowing under constant stress, store some of the energy input, instead

of dissipating it all as heat; and it may recover part of its deformation when the stress is removed (elastic recoil). When such bodies are subjected to sinusoidally oscillating stress, the strain is neither exactly in phase with the stress (as it would be for a perfectly elastic solid) nor 90° out of phase (as it would be for a perfectly viscous liquid) but is somewhere in between. Some of the energy input is stored and recovered in each cycle, and some is dissipated as heat. Materials whose behavior exhibits such characteristics are called viscoelastic. If both strain and rate of strain are infinitesimal, and the time-dependent stress-strain relations can be described by linear differential equations with constant coefficients, we have *linear* viscoelastic behavior; then, in a given experiment the ratio of stress to strain is a function of time (or frequency) alone, and not of stress magnitude.

The relations between stress, strain, and their time dependences are in general described by a "constitutive equation" or "rheological equation of state." If strains and/or rates of strain are finite, the constitutive equation may be quite complicated. If they are infinitesimal, however, corresponding to linear viscoelastic behavior, the constitutive equation is relatively simple, and most of the phenomena described in this book fall under its jurisdiction.

In many of the materials of interest in classical physics, as well as of practical importance in engineering, viscoelastic anomalies are negligible or of minor significance. Though the foundations of the phenomenological theory of linear viscoelasticity were inspired by creep and relaxation experiments on fibers of metal and glass,[1-4] and the dissipation of energy in sinusoidally oscillating deformations has provided valuable information about the structure of metals,[5] the deviations from perfect elasticity here are small. In polymeric systems, by contrast, mechanical behavior is dominated by viscoelastic phenomena which are often truly spectacular.

The prominence of viscoelasticity in polymers is not unexpected when one considers the complicated molecular adjustments which must underlie any macroscopic mechanical deformation. In deformation of a hard solid such as diamond, sodium chloride, or crystalline zinc, atoms are displaced from equilibrium positions in fields of force which are quite local in character; from knowledge of the interatomic potentials, elastic constants can be calculated.[6] Other mechanical phenomena reflect structural imperfections involving distances discontinuously larger than atomic dimensions.[5,6] In an ordinary liquid composed of small molecules, viscous flow reflects the change with time, under stress, of the distribution of molecules surrounding a given molecule; here, too, the relevant forces and processes of readjustment are quite local in character, and from knowledge of them the viscosity can in principle be calculated.[7] In a polymer, on the other hand, each flexible threadlike molecule pervades an average volume much greater than atomic dimensions and is continually changing the shape of its contour as it wriggles and writhes with its thermal energy. To characterize the various configurations or contour shapes which it assumes, it is necessary to consider (qualitatively speaking) gross long-range contour relationships, somewhat more local relationships seen with a more detailed scale, and so on, eventually including the orientation of bonds in the chain backbone with respect to each other on a scale of atomic dimensions,

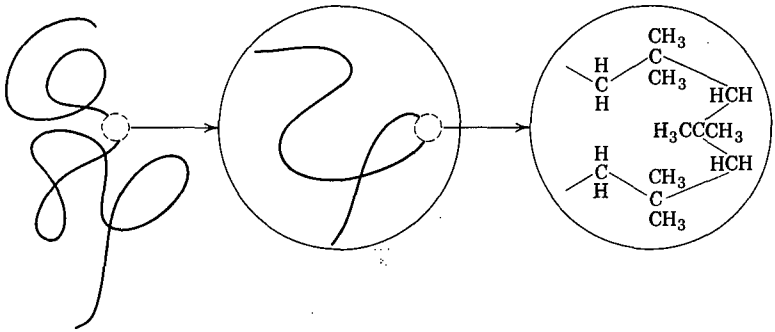


FIG. 1-1. Symbolic representation of long-range and short-range contour relationships in a flexible polymer molecule (polyisobutylene).

as symbolized in Fig. 1-1. Alfrey[8] referred to these spatial relationships, viewed over progressively longer ranges, as "kinks, curls, and convolutions." Rearrangements on a local scale (kinks) are relatively rapid, on a long-range scale (convolutions) very slow. Under stress, a new assortment of configurations is obtained; the response to the local aspects of the new distribution is rapid, the response to the long-range aspects is slow, and all told there is a very wide and continuous range of time scale covering the response of such a system to external stress.

Every amorphous polymeric system has a glass transition temperature below which the writhing thermal motions essentially cease. Here, long-range convolutional readjustments are severely restricted; there is still a wide range of response rates to external stress, but different in nature. The significance of the glass transition in both polymeric systems and liquids of low molecular weight is discussed in Chapter 11.

From measurements of viscoelastic properties of polymers, information can be obtained about the nature and the rates of the configurational rearrangements, and the disposition and interaction of the macromolecules in both their short-range and their long-range interrelations. From the standpoint of the physical chemist, this provides a field of inquiry with unique features of interest. Investigation of viscoelastic properties of polymers has also been greatly stimulated, of course, by the practical importance of mechanical behavior in the processing and utilization of rubbers, plastics, and fibers. As a result, a very high proportion of all studies on viscoelasticity in the past four decades has been devoted to the viscoelasticity of polymers.

B. STRAIN, STRESS, AND LINEAR CONSTITUTIVE EQUATIONS FOR SIMPLE SHEAR

The principal purpose of this book is to relate the viscoelasticity of polymers to molecular structure and modes of molecular motion, and to describe the dependence of viscoelastic properties on molecular weight, molecular weight distribution,

temperature, concentration, chemical structure, and other variables. However, it is necessary first to provide a phenomenological background with definitions of strain and stress and their interrelations in a medium regarded as a continuum.

1. Equations of Change

Experimental measurements of mechanical properties are usually made by observing external forces and changes in external dimensions of a body with a certain shape—a cube, disc, rod, or fiber. The connection between forces and deformations in a specific experiment depends not only on the stress-strain relations (the constitutive equation) but also on two other relations.[9,10] These are the equation of continuity, expressing conservation of mass:

$$\frac{\partial}{\partial t}\rho = -\sum_{i=1}^{3}\frac{\partial}{\partial x_i}(\rho v_i) \tag{1}$$

and the equation of motion, expressing conservation of momentum, with three components of the form:

$$\rho\left(\frac{\partial}{\partial t}v_j + \sum_{i=1}^{3} v_i\frac{\partial}{\partial x_i}v_j\right) = \sum_{i=1}^{3}\frac{\partial}{\partial x_i}\sigma_{ij} + \rho g_j \tag{2}$$

Here ρ is the density, t the time, x_i the three Cartesian coordinates, and v_i the components of velocity in the respective directions of these coordinates. In equation 2, the index j may assume successively the values 1, 2, 3; g_j is the component of gravitational acceleration in the j direction, and σ_{ij} the appropriate component of the stress tensor (see below). (A third equation, describing the law of conservation of energy, can be omitted for a process at constant temperature; the discussion in this chapter is limited to isothermal conditions.) Now, many experiments are purposely designed so that both sides of equation 1 are zero, and so that in equation 2 the inertial and gravitational forces represented by the first and last terms are negligible. In this case, the internal states of stress and strain can be calculated from observable quantities by the constitutive equation alone. For infinitesimal deformations, the appropriate relations for viscoelastic materials involve the same geometrical form factors as in the classical theory of equilibrium elasticity; they are described in connection with experimental methods in Chapters 5–8 and are summarized in Appendix C.

2. Infinitesimal Strain Tensor

In a viscoelastic as in a perfectly elastic body, the state of deformation at a given point is specified by a strain tensor which represents the relative changes in dimensions and angles of a small cubical element cut out at that position. The rate of strain tensor expresses the time derivatives of these relative dimensions and angles. Similarly, the state of stress is specified by a stress tensor which represents the forces acting on different faces of the cubical element from different directions. For details, the reader is referred to standard treatises.[8–16]

For an infinitesimal deformation, the components of the infinitesimal strain tensor in rectangular coordinates with the three Cartesian directions denoted by the subscripts 1, 2, 3 are

$$\gamma_{ij} = \begin{pmatrix} 2\partial u_1/\partial x_1 & \partial u_2/\partial x_1 + \partial u_1/\partial x_2 & \partial u_3/\partial x_1 + \partial u_1/\partial x_3 \\ \partial u_2/\partial x_1 + \partial u_1/\partial x_2 & 2\partial u_2/\partial x_2 & \partial u_2/\partial x_3 + \partial u_3/\partial x_2 \\ \partial u_3/\partial x_1 + \partial u_1/\partial x_3 & \partial u_2/\partial x_3 + \partial u_3/\partial x_2 & 2\partial u_3/\partial x_3 \end{pmatrix} \quad (3)$$

where x_i and u_i are respectively the coordinates of the point where the strain is specified and its displacement in the strained state; *i.e.*, $u_i = x_i - x_i^0$, where the superscript 0 refers to the unstrained state. The rate of strain tensor, $\dot{\gamma}_{ij}$, is formulated similarly with u_i replaced by v_i, the velocity of displacement $(= \partial u_i/\partial t)$.

In most treatises,[11-13,16] the strain tensor is defined with all components smaller by a factor of $\frac{1}{2}$ than in equation 3, so that $\gamma_{11} = \partial u_1/\partial x_1$ and $\gamma_{21} = \frac{1}{2}(\partial u_2/\partial x_1 + \partial u_1/\partial x_2)$. However, such a definition makes discussion of shear or shear flow somewhat clumsy: either a "practical" shear strain and "practical" shear rate must be introduced which are twice γ_{21} and $\dot{\gamma}_{21}$ respectively, or else a factor of 2 must be carried in the constitutive equations. Since most of the discussion in this book is concerned with shear deformations, we use the definition of equation 3 which follows Bird and his school[10] and Lodge.[14,17] This does cause a slight inconvenience in the discussion of compressive and tensile strain, where a "practical" measure of strain is subsequently introduced (Section F below). In older treatises on elasticity,[15] strains are defined without the factor of 2 appearing in the diagonal components of equation 3, but with the other components the same.

For large deformations or rates of deformation, definition of the strain tensor or rate of strain tensor becomes extremely complicated and there are various different alternatives. A thorough discussion is presented in Chapters 7–9 of reference 10.

3. Stress Tensor

The stress components of σ_{ij} which appear in equation 2 may also be displayed in matrix form as follows:

$$\sigma_{ij} = \begin{pmatrix} \sigma_{11} & \sigma_{12} & \sigma_{13} \\ \sigma_{21} & \sigma_{22} & \sigma_{23} \\ \sigma_{31} & \sigma_{32} & \sigma_{33} \end{pmatrix} \quad (4)$$

where σ_{ij} is the component, parallel to the j direction, of the force per unit area acting on the face of a cubical element which is perpendicular to the i direction. The normal stresses σ_{ii} are taken as positive for tension and negative for compression. (This convention is not universal; the opposite signs are sometimes

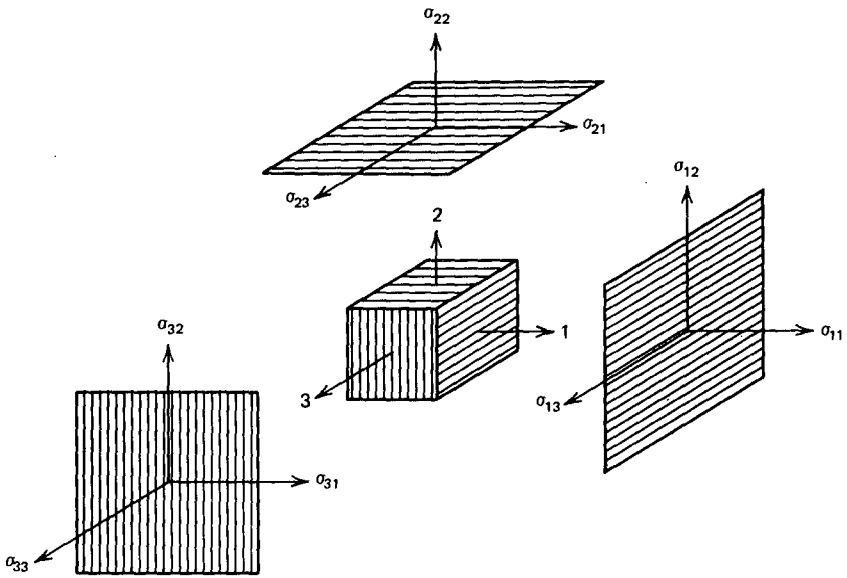


FIG. 1-2. Identification of the components of the stress tensor.

used.[9,10]) The components of the stress tensor are illustrated graphically in Fig. 1-2.

4. Constitutive Equation for Linear Viscoelasticity in Simple Shear

If the deformation is uniform (homogeneous), the stress and strain components do not vary with position and are independent of x_i. There are several specific types of uniform deformation for which the strain and stress tensors assume a relatively simple form. One that corresponds to a commonly used experimental geometry is simple shear, where two opposite faces of the cubical element are displaced by sliding, as illustrated in Fig. 1-3. Conventionally, the 13 plane slides in the 1 direction; the strains and stresses are then

$$\gamma_{ij} = \begin{pmatrix} 0 & \gamma_{21} & 0 \\ \gamma_{12} & 0 & 0 \\ 0 & 0 & 0 \end{pmatrix} \tag{5}$$

where $\gamma_{21} = \gamma_{12} = \partial u_1/\partial x_2 = \tan \alpha \cong \alpha$, and

$$\sigma_{ij} = \begin{pmatrix} -P & \sigma_{12} & 0 \\ \sigma_{21} & -P & 0 \\ 0 & 0 & -P \end{pmatrix} \tag{6}$$

where P is an isotropic pressure. The strain γ_{21} and stress σ_{21} are functions of time,

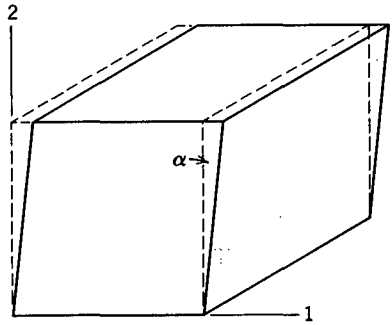


FIG. 1-3. Illustration of simple shear of a cubical element.

and they are connected by a constitutive equation for linear viscoelasticity which for simple shear has a very simple form.

This linear constitutive equation is based on the principle that the effects of sequential changes in strain are additive:[13,16]

$$\sigma_{21}(t) = \int_{-\infty}^{t} G(t - t')\dot{\gamma}_{21}(t')dt' \tag{7}$$

where $\dot{\gamma}_{21} = \partial\gamma_{21}/\partial t$ is the shear rate, $G(t)$ is called the relaxation modulus, with a physical significance which will be apparent later, and the integration is carried out over all past times t' up to the current time t.

If the function $G(s)$ approaches zero as s approaches infinity (a condition which as we shall see corresponds to a viscoelastic *liquid*), there is an alternative formulation[10,14] expressed in terms of the history of the strain rather than that of the rate of strain:

$$\sigma_{21}(t) = -\int_{-\infty}^{t} m(t - t')\gamma_{21}(t, t')dt' \tag{8}$$

in which $m(t)$, the memory function, is $-dG(t)/dt$. To specify the strain, a reference state must be selected; $\gamma_{21}(t, t')$ means the shear strain at time t' relative to that at time t. If the function $G(s)$ remains finite for large s (corresponding to a viscoelastic *solid*), equation 8 does not contain all the information of equation 7 and another term must be added.

An alternative constitutive equation can be written to express the strain in terms of the history of the time derivative of the stress, in the form

$$\gamma_{21}(t) = \int_{-\infty}^{t} J(t - t')\,\dot{\sigma}_{21}(t')dt' \tag{9}$$

where $\dot{\sigma}_{21} = d\sigma_{21}/dt$ and $J(t)$ is called the creep compliance because of its physical significance to be described later. There is also an equation in terms of the history of the stress, corresponding to equation 8.[12]

From knowledge of the shear relaxation modulus, the memory function, or the creep compliance function of a particular material, its stress-strain relations for

any kind of experiment in shear with a prescribed time dependence of stress or strain can be predicted as long as the motions are sufficiently small and/or sufficiently slow. Some time-dependent patterns of particular interest are described in the following section and analyzed in terms of equation 7. Equation 9 will be used to illustrate certain other experimental patterns in Section E.

C. DESCRIPTION OF LINEAR TIME-DEPENDENT EXPERIMENTS IN SHEAR

The constitutive equations of the preceding section can be used to describe the response of a linear viscoelastic material to various kinds of time-dependent patterns of stress and strain in simple shear. In this section, the subscript 21 will be omitted with the understanding that all equations refer to simple shear.

1. Stress Relaxation after Sudden Strain

Suppose a shear strain γ is imposed within a brief period of time ξ by a constant rate of strain $\dot{\gamma} = \gamma/\xi$ (Fig. 1-4). Equation 7 can then be expressed as

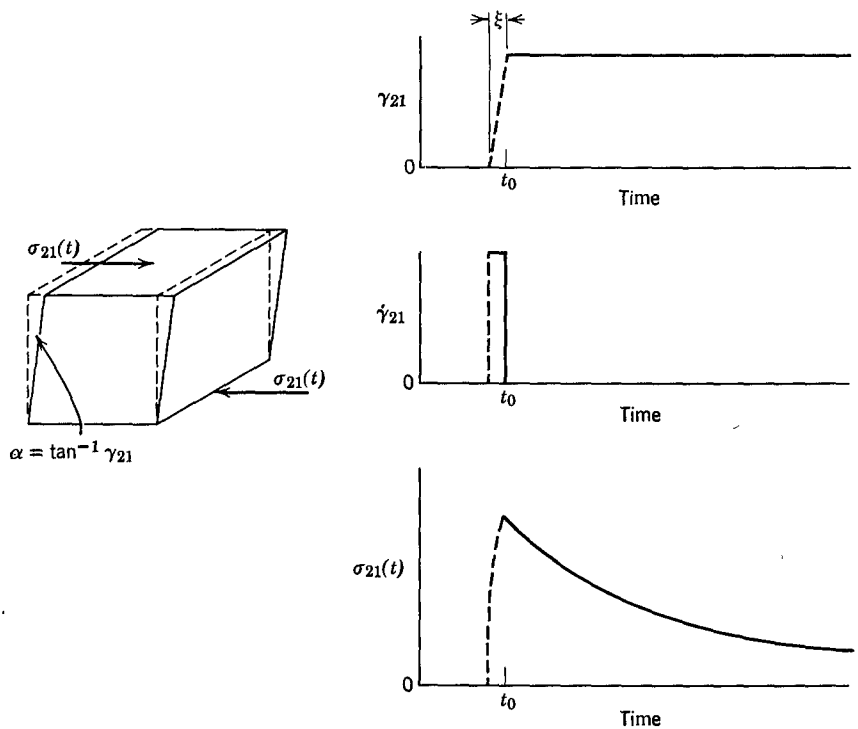


FIG. 1-4. Geometry and time profile of a simple shear stress relaxation experiment following sudden strain.

$$\sigma(t) = \int_{t_0-\xi}^{t_0} G(t - t')(\gamma/\xi)dt' \tag{10}$$

where t_0 is the time at which the strain is complete, since the rate of strain is zero both before and after the interval represented by this integral. By the Theorem of the Mean, equation 10 can be written

$$\sigma(t) = (\gamma/\xi)\xi G(t - t_0 + \epsilon\xi), \quad 0 \leq \epsilon \leq 1$$

Thus, if t_0 is set equal to 0,

$$\sigma(t) = \gamma G(t + \epsilon\xi) \tag{11}$$

and for times long compared with ξ, the loading interval, this is indistinguishable from

$$\sigma(t) = \gamma G(t) \tag{12}$$

The physical meaning of the relaxation modulus $G(t)$ is apparent in terms of this simple experiment. In general, the ratio of a stress to the corresponding strain is called a modulus, and for a perfectly elastic solid the equilibrium shear modulus G is defined as σ/γ; $G(t)$ is its time-dependent analog as measured in an experiment with this particular time pattern. This experiment can be performed on both viscoelastic liquids and viscoelastic solids.

2. Stress Relaxation after Cessation of Steady Shear Flow

There is another kind of stress relaxation experiment that is applicable only to viscoelastic liquids, which are capable of steady-state shearing deformation at a constant strain rate $\dot{\gamma}$. The stress during steady flow (sufficiently slow to ensure linear behavior) is $\sigma = \dot{\gamma}\eta_0$, where η_0 is the viscosity corresponding to vanishing shear rate. If the flow is abruptly stopped, the stress will gradually decay (Fig. 1-5). Its time dependence can be shown to be given by

$$\sigma^{ss}(t) = \dot{\gamma} \int_t^\infty G(s)ds \tag{13}$$

The time-dependent stress $\sigma^{ss}(t)$ corresponds to the notation $\eta^-(t)\dot{\gamma}_0$ in the treatise of Bird, Armstrong, and Hassager.[10]

3. Stress Growth after Initiation of a Constant Shear Rate

If a viscoelastic liquid at rest is suddenly subjected to a constant shear strain rate $\dot{\gamma}$, the stress will increase gradually to approach asymptotically the value $\dot{\gamma}\eta_0$. Its time dependence can be shown to be given by

$$\sigma(t) = \dot{\gamma} \int_0^t G(s)ds \tag{14}$$

This time-dependent stress corresponds to $\eta^+(t)\dot{\gamma}_0$ in Bird, Armstrong, and Hassager.[10]

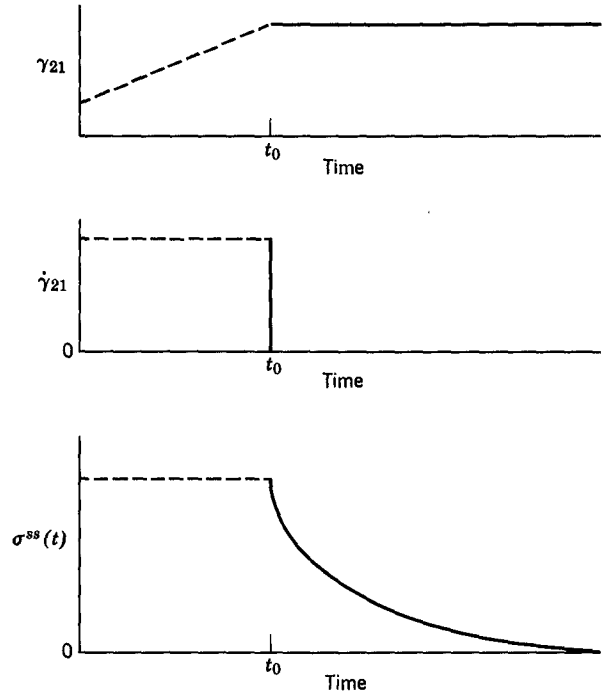


FIG. 1-5. Time profile of a simple shear stress relaxation experiment following cessation of steady-state flow.

4. Creep after Sudden Stress

In an experiment which is the opposite of stress relaxation after sudden strain, a shear stress σ may be applied within a very brief period before time 0 and then maintained constant (Fig. 1-6). The dependence of the strain γ on time can be derived from equation 9 exactly as equation 12 is obtained from equation 7, with the result

$$\gamma(t) = \sigma J(t) \tag{15}$$

This shows the physical meaning of the creep compliance $J(t)$, which has the dimensions of reciprocal modulus and is a monotonically nondecreasing function of time. For a perfectly elastic solid $J = 1/G$. However, for a viscoelastic material, $J(t) \neq 1/G(t)$, because of the difference between the two experimental time patterns; interrelations between the two functions will be given Chapters 3 and 4.

5. Other Types of Transient Experiments

In deformation with a constant rate of strain, γ is increased linearly with time (at constant $\dot{\gamma}$); if the total deformation is small, $\sigma(t)$ can be rather simply related to $G(t)$. In deformation with a constant rate of stress loading, σ is increased linearly with time; then $\gamma(t)$ can be rather simply related to $J(t)$. These relations will be

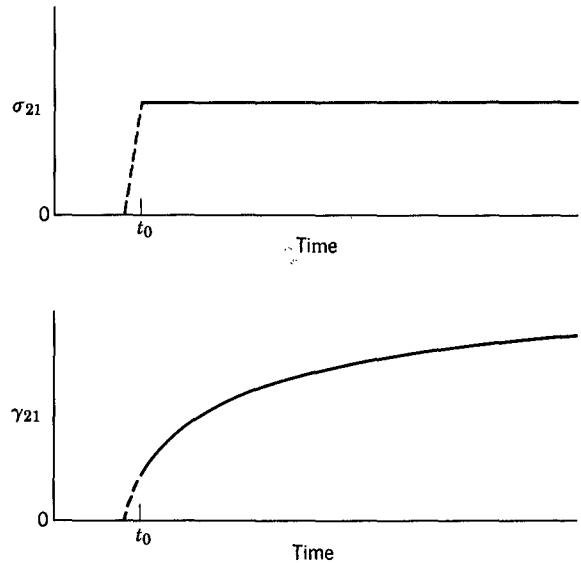


FIG. 1-6. Time profile of a shear creep experiment.

given in Chapters 3 and 4. Another pattern of interest involves removal of stress after it has been applied for a sufficiently long time to achieve either a constant strain or a constant rate of strain. This type of experiment will be discussed in Section E.

6. Periodic or Dynamic Experiments

To supplement the above transient (*i.e.*, nonperiodic) experiments and provide information corresponding to very short times, the stress may be varied periodically, usually with a sinusoidal alternation at a frequency ν in cycles/sec (Hz) or $\omega(=2\pi\nu)$ in radians/sec. A periodic experiment at frequency ω is qualitatively equivalent to a transient experiment at time $t = 1/\omega$, as will be evident in the examples shown in Chapter 2. If the viscoelastic behavior is linear, it is found that the strain will also alternate sinusoidally but will be out of phase with the stress (Fig. 1-7). This can be shown from the constitutive equation as follows. Let

$$\gamma = \gamma^0 \sin \omega t \tag{16}$$

where γ^0 is the maximum amplitude of the strain. Then

$$\dot{\gamma} = \omega\gamma^0 \cos \omega t \tag{17}$$

Substituting in equation 7, denoting $t - t'$ by s, we have

$$\sigma(t) = \int_0^\infty G(s)\omega\gamma^0 \cos[\omega(t-s)]ds$$

$$= \gamma^0\left[\omega \int_0^\infty G(s) \sin \omega s \, ds\right] \sin \omega t + \gamma^0\left[\omega \int_0^\infty G(s) \cos \omega s \, ds\right] \cos \omega t \tag{18}$$

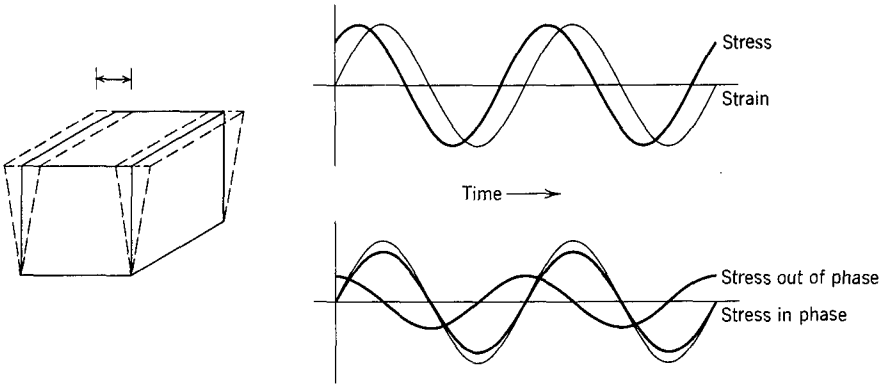


FIG. 1-7. Geometry and time profile of a simple shear experiment with sinusoidally varying shear.

The integrals converge only if $G(s) \to 0$ as $s \to \infty$; otherwise they must be formulated somewhat differently (Chapter 3). It is clear that the term in $\sin \omega t$ is in phase with γ and the term in $\cos \omega t$ is 90° out of phase; σ is periodic in ω but out of phase with γ to a degree depending on the relative magnitudes of these terms. The quantities in brackets are functions of frequency but not of elapsed time, so equation 18 can be conveniently written

$$\sigma = \gamma^0 (G' \sin \omega t + G'' \cos \omega t) \tag{19}$$

thereby defining two frequency-dependent functions—the shear storage modulus $G'(\omega)$ and the shear loss modulus $G''(\omega)$.

It is instructive to write the stress in an alternative form displaying the *amplitude* $\sigma^0(\omega)$ of the stress and the *phase angle* $\delta(\omega)$ between stress and strain. From trigonometric relations,

$$\sigma = \sigma^0 \sin (\omega t + \delta) = \sigma^0 \cos \delta \sin \omega t + \sigma^0 \sin \delta \cos \omega t \tag{20}$$

Comparison of equations 19 and 20 shows that

$$G' = (\sigma^0/\gamma^0) \cos \delta \tag{21}$$

$$G'' = (\sigma^0/\gamma^0) \sin \delta \tag{22}$$

$$G''/G' = \tan \delta \tag{23}$$

It is evident that each periodic, or dynamic, measurement at a given frequency provides simultaneously *two* independent quantities, either G' and G'' or else $\tan \delta$ and σ^0/γ^0, the ratio of peak stress to peak strain. (Over a sufficiently wide range of frequencies, however, G' and G'' are not independent and can be interrelated as discussed in Chapters 2, 3, and 4.)

It is usually convenient to express the sinusoidally varying stress as a complex quantity, as explained in Supplement 2 at the end of this Chapter.

Then the modulus is also complex, given by

$$\sigma^*/\gamma^* = G^* = G' + iG'' \tag{24}$$

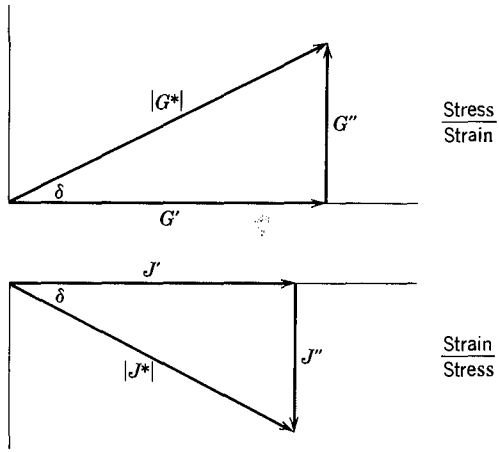


FIG. 1-8. Vectorial resolution of components of complex modulus and compliance in sinusoidal shear deformations.

$$|G^*| = \sigma^0/\gamma^0 = \sqrt{G'^2 + G''^2} \tag{25}$$

This corresponds to a vectorial resolution of the components in the complex plane as shown in Fig. 1-8. It is evident that G' is the ratio of the stress in phase with the strain to the strain, whereas G'' is the ratio of the stress 90° out of phase with the strain to the strain.

The data from sinuosidal experiments can also be expressed in terms of a complex compliance

$$J^* = \gamma^*/\sigma^* = 1/G^* = J' - iJ'' \tag{26}$$

The storage compliance J' is the ratio of the strain in the phase with the stress to the stress, whereas the loss compliance J'' is the ratio of the strain 90° out phase with the stress to the stress (Fig. 1-8). The storage modulus G' and compliance J' are so named because they are directly proportional to the average energy storage in a cycle of deformation. The loss modulus G'' and compliance J'' are directly proportional to the average dissipation or loss of energy as heat in a cycle of deformation. Note that $J''/J' = G''/G' = \tan\delta$.

Reference to the complex modulus G^* may be regarded as abbreviated language for talking about G' and G'' simultaneously, and similarly for J^*.

Although $J^* = 1/G^*$, their individual components are not reciprocally related, but are connected by the following equations:

$$J' = \frac{G'}{(G'^2 + G''^2)} = \frac{1/G'}{1 + \tan^2\delta} \tag{27}$$

$$J'' = \frac{G''}{(G'^2 + G''^2)} = \frac{1/G''}{1 + (\tan^2\delta)^{-1}} \tag{28}$$

$$G' = \frac{J'}{(J'^2 + J''^2)} = \frac{1/J'}{1 + \tan^2\delta} \tag{29}$$

$$G'' = \frac{J''}{(J'^2 + J''^2)} = \frac{1/J''}{1 + (\tan^2 \delta)^{-1}} \tag{30}$$

Periodic measurements can be made, depending on circumstances, at frequencies from 10^{-5} to 10^{8} Hz; usually a given experimental method will cover only 2 to 3 powers of ten, but a great variety of methods is available, as will be seen in Chapters 5–8.

As an alternative to G^*, the phase relationships can equally well be expressed by a complex viscosity $\eta^* = \eta' - i\eta''$, which is frequently used to describe viscoelastic liquids. The ratio of stress in phase with rate of strain to the rate of strain is η', and η'' is the stress 90° out of phase with the rate of strain divided by the rate of strain. Thus the phase relations are the opposite of those for G^*, and the individual components are given by

$$\eta' = G''/\omega \tag{31}$$

$$\eta'' = G'/\omega \tag{32}$$

The in-phase or real component η' for a viscoelastic liquid approaches the steady-flow viscosity η_0 as the frequency ω approaches zero.

7. Correlation of Experimental Data to Provide Information over Wide Ranges of Time Scale

To cover a wide enough time scale to reflect the variety of molecular motions in polymeric systems, often 10 to 15 logarithmic decades, one must usually combine information from transient and sinusoidal experiments. It is then necessary to calculate from the results of one type of measurement what would have been observed in the other, in the same range of time (or inverse radian frequency). Fortunately, this is possible, provided the viscoelastic behavior is linear. In principle, knowledge of any one of the functions $J(t)$, $G(t)$, $G'(\omega)$, $G''(\omega)$, $J'(\omega)$, $J''(\omega)$ over the entire range of time or frequency (plus in certain cases one or two additional constants) permits calculation of all the others. Even if the values are not available over the entire range of the argument, approximation methods can be applied. These calculations are treated in detail in Chapters 3 and 4.

Since each of the preceding functions can be calculated from any other, it is an arbitrary matter which is chosen to depict the behavior of a system and to correlate with theoretical formulations on a molecular basis. In fact, two other derived functions are sometimes used for the latter purpose—the relaxation and retardation spectra, H and L, which will be defined in Chapter 3. Actually, different aspects of the viscoelastic behavior, and the molecular phenomena which underlie them, have different degrees of prominence in the various functions enumerated above, so it is worthwhile to examine the form of several of these functions even when all are calculated from the same experimental data. A qualitative survey of their appearance will be presented in Chapter 2.

Even when only one experimental method is available, covering perhaps two or three decades of logarithmic time or frequency scale, the viscoelastic functions can

be traced out over a much larger effective range by making measurements at different temperatures, and using a sort of principle of viscoelastic corresponding states. In many cases, an increase in temperature is nearly equivalent to an increase in time or a decrease in frequency in its effect on a modulus or compliance, and a temperature range of 100° may provide an effective time range of 10 logarithmic decades. This scheme must be used judiciously, with regard to the reservations in the theories which support it, and to previous experimental experience; it is critically discussed in Chapter 11. When properly applied, it yields plots in terms of reduced variables which can be used with considerable confidence to deduce molecular parameters as well as to predict viscoelastic behavior in regions of time or frequency scale not experimentally accessible.

D. MECHANICAL MODEL ANALOGIES OF LINEAR VISCOELASTIC BEHAVIOR

The form of the time dependence of $J(t)$ or $G(t)$, or of the frequency dependence of $G'(\omega)$, $G''(\omega)$, $J'(\omega)$, or $J''(\omega)$, can be imitated by the behavior of a mechanical model with a sufficient number of elastic elements (springs) and viscous elements (dashpots imagined as pistons moving in oil).[8,12] Examples are shown in Figs. 1-9 and 1-10. Here force applied to the terminals of the model is analogous to σ, the relative displacement of the terminals is analogous to γ, and the rate of displacement is analogous to $\dot{\gamma}$. Each spring element is assigned a stiffness (force/displacement) analogous to a shear modulus contribution G_i, and each dashpot is assigned a frictional resistance (force/velocity) analogous to a viscosity contribution η_i. The dimensions do not correspond (force/displacement is dynes/cm and modulus is dynes/cm^2) and the geometry looks like extension rather than shear, but the mathematical analogy is satisfactory.

For example, when the Maxwell model, Fig. 1-9, is subjected to a stress relaxation experiment as in Fig. 1-4, the force on each spring-dashpot pair relaxes exponentially; expressed in terms of the modulus analogy, we have the contribution of the ith pair to the modulus, $G_i(t)$, given by

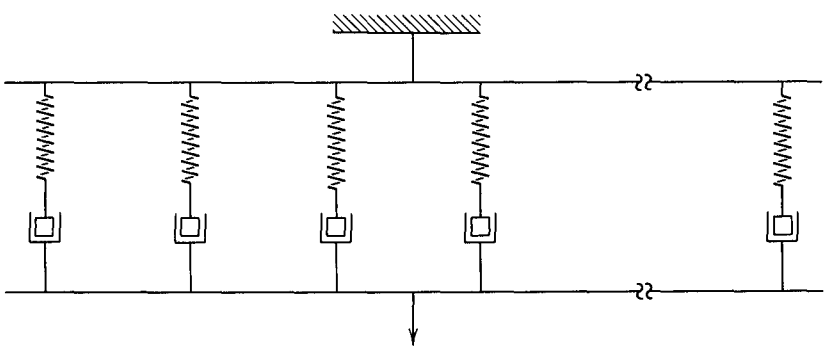


FIG. 1-9. Generalized Maxwell model.

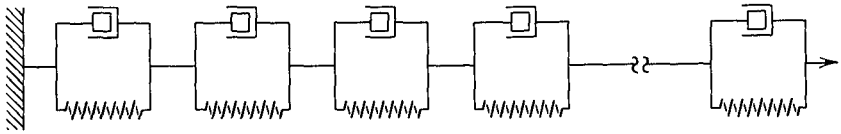


FIG. 1-10. Generalized Voigt model.

$$G_i(t) = G_i e^{-tG_i/\eta_i} \equiv G_i e^{-t/\tau_i} \tag{33}$$

in which the time constants τ_i, the relaxation times, are defined as η_i/G_i. Then

$$G(t) = \sigma(t)/\gamma = \sum_i G_i e^{-t/\tau_i} \tag{34}$$

The corresponding constitutive equation analogous to equation 8 is

$$\sigma(t) = -\int_{-\infty}^{t} \left\{ \sum_i (G_i/\tau_i) e^{-(t-t')/\tau_i} \right\} \gamma(t, t') dt' \tag{35}$$

in which the quantity in brackets corresponds to the memory function. (Note that the model as drawn depicts a viscoelastic liquid since the stress will relax to zero at long times.) With a sufficient number of elements the continuous functions $G(t - t')$ and $m(t - t')$ can be represented by the sums indicated. If appropriate values for all G_i and τ_i (or η_i) have been assigned, in principle all the viscoelastic functions can be calculated by formulas to be given in Chapter 3. In practice, such a procedure is rarely attempted, except for rough calculations. The chief value of a model is as a guide for qualitative thinking.

The models of Figs. 1-9 and 1-10 are equivalent with an appropriate assignment of parameters subject to certain requirements which depend on whether the system is a viscoelastic liquid or a viscoelastic solid. These terms have been used several times in preceding sections and will now be clarified. To make such a dichotomy may seem paradoxical since all viscoelastic materials are intermediate between solids and liquids. However, it is usually possible to distinguish between those which in a creep experiment eventually achieve steady flow or linearly increasing deformation with time (liquids) and those which eventually closely approach an equilibrium deformation or zero strain rate (solids). For liquids, $G(t)$ approaches zero as $t \to \infty$; for solids, $G(t)$ approaches a constant finite value (G_e). Only in systems with exceedingly long relaxation times is the distinction uncertain (*cf.* Chapters 13-15). For a *liquid,* all viscosities in the Maxwell model if Fig. 1-9 must be finite and one spring in the Voigt model of Fig. 1-10 must be zero. For a *solid,* one viscosity in the Maxwell model must be infinite (resulting in an added constant term G_e in equation 34) and all springs in the Voigt model must be nonzero. It should be noted that a viscoelastic liquid, in this sense, may have a very high viscosity with the superficial appearance of a solid.

It was pointed out by Poincaré[18] that if a physical phenomenon can be represented by one mechanical model it can also be represented by many other models. Thus, springs and dashpots could be arranged in many different patterns, as dis-

cussed by Kuhn,[19] all of them equivalent. In particular, there are rules for interrelating the parameters of the equivalent Maxwell and Voigt models.[8]

As an example of the qualitative usefulness of mechanical models, the difference between the two stress relaxation experiments portrayed in Figs. 1-4 and 1-5 can be easily understood in terms of the model of Fig. 1-9. If the strain is suddenly imposed (Fig. 1-4), the individual forces on the spring-dashpot pairs of the model are initially distributed in proportion to the relative stiffnesses of the *springs*. Subsequently, each contribution to the total force relaxes according to its own relaxation time. By contrast, if the experiment begins with a state of steady flow (Fig. 1-5), the individual forces on the spring-dashpot pairs are initially distributed in proportion to the relative frictional resistances of the *dashpots*. In the subsequent relaxation, the relaxation times are the same, but the magnitudes of the relaxing force contributions are different, so the course of the total force as a function of time is entirely different.

E. THE BOLTZMANN SUPERPOSITION PRINCIPLE; ELASTIC RECOVERY

Equations 7 and 9 are two of many possible expressions of the Boltzmann superposition principle[1,20] that the effects of mechanical history are linearly additive, where the stress is described as a function of rate of strain history or alternatively the strain is described as a function of the history of rate of change of stress. Many early treatises have elaborated on the effects of different sequences of stressing or straining according to this principle, and it has been tested by a variety of experiments. The procedure may be illustrated by some characteristic sequences of stress history.

We take first a trivial example of just two events in stress history, continuing to omit the subscripts 21 but with the understanding tha the deformation is simple shear. If a stress σ_A is applied at $t = 0$ and an additional stress σ_B is applied at $t = t_1$, the total strain at time t is found by applying equation 9 to be

$$\gamma(t) = \sigma_A J(t) + \sigma_B J(t - t_1) \tag{36}$$

namely, the linear superposition of the two strains specified by the creep compliances at their respective elapsed times. This can be generalized for a sequence of finite stress changes σ_i, each at a time point u_i, to give

$$\gamma(t) = \sum_{u_i=-\infty}^{u_i=t} \sigma_i J(t - u_i) \tag{37}$$

A sequence of particular interest is the case where a creep experiment has progressed for some time and the stress is then suddenly removed. The rate of deformation will change sign and the body will gradually return more or less toward its initial state (*i.e.*, for shear deformation, toward its initial shape). The course of this reverse deformation is called creep recovery. The results depend in a critical manner on whether the material is a viscoelastic solid or a viscoelastic liquid as distinguished

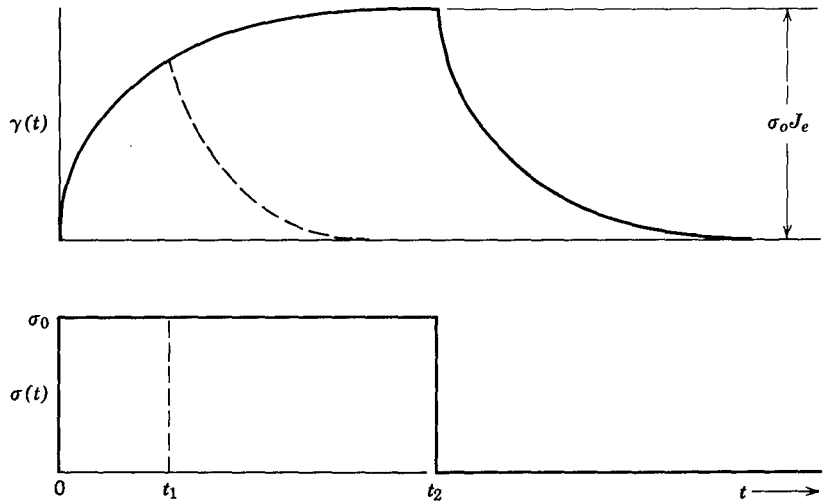


FIG. 1-11. Shear creep and creep recovery shown schematically for a viscoelastic solid, *e.g.*, a cross-linked polymer.

in Section D above; *i.e.*, whether or not it eventually reaches an equilibrium deformation in creep, characterized by an equilibrium compliance (in shear, J_e). As explained above, attainment of equilibrium corresponds to a Maxwell model (Fig. 1-9) in which one dashpot is missing—a viscoelastic solid. In bulk compression (see Section F below), an equilibrium compliance no doubt always exists—it is simply the thermodynamic compressibility. For shear and other deformations of polymers, the presence or absence of an equilibrium compliance corresponds approximately to the presence or absence of a cross-linked network in the molecular structure.

In a cross-linked polymer, shear creep followed by creep recovery is essentially as shown schematically in Fig. 1-11. If the stress σ_0 has been applied for a time t_2 long enough for the strain to reach within experimental error its equilibrium value $\gamma(\infty) = \sigma_0 J_e$, then in accordance with equation 37 the course of creep recovery will be given by

$$\gamma_r(t) = \sigma_0[J_e - J(t - t_2)] \tag{38}$$

(noting that removal of stress is equivalent to applying an additional stress $-\sigma_0$). This is just a mirror image of the creep itself in the time axis, displaced vertically by $\gamma(\infty)$ and horizontally by t_2. If, on the other hand, the load is removed at a time t_1 before $\gamma(\infty)$ is reached, the course of recovery will be

$$\gamma_r(t) = \sigma_0[J(t) - J(t - t_1)] \tag{39}$$

which, although not a simple mirror image, is readily susceptible of experimental test by calculating the right side of the equation from a duplicate creep run carried to longer times. The results of numerous such tests, which support the validity of the superposition principle and equations 7 and 8, have been summarized by

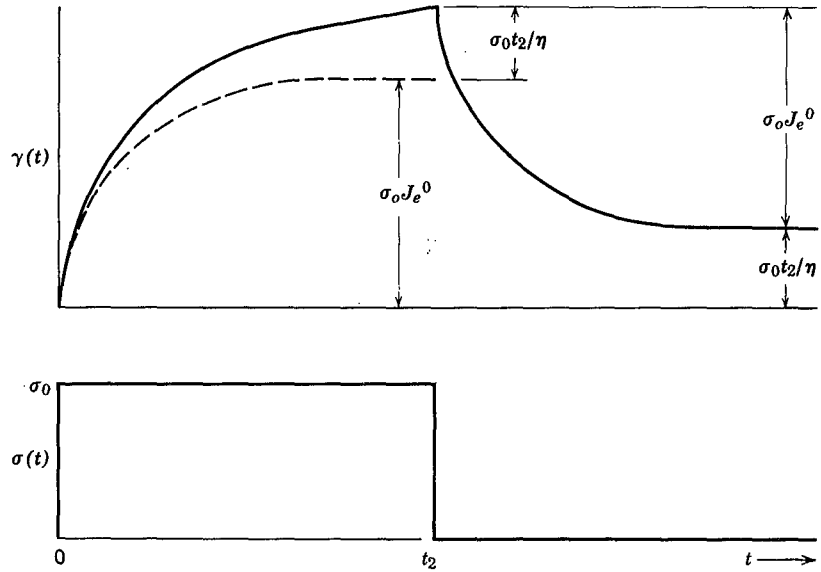


FIG. 1-12. Shear creep and creep recovery shown schematically for a viscoelastic liquid, *e.g.*, an uncross-linked polymer.

Leaderman.[1] These tests have more often been performed for deformation in simple extension than in shear; then equations 38 and 39 hold with D (defined in Section F below) substituted for J and appropriate changes in the stress and strain components.

If the deformations are not kept small, but are carried to the point where the elastic behavior is nonlinear, equations 38 and 39 do not hold. For soft polymeric solids, deviations from linearity appear sooner (*i.e.*, at smaller strains) in extension than in shear, because of the geometrical effects of finite deformations. At substantial deformations, the relations between creep and recovery are much more complicated than those given above, and require formulation by nonlinear constitutive relationships.

As explained in Section D, a viscoelastic liquid, such as an uncross-linked polymer whose threadlike molecules are not permanently attached to each other, has no equilibrium compliance. Then under constant stress the rate of strain approaches a limiting value, and a situation of steady-state flow is eventually attained, governed by a Newtonian viscosity η_0 which is most readily visualized as the sum of all the viscosities in Fig. 1-9. Concomitantly, in this steady state the springs of the models are stretched to equilibrium extensions, representing elastic energy storage which is recoverable after the stress is removed. Thus, even though there is no equilibrium compliance, there is a steady-state compliance which is most readily visualized as the sum of the deformations of the springs in Fig. 1-10 (equipped with a viscosity in series to make it a viscoelastic liquid) divided by the stress.

For such a material, the shear creep followed by creep recovery is shown schematically in Fig. 1-12. The creep is the sum of a deformation approaching a con-

stant value $J_e^0\sigma_0$, analogous to $J_e\sigma_0$ in Fig. 1–11, plus a viscous flow contribution $\sigma_0 t/\eta_0$. Here J_e^0 is the steady-state compliance, a measure of the elastic deformation during steady flow. After a sufficiently long time (but before the stress is removed at t_2) the creep strain is given by

$$\gamma(t) = \sigma_0(J_e^0 + t/\eta_0) \tag{40}$$

Thus both J_e^0 and η_0 can be obtained from the geometry of a linear plot in this region; whereas the strain during the recovery is given by

$$\gamma(t) = \sigma_0[J_e^0 + t/\eta_0 - J(t - t_2)] \tag{41}$$

and it approaches a final value of $\sigma_0 t_2/\eta_0$, providing an alternative determination of η_0. At stresses sufficiently high to evoke substantial strain rates, these linear equations do not hold, and elastic recovery must be formulated in a much more complicated manner.

Equations 36 to 41 are written for simple shear. Analogous relations hold for simple extension with all J's replaced by D's and the shear viscosity η_0 replaced by the tensile viscosity $\bar{\eta}_0$, which is defined as $\sigma_T/\dot{\epsilon}$ in steady flow (see Section F below).

The sharp dichotomy between viscoelastic solids (ordinarily, cross-linked polymer systems) and viscoelastic liquids (ordinarily, uncross-linked polymer systems) is apparent in all the time-dependent and frequency-dependent viscoelastic functions which describe their mechanical behavior in small deformations. Examples of these functions for various types of each of the two classes will be surveyed in the next chapter.

F. LINEAR STRESS-STRAIN RELATIONS FOR OTHER TYPES OF DEFORMATION

In simple shear, the change in shape is not accompanied by any change in volume; this feature facilitates interpretation of the mechanical behavior in molecular terms. There are other deformation geometries which are characterized by a change in volume or combined change in volume and shape. To describe the mechanical behavior under such conditions it is necessary to introduce a more complicated constitutive equation including all components of the stress tensor with two time-dependent functions.[21]

$$\sigma_{ij} = \int_{-\infty}^{t} \{G(t - t')[\dot{\gamma}_{ij}(t') - \tfrac{1}{3}\textstyle\sum \dot{\gamma}_{kk}(t')\,\delta_{ij}] + \tfrac{3}{2}K(t - t')\,[\tfrac{1}{3}\textstyle\sum \dot{\gamma}_{kk}(t')\,\delta_{ij}]\}\,dt' \tag{42}$$

where δ is the Kronecker delta. Here $G(t)$ is the same shear stress relaxation modulus as in the preceding section; $K(t)$ has the physical significance of a volumetric relaxation modulus as will be shown by treatment of a bulk compression experiment, below.

When perceptible changes in volume occur, both $G(t)$ and $K(t)$ are found to depend strongly on the density or degree of compression or dilatation (Chapters 11 and 18). Hence linear behavior must be limited to extremely small volume changes.

1. Bulk Compression or Dilatation

If the dimensions of an isotropic cubical element are increased or decreased uniformly by application of normal forces on all faces (Fig. 1-13), $\sigma_{11} = \sigma_{22} = \sigma_{33} = -P$, the hydrostatic pressure, and all other stress components are zero; and the three $\dot{\gamma}_{kk}$ are equal. Equation 42 then becomes

$$-P = \tfrac{3}{2} \int_{-\infty}^{t} K(t - t')\dot{\gamma}_{kk}(t')dt' \tag{43}$$

A calculation corresponding to that of equations 10 and 12 will provide the time dependence of pressure following a sudden voluminal deformation. For this purpose, the voluminal strain may be defined as the relative change in volume,

$$(V - V_0)/V_0 = (1 + \gamma_{11}/2)(1 + \gamma_{22}/2)(1 + \gamma_{33}/2) - 1 \tag{44}$$

For very small strains, this is $\frac{1}{2}\Sigma_k \gamma_{kk}$, the so-called dilation Δ_v; for compression, Δ_v is negative. After an initial change Δ_v accomplished within a very small time interval at $t = 0$, we have by an operation analogous to the derivation of equation 12:

$$P(t) = -\Delta_v K(t) \tag{45}$$

analogous to equation 12 for shear; $K(t)$ is termed the bulk relaxation modulus. (If the reference state is ambient pressure P_a, then $P(t)$ in this and equation 46 should strictly be replaced by $P(t) - P_a$; experiments usually involve rather high pressures so the difference is slight.) Alternatively, if the pressure P is applied suddenly and the volume change is followed as a function of time, the bulk creep experiment is described by the analog of equation 15,

$$\Delta_v(t) = -PB(t) \tag{46}$$

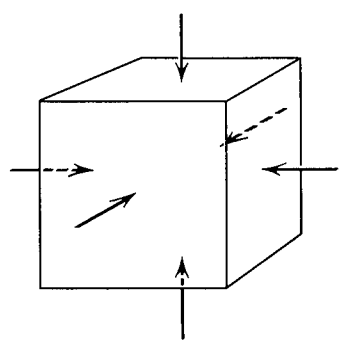


FIG. 1-13. Geometrical arrangement for bulk compression.

where $B(t)$ is the bulk creep compliance. The complex dynamic modulus K^* and compliances B^* can be defined in the same way as those for shear, with $K^* = K' + iK''$ and $B^* = B' - iB''$. The storage bulk modulus K' is the component of bulk stress in phase with the volume strain divided by the strain, etc. A summary of all moduli and compliances is given in Supplement 1 at the end of this chapter. For a solid or liquid in which there is no time-dependent response, or for any material at equilibrium under pressure, $B(t)$ and B^* become the thermodynamic compressibility $\beta = -(1/V)(\partial V/\partial P)_T$ (since $V \cong V_0$ for small deformations); and $K(t)$ and K^* become the equilibrium bulk modulus K.

Bulk compression would not be expected to involve changes in long-range molecular configuration or contour shape, and in fact the differences between polymers and ordinary liquids and solids are not so striking in compression as in shear.

The subscript T in the above partial derivative implies an isothermal measurement, and indeed all of the experimental examples given here are supposed to be carried out isothermally. The relation between isothermal and adiabatic moduli is considered in Chapter 5.

2. Simple Extension

If an isotropic cubical element is elongated in one direction and the dimensional changes in the two mutually perpendicular directions are equal (Fig. 1-14), the experiment is termed simple extension; if γ_{11} is positive, γ_{22} and γ_{33} are equal to each other and negative (or possibly zero). The stresses are $\sigma_{11} = \sigma_T - P_a$, $\sigma_{22} = \sigma_{33} = -P_a$, where σ_T is the tensile stress resulting from the applied force and P_a is the ambient pressure. This type of deformation results when a rod, strip, or fiber is subjected to a tensile force. Equation 42 for this case becomes[22]

$$\sigma_{11}(t) = \int_{-\infty}^{t} \{\tfrac{2}{3}G(t-t')[\dot{\gamma}_{11}(t') - \dot{\gamma}_{22}(t')] + \tfrac{1}{2}K(t-t')[\dot{\gamma}_{11}(t') + 2\dot{\gamma}_{22}(t')]\}dt' \quad (47)$$

also, since $\sigma_{22}(t) = -P_a$,

$$\int_{-\infty}^{t} \{\tfrac{1}{3}G(t-t')[\dot{\gamma}_{22}(t) - \dot{\gamma}_{11}(t)] + \tfrac{1}{2}K(t-t')[\dot{\gamma}_{11}(t') + 2\dot{\gamma}_{22}(t')]\}dt = -P_a \quad (48)$$

Elimination of $K(t)$ from equations 47 and 48 gives the analog of equation 7 for this deformation:

$$\sigma_{11}(t) = \int_{-\infty}^{t} G(t-t')\dot{\gamma}_{11}(t')dt' - \int_{-\infty}^{t} G(t-t')\dot{\gamma}_{22}(t')dt' - P_a \quad (49)$$

Although γ_{11} is constant by definition during the stress relaxation experiment, γ_{22} will in general change. The relation between axial extension and lateral contraction for a perfectly elastic solid is specified by Poisson's ratio μ:

$$\mu = -\gamma_{22}/\gamma_{11} = \frac{1 - \Delta_v/\epsilon}{2} \quad (50)$$



FIG. 1-14. Geometrical arrangement for simple extension.

where ϵ is the practical tensile strain, $\partial u_1/\partial x_1 = \frac{1}{2}\gamma_{11}$. In a viscoelastic material. μ is a function of time. An operation analogous to the derivation of equation 12 then gives[22]

$$\sigma_{11}(t) = \gamma_{11}[G(t) + \int_{-\infty}^{t} G(t - t')\dot{\mu}(t')dt'] - P_a$$

and the tensile stress is

$$\sigma_T(t) = \gamma_{11}[G(t) + \int_{-\infty}^{t} G(t - t')\mu(t')dt'] \tag{51}$$

The quantity in brackets is[22] $E(t)/2$, where $E(t)$ is the tensile relaxation modulus or time-dependent Young's modulus. Hence,

$$\sigma_T(t) = \epsilon E(t) \tag{52}$$

the analog of equation 12 for shear.

For a perfectly elastic solid, or a viscoelastic solid at equilibrium, the equilibrium Young's modulus is related to the shear and bulk moduli more simply as follows:[8,9]

$$E_e = \frac{9G_eK_e}{G_e + 3K_e} = 2G_e(1 + \mu_e) \tag{53}$$

but when G and K are time-dependent, $E(t)$ must be specified in terms of G and

μ by the integral in equation 51; the reader is referred to the treatise of Tschoegl[22] for its derivation.

For creep in extension, the shear and bulk functions combine in a somewhat simpler manner. A sudden tensile stress σ_T produces a time-dependent strain

$$\epsilon(t) = \sigma_T D(t) \tag{54}$$

where $D(t)$ is the tensile creep function, which is related to shear and bulk creep thus:

$$D(t) = J(t)/3 + B(t)/9 \tag{55}$$

The complex dynamic tensile modulus $E^* = E' + iE''$ and compliance $D^* = D' - iD''$ are defined by analogs of equations 19–30.

Tensile experiments are often easy to perform but have the disadvantage that simultaneous changes in both shape and volume make the behavior more difficult to interpret on a molecular basis; moreover, perceptible volume changes may significantly modify the relaxation functions as mentioned above. However, in polymeric systems, in certain broad ranges of time scale, $K(t)$ is often greater than $G(t)$ by two orders of magnitude or more. This condition corresponds to a Poisson's ratio μ very close to $\frac{1}{2}$ (*e.g.*,.0.499), and in this case equations 51 and 55 become

$$E(t) = 3G(t) \tag{56}$$

$$D(t) = J(t)/3 \tag{57}$$

Then simple extension gives the same information as simple shear, and the results of the two experiments are interconvertible. Physically, this fact arises because the change in volume caused by the extension is negligible in comparison with the change in shape. When $J \gg B$ or $G \ll K$, the material is often loosely but inaccurately called "incompressible"; a "soft elastic solid" might be better. (In fact, the equilibrium compressibility β is generally *higher* for such solids than for "hard solids" for which G and K are similar in magnitude.) For any viscoelastic material, there will in general be some conditions (especially short times or high frequencies) under which G will approach K in magnitude and the approximations of equations 56 and 57 will not be applicable. This situation corresponds to a value of μ substantially less than $\frac{1}{2}$; the minimum value ordinarily observed is about 0.2 for homogeneous, isotropic materials, but it may be smaller for certain heterogeneous materials such as cork or sponge rubber. (A value of $\mu = 0$ would mean that $\Delta_v = \epsilon$ and axial extension would be accompanied by no lateral contraction at all.)

The statement in connection with equations 56 and 57 that simple extension gives the same information as simple shear is limited not only to materials with μ very near $\frac{1}{2}$ but also to small deformations. With large deformations and/or large rates of deformation, the two types of strain show very different behavior. For example, in steady-state flow, the apparent shear viscosity (ratio of stress to rate of strain) commonly decreases with increasing rate of strain, whereas the apparent elongational viscosity may remain constant or increase. Some examples will be shown in Chapters 13 and 17.

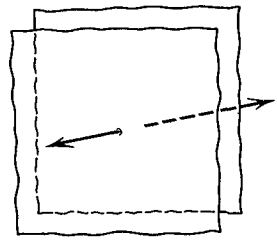


FIG. 1-15. Geometrical arrangement for bulk longitudinal deformation.

3. One-Dimensional Extension in Infinite Medium (Bulk Longitudinal Deformation)

An alternative version of extension occurs when the dimensions change in one direction and are constrained to be constant in the two mutually perpendicular directions. This is achieved by placing a thin flat sample, whose faces are bonded to rigid members, under tension or compression in the thin direction, colloquially termed "poker chip geometry" (Fig. 1-15), or by axial compression of a cylinder confined by a rigid cylindrical wall. Under these conditions, $\gamma_{22} = \gamma_{33} = 0$. If a sudden tensile strain $\epsilon = \frac{1}{2}\gamma_{11}$ is accomplished and the stress relaxation is followed as a function of time, a calculation analogous to that of the preceding section gives

$$\sigma_T(t) = \epsilon[K(t) + (4/3)G(t)] \tag{58}$$

The quantity in brackets is denoted by $M(t)$, and may be called the bulk longitudinal relaxation modulus. For a soft elastic solid with μ only slightly different from $\frac{1}{2}$ and $K \gg G$, $M(t)$ is evidently indistinguishable from the bulk modulus. The corresponding complex dynamic modulus $M^* = M' + iM''$ can be defined in the usual manner. The propagation of a longitudinal elastic wave in a medium all of whose dimensions are large compared with the wavelength is specified by M^* and the density of the medium (Chapter 8); M^* is much more commonly measured experimentally than $M(t)$.

4. Inhomogeneous Deformations

The relations discussed above can be applied directly to homogeneous deformations of a body in which the strains are the same everywhere in the sample and the macroscopic deformation of the sample is essentially the same as that of any infinitesimal element of it. In many deformation geometries commonly used for experimental measurements, however, such as torsion between coaxial cylinders, torsion of a cylindrical rod, flow through a tube, flexure, etc., the magnitudes of the strains and rates of strain vary from point to point. Application of the equations of continuity and motion and integration over the sample geometry are then necessary to relate external forces and displacements to the viscoelastic functions. For some cases, if the deformations are small, the geometry is no real complication;

for example, in any kind of torsion, a sudden angular deformation followed by measurement of the torque as a function of time will provide the shear relaxation modulus $G(t)$. For large deformations, however, different experimental geometries provide different kinds of information. Specific examples will be given in Chapters 5–8.

G. FINITE STRAINS AND LARGE STRAIN RATES

When strains are not infinitesimal, the definitions of equation 3 are inapplicable; there are then various alternative ways of defining finite strain. One fortunate simplification is that for most viscoelastic substances which are sufficiently soft to support substantial deformations without breaking, $K \gg G$ and so volume changes can be neglected; *i.e.*, the material is treated as incompressible. (Although, as stated previously, there will in general be some range of time or frequency where this inequality does not hold, large deformations will usually be possible only under conditions where it does.) In this case, relations between stress and strain involve only characteristic functions which are analogous to shear relaxation moduli or memory functions.

For infinitesimal deformations of materials for which volume changes can be neglected, equation 7 can then be generalized to include all components of the total stress tensor:

$$\sigma_{ij}(t) = -P\delta_{ij} + \int_{-\infty}^{t} G(t - t')\dot{\gamma}_{ij}(t')dt' \tag{59}$$

Because of the assumption of incompressibility, the pressure P is no longer the thermodynamic pressure which is the variable in Section F1 above; in fact, P is now not a single-valued function of the density ρ. However, P is irrelevant to rheological behavior since only differences of the normal stresses σ_{ii} are considered and hence the pressure term cancels, as shown below. (However, even with $K \gg G$, a small finite compressibility will cause $G(t)$ to be a function of P, as discussed in Chapter 11.)

At finite deformations, equation 59 can be shown to be incorrect[10] because it is not "objective"; *i.e.*, it predicts results which erroneously depend on the orientation of the sample with respect to laboratory coordinates. This error can be eliminated by replacing $\dot{\gamma}_{ij}$ in equation 59 by the components of a "corotational" rate-of-strain tensor or the components of one of several possible "codeformational" rate-of-strain tensors; either of these replacements ensures that the unwanted dependence of σ_{ij} on the instantaneous orientation of a fluid particle in space is removed. If the stress-strain relations are linear within the changing coordinate frame, equation 59 is modified only be replacing $\dot{\gamma}_{ij}$ with a different strain rate tensor whose definition is complicated and beyond the scope of this discussion.[10] The corresponding corotational model is that of Goddard and Miller[23] and the codeformational models correspond to those of Lodge[14,24] or Oldroyd,[25] Walters,[26] and Fredrickson.[27]

A modification of equation 59 in which the rate of strain tensor is replaced by

an appropriate derivative has been called the equation of finite linear viscoelasticity.[21,28,29] In finite linear viscoelasticity, time dependence is still described by the Boltzmann superposition integral (or equivalently, by linear differential equations with constant coefficients), but the infinitesimal strain is replaced by a finite strain. An example which has been extensively applied to describe experimental data successfully is the equation of Tschoegl and co-workers[30–32] in which $\dot{\gamma}_{ij}$ in equation 59 is replaced by the derivative of an objective nonlinear strain measure.

These single-integral constitutive equations are special cases of multiple memory integral expansions which involve additional functions analogous to $G(t)$ but dependent on more than one time interval together with combinations of strain or strain rate tensors specified at those time intervals. A thorough analysis of many specific equations and their interrelations is given in the treatise of Bird, Armstrong, and Hassager.[10]

1. Normal Stress Differences

A consequence of finite deformations is the appearance of normal stresses in simple shearing deformations. Thus, even in steady-state simple shear flow (Fig. 1-16) where the rate of strain tensor (*cf.* equations 3 and 5) is

$$\dot{\gamma}_{ij} = \begin{pmatrix} 0 & 1 & 0 \\ 1 & 0 & 0 \\ 0 & 0 & 0 \end{pmatrix} \dot{\gamma} \tag{60}$$

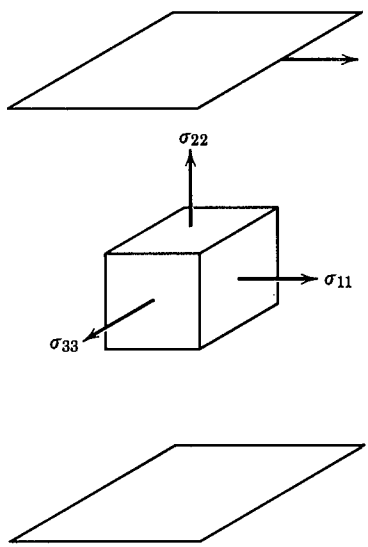


FIG. 1-16. Normal stresses in steady-state shear flow.

the stress tensor has different diagonal components:

$$\sigma_{ij} = \begin{pmatrix} \sigma_{11} & \sigma_{12} & 0 \\ \sigma_{21} & \sigma_{22} & 0 \\ 0 & 0 & \sigma_{33} \end{pmatrix} \tag{61}$$

The normal stresses σ_{ii} cannot be specified on an absolute basis because of the arbitrary hydrostatic pressure in equation 59, but their differences are predicted by continuum mechanics and several molecular theories and can be measured. The primary and secondary normal stress differences are defined as $\sigma_{11} - \sigma_{22}$ and $\sigma_{22} - \sigma_{33}$ respectively. Data are often expressed in terms of the primary normal stress coefficient

$$\Psi_1 = (\sigma_{11} - \sigma_{22})/\dot{\gamma}^2 \tag{62}$$

and the secondary normal stress coefficient

$$\Psi_2 = (\sigma_{22} - \sigma_{33})/\dot{\gamma}^2 \tag{63}$$

At low values of $\dot{\gamma}$, the coefficients Ψ_1 and Ψ_2 approach the "zero-shear-rate" limits of $\Psi_{1,0}$ and $\Psi_{2,0}$ respectively. All the single-integral equations mentioned above predict for the limiting primary normal stress coefficient:

$$\Psi_{1,0} = 2\int_0^\infty tG(t)dt \tag{64}$$

It will be shown in Chapter 3 that this relation is equivalent to $\Psi_{1,0} = 2\eta_0^2 J_e^0$. The predictions of different nonlinear models for the magnitude of Ψ_2 vary considerably, but for most materials investigated thus far Ψ_2 is found to be less than Ψ_1 and of opposite sign.

If steady shear flow of a viscoelastic liquid is abruptly halted, the normal stress differences $\sigma_{11} - \sigma_{22}$ and $\sigma_{22} - \sigma_{33}$ decay gradually with time but fall off more rapidly than does the shear stress σ_{12} (Fig. 1-5). Also, for sinusoidally varying shear strains, each normal stress difference is a sinusoidal function of time, with oscillatory components at twice the frequency of the shear strain about a nonzero mean value. Some of these relations are given in Chapter 3. Other time-dependent experimental patterns of strain or stress history evoke various characteristic nonlinear phenomena.

A perfectly elastic solid subjected to large shear deformations also exhibits normal stress differences.[33] At equilibrium these are constant and strictly speaking outside the scope of viscoelasticity. The simplest extension beyond infinitesimal deformations leads to the relation[14]

$$\sigma_{11} - \sigma_{22} = G_e\gamma_{21}^2 = \sigma_{21}^2/G_e \tag{65}$$

For viscoelastic solids, time-dependent shearing deformations produce normal stress differences which are time or frequency dependent.

For both viscoelastic liquids and viscoelastic solids, combinations of large shear rates or large static deformations, respectively, with small time-dependent deformations result in a variety of characteristic behavior, some examples of which will be given in subsequent chapters.

2. Non-Newtonian Flow

In polymeric liquids, the ratio $\sigma_{21}/\dot{\gamma}_{21}$ in steady shearing flow is independent of $\dot{\gamma}_{21}$ when $\dot{\gamma}_{21}$ is vanishingly small, but at higher shear rates it falls with increasing $\dot{\gamma}_{21}$, sometimes by several orders of magnitude. This ratio for a Newtonian liquid is of course a constant, the viscosity. For polymeric liquids it is called the non-Newtonian viscosity η, and its value at vanishing $\dot{\gamma}_{21}$ ("zero-shear viscosity") is written as η_0.

At very low shear rates, the normal stress coefficients $\Psi_{1,0}$ and $\Psi_{2,0}$ are also independent of $\dot{\gamma}_{21}$; *i.e.*, the normal stress differences are proportional to $\dot{\gamma}_{21}^2$. At higher shear rates, Ψ_1 and Ψ_2 are observed to decrease. The course of stress relaxation after cessation of steady-state flow and the magnitude of the steady-state compliance J_e^0 are also strongly affected at high shear rates. In general, description of these phenomena requires more complicated constitutive equations than the single-integral models mentioned above.

3. Other Time-Dependent Phenomena

In addition to the normal stress differences and manifestations of non-Newtonian flow mentioned above, all the viscoelastic experiments described in Section C above (stress relaxation after sudden strain, stress relaxation after cessation of steady flow, creep, creep recovery, behavior in oscillating deformations, etc.) become much more complicated when deformations are large. A few examples will be shown in Chapter 2 and others in Chapters 13 and 17.

The writer is particularly indebted to Professors R. B. Bird, N. W. Tschoegl, and M. W. Johnson for advice in formulating this chapter.

SUPPLEMENT 1: SUMMARY OF MODULI AND COMPLIANCES

The various moduli and compliances which have been introduced for infinitesimal deformations are summarized in Table 1-I, including the glasslike modulus and compliance which will be explained in Chapter 2. All moduli have the dimensions of stress (units usually dynes/cm^2 or alternatively Pa); all compliances have the dimensions of reciprocal stress (usually cm^2/dyne or Pa^{-1}). Certain quantities in any row of the table can be interrelated by equations of the form of 55 and 58. The symbols follow rather closely the recommendations of a Committee of the Society of Rheology.[34]

Table 1-I

SUMMARY OF MODULI AND COMPLIANCES

Deformation	Simple Shear	Bulk Compression	Simple Extension[a]	Bulk Longitudinal
Relaxation Modulus	$G(t)$	$K(t)$	$E(t)$	$M(t)$
Creep Compliance	$J(t)$	$B(t)$	$D(t)$	—
Complex Modulus	$G^*(\omega)$	$K^*(\omega)$	$E^*(\omega)$	$M^*(\omega)$
Storage Modulus	$G'(\omega)$	$K'(\omega)$	$E'(\omega)$	$M'(\omega)$
Loss Modulus	$G''(\omega)$	$K''(\omega)$	$E''(\omega)$	$M''(\omega)$
Complex Compliance	$J^*(\omega)$	$B^*(\omega)$	$D^*(\omega)$	—
Storage Compliance	$J'(\omega)$	$B'(\omega)$	$D'(\omega)$	—
Loss Compliance	$J''(\omega)$	$B''(\omega)$	$D''(\omega)$	—
Equilibrium Modulus	G_e	K_e	E_e	M_e
Glasslike Modulus	G_g	K_g	E_g	M_g
Equilibrium Compliance	J_e	$B_e(=\beta)$	D_e	—
Glasslike Compliance	J_g	B_g	D_g	—
Steady-State Compliance	J_e^0	—	D_e^0	—
Steady-Flow Viscosity[b]	η_0	—	$\bar{\eta}_0$	—
Dynamic Viscosity	$\eta'(\omega)$	$\eta_v'(\omega)$	$\bar{\eta}'(\omega)$	$\eta_m'(\omega)$

[a] For this type of deformation each modulus may be called a Young's modulus (relaxation Young's modulus, storage Young's modulus, etc.).

[b] At vanishing shear rate.

SUPPLEMENT 2: COMPLEX NOTATION FOR DYNAMIC (SINUSOIDAL) STRESS-STRAIN RELATIONS

In Section C6, a sinusoidally varying shear strain was expressed as

$$\gamma = \gamma^0 \sin \omega t \tag{16}$$

For comparison with complex notation, it is more convenient to change the phase by $\pi/2$ and write

$$\gamma = \gamma^0 \cos \omega t \tag{66}$$

In this case, the shear stress for linear viscoelastic behavior will be

$$\sigma = \gamma^0(G' \cos \omega t - G'' \sin \omega t) = \gamma^0 \sqrt{G'^2 + G''^2} \cos(\omega t + \delta) \tag{67}$$

To derive this relation with complex notation, a complex time-dependent strain and stress are defined as

$$\gamma^* = \gamma^0 e^{i\omega t} \tag{68}$$

$$\sigma^* = \sigma^0 e^{i(\omega t + \delta)} \tag{69}$$

where γ^0 and σ^0 are the magnitudes of the corresponding complex quantities. The complex shear modulus, which unlike the ratio σ/γ is time invariant, is

$$G^* = G' + iG'' = \sigma^*/\gamma^* = (\sigma^0/\gamma^0)e^{i\delta} = (\sigma^0/\gamma^0)(\cos\delta + i\sin\delta) \quad (70)$$

Comparison of the real and imaginary parts in equation 70 shows that

$$G' = (\sigma^0/\gamma^0)\cos\delta \quad (21)$$

$$G'' = (\sigma^0/\gamma^0)\sin\delta \quad (22)$$

as stated earlier.

The loss modulus G'' and compliance J'' are often called the "imaginary" parts of their complex counterparts by analogy with the language of dielectrics and optics in which such notation is conventional. However, G'' and J'' are of course real quantities which are the coefficients of the imaginary terms in equations 24 and 26. The complex notation is particularly convenient for interconverting modulus and compliance as expressed by equations 27 to 30.

REFERENCES

1. H. Leaderman, *Elastic and Creep Properties of Filamentous Materials and Other High Polymers,* The Textile Foundation, Washington, 1943.
2. W. Weber, *Pogg. Ann.*, (2) **4**, 247 (1835).
3. R. Kohlrausch, *Pogg. Ann.*, (3) **12**, 393 (1847).
4. L. Boltzmann, *Wied. Ann.*, **5**, 430 (1878).
5. C. Kittel, *Introduction to Solid-State Physics,* 4th ed., Wiley, New York, 1971.
6. N. Ashcroft, *Solid-State Physics,* Rinehart and Winston, New York, 1976.
7. J. G. Kirkwood, *J. Chem. Phys.*, **14**, 180 (1946); S. A. Rice and J. G. Kirkwood, *ibid.*, **31**, 901 (1959).
8. T. Alfrey, Jr., *Mechanical Behavior of High Polymers,* Interscience, New York, 1948.
9. R. B. Bird, W. E. Stewart, and E. N. Lightfoot, *Transport Phenomena,* Wiley, New York, 1960.
10. R. B. Bird, R. C. Armstrong, and O. Hassager, *Dynamics of Polymeric Liquids,* Volume I, Wiley, New York, 1977.
11. L. D. Landau and E. M. Lifschitz, *Theory of Elasticity,* Pergamon Press, London, 1959.
12. N. W. Tschoegl, *The Theory of Linear Viscoelastic Behavior,* Springer-Verlag, to be published.
13. A. G. Frederickson, *Principles and Applications of Rheology,* Prentice-Hall, Englewood Cliffs, N. J., 1964.
14. A. S. Lodge, *Elastic Liquids,* Academic Press, New York, 1964.
15. A. E. H. Love, *A Treatise on the Mathematical Theory of Elasticity,* 4th ed., Dover, New York, 1944.
16. Y. C. Fung, *Foundations of Solid Mechanics,* Prentice-Hall, Englewood Cliffs, N. J., 1965.
17. A. S. Lodge, *Body Tensor Fields in Continuum Mechanics,* Academic Press, New York, 1974.
18. H. Poincaré, *The Foundations of Science,* Science, New York, 1929, p. 181.
19. W. Kuhn, *Helv. Chim. Acta.*, **30**, 487 (1947).
20. L. Boltzmann, *Pogg. Ann. Phys.*, **7**, 624 (1876).
21. B. D. Coleman and W. Noll, *Rev. Mod. Phys.*, **33**, 239 (1961).
22. N. W. Tschoegl, *The Theory of Linear Viscoelastic Behavior,* Academic Press, 1981, Section 11-4.
23. J. D. Goddard and C. Miller, *Rheol. Acta,* **5**, 177 (1966).
24. A. S. Lodge, *Trans. Faraday Soc.*, **52**, 120 (1956).
25. J. G. Oldroyd, *Proc. R. Soc.*, **A200**, 45 (1950).

26. K. Walters, *Q. J. Mech. Appl. Math.*, **13,** 444 (1960).
27. A. G. Frederickson, *Chem. Eng. Sci.*, **17,** 155 (1962).
28. H. Markovitz and B. D. Coleman, *Adv. Appl. Mech.*, **8,** 69 (1964).
29. W. R. Schowalter, *Mechanics of Non-Newtonian Fluids,* Pergamon Press, New York, 1978, pp. 180–183.
30. W. V. Chang, R. Bloch, and N. W. Tschoegl, *J. Polym. Sci., Polym. Phys. Ed.*, **15,** 923 (1977).
31. R. Bloch, W. V. Chang, and N. W. Tschoegl, *J. Rheol.*, **22,** 1 (1978).
32. W. V. Chang, R. Bloch, and N. W. Tschoegl, *Rheol. Acta,* **15,** 367 (1976).
33. R. S. Rivlin, in *Rheology,* edited by F. R. Eirich, Volume I, Chapter 10, Academic Press, New York, 1956.
34. C. L. Sieglaff, *Trans. Soc. Rheol.*, **20,** 311 (1976).

CHAPTER 2

Illustrations of Viscoelastic Behavior of Polymeric Systems

It seems desirable at this point to familiarize the reader with some concrete examples of the viscoelastic phenomena defined in the preceding chapter, and to provide an idea of their character as exhibited by various types of polymeric systems. Linear viscoelastic behavior in shear will be illustrated in considerable detail, with a few additional examples of bulk viscoelastic behavior and nonlinear phenomena. The examples are accompanied by some qualitative remarks about molecular interpretation, anticipating Chapters 9 and 10 where molecular theories will be discussed more quantitatively.

A. LINEAR VISCOELASTIC BEHAVIOR IN SHEAR OR SIMPLE EXTENSION

When the shear creep compliance or the shear relaxation modulus for a particular polymer is plotted against time, or any one of the dynamic functions is plotted against frequency, the most striking feature is the enormous range of magnitudes which the ordinate can assume, changing over several powers of 10. Concomitantly, a still larger range of time or frequency is required on the abscissa scale to encompass these changes. As a result, both coordinates are usually plotted logarithmically. Inspection of such logarithmic graphs reveals a pattern of certain zones on the time (or frequency) scale, where the viscoelastic functions have characteristic shapes: the transition zone from glasslike to rubberlike consistency, the plateau zone, the pseudo-equilibrium zone (in cross-linked polymers), the terminal zone (in uncross-linked polymers), etc. These regions can be associated qualitatively with different kinds of molecular responses, and appear with different degrees of

prominence depending on whether the polymer is of low or high molecular weight, amorphous or crystalline, above or below its glass transition temperature, and undiluted or mixed with solvent.

Eight polymeric systems have been chosen as examples of these alternatives to illustrate the variety of viscoelastic responses and the gross correlation of behavior in different time and frequency zones with molecular structure. The graphs to be portrayed here represent experimental data from the literature which have been combined by the method of reduced variables (alluded to in the preceding chapter, and discussed in detail in Chapter 11) to cover as wide a range as possible of the effective time or frequency scale. All the measurements were made on isotropic materials at sufficiently low stresses so that the viscoelastic behavior was linear, and the deformation was usually simple shear though in two cases it was simple extension (in which the shear effects predominate). It was necessary in all cases to calculate some of the viscoelastic functions indirectly from others that were directly measured, using the interconversion methods which were alluded to in the preceding chapter and which will be spelled out in detail in Chapters 3 and 4.

1. Description of the Polymers Chosen for Illustration

The first four systems involve uncross-linked polymers; they are viscoelastic liquids in the sense that they do not possess any equilibrium compliance and exhibit viscous flow at sufficiently long times. (The reader is reminded, however, that such a viscoelastic liquid may have a very high viscosity and the superficial appearance of a rubbery solid.)

I. To illustrate a *dilute polymer solution,* in which the viscoelasticity is a relatively minor perturbation of the Newtonian behavior of the solvent: a solution of atactic polystyrene, 0.015 g/ml in Aroclor 1248, a chlorinated diphenyl with viscosity 2.57 poise at 25°C. The weight-average molecular weight was 860,000 with narrow molecular weight distribution. Dynamic shear data by Massa, Schrag, and Ferry[1] are reduced to 25°C.

The significance of the reference temperature is that the reduced curves represent the viscoelastic functions as they would have been measured at 25°C over a much wider range of time or frequency scale than the actual experimental measurements provided; *cf.* Chapter 11.

Dilute solutions such as this are of considerable interest because they represent the only type of system to which the molecular theories to be discussed in Chapter 9 are clearly applicable; the polymer molecules are sufficiently separated to move fairly independently without much interaction. The remaining examples described here are all undiluted polymers in which the molecules are extensively intertwined.

II. To illustrate an *amorphous polymer of low molecular weight:* a fractionated poly(vinyl acetate) with molecular weight 10,500. Shear creep data of Ninomiya and Ferry[2] were employed, reduced to 75°C. For a linear molecule as short as these (degree of polymerization about 120), the effects of neighboring molecules on

viscoelastic properties can be rather well described in terms of the local frictional forces encountered by a short segment of a moving chain (Chapter 10, Section A).

III. To illustrate an *amorphous polymer of high molecular weight:* an atactic polystyrene with narrow molecular weight distribution, molecular weight 600,000. Shear creep data of Plazek and O'Rourke[3] were employed, reduced to 100°C. Interconversion of viscoelastic functions was performed by S. J. Orbon.[4] Some of the data are tabulated in Appendix D. This is sharply differentiated from the preceding example by its higher molecular weight. Above a critical molecular weight, which for different polymers is of the order of 4000 to 30,000, the effect of neighbors on molecular motion can no longer be described solely in terms of local frictional forces; the viscoelastic properties reveal a strong additional coupling to neighbors which acts as though it were localized at a few widely separated points along the molecular chain. This phenomenon, generally known as entanglement coupling, is imperfectly understood, but it clearly prolongs very greatly any molecular rearrangements which are sufficiently long range to involve regions of a molecule separated from each other by one or more entanglement points. The term "entanglement" has come to be employed in this special sense, and is not currently applied to the short-range intermolecular entwining which must exist in all polymeric systems (other than very dilute solutions) regardless of their molecular length. An alternative model for the topological restraints represented by entanglements is that of a tube which surrounds each molecule along its contorted contour and to a considerable extent restricts its long-range motions to sliding along that contour. Here the average tube diameter has the same role as the average spacing between entanglements. These concepts will be discussed in more detail in Chapters 10 and 13.

IV. To illustrate an *amorphous polymer of high molecular weight with long side groups:* a fractionated poly(*n*-octyl methacrylate) of weight-average molecular weight 3,620,000. Dynamic and shear creep data of Dannhauser, Child, and Ferry[5] and Berge, Saunders, and Ferry[6] were employed, after reduction to a reference temperature of 100°C. Some of the data are tabulated in Appendix D.

The molecule differs from the preceding in that each monomer unit, with two chain atoms, carries a flexible side ester group which now comprises nearly three-fourths of the monomeric molecular weight. Thus only a small proportion of the total volume is occupied by the chain backbones.

The remaining four examples are viscoelastic solids in the sense that they do not exhibit viscous flow and under a constant stress they eventually reach (or closely approach) an equilibrium deformation.

V. To illustrate an *amorphous polymer of high molecular weight below its glass transition temperature:* a poly(methyl methacrylate) of high molecular weight. Shear stress relaxation[7] and shear creep[8] data of Iwayanagi were employed, reduced to a reference temperature of −22°C.

The distinguishing feature of this example is that the measurements are all far below the glass transition temperature (about 100°C) where the chain backbone

configurations are largely immobilized. Hence the response to external stress involves primarily very local adjustments somewhat similar to those in the mechanical deformation of an ordinary hard solid (amorphous glucose, for example).

For the present, the glass transition temperature T_g of any amorphous substance, whether polymeric or not, may be defined as the point where the thermal expansion coefficient α undergoes a discontinuity. Above this temperature, α has the magnitude generally associated with liquids—6 to 10×10^{-4} deg^{-1}. Decrease in temperature is accompanied by collapse of free volume which is made possible by configurational adjustments. Eventually, the free volume becomes so small that further adjustments are extremely slow or even impossible; then it no longer decreases and the further contraction in total volume with decreasing temperature is much less, so α drops suddenly to between 1 and 3×10^{-4} deg^{-1}.

In polymers, there may be more than one discontinuity in α. The highest is usually associated with the loss of the molecular mobility which permits configurational rearrangements of the chain backbones, and it profoundly alters the viscoelastic behavior; this is "the" glass transition. Others may be associated with the loss of much more specific, local motions, such as the rearrangements of short side groups.

The subject of the glass transition temperature is discussed at greater length in Chapter 11.

VI. To illustrate a *lightly cross-linked amorphous polymer:* lightly vulcanized Hevea rubber, vulcanized with sulfur and an accelerator to an equilibrium tensile modulus E_e of about 7×10^6 dynes/cm^2. Dynamic data, in simple extension, of Cunningham and Ivey[9] and Payne,[10] together with creep data in simple extension of Martin, Roth, and Stiehler,[11] were employed, all reduced to a reference temperature of 25°C. Certain minor adjustments in the data are described elsewhere.[12]

The molecular structure is a network of highly flexible threadlike strands whose average molecular weight between cross-links is about 4000. Relatively short-range segmental rearrangements are oblivious of the presence of the linkage points, but of course long-range rearrangements are profoundly affected.

VII. To illustrate a *very lightly cross-linked amorphous polymer:* a styrene-butadiene random copolymer with 23.5% styrene by weight, vulcanized with dicumyl peroxide to an equilibrium shear modulus G_e of about 1.5×10^6 dynes/cm^2. Dynamic shear data and shear creep data of Mancke and Ferry[13] were combined and reduced to 25°C. The feature which differentiates this example from the preceding one is the paucity of cross-links. The molecular weight between cross-linking points is about 23,000, and since the number-average molecular weight before cross-linking was about 100,000, there are only a few cross-linked points per initial molecule on the average. The network topology is then expected to include dangling branched structures[14,15] which are extensively entangled because the molecular weight between coupling entanglements[16] is only about 3000. Associated with these are prominent differences in the viscoelastic functions.

VIII. To illustrate a *highly crystalline polymer:* a linear polyethylene with a density of 0.965 g/ml at room temperature, corresponding to a high degree of crystallinity. Stress relaxation data of Faucher[17] in simple extension were employed,

reduced to a reference temperature of 20°C. (There was no evidence of a change in crystallinity over the temperature range within which experiments were utilized for reduction, *viz.*, −70° to 70°.)

The polymer may be pictured as a matrix of crystalline material with units of various forms such as lamellae and fibrils, containing various kinds of crystal defects and interfaced by regions of greater disorder. Both ordered and disordered regions will contribute to the viscoelastic behavior.

The characteristic linear viscoelastic behavior (in shear except for Examples VI and VIII, which are in extension) of these eight representative systems will now be reviewed.

2. The Creep Compliance

Plotted on a linear scale, the creep compliance of a viscoelastic liquid would look like the creep deformation as shown in Fig. 1-6, differing only by a proportionality factor of the stress. In analyzing creep experiments, such linear plots are invariably made to determine the quantities J_e^0 and η_0. But in presenting the overall aspect of $J(t)$, the ranges of both the magnitude of $J(t)$ and the time scale are so enormous (as mentioned above) that the only way to give a complete representation in a single graph is to make both coordinates logarithmic. This procedure is followed here for depicting all the viscoelastic functions. Both cgs and SI units usually appear on these graphs. A modulus is in dynes/cm^2 or pascals (Pa, or N/m^2) respectively; a compliance is in cm^2/dyne or Pa^{-1}. The conversion is 1 dyne/cm^2 = 0.1 Pa.

In comparing different structural types of polymers, it is the shapes and the magnitudes of the functions which are important; the positions of the curves on the logarithmic time scale are in a sense irrelevant since they depend sharply on the temperature and in any case the reference temperatures for the polymers compared here are not all the same. Purely for clarity in distinguishing the curves, arbitrary shifts along the logarithmic time (or frequency) axis have been made by adding to log t (subtracting from log ω) a constant A with the following values: I, −5; II, −6; III, −9; IV, 0; V, −7; VI, 0; VII, −1; VIII, 2. The same values of A have been used throughout this chapter. Thus the relative horizontal positions of the curves have no significance; it is their shapes and vertical positions which are to be scrutinized. The vertical positions of curve VI and VII will not be directly comparable with the others, because they represent deformation in extension instead of shear; the compliances will be lower and the moduli higher by about half an order of magnitude (factor of 2.5 to 3), as discussed in Section F2 of Chapter 1.

Figure 2-1 shows the creep compliance thus plotted for the eight typical systems, with the liquids on the left and the solids on the right. The tremendous range of time scale over which response to stress is achieved is immediately apparent.

At short times, $J(t)$ approaches a value of the order of 10^{-10} cm^2/dyne (10^{-9} Pa^{-1}), characteristic of a hard glasslike solid. The corresponding region of the time scale is sometimes called the glassy zone. This small compliance corresponds to the absence of any configurational rearrangements of the chain backbones within the interval of the experiment; indeed, curve V shows that below the glass transition

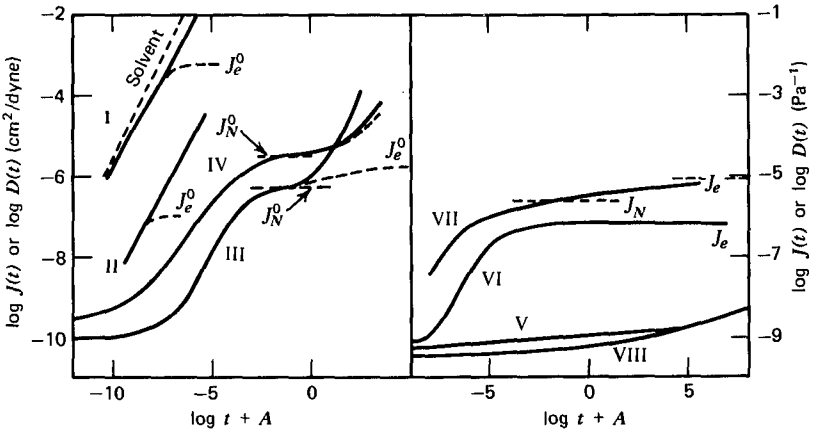


FIG. 2-1. Creep compliance plotted logarithmically for eight typical polymer systems: viscoelastic liquids on left, viscoelastic solids on right, identified by numbers as described in the text. Deformation is shear, $J(t)$, except for curves VI and VIII, which are for simple extension, $D(t)$. The dashed curves represent the compliance after subtraction of the flow contribution t/η_0. The solvent for the dilute solution, example I, is also shown as a dashed line.

temperature, where the backbone configurations are immobilized, $J(t)$ has this order of magnitude throughout the time scale. Approximately, $J(t)$ may be regarded as possessing a limiting value $J(0)$ at zero time, often written J_g, the subscript standing for glass. This value is often not very well defined operationally, however.

At long times, $J(t)$ for the viscoelastic liquids increases without limit, because it includes a contribution from viscous flow. But if the latter is subtracted, the remainder $J(t) - t/\eta_0$ approaches a limiting value J_e^0 (*cf.* equation 40 of Chapter 1). This value has been attained in examples I ($10^{-3.2}$ cm^2/dyne), II (10^{-7} cm^2/dyne), and III ($10^{-5.8}$ cm^2/dyne), but not in example IV because the very high molecular weight, together with coupling entanglements, greatly prolongs the time necessary for long-range configurational changes, and at the end of the experiment $J(t) - t/\eta_0$ is still increasing. In terms of models, J_e^0 is a measure of the energy stored in all the springs (Fig. 1-9) during steady-state flow; in molecular terms, it measures the average distortion of the polymer coils during flow, when ample time has been allowed for the molecular distribution function to become independent of time.

For the cross-linked rubbers, VI and VII, $J(t)$ at long times approaches a limiting value J_e, the equilibrium compliance, which according to the theory of rubberlike elasticity[18] is proportional to the number-average molecular weight of the network strands. A strand is often defined as a segment between cross-links, but trapped entanglements must also be taken into account in defining a strand, as discussed in Chapter 14. Both J_e^0 and J_e are measures of energy storage but are distinguished since the former refers to steady-state flow and the latter to elastic equilibrium.

The other viscoelastic solids, V and VIII, exhibit creep compliance which is still increasing slowly with time at the longest times of observation.

The creep compliance of the dilute solution, I (which could hardly be measured directly but must be calculated from dynamic measurements), is compared with a calculated curve for the solvent. For the latter, a Newtonian liquid, $J(t)$ is simply t/η_s. The solution compliance is lower than that of the solvent by an amount which is quite small at short times but somewhat larger at long times. The inflection between these regions lies at a point on the time scale related to the relaxation times for configurational rearrangements, to be discussed in detail in Chapter 9.

At intermediate times there is for each of the undiluted polymers, except the glasslike (V) and the highly crystalline (VIII), a gradual increase of $J(t)$, which rises by several powers of 10. This reflects the increasing response to external stress by configurational rearrangements, first of the relative positions of chain backbone segments near each other, then farther and farther apart, requiring more and more mutual cooperation and therefore more and more time (*cf.* Fig. 1-1). In the low molecular weight (II) and the moderately cross-linked polymers (VI) this rise occurs in a single stage, usually called the transition from glasslike to rubberlike consistency. It is not a transition in any thermodynamic sense, but merely reflects a change in the response of the system to experiments of different time scales. At the end of the transition zone, the elapsed time has become long compared with the time required for the slowest rearrangement of a molecule (in the cross-linked polymers, of a strand between two cross-linking points), and the average molecular distortion has approached its maximum. In the uncross-linked polymers of high molecular weight (III, IV) and the very lightly cross-linked network (VII), there are two stages. The first reflects the relative motion of chain segments between the entanglement coupling loci, and corresponds to the glass-rubber transition. At the end of this stage, $J(t)$ tends to level off at a value denoted by J_N^0 for the uncross-linked and J_N for the cross-linked systems, often called the plateau compliance. Here the entanglements (whether trapped or not) suppress long-range configurational rearrangements almost as though they were cross-links. The values of J_N^0 cannot usually be determined by inspection, since the curves do not really become flat in this region, but they can be calculated indirectly as described in Chapters 3 and 13. They are approximately proportional to the spacings between entanglement loci; the average spacing is evidently greater in Example IV than in Example III. In the second stage, where $J(t)$ rises from J_N^0 to J_e^0 for Example III (not achieved in IV), the entanglements slip so that configurational rearrangements of segments separated by entanglements can take place. The corresponding rise from J_N to J_e in Example VII is probably attributable to slippage of entanglements on branched structures which are incompletely attached to the network. At a higher degree of cross-linking (VI) such structures do not exist and the second inflection is eliminated.

The topological constraints which are described here in the framework of the concept of entanglement coupling can also be described in terms of obstacles which

tend to limit motion of a contorted molecule to sliding along its own contour, as will be discussed in Chapter 10.[19-21]

3. The Stress Relaxation Modulus

The modulus $G(t)$, defined as the stress/strain ratio at constant deformation, is plotted against t with logarithmic scales in Fig. 2-2. In certain regions, $G(t)$ is approximately $1/J(t)$, so that the logarithmic plots have roughly the appearance of mirror images of those in Fig. 2-1 reflected in the time axis. The more slowly $J(t)$ changes with time, the more nearly is the reciprocal relation approached. Thus, at short times, $G(t)$ appears to approach a limiting value which (if it exists) is $G_g = 1/J_g$, of the order of 10^{10} dynes/cm^2 (10^9 Pa), and represents the rigidity in the absence of backbone rearrangements. At long times, $G(t)$ for the cross-linked networks VI and VII approaches values which are again nearly constant, written $G_e = 1/J_e$ and representing the equilibrium shear modulus as treated by the theory of rubberlike elasticity.

At long times for the uncross-linked polymers, however, $G(t)$ falls rapidly and eventually vanishes. In terms of mechanical models, this corresponds to the complete relaxation of all springs in an array such as Fig. 1-9; in molecular terms, it corresponds to the resumption of random average configurations by the macromolecular coils, which have completely freed themselves from the constraints originally imposed on them, even though the external dimensions of the sample remain deformed. (The final residual deformation corresponds to the flow contribution to a creep experiment.) The region of time scale in which $G(t)$ falls sharply is often called the terminal zone. If the viscoelastic behavior is represented by a finite mechanical model such as Fig. 1-9, the decay of $G(t)$ must at the end become exponential, proportional to e^{-t/τ_1} where τ_1 is the terminal relaxation time. According to some molecular theories (Chapters 9 and 10), a well-defined terminal relaxation time should be observed for a polymer with uniform molecular weight, but for a broad

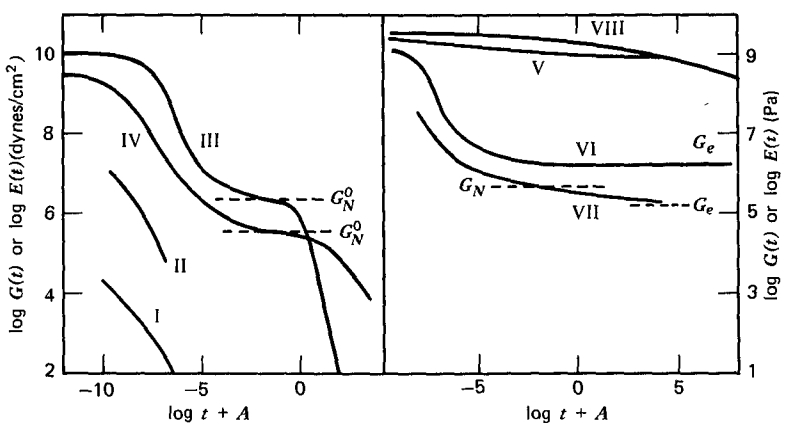


FIG. 2-2. Stress relaxation modulus for the eight systems identified as in Fig. 2-1.

molecular weight distribution the final stage of exponential relaxation may not be attainable. The much sharper drop in Example III compared with Example IV is due to the narrow molecular weight distribution of the former.

At intermediate times, the stress gradually falls as the distortion of the chain backbone adjusts itself through Brownian motion, first of segments with respect to closely neighboring segments, then with respect to those farther removed along the backbone contour, and so on (*cf.* Fig. 1-1). The drop occurs in two stages for the uncross-linked polymers of high molecular weight III and IV and the very lightly cross-linked network VII, just as the creep compliance rises in either one or two stages, and for the same reasons. Between the transition and terminal zones of III and IV, and the transition and slow relaxation zones of VII, $G(t)$ flattens somewhat at a level which again is associated with the average spacing between entanglement coupling points, and is approximately the reciprocal of J_N^0 or J_N respectively, *viz.*, G_N^0 or G_N. From the Boltzmann superposition principle it can be shown that $J(t)G(t) \leq 1$ for all values of t, so each drop in G(t) always occurs at somewhat shorter times than the corresponding rise in $J(t)$.

In the glassy polymer, V, there is very little stress relaxation over many decades of logarithmic time, since no backbone contour changes occur; in the densely crystalline polymer, VIII, there is some relaxation at very long times through whatever mechanism is responsible for the creep which also occurs in this region. Examples of stress relaxation after cessation of steady-state flow (Fig. 1-5) are not included here because of the limited applicability of this type of experiment. Such stress relaxation is of particular interest in connection with nonlinear phenomena, however, and will be illustrated in Section C below.

4. The Storage Modulus

The modulus $G'(\omega)$ is defined as the stress in phase with the strain in a sinusoidal shear deformation divided by the strain; it is a measure of the energy stored and recovered per cycle, when different systems are compared at the same strain amplitude. It is plotted against the radian frequency ω with logarithmic scales in Fig. 2-3. Since both $G(t)$ and $G'(\omega)$ are measures of stored elastic energy, and a dynamic measurement at frequency ω is qualitatively equivalent to a transient one at $t = 1/\omega$, these graphs are approximately mirror images of those for the relaxation modulus, reflected in the modulus axis. In particular, when $G(t)$ is changing very slowly, $G(t) \cong G'(1/t)$, so the values G_g and G_e characteristic of high and low frequencies are the same as those characteristic of short and long times respectively.

At long times for the viscoelastic liquids on the left of the figure, $G'(\omega)$ approaches 0 with decreasing frequency, just as $G(t)$ does with increasing t; macroscopically, this means that the phase angle between stress and strain approaches 90° as the stored energy per cycle of deformation becomes negligible compared with that dissipated as heat. However, the shape of the curve is somewhat different and $G'(1/t) > G(t)$ at all times. At the end of the terminal zone at the left, G' becomes proportional to ω^2 instead of exponentially dependent on t; this relation is

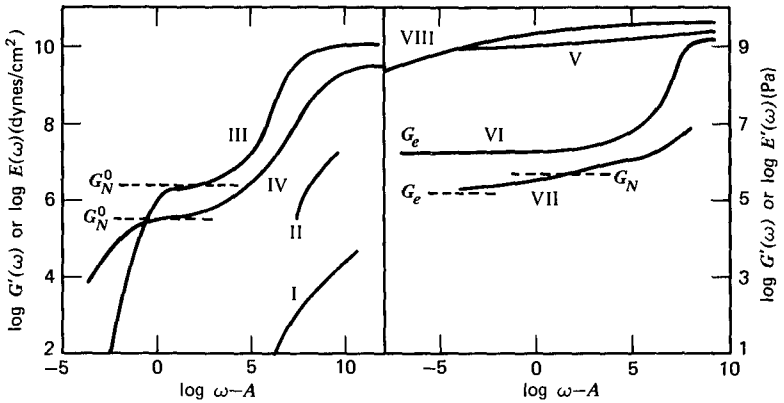


FIG. 2-3. Storage modulus plotted against frequency, with logarithmic scales, for the eight systems identified as in Fig. 2-1.

seen in the terminal slope of 2 for Example III and would be seen in the other viscoelastic liquids at lower frequencies. It can be derived readily from model analogies as will be seen in Chapter 3. The exponent 2 is independent of whether the molecular weight is uniform or not. The proportionality constant $A_G = G'/\omega^2|_{\omega\to 0}$, however, is strongly dependent on molecular weight distribution.

At intermediate times, the behavior is very similar to what has already been described for $G(t)$, except that $G'(1/t)$ always exceeds $G(t)$ to some extent. On a molecular basis, the magnitude of G' depends on what contour rearrangements can take place within the period of the oscillatory deformation.

5. The Loss Modulus

The modulus $G''(\omega)$ is defined as the stress 90° out of phase with the strain divided by the strain; it is a measure of the energy dissipated or lost as heat per cycle of sinusoidal deformation, when different systems are compared at the same strain amplitude. It is plotted with logarithmic scales in Fig. 2-4.

Observation of these curves reveals a feature which can be stated qualitatively as follows. In frequency regions where $G'(\omega)$ changes slowly (undergoes little dispersion), corresponding to very little stress relaxation in the equivalent plot of $G(t)$, the behavior is more nearly perfectly elastic; hence comparatively little energy is dissipated in periodic deformations. Thus, in such regions G'' tends to be considerably less than G'. This effect is prominent in the locations of G'' for the glass (V) and the crystalline polymer (VIII), whose G' curves are relatively flat throughout; G'' is so low that it intersects some of the other curves. Also, the flattening of G' at frequencies below the transition zone for the polymers which exhibit effects of entanglement coupling (III, IV, and VII) is accompanied by a plateau or minimum in G''.

At high frequencies, a mechanical model such as Fig. 1-9 would be expected to approach perfect elastic behavior, as the motion of the dashpots became negligible

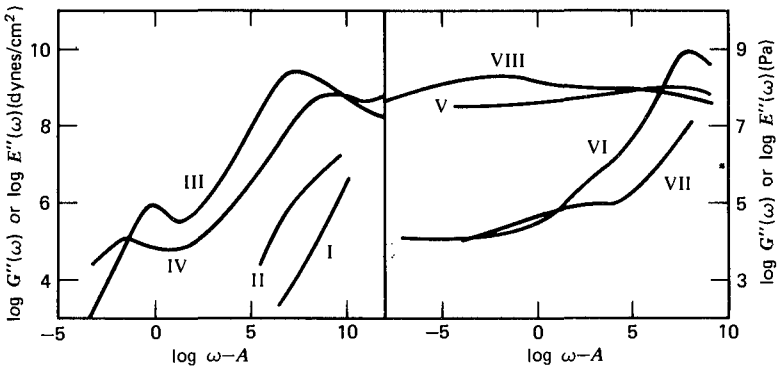


FIG. 2-4. Loss modulus plotted logarithmically for the eight systems identified as in Fig. 2-1.

compared with that of the springs; then G'' should approach zero. On a molecular basis, this would correspond to the absence of any molecular or atomic adjustments capable of dissipating energy within the period of deformation. This situation is not in fact achieved for high polymers or indeed any other solids of simpler structure; however, maxima in G'' appear for the soft polymers III, IV, and VI at rather high frequencies beyond which the losses due to backbone configurational changes diminish. Other maxima, in V and VIII, represent peaks in other dissipative processes.

At very low frequencies, G'' for a viscoelastic liquid should be directly proportional to ω, with a slope of 1 on a logarithmic plot. This is evident in Examples I, II, and III. The proportionality constant is the Newtonian steady-flow viscosity η_0, as shown below. For a simple Newtonian liquid, $G'' = \omega\eta_0$ over the entire frequency range; this would be represented by a straight line with unit slope for the solvent of the dilute solution, Example I.

For a viscoelastic solid with linear viscoelasticity corresponding to a model with springs and dashpots such as Fig. 1-9 or 1-10, G'' should also be directly proportional to ω at very low frequencies. Such behavior is not observed for the examples on the right side of Fig. 2-4; experiments have never been carried to sufficiently low frequencies to test this prediction.

6. The Dynamic Viscosity

The real or in-phase component η' of the complex dynamic viscosity is related to the loss modulus by the equation $\eta' = G''/\omega$ (equation 32 of Chapter 1). It is mostly useful for viscoelastic liquids because at low frequencies it approaches the steady-flow viscosity η_0. It is plotted with logarithmic scales in Fig. 2-5.

As is obvious from the above relation, in regions where G'' is flat, η' is inversely proportional to frequency; whereas when G'' rises steeply, on the left side of the maximum, η' may flatten out, as seen particularly in the cross-linked rubber, Example VI. But it decreases monotonically with increasing frequency and falls by many orders of magnitude.

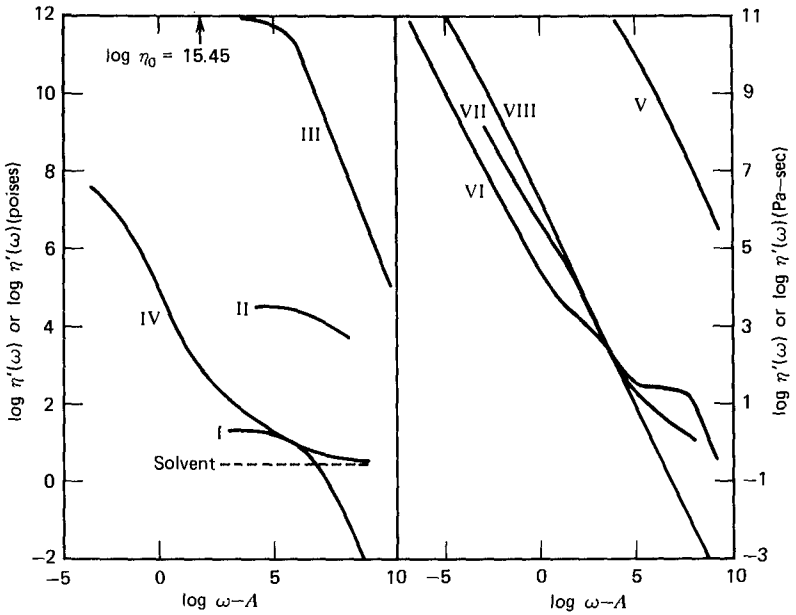


FIG. 2-5. Real part of the complex dynamic viscosity, plotted logarithmically for the eight systems identified as in Fig. 2-1.

The low-frequency limiting value of η_0 is attained for the viscoelastic liquids I and II (also for III, but the very high value does not appear on the graph). Its magnitude depends of course on temperature, molecular weight, and (for solutions) polymer concentration. For Example IV, data do not extend to low enough frequencies to reach the limiting value. For the dilute solution, I, the steady-flow viscosity η_0 is about eight times that of the solvent. With increasing frequency, η' falls and approaches a limiting value at high frequencies which is about 1.3 times that of the solvent. The frequency region in which the transition occurs is, again, related to configurational relaxation times. For a viscoelastic solid, such as a cross-linked polymer, η_0 is of course infinite, but if the viscoelastic behavior can be represented by a finite mechanical model, η' should approach a finite limiting value at low frequencies; for example, in Fig. 1-9, if one of the viscosities is infinite, there is no finite steady-flow viscosity, but the low-frequency limit of η' is finite and equal to the sum of all the other viscosities. To the author's knowledge, this situation has never been experimentally observed in a cross-linked polymer.

An alternative frequency-dependent viscosity, which could also be called the dynamic viscosity, is the absolute value $|\eta^*| = (\eta'^2 + \eta''^2)^{1/2} = (G'^2 + G''^2)^{1/2}/\omega$.

7. The Storage Compliance

The compliance $J'(\omega)$ is defined as the strain in a sinusoidal deformation in phase with the stress divided by the stress; it is a measure of the energy stored and re-

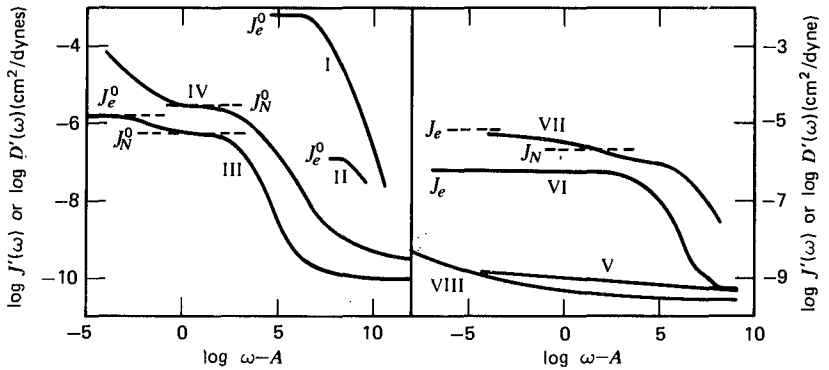


FIG. 2-6. Storage compliance plotted logarithmically for the eight systems identified as in Fig. 2-1.

covered per cycle, when different systems are compared at the same stress amplitude. It is plotted with the usual logarithmic scales in Fig. 2-6. For the same reason that $G'(\omega)$ resembles $G(t)$ plotted backwards, $J'(\omega)$ resembles $J(t)$ reflected in the compliance axis. An important distinction, however, appears in those polymers which are viscoelastic liquids: the elastic (recoverable) part of the creep is obtained only after subtracting t/η_0, and it is the difference $J(t) - t/\eta_0$ which approaches a limiting value J_e^0; but for J' the phase specification automatically eliminates any flow contribution, so J' itself approaches J_e^0 at low frequencies. This is seen in curves I, II, and III.

In the transition zone and other regions where J' changes rapidly, the shapes of $J'(\omega)$ and $J(t)$ differ such that $J'(1/t) < J(t)$ at all times. From equation 27 of Chapter 1 it is evident also that $J'(\omega) < 1/G'(\omega)$. The magnitudes of the two compliances and reciprocal moduli fall in the following order: $J'(1/t) < J(t) - t/\eta_0 < 1/G'(1/t) < 1/G(t)$. It is also evident from equations 25 and 26 of Chapter 1 that $J' < |J^*| = 1/|G^*| < 1/G'$. In practice $J(t)$ often lies quite close to $|J^*|$.

8. The Loss Compliance

The compliance $J''(\omega)$ is defined as the strain 90° out of phase with the stress divided by the stress; it is a measure of the energy dissipated or lost as heat per cycle of sinusoidal deformation, when different systems are compared at the same stress amplitude. It is plotted with logarithmic scales in Fig. 2-7.

For a Newtonian liquid, $J'' = 1/\omega\eta_0$ over the entire frequency range, as illustrated by the solvent for the dilute solution, Example I, with a slope of -1 on the logarithmic scale. For viscoelastic liquids, J'' becomes equal to $1/\omega\eta_0$ at very low frequencies; this is seen in examples I, II, and III, where slopes of -1 are attained.

A characteristic feature of J'' for viscoelastic solids which are lightly cross-linked networks or polymeric viscoelastic liquids of high molecular weight is a rather broad maximum whose location on the frequency scale corresponds to the low-frequency end of the transition zone as seen in the storage modulus (Fig. 2-3). This is asso-

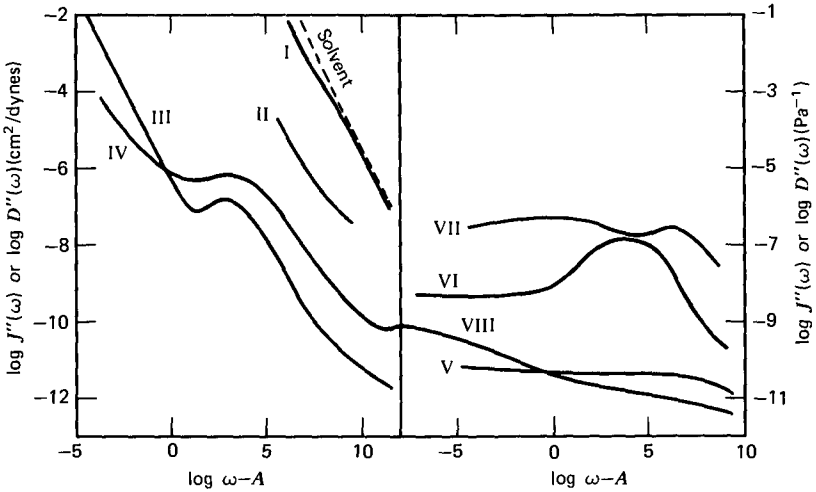


FIG. 2-7. Loss compliance plotted logarithmically for the eight systems identified as in Fig. 2-1.

ciated with configurational rearrangements of the strands of a network structure. The maximum for an uncross-linked polymer of high molecular weight, curves III and IV, is attributable to the entanglement network, in which the entanglements suppress long-range configurational rearrangements almost as though they were cross-links. In this case, there is a minimum on the low-frequency side of the maximum, and at still lower frequencies J'' rises to become inversely proportional to ω. For a cross-linked polymer, curve VI of Fig. 2-7, the maximum is attributable to the network netted by the chemical cross-links together with the entanglements which were present before cross-linking.

For the very lightly cross-linked network, curve VII of Fig. 2-7, there are *two* maxima. The one at higher frequencies corresponds to a network consisting of all strands terminated either by cross-links or by entanglements (which here considerably outnumber the cross-links). The other at the left can be attributed to the network which remains after subtraction of those entanglements which are capable of slippage because they are on structures incompletely attached to the chemically cross-linked network, as outlined in the discussion of creep compliance, Section 2 above.

9. The Loss Tangent

A useful parameter which is dimensionless and conveys no physical magnitude but is a measure of the ratio of energy lost to energy stored in a cyclic deformation is the loss tangent, $\tan\delta = G''/G' = J''/J'$ (equation 23, Chapter 1). The logarithmic plots in Fig. 2-8 reveal several characteristic levels of $\tan\delta$. First, for the dilute solution (curve I) $\tan\delta$ is very high because both solvent and solute contribute to G'' but only the solute contributes to G'. It goes through a minimum in the frequency range where the transition occurs in η' (*cf.* Fig. 2-5) and the other dynamic func-

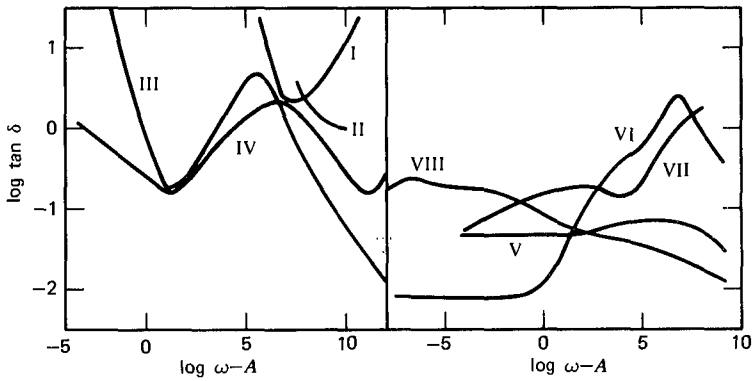


FIG. 2-8. Loss tangent plotted logarithmically for the eight systems identified as in Fig. 2-1.

tions. At low frequencies, tan δ is large for all the uncross-linked polymers (curves I, II, III, IV) and in fact becomes inversely proportional to the frequency. (We recall that in this region G'' is proportional to ω and G' to ω^2; alternatively, J'' is proportional to ω^{-1} and J' approaches a constant; so from either G''/G' or J''/J' it is clear that tan δ is proportional to ω^{-1}.) Second, all the amorphous polymers, whether cross-linked or not, have values in the transition zone which are in the neighborhood of tan $\delta = 1$, ranging perhaps from 0.2 to 3. Third, the glassy and crystalline polymers, V and VIII, have values in the general neighborhood of 0.1; and, finally, the lightly cross-linked polymer attains an extremely small value at low frequencies, of the order of 0.01.

In the transition zone between glasslike and rubberlike consistency, the loss tangent goes through a pronounced maximum for both uncross-linked polymers of high molecular weight (III and IV) and lightly cross-linked polymers (VI and VII, though the right side of the latter maximum is not encompassed). It is of interest that the maxima in J'' occur to the left of those in tan δ, and the maxima in G'' occur to the right of those in tan δ on the frequency scale; the differences amount to several logarithmic decades. Each of these three functions is a measure of elastic losses or heat dissipation, but it is clear that the frequency region in which the "loss" occurs depends on the choice of function by which the loss is specified.

For the very lightly cross-linked polymer (curve VII), there is a subsidiary maximum at lower frequencies associated with the losses involved in entanglement slippage as discussed in connection with $J(t)$ and J''. In this case, also, the maximum in J'' lies to the left of that in tan δ. Smaller maxima occur in the curves for the glassy and highly crystalline polymers, reflecting other dissipative mechanisms.

The loss tangent determines such macroscopic physical properties as the damping of free vibrations, the attenuation of propagated waves, and the frequency width of a resonance response. It can often be more conveniently measured than any other viscoelastic function, by observations of these phenomena, and is of considerable practical interest. It is less susceptible of direct theoretical interpretation than the other functions, however.

B. LINEAR VISCOELASTIC BEHAVIOR IN BULK (VOLUMINAL) DEFORMATION

As explained in Chapter 1, shear and bulk deformations are essentially different in character, one involving a shape change and the other a volume change; and they are accompanied by quite different molecular processes. There are far fewer experimental data available on bulk viscoelastic properties; however, a much narrower range of behavior among various types of polymeric systems may be expected, since voluminal changes should be dominated by local configurational rearrangements and these are scarcely affected by molecular weight (if sufficiently high), entanglements, or cross-links in moderate numbers.

As an example of bulk viscoelastic behavior, data for a poly(vinyl acetate) of moderately high molecular weight are shown in Fig. 2-9. Measurements by McKinney and Belcher[22] of the storage and loss bulk compliance B' and B'' at various temperatures and pressures are plotted after reduction to a reference temperature and pressure of 50°C and 1 atm respectively (see Chapter 11). The complex bulk compliance is formally analogous to the complex shear compliance, but the two functions present several marked contrasts.

The storage bulk compliance B' falls from a low-frequency limiting value to a high-frequency limiting value, but the change (shown here on a linear scale) is less than a factor of two instead of the many powers of 10 displayed by the shear compliance in Fig. 2-6. On a qualitative molecular basis, the low-frequency value reflects volume decreases under pressure due to reduction of atomic and molecular dimensions together with collapse of free volume involving local configurational adjustments which require a finite time. The high-frequency value reflects the volume decrease due to reduction of atomic and molecular dimensions alone. The frequency region in which the transition occurs depends on the relation of the time required for configurational adjustments to the period for cyclic deformation. It is somewhat narrower than the dispersion region for shear viscoelasticity, but it still covers several decades. The maxima in the loss tangents for shear and bulk deformation of this polymer occur at approximately the same frequency when compared at the same temperature, but in general no simple relation between the two can be expected. The loss bulk compliance B'' is zero within experimental error at both low and high frequencies and it passes through a maximum in the region of transition. The maximum loss tangent is of the order of 0.1.

Since the loss tangent is never very large, the storage modulus is nearly the reciprocal of the storage compliance (equation 27 of Chapter 1 with appropriate substitutions) and the loss modulus K'' is nearly B''/B'^2 (analog of equation 30, Chapter 1). It is easy to visualize the appearance of these functions. The corresponding transient functions, $B(t)$ and $K(t)$, can be visualized by reflecting mirror images of $B'(\omega)$ and $K'(\omega)$ in the ordinate axis.

Viscoelastic behavior in simple extension or in bulk longitudinal deformation will in general combine the features of shear and bulk viscoelasticity, since the moduli $E(t)$ and $M(t)$ depend on both $G(t)$ and $K(t)$, as shown by equations 51 and 58 of Chapter 1 (and analogous relations for E^* and M^*). However, as already pointed out, shear effects predominate in $E(t)$ and E^*, and bulk effects predominate

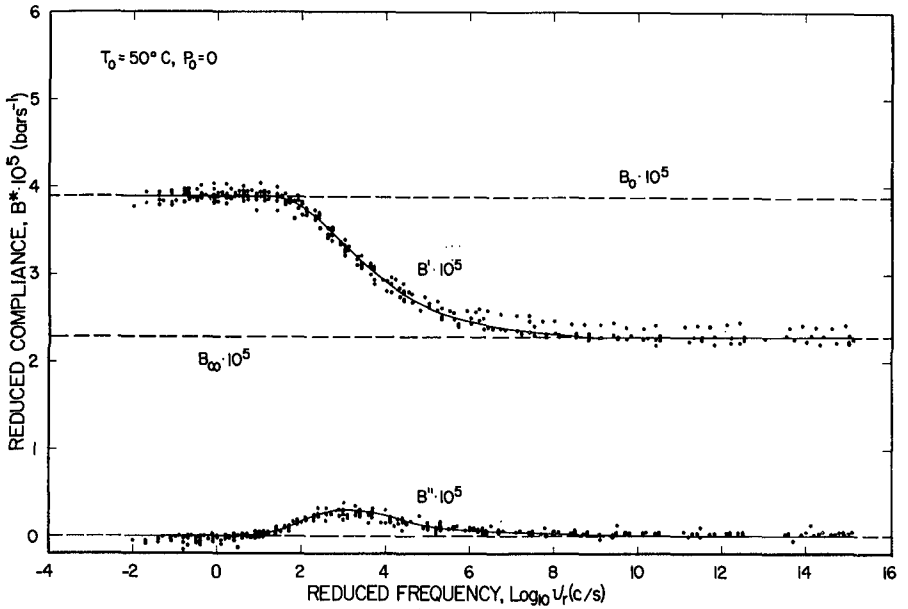


FIG. 2-9. Storage and loss bulk compliance plotted logarithmically against frequency, for a poly(vinyl acetate) reduced to 50°C and 1 atm, as described in text.[22]

in $M(t)$ and M^*, so the qualitative behavior is evident from the examples already given.

C. NONLINEAR VISCOELASTIC PHENOMENA IN SHEAR

When finite strains and or strain rates are allowed, the variety of behavior is enormously multiplied. As pointed out in Section G, Chapter 1, for such situations the simplification $K(t) \gg G(t)$ usually applies, so volume changes can be ignored. However, it is no longer possible to predict behavior in extension from behavior in shear by applying a factor of 3, as in linear viscoelasticity (equations 56 and 57 in Chapter 1); entirely different phenomena may be observed in the two deformational modes. Moreover, different experimental geometries such as torsion and flow through an annulus, which for linear viscoelasticity yield equivalent information concerning the time or frequency-dependent shear modulus, may now give quite different kinds of information; so a variety of experimental arrangements is desirable not merely for improved accuracy or convenience but to obtain information otherwise inaccessible. Only a few of the many nonlinear viscoelastic manifestations are mentioned here.

1. Normal Stress Differences

The well-known normal stress differences which appear in the shearing deformation of a rubberlike solid in large strains at mechanical equilibrium[23,24] are

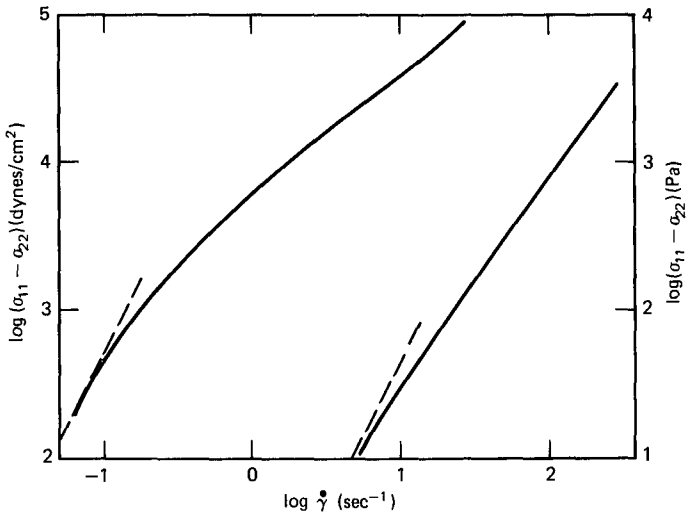


FIG. 2-10. Primary normal stress difference plotted logarithmically against shear rate, for two solutions of polystyrene with concentrations indicated, as described in the text.[25] Dashed lines have slope of 2.

strictly speaking outside the domain of viscoelasticity. However, the normal stresses in time-dependent deformation of viscoelastic liquids, in either steady flow or other time patterns, and in viscoelastic solids for oscillatory or other time-dependent deformations, represent combinations of elastic and viscous effects.

The primary normal stress difference in steady shear flow of moderately dilute polymer solutions is illustrated in Fig. 2-10, which shows measurements by Ashare[25] on solutions of a polystyrene of weight-average molecular weight ($\overline{M}_w$) 1,800,000 and number-average molecular weight ($\overline{M}_n$) 1,500,000 in a highly viscous solvent (a chlorinated diphenyl with viscosity 3 poises at 25°C). The primary normal stress difference $\sigma_{11} - \sigma_{22}$ (*cf.* Fig. 1-16) is plotted logarithmically against the shear rate $\dot{\gamma}_{21}$. Qualitatively, this quantity represents a tension along streamlines. It increases monotonically with $\dot{\gamma}_{21}$ and at low $\dot{\gamma}_{21}$ appears to approach the proportionality to $\dot{\gamma}_{21}^2$ predicted by equation 62 of Chapter 1 (slope of 2 on logarithmic plot). Other measurements at lower shear rates have shown exact proportionality.[26] Thus, $\sigma_{11} - \sigma_{22}$ as a function of $\dot{\gamma}$ is similar to G' as a function of ω for small values of the respective arguments. Aspects of this analogy are discussed in Chapter 3. The curve for 5% concentration has an inflection reminiscent of, though far less prominent than, the inflections in G' as a function of ω in Fig. 2-3. It is probably associated with the presence of some degree of entanglement coupling at this concentration, whereas at 1% the molecules do not pervade each other's domains sufficiently for entanglement to occur (Chapters 9 and 10). (This statement calls attention to the importance of polymer concentration in determining the degree of entanglement, while in the preceding discussion of linear viscoelastic behavior the dependence of entanglement on molecular weight was stressed. The interaction of these two variables is discussed in Chapter 17.)

The secondary normal stress difference in steady shear flow, $\sigma_{22} - \sigma_{33}$, has been studied much less extensively.[27] It has a similar dependence on $\dot{\gamma}_{21}$ but is smaller than $\sigma_{11} - \sigma_{22}$ by roughly an order of magnitude and is negative.

2. Non-Newtonian Flow

Examples of non-Newtonian flow in several very different types of polymeric systems are shown in Fig. 2-11, where the non-Newtonian viscosity $\eta = \sigma_{21}/\dot{\gamma}_{21}$ is plotted logarithmically against $\dot{\gamma}_{21}$.

First, an extremely dilute solution in which the polymer molecules move essentially independently of each other is represented by curve A, for a polystyrene with molecular weight 6.2×10^6 and sharp molecular weight distribution at a concentration of 0.05 g/dl in benzene at 30°C: data of Suzuki, Kotaka, and Inagaki.[28] From the low-shear rate limiting value of η_0 there is a slight but definite drop in η with increasing $\dot{\gamma}$, amounting to about 20% in the range investigated. Such dilute

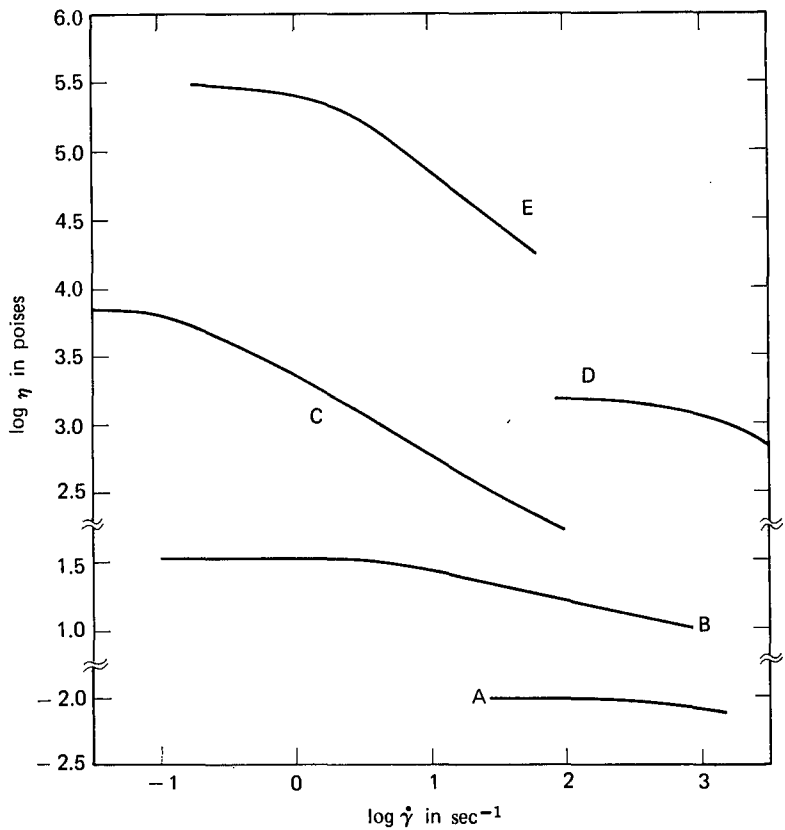


FIG. 2-11. Non-Newtonian viscosity plotted logarithmically against shear rate, for polymer solutions and undiluted polymers as described in the text.

solution measurements are often extrapolated to infinite dilution and expressed as a shear-rate-dependent intrinsic viscosity.

Second, data for the somewhat more concentrated polystyrene solutions of Ashare[25] whose primary normal stress differences are portrayed in Fig. 2-10 are represented by curves B and C. At 1% concentration, where the molecules overlap somewhat but are probably not entangled, there is a moderate drop in η, somewhat more than in the extremely dilute solution; at 5% concentration, where entanglements probably exist, the non-Newtonian effect is much more pronounced and, over about two decades of $\dot{\gamma}$, η follows rather closely a power-law relation. It is of interest that the onset of non-Newtonian flow occurs at a much higher shear rate for 1% than for 5% concentration, just as the normal stress differences achieve significant magnitudes at a higher shear rate for 1% than for 5% concentration in Fig. 2-10. Quantitative correlations will be introduced in later chapters.

Finally, data for *undiluted* polystyrenes at elevated temperature are represented in curves D and E, from experiments by Stratton.[29] The molecular weights (D: $\overline{M}_w$ = 48,000, $\overline{M}_n$ = 45,000; E: $\overline{M}_w$ = 242,000, $\overline{M}_n$ = 236,000) are sufficiently high for entanglements to be present, though for curve D only barely. Qualitatively, curves D and E resemble curves B and C respectively, though the power law region in curve E has a steeper slope. The positions on the abscissa scale do not have direct significance, because they depend on temperature, concentration, and the solvent viscosity in the case of the solutions.

All these examples are for sharp molecular weight distribution. The form of the dependence on η on $\dot{\gamma}$ is strongly dependent on the spread of molecular weights; a broad distribution causes a more gradual change of η at low $\dot{\gamma}$ where the limiting value η_0 is approached.

It may be remarked that the nonlinear behavior of the elongational viscosity, $\bar{\eta}$, is entirely different; it remains constant[30] up to rather high values of $\dot{\gamma}_{11}$ or $\dot{\epsilon}$ and then may increase, passing through a maximum. Measurements of $\bar{\eta}$ in the steady state are extremely difficult.[31]

3. Stress Relaxation after Large Sudden Strains

For small shear strains, the relaxation modulus described in Section C1 of Chapter 1 is of course independent of shear magnitude γ_{21}. At large strains, it decreases dramatically with increasing strain, as illustrated in Fig. 2-12. These are measurements by Einaga and collaborators[32] on a 20% solution of polystyrene with $\overline{M}_w = 1.80 \times 10^6$ and narrow molecular weight distribution, in chlorinated diphenyl at 33.5°C. The strains imposed range from 0.41 to 25.4; up to $\gamma_{21} = 1.87$, the viscoelastic behavior is linear, but at the highest strain $G(t)$ is smaller by nearly two orders of magnitude. The shapes of the curves are similar and they can be superimposed (except at the shortest times) by vertical shifts.

4. Stress Relaxation after Cessation of Steady-State Non-Newtonian Flow

The alternative type of stress relaxation experiment portrayed in Fig. 1-5, which

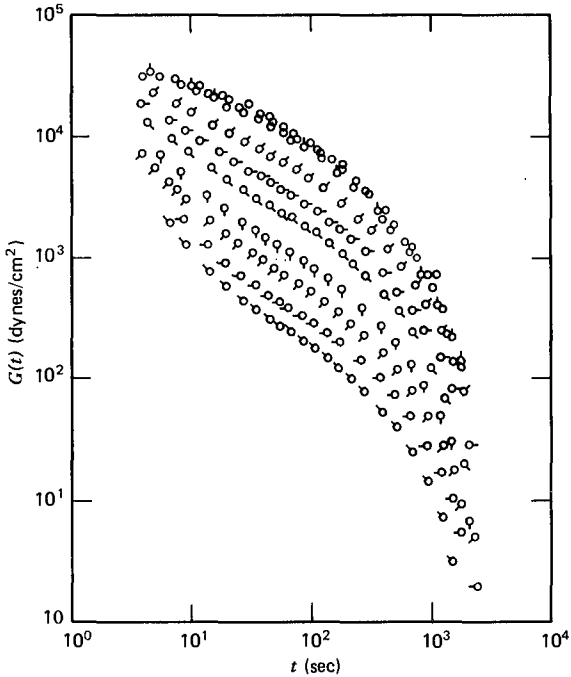


FIG. 2-12. Apparent shear relaxation modulus $\sigma(t)/\gamma$ plotted logarithmically against time for a 20% solution of polystyrene, $\overline{M}_w = 1.80 \times 10^6$, in chlorinated diphenyl at 33.5°C. Values of strain γ as follows: open circles without pip, 0.41; pip up, 1.87; pip with successive 45° rotations clockwise, 3.34, 5.52, 6.68, 10.0, 13.4, 18.7, and 25.4. (Einaga and collaborators.[32]) Reproduced, by permission, from *Polymer Journal*.

follows cessation of steady-state flow, has not been illustrated until now. If the shear rate during the steady flow is sufficiently high so non-Newtonian viscosity is observed, the course of the subsequent relaxation also depends strongly on shear rate. This is illustrated in Fig. 2-13 for a 4% solution of polystyrene, with molecular weight 1.8×10^6 (rather sharp distribution) in a viscous chlorinated diphenyl solvent, by data of Macdonald.[33] Here $\sigma_{21}{}^{ss}(t)$ refers to the shear stress as a function of time in this type of experiment. When the shear rate preceding the relaxation experiment is high, the relaxation is much more rapid. If a suitable constitutive equation were available to describe this behavior accurately, it could be used to predict the course of the relaxation following infinitesimal shear rate, which in this case is not accessible experimentally. This function would be related to the linear viscoelastic functions of Section A as will be shown in Chapter 3.

The normal stresses present during the steady-state flow also relax after its cessation, and the course of the primary normal stress difference, $(\sigma_{11} - \sigma_{22})^{ss}(t)$, where the superscript *ss* again refers to this particular type of experiment, is also shown in Fig. 2-13. Here, also, the relaxation is the more rapid, the higher the shear rate which precedes it. However, the normal stress difference relaxes more slowly than the shear stress.

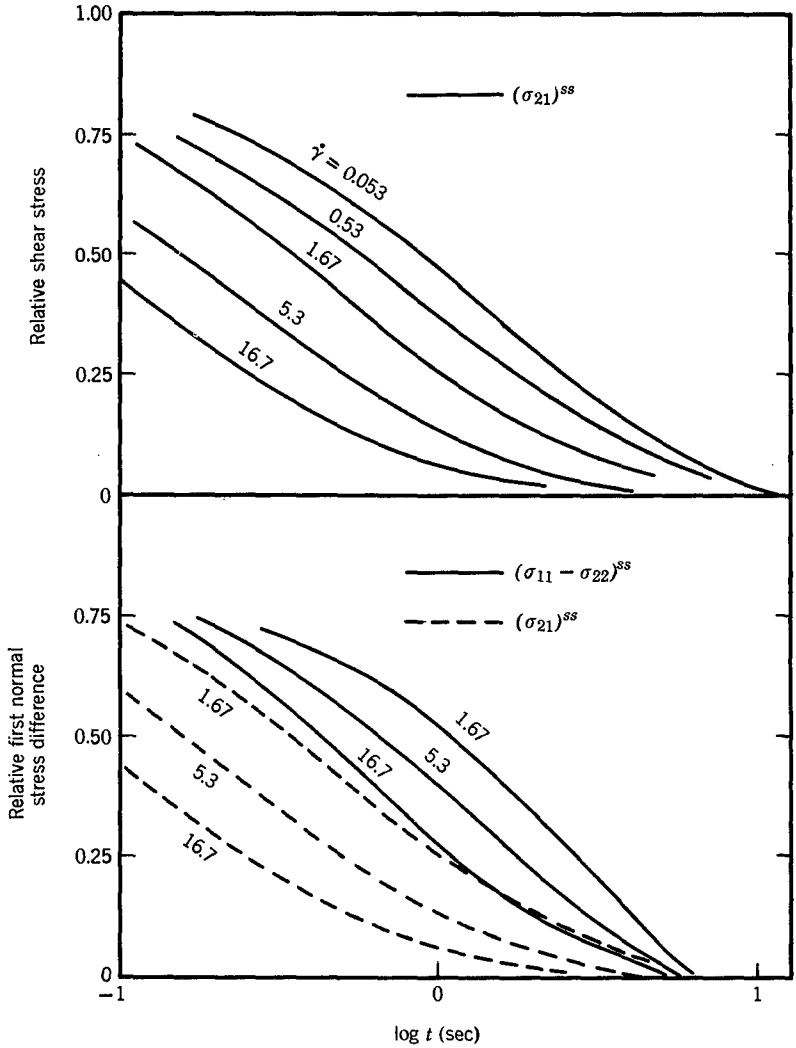


FIG. 2-13. Relaxation of shear stress and primary normal stress difference after cessation of steady state flow, for a 4% solution of polystyrene with molecular weight 1.8×10^6 in chlorinated diphenyl as described in the text.[33] Numbers refer to the shear rate preceding cessation of flow.

D. CONCLUSIONS

The foregoing examples are intended to provide some familiarity with the character and scope of the time-dependent viscoelastic behavior in polymeric systems, and a rough qualitative idea of its origin in molecular processes. Before returning in later chapters to a more detailed discussion of theoretical interpretations and correlations with molecular structure, we shall digress to consider the purely

phenomenological theory of interrelations among the different viscoelastic functions, and also methods of experimental measurements.

REFERENCES

1. D. J. Massa, J. L. Schrag, and J. D. Ferry, *Macromolecules,* **4,** 210 (1971).
2. K. Ninomiya and J. D. Ferry, *J. Phys. Chem.,* **67,** 2292 (1963).
3. D. J. Plazek and V. M. O'Rourke, personal communication.
4. S. J. Orbon, Ph.D. thesis, University of Pittsburgh, 1978.
5. W. Dannhauser, W. C. Child, Jr., and J. D. Ferry, *J. Colloid Sci.,* **13,** 103 (1958).
6. J. W. Berge, P. R. Saunders, and J. D. Ferry, *J. Colloid Sci.,* **14,** 135 (1959).
7. S. Iwayanagi, *J. Sci. Res. Inst. Jpn.,* **49,** 4 (1955).
8. K. Sato, H. Nakane, T. Hideshima, and S. Iwayanagi, *J. Phys. Soc. Jpn.,* **9,** 413 (1954).
9. J. R. Cunningham and D. G. Ivey, *J. Appl. Phys.,* **27,** 967 (1956).
10. A. R. Payne, in P. Mason and N. Wookey, *Rheology of Elastomers,* Pergamon, London, 1958, p. 86.
11. G. M. Martin, J. L. Roth, and R. D. Stiehler, *Trans. Inst. Rubber Ind.,* **32,** 189 (1956).
12. J. D. Ferry and K. Ninomiya, in *Viscoelasticity—Phenomenological Aspects,* edited by J. T. Bergen, Academic Press, New York, 1960, p. 55.
13. R. G. Mancke and J. D. Ferry, *Trans. Soc. Rheol.,* **12,** 335 (1968).
14. N. R. Langley, *Macromolecules,* **1,** 348 (1968).
15. D. S. Pearson and W. W. Graessley, *Macromolecules,* **11,** 528 (1978).
16. J. F. Sanders, R. H. Valentine, and J. D. Ferry, *J. Polym. Sci.,* A-2, **6,** 967 (1968).
17. J. A. Faucher, *Trans. Soc. Rheol.,* **3,** 81 (1959).
18. L. R. G. Treloar, *The Physics of Rubber Elasticity,* 3rd ed., Oxford, 1975.
19. S. F. Edwards, *Proc. Phys. Soc.,* **92,** 9 (1967).
20. P. G. de Gennes, *J. Chem. Phys.,* **55,** 572 (1971).
21. M. Doi and S. F. Edwards, *J. Chem. Soc., Faraday Trans. II,* **14,** 1789, 1802, 1818 (1978).
22. J. E. McKinney and H. V. Belcher, *J. Res. Nat. Bur. Stand.,* **67A,** 43 (1963).
23. R. S. Rivlin, in *Rheology,* Volume I, edited by F. R. Eirich, Academic Press, New York, 1956.
24. R. S. Rivlin and D. W. Saunders, *Trans. Faraday Soc.,* **48,** 200 (1952).
25. E. Ashare, *Trans. Soc. Rheol.,* **12,** 535 (1968).
26. W. W. Graessley and L. Segal, *Macromolecules,* **2,** 49 (1969).
27. R. B. Bird, R. C. Armstrong, and O. Hassager, *Dynamics of Polymeric Liquids,* Volume I, Wiley, New York, p. 146 *ff.*
28. H. Suzuki, T. Kotaka, and H. Inagaki, *J. Chem. Phys.,* **51,** 1279 (1969).
29. R. A. Stratton, *J. Colloid Interface Sci.,* **22,** 517 (1966).
30. J. F. Stevenson, *Am. Inst. Chem. Eng. J.,* **18,** 540 (1972).
31. K. Walters, *Rheometry,* Wiley, New York, 1975.
32. Y. Einaga, K. Osaki, M. Kurata, S. Kimura, and M. Tamura, *Polym. J.,* **2,** 550 (1971).
33. I. F. Macdonald, Ph.D. thesis, University of Wisconsin, 1968.

CHAPTER 3

Exact Interrelations among the Viscoelastic Functions

The linear viscoelastic phenomena described in the preceding chapter are all interrelated. From a single quite simple constitutive equation, equation 7 of Chapter 1, it is possible to derive exact relations for calculating any one of the viscoelastic functions in shear from any other provided the latter is known over a sufficiently wide range of time or frequency. The relations for other types of linear deformation (bulk, simple extension, etc.) are analogous. Procedures for such calculations are summarized in this chapter, together with a few remarks about relations among nonlinear phenomena.

A considerable literature has accumulated on the phenomenological theory of linear viscoelasticity.[1-13] Interest in it stems from several sources. In the first place, such calculations are usually necessary to map out the behavior of any one function over the complete panorama of time or frequency scale, by combining the results of different sorts of measurements. Most of the curves in Chapter 2 were in fact obtained in this manner. Second, the calculations are of practical value in permitting prediction of the behavior of a plastic or rubber in a certain situation, perhaps inaccessible to direct experiment, from measurements made under other more readily realizable conditions. Finally, the phenomenological theory offers some mathematical challenges and its structure can be summarized in a rather elegant and attractive form. Moreover, it is a special case of the more general theory of linear transformations, which is widely used in the analysis of electrical circuits. In the present chapter, the concepts and results of the theory will be presented without going into its more abstract aspects, involving Fourier and Laplace transforms.[4,10,13] For derivations of the equations given here, and additional relationships, the reader is referred especially to the very thorough treatise by Tschoegl.[13]

The equations in this chapter are formulated in terms of shear deformation, but analogous relations exist for bulk compression, simple extension, etc.

It is helpful to begin the development on the basis of mechanical models such

as Figs. 1-9 and 1-10, which are equivalent to equations 7 or 9 of Chapter 1 as long as the discussion is restricted to linear behavior. These lead to the introduction of two additional derived functions, the relaxation and retardation spectra.

A. MECHANICAL MODEL ANALOGIES

The simplest mechanical model analogous to a viscoelastic system is one spring combined with one dashpot, either in series (Fig. 3-1) or in parallel (Fig. 3-2).

1. The Maxwell Element

Figure 3-1 represents a Maxwell element. If the spring corresponds to a shear rigidity $G_i = 1/J_i$ (we choose shear as the type of deformation to be worked out in detail, though any other deformation would do as well) and the dashpot to a viscosity η_i, then the *relaxation time* of the element is defined as $\tau_i = \eta_i/G_i$, and is a measure of the time required for stress relaxation. If η_i is in poises and G_i in dynes/cm^2, τ_i is in seconds.

The viscoelastic functions exhibited by the Maxwell element can be easily derived and are summarized as follows:

$$J(t) = J_i + t/\eta_i \tag{1}$$

$$G(t) = G_i e^{-t/\tau_i} \tag{2}$$

$$G'(\omega) = G_i \omega^2 \tau_i^2 (1 + \omega^2 \tau_i^2) \tag{3}$$

$$G''(\omega) = G_i \omega \tau_i / (1 + \omega^2 \tau_i^2) \tag{4}$$

$$\eta'(\omega) = \eta_i / (1 + \omega^2 \tau_i^2) \tag{5}$$

$$J'(\omega) = J_i \tag{6}$$

$$J''(\omega) = J_i / \omega \tau_i = 1/\omega \eta_i \tag{7}$$

$$\tan \delta = 1/\omega \tau_i \tag{8}$$



FIG. 3-1. The Maxwell element.

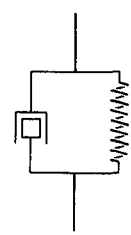


FIG. 3-2. The Voigt element.

2. The Voigt Element

Figure 3–2 represents a Voigt element. If the spring and dashpot have the same significance as before, their ratio τ_i is defined as the *retardation time* and is a measure of the time required for the extension of the spring to its equilibrium length while retarded by the dashpot.

The viscoelastic functions exhibited by the Voigt element are as follows:

$$J(t) = J_i(1 - e^{-t/\tau_i}) \tag{9}$$

$$G(t) = G_i \tag{10}$$

$$G'(\omega) = G_i \tag{11}$$

$$G''(\omega) = G_i\omega\tau_i = \omega\eta_i \tag{12}$$

$$\eta'(\omega) = \eta_i \tag{13}$$

$$J'(\omega) = J_i/(1 + \omega^2\tau_i^2) \tag{14}$$

$$J''(\omega) = J_i\omega\tau_i/(1 + \omega^2\tau_i^2) \tag{15}$$

$$\tan\delta = \omega\tau_i \tag{16}$$

Graphs of these functions have been given in many places,[11–15] but will not be reproduced here because they are too drastically simplified to correspond to real viscoelastic behavior. The Maxwell element cannot describe creep and the Voigt element cannot describe stress relaxation. The Maxwell does describe stress relaxation and the Voigt does describe creep, but as exponential functions of time. Most observed creep and relaxation processes in polymers progress more gradually. The components of the complex modulus for the Maxwell element, and those of the complex compliance for the Voigt element, depend on frequency in a manner reminiscent of the Debye dispersion of the complex dielectric constant. Again, observed moduli and compliances change with frequency more gradually than this. These elements may be considered as building blocks for useful models.[13]

The time-dependent behavior of the Maxwell and Voigt elements is in fact exactly analogous to the time-dependent electrical behavior of combinations of resistances and capacities or resistances and inductances. There are several possible ways of setting up the analogy. In particular, if capacities are equated to springs and dashpots to resistances, the storage and dissipative units correspond correctly physically, but the topology is backwards—*i.e.*, parallel mechanical connections correspond to series electrical connections. If resistances are equated to springs and capacities to dashpots, the two topologies are identical but the physical analogy is less satisfactory. A large literature has been devoted to this subject.[13,16–18] The analog of the Boltzmann superposition principle in the electrical case is known as the Hopkinson superposition principle.

3. Discrete Viscoelastic Spectra

Any number of Maxwell elements in series have the properties of a single Maxwell element with $J = \Sigma J_i$ and $1/\eta_0 = \Sigma(1/\eta_i)$; any number of Voigt elements

in parallel have the properties of a single Voigt element with $G = \Sigma G_i$ and $\eta_0 = \Sigma \eta_i$. However, Maxwell elements in parallel or Voigt elements in series, as in Figs. 1-9 and 1-10, obviously have much more complicated properties.

A group of Maxwell elements in parallel represents a discrete spectrum of relaxation times, each time τ_i being associated with a spectral strength G_i. Since in a parallel arrangement the forces (or stresses) are additive, it can readily be shown that for the Maxwell model, Fig. 1-9, the viscoelastic functions $G(t)$, $G'(\omega)$, $G''(\omega)$, and $\eta'(\omega)$ are obtained simply by summing the expressions in equations 2 to 5 over all the parallel elements; thus, if there are n elements,

$$G(t) = \sum_{i=1}^{n} G_i e^{-t/\tau_i} \tag{17}$$

etc.

For a viscoelastic solid, one of the relaxation times must be infinite and the corresponding modulus contribution is G_e, the equilibrium modulus. The functions $J(t)$, $J'(\omega)$, and $J''(\omega)$ can also be calculated, but not in a simple manner.

A group of Voigt elements in series represents a discrete spectrum of retardation times, each time τ_i being associated with a spectral compliance magnitude J_i. Since in a series arrangement the strains are additive, it turns out that for the Voigt model, Fig. 1-10, the viscoelastic functions $J(t)$, $J'(\omega)$, and $J''(\omega)$ are obtained by summing the expressions in equations 9, 14, and 15 over all the series elements; thus

$$J(t) = \sum_{i=1}^{n} J_i(1 - e^{-t/\tau_i}) \tag{18}$$

(to which a term t/η_0 must be added if one of the springs has zero rigidity, as must be the case for an uncross-linked polymer), etc. The functions $G(t)$, $G'(\omega)$, $G''(\omega)$, and $\eta'(\omega)$ cannot be simply expressed for this model.

Any experimentally observed stress relaxation curve which decreases monotonically can in principle be fitted with any desired degree of accuracy to a series of terms as in equation 17 by taking n sufficiently large, and this would amount to determining the discrete spectrum of "lines," each with a location τ_i and intensity G_i. Similarly, fitting creep data to equation 18 would amount to experimental determination of the discrete retardation spectrum. The process is discussed in detail by Tschoegl.[13] Certain molecular theories, as described in Chapters 9 and 10, do indeed predict discrete spectra corresponding to equations 17 and 18. In the analysis of experimental data, however, it is difficult or impossible to resolve more than a few lines. The contributions with the longest relaxation times can in principle be separated from a stress relaxation experiment by a procedure analogous to the analysis of radioactive decay in a mixture of radioactive species.[19-21] Beyond this, the empirical choice of parameters τ_i and G_i (or J_i) would be largely arbitrary. Although an arbitrary set of parameters would suffice to predict macroscopic behavior, it would not be unique and would be of little value for theoretical interpretation. This difficulty can be avoided, however, by substituting continuous spectra.

B. THE RELAXATION AND RETARDATION SPECTRA

1. The Relaxation Spectrum

If the number of elements in the Maxwell model of Fig. 1-9 is increased without limit, the result is a continuous spectrum in which each infinitesimal contribution to rigidity $F\,d\tau$ is associated with relaxation times lying in the range between τ and $\tau + d\tau$. Actually, experience has shown that a logarithmic time scale is far more convenient; accordingly the continuous relaxation spectrum is defined as $H\,d\ln\tau$, the contribution to rigidity associated with relaxation times whose logarithms lie in the range between $\ln\tau$ and $\ln\tau + d\ln\tau$, a measure of the population of relaxation mechanisms with relaxation times in this interval. (Evidently, $H = F\tau$.) For the continuous spectrum, equation 17 becomes

$$G(t) = G_e + \int_{-\infty}^{\infty} He^{-t/\tau}\,d\ln\tau \tag{19}$$

which may alternatively be taken as a mathematical definition of H in terms of the relaxation function $G(t)$ which is introduced in the basic constitutive equation, equation 7 of Chapter 1. The constant G_e is added to allow for a discrete contribution to the spectrum with $\tau = \infty$, for viscoelastic solids; for viscoelastic liquids (uncross-linked polymers), of course, $G_e = 0$.

Here we continue to follow the notation recommended by the Committee on Nomenclature of the Society of Rheology. Various other symbols have been used for H, and in some cases a spectrum has been defined by an equation analogous to 19 with $d\log_{10}\tau$ instead of $d\ln\tau$, thereby differing by a factor of 2.303.

Plots of H for the eight polymer types surveyed in Chapter 2 are shown in Fig. 3-3. The constant A has the same significance as before. Their shapes are rather similar to those of G'', reflected in the modulus axis. Their maxima represent concentrations of relaxation processes in certain regions of the logarithmic time scale. At long times, in uncross-linked viscoelastic liquids, when steady-state flow is reached, H should vanish; it does become very small on the logarithmic scale. The contrast between the sharp drop in Example III and the more gradual drop in Example IV is due to the much narrower molecular weight distribution of the former. For the viscoelastic solids on the right, H attains quite low values at long times but gives no evidence of approaching zero; this behavior is associated with the persistence of a small negative slope in stress relaxation (Fig. 2-2), showing that some degree of relaxation continues to long times. At very short times, if the mechanical behavior approaches perfect elasticity, H should also vanish; actually, it remains finite, and in these polymers at a rather high level, since some relaxation processes occur even at the shortest times (dissipative processes at the highest frequencies).

The characteristic zones of the viscoelastic time scale are clearly apparent in H: the glassy zone to the left of the principal maximum, the transition zone where

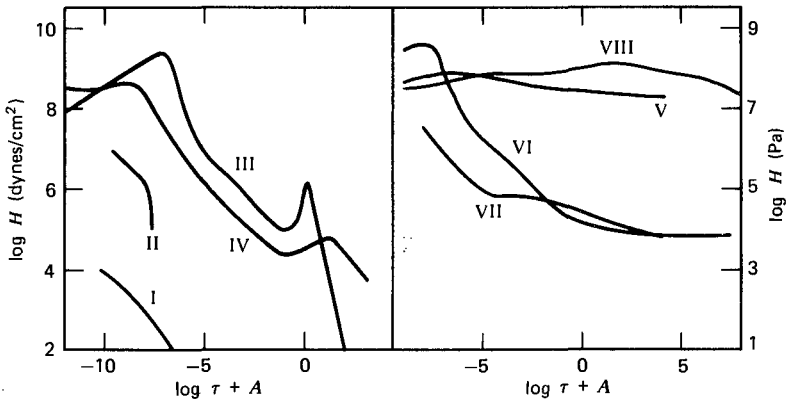


FIG. 3-3. The relaxation spectrum, plotted with logarithmic scales for the eight typical polymer systems described in Chapter 2, viscoelastic liquids on left, viscoelastic solids on right, identified by numbers as described in the text.

H drops steeply, the terminal zone where it approaches zero, and a region to the right of the transition zone in examples III, IV, and VII where H is relatively flat (the plateau) or passes through a minimum.

2. The Retardation Spectrum

In an entirely analogous manner, if the Voigt model in Fig. 1-10 is made infinite in extent, it represents a continuous spectrum of retardation times, L, alternatively defined by the continuous analog of equation 18:

$$J(t) = J_g + \int_{-\infty}^{\infty} L(1 - e^{-t/\tau})\, d \ln \tau + t/\eta_0 \qquad (20)$$

In this case an instantaneous compliance J_g must be added to allow for the possibility of a discrete contribution with $\tau = 0$. (Although J_g may be inaccessible experimentally, its presence must be inferred or else instantaneous deformation would require infinite stress.[4])

Plots of L for the eight polymer types are shown in Fig. 3-4. Their shapes, correspondingly, resemble those of J'' reflected in the compliance axis. Their maxima represent a concentration of retardation processes, measured by their contributions to compliance rather than modulus, in certain regions of the logarithmic time scale; they occur at quite different locations from the maxima in H.

At long times, L, like H, should vanish when an uncross-linked viscoelastic liquid polymer reaches the state of steady flow. This condition is observed for Examples I, II, and III. For Example IV, there are compliance mechanisms persisting beyond the longest times for which data are available. The plateau or minimum in the spectrum H corresponds very roughly to a maximum in the spectrum L.

The two spectra are of the nature of distribution functions, although they have the dimensions of a modulus (H) and a compliance (L) respectively, rather than the dimensionless

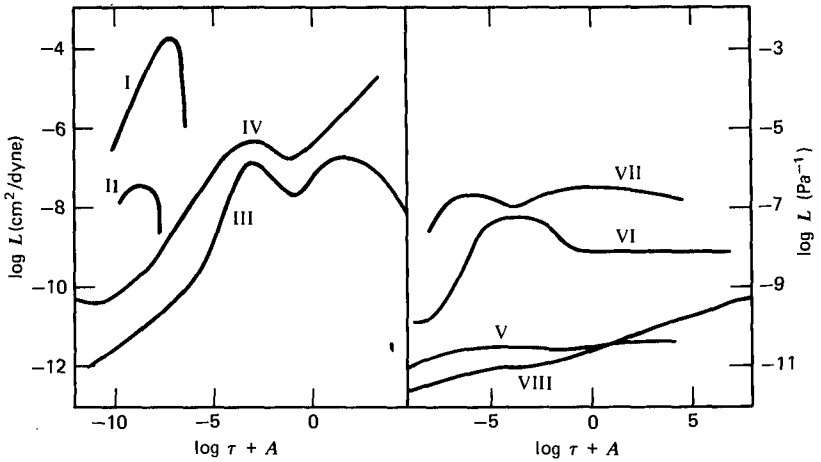


FIG. 3-4. The retardation spectrum, plotted logarithmically for the eight systems, identified as in Fig. 3-3 and Chapter 2.

character of the usual distribution function. In some treatments of linear viscoelastic behavior, normalized dimensionless distributions are employed:

$$h = H/G_g$$

$$l = L/(J_e - J_g)$$

where G_g is the stress/strain ratio for an instantaneous deformation and, for a viscoelastic solid, J_e is the equilibrium compliance; for a viscoelastic liquid, J_e would be replaced by J_e^0. Although these functions have mathematical convenience (their integrals over $d \ln \tau$ from $-\infty$ to ∞ are unity), they are less practical to apply to experimental data, because the normalizing factors are usually known only with poor precision or else are operationally inaccessible. Hence the nonnormalized functions H and L will be used throughout this book.

As defined in the preceding equations, the spectra H and L refer to deformation in shear. Similar spectra can of course be used for other types of deformation, and are specified by modified symbols, *e.g.*, H_v for bulk compression and $\overline{H}$ for simple elongation; thus, curves VI and VIII in Fig. 3-3 are actually $\overline{H}$. Often in the literature H and $\overline{H}$ are not clearly distinguished.

It should be repeated that H and L are not essential to the treatment of linear viscoelastic behavior. The predictions of molecular theories can, for example, be expressed in the form of directly measurable quantities such as $G(t)$, $G'(\omega)$, and $G''(\omega)$, and compared directly with experiments. Also, simultaneous measurements of $G'(\omega)$ and $G''(\omega)$ over a range of frequencies can in principle be interconverted by approximation formulas to check the internal consistency of experiments. However, an easy method of testing the consistency of measured values of G', G'', and $G(t)$ is to convert all of them to H by the simple approximation formulas given in Chapter 4; and a simple way to compare J', J'', and $J(t)$ is through the function L. Moreover, the spectra H and L are useful qualitatively in gauging the distribution

of relaxation or retardation mechanisms in different regions of the time scale. Hence they are included here together with their relations with various other functions.

3. Interrelations between the Spectra

If one spectrum is known over the entire range of time scale, together with certain limiting values such as G_e, J_g, and η_0, the other spectrum can be calculated.[4] The necessary equations are:

$$L = \frac{H}{\left[G_e - \int_{-\infty}^{\infty} \frac{H(u)}{\tau/u - 1}\, d \ln u\right]^2 + \pi^2 H^2} \tag{21}$$

$$H = \frac{L}{\left[J_g + \int_{-\infty}^{\infty} \frac{L(u)}{1 - u/\tau}\, d \ln u - \frac{\tau}{\eta_0}\right]^2 + \pi^2 L^2} \tag{22}$$

For an uncross-linked polymer, $G_e = 0$; for a cross-linked one, $\eta_0 = \infty$. The fact that J_g is generally not known with any degree of accuracy is unimportant, since it ordinarily makes a negligible contribution to the denominator of equation 22.

To calculate L from H, for example, it is necessary for each point desired to evaluate the integral in the denominator of equation 21 graphically or numerically from knowledge of H over its entire range. A graph of the integrand is shown in Fig. 3-5 for a representative case. The integration is carried up to within a small

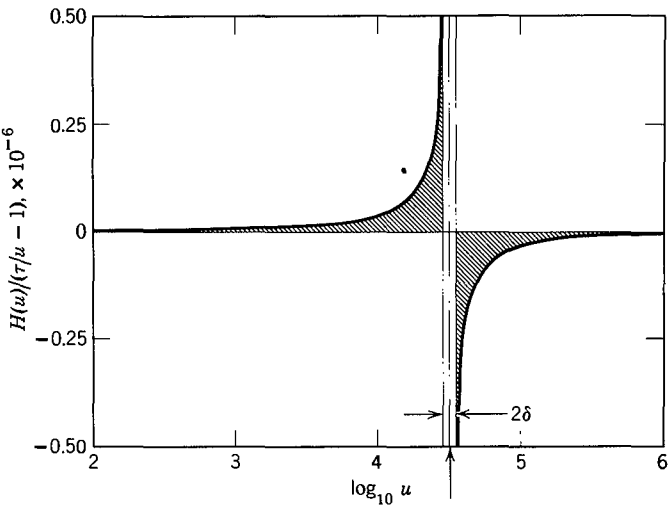


FIG. 3-5. Graphical evaluation of integral in equation 21, for poly(vinyl acetate) (weight-average molecular weight 3×10^5) at $\log \tau = 4.5$. For convenience, logarithms to the base 10 are used, and the net area is multiplied by 2.303. At the arrow, $u = \tau$. The integral is the difference between the positive and negative contributions, $(6.9 - 5.6) \times 10^4 = 1.3 \times 10^4$; $H = 0.51 \times 10^5$; $G_e = 0$; thence $L = 1.9 \times 10^{-6}$ cm^2/dyne. The calculation was carried out by K. Ninomiya for reference 12 of Chapter 2.

distance of the singularity, and the positive and negative contributions within the interval $\ln \tau - \delta$ to $\ln \tau + \delta$ will cancel if H is changing slowly. (A closer approximation can be made by assuming H to be linear in the interval with the slope of its tangent at $u = \tau$, as illustrated by Silva and Gross[22] for a similar integration relating dielectric properties.) Although this calculation is not particularly difficult, it involves two areas of similar magnitude and opposite sign, with attendant loss of precision. The reader may be assured that far simpler approximation methods exist, adequate for most situations, which will be introduced in Chapter 4.

Interconversion formulas for the corresponding discrete viscoelastic spectra have also been given by Gross.[4]

The existence of equations 21 and 22 raises the question as to why one should bother to deal with both spectra since they are interrelated and they present in principle the same information. But the viscoelastic behavior is seen differently in the two, since H weights contributions to modulus and L contributions to compliance. Generally, short-time processes are revealed in more detail in H, and long-time processes in L. Accordingly, it is worthwhile to examine both spectra.

C. CALCULATION OF VISCOELASTIC FUNCTIONS AND CONSTANTS FROM THE SPECTRA

Equation 19 permits calculation of the relaxation modulus $G(t)$ when H is known. Similarly, the other moduli can be obtained by integrations which are equivalent to summing over all the elements of an infinite Maxwell model:

$$G' = G_e + \int_{-\infty}^{\infty} [H\omega^2\tau^2/(1 + \omega^2\tau^2)]\, d \ln \tau \tag{23}$$

$$G'' = \int_{-\infty}^{\infty} [H\omega\tau/(1 + \omega^2\tau^2)]\, d \ln \tau \tag{24}$$

$$\eta' = \int_{-\infty}^{\infty} [H\tau/(1 + \omega^2\tau^2)]\, d \ln \tau \tag{25}$$

The compliances cannot be calculated from H in a simple manner, but they can be obtained from L by integrations which are equivalent to summing over all the elements of an infinite Voigt model. Equation 20 provides $J(t)$; the dynamic compliances are given by

$$J' = J_g + \int_{-\infty}^{\infty} [L/(1 + \omega^2\tau^2)]\, d \ln \tau \tag{26}$$

$$J'' = \int_{-\infty}^{\infty} [L\omega\tau/(1 + \omega^2\tau^2)]\, d \ln \tau + 1/\omega\eta_0 \tag{27}$$

Each of these equations requires in principle knowledge of the spectrum over a wide range of time scale, depending on how fast the integrand converges. The kernel (that part of the integrand exclusive of H or L) approaches zero at low τ

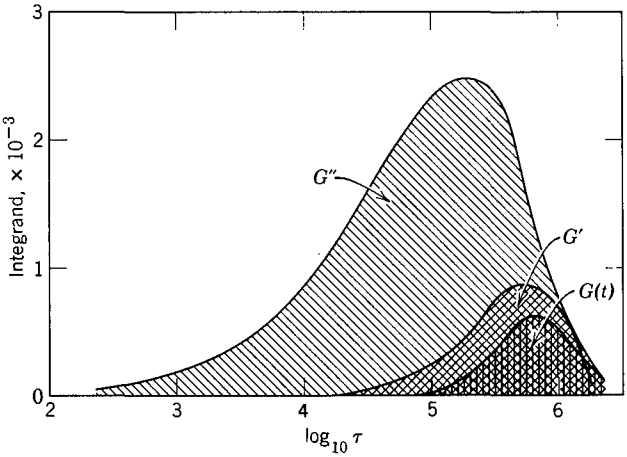


FIG. 3-6. Graphical evaluation of equations 19, 23, and 24, for a poly(vinyl acetate) in the terminal zone, at $\log t = 6.0$ for $G(t)$, $\log \omega = -6.0$ for $G'(\omega)$ and $G''(\omega)$. The integrals give $G(t) = 1.06 \times 10^3$, $G' = 1.96 \times 10^3$, $G'' = 1.00 \times 10^4$. (Calculations by K. Ninomiya.)

in equations 19 and 23; at high τ in 20 and 26; and at both ends in 24, 25, and 27. The spectra themselves approach zero rather rapidly in certain regions: L at low τ, and H at high τ for uncross-linked polymers.

An example of graphical integration of equations 19, 23, and 24 for a favorable case of convergence, near the terminal zone of the spectrum H, is shown in Fig. 3-6.

Certain viscoelastic constants can also be obtained by integration over the spectra. Thus for an uncross-linked polymer (viscoelastic liquid), by setting $\omega = 0$ in equation 25, we obtain for the steady-flow viscosity

$$\eta_0 = \int_{-\infty}^{\infty} H\tau \, d \ln \tau \tag{28}$$

For cross-linked polymers, there is some question as to whether the above integral is always finite. In this case it does not represent the steady-flow viscosity η_0, which is infinite, but if H vanishes at long times, the integral should represent a finite low-frequency limiting value of η'.

By setting $\omega = \infty$ in equation 23 we obtain for the instantaneous modulus

$$G_g = \int_{-\infty}^{\infty} H \, d \ln \tau + G_e \tag{29}$$

It will be recalled that there is some operational uncertainty in the definition of G_g and its reciprocal J_g, since H usually does not drop rapidly enough at the shortest times experimentally accessible to provide a converging integral in equation 29. Even if it does, there may be further contributions from some other viscoelastic mechanism at still shorter times which would be reflected in a further rise in G_g with extension of the time scale.

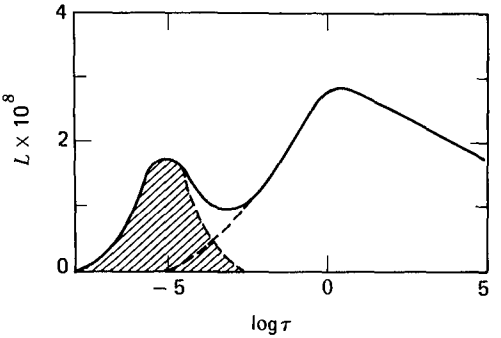


FIG. 3-7. Retardation spectrum for a styrene-butadiene rubber (curve VII of Fig. 3-4), reduced to 25°C and plotted linearly against log τ to illustrate partial integration by equation 33 to determine $J_N = 1.13 \times 10^{-7}$ cm²/dyne.

From equation 26, setting $\omega = 0$, we have for the equilibrium compliance J_e in a viscoelastic solid or the steady-state compliance J_e^0 in a viscoelastic liquid:

$$J_e = \int_{-\infty}^{\infty} L \, d \ln \tau + J_g \tag{30}$$

$$J_e^0 = \int_{-\infty}^{\infty} L \, d \ln \tau + J_g \tag{31}$$

where J_g is ordinarily negligible in comparison with the integral. If L is available from measurements which encompass steady-state flow, the integral in equation 31 is finite; the integral in equation 30 should be finite if L is available from measurements carried to sufficiently long times.

The steady-state compliance J_e^0 can also be calculated from H by the following relation:[13,43]

$$J_e^0 = \int_{-\infty}^{\infty} H\tau^2 \, d \ln \tau \Big/ \left[\int_{-\infty}^{\infty} H\tau \, d \ln \tau \right]^2 \tag{32}$$

When a spectrum has more than one maximum and the maxima are fairly well separated, integrations such as those in equation 29 or 30 can be made over limited regions of the time scale to determine the contribution to G_g, or J_e, associated with a particular class of mechanisms. For example, the data of example VII in Fig. 3-4 are plotted with a linear ordinate scale in Fig. 3-7. The curve can be decomposed in the neighborhood of the minimum, somewhat arbitrarily, into two components which add up to the observed values, and the integration is carried out over a sufficient range for convergence:

$$\int_a^b L \, d \ln \tau = J_N \tag{33}$$

where L is represented by the dashed curve on the right in Fig. 3-7. Strictly, a term J_g should be added, but it is entirely negligible. The significance of the quantity

J_N is discussed in Chapter 14. It may be noted that for viscoelastic liquids at very low frequencies equations 23 and 24 reduce to

$$G' = \omega^2 \int_{-\infty}^{\infty} H\tau^2 \, d \ln \tau = A_G \omega^2 = J_e^0 \eta_0^2 \omega^2 \tag{34}$$

$$G'' = \omega \int_{-\infty}^{\infty} H\tau \, d \ln \tau = \omega \eta_0 \tag{35}$$

giving the proportionalities to ω^2 and ω, respectively, that were observed in Figs. 2–3 and 2–4. The constant A_G will be discussed in connection with molecular theories in Chapter 9.

D. CALCULATION OF RELAXATION AND RETARDATION SPECTRA FROM EXPERIMENTALLY DETERMINED VISCOELASTIC FUNCTIONS

Although it is relatively easy to obtain the viscoelastic functions from the spectra, the reverse process is difficult, and usually involves successive approximations of some kind as described in Chapter 4. However, if the dynamic viscoelastic functions can be expressed analytically, the spectra can be obtained directly therefrom by a substitution involving complex algebra,[4,5,13] derived for the analogous case of dielectric properties by Fuoss and Kirkwood.[23] In practice, the functional forms of G', G'', J', and J'' are so complicated, with inflections, maxima, and minima, as seen in Chapter 2, that usually no attempt is made to represent them by analytical expressions, and the data remain in tabular or graphical form. Thus the relations referred to are rarely used for processing experimental data. They might be useful, however, for manipulating the results of theories (Chapters 9 and 10).

If, within a particular zone of viscoelastic behavior, an empirical equation can be used to fit a viscoelastic function, an exact expression for the corresponding spectrum can sometimes be derived, as shown by Smith.[24]

The retardation spectrum can be calculated from numerical data for the recoverable creep compliance (*i.e.*, $J(t) - t/\eta_0$) by iterative computer techniques developed by Plazek and Orbon.[25] An approximate set of numerical values defining L, obtained by one of the methods of Chapter 4, is inserted into equation 20 and corrections are made until the experimentally determined creep function is reproduced. Although the limits of the integral in equation 20 must be changed to finite values, if the data cover a sufficiently wide range of time scale it is still possible to obtain convergence for practical purposes. However, the inevitable noise in the data can lead to nonunique assignments of L in certain regions of time, and even false ripples in its shape, so judgment is necessary as well as preferably comparison of the results for several closely related polymer systems (different molecular weights or concentrations) to ensure reliability of the calculation. Once L has been determined in this manner, an exact numerical calculation of H can be made by equation 22, and all the linear viscoelastic functions can be obtained from the equations of Section C above.

E. CALCULATION OF ONE EXPERIMENTALLY OBSERVABLE VISCOELASTIC FUNCTION FROM ANOTHER

1. Interrelation of the Two Transient Functions

The creep compliance and the relaxation modulus are connected by the relations

$$\int_0^t G(\tau)J(t-\tau)d\tau = t \tag{36}$$

$$\int_0^t J(\tau)G(t-\tau)d\tau = t \tag{37}$$

from which it follows[13] that $J(t)G(t) \leq 1$ as mentioned in Chapter 2. An efficient method for numerical evaluation of this convolution integral has been outlined and illustrated by Hopkins and Hamming;[26] values of $G(t)$ spaced at log t intervals of 0.2 are used, for example, to calculate $J(t)$, by a progressive operation starting at $t = 0$.

Alternatively, the Laplace transforms of $J(t)$ and $G(t)$ are reciprocally related:

$$p\mathcal{L}\{J(t)\} = 1/p\{\mathcal{L}G(t)\} \tag{38}$$

from which, in principle, if one function is given analytically, the other can be calculated.

2. Interrelation of a Transient with the Corresponding Dynamic Functions

The components of the complex dynamic modulus are obtainable from the relaxation modulus by the Fourier transforms

$$G'(\omega) = G_e + \omega \int_0^\infty [G(t) - G_e] \sin \omega t \, dt \tag{39}$$

$$G''(\omega) = \omega \int_0^\infty [G(t) - G_e] \cos \omega t \, dt \tag{40}$$

which have already been given in Chapter 1, derived from the constitutive equation, equation 7 of that Chapter, for the case of $G_e = 0$, *i.e.*, for a viscoelastic liquid. Otherwise, G_e is the equilibrium modulus. The corresponding relations to obtain $G(t)$ from G' or G'' are

$$G(t) = G_e + \frac{2}{\pi} \int_0^\infty [(G' - G_e)/\omega] \sin \omega t \, d\omega \tag{41}$$

$$G(t) = G_e + \frac{2}{\pi} \int_0^\infty (G''/\omega) \cos \omega t \, d\omega \tag{42}$$

In principle, these integrals can be performed numerically or graphically if the starting function is known over a sufficiently wide range of time or frequency.

Equations 39–42 can be expressed[27] alternatively in terms of the memory function $m(t)$ instead of the relaxation modulus $G(t)$, making use of equation 8 of Chapter 1.

For relating the real component G' to $G(t)$, a far more convenient formulation can be made utilizing the fact that the difference $G'(\omega) - G(t)$ for $t = 1/\omega$ is relatively small, and can be expressed in terms of the relaxation spectrum by equations 19 and 23, as pointed out by Marvin:[28]

$$G'(\omega)|_{1/\omega=t} - G(t) = \int_{-\infty}^{\infty} H\left(\frac{\tau^2}{t^2+\tau^2} - e^{-t/\tau}\right) d \ln \tau \tag{43}$$

Even though this still contains an integral to be evaluated graphically or numerically, and moreover another function H which must also be determined approximately from whichever of the moduli is known at the start of the problem, the right side of equation 43 represents a minor correction which need not be calculated with great precision. With it, $G'(\omega)$ can be obtained from $G(t)$ or vice versa.

Analogous relations to equations 39 to 43 connect the creep compliance with the components of the complex dynamic compliance. As formulated by Dr. R. S. Marvin, they are:

$$J'(\omega) = J_e^0 - \omega \int_0^{\infty} [J_e^0 - J(t) + t/\eta_0] \sin \omega t \, dt \tag{44}$$

$$J''(\omega) = \omega \int_0^{\infty} [J_e^0 - J(t) + t/\eta_0] \cos \omega t \, dt + 1/\omega\eta_0 \tag{45}$$

$$J(t) = J_g + \frac{2}{\pi} \int_0^{\infty} [(J' - J_g)/\omega] \sin \omega t \, d\omega + t/\eta_0 \tag{46}$$

$$J(t) = J_g + \frac{2}{\pi} \int_0^{\infty} (J''/\omega - 1/\omega^2\eta_0)(1 - \cos \omega t) d\omega + t/\eta_0 \tag{47}$$

$$J'(\omega)|_{1/\omega=t} - J(t) + t/\eta_0 = \int_{-\infty}^{\infty} L\left(e^{-t/\tau} - \frac{\tau^2}{t^2+\tau^2}\right) d \ln \tau \tag{48}$$

Since J_e^0 appears in equations 44 and 45, they apply to viscoelastic liquids; for viscoelastic solids, J_e^0 would be replaced by J_e and the term t/η_0 would be omitted. In applications of these equations, J_g is often relatively so small that it does not matter whether it is known accurately. Although the integral in equation 43 is always positive, that in equation 48 is always negative, confirming the relative magnitudes $J'(1/t) < J(t) - t/\eta_0 < 1/G'(1/t) < 1/G(t)$, as stated in Chapter 2.

3. Interrelations between the Components of a Complex Dynamic Function

If both components of G^* are known at a single frequency, both components of J^* can be very simply calculated by equations 27 to 30 of Chapter 1. On the other hand, if *one* component is known over the whole frequency range, the other can be obtained from it by mechanical analogs of the Kronig-Kramers relations.[29–31]

Thus, for the compliances,

$$J'(\omega_1) = J_g + \frac{2}{\pi}\int_{-\infty}^{\infty} [(J''\omega^2 - \omega/\eta_0)/(\omega^2 - \omega_1^2)]\, d\ln\omega \tag{49}$$

$$J''(\omega_1) = \frac{2}{\pi}\int_{-\infty}^{\infty} [(J' - J_g)\omega_1\omega/(\omega_1^2 - \omega^2)]\, d\ln\omega + 1/\omega_1\eta_0 \tag{50}$$

To calculate J' from J'', for example, it is necessary, for each point desired (ω_1), to evaluate the integral of equation 49 graphically or numerically. The integration has features similar to those of equations 21 and 22 which connect the relaxation and retardation spectra.[22] There are analogous interrelations between G' and G''.[13]

4. Evaluation of Viscoelastic Constants

There are some interesting relations which can be obtained from equations 23 to 31 (or by alternative derivations) to connect the steady-flow viscosity and the steady-state compliance, for uncross-linked polymers (viscoelastic liquids), with experimentally measured functions:[4,13,32]

$$\eta_0 = \int_{-\infty}^{\infty} tG(t)\, d\ln t \tag{51}$$

$$\eta_0 = \frac{2}{\pi}\int_{-\infty}^{\infty} \frac{G'(\omega)}{\omega}\, d\ln\omega \tag{52}$$

$$J_e^0 = J_g + \frac{2}{\pi}\int_{-\infty}^{\infty} (J''(\omega) - 1/\omega\eta_0)\, d\ln\omega \tag{53}$$

$$J_e^0 = \frac{1}{\eta_0^2}\int_{-\infty}^{\infty} t^2G(t)\, d\ln t \tag{54}$$

$$G_g = G_e + \frac{2}{\pi}\int_{-\infty}^{\infty} G''\, d\ln\omega \tag{55}$$

Equation 53 is equally applicable to cross-linked viscoelastic solids with J_e^0 replaced by J_e and the term $1/\omega\eta_0$ omitted. Equation 55 is actually written in the appropriate form for a viscoelastic solid; for an uncross-linked polymer, G_e would be omitted. These equations are useful as sensitive tests of the accuracy of the experimental functions $G(t)$, $G'(\omega)$, etc., near the limits of the range of measurements, provided η_0 and J_e^0 are known from other sources.

A relatively isolated maximum in L associated with a particular class of retardation mechanisms as in Fig. 3–7 implies a similar maximum in J'' (*cf.* Figs. 2–7 and 3–4). Equation 53 can be used to integrate over this maximum between appropriate limits as an alternative means of estimating the contribution of this class of mechanisms to J_e or J_e^0. This integration is shown in Fig. 3–8 for the same example as Fig. 3–7, *i.e.*, Example VII of Fig. 2–7 plotted with a linear scale. The term J_g in equation 53 is negligible and $1/\omega\eta_0$ is zero because the polymer is

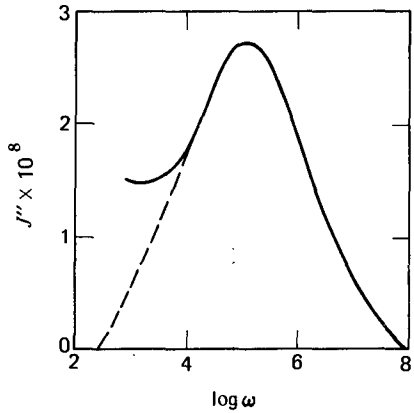


FIG. 3-8. Loss compliance for system of Fig. 3-7 (curve VII of Fig. 2-7), reduced to 25°C. and plotted linearly against log ω to illustrate partial integration by equation 53 (with finite limits) to determine $J_N = 1.11 \times 10^{-7}$ cm^2/dyne.

cross-linked. Similarly, equation 55 can be used to integrate over a relatively isolated maximum in G'', instead of between $-\infty$ and ∞, to obtain the contribution to G_g from the particular class of relaxation mechanisms it represents.

F. CALCULATION OF MORE COMPLICATED EXPERIMENTAL FUNCTIONS

There are other more complicated experimental situations where viscoelastic behavior can also be predicted in terms of the relaxation and retardation spectra or other functions. These include deformations at constant rate of strain and constant rate of stress increase, stress relaxation after cessation of steady-state flow, and creep recovery or elastic recoil, all of which were mentioned in Chapter 1, as well as nonsinusoidal periodic deformations.[13] In referring to stress σ, strain γ, and rate of strain $\dot{\gamma}$, the subscript 21 will be omitted here although it is understood that the discussion applies to shear unless otherwise specified.

1. Deformation at Constant Rate of Strain

If, starting from the undeformed or stressfree state, the strain is made to increase at a constant rate $\dot{\gamma}$, its value at time t will be $\gamma = \dot{\gamma}t$, and the stress σ will represent the superposition of a series of partially relaxed stresses up to that instant. In terms of the relaxation spectrum, two alternative formulations can be given:[33]

$$\sigma(t) = \dot{\gamma} \int_{-\infty}^{\infty} \tau H(1 - e^{-t/\tau}) d \ln \tau + G_e \dot{\gamma} t \tag{56}$$

$$\sigma(t) = \dot{\gamma} \int_{0}^{t} \int_{-\infty}^{\infty} H e^{-u/\tau} \, d \ln \tau \, du + G_e \dot{\gamma} t \tag{57}$$

In terms of the relaxation modulus, equation 7 of Chapter 1 gives

$$\sigma(t) = \dot{\gamma} \int_0^t G(t-u)du \tag{58}$$

A plot of σ against γ (equivalent, with a change of scale, to plotting σ against t) gives a stress-strain curve at constant rate of strain.

Differentiation of the stress-strain curve yields the relaxation modulus:

$$d\sigma/d\gamma = (1/\dot{\gamma})d\sigma/dt = \int_{-\infty}^{\infty} He^{-t/\tau}\, d\ln\tau + G_e = G(t) \tag{59}$$

and calculations of this sort have been successfully made by Smith,[34] the results agreeing with direct measurements, with data for simple extension at moderate elongations; here σ is the tensile stress, and γ and G are replaced by ϵ and E respectively.

For deformation in simple extension at constant rate of (practical) strain $\dot{\epsilon}$, for which $G(t)$ is replaced by $E(t)$, Smith has pointed out that it is convenient to define a constant-strain-rate modulus $F(t) \equiv \sigma_T(t)/\epsilon(t)$. This is related to the relaxation modulus by the equation[35-37]

$$E(t) = F(t)\left[1 + \frac{d\log F(t)}{d\log t}\right] \tag{60}$$

For a viscoelastic liquid in shear, the ratio $\sigma_{21}(t)/\dot{\gamma}$ in equations 56 to 58 is sometimes treated as a time-dependent viscosity $\eta^+(t)$ which increases monotonically (provided the viscoelasticity is linear) to approach the steady-state viscosity η_0.[38-40] Meissner[41] has pointed out that, in an experiment involving deformation at constant strain rate followed by stress relaxation at constant deformation, viscoelastic information can be obtained without imposing the restriction in equation 11 of Chapter 1 that the loading interval ξ is small compared with the time elapsed at the first experimental stress measurement.[42]

2. Deformation at Constant Rate of Stress Loading

If the stress is increased linearly starting from zero, on the other hand, the resulting strain will reflect the superposition of a series of retarded compliances. Then, if $\dot{\sigma}$ is the rate of stress increase,

$$\gamma = \dot{\sigma}tJ_g + \dot{\sigma}\int_0^t \int_{-\infty}^{\infty} L(1-e^{-u/\tau})\, d\ln\tau\, du + \frac{\dot{\sigma}t^2}{2\eta_0} \tag{61}$$

$$\gamma = \dot{\sigma}tJ_g + \dot{\sigma}\int_{-\infty}^{\infty} L[t-\tau(1-e^{-t/\tau})]\, d\ln\tau + \frac{\dot{\sigma}t^2}{2\eta_0} \tag{62}$$

When the strain-stress curve obtained under these conditions is differentiated, the result is the creep compliance:

$$d\gamma/d\sigma = (1/\dot{\sigma})\, d\gamma/dt = J_g + \int_{-\infty}^{\infty} L(1-e^{-t/\tau})\, d\ln\tau + t/\eta_0 = J(t) \tag{63}$$

The restriction of linear viscoelastic behavior—small deformations—is more serious for equations 56 to 63 than for most of the preceding treatments, because with constantly increasing strain or stress the nonlinear regime may soon be reached. Then formulation in terms of a more complicated constitutive equation is necessary.

3. Stress Relaxation after Cessation of Steady-State Flow

If, following steady shear flow of a viscoelastic liquid at a shear rate $\dot{\gamma}$, the flow is abruptly halted, the stress (initially equal to $\eta_0\dot{\gamma}$) decays with a time dependence given by[43]

$$\sigma^{ss}(t) = \dot{\gamma} \int_{-\infty}^{\infty} H\tau e^{-t/\tau}\, d \ln \tau \tag{64}$$

Comparison of this with equation 19 shows that the longer relaxation times are weighted relative to stress relaxation after sudden strain. Equation 64 can be inverted to obtain H from $\sigma^{ss}(t)$ by approximation procedures (Chapter 4). Alternatively, in terms of the relaxation modulus $G(t)$, as given in equation 13 of Chapter 1,

$$\sigma^{ss}(t) = \dot{\gamma} \int_{t}^{\infty} G(s)\, ds \tag{65}$$

from which we have by differentiation

$$-(1/\dot{\gamma})\, d\sigma^{ss}(t)/dt = G(t) \tag{66}$$

The steady-state compliance can also be related to $\sigma^{ss}(t)$ by an equation[44] related to equation 54:

$$J_e^0 = \frac{1}{\dot{\gamma}\eta_0^2} \int_{-\infty}^{\infty} t\sigma^{ss}(t)\, d \ln t \tag{67}$$

These equations can be applied to elongational flow in the linear regime with appropriate substitutions.

4. Creep Recovery or Elastic Recoil

An alternative to the preceding experiment is, after steady shear flow of a viscoelastic liquid under stress σ, to remove the stress at time t_2 and observe the decreasing strain as a function of time (Fig. 1-12). It has already been pointed out in Chapter 1 (equation 41) that the ensuing creep recovery is simply given by the creep function. The strain at t_2 is $\gamma(t_2) = \sigma(J_e^0 + t_2/\eta_0)$; the strain during the recovery is

$$\gamma_r(t) = \sigma[J_e^0 + t/\eta_0 - J(t - t_2)] \tag{68}$$

and so the recovered strain is

$$\gamma(t_2) - \gamma_r(t) = \sigma[J(t - t_2) - (t - t_2)/\eta_0] \tag{69}$$

the final value of which at $t \to \infty$ is $\gamma_\infty = \sigma J_e^0$. The latter conclusion can also be reached by setting the right side of equation 7 of Chapter 1 equal to zero with the appropriate boundary conditions,[40] from which it is found that

$$\gamma_\infty = \dot{\gamma} \frac{\int_{-\infty}^{\infty} t^2 G(t)\, d \ln t}{\int_{-\infty}^{\infty} tG(t)\, d \ln t} = \eta_0 \dot{\gamma} J_e^0 = \sigma J_e^0 \tag{70}$$

where $\dot{\gamma}$ refers to the rate of strain prior to removal of stress. The final residual strain after recovery is $\sigma t_2/\eta_0$, sometimes called the permanent set. (Permanent set can also appear in experiments on viscoelastic solids if chemical or structural changes occur in the strained state, as discussed in Chapter 14.)

5. Recovery after Partial Stress Relaxation

In an experiment which combines stress relaxation and recovery, sudden shear strain γ_0 is applied to a viscoelastic liquid at time $t = -t_1$, and stress relaxation is observed until a time $t = 0$ at which there is still some residual stress. Then the stress is removed and the decreasing strain is observed as a function of time. It is given by[45]

$$\gamma(t) = -\gamma_0 \int_{-t_1}^{0} G(s + t_1) \frac{dJ\,(t - s)}{ds}\, ds \tag{71}$$

The total recoverable strain is

$$\gamma_0 - \gamma_\infty = (\gamma_0/\eta_0) \int_{t_1}^{\infty} G(s)\, ds \tag{72}$$

and the final residual strain or permanent set corresponding to $t = \infty$ in equation 71 is

$$\gamma_\infty = (\gamma_0/\eta_0) \int_0^{t_1} G(s)\, ds \tag{73}$$

which may be recognized as the flow occurring in the interval from $t = -t_1$ to $t = 0$ under time-varying stress.

G. COMMENTS ON THE PHENOMENOLOGICAL THEORY OF LINEAR VISCOELASTICITY

All the relations in Sections B to F above may be regarded as originating in the Boltzmann superposition principle or the constitutive equation of Chapter 1, equation 7. The foundation of the theory has also been related to the principles of linear irreversible thermodynamics.[46,47] It has been pointed out by Meixner[9,48] that certain other postulates are taken for granted. Many of the specific predictions

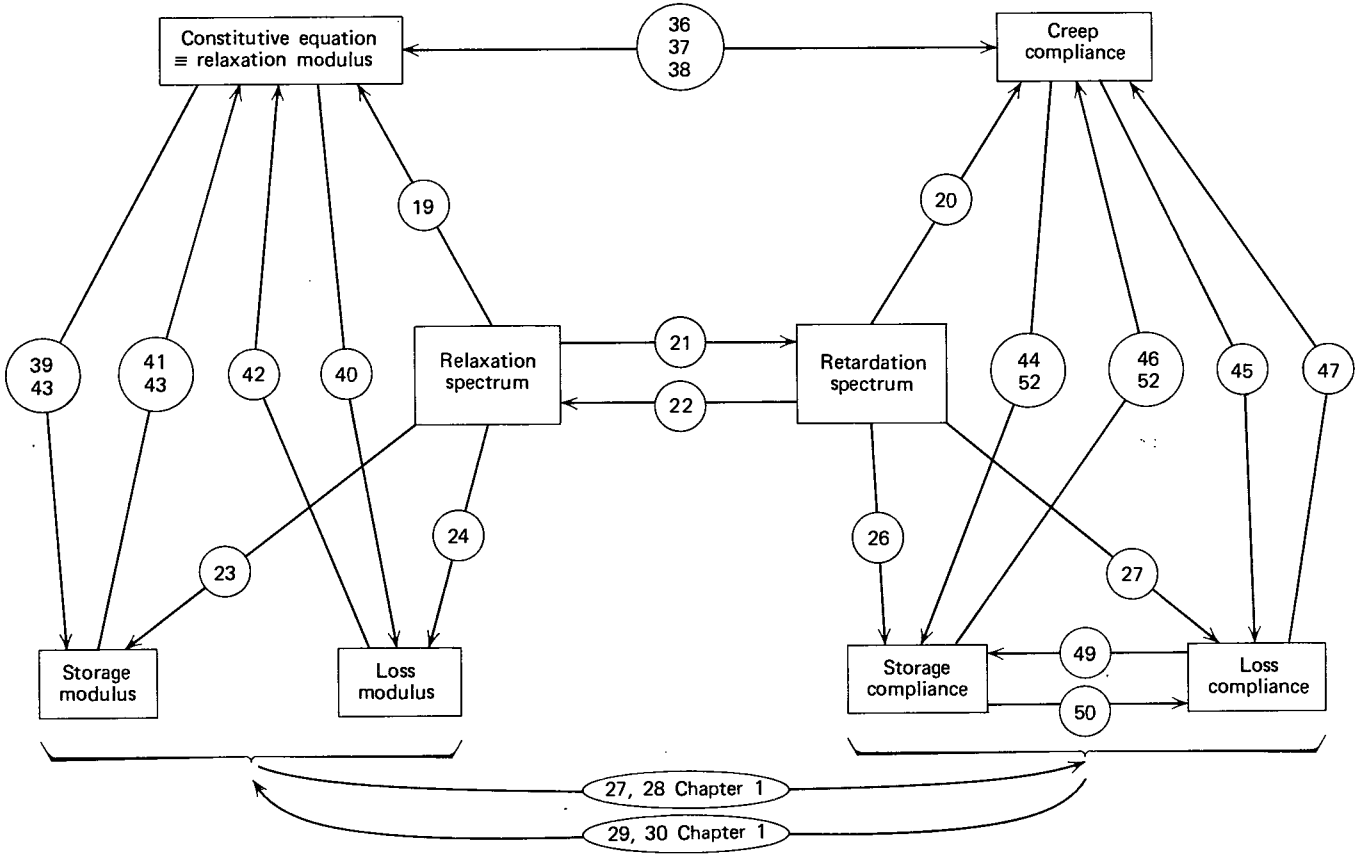


FIG. 3-9. Relations among the linear viscoelastic functions with numbers of equations (in this chapter unless otherwise specified).

TABLE 3-I

SUMMARY OF EQUATIONS FOR VISCOELASTIC CONSTANTS

From	η_0	G_g	J_e	J_e^0
Relaxation spectrum, H	28	29		32
Retardation spectrum, L			30	31
Relaxation modulus, $G(t)$	51			54
Storage modulus, G'	52			
Loss modulus, G''		55		
Creep compliance, $J(t)$	40[a]			40[a]
Loss compliance, J''			53	53

[a] Chapter 1.

of the theory have been repeatedly confirmed experimentally, although there are occasional reports of puzzling discrepancies.[49]

The relations among the various types of linear viscoelastic functions are summarized in Fig. 3-9 with equation numbers identified. The equation numbers for calculation of viscoelastic constants are identified in Table 3-I.

For further details on the theory of linear viscoelasticity, the treatise of Tschoegl[13] may be consulted.

H. RELATIONS FROM NONLINEAR CONSTITUTIVE EQUATIONS

The interrelationships for linear viscoelasticity in Sections B to F are accepted with almost the confidence given deductions from the laws of thermodynamics. Relations from nonlinear viscoelasticity theory are less well established. Many nonlinear constitutive equations have been proposed. Some predict certain relations which are in close accord with experiment and can be accepted with confidence but fail in other respects. A very thorough analysis with emphasis on viscoelastic liquids is provided by the treatise of Bird, Armstrong, and Hassager.[40]

The first manifestation of nonlinear behavior with increasing strain or strain rate is the appearance of normal stress differences in shearing deformation. For steady-state shear flow at small shear rates, several nonlinear models[50-53] predict the relation for the primary normal stress difference given as equation 62 of Chapter 1, which, combined with equation 54, gives

$$\sigma_{11} - \sigma_{22} \equiv \Psi_{1,0}\dot{\gamma}^2 = 2\eta_0^2 J_e^0 \dot{\gamma}^2 \tag{74}$$

Combination with equation 34 provides the relation

$$\lim_{\dot{\gamma}\to 0} \Psi_1 = \Psi_{1,0} = 2A_G \tag{75}$$

Thus the primary normal stress difference in steady flow at *small* $\dot{\gamma}$ gives the same information as G' at *low* frequencies. At higher values of the respective arguments,

there is no rigorous method for predicting one function from the other. The decrease in Ψ_1 with increasing $\dot{\gamma}$ appears together with the non-Newtonian decrease in η, and is related to it by some nonlinear models such as that of Goddard and Miller.[54]

A sinusoidally varying shear strain rate with small amplitude, such that $\dot{\gamma}_{21} = \gamma_{21}^0 \cos \omega t$, evokes a sinusoidally varying normal stress difference $\sigma_{11} - \sigma_{22}$ but at *twice* the frequency of the strain. This result, which would be expected from symmetry considerations because of the proportionality to $\dot{\gamma}_{21}^2$, is predicted by the phenomenological models previously quoted.[50-54] The oscillatory stress difference is superposed on a constant stress and both are proportional to $\dot{\gamma}_{21}^2$ if $\dot{\gamma}_{21}$ is small. The coefficient Ψ_1 is now defined as the ratio $(\sigma_{11} - \sigma_{22})/(\dot{\gamma}_{21}^0)^2$. It is the sum of a constant term and two oscillating terms:

$$\Psi_1 = \Psi_1^d + \Psi_1' \cos 2\omega t - \Psi_1'' \sin 2\omega t \tag{76}$$

The individual coefficients can be related to η' and η'' as follows:

$$\Psi_1^d = \eta''/\omega \tag{77}$$

$$\Psi_1'(\omega) = [-\eta''(\omega) + \eta''(2\omega)]/\omega \tag{78}$$

$$\Psi_1''(\omega) = [\eta'(\omega) - \eta'(2\omega)]/\omega \tag{79}$$

Thus oscillatory measurements of the primary normal stress difference give the same information as oscillatory shear stress measurements. Oscillatory measurements of the secondary normal stress difference, however, would provide additional information.

The relaxation of the primary normal stress difference after cessation of steady-state flow at strain rate $\dot{\gamma}$ can also be expressed in terms of linear viscoelastic properties by these models. For example, in terms of the relaxation spectrum, the rubberlike liquid theory of Lodge[50] provides[55]

$$(\sigma_{11} - \sigma_{22})^{ss}(t) = \dot{\gamma}^2 \int_{-\infty}^{\infty} H(\tau) \left[2 \int_0^t s e^{-s/\tau}\, ds \right] d \ln \tau \tag{80}$$

and, in terms of the relaxation modulus,

$$(\sigma_{11} - \sigma_{22})^{ss}(t) = 2\dot{\gamma}^2 \int_0^t sG(s)\, ds \tag{81}$$

The primary normal stress coefficient during steady-state shear flow is also related to the relaxation of *shear* stress after cessation of steady-state flow, as shown by combining equations 67 and 74;

$$\Psi_1 = (2/\dot{\gamma}) \int_{-\infty}^{\infty} t\sigma^{ss}(t)\, d \ln t \tag{82}$$

This relation can be derived from several phenomenological models and also from molecular theory.[56] According to the constitutive equation of Bird and Carreau,[57] it holds for finite $\dot{\gamma}$ even though equations 67 and 74 are limited to small $\dot{\gamma}$.

With large deformations or large strain rates, other nonlinear phenomena will

appear, including decrease in η (non-Newtonian viscosity), decrease in Ψ_1, deviations from the predictions of linear viscoelasticity for shear stress growth after sudden imposition of shear rate and for relaxation after sudden strain or after cessation of steady-state flow, corresponding behavior of the primary normal stress difference, etc. For other predictions of various phenomenological models concerning these phenomena, as well as the second normal stress difference, the reader is referred to some additonal reviews[40,58]

REFERENCES

1. W. Kuhn, *Z. Phys. Chem.*, **B42,** 1 (1939).
2. K. Bennewitz and H. Rötger, *Phys. Z.*, **40,** 416 (1939).
3. T. Alfrey and P. Doty, *J. Appl. Phys.*, **11,** 700 (1945).
4. B. Gross, *Mathematical Structure of the Theories of Viscoelasticity,* Hermann et Cie., Paris, 1953.
5. J. Schrama, Ph.D. dissertation, Leiden, 1957.
6. S. Kästner and E. Schlosser, *Kolloid-Z.*, **152,** 116 (1957).
7. J. R. Macdonald and M. K. Brachman, *Rev. Mod. Phys.*, **28,** 393 (1956); J. R. Macdonald and C. A. Barlow, Jr., *ibid.*, **35,** 940 (1963).
8. S. Goldman, *Transformation Calculus and Electrical Transients,* Prentice-Hall, Englewood Cliffs, N. J., 1949.
9. J. Meixner and H. König, *Rheol. Acta,* **1,** 190 (1958).
10. D. R. Bland, *Theory of Linear Viscoelasticity,* Pergamon, Oxford, 1960.
11. A. J. Staverman and F. Schwarzl, in *Die Physik der Hochpolymeren,* Volume IV, edited by H. A. Stuart, Chapter I, Springer-Verlag, Berlin, 1956.
12. T. Alfrey, Jr., *Mechanical Behavior of High Polymers,* Interscience, New York, 1948.
13. N. W. Tschoegl, *The Theory of Linear Viscoelastic Behavior,* Academic Press, 1981.
14. J. D. Ferry, W. M. Sawyer, and J. N. Ashworth, *J. Polym. Sci.*, **2,** 593 (1947).
15. J. J. Aklonis, W. J. MacKnight, and M. Shen, *Introduction to Polymer Viscoelasticity,* Wiley, New York, 1972.
16. H. F. Olson, *Dynamical Analogies,* Van Nostrand, New York, 1943.
17. G. Kegel, *Kolloid-Z.*, **135,** 125 (1954).
18. B. Gross, *J. Polym. Sci.*, **20,** 371 (1956).
19. M. Curie, *Radioactivité,* Volume I, Hermann, Paris, 1935.
20. A. V. Tobolsky, *Properties and Structure of Polymers,* Wiley, New York, 1960, pp. 188–194.
21. R. L. Bergen, Jr., and W. E. Wolstenholme, *Soc. Pet. Eng. J.*, **16,** 1235 (1960).
22. H. Silva and B. Gross, *Phys. Rev.*, **60,** 684 (1941).
23. R. M. Fuoss and J. G. Kirkwood, *J. Am. Chem. Soc.*, **63,** 385 (1941).
24. T. L. Smith, *J. Polym. Sci.*, **C35,** 39 (1971).
25. D. J. Plazek and S. J. Orbon, in preparation; S. J. Orbon, Ph.D. thesis, University of Pittsburgh, 1978.
26. I. L. Hopkins and R. W. Hamming, *J. Appl. Phys.*, **28,** 906 (1957); W. F. Knoff and I. L. Hopkins, *J. Appl. Polym. Sci.*, **16,** 2963 (1972).
27. A. S. Lodge, *Elastic Liquids,* Academic Press, London and New York, 1964.
28. R. S. Marvin, *Phys. Rev.*, **86,** 644 (1952).
29. R. de L. Kronig, *J. Opt. Soc. Am.*, **12,** 547 (1926).
30. H. A. Kramers, *Atti Cong. dei Fisici,* Como, 1927, p. 545.
31. J. H. Van Vleck, in *Properties of Short Radio Waves,* edited by D. E. Kerr, McGraw-Hill, New York, 1951, p. 641.
32. H. Fujita, personal communication.

33. R. Sips, *J. Polym. Sci.*, **5,** 69 (1950); **6,** 285 (1951).
34. T. L. Smith, *J. Polym. Sci.*, **20,** 89 (1956).
35. T. L. Smith, *Trans. Soc. Rheol.*, **6,** 61 (1962).
36. T. L. Smith, *Trans. Soc. Rheol.*, **20,** 103 (1976).
37. T. L. Smith, *Treatise on Materials Science and Technology,* Volume 10, Part A, Academic Press, New York, 1977, p. 369.
38. N. W. Tschoegl, *Kolloid-Z.*, **174,** 113 (1961).
39. J. Meissner, *J. Appl. Polym. Sci.*, **16,** 2877 (1972).
40. R. B. Bird, R. C. Armstrong, and O. Hassager, *Dynamics of Polymeric Liquids,* Volume I, Wiley, New York, 1977.
41. J. Meissner, *J. Polym. Sci., Polym. Phys. Ed.*, **16,** 915 (1978).
42. R. E. Kelchner and J. J. Aklonis, *J. Polym. Sci., Polym. Phys. Ed.*, **9,** 609 (1971).
43. F. W. Schremp, J. D. Ferry, and W. W. Evans, *J. Appl. Phys.*, **22,** 711 (1951).
44. R. A. Stratton and A. F. Butcher, *J. Polym. Sci., Polym. Phys. Ed.*, **11,** 1747 (1973).
45. S. Ohta, Y. Einaga, K. Osaki, and M. Kurata, *Bull. Inst. Chem. Res., Kyoto Univ.*, **51,** 220 (1973).
46. J. Meixner, *Kolloid-Z.*, **134,** 3 (1953); *Z. Naturforsch.*, **9a,** 654 (1954).
47. A. J. Staverman, *Kolloid-Z.*, **134,** 189 (1953).
48. J. Meixner, *Z. Phys.*, **139,** 30 (1954).
49. W. Sommer, *Kolloid-Z.*, **167,** 97 (1959).
50. A. S. Lodge, *Rheol. Acta,* **1,** 158 (1958).
51. B. D. Coleman and H. Markovitz, *J. Appl. Phys.*, **35,** 1 (1964).
52. B. D. Coleman and W. Noll, *Rev. Mod. Phys.*, **33,** 239 (1961).
53. A. G. Fredrickson, *Chem. Eng. Sci.*, **17,** 155 (1962).
54. Reference 40, p. 343.
55. F. H. Gortemaker, M. G. Hansen, B. de Cindio, H. M. Laun, and H. Janeschitz-Kriegl, *Rheol. Acta,* **15,** 256 (1976).
56. R. B. Bird, O. Hassager, R. C. Armstrong, and C. F. Curtiss, *Dynamics of Polymeric Liquids,* Volume II, Wiley, New York, 1977, p. 601.
57. R. B. Bird and P. J. Carreau, *Chem. Eng. Sci.*, **23,** 427 (1968).
58. C. M. Vrentas and W. W. Graessley, *S. Non-Newt. Mech.*, **9,** 339 (1981).

CHAPTER 4

Approximate Interrelations among The Linear Viscoelastic Functions

Many of the equations in Sections B to F of the preceding chapter, although accurate within the assumptions of linear viscoelasticity, fail to meet practical needs for converting one viscoelastic function into another. Usually, an integration from $-\infty$ to ∞ is required, and the function which is known initially may not be available over a wide enough range of time or frequency to give convergence of the integral; or even if it is, the integration may be tedious, and sensitive to errors through addition of terms of opposite sign as in Fig. 3-5. For these reasons, a variety of approximation methods have been developed for performing such calculations.

Most of the approximation procedures involve taking derivatives either of the initial function or of related functions, either graphically or by a numerical differencing process. Some can be extended in principle to utilize second and higher derivatives, but it is rare (except in isolated cases where curvature changes sharply) that experimental data are sufficiently precise to make any derivatives beyond the second worthwhile. For determining derivatives, graphical methods are often used. They can also be obtained from computer calculations after numerical data have been smoothed and interpolated, for example by spline functions (or spline in tension).[1-3] If a computer is used, the results should be monitored by graphical plots or display to avoid spurious effects from fluctuations in the data. Methods based on numerical differencing are easily adapted to computer calculation if the experimental data are spaced closely enough on the time or frequency scale to obtain reliable interpolated values at equal logarithmic intervals.

Generally, the approximation methods have an analytical foundation based on the properties of the integrands of the corresponding exact equations. Such an integrand is usually the product of the viscoelastic function initially known and an

additional dimensionless intensity function. For example, in equation 19 of Chapter 3,

$$G(t) = G_e + \int_{-\infty}^{\infty} He^{-t/\tau}\, d \ln \tau \tag{1}$$

the initial function H is multiplied by the kernel function $e^{-t/\tau}$ which goes from 0 at $\tau = 0$ to 1 at $\tau \to \infty$. If the latter were approximated by a step function going from 0 to 1 at $\tau = t$, we would have

$$G(t) \cong G_e + \int_{\ln t}^{\infty} H\, d \ln \tau \tag{2}$$

and the integral would not be grossly different. Moreover, by differentiating equation 2 with respect to the limit $\ln t$, we obtain

$$-\frac{dG(t)}{d \ln t}\bigg|_{t=\tau} \cong H(\tau) \tag{3}$$

so the relaxation spectrum at $\tau = t$ is obtainable in first approximation as the negative slope of the relaxation modulus. This is Alfrey's rule.[4]

Equations 2 and 3 are not sufficiently accurate unless H changes very slowly with time. To achieve a better approximation, there are two approaches: to develop the problem analytically[5-18] or to proceed semiempirically[19,20] with a set of correction factors based on an assumed form for H. If the assumed form fits H over a relatively limited region of time scale, this is ordinarily sufficient.

In other cases, simple explicit solutions can be obtained for integrals in equations such as 21 and 22 of Chapter 3 if the viscoelastic function in the integrand is assumed to have a certain form and the intensity function is retained without approximation. Again, it may be sufficient for the form assumed for the viscoelastic function to be valid over perhaps two decades of logarithmic time scale.

In the following summary of approximation methods, no derivations will be given; these are in the original literature. Many are presented in a critical review by Schwarzl and Struik,[15] and a general treatment and critique of the whole subject has been given by Tschoegl.[14] Some comments on utility will be made, however. Methods involving graphical differentiation are usually outlined in terms of slopes measured on logarithmic plots like those in Chapter 2.

A. CALCULATION OF SPECTRA FROM EXPERIMENTAL FUNCTIONS

This is the most important application of approximation methods, since exact methods are of such limited use.

1. Relaxation Spectrum from Relaxation Modulus

The method of Ferry and Williams[20] provides

$$H(\tau) = -M(m)G(t)\, d \log G(t)/d \log t\big|_{t=\tau} \tag{4}$$

where $M(m) = 1/\Gamma(m+1)$ and $-m$ is the slope of a doubly logarithmic plot of H against τ; Γ is the gamma function. (The method is limited to positive values of m.) The procedure is to make a tentative (first approximation) calculation of H by setting $M = 1$ in equation 4. Ordinarily, a series of points equally spaced on the logarithmic time scale is chosen, each providing a value of H at $\tau = t$. Then from a tentative logarithmic plot of H against τ, the slope $-m$ is measured at each point; the corresponding value of M is obtained and multiplied by the provisional value of H. Tables of M and other useful correction factors are given at the end of this chapter. Graphs of log M against m are also very convenient.

The second approximation method of Schwarzl and Staverman[5] provides

$$H(\tau) = -dG(t)/d \ln t + d^2G(t)/d(\ln t)^2|_{t=2\tau} \tag{5}$$

or, in terms of log-log plots,

$$H(\tau) = -G(t)[d \log G(t)/d \log t - (d \log G(t)/d \log t)^2 - (1/2.303)\, d^2 \log G(t)/d(\log t)^2]|_{t=2\tau} \tag{6}$$

Here both first and second derivatives of $G(t)$ must be measured, and the calculated value of H corresponds not to $\tau = t$ but to $\tau = t/2$. The two methods really use equivalent information, since the first derivative of H, needed for m in equation 4, is closely related to the second derivative of $G(t)$.

A variety of expressions involving second and higher derivatives has been derived by Tschoegl.[13,14] For example, as an alternative to equation 5:

$$H(\tau) = -dG(t)/d \ln t + \tfrac{1}{3}d^2G(t)/d(\ln t)^2|_{t=\tau/\sqrt{2}} \tag{7}$$

In comparing equations 5 and 7, the neglect of a third derivative is probably more serious in equation 7, but the latter has the advantage that the second derivative, more difficult to measure than the first derivative, makes a smaller contribution.[13]

An example of the third-order approximations of Tschoegl, employing the third derivative of $G(t)$, is

$$H(\tau) = -dG(t)/d \ln t + \tfrac{3}{2}d^2G(t)/d(\ln t)^2 - \tfrac{1}{2}d^3G(t)/d(\ln t)^3|_{t=3\tau} \tag{8}$$

Very precise data would be required to make a third or higher order approximation worthwhile. A modification of this type of calculation involving an iterative procedure has been proposed by Hlaváček and collaborators,[11,21] with much improved resolution if sharp peaks are present in the spectrum. Numerical differentiation methods such as that of Ninomiya and Ferry described in Section 3 below can also be applied.[9a,14]

2. Retardation Spectrum from Creep Compliance

The analog of the Ferry-Williams calculation, as shown by Stern,[22] is:

$$L(\tau) = M(-m)[J(t) - t/\eta_0]\, d \log [J(t) - t/\eta_0]/d \log t|_{t=\tau} \tag{9}$$

where M is the same function as before and $+m$ is the slope of a doubly logarithmic

plot of L against τ. The calculation is carried out in two stages as with equation 4.

The second approximation method of Schwarzl and Staverman gives

$$L(\tau) = dJ(t)/d \ln t - d^2J(t)/d(\ln t)^2|_{t=2\tau} \tag{10}$$

or

$$L(\tau) = (d/d \ln t)[J(t) - dJ(t)/d \ln t]|_{t=2\tau} \tag{11}$$

and has the advantage, not possessed by equation 9, that the flow term t/η_0 need not be subtracted from $J(t)$ before making the calculation. (Actually, equations 10 and 11 are unchanged[23] by substituting $J(t) - t/\eta_0$ for $J(t)$.) When creep experiments on uncross-linked polymers have not been carried far enough to determine η_0 with confidence, the Ferry-Williams method cannot be applied. The use of spline functions in computer processing of $J(t)$ data for second-approximation calculations has been described by Plazek and associates.[1-3]

Alternative second approximations, and third and higher approximations in alternative forms, are provided by the method of Tschoegl.[13,14]

3. Relaxation Spectrum from Storage Modulus

The method of Williams and Ferry[24] provides two formulas depending on whether m, the negative slope of H on a doubly logarithmic plot, is greater or less than 1. Almost invariably, $m < 1$, in which case:

$$H(\tau) = AG' \, d \log G'/d \log \omega|_{1/\omega=\tau} \tag{12}$$

where

$$A = (2 - m)/2\Gamma\left(2 - \frac{m}{2}\right)\Gamma\left(1 + \frac{m}{2}\right) = \frac{\sin(m\pi/2)}{m\pi/2} \tag{13}$$

If, on the other hand, $1 < m < 2$, the corresponding formula is

$$H(\tau) = A'G'(2 - d \log G'/d \log \omega)|_{1/\omega=\tau} \tag{14}$$

where

$$A' = m/2\Gamma\left(1 + \frac{m}{2}\right)\Gamma\left(2 - \frac{m}{2}\right) = \frac{\sin(m\pi/2)}{\pi(1 - m/2)} \tag{15}$$

As with equation 4, the calculation is carried out in two stages; first A is set equal to unity, and a preliminary calculation is made with each point at a given value of ω yielding a value of H at $\tau = 1/\omega$. From a tentative graph of H, the value of m is measured at each point, and the appropriate correction factor A is applied. Values of A and A' are also given at the end of the chapter.

The second order approximation formulas of Tschoegl[13a,14] are probably more accurate:

$$H(\tau) = dG'/d \ln \omega + \tfrac{1}{2}d^2G'/d(\ln \omega)^2|_{1/\omega=\sqrt{2\tau}} \tag{16}$$

$$H(\tau) = dG'/d \ln \omega - \tfrac{1}{2}d^2G'/d(\ln \omega)^2|_{1/\omega=\tau/\sqrt{2}} \quad (17)$$

Equation 16 is used when the slope of $H(\tau)$ is positive (m negative) and equation 17 when the slope is negative (m positive). In terms of log-log plots, equation 17 is

$$H(\tau) = G'[d \log G'/d \log \omega - \tfrac{1}{2}(d \log G'/d \log \omega)^2 - (1/4.606)d^2 \log G'/d(\log \omega)^2]|_{1/\omega=\tau/\sqrt{2}} \quad (18)$$

An example of a third-order approximation from the method of Tschoegl is, for m positive,

$$H(\tau) = dG'/d \ln \omega - \tfrac{3}{8}d^2G'/d(\ln \omega)^2 - \tfrac{1}{8}d^3G'/d(\ln \omega)^3|_{1/\omega=\tau/\sqrt{3}} \quad (19)$$

For m negative, the sign of the second derivative is changed and $1/\omega$ corresponds to $\sqrt{3}\tau$ instead of $\tau/\sqrt{3}$.

As an example of a numerical differencing procedure in which derivatives are not explicitly calculated, the method of Ninomiya and Ferry[9] requires values of G', spaced at equal intervals on a logarithmic frequency scale above and below the frequency $\omega = 1/\tau$ corresponding to the value of τ for which H is desired: *viz.*, at ω/a^2, ω/a, $a\omega$, and $a^2\omega$, with a suitable choice of a. Then

$$H(\tau) = \frac{G'(a\omega) - G'(\omega/a)}{2 \ln a} - \frac{a^2}{(a^2-1)^2}\frac{G'(a^2\omega) - G'(\omega/a^2) - 2G'(a\omega) + 2G'(\omega/a)}{2 \ln a}\Bigg|_{1/\omega=\tau} \quad (20)$$

In practice $\log a = 0.2$ to 0.4 is a reasonable choice; with larger values the approximation is poorer, and with smaller values the limitations in accuracy of the experimental values of G' may cause serious fluctuations in the differencing.

Finally, Roesler[25] and Roesler and Twyman[26] have outlined more complicated numerical methods, and Hlaváček and Kotrba[11] have presented an iterative procedure starting from a third-order approximation of Schwarzl and Staverman.[5]

4. Retardation Spectrum from Storage Compliance

These are analogs to equations 12 to 20, some of which follow. By the method of Williams and Ferry, when m, the (positive) slope of a doubly logarithmic plot of L, is less than 1:

$$L(\tau) = -AJ'\, d \log J'/d \log \omega|_{1/\omega=\tau} \quad (21)$$

and in the rare event that $m > 1$

$$L(\tau) = A'J'(2 + d \log J'/d \log \omega)|_{1/\omega=\tau} \quad (22)$$

with A and A' defined in terms of m by equations 13 and 15 above. By the method of Tschoegl,[13a,14] in second-order approximation,

$$L(\tau) = -[dJ'/d \ln \omega + \tfrac{1}{2}d^2J'/d(\ln \omega)^2]|_{1/\omega=\sqrt{2}\tau} \tag{23}$$

$$L(\tau) = -[dJ'/d \ln \omega - \tfrac{1}{2}d^2J'/d(\ln \omega)^2]|_{1/\omega=\tau/\sqrt{2}} \tag{24}$$

Equation 23 is used when the slope of $L(\tau)$ is negative and equation 24 when it is positive. The corresponding equation from the method of Ninomiya and Ferry[9] is

$$L(\tau) = \frac{J'(\omega/a) - J'(a\omega)}{2 \ln a} - \frac{a^2}{(a^2-1)^2} \frac{J'(\omega/a^2) - J'(a^2\omega) - 2J'(\omega/a) + 2J'(a\omega)}{2 \ln a}\Bigg|_{1/\omega=\tau} \tag{25}$$

5. Relaxation Spectrum from Loss Modulus

In zero approximation, the loss modulus at ω has sometimes been directly taken as the relaxation spectrum at $\tau = 1/\omega$, but there is no need to use such a crude approximation when very simple methods are available to improve it.

The method of Williams and Ferry again provides two alternative formulas depending on whether m is positive or negative, but these can be readily synthesized by using the absolute values of m and of the slope $d \log G''/d \log \omega$:

$$H(\tau) = BG''(1 - |d \log G''/d \log \omega|)|_{1/\omega=\tau} \tag{26}$$

where

$$B = (1 + |m|)/2\Gamma\left(\frac{3}{2} - \frac{|m|}{2}\right)\Gamma\left(\frac{3}{2} + \frac{|m|}{2}\right) = \frac{\sin[\pi(1 + |m|)/2]}{\pi(1 - |m|)/2} \tag{27}$$

or[14]

$$B = \frac{\cos m\pi/2}{1 \pm m\beta^m}, \tag{28}$$

$\beta = \sqrt{3}$ if sign in denominator is $-$, $1/\sqrt{3}$ if $+$

The calculation proceeds in two steps as in the other Williams-Ferry methods; values of B from equation 27 are given at the end of the chapter.

The first-order approximations of Tschoegl[13a,14] give

$$H(\tau) = (2/\pi)[G'' + dG''/d \ln \omega]|_{1/\omega=\sqrt{3}\tau} \tag{29}$$

$$H(\tau) = (2/\pi)[G'' - dG''/d \ln \omega]|_{1/\omega=\tau/\sqrt{3}} \tag{30}$$

Equation 29 is used when the slope of $H(\tau)$ is positive and equation 30 when it is negative.

An equation of Schwarzl and Staverman uses only the second derivative:

$$H(\tau) = (2/\pi)[G'' - d^2G''/d(\ln \omega)^2]/_{1/\omega=\tau} \tag{31}$$

and the method of Tschoegl provides alternative second-order approximations which

use both first and second derivatives, such as

$$H(\tau) = (2/\pi)[G'' + \tfrac{4}{3}dG''/d \ln \omega + \tfrac{1}{3}d^2G''/d(\ln \omega)^2]|_{1/\omega=\tau/\sqrt{5}} \quad (32)$$

which is applicable when the slope of $H(\tau)$ is positive. If the latter is negative, the sign of the first derivative term in equation 32 is changed and $1/\omega$ corresponds to $\sqrt{5}\tau$.

It may be noted that the value of B for $m = 0$ (and $d \ln G''/d \ln \omega = 0$) is also $2/\pi = 0.637$, so for this case equations 26 and 31 agree except for the second derivative in the latter. When the second derivative is substantial, equation 31, or better 32, is preferable.

The method of Ninomiya and Ferry (first approximation) for this calculation involves three values of G'', equally spaced on the logarithmic frequency scale with a spacing of log a:

$$H(\tau) = \frac{2}{\pi}\left[G''(\omega) - \frac{a}{(a-1)^2}\{G''(a\omega) + G''(\omega/a) - 2G''(\omega)\}\right]\Bigg|_{1/\omega=\tau} \quad (33)$$

There are also the iterative numerical methods of Roesler and Twyman[26] and the eigenfunction expansion method of Roesler and Pearson[27] which in principle can be carried to any degree of approximation desired.

6. Retardation Spectrum from Loss Compliance

The Williams-Ferry formula for this calculation is

$$L(\tau) = BJ''(1 - |d \log J''/d \log \omega|)|_{1/\omega=\tau} \quad (34)$$

with B the same function of $|m|$ as before. For an uncross-linked polymer, at very low frequencies, J'' approaches $1/\omega\eta_0$; hence the calculation becomes numerically uncertain, with J'' increasing without limit and the quantity in parentheses approaching zero. Mathematically, of course, L approaches zero at low frequencies as it must if there is a finite number of relaxation mechanisms. The numerical uncertainty can be avoided, or shifted to an earlier stage in the data processing, if η_0 is known and $J'' - 1/\omega\eta_0$ is substituted for J'' in the formula.

The Tschoegl, Schwarzl-Staverman, and Ninomiya-Ferry approximations can be obtained simply by substituting either J'' or $J'' - 1/\omega\eta_0$ for G'' in equations 28 to 32. Equations 28 and 31 are applicable for negative slope of $L(\tau)$.

7. Criteria of Applicability of Various Approximations

The degree of error in an approximate calculation of a relaxation or retardation spectrum can be gauged in various ways. The original experimental function from which it was derived can be reconstructed by an integration such as equation 1, and compared with the initial data; this is not a very critical test and has rarely been undertaken. An iterative method such as that of Roesler and Pearson can be carried to convergence and used to check a simpler method; in one test of this sort,[27] the Williams-Ferry equation 26 was rather closely confirmed except near the maximum

in H. More commonly, the values of H obtained by approximations from different experimental functions are compared. This is almost always possible in analyzing dynamic measurements, where G' and G'' (or J' and J'') are determined simultaneously. Failure of the spectra calculated from the storage and loss components to agree indicates that at least one is in error, whereas agreement is reasonable evidence of a satisfactory calculation since both would not be expected to deviate in the same manner.

Sharp peaks in the spectra can be distinguished in approximation calculations only if many iterations are performed, as by Stanislav and Hlaváček.[21] However, when such discrete relaxation mechanisms appear (as in dilute solutions of polymers of uniform molecular weight) is it not customary to express results in terms of spectra. In regions where m changes slowly (corresponding to small second derivatives of G'', J'', H, or L, or small third derivatives of G', J', $G(t)$ or $J(t)$), the Williams-Ferry formulas have repeatedly given agreement between the calculations from storage and loss components to 0.05 log unit (10%) or better, which is probably as much as can be expected from most experimental data. These formulas are susceptible of rapid and easy calculation, although some judgment is needed in measuring slopes graphically. They cannot be relied upon, however, under circumstances where the correction factors (M, A, B, etc.) are smaller than $\frac{1}{2}$. They fail where there is sharp curvature in H and L, such as near the maxima and minima in Curves IV and VII of Figs. 3-3 and 3-4. In such regions, the Tschoegl methods[13,13a,14] are preferable. The numerical differentiation methods such as that of Ninomiya and Ferry lend themselves to routine calculation, but require carefully smoothed original data.

B. INTERRELATIONS BETWEEN THE SPECTRA

Equations 21 and 22 of Chapter 3 can be modified in various ways for simpler calculation of H from L and vice versa. Most of the resulting formulas have been given by Smith,[28] and are based on two principles: (a) if H is known, it has ordinarily been obtained from either $G(t)$ or G' and G'', so these latter functions can be utilized to aid in the calculation of L, and *mutatis mutandis* compliances can be utilized in the calculation of H from L; (b) over a limited range of logarithmic time scale, H can be assumed proportional to τ^{-m}, and L proportional to τ^{m}, *viz.* they can be characterized by the logarithmic slope m as used in the Williams-Ferry approximation methods.

1. One Spectrum and Transient Known

To obtain L from H and $G(t)$, the formula is

$$L(\tau) = \frac{H(\tau)}{\left\{G(t) + H(\tau)\left[\frac{\pi}{2}\left(\csc\frac{m\pi}{2} - \sec\frac{m\pi}{2}\right) - \Gamma(m) + 1.37\right]\right\}^2 + \pi^2 H^2} \qquad (35)$$

where m is the negative slope of a logarithmic plot of H, measured of course separately point by point; and to obtain H from L and $J(t)$,

$$H(\tau) = \frac{L(\tau)}{\left\{J(t) - 2t/\eta + L(\tau)\left[\frac{\pi}{2}\left(\csc\frac{m\pi}{2} - \sec\frac{m\pi}{2}\right) + \Gamma(-m) + 1.37\right]\right\}^2 + \pi^2 L^2} \tag{36}$$

where m is the positive slope of a logarithmic plot of L. These formulas are limited to $-1 < m < 1$.

2. One Spectrum and Dynamic Data Known

In this case, the slopes m are not necessary. To obtain L from H, G', and G'', we have

$$L(\tau) = \frac{H(\tau)}{[G'(1/\tau) - G''(1/\tau) + 1.37H(\tau)]^2 + \pi^2 H^2(\tau)} \tag{37}$$

and to obtain H from L, J', and J'', the corresponding approximation is

$$H(\tau) = \frac{L(\tau)}{[J'(1/\tau) - J''(1/\tau) + 1.37L(\tau)]^2 + \pi^2 L^2(\tau)} \tag{38}$$

3. One Spectrum Known with Constant Logarithmic Slope

There are two cases of interest where additional data are not required for the interconversion provided the given spectrum has a constant logarithmic slope over a wide range of time scale. When this is so, the exponents m in the expressions $H \propto \tau^{-m}$ and $L \propto \tau^m$ are equal. If $m = \frac{1}{2}$

$$H(\tau)L(\tau) = 1/\pi^2 \tag{39}$$

which is approximately applicable in the transition zone from rubberlike to glasslike consistency where $\log H$ has a slope near $-\frac{1}{2}$ and $\log L$ near $\frac{1}{2}$ (Figs. 3-3 and 3-4, curves III, IV, VI, and VII). Thus in such a zone $H(\tau) \cong 0.1/L(\tau)$.

If, on the other hand, $m \ll 1$, so that H falls very slightly and L rises very slightly, as in curves V and VIII at long times, Figs. 3-3 and 3-4,

$$H(\tau)L(\tau) = m^2 \tag{40}$$

so that in such extended plateau regions $H(\tau) \ll 1/L(\tau)$, as observed for the curves cited.

C. CALCULATION OF VISCOELASTIC FUNCTIONS FROM THE SPECTRA

Simplified methods for this type of calculation have not been widely developed,

partly because the problem seldom arises in practice and partly because the exact formulas, involving integrals such as equation 1 with reasonably rapid convergence, are not difficult to evaluate. However, Smith[28] has quoted two formulas, obtained by rearranging equations 25 and 36, from which the transient experimental functions can be calculated if both spectra are known:

$$G(t) = [H/L - \pi^2 H^2]^{1/2} - H\left[\frac{\pi}{2}\left(\csc\frac{m\pi}{2} - \sec\frac{m\pi}{2}\right) - \Gamma(m) + 1.37\right] \quad (41)$$

where m refers to the negative logarithmic slope of H; and

$$J(t) = [L/H - \pi^2 L^2]^{1/2} - L\left[\frac{\pi}{2}\left(\csc\frac{m\pi}{2} - \sec\frac{m\pi}{2}\right) + \Gamma(-m) + 1.37\right] + \frac{2t}{\eta_0} \quad (42)$$

where m refers to the (positive) logarithmic slope of L. For these formulas, m must be measured separately at each value of τ corresponding to the value of t at which the transient function is desired.

Two experimental functions which are quite easily derivable from the spectra are the closely related dynamic loss functions. Equations 26 and 34 can be rearranged to give

$$G''(\omega) = H/B(1 - |m|)|_{\tau=1/\omega} \quad (43)$$

$$J''(\omega) = L/B(1 - |m|) + \tau/\eta_0|_{\tau=1/\omega} \quad (44)$$

where m has its usual significance and at each point B is determined by the value of m. Some alternative equations have been given by Smith:[19]

$$G''(\omega) = (H\pi/2)\sec(m\pi/2)|_{\tau=1/\omega} \quad (45)$$

$$J''(\omega) = (L\pi/2)\sec(m\pi/2) + \tau/\eta_0|_{\tau=1/\omega} \quad (46)$$

D. CALCULATION OF ONE EXPERIMENTALLY OBSERVABLE VISCOELASTIC FUNCTION FROM ANOTHER

1. Interrelation of the Two Transient Functions

From equation 36 of Chapter 3, an approximate relation can be derived by assuming, for example, that $\log J(t)$ is a linear function of $\log t$ over a moderate interval of time scale, the slope of the function being as usual denoted by m. Then[23]

$$G(t) = (\sin m\pi)/m\pi J(t) \quad (47)$$

The same equation may be used to obtain $J(t)$ from $G(t)$, with m the slope of the doubly logarithmic plot of $G(t)$. A table of $(\sin m\pi)/m\pi$ is given at the end of the chapter. It has been emphasized by Aklonis and Tobolsky[29] that equation 47 is valid only for $m < 1$; even for m as large as 0.8, the correction factor is so far from unity

that the calculation is doubtful. When $m > 1$, as may be observed experimentally, the exact methods of Section E1 of Chapter 3 must be employed.

It may be noted that with $m \ll 1$, $G(t)$ becomes simply the reciprocal of $J(t)$, as mentioned in Chapter 2; otherwise, $G(t) < 1/J(t)$. Moreover, when an uncross-linked polymer reaches a steady-state condition of flow, $m \to 1$ (since $J(t) = t/\eta_0 +$ other terms which eventually become negligible by comparison); then according to equation 47, $G(t) \to 0$, as it must (Chapter 2).

2. Interrelation of a Transient with the Corresponding Dynamic Functions

If both dynamic components are known, the transient function can be calculated by the method of Ninomiya and Ferry. Thus, for relaxation:

$$G(t) = G'(\omega) - 0.40G''(0.40\omega) + 0.014G''(10\omega)\big|_{\omega=1/t} \tag{48}$$

requiring G' at the corresponding frequency $\omega = 1/t$ and G'' at two other frequencies. Similarly, for creep:

$$J(t) = J'(\omega) + 0.40J''(0.40\omega) - 0.014J''(10\omega)\big|_{\omega=1/t} \tag{49}$$

Alternatively, if $G(t)$ and G'' are known, G' can be calculated. The limits of error of these formulas have been examined by Schwarzl and Struik.[15]

More elaborate formulas have been derived by Schwarzl[17] for calculating $J(t)$ from one value of J' at $\omega = 1/t$ and several values of J'' at frequencies equally spaced logarithmically from $\omega/16$ to 8ω, or alternatively from one value of J'' at $\omega = 1/t$ and several values of J' at frequencies equally spaced logarithmically from $\omega/4$ to 64ω. The error bounds of the approximation have been carefully examined. This type of calculation is easily performed by computer if smoothed interpolated data for J' and J'' are available. In either the Ninomiya or the Schwarzl method, $J(t)$ is of course obtained over a somewhat narrower time range than the frequency range of the original data.

A rough relation which is sometimes useful[30] is that $J(t) \cong J''(1/t)$, though a better approximation is $J(t) \cong |J^*|(1/t)$, as mentioned in Chapter 2.

If either $G(t)$ or G' is known together with H, the other experimental function can be calculated by a simplification of equation 43 of Chapter 3 which avoids performing the integration, as introduced by Catsiff and Tobolsky:[31]

$$G'(\omega)\big|_{\omega=1/t} - G(t) = H(\tau)\psi(m)\big|_{\tau=t} \tag{50}$$

where H can be obtained from equation 4 or 12, depending on which of the experimental functions is given initially; m is as usual the negative slope of a plot of log H against log τ at the point $\tau = t$, and $\psi(m) = (\pi/2)\csc(m\pi/2) - \Gamma(m)$. A table of $\psi(m)$ is given at the end of the chapter. With equation 50, $G'(\omega)$ can be calculated from $G(t)$ or vice versa.

The analogous equation connecting the compliance functions is[28]

$$J'(\omega)\big|_{\omega=1/t} - J(t) + t/\eta_0 = L(\tau)\psi'(m)\big|_{\tau=t} \tag{51}$$

where m is the (positive) slope of a plot of log L against log τ at the point $\tau = t$, and

$\psi'(m) = (\pi/2)\csc(m\pi/2) + \Gamma(-m)$. A table of $\psi'(m)$ is also given at the end of the chapter; it is negative, as required by the fact that $J(t) > J'(1/t)$, even after subtraction of t/η_0.

If $G'(\omega)$ is very flat, H (which reflects the slope of G') is small by comparison, and as a result G' and $G(t)$ are almost identical, as seen in Chapter 2. Similarly, if J' is very flat, it is almost identical with $J(t) - t/\eta_0$. Another specific case of some interest occurs when $G' = G''$ and both are proportional to $\omega^{1/2}$, as specified in certain theories (Chapters 9 and 10) and roughly fulfilled in the transition region between glasslike and rubberlike consistency; then equation 50 reduces to $G(t) = 0.79G'(1/t)$. Still another example is given by the so-called Andrade creep behavior of cross-linked systems at long times (Chapter 13), where the compliance can be represented by the empirical equation $J(t) = J_A + \beta t^{1/3}$. At an equivalent frequency $\omega = 1/t$, the dynamic compliances are then given by[32]

$$J'(\omega) = J_A + [\beta\Gamma(\tfrac{1}{3})/2\sqrt{3}]\omega^{-1/3} = J_A + 0.773\beta\omega^{-1/3} \tag{52}$$

$$J''(\omega) = [\beta\Gamma(\tfrac{1}{3})/6]\omega^{-1/3} = 0.446\beta\omega^{-1/3} \tag{53}$$

and at frequencies sufficiently low that the term J_A in equation 51 can be neglected,

$$J''/J' = 1/\sqrt{3} = 0.577 \tag{54}$$

Analogs of equations 48 and 49 have been developed by Yagii and Maekawa[33] to calculate G' and G'' from $G(t)$ and the corresponding dynamic compliances from the creep compliance. If $G(t)$ is known at several times between $0.158t$ and $2.50t$, $G'(\omega)$ and $G''(\omega)$ where $\omega = 1/t$ can be estimated. More elaborate formulas of Schwarzl[18] provide for calculating G' and G'' from a series of $G(t)$ values at times equally spaced logarithmically over a wider range. The corresponding calculations of J' and J'' from a series of $J(t)$ values have also been derived.[16] For example, the best approximation for J' at the frequency $\omega = 1/t$ involves nine values of $J(t)$ from $t/8$ to $32t$ and an equation with 13 terms. The calculation can be easily programmed on a computer.

Some empirical interrelations for obtaining J' and J'' from the *recoverable* creep compliance, $J_r(t) = J(t) - t/\eta_0$, have been given by Plazek and Raghupathi.[34] These are

$$J'(\omega) = [1 - m(2t)]^{0.8} J_r(t)\big|_{t=1/\omega} \tag{55}$$

$$J''(\omega) = [m(\tfrac{2}{3}t)]^{0.8} J_r(t) + 1/\omega\eta_0\big|_{t=1/\omega} \tag{56}$$

where $m = d \log J_r(t)/d \log t$.

If the slope m of the creep function $J(t)$ on a doubly logarithmic plot is quite small (precluding the presence of viscous flow, of course), it is related to the loss tangent J''/J' by the equation[35]

$$\tan\delta = J''/J' = G''/G' = m\pi/2, \qquad m\pi/2 \ll 1 \tag{57}$$

Thus under certain circumstances $\tan\delta$ is independent of frequency, as seen in Fig. 2-8 (curves IV and V at low frequencies).

An elegant method has been described by Vinh[12] for converting $|G^*|$ and tan δ as functions of ω to $G(t)$, by Laplace and Carson transforms. The data are processed numerically with the aid of graphical devices, and the result is obtained in the form of an analytic function.

Finally, a numerical method has been outlined by Benbow[35] for calculating the components of the dynamic compliance from the creep compliance, based on a Fourier analysis of the latter.

3. Interrelation between the Components of a Complex Dynamic Function

Two relations have been given by Staverman and Schwarzl[36] relating the values of G' at two frequencies ω_1 and ω_2:

$$G'(\omega_2) - G'(\omega_1) \cong \frac{2}{\pi} \int_{\ln \omega_1}^{\ln \omega_2} G''(\omega)\, d \ln \omega \tag{58}$$

$$\ln G'(\omega_2)/G'(\omega_1) \cong \frac{2}{\pi} \int_{\ln \omega_1}^{\ln \omega_2} \tan \delta\, d \ln \omega \tag{59}$$

4. Criteria of Applicability

It is difficult to generalize in appraising the possible errors in the various approximations given here, which can range from within the experimental error of any measurements to deviations of 25% or more, depending on the features of the functions employed. The most complete analyses have been made by Schwarzl[15-19] and Tschoegl.[13,14] Smith[28] has compared approximate with exact calculations in a number of cases and found that over a wide range of circumstances the respective logarithms did not differ by more than 0.1. In general, results which involve subtraction of two numbers similar in magnitude, or the product of one quantity which is rapidly increasing and another which is approaching zero, should be regarded with skepticism; they can be distinguished by arithmetic common sense.

E. CALCULATION OF SPECTRA FROM MORE COMPLICATED EXPERIMENTAL FUNCTIONS

In Section F of Chapter 3, some more complicated viscoelastic experiments were formulated. The stress-strain or strain-stress curves can provide spectra through first differentiating to give the transient functions (equations 59 and 63 of Chapter 3) and then applying formulas such as equations 4 to 11. The stress relaxation after cessation of steady-state flow can provide the spectrum H through the following approximation relation:

$$H(\tau) = -(N/\dot{\gamma}t)\, d\sigma^{ss}/d \ln t\,|_{t=\tau} \tag{60}$$

where $\dot{\gamma}$ is the rate of shear during flow and $N = 1/\Gamma(m)$. A table of N is also given

Table 4-I

FUNCTIONS OF THE LOGARITHMIC SLOPE m USED IN APPROXIMATION CALCULATIONS

m	M	A	A'	B	N	ψ	ψ'	$\frac{\sin m\pi}{m\pi}$	m
−1.1							−0.639		−1.1
−1.0		0.637		1.000			−0.571		−1.0
−0.9		0.699		0.996			−0.521		−0.9
−0.8		0.757		0.984			−0.487		−0.8
−0.7		0.810		0.963			−0.464		−0.7
−0.6		0.858		0.936		1.757	−0.453		−0.6
−0.5		0.900		0.900		1.324	−0.449		−0.5
−0.4	0.672	0.936		0.858		1.052	−0.454		−0.4
−0.3	0.771	0.963		0.810		0.868	−0.468		−0.3
−0.2	0.859	0.984		0.757		0.737	−0.492		−0.2
−0.1	0.935	0.996		0.699		0.645	−0.527		−0.1
0	1.000	1.000		0.637		0.577	−0.577	1.000	0
0.1	1.051	0.996		0.699		0.527	−0.649	0.984	0.1
0.2	1.089	0.984		0.757		0.493	−0.737	0.935	0.2
0.3	1.114	0.963		0.810		0.470	−0.864	0.858	0.3
0.4	1.127	0.936		0.858		0.454	−1.050	0.757	0.4
0.5	1.128	0.900		0.900		0.449	−1.323	0.637	0.5
0.6	1.119	0.858		0.936	0.672	0.454	−1.755	0.505	0.6
0.7	1.101	0.810		0.963	0.771	0.465		0.368	0.7
0.8	1.074	0.757		0.984	0.859	0.488		0.234	0.8
0.9	1.040	0.699		0.996	0.935	0.523		0.109	0.9
1.0	1.000	0.637	0.637	1.000	1.000	0.571			1.0
1.1	0.956		0.699	0.996	1.050	0.640			1.1
1.1	0.908		0.757	0.984	1.089	0.732			1.2
1.3	0.857		0.810	0.963	1.114	0.866			1.3
1.4	0.805		0.858	0.936	1.127	1.057			1.4
1.5	0.753		0.900	0.900	1.128	1.336			1.5
1.6	0.700		0.936	0.858	1.119	1.783			1.6
1.7	0.647		0.963	0.810	1.100				1.7
1.8	0.597		0.984	0.757	1.074				1.8
1.9	0.547		0.996	0.699	1.040				1.9
2.0	0.500		1.000	0.637	1.000				2.0
Used in equations:	4	12 21	14 22 43 44	26 34	60	50	51	47	

at the end of the chapter. It should be remarked that equation 60 holds only when the stress relaxation is in the regime of linear viscoelasticity, and this condition is often not met experimentally.[37]

Once again the reader is reminded that, although all the equations in this chapter refer to deformation in shear, they are equally applicable to other types of deformation if the shear moduli, compliances, and spectra are replaced by the corresponding functions appropriate to extension or bulk compression, etc.

F. TABLE OF CORRECTION FACTORS

For convenience in calculation, Table 4-I gives values of the correction factors M, A, A', B, N, ψ, ψ', and $(\sin m\pi)/m\pi$ as functions of m. It will be recalled that, depending on the equation used, m is the negative slope of log H against log τ, the positive slope of log L against log τ, the positive slope of log $J(t)$ against log t, or the negative slope of log $G(t)$ against log t.

REFERENCES

1. E. Riande, H. Markovitz, D. J. Plazek, and N. Raghupathi, *J. Polym. Sci.*, **C50**, 405 (1975).
2. S. J. Orbon, Ph.D. thesis, University of Pittsburgh, 1978.
3. D. J. Plazek and S. J. Orbon, in preparation.
4. T. Alfrey and P. Doty, *J. Appl. Phys.*, **16**, 700 (1945).
5. F. Schwarzl and A. J. Staverman, *Appl. Sci. Res.*, **A4**, 127 (1953).
6. H. Leaderman, *J. Appl. Phys.*, **25**, 294 (1954).
7. M. Okano, *Busseiron Kenkyu*, **3**, 493 (1958).
8. H. Fujita, *J. Appl. Phys.*, **29**, 943 (1958).
9. K. Ninomiya and J. D. Ferry, *J. Colloid Sci.*, **14**, 36 (1959).
9a. G. Yasuda and K. Ninomiya, *Nippon Gomu Kyokaishi*, **59**, 81 (1966).
10. R. A. Schapery, *Proc. 4th U.S. Cong. Appl. Mech.*, 1961, p. 1075.
11. B. Hlaváček and V. Kotrba, *Rheol. Acta*, **6**, 288 (1967).
12. N. P. Vinh Tuong, *Mem. Artillerie Fr.*, 1967, p. 725; R. Veysseyre and N. P. Vinh Tuong, *C. R.*, **266**, 366 (1968).
13. N. W. Tschoegl, *Rheol. Acta*, **10**, 595 (1971).
13a. N. W. Tschoegl, *Rheol. Acta*, **10**, 582 (1971); **12**, 82 (1973).
14. N. W. Tschoegl, *The Theory of Linear Viscoelastic Behavior*, Springer-Verlag to be published.
15. F. R. Schwarzl and L. C. E. Struik, *Adv. Mol. Relaxation Processes*, **1**, 201 (1967–1968).
15a. F. R. Schwarzl, *Pure Appl. Chem.*, **23**, 219 (1970).
16. F. R. Schwarzl, *Rheol. Acta*, **8**, 6 (1969).
17. F. R. Schwarzl, *Rheol. Acta*, **9**, 382 (1970).
18. F. R. Schwarzl, *Rheol. Acta*, **10**, 166 (1971).
19. R. D. Andrews, *Ind. Eng. Chem.*, **44**, 707 (1952).
20. J. D. Ferry and M. L. Williams, *J. Colloid Sci.*, **7**, 347 (1952).
21. J. Stanislav and B. Hlaváček, *Trans. Soc. Rheol.*, **17**, 331 (1973).
22. D. M. Stern, Ph.D. thesis, University of Wisconsin, 1957.
23. H. Leaderman, in *Rheology*, Vol. II, edited by F. R. Eirich, Academic Press, New York, 1958.
24. M. L. Williams and J. D. Ferry, *J. Polym. Sci.*, **11**, 169 (1953).
25. F. C. Roesler, *Proc. Phys. Soc.*, **B68**, 89 (1955).
26. F. C. Roesler and W. A. Twyman, *Proc. Phys. Soc.*, **B68**, 97 (1955).
27. F. C. Roesler and J. R. A. Pearson, *Proc. Phys. Soc.*, **B67**, 338 (1954).

28. T. L. Smith, *Trans. Soc. Rheol.*, **2,** 731 (1958).
29. J. J. Aklonis and A. V. Tobolsky, *J. Appl. Phys.*, **36,** 3483 (1965).
30. E. Riande and H. Markovitz, *J. Polym. Sci., Polym. Phys. Ed.*, **13,** 947 (1975).
31. E. Catsiff and A. V. Tobolsky, *J. Colloid Sci.*, **10,** 375 (1955).
32. D. J. Plazek, *J. Colloid Sci.*, **15,** 50 (1960).
33. K. Yagii and E. Maekawa, *Nippon Gomu Kyokaishi,* **40,** 46 (1967).
34. D. J. Plazek, N. Raghupathi, and S. J. Orbon, *J. Rheol.*, **23,** 477 (1979).
35. J. J. Benbow, *Proc. Phys. Soc.*, **B69,** 885 (1956).
36. A. J. Staverman and F. Schwarzl, in *Die Physik der Hochpolymeren,* edited by H. A. Stuart, Vol. IV, Chapter 1, Springer-Verlag, Berlin, 1956.
37. F. W. Schremp, J. D. Ferry, and W. W. Evans, *J. Appl. Phys.*, **22,** 711 (1951).

CHAPTER 5

Experimental Methods for Viscoelastic Liquids

We now devote several chapters to the experimental determination of the viscoelastic properties whose general features have been surveyed in Chapter 2 and whose interrelations have been summarized in Chapters 3 and 4.

Experimental methods depend greatly on the consistencies of the materials to be studied, and are classified accordingly in the next three chapters. In Chapters 1 and 2, a "viscoelastic liquid" was identified as a material which, in a creep experiment, approaches steady-state flow after a constant stress has been applied for a sufficiently long period. Such a material must usually be suitably confined to prevent flow under the action of gravitational forces during an experiment, and most of the methods described in this chapter provide for this, though in some cases thin films are held in place primarily by surface tension. Polymeric liquids of extremely high viscosity can, on the other hand, often be studied in equipment designed for soft viscoelastic solids as described in Chapter 6, where no provision is made to contain the sample against gravitational forces.

As pointed out in Chapter 1, the forces and displacements which are measured in a mechanical experiment are related to the states of stress and strain by the constitutive equation which describes the viscoelastic properties sought, as well as the equations of motion and continuity (equations 1 and 2 of Chapter 1). Ordinarily, there is considerable simplification because there is no change in density with time, and because gravitational forces can be neglected. In transient experiments (creep and stress relaxation), inertial forces can also be neglected by suitable restriction of the time scale, eliminating short times. In periodic (oscillatory) experiments, inertial forces may or may not play an important role depending on the frequency, sample dimensions, and mechanical consistency as described in Section D below.

When inertial forces can be neglected and the deformations are infinitesimal, strain/stress ratios can be related to displacement/force ratios (or angular dis-

placement/torque ratios) by form factors which depend on apparatus geometry. For most measurements on viscoelastic liquids, the deformation corresponds to simple shear; the most useful geometries are sketched in Fig. 5–1, as follows: (*a*)

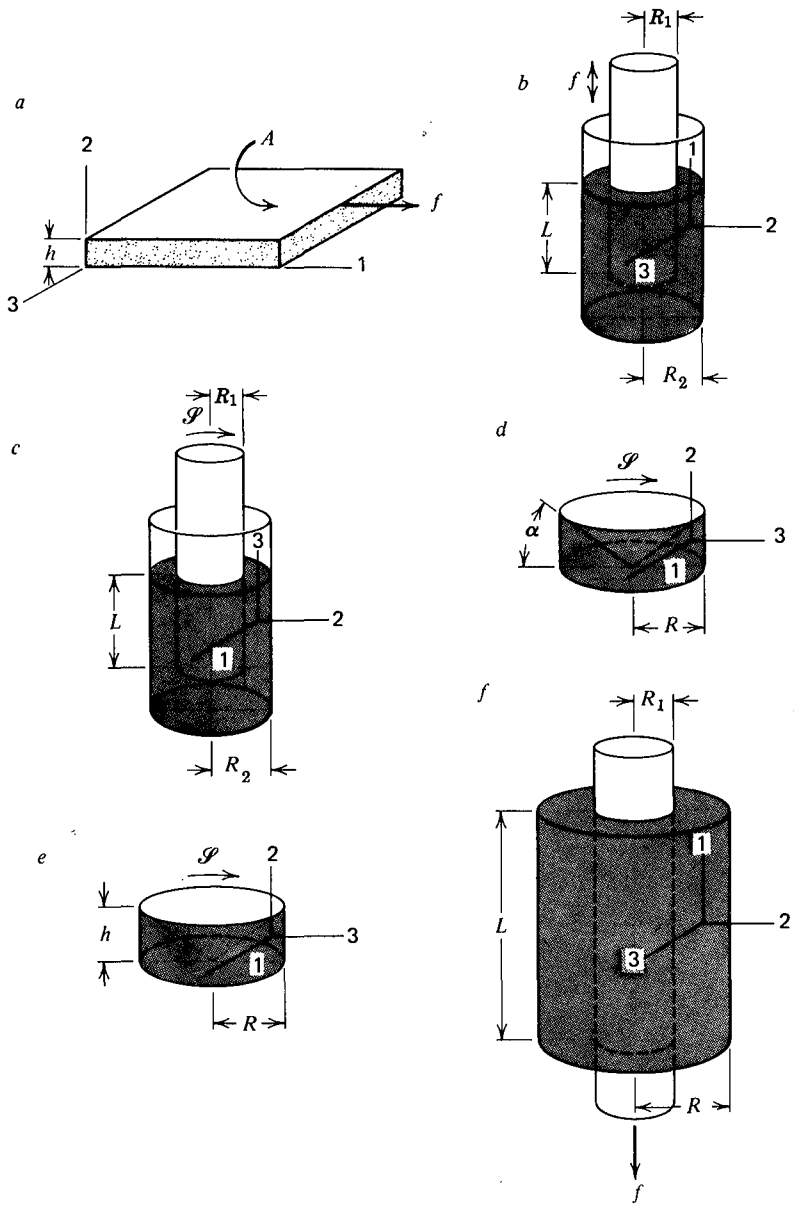


FIG. 5–1. Geometries, coordinates, and dimensions for investigations of viscoelastic liquids. (*a*) parallel plate simple shear; (*b*) annular pumping; (*c*) rotation between coaxial cylinders; (*d*) torsion between cone and plate; (*e*) torsion between parallel plates; (*f*) axial motion between coaxial cylinders.

parallel plate simple shear; (*b*) annular pumping; (*c*) rotation between coaxial cylinders; (*d*) torsion between cone and plate; (*e*) torsion of cylindrical disc between parallel plates; (*f*) axial motion between coaxial cylinders. Of these, (*a*) and (*d*) have the advantage that the strain is nearly homogeneous throughout the sample. All these geometries give equivalent information for the shear strain/stress ratio, γ_{21}/σ_{21}, in small deformations (though this is not true for normal stresses, discussed in Section C below). In the ratio γ_{21}/σ_{21}, γ_{21} is time dependent in creep; σ_{21} is time dependent in stress relaxation; and both are periodic with a phase difference (expressible by complex notation) in oscillatory experiments. The geometrical factors (which are discussed in more detail in a review by Philippoff[1]) are expressed as follows:

(*a*) Parallel plate simple shear:

$$\gamma_{21}/\sigma_{21} = bx_1/f \tag{1}$$

$$b = A/h \tag{2}$$

(*b*) Annular pumping:

$$\gamma_{21}/\sigma_{21} = bx_1/f \tag{3}$$

$$b = \frac{2\pi L}{\ln q - (q^2 - 1)/(q^2 + 1)} \tag{4}$$

$$q = R_2/R_1 \tag{5}$$

(*c*) Rotation between coaxial cylinders:

$$\gamma_{21}/\sigma_{21} = b\alpha\mathcal{S} \tag{6}$$

$$b = 4\pi L/(1/R_1^2 - 1/R_2^2) \tag{7}$$

(*d*) Torsion between cone and plate:

$$\gamma_{21}/\sigma_{21} = b\alpha/\mathcal{S} \tag{8}$$

$$b = 2\pi R^3/3\theta \tag{9}$$

(*e*) Torsion between parallel plates:

$$\gamma_{21}/\sigma_{21} = b\alpha/\mathcal{S} \tag{10}$$

$$b = \pi R^4/2h \tag{11}$$

(*f*) Axial motion between coaxial cylinders:

$$\gamma_{21}/\sigma_{21} = bx/f \tag{12}$$

$$b = 2\pi L/\ln (R_2/R_1) \tag{13}$$

(Configuration *f*, known as Segel[2] or Pochettino[3] geometry, is applicable to viscous liquids only if the sample is sufficiently viscous or is prevented somehow from running out of the open gap, as by a thin foil of negligible mechanical stiffness.[4])

b = form factor—dimensions cm in (a), (b), and (f); cm^3 in (c), (d), and (e)
x_1 = linear displacement
f = force
A = area (of sample in contact with plates)
h = thickness of sample (see Fig. 5-1)
L = length of sample (see Fig. 5-1)
R_2 = radius of outer cylinder
R_1 = radius of inner cylinder
R = radius of sample (in cone and plate or parallel plate)
α = angular displacement (radians)
$\mathcal{S}$ = torque
θ = angle between cone and plate

All these formulas are approximations in that various edge and end effects have been neglected, as well as states of strain and flow which may be somewhat more complicated than the simple forms assumed from the geometry. In some cases, better approximations have been introduced for specific experimental methods. The possible effect of surface tension on the mechanical measurements is usually not considered, but may be important if there is a change in surface area with the mechanical deformation.

Transient experiments will be discussed first, then oscillatory experiments.

A. CREEP

For creep of viscoelastic liquids, one of the rotational geometries is usually chosen. A constant torque is suddenly applied (actually, within a small time interval t_1) and after lapse of a period somewhat longer than t_1 the angular displacement is followed as a function of time. After steady-state flow has been achieved, it is desirable to remove the torque and follow the creep recovery as described in Chapter 1, Section E. Absence of perceptible friction is essential. For temperature control, which is important because of the strong dependence of viscoelastic properties on temperature, there must be no heat leakage through the device used to apply the torque; connecting members of low thermal conductivity are useful.

1. Rotation between Coaxial Cylinders

The apparatus of Overberg and Leaderman[5] is an excellent example of a carefully designed coaxial cylinder device (Fig. 5-2). The torque is applied by weights over pulleys and the rotor is held by ball bearings with low friction. The stator (outer cylinder) is made of glass to permit observation of the sample. For measurement of creep recovery, the torque can be quickly disengaged by a solenoid. The angular displacement is measured by reflection of a light beam from a system of multiple mirrors, which provide high sensitivity and at the same time permit the rotation to be followed through large angles; it can be recorded by a photoelectric recorder.

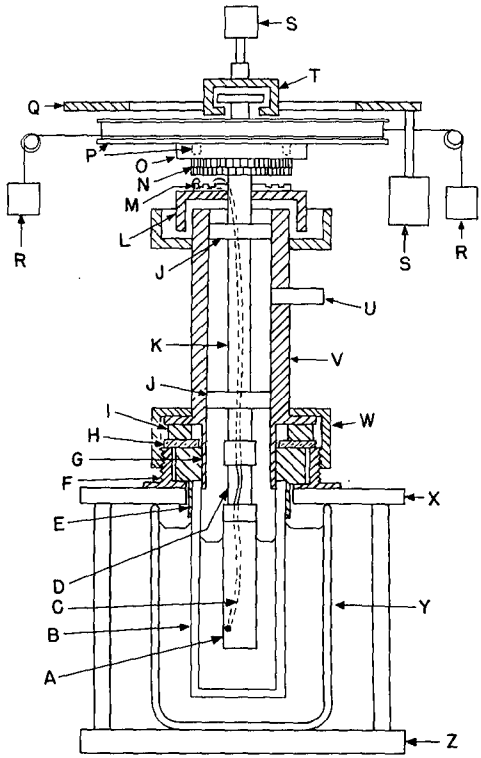


FIG. 5-2. Coaxial cylinder apparatus of Overberg and Leaderman[5] for measurement of creep and creep recovery. (A) Interchangeable rotor; (B) precision-bore glass stator; (C) rotor thermocouple; (D) Kovar-glass insulating link; (E) collar; (F) support ring; (G) stator centering sleeve; (H) spacing ring; (I) gauge blocks; (J) axial thrust ball bearings; (K) rotor shaft; (L) mercury seal; (M) mercury slip-rings for thermocouple contacts; (N) multiple mirror; (O) torque drum adapter; (P) torque drum; (Q) torque drum arresting ring; (R) weights; (S, S′) solenoids; (T) drum removal device; (U) gas inlet tube; (V) rotor shaft housing; (W) locking ring; (X) upper platform; (Y) Dewar vessel; (Z) sub-base.

The use of different torque drums and cylinder dimensions permits measurements of materials over a wide range of consistencies. Good thermal isolation is achieved by a glass section in the torque rod.

In this geometry, the strain and rate of strain are not homogeneous, but diminish from the inner cylinder outwards. For Newtonian liquids, they are proportional to $1/r^2$, where r is the distance from the center of rotation; for non-Newtonian liquids, the distribution is more complicated.[6] Corrections must be made for end effects of the cylinders[7] and can be checked by filling the apparatus to different levels or varying the end clearance.[5] Filling is difficult with liquids of very high viscosity.

Since in equation 6 the ratio $\gamma_{21}(t)/\sigma_{21}$ is the creep compliance $J(t)$, the latter is obtained directly by substituting in this equation the time-dependent angular displacement $\alpha(t)$.

The torques must be kept small to approach linear viscoelastic behavior. A large viscous deformation does not necessarily imply departure from linear behavior if the associated elastic deformation (as measured by the recoverable strain after removal of the torque) is small; as a rule of thumb, the product $\sigma_{21}J_e^0$ should perhaps be less than 0.1. The maximum value of σ_{21} (at the inner cylinder wall) can be calculated from the torque; formulas for all geometries are given in Appendix C.

Another serious limitation on the magnitude of the torque is avoidance of the Weissenberg effect in which, owing to normal stresses (Section C below), the liquid climbs up the inner cylinder during rotation. This alters the geometry and falsifies the form factor b calculated from equation 7. Observation of the sample is therefore highly desirable to make sure that the torque is sufficiently small to render this effect negligible.

2. Torsion between Parallel Plates or Cone and Plate

The apparatus of Plazek[8] (Fig. 5-3) is an exceptionally precise and versatile torsion instrument. The rotating system is magnetically suspended and the torque is applied magnetically by a drag cup motor; hence the rotor touches nothing but the sample and is wholly devoid of friction. The sample is contained between two parallel circular surfaces which, for a liquid of low viscosity, can be close together to provide a thin disc, or, for a liquid of very high viscosity, can be more widely separated. A single sample can be measured with different geometries over a wide temperature range by starting with a relatively thin disc at high temperatures and increasing the thickness as the temperature is lowered. (In this case, the sample contracts laterally and loses its cylindrical shape, so equation 11 does not apply; but the form factor b can be determined empirically after each change in dimensions from a measurement at the same temperature with the preceding configuration.) The angular deformation is measured by a light beam and multiple mirrors with a photocell recorder. The sample can be inspected visually and its thickness measured *in situ*. The sample chamber can be filled with inert gas or pumped to a low vacuum. The creep compliance is obtained from equation 10, using the time-dependent angle $\alpha(t)$.

A modification of this apparatus by Berry and Wong[9] provides for an alternative mode of operation in which a steady shear rate is imposed and stress growth and relaxation can be measured (Section B below); it is also adapted to the use of corrosive liquids which must be protected from atmospheric moisture, and can be operated at temperatures up to 200°C.

Numerous less elaborate devices with parallel plate or cone and plate geometry have been described in the literature.[10-12] Application of torque by a torsion wire from which the rotating element of the apparatus is suspended can be quite satisfactory for creep if the torsional stiffness of the wire is small and the top is turned through a large angle; then the torque remains essentially constant despite the small angular displacement at the bottom of the wire.[9] It is difficult to perform creep recovery experiments with a torsion wire, but these can be accomplished if the

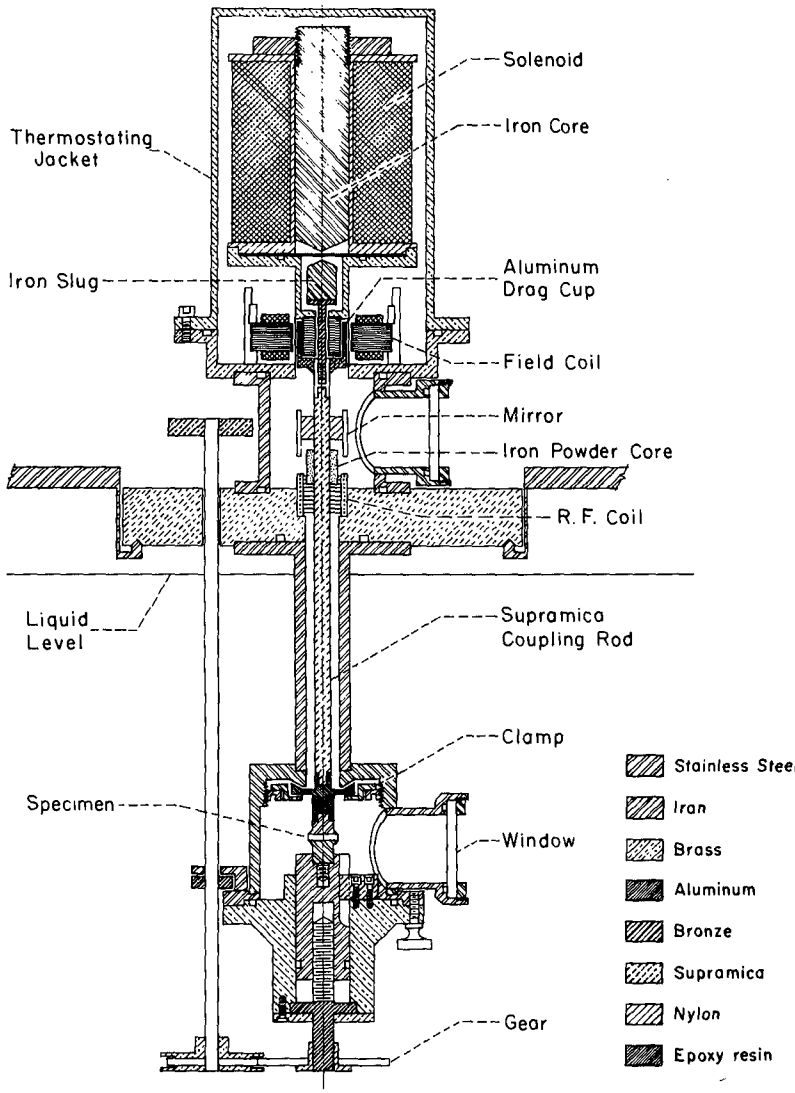


FIG. 5-3. Magnetic bearing parallel plate apparatus of Plazek[8] for measurement of creep and creep recovery.

torsion wire is in turn suspended by a silk thread of negligible torsional stiffness.[12]

It should be noted that there is a potential complication from secondary flow patterns in all geometries,[13,14] but these are probably unimportant at low shear rates.

3. Calculation of η_0 and J_e^0 from Creep Measurements in the Terminal Zone

The steady-flow viscosity η_0 and the steady-state compliance J_e^0 can easily be determined from creep data in the region of linear viscoelastic behavior as shown in Fig. 1–12, from equation 40 of Chapter 1, provided steady-state flow has been attained. However, it is easy to be misled into believing prematurely that the linear portion of the creep curve has been reached; in general, it cannot be expected to become linear until the flow term t/η_0 is at least as large as the intercept J_e^0. It is always desirable to perform the recovery experiment shown in Fig. 1–12 to confirm the calculation.

Assistance in estimating η_0 and J_e^0 in creep experiments of long duration can be provided by the extrapolation method of Ninomiya,[15] as follows. First log $J(t)$ is plotted against log t and the slope of the curve, m, is measured at suitable intervals. Then $J(t)/t$ and also $mJ(t)/t$ are plotted against $1/t$ as illustrated in Fig. 5–4. The limiting intercept of both curves is $1/\eta_0$. This is obtained first by extrapolating $mJ(t)/t$, which is nearly linear. Then $J(t)/t$ is extrapolated, and its limiting slope is J_e^0. For application of this method, the experiment must approach closely enough to steady-state flow so that m is at least as large as 0.7. It is evident that J_e^0 is less reliable than η_0. For a really confident determination of J_e^0, a creep recovery experiment should be made with a frictionfree apparatus.

To make an order-of-magnitude rule about the duration of a creep experiment, it may be noted that the terminal retardation time is very roughly equal to the product $J_e^0\,\eta_0$ (*cf.* equations 10 and 11 of Chapter 10, recalling that the terminal relaxation and retardation times are similar in magnitude). Though J_e^0 depends on polymer concentration, molecular weight, and molecular weight distribution, it is often of the order of 10^{-6} to 10^{-5} cm^2/dyne (10^{-5} to 10^{-4} Pa^{-1}). This sets both

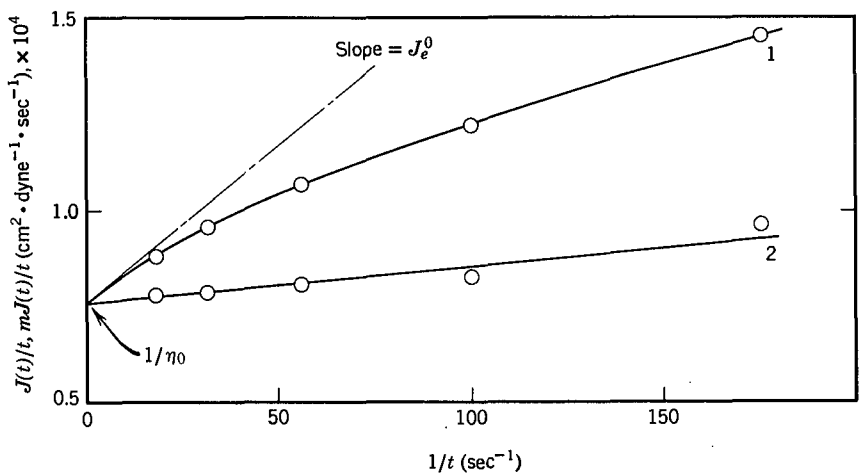


FIG. 5–4. Example of Ninomiya extrapolation method[15] to obtain J_e^0 and η_0 from creep measurements: data for a polyisobutylene with weight-average molecular weight 16,000, reduced to 30°C from measurements at low temperatures. 1, $J(t)/t$; 2, $mJ(t)/t$.

upper and lower limits on the practicality of creep measurements depending on the magnitude of η_0.

4. Nonlinear Creep and Non-Newtonian Viscosity

If the linear viscoelastic properties are sought, creep experiments should be made at more than one torque to ensure that $J(t)$ is independent of stress. Otherwise, to study nonlinear behavior in creep, it is necessary to follow creep and creep recovery at various stresses or shear rates, preferably under homogeneous shearing conditions as provided by torsion between cone and plate, and to obtain the non-Newtonian viscosity (η) and shear-rate-dependent steady-state compliance ($R_{\dot{\gamma}}$) corresponding to each level of shear rate.[16] However, if only η is desired, it is only necessary to ensure that steady-state flow has been achieved before the stress and shear rate are determined. Many elaborate instruments for this purpose have been described, including the Weissenberg rheogoniometer,[17] the Képès cone and plate viscometer,[18] the coaxial cylinder rheometer of Horio, Onogi, and Ogihara,[19] the high-shear rheometer of Porter and Johnson,[20] the Ferranti-Shirley viscometer,[21] and the Rheometrics Mechanical Spectrometer[22,22a] (some of which perform other rheological measurements in different modes). A review of such methods is beyond the scope of this chapter; other sources are available.[23–25]

B. SHEAR STRESS RELAXATION AND STRESS GROWTH

Stress relaxation following large sudden shear strains (Fig. 1-4) can be measured with cone and plate geometry;[24–27] the torque is measured by the angular deformation of a torsion wire which is sufficiently stiff so that its rotation is much smaller than the rotation imposed to produce the strain, and the magnitude of the strain does not change significantly during the relaxation process.

More commonly, for viscoelastic liquids, stress relaxation is measured after cessation of steady-state flow (Fig. 1-5). The geometry may be again either coaxial cylinders,[28] parallel plates,[17] cone and plate,[17,22,29] or two cones with different apex angles.[30,31] After cessation of flow, the member which was originally rotating is held fixed and the torque exerted at rest is measured by a suitable sensing device such as a strain gauge, differential transformer, or simply the untwisting of a very stiff torque element between the system and a rigid clamp. Actually, any of these devices must admit a very small motion within the sample, since the measurement determines a strain to which the torque is proportional; but it is sufficient to keep the motion of the measuring element much smaller than the angle corresponding to γ_e, the elastic strain during steady-state flow [$= J_e^0 \sigma^{ss}(0)$, where $\sigma^{ss}(0)$ is the shear stress—maximum value, if inhomogeneous in the sample—during steady-state flow preceding the stress relaxation]. The Weissenberg rheogoniometer,[17] especially as modified by Meissner,[32] and the modification by Pierson and Kovacs[29] of the Képès viscosimeter,[18] have been extensively used for this purpose, especially to study nonlinear stress relaxation following cessation of non-Newtonian flow.

The increase of stress during approach to steady-state flow can also be studied; it often passes through a maximum. With the device of Pierson and Kovacs,[29] a small correction is made for the compliance of the apparatus. To obtain the normalized stress relaxation function, $\sigma^{ss}(t)/\sigma^{ss}(0) = \mathcal{S}^{ss}(t)/\mathcal{S}^{ss}(0)$, no form factor b is necessary. It may be noted, however, that the viscosity (in general non-Newtonian) is $\mathcal{S}^{ss}(0)/b\dot{\alpha}$, where $\dot{\alpha}$ is the steady-state angular velocity preceding cessation of flow.

Many of the devices mentioned in the preceding paragraph can also be used to measure stress growth following the inception of shear at a constant shear rate, as the condition of steady-state shear flow is approached.

C. NORMAL STRESS MEASUREMENTS

Measurements of normal stress differences during steady shear flow, and of normal stress growth approaching steady-state flow and stress relaxation after cessation of flow, provide additional information about nonlinear viscoelastic properties. The conventional identifications of the normal stresses for simple shear have been shown in Fig. 1-16; their orientations in several examples of experimental geometry are sketched in Fig. 5-5.

Although, in studying linear viscoelastic properties, the geometries of Fig. 5-1 or Fig. 5-5 all yield equivalent information, this is not the case for normal stresses, and different configurations give different combinations of σ_{11}, σ_{22}, and σ_{33}. A

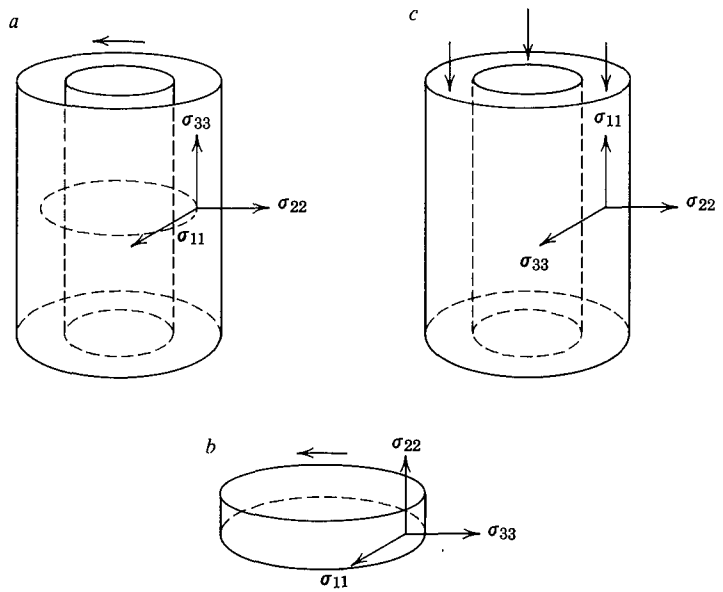


FIG. 5-5. Identification of normal stresses in different experimental geometries. (*a*), rotation between coaxial cylinders; (*b*), torsion between cone and plate or parallel plates; (*c*) annular axial flow between coaxial cylinders.

detailed discussion of the theory of such measurements and derivation of the equations which follow have been given by Lodge[33] and Walters.[17]

1. Measurements of Total Thrust

For cone and plate geometry, the primary normal stress difference $\sigma_{11} - \sigma_{22}$ can be obtained from the vertical thrust force F tending to separate the two surfaces, and this can be measured by a force transducer as in the Weissenberg rheogoniometer;[17,32] the relation is

$$\sigma_{11} - \sigma_{22} = 2F/\pi R^2 \tag{14}$$

The derivation of this equation assumes that the free surface at the rim of cone and plate has a shape corresponding to part of a sphere of radius R, but experiments with intentionally different surface shapes indicate that for small cone angles the results are insensitive to this feature.[34]

For parallel plate geometry, the vertical thrust depends on both primary and secondary normal stress differences. A device for providing this measurement at very high shear rates has been described by Walters.[35]

2. Measurements of Pressure Gradients

Another source of normal stress information is the measurement of pressure differences at various radial locations in cone and plate or parallel plate geometry, or between the inner and outer cylinders in coaxial cylinder geometry. The pressures are sometimes measured by tapping small holes in the appropriate surfaces to which vertical tubes are attached, and noting the heights to which the viscoelastic liquid (or another liquid with which it is in contact) rises in the steady state, or by pressure transducers either in cavities below the surface or flush-mounted in the surface. Since the pressures at surface and in a cavity are not the same during flow of a viscoelastic liquid,[36,37] the difference being due to distortion of the streamlines and termed the hole pressure error, cavities can be used only in configurations where the hole pressure error cancels out in the calculations. (However, hole pressure differences can be used to determine normal stress differences, as described in Section 3 below.)

For cone and plate geometry, $\partial P/\partial r$, the gradient of pressure with respect to radius, is related to the normal stress differences as follows:

$$-r\partial P/\partial r = \sigma_{11} + \sigma_{22} - 2\sigma_{33} \tag{15}$$

The form of this equation implies that P is a linear function of $\ln r$, as is found experimentally. Apparatus for this purpose has been described by several authors.[38–41] By combining equations 14 and 15, the secondary normal stress difference, $\sigma_{22} - \sigma_{33}$, can be obtained.

For parallel plate geometry, the radial gradient of pressure (measured at the surface) is related to normal stress differences as follows:

$$-r\partial P/\partial r = \sigma_{11} - \sigma_{33} + r\partial(\sigma_{22} - \sigma_{33})/\partial r \tag{16}$$

A combination of these geometries is provided by the plate and truncated cone apparatus of Lodge,[42,43] which provides the radial gradient of pressure in the outer cone region as well as the pressure at the center of the truncated (parallel plate) area. From these measurements, both primary and secondary normal stress differences can be obtained in principle; preliminary work suggests, however, that the accuracy obtainable for $\sigma_{22} - \sigma_{33}$ is unacceptably low.

For rotating coaxial cylinder geometry, the radial gradient in pressure across the gap between the cylinders, measured at a point well removed from either end, would in the absence of hole effects be related to the primary normal stress difference:

$$-r\partial P/\partial r = \sigma_{11} - \sigma_{22} \tag{17}$$

Apparatus for measuring the pressure difference between the walls of the two cylinders has been described by Markovitz[44] and Lodge.[45]

Still another method for obtaining information about the second normal stress difference involves measuring the pressure difference between the walls of two coaxial cylinders between which annular flow is occurring.[46,47] The reduction of the data is complicated, however. Also, flow through a tube can be employed.[33]

3. Measurements Involving Hole Pressures

The difference between the pressure measured flush with the surface (P_1) and at the bottom of a hole (P_2) during steady-state flow through a channel (slit-die apparatus) can also provide information on normal stress differences, as shown by Lodge and associates.[48–50] The relations have been derived by Higashitani and Pritchard[51] subject to certain assumptions concerning the nature of the viscoelastic liquid and the flow pattern; they can be expressed in terms of $P_1 - P_2$ as a function of σ_{12} for steady-state flows with different shear rates. If the hole is a slot perpendicular to the flow direction,

$$\sigma_{11} - \sigma_{22} = 2\sigma_{12}d(P_1 - P_2)/d\sigma_{12} \tag{18}$$

where σ_{12} is the shear stress at the surface (channel wall), unperturbed by the hole. Thus the primary normal stress difference can be obtained from measurements at various shear rates to determine $P_1 - P_2$ as a function of σ_{12}. If the hole is a slot parallel to the flow direction, the theory provides the secondary normal stress difference, and if the hole is circular the difference $\sigma_{11} - \sigma_{33}$ can be obtained.

D. DYNAMIC (OSCILLATORY) MEASUREMENTS WITHOUT SAMPLE INERTIA EFFECTS ("GAP LOADING")

The remaining sections of this chapter treat dynamic or oscillatory measurements of viscoelastic properties. Here, in simple shear, the experimental determination is usually a complex ratio of force to displacement (or torque to angular displacement) measured at a surface in contact with the sample; or else a force measured

at one surface and a displacement at another with a gap between, in which the sample is contained. As pointed out at the beginning of this chapter, conversion of the experimental measurement to the desired complex ratio $\sigma_{21}^*/\gamma_{21}^*$ depends critically on whether the inertia of the sample must be taken into account in its periodic motions. The inertial forces will be small if the density ρ is small compared with $G'/h^2\nu^2$ or $G''/h^2\nu^2$, where h is the thickness of the sample as in equations 2 and 11 or $R_2 - R_1$ in equations 5 and 7, depending on the geometry (*i.e.*, the direction of axis x_2 in Figs. 5–1 and 5–5), and ν is the oscillatory frequency in Hz. The first criterion is equivalent to saying that the sample thickness is small compared with the wavelength of a shear wave propagated through the medium; the second, to saying that the shear disturbance experiences negligible attenuation within the gap. The states of stress and strain are then uniform, or vary monotonically, across the gap in the x_2 direction, and they experience no periodic spatial variation. The driving surface feels a "gap loading" which is a decreasing function of the gap thickness.

If, on the other hand, the sample thickness in the x_2 direction is large compared with the wavelength of a shear wave, waves are propagated in the medium, and they decay in amplitude as they progress from the driving surface to the opposite side. In viscoelastic liquids, the gap can usually be made sufficiently large so that the amplitude becomes negligible before the opposite side is reached and no reflection occurs; in fact, in some cases the amplitude vanishes within an extremely short distance of the driving surface. Then the viscoelastic properties can be calculated from force/displacement ratios at the surface (characteristic impedance methods of Section E). The driving surface feels a "surface loading" which is oblivious of the existence of the other side of the gap. Alternatively, if the damping is not too severe, the propagation of the wave itself can be examined to determine the viscoelastic properties (Section F).

The criteria for gap loading and surface loading conditions and the magnitude of errors introduced for finite ratios of gap thickness to shear wavelength have been critically examined by Schrag.[52]

In principle there is an intermediate case where the gap corresponds to one or several wavelengths and standing waves can be set up. This feature is rarely exploited in viscoelastic liquids because of their high damping characteristics.

This section deals with methods in the first category, where the gap in the x_2 direction is small compared with the shear wavelength, and the driving surface feels a "gap loading." Ordinarily, inertial effects are neglected entirely, but correction terms for small effects can be introduced from the calculations of Markovitz[53] and Oka[54] for rotating coaxial cylinder geometry and Markovitz[53] for annular pumping, corresponding to diagrams (*c*) and (*b*) of Fig. 5–1.

1. Direct Measurements of Sinusoidally Varying Stress and Strain

The simplest oscillatory experiment is based on driving one surface with a known periodic displacement and measuring the periodic force at the surface on the other side of the gap with a sensing device of negligible motion, such as a ceramic pi-

ezoelectric transducer.[55] The force is proportional to stress and the displacement to strain, so monitoring these sinusoidal functions is equivalent to tracing out the sinusoidal variation of stress and strain with time in Fig. 1–7. The phase angle between force and displacement is the same as that between stress and strain (δ), and the ratios of the maximum magnitudes are given by the same equations 1 to 13 which apply to transient experiments. For parallel plates in simple shear, for example, combination of equation 1 of this chapter with equations 21 and 22 of Chapter 1 gives for the components of the complex shear modulus:

$$G' = (f_0/bx_{01}) \cos \delta \tag{19}$$

$$G'' = (f_0/bx_{01}) \sin \delta \tag{20}$$

where f_0 and x_{01} are maximum (peak) values of force and displacement, and b is specified by equation 2. The apparatus of Miles[55,56] shown in Fig. 5–6 has this conceptual simplicity; f_0 and x_{01} are read as voltage outputs of transducers with appropriate calibration, and δ is measured on a dual beam oscilloscope. The liquid must be held in the gap by capillary action. A range of frequencies from 20 to 1000 Hz can be covered. This device is not adapted to highly precise measurements, however.

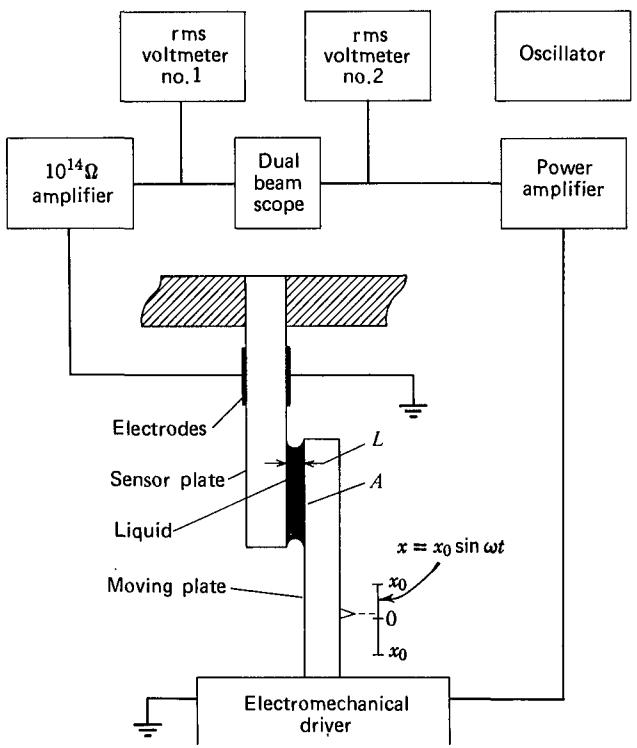


FIG. 5–6. Schematic diagram of simple shear vibrator of Miles.[55] The displacement is specified at the moving plate and the force is measured at the sensor plate.

With a similar principle, the apparatus of Chompff[4] uses Segel-Pochettino geometry (*f* of Fig. 5-1) with a thin foil to contain the viscoelastic liquid between the cylinders. The displacement of the inner cylinder is measured by a differential transformer and the force on the outer cylinder by a ferroelectric ceramic transducer. The frequency range is from 1 to 2500 Hz, and good temperature control is provided over an extremely wide range. The moduli G' and G'' are obtained as in equations 19 and 20, with the form factor b specified by equation 13. A related apparatus with continuous recording at constant frequency has been described by Date.[57]

The Weissenberg rheogoniometer[17,32,33] and the Rheometrics Mechanical Spectrometer[22,22a] can be used for oscillatory measurements in this manner with either parallel plate or cone and plate geometry. A sinusoidally varying angular displacement is imposed on one surface by a mechanical drive and the resulting torque on the other surface is measured with a transducer. Analyses of the performance of the Weissenberg instrument have been made by Nally,[58] Bogie and Harris,[59] and Walters[17]; and an improved method[60] for measuring the phase angle has been discussed by Prest and O'Reilly.[61] From maximum values of torque and angular displacement, G' and G'' can be calculated with equations analogous to 19 and 20 and the appropriate form factors from equation 9 or 11. The Rheometrics Spectrometer can be automated with computerized data acquisition and processing.[22]

To remain within the linear range of viscoelastic behavior, the periodic displacements must be kept small; linearity can always be tested by varying the amplitude. The Rheometrics Spectrometer can also be operated at large amplitudes.

The sample must be sufficiently compliant so the displacement due to its deformation is large compared with that of the force-sensing element, which cannot be zero, or of other parts of the apparatus structure.[32] This requirement may set the high-frequency limit of operation.

Oscillating normal stresses[17,22,62] can be measured in a similar manner, usually with cone and plate geometry.[63]

2. Measurements Involving the Mechanical Impedance of a Moving Element

If the force-sensing element has perceptible motion, or if the force and displacement are measured at the same surface, motion of a part of the apparatus must be specifically taken into account. In the latter case, it is convenient to discuss the mechanical impedance Z^*_M, or complex ratio of force to velocity, of the moving element; this includes contributions from the surface in contact with the sample, but also the inertia, elastance, and frictance of the moving element itself. The principles may be illustrated by a schematic diagram of the Birnboim apparatus[64] as modified by Massa and Schrag,[65] in Fig. 5-7. (It will be described in more detail below.) It employs either annular pumping or Segel-Pochettino geometry. The force and motion are both measured on the moving element. To the approximation that inertial effects in the sample can be neglected, the following quantities control the

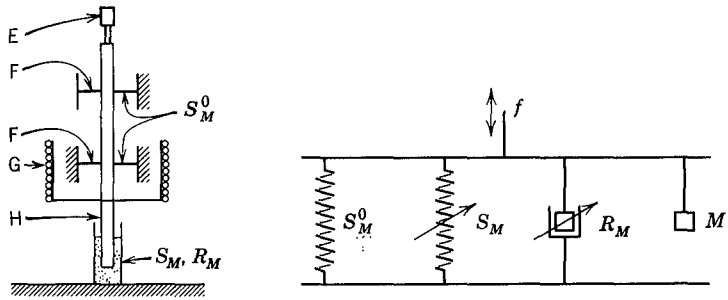


FIG. 5-7. Schematic diagram of moving element in the Birnboim apparatus,[64] with equivalent mechanical model. Letters at left identify components of the moving element as defined in the legend of Fig. 5-8. Symbols at right correspond to the components of the equivalent mechanical model.

dynamic response: M, the mass of the moving element (here about 20 g); S_M^0, the elastance or force per unit displacement in the axial direction of the springs which support and center the moving unit; S_M, the elastance of the sample, or force per unit displacement in phase with displacement; and R_M, the frictance of the sample or force per unit velocity in phase with velocity. Any frictance contributed by the mounting (or air resistance) is neglected here, though it can easily be added as a further correction. The quantities S_M and R_M depend on frequency as symbolized by the slanting arrows and they are related to the viscoelastic properties sought (provided sample inertia plays no role) by the simple relations $G' = S_M/b$ and $G'' = \omega R_M/b$, where b is the form factor of equation 4 or 13. The response can be simulated by the mechanical model in Fig. 5-7, in which the springs and dashpot differ from those of Figs. 1-9 and 1-10 because they represent elastances and a frictance, respectively, rather than moduli and viscosities. The application of such models to calculations of the dynamic response of apparatus follows rules which have been clearly formulated by Tschoegl.[66]

Analysis of the equation of motion for driving with a sinusoidal force gives a simple expression for the mechanical impedance of the moving element:

$$Z_M^* \equiv f^*/v \equiv R_M + iX_M = R_M + i(\omega M - S_M/\omega - S_M^0/\omega) \tag{21}$$

whence

$$G' = (-\omega X_M + \omega^2 M - S_M^0)/b \tag{22}$$

$$G'' = \omega R_M/b \tag{23}$$

Here ω is the radian frequency $2\pi\nu$, f^* is the complex force with a real component in phase with the velocity v and an imaginary component 90° out of phase, these components being measurable separately in an experiment, and R_M and X_M are defined as the mechanical resistance and mechanical reactance by analogy with the treatment of electrical circuits with alternating current. (The equations actually used with the Birnboim apparatus are more complicated because they include an approximate correction for sample inertia.[53])

Certain important restrictions are inherent in equations 21 and 22. Obviously

S_M^0 should be small compared with S_M to avoid loss of precision with subtraction; since G' and S_M decrease with decreasing frequency, this may set a low-frequency limit. At high frequencies, the term $\omega^2 M$ in equation 22 becomes large and subtraction from ωX_M may leave no precision; in this case the measurement senses only the inertia of the moving element of the apparatus. At the system resonance frequency $\omega_0 = [(S_M^0 + S_M)/M]^{1/2}$, X_M becomes zero and the system may be too sensitive to permit measurements (though in some other methods this feature is exploited; in particular, force and velocity are in phase at this point and only R_M and G'' determine the response). When the phase angle θ between force and displacement (whose magnitude is $\pi/2$ minus the phase angle between force and velocity, and equal to $\tan^{-1} R_M/X_M$) is near zero, G' can be measured but there is little precision for G''. (A similar phase angle restriction applies to the direct measurements described in the preceding section, but there the relevant phase angle is δ in equations 19 and 20, which is simply $\tan^{-1} G''/G'$; in the methods with apparatus inertia, the angle θ has no simple relation to δ, though it becomes equal to δ when S_M^0 and M can be neglected.)

As with the methods of the preceding section, the basic measurements are the ratio of peak values of force, f_0, and displacement, x_0 (or velocity, v_0) and the phase angle θ between them. Then Z_M^* is calculated as

$$Z_M^* = (f_0/v_0)(\sin\theta - i\cos\theta) = (f_0/\omega x_0)(\sin\theta - i\cos\theta) \qquad (24)$$

and G' and G'' can be obtained from equations 21 to 23. The phase angle θ can in principle be measured on an oscilloscope (with ellipse geometry, for example); or more accurately, with a suitably designed phase meter.[60,64] However, the most accurate measurements are obtained with a computerized data acquisition and processing system which performs cross-correlation calculations,[65] especially when improved by signal averaging.[65a]

As an example of this kind of device, a more complete diagram of the Birnboim apparatus[64,65] is shown in Fig. 5-8. The sample volume is only about 1 cm^3. The force is measured by the magnitude of the alternating current passing through the driving coil, which is in the field of a permanent magnet; the displacement is measured by a coaxial capacitor which changes the frequency of a 4.5 MHz oscillator. A modified FM discriminator detects these changes and can sense extremely small excursions, of the order of 10 Å. The data acquisition system performs a large number of force and displacement measurements to construct their sinusoidal time dependences, and the computer combines signal averaging and cross-correlation calculations[67] to determine f_0, x_0, and θ with elimination of noise and harmonics. The frequency range is from 0.01 to about 500 Hz and the frequencies can be spaced as closely as desired. The temperature can be accurately controlled over a very wide range because the entire apparatus can be submerged in a thermostat.

A sinusoidally driven vibrator described by Philippoff[68,69] also belongs in this category, although under most circumstances its inertia and elastance can be neglected. It employs annular pumping geometry for liquid samples, and other geometries for different kinds of viscoelastic materials which will be mentioned

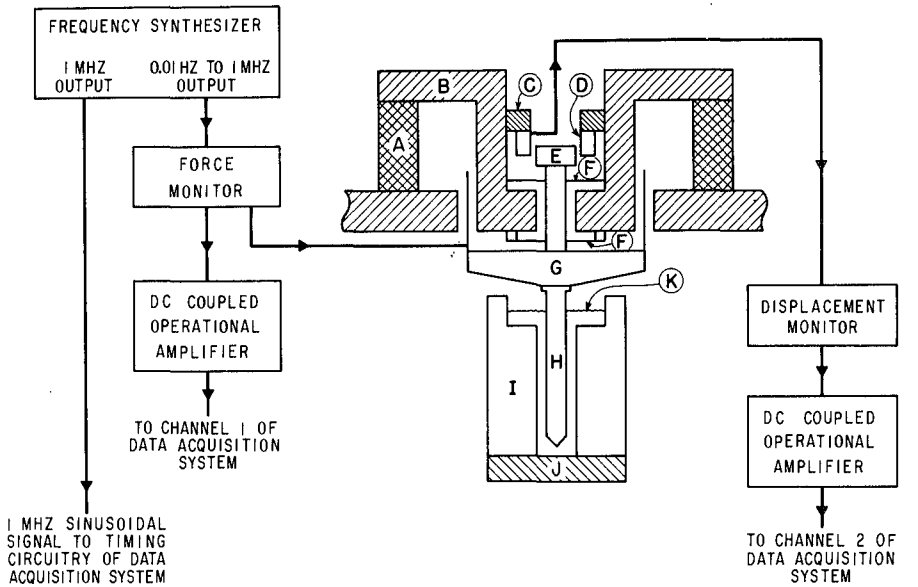


FIG. 5-8. Simplified diagram of the modified Birnboim transducer and the associated electronics. (A) Permanent magnet; (B) soft iron pole pieces; (C) Delrin insulator; (D) fixed element of displacement monitoring capacitor; (E) moving element of capacitor; (F) suspension springs; (G) drive-coil assembly; (H) driving rod; (I) sample cell; (J) glass cell bottom; (K) fluid level. (Massa and Schrag.[65]) Reproduced, by permission, from the *Journal of Polymer Science.*

in Chapters 6 and 7. The force and displacement are measured by strain gauge transducers whose outputs can trace an ellipse on an oscilloscope. The frequency range is from 3×10^{-5} to 10 Hz, the apparatus being especially suitable for extremely low frequencies, and large forces and displacements can be used if desired.

In rotational instruments, also, dynamic torques and angular displacements can be measured simultaneously on the same surface in contact with the sample, as in the coaxial cylinder instruments of Morrison, Zapas, and DeWitt[70] and Kambe and Takano,[71] and the cone and plate instrument of the latter authors.[72] The equation of motion must be reformulated with torsional stiffness constants substituted for elastances and moment of inertia substituted for mass.[70] The torque is applied electromagnetically to the inner cylinder (or to the cone) and the displacement is measured by deflection of a light beam[70,73] or an electromagnetic pickup.[71,72]

A somewhat less direct method in which there is no specific determination of force involves coaxial cylinder geometry in which the outer cylinder is oscillated through a small angle. The inner cylinder, suspended from a torsion wire of suitable stiffness, responds with an angular oscillation whose amplitude and phase depend on the viscoelastic properties of the material in the gap as well as the moment of inertia of the inner cylinder and the stiffness of its support. From the ratio of amplitudes and the phase difference between the two motions, which are usually de-

termined by reflection of light beams or electromagnetic pickups, the viscoelastic properties can be calculated by some rather complicated equations. Apparatus of this type has been described by Markovitz, De Witt, and collaborators,[74] Horio and Onogi,[19,75] Duiser,[76] den Otter,[77] and Harrison.[78] The frequency range is generally in the region from 0.1 to 100 Hz.

With a suitable mechanical drive, small angular oscillating deformations can be imposed on steady rotation at various shear rates, using either coaxial cylinder[78a] or cone and plate[79] geometry, and the dynamic mechanical properties can be measured under conditions of non-Newtonian flow. By use of annular pumping geometry with steady rotation of the outer cylinder, the viscoelastic properties under conditions of non-Newtonian flow perpendicular to the oscillatory motion can be measured.[80]

3. Transducer Measurements by Electrical Impedance

The methods of Sections 1 and 2 above require measurements of the magnitudes of force and displacement (or torque and angular displacement), often by electromechanical transducers; if the deformations are in the linear range of viscoelastic behavior, these quantities are very small and require sensitive detectors for adequate precision. An alternative application of electromechanical transducers involves measurement of voltage/current ratios (*i.e.*, electrical impedance) from which force/velocity ratios (*i.e.*, mechanical impedance) are calculated, without any need to know the magnitude of either as long as the experiment is conducted in the linear regime. The electrical measurements, made ordinarily by adjusting resistances and capacities to balance an impedance bridge, are capable of high precision. This principle may be illustrated by an earlier alternative mode of operation of the Birnboim apparatus[64] illustrated in Figs. 5-7 and 5-8, the "impedance measurement mode."

The electrical impedance $Z^* = R + iX$ of the driving coil is measured while in motion subjecting the sample to periodic deformations, and again when the coil is firmly clamped to prevent motion ($Z_0^* = R_0 + iX_0$). Here the R's are the resistances and the X's the reactances. From these four quantities, the components of the mechanical impedance Z_M^* as defined in the preceding section are calculated as follows.[81,82] The force exerted on the moving mechanical system is $f^* = Bli^*$, where B is the flux density of the magnetic field, l is the length of wire in the coil, and i^* is the driving current. The system will respond with a velocity $v = f^*/Z_M^*$, in accordance with equation 21. The motion of the coil will generate a back emf given by $e = Blv$. The applied total emf is $Z_0^* i^* + e = Z^* i^*$. Thus[81]

$$(Z^* - Z_0^*)i^* = Blv = (Bl)^2 i^*/Z_M^* \tag{25}$$

Separation of the complex quantities into real and imaginary parts yields

$$R_M = \frac{(Bl)^2(R - R_0)}{(R - R_0)^2 + (X - X_0)^2} \tag{26}$$

$$X_M = \frac{-(Bl)^2(X - X_0)}{(R - R_0)^2 + (X - X_0)^2} \tag{27}$$

Thus, once the apparatus is calibrated, only electrical measurements are necessary. The key to the calibration is M, the mass of the moving unit—the coil and inner cylinder. The constant $(Bl)^2$ can be determined from the frequency dependence of $(X - X_0)/[(R - R_0)^2 + (X - X_0)^2]$ with no sample present; in this case $S_M = 0$ in equation 20 and the above quantity times ω plotted against ω^2 gives a straight line whose slope is $M/(Bl)^2$ and intercept $S_M^0/(Bl)^2$. Alternatively, at high frequencies where the term S_M^0/ω can be neglected in equation 21, $(Bl)^2 = -\omega M[(R - R_0)^2 + (X - X_0)^2]/(X - X_0)$. The spring constant S_M^0 can also be measured from a transient response with the cell filled by a Newtonian liquid of known viscosity. The impedance components at rest, R_0 and X_0, are determined for every measurement immediately before R and X since the differences are sometimes small and the temperature, frequency, and thermal history must correspond exactly. Finally G' and G'' are calculated from X_M and R_M by equations 22 and 23. The capacitative displacement sensor in Figs. 5–7 and 5–8 is not used in this mode of measurement.

This transducer impedance method has been utilized up to frequencies of several hundred hertz. For a given mass and sample consistency, there is a system resonance frequency at which $X_M = 0$ because of cancellation of terms in equation 21; near this, the impedance bridge balance is sensitive and difficult. On the other hand, at frequencies too far from the resonance on either side, the differences in R and X become too small to measure accurately. Although the magnitude of the driving current is not needed for calculations, it is usually measured to provide a gauge of the peak force applied. Variation of the driving current provides a sensitive test of whether the viscoelastic behavior is truly linear; if the impedance bridge is balanced at one current level, it should remain balanced when the current is increased say 10-fold. In making impedance measurements, this test is used routinely.

A warning should be added that because of the small amplitudes of motion in the sample there is a risk of falsification by small vibrations or lack of complete rigidity in the apparatus itself. Careful design and tests with materials of known properties can eliminate this danger.

An early version of this method with annular pumping geometry was described by Smith, Ferry, and Schremp.[82] A similar principle with oscillating rotation between coaxial cylinders has been utilized by Lamb and Lindon[83] in a carefully designed apparatus. Here there are separate driving and pickup coils and the transfer impedance (ratio of voltage in one to current in the other) is measured by a null device; the change in electrical impedance with depth of liquid in the gap between cylinders is used to eliminate the need for clamped impedance measurements as well as end effects. The frequency range is from 20 to 1500 Hz. The gap between cylinders is not necessarily small compared with the wavelength of shear waves, and complicated calculations are used to obtain G' and G'' under circumstances where standing waves are propagated in the gap.

E. DYNAMIC (OSCILLATORY) MEASUREMENTS OF CHARACTERISTIC IMPEDANCE ("SURFACE LOADING")

If the gap in the x_2 direction (Fig. 5-1) is so large that shear waves are propagated from the driving surface and die off before they reach the opposite surface, the driving surface is oblivious of the latter and feels only "surface loading." In curved geometries the radius of curvature is usually large compared with the wavelength and the only dimension that matters is the area of the driving surface. In experiments, the quantities measured are the components of the complex characteristic impedance, or impedance per unit area of driving surface, $\mathcal{R}_M + i\mathcal{X}_M$, due to contact with the sample. Whereas in gap loading R_M is related only to G'' and X_M only to G', in surface loading both G' and G'' depend on both impedance components, as follows:[84]

$$\mathcal{R}_M = (\rho/2)^{1/2}(\sqrt{G'^2 + G''^2} + G')^{1/2} \tag{28}$$

$$\mathcal{X}_M = (\rho/2)^{1/2}(\sqrt{G'^2 + G''^2} - G')^{1/2} \tag{29}$$

and so G', G'', and η' can be obtained by rearrangement in the form

$$G' = (\mathcal{R}_M^2 - \mathcal{X}_M^2)/\rho \tag{30}$$

$$G'' = 2\mathcal{R}_M\mathcal{X}_M/\rho \tag{31}$$

$$\eta' = 2\mathcal{R}_M\mathcal{X}_M/\omega\rho \tag{32}$$

The density ρ enters because the inertia of the sample plays an essential role in the wave propagation. For a purely viscous liquid, $\mathcal{R}_M = \mathcal{X}_M$ and $\eta_0 = 2\mathcal{R}_M^2/\omega\rho$. The total mechanical impedance $R_M + iX_M$ is $(\mathcal{R}_M + i\mathcal{X}_M)$ times the area of contact A *plus* the contributions from whatever inertia, elastance, and frictance must be attributed to the apparatus itself.

Most characteristic impedance devices are operated near a system resonance to achieve high sensitivity. This feature has the disadvantage that measurements can be made only at a single frequency, or a few discrete frequencies, instead of the continuously variable frequency range provided by the methods of the preceding sections. However, only such devices have provided measurements on viscoelastic liquids with very low viscosity and rigidity.

A very sensitive device operating at about 100 Hz has been described by Konno, Makino, and Kaneko,[85] shown in Fig. 5-9. A very thin microscope slide immersed in the viscoelastic liquid to be measured is oscillated by a coil moving in a magnetic field. The resonance frequency is determined with and without sample present; the resonance frequencies, ω_0 and ω_0^0 respectively, are identified by an oscilloscope pattern and measured to many significant figures by a frequency counter. From relations analogous to equation 21, setting $X_M = 0$ for the two cases, we obtain $\omega_0^2 - (\omega_0^0)^2 = -\mathcal{X}_M A\omega_0/M$, and since the difference $\Delta\omega_0$ between ω_0 and ω_0^0 is very small, this reduces approximately to

$$\mathcal{X}_M = -2\Delta\omega_0 M/A \tag{33}$$

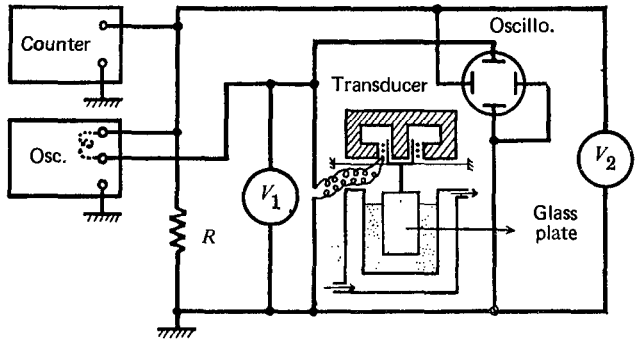


FIG. 5-9. Schematic diagram of apparatus of Konno, Makino, and Kaneko[85] for characteristic impedance measurements on solutions of very low viscosity and rigidity. R is a known resistance, V_1 and V_2 are vacuum tube voltmeters.

The characteristic resistance $\mathcal{R}_M$ is obtained from equation 26, noting that when the apparatus is driven at resonance $X = X_0$ so

$$\mathcal{R}_M = (Bl)^2/(R - R_0)A - R_M^0 \tag{34}$$

where R_M^0 is a frictional correction for the apparatus itself, which was not needed in previous applications of the impedance method. Measurements of the electrical resistance of the driving coil when in motion and when clamped, therefore, suffice to determine $\mathcal{R}_M$. Finally, G' and G'' are calculated from equations 30 and 31. Measurements can be made on liquids with viscosities as low as 1 centipoise and rigidities (at 100 Hz) as low as 1 dyne/cm^2.

For somewhat higher frequencies, in the range from 200 to 2500 Hz, a hollow torsion pendulum designed by Sittel, Rouse, and Bailey[86] has been used. The viscoelastic liquid fills the sample holder and is subjected to periodic motion near the inside surface when the holder is excited in free torsional oscillations with a very small amplitude. The wavelength is so small that the geometry is negligibly different from that of plane surfaces. The characteristic reactance $\mathcal{X}_M$ is determined from the precise value of the characteristic frequency for free oscillations, analogous to the resonance frequency in the preceding paragraph; it is necessary to use a different torsion rod for each frequency desired. The characteristic resistance $\mathcal{R}_M$ is determined from the logarithmic decrement in amplitude of free oscillations, the principles of which will be discussed in Chapter 6. The necessary apparatus constants are obtained by calibration with liquids of known viscosity.

In the multiple-lumped resonator proposed by Birnboim[87] and developed by Schrag,[88,89] the viscoelastic liquid is in contact with the outside rather than the inside of a torsionally oscillating element. This is a stack of five cylinders machined from a single piece of low-loss aluminum[88] or titanium[90] alloy and connected by torsion rods of different thicknesses (Fig. 5-10). It oscillates in five different modes so resonance measurements can be made at five frequencies without changes in the apparatus. One change of resonators can provide five additional frequencies. The resonator is driven by a magnet in an oscillating magnet field whose frequency

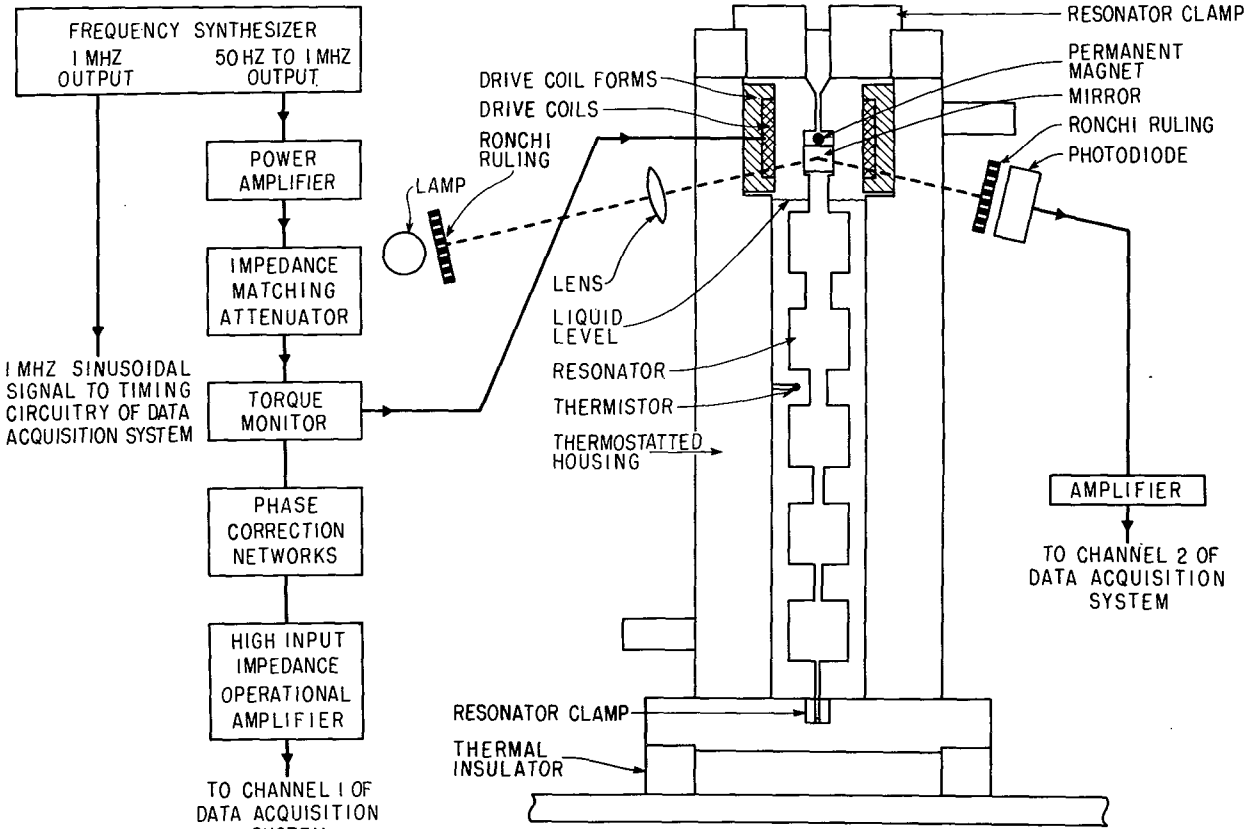


FIG. 5-10. Simplified diagram (to scale) of multiple-lumped resonator apparatus and auxiliary electronics. (Schrag and Ferry.[89]) Reproduced, by permission from the American Institute of Physics, from *The Review of Scientific Instruments*, **42**, 224 (1971).

can be varied and specified with high precision. The torque and angular displacement are measured by the current in the driving coil and the reflection of a light beam through a Ronchi grating, respectively. In the vicinity of each resonance, the phase angle between torque and angular displacement is determined with high accuracy by computerized measurements with signal averaging and cross-correlation calculations as described for the modified Birnboim apparatus above.[65,65a] From the frequencies corresponding to phase angles of 45°, 90°, and 135°, together with calibration data which depend on the moments of inertia of the cylinders and the torsional stiffnesses of the connectors, the mechanical resistance and reactance can be calculated, as explained in the discussion of resonance devices in Chapter 6. Conversion to $\mathcal{R}_M$ and $\mathcal{X}_M$ and subsequently to G' and G'' involves additional calibration data which depend on the dimensions of the cylinders and are obtained in practice from measurements in Newtonian liquids and in air. The frequency range is about 100 to 8000 Hz and measurements can be made on viscoelastic liquids in the viscosity range from 0.005 to 0.5 poise. Very small values of G', of the order of 1 dyne/cm^2, can be measured.

For higher frequencies, of the order of 20 to 100 kHz, the cylindrical torsionally oscillating quartz crystals introduced by Mason[84] have been widely used and further developed.[91–97] The crystal is immersed in the viscoelastic liquid to be measured and driven piezoelectrically by appropriately positioned electrodes. The geometry of the disturbance at the surface can usually again be approximated by plane waves, though the cylindrical features can be taken into account by more complicated calculations.[98] The resonant frequency and electrical resistance of the crystal at resonance are measured first in a vacuum and then while immersed in the liquid, and $\mathcal{R}_M$ and $\mathcal{X}_M$ are calculated from the differences.[84,98] Then G' and G'' are obtained in turn from equations 30 and 31. A separate crystal is usually employed for each frequency desired, though higher frequency harmonics have also been utilized. Application of a phase-sensitive detector[99] for the resistance measurement has been introduced by Tanaka and Sakanishi.[94] This method is excellent for very dilute polymer solutions.

More versatility is obtained by immersing a long thin rod, usually of quartz, in the liquid and exciting torsional oscillations by a piezoelectric crystal attached to the top.[93,96,100] In the torsional traveling wave method,[96] $\mathcal{R}_M$ and $\mathcal{X}_M$ are obtained from measurements of phase shift and attenuation of reflected torsional pulses as they return from the bottom of the rod to the crystal driver. The frequency range is from about 16 to 500 kHz. In the torsional free-decay method,[100] the change in resonant frequency and decay rate of a torsional pulse are measured. The frequency range is from about 2 to 20 kHz.

An alternative crystal geometry is the quartz piezoelectric tuning fork of Mason,[98] whose wide, thin arms oscillate in their own planes and set up primarily plane shear waves in the liquid surrounding them. The components $\mathcal{R}_M$ and $\mathcal{X}_M$ are again obtained from measurements of the change in resonant frequency and electrical resistance produced by the presence of the liquid. The frequency range is from 0.5 to 10 kHz. Pulsed waves in a metal plate immersed in the liquid can be followed to determine viscoelastic properties in the range from 1 to 7 MHz.[101]

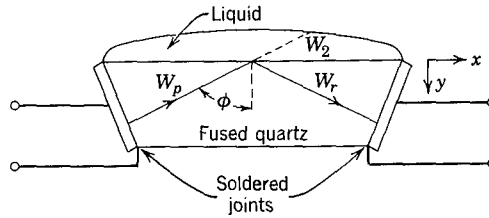


FIG. 5–11. Apparatus of Mason and McSkimin[106] for characteristic impedance measurements at extremely high frequencies by reflection of a shear wave at a fused quartz interface.

There are some other characteristic impedance methods in the medium frequency range which measure only the resistive component $\mathcal{R}_M$. That of Zimm[102] employs longitudinal vibrations of the walls of a glass container, which set up shear waves in the liquid. The driver is electromagnetic and the amplitude detector is piezoelectric; $\mathcal{R}_M$ is obtained from the decay in amplitude after the driver is shut off. There is a rather wide choice of frequencies by utilizing various overtones. The Nametre oscillating sphere viscometer[103,104] employs a sphere immersed in the liquid and driven in small torsional oscillations at a fixed frequency; the power consumption required to maintain a given amplitude of oscillation is proportional to $\mathcal{R}_M$. (It is possible to determine $\mathcal{X}_M$ also from a shift in resonance frequency.) The Ultraviscoson viscometer[105] employs a magnetostrictive rod immersed in the liquid, whose longitudinal vibrations again excite shear waves, at a fixed frequency. The basic viscoelastic functions cannot of course be obtained from measurements of $\mathcal{R}_M$ alone; in terms of dynamic viscosity, $\mathcal{R}_M = (\omega\rho/2)^{1/2}(|\eta^*| + \eta'')^{1/2}$. Only a "nominal" frequency-dependent viscosity $\eta_n = |\eta^*| + \eta''$ can thus be calculated. Nevertheless, experimental determinations of $\mathcal{R}_M$ or η_n can be used for comparisons with theory, for example, by expressing the latter in the form of the right side of equation 28.[102,104]

For still higher frequencies, in the megacycle range, shear waves are propagated through a block of quartz and the reflection coefficient at an interface between the quartz and the viscoelastic liquid is measured. An example is the method illustrated in Fig. 5–11 in which a shear wave generated by a piezoelectric crystal transmitter passes through fused quartz, is reflected from the horizontal interface with the liquid at a suitable angle, and is detected by a second piezoelectric crystal. A very thin film of liquid suffices. From the differences in amplitude and phase between the incident and reflected waves, the components $\mathcal{R}_M$ and $\mathcal{X}_M$ of the characteristic impedance at the liquid surface can be calculated. The frequency range is from 3 to 100 MHz, and the range of liquid consistencies which can be measured is very broad. The method has been used extensively to follow changes in viscoelastic properties during polymerization or cross-linking in a thin film.[108] In a modification introduced by Lamb and collaborators, the second transducer can be omitted. By utilizing reflection at the surface of a suitably cut quartz crystal with normal incidence,[109,110] measurements can be made at considerably higher frequencies, from 40 to 1500 MHz. A method based on a quartz disc in a resonant cavity has been designed by Lamb and Seguin[111] for measurements at 3000 MHz. Some of these

ultrasonic methods have been reviewed in detail by Lamb and collaborators[93] and by McSkimin.[112]

A somewhat indirect method for measuring characteristic impedance at low frequencies is used in the acoustic streaming device of Thurston,[113] in which the liquid is pumped back and forth through parallel capillaries. It is appropriate for liquids of very low viscosity in a continuous frequency range from 10 to 300 Hz.

F. SHEAR WAVE PROPAGATION

In the methods of the preceding section, the propagation of a shear wave into the viscoelastic liquid is not observed directly; only its effect on the propagating surface is detected and measured. On the other hand, if the damping is not too severe, so that a wave train of several maxima and minima is perceptible, the wavelength and attenuation can be measured directly, as described in this section. The sample must be sufficiently large so that the waves are attenuated before they can experience reflection.

For a shear wave traveling under conditions where it approximates a one-dimensional disturbance in the x direction, the damping is exponential and the amplitude (shear displacement, u) can be represented as

$$u = u_0 e^{i(\omega t - 2\pi x/\lambda) - x/x_0} \tag{35}$$

where λ is the wavelength and x_0 is the distance within which the amplitude falls off by a factor $1/e$ (Fig. 5-12). The attenuation α in nepers/cm is $1/x_0$; the velocity v in cm/sec is $\omega\lambda/2\pi = \nu\lambda$. The complex propagation constant used in discussions of acoustics[98] is

$$\Gamma = A - iB = 2\pi/\lambda - i/x_0 = [\rho\omega^2/(G' + i\omega\eta')]^{1/2} \tag{36}$$

where ρ is the density of the medium. The acoustic attenuation in decibels/cm is 8.686α.

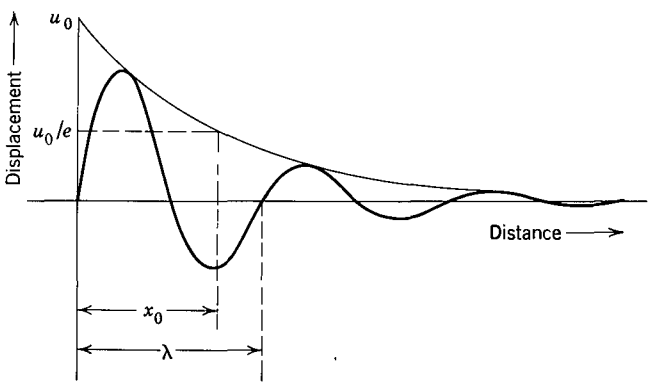


FIG. 5-12. Exponentially damped shear wave with definitions of characteristic parameters (from reference 116).

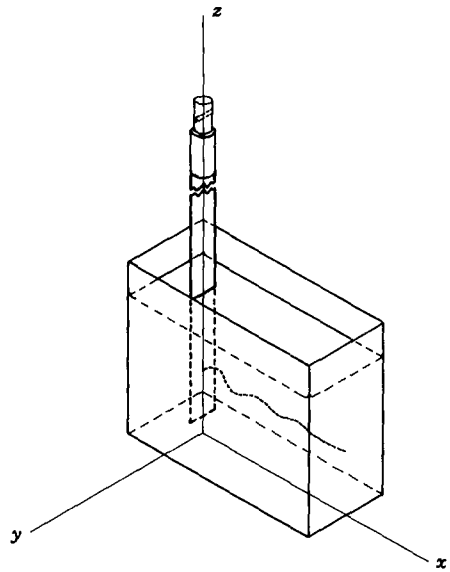


FIG. 5-13. Shear wave propagation in a rectangular vessel (from reference 114).

From measurements of the wavelength and attenuation the components of the complex shear modulus can be calculated by the following equations:[114]

$$G' = \frac{\omega^2\lambda^2\rho[4\pi^2 - (\lambda/x_0)^2]}{[4\pi^2 + (\lambda/x_0)^2]^2} \tag{37}$$

$$\eta' = \frac{4\pi\omega\lambda^2\rho(\lambda/x_0)}{[4\pi^2 + (\lambda/x_0)^2]^2} \tag{38}$$

or in different form,[115]

$$G' = \rho v^2(1 - r^2)/(1 + r^2)^2 \tag{39}$$

$$G'' = 2\rho v^2 r/(1 + r^2)^2 \tag{40}$$

where $r = \lambda/2\pi x_0 = \alpha\lambda/2\pi$. It is clear from equations 37 and 39 that if the damping per wavelength is small, the attenuation enters the calculation of G' only as a minor correction; hence the approximate relation stated previously that $\lambda \cong (G'/\rho)^{1/2}/\nu$, *i.e.*, $v \cong (G'/\rho)^{1/2}$. For convenience, an auxiliary parameter $\tilde{G} = \rho v^2$ (the "wave rigidity modulus") is sometimes calculated and then subsequently converted to G' by the correction factor $(1 - r^2)/(1 + r^2)^2$, for which only a rough estimate of the damping is needed. The frequency dependence of $\tilde{G}$ corresponding to certain mechanical models has been calculated,[116] and has been useful for analyzing measurements in which only the wavelength and not the damping was provided.[117] On the other hand, η' and G'' are directly proportional to the attenuation and require a precise determination of the latter.

Experimentally, a disturbance approximating a plane shear wave can be set up by vibrating a plate in a rectangular vessel[118,119] (Fig. 5-13); and, provided the

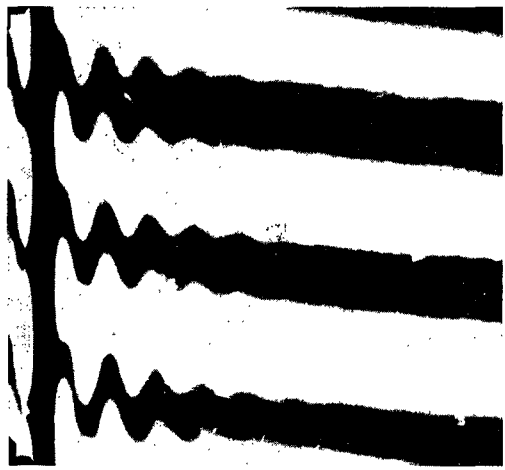


FIG. 5-14. Stroboscope photograph of a wave of shear strain double refraction in a 1% solution of sodium deoxyribonucleate at 25°C, frequency 125 Hz. The driving plate is oscillated vertically; shear waves propagated horizontally to the right produce patterns of strain double refraction. Each boundary between black and white provides the same information; the inclination of the base lines is specified by the angle between the axes of the Babinet compensator and the analyzing Polaroid (from reference 117).

viscoelastic liquid is transparent and becomes birefringent with straining, the wave can be observed and photographed stroboscopically (Fig. 5-14) using a suitable optical system with a Babinet compensator between crossed Polaroid plates; the axis of the compensator is inclined at a small angle to the axis of the analyzing Polaroid, and this feature magnifies the wave pattern seen. [The displacements seen in the optical pattern are not directly proportional to the shear strain, but are proportional to the arctangents of the relative retardation (phase difference) in the components of polarized light passing through the strained medium. The relative retardation is assumed to be proportional in turn to the shear strain.]

The effects of the container walls in the arrangement of Fig. 5-13 have been investigated theoretically.[114] The deviations from the one-dimensional wave assumed in equations 35 to 40 are not serious unless the damping λ/x_0 is rather small, in which case reflections from the walls may cause the observed damping to appear erroneously magnified. This situation is not encountered in polymeric liquids, though it may be in gels. At the other extreme, if λ/x_0 is too large, the wave will be too attenuated to measure even the wavelength; an upper limit would ordinarily be $\lambda/x_0 = 3$. It may be noted from equations 37 and 38 that, when the damping is small, $\lambda/x_0 \cong \pi G''/G'$, so this limit corresponds roughly to a loss tangent of unity.

The shear wave method described here has been used at frequencies from 4 to 5000 Hz. Its most important advantage is that no dimensions of the sample need be known; there is no form factor b such as enters into the calculations of the other

low-frequency methods of Section D, so it is attractive for absolute measurements. On the other hand, it is somewhat inferior in precision.

Both viscoelastic and birefringence data can be obtained from examination of the propagation of shear waves with a very small optical probe beam,[114a] and a wide range of solution viscosities can be investigated.

At much higher frequencies, bulk longitudinal waves can be propagated in polymeric liquids, and these may yield indirectly some information about shear properties. Since their behavior is dominated by the bulk compressional viscoelasticity, however, discussion of them will be postponed to Chapter 8.

G. DYNAMIC MEASUREMENTS ON LIQUIDS IN SOLID MATRICES

Brief mention may be made of some methods in which apparatus designed for viscoelastic solids is applied to study of viscoelastic liquids compounded with solid matrices. Such measurements usually provide the loss tangent only and are not appropriate for absolute measurements of viscoelastic properties, though they can give a semiquantitative view of changes in properties over wide ranges of temperature.

In the method of Illers,[120] the liquid is dispersed as droplets in a block of polymeric solid which experiences very little mechanical loss in the range of frequencies and temperatures to be investigated. Then, in measurements of the type described in Chapter 7, observed losses may be largely ascribed to the liquid phase. Experiments may be carried through the temperature range in which the liquid experiences transition from fluid to glasslike consistency.

In the so-called torsional braid analysis,[121-124] the liquid is absorbed in a long strip of soft braided thread or filter paper which has very slight torsional stiffness, and torsion pendulum measurements are made by the methods of Chapters 6 and 7. Both storage and loss components of the dynamic torsional response may be attributed primarily to the viscoelastic liquid, and examined on a relative basis, although absolute measurements are not possible. Care must be taken that a contribution from the braid does not lead to erroneous conclusions about the properties of the viscoelastic liquid.[125,125a]. A flexural braid method has also been utilized.[126]

H. MEASUREMENT OF DYNAMIC VISCOELASTIC FUNCTIONS BY ECCENTRIC STEADY FLOW INSTRUMENTS

It is possible to subject a viscoelastic liquid to oscillating deformation without applying oscillating stress if certain eccentric geometries are used. In the orthogonal rheometer geometry, the sample is contained between parallel plates which are rotated with the same constant angular velocity but whose axes are slightly displaced with respect to each other; this is an option for the Rheometrics Mechanical Spectrometer[22,127] and the Instron rotary rheometer.[128] Although the instrumental angular velocity is constant, the material experiences sinusoidal deformations which

vary from point to point. The two components of the tangential force on one of the plates are measured, and from them η' and η'' can be calculated corresponding to a radian frequency equal to the angular velocity. In the Képès balance rheometer,[129] the liquid is contained between a sphere and a spherical cup which rotate about axes inclined to each other at a small angle. It is also possible to use coaxial cylinder geometry with eccentric axes.[130] The theory for obtaining η' and η'' from such measurements has been critically discussed by Walters.[17]

I. ISOTHERMAL AND ADIABATIC MEASUREMENTS

The viscoelastic functions as defined refer to isothermal changes of state, and indeed the control of constant temperature is an important feature of all the experimental methods described in this chapter. It is evident, however, that the dynamic measurements described in some of the preceding sections must in fact be adiabatic rather than isothermal, because of failure to reach thermal equilibrium within the period of deformation. This distinction has usually been ignored, and reasonably so since the difference between the adiabatic and isothermal quantities is in most cases negligible. For the sake of completeness, however, some general features of the problem are mentioned here.

1. Difference between Adiabatic and Isothermal Moduli for Perfect Elastic Materials

The magnitude of the difference for viscoelastic materials can be gauged by making the calculation without considering time-dependent effects. Although the experimental methods in this chapter deal solely with shear deformations, it is useful for orientation to refer here first to deformation in bulk compression, for which the result is well known from thermodynamics[131,132] and is applicable to solids, liquids, and gases alike:

$$K_{ad} = K_{is}(1 + \alpha^2 T K_{is}/\rho C_v) \tag{41}$$

where K_{ad} and K_{is} are the adiabatic and isothermal bulk moduli, α the (volume) thermal expansion coefficient, ρ the density, and C_v the heat capacity per gram at constant volume. By substituting representative values, it is found that K_{ad} and K_{is} rarely differ by more than a few percent except possibly for liquids and very soft solids.

For shear, it is usually stated that at small strains the moduli G_{ad} and G_{is} are identical in isotropic solids.[132,133] For a solid in which G is directly proportional to T, as is closely approximated by soft rubbers, a thermodynamic calculation[134] gives

$$G_{ad} = G_{is} + [(\partial G/\partial T)^2 T/C_\gamma \rho]\gamma^2 \tag{42}$$

where γ is the strain and C_γ the heat capacity per gram at constant strain. The correction term does vanish at small strains, and is entirely negligible for the strain

magnitudes limited by the conditions of linear viscoelastic behavior; for a soft rubber, the coefficient of γ^2 is of the order of 10^2 to 10^3 dynes/cm^2.

2. Critical Frequencies for Isothermal-Adiabatic Transitions

An elementary calculation shows that failure to attain thermal equilibrium with the surrounding medium will set in when the frequency (or reciprocal time in a transient experiment) exceeds the order of $\kappa/C_p\rho x^2$, where κ is the thermal conductivity (of the order of 4×10^{-4} cal/cm deg sec for polymeric liquids and solids), C_p the heat capacity per gram at constant pressure (of the order of 0.4 cal/deg g), and x the thickness of the sample. For $x = 0.1$ cm, the critical frequency is of the order of 0.1 Hz, so the majority of dynamic measurements are indeed adiabatic. At very high frequencies, however, where the experiment involves wave propagation or else characteristic impedance measurements at a wave-propagating surface, the wavelength becomes so short that thermal conduction prevents development of temperature gradients within a cycle, and the deformation is again isothermal. For shear, the critical frequency for this second transition is[132,133]

$$\nu = G'C_p/2\pi\kappa \tag{43}$$

For a viscoelastic liquid with $G' = 10^4$, the corresponding frequency is about 10^6 Hz; for a soft polymeric solid with $G' = 10^7$, 10^9 Hz; for a hard solid with $G' = 10^{10}$, 10^{12} Hz. Only in rare cases—possibly for dilute polymer solutions in the megacycle range—would this transition be crossed, since G' always increases with frequency.

3. Time-Dependent Effects Associated with Heat Flow

Although the change in the real part of the modulus, G' or K', accompanying the change from isothermal to adiabatic conditions may be expected to be negligibly small on the basis of the above estimates, it is accompanied by a contribution to G'' or K'' associated with the dissipation of energy by heat flow. In the viscoelastic liquids discussed in the present chapter, the effect on G'' will certainly also be negligibly small compared with contributions from ordinary viscous losses. The phenomenon may appear, however, in E'' and K'' for hard solids whose losses due to coordinated molecular motions are very small (Chapters 7 and 8).

An analysis of viscoelasticity by the methods of irreversible thermodynamics[135,136] shows that under adiabatic conditions the relaxation spectrum lies at slightly shorter times than under isothermal conditions.

In Appendix B at the end of the book, the experimental methods described in this and the following chapters are summarized with a tabulation of their ranges of applicability.

REFERENCES

1. W. Philippoff, in *Physical Acoustics*, edited by W. P. Mason, Vol. IIB, Academic Press, New York, 1965, p. 1.

2. M. Segel, *Phys. Z.*, **4**, 493 (1903).
3. A. Pochettino, *Nuovo Cimento*, **8**, 77 (1914).
4. A. J. Chompff, thesis, Delft, 1965.
5. R. J. Overberg and H. Leaderman, *J. Res. Nat. Bureau Stand.*, **65C**, 9 (1961).
6. W. Tillmann, *Kolloid-Z.*, **131**, 66 (1953).
7. H. Goldberg and O. Sandvik, *Anal. Chem.*, **19**, 123 (1947).
8. D. J. Plazek, *J. Polym. Sci.*, A-2, **6**, 621 (1968).
9. G. C. Berry and C.-P. Wong, *J. Polym. Sci., Polym. Phys. Ed.*, **13**, 1761 (1975).
10. D. J. Plazek, M. N. Vrancken, and J. W. Berge, *Trans. Soc. Rheol.*, **2**, 39 (1958).
11. D. J. Plazek, *Trans. Soc. Rheol.*, **7**, 61 (1963).
12. K. Osaki, Y. Einaga, M. Kurata, and M. Tamura, *Macromolecules*, **4**, 82 (1971).
13. H. Giesekus, *Rheol. Acta*, **4**, 85 (1965).
14. W. H. Hoppmann, II, and C. E. Miller, *Trans. Soc. Rheol.*, **7**, 181 (1963).
15. K. Ninomiya, *J. Phys. Chem.*, **67**, 1152 (1963).
16. G. C. Berry, B. L. Hager, and C.-P. Wong, *Macromolecules*, **10**, 361 (1977).
17. K. Walters, *Rheometry*, Wiley, New York, 1975.
18. A. Kèpès, *J. Polym. Sci.*, **22**, 409 (1956).
19. M. Horio, S. Onogi, and S. Ogihara, *J. Jpn. Soc. Testing Mater.*, **10**, 350 (1961).
20. R. S. Porter and J. F. Johnson, *J. Appl. Polym. Sci.*, **3**, 200 (1960).
21. Ferranti Electric Inc., Plainview, N.Y. 11803.
22. C. W. Macosko and J. M. Starita, *Soc. Plast. Eng. J.*, **17**, 38 (November 1971); C. W. Macosko, R. G. Garritano, and J. M. Starita, *Soc. Plast. Eng. Tech. Pap.*, **24**, 2 (1978).

22a. C. W. Macosko and F. C. Weissert, in *Rubber and Related Products—New Methods for Testing and Analyzing*, edited by W. H. King and T. H. Rogers, ASTM STP 553, 1974, p. 127.

23. S. Oka, in *Rheology*, edited by F. R. Eirich, Volume 3, Academic Press, New York, 1960, p. 18.
24. J. R. Van Wazer, J. W. Lyons, K. Y. Kim, and R. E. Colwell, *Viscosity and Flow Measurement*, Wiley-Interscience, New York, 1963.
25. A. Ram, in *Rheology*, edited by F. R. Eirich, Volume 4, Academic Press, New York, 1967, p. 251.
26. Y. Einaga, K. Osaki, M. Kurata, S. Kimura, and M. Tamura, *Polym. J.*, **2**, 550 (1971).
27. S. Ohta, Y. Einaga, K. Osaki, and M. Kurata, *Bull. Inst. Chem. Res. Kyoto Univ.*, **51**, 220 (1973).
28. F. W. Schremp, J. D. Ferry, and W. W. Evans, *J. Appl. Phys.*, **22**, 711 (1951).
29. J. F. Pierson, thesis, University of Strasbourg, 1968.
30. J. M. Watkins, *J. Appl. Phys.*, **27**, 419 (1956).
31. J. M. Watkins, R. D. Spangler, and E. C. McKannan, *J. Appl. Phys.*, **27**, 685 (1956).
32. J. Meissner, *J. Appl. Polym. Sci.*, **16**, 2877 (1972).
33. A. S. Lodge, *Elastic Liquids*, Academic Press, New York, 1964.
34. J. D. Huppler, E. Ashare, and L. A. Holmes, *Trans. Soc. Rheol.*, **11:2**, 159 (1967).
35. K. Walters, *Proc. 7th Intern. Congr. Rheology*, edited by C. Klason and J. Kubat, Chalmers Inst. Tech., Gothenburg, 1977, p. 147.
36. J. M. Broadbent, A. Kaye, A. S. Lodge, and D. G. Vale, *Nature*, **217**, 55 (1968).
37. J. M. Broadbent and A. S. Lodge, *Rheol. Acta*, **10**, 557 (1972).
38. M. C. Williams, *Am. Inst. Chem. Eng. J.*, **11**, 467 (1965).
39. H. W. Greensmith and R. S. Rivlin, *Phil. Trans. R. Soc.*, **A245**, 399 (1953).
40. N. Adams and A. S. Lodge, *Phil. Trans. R. Soc.*, **A256**, 149 (1964).
41. H. Markovitz and D. R. Brown, *Proc. Intern. Symp. on Second-Order Effects*, Jerusalem Academic Press, Haifa, 1964.
42. A. S. Lodge, *Rheol. Acta*, **10**, 554 (1971).
43. A. S. Lodge and T. H. Hou, Rheol. Acta, **20**, 247 (1981).
44. H. Markovitz, *J. Polym. Sci.*, **B3**, 3 (1965).
45. J. M. Broadbent and A. S. Lodge, *Rheol. Acta*, **10**, 557 (1972).

46. J. D. Huppler, *Trans. Soc. Rheol.*, **9:2,** 273 (1965).
47. R. I. Tanner, *Trans. Soc. Rheol.*, **11,** 347 (1967).
48. K. Higashitani and A. S. Lodge, *Trans. Soc. Rheol.*, **19,** 307 (1975).
49. D. G. Baird, *J. Appl. Polym. Sci.*, **20,** 3155 (1976).
50. Seismographic Service Corporation, Technical Bulletin on Seiscor-Lodge Stressmeter, Tulsa, Oklahoma, 1978.
51. K. Higashitani and W. G. Pritchard, *Trans. Soc. Rheol.*, **16,** 687 (1972).
52. J. L. Schrag, *Trans. Soc. Rheol.*, **21,** 399 (1977).
53. H. Markovitz, *J. Appl. Phys.*, **23,** 1070 (1952).
54. S. Oka and A. Takami, *Jpn. J. Appl. Phys.*, **4,** 803 (1965).
55. D. O. Miles, *J. Appl. Phys.*, **33,** 1422 (1962).
56. D. O. Miles and G. C. Knollman, *J. Appl. Phys.*, **35,** 2549 (1964).
57. M. Date, *Rep. Progr. Polym. Phys. Jpn.*, **7,** 183 (1964); *Kinzoku Butsuri*, **11,** 233 (1965).
58. M. C. Nally, *Br. J. Appl. Phys.*, **16,** 1023 (1965).
59. K. Bogie and J. Harris, *Rheol. Acta*, **5,** 212 (1966).
60. M. H. Birnboim, U. S. Patent 3,286,176 (1966).
61. W. M. Prest, R. S. Porter, and J. M. O'Reilly, *J. Appl. Polym. Sci.*, **14,** 2697 (1970).
62. M. C. Williams and R. B. Bird, *Ind. Eng. Chem., Fundam.*, **3,** 42 (1964).
63. E. B. Christiansen and W. R. Leppard, *Trans. Soc. Rheol.*, **18,** 65 (1974).
64. M. H. Birnboim and J. D. Ferry, *J. Appl. Phys.*, **32,** 2305 (1961).
65. D. J. Massa and J. L. Schrag, *J. Polym. Sci.*, A-2, **10,** 71 (1972).

65a. A. L. Soli, Ph. D. thesis, University of Wisconsin, 1978.

66. N. W. Tschoegl, *Kolloid-Z.*, **174,** 113 (1961); *Aust. J. Phys.*, **14,** 307 (1961).
67. M. H. Birnboim, J. S. Burke, and R. L. Anderson, in *Proc. 5th Intern. Cong. Rheology*, edited by S. Onogi, University Park Press, Baltimore, 1969, Vol. 1, p. 409.
68. W. Philippoff, *J. Appl. Phys.*, **24,** 685 (1953).
69. W. Philippoff, *J. Appl. Phys.*, **25,** 1102 (1954).
70. T. E. Morrison, L. J. Zapas, and T. W. DeWitt, *Rev. Sci. Instrum.*, **26,** 357 (1955).
71. H. Kambe and M. Takano, *Rep., Aeronaut. Res. Inst., Univ. Tokyo*, **28,** 159 (1963).
72. H. Kambe and M. Takano, *Rep., Aeronaut. Res. Inst., Univ. Tokyo*, **28,** 175 (1963).
73. R. H. Shoulberg, F. H. Zimmerli, and O. C. Kohler, *Trans. Soc. Rheol.*, **3,** 27 (1959).
74. H. Markovitz, P. M. Yavorsky, R. C. Harper, Jr., L. J. Zapas, and T. W. DeWitt, *Rev. Sci. Instrum.*, **23,** 240 (1952).
75. M. Horio, T. Fujii, and S. Onogi, *J. Phys. Chem.*, **68,** 778 (1964).
76. J. A. Duiser, thesis, Leiden, 1965.
77. J. L. den Otter, thesis, Leiden, 1967.
78. G. Harrison, *Rheol. Acta*, **13,** 536 (1974).

78a. K. Osaki, M. Tamura, M. Kurata, and T. Kotaka, *J. Phys. Chem.*, **69,** 4183 (1965).

79. H. C. Booij, *Rheol. Acta*, **5,** 215 (1966).
80. J. M. Simmons, *Rheol. Acta*, **7,** 184 (1968).
81. W. P. Mason, *Electromechanical Transducers and Wave Filters*, Van Nostrand, New York, 1942.
82. T. L. Smith, J. D. Ferry, and F. W. Schremp, *J. Appl. Phys.*, **20,** 144 (1949).
83. J. Lamb and P. Lindon, *J. Acoust. Soc. Am.*, **41,** 1032 (1967).
84. W. P. Mason, *Trans. ASME*, **69,** 359 (1947).
85. A. Konno, S. Makino, and M. Kaneko, *Jpn. J. Appl. Phys.*, **7,** 89 (1968).
86. K. Sittel, P. E. Rouse, Jr., and E. D. Bailey, *J. Appl. Phys.*, **25,** 1312 (1954).
87. M. H. Birnboim and L. J. Elyash, *Bull. Am. Phys. Soc.*, [2] **11,** 165 (1966).
88. J. L. Schrag and R. M. Johnson, *Rev. Sci. Instrum.*, **42,** 224 (1971).
89. J. L. Schrag and J. D. Ferry, *Faraday Symp. Chem. Soc.*, **6,** 182 (1972).
90. N. Nemoto, J. L. Schrag, J. D. Ferry, and R. W. Fulton, *Biopolymers*, **14,** 409 (1975).
91. P. E. Rouse, Jr., and K. Sittel, *J. Appl. Phys.*, **24,** 690 (1953).
92. W. Philippoff, *J. Appl. Phys.*, **34,** 1507 (1963).
93. A. J. Barlow, G. Harrison, J. Richter, H. Seguin, and J. Lamb, *Lab. Pract.*, **10,** 786 (1961).

94. H. Tanaka, A. Sakanishi, and J. Furuichi, *Zairyo,* **15,** 438 (1966).
95. H. Tanaka and A. Sakanishi, *Kobunshi,* **17,** 954 (1968).
96. H. J. McSkimin, *J. Acoust. Soc. Am.,* **24,** 355 (1952).
97. H. Nomura, T. Konaka, H. Shimizu, S. Kato, and Y. Miyahara, *Rep. Prog. Polym. Phys. Jpn.,* **20,** 127 (1977).
98. W. P. Mason, *Physical Acoustics and the Properties of Solids,* Van Nostrand, New York, 1958.
99. N. A. Schuster, *Rev. Sci. Instrum.,* **22,** 254 (1951).
100. H. Nakajima and Y. Wada, *Polym. J.,* **1,** 727 (1970); H. Nakajima, H. Okamoto, and Y. Wada, *Polym. J.,* **5,** 268 (1973).
101. D. L. Hunston, R. R. Myers, and M. B. Palmer, *Trans. Soc. Rheol.,* **16,** 33 (1972).
102. B. J. Zimm, *J. Polym. Sci.,* **26,** 101 (1957).
103. J. V. Fitzgerald, F. J. Matusik, and H. R. Oppliger, *Meas. Data,* 65 (May 1975).
104. J. D. Ferry, P. A. Janmey, F. H. M. Nestler, and R. W. Rosser, *Meas. Control,* 113 (April 1979).
105. W. Roth and S. R. Rich, *J. Appl. Phys.,* **24,** 950 (1953).
106. W. P. Mason, W. O. Baker, J. H. McSkimin, and J. H. Heiss, *Phys. Rev.,* **75,** 936 (1949).
107. A. J. Barlow and J. Lamb, *Proc. R. Soc.,* **A253,** 52 (1959).
108. R. R. Myers and C. J. Knauss, *J. Coatings Tech.,* **40:**523, 315 (1968).
109. R. S. Moore, H. J. McSkimin, C. Gieniewski, and F. Andreatch, *J. Chem. Phys.,* **47,** 3 (1967).
110. A. J. Barlow, J. Lamb, A. J. Matheson, P. R. K. L. Padmini, and J. Richter, *Proc. R. Soc.,* **A298,** 467 (1967).
111. J. Lamb and H. Seguin, *J. Acoust. Soc. Am.,* **30,** 519 (1966).
112. H. J. McSkimin, in *Physical Acoustics,* edited by W. P. Mason, Vol. IA, Academic Press, New York, 1964, Chapter 4.
113. G. B. Thurston, *J. Acoust. Soc. Am.,* **32,** 210 (1960); **33,** 1091 (1961).
114. F. T. Adler, W. M. Sawyer, and J. D. Ferry, *J. Appl. Phys.,* **20,** 1036 (1949).
114a. G. B. Thurston and J. L. Schrag, *J. Appl. Phys.,* **35,** 144 (1964).
115. A. W. Nolle and P. W. Sieck, *J. Appl. Phys.,* **23,** 888 (1952).
116. J. D. Ferry, W. M. Sawyer, and J. N. Ashworth, *J. Polym. Sci.,* **2,** 593 (1947).
117. J. D. Ferry and F. E. Helders, *Biochim. Biophys. Acta,* **23,** 569 (1967).
118. J. D. Ferry, *Rev. Sci. Instrum.,* **12,** 79 (1941).
119. D. J. Plazek, Ph. D. thesis, University of Wisconsin, 1956.
120. K. H. Illers, *Rheol. Acta,* **4,** 185 (1964).
121. D. Kutz, B. S. thesis, Lehigh University, 1958.
122. A. F. Lewis and J. K. Gilham, *J. Appl. Polym. Sci.,* **6,** 422 (1962); **7,** 685 (1963).
123. J. A. Faucher and J. V. Koleske, *Phys. Chem. Glasses,* **7,** 202 (1966).
124. R. R. Myers, *J. Polym. Sci.,* **C35,** 3 (1971).
125. R. M. Neumann, G. A. Senich, and W. J. MacKnight, *Polym. Eng. Sci.,* **18,** 624 (1978).
125a. D. J. Plazek, *J. Polym-Sci., Polym. Phys. Ed.,* **20,** 1533, 1551 (1982).
126. A. F. Lewis and M. C. Tobin, *Trans. Soc. Rheol.,* **6,** 27 (1962).
127. W. M. Davis and C. W. Macosko, *AIChE J.,* **20,** 600 (1974).
128. Instron Corporation, Canton, Massachusetts 02021.
129. K. Walters, *J. Fluid Mech.,* **40,** 191 (1970).
130. D. G. Knight and K. Walters, *Rheol. Acta,* **12,** 524 (1973).
131. M. Zemansky, *Heat and Thermodynamics,* McGraw-Hill, New York, 1951.
132. W. P. Mason, *Piezoelectric Crystals and Their Application to Ultrasonics,* Van Nostrand, New York, 1950.
133. K. Okano, *Reports on Progress in Polymer Physics in Japan,* Kobayasi Institute of Physical Research, Tokyo, 1958, p. 64.
134. J. D. Ferry, unpublished calculations.
135. J. Meixner, *Z. Naturforsch.,* **4a,** 594 (1949).
136. J. Meixner, *Z. Naturforsch.,* **9a,** 654 (1954).

CHAPTER 6

Experimental Methods for Soft Viscoelastic Solids and Liquids of High Viscosity

The boundary between this chapter and the preceding one is rather arbitrarily drawn; we now describe methods for materials with high enough viscosity, or if cross-linked with high enough equilibrium modulus, to support their own weight under gravitational forces. For such materials, there is considerably more freedom of choice in sample geometry and types of deformation. By specifying that the materials are "soft," *i.e.*, with a shear modulus less than something like 10^8 to 10^9 dynes/cm^2 (10^7 to 10^8 Pa), the problems of measurement are further facilitated. There is no difficulty in making the structural parts of the apparatus much more rigid than the sample, so that their compliance can be neglected. Moreover, deformations in shear and in simple extension can be used interchangeably to yield the same information provided the deformations are small. This follows because with $\mu \cong \frac{1}{2}$, in accordance with equation 56 of Chapter 1, $E = 3G$; and any extensional viscoelastic function is related to the corresponding shear function by a factor of 3.

There is one type of soft solid for which recourse must be had to the apparatus described in Chapter 5—very weak gels which, though their viscosity may be infinite, have insufficient rigidity to prevent gross distortion under gravitational forces unless supported in containers. For example, stress relaxation in shear between coaxial cylinders can be followed after initial twist through a small angle;[1] and by placing a small differential pressure on a plug of gel in a cylindrical tube, shear experiments can be performed with the same deformation geometry as for liquid flow in a capillary.[2]

Whether or not a given polymeric system is "soft" or "hard" depends of course on the frequency range as well as the temperature. At high frequencies and low temperatures the methods described in this chapter must be replaced by those of

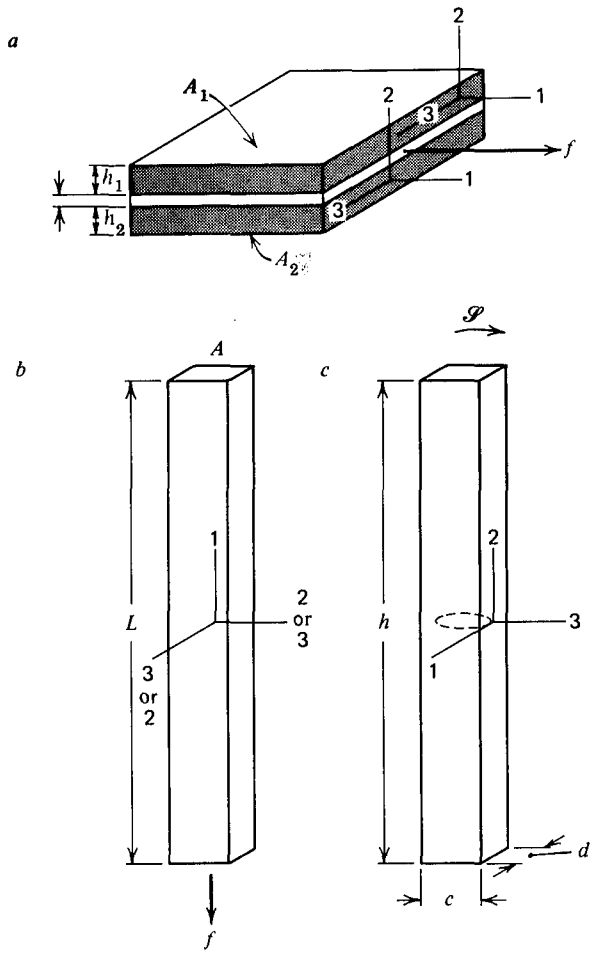


FIG. 6-1. Geometries, coordinates, and dimensions for investigation of soft viscoelastic solids (in addition to those shown in Fig. 5-1). (*a*) simple shear sandwich; (*b*) simple elongation; (*c*) torsion of bar with rectangular cross-section.

Chapter 7. Detailed reviews of experimental methods to supplement Chapters 6 and 7 may be found in the literature.[3-6]

All the experimental geometries described in the preceding chapter and illustrated in Fig. 5-1 can be used for measurements of viscoelastic properties of soft solids, though confinement of the sample between coaxial cylinders is rather unusual[7,8] because of the difficulty in filling. In addition, three other geometries which are common are sketched in Fig. 6-1. In creep, stress relaxation, and dynamic experiments without sample inertia effects, the shear (or simple extension) strain stress ratios can be obtained from displacement/force ratios by geometrical factors which supplement the list given in Chapter 5 as follows:

(a) Simple shear sandwich:

$$\gamma_{21}/\sigma_{21} = bx_1/f \tag{1}$$

$$b = A_1/h_1 + A_2/h_2 \tag{2}$$

(b) Simple extension:

$$\epsilon/\sigma_T = bx_1/f \tag{3}$$

$$b = A/L \tag{4}$$

(c) Torsion of bar with rectangular cross-section:

$$\gamma_{21}/\sigma_{21} = b\alpha/\mathcal{S} \tag{5}$$

$$b = cd^3q(c/d)/16h \tag{6}$$

b = form factor—dimensions in cm in (a) and (b); cm^3 in (c)
x_1 = linear displacement
f = force
A_1, A_2 = areas of sandwich samples
h_1, h_2 = thicknesses of sandwich samples
ϵ = practical tensile strain (*cf.* equation 52 of Chapter 1)
A = cross-section area
L = length of sample
α = angular displacement (rad)
$\mathcal{S}$ = torque
c = width of torsion bar
d = thickness of torsion bar
$q(c/d)$ = numerical factor[9,10] between 2.249 and 5.333

These formulas, like the corresponding ones in Chapter 5, imply small deformations and are approximations based on simplified representations of the states of strain. Corrections may be made for edge effects[11] and bulging of the sides[12] of shear sandwich samples of appreciable thickness, and for a more complete description of the state of strain in a twisted rod of rectangular cross-section.[13]

A. CREEP

Because of the simplicity of a creep experiment, a wide variety of arrangements have been used in different laboratories, and many have never been described in publications. The constant force is often applied by a dead weight, and the displacement is measured by a differential transformer, traveling microscope, or deflection of a light beam. Simple shear sandwich geometry is convenient,[14,15] though in vertical orientation a clear-cut creep recovery experiment is not possible because after removal of the applied force the weight of the center plate produces a small continuing stress in the original direction (Fig. 5-1a). Since the areas in equation 2 may not be easy to measure *in situ*, b can be calculated alternatively as $b = (m_1/h_1^2$

$+ m_2/h_2^2)/\rho$, where the m's are the sample masses and ρ is the density. The shape of the cross-section area does not matter. In accordance with equation 1 with constant σ_{21} and time-dependent γ_{21}, the creep compliance $J(t)$ is given by $bx_1(t)/f$. Torsion of a thin disc as in the creep apparatus of Plazek[16] described in Chapter 5 or its earlier version,[17] as well as in other torsional devices,[18,19] is applicable also to soft uncross-linked polymers of high molecular weight or even soft cross-linked solid samples provided they adhere to the parallel plate surfaces. Here, also, measurement of sample mass m can be substituted for that of radius R by calculating b as $m^2/2\pi h^3/\rho^2$ instead of from equation 11 of Chapter 5. The height h must be measured *in situ* with great precision—at each temperature, since it is affected perceptibly by thermal expansion of the sample housing. Longer rods or bars may also be studied in torsion.[20]

If the sample is not too soft to attach clamps of some sort, it can be formed in strips, rods, dumbbells, or rings and the creep can be measured in simple extension rather than shear. If the tensile strain is very small, the tensile compliance is given by $D(t) = J(t)/3 = bx_1(t)/f$, with b from equation 4. With somewhat larger strains, even though the stress may be small enough to fulfill the requirements of linear viscoelastic behavior, a difficulty is encountered because A and L change continuously throughout the experiment (in inverse proportion, since we are dealing in this chapter with materials whose Poisson's ratio is near $\frac{1}{2}$ and whose volume change in simple extension is very small). The tensile stress can be maintained constant, as demanded by the definition of the creep compliance, by decreasing the force f in proportion to A; this can be accomplished by automatic devices or a buoyancy correction.[21-23] However, $D(t)$ cannot be obtained from $x_1(t)$ with a constant form factor. The extension should be measured by displacements of fiducial marks on the sample rather than separation of the clamps, since the strain may be inhomogeneous near the clamps; homogeneity in the portion where the strain is measured should be checked by following the displacement of several fiducial marks. Experiments in extension with very large deformations may require a complicated constitutive equation for their interpretation and may yield quite different information from creep in shear. Only for small strains, in soft solids where Poisson's ratio μ is negligibly different from $\frac{1}{2}$, is $J(t)$ equal to $3D(t)$.

Any uncross-linked polymer system with a viscosity high enough to be studied by the methods described in this section will be very slow in coming to steady-state flow; attempts to obtain η_0 and J_e^0 from linear plots such as Fig. 1-12 should be approached with caution and skepticism, and if possible tested by creep recovery experiments. From the methods described in Chapter 4, it is possible to calculate the retardation spectrum L from $J(t)$ even if one is not sure whether steady-state flow has been achieved.

B. STRESS RELAXATION

Any of the arrangements described in the preceding section can in principle be used for studying stress relaxation if the force can be measured as a function of time

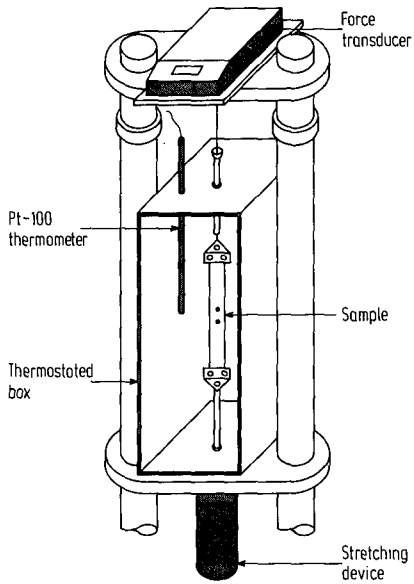


FIG. 6-2. Apparatus of Kramer[26] for measuring stress relaxation in simple extension. The stretching device can be operated at a controlled rate of extension prior to the relaxation at constant extension.

$f(t)$, while the deformation is maintained constant. There are in general three ways of keeping constant strain: by continuous adjustment of the force as the stress in the sample relaxes, which can be done by an automatic servomechanism;[24] by applying more than enough force, with a stop to limit the deformation, and making measurements at intervals by accurately balancing of the force so that the deformation just clears the stop;[25] and by straining a stiff spring element in series with the sample. In the latter case, the strain of the sample is not strictly constant, since it increases slightly as the spring element contracts in response to the relaxing stress. However, if the force per unit deformation is far larger for the spring than for the sample, the relaxation will approximate conditions of constant strain, and if the spring element carries a strain gauge or a differential transformer, a continuous recording of the stress relaxation can be made, with a digital printout if desired. An example is shown in Fig. 6-2, where a force transducer records the stress with an automatic adjustment to zero displacement. Experimental methods and procedures for stress relaxation have been reviewed in detail by Bergen.[27]

In practice, most stress relaxation measurements on soft solids are made in simple extension.[28] For small deformations, the tensile relaxation modulus is obtained by inverting equation 3 with time-dependent force:

$$E(t) = f(t)/bx_1 \tag{7}$$

and, if μ is close to $\frac{1}{2}$, $G(t) = E(t)/3$. For larger deformations, it has been sometimes found[29-34] that the time-dependent tensile stress can be factored into a function of time and a function of strain:

$$\sigma_T(t, \lambda_1) = \mathcal{F}(\lambda_1)E(t) \tag{8}$$

where λ_1, the extension ratio, is simply $\epsilon + 1$ (a measure of tensile strain more commonly used in this context) and $\mathcal{F}(\lambda_1)$ is some function of λ_1 which approaches $\lambda_1 - 1 = \epsilon$ as ϵ approaches zero, thus giving equation 52 of Chapter 1 as a limiting relation. In other cases, in particular for uncross-linked polymers over a wide range of time scale, the two dependences cannot be factored.[35-37] A portion of the strain dependence $\mathcal{F}(\lambda_1)$ is sometimes expressed in terms of the formulation of the Gaussian theory of rubberlike elasticity, which predicts[38] for the equilibrium stress of a cross-linked polymer in simple extension

$$\sigma_T = (E_e/3)(\lambda_1^2 - \lambda_1^{-1}) \tag{9}$$

The apparent Young's modulus[36,37] or "reduced force"[39] is then calculated as

$$E_a(t, \lambda_1) = 3\sigma_T/(\lambda_1^2 - \lambda_1^{-1}) = \frac{3f(t)/A_0}{(\lambda_1 - \lambda_1^{-2})} \tag{10}$$

where A_0 is the initial cross-section area. The dependence of E_a on λ_1 is of course much less than that of σ_T, and E_a approaches the linear Young's relaxation modulus $E(t)$ as $\lambda_1 \to 1$. Interpretation of such data will be discussed in Chapter 13.

When stress relaxation experiments are performed on uncross-linked polymers which are viscoelastic liquids of very high viscosity, the stress eventually decays to zero and small forces must be measured with a sensitive detector toward the end of the experiment.[26,28] On the other hand, in cross-linked polymers which are soft viscoelastic solids the stress approaches a limiting value and it is necessary to determine small changes toward the end of the experiment, requiring measurements to several significant figures.[32] Several installations with different sensitivities are usually needed to cover a wide range of sample properties.[28] Automatic recording with a digital printer is often used, and the recording intervals can be spaced logarithmically with a suitable logarithmic clock,[40,41] as in the "Logtimer."[41]

C. DYNAMIC MEASUREMENTS WITHOUT SAMPLE INERTIA EFFECTS

Measurements on soft solids with sinusoidally varying deformations may be classified in the same way as those on liquids discussed in the preceding chapter. If the sample thickness is small compared with the wavelength of a shear wave, sample inertia effects may be neglected and the form factors defined in connection with Figs. 5-1 and 6-1 can be used just as in transient measurements.

1. Direct Measurements of Sinusoidally Varying Stress and Strain

The methods described in Sections D1 and D2 of Chapter 5 for tracing directly the sinusoidally varying stresses and strains, or for measuring the mechanical im-

pedance in case inertia and/or elastance of a moving element of the apparatus must be taken into account, can be applied to soft solids with very little change. The mechanically driven vibrator of Philippoff[42] is used by substituting the shear sandwich geometry of Fig. 6-1*a* for the annular pumping geometry of Fig. 5-1*b*. Similar devices, with other means for following force and displacement, have been employed by other investigators for both shear and longitudinal deformations.[43-45] Instead of tracing an ellipse, both force and displacement can be automatically recorded against time; a versatile arrangement of Koppelmann[46] permits deformation in simple shear, simple extension, torsion, or flexure by interchange of mountings. In the uniaxial extension viscoelastic spectrometer of Kawai and associates,[47,48] force and displacement are measured with differential transformers at opposite ends of a long strip. The phase angle δ is determined by a phase meter. The frequency range is from 0.1 to 100 Hz. A constant static strain, controlled by a differential transformer and a servomechanism, can be imposed during the dynamic measurements. The Rheovibron device of Takayanagi and Yoshino[49-51] uses similar geometry but has a more restricted frequency range; the apparatus is designed for very small, delicate samples. The phase angle is measured by a vector subtraction method, similar to that used earlier by Marvin[52] and Painter;[53] values of loss tangent as small as 0.001 can be determined. If the sample modulus is rather high (approaching a glasslike value), correction should be made for several sources of error involving compliance of the apparatus.[54,55] The Rheometrics Mechanical Spectrometer[56] can be used for solids as well as liquids in several different geometries, and can be automated. In the carefully designed apparatus of Wetton and Allen,[57] a cylindrical rod of circular cross-section is subjected to sinusoidally varying torsional deformation, the angular deformation being measured by a capacitance transducer; an unusually wide frequency range of 10^{-2} to 10^{3} Hz is encompassed.

The two devices of De Witt and associates[58] can be modified by replacing the coaxial cylinders for liquids by a cylindrical solid sample which is deformed in torsion through a small angle. The sample form factor is then given by equation 11 of Chapter 5, but the calculations involve the moment of inertia and the stiffness of the supporting wire in a rather complicated way as before. The "thickness" of the sample which must be small compared with the shear wavelength in this case the length of the cylinder, which is often its largest dimension; similarly for extensional devices the length of the strip.[47-51]

2. Transducer Measurements by Electrical Impedance

The electrical impedance method, in which complex voltage/current ratios are measured without the need to determine absolute values of force, displacement, or velocity, can also be applied to soft solids; the Fitzgerald transducer apparatus,[12,59] which uses shear sandwich geometry, is an example which provides considerable versatility and precision.

In this device, shown in Fig. 6-3, two disc-shaped samples are periodically sheared between flat surfaces inside a thin cylindrical driving tube and a heavy,

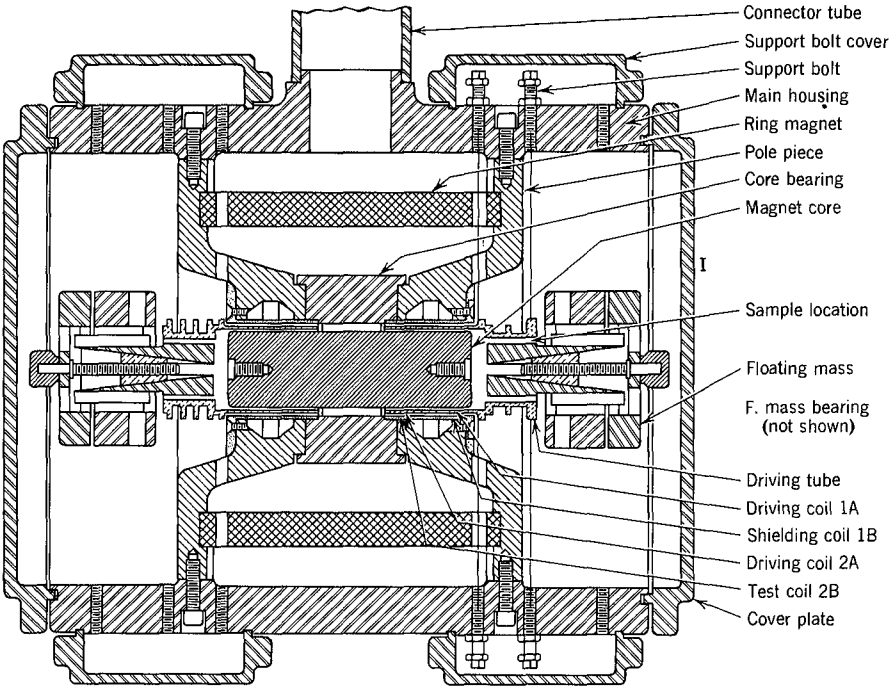
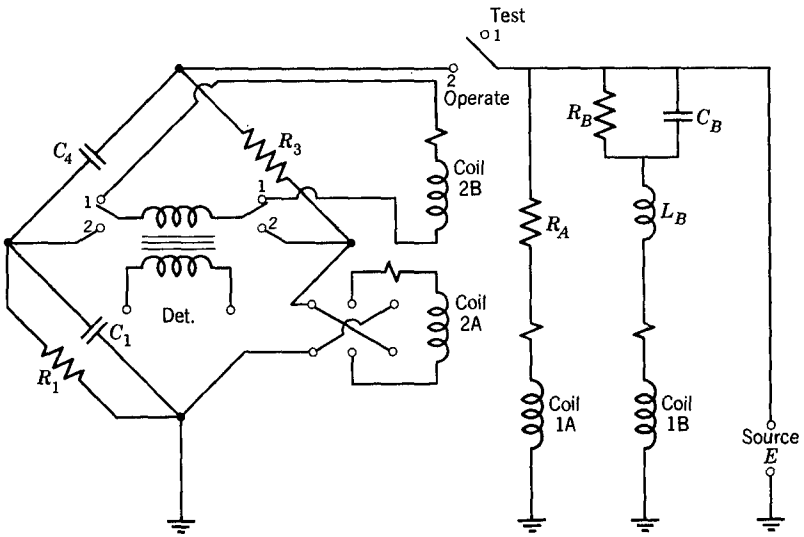


FIG. 6-3. Electromagnetic transducer apparatus of Fitzgerald[59] for dynamic measurements on soft solids, comprising two complete electromechanical units in one housing.

freely suspended floating mass. Both tube and mass are supported by fine wires which center them radially but permit longitudinal motion. Two coils around the driving tube, each in a radial magnetic field, carry an alternating current which produces a longitudinal oscillation with small amplitude. The floating mass moves with a much smaller amplitude, whose magnitude and phase are determined by its inertia and the elastance of its supports. The electrical impedance of one of the driving coils is measured with a bridge while in motion. From this, the mechanical impedance of the oscillating system can be calculated; the basic transducer equation is the same as equation 25 of Chapter 5, but the rest impedance Z_0^* is eliminated by making two measurements of Z^* with different ratios, r, of the driving currents in the two coils.

The electrical circuit of the Fitzgerald transducer is shown in Fig. 6-4, where coils 1A and 2A are the driving coils. There are several procedures for varying the ratio of the two driving currents, by changing R_3 or R_A or by reversing the direction in coil 2A. An important feature of the method is the elimination of the emf in coil 2A, whose impedance is being measured, due to mutual inductance from the current in coil 1A. This is accomplished by a current in the reverse direction in coil 1B, which is stationary and very close to 1A on the outside. The magnitude and phase of the current in 1B are adjusted by varying R_B, C_B, and L_B until the emf in coil 2B (measured in the "test" position) vanishes. Coil 2B is stationary outside and very close to 2A. This mutual inductance balance must be made before each



(Coils 1A and 2A are mechanically coupled)

FIG. 6–4. Electrical circuit of Fitzgerald apparatus (showing only one electromechanical unit).

bridge measurement of the impedance, Z_2^*, of coil 2A; without it, the useful frequency range would not go much above 100 Hz.

The mechanical impedance of the moving system is calculated as

$$Z_M^* = -K^2 \Delta r / \Delta Z_2^* \tag{9}$$

where Δ refers to the difference between two sets of readings, and K^2 corresponds to $(Bl)^2$ in equation 25 of Chapter 5 except that it is the product of the magnetic field intensities and wire lengths for the two coils 1A and 2A.

From measurements on the driving tube alone, its mechanical impedance Z_{Mt}^* can be determined, as well as the constant K^2, making use of the known mass of the tube M, and the fact that at high frequencies X_{Mt} approaches ωM (*cf.* equation 20 of Chapter 5). The difference $Z_M^* - Z_{Mt}^* - i\omega m/3$ gives the mechanical impedance Z_{AB}^* due to motion of the samples and the floating mass. The term in m (the combined masses of the samples $m_1 + m_2$) represents a first-order correction for sample inertia.[60] The correction is valid only when it is small compared with the imaginary part of Z_M^*. In practice, it is often quite negligible. The motions of the samples and the floating mass add as reciprocal impedances or admittances (Y) since their displacements are in series; thus

$$1/Z_{AB}^* = Y_{AB}^* = Y_{Ms}^* + Y_{Mm}^* \tag{10}$$

so if Y_{Mm}^*, the reciprocal impedance of the floating mass, is known from a separate calibration with the driving tube and mass coupled rigidly together, the reciprocal impedance Y_{Ms}^* of the samples can be obtained by a second subtraction.

In making the two subtractions to obtain Y_{Ms}^* (each of which is a complex operation with a real and an imaginary part), it is necessary to keep Z_{Mt}^* and Y_{Mm}^* relatively small, or at least not overwhelmingly large, compared with the respective remainders. To cover a wide range of frequencies, samples of different sizes and shapes may be necessary.

Finally, the real and imaginary parts of the complex compliance of the material are calculated as

$$J' - iJ'' = -ibY^*_{Ms}/\omega \tag{11}$$

The form factor b is given by equation 2, subject to corrections for stress distribution and bulging. The components J' and J'' can of course be converted to G' and G'' by equations 29 and 30 of Chapter 1.

The Fitzgerald apparatus has been used at frequencies from 10 to 6000 Hz. It can be operated over an unusually wide temperature range, from −60° to 155°C. The temperature control is very good because the entire apparatus is immersed in a liquid bath. Like the electrical impedance transducers described in Chapter 5, it is operated with exceedingly small stresses and deformations because neither needs to be measured directly; and stability of the bridge balance with changing driving current provides a sensitive test of linearity of the viscoelastic behavior of the sample. The wave form of the driving current should be monitored as an additional test of linear viscoelasticity as well as possible spurious resonances in the apparatus.

Another electrical impedance device for measurements on soft (and very soft) solids has been described by Keiper.[61] The electrical measurements are similar to those of the apparatus of Smith, Ferry, and Schremp[62] or the impedance mode of the Birnboim apparatus[63] (equations 26 and 27 of Chapter 5); the elastance and frictance of the moving element are eliminated by use of a gas bearing, and its inertia is very small. It can be used with various sample geometries;[64] the frequency range is from 1 to 400 Hz.

3. Compound Resonance Devices with Forced Oscillations

Reference has already been made in Chapter 5 to the exploitation of a resonance oscillation of a moving apparatus element in the measurement of dynamic viscoelastic properties, commonly used in characteristic impedance determinations. This principle is frequently employed for measurements on soft solids and will now be described in more detail.

A simple illustration is shown in Fig. 6–5; an electromagnetic drive causes periodic shearing of two discs with shear sandwich geometry.[65] The complex ratio of driving force to velocity is the same as that given in equations 21 to 23 of Chapter 5:

$$f^*/v = Z^*_M = bG''/\omega + i(\omega M - S^0_M/\omega - bG'/\omega) \tag{12}$$

where the symbols have their usual significance (*cf.* the mechanical model in Fig. 5–7); M is of course the mass of the entire moving system, not just the principal inertial member illustrated in Fig. 6–5, and the elastance S^0_M is ordinarily kept small compared with bG' by using supports which yield freely in the direction of motion. The form factor b is given by equation 2.

At the resonance frequency, ω_0, the imaginary term vanishes and the force and velocity are in phase; the force and displacement are out of phase by 90°, and this

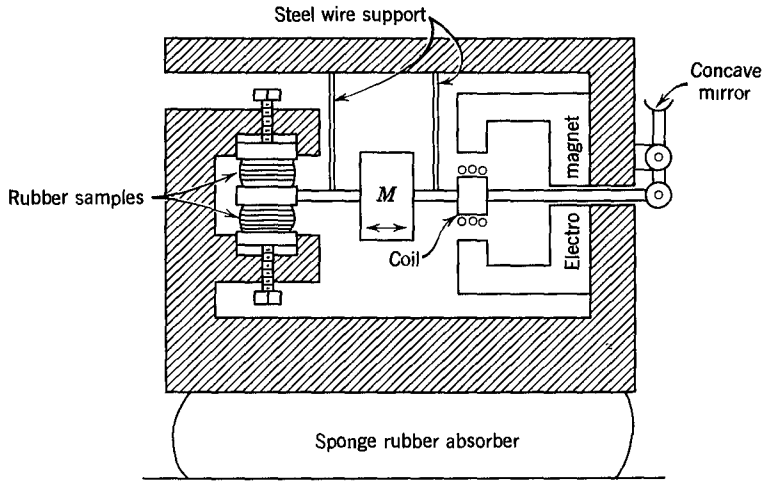


FIG. 6-5. Resonance apparatus for dynamic measurements on soft solids. (Dillon, Prettyman, and Hall.[65])

phase angle specification provides the most precise determination[66] of ω_0. More often, however, ω_0 is determined as the frequency of maximum velocity, or (very nearly) that of maximum displacement, for a given peak driving force, since at ω_0 the response is determined only by G'' and both displacement and velocity pass through maxima as a function of frequency. In electrical impedance transducers such as those of Figs. 5-8 and 6-3 and 6-4, the immediate vicinity of the resonance is to be avoided because of extreme sensitivity. But advantage of the resonance may now be taken by solving for G' in terms of ω_0:

$$G' = \omega_0^2 M/b - S_M^0/b \tag{13}$$

Ordinarily, G'' is obtained by either of two procedures: measurement of the absolute values of peak displacement $|x^*|$ and peak force $|f^*|$ at resonance, in which case

$$G'' = |f^*|/b|x^*| \tag{14}$$

or else measurement of the relative values of $|x^*|$ at a series of frequencies near ω_0 and construction of a response curve from which the half-width, $\Delta\omega$, corresponding to the difference between the frequencies at which $|x^*|$ is half its maximum value, is read. Then

$$G'' = G'\Delta\omega/\omega_0\sqrt{3} \tag{15}$$

[Alternatively, if $(\Delta\omega)'$ is the difference between frequencies at which $|x^*|$ is $1/\sqrt{2}$ of its maximum value, $G'' = G'(\Delta\omega)'/\omega_0$.] A third method[66] is based on measuring the frequency at which the phase angle between force and displacement is 45° and/or 135°. The above formulas assume that the sample itself makes a negligible contribution to M, in contrast to the situation to be described in Chapter 7 where

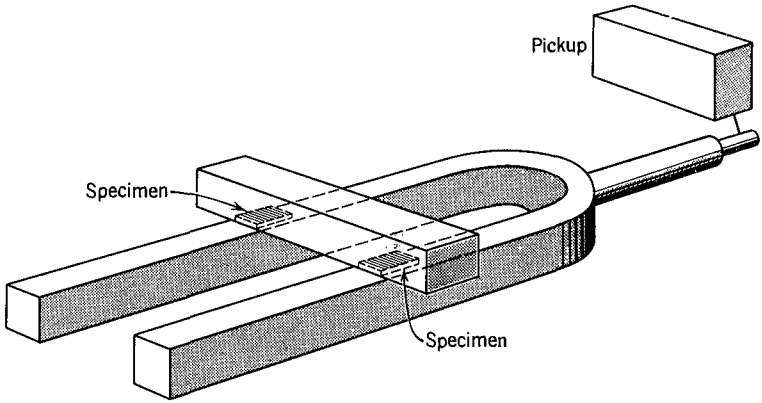


FIG. 6-6. Tuning fork compound resonator for dynamic measurements on soft solids. (Rorden and Grieco,[74] and Hopkins.[75])

the resonance is determined by the inertia of the sample itself. Moreover, it is assumed that $R_M \ll \omega M$, or $\tan\theta \ll 1$ (*cf.* equation 24 of Chapter 5); only under these conditions is a sharply defined resonance obtained. If S_M^0 is small compared with bG', so that the elastance is largely contributed by the sample, this is equivalent to specifying that $\tan\delta \ll 1$. The resonance corresponds to maximum velocity $|v^*|$ and nearly to maximum $|x^*|$.

The measurement can of course be made at only one frequency ω_0, although that can be adjusted by varying the mass M and/or the form factor of the sample. There are various modifications of this principle, employing deformation in shear,[67] extension-compression,[68-70] and shear between coaxial cylinders[71,72] (for very soft gels). In the latter case, the resonance frequency corresponds to torsional oscillations of a suspended system.

If G' is small (and it will generally not be over 10^7 dynes/cm^2 for the low-loss soft solids handled by these methods), the upper limit of the frequency range is rather restricted by limitations of convenience and design on the smallness of M and the largeness of b. Higher frequencies can be used by increasing the magnitude of the term S_M^0/b in equation 13; but then the calculation of G' loses precision by becoming a small remainder of a subtraction, and the result may be that only the component G'' can be determined.[73]

If S_M^0 is made large and provision is made for an accurate subtraction, the equations can be formulated somewhat differently in terms of resonant frequencies with and without presence of the sample. With this modification, it is no longer necessary to have $\tan\delta \ll 1$ for the material of the sample; a sharp resonance is obtained so long as $\tan\theta \ll 1$, *viz.*, $R_M \ll S_M^0/\omega$ (*i.e.*, $G'' \ll S_M^0/b$), and high-loss as well as low-loss materials can be studied. For example, in the method of Rorden and Grieco,[74] the resonant frequency and the response width $\Delta\omega$ of an electrically driven tuning fork are modified by deforming two soft samples in simple shear between the fork and an inertia bar (Fig. 6-6). The storage modulus G' is obtained from the difference between the two resonant frequencies with and without samples,

and the loss modulus G'' from the difference between the two $\Delta\omega$ values. Because of the complex vibration modes of a tuning fork, the relations involve some rather complicated calibration parameters which will not be described here. (This method has been modified by Hopkins[75,76] for high-viscosity polymeric liquids.)

The frequency range of the forced-oscillation resonance devices described in this section is generally from 10 to a few thousand Hz. It should be emphasized that we are still dealing with situations where the dimensions of the sample (thickness in the case of shear, length for torsion or extension, etc.) are small compared with the wavelength of an elastic wave corresponding to the type of deformation used. Thus, the inertia of the sample itself does not enter into the calculations.

4. Compound Resonance Devices with Free Oscillations

Any one of the forced-oscillation arrangements described above can in principle be operated in free vibrations; the system is set into oscillation and it continues freely with a constant frequency ω_c and a gradually decreasing amplitude. The viscoelastic properties are calculated from the characteristic frequency ω_c and the decrement. It is again important that $G'' \ll G' + S_M^0/b$, so that either $\tan\delta$ must be small (material of low loss) or (rarely) S_M^0 must be made deliberately large. Otherwise, the relations between the measured quantities and the viscoelastic functions are very complicated; the relations have been critically discussed with evaluation of error bounds by Struik[77] and Roscoe.[78] An iterative procedure for reducing such data has been proposed.[79] Moreover, if G'' is the same order of magnitude as $G' + S_M^0/b$, the amplitude will decay too rapidly to establish a characteristic frequency. For linear oscillations, if S_M^0 makes a negligible contribution and $G'' \ll G'$,

$$G' = (\omega_c^2 M/b)(1 + \Delta^2/4\pi^2) \tag{16}$$

$$G'' = (\omega_c^2 M/b)\Delta/\pi \tag{17}$$

where Δ is the logarithmic decrement (natural logarithm of the ratio between two successive displacements), and b is the appropriate form factor from equation 2 or 4 of this chapter or equation 2 or 13 of Chapter 5. The corresponding equations for torsional oscillations of a cylindrical or prismatic sample are identical except that I, the moment of inertia of the oscillating system, must be substituted for M; and b, in units of cm^3, is now given by equation 6 of this chapter or equation 7 or 9 of Chapter 5.

An example of a free oscillation device whose deformation geometry is torsion of a circular cylinder is shown in Fig. 6–7. The apparatus of Plazek, Vrancken, and Berge[17] mentioned above under creep is equipped here with a moment arm to provide an adjustable moment of inertia. The oscillations are followed by reflection of a light beam from a mirror attached to the rotating unit onto a photocell, whose output is automatically recorded. From the trace (Fig. 6–8), the characteristic frequency ω_c and the decrement Δ can be obtained; it is convenient to match with an adjustable enlarger to standard exponential envelopes.[80] The decrement is proportional to the slope of a plot of the logarithm of the maximum amplitude

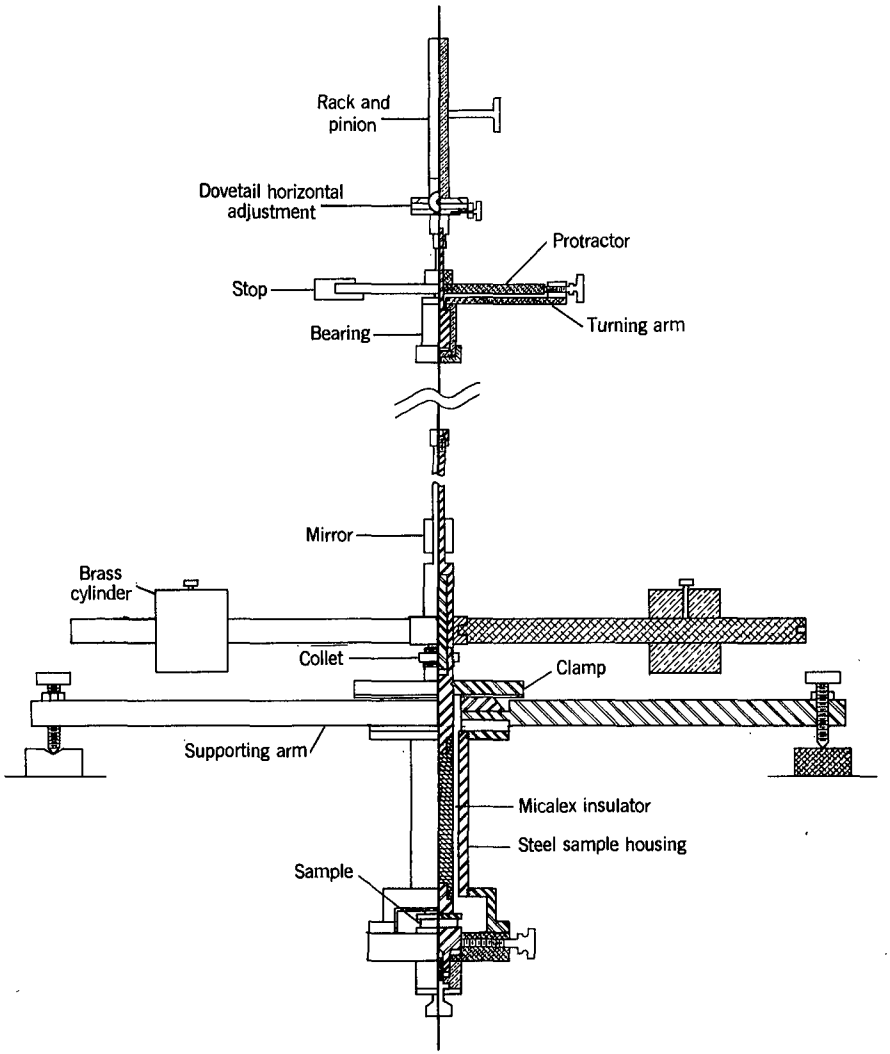


FIG. 6–7. Torsion pendulum for dynamic measurements on soft solids with free oscillations (Plazek, Vrancken, and Berge[17]), with modified moment arms.

against number of oscillations (Fig. 6–9). This particular design is especially suited for very soft solids with low loss. In other modifications with torsional geometry, the sample is held in place with clamps,[81–85] and the oscillations are followed by the tangential motion of a differential transformer,[81] induction of an emf in a coil attached to the rotating system (from a stationary coil at right angles energized with a carrier frequency[82,84,85]), or even by a trace of light on a photographic film. It is possible to use an electrical recorder whose trace amplitude is proportional to the logarithm of the signal,[46,82] so that Δ can be obtained directly from the slope

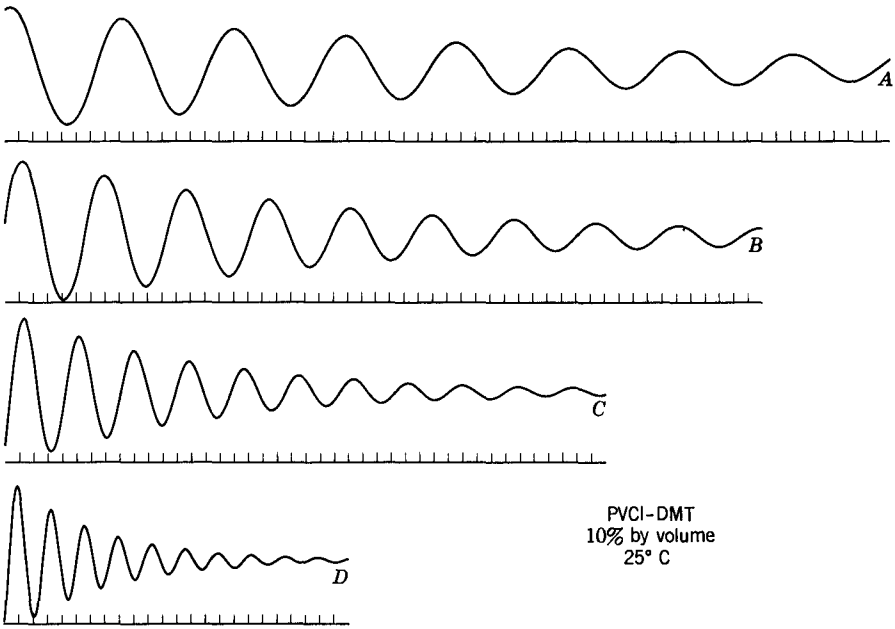


FIG. 6-8. Automatic recording of angular deflection *vs.* time in free torsional oscillations for a 10% polyvinyl chloride gel at 25°C with four different moments of inertia. (Plazek, Vrancken, and Berge.[17])

of the envelope of the maxima (Fig. 6-10), eliminating the need for constructing a second logarithmic graph like Fig. 6-9. Free oscillations in simple extension can also be used;[86] in this case the real and imaginary components of Young's modulus, E' and E'', are given by equations 13 and 14 with b from equation 4. For soft solids, then, $G' = E'/3$ and $G'' = E''/3$.

The free oscillation devices cover in general a frequency range of 0.01 to 25 Hz. The precise temperature control needed for all viscoelastic measurements can be achieved by suitable design; any mechanical connections with parts of the apparatus outside the thermostat must be made through members of low heat conductivity.

D. WAVE PROPAGATION

At higher frequencies, the wavelength of shear or extensional waves becomes too short to satisfy the requirement in Section C that the critical dimension of the sample must be small compared with a wavelength. At the other extreme, as in Chapter 5, when the sample is large compared with the wavelength, the propagation of traveling waves may be observed. For soft solids, the usual geometry is simple extension, requiring the propagation of longitudinal waves along thin strips[86] whose lateral dimensions are *small* compared with a wavelength. The velocity and at-

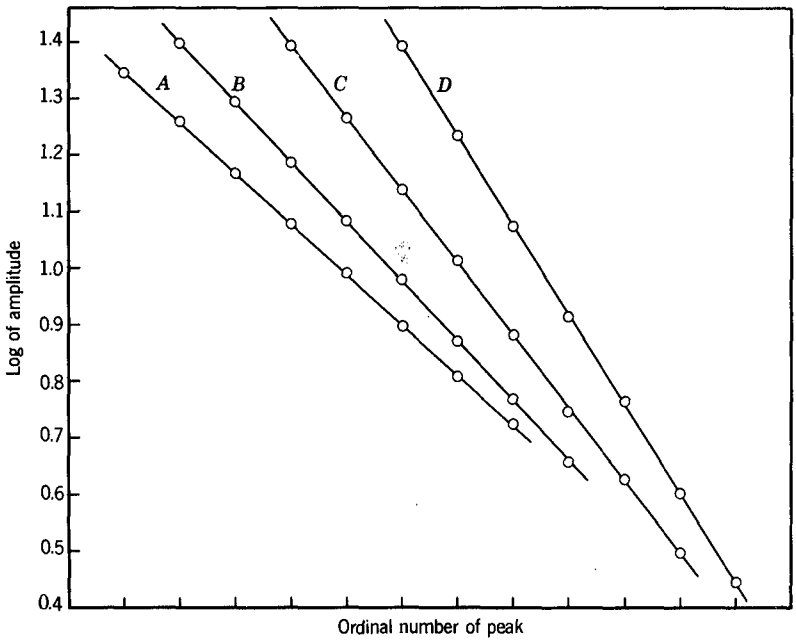


FIG. 6–9. Logarithmic plots of the maximum amplitude obtained from Fig. 6–8 *vs.* oscillation number, to determine logarithmic decrement.

tenuation here provide the components of the complex Young's modulus; equations 39 and 40 of Chapter 5 give E' and E'' instead of G' and G'' if v and r are the velocity and damping ratio respectively of a *longitudinal* wave. A nomograph for the calculation has been drawn by Nolle.[86] The strip is placed under slight constant tension to keep it taut, and longitudinal vibrations are excited in the long direction by an electromechanical driver such as a phonograph cutting head. An electromechanical pickup is then moved along the strip with constant velocity, and its output is compared in amplitude and phase with the driving signal. An automatic

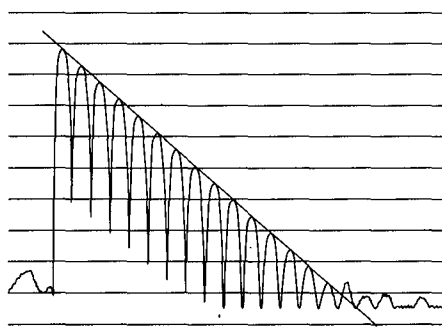


FIG. 6–10. Automatic recording of free torsional oscillations with logarithmic amplitudes. (Koppelmann.[82])

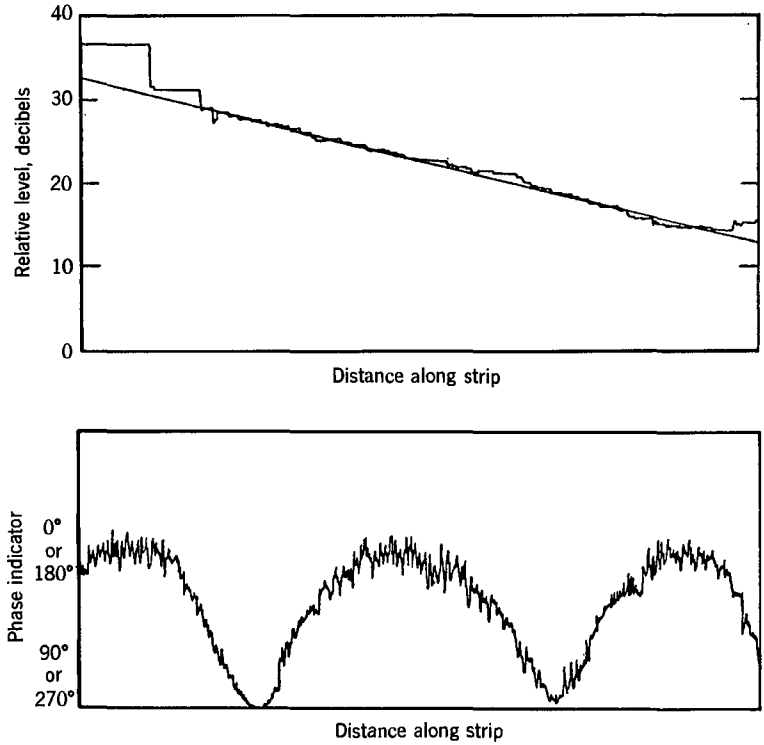


FIG. 6-11. Automatic recording of longitudinal wave propagation along thin strips. (Nolle.[86])

plot of the phase difference gives the wavelength, and the amplitude of the pickup gives the attenuation (Fig. 6-11). It may be noted[87] that the linearity of the plots of logarithm of amplitude and a number of wavelengths against distance is a sensitive test of the linearity of the viscoelastic behavior. The attenuation must be high enough so that no appreciable reflection occurs from the far end of the strip. At the same time, of course, the attenuation cannot be too high, or an insufficient number of wavelengths will be detectable. The coupling with the pickup must be light to prevent reflection back from its point of contact; it is sometimes worthwhile to adjust the contact pressure at each point of measurement,[87] even though this practically eliminates automatic recording.

An alternative is to use flexural waves, excited by transverse motions of an electromechanical driver.[88] A flexural (bending) deformation of a rod or strip measures Young's modulus because one side of the sample is stretched and the other compressed at a bend. For traveling flexural waves, the analogs of equations 39 and 40 of Chapter 5 are (for small damping, $r \ll 1$):[88]

$$E' = (3/\pi^2)\rho v^2(\lambda/d)^2 \tag{18}$$

$$E'' = (12/\pi^2)\rho v^2 r(\lambda/d)^2 \tag{19}$$

where d is the thickness of the strip in the direction of the bending displacement.

In this case, one dimension of the sample must be known with considerable accuracy, in contrast to the extensional waves described above and the shear waves described in Chapter 5 where no dimensions are needed at all. The frequency range is from 100 to 10,000 Hz.

If reflection of the waves occurs at the opposite end of the sample, standing waves can be set up and resonance with high amplitudes is observed when the sample length is an integral number of wavelengths. For this purpose, the sample dimension in the direction of wave propagation should be of the order of several wavelengths rather than very much greater than λ. The damping can be calculated from the shape of a response curve with the frequency varied in the immediate neighborhood of the resonance value, as described in connection with equation 15. This method has been used by Koppelmann[82] with torsional waves in a strip of rectangular cross-section, at frequencies up to 10,000 Hz. Such resonance vibrations are applied much more commonly to measurements on hard solids, as described in Chapter 7.

Longitudinal and flexural waves in thin strips can in general cover a frequency range from the order of 100 to 40,000 Hz, and the frequency can be continuously varied. At much higher frequencies, where the wavelengths are too small to measure conveniently and the requirement that the lateral dimensions are small compared with the wavelength is no longer satisfied, information about dynamic shear behavior can still be obtained by following the propagation of transverse waves in another way. The transit of a shear wave pulse through a sample of known thickness is timed and its decrease in amplitude in transit is also measured. The attenuation and velocity thus determined are substituted directly into equations 39 and 40 of Chapter 5 to calculate G' and G''. In the apparatus of Nolle and Sieck,[89] a shear wave from a suitably cut piezoelectric crystal is sent through two transmission blocks of a hard solid (in this case, glass) separated by a soft polymeric solid of the order of a millimeter thick to a second crystal which serves as a detector. The transit time for wave pulses (several hundred per second) and attenuation are determined by comparing the input and output signals, and correcting for the path in the glass blocks as well as the effects of partial reflection at the interfaces. It is usually necessary, unfortunately, to use thin films of cement between the polymer and the transmitting blocks for mechanical contact; the complications thus introduced can be minimized by comparison with a duplicate system in which the polymer sample has a different thickness, as in the apparatus of Cunningham and Ivey[90] (Fig. 6–12). (Here the transmitting blocks are aluminum.) The method has been used in the range from 0.2 to 10 MHz.

Shear waves can also be propagated through a viscoelastic solid by the incidence of a longitudinal wave through a surrounding liquid which strikes the surface of the solid at a suitable angle. This arrangement is the basis of the methods of Kono[91] and Waterman[92] which will be described in Chapter 8 in connection with bulk longitudinal wave propagation measurements.

The characteristic impedance method with reflection of a shear wave from a quartz surface[93] as described for liquids in Chapter 5 may also be used for soft solids in the megacycle range. In this case, where reflection occurs at an angle, there should be direct contact between the quartz and the sample.

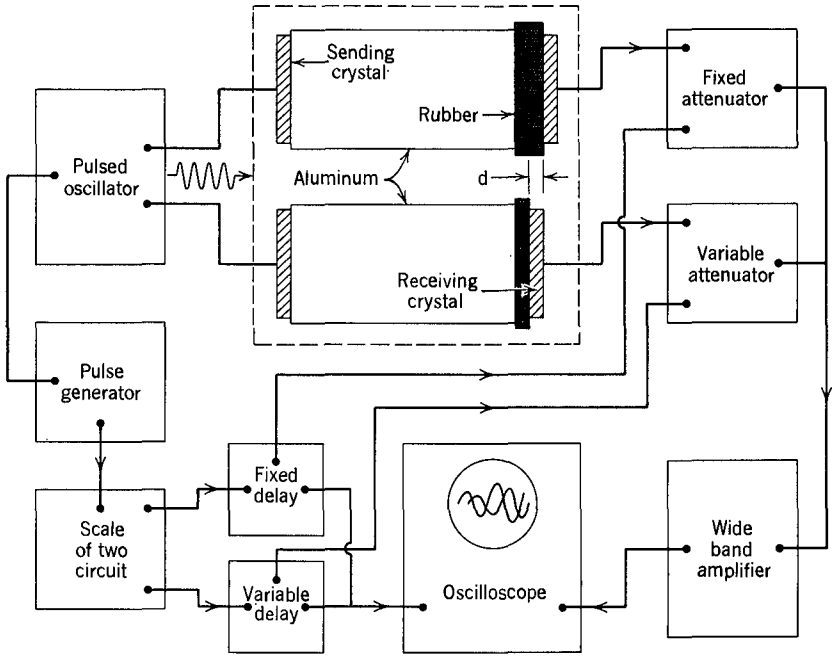


FIG. 6-12. Shear wave pulse apparatus for measuring the components of the dynamic shear modulus in the megacycle range (Cunningham and Ivey[90]).

The discussion of transitions between adiabatic and isothermal conditions in dynamic measurements as given in Chapter 5 is of course relevant to measurements on soft solids as well as on viscoelastic liquids.

E. METHODS WITH OTHER FEATURES

Some other experimental methods with features which do not fit into the preceding classifications will now be mentioned briefly.

1. Simple Extension at Constant Strain Rate

At small deformations, viscoelastic information can in principle be obtained from stress-strain measurements at a constant strain rate, as shown for shear deformations in equations 56 to 59 of Chapter 3. Such experiments are often made in simple extension, but the deformations can become rather large so there are marked deviations from linear viscoelastic behavior. The most commonly used instrument is the Instron tester;[94,95] other carefully designed devices have been described.[96,97] The sample is usually a dumbbell or a ring.[96] In the former case, the strain in the narrow section as checked by separations of several fiducial marks can be calculated from the separation between the clamps by a suitable multiplication factor.[98] In

the latter case, it may be necessary to rotate the sample around the pulleys that stretch it, in order to avoid spurious loss effects.[96]

If the practical tensile strain is defined as $\epsilon = L/L_0 - 1$, where L and L_0 are the stretched and unstretched lengths respectively, the practical tensile strain rate $\dot{\epsilon}$ is $(1/L_0)dL/dt$ (*cf.* equation 60 of Chapter 3), and a constant $\dot{\epsilon}$ can be achieved by pulling the clamps apart at a constant rate.[98] However, if the elongational strain rate is defined as the ratio of the velocity of a material point to its displacement, this quantity, denoted $\dot{\epsilon}_1$, is $(1/L)dL/dt$ and it will remain constant only if the clamps are pulled apart at a rate which increases exponentially with time.[99] Several instruments which accomplish this have been described.[97,100–102a] In that of Münstedt,[102a] very large strains can be accomplished and a variety of stretching patterns including creep, stress relaxation, recovery, and oscillatory deformations can be programmed by computer. An effective alternative is to replace the two clamps by pairs of gears which rotate at a fixed rate to stretch the sample;[103] the length being stretched then remains constant. For a viscoelastic liquid of high viscosity (uncross-linked polymer), this provides the possibility of achieving steady-state elongational flow from which the elongational viscosity $\bar{\eta}$ can be calculated. In the apparatus of Meissner,[103] the sample while being stretched floats on a bath of silicone oil and at a specified time can be cut into several free segments so that their subsequent retraction (recoverable strain) can be determined. Moreover, this instrument can also be used for measurements of elongational creep at constant stress, or various other stress or strain histories. The results of this type of experiment may be expressed in terms of stress growth $\sigma_T(t)$ or a time-dependent extensional viscosity $\bar{\eta}^+(t) = (1/\dot{\epsilon}_1)\sigma_T(t)$.

2. Impact Measurements

When a moving body with a certain momentum strikes another body with high inertia, the detailed course of its deceleration and rebound depends on viscoelastic properties. Such an experiment has been used by Vinh[104] as a source of viscoelastic information. A modified Hopkinson pendulum,[105] with mass about 0.75 kg, swings from fine wires so that a hemispherical surface of steel strikes the flat surface of a thick block of the material to be investigated. The block is very rigidly mounted on concrete. The projectile carries a piezoelectric accelerometer and its position along the direction of swing is monitored by the approach of a steel vane to an inductive unit whose changing inductance causes imbalance of an impedance bridge. A curve of acceleration versus displacement is traced on an oscilloscope. Characteristic shapes are obtained for polymers of different viscoelastic properties. For quantitative evaluation, the experimental curves are matched with simulated curves produced by an analog computer.

3. Sinusoidal Deformations with Large Amplitudes

For investigations of sinusoidally oscillating deformations outside the range of linear viscoelastic behavior, with large amplitudes, a higher power input is necessary

than for the very small deformations used in study of linear viscoelasticity. Care must be taken that heat generation does not alter the sample temperature. Heavy instruments with mechanical drives, especially those of Philippoff[42,106] and Painter,[53] have been useful for this purpose. A device for performing large sinusoidal deformations in shear, extension, or compression has been described by Prevorsek;[107] it provides also for superimposing small deformations at a higher frequency.

4. Combined Static and Dynamic Measurements

Many of the methods previously described can be adapted to measurements with sinusoidal deformations of small amplitude superimposed on large static deformations. In the apparatus of Kawai[47,48] and that of Meinecke,[108] direct measurements of oscillating stress and strain in simple extension can be made in this manner; the Rheovibron has also been used for this purpose.[109] Propagation of longitudinal waves along thin strips which are stretched to a high elongation has been studied by Mason[110] with apparatus similar to that of Nolle.[86] In these examples, the static and dynamic strains are in the same directions. Various other combinations are possible; in the Fitzgerald apparatus,[59] static simple extension can be combined with simple shear, with either the x_1 or the x_3 direction (Fig. 6-1) parallel to the direction of stretch.[111]

5. Dynamic Mechanical Measurements Combined with Other Physical Properties

Considerable information about molecular motions and grosser structural features can be obtained from other physical measurements on polymeric systems which are subjected to sinusoidally varying deformations. This subject is beyond the scope of this book, but reference may be made to dynamic investigations of birefringence,[112-117] infrared absorption,[117-118] light scattering,[119] X-ray scattering,[120,121] dielectric constant,[122] and piezoelectricity,[123,124] as well as studies of simultaneous stress relaxation and time-dependent infrared dichroism by a differential method.[125,126] They have been particularly useful in the study of partially crystalline polymers.

REFERENCES

1. M. Miller, J. D. Ferry, F. W. Schremp, and J. E. Eldridge, *J. Phys. Colloid Chem.*, **55**, 1387 (1951).
2. P. R. Saunders and A. G. Ward, *Proc. 2nd Inter. Congr. Rheol.*, Oxford, 1953, p. 284.
3. H. Oberst, in *Kunststoffe*, edited by Nitsche and K. Wolf, Volume 2, Springer-Verlag, Berlin, 1961, p. 148.
4. W. Philippoff, in *Physical Acoustics*, edited by W. P. Mason, Volume 11B, Academic Press, New York, 1965, p. 1.
5. A. R. Payne, in *Progress in High Polymers*, edited by J. C. Robb and F. W. Peaker, Volume 2, Heywood Books, London, 1968.

6. I. M. Ward, *Mechanical Properties of Solid Polymers,* Wiley-Interscience, London, 1971.
7. T. G. Fox and P. J. Flory, *J. Am. Chem. Soc.,* **70,** 2384 (1948).
8. D. M. Stern, Ph. D. thesis, University of Wisconsin, 1957.
9. L. R. Nielsen, Am. Soc. Testing Matls. Bull. No. 165, p. 48 (1950).
10. C. J. Nederveen and C. W. van der Wal, *Rheol. Acta,* **6,** 316 (1956).
11. W. T. Read, *J. Appl. Mech.,* **17,** 349 (1950).
12. E. R. Fitzgerald and J. D. Ferry, *J. Colloid Sci.,* **8,** 1 (1953).
13. K. Vogel and G. W. Becker, *PTB—Mitt.,* **4,** 332 (1965).
14. K. E. Van Holde and J. W. Williams, *J. Polym. Sci.,* **11,** 243 (1953).
15. J. W. Berge, Ph. D. thesis, University of Wisconsin, 1958.
16. D. J. Plazek, *J. Polym. Sci.,* A-2, **6,** 621 (1968).
17. D. J. Plazek, M. N. Vrancken, and J. W. Berge, *Trans. Soc. Rheol.,* **2,** 39 (1958).
18. G. C. Berry and C.-P. Wong, *J. Polym. Sci., Polym. Phys. Ed.,* **13,** 1761 (1975).
19. K. Walters, *Rheometry,* Chapman and Hall, London, 1975.
20. C. W. van der Wal and R. H. J. W. A. Drent, *Rheol. Acta,* **7,** 265 (1968).
21. W. L. Holt, E. O. Knox, and J. L. Roth, *J. Res. Nat. Bur. Stand.* **41,** 95 (1948).
22. E. N. da C. Andrade, *Proc. R. Soc. (London),* **A84,** 1 (1910); **A90,** 339 (1914).
23. C. A. Dahlquist, J. O. Hendricks, and N. W. Taylor, *Ind. Eng. Chem.,* **43,** 1404 (1951).
24. R. S. Stein and H. Schaevitz, *Rev. Sci. Instrum.,* **19,** 835 (1948).
25. R. D. Andrews, N. Hofman-Bang, and A. V. Tobolsky, *J. Polym. Sci.,* **3,** 669 (1948).
26. O. Kramer, Private communication.
27. R. L. Bergen, in *Testing of Polymers,* edited by J. V. Schmitz, Volume 2, Wiley, New York, 1966, p. 1.
28. A. V. Tobolsky, *J. Appl. Phys.,* **27,** 673 (1956).
29. A. V. Tobolsky and R. D. Andrews, *J. Chem. Phys.,* **13,** 3 (1945).
30. E. Guth, P. E. Wack, and R. L. Anthony, *J. Appl. Phys.,* **17,** 347 (1946).
31. R. D. Andrews and A. V. Tobolsky, *J. Polym. Sci.,* **7,** 221 (1951).
32. P. Thirion and R. Chasset, *Rev. Gen. Caoutch.* **41,** 271 (1964); *Chim. Ind.,* **97,** 617 (1967).
33. R. F. Landel and R. F. Fedors, in *Fracture Processes in Polymeric Solids,* edited by B. Rosen, Interscience, New York, 1964.
34. W. V. Chang, R. Bloch, and N. W. Tschoegl, *J. Polym. Sci., Polym. Phys. Ed.,* **15,** 923 (1977).
35. K. Arai and M. Niinomi, *Kogyo Kagaku Zasshi,* **74,** 2525 (1971).
36. C. R. Taylor, R. Greco, O. Kramer, and J. D. Ferry, *Trans. Soc. Rheol.,* **20,** 141 (1976).
37. J. W. M. Noordermeer and J. D. Ferry, *J. Polym. Sco., Polym. Phys. Ed.,* **14,** 509 (1976).
38. L. R. G. Treloar, *The Physics of Rubber Elasticity,* Oxford, 1975..
39. J. E. Mark, *Rubber Chem. Tech.,* **48,** 495 (1975).
40. L. C. E. Struik and G. A. Schwippert, *TNO Nieuws,* **21,** 285 (1966).
41. K. Arai, *Rep. Prog. Polym. Phys. Jpn.,* **20,** 317 (1977).
42. W. Philippoff, *J. Appl. Phys.,* **24,** 685 (1953).
43. H. Roelig, *Proc. Rubber Technol. Conf.,* 1938, pp. 821–829.
44. L. Mullins, *Trans. Inst. Rubber Ind.,* **26,** 27 (1950).
45. W. P. Fletcher and A. N. Gent, *J. Sci. Instrum.,* **29,** 186 (1952).
46. J. Koppelmann, *Rheol. Acta,* **1,** 20 (1958).
47. K. Fujino, I. Furuta, S. Kawabata, and H. Kawai, *Zairyo,* **13,** 404 (1964).
48. M. Nakatani, K. Iijima, A. Suganuma, and H. Kawai, J. Macromol. *Sci., Phys.,* **B2,** 55 (1968).
49. M. Yoshino and M. Takayanagi, *Zairyo,* **8,** 330 (1959).
50. M. Takayanagi, *Mem. Fac. Eng. Kyushu Univ.,* **23,** 41 (1963); *Proc. 4th Int. Congr. Rheology,* Part 1, Interscience, 1965, p. 161.
51. A. F. Yee and M. T. Takemori, *J. Appl. Polym. Sci.,* **21,** 2597 (1977).
52. R. S. Marvin, E. R. Fitzgerald, and J. D. Ferry, *J. Appl. Phys.,* **21,** 197 (1950).
53. G. W. Painter, *ASTM Bull.,* **177,** 45 (1951).
54. D. J. Massa, *J. Appl. Phys.,* **44,** 2595 (1973).

55. A. R. Ramos and R. E. Cohen, *Polym. Eng. Sci.*, **17,** 639 (1977).
56. C. W. Macosko, R. G. Garritano, and J. M. Starita, *SPE Tech. Papers*, **36,** 2 (1978); W. M. Davis and C. W. Macosko, *Polym. Eng. Sci.*, **17,** 32 (1977).
57. R. E. Wetton and G. Allen, *Polymer*, **7,** 331 (1966).
58. T. E. Morrison, L. J. Zapas, and T. W. DeWitt, *Rev. Sci. Instrum.*, **26,** 357 (1955); H. Markovitz, P. M. Yavorsky, R. C. Harper, Jr., L. J. Zapas, and T. W. DeWitt, *Rev. Sci. Instrum.*, **23,** 430 (1952).
59. E. R. Fitzgerald, *Phys. Rev.*, **108,** 690 (1957).
60. R. S. Marvin, Ph. D. thesis, University of Wisconsin, 1949.
61. D. A. Keiper, *Rev. Sci. Instrum.*, **33,** 1181 (1962).
62. T. L. Smith, J. D. Ferry, and F. W. Schremp, *J. Appl. Phys.*, **20,** 144 (1949).
63. M. H. Birnboim and J. D. Ferry, *J. Appl. Phys.*, **32,** 2305 (1961).
64. C. W. Hargens, private communication.
65. J. H. Dillon, I. B. Prettyman, and G. L. Hall, *J. Appl. Phys.*, **15,** 309 (1941).
66. J. L. Schrag and R. M. Johnson, *Rev. Sci. Instrum.*, **42,** 224 (1971).
67. R. S. Enabnit and S. D. Gehman, *Ind. Eng. Chem.*, **43,** 346 (1951).
68. C. W. Kosten and C. Zwikker, *Physica*, **4,** 221 (1937).
69. W. J. S. Naunton and J. R. S. Waring, *Trans. Inst. Rubber Ind.*, **14,** 340 (1939).
70. S. D. Gehman, D. E. Woodford, and R. B. Stambaugh, *Ind. Eng. Chem.*, **33,** 1032 (1941).
71. H. Goldberg and O. Sandvik, *Ind. Eng. Chem., Anal. Ed.*, **19,** 123 (1947).
72. J. R. Van Wazer and H. Goldberg, *J. Appl. Phys.*, **18,** 207 (1947).
73. W. Philippoff, *Phys. Z.*, **35,** 884 (1934).
74. H. C. Rorden and A. Grieco, *J. Appl. Phys.*, **22,** 842 (1951).
75. I. L. Hopkins, *Trnas. ASME*, **73,** 195 (1951).
76. I. L. Hopkins, *J. Appl. Phys.*, **24,** 1300 (1953).
77. J. Struik, *Rheol. Acta*, **6,** 119 (1967).
78. R. Roscoe, *Br. J. Appl. Phys., Ser. 2*, **2,** 1261 (1969).
79. I. L. Hopkins, *J. Appl. Polymer Sci.*, **7,** 971 (1963).
80. R. A. Dickie and J. D. Ferry, *J. Phys. Chem.*, **70,** 2594 (1966).
81. L. E. Nielsen, *Rev. Sci. Instrum.*, **22,** 690 (1951).
82. J. Koppelmann, *Kolloid-Z.*, **144,** 12 (1955).
83. W. Kuhn and O. Künzle, *Helv. Chim. Acta*, **30,** 839 (1947).
84. K. H. Illers and H. Breuer, *Kolloid-Z.*, **176,** 110 (1961).
85. E. E. Schäfer, Thesis, Aachen, 1966.
86. A. W. Nolle, *J. Appl. Phys.*, **19,** 753 (1948).
87. P. Mason, private communication.
88. G. W. Becker, *Kolloid-Z.*, **140,** 1 (1955).
89. A. W. Nolle and P. W. Sieck, *J. Appl. Phys.*, **23,** 888 (1952).
90. J. R. Cunningham and D. G. Ivey, *J. Appl. Phys.*, **27,** 967 (1956).
91. R. Kono, *J. Phys. Soc. Jpn.*, **15,** 718 (1960); **16,** 1580 (1961).
92. H. A. Waterman, *Kolloid-Z.*, **192,** 1 9 (1963).
93. W. P. Mason, W. O. Baker, J. H. McSkimin, and J. H. Heiss, *Phys. Rev.*, **75,** 936 (1949).
94. H. Hindman and G. S. Burr, *Trans. ASME*, **71,** 789 (1949).
95. Instron Corporation, Canton, Massachusetts.
96. P. Thirion and R. Chasset, *Nippon Gomu Kyokaishi*, **41,** 1122 (1968); *Rev. Gen. Caoutch. Plast.*, **47,** 427 (1970).
97. G. V. Vinogradov, V. D. Fikhman, B. V. Radushkevich, and A. Ya. Malkin, *J. Polym. Sci.*, A-2, **8,** 657 (1970).
98. T. L. Smith, *Trans. Soc. Rheol.*, **20,** 103 (1976).
99. P. Heydemann, *Acustica*, **16,** 124 (1965/66).
100. R. T. Ballman, *Rheol. Acta*, **4,** 137 (1965).
101. T. J. Peng, *JPL Q. Rev.*, **2,** 40 (1972).
102. G. V. Vinogradov, V. D. Fikhman, and V. M. Alekseyeva, *Polym. Eng. Sci.*, **12,** 317 (1972).

102a. H. Münstedt, *J. Rheol.*, **23,** 421 (1979).
103. J. Meissner, *Trans. Soc. Rheol.*, **16,** 405 (1972).
104. N. P. Vinh Tuong, *Mem. Artillerie Fr.*, 1965, p. 67.
105. B. Hopkinson, *Phil. Trans. R. Soc.*, **A213,** 437 (1914).
106. W. Philippoff, *Trans. Soc. Rheol.*, **10,** 317 (1966).
107. Y. D. Kwon, R. K. Sharma, and D. C. Prevorsek, *Polym. Prepr. Am. Chem. Soc.*, **18,** No. 2, 99 (1977).
108. E. A. Meinecke, *Rheol. Acta,* **10,** 302 (1971).
109. A. Voet and J. C. Morawski, *Rubber Chem. Tech.*, **47,** 758 (1974).
110. P. Mason, *J. Appl. Polym. Sci.*, **1,** 63 (1959).
111. E. R. Fitzgerald, *J. Acoust. Soc. Am.*, **33,** 1305 (1961).
112. R. S. Stein, S. Onogi, and D. A. Keedy, *J. Polym. Sci.*, **57,** 801 (1962).
113. D. G. LeGrand and P. F. Erhardt, *Trans. Soc. Rheol.*, **6,** 301 (1962).
114. R. S. Stein, Ed., *Rheo-optics of Polymers* (*J. Polym. Sci.*, **C5**), Interscience, New York, 1964.
115. B. E. Read, *Polymer,* **5,** 1 (1964).
116. S. Onogi, T. Asada, Y. Fukui, and T. Fujisawa, *J. Polym. Sci.*, **5,** 1067 (1967).
117. S. Onogi, T. Sato, T. Asada, and Y. Fukui, *J. Polym. Sci.*, A-2, **8,** 1211 (1970).
118. S. Onogi and T. Asada, *J. Polym. Sci.*, **C16,** 1445 (1967).
119. P. F. Erhardt and D. G. LeGrand, *J. Appl. Phys.*, **34,** 68 (1963).
120. T. Kawaguchi, T. Ito, H. Kawai, D. Keedy, and R. S. Stein, *Macromolecules,* **1,** 126 (1968); H. Kawai, *Rheol. Acta,* **14,** 27 (1975).
121. S. Suehiro, T. Yamada, H. Inagaki, and H. Kawai, *Polym. J.*, **10,** 315 (1978).
122. E. R. Fitzgerald, unpublished experiments.
123. E. Fukada, *Biorheology,* **5,** 199 (1968).
124. K. Koga, T. Kajiyama, and M. Takayanagi, *J. Phys. E,* **8,** 299 (1975).
125. R. Gotoh, T. Takenaka, and N. Hayama, *Bull. Inst. Chem. Res., Kyoto Univ.*, **43,** 369 (1965).
126. R. Gotoh, T. Takenaka, J. Uemura, and S. Hayashi, *Bull. Inst. Chem. Res., Kyoto Univ.*, **44,** 286 (1966).

CHAPTER 7

Experimental Methods for Hard Viscoelastic Solids

The devices of the preceding chapter are designed for viscoelastic solids with moduli in the general range from 10^6 to 10^8 dynes/cm^2 (10^5 to 10^7 Pa); some are appropriate for low values of tan δ, others for intermediate to high tan δ. For harder solids with moduli in the range of 10^9 to 10^{11} dynes/cm^2 (10^8 to 10^{10} Pa), there is no difference in principle in the application of the same experimental methods, and indeed some of them can be used without modification, but some new features appear with the increase in stiffness of several orders of magnitude.

Since $J(t)$ and $J^*(\omega)$ are now not much greater than $B(t)$ and $B^*(\omega)$—*i.e.*, μ is perceptibly less than $\frac{1}{2}$—shear and elongation do not yield equivalent information. Experiments with simple shear or torsion give time-dependent shear moduli and compliances, whereas experiments with simple extension or flexure give time-dependent Young's moduli. The ratio between the respective moduli is itself time-dependent, corresponding to the variable μ in equation 51 of Chapter 1. The shear moduli, $G(t)$ and $G^*(\omega)$, representing the resistance to change in shape alone, are more readily interpretable in terms of molecular properties; nevertheless, Young's modulus, $E(t)$ or $E^*(\omega)$, is often the experimenter's choice, since its measurement is somewhat simpler for hard materials. When $E(t)$ is measured, $G(t)$ can be obtained from it only if $B(t)$ or $K(t)$ or $\mu(t)$ is also known.

When $G > 10^9$ dynes/cm^2, the stiffness of the sample approaches that of structural parts of the apparatus, and the sample shape must be chosen to keep the form factor b as small as possible. Simple shear sandwich geometry is practically eliminated; torsion is applied to long thin rods instead of squat discs; extension is applied to long thin strips, and flexural geometry is especially favored because it can give relatively large displacements. There are several alternative arrangements for the latter, which are illustrated in Fig. 7-1. The extensional strain/stress ratios are obtained from displacement/force ratios for these configurations by equations which supplement those given at the beginning of Chapters 5 and 6. The following

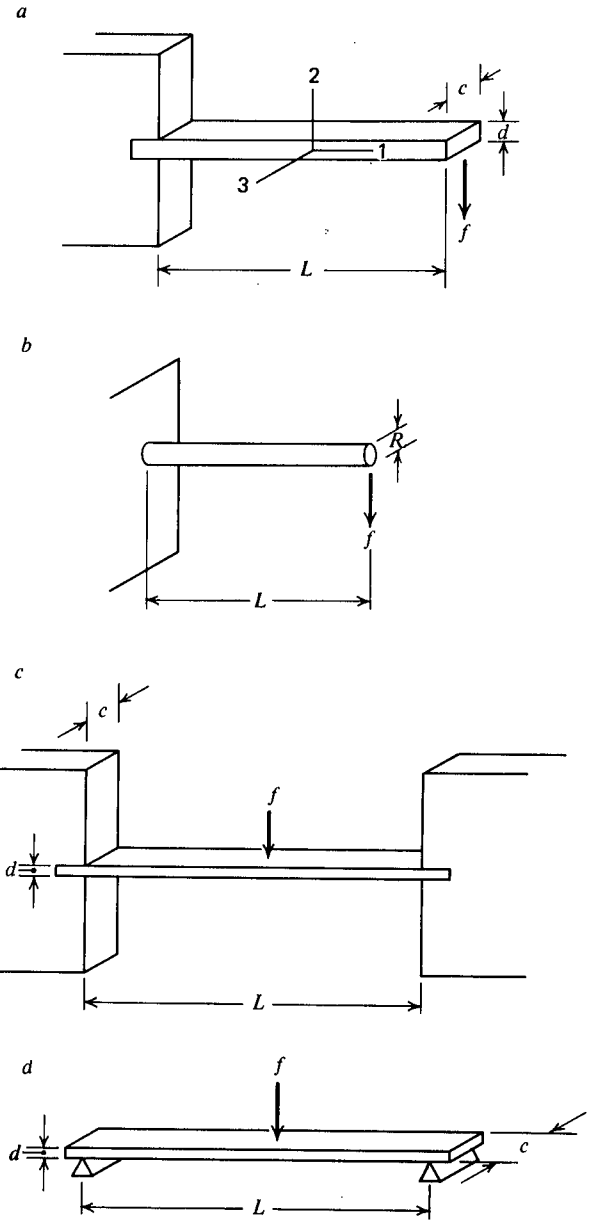


FIG. 7-1. Geometries, coordinates, and dimensions for investigation of hard viscoelastic solids (in addition to some shown in Figs. 5-1 and 6-1). (*a*) cantilever with rectangular cross-section; (*b*) cantilever with circular cross-section; (*c*) flexure of rectangular bar with both ends clamped; (*d*) flexure of rectangular bar with knife edge support.

equation holds for all flexural arrangements:

$$\epsilon/\sigma_T = bx_2/f \tag{1}$$

and the form factor b (dimensions cm) depends on the experimental configuration as follows:

(a) Cantilever flexure, one end clamped, rectangular cross-section:

$$b = cd^3/4L^3 \tag{2}$$

(b) Cantilever flexure, one end clamped, circular cross-section:

$$b = 3\pi R^4/4L^3 \tag{3}$$

(c) Flexure of bar with both ends clamped, rectangular cross-section:

$$b = 16cd^3/L^3 \tag{4}$$

(d) Flexure of bar with knife edge support:

$$b = 4cd^3/L^3 \tag{5}$$

x_2 = linear displacement (perpendicular to direction of stretch in sample)
f = force
c = width of bar
d = thickness of bar (dimension in x_2 direction)
L = length of bar
R = radius of bar of circular cross-section

A modification of arrangement (d) in which the load is applied by two knife edge contacts has also been used.[1]

A. CREEP AND STRESS RELAXATION

For transient experiments the applied stress must often be large, requiring massive construction, and small displacements must be measured accurately. It will suffice to quote a few representative references for specific details: for creep in torsion;[2–4] creep in extension;[5,6] stress relaxation in torsion;[7] and stress relaxation in tension.[8,9] Since the strains are always small, there is no trouble with nonlinear problems arising from large extensions as in the preceding chapter. Care must be taken, however, that the stresses do not exceed the limits of linear viscoelastic behavior; it is desirable to make plots of stress against strain interpolated at equal time intervals (from several relaxation experiments at different strains, or several creep experiments at different stresses) to ensure linearity.[10] A versatile commercial instrument for transient experiments is the Instron Tester mentioned in the preceding chapter,[11] in which the stress is determined by a strain gauge and can be continuously recorded. A device for measuring extremely small elongations and tensile forces on single polymer crystals has been described by Andeen and Hoffman.[12]

An extremely versatile and accurate instrument designed by Sternstein[12a] has been used to subject hard polymeric solids to combined tension and torsion and can be programmed for computerized data acquisition and processing with a variety of loading patterns including creep, relaxation, and recovery.

B. DIRECT MEASUREMENTS OF SINUSOIDALLY VARYING STRESS AND STRAIN

A stress-strain ellipse can be traced for sinusoidal deformations of a hard solid with the methods described previously after suitable modifications in the sample mounting. For example, the versatile apparatus of Philippoff[13] described in Chapters 5 and 6 can be further modified for measurements of hard solids in flexure, using a configuration similar to that of (*c*) in Fig. 7-1. Configuration (*a*) is used by Koppelmann.[14] The calculation of dynamic properties from equation 1 with both f and x_2 sinusoidally varying is analogous to equations 19 and 20 of Chapter 5, except that now the two components of Young's modulus are determined:

$$E' = (f_0/bx_{02}) \cos \delta \tag{6}$$

$$E'' = (f_0/bx_{02}) \sin \delta \tag{7}$$

An ingenious method for steady-state dynamic measurements[15,16] has been applied to hard polymeric solids by Maxwell.[17] A rod of circular cross-section is rotated at a given frequency and simultaneously flexed by a yoke with negligible friction (Fig. 7-2). Each element of the rod undergoes a sinusoidally varying strain in extension; if $\tan \delta \neq 0$, the rod will have a steady-state deflection with components both in the direction of the flexing force (A) and perpendicular to it (B), and the two components are inversely proportional to E' and E'' respectively, thus:

$$E' = f/bA \tag{8}$$

$$E'' = f/bB \tag{9}$$

where the form factor b is given by equation 3. This method has been used over a frequency range from somewhat less than 0.001 to somewhat over 100 Hz. A discussion of the theory of this experiment, and of a related experiment in which

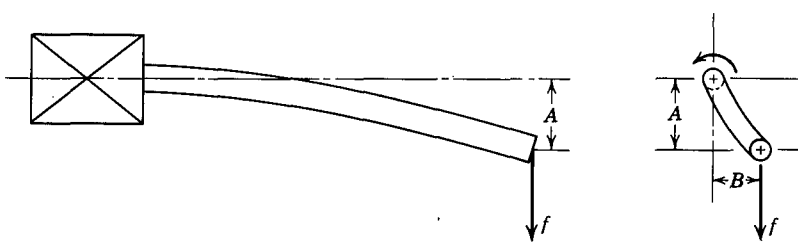


FIG. 7-2. Apparatus for dynamic measurements by a rotating rod strained in flexure. (Maxwell.[17])

sufficient lateral force is applied (and measured) to prevent the horizontal displacement B, has been given by Kaelble.[18]

For measuring G' and G'', the usual geometry is torsion, with the end of a long rod, bar,[14,18a] or tube[19] oscillated through a small angular rotation. The torque and angular displacement can be measured by any of the methods previously described. A torsion pendulum for accurate measurements on hard solids has been described by Cayrol.[20] The form factors for rods and bars are those given by equations 11 of Chapter 5 and 6 of Chapter 6, respectively. That for tubes is $b = \pi(R_2^4 - R_1^4)/2L$, where R_1 and R_2 are the inner and outer radii, and L the length. Apparatus for torsion of bars with direct measurements of torque (by strain gauge transducers) and angle (by deflection of a light beam) has been described by Heydemann.[21] By interfacing to a computer, the relative amplitudes and phase of torque and deflection can be obtained by a cross-correlation analysis which rejects noise and distortion.[22]

C. RESONANCE VIBRATIONS

The methods of the preceding section are of course subject to the usual restriction for direct sinusoidal measurements that the critical dimension of the sample must be small compared with the wavelength of the corresponding elastic wave (flexural or torsional respectively). The opposite extreme is attainable for hard solids only at very high frequencies, since the wavelength is proportional to the square root of the modulus, other things being equal, and we are dealing here with moduli of the order of 10^{10} dynes/cm^2; thus wave propagation is studied only at high frequencies. However, an intermediate situation is readily achieved, where the wavelength is the same order of magnitude as the sample dimensions. Then, at specified frequencies, standing waves can be set up within the sample; *i.e.*, it vibrates in various characteristic modes. This phenomenon was mentioned briefly in Chapter 6 in connection with torsional waves in bar-shaped samples of soft solids. For optimum measurements, it is necessary that $\tan \delta$ be quite small, but for hard viscoelastic solids this is usually the case.

The available frequencies are limited to discrete values corresponding to different vibrational modes, though several sets can be obtained by using samples of different shapes and sizes. Determination of a resonant frequency (in forced vibrations) or characteristic frequency (in free vibrations) permits calculation of the storage modulus; and the corresponding loss tangent is obtained just as in the compound resonance devices discussed in Chapter 6—for forced vibrations, by measurement of the absolute value of the amplitude at resonance, or by constructing a response curve around the resonance frequency and measuring its width, $\Delta\omega$ or $(\Delta\omega)'$; for free vibrations, by measuring the logarithmic decrement Δ.

Since the resonance is determined by the inertia of the sample, and there is no added mass associated with the apparatus, the density ρ enters all the calculations of the storage modulus. The details depend on the sample geometry. Thus, for forced vibrations of a bar or reed in flexure (sample mounted as in Fig. 7-1*a* but with

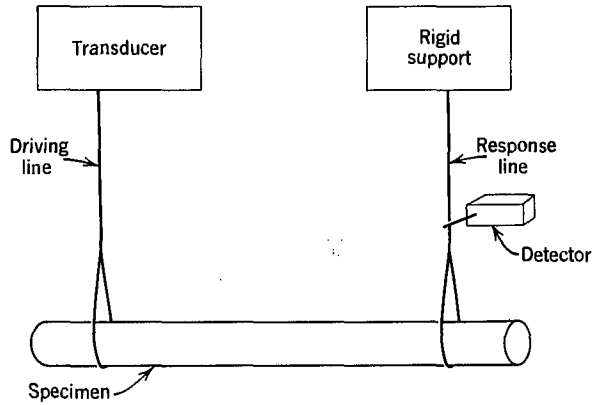


FIG. 7–3. Apparatus for measuring flexural vibrations in a freely suspended rod (Kline.[31])

nothing attached to the free end), the components of the dynamic Young's modulus are given by[23–25]

$$E' = \rho B_n (L^4/d^2)[\omega_0^2 + (\Delta\omega)'^2/2] \tag{10}$$

$$E'' = E' \tan \delta = \rho B_n (L^4/d^2)\omega_0(\Delta\omega)' \tag{11}$$

where L and d are the length and thickness of the reed, and ω_0 and $(\Delta\omega)'$ are defined as in Section C3 of Chapter 6. The numerical coefficients B_n are equal to 0.974, 0.0247, and 0.00315 for the fundamental and first and second harmonic modes of vibration respectively. (Some treatments[26,27] give different results for the last term in equation 10, but this term is usually a very small correction in any case; a general analysis, leading to some rather complicated relations, has been given by Bland and Lee.[28] Correction for the effect of gravity, which may be important at low frequencies, on the reed has been treated by Onogi, Kondo, and Tabata.[29]) In the corresponding equations for free vibration, ω_0 is replaced by ω_c and $(\Delta\omega)'/\omega_0$ by Δ/π. Obviously the dimensions of the sample must be known with high precision. Uniformity of the sample shape is sometimes a troublesome problem. If it is molded, it must be free from anisotropy (*cf.* Section F below), and if it is machined, alteration of the surface must be avoided. In a modification of the geometry of Fig. 7–1*a*, described by Vinh,[24] the sample is clamped at the middle and both ends vibrate.

Flexural vibrations can also be excited in a rod of circular cross-section which is not clamped at all but suspended by fine threads looped around it and subjected to slight oscillating tension at the chosen frequency[30,31] (Fig. 7–3). For vibration in the first transverse mode, the components of Young's modulus are obtained by the equations

$$E' = 12.54\rho(L^4/R^2)\omega_0^2 \tag{12}$$

$$E'' = 12.54\rho(L^4/R^2)\omega_0(\Delta\omega)' \tag{13}$$

where the symbols have their usual significance. In a modification by Shen,[32] a rod

of rectangular cross-section is supported on knife edges and excited in flexural vibrations by small magnets attached to the ends. This device can be operated automatically[33] by a computer, which sweeps through a frequency range near the resonance in three sequences and determines ω_0 and $(\Delta\omega)'$ successively.

Longitudinal resonance vibrations in reeds[34] have also been used to determine E' and E'', and torsional vibrations in rods[35-38] to determine G' and G'' of hard polymeric solids. In longitudinal vibrations, only the length of the sample enters the calculation, and only to the first power, in contrast to the high powers of L, d, and R in equations 10 to 13.

The frequency range of devices of this sort is of the order of 10 to 5000 Hz. Since neither the frequency response curve nor the logarithmic decrement requires an absolute measurement of amplitude, the relative amplitudes are rather easily measured by optical or electrical elements or even by observation with a microscope.[19] The limited choice of frequencies is a serious drawback, however. Usually only a few harmonics can be applied, and, in contrast to the flexibility of the compound resonance devices in Chapter 6, whose frequencies can be adjusted by changing the mass or moment of inertia of the apparatus, a new set of values can be obtained only by shaping a new sample. Temperature control can be satisfactorily arranged, since the mechanical system can easily be isolated in a thermostat, and in fact measurements have been made[39] at temperatures down to 4.2°K.

D. COMPOUND RESONANCE VIBRATION DEVICES

The method of resonance vibrations can be made more versatile by attaching to the sample elements of additional inertia and/or elastance with known properties. These influence its motions in a manner which is analogous to the role of the apparatus inertia in Sections C3 and C4 of Chapter 6 but is much more complicated to analyze. In a comparatively simple example,[40] inertial members are attached to the ends of a bar which undergoes either forced or free vibrations in either flexure or torsion. In a more elaborate arrangement, a layer of polymer is attached to a layer of a high-modulus, low-loss solid. Usually long, narrow metal strips are employed, covered with a uniform thickness of polymer on one or both sides, and suspended from threads or supported on knife edges at nodal points. Flexural vibrations are excited; the resonance frequencies ω_0 and response half-widths $\Delta\omega$ or $(\Delta\omega)'$ depend on the properties of both materials. By knowing the properties of the metal, the corresponding quantities for the polymer alone can be calculated by solving some rather complicated expressions. The theory has been given by van Oort[41] and Oberst.[42]

This method can be used for materials which are too soft or too lossy to support resonance vibrations alone. By making measurements at various vibration modes (up to 20 nodes along the sample length), a considerable frequency range can be obtained with a single sample. The choice of the thickness ratio for the two layers depends on their modulus and loss tangent ratios. Interest in such measurements stems not only from the opportunity of deriving viscoelastic data but also from the

importance of polymeric coatings in reducing vibrational noise of metal plates (Chapter 19).

E. WAVE PROPAGATION

Attenuation and velocity measurements of periodic shear wave pulses can be made on hard solids by the methods described in Section D of the preceding chapter, as well as by the methods of Kono[43] and Waterman[44] to be described in Chapter 8, and the moduli G' and G'' can be calculated from them. In another type of experiment, a single compressive pulse is sent into a rod, such as by detonation of an explosive at one end;[45] the deformation is equivalent to a group of Fourier components with a wide range of frequencies, and in a polymeric material these of course travel with different velocities, so the pulse is distorted and broadened in transit.[46] If the length of the pulse well exceeds the thickness of the rod, the form of E' should in principle be obtainable from studies of the change in shape as determined by recording the deformation-time patterns at the opposite ends of rods of different lengths. The reverse calculation has been successfully made.[47] For thicker rods, however, there is additional distortion from other causes which are mentioned in the following chapter.

A variety of experimental devices similar to those described in this chapter have been devised for study of metals and other nonpolymeric solids.[48-54] In principle, the distinction between isothermal and adiabatic measurements should again be drawn, but in practice the difference between the two will be small.

F. METHODS ADAPTED TO FIBERS

Methods suitable for hard viscoelastic solids in fiber form require some special attention because of the restrictions imposed by sample size and shape. In particular, the sample shape cannot be chosen to suit the experimenter's convenience; often the only dimension which can be adjusted is the length.

Frequently, a fiber is anisotropic, with different properties in different directions.[55] For practical purposes, the only types of deformation which can be readily measured are simple extension, torsion, and flexure. Extension and flexure should both measure Young's modulus E for elongation in the fiber direction, and should therefore yield the same result. Torsion measures the shear modulus G for a direction of slide *perpendicular* to the fiber direction, and in case of anisotropy these moduli E and G are not connected in any simple manner. Some examples of such behavior will be given in Chapter 16.

The fiber cross-section frequently has a shape other than circular, such as the "racetrack" or "dogbone" contours. Although this causes no particular complication for measurements in extension, where the sample coefficient is determined directly by the cross-section area, it makes difficult the calculation of absolute values of viscoelastic properties from measurements in torsion or flexure, which involve higher

moments of the area.[56] Moreover, the lateral dimensions are usually far from uniform.[57]

Another special problem which enters into measurements on a fiber is the necessity of maintaining its content of moisture (or other diluent) constant by equilibrium with a liquid or a vapor of known composition. Although fibers are no more sensitive to traces of diluent than are other hard polymers (glassy or crystalline), their small diameter enables them to absorb or lose diluent rapidly if the composition of the environment fluctuates.

1. Creep and Stress Relaxation

Transient viscoelastic measurements are usually made in simple extension,[58-62] but occasionally in torsion.[63,64] The principal problem is the measurement of rather small deforming forces, since the cross-section area is very small though the modulus is high. Beam balances and electrical (resistance) strain gauges have been successfully employed for extension. In torsion, the concomitant twist of a torsion member in series with the sample (the angle of twist of the torsion member being comparatively small, for stress relaxation, or comparatively large, for creep) can be measured. Even for small forces, the stresses are high, and frequently the smallest experimentally practicable stresses exceed the limits of linear viscoelastic behavior, as illustrated for polycrystalline fibers in Chapter 16.

Stress-strain curves at constant rate of loading or of elongation are also measured by various devices, often with cycling of the loading pattern, and often with automatic recording.[65,66]

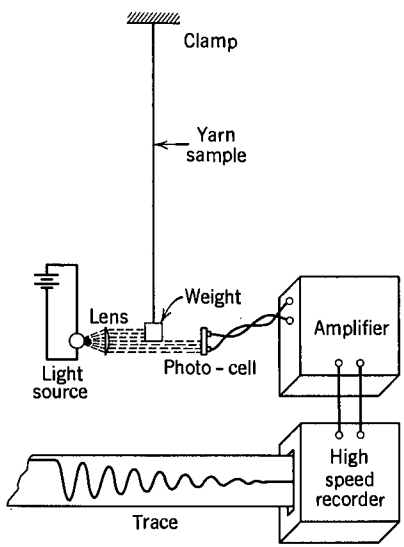


FIG. 7-4. Apparatus of Ballou and Smith[71] for measurement of dynamic Young's modulus of fibers by free vibrations.

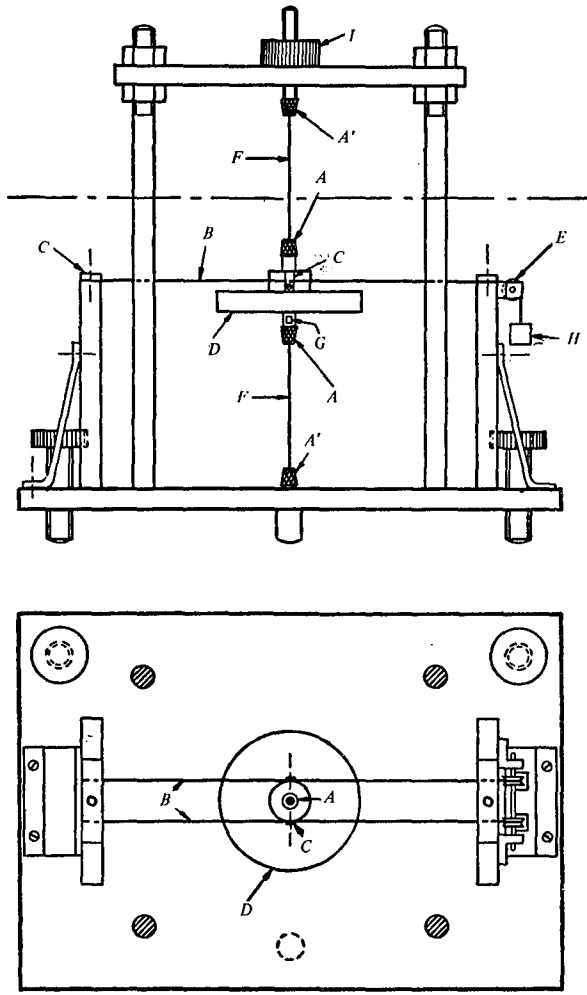


FIG. 7-5. Apparatus of Fujino, Kawai, and Horino[72] for measurement of dynamic Young's modulus of fibers by free vibrations. (*A*, *A'*) Chucks; (*B*) sample fibers; (*C*) clamps; (*D*) inertial disc; (*E*) idler pulleys; (*F*) piano wire; (*G*) mirror to reflect light beam; (*H*) weight to adjust static tension.

2. Dynamic Measurements

Most of the various types of dynamic methods described in preceding chapters have been applied to fibers. The simplest principle, that of direct measurement of sinusoidally varying stress and strain, has been employed below 0.5 Hz by mechanical deformation and optical recording of both stress and strain with rotating mirrors,[67] somewhat in the manner of the corresponding device of Roelig[68] for soft rubberlike polymers (Chapter 6). The Rheovibron of Takayanagi[69] is well adapted to measurements on fibers. At lower frequencies (down to 10^{-3} Hz) an instrument

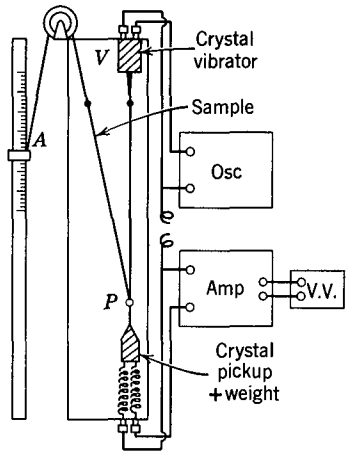


FIG. 7-6. Apparatus for measurement of longitudinal wave propagation in fibers. (Tokita.[73])

with a mechanical drive that rejects noise by cross-correlation analysis has been described by Pinnock and Ward.[70]

Compound resonance devices in free oscillations, where the measurements are a characteristic frequency and a logarithmic decrement of amplitude (Section C4 of Chapter 6), have been widely used. In its simplest form, a mass serves to keep the fiber taut under static stress and also functions as the inertia in longitudinal oscillation[71] (Fig. 7-4). This device is operated in the range from 2 to 20 Hz. Similar geometry, but with horizontal orientation and independent adjustments of inertial mass and static stress, and operation in forced rather than free resonance vibrations, is used in the apparatus of Fujino, Kawai, and Horino[72] which covers the range from 50 to 500 Hz. At lower frequencies, down to 0.04 Hz, torsion pendulums have been used[72,73] in which the samples (two fibers) are actually deformed in extension although the free oscillations of the apparatus are torsional (Fig. 7-5). In other frequency ranges, a rocking beam balance can be used to deform fibers in extension, either freely rocking or attached to a torsion wire at right angles to increase the characteristic frequency.[73] Use of forced oscillations can extend the frequency range to 5 kHz.[74]

Propagation of longitudinal waves along the fiber direction provides measurements of the components of the complex Young's modulus, in accordance with Section D of Chapter 6, in the range from 4 to 200 kHz.[72,73,75] Figure 7-6 shows an example of such an apparatus, in which piezoelectric Rochelle salt crystals are used as driver and pickup. The fiber is doubled back at the pickup, which slides up and down to vary the path length; a more positive contact than the slight sideways pressure used for rubber strips is desirable. The equations for calculation are, as before, the same as 39 and 40 of Chapter 5, which when applied to data for longitudinal waves give E' and E'' instead of G' and G''. In the case of high damping, the pickup amplifier can be lightly coupled to the oscillator so that it records a vector sum of pickup and (attenuated) driving voltages; this permits observing a sufficient number of wavelengths to determine the velocity of propagation.[73] The method

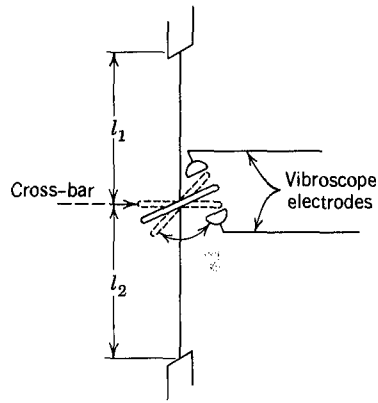


FIG. 7–7. Measurement of dynamic shear modulus of a fiber by forced torsional vibrations. (Wakelin *et al.*[57])

has been adapted to measurements of high precision by Dick and Müller.[76] In another modification,[77,78] longitudinal wave pulses are sent down the fiber (*cf.* Section D of Chapter 6 and Section B3 of Chapter 8).

The method of resonance vibrations (Section C above) has also been used, in the form of standing longitudinal wave measurements[70,73] and flexural vibrations of short fiber segments.[57,69,79,80] In the latter case, the fiber cross-section shape and dimensions must be known with high accuracy; the equations for calculating E' and E'' are similar to equations 12 and 13 (for circular cross-section) but with different numerical coefficients for one end clamped and one free. Despite the small flexural stiffness of thin fibers, this method has been employed on filaments as thin as 0.03 mm^2.

All the dynamic measurements thus far mentioned furnish the complex Young's modulus in the fiber direction. The shear modulus at right angles can be measured by torsional vibrations of the fiber itself, using a light crossbar or disc to provide the amount of inertia for a compound oscillating system in forced[57] or free[56] vibration. An example[57] is shown in Fig. 7–7, where the forced vibrations are driven by an electrostatic device.[81] Here the analog of equation 13 of Chapter 6 is[57]

$$G' = \rho' A' L'^3 \omega_0^2 / 6\pi R^4 [1/L_1 + 1/L_2] \tag{14}$$

where ρ', A', and L' are the density, cross-section area, and length of the crossbar, R is the fiber radius, and L_1 and L_2 are the lengths of the fiber above and below the crossbar attachment.

Apparatus has also been devised for continuous measurement of dynamic mechanical properties during drawing or processing.[82,83]

REFERENCES

1. H. Högberg, *Symposium on Plastics Testing and Standardization,* American Society for Testing Materials, Special Technical Publication No. 247, 1958, p. 95.

2. W. Lethersich, *J. Sci. Instrum.*, **24,** 66 (1947).
3. K. Sato, H. Nakane, T. Hideshima, and S. Iwayanagi, *J. Phys. Soc. Jpn.*, **9,** 413 (1954).
4. J. J. Benbow, in P. Mason and N. Wookey, *Rheology of Elastomers,* Pergamon, London, 1958.
5. K. Van Holde, *J. Polymer Sci.*, **24,** 417 (1957).
6. J. A. Sauer, J. Marin, and C. C. Hsiao, *J. Appl. Phys.*, **20,** 507 (1949).
7. S. Iwayanagi, *J. Sci. Res. Inst. Jpn.*, **49,** 4 (1955).
8. J. R. McLoughlin, *Rev. Sci. Instrum.*, **23,** 459 (1952).
9. K. Nagamatsu, T. Yoshitomi, and T. Takemoto, *J. Colloid Sci.*, **13,** 257 (1958).
10. H. Sommer, Ph. D. thesis, University of Braunschweig, 1958.
11. H. Hindman and G. S. Burr, *Trans. ASME,* **71,** 789 (1949).
12. C. G. Andeen and R. W. Hoffman, *Polym. repr. Am. Chem. Soc.*, **18,** No. 2, 97 (1977).
12a. S. S. Sternstein, U. S. Patent 4096, 741 (1978).
13. W. Philippoff, *J. Appl. Phys.*, **25,** 1102 (1954).
14. J. Koppelmann, *Rheol. Acta,* **1,** 20 (1958).
15. W. Mason, *Engineering;* **115,** 698 (1923).
16. A. L. Kimball and D. E. Lovell, *Trans. ASME,* **48,** 479 (1926).
17. B. Maxwell, *J. Polym. Sci.*, **20,** 551 (1956).
18. D. H. Kaelble, *J. Appl. Polym. Sci.*, **9,** 1201 (1965).
18a. W. M. Davis and C. W. Macosko, *Polym. Eng. Sci.*, **17,** 32 (1977).
19. W. Lethersich, *J. Sci. Instrum.*, **27,** 303 (1950).
20. B. Cayrol, Ph. D. thesis, McGill University, 1972.
21. P. Heydemann, *Acustica,* **16,** 124 (1965–1966).
22. M. H. Birnboim, J. S. Burke, and R. L. Anderson, *Proc. 5th Intern. Congress Rheology,* edited by S. Onogi, University Park Press, Baltimore, 1969, Vol. 1, p. 409.
23. A. W. Nolle, *J. Appl. Phys.*, **19,** 753 (1948).
24. N. P. Vinh Tuong and P. Sorin, *Mem. Artillerie Fr.*, 1963, p. 1979.
25. D. W. Robinson, *J. Sci. Instrum.*, **32,** 2 (1955).
26. M. Horio and S. Onogi, *J. Appl. Phys.*, **22,** 977 (1951).
27. G. W. Becker, *Kolloid-Z.*, **140,** 1 (1955).
28. D. R. Bland and E. H. Lee, *J. Appl. Phys.*, **26,** 1497 (1955).
29. S. Onogi, T. Kondo, and Y. Tabata, *Polym. J.*, **4,** 61 (1973).
30. F. Förster, *Z. Metallkd.*, **29,** 109 (1937).
31. D. E. Kline, *J. Polym. Sci.*, **22,** 449 (1956).
32. M. Shen, J. D. Strong, and F. J. Matusik, *J. Macromol. Sci., Phys.*, **B1,** 15 (1967).
33. M. Shen and H. Schlein, *ACS Polymer Prepr.*, **9,** 1121 (1968).
34. H. S. Sack, J. Motz, H. L. Raub, and R. N. Work, *J. Appl. Phys.*, **18,** 450 (1947).
35. K. Schmieder and K. Wolf, *Kolloid-Z.*, **127,** 65 (1952).
36. J. J. Benbow, *J. Sci. Instrum.*, **30,** 412 (1953).
37. I. Heyboer, P. Dekking, and A. J. Staverman, *Proc. 2nd Intern. Congress Rheology,* Butterworths, London, 1954, p. 123.
38. E. Jenckel, *Kolloid-Z.*, **136,** 142 (1954).
39. K. M. Sinnott, *J. Appl. Phys.*, **29,** 1433 (1958).
40. C. J. Nederveen, *Rheol. Acta,* **3,** 2 (1963).
41. W. P. Van Oort, *Microtecnic,* **7,** 246 (1952).
42. H. Oberst, *Akust. Beih.*, **1952,** p. AB181.
43. R. Kono, *J. Phys. Soc. Jpn.*, **15,** 718 (1960); **16,** 1580 (1961).
44. H. A. Waterman, *Kolloid-Z.*, **192,** 1, 9 (1963).
45. H. Kolsky, *Stress Waves in Solids,* Clarendon, Oxford, 1953.
46. H. Kolsky, *Proc. 2nd Intern. Congress Rheology,* Butterworths, London, 1954, p. 79.
47. H. Kolsky, *Phil. Mag.* [8], **1,** 693 (1956).
48. C. Zener, *Elasticity and Anelasticity of Metals,* University of Chicago Press, 1948.
49. R. L. Wegel and H. Walther, *Physics,* **6,** 141 (1935).
50. F. Birch, *J. Appl. Phys.*, **8,** 129 (1937).

51. F. Birch and D. Bancroft, *J. Geol.*, **46,** 59, 113 (1938).
52. A. Gemant, *J. Appl. Phys.*, **14,** 204 (1943).
53. T. S. Kê, *Phys. Rev.*, **71,** 533 (1947); **72,** 41 (1947).
54. W. N. Findley and W. J. Worley, *Proc. Soc. Exp. Stress Anal.*, **17,** 15 (1959).
55. I. M. Ward, *Mechanical Properties of Solid Polymers,* Wiley, 1971, p. 24 *ff.*
56. R. Meredith, *J. Text. Inst.*, **45,** T489 (1954).
57. J. H. Wakelin, E. T. L. Voong, D. J. Montgomery, and J. H. Dusenbury, *J. Appl. Phys.*, **26,** 786 (1955).
58. H. Leaderman, *Elastic and Creep Properties of Filamentous Materials and Other High Polymers,* The Textile Foundation, Washington, 1943.
59. R. Meredith, *J. Text. Inst.*, **45,** T438 (1954).
60. W. J. Thorsen, *Text. Res. J.*, **22,** 765 (1952).
61. E. T. Kubu, *Text. Res. J.*, **22,** 765 (1952).
62. W. H. Howard and M. L. Williams, *Text. Res. J.*, **33,** 689 (1963).
63. W. G. Hammerle and D. J. Montgomery, *Text. Res. J.*, **23,** 595 (1953).
64. T. Yoshitomi, K. Nagamatsu, and K. Kosiyama, *J. Polym. Sci.*, **27,** 335 (1958).
65. W. Meskat and O. Rosenberg, in H. A. Stuart, *Die Physik der Hochpolymeren,* Volume IV, Springer-Verlag, Berlin, 1956, p. 235.
66. R. Meredith, editor, *Mechanical Properties of Textile Fibers,* North Holland, Amsterdam, 1956.
67. W. Wegener, in E. Wagner, *Mechanische technologische Textilprüfungen,* Wuppertal, 1953, p. 206.
68. H. Roelig, Proc. Rubber Technol. Conf., pp. 821–829 (1938).
69. M. Takayanagi, Proc. 4th Int. Congr. Rheology, Part 1, Interscience, 1965, p. 161.
70. P. R. Pinnock and I. M. Ward, *Proc. Phys. Soc.*, **81,** 261.
71. J. W. Ballou and J. C. Smith, *J. Appl. Phys.*, **20,** 493 (1949).
72. K. Fujino, H. Kawai, and T. Horino. *Text. Res. J.*, **25,** 722 (1955).
73. N. Tokita, *J. Polym. Sci.*, **20,** 515 (1956).
74. B. A. Dunnell and J. H. Dillon, *Text. Res. J.*, **21,** 393 (1951).
75. K. W. Hillier and H. Kolsky, *Proc. Phys. Soc.*, **62B,** 701 (1949).
76. W. Dick and F. H. Müller, *Kolloid-Z.*, **166,** 113 (1959).
77. M. Chaikin and N. H. Chamberlain, *J. Text. Inst.*, **46,** T25 (1955).
78. H. M. Morgan, *Text. Res. J.*, **32,** 866 (1962).
79. J. P. A. Lochner, *J. Text. Inst.*, **40,** T220 (1949).
80. J. C. Guthrie, D. H. Morton, and P. H. Oliver, *J. Text. Inst.*, **45,** T912 (1954).
81. D. J. Montgomery and W. T. Milloway, *Text. Res. J.*, **22,** 729 (1952).
82. F. Breazeale and J. Whisnant, *J. Appl. Phys.*, **20,** 621 (1949).
83. W. Meskat and O. Rosenberg, Reference 65, p. 286.

CHAPTER 8

Experimental Methods for Bulk Measurements

The two basic types of mechanical deformation, from a physical and molecular standpoint, are shear and dilatation. The experimental methods described in the preceding three chapters yield information primarily about shear; only in extension measurements on hard solids does a perceptible volume change influence the results. By combining shear and extension measurements, the bulk properties can be calculated by difference, as for example in creep by equation 55 of Chapter 1, but the subtraction is unfavorable for achieving a precise result. Alternatively, bulk properties can be measured directly, or they can be obtained by combining data on shear and bulk longitudinal deformations (corresponding to the modulus M discussed in Chapter 1), where the subtraction does not involve such a loss of precision. Methods for such measurements will now be described. They have been reviewed in more detail by Marvin and McKinney.[1]

An unfortunate usage of the term "bulk viscosity" is common among polymer chemists, in the sense of the ordinary shear viscosity of a polymer "in bulk," as contrasted with its viscosity in dilute solution. In acoustics, "bulk viscosity" means the viscosity associated with a change in volume, and this definition fits in best with the nomenclature of viscoelasticity. In this book, the complex dynamic bulk viscosity refers to $\eta_v^* = K^*/i\omega$.

A. BULK TRANSIENT MEASUREMENTS

In the bulk analog of a stress relaxation experiment, the sample is suddenly compressed to a smaller volume and the pressure required to hold it at constant volume is recorded as a function of time. Apparatus for this purpose has been described by Matsuoka and Maxwell.[2] In practice, it is more often used to obtain pressure-volume curves at a constant rate of volume decrease, from which the bulk relaxation modulus can be obtained by differentiation; equation 59 of Chapter 3

would be applied, with Δ (volume strain or dilation), P, and $K(t)$ replacing γ, σ, and $G(t)$. Measurements of this sort require the techniques of high-pressure physics;[3,4] in particular, freedom from voids and gas bubbles is naturally very important.

Alternatively, in the bulk analog of a creep experiment, the pressure is maintained constant and the decrease in volume is followed with time. Apparatus for very precise measurements at moderate pressures has been described by Goldbach and Rehage;[5] the volume change is measured by motion of mercury in a capillary. Other devices, suitable for higher pressures, have been used by Mandelkern[6] and by Findley,[7] who measured voluminal deformation by strain gauges.

Closely related information can be obtained without actually changing the external pressure, in an experiment which involves an abrupt temperature change followed by precise measurements of change in volume. If the final temperature is near the glass transition, the volume change is time dependent with a time scale which may extend over many hours.[4,8-10] Though this experiment does not correspond exactly to either creep or stress relaxation, it yields essentially equivalent information, as discussed in Chapter 18. Its applicability is, however, restricted to the immediate vicinity of the glass transition temperature.

B. BULK DYNAMIC MEASUREMENTS

Measurements of bulk viscoelastic properties in sinusoidally oscillating deformations, like those of shear properties, can be classified depending on whether the ratio of sample dimensions to the wavelength of waves propagated at the chosen frequency is small (so that inertial effects can be neglected and the deformation is homogeneous throughout the sample) or large (so that the sample contains a train of waves). The intermediate case where resonance effects are observed has also been exploited. Since the bulk moduli are always of the order of 10^{11} dynes/cm^2, the critical conditions for comparing wavelength with sample size correspond to considerably larger sample dimensions and/or higher frequencies than for shear measurements on liquids or soft solids as described in Chapters 5 and 6.

1. Homogeneous Deformation with Direct Measurement of Pressure

If pressure variations are imposed on material contained within a cavity whose dimensions are small compared to the wavelength of any type of wave which could be propagated through such material, the pressure at every instant can be regarded as constant throughout the cavity. This condition holds in a method described by Philippoff and Brodnyan[11] with direct observation of sinusoidally varying pressure and volume, at frequencies from 3×10^{-4} to 6 Hz. The versatile apparatus of Philippoff,[12] already quoted in connection with shear measurements on liquids and soft solids (Chapters 5 and 6) and flexure of hard solids (Chapter 7), was provided with another attachment for bulk compression measurements; the sample was confined under mercury and compressed by an oil-sealed plunger. From the

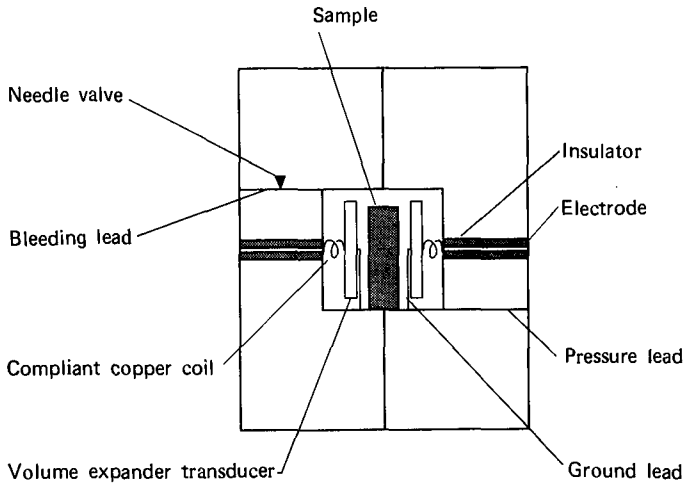


FIG.8-1. Diagram of method of McKinney, Edelman, and Marvin[13] for measuring dynamic bulk viscoelastic properties.

stress-strain ellipse geometry, the components K' and K'' of the complex bulk modulus were obtained after correcting for the compression of the mercury and slight compliances of the apparatus itself. Correction for friction of the plunger was somewhat uncertain.

A method described by McKinney, Edelman, and Marvin[13] provides measurements at considerably higher frequencies, from 50 to 5000 Hz. The sample is confined in a cavity under an inert liquid (Fig. 8-1). Periodic volume changes are imposed by a piezoelectric transducer; a second transducer detects the periodic pressure changes specified by the volume changes and the bulk compliance of the cavity and contents. From the (complex) ratio of the input and output voltages, the components K' and K'' of the dynamic bulk modulus can be calculated, again after correction for the compliances of the oil and the block containing the cavity. The cavity is small compared with the wavelength of a compressional wave at the frequencies employed, so the method is analogous to the shear transducer methods described in Chapter 5, Section D, and Chapter 6, Section C; the inertia of the sample plays no role. A static pressure of the order of 100 kg/cm^2 is imposed initially to force any residual air into solution. Afterwards, measurements may be made at any pressure from 1 to 1000 atm.

The frequency ranges of the two devices described above are such that they measure primarily isothermal and adiabatic moduli respectively (Chapter 5); and the difference between the two will be larger for bulk compression than for any other type of deformation. For a soft polymeric solid with $\alpha = 6 \times 10^{-4}$ deg^{-1} and $K_{is} = 3 \times 10^{10}$ dynes/cm^2, K_{ad} would be higher than K_{is} by about 20% (Chapter 5, equation 41).

2. Homogeneous Deformation by Longitudinal Waves in a Confining Liquid

If a sample immersed in an inert liquid through which traveling or standing

longitudinal waves are propagated has dimensions small compared with the wavelength of such waves, it will undergo uniform periodic compression. A single specimen immersed in a liquid with standing waves with linear geometry has been used by several investigators;[14-16] K' and K'' are derived from the shifts in resonance frequency and half-width of frequency response caused by insertion of the specimen, the method being somewhat analogous to the compound resonance devices of Section C3, Chapter 6. Spherical geometry with a single small specimen at the center of a spherical shell containing the transmitting liquid has been used by Hueter and Blanchard.[17]

Instead of immersing a single specimen, many small particles of polymer may be suspended in the transmitting liquid. The calculation of the bulk viscoelastic properties of the suspended phase from longitudinal wave propagation in the suspension is based on theories by Herzfeld[18] and Urick.[19,20] This method, as exploited by Wada and collaborators,[21,22] is capable of high precision. The particles must be small compared with the wavelength of longitudinal waves in the suspending liquid (ratio of 1/20 or less) and preferably spherical in shape, and must be wetted but not swollen by the liquid; the concentration of particles must be sufficiently small so that the velocity and attenuation of longitudinal waves propagated through the suspension are linear functions of concentration. In practice, a concentration of the order of 10% by volume is usually employed, though it may[22] be as low as 1.6%; and the particle diameter is of the order of 1 micron. Suitable samples are easily obtained by diluting polymer latices prepared by emulsion polymerization. The frequency range is from 1 to 10 MHz, and a range of temperatures can be covered.

The calculation of K' and K'' of the polymer from the velocity and attenuation measurements requires knowledge of the corresponding properties of the suspending liquid and also corrections for scattering and viscous drag of the particles.[21] The method is particularly valuable for investigation of single crystals of polymers.[22]

3. Longitudinal Bulk Wave Propagation

In the compound systems described above, the polymer is subjected to compressional stress only, with no shear components, because the confining liquid transmits no perceptible shear stresses. If, however, longitudinal waves are propagated in a continuous specimen of polymer with at least one dimension large compared with the wavelength, the sample experiences both bulk and shear stresses and deformations which are combined in a manner dependent on the sample shape.

When longitudinal waves are propagated along thin strips, as described for soft solids in Chapter 6, and the wavelength is large compared to the sample thickness but small compared to its length, the deformation corresponds to simple extension and the components of the complex Young's modulus E^* are measured. When the thickness is an appreciable fraction of the wavelength, complications ensue because the lateral contraction characteristic of simple extension is opposed by the elasticity and inertia of the material. The resulting effects, predicted for cylindrical rods by

the Pochhammer-Cree equations, have been discussed by various authors;[23-25] the phase and group velocities differ, and both depend on the ratio of radius to wavelength. The effects are particularly noticeable in the distortion of pulses over and above the distortion due to dispersion such as discussion in Section E of the preceding chapter.

When, at the other extreme, the sample dimension normal to the stress is large compared with the wavelength, the situation becomes relatively simple again and the wave propagation is governed by the complex modulus M^*:

$$M^* = K^* + (\tfrac{4}{3})G^* \tag{1}$$

defined by analogy with equation 50 of Chapter 1. The components of M^* can be calculated from the velocity and attenuation by the analogs of equations 39 and 40 of Chapter 5, with M' and M'' replacing G' and G''.

If the components of G^* have been determined in a separate experiment, those of K^* can be obtained from M^* by difference.[26,27]

$$K' = M' - (\tfrac{4}{3})G' \tag{2}$$

$$K'' = M'' - (\tfrac{4}{3})G'' \tag{3}$$

For a soft solid, in a frequency range where $G' \ll K'$, M' is practically equal to K' and no subtraction is necessary; but K'' and G'' may be of comparable magnitude.

Direct measurements of velocity and attenuation are often made by passage of a train of pulses which is sufficiently long to approximate steady-state oscillating deformation at the chosen frequency—from 0.1 to 30 MHz. The shear wave pulse system of Nolle and Sieck as described in Chapter 6 can be modified by substituting piezoelectric crystals cut to produce longitudinal vibrations, in this case with transmission blocks of aluminum.[28] Alternatively, a liquid can be used as a transmission medium between the crystal and the polymer;[29-31] measurements are made first with, then without, a sample of polymer inserted in the wave path through the liquid, determining the changes in amplitude and phase of a signal echoed back from a reflector (Fig. 8-2) or of a signal sent from a transmitter to a receiver.[31] Since the measurement gives the difference between the bulk longitudinal properties of the polymer and the liquid, the latter must of course be known. The liquid medium has the advantage that no cement is required to establish mechanical coupling, but the liquid must be chosen carefully to avoid swelling the polymer even to a slight extent and thereby modifying the mechanical properties (*cf.* Chapter 17).

Since the subtractions indicated in equations 2 and 3 may cause loss of precision, it is desirable to measure both M^* and G^* in the same experiment with as little manipulation of the apparatus as possible. This can be achieved by propagating both longitudinal and transverse waves through the same sample; the velocity and attenuation of the latter provide G' and G'' in accordance with equations 39 and 40 of Chapter 5. Methods for these measurements have been described by Bradfield,[32] Wada,[33], Kono,[34] and Waterman.[35] In the latter two, the sample in the form of a plate is placed between a transmitting and a receiving transducer as in Fig. 8-2

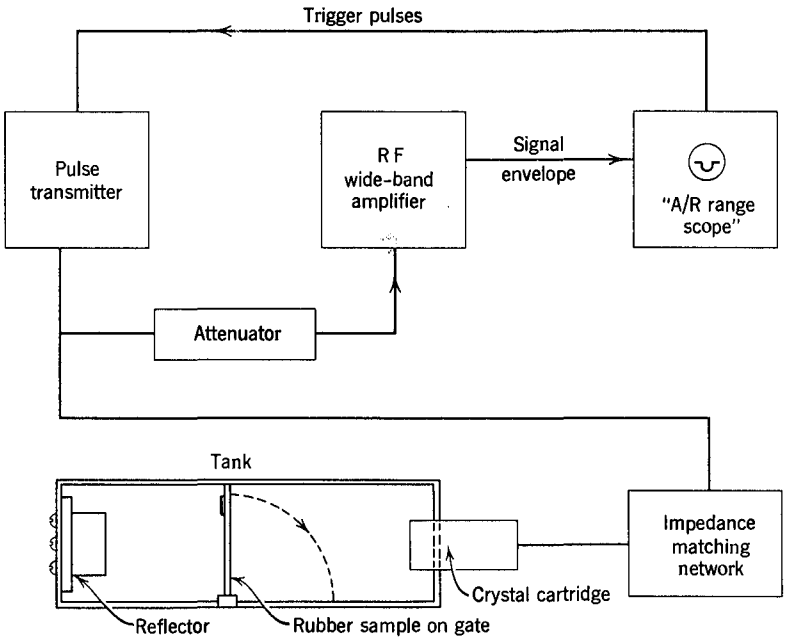


FIG.8-2. Apparatus for longitudinal bulk wave propagation measurements, by echoing longitudinal pulses through a liquid with and without a polymeric sample in the path. (Nolle and Mowry.)[29]

but is rotated at various angles (Fig. 8–3). At normal incidence ($\theta = 0$), only a longitudinal wave is transmitted through the sample; at small angles of incidence, both longitudinal and transverse waves; and at the critical angle for total reflection (θ_l), only a transverse wave. (The transverse wave is transformed to a longitudinal wave when it emerges from the sample back into the liquid.) The value of θ_l provides an alternative determination of longitudinal wave velocity. The transverse wave velocity and attenuation are obtained from measurements at different angles or different sample thicknesses.[33,34] The frequency range for such measurements is from about 0.5 to 5 MHz.

At somewhat lower frequencies, from 30 to 300 kHz, standing waves may be employed in a method devised by Koppelmann,[31] which really belongs in the classification of resonance vibrations rather than wave propagation. Longitudinal "thickness" vibrations are excited across a plate of known thickness d, which is lightly supported at only a few points, by an electrostatically vibrated metal membrane; a second membrane serves as a detector. A series of resonances ω_{0n} is observed, whence the velocity is $v = d\omega_{0n}/n\pi$; the loss tangent is determined from the width of a frequency response curve or from the logarithmic decrement of free vibrations after the driving potential has been switched off. By using periodic on-off pulses, the decrement can be portrayed on an oscilloscope.

In a polymeric liquid with low enough viscosity to permit a receiving element to be moved through it, the liquid itself can be the sole transmitting medium for a bulk longitudinal wave and the attenuation and phase shift can be measured as

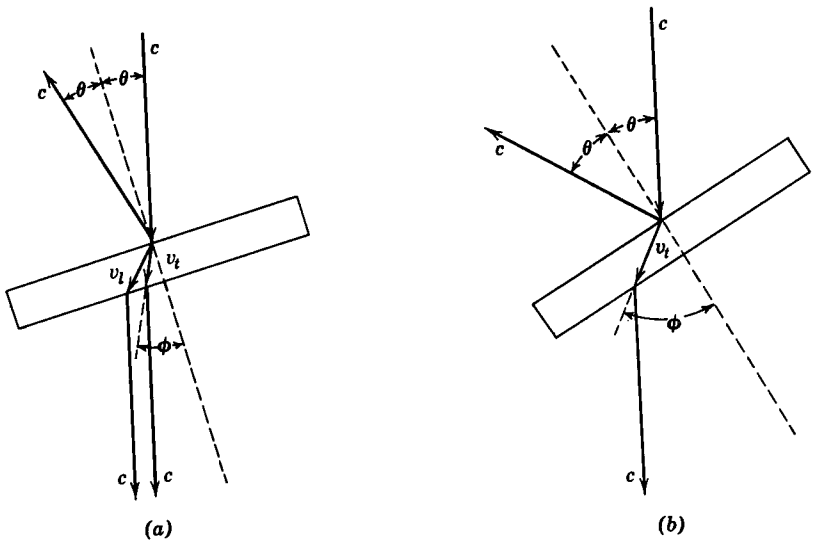


FIG.8-3. Rotating plate method for measurements of longitudinal and transverse wave propagation. The velocity in the liquid medium is c; longitudinal and transverse velocities in the sample are v_t and v_l respectively; θ is angle of incidence, ϕ is angle of refraction for transverse propagation. (a) Partial transmission of longitudinal wave; (b) total reflection of longitudinal wave. (After Marvin.[1])

a function of the distance between the sending and receiving piezoelectric crystals[36] (Fig. 8–4). The calculations are analogous to those for longitudinal wave transmission in thin strips as described in Section G of Chapter 6. The wavelength and attenuation of the traveling wave can also be determined from diffraction of a laser light beam at the Bragg angle;[37] this method is applicable from 50 to 110 MHz. Alternatively, the positions of nodes in standing waves can be determined,[38] with

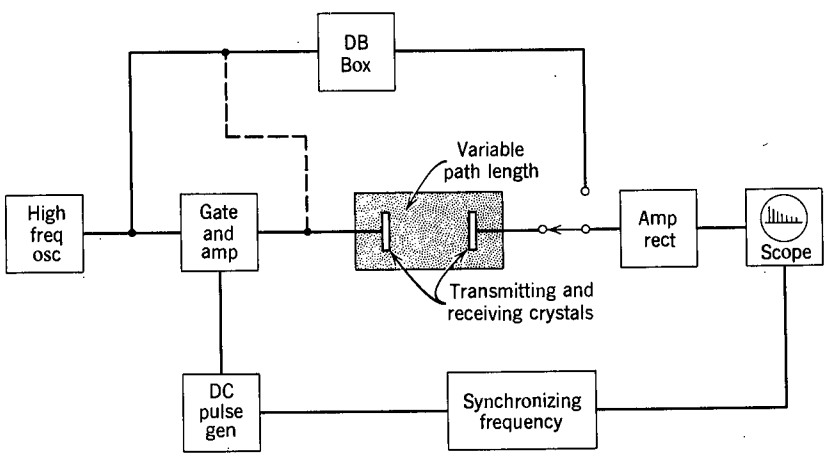


FIG.8-4. Apparatus for longitudinal bulk wave propagation measurements in a viscoelastic liquid, with variable path length. (Mason, Baker, McSkimin, and Heiss.[36])

transducer measurements of attenuation in terms of the electrical resistance of the propagating crystal.

For studies of dilute polymer solutions, measurements of high precision are necessary to obtain the small differences between the properties of solutions and solvent. Apparatus for pulse propagation in such solutions at 20 MHz has been described by Miyahara,[39] Wada,[37] and Hässler,[40] and for variable path interferometry by Cerf,[41] and for standing waves by Miyahara.[42] In the latter method, the frequency can be varied continuously from 1 to 20 MHz. At lower frequencies (10 to 700 kHz), the free decay of waves in a spherical vessel can be measured.[37,43] In such measurements, the data are ordinarily left in terms of M^* (or simply velocity and attenuation, or the acoustic absorption coefficient identified in Chapter 18) with no attempt to convert them to K^*.

REFERENCES

1. R. S. Marvin and J. E. McKinney, in *Physical Acoustics,* edited by W. P. Mason, Volume IIB, Academic Press, New York, 1965.
2. S. Matsuoka and B. Maxwell, *J. Polym. Sci.,* **32,** 131 (1958).
3. P. W. Bridgman, *The Physics of High Pressure,* G. Bell and Sons, London, 1952.
4. R. S. Bradley, *High Pressure Physics and Chemistry,* Academic Press, New York, 1963, Vols. I and II.
5. G. Goldbach and G. Rehage, *Rheol. Acta,* **6,** 30 (1967); *J. Polym. Sci.,* **C16,** 2289 (1967).
6. G. M. Martin and L. Mandelkern, *J. Appl. Phys.,* **34,** 2312 (1963).
7. W. N. Findley, R. M. Reed, and P. Stern, *J. Appl. Mech.,* **34,** 895 (1967).
8. E. Jenckel, in *Die Physik der Hochpolymeren,* edited by H. A. Stuart, Volume III, pp. 621–629, Springer-Verlag, Berlin, 1957.
9. R. O. Davies and G. O. Jones, *Proc. R. Soc.,* **A217,** 26 (1953).
10. A. Kovacs, Sc.D. thesis, University of Paris, 1955; *Adv. Polym. Sci.,* **3,** 394 (1964).
11. W. Philippoff and J. Brodnyan, *J. Appl. Phys.,* **26,** 846 (1955).
12. W. Philippoff, *J. Appl. Phys.,* **24,** 685 (1953).
13. J. E. McKinney, S. Edelman, and R. S. Marvin, *J. Appl. Phys.,* **27,** 425 (1956); J. E. McKinney, H. V. Belcher, and R. S. Marvin, *Trans. Soc. Rheol.,* **4,** 346 (1960).
14. E. Meyer and K. Tamm, *Akust. Z.,* **7,** 4 (1942).
15. C. S. Sandler, *J. Acoust. Soc. Am.,* **22,** 685 (1950).
16. W. S. Cramer and I. Silver, *Navord Report 1778* (1951).
17. T. F. Hueter and B. E. Blanchard, quoted in reference 1 (1957).
18. K. F. Herzfeld, *Phil. Mag.,* [7], **9,** 752 (1930).
19. R. J. Urick, *J. Appl. Phys.,* **18,** 983 (1947).
20. R. J. Urick and W. S. Ament, *J. Acoust. Soc. Am.,* **21,** 115 (1949).
21. Y. Wada, H. Hirose, H. Umebayashi, and M. Otomo, *J. Phys. Soc. Jpn.,* **15,** 2324 (1960).
22. K. Arai, O. Yano, and Y. Wada, *Rep. Progr. Polym. Phys. Jpn.,* **11,** 267 (1968).
23. H. Kolsky, *Stress Waves in Solids,* Clarendon, Oxford, 1953.
24. W. P. Mason, *Piezoelectric Crystals and Their Applications in Ultrasonics,* Van Nostrand, New York, 1950.
25. W. P. Mason, *Physical Acoustics and Properties of Solids,* Van Nostrand, New York, 1958.
26. R. S. Marvin, R. Aldrich, and H. S. Sack, *J. Appl. Phys.,* **25,** 1213 (1954).
27. K. F. Herzfeld and T. A. Litovitz, *Absorption and Dispersion of Ultrasonic Waves,* Academic Press, New York, 1959.
28. A. W. Nolle and P. W. Sieck, *J. Appl. Phys.,* **23,** 888 (1952).
29. A. W. Nolle and S. C. Mowry, *J. Acoust. Soc. Am.,* **20,** 432 (1948).

30. H. S. Sack and R. W. Aldrich, *Phys. Rev.*, **75,** 1285 (1949).
31. J. Koppelmann, *Kolloid-Z.*, **144,** 12 (1955).
32. G. Bradfield, *Fourth Intern. Congr. Acoustics,* Copenhagen, 1962, Paper K-17.
33. Y. Wada, H. Hirose, T. Asano, and S. Fukutomi, *J. Phys. Soc. Jpn.*, **14,** 1064 (1959).
34. R. Kono, *J. Phys. Soc. Jpn.*, **15,** 718 (1960); **16,** 1580 (1961).
35. H. A. Waterman, *Kolloid-Z.*, **192,** 1, 9 (1963).
36. W. P. Mason, W. O. Baker, H. J. McSkimin, and J. H. Heiss, *Phys. Rev.*, **73,** 1074 (1948); *ibid.*, **74,** 1874 (1949).
37. K. Ono, H. Shintani, O. Yano, and Y. Wada, *Polym. J.*, **5,** 164 (1973).
38. R. Cerf and G. Laville, *J. Chim. Phys.*, **53,** 292 (1956).
39. H. Nomura, S. Kato, and Y. Miyahara, *Mem. Fac. Eng. Nagoya Univ.*, **27,** 72 (1975).
40. H. Hässler and H. J. Bauer, *Kolloid-Z., Z. Polymere,* **230,** 194 (1969).
41. R. Cerf, *Acustica,* **13,** 57, 417 (1963).
42. S. Kato, H. Nomura, and Y. Miyahara, *Polymer J.*, **11,** 455 (1979).
43. T. Ohsawa and Y. Wada, Japan, *J. Appl. Phys.*, **6,** 135 (1967).

CHAPTER 9

Dilute Solutions: Molecular Theory and Comparison with Experiments

Although the phenomenological theory of viscoelasticity, whose results were summarized in Chapters 3 and 4, is of great value for interrelating different kinds of experimental measurements, and for formulating certain limits on the behavior of polymeric systems, it provides no insight into the molecular origin of viscoelastic behavior. Qualitatively, we have seen in Chapter 1 that the prominence of viscoelastic phenomena in polymers is associated with the versatility of movement of flexible threadlike macromolecules. In Chapters 2 and 3, scrutiny of the shapes of the viscoelastic functions revealed certain characteristic features which were roughly correlated with different types of molecular motions. We must now examine these processes in more detail and attempt to relate quantities with molecular parameters. The discussion is largely limited to linear viscoelastic behavior.

The simplest example in Chapter 2 was a dilute solution of a linear polymer, for which no complications attributable to entanglements appeared, despite a rather high molecular weight. Development of molecular theory has progressed farthest for this type of system, in which the molecules can be considered as essentially isolated from each other and the treatment of a single molecule suffices. Experimental data are in practice never taken at concentrations sufficiently low to eliminate all intermolecular interactions and hence must be extrapolated to infinite dilution to compare with molecular theory. For reliable extrapolation, the concentrations (c) must usually be less than 10^{-2} g polymer per cm^3 solution, and for this requirement very sensitive measurements are needed.

The appropriate viscoelastic functions are ordinarily the complex modulus or the complex viscosity, and the corresponding quantities extrapolated to infinite dilution are the intrinsic storage and loss moduli

$$[G'] = \lim_{c \to 0} G'/c \tag{1}$$

$$[G''] = \lim_{c \to 0} (G'' - \omega\eta_s)/c \tag{2}$$

or the corresponding intrinsic viscosities (*cf.* equations 31 and 32, Chapter 1)

$$[\eta'] = \lim_{c \to 0} (\eta' - \eta_s)/\eta_s c \tag{3}$$

$$[\eta''] = \lim_{c \to 0} \eta''/\eta_s c \tag{4}$$

where ω is radian frequency and η_s solvent viscosity. The contribution of the solvent has been subtracted in equations 2 and 3. The adjective "intrinsic" is of course used by analogy with the familiar intrinsic viscosity, which is

$$[\eta] = \lim_{c \to 0} (\eta_0 - \eta_s)/\eta_s c = \lim_{\omega \to 0} [\eta'] = \lim_{\omega \to 0} [G'']/\omega\eta_s \tag{5}$$

where η_0 is the steady-flow solution viscosity (at vanishing shear rate).

In the theories for many molecular models, $[G']$ and $[G'']$ are predicted to be proportional to RT/M, where M is molecular weight (if uniform). Hence theoretical predictions are conveniently expressed by the reduced dimensionless intrinsic moduli

$$[G']_R = [G']M/RT \tag{6}$$

$$[G'']_R = [G'']M/RT \tag{7}$$

This chapter describes theories based on various models for rigid and flexible molecules and their comparison with experiment. The effects of intermolecular interaction at finite but low concentrations are discussed; extensions of theory to higher concentrations, undiluted polymers, and cross-linked systems are treated in Chapter 10.

In general, dilute-solution theory of linear viscoelastic properties describes a transition from a *low-frequency* regime in which a Newtonian viscosity is measured but elastic energy is stored during flow and normal stresses appear, to a *high-frequency oscillatory* regime. In the former, rotations of rigid molecules and all possible configurational rearrangements of flexible molecules occur within the period of oscillation. In the latter, neither type of motion occurs within the period; it corresponds in a sense to the glasslike response of an undiluted polymer at high frequencies (Chapter 2), but differs in that the mechanical behavior is still dominated by the Newtonian viscosity of the solvent; the solute represents a minor perturbation of the solvent flow throughout the range of times or frequencies.

The results of molecular theory are presented here without derivations, which can be found in the references cited. The most complete treatment is given by Bird and coauthors.[1]

A. RIGID SOLUTE MOLECULES

Any rigid solute molecule will have a finite $[\eta]$ and $[G'']_R$; it may also be expected to have a finite $[G']_R$ at sufficiently high frequencies if it is asymmetric.[2] When a dilute solution of asymmetric molecules is subjected to steady shear flow, the distribution of orientations departs from spherical symmetry, as is well known from the classical theory of flow birefringence;[3] the resulting decrease in entropy corresponds to a storage of elastic energy. The orientation is opposed by Brownian motion, in which random thermal movements tend to produce a uniform distribution of orientations. The rate of such motion for an axisymmetric molecule can be characterized by a rotatory diffusion coefficient D, or by a relaxation time $\tau = 1/6D$ which is a measure of the time required for end-over-end rotation; it has the physical significance that an imposed preferred orientation reverts to random orientation with an exponential time decay, proportional to $e^{-t/\tau}$. For sinusoidally oscillating flow at frequencies $\omega \gg 1/\tau$, the orientation cannot keep pace with the alternating shear rate and less energy is dissipated, so the dynamic viscosity falls with increasing frequency to a value characteristic of the high-frequency regime. There are a few macromolecules which behave in this manner, mostly of biological origin.

1. Elongated Rodlike Models

Several theories based on elongated rigid axisymmetric models for a macromolecule predict frequency dependence of the dynamic shear moduli and intrinsic viscosities which can be expressed in the following form:

$$[G']_R = m_1\omega^2\tau^2/(1 + \omega^2\tau^2) \tag{8}$$

$$[G'']_R = \omega\tau[m_1/(1 + \omega^2\tau^2) + m_2] \tag{9}$$

$$\tau \doteq m[\eta]\eta_s M/RT, \qquad m = (m_1 + m_2)^{-1} \tag{10}$$

$$[\eta']/[\eta] = m[m_1/(1 + \omega^2\tau^2) + m_2] \tag{11}$$

$$[\eta'']/[\eta] = mm_1\omega\tau/(1 + \omega^2\tau^2) \tag{12}$$

The numerical coefficients m_1 and m_2 depend on the details of the model. Several are given in Table 9-I for highly elongated rodlike molecules of various shapes. The "shishkebab" is a linear array of centers of frictional resistance ("beads") spaced by a uniform distance b; the length is $L \gg b$. For the prolate ellipsoid, $L \gg B$ where B is the minor axis. For the cylinders, values for L and the diameter d must be assigned, and the examples are taken from specific applications in the literature. The differences among the models are not great.

Table 9-I also includes values of the reduced intrinsic steady-state compliance, j^0_{eR}, which is defined as

$$j^0_{eR} = \frac{RT}{M[\eta]^2} \lim_{c\to 0} J^0_e/c \tag{13}$$

Table 9-I

NUMERICAL COEFFICIENTS FOR HIGHLY ELONGATED RODLIKE MACROMOLECULES

Model	Author	m_1	m_2	m^*	j^0_{eR}	Condition	Ref.
Shishkebab	Kirkwood, Auer	3/5	1/5	5/4	15/16	$L/b \gg 1$ [a]	4
Prolate ellipsoid	Cerf	3/5	6/25	25/21	0.85	$L/B \gg 1$	5
Rigid dumbbell [b]	Bird	3/5	2/5	1	3/5	—	6
Cylinder	Ullman	0.46	0.16	1.61	1.19	[c]	7,8
Cylinder	Yamakawa	3/5	0.29	1.15	0.79	[d]	9,10

[a] I.e., the number of beads is large.

[b] This result is for absence of hydrodynamic interaction (*cf.* Section B2 below). For the effect of hydrodynamic interaction, and the extension of the rigid dumbbell to the shishkebab model, the reader is referred to the treatise by Bird and coauthors,[1] Chapter 11.

[c] $L = 3870$ Å, $d = 25$ Å.

[d] $L/d = 150$.

where J^0_e is the steady-state compliance, which would in principle be measured from a creep experiment or calculated from G' at very low frequencies by equation 34 of Chapter 3. Note that j^0_{eR} is the zero-frequency limit of $[G']_R/[G'']^2_R$. For these

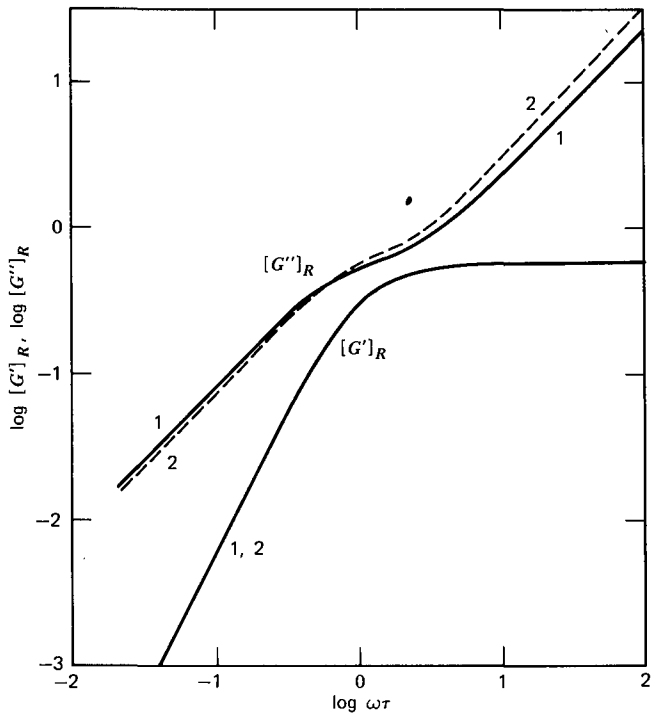


FIG. 9-1. Logarithmic plots of $[G']_R$ and $[G'']_R$ against $\omega\tau$ from equations 8 and 9, for Cerf prolate ellipsoid (1) and Yamakawa cylinder (2) with coefficients m_1 and m_2 as given in Table 9-I.

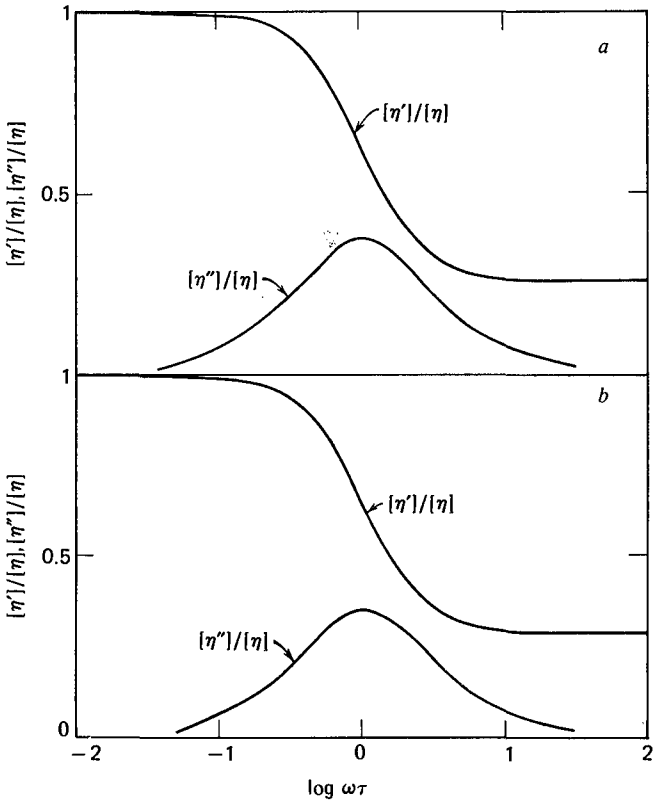


FIG. 9-2. Plots of $[\eta']/[\eta]$ and $[\eta'']/[\eta]$ against log $\omega\tau$ from equations 11 and 12, for Kirkwood-Auer shishkebab (*a*) and Cerf prolate ellipsoid (*b*).

models, $j^0_{eR} = m_1 m^2$. [In the terminology of Bird and collaborators,[1] $j^0_{eR} = nkT\alpha_2/(\alpha_1 - \eta_s)^2$.]

Curves corresponding to equations 8 and 9 are plotted against log $\omega\tau$ in Fig. 9-1 for the Cerf ellipsoid and the Yamakawa cylinder with coefficients from Table 9-I, and curves corresponding to equations 11 and 12 are plotted in Fig. 9-2 for the Kirkwood-Auer shishkebab and the Cerf ellipsoid. There are characteristic abrupt changes in the frequency dependence of each function near $\omega\tau = 1$; at high frequencies, $[G']_R$ levels at the value m_1 and $[\eta']/[\eta]$ becomes equal to mm_2.

The rotational relaxation time can be calculated from molecular dimensions; except for the dumbbell, it is

$$\tau = (\pi\eta_s L^3/18kT)\, F(L/d) \tag{14}$$

where k is Boltzmann's constant and F is a slowly varying function of L/d (or L/b, or L/B) which depends on the individual model. For homologous macromolecules with the same cross-section area, τ is nearly proportional to L^3. For the dumbbell model, τ is proportional to L^2.

Two systems have been investigated which show this rigid elongated rodlike

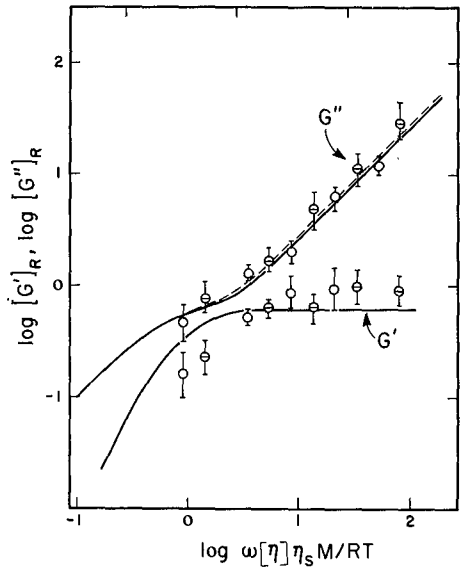


FIG. 9-3. Logarithmic plots of $[G']_R$ and $[G'']_R$ against $\omega[\eta]\eta_s M/RT$, for tobacco mosaic virus in 50.7% aqueous glycerol solvent. Open circles at 37.8°C; slotted circles at 25.0°C. Solid curves, Kirkwood-Auer theory; dashed curves, Cerf ellipsoid theory.

behavior. One is tobacco mosaic virus[11] ($M = 39 \times 10^6$, $L = 3000$ Å), for which $[G']_R$ and $[G'']_R$ are compared with theory in Fig. 9-3. (Here the reduced frequency is conveniently chosen as $\log \omega[\eta]\eta_s M/RT$, since τ is not known *a priori;* it differs from $\log \omega\tau$ only by $\log m$, which must be determined from the choice of model.) The agreement is reasonably good within the large uncertainty of the very small values of $[G']$ and $[G'']$ associated with such a high molecular weight (note equations 6 and 7). The relaxation time agrees rather well with that calculated from molecular dimensions by equation 14 with F taken from a theory for rods by Broersma.[12] Linearly aggregated tobacco mosaic virus with an average of three to four rods joined end-to-end was also found to have $[G']_R$ and $[G'']_R$ (measured only for $\omega\tau \gg 1$) in agreement with theory. The other macromolecule that has been found to be rodlike is fibrin oligomer, formed by partial polymerization of fibrinogen in the presence of an inhibitor to prevent complete polymerization to a fibrin clot (gel).[10] The rigidity of the oligomer may have important implications concerning the structure of the clot.

Values of τ determined in this manner may be compared with estimates from other physical measurements such as flow birefringence, electrical birefringence, and forward depolarized Rayleigh spectra.

2. Other Rigid Models

Models with arbitrary rigid arrays of equally spaced centers of frictional resistance (rigid bead-rod models) that are axisymmetric, *i.e.*, have two equal moments

of inertia, also have frequency-dependent moduli and intrinsic viscosities which are given by equations 8, 9, 11, and 12. Several cases have been treated by Hassager.[2,13] For a rigid "tridumbbell," with a central bead and six rods of equal length terminated by beads, $m_1 = 0$, $m_2 = \frac{3}{2}$; there is no viscoelasticity and the intrinsic viscosity is independent of frequency. However, if one arm of the model is extended by two more colinear rods and beads, $m_1 = 0.31$ and $m_2 = 0.83$ (in Hassager's notation, $m_1 = b$ and $m_2 = a\lambda/2$). The relaxation times, in terms of molecular dimensions, are expressed in terms of the spacing between beads (rod length) and the friction coefficient (force per unit velocity) of a bead. Various macromolecules of biological origin might be modeled in this way.

3. Jointed Bead-Rod Model, Three Beads

A model of three beads joined by two rigid rods but with a universal joint at the center has also been treated by Hassager.[13] Here $[G']_R$ is expressed by several terms with the form of the right side of equation 8; most of the contribution is from two longest relaxation times in the ratio of 1:0.437, with small contributions from shorter relaxation times. The other functions have corresponding added terms. The fibrinogen molecule has been modeled in this way,[10] although recent work[13a] suggests that there are flexible regions in the middle of each rod instead of at the center bead.

B. LINEAR FLEXIBLE RANDOM COILS: THE BEAD-SPRING MODEL

More commonly, a linear polymer molecule does not have internal structure that endows it with rodlike rigidity, but rather has a randomly contorted configuration which is continually changing as rotation occurs around the bonds of the chain backbone. The average configuration of such a molecule in dilute solution is determined by the relative energy minima of various isomeric conformations involving sequences of three or four monomer units,[14,15] as well as by thermodynamic interaction with the solvent. The rapidity with which the configuration changes depends on energy maxima separating these conformations, which may be affected also by the nature of the solvent, and also on the viscous resistance encountered by portions of the chain as they move through the solvent. The driving force for these changes (Brownian motions) is the thermal energy. There will clearly be many kinds of configurational changes; those involving relative motions of parts of the chain close to each other may depend primarily on the internal structure of the molecule, and those involving relative motions of parts widely separated probably depend primarily on viscous resistance of the solvent.

If external shearing forces are applied to the dilute solution, and they are small enough to correspond to the usual restrictions of linear viscoelastic behavior, the assortment of configurations and the rates of configurational change are only slightly disturbed; the Brownian motions go on just the same. But these motions

are influenced by the applied forces so that the response is not the simple shear flow which would be observed for the solvent without the polymeric solute.

A qualitative discussion could be pursued in terms of any of the viscoelastic functions surveyed in Chapter 2. It is convenient for the moment to choose the components of the dynamic modulus, G' and G''. For a periodic strain, the energy storage per cycle depends on G', and is contributed by the polymeric solute molecules alone; the energy dissipation depends on G'', and has contributions from both solute and solvent. The relative contributions of the solute to G' and G'' depend on the extent to which the Brownian motions are correlated with the external forces. Force in phase with displacement corresponds to energy storage, but force in phase with velocity corresponds to energy dissipation.

On a scale of atomic dimensions (*cf.* Fig. 1-1), the configurational motions must be accounted for by rotations around all the bonds in the chain backbone. For complete specification of a configuration, with all the positions of jP backbone atoms relative to each other (P being the degree of polymerization, and j the number of chain atoms per monomer unit—often 2), a point in configuration space with $3jP$ dimensions would be required.[16-18] It can be seen qualitatively that for very high frequencies there will be no time for any internal rotations within a period of alternation and the response of the polymer molecule will be limited to bending and stretching chemical bonds; it can be thought of as a random coil of stiff wire, and G' for the solution should be frequency independent and relatively high (though not high on an absolute basis, because there are only a few such coils per unit volume in a dilute solution). At such high frequencies, G'' will be proportional to ω, reflecting a viscosity $\eta' = G''/\omega$ which is slightly higher than that of the solvent because of the volume occupied by the effectively immobile coils. At lower frequencies, regions of the chain not too far removed from each other have time to change their relative positions within a period of cyclic deformation; each coil deforms more easily and G', which is contributed solely by these coils, is smaller. Also, G'' will be somewhat smaller; the relative magnitudes of G' and G'' depend on the phase relations of configurational changes. At very low frequencies, all possible configurational rearrangements occur within the period of a cycle, and the coils deform so easily that the force in phase with displacement is negligible; G', which the phenomenological theory of Chapter 3 shows must become proportional to ω^2, vanishes compared to G'', which is proportional to ω. The ratio G''/ω at low frequencies becomes the steady-flow viscosity which has a substantial contribution from the polymer solute as prescribed by the well-known features of intrinsic viscosity.[19]

The complete specification of molecular configuration would require a detailed knowledge of the dimensions and shapes of the monomeric units, local packing effects, and interactions with the solvent molecules. A valuable simplification can be made if one is willing to sacrifice consideration of short-range relationships and attendant behavior at the very highest frequencies. It utilizes the principle from polymer chain statistics that any two points on the chain backbone separated by perhaps 50 or more chain atoms will be related to each other in space in accordance with a Gaussian distribution of vectors,[19,20] provided the solvent is a Θ-solvent. In

the absence of external forces, the form of this distribution holds regardless of bond distances and angles and the relative probabilities of local isomeric conformations.[14,15] Thus the root-mean-square distance between two points separated by q monomer units ($qj \gtrsim 50$) is $\sigma = a\sqrt{q}$, where j is the number of bonds per monomer unit (often 2) and the length a depends on local geometric parameters; it is generally of the order of several times the length of a single chain bond.

A numerical parameter that is commonly used to characterize molecular dimensions of random coils is the "characteristic ratio" $C_\infty = \overline{r_0^2}/nl^2$, where $\overline{r_0^2}$ is the mean-square end-to-end distance, n the number of chain bonds (in this expression only), and l the bond length.[15] In terms of C_∞, $a = (C_\infty j)^{1/2} l$.

Elementary random-walk arguments show that the fluctuations in length of such a chain segment cause it to act like a Hooke's law spring under tension, storing energy because of the entropy decrease associated with restrictions on the assortment of configurations it can assume.[21] The force constant (force per unit displacement) of the spring is $3kT/qa^2$. The flexible polymer molecule is thus represented as a chain of N Gaussian submolecules. The root-mean-square end-to-end length of the entire molecule is $(\overline{r_0^2})^{1/2} = \sigma\sqrt{N} = a\sqrt{P}$, where σ is thus the root-mean-square end-to-end length of a submolecule. Fortunately, for many purposes, the arbitrary quantities q, σ, and N cancel out and do not need to be specified, but the high-frequency limits of applicability of the theories depend on them.

For the sake of mathematical simplification, the frictional interaction with the solvent medium is supposed to be restricted to the $N + 1$ ends of the submolecules ("beads"). When a dilute solution of polymer molecules is subjected to shearing stress, the flowing solvent distorts each molecule, acting on the beads, so that the assortment of vectors between two chain atoms q units apart is slightly perturbed from a Gaussian distribution. The Brownian motion will result in a diffusion back to approach this distribution, however, and the viscoelastic behavior is determined by the interaction between these two effects. In some theoretical treatments, the storage of free energy associated with an entropy decrease resulting from the change in distribution is specifically calculated; in others, the submolecules are simply represented as "entropy springs" with spring constants $3kT/qa^2$; hence the term "bead-spring model" (Fig. 9–4).

1. The Bead-Spring Model with no Hydrodynamic Interaction among Beads

In the theory of Rouse,[22] and in one limiting case of that of Zimm[23] which employs a different method but reaches the same result, hydrodynamic interaction between the motions of the submolecule junctions is ignored (Fig. 9–5); this corresponds to the "free-draining" assumption in calculations of the intrinsic viscosity.[24] A similar model, but not specifically designated for dilute solutions, was used by Bueche.[25] The resistance encountered by a submolecule junction moving through its surroundings is characterized by a friction coefficient f_0, and it is assumed that an average value can be used for all such junctions; f_0 is proportional to q. (Specifically, $f_0 = q\zeta_0$, where ζ_0 is the monomeric friction coefficient.) No intramolecular friction (internal viscosity) is taken into account.

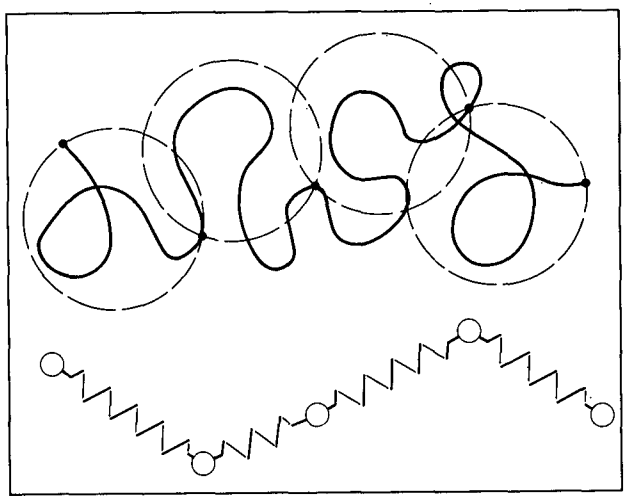


FIG. 9-4. Representation of flexible randomly coiled macromolecule by the bead-spring model.

The simultaneous motions of all segment junctions can be described through a transformation of coordinates as a series of cooperative modes. Each mode represents motion away from a given instantaneous configuration in which the segments are coordinated along the molecular contour similarly to the segments of a vibrating string. In Fig. 9-6, the "zero" mode is uniform translation and does not contribute to viscoelasticity. The next, in three dimensions, can be resolved into two rotational motions and the stretching motion shown. There are a total of N modes.

The theory of Rouse[22] is based on the change in free energy associated with the entropy decrease for nonrandom configurations and the tendency of the system to diffuse toward a random state; from this, the energy dissipation and storage in

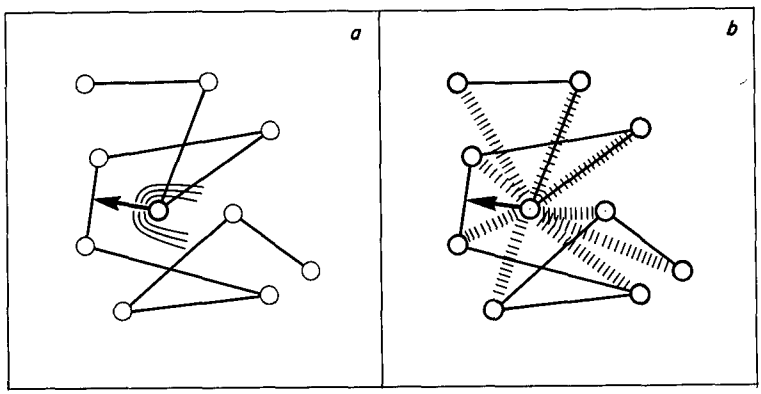


FIG. 9-5. Representation of frictional resistance encountered by a bead for (a) negligible hydrodynamic interaction or free draining, (b) dominant hydrodynamic interaction.

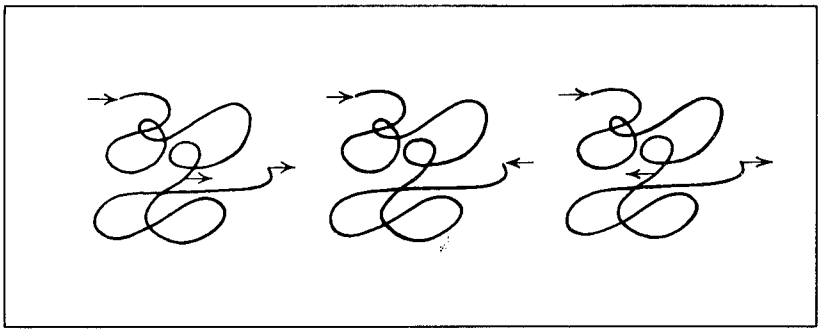


FIG. 9-6. Representation of characteristic modes of coordinated motion of a flexible macromolecule. The first is the "zero" mode; the next corresponds to τ_1.

sinusoidally oscillating deformations are calculated, and thence the complex viscosity or complex modulus. In the theory of Zimm,[23] the force on each bead is calculated as the sum of the hydrodynamic drag force by the solvent, the force associated with the Brownian motion, and the Hookean springlike forces exerted by the two neighboring submolecules. Inertial forces are neglected. The contribution of the solute to the shear stress for oscillating deformations is derived, from which the complex viscosity and modulus follow directly.

For the details of the calculation, the reader is referred to the original papers by Rouse[22] and Zimm[23] as well as to later treatises by Bird and collaborators,[1] Osaki,[26] Yamakawa,[27] and Berry and Casassa.[28] The relation between the Rouse and Zimm treatments is thoroughly elucidated by Bird (Chapter 12).[1] Both treatments give the same result for linear viscoelastic behavior so long as hydrodynamic interaction is neglected; this result is usually identified as the Rouse theory. Expressed in terms of the intrinsic moduli for a polymer homogeneous with respect to molecular weight, the Rouse theory specifies

$$[G']_R = \sum_{p=1}^{N} \omega^2\tau_p^2/(1 + \omega^2\tau_p^2) \tag{15}$$

$$[G'']_R = \sum_{p=1}^{N} \omega\tau_p/(1 + \omega^2\tau_p^2) \tag{16}$$

$$\tau_p = \sigma^2 f_0/24kT \sin^2[p\pi/2(N + 1)] \tag{17}$$

(An alternative formulation of τ_p containing only experimentally observable quantities will follow in equation 27.)

At a finite concentration sufficiently small that $[G']_R$ can be approximated by $G'M/cRT = G'/nkT$ where n is the number of polymer molecules per cubic centimeter, equation 15 can be written

$$G' = nkT \sum_{p=1}^{N} \omega^2\tau_p^2/(1 + \omega^2\tau_p^2) \tag{18}$$

From equations 23 and 24 of Chapter 3, it is evident that the contribution of the

solute to the complex modulus corresponds to a discrete relaxation spectrum (equivalent to a generalized Maxwell model) in which each contribution (G_p, corresponding to G_i in equation 17 of Chapter 3) has the magnitude nkT and the relaxation times are given by equation 17. Other viscoelastic functions can accordingly be easily written such as

$$G(t) = nkT \sum_{p=1}^{N} e^{-t/\tau_p} \tag{19}$$

$$\eta'(\omega) = \eta_s + nkT \sum_{p=1}^{N} \tau_p/(1 + \omega^2\tau_p^2) \tag{20}$$

or, at infinite dilution,

$$[\eta'] = \frac{RT}{M\eta_s} \sum \tau_p/(1 + \omega^2\tau_p^2) \tag{21}$$

The relaxation times become progressively more closely spaced with increasing p (Fig. 9-7). The finite limit of the sum at $p = N$ is an artificial consequence of the

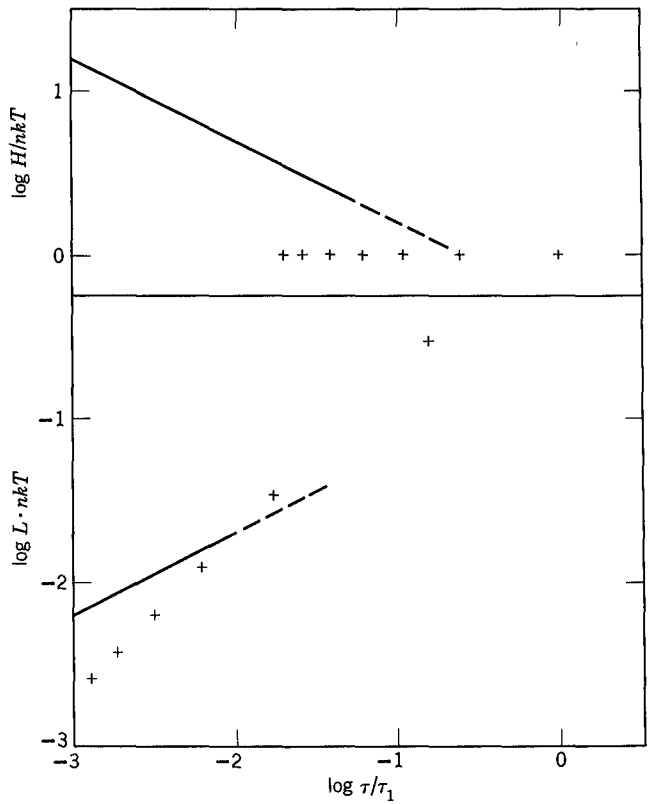


FIG. 9-7. Line spectra (crosses) for relaxation and retardation as predicted by the Rouse theory, with equivalent continuous spectra at short times (solid lines); τ_1 is longest or terminal relaxation time.

submolecular model, and if the higher terms where $p \to N$ make an appreciable contribution, the treatment is inapplicable because configurational changes within the segments are ignored. It can be applied only where the series converges for $p < N$; specifically, if it is limited to $p < N/5$, equation 17 can be replaced by the much more convenient approximation

$$\tau_p = \sigma^2 N^2 f_0/6\pi^2 p^2 kT = a^2 P^2 \zeta_0/6\pi^2 p^2 kT \tag{22}$$

The convergence requirements restrict the applicability to times or reciprocal frequencies greater than $5\tau_N \cong 0.1a^2q^2\zeta_0/kT$. However, the values of τ_p fortunately depend only on ζ_0 and a, not on any properties of the artificial submolecule.

The retardation spectrum corresponding to the Rouse theory is also discrete, equivalent to a generalized Voight model, but not with equal magnitudes of compliance contributions; the pth contribution J_p to the compliance falls off rapidly with increasing p, being approximately proportional to the retardation time itself as well as to $1/nkT$. They have been calculated by Berry;[29] the retardation times are spaced between the relaxation times, as shown in the lower panel of Fig. 9-7. From the discrete retardation times and J_p values, the creep compliance can be calculated in principle by equation 18 of Chapter 3.

Except for the two or three longest relaxation (or retardation) times, the contributions in Fig. 9-7 are closely enough spaced to be well approximated by continuous spectra. The appropriate equations are[30]

$$H = (aPn/2\pi)(\zeta_0 kT/6)^{1/2}\,\tau^{-1/2} \tag{23}$$

$$L = (2/\pi aPn)(6/\zeta_0 kT)^{1/2}\,\tau^{1/2} \tag{24}$$

Thus these functions plotted with logarithmic scales are linear with slopes of $-\frac{1}{2}$ and $\frac{1}{2}$ respectively, as drawn in Fig. 9-7.

The limit of applicability of equations 23 and 24 is set at long times roughly by $\tau < \tau_3$, corresponding to $H > \frac{3}{2}nkT$, or $L < \frac{2}{3}(\pi^2 nkT)^{-1}$; at short times, it is set by the requirement that $\tau > 0.1a^2q^2\zeta_0/kT$, corresponding to $H < 0.1(P/q)nkT$, or $L > 1/(P/q)nkT$. If $q = 25$ and $P = 10^4$ (*e.g.*, molecular weight of 10^6 and monomer molecular weight of 10^2), the linear logarithmic plot would be expected over about one and a half decades of H or L, or three decades of time scale. In the corresponding range of frequency scale, G' and $G'' - \omega\eta_s$ are equal and proportional to $\omega^{1/2}$; thus, for very low but finite concentration,

$$G' = G'' - \omega\eta_s = (aPn/4)(\zeta_0 kT/3)^{1/2}\omega^{1/2}. \tag{25}$$

It may be noted that, for a given weight concentration of solute, Pn is independent of molecular weight, so that in this region of frequency the effect of molecular weight would enter (if at all) only through the monomeric friction coefficient ζ_0. Actually, the assumption that f_0 and ζ_0 are the same for all segments of the molecule implies that they must also be independent of molecular weight, so G' and $G'' - \omega\eta_s$ should not depend on M in the $\omega^{1/2}$ region, provided M is sufficiently high that

N can be considered large. The behavior at higher frequencies is described in Section E below.

Although equations 18 to 25 have been written for finite concentration to show the roles of M and ζ_0, comparisons with experiment should be based on extrapolations to infinite dilution, and for this purpose the relaxation times can be reformulated in terms of the intrinsic viscosity to eliminate quantities not directly measurable. From equation 21 it follows that as ω approaches zero

$$[\eta] = \frac{RT}{M\eta_s}\sum\tau_p = \frac{RT\tau_1 S_1}{M\eta_s} \tag{26}$$

where S_1 is defined as $\Sigma\tau_p/\tau_1$. This holds for any set of relaxation times associated with equal modulus contributions; specifically, for the Rouse relaxation time spacings (equation 22), $S_1 = \Sigma(1/p^2) = \pi^2/6$. Note that equation 26 is the same as equation 10 for rigid rods with S_1^{-1} substituted for m. Thus for the Rouse relaxation spectrum

$$\tau_p = 6[\eta]\eta_s M/\pi^2 p^2 RT \tag{27}$$

With this substitution, equations 23 to 25 can be rewritten without the elusive quantity ζ_0; for example, in the frequency region of $\omega^{1/2}$ dependence, equation 25 becomes

$$[G']_R = [G'']_R = (\pi/2\sqrt{2})(\omega\tau_1)^{1/2} \tag{28}$$

The reduced intrinsic moduli as functions of $\omega\tau_1$ are independent of M; and as long as $\omega\tau_1$ is not too large, the sums are essentially independent of N, the arbitrary number of submolecules; *i.e.*, they are indistinguishable from the corresponding sums with $N = \infty$. The reduced moduli are plotted logarithmically in Fig. 9-8-I,

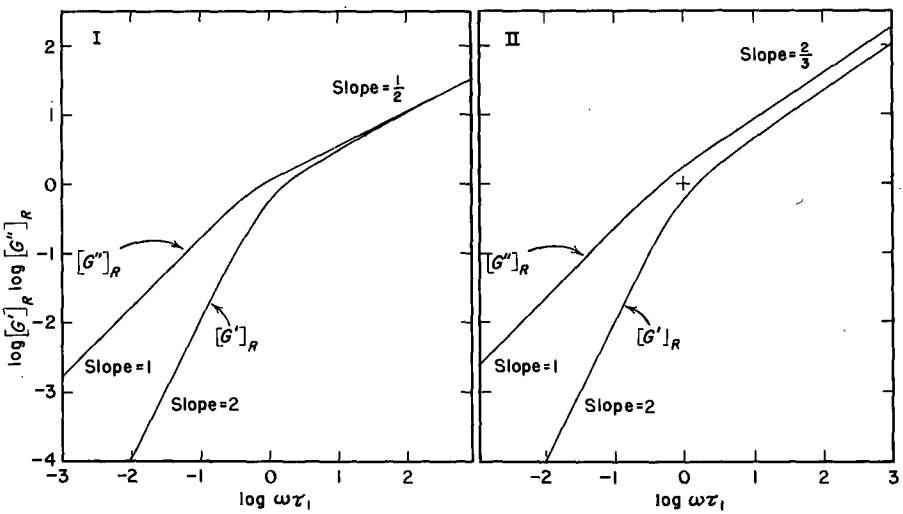


FIG. 9-8. Logarithmic plots of $[G']_R$ and $[G'']_R$ against $\omega\tau_1$ for bead-spring theories. (I) Rouse (negligible hydrodynamic interaction); (II) Zimm (dominant hydrodynamic interaction).

showing the low-frequency slopes of 2 and 1 respectively expected for any linear viscoelastic liquid, and the high-frequency slope of $\frac{1}{2}$ specified by equation 28 where $[G']_R$ and $[G'']_R$ are identical. A table of numerical values is given in Appendix E.

It is clear from a combination of equations 22 and 26 that (since a and ζ_0 are independent of M and P is proportional to M, in a series of molecular weights for the same polymer) $[\eta]$ should be proportional to M, and this is obviously experimentally incorrect, though it is a well-known feature of the theory of free-draining hydrodynamics.[24] In a Θ-solvent, $[\eta]$ is proportional to $M^{1/2}$, and in good solvents the exponent is not higher than 0.8. This discrepancy is removed by inclusion of hydrodynamic interaction. (However, the Rouse form of the frequency dependence is applicable with certain limitations to concentrated solutions and undiluted polymers, as shown in subsequent chapters.)

2. The Bead-Spring Model with Dominant Hydrodynamic Interaction

The Zimm theory[23] includes an alternative treatment in which frictional resistance to motion of the beads in the bead-spring chain is dominated by the viscous drag from other beads in the same chain (dominant hydrodynamic interaction, Fig. 9-5-II). The interaction is treated approximately as in the theory of Kirkwood and Riseman[32] for the intrinsic viscosity of dilute polymer solutions, by use of the equilibrium-averaged Oseen tensor for the influence of the motion of one bead on another; the average distances between pairs of beads are supposed to correspond to those in a Θ-solvent.

This treatment has become conveniently but imprecisely known as "the" Zimm theory, so that the names of Zimm and Rouse are labels for dominant hydrodynamic interaction and free draining, respectively.

Analysis of the normal modes and transformation of the coordinates leads to another discrete spectrum which differs from that of the Rouse theory only in the values of the relaxation times. Thus, equations 15, 16, 21, and 26 are unchanged, but the relaxation times are obtained from the eigenvalues of a complicated matrix which includes the pairwise hydrodynamic interactions.[23,33,34] The strength of the latter is measured by either of two parameters:

$$h = N^{1/2} f_0/(12\pi^3)^{1/2}\eta_s\sigma$$

or

$$h^* = h/N^{1/2} = f_0/(12\pi^3)^{1/2}\eta_s\sigma \tag{29}$$

For very large values of h, or for a specific value of h^* which may be 0.25 or about 0.22 depending on the method of evaluating the eigenvalues,[33,34] the hydrodynamic interaction is dominant ("nonfree-draining"), and the spacing of the relaxation times leads to the following relations:

$$[\eta] = 0.47(RT/M)a^3P^{3/2} \tag{30}$$

$$S_1 = 2.369 \tag{31}$$

and, at higher frequencies, $[G']_R$ and $[G'']_R$ are proportional to $\omega^{2/3}$ and are not equal but differ by a factor of $\sqrt{3}$:

$$[G']_R = 1.05\,(\omega\tau_1)^{2/3} \tag{32}$$

$$[G'']_R = 1.82\,(\omega\tau_1)^{2/3} \tag{33}$$

Equation 30 gives the experimentally observed proportionality of $[\eta]$ to $M^{1/2}$ in a Θ-solvent. Again the reduced intrinsic moduli as functions of $\omega\tau_1$ are independent of M. They are plotted in Fig. 9-8-II. As with the Rouse theory, the results are insensitive to N so long as the frequency is not too high. The slope of $\frac{2}{3}$ on the logarithmic plot at higher frequencies corresponds to a relaxation spectrum in which all τ_p except the first few are proportional to $p^{-3/2}$ instead of to p^{-2} as in the free-draining case.

3. Partial Hydrodynamic Interaction

For $h = 0$ or $h^* = 0$, the Zimm theory reduces to the Rouse theory. For values of h neither 0 nor ∞, a solution of the frequency dependence of $[G']_R$ and $[G'']_R$ corresponding to very large N was obtained to Tschoegl;[35] with increasing h, the shapes of the calculated curves progressed from those of Fig. 9-8-I to those of Fig. 9-8-II. Exact eigenvalues for various values of h^* over wide ranges of N have been evaluated with the use of a high-speed computer by Lodge and Wu.[35] At high N, they are insensitive to N except at high frequencies; they provide frequency dependences of $[G']_R$ and $[G'']_R$ which, in the power law region, again change progressively from free-draining ("Rouselike") to nonfree-draining ("Zimmlike") behavior as h^* increases. Some examples are shown in Fig. 9-9. Equation 26 holds

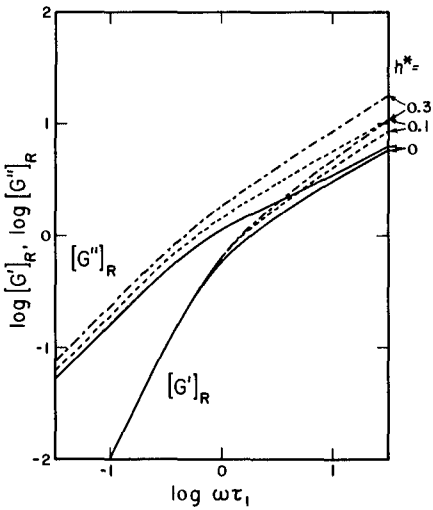


FIG. 9-9. Logarithmic plots of $[G']_R$ and $[G'']_R$ against $\omega\tau_1$ from Zimm theory with exact eigenvalues evaluated by Lodge and Wu,[35] for $N = 200$ and three values of h^* as indicated.

in every case to enable τ_1 to be expressed in terms of $[\eta]$, but the value of S_1 depends on the value of h^*.

From the theory of Kirkwood and Riseman[32] it would be expected that, for exceedingly dilute solutions in a Θ-solvent, h would increase from 0 to ∞ with molecular weight and reach ∞ at a moderately low molecular weight; so Zimmlike behavior (Fig. 9-8-II) should be the norm, and Rouselike behavior (Fig. 9-8-I) should appear only for very low molecular weights. Actually, Zimmlike behavior is indeed the norm but a transition toward Rouselike behavior at low molecular weights has not been observed. At finite concentrations, such a transition occurs with *increasing* molecular weights because of interaction between molecules, as described in Section D.

4. Non-Θ-Solvents

It should be emphasized that all of the preceding discussion applies only to solutions in Θ-solvents, since the distribution of molecular configurations is supposed to be Gaussian; the length σ and the length $(\overline{r_0^2})^{1/2}$ are proportional to $P^{1/2}$ (or to $M^{1/2}$), and the intrinsic viscosity $[\eta]$ is proportional to $P^{1/2}$ or $M^{1/2}$ (except for very low molecular weights), as derived from equation 30 and observed experimentally. For solutions in good solvents, the molecular configurations are expanded; $(\overline{r_0^2})^{1/2}$ and $[\eta]$ are larger than in a Θ-solvent and they increase with M more rapidly than proportional to $M^{1/2}$. The extent of expansion can be approximated[36] by a parameter ϵ, defined such that the mean-square distance between any two points on the chain separated by n bonds is proportional to $n^{1+\epsilon}$ instead of to n as it would be in a Θ-solvent. The limiting values of ϵ are 0 and $\frac{1}{3}$.

The theory of Zimm was modified by Ptitsyn and Eizner[37,38] in this manner. The result, for the maximum value of ϵ, is to shift the form of the frequency dependence slightly in the direction of Rouselike behavior.[39] For intermediate values of ϵ, curves of intermediate shapes are obtained.

The frequency dependence for any arbitrary value of ϵ and any arbitrary value of h was calculated by Tschoegl.[39] For this purpose, h is given by

$$h = 2^{\epsilon/2} N^{(1-\epsilon)/2} f_0 / (12\pi^3)^{1/2} \eta_s \sigma \tag{34}$$

With increasing ϵ and/or decreasing h, the form of the frequency dependence changes gradually from that of Fig. 9-8-II to that of Fig. 9-8-I. For a given polymer–solvent system, ϵ can be obtained from the dependence of intrinsic viscosity on molecular weight,[39] and h can be chosen as an adjustable parameter. In practice, the observed frequency dependence in non-Θ-solvents can be fitted quite well by a single adjustment of the hydrodynamic interaction as measured by h^*, as will be seen in Section 6, without introduction of ϵ. Strictly speaking, this is inconsistent since it implies a Gaussian distribution of configurations in good solvents, but qualitatively the appropriate change of h^* with choice of solvent can be understood in terms of the expansion of the molecule as revealed by the intrinsic viscosity (Section 4).

Many other modifications and elaborations of these theories have been made,

but they are outside the scope of this chapter. Information can be found in reviews already cited[1,26-28] and other sources.[40-42] Also, the dynamics of flexible polymers has been extensively treated by stochastic methods with computer simulation[43] involving motions of a jointed chain on a lattice or much more realistic representation of a molecule with constraints on bond lengths and angles and rotational barriers.[44]

5. Comparisons of Characteristic Parameters for Bead-Spring Model Theories

For all the theories thus far described, equations 15, 16, and 26 hold; only the spacings among the relaxation times differ. Another relation which follows from equation 15 and is valid for all these theories is

$$[A_G] = (RT/M)\tau_1^2 S_2 \tag{35}$$

where $[A_G]$ is the zero-concentration limit of A_G/c, A_G is the zero-frequency limit of G'/ω^2 (*cf.* equation[34] of Chapter 3), and

$$S_2 = \sum_{p=1}^{N} (\tau_p/\tau_1)^2 \tag{36}$$

From equations 13, 26, and 35 it follows that

$$j_{eR}^0 = S_2/S_1^2 \tag{37}$$

when it is recalled that

$$S_1 = \sum_{p=1}^{N} \tau_p/\tau_1. \tag{38}$$

(The definitions of the sums S_1 and S_2 given here hold for linear polymers in which all contributions to modulus associated with different relaxation times have the same magnitudes; for branched polymers or semirigid polymers with hybrid spectra they will be defined somewhat differently.)

The low-frequency limiting viscoelastic behavior is thus governed by the sums S_1 and S_2. Values of these, together with S_2/S_1^2 and the first two relaxation time ratios, are given in Table 9–II for several choices of h^* and other parameters. The greatest differences are seen in the ratio S_2/S_1^2 to which the steady-state compliance J_e^0 is proportional. The table also includes some data for branched polymers which will be discussed in Section 8.

6. Comparison of Theory for Linear Molecules with Experiment

To compare experimental data with the predictions of equations 15, 16, and 26, it is necessary to have a linear polymer with narrow molecular weight distribution and to extrapolate data at each frequency of measurement to infinite dilution. For $[G'']$, the right side of equation 2 plotted against c gives a satisfactory linear plot

Table 9–II

CHARACTERISTIC PARAMETERS PREDICTED BY BEAD-SPRING MODEL THEORIES

Theory	S_1	S_2	S_2/S_1^2	τ_2/τ_1	τ_3/τ_1
Linear Molecules					
Rouse, $h^* = 0$	1.645	1.082	0.400	0.250	0.111
Zimm, $h^* = 0.25$ (Θ-solvent)	2.369	1.156	0.206	0.316	0.167
Zimm, $h^* = 0.10$	2.066	1.139	0.267	0.305	0.156
Ptitsyn-Eizner-Tschoegl, $h = \infty$, $\epsilon = 0.33$	2.003	1.123	0.280	0.291	0.145
Branched Molecules					
Star, $f = 8$, $h^* = 0.25$, $N_b = 100$	11.43	7.337	0.056	0.230	0.167
Comb, $f = 8$, $h^* = 0.25$, $N_s = 5$, $N_b = 5$	3.05	1.274	0.137	0.355	0.214
Comb, $f = 8$, $h^* = 0.25$, $N_s = 1$, $N_b = 8$	6.11	0.276	0.074	0.612	0.538

(like that of η_{sp}/c to arrive at $[\eta]$); for $[G']$, it can be inferred from the form of equation 15 that $(G'/c)^{1/2}$ against c will be more nearly linear than G'/c. Examples are shown in Fig. 9–10.[45]

The first comparisons of data extrapolated to infinite dilution with molecular theory were made by Tanaka, Sakanishi, Kaneko, and Furuichi.[46–49] Rather good agreement with the Zimm theory was obtained, especially in Θ-solvents, but with a relatively narrow frequency range. A wider range has been covered more recently with the Birnboim-Schrag multiple-lumped resonator.[50]

The reduced intrinsic moduli $[G']_R$ and $[G'']_R$ are plotted logarithmically against $\omega[\eta]\eta_s M/RT$ in Fig. 9–11 for a polystyrene with $M = 0.86 \times 10^6$ in two Θ-solvents, each at its Θ-temperature.[45] The solvent viscosities are quite different and this feature extends the effective frequency range. The reduced frequency used for the abscissa again permits the plot to be constructed from experimental data only and differs from the dimensionless frequency $\omega\tau_1$ only by the factor S_1 which must be determined by the choice of h^*. (Also, in this type of plot the abscissa and ordinate are identical at the low-frequency end of $[G'']_R$.) In this case there is a good fit to theoretical curves drawn with N large, $h^* = 0.25$, hence $S_1 = 2.369$, confirming the Zimm theory for dominant hydrodynamic interaction in a Θ-solvent. Not only the shapes but also the magnitudes are confirmed. (Strictly speaking, a more fundamental test of the Zimm theory could be made by substituting for $[\eta]$ the value in terms of molecular dimensions given by equation 30, but this substitution would be irrelevant to the form of the frequency dependence.)

A similar plot is shown in Fig. 9–12 for the same polystyrene in two good solvents whose thermodynamic interaction with the polymer is about the same as evidenced by nearly equal intrinsic viscosities, but whose different solvent viscosities again extend the effective frequency range. The fit is good with N large, $h^* = 0.15$, corresponding to intermediate hydrodynamic interaction (Section 3).

In other examples, experimental data have been fitted to the Zimm theory

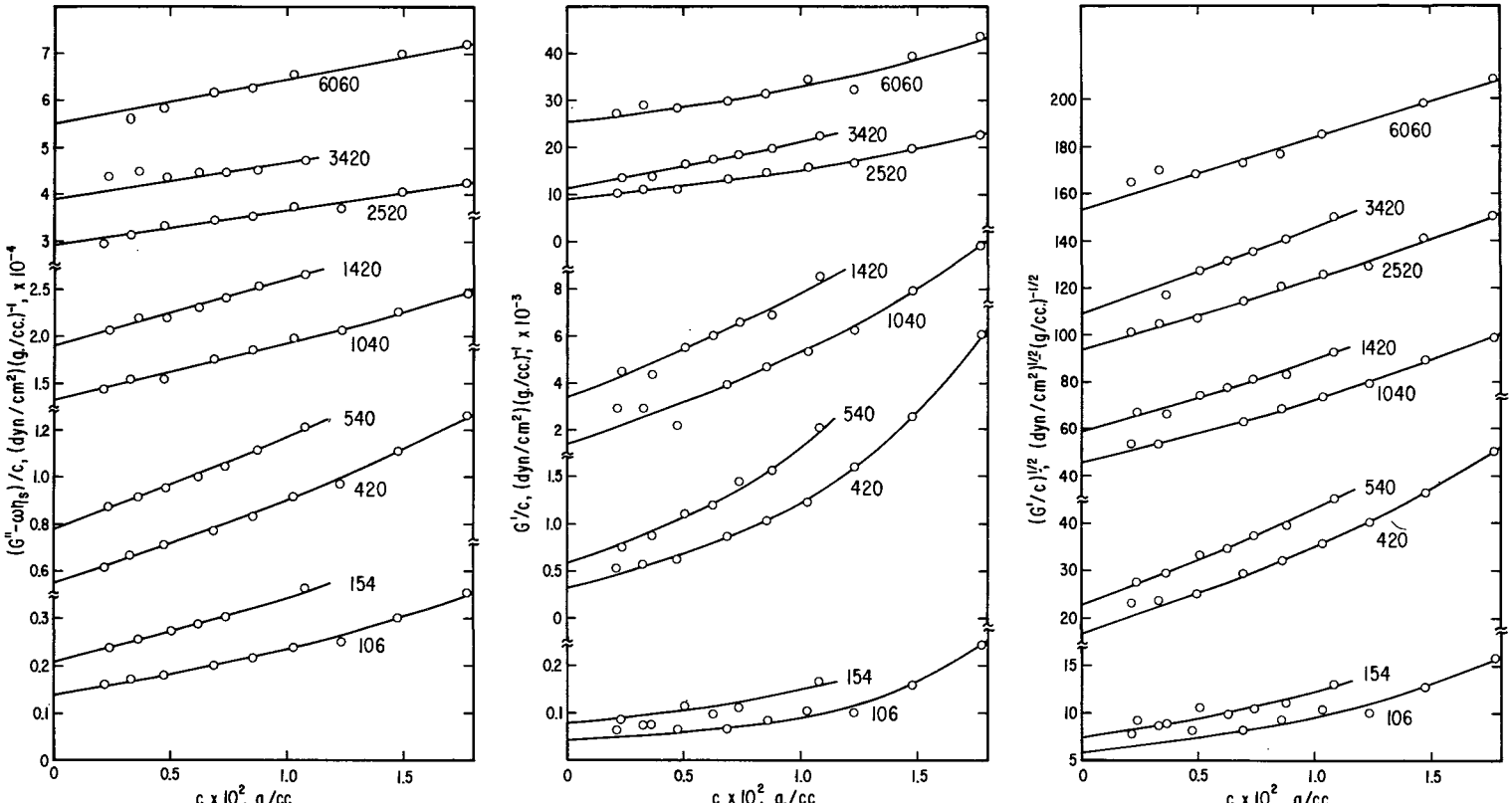


FIG. 9–10. Plots of $(G'' - \omega\eta_s)/c$, G'/c, and $(G'/c)^{1/2}$ against c, each at nine frequencies as indicated, for polystyrene with $M = 0.86 \times 10^6$ in Decalin.[45] Note that several different ordinate scales are used in each panel. Reproduced, by permission, from *Polymer Journal*.

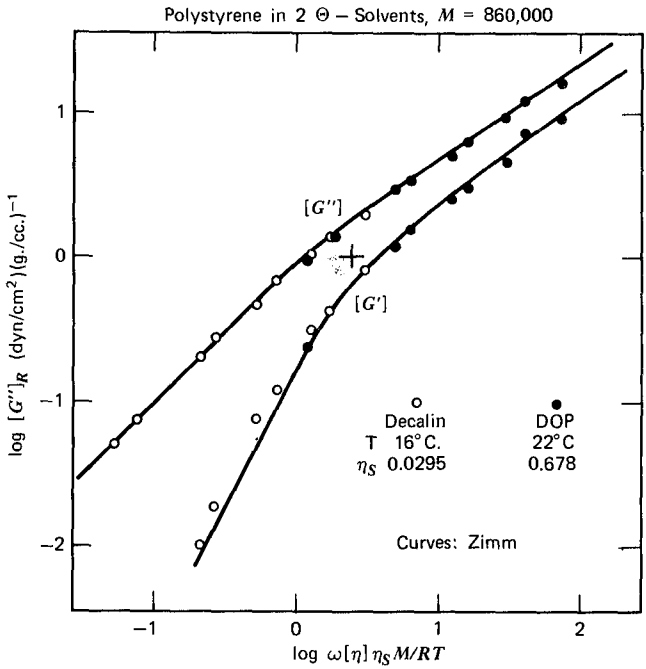


FIG. 9-11. Logarithmic plots of $[G']_R$ and $[G'']_R$ against $\omega[\eta]\eta_s M/RT$ for polystyrene with $M = 0.86 \times 10^6$ in two Θ-solvents, Decalin and di-2-ethylhexyl phthalate (DOP), at their respective Θ temperatures. Curves for Zimm theory with $h = \infty$.[45]

evaluated with Lodge-Wu eigenvalues (Section 3) corresponding to empirically chosen values of h^*, and N large, for poly(α-methyl styrene),[51] polybutadiene,[52] and poly(dimethyl siloxane).[53] With increasing solvent power, h^* decreases; the product $h^*\alpha_\eta$, where $\alpha_\eta = ([\eta]/[\eta]_\Theta)^{1/3}$ is a measure of the linear coil dimensions in a good solvent relative to those in a Θ solvent, is approximately constant at 0.21. This is close to the value of about 0.22 obtained from exact eigenvalue calculations.[33]

The above relation can be qualitatively understood[51] if the bead friction coefficient f_0 is approximated by the Stokes value for a sphere of radius r, namely, $6\pi\eta_s r$. The equation 29 becomes

$$h^* = 0.98\, r/\sigma \tag{39}$$

Thus h^* may be regarded as a measure of the ratio of the bead "diameter" to the separation between beads, and diminishes with increasing σ, which is proportional to α_η. Strictly, this view is inconsistent because it implies that in a good solvent the coil is expanded but still Gaussian. In fact, excluded volume should be taken into account as mentioned in Section 4. However, the bead-spring model appears to account rather well for the magnitudes and frequency dependences of viscoelastic properties of linear polymers in Θ and good solvents—if the frequency range does not extend too high.

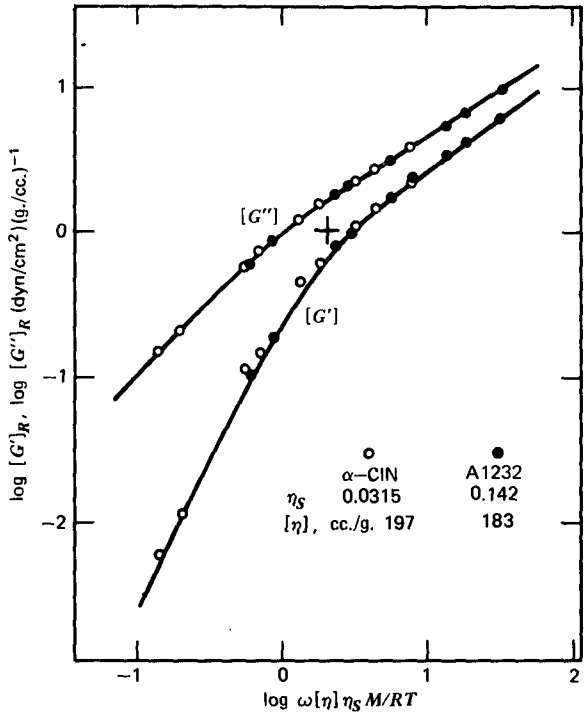


FIG. 9-12. Logarithmic plots of $[G']_R$ and $[G'']_R$ against $\omega[\eta]\eta_s M/RT$ for the polystyrene of Figs. 9-10 and 9-11 in two good solvents (α-chloronaphthalene and Aroclor 1232) at 25°, with similar expansion factors α_η as evidenced by the similar intrinsic viscosities.[45] Curves were drawn from Tschoegl theory[39] with $h = 40$, $\epsilon = 0.13$, but are also reproduced by exact eigenvalue calculations[35] with N large and $h^* = 0.15$.

7. Effect of Molecular Weight Distribution

In very dilute solution, the contributions of solute species of different sizes to the components of the modulus (and to dissipation and storage of energy) should simply be additive. Since the friction coefficients f_0 and ζ_0 in the Rouse theory are independent of molecular weight, τ_p depends on it only through the factor P^2 in equation 22; and in the Zimm theory with $h^* = 0.25$ only through the factor $P^{3/2}$ in equation 30. It is possible then to integrate over the contributions to G' and G'' for any arbitrary distribution of molecular weights.[54,55] At high frequencies, G' and G'' are independent of molecular weight distribution because they are independent of molecular weight (equations 25, 32, 33). At low frequencies, they can be expressed in terms of conventional molecular weight averages.[54] For example, the Rouse theory for uniform molecular weight gives for $[A_G]$ (from equations 35 and 22):

$$[A_G] = S_2(RT/M)(a^2\zeta_0/6\pi^2 kT)^2 P^4 \tag{40}$$

and the corresponding expression[54] for arbitrary molecular weight distribution is

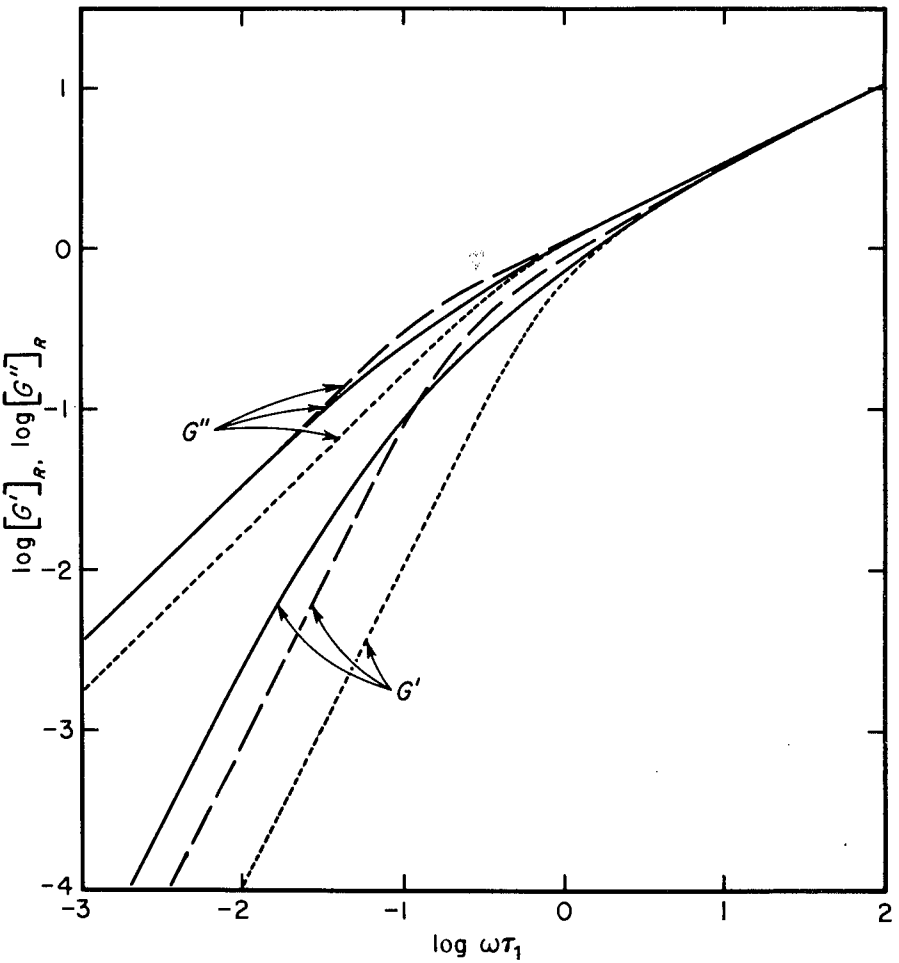


FIG. 9–13. Logarithmic plots of $[G']_R$ and $[G'']_R$ against $\omega\tau_{1n}$ for the Rouse theory with a most probable molecular weight distribution (solid curves). The relative positions (on unreduced scales) of the moduli for monodisperse polymers of the same $\overline{M}_n$ and $\overline{M}_w$ are shown by the curves with short and long dashes, respectively.

$$[A_G] = S_2(RT/\overline{M}_n)(a^2\zeta_0/6\pi^2kT)^2\overline{P}_{z+1}\overline{P}_z\overline{P}_w\overline{P}_n \tag{41}$$

Here $\overline{P}_{z+1} = \overline{M}_{z+1}/M_0$ where M_0 is the monomer molecular weight, etc. Thus the low-frequency storage modulus, at equal weight concentration and frequency, is always higher for a polymer with molecular weight distribution than for a homogeneous sample with the same number-average molecular weight; and to a degree that is strongly weighted by high-molecular-weight components.

Plots of $[G']_R$ and $[G'']_R$ against $\omega\tau_1$ for a most probable molecular weight distribution are shown for the Rouse theory in Fig. 9–13, and compared with uniform samples of the same number-average and weight-average molecular weights.

Numerical values are given in Appendix E. Here the subscript n means that $\overline{M}_n$ is used for M in the defining equations for the reduced variables (equations 36 and 37); also $\overline{P}_n$ for P in specifying τ_1 in the product $\omega\tau_1$. Although $[G'']_R$ is not markedly affected, $[G']_R$ is higher by a factor of 24 at low frequencies than for a uniform sample of the same number-average molecular weight. Strictly speaking, this calculation is inconsistent because the lowest molecular weights will not conform to the requirement that N be large in applying the Rouse theory (*cf.* the discussion in connection with equations 23 and 24). However, the contributions from the low molecular weight species will be very small at low frequencies where the effects of molecular weight distribution are most apparent.

Corresponding integrations can be performed for the Zimm theory; the results are similar[54] but the effects of molecular weight distribution are smaller. For example, with a most probable distribution, $[G']_R$ is higher by a factor of 6 at low frequencies than for a uniform sample with the same number-average molecular weight.

In making these comparisons, it is assumed that the characteristic length a is independent of molecular weight, and this will not be the case if excluded volume must be taken into account. However, it is clear that molecular weight distribution has a very large effect on $[G']_R$ at low frequencies, and also on the steady-state compliance through the relation $j_{eR}^0 = \lim_{\omega\to 0}[G']_R/[G'']_R^2$. These features also appear in concentrated solutions and undiluted polymers (for which the effect of molecular weight distribution was first derived[54]).

It is evident that a very sharp molecular weight distribution is required if experimental data are to be compared with the theories as formulated for uniform molecular weight as in Section 6 above.

8. Branched Flexible Random Coils

The bead-spring model with dominant hydrodynamic interaction was extended to star-shaped branched molecules by Zimm and Kilb.[56] For f branches of equal length, each with N_b submolecules, equations 15, 16, 36, and 38 are replaced by

$$[G']_R = (f-1)\sum_{\substack{p=1\\ \text{odd}}}^{2N_b-1} \omega^2\tau_p^2/(1+\omega^2\tau_p^2) + \sum_{\substack{p=2\\ \text{even}}}^{2N_b} \omega^2\tau_p^2/(1+\omega^2\tau_p^2) \tag{42}$$

$$[G'']_R = (f-1)\sum_{\substack{p=1\\ \text{odd}}}^{2N_b-1} \omega\tau_p/(1+\omega^2\tau_p^2) + \sum_{\substack{p=2\\ \text{even}}}^{2N_b} \omega\tau_p/(1+\omega^2\tau_p^2) \tag{43}$$

$$S_1 = (f-1)\sum_{\substack{p=1\\ \text{odd}}}^{2N_b-1} \tau_p/\tau_1 + \sum_{\substack{p=2\\ \text{even}}}^{2N_b} \tau_p/\tau_1 \tag{44}$$

$$S_2 = (f-1)\sum_{\substack{p=1\\ \text{odd}}}^{2N_b-1} (\tau_p/\tau_1)^2 + \sum_{\substack{p=2\\ \text{even}}}^{2N_b} (\tau_p/\tau_1)^2 \tag{45}$$

Equation 26 still holds with the new definition of S_1. The average distances between

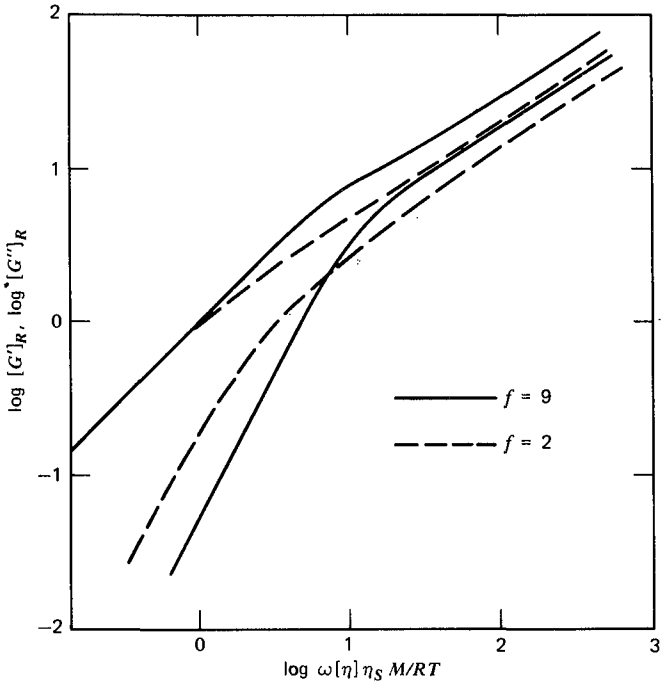


FIG. 9–14. Logarithmic plots of $[G']_R$ and $[G'']_R$ against $\omega[\eta]\eta_s M/RT$ for linear ($f = 2$) and nine-arm star ($f = 9$) calculated from Zimm-Kilb theory for $h^* = 0.25$ and $N_b = 100$.[57,58] Reproduced, by permission, from *Polymer Journal*.

pairs of beads, whether in the same branch or different branches, are taken again as proportional to the square root of the number of intervening submolecules, and the hydrodynamic interactions are included in a matrix whose eigenvalues provide the relaxation times. For partial hydrodynamic interaction, the relaxation times depend on the choice of h^*; exact values have been evaluated, following the procedure of Lodge and Wu,[35] for various values of f, N_b, and h^* by Osaki and Schrag.[57] Large values of N_b are needed for a realistic model; the maximum value of fN_b in these calculations was 800 because of computer limitations, but this is adequate if f is not too large.

Comparison of the frequency dependence of G' and G'' for linear and star molecules depends on how the coordinates are scaled. If the reduced variables are plotted as in Figs. 9–11 and 9–12, $[G'']_R$ at low frequencies is a line of identity for any molecule. A linear and nine-armed star are compared in this manner for $h^* = 0.25$ (Θ-solvent) and a somewhat unrealistically low value of $N_b = 100$ in Fig. 9–14.[58] The branched molecule differs in displaying a "bump" near 1 on the abscissa scale (related to the large spacing between the first and third relaxation times which dominate the low-frequency behavior) and in having a much lower $[G']_R$ at low frequencies. The latter is reflected in low values of $[A_G]$ and j^0_{eR}; note that this effect of branching is opposite to that of molecular weight distribution.

On the other hand, if one plots $[G']$ and $[G'']$ logarithmically against frequency

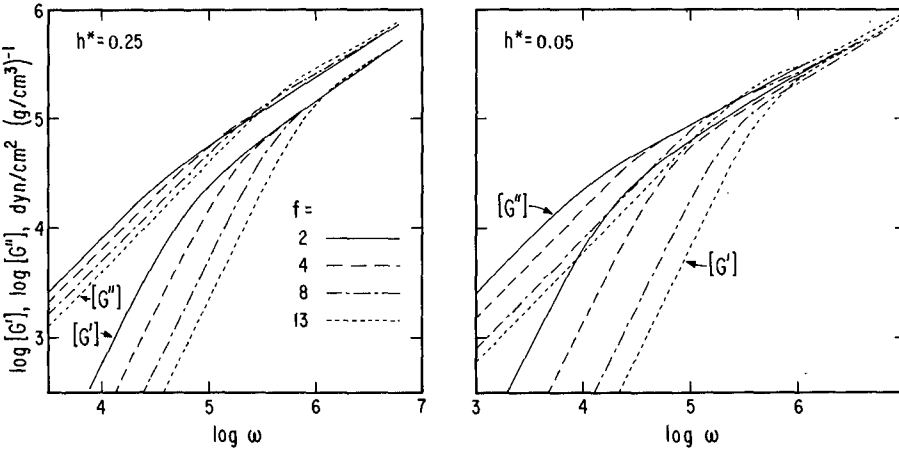


FIG. 9-15. Logarithmic plots of $[G']$ and $[G'']$ against frequency (unreduced) calculated from Zimm-Kilb theory for star-branched polystyrenes with molecular weight 10^6 in a solvent with viscosity 0.01 poise at 25°C, with large N and $h^* = 0.25$ or 0.05, and different degrees of branching from $f = 2$ (linear) to $f = 13$.

without such scaling, a different comparison emerges as shown in Fig. 9-15. For this purpose it is necessary to choose specific conditions; the example is for polystyrenes with molecular weight 10^6, solvent viscosity 0.01 poise at 25°C, intrinsic viscosity for the linear molecule ($f = 2$) of 82 ml/g in a Θ-solvent ($h^* = 0.25$), and 250 ml/g in a good solvent ($h^* = 0.05$); intrinsic viscosities for branched molecules are estimated from related data in the literature.[59] Now the curves for different degrees of branching all merge at high frequencies, naturally because the behavior there is dominated by short-range configurational changes which are oblivious of branch points. At low frequencies, the ratio G''/ω diminishes with increasing branching and reflects the well-known effect of branching on intrinsic viscosity as expressed by the coefficient g'.[56] The ratio G'/ω^2 at low frequencies decreases enormously with increasing branching. This effect would also appear in the primary normal stress difference. The "bump" of Fig. 9-14 is also apparent in the curves of Fig. 9-15.

In a third method of comparison[59a] (not shown), the dimensionless ratios $[G']M_b/RT$ and $[G'']M_b/RT$, where M_b is the molecular weight of one branch of the star, are plotted logarithmically against $\omega\tau_1$ for stars with equal M_b but different branch numbers f. In this case the curves all lie close together and the differences in f are apparent primarily in the size of the "bump".

An example of comparison with experiment is shown in Fig. 9-16.[58] Good agreement is obtained for a 9-arm star polystyrene with molecular weight 5.0×10^6. (A better fit is shown with an unrealistically high value of $h^* = 0.40$ than with $h^* = 0.25$, but the fit is equally good with $h^* = 0.25$ and a smaller value of f, and the functionality of 9 may be uncertain.[59a]) Good agreement has also been obtained for a 4-arm star polybutadiene[52] and 4-arm star polystyrenes.[60]

Similar calculations have also been made for comb polymers with various regular structures by Osaki and coauthors.[61] In this case the matrices are very complicated

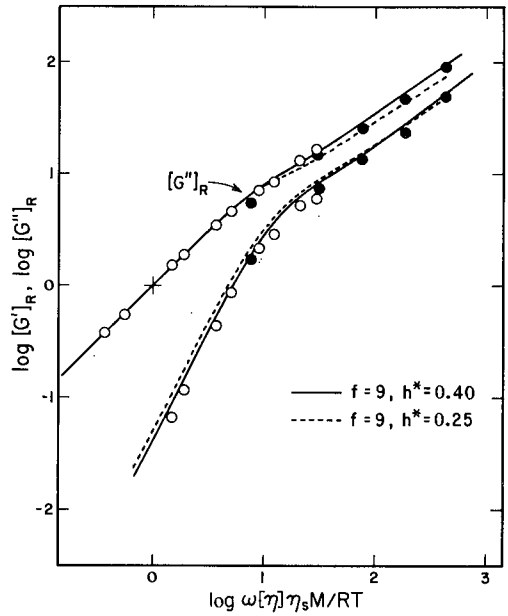


FIG. 9-16. Logarithmic plots of $[G']_R$ and $[G'']_R$ against $\omega[\eta]\eta_s M/RT$ for a nine-arm star polystyrene with $M = 5.0 \times 10^6$ in two Θ-solvents, Decalin (black circles), and DOP (open circles).[58] Curves: exact eigenvalue evaluation[57] of Zimm-Kilb theory with $f = 9$, $N_b = 100$, $h^* = 0.40$ and 0.25, identified as shown. Reproduced, by permission, from *Deformation and Fracture of High Polymers*, edited by H. H. Kausch, J. A. Hassell, and R. I. Jaffee, Plenum Press, New York, 1973.

and computer limitations prevent solution of eigenvalues with more than rather small numbers of submolecules on the comb arms (N_b) and between branch points on the backbone (N_s), so the predictions may not be very realistic. A comparison is shown in Fig. 9-17 for the relaxation spectra of a linear molecule, eight-arm star, and two eight-arm combs with long and short branches respectively; $h^* = 0.25$. For the combs, contributions with relaxation times nearly identical have been lumped together. The corresponding frequency dependences of $[G']_R$ and $[G'']_R$ are plotted in Fig. 9-18 with the usual reduced variables. It is evident that in most respects the combs are intermediate between the linear and the star. Differences are most prominent in $[G']_R$ at low frequencies where the behavior can be compared in terms of $j^0_{eR} = \lim_{\omega\to 0}[G']_R/[G'']^2_R = S_2/S_1^2$. Values of S_1, S_2, and S_2/S_1^2 are given in Table 9-II for these specific examples.

Comparisons with experiment[62] show that the differences between comb and linear polymers are generally less than predicted from these calculations; the assumption of Gaussian distributions of configurations involving all parts of a comb may not be applicable.

Some measurements have also been made on randomly branched polymers[63] and indicate that as little as one branch per molecule can be detected from the value of j^0_{eR} ($= [G']_R/[G'']^2_R$) provided the molecular weight distribution is not too broad and enough is known about it to correct for its effect on j^0_{eR}.

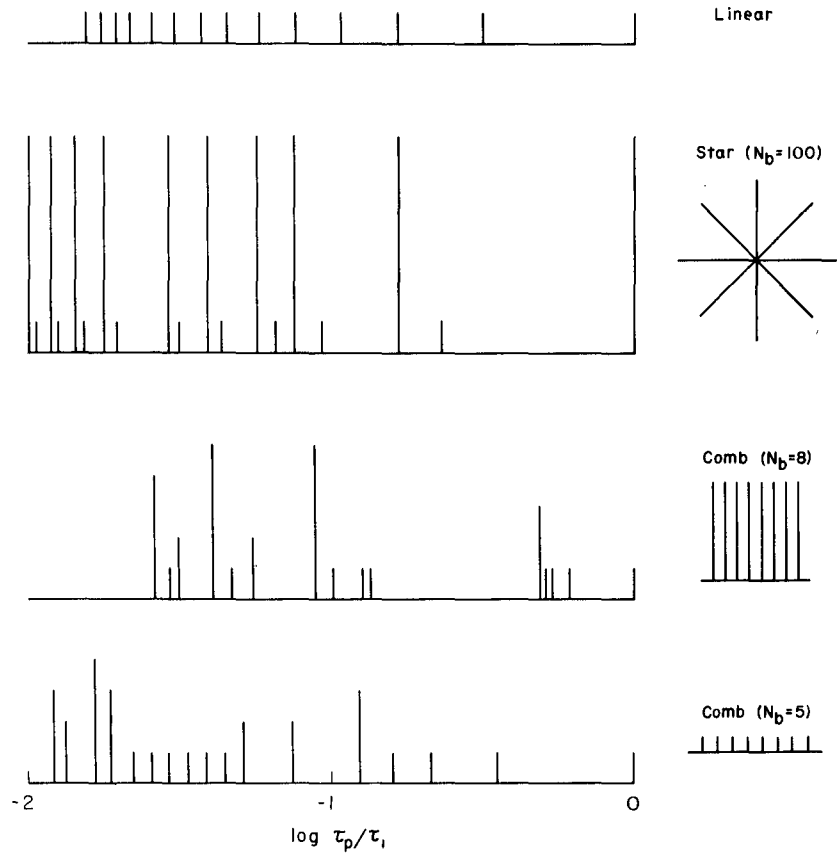


FIG. 9-17. Relaxation time spectra for polymers in very dilute solution. Linear, Zimm theory evaluated by Lodge and Wu;[35] branched, Zimm-Kilb theory evaluated by Osaki and Schrag.[57,61] For the comb polymers, some very closely spaced mechanisms have been arbitrarily combined. N_b is the number of submolecules per branch. Minimum height represents a modulus contribution of cRT/M. Reproduced, by permission, from the same source as Fig. 9-16.

C. PARTIALLY FLEXIBLE ELONGATED MOLECULES

Intermediate between flexible random coils and rigid rods, there can be classified certain macromolecules which are highly extended so that the average end-to-end distance is much greater than that of a flexible Gaussian coil with a normal characteristic ratio $\bar{r}_0^2/nl^2$ (or length parameter a) but nevertheless possess some degree of flexibility. Examples are helical structures [single helices such as poly(α-amino acid)s or double helices such as DNA] and highly charged polyelectrolytes in solvents of low ionic strength. The high extension is at once obvious from the enormous magnitude of the intrinsic viscosity. Studies of intrinsic viscosity, light scattering, and dipole moment show that such molecules are actually somewhat less than completely linearly extended but do not provide information on rates of their internal motions.

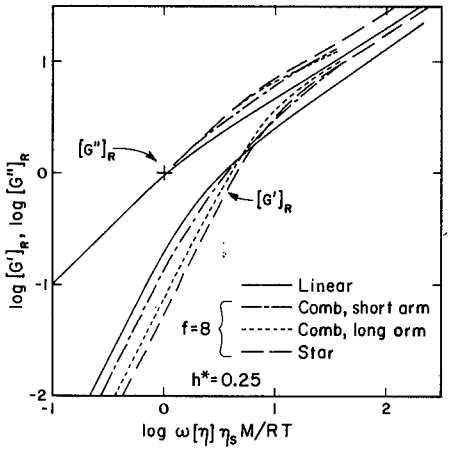


FIG. 9-18. Logarithmic plots of $[G']_R$ and $[G'']_R$ against $\omega[\eta]\eta_s M/RT$ calculated from the relaxation spectra of Fig. 9-17.

1. Helical Macromolecules

The average dimensions of helical molecules have been usually described by a wormlike coil model[64,65] with a stiffness described by the persistence length q, defined as the average projection of the end-to-end vector of a very long molecule on a single bond direction; for some helical structures, it is typically of the order of 1000 Å.[66] For helix lengths L less than q, the behavior approaches that of a rigid rod; for $L \gg q$, the behavior approaches that of a random coil. The model is not always successful because the characteristic length q sometimes appears to decrease with increasing molecular weight instead of being constant for a given helical structure.[67]

Introduction of stiffness into the bead-spring model by increasing the persistence length, as shown by Bixon and Zwanzig,[68] has the effect of prolonging the longest relaxation time τ_1 and separating it from the others. Stockmayer[69] has suggested that increasing stiffening of a flexible macromolecule should cause the longest mode to split into two rotational degrees of freedom with a very long relaxation time and a third which represents the end-to-end separation characterized by τ_1 in the bead-spring model.

Good agreement with experimental viscoelastic measurements on several helical polymers has been obtained with an empirical hybrid relaxation spectrum in which a separate rotational mode (relaxation time τ_0) has been added to a set of mechanisms attributed to internal motions and spaced in accordance with the Zimm spectrum $(\tau_1, \tau_2, \ldots)$.[8,70] The appropriate equations for $[G']_R$ and $[G'']_R$ are as follows:

$$[G']_R = m_1\omega^2\tau_0^2/(1 + \omega^2\tau_0^2) + zZ'(\omega\tau_1) \tag{46}$$

$$[G'']_R = \omega\tau_0[m_1/(1 + \omega^2\tau_0^2) + m_2] + zZ''(\omega\tau_1) \tag{47}$$

Here the terms in τ_0 are taken from equations 8 and 9, and the functions Z' and

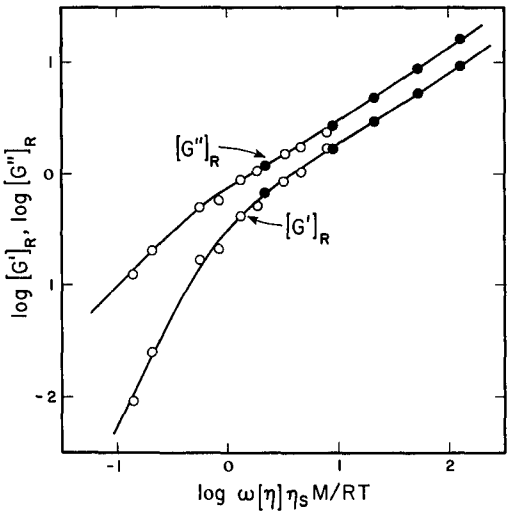


FIG. 9-19. Logarithmic plots of $[G']_R$ and $[G'']_R$ against $\omega[\eta]\eta_s M/RT$ for poly(γ-benzyl-L-glutamate) with $\overline{M}_w = 57 \times 10^4$ in dimethyl formamide (open circles) and *n*-cresol (black circles).[8] The different solvent viscosities extend the effective frequency range. Curves drawn from equations 46 and 47 with $m_1 = 0.555$, $m_2 = 0$, $\tau_1/\tau_0 = 0.211$, and $z = 1$. Reproduced, by permission, from *Biopolymers*.

Z'' are given by equations 15 and 16, reformulated in terms of τ_p/τ_1:

$$Z'(\omega\tau_1) = \sum_{p=1}^{N} \frac{(\omega\tau_1)^2(\tau_p/\tau_1)^2}{1 + (\omega\tau_1)^2(\tau_p/\tau_1)^2}$$

$$Z''(\omega\tau_1) = \sum_{p=1}^{N} \frac{(\omega\tau_1)(\tau_p/\tau_1)}{1 + (\omega\tau_1)^2(\tau_p/\tau_1)^2}$$

with the ratios τ_p/τ_1 specified by the Zimm spectrum for dominant hydrodynamic interaction. The numerical coefficients m_1 and m_2 and the relaxation time τ_0 are associated with end-over-end rotation as for the rigid rods treated in Section A; τ_0 is still given by equation 10 with

$$m = (m_1 + m_2 + zS_{1z}\tau_1/\tau_0)^{-1} \tag{48}$$

where S_{1z} is the Zimm summation in Table 9-I (=2.37). The coefficient z is a weighting factor, in practice set equal to unity.

An example is shown in Fig. 9-19 for poly(γ-benzyl-L-glutamate)[8] with a helix length about three times the persistence length. The slopes of and spacing between the lines at higher frequencies accurately specify a Zimm spectrum in which τ_p is proportional to $p^{-3/2}$. However, the motions associated with these relaxation times are not believed to be random configurational changes as in a flexible coil but rather bending modes of a rather stiff structure as described below. A rather large separation between τ_0 and τ_1 causes a bump in the curves somewhat like the effect of branching in Fig. 9-14. Similar agreement with equations 46 and 47 has also been found for poly(*n*-hexyl isocyanate)[71] provided the molecular weight is

sufficiently small and for the protein paramyosin,[72] which consists of two helices coiled around each other. It is of interest that $m_2 = 0$ for the single helices but for paramyosin has a nonzero value of 0.1. It may be recalled that for completely rigid rods m_2 is always finite (Table 9–I).

For several samples of poly(γ-benzyl-L-glutamate) with molecular weights between 6.4×10^4 and 57×10^4, Wada and collaborators[72] showed by combining data from two laboratories that τ_0 (or its equivalent in a somewhat different analysis) conformed to equation 14 with the correct, very strong dependence on molecular length; so this relaxation time clearly represents end-over-end rotation. The others ($\tau_1, \tau_2, \ldots$) might be attributed either flexural or accordionlike elongational modes. For the former, the fundamental relaxation time has been calculated[72] as

$$\tau_F = 5.53 \times 10^{-3} \pi \eta_s L^4 / B \ln(L/d) \tag{49}$$

where B is the flexural rigidity, a measure of resistance to bending. If this is identified with τ_1, comparison with equation 14 shows that with increasing L the spacing between τ_0 and τ_1 narrows and eventually the rotational motion will be obscured by internal motions—the behavior approaches that of a flexible coil. This is clearly observed in poly(*n*-hexyl isocyanate)[71] and there is a suggestion of it in the poly(γ-benzyl-L-glutamate) of highest molecular weight.[69,72] For extensional modes, the fundamental relaxation time is approximately proportional to L^2 and the spacing between τ_0 and τ_1 would widen with increasing L.[73]

From the observed ratio τ_0 and τ_1 and equations 14 and 49, the flexural rigidity B can be calculated[72] and from it the Young's modulus of the helix considered as a uniform rod.[70] This is about 0.2×10^{10} dynes/cm^2 for poly(γ-benzyl-L-glutamate) and 1.2×10^{10} dynes/cm^2 for paramyosin. However, the relation between rotational and internal motions represented by the empirical hybrid spectrum should be modified to conform to improved theory.[68,69]

Equations 46 and 47 have also been applied by Amari and collaborators[74] to describe the frequency dependence of $[G']_R$ and $[G'']_R$ for aqueous solutions of the amylose–iodine complex. A large τ_0/τ_1 ratio indicates that this is a very rigid macromolecule.

2. Polyelectrolytes

A strong polyelectrolyte such as the sodium salt of poly(styrene sulfonate) is also highly extended in a solvent of low ionic strength, as evidenced by an enormous intrinsic viscosity. An indication of the effect of this expansion on viscoelastic properties has been provided by Wada, Doi, and collaborators,[75] who treated a bead-spring model with a small number of charged beads by computer simulation. It was found that with increasing charge the longest relaxation time increased rapidly and approached proportionality to N^3, where N is the number of beads; it corresponds to end-over-end rotation. The next longest relaxation time, attributed to configurational change, was proportional to N^2.

Experimental measurements on polyelectrolytes must be extrapolated to infinite

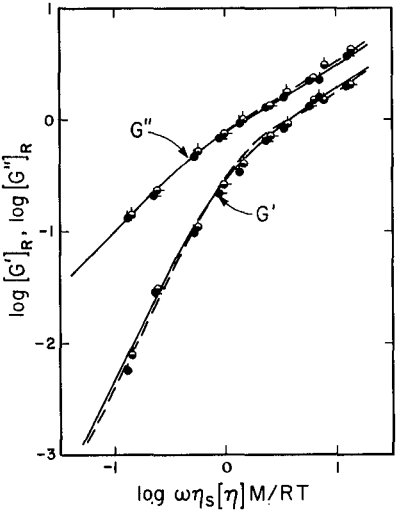


FIG. 9-20. Logarithmic plots of $[G']_R$ and $[G'']_R$ against $\omega[\eta]\eta_s M/RT$ for sodium poly(styrene sulfonate) in 25% aqueous glycerol solvent. Different points refer to sodium concentrations (0.002M and 0.005M) and temperatures (1.0° and 15.0°C). Solid curves drawn from equations 46 and 47 with $m_1 = 0.6$, $m_2 = 0$, $\tau_1/\tau_0 = 0.25$, and $z = 1$. Dashed curves are alternative fit mentioned in text. Reproduced, by permission, from the *Journal of Polymer Science*.[78]

dilution with care to avoid complications due to changing ionic atmospheres of counterions. In the isoionic extrapolation method,[76] the mean activity of a small amount of added salt (with the same ion as the polyelectrolyte counterion) is kept constant.[77] In such a study of sodium poly(styrene sulfonate),[78] the frequency dependences of the intrinsic moduli $[G']_R$ and $[G'']_R$ were found to agree with predictions of the hybrid spectrum of equations 46 and 47 with $m_2 = 0$; an example is shown in Fig. 9-20. An equally good fit is obtained without introducing an additional relaxation time τ_0 but by arbitrarily increasing the first Zimm relaxation time τ_1 by a factor of 2.4 and leaving the other spacings unaltered; this is more nearly consistent with the theory described above.

In this treatment, the shorter relaxation times are attributed not to flexural motions as for the helices described in Section C1, but rather to configurational changes as in the original bead-spring model. The longest relaxation time τ_0 obtained by fitting data to the hybrid spectrum increased with molecular weight (with the 1.7 power, indicating chain extension somewhat short of the maximum which should give nearly a power of 3), and decreased with increasing content of added salt or glycerol.

Measurements on poly(acrylic acid)[79] and poly(methacrylic acid)[80] by Wada and collaborators at very low but finite concentrations led to similar conclusions. Here, since the polyelectrolyte is weak, the degree of neutralization is an additional variable; with decreasing neutralization and average charge per molecule, the longest relaxation time drops rapidly and the end-over-end rotational mode disappears.

D. BEHAVIOR AT FINITE CONCENTRATIONS

Even at very low concentrations, the viscoelastic properties are affected by intermolecular interactions as evidenced by the extrapolation plots of Fig. 9–10. A simple analysis of the initial concentration dependence has suggested that the first effect is an increase in the longest relaxation time.[45] Recent theoretical calculations of Muthukumar and Freed,[81] based on the Freed-Edwards theory of concentration dependence of viscosity in polymer solutions,[82] show that the pth relaxation time has a concentration dependence of the form

$$\tau_p = \tau_p^0(1 + c\mathcal{A}p^{-\kappa}) \tag{50}$$

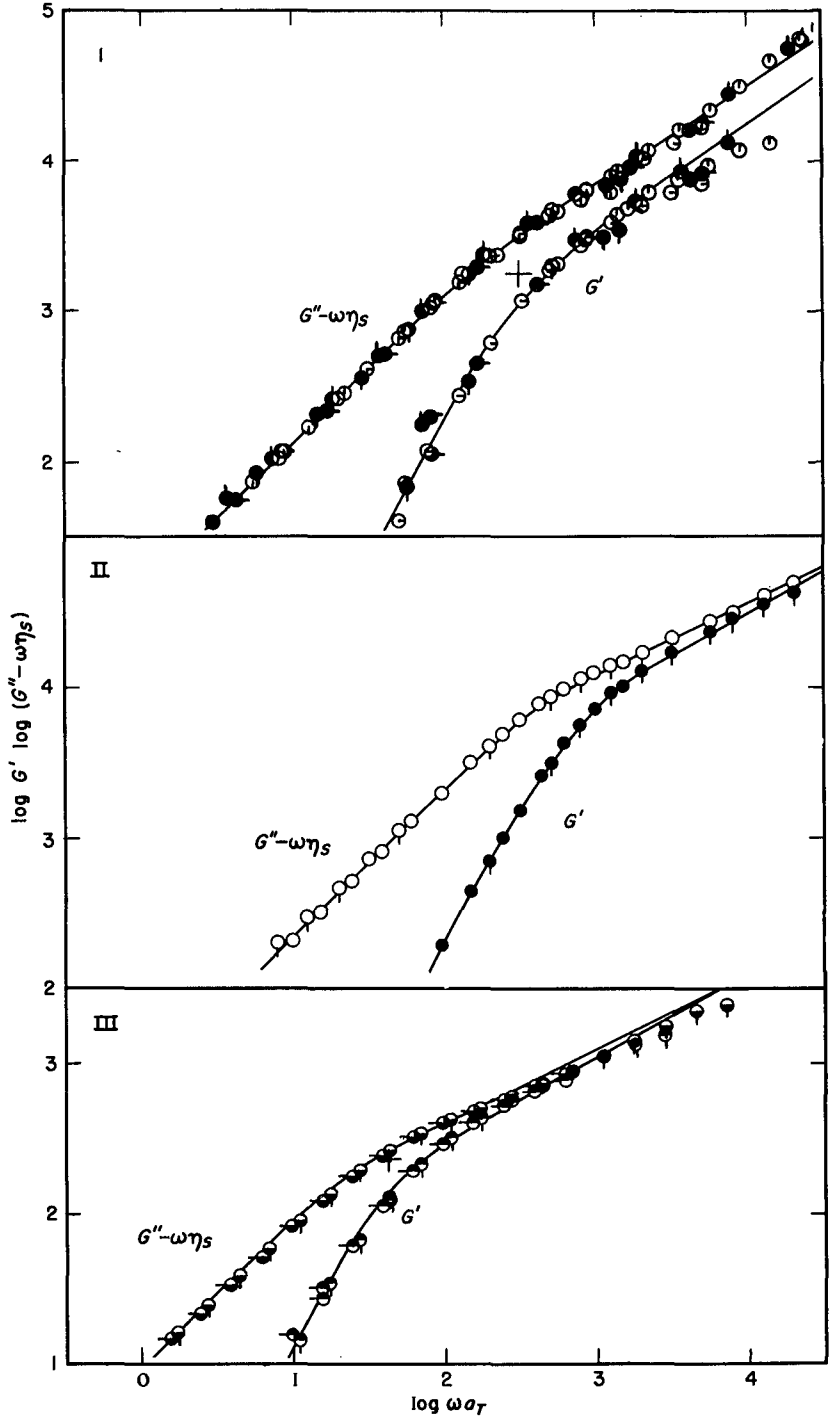
where $\mathcal{A}$ is a constant depending on the extent of the excluded volume effect and the exponent κ is $\frac{1}{2}$ for Θ-solvents and somewhat larger for good solvents. Thus, the effect of concentration in increasing the relaxation times diminishes with increasing mode number p. At higher concentrations, there is increasing interpenetration of the domains of neighboring molecules and the form of the relaxation spectrum is progressively altered. At still higher concentrations, the phenomenon of entanglement coupling, described qualitatively in Chapter 2, can be expected to appear and cause profound changes in the relaxation spectrum. These effects are observed and can be at least qualitatively understood.

1. Effects of Domain Overlap

At finite concentrations, the frequency dependence of G' and $G'' - \omega\eta_s$ can be examined directly without scaling the coordinates as in preceding figures. However, measurements at different temperatures may be combined by reduction to a standard temperature T_0: G' and $G'' - \omega\eta_s$ are multiplied by T_0c_0/Tc and ω is multiplied by a shift factor a_T which is given by $(\eta_0 - \eta_s)_0cT/(\eta_0 - \eta_s)c_0T_0$. Here η_0 is the steady-flow (vanishing shear rate) viscosity and the subscript 0 otherwise refers to the reference temperature. This is the method of reduced variables which will be discussed fully in Chapter 11 with explanation of its rationale, and affords an extension of the effective frequency range.

Examples of experimental data at finite concentration are shown in Fig. 9–21 for three polystyrene solutions[83–85] with sharp molecular weight distribution. In I, the curves for a sample with $M = 267{,}000$ and $c = 0.0286$ g/cm^3 conforms rather closely in shape to the Zimm theory (*cf.* Fig. 9–8–II). In II, the same polymer at $c = 0.124$ conforms more nearly to the Rouse theory (*cf.* Fig. 9–8–I). In III, a sample of higher molecular weight (1,700,000) but the same concentration as I also conforms rather closely to the Rouse theory.

The results illustrate principles which have been observed repeatedly. At low finite concentrations, the form of the frequency dependence approaches the Zimm theory, especially in a Θ-solvent. At somewhat higher concentrations, the shape of the frequency dependence changes progressively toward the Rouse theory. The higher the molecular weight, and the better the solvent, the lower the concentration at which the change in behavior is accomplished.


I
II
III
G''-ωηs
G'
log G' log (G''-ωηs)
log ωaT
0
1
2
3
4
5

The above comparisons with theory are concerned only with the shapes of the logarithmic plots. Quantitative agreement with magnitudes can be obtained only with the introduction of adjustable parameters. Thus, at finite concentrations, $[G']_R$ and $[G'']_R$ in equations 15 and 16 could be replaced by $G'M_{ve}/cRT$ and $G''M_{ve}/cRT$; the apparent molecular weight M_{ve} must be chosen somewhat larger than the true molecular weight M. The terminal relaxation time τ_1 can be obtained as $S_1A_G/S_2(\eta_0 - \eta_s)$; it is larger than the value at infinite dilution but is still proportional to η_s when data in different solvents are compared.[86]

A different index of the change from Zimmlike to Rouselike behavior with increasing concentration can be obtained from the limiting behavior at low frequencies. This does not involve differences in frequency dependence, since G' and $G'' - \omega\eta_s$ are proportional to ω^2 and ω respectively in this region for all theories; instead, it depends on the magnitudes of the respective proportionality constants, which are A_G and $\eta_0 - \eta_s$. In connection with Table 9–II, it was noted that the parameter S_2/S_1^2 varies from 0.2 to 0.4 for the change from free draining to dominant hydrodynamic interaction. For finite concentrations this parameter can be identified[85] with

$$J_{eR}^0 = A_G cRT/M(\eta_0 - \eta_s)^2 \tag{51}$$

At infinite dilution, this reduces to equation 37. The ratio S_2/S_1^2 can also be obtained from normal stress difference measurements at low $\dot{\gamma}$ through the relation $\Psi_{1,0} = 2A_G$ (equation 74 of Chapter 3).[90–92] From measurement of A_G and η_0, it is found that (provided the molecular weight distribution is very narrow) J_{eR}^0 does indeed increase from 0.2 to 0.4 as the product $c[\eta]$ goes from 0 to about 5;[85] the higher the molecular weight, the lower the concentration at which the change occurs, and the dependence on $c[\eta]$ suggests that the critical feature is the degree of coil overlap as gauged by this product,[87] and that the critical value of the product is about 3. However, at higher concentrations J_{eR}^0 may rise above 0.4 and depend on concentration in a complicated manner.[88,89]

The change from Zimmlike to Rouselike behavior apparent in both these symptoms suggests that coil overlap (in the concentration range sometimes described as "semidilute") nullifies the hydrodynamic interaction between different portions of the same molecule as they are shielded from each other by interpenetration of foreign polymer segments. In the theory of Wang and Zimm,[93] this shielding is treated in terms of the bead-spring model of a single chain with a background of uniformly distributed beads, and described by a screening parameter which is a function of $c[\eta]$ and can be correlated with S_2/S_1^2. The predicted frequency dependence at finite concentrations gives very good agreement with experiment. Further details of the concentration dependence of viscoelastic properties are provided by the theory of Muthukumar and Freed.[81]

FIG. 9–21. Logarithmic plots of G' and $G'' - \omega\eta_s$ against frequency reduced to a reference temperature of 25.0°C for polystyrenes with narrow molecular weight distribution in chlorinated diphenyl.[83–85] (I) M = 267,000, c = 0.0286 g/cm^3, measurements at several temperatures from 10.0° to 30.0°C. (II) M = 267,000, c = 0.124, measurements at 0° and 25°C. (III) M = 1,700,000, c = 0.0253, measurements at 10° and 25°C.

De Gennes[94] and Adam and Delsanti[95] have discussed the properties of solutions in the concentration range of coil overlap in terms of a critical concentration c^* which is defined as $M/N_0 s^3$, where s is the radius of gyration and N_0 is Avogadro's number. This is similar in magnitude to the concentration defined by $c[\eta] = 3$. Above the c^*, the solution is termed semidilute.

2. Onset of Entanglement Coupling

At still higher concentrations, the form of the frequency dependence changes entirely and a region appears in which $G'' - \omega\eta_s$ is actually smaller than G' so that the curves cross, as illustrated in Fig. 9-22.[86] The width of the "crossover" region increases rapidly with c, and also with M. The behavior corresponds to the development of a plateau zone as seen in undiluted polymers of high molecular weight in Figs. 2-3 and 2-4; it is attributable to entanglement coupling, and its onset corresponds to a critical value of $cM/\rho M_C^0$, where M_C^0 is a characteristic molecular weight of the undiluted polymer and ρ is its density, as will be discussed in Chapter

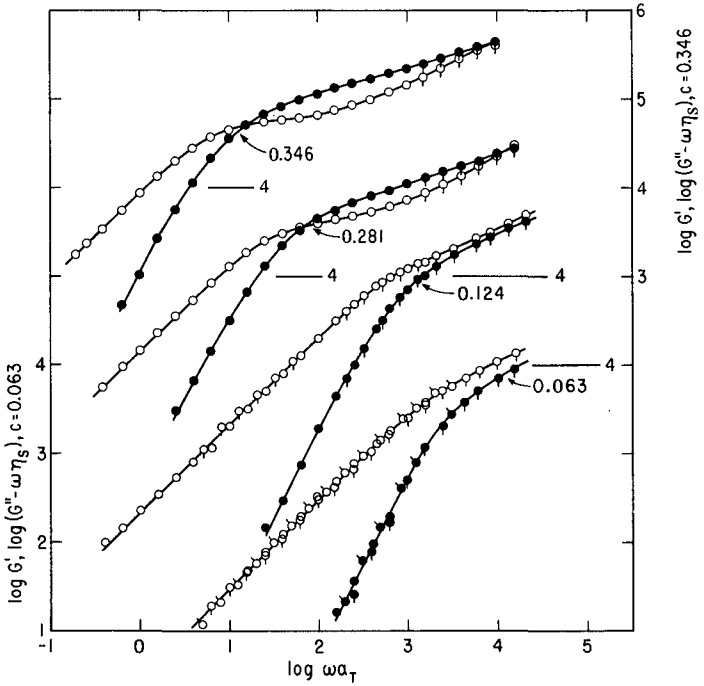


FIG. 9-22. Logarithmic plots of G' (black circles) and $G'' - \omega\eta_s$ (open circles) against frequency reduced to a reference temperature of 25.0°C for polystyrene with M = 267,000 in chlorinated diphenyl (Aroclor 1232).[86] Ordinates displaced as shown by respective locations of 4 on the vertical scale. Numbers refer to concentrations c in g/cm^3; tags on points to different temperatures of measurement, between 0° and 25°C. Reproduced, by permission, from the *Journal of Polymer Science.*

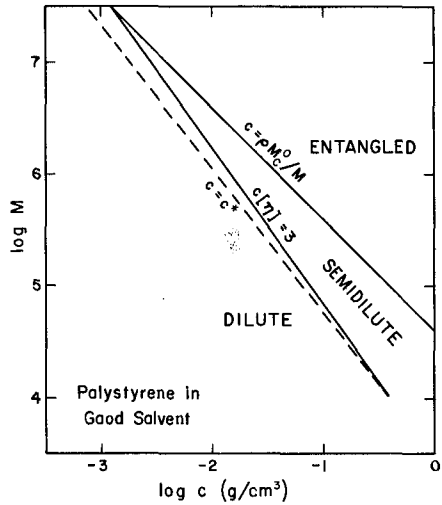


FIG. 9-23. Schematic delineation of dilute, semidilute, and entangled regions on a logarithmic map of M against c for polystyrenes in a good solvent.

17. Thus while the product $c[\eta]$ controls the change in behavior seen in Fig. 9-21, the product cM controls that seen in Fig. 9-22. The relation between these dependences is shown in Fig. 9-23 for polystyrene in a good solvent where $[\eta]$ can be taken as 1.00×10^{-2} $M^{0.72}$ and M_C^0 is taken as 36,000 (Chapter 13). For $M < 10^7$, the solutions progress with increasing concentration from dilute to semidilute to entangled. For higher molecular weights, the lines appear to cross; this unrealistic result is probably due to failure of the entanglement criterion when the density of polymer segments in a coil domain is highly nonuniform. Since the concentration range in which entanglement coupling appears is well outside the dilute range which is the subject of this chapter, further discussion of this phenomenon is postponed to Chapters 10 and 17.

3. Rigid Rodlike Macromolecules

The concentration of rigid rodlike molecules cannot be increased very much before spontaneous separation occurs into a concentrated ordered and a very dilute disordered phase, as required by thermodynamic relations,[96] although the separation may occur at higher concentrations if there is some degree of flexibility,[97] and may be delayed by steric hindrance so that a metastable disordered state may persist. The rotation of rigid rods at finite concentration is impeded by collisions and the rotatory relaxation time should increase rapidly with concentration. The theory has been treated by Doi[98] and Doi and Edwards,[99] who conclude that the relaxation time is approximately proportional to c^2L^6, where L is the molecular length.

E. BEHAVIOR AT HIGH FREQUENCIES AND IN HIGH-VISCOSITY SOLVENTS

The bead-spring model theories of Section B imply that the solute molecule is completely limp with no internal resistance to configurational change; more precisely, internal resistance is evaded by restricting the treatment to long-range configurational changes (index p not too high) for which the frictional resistance of the medium dominates. Under these circumstances, G' and $G'' - \omega\eta_s$ increase steadily with frequency as in Fig. 9-8; but this type of frequency dependence cannot extend indefinitely. At very high frequencies, it is found that G'' becomes directly proportional to ω instead of to a fractional power, so that η' approaches a constant value somewhat higher than the solvent viscosity. There is an indication that G' is approaching a limiting value, but this is uncertain because of the difficulty of measurement. This behavior is illustrated in Fig. 9-24 for a polystyrene of molecular weight 860,000 in a solvent whose viscosity is very high and strongly temperature dependent, so that the relaxation times are very long at low temperatures and very high values of the product $\omega\tau_1$ are achieved.[100] The temperature dependence is taken care of by the shift factor a_T mentioned in Section D1 (see Chapter 11). This observation represents no real conflict with the theories of Section B, since at frequencies sufficiently high that equations 15 and 16 fail to converge for $p < N$

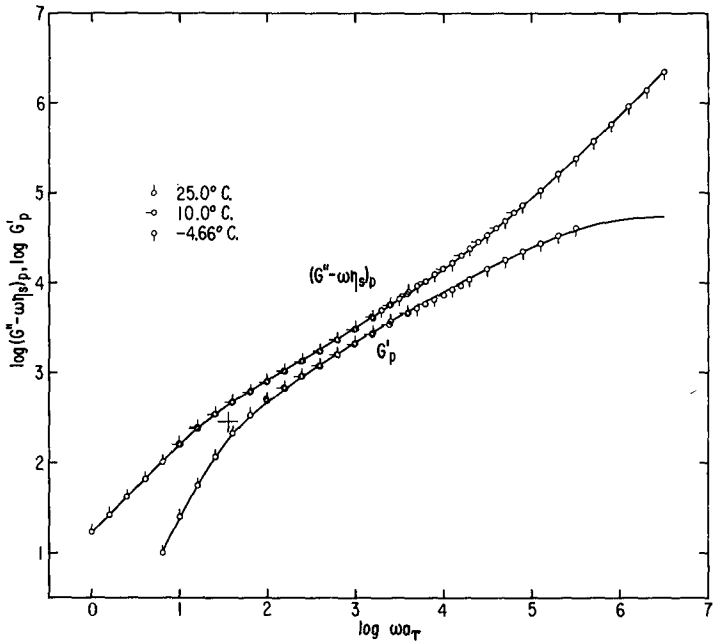


FIG. 9-24. Logarithmic plots of G' and $G'' - \omega\eta_s$ against frequency reduced to 25°C for polystyrene with M = 860,000 in chlorinated diphenyl, c = 0.015 g/cc. Subscript p denotes multiplication by $T_0\rho_0/T\rho$ where ρ's are solution densities and subscript 0 refers to 298° K.[100] Reprinted with permission from Macromolecules, **4**, 210 (1971). Copyright by the American Chemical Society.

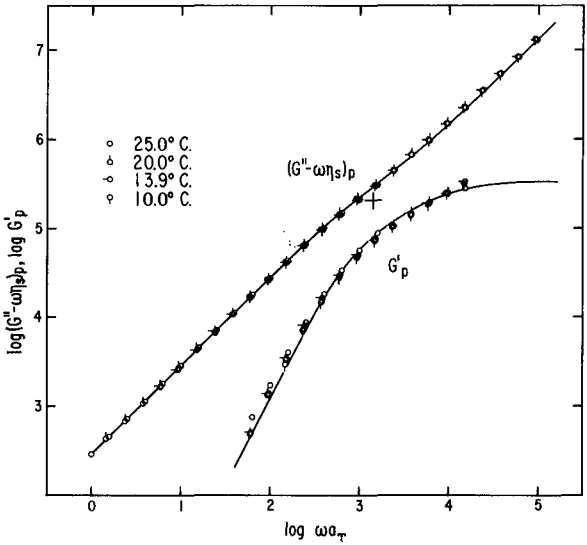


FIG. 9-25. Plots analogous to Fig. 9-24 for polystyrene with M = 19,800, c = 0.076 g/cm^3.[100] Reprinted with permission from Macromolecules, **4**, 210 (1971). Copyright by the American Chemical Society.

with a reasonable finite value of N, the approximations used in equation 22 are inapplicable. Because N, though unspecified, is proportional to M, this restriction will be more serious at low molecular weights, and at sufficiently low molecular weights the size of the submolecule cannot be eliminated from the theory. For example, in Fig. 9-25 for a polystyrene of molecular weight 19,800, the usual intermediate region with a slope between $\frac{1}{2}$ and $\frac{2}{3}$ has almost completely disappeared.

Although the high-frequency behavior of G' is somewhat in doubt, the approach of $G''/\omega = \eta'$ to a limiting value higher than η_s is well established for several polymers with a wide range of molecular weights, and both linear and branched.[100-103] An alternative illustration is shown in Fig. 9-26 and two others with a linear plot of $(\eta' - \eta_s)/a_T$.[100] The limiting value of η' has been denoted η'_∞ although the subscript may be misleading because there is evidence of another dispersion at still higher frequencies followed by a lower plateau in η'.[26,104]

It is found empirically that the concentration dependence of η'_∞ can be expressed by proportionality of $\ln(\eta'_\infty/\eta_s)$ to c, and the proportionality constant can be shown to be the high-frequency intrinsic viscosity $[\eta']_\infty$. An example is shown in Fig. 9-27 for five linear polystyrenes with widely different molecular weights and three branched samples.[102] The high-frequency intrinsic viscosity is independent of branching as would be expected for a quantity which reflects a very local motion within the molecule; it is also independent of molecular weight for $M \geq$ 19,800. At M = 19,800, it is almost equal to the ordinary (steady-flow) intrinsic viscosity. However, $[\eta']_\infty$ does depend on detailed chemical structure as shown in Fig. 9-28, where data for several polymers are similarly plotted.[103] Thus the high-frequency behavior is in a sense just the opposite of the low-frequency viscoelastic behavior

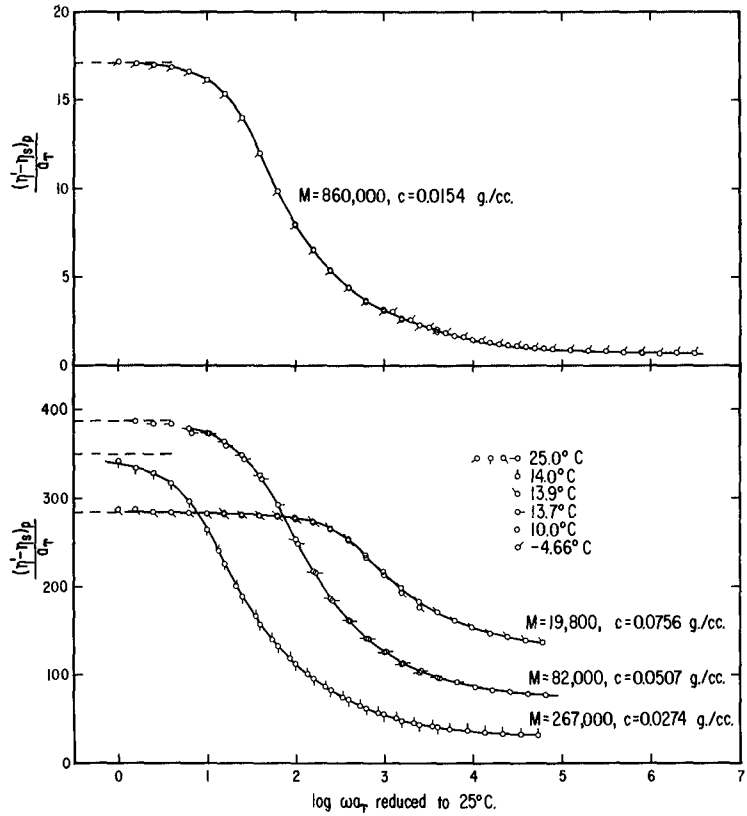


FIG. 9-26. Plot of $(\eta' - \eta_s)/a_T$ against log ωa_T reduced to 25.0°C for data of Figs. 9-24 and 9-25 and two other polystyrenes of intermediate molecular weights. Reprinted with permission from Macromolecules, **4**, 210 (1971). Copyright by the American Chemical Society.

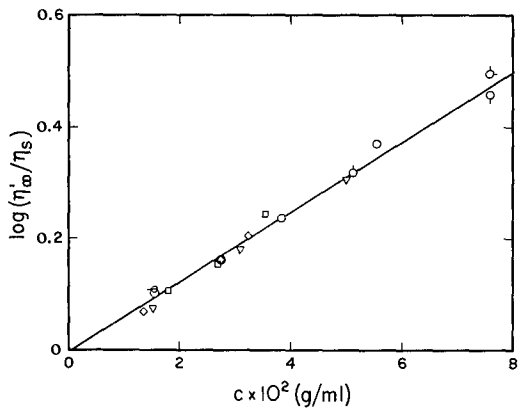


FIG. 9-27. Plot of log (η_∞'/η_s) against concentration for five linear, two star-branched, and one comb-branched polystyrene in chlorinated diphenyl. Circles with different pips, linear with M = 19,800 to 860,000; square, four-arm star; triangle, nine-arm star; diamond, 24-arm comb.[102] Reprinted with permission from Macromolecules, **8**, 539 (1975). Copyright by the American Chemical Society.

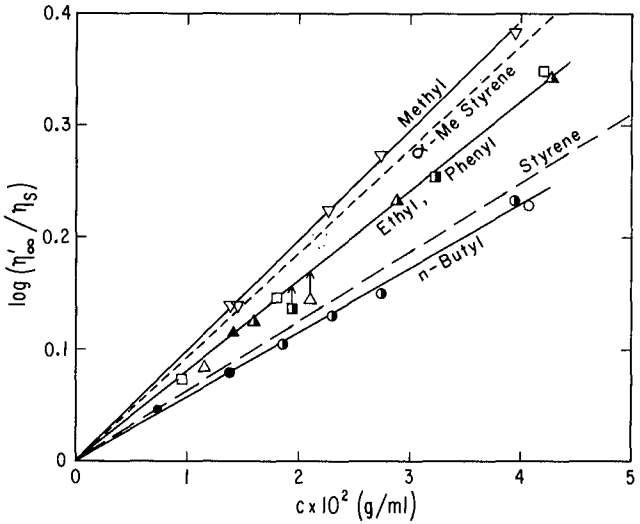


FIG. 9-28. Plots analogous to Fig. 9-27 for polystyrene, poly(α-methyl styrene), and four poly(2-substituted methyl acrylate)s identified by their substituents (methyl, ethyl, *n*-butyl, and phenyl). Open, half black, and black points refer to different molecular weights. Reprinted with permission from Macromolecules, **8**, 672 (1975). Copyright by the American Chemical Society.

which is independent of detailed chemical structure but strongly dependent on molecular weight, molecular weight distribution, and branching.

The data shown in Figs. 9-24 to 9-28 were all obtained at moderate frequencies in high-viscosity solvents. A few data are available from the much more difficult experiment at very high frequencies in low-viscosity solvents.[105] Both sources for $[\eta]_\infty$ are compared in Table 9-III. The agreement between values measured under these extremely different conditions in two cases indicates that the methods are essentially equivalent.

The finite values of $[\eta]_\infty$ imply additional dissipation of energy by mechanisms other than the frictional resistance of beads in the bead-spring model. Theories have

Table 9-III

HIGH-FREQUENCY INTRINSIC VISCOSITIES, $[\eta]_\infty$ (ml/g)

Polymer	Moderate Frequency High-η Solvent	Frequency $\sim 10^5$ Hz Low-η Solvent	Ref.
Polystyrene	14.3	15	100,102,105
Poly(α-methyl styrene)	22.2	18	101,105
Poly(1,4-butadiene)		8	105
Polyisobutylene		7	105
Poly(methyl methacrylate)	22.8		103
Poly(methyl-2-ethyl acrylate)	18.5		103
Poly(methyl-2-*n*-butyl acrylate)	13.3		103
Poly(methyl-2-phenyl acrylate)	18.5		103

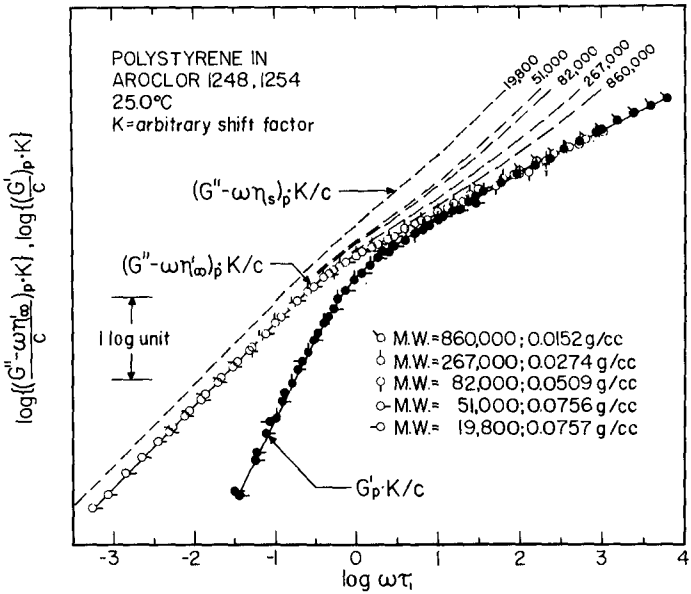


FIG. 9-29. Logarithmic plots of G'/c and $(G'' - \omega\eta_\infty)/c$ against $\omega\tau_1$, reduced to 25.0°C, for polystyrenes of five different molecular weights in chlorinated diphenyl. Dashed lines correspond to $(G'' - \omega\eta_s)/c$ as plotted in Figs. 9-24 and 9-25.[118] Reprinted with permission from Macromolecules, **11**, 119 (1978). Copyright by the American Chemical Society.

been developed to describe this by an internal viscosity either with retention of the bead-spring framework[105-112] or replacement of it by a more detailed model with fixed bond lengths and rotation barriers,[113,114] usually with application of computer simulation.[115] The bead-spring model can be modified to include side-group motions.[111] The additional dissipation has also been ascribed to friction between monomer units widely separated along the molecular contour but adjacent in space.[116] The theory is currently in a stage of rapid development.

The existence of a limiting high-frequency viscosity η'_∞ which is higher than η_s had led to examination of the frequency dependence of $G'' - \omega\eta'_\infty$ instead of $G'' - \omega\eta_s$ and comparisons of it with predictions of the bead-spring theory. This was observed by Lamb and Matheson,[117] who found that an empirical assignment of η'_∞ resulted in frequency dependence resembling the Rouse free-draining form. Schrag and collaborators[118] have used experimental values of η'_∞ in an extensive series of comparisons and found close agreement with the Rouse theory, $h^* = 0$, for several polymers with a wide range of molecular weights and concentrations; an example is shown in Fig. 9-29. When described in this manner, the free-draining behavior characteristic of finite concentrations with molecular overlap as in Section D1 appears at a much lower concentration. In one example,[118] data even at infinite dilution when plotted as $[G'' - \omega\eta'_\infty]$ correspond to an unusually low h^*. The significance of these observations has not yet been clearly resolved.

F. NON-NEWTONIAN FLOW

Very dilute solutions of axisymmetric rigid molecules exhibit not only frequency-dependent viscoelastic properties but also an apparent viscosity which depends on shear rate. This non-Newtonian flow is predicted by theory for elongated ellipsoids[5,119,120] and rigid dumbbells,[121] and the theoretical results have been widely applied for certain biological macromolecules. The shear-rate dependent viscosity η is defined as the ratio of shear stress σ to shear rate $\dot{\gamma}$, and the intrinsic viscosity as defined by equation 5 with η substituted for η_0 is then in general a function of $\dot{\gamma}$. At low shear rates, the shear-dependent intrinsic viscosity has the form

$$[\eta] = [\eta]_0(1 - A\beta^2 + \text{higher terms in even powers of } \beta) \tag{52}$$

where $\beta = ([\eta]_0\eta_s M/RT)\dot{\gamma}$, and $[\eta]_0$ is the limiting value of $[\eta]$ at vanishing shear rate. The dimensionless numerical coefficient A is near unity and depends on the details of the model.

For flexible coils, the bead-spring theories with Hookean springs predict no non-Newtonian behavior; η is independent of $\dot{\gamma}$. In fact, measurements on very dilute solutions do show a small effect, describable at low values of β by equation 52 with much smaller values of A; decreases of $[\eta]/[\eta]_0$ from 1 down to about 0.7 have been observed.[122-124] The failure of the bead-spring model with Hookean springs to predict any shear rate dependence of $[\eta]$ is evidently associated with the unrealistic unlimited extensibilities of the springs.[1,125,126] Rather good agreement of experimental results has been observed with the theory of Fixman,[127] in which the decrease in intrinsic viscosity with increasing $\dot{\gamma}$ is attributed to the effect of molecular distortion on excluded volume.

At higher concentrations, where the molecules are substantially entangled, the non-Newtonian behavior is enormously amplified, and η/η_0 may fall by several orders of magnitude. This phenomenon, as in undiluted polymers, is associated with topological restraints that can be represented by entanglement coupling or tube constraints, and will be discussed in Chapters 10, 13, and 17.

G. PRACTICAL ASPECTS OF VISCOELASTICITY OF DILUTE SOLUTIONS

Although the applications of dilute polymer solutions in which viscoelasticity is important are few, two examples may be cited. In the phenomenon of drag reduction, frictional resistance associated with turbulent flow of a liquid is substantially reduced by exceedingly small concentrations of dissolved polymer.[128,129] Although the mechanism is not clearly established, it is evidently related to viscoelastic properties.[130] Another phenomenon associated with polymers in dilute solution is vortex inhibition.[131] Lubrication in bearings and gears is associated with periodic loading patterns, and because of the wide use of oils with polymeric ad-

ditives the relation of viscoelastic properties to the effectiveness of lubrication, dissipation of energy, and wear of lubricated surfaces is of considerable interest.[132-134]

REFERENCES

1. R. B. Bird, O. Hassager, R. C. Armstrong, and C. F. Curtiss, *Dynamics of Polymeric Liquids*, Volume II, Wiley, New York, 1977.
2. Reference 1, p. 642.
3. A. Peterlin and H. A. Stuart, *Ann. Phys.*, **112**, 1, 129 (1939).
4. J. G. Kirkwood and P. L. Auer, *J. Chem. Phys.*, **19**, 281 (1951).
5. R. Cerf, *C. R.*, **234**, 1549 (1952).
6. Reference 1, p. 545.
7. R. Ullman, *Macromolecules*, **2**, 27 (1969).
8. T. C. Warren, J. L. Schrag, and J. D. Ferry, *Biopolymers*, **12**, 1905 (1973).
9. H. Yamakawa, *Macromolecules*, **8**, 339 (1975).
10. N. Nemoto, F. H. M. Nestler, J. L. Schrag, and J. D. Ferry, *Biopolymers*, **16**, 1957 (1977).
11. N. Nemoto, J. L. Schrag, J. D. Ferry, and R. W. Fulton, *Biopolymers*, **14**, 409 (1975).
12. S. Broersma, *J. Chem. Phys.*, **32**, 1626 (1960).
13. O. Hassager, *J. Chem. Phys.*, **60**, 4001 (1974).

13a. R. F. Doolittle, D. M. Goldbaum, and L. R. Doolittle, *J. Mol. Biol.*, **120**, 311 (1978).

14. M. V. Vol'kenshtein, *Configurational Statistics of Polymeric Chains*, Interscience, London, 1963.
15. P. J. Flory, *Statistical Mechanics of Chain Molecules*, Interscience, New York, 1969.
16. J. G. Kirkwood and R. M. Fuoss, *J. Chem. Phys.*, **9**, 329 (1941).
17. J. G. Kirkwood, *Rev. Trav. Chim.*, **68**, 649 (1949).
18. J. G. Kirkwood, *J. Polym. Sci.*, **12**, 1 (1954).
19. W. H. Stockmayer and M. Kurata, *Adv. Polym. Sci.*, **3**, 196 (1963).
20. P. J. Flory, *Principles of Polymer Chemistry*, Chapter X, Cornell University Press, Ithaca, N. Y., 1953.
21. L. R. G. Treloar, *The Physics of Rubberlike Elasticity*, 3rd ed., Clarendon Press, Oxford, 1975.
22. P. E. Rouse, Jr., *J. Chem. Phys.*, **21**, 1272 (1953).
23. B. H. Zimm, *J. Chem. Phys.*, **24**, 269 (1956).
24. P. Debye, *J. Chem. Phys.*, **14**, 636 (1946).
25. F. Bueche, *J. Chem. Phys.*, **22**, 603 (1954).
26. K. Osaki, *Adv. Polym. Sci.*, **12**, 1 (1973).
27. H. Yamakawa, *Modern Theory of Polymer Solutions*, Harper and Row, New York, 1971.
28. G. C. Berry and E. F. Casassa, *Macromol. Rev.*, **4**, 1 (1970).
29. B. Gross, *J. Polym. Sci.*, **20**, 123 (1956).
30. J. D. Ferry, in *Die Physik der Hochpolymeren*, H. A. Stuart, editor, Volume IV, Springer-Verlag, Berlin, 1956, p. 96.
31. H. Giesekus, *Kolloid-Z.*, **147**, 29 (1956); *Rheol. Acta*, **5**, 29 (1966).
32. J. G. Kirkwood and J. Riseman, *J. Chem. Phys.*, **16**, 565 (1948).
33. A. S. Lodge and Y.-J. Wu, *Rheol. Acta*, **10**, 539 (1971); Mathematics Research Center Technical Summary Report No. 1250, University of Wisconsin, October, 1972.
34. K. Osaki, *Macromolecules*, **5**, 141 (1972).
35. N. W. Tschoegl, *J. Chem. Phys.*, **39**, 149 (1963).
36. A. Peterlin, *J. Chem. Phys.*, **23**, 2464 (1955).

37. O. B. Ptitsyn and Yu. E. Eisner, *Zh. Fiz. Khim.*, **32,** 2464 (1958).
38. O. B. Ptitsyn and Yu. E. Eisner, *Zh. Tekh. Fiz.*, **29,** 1117 (1959).
39. N. W. Tschoegl, *J. Phys. Chem.*, **40,** 473 (1964).
40. H. Yamakawa, *Ann. Rev. Phys. Chem.*, **25,** 179 (1974).
41. M. Bixon, *Ann. Rev. Phys. Chem.*, **27,** 65 (1976).
42. M. C. Williams, *AIChE J.*, **21,** 1 (1975).
43. P. H. Verdier and W. H. Stockmayer, *J. Chem. Phys.*, **36,** 227 (1962).
44. M. Fixman, *J. Chem. Phys.*, **69,** 1527, 1538 (1978).
45. R. M. Johnson, J. L. Schrag, and J. D. Ferry, *Polym. J.*, **1,** 742 (1970).
46. H. Tanaka, A. Sakanishi, M. Kaneko, and J. Furuichi, *J. Polym. Sci.*, **C15,** 317 (1966); A. Sakanishi, *J. Chem. Phys.*, **48,** 3850 (1968).
47. A. Sakanishi and H. Tanaka, *J. Phys. Soc. Jpn.*, **24,** 222 (1968).
48. A. Sakanishi, *J. Chem. Phys.*, **48,** 3850 (1968).
49. H. Tanaka and A. Sakanishi, *Proc. 5th Intern. Cong. Rheology*, Volume 4, University of Tokyo Press, 1970, p. 243.
50. J. L. Schrag and R. M. Johnson, *Rev. Sci. Instrum.*, **42,** 224 (1971).
51. K. Osaki, J. L. Schrag, and J. D. Ferry, *Macromolecules*, **5,** 144 (1972).
52. K. Osaki, Y. Mitsuda, R. M. Johnson, J. L. Schrag, and J. D. Ferry, *Macromolecules*, **5,** 17 (1972).
53. T. C. Warren, J. L. Schrag, and J. D. Ferry, *Macromolecules*, **6,** 467 (1973).
54. S. E. Lovell and J. D. Ferry, *J. Phys. Chem.*, **65,** 2274 (1961).
55. E. Menefee and W. L. Peticolas, *J. Chem. Phys.*, **35,** 947 (1961).
56. B. H. Zimm and R. W. Kilb, *J. Polym. Sci.*, **37,** 19 (1959).
57. K. Osaki and J. L. Schrag, *J. Polym. Sci., Polym. Phys. Ed.*, **11,** 549 (1973).
58. Y. Mitsuda, K. Osaki, J. L. Schrag, and J. D. Ferry, *Polym. J.*, **4,** 24 (1973).
59. G. C. Berry, *J. Polym. Sci.*, A-2, **9,** 687 (1971).

59a. M. G. Dibbs, Ph.D. Thesis, University of Wisconsin, 1983.

60. Y. Mitsuda and J. D. Ferry, *Kobunshi Ronbunshu*, **31,** 135 (1974).
61. K. Osaki, Y. Mitsuda, J. L. Schrag, and J. D. Ferry, *Trans. Soc. Rheol.*, **18,** 395 (1974).
62. Y. Mitsuda, J. L. Schrag, and J. D. Ferry, *Polym. J.*, **4,** 668 (1973).
63. Y. Mitsuda, J. L. Schrag, and J. D. Ferry, *J. Appl. Polym. Sci.*, **18,** 193 (1974); N. Nemoto, Y. Mitsuda, J. L. Schrag, and J. D. Ferry, *Macromolecules*, **7,** 253 (1974).
64. O. Kratky and G. Porod, *Rec. Trav. Chim.*, **68,** 1106 (1949).
65. H. Yamakawa and M. Fujii, *Macromolecules*, **6,** 407 (1973).
66. M. T. Record, Jr., C. P. Woodbury, and R. B. Inman, *Biopolymers*, **14,** 393 (1975).
67. C. D. Han and H. Yu, *J. Chem. Phys.*, **61,** 2650 (1974).
68. M. Bixon and R. Zwanzig, *J. Chem. Phys.*, **68,** 1896 (1978).
69. W. H. Stockmayer, in *Molecular Fluids*, edited by R. Balian and G. Weill, Gordon and Breach, London, 1976.
70. R. W. Rosser, J. L. Schrag, J. D. Ferry, and M. Greaser, *Macromolecules*, **10,** 978 (1977).
71. N. Nemoto, J. L. Schrag, and J. D. Ferry, *Polym. J.*, **7,** 195 (1975).
72. N. Ookubo, M. Komatsubara, H. Nakajima, and Y. Wada, *Biopolymers*, **15,** 929 (1976).
73. R. W. Rosser, *Macromolecules*, **12,** 153 (1979).
74. T. Amari, K. Watanabe, and M. Nakamura, *Proc. VI Intern. Congress on Rheology*, Gothenberg, 1976, p. 490.
75. S. Fujimori, H. Nakajima, Y. Wada, and M. Doi, *J. Polym. Sci., Polym. Phys. Ed.*, **13,** 2135 (1975).
76. D. T. F. Pals and J. J. Hermans, *J. Polym. Sci.*, **5,** 733 (1950).
77. E. F. Casassa and H. Eisenberg, *J. Phys. Chem.*, **64,** 753 (1960).
78. R. W. Rosser, N. Nemoto, J. L. Schrag, and J. D. Ferry, *J. Polym. Sci., Polym. Phys. Ed.*, **16,** 1031 (1978).

79. H. Okamoto, H. Nakajima, and Y. Wada, *J. Polym. Sci., Polym. Phys. Ed.*, **12,** 1035 (1974).
80. H. Okamoto and Y. Wada, *J. Polym. Sci., Polym. Phys. Ed.*, **12,** 2413 (1974).
81. M. Muthukumar and K. F. Freed, *Macromolecules,* **11,** 843 (1978).
82. K. F. Freed and S. F. Edwards, *J. Chem. Phys.*, **61,** 3626 (1974); **62,** 4032 (1975).
83. R. B. DeMallie, Jr., M. H. Birnboim, J. E. Frederick, N. W. Tschoegl, and J. D. Ferry, *J. Phys. Chem.*, **66,** 536 (1962).
84. J. E. Frederick, N. W. Tschoegl, and J. D. Ferry, *J. Phys. Chem.*, **68,** 1974 (1964).
85. L. A. Holmes and J. D. Ferry, *J. Polym. Sci.*, **C23,** 291 (1968).
86. L. A. Holmes, S. Kusamizu, K. Osaki, and J. D. Ferry, *J. Polym. Sci.*, A-2, **9,** 2009 (1971).
87. R. Simha and J. L. Zakin, *J. Colloid Sci.*, **17,** 270 (1962).
88. K. Osaki and Y. Einaga, *Prog. Polym. Sci. Jpn.*, **1,** 321 (1970).
89. H. Janeschitz-Kriegl, *Adv. Polym. Sci.*, **6,** 170 (1969).
90. M. C. Williams, *J. Chem. Phys.*, **42,** 2988 (1965); **43,** 4542 (1965).
91. E. Ashare, *Trans. Soc. Rheol.*, **12,** 535 (1968).
92. W. W. Graessley and L. Segal, *Macromolecules,* **2,** 49 (1969).
93. F. W. Wang and B. H. Zimm, *J. Polym. Sci., Polym. Phys. Ed.*, **12,** 1619, 1639 (1974).
94. P. G. de Gennes, *Macromolecules,* **9,** 587 (1976).
95. M. Adam and M. Delsanti, *Macromolecules,* **10,** 1229 (1977).
96. P. J. Flory, *Proc. R. Soc.*, **A234,** 73 (1956).
97. L. P. McMaster, in *Copolymers, Polyblends, and Composites,* edited by N. A. J. Platzer, Adb. Chem. No. 142, American Chemical Society, Washington, D. C., 1975.
98. M. Doi, *J. Phys.*, **36,** 607 (1975).
99. M. Doi and S. F. Edwards, *J. Chem. Soc., Faraday Trans. II,* **74,** 560, 918 (1978).
100. D. J. Massa, J. L. Schrag, and J. D. Ferry, *Macromolecules,* **4,** 210 (1971).
101. K. Osaki and J. L. Schrag, *Polym. J.*, **2,** 541 (1971).
102. J. W. M. Noordermeer, O. Kramer, F. H. M. Nestler, J. L. Schrag, and J. D. Ferry, *Macromolecules,* **8,** 539 (1975).
103. J. W. M. Noordermeer, J. D. Ferry, and N. Nemoto, *Macromolecules,* **8,** 672 (1975).
104. R. S. Moore, H. J. McSkimin, C. Gieniewski, and P. Andreatch, Jr., *J. Chem. Phys.*, **50,** 5088 (1969).
105. B. J. Cooke and A. J. Matheson, *J. Chem. Soc., Faraday Trans. II,* **3,** 679 (1976).
106. R. Cerf, *Adv. Polym. Sci.*, **1,** 382 (1959).
107. A. Peterlin, *Rheol. Acta,* **12,** 496 (1973).
108. J. T. Fong and A. Peterlin, *J. Res. Nat. Bur. Stand.*, **80B,** 273 (1976).
109. R. Cerf, *J. Phys.*, **38,** 357 (1977).
110. S. A. Adelman and K. F. Freed, *J. Chem. Phys.*, **67,** 1380 (1977).
111. T. S. Adler and K. F. Freed, *Macromolecules,* **11,** 1508 (1978).
112. D. A. MacInnes, *J. Polym. Sci., Polym. Phys. Ed.*, **15,** 657 (1977).
113. M. Fixman and G. T. Evans, *J. Chem. Phys.*, **64,** 3474 (1976).
114. M. Doi, H. Nakajima, and Y. Wada, *Coll. Polym. Sci.*, **254,** 559 (1976).
115. M. Fixman, *J. Chem. Phys.*, **69,** 1527, 1538 (1978).
116. P. G. de Gennes, *J. Chem. Phys.*, **66,** 5825 (1977).
117. J. Lamb and A. J. Matheson, *Proc. R. Soc.*, **A281,** 207 (1964).
118. B. G. Brueggeman, M. G. Minnick, and J. L. Schrag, *Macromolecules,* **11,** 119 (1978).
119. G. B. Jeffrey, *Proc. R. Soc.*, **A102,** 161 (1922–23).
120. N. Saito, *J. Phys. Soc. Jpn.*, **6,** 297 (1951); **7,** 554 (1952).
121. Reference 1, p. 536.
122. I. Noda, Y. Yamada, and M. Nagasawa, *J. Phys. Chem.*, **72,** 2890 (1968).
123. H. Suzuki, T. Kotaka, and H. Inagaki, *J. Chem. Phys.*, **51,** 1279 (1969).
124. Y. Ito and S. Shishido, *J. Polym. Sci., Polym. Phys. Ed.*, **16,** 725 (1978).
125. R. C. Armstrong, *J. Chem. Phys.*, **60,** 724, 729 (1974).

126. R. L. Christiansen and R. B. Bird, *J. Non-Newt. Fluid Mech.*, **3**, 161 (1977/8); **5**, 1 (1979).
127. M. Fixman, *J. Chem. Phys.*, **45**, 793 (1966).
128. B. A. Toms, *Proc. Intern. Cong. Rheology*, North-Holland, Amsterdam, p. II-135 (1948).
129. J. L. Lumley, *Macromol. Rev.*, **7**, 263 (1973).
130. R. Y. Ting and D. L. Hunston, *Ind. Eng. Chem., Prod. Res. Dev.*, **16**, 129 (1977).
131. R. J. Gordon and C. Balakrishnan, *J. Appl. Polym. Sci.*, **16**, 1629 (1972).
132. A. Dyson, *Phil. Trans. R. Soc.*, **A266**, 1 (1970).
133. W. Hirst and M. G. Lewis, *Proc. Roy. Soc.*, **A334**, 1 (1973).
134. *The Rheology of Lubricants*, edited by T. C. Davenport, Halsted Press, London, 1973.

CHAPTER 10

Molecular Theory for Undiluted Amorphous Polymers and Concentrated Solutions; Networks and Entanglements

The theories outlined in the preceding chapter provide considerable insight into the relations between viscoelastic properties and the structure and motions of individual polymer molecules. They are, however, restricted to a range of very low concentrations where experiments are difficult and the phenomena have relatively few practical applications. In more concentrated solutions and in undiluted polymers, viscoelastic properties are much easier to measure and are very important in many technological problems. The application of molecular theory to such systems will now be discussed. Further simplifying assumptions are naturally required. Comparisons with experiment are mostly deferred to subsequent chapters. The discussion is largely limited to linear viscoelastic properties in shear. Most of the principles introduced in this chapter are applicable to both undiluted polymers and concentrated solutions, but undiluted polymers are emphasized. Specific features of the dependence of viscoelastic properties on concentration are discussed in Chapter 17 together with various phenomena which have been studied principally in concentrated solutions.

A. UNDILUTED POLYMERS OF LOW MOLECULAR WEIGHT

A useful principle was proposed by Bueche[1] in 1952; the character of molecular motions and configurational changes as described for dilute solutions is much the same in concentrated solution or even undiluted polymer as long as the molecular weight is sufficiently low so that the coupling entanglements discussed qualitatively

in Chapter 2 do not occur. The only effect of changing the surrounding medium from solvent molecules to other polymer molecules is to change (ordinarily, increase) the relaxation times, all by the same factor. In applying bead-spring theory to this situation, the simple Rouse formulation is chosen since hydrodynamic interaction is presumably abolished by the presence of foreign segments within the domain of a given polymer molecule. The discussion in this section is restricted to molecular weights below of the order of 20,000; the limit depends on the chemical structure of the polymer and it is approximately inversely proportional to polymer concentration in the case of concentrated solutions.

1. Modified Rouse Theory

In an undiluted polymer, the number of polymer molecules per cubic centimeter, n, is $\rho N_0/M$ rather than cN_0/M, where ρ is the density. Equations 18 and 19 of Chapter 9 and the corresponding equation for G'' then become[2]

$$G' = (\rho RT/M) \sum_{p=1}^{N} \omega^2\tau_p^2/(1 + \omega^2\tau_p^2) \tag{1}$$

$$G'' = (\rho RT/M) \sum_{p=1}^{N} \omega\tau_p/(1 + \omega^2\tau_p^2) \tag{2}$$

(here, the term $\omega\eta_s$ is ignored because there is no solvent) and

$$G(t) = (\rho RT/M) \sum_{p=1}^{N} e^{-t/\tau_p} \tag{3}$$

Equation 22 of Chapter 9 is unchanged:

$$\tau_p = a^2P^2\zeta_0/6\pi^2p^2kT \tag{4}$$

The characteristic length a will correspond to that in dilute solution in a Θ-solvent. Since the low-frequency limit of G'' is $\omega\eta_0$, the friction coefficient ζ_0 can be expressed in terms of η_0 by a calculation analogous to the derivation of equation 27 of Chapter 9:

$$\zeta_0 = 36\eta_0M_0^2/\rho a^2MN_0 \tag{5}$$

where $M_0 = M/P$ is the monomer molecular weight and N_0 is Avogadro's number. It follows that

$$\tau_p = 6\eta_0M/\pi^2p^2\rho RT \tag{6}$$

In the terminal zone of the frequency scale (*cf.* Chapter 2, Section A3) the properties are dominated by the terminal relaxation time,

$$\tau_1 = 6\eta_0M/\pi^2\rho RT \tag{7}$$

which has several qualitative aspects of practical interest. It is a measure of the time required for internal stresses to relax during an annealing process, and also (since it differs from the terminal retardation time only by a small numerical factor) of the time required to attain steady-state flow under constant stress, or for elastic

recoil to be accomplished after removal of stress (always assuming linear viscoelastic behavior). It also represents in order of magnitude the ratio of energy stored to energy dissipated per second during steady-state flow.

The terminal segments of G' and G'' plotted against ω are described by the equations (in which $1.08 = S_2$ for the Rouse theory)

$$G' = 1.08(\rho RT/M)\omega^2\tau_1^2 \tag{8}$$

$$G'' = \omega\eta_0 \tag{9}$$

Other features of the viscoelastic behavior in the terminal zone are represented by the constants η_0 and J_e^0. Rearrangement of equations 7 and 9, together in the equation 51 of Chapter 9 with omission of η_s as appropriate for undiluted polymer, gives for these quantities

$$\eta_0 = (\rho RT/M)\tau_1 S_1 \tag{10}$$

$$J_e^0 = (\rho RT/M)\tau_1^2 S_2/\eta_0^2 = (M/\rho RT)S_2/S_1^2 \tag{11}$$

where $S_1 = 1.645$ and $S_2/S_1^2 = 0.40$. In the summations S_1 and S_2, which are applicable only for a polymer of uniform molecular weight, the first term contributes 61% of the total viscosity and 92% of the total compliance. Since the first mode of motion corresponds to coordinated movement of the molecule as a whole, the properties in the terminal zone are sensitive to the long-range features of molecular topology, such as molecular weight, molecular weight distribution, and branching.

In the frequency region where G' and G'' are proportional to $\omega^{1/2}$, the continuous relaxation and retardation spectra in equations 23 and 24 of Chapter 9 hold and can be formulated in terms of η_0 by use of equation 5. The frequency dependence of the storage and loss modulus can be expressed either in terms of η_0:

$$G' = G'' = (\sqrt{3}/2)(\rho RT\eta_0/M)^{1/2}\omega^{1/2} \tag{12}$$

or of ζ_0:

$$G' = G'' = (a\rho N_0/4M_0)(\zeta_0 kT/3)^{1/2}\omega^{1/2} \tag{13}$$

where as before N_0 is Avogadro's number and M_0 the monomer molecular weight. This represents the transition zone of viscoelastic behavior where G' is increasing with frequency toward a value characteristic of a hard solid.

The friction coefficient ζ_0 now represents the frictional force per monomer unit per unit velocity encountered by a submolecule junction as it moves through a medium consisting of other polymer molecules; it is ordinarily considerably higher than the ζ_0 of dilute solution theory, which is approximately proportional to solvent viscosity.

If ζ_0 were independent of molecular weight, G' and G'' would be also. Actually, ζ_0 can be readily determined from experimental viscoelastic data by equation 13 or the equivalent for transient properties; with increasing M it increases at first and then approaches an asymptotic limiting value (Fig. 10-1-I). Similar information can be obtained from steady-flow viscosity;[3] from equation 5 it is evident

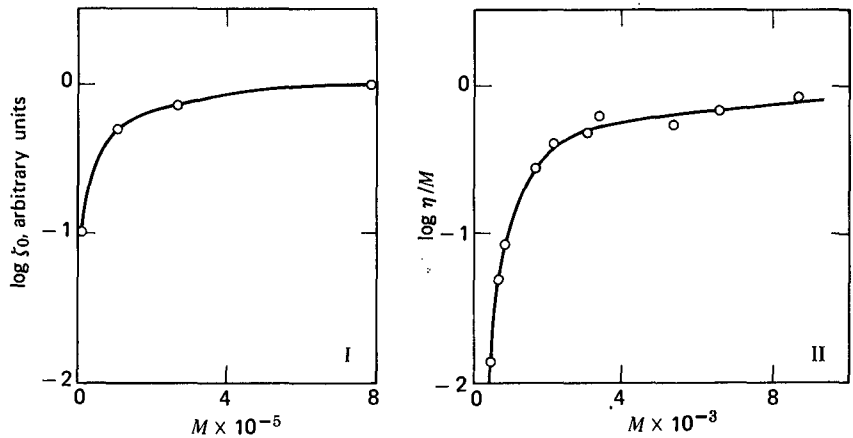


FIG. 10-1. (I) Log ζ_0 plotted against M, for poly(vinyl acetate) fractions at 40°C (data from Reference 67). (II) Log η_0/M plotted against M, for polyisobutylene fractions at 30°C. (Data of Fox and Flory quoted in reference 3.)

that η_0/M is proportional to ζ_0. The ratio η_0/M increases at first and approaches an asymptotic limiting value so long as M does not exceed the minimum value for entanglement coupling (Fig. 10-1-II).

The molecular weight dependence of ζ_0 and η_0/M is attributed to additional free volume associated with molecular ends, as discussed more fully in Chapter 11. The number of molecular ends per unit volume is proportional to $1/M$ and so their influence diminishes with increasing M and then becomes negligible. As will be shown in Chapter 11, the dependence is given approximately as follows at a fixed temperature:

$$\log \zeta_0 = \log \zeta_{00} + (B/2.303)(1/f_M - 1/f_0) \tag{14}$$

$$f_M = f_0 + A/M \tag{15}$$

where f_M is the fractional free volume at molecular weight M, f_0 and ζ_{00} are limiting values at high molecular weight, B is a numerical constant close to unity, and A is a constant related to the excess molar free volume accompanying molecular ends. From f_0, ζ_{00}, and A for a particular polymer, the dynamic viscoelastic properties can be calculated for any (uniform) molecular weight. The significance of the fractional free volume will be explained in Chapter 11. Quite a good picture can be obtained in the form of three straight lines on a logarithmic plot from equations 8, 9, and 13. Schematic plots are illustrated in Fig. 10-2.

The range of applicability of the square-root law, equation 13, is quite restricted. With increasing frequency, it begins at about $\omega\tau_1 = 1$ (Fig. 9-8); here, G' is given by equations 12 and 7 as being close to $\rho RT/M$, which for a maximum M of about 20,000 is 1.2×10^6 dynes/cm^2 at room temperature. It fails, according to the criterion stated in connection with equations 23 and 24 of Chapter 9, when motions within submolecules can no longer be ignored at a frequency corresponding to about $0.5\ \rho RT/qM_0$, where qM_0 is the molecular weight of a submolecule. For $qM_0 =$

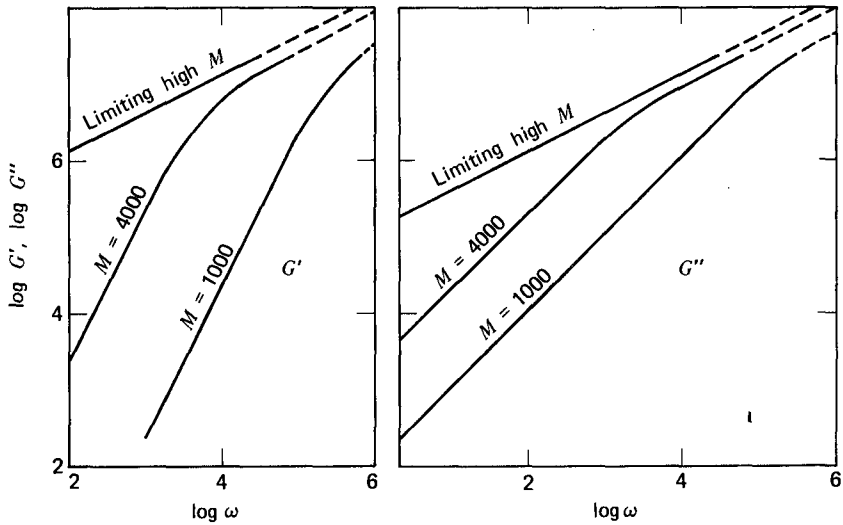


FIG. 10-2. Schematic dependence of G' and G'' on frequency and molecular weight, calculated from equations 7, 8, 9, 12, 14, and 15 and the data of Fig. 10-1-II, for polyisobutylenes at 30°C.

500, for example, the upper limit of G' is 2.5×10^7 (above which the curves in Fig. 10-2 are dashed). One cannot expect the square-root law to be applicable over much more than a G' range of a power of 10, therefore. In the remainder of the transition zone where G' increases toward something like 10^{10} dynes/cm^2, some other theoretical treatment will be necessary. This limitation was emphasized by Williams[4] with a somewhat different calculation. (In dilute solution, the power-law region can extend considerably farther because there is no restriction to a minimum molecular weight of 20,000; very large molecules can coexist without entanglements.)

For undiluted polymers, unlike dilute solutions, the viscoelastic behavior in stress relaxation and creep is of considerable interest as well as dynamic properties. The functions $G(t)$ and $J(t)$ as predicted by the Rouse theory have been numerically evaluated by Tschoegl,[5] and are tabulated in reduced dimensionless form in Appendix E.

2. Closed Form of Rouse Theory: Ladder Networks

The results of the Rouse theory are usually left in the form of sums because with high-speed computers there is no difficulty in evaluating them. It can be shown, however,[6] that equations 1 and 2 with the summations carried to $N = \infty$ (satisfactory within the restrictions discussed in the preceding paragraph) correspond to the following closed form complex expression for G' and G'':

$$G' + iG'' = (\rho RT/2M)(y \coth y - 1)$$

$$y = (6i\omega\eta_0 M/\rho RT)^{1/2} = (i\pi^2\omega\tau_1)^{1/2} \qquad (16)$$

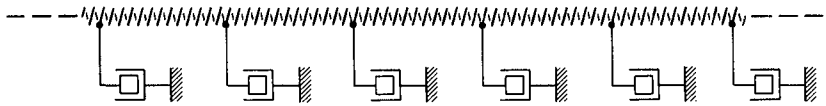


FIG. 10-3. Ladder network of Blizard for uncross-linked polymer of low molecular weight.

which is simpler as a starting point for certain modifications that have been introduced for undiluted polymers. An equation of this form was obtained long ago by Blizard[7] by analogy with a concept of springlike molecules moving in a viscous medium, but only in terms of unspecified constants which provided no information about the absolute magnitudes of the moduli or the location of the frequency scale. It corresponds to the mechanical model shown in Fig. 10-3, analogous to the ladder network in electrical network theory.[8]

A similar ladder network model in which the line of springs is fixed at one end has been used by Marvin and Oser[6,9,10] with various modifications which will be mentioned below. In this case the complex modulus is given by

$$G' + iG'' = (\rho RT/2M)(x \coth x - x/\sinh x)$$
$$x = (2i\pi^2\omega\tau_1/3)^{1/2} \tag{17}$$

which is essentially indistinguishable from equation 15 except for a slight shift in the frequency scale.

3. Effect of Molecular Weight Distribution

In dilute solutions, molecular weight distribution can be rather easily introduced with the assumption that the friction coefficient ζ_0 is the same for all species (Chapter 9, Section B7). In undiluted polymers, ζ_0 may still be taken as the same for all species in a particular mixture, but when species of low molecular weight are present, the uniform value of ζ_0 in the mixture (ζ_{0b}) will depend on the concentration of molecular ends through the free volume, in accordance with equations 14 and 15. Since the number of ends is inversely proportional to the number-average molecular weight, it may be expected that ζ_{0b} can be evaluated from these equations if M in equation 15 is replaced by $\overline{M}_n$. (In Fig. 11-13, data for blends are included in this manner.) Then, provided there are *no* species with molecular weights high enough to participate in coupling entanglements, the contributions of different species to G' and G'' may be considered additive as they are in dilute solution.

The additivity may be illustrated by considering a binary blend of two species of the same polymer with molecular weight M_1 and M_2 ($M_2 > M_1$, but both $< M_C$, where M_C is the minimum molecular weight for the influence of coupling entanglement formation on viscosity). The number of molecules per cubic centimeter, n_i, will be $w_i\rho N_0/M_i$, where w_i is the weight fraction. Thus the magnitude $n_i kT$ of contributions of species i to the relaxation spectrum will be $w_i\rho RT/M_i$. The stress relaxation and dynamic moduli then become

$$G_b(t) = (w_1\rho RT/M_1)\sum_{p=1}^{N} e^{-t/\tau_{p1}} + (w_2\rho RT/M_2)\sum_{p=1}^{N} e^{-t/\tau_{p2}} \tag{18}$$

$$G_b' = (w_1\rho RT/M_1)\sum \omega^2\tau_{p1}^2/(1+\omega^2\tau_{p1}^2) + (w_2\rho RT/M_2)\sum \omega^2\tau_{p2}^2/(1+\omega^2\tau_{p2}^2) \quad (19)$$

$$G_b'' = (w_1\rho RT/M_1)\sum \omega\tau_{p1}/(1+\omega^2\tau_{p1}^2) + (w_2\rho RT/M_2)\sum \omega\tau_{p2}/(1+\omega^2\tau_{p2}^2) \quad (20)$$

$$\tau_{p1} = a^2P_1^2\zeta_{0b}/6\pi^2p^2kT \quad (21)$$

$$\tau_{p2} = a^2P_2^2\zeta_{0b}/6\pi^2p^2kT \quad (22)$$

where the subscript b refers to the blend. When the relaxation times are recalculated in terms of the steady-flow viscosity of the blend, η_b, they become

$$\tau_{p1} = 6\eta_bM_1^2/\pi^2p^2\rho\overline{M}_wRT \quad (23)$$

$$\tau_{p2} = 6\eta_bM_2^2/\pi^2p^2\rho\overline{M}_wRT \quad (24)$$

where $\overline{M}_w$ is the weight-average molecular weight; the ratio $M_i^2/\overline{M}_w$ replaces the factor M appearing in the corresponding expression for a homogeneous polymer (equation 6).

Equations 18 to 20 specify that the contributions of the components to the moduli are additive by mole fraction, on an absolute basis, since the mole fraction is proportional to w_i/M_i. However, if the moduli are expressed in terms of the corresponding properties of the individual pure components, the latter are additive by weight fraction (or more strictly, volume fraction, if their densities are not quite identical). Thus, if $G_1(t)$ and $G_2(t)$ are the relaxation moduli of the respective individual components, equation 18 can be written

$$G_b(t) = v_1G_1(t\eta_1\overline{M}_w/\eta_bM_1) + v_2G_2(t\eta_2\overline{M}_w/\eta_bM_2) \quad (25)$$

(Here the transition from w_i to the volume fraction v_i involves the relation $v_i = w_i\rho/\rho_i$, where ρ_i is the density of the ith component.) The time scale for each component has been shifted by the factor $\eta_i\overline{M}_w/\eta_bM_i$; for the storage and loss moduli, the frequency scale would be shifted to the reciprocal of this factor, and the components would then be additive in the volume fraction in the same manner.

Equation 25 is a special case of a blending law extensively discussed by Ninomiya:[11-13]

$$G_b(t) = v_1G_1(t/\lambda_1) + v_2G_2(t/\lambda_2) \quad (26)$$

where λ_1 (>1) is the factor by which all the relaxation times of a molecule of component 1 in the blend are increased relative to their values when the molecule is surrounded by others of its own kind; and λ_2 (<1) expresses the same ratio for component 2. For the Rouse theory, $\lambda_i = \eta_bM_i/\eta_i\overline{M}_w$.

For undiluted polymers of low molecular weight to which the Rouse theory is applicable, the λ factors are actually determined entirely by ζ_0. Comparison of equations 4, 6, 21, and 23 shows that

$$\lambda_i = \eta_bM_i/\eta_i\overline{M}_w = \zeta_{0b}/\zeta_{0i} \quad (27)$$

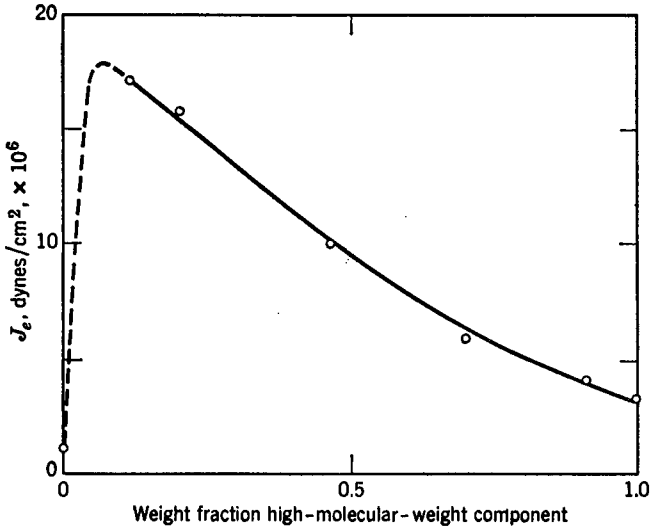


FIG. 10–4. Steady-state shear compliances of blends of two polyisobutylene fractions with weight-average molecular weights of 1.60 and 13.1 × 10^4, plotted against the weight fraction of the component of higher molecular weight. (Data of Leaderman, Smith and Williams.[15])

This is equivalent to the statement that the steady-flow viscosity when corrected for differences in free volume is directly proportional to molecular weight when the latter is below the minimum value for entanglement coupling.[3] The latter relation has been confirmed experimentally for several systems.[3] Also, equation 27 has been confirmed directly (for $i = 2$) from viscoelastic measurements[14] on blends of two polyvinyl acetate fractions of molecular weight 5500 and 10,500.

If equation 25 holds, the viscosity and steady-state compliance of the blend in terms of those of the individual pure components are

$$\eta_b = v_1\lambda_1\eta_1 + v_2\lambda_2\eta_2 \tag{28}$$

$$J^0_{eb} = (\lambda_1^2\eta_1^2 v_1 J^0_{e1} + \lambda_2^2\eta_2^2 v_2 J^0_{e2})/\eta_b^2 \tag{29}$$

For the Rouse theory case, substitution of equation 27 gives

$$\eta_b = v_1\eta_1\zeta_{0b}/\zeta_{01} + v_2\eta_2\zeta_{0b}/\zeta_{02} \tag{30}$$

$$J^0_{eb} = v_1 J^0_{e1}(M_1/\overline{M}_w)^2 + v_2 J^0_{e2}(M_2/\overline{M}_w)^2 \tag{31}$$

Although η_b always lies between η_1 and η_2, J^0_{eb} can exceed both J^0_{e1} and J^0_{e2} especially if $M_2 \gg M_1$ and $w_2 < w_1$. This somewhat surprising fact is illustrated in Fig. 10–4 for some data of Leaderman and associates[15] (though, strictly, one component of this mixture is long enough to participate in coupling entanglements.) Qualitatively, it can be anticipated from equation 11 for the extreme case of a polymer dissolved in a homologous solvent of low molecular weight. Here the density ρ would be replaced by polymer concentration c in g/cc (since $n = cN_0/M$); J^0_e is then inversely proportional to c, and it is higher for the solution than for the pure polymer.

Equation 31 can also be written, after substituting the values of J_{e1}^0 and J_{e2}^0:

$$J_{eb}^0 = (\tfrac{2}{5})\overline{M}_{z+1}\overline{M}_z/\overline{M}_w\rho RT \qquad (32)$$

where $\overline{M}_z$ and $\overline{M}_{z+1}$ are the usual progressively higher moments of the molecular weight distribution. This relation emphasizes the importance of the higher averages in determining the steady-state compliance, and hence the energy stored in steady-state flow.

All the above relations for blends reduce to the correct equations for concentrated soltuions when component 1 is taken as a solvent of low molecular weight. In this case, $\overline{M}_w$ averaged over polymer and solvent is negligibly different from w_2M_2 (unless the solution is extremely dilute), and $\overline{M}_z \cong \overline{M}_{z+1} \cong M_2$. Then equation 24 becomes $\tau_p = 6\eta_0 M_2/\pi^2 p^2 cRT$, and equation 32 becomes $J_e^0 = (\frac{2}{5})M_2/cRT$. These are the same as equations 6 and 11 respectively, with c $(= w_2\rho)$ substituted for ρ.

The calculations for a blend can be readily extended to a continuous distribution of molecular weights.[16-18] The result is the same as that discussed for dilute solutions in Chapter 9, Section B7; the numerical values for a most probable molecular weight distribution are applicable. The steady-state compliance of a polymer with a continuous distribution of molecular weights is given[19] by equation 32 regardless of the form of the distribution. However, all this discussion of molecular weight distribution is limited to the very restricted case that no molecular species long enough to participate in coupling entanglements are present. Otherwise, more complicated behavior is observed which cannot be described by any simple theory (see Chapter 13).

In dealing with a concentrated solution of a polymer with a continuous molecular weight distribution, one normally does not include the solvent in the molecular weight averages, of course; the example given above was calculated in this manner merely to show the consistency of the equations for solutions and blends. If the averages are calculated over the polymer components only, equation 32 and the results of the integrations described above hold with c substituted for ρ. This is quite satisfactory as long as the smallest polymer component is large compared with the solvent molecule. But if there is a continuous spread of polymer components down to monomeric dimensions, the smaller species will not have Rouselike behavior and the problem is not easily formulated.

4. Effect of Branching

For the restricted case of low molecular weights and no coupling entanglements, the viscoelastic properties of star-branched undiluted polymers can be described by a special case of the Zimm-Kilb theory[20] in which there is no hydrodynamic interaction. Calculations were made by Ham[21] by use of a method which is somewhat different from that of Rouse but yields the same results for unbranched molecules. Stars with arms of unequal length were included. For such a branched molecule, the terminal relaxation time τ_1, the viscosity η_0, and the steady-state compliance J_e^0 are always smaller than for an unbranched molecule of the same molecular weight; the more branches and the more nearly equal their lengths, the

Table 10–I

COMPARISONS OF τ_1, η_0, AND J_e^0 FOR BRANCHED AND LINEAR STAR POLYMERS OF THE SAME MOLECULAR WEIGHT[21]

Lengths of Branches	$\tau_{1,B}/\tau_{1,L}$	η_{0B}/η_{0L}	$J^0_{e,B}/J^0_{e,L}$
1/4, 1/4, 1/2	0.68	0.81	0.76
1/5, 1/5, 3/5	0.80	0.86	0.89
1/5, 2/5, 2/5	0.64	0.81	0.73
1/4, 1/4, 1/4, 1/4	0.25	0.63	0.46
1/5, 1/5, 1/5, 2/5	0.48	0.66	0.60
1/6, 1/6, 1/3, 1/3	0.60	0.67	0.58
1/5, 1/5, 1/5, 1/5, 1/5	0.16	0.52	0.36
1/6, 1/6, 1/6, 1/6, 1/3	0.48	0.56	0.49

greater the discrepancy. The appropriate ratios are listed in Table 10–I for several examples. The terminal relaxation time is the most sensitive of the three quantities.

For a complete prediction of the viscoelastic behavior, it would be necessary to substitute the individual relaxation times, which are given by Ham for a number of topologies, into equations 1 to 3. For many purposes, however, Table 10–I combined with equations 7 and 11 will provide useful information. At very short times, where the effects of branching vanish, G' and G'' should be given by equation 13 without modification, noting however that η_0 will not be the same as for an unbranched polymer of the same molecular weight.

It should be emphasized again that these statements about branching apply only to molecules which are short enough, and all of whose branches are short enough, so that there is no participation in coupling entanglements. If entanglements occur, τ_1, η_0, and J_e^0 may all be greater, rather than less, than for an unbranched molecule of the same molecular weight (Chapter 13).

B. CROSS-LINKED NETWORKS

For application to a lightly chemically cross-linked polymer, such as the vulcanized rubbers, Examples VI and VII of Section A of Chapter 2, some modifications in the Rouse theory are clearly necessary. The short-range configurational changes should be oblivious of the presence of cross-links, just as they are of free ends (if the molecular weight is sufficiently high) and of branch points (for long branches); therefore the storage and loss moduli in the transition zone should be given by equation 13 for cross-linked and uncross-linked polymers alike, though the value of ζ_0 may possibly depend slightly on the cross-linking density. At zero frequency or long times, however, the theory for a cross-linked system must diverge and predict an essentially constant finite modulus and infinite viscosity instead of

a zero modulus and finite viscosity. The fact that η_0 is infinite makes equation 12 and all other previous formulations in terms of η_0 meaningless.

1. Idealized Network with Fixed Cross-Links

A common idealization of a lightly cross-linked rubber is a network of tetrafunctional connectivity in which four strands radiate from each cross-link; the strands are of equal length; dangling molecular ends are negligible (equivalent to a very high molecular weight of the linear polymer prior to cross-linking); the density of cross-links exceeds the density of entanglement loci present before vulcanization; and the cross-links are fixed in the sense that when the external sample dimensions change with deformation the cross-links move in an affine manner.

The classical theory of rubberlike elasticity[22,23] specifies for this case that the equilibrium shear modulus in infinitesimal deformations is given by

$$G_e = g(\overline{r_E^2}/\overline{r_0^2})\nu RT \tag{33}$$

where ν is the moles of network strands per cubic centimeter and g is a numerical factor not far from unity. The ratio $\overline{r_E^2}/\overline{r_0^2}$, where $\overline{r_E^2}$ is the mean square end-to-end distance of a strand and $\overline{r_0^2}$ is the mean square end-to-end distance which strands of the same length would assume if not constrained by cross-links,[24,25] is probably unity at the temperature and concentration at which the network was formed, and will frequently be omitted in future use of this equation. The factor g may include several contributions;[26–28] in particular, if the cross-links are mobile and experience fluctuations instead of moving affinely, there is a factor of $(f-2)/f$, where f is the functionality of a cross-link (factor of $\frac{1}{2}$ for the usual tetrafunctional cross-link.[27,28] Introduction of this factor corresponds to replacing ν by $\nu - \mu$ is the moles of junction points per cubic centimeter.[28] There may be an intermediate degree of mobility depending on the severity of constraints in the medium surrounding the cross-links.[27] It is rarely possible to determine ν and μ accurately by independent means, although end-linked networks of difunctional oligomers provide an opportunity for this.[29,30] Possible contributions to the modulus from trapped entanglements will be discussed in Chapter 14.

The Rouse modes of motion of a molecule whose ends are fixed were examined by Mooney,[31] who found that the relaxation spectrum was the same as that corresponding to equations 1 to 4 with ν substituted for ρ/M except for an additional contribution to the modulus with infinite relaxation time and magnitude νkT. Thus, the relaxation and dynamic moduli are given by

$$G(t) = \nu RT[1 + \sum e^{-t/\tau_p}] \tag{34}$$

$$G' = \nu RT[1 + \sum \omega^2\tau_p^2/(1 + \omega^2\tau_p^2)] \tag{35}$$

$$G'' = \nu RT \sum \omega\tau_p/(1 + \omega^2\tau_p^2) \tag{36}$$

$$\tau_p = a^2P_c^2\zeta_0/6\pi^2p^2kT \tag{37}$$

The quantity P_c refers to a strand ($P_c = \rho/\nu M_0$, where M_0 is the monomer molecular weight). The long-time and low-frequency limiting values of $G(t)$ and G',

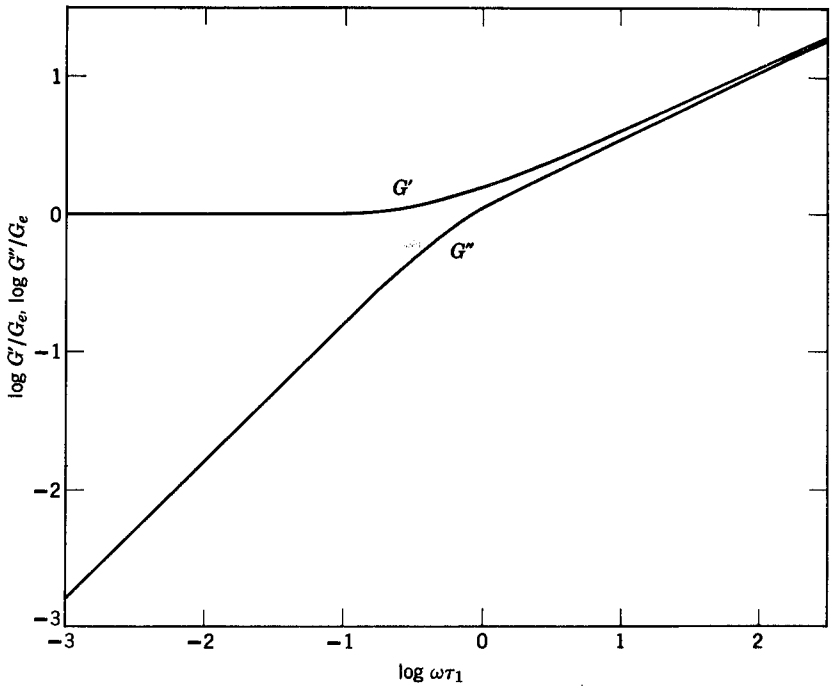


FIG. 10–5. Storage and loss shear moduli, normalized by the equilibrium modulus, plotted logarithmically against frequency for the Mooney[31] modification of the Rouse theory.

respectively, must be G_e; in this treatment, the front factor g and the ratio $\overline{r_E^2}/\overline{r_0^2}$ have been assumed to be unity, and contributions from trapped entanglements, if any, are lumped in together with ν. Logarithmic plots of G'/G_e and G''/G_e are illustrated in Fig. 10–5. Although objections have been raised to the use of such normal mode analysis for a network structure,[32] equations 35 and 36 portray approximately the features of behavior in the transition zone, as will be seen in Chapter 14.

A closed-form expression corresponding to equations 35 and 36 (*cf.* equation 16) is

$$G' + iG'' = (\nu RT/2)y \coth y \tag{38}$$

$$y = (i\pi^2\omega\tau_1)^{1/2} \tag{39}$$

An equation of this form, but without specifying the constants in molecular terms, was obtained by Blizard[7] on the basis of a ladder network model similar to Fig. 10–3 but with both ends fixed.

The square-root law region of G' and G'' is given by equation 13, unchanged for a cross-linked network; it is independent of the degree of cross-linking. It should be noted, however, that the expected range of applicability of this equation is very restricted. If the molecular weight between cross-links is of the order of 5000, arguments similar to those in Section A1 above suggest that the $\omega^{1/2}$ proportionality

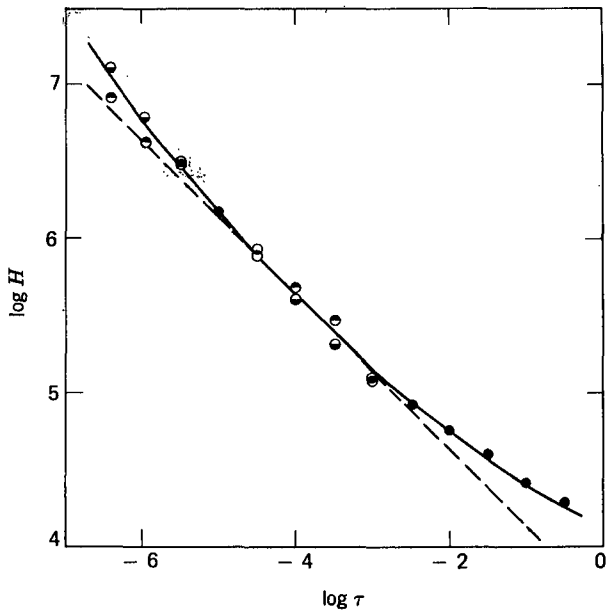


FIG. 10-6. Relaxation spectrum H in dynes/cm^2, plotted logarithmically, for natural rubber lightly cross-linked by dicumyl peroxide with $\nu = 1.86 \times 10^{-4}$ moles/cm^3, and tangent with slope $-\frac{1}{2}$ to calculate ζ_0 from equation 39. Points top black, from G'; bottom black, from G''. (Data of Dickie and Ferry.[33])

should hold only over a frequency range of a factor of 5, or 0.7 on a logarithmic scale. In fact, experiments often show a gradually increasing slope on a logarithmic plot and the only way to fit it with the theoretical slope of $\frac{1}{2}$ is to draw a tangent. Usually the comparison is made with the relaxation spectrum H, derived from both G' and G'' data by the methods of Sections A3 and A5 of Chapter 4. In the square-root law region, H is given by (*cf.* equation 23 of Chapter 9):

$$H = (a\rho_0 N_0/2\pi M_0)(\zeta_0 kT/6)^{1/2}\tau^{-1/2} \tag{40}$$

An example[33] is illustrated in Fig. 10-6. Although the region of fit with the square-root law is very limited, the prediction of the theory that G', G'', and H should be independent of the degree of cross-linking is usually fulfilled throughout the entire transition zone. Effects of cross-link density are very slight unless the cross-linking process changes the chemical composition of the polymer and hence affects ζ_0 (Chapter 14).

Bueche[34] applied the bead-spring normal coordinate treatment to a cross-linked network to calculate the retardation spectrum and the creep, storage, and loss compliances, L, $J(t)$, J', and J'', rather than H, $G(t)$, G', and G''. The results were equivalent to equations 34 to 37 except for numerical factors close to unity. A similar calculation was made by Nakada,[35] and by Ham,[21] who considered different models of lattice connectivity.

The compliances are probably more instructive than the moduli in describing the viscoelastic behavior of networks, because of the maximum in the loss compliance, J'', which is characteristic of networks as pointed out in Chapter 2. This is shown for the Rouse-Mooney theory, equations 35 to 37, in Fig. 10–7 together with some modifications to be described in the following section. Here J'' is calculated simply as $G''/(G'^2 + G''^2)$, equation 28 of Chapter 1, and then normalized by dividing by J_e $(= 1/G_e)$. The frequency scale is normalized by τ_1.

The longest relaxation time in the transition zone, τ_{tr}, can be calculated from equation 37 with $p = 1$. It is close to the reciprocal of a characteristic frequency ω_{tr} obtained as the intersection of the two linear segments of log G' in Figure 10–5; ω_{tr} may be regarded as defining the boundary between the equilibrium and transition zones.[36]

2. Network with Mobile Cross-Links

In the ladder model treatment of Blizard,[7] an alternative termination of the line of springs (Fig. 10–3) was considered in which each end, rather than being fixed, is attached to three other such lines, each of these to three more, and so on indefinitely, thus reproducing the connectivity of a tetrafunctional network. This provision increases the equilibrium compliance by a factor of 2 (corresponding to the factor of $(f - 2)/f$ mentioned in Section 1 above), and it modifies the frequency dependence, which is now expressed by a rather complicated combination of hyperbolic functions. This frequency dependence of J'' is also shown[37] in Fig. 10–7; the maximum is slightly broader than for fixed cross-links (*i.e.*, cross-links with affine deformation).

A more complete analysis of the normal modes of motion in a network with tetrafunctional cross-linking was made by Staverman, Chompff, and Duiser.[26] The motions were first analyzed for a model of the Rouse type with four interconnecting strands whose outer ends are fixed (Fig. 10–8–I). If one begins by considering the line *APC*, the junction point *P* has wide latitude of mobility. Once the line *APC* has a chosen configuration, however, the point *P* is fixed as far as the strands *BP* and *DP* are concerned. It can be shown that the matrix describing the modes of motion is identical with that for Fig. 10–8–II, so the behavior really corresponds to three network strands instead of four. This principle can be extended to a large tetrafunctionally connected network by an iterative process. The result is, first, an equilibrium compliance larger by a factor of 2 than in the simple rubberlike elasticity theory, as deduced from cross-link mobility in Blizard's ladder mechanical model or from the theories of Graessley[28] and that of Flory[27] for the case of maximum cross-link mobility. The treatment also modifies the nature of the relaxation spectrum; its comparison with that of the Rouse-Mooney theory is most easily seen by examining the equivalent continuous spectra. The Rouse-Mooney relaxation spectrum is the same as that of the original Rouse theory except for one additional contribution of νRT at infinite time; over most of the range it is given by equation 23 of Chapter 9, which can be written (with $n = \nu N_0$, and τ_{tr} given by equation 37

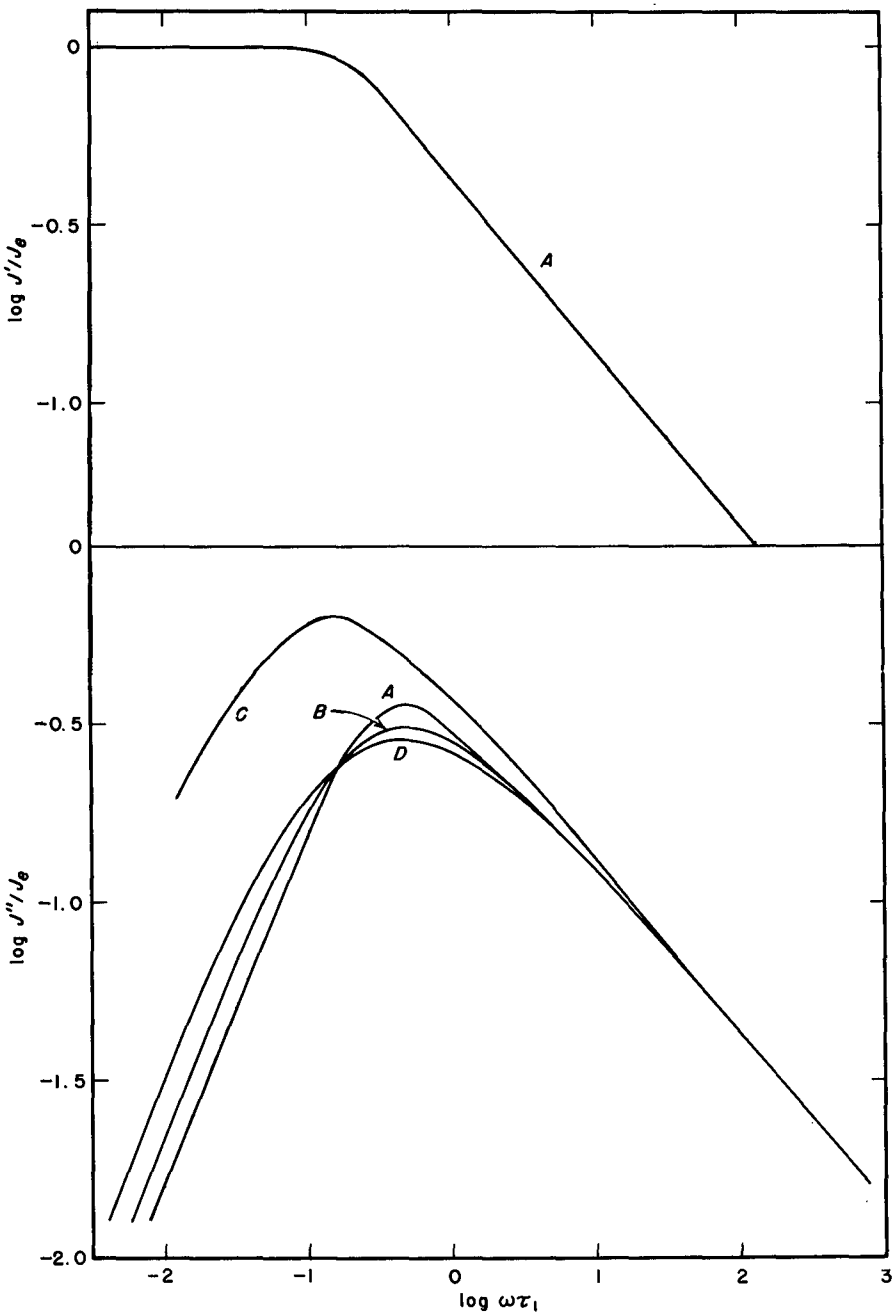


FIG. 10-7. Storage and loss shear compliances, normalized by the equilibrium compliance, plotted logarithmically against frequency for various network theories. (*A*) Mooney-Rouse theory,[31] corresponding to Fig. 10-5; (*B*) Blizard model with trifurcate branching corresponding to tetrafunctional connectivity[37]; (*C*) tetrafunctional model of Chompff and Duiser[26]; (*D*) Mooney-Rouse theory with most probable distribution of strand lengths.

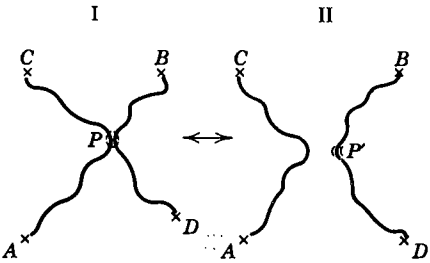


FIG. 10–8. Chompff-Duiser network model. (I) Unit of tetrafunctional network; (II) decoupled mathematical equivalent.[26]

with $p = 1$)

$$H = (\nu RT/2)(\tau_{tr}/\tau)^{1/2} \tag{41}$$

The Chompff-Duiser relaxation spectrum for a network with mobile crosslinks is the same as equation 41 for $\tau \leq 2.4\tau_{tr}$. For $\tau > 2.4\tau_{tr}$ it is given by

$$H = 1.56(\nu RT/2)(\tau_{tr}/\tau) \tag{42}$$

plus one additional contribution of $\nu RT/2$ at infinite time. In other words, there is a distribution of relaxation processes with times longer than the relaxation time τ_{tr} which represents the slowest configurational rearrangement for a single network strand. Equation 41 describes the motions within a single strand; equation 42 describes cooperative motions extending over larger portions of the network, in which cross-links participate.

Integration over equations 41 and 42 with appropriate limits by equations 19, 23, and 24 of Chapter 3 and addition of $\nu RT/2$ in the first two cases provides the viscoelastic functions $G(t)$, G', and G'' for the Chompff-Duiser theory. The corresponding curve for the loss compliance J'' is included in Fig. 10–7. It extends farther to the low-frequency side than the others, as would be expected from the additional slow relaxation mechanisms.

3. Network with Random Distribution of Strand Lengths

In all the preceding network calculations, it has been assumed that the strands were of uniform length corresponding to a degree of polymerization P_c or molecular weight between cross-links $M_c = P_c M_0$. Except under very specific conditions of network formation, such as end-linking of oligomers of nearly uniform molecular weight, there will certainly be a distribution of strand lengths, the form of which will depend on the cross-linking process. The equilibrium modulus can still be expressed by equation 33, however; $\nu = \rho/\overline{M}_{nc}$, where $\overline{M}_{nc}$ is the number-average molecular weight between cross-links.

If the cross-links are considered as fixed, the Rouse-Mooney theory can be readily modified[36] by exactly the same procedures as for molecular weight distribution in uncross-linked polymers (Section A3 above) or dilute solutions (Section B7, Chapter 9). The result is a somewhat more gradual frequency or time dependence

of the viscoelastic functions. The calculated curve for J'' for a most probable distribution of strand lengths is included in Fig. 10–7.

4. Role of Network Defects

A real network differs also from the idealized concept of Section 1 above because of irregularities in the structure. The three most important are probably the presence of dangling ends due to the finite molecular weight of the polymer prior to cross-linking, the presence of coupling entanglements which existed in the linear polymer before network formation and became permanently trapped in the course of the cross-linking process, and the presence of sol fraction (*i.e.*, molecular species not attached to the network at all). The dangling ends and the sol fraction do not contribute to the equilibrium modulus because they cannot store elastic energy at equilibrium; the trapped entanglements add because they represent additional restraints which magnify the change of entropy with deformation. In the theory of Langley,[38,39] all these features are taken into account and the effective network strand density for random tetrafunctional cross-linking is given by

$$\nu = (q\rho/M_0)w_g T_e^{1/2} + 2\varepsilon T_e \tag{43}$$

where q is the probability that a monomer unit participates in a cross-link, ρ the density, M_0 the monomer molecular weight, w_g the gel weight fraction ($= 1 - w_s$, where w_s is the sol weight fraction), T_e the probability that an entanglement is trapped (*i.e.*, all four strands leading from it are attached to the gel fraction), and ε the effective total concentration of entanglements. By "effective" concentration is meant that the entanglements are counted as though they affected the strain entropy to the same degree as cross-links. If not, the concentration includes an effectiveness factor.[38] The values of w_g and T_e depend on q and the molecular weight distribution. The equilibrium modulus G_e is then given by equation 33 with ν substituted from equation 43.

If the sol fraction consists of relatively short, unbranched molecules, its contributions to the relaxation or dynamic moduli may be estimated by equations 1 to 4, preferably integrated over a suitable distribution of molecular lengths as described in Section A3, and multiplied by the factor w_s. However, it is uncertain whether the longest relaxation times are the same for a loose molecule threaded through a network as they are in a linear polymer, even if the molecules are short enough not to participate in coupling entanglements. If they are long, branched, or both, their motions will be very different from those described by the Rouse theory and their longest relaxation times will be much longer than given by equation 37. This will be discussed in Chapter 14.

If the dangling ends are short and unbranched, their contributions to the relaxation or dynamic moduli have in principle a time or frequency dependence almost indistinguishable from that of the completely unattached sol fraction; both Mooney[31] and Blizard[7] have treated the case of a linear molecule attached at only one end and reached this conclusion. If the dangling ends are long, branched, or both, the behavior is quite complicated and it will also be discussed in Chapter 14.

C. UNCROSS-LINKED POLYMERS OF HIGH MOLECULAR WEIGHT

In interpreting the viscoelastic properties of undiluted polymers of high molecular weight, the concept of entanglement coupling plays a crucial role. This was introduced qualitatively in Chapter 2 to explain the inflections in $J(t)$, $G(t)$, G', and J', and the double maxima in J'' and G'' (also in the spectra H and L, Chapter 3), for examples III and IV. It has been necessary to allude to it several times without further explanation, as in Section A above where polymers of "low" molecular weight are defined as those sufficiently low so that entanglement coupling does not occur in the undiluted state, and in Section B where the contribution of trapped entanglements to the equilibrium modulus was formulated. We must now examine this concept in more detail.

1. The Nature of Entanglement Coupling

One of the first allusions to some kind of intermolecular coupling at widely separated points in uncross-linked rubbery polymers was that of Treloar,[40] based on the behavior of unvulcanized natural rubber. Under constant force, this polymer first stretches very rapidly, then undergoes very slow additional deformation; upon removal of stress, most of the deformation is recoverable, rather closely resembling the behavior of a cross-linked rubber. Yet there cannot be a cross-linked network, since the material is completely soluble in suitable solvents. This observation suggested some kind of temporary network structure in which the junctions are not chemical cross-links but points coupled by twisting or looping. Between these points, the frictional resistance to configurational changes is low; but the slow motion at these points gives a high macroscopic viscosity. Similar arguments were advanced later by Nielsen and Buchdahl.[41] These observations, though made at high deformation, are essentially creep and creep recovery experiments stopping somewhere in the first plateau shown in Fig. 2-1 for Examples III and IV. Of course, low molecular weight polymers exhibit time-dependent creep and creep recovery too, but there is a qualitative difference. This is illustrated in Fig. 10-9, where the Rouse theory recoverable creep compliance[5] is plotted with dimensionless variables to give a master curve which should hold for any molecular weight in the subentanglement range. Experimental data for polymers of low molecular weight conform reasonably well to this (Chapter 12). By contrast, experimental data for a high molecular weight polymer such as Example III of Chapter 2, Section A, also plotted in Fig. 10-9, show a different shape with a long plateau where the compliance changes slowly with time.

The extensive stress relaxation experiments of Tobolsky on uncross-linked polymers of high molecular weight[42,43] similarly showed two stages of relaxation (like those in Examples III and IV of Fig. 2-2) with a period in the time scale where the stress relaxed very slowly, leading to the concept of an entangled network structure.

The essential feature of these observations is that there are two sets of relaxation or retardation times with very different magnitudes, represented by the two maxima

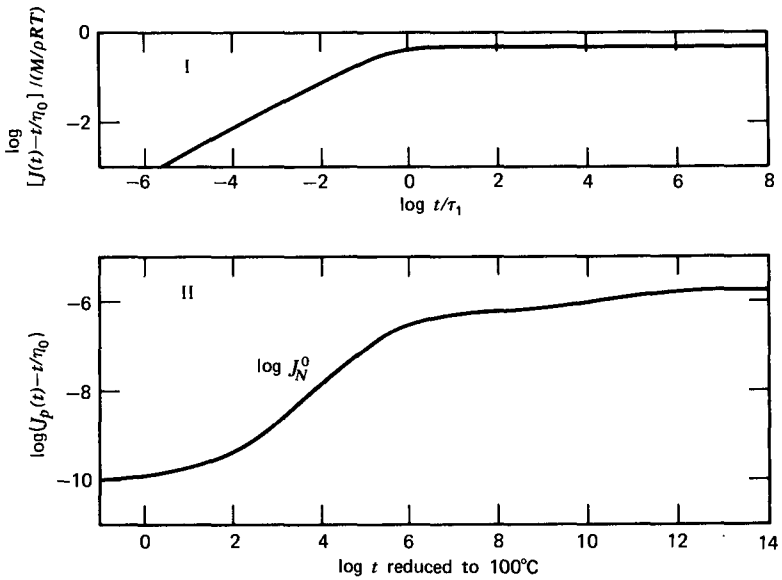


FIG. 10-9. Normalized logarithmic recoverable creep compliance plot for Rouse theory (I) and for polystyrene of high molecular weight (II) (Example III of Fig. 2-1).

in the relation and retardation spectra in the corresponding curves in Figs. 3-3 and 3-4.

A quite different type of observation which leads also to the concept of an entanglement network is the dependence of viscosity on molecular weight in undiluted polymers or at constant concentration in concentrated solutions, as advanced by Bueche.[1,44] This is illustrated in Fig. 10-10 for fractions of polystyrene.[45] At low molecular weights, η_0 increases only slightly more rapidly than directly proportional to M, and its magnitude is actually predicted by the Rouse theory, in accordance with the principle of Bueche.[1] Thus, from equations 4 and 6, η_0 is given by

$$\eta_0 = (a^2\rho N_0/36M_0^2)\zeta_0 M \tag{44}$$

The ratio η_0/M depends on molecular weight only through the friction coefficient ζ_0; and if the latter is corrected to its limiting high molecular weight value ζ_{00} by equations 14 and 15, it is found that $\eta_0\zeta_{00}/\zeta_0$ is indeed exactly proportional to M, as shown for many polymers by Berry and Fox[3] and illustrated in Fig. 10-11. Moreover, the value of ζ_{00} determined experimentally from equation 44 agrees approximately with that derived independently from viscoelastic measurements.[3]

At *high* molecular weights, however, η_0 increases with the 3.4 power of the molecular weight, as evident in both Fig. 10-10 and Fig. 10-11. (In this region, there is no variation of ζ_0, which has reached its limiting value of ζ_{00}.) This highly exaggerated molecular weight dependence was attributed by Bueche to entanglement coupling, and on the basis of the dragging of one molecule by another he calculated[1,44] that the viscosity should be proportional to $M^{3.5}$. The magnitude of

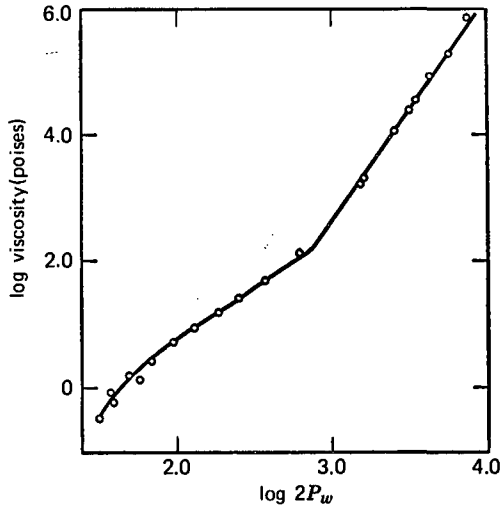


FIG. 10–10. Dependence of steady-flow viscosity on number of chain atoms per molecule for polystyrene fractions at 217°C. (Fox, Gratch, and Loshaek.[45])

M at which the slope changes is a characteristic value, M_C, which according to the Bueche theory[44] is related to the average molecular weight spacing between entanglement points, M_e, in a rather complicated manner; approximately, $M_C \cong 2 M_e$. Because the change in slope is of course not really a discontinuity, there has been some skepticism of a real qualitative difference between the regions $M < M_C$ and $M > M_C$. However, in the relaxation and retardation spectra there is a clear difference; only for $M > M_C$ do two maxima appear.

Though the phenomenon is evident, the nature of the coupling is still speculative. The notion of coupling at widely separated points, necessary to explain the two widely separated sets of relaxation times, led to the concept of adherence of the polymer molecules at specific loci (Fig. 10–12–I). Such a locus is a temporary cross-link; kinetics of formation and dissociation of these junctions have been treated, and viscoelastic properties have been calculated from them.[46–48] Adherence at widely separated points corresponding to degrees of polymerization of the order of 100 would, however, imply some kind of chemical or structural inhomogeneity along the polymer molecule. It is conceivable that specific spots of strong attraction could occur, due to a copolymeric impurity (which can produce marked effects when introduced by design[49,50]) or regions of tactic ordering.[51] Also, viscoelasticity controlled by association and dissociation of such reversible linkages would seem quite reasonable in solutions of polyvalent metallic soaps[52,53] where the structure does not involve long sequences of primary chemical bonds. However, the effects of entanglement coupling appear universally; examples include such nonpolar polymers as polyisobutylene and polystyrene where the intermolecular attractive forces are small and there is no suspicion of structural heterogeneity. It seems, therefore, that the coupling must be topological rather than due to intermolecular forces, thus justifying the term "entanglement." A concept which retains the idea

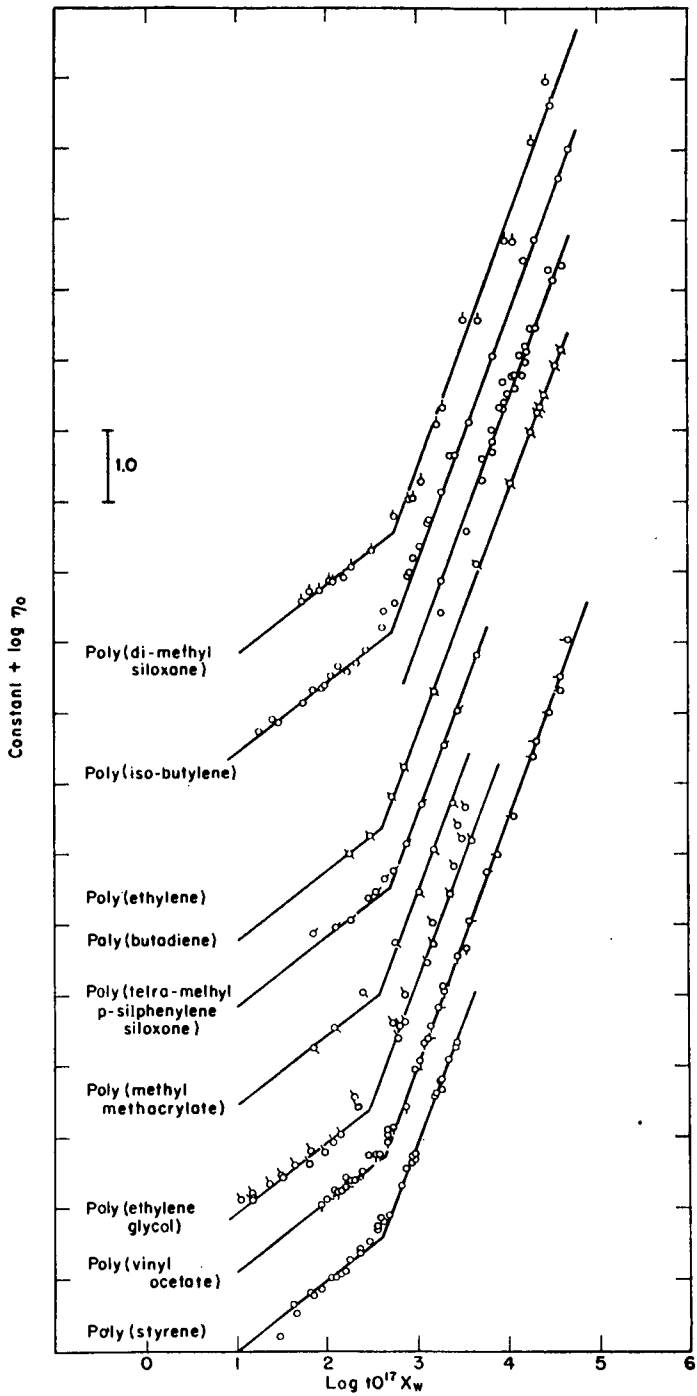


Fig. 10–11. Log $\eta_0\zeta_{00}/\zeta_0$ + const. plotted against an abscissa which for each polymer is log M + const., for nine different polymers. The lines have slope 1.0 on the left and 3.4 on the right. (Berry and Fox.[3])

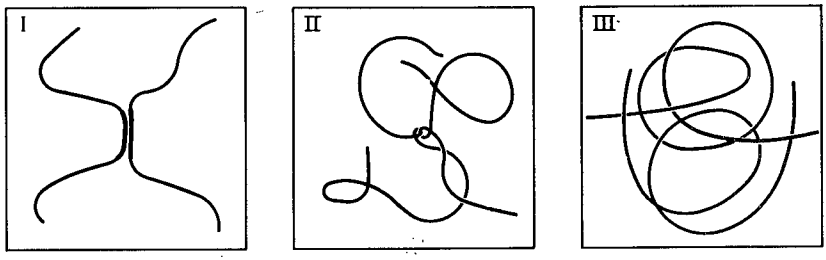


FIG. 10–12. Concepts of entanglement coupling. (I) Locus of adherence or temporary cross-link; (II) local kink; (III) long-range contour loop.

of a specific locus is an entanglement where two chains are tightly kinked around each other by bending back on themselves in short-range contour (Fig. 10–12–II). However, molecules which are relatively stiff and extended such as cellulose derivatives[54] and even deoxyribonucleic acid[55,56] and a helical poly(amino acid),[57] and a very rigid heterocyclic polymer[58] (all in concentrated solution) exhibit the effects of entanglement coupling even more prominently than do highly flexible polymers. Moreover, the presence of enormous bulky side groups does not markedly inhibit the entanglement coupling.[59] It seems probable, therefore, that the coupling involves looping of chains around each other in their long-range contour[44,60,61] (Fig. 10–12–III). Hoffmann[62,63] calculated by simple geometrical arguments the probability that the four chains radiating from two juxtaposed segments on different chains cannot easily disentangle, and obtained a value of 0.017; a plausible estimate of the total number of juxtaposed segments from different chains leads to an entanglement density of the correct order of magnitude. Alternatively, the existence of an entanglement can be formulated in terms of random-walk statistics and the probability that a closed loop will exist. The geometry of such topological constraints has been extensively discussed by Edwards[64,65] and Ziabicki.[66–67a]

Additional evidence that the constraints called entanglements are topological and not dissociable junctions comes from the behavior of networks cross-linked in strained states.[68] A linear polymer of high molecular weight is stretched in simple extension slightly above the glass transition temperature to a stretch ratio λ_0, cooled to eliminate long-range configurational motions and rearrangement of entanglements, and cross-linked by γ-irradiation. The cross-links trap the entanglements so that subsequent disentanglement is not possible, just as in ordinary networks as discussed in Section B4 above; and the state of lowest free energy for the network strands terminated by cross-links corresponds to the deformed dimensions. Upon release and warming, the sample retracts to a state of ease with stretch ratio λ_s in which the forces associated with the cross-links and the trapped entanglements are equal and opposite. The ratio of cross-links to trapped entanglements can be calculated from λ_0 and λ_s; and the concentration of strands contributed by trapped entanglements, $\nu_N = 2\varepsilon T_e$, can be calculated from the equilibrium stress measured in the same state of deformation λ_0 as during cross-linking, since the cross-links make no contribution here and the first term on the right side of equation 43 is absent. If the constraints were simply dissociable junctions, trapping would not

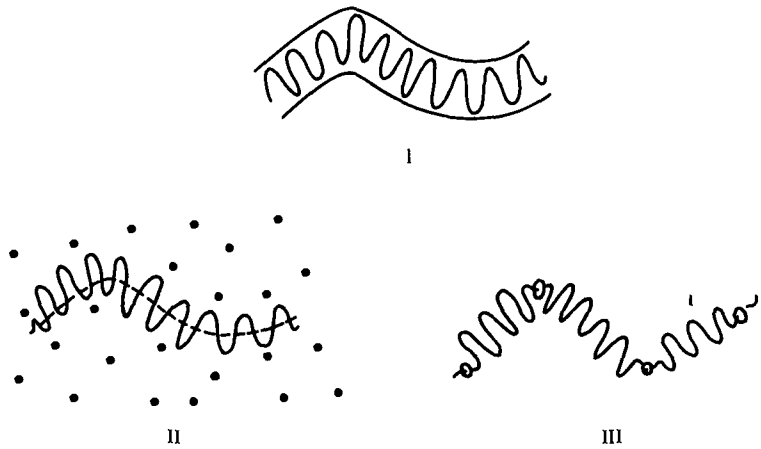


FIG. 10-13. Models of topological restraints. (I) virtual tube; (II) point obstacles; (III) slip links. (Doi and Edwards.[72]) Reproduced, by permission, from Journal of the Chemical Society Faraday Transactions II.

take place; there would still be an equilibrium stress at λ_0 because of a configurational memory effect,[69] but considerably smaller than that observed.[69a]

Since an entanglement, whether trapped or not, is pictured as being able to slide along the contours of the two molecules participating in it, and continually changes its position with thermal motions, it is somewhat misleading to speak of entanglement "points" or "loci." A somewhat different model which introduces topological restraint without placing it at a specific point is that of a tube or tunnel that surrounds a given polymer molecule and conforms to its contorted contour, as introduced by Edwards[70] and treated by de Gennes,[71] Doi and Edwards,[72-74] and Klein.[75] The constraint of the tube (Fig. 10-13-I) corresponds to a set of obstacles[71] (Fig. 10-13-II) or a sequence of slip links[72] (Fig. 10-13-III) which replace the entanglement points of the entanglement conceptual scheme. The two sets of relaxation or retardation times evident in Fig. 10-9 then correspond to short-range configurational changes within the confines of the tube (rapid) and long-range configurational changes which necessitate escape from the tube (much slower). As pointed out by de Gennes,[71] the easiest escape for sufficiently long chains will be achieved by sliding along the contorted contour (reptation). Long-range configurational changes could also be achieved if the obstacles rearrange themselves ("tube reorganization" [76]), but this process should not make a very significant contribution except where M/M_C is only slightly greater than 1 and entanglement behavior is only incipient.[75]

Although the tube model avoids the specification of an average molecular weight M_e between entanglement points, the diameter d of the tube is an equivalent parameter and the average number of entanglements per molecule, M/M_e, can be identified approximately with L/d, where L is the contour length of a random walk with M/M_e steps.[77] (In the theory of Klein,[75] M/M_e can be identified approximately with $\mathcal{N}/13$, where $\mathcal{N}$ is his number of entanglement points per molecule.) In spite of these different alternatives, the parameter M_e will be retained here as a measure

of the topological restraints which are responsible for very slow relaxation processes, and some of the discussion will be worded as though the restraints were located at specific points, with the understanding that this description should not be taken literally.

2. Behavior in the Transition Zone

In the transition zone of time or frequency, the viscoelastic behavior of an uncross-linked polymer is dominated by configurational changes of regions of the molecule which are shorter than the distance between entanglements (or, in the tube model, shorter than the tube diameter). These motions are oblivious of the topological restraints described above and can be expressed by Rouse modes in the manner of the Rouse-Mooney theory discussed for cross-linked networks in Section B1 above. The longest relaxation time associated with these motions, τ_{tr}, can be estimated from equation 37 with $p = 1$ and P_c replaced by P_e, where $P_e = M_e/M_0$. In this zone, high molecular weights are in a sense simpler than low molecular weights because there is no dependence of ζ_0 on M. In equations 14 and 15, f_M and ζ_0 have their limiting values f_0 and ζ_{00}, and the storage and loss moduli as given by equation 13 are quite independent of molecular weight. However, equation 12 is not applicable at all because the steady flow viscosity is determined by a different set of molecular motions involving the slow slippage of the entanglements.

The remarks made in Section B1 above about the very limited frequency range of applicability of Equation 13 in cross-linked networks apply equally to entanglement networks. The average molecular weight between entanglement loci, though it varies considerably among polymers (Chapter 13), is often of the order of 5000, and as would be expected from the arguments of Section A1 the square-root relations of equations 13 and 40 are rarely found to hold over much more than a decade of the time or frequency scale. Nevertheless, equation 40 has been used extensively to estimate the value of ζ_0 (actually ζ_{00}, in the sense of equation 14) from viscoelastic measurements on uncross-linked polymers of high molecular weight. The appropriate expression, solving equation 40 for ζ_0, is

$$\log \zeta_0 = 2 \log H + \log \tau + \log (6/kT) + 2 \log (2\pi M_0/a\rho N_0) \qquad (45)$$

where H and τ are taken from any point in the square-root-law region. These data will be reviewed in Chapter 12.

The prediction of the theory that the properties throughout the transition zone are independent of molecular weight, so long as the latter is high enough for ζ_0 to have its limiting value ζ_{00}, has been abundantly confirmed experimentally even though the shape of the time or frequency dependence is more complicated than the simple square-root law (*e.g.*, equation 13).

3. Behavior in the Terminal Zone

In the terminal zone where G' and G'' are proportional to ω^2 and ω respectively, the viscoelastic properties are dominated by the longest relaxation times and these are determined by long-range motions in which a molecule of high molecular weight

may be constrained by of the order of 100 entanglements (or as though in a contorted tube with a length/diameter ratio of 100). The simplest approach to modifying the bead-spring theories is to assume that the relaxation times for these long-range motions are still given by equation 4 with a uniformly effective friction coefficient which is much higher than that governing the short-range motions.[1] This principle was used in several early modifications of the Rouse theory[2,78,79] or mechanical models with similar features.[80] For a polymer of uniform molecular weight, the three or four longest relaxation times are sufficient to calculate the important constants η_0 and J_e^0, since they contribute most of S_1 and S_2 in equations 10 and 11. If, for these three or four, equation 4 is modified by a factor Q_e representing the enhancement of friction by entanglement restraints,

$$\tau_p = a^2P^2Q_e\zeta_0/6\pi^2p^2kT \tag{46}$$

and equation 10 becomes

$$\eta_0 = \rho N_0 a^2 M Q_e \zeta_0/36M_0^2 \tag{47}$$

Since for $M > M_C$, η_0 is observed experimentally to be proportional to M,[3,4] this behavior can be reproduced by setting

$$Q_e = (M/M_C)^{2.4}, \qquad M > M_C \tag{48}$$

The calculation of J_e^0 is unaltered by the introduction of Q_e, which cancels out in equation 11, so

$$J_e^0 = 0.40M/\rho RT \tag{49}$$

as long as Q_e is the same for a few of the longest relaxation times. Combination of equations 46 and 48 shows that the longest relaxation time, τ_1, should be proportional to $M^{4.4}$. By combining equations 47 and 48, one obtains a semiempirical relation,

$$\eta_0 \cong 0.028\rho N_0 a^2 \zeta_0 M^{3.4}/M_C^{2.4}M_0^2 \tag{50}$$

which has the correct molecular weight dependence and reproduces experimental data within better than an order of magnitude. However, failure of equation 49 to agree with experiment gives clear evidence of the inadequacy of this type of modification of the Rouse theory, as first pointed out by Tobolsky;[81] although it holds at low molecular weight in accordance with the discussion in Section A1, when M is greater than a critical value M_C' (empirically several times M_C) J_e^0 is *independent* of M instead of directly proportional to it.[60] This is illustrated for polystyrene in Fig. 10-14.[82] Also, τ_1 is found to be proportional to $M^{3.4}$ instead of to $M^{4.4}$ as would follow by combining equation 46 and 48.[60] Finally, the observed frequency dependence in the terminal zone for polymers with narrow molecular weight distribution corresponds almost to a single terminal relaxation time τ_1 rather than a sequence with the Rouse spacings; the terminal zone where $G' \propto \omega^2$ is followed directly by the plateau zone where G' is virtually independent of ω, with no intermediate $\omega^{1/2}$ dependence as would be provided by a Rouse relaxation spectrum.[60,83] (Some of this evidence is from data on concentrated solutions which are discussed in Chapter 17.)

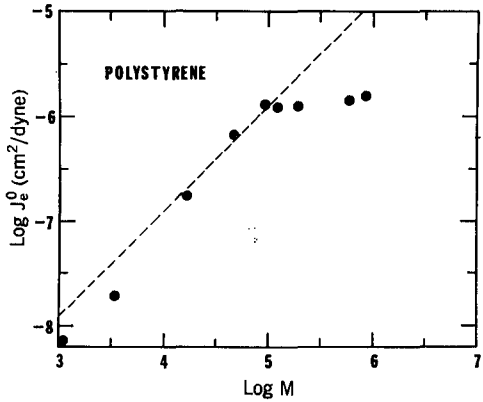


FIG. 10–14. Logarithmic plot of J_e^0 against molecular weight for polystyrenes of narrow molecular weight distribution. (Plazek and O'Rourke.[82])

It may be concluded that when entanglements are present the molecular motions do not correspond to the normal modes of the Rouse theory. Indeed, the topological restraints must necessitate very different motions to achieve configurational rearrangements, and other models have been proposed to describe them.

In the "uncorrelated drag model" of Graessley,[84] entanglement loci are assigned friction coefficients which increase rapidly with distance from the chain ends, and their motions are associated also with spring constants which are governed by the mean equilibrium distance from the center of mass. The result is a much sharper relaxation spectrum in the terminal zone; it predicts, for $M > M_C$ and $M > M_C'$ respectively,

$$\eta_0 \cong 0.0027 \rho N_0 a^2 \zeta_0 M^{3.5} / M_e^{2.5} M_0^2 \tag{51}$$

$$J_e^0 = 1.798\, M_e / \rho RT \tag{52}$$

$$\tau_w = 1.798\, M_e \eta_0 / \rho RT = \eta_0 J_e^0 \tag{53}$$

where τ_w is the weight-average relaxation time for a narrow distribution of relaxation times that is predicted in the terminal zone (discussed in more detail in Section C3 of Chapter 13). Equation 51 is very similar to equation 50, allowing for the difference between M_C and M_e; but now equation 52 gives the correct molecular weight independence of J_e^0 for $M > M_C'$. Moreover, τ_w is correctly predicted to have the same molecular weight dependence as η_0. The relaxation modulus $G(t)$ in the terminal zone is plotted in Fig. 10–15 and compared with that for a Rouse spectrum and also for a single relaxation time; it has the sharpness which has been observed experimentally.

Friction coefficients which vary with position and elastic coupling have also been introduced by Hansen, Williams, and Shen,[85] as well as intramolecular entanglement coupling;[86] Hayashi[87] treats an entangled molecule as moving in a viscoelastic medium. A detailed discussion of some of these theories has been presented by Graessley.[60]

In the framework of the tube model, configurational rearrangements in the

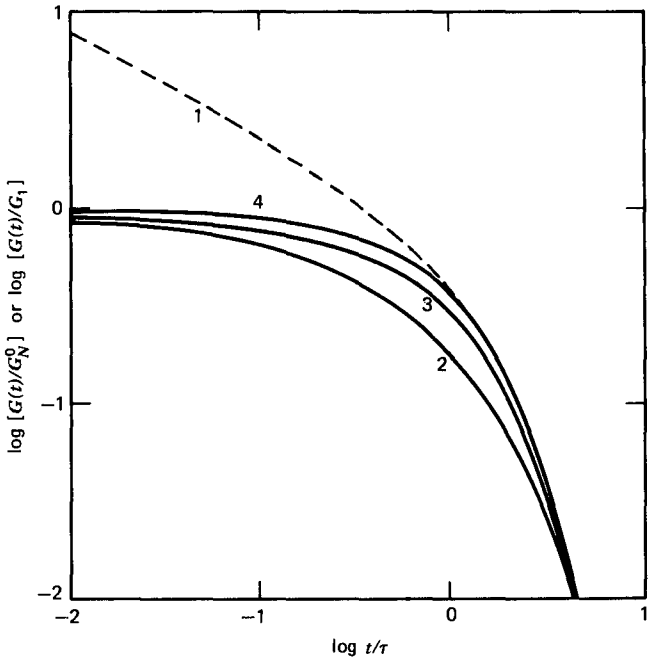


FIG. 10–15. Logarithmic plot of relaxation modulus in the terminal zone as predicted by the relaxation spectra of Rouse (1), Graessley (2), and Doi and Edwards (3); and for a single terminal relaxation time (4). Values normalized by G_N^0 except for (4) which is normalized by G_1; τ is τ_1, τ_w, or τ_d depending on theory.

terminal zone are accomplished by reptation of a molecule back and forth along its contour with random choice of new paths so that the original tube "evaporates" as portrayed in Fig. 10–16. This also corresponds to a very narrow distribution of relaxation times and a relaxation modulus given by Doi and Edwards[72] as

$$G(t) = G_N^0 \frac{8}{\pi^2} \sum_{p \text{ odd}} \frac{1}{p^2} e^{-tp^2/\tau_d} \tag{54}$$

where G_N^0 is the plateau modulus (*cf.* Fig. 2–2) and τ_d is the longest relaxation time corresponding to disengagement from the tube by the reptation process; because of the $1/p^2$ factor, this scarcely differs from relaxation with a single relaxation time, as shown in Fig. 10–15 where this function is also plotted. The viscoelastic constants have been calculated by Graessley[77] and can be expressed in terms of M_e, provided M/M_e is identified with L/d (Section 1 above), as follows:

$$\eta_0 = (\tfrac{1}{15})\rho N_0 a^2 \zeta_0 M^3 / M_e^2 M_0^2 \tag{55}$$

$$J_e^0 = (\tfrac{2}{5})M_e/\rho RT \tag{56}$$

$$\tau_d = (15/\pi^2)M_e\eta_0/\rho RT = (10/\pi^2)\eta_0 J_e^0 \tag{57}$$

alternatively,

$$\tau_d = a^2\zeta_0 M^3/M_e M_0^2 \pi^2 kT \tag{57a}$$

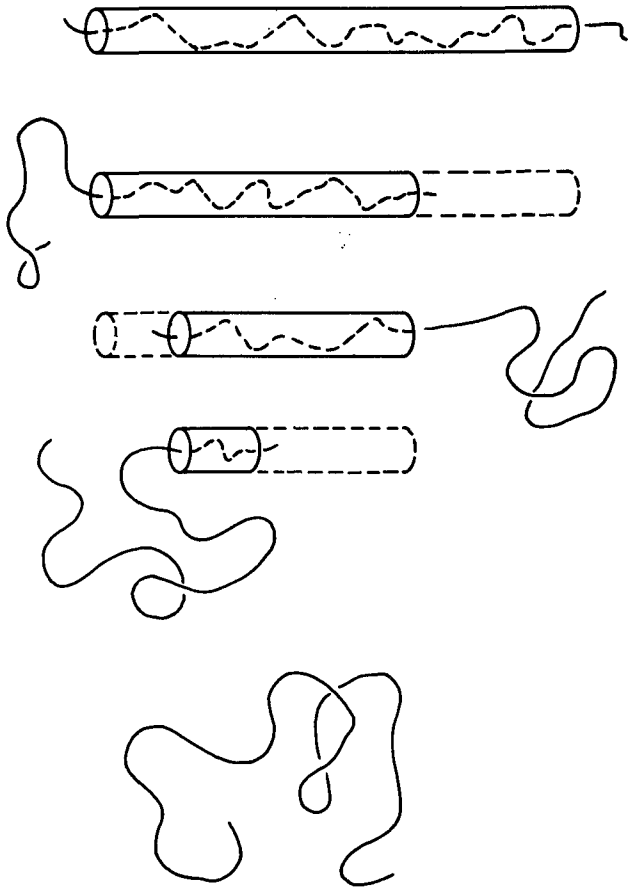


FIG. 10–16. Schematic diagram of the escape of a constrained molecule from its original virtual tube. (After Graessley.) Of course, the axis of the original tube is not really a straight line.

Again J_e^0 is correctly predicted to be independent of molecular weight, and the molecular weight dependences of η_0 and τ_d are the same. However, they are proportional to M^3 (the proportionality of τ_d to M^3 was derived earlier by de Gennes[71]) instead of $M^{3.4}$ as observed experimentally. It has been suggested by Graessley[77] that the exponent of 3 is correct for extremely high molecular weight and that the deviation is due to contributions to relaxation from other mechanisms than reptation which become more important with decreasing molecular weight.

The effects of branching and molecular weight distribution when entanglements dominate the terminal zone are not well understood theoretically; experimental results will be reviewed in Chapters 13 and 17. It may be mentioned that branching should strongly inhibit the reptation mechanism for configurational rearrangements[88] and hence should greatly increase τ_1 compared with that of a linear molecule of the same molecular weight. The effect of molecular weight distribution on η_0 can be described simply by the well-known relation that η_0 is determined by $\overline{M}_w$ except possibly at very high molecular weights.[60] The presence of molecular

weight distribution always increases J_e^0. For example, when two samples with uniform molecular weight, whose molecular weights are well above M_C' and whose values of J_e^0 are therefore equal, are blended in various proportions, J_e^0 goes through a maximum as a function of composition which may be higher than the value for the components by more than an order of magnitude.[89-91] Various blending laws have been proposed to describe viscoelastic properties;[84,92-95] usually several adjustable parameters are needed for good agreement with experimental results, although the theory of Graessley[84] provides this without adjustable parameters if the molecular weights of the components do not differ by too large a factor.

4. Transient Network Models for Viscoelastic Properties in the Terminal Zone

A different approach to terminal zone viscoelasticity of a linear polymer of high molecular weight, either undiluted or in concentrated solution, is based on the transient network model.[46-48,96,97] The strands of the network support stress and store elastic energy just as in a permanently cross-linked network at equilibrium (equation 33). The time-dependent properties are supposed to arise not from delayed configurational changes within the network strands as in Section B above, but from the concept that strands are continually leaving and joining the network as the transient junctions are formed and released. In entanglement terms, this corresponds to the continual rearrangment of entanglement loci by thermal motion. In tube model terms, it corresponds in a sense to a molecule sliding out of one virtual tube and entering another. "Joining" may be interpreted as the formation of a network strand by establishing two entanglement loci which constitute its ends; "leaving" is the disappearance of such a strand by spontaneous disentanglement. Neglect of relaxation processes within the network strands is perfectly satisfactory for the terminal zone, since the relaxation times for motions between entanglements are far smaller than those in which entanglements participate.

The strands are classified in the most general case[96] by Lodge according to length (subscript e) and complexity of their junctions with the network (subscript κ). Then, if $\nu_{\kappa e}$ is the moles of strands with given values of e and κ per unit volume at any instant, and $\tau_{\kappa e}^{-1}$ is the probability that any one such strand will leave the network in unit time, the linear viscoelastic properties are given by

$$G(t) = RT \sum_{\kappa,e} \nu_{\kappa e}\, e^{-t/\tau_{\kappa e}} \tag{58}$$

$$G'(\omega) = RT \sum \nu_{\kappa e}\omega^2\tau_{\kappa e}^2/(1 + \omega^2\tau_{\kappa e}^2) \tag{59}$$

$$G''(\omega) = RT \sum \nu_{\kappa e}\omega\tau_{\kappa e}/(1 + \omega^2\tau_{\kappa e}^2) \tag{60}$$

$$\eta_0 = RT \sum \nu_{\kappa e}\tau_{\kappa e} \tag{61}$$

$$J_e^0 = (1/RT)(\sum \nu_{\kappa e}\tau_{\kappa e}^2)/(\sum \nu_{\kappa e}\tau_{\kappa e})^2 \tag{62}$$

For a polymer solution, η_0 in equation 61 should strictly be replaced by $\eta_0 - \eta_s$, but it is probable that in any solution concentrated enough to have a transient network η_s would be negligible.

Comparison of the forms of equations 58 to 61 with equations 21 to 23 of Chapter 9 and equations 23 and 24 of Chapter 3 shows that the time and frequency dependence correspond to a generalized Maxwell model as in the Rouse theory and its various modifications, but here the spring constants (or discrete contributions to the relaxation spectrum) are not necessarily all equal; they are proportional to the concentrations of the various types of strands, $\nu_{\kappa e}$. The molecular weight does not enter explicitly, but it may be expected that the higher the molecular weight the greater the concentrations of strands which find it difficult to leave the network and hence have large values of the time parameter $\tau_{\kappa e}$.

Without knowledge of the relations between $\nu_{\kappa e}$ and $\tau_{\kappa e}$, it is impossible to formulate the viscoelastic properties more specifically. The fact that J_e^0 is independent of M for high uniform molecular weight suggests that there is a rather narrow distribution of $\tau_{\kappa e}$'s in this case.

The network theory of Lodge[96,97] also predicts normal stresses in both steady and oscillating flow and can be extended to predict a variety of nonlinear phenomena.

5. Practical Aspects of Behavior in the Terminal Zone

The practical significance of the terminal relaxation time τ_1 in several qualitative aspects of behavior has already been mentioned in connection with equation 7 for polymers of low molecular weight. The same considerations apply to polymers of high molecular weight, where τ_1 (or τ_d, in the framework of the tube model) and the other two viscoelastic constants η_0 and J_e^0 which characterize the terminal zone are even more important in the processing and use of polymeric materials. Rough estimates of these quantities can sometimes be made from the equations in Section C3 above for practical purposes.

The constants η_0 and J_e^0 are important in extrusion and molding processes. The former is a measure of the energy expended in flow; the latter is a measure of the energy stored, which can cause distortion of an extruded object when it emerges, or frozen-in strain if a molded object is cooled below its glass transition temperature without annealing. The values of η_0 and J_e^0 can be varied independently to a considerable extent by controlling the molecular weight distribution and branching. Also, η_0 is much more dependent on temperature than J_e^0. In applying the theoretical predictions to practical cases, however, it must be remembered that the theory applies only to small stresses. At high stresses, the apparent viscosity η will be less than η_0 because of non-Newtonian behavior (Section E). On the other hand, a high confining pressure will cause the viscosity to be higher than at atmospheric pressure, because of the diminution of free volume (Chapter 11, Section D). However, J_e^0 is affected to a lesser degree by high stresses[98] and probably very little by high confining pressures.

The magnitudes of the terminal relaxation time (and the terminal retardation time, which differs from it only by a small factor) are also of considerable importance (*cf.* equation 7). For a polymer homogeneous with respect to molecular weight, τ_1 can be estimated from the viscosity by equation 7 if $M < M_C$ and by

equation 53 or 57 if $M > M_C$. For a heterogeneous polymer, small amounts of components with very high molecular weights will cause small residual stresses, residual recoil, etc., at very long times; specification of a terminal relaxation time is essentially impossible. An empirical approach to defining a characteristic terminal time[99] τ_m is to draw a tangent to the relaxation modulus curve, $\log G(t)$ *vs.* $\log t$ (Fig. 2–2) with a slope of -1. The location of this tangent on the time scale specifies $t = \tau_m$. For a single Maxwell element, τ_m would be identical with the relaxation time τ_1.

6. Behavior in the Plateau Zone

The characteristic feature of viscoelastic properties of linear polymers of high molecular weight is the presence of two sets of relaxation times relating to configurational rearrangements between entanglements (short) and beyond entanglements (long) respectively. In the transition zone of time or frequency, the latter can be ignored; in the terminal zone, the former can be ignored. At intermediate times or frequencies, in the plateau zone, it might be expected that neither set would make a substantial contribution to relaxation; in this case, $G(t)$ and $G'(\omega)$ would be quite independent of time and frequency respectively, and losses would be extremely small with a deep minimum of G'' or $\tan \delta$, corresponding to the qualitative description of the plateau zone as the region of time scale in which there is no rearrangement of entanglements but the configurational changes of strands between entanglements are rapid. The modified Rouse theories of Section C3 do predict this behavior, even though they are unsatisfactory in the terminal zone; the uncorrelated drag model and the tube model, which are much more successful in the terminal zone, also provide a flat plateau in $G(t)$ or $G'(\omega)$. The plateau level G_N^0 is $\rho RT/M_e$. In the tube model with the identification $L/d = M/M_e$, there is a small relaxation in the plateau zone from a modulus of $\rho RT/M_e$ to $(\frac{4}{5})\rho RT/M_e$. Actually, the experimental G' is usually less flat and the minimum in G'' is less deep than predicted. A rather good fit is provided by the position-dependent friction coefficients with elastic coupling in the model of Hansen, Williams, and Shen,[85] but with several arbitrary parameters. Another very different approach which successfully describes the plateau zone is that of Thirion,[100] in which the friction of the beads of the Rouse model is made time dependent with a micro-memory function which reflects the entanglement effects. With a suitable form for the memory function and three adjustable parameters, the experimental frequency dependence of G' and G'' in both plateau and terminal zones can be reproduced. For large strains, relaxation in the plateau zone may become prominent, as mentioned in Section E3 below.

D. BEHAVIOR IN AND NEAR THE GLASSY ZONE

It has already been pointed out that the bead-spring model on which the discussion of Sections B1 and C2 has been based to describe the transition zone cannot

be expected to predict correctly storage or relaxation moduli in excess of the order of 10^8 dynes/cm^2 (10^7 Pa), for either cross-linked or uncross-linked polymers. With increasing frequency (and correspondingly for decreasing time), there are progressive deviations from the square-root proportionality to ω given in equations 12 and 13, and at high frequencies G' approaches a limiting value G_g. Obviously, when chain units very close to each other rearrange their relative positions, their configurations do not have a Gaussian distribution, and the energy changes do not correspond to the stretching of an entropy spring. Moreover, the resistance to motion cannot be described by an average viscous friction. It depends on details of local geometry, and at frequencies so high that no configurational rearrangements are possible it develops an elastic rather than a viscous character; whatever slight motions are accomplished involve bending and stretching of chemical bonds.

1. Limiting Behavior at High Frequencies

An extension to the flexible chain theory taking into account the elastic reaction of high frequencies was introduced by Marvin.[6,9] Essentially, it replaces the viscous force by an elastic and a viscous force in series, so ζ_0 becomes $\zeta_0(1 - i\omega\zeta_0/\zeta_E)/(1 + \omega^2\zeta_0^2/\zeta_E^2)$. At low frequencies, the force per unit velocity is ζ_0 as before; at high frequencies, it is $-i\zeta_E/\omega$, where ζ_E is the force per unit displacement of a monomer unit. The value of ζ_E is chosen to give the proper limiting value of G_g at high frequencies; $\zeta_E = 24G_g^2v_0^2/a^2kT$, where v_0, the volume per monomer unit, is $M_0/N_0\rho$. Otherwise there are no additional adjustable parameters. (The coefficient ζ_0 is of course determined empirically in any case.) The calculation is made by the equivalent ladder network model illustrated in Fig. 10–17. The results predict a rather abrupt transition from the square-root relations of equations 12 and 13 to the properties of a single Maxwell element (equations 1 to 8 of Chapter 3) with $G_i = G_g$ and $\eta_i = G_g\zeta_0/\zeta_E$. Correspondingly, the spectra H and L are cut off at a time of the order ζ_0/ζ_E. The functions G', $G(t)$, J', and $J(t)$ approach their proper asymptotic values, and, in agreement with experiment (Fig. 2–4), G'' passes through a maximum. Beyond this maximum, both G'' and J'' are inversely proportional to the first power of the frequency. The theory predicts the height of the maximum to be $0.613G_g$, and its location on the frequency scale to be at $\omega_M = 0.576\zeta_E/\zeta_0$. Experimentally, the maxima in Fig. 2–4 (except for that of rubber, curve VI, which is unusually sharp) correspond to $G''_M/G_g \cong 0.2$ to 0.3, so the entrance into the glassy zone is somewhat more gradual than predicted by the theory.

The minimum relaxation time ζ_0/ζ_E in the Marvin theory can be shown to be equal to the time at which the Rouse expression for H, as given by equation 23 of Chapter 9, has the value G_g/π.

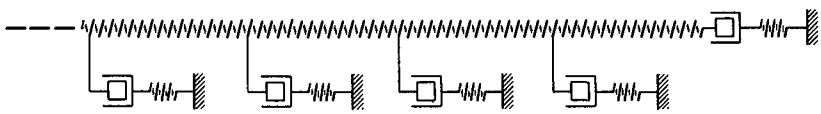


FIG. 10–17. Modification of ladder network by Marvin[9] to account for limiting value of modulus at high frequencies and short times.

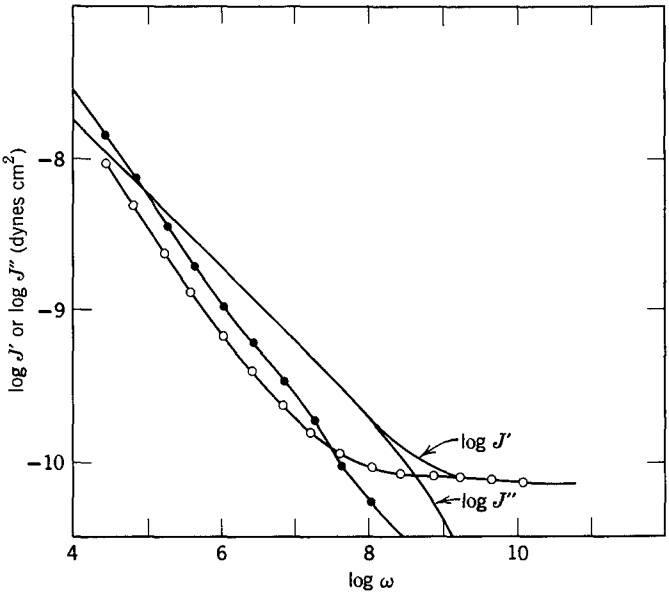


FIG. 10-18. Comparison of calculated curves for J' and J'' for polyisobutylene, by the ladder network model of Fig. 10-17, with experimental results reduced to 25°C. Curves without points, theory; open circles, experimental J'; black circles, experimental J''.

A detailed comparison of theory with experiment is given for polyisobutylene in Fig. 10-18, where the components of the complex compliance are chosen for representation. The general aspects of the onset of the glassy zone are evidently semiquantitatively reproduced. However, the distinct difference in slope between theory and experiment for values of J' and J'' less than 10^{-8} cm^2/dyne is apparent. A similar treatment was made by Shibayama and collaborators,[101] who also introduced varying parameters for the springs and dashpots in the ladder model to modify the shapes of the viscoelastic functions predicted. But a more detailed picture of local molecular motions is needed to explain viscoelastic behavior near the glassy zone.

2. Persistence of Relaxation and Retardation Spectra into the Glassy Zone

In the Marvin modification of the flexible chain theory for the glassy end of the transition, the minimum retardation time ($= \zeta_0/\zeta_E$) and minimum relaxation time occur near $1/\omega_M$, and at shorter times H and L vanish. Actually, although H goes through a maximum with decreasing τ, it does not vanish but persists at a rather high level (Fig. 3-3). This corresponds to the fact that G' and $G(t)$ do not really approach an upper asymptotic value of G_g, but continue to change slightly (Figs. 2-2 and 2-3). From the behavior of polymers below their glass transition temperatures (curves V in the figures quoted), it may be inferred that contributions to H and L extend practically indefinitely out in the short-time direction. No clear in-

terpretation of this background for the relaxation and retardation spectra has been given.

Superimposed on the background of the spectra are perceptible maxima and minima. These features are visible in curves V of Figs. 3-3 and 3-4 and can be seen more readily with an enlarged scale, revealing characteristic shapes. They can be attributed partly to very local motions of the chain backbone and partly to motions of side groups. Correlations of these loss mechanisms with structure will be discussed in Chapter 15.

E. NONLINEAR BEHAVIOR IN UNCROSS-LINKED POLYMERS OF HIGH MOLECULAR WEIGHT

1. Apparent Viscosity in Non-Newtonian Flow

Nonlinear viscoelastic behavior in amorphous, homogeneous polymers is most prominent in the terminal zone, and its most spectacular manifestation is non-Newtonian flow, *i.e.*, the enormous decrease in apparent viscosity η with increasing shear rate $\dot{\gamma}$. In contrast to the case for dilute solutions of flexible macromolecules mentioned in Section F of Chapter 9, where decreases of 30% are observed and attributed to intramolecular effects, in concentrated solutions and undiluted uncross-linked polymers decreases of several orders of magnitude are found. Shear rate dependence may appear at very low shear rates. Indeed, as mentioned in Chapter 1, it may be difficult to perform experiments at sufficiently low $\dot{\gamma}$ to determine the limiting vanishing-shear viscosity η_0. For these systems the phenomenon can be attributed primarily to intermolecular effects, since the viscosity is dominated by the longest relaxation times and these are associated with entanglements, which are inherently intermolecular. As pointed out by Graessley,[60] this conclusion is reinforced by the minimum value of $\dot{\gamma}$ at which non-Newtonian behavior appears, *i.e.*, at which η/η_0 falls to a characteristic value significantly smaller than unity. The reciprocal of this $\dot{\gamma}$ is a characteristic time τ_η which is found to be similar in magnitude to the longest relaxation time in the terminal zone or to the weight-average terminal relaxation time τ_w of equation 53, so the onset of non-Newtonian behavior is related to the time required for complete configurational rearrangement of an entangled molecule.

Several molecular theories for non-Newtonian flow have been advanced;[44,73,102-104] the earlier ones have been reviewed in detail by Graessley.[60]

Very good agreement with experiment for undiluted polymers with sharp molecular weight distribution is obtained for the theory of Graessley,[102] which is based on the following features. There is a dynamic steady state in the formation and disappearance of entanglements; with increasing shear rate, the concentration of entanglements is diminished, primarily because the transit time during which a pair of molecules pervade each others' domains as they shear past becomes smaller compared with the time required to form an entanglement; and the time required to form an entanglement is proportional to the viscosity η at the existing shear rate.

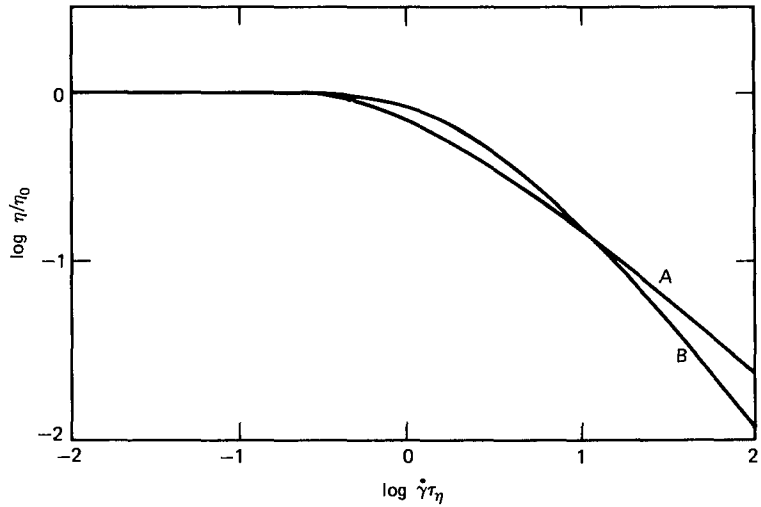


FIG. 10–19. Dependence of non-Newtonian viscosity on shear rate: log η/η_0 plotted against log $\dot{\gamma}\tau_\eta$. (A) Theory of Graessley;[102] (B) theory of Williams.[107]

The resulting prediction for the non-Newtonian viscosity is

$$\frac{\eta}{\eta_0} = \left(\frac{2}{\pi}\right)^{5/2}\left[\cot^{-1}\theta + \frac{\theta(1-\theta^2)}{(1+\theta^2)^2}\right]\left[\cot^{-1}\theta + \frac{\theta}{1+\theta^2}\right]^{3/2} \tag{63}$$

where $\theta = (\eta/\eta_0)(\dot{\gamma}\tau_\eta/2)$. At very small shear rates, the initial decrease in viscosity is given by the expansion

$$1 - \eta/\eta_0 = (5/24\pi)(\dot{\gamma}\tau_\eta)^3 + \text{higher terms} \tag{64}$$

(Since odd terms are involved, the absolute value of $\dot{\gamma}$ must be used.) At high shear rates, on the other hand, η becomes proportional to $\dot{\gamma}^{-9/11}$. This exponent of -0.818 has been observed for polystyrenes[105] and poly(dimethylsiloxane)s.[106] The characteristic value of η/η_0 which may be regarded as the onset of non-Newtonian behavior, *i.e.*, where $\dot{\gamma} = \tau_\eta^{-1}$, is for uniform molecular weight distribution approximately 0.83; for a small departure from uniform distribution ($\overline{M}_w/\overline{M}_n = 1.09$) it corresponds to about 0.78.

In Fig. 10–19, η/η_0 is plotted logarithmically against $\dot{\gamma}\tau_\eta$ for the Graessley theory, as well as for a theory of Williams[107] for concentrated polymer solutions which involves the intermolecular potential between neighboring segments and a friction coefficient between segments. These plots correspond to a polymer of uniform molecular weight, but the effect of molecular weight distribution can be introduced on an additive basis. The integration is analogous to that used for viscoelastic properties. An example of comparison with experiment is shown in Fig. 10–20, where η/η_0 is plotted logarithmically against $\dot{\gamma}\tau_\eta/2$ for a polystyrene[108] with sharp molecular weight distribution and $\overline{M}_w = 180{,}000$ at five different temperatures and compared with the Graessley theory (equation 63). The agreement is very good; similar agreement has been found for other narrow-distribution

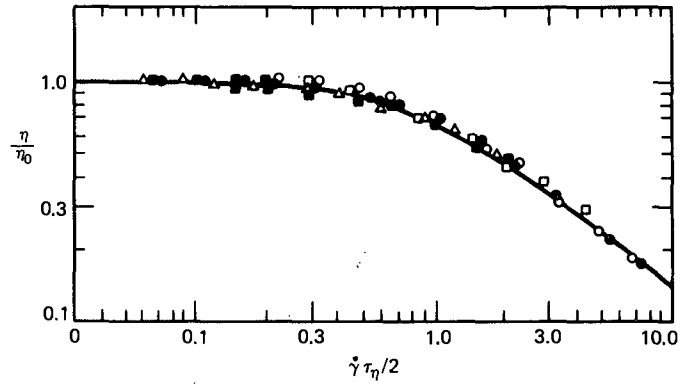


FIG. 10-20. Logarithmic plot of η/η_0 against $\dot{\gamma}\tau_\eta/2$ for narrow-distribution polystyrene with M_w = 180,000. Different symbols refer to five different temperatures from 142° to 174.5°C. Curve drawn from Graessley theory. (Penwell, Graessley, and Kovacs.[108]) Reproduced, by permission, from the Journal of Polymer Science.

polystyrenes,[109] poly(dimethylsiloxane)s,[106] and polybutadienes.[110] The characteristic time τ_η is found almost always to be 2 to 3 times τ_w as calculated from equation 53 over wide ranges of molecular weight, in confirmation of the concept that the longest relaxation time governs the onset of the non-Newtonian behavior with increasing shear rate.

2. Steady-State Compliance and Normal Stress Differences

The concept of the Graessley theory that the steady-state concentration of entanglements is diminished during flow at high shear rates implies that the steady-state compliance $R_{\dot{\gamma}}$ observed in recovery after cessation of steady-state flow will be larger than J_e^0 and given by the equation

$$R_{\dot{\gamma}} = J_e^0/(2/\pi)[\cot^{-1}\theta + \theta/(1+\theta^2)] \tag{65}$$

where θ is defined as in equation 63. An increase in $R_{\dot{\gamma}}$ with $\dot{\gamma}$ has been sometimes, but not always, observed; the behavior appears to be strongly affected by molecular weight distribution.

The primary normal stress coefficient at low shear rates according to equation 74 of Chapter 3 is given by $\Psi_{1,0} = 2\eta_0^2 J_e^0$. At high shear rates, relations between $\Psi_1(\dot{\gamma})$ and $\eta(\dot{\gamma})$ are provided by some phenomenological theories;[111] from a qualitative molecular standpoint, it may be inferred that the decrease in Ψ_1 with increasing $\dot{\gamma}$ is related to the drop in η and hence, in the framework of the entanglement model, to a decrease in the steady-state concentration of entanglements.

3. Other Manifestations of Nonlinear Behavior

Stress relaxation following sudden strain for large deformations in both shear and simple extension has been treated for the tube model by Doi and Edwards.[73,74]

If the time scale is limited to the terminal zone ($t \geq \tau_d$), the time-dependent stress can be factored into a function of time and a function of strain (*cf.* equation 8 of Chapter 6); thus, for shear,

$$\sigma_{21}(t) = \mathcal{F}_{21}(\gamma)G(t) \tag{66}$$

and for elongation

$$\sigma_T(t) = \mathcal{F}_T(\lambda)E(t) \tag{67}$$

in which $\mathcal{F}_{21}$ and $\mathcal{F}_T$ are rapidly decreasing functions of their arguments; $G(t)$ is given by equation 54 and $E(t) = 3G(t)$.

However, near the boundary between the plateau and terminal zone, the time and strain dependences cannot be factored, as shown experimentally for both shear[113] and elongation.[112] Account must be taken of another relaxation process which precedes the disengagement of a molecule from its tube.[74] At large strains, segments of the molecule of length the order of the tube diameter (or the distance between slip links or entanglements) are deformed to different degrees; depending on orientation, some parts will be stretched and others compressed. These differences can be equalized by motion of the molecule within the tube with a characteristic relaxation time τ_{eq} which is proportional to M^2. The time τ_{eq} lies between τ_d, which corresponds to diffusion of the entire molecule along its contour to escape from the tube, and the longest relaxation time in the transition zone, τ_{tr}, which corresponds to rearrangement over a distance equivalent to the tube diameter (or to the length of a strand of the entanglement network), as discussed in Section C2 above. In fact, τ_{eq} is approximately equal to τ_1 as defined by equation 4 with $p = 1$ and therefore corresponds to the longest relaxation time the molecule would have in the *absence* of the topological restraints imposed by the entanglements or slip links. Then in equation 67 another factor is added which is a function of both λ and t/τ_{eq} but approaches unity as $\lambda \to 1$; and similarly for equation 66. The result,[74] which will be given in more detail in Section E1 of Chapter 13, describes very well the large nonlinear effects observed in simple extension[112] as well as, reasonably well, the very large effects observed in shear.[113]

The dependence of stress on strain, strain rate, and time for both shear and elongational deformation can also be described by various other constitutive equations.[97,114-119] Some of these involve specially defined measures of strain.[116,117] In some, the strain dependence and time dependence of stress are factored as in equations 66 and 67.[116,118] Experimental data are fitted very closely but detailed molecular interpretations are not provided.

Other manifestations of nonlinear behavior include growth of shear and normal stresses following imposition of a large strain rate and relaxation of these stresses after cessation of flow, extensional viscosity as a function of strain rate, and combination of steady state shear flow with oscillating deformations either in the flow direction or at right angles. These can be related to the dependence of η on $\dot{\gamma}$ by various phenomenological constitutive equations,[111] and can be understood qualitatively in terms of a reduced concentration of entanglements during steady-state flow and the rates of disentanglement and entanglement formation.[120] These

phenomena have also been predicted from the tube model by the theory of Doi and Edwards[73,74] in qualitative agreement with experiment.

A detailed and rigorous theory of linear and non-linear viscoelasticity for a different model of constraints to the motion of a macromolecule has been developed by Curtiss and Bird.[121]

More detailed comparisons of the theoretical predictions discussed in this chapter with experimental results will be presented in later chapters.

REFERENCES

1. F. Bueche, *J. Chem. Phys.*, **20,** 1959 (1952).
2. J. D. Ferry, R. F. Landel, and M. L. Williams, *J. Appl. Phys.*, **26,** 359 (1955).
3. G. C. Berry and T. G. Fox, *Adv. Polym. Sci.*, **5,** 261 (1968).
4. M. L. Williams, *J. Polym. Sci.*, **62,** 57 (1962).
5. N.W. Tschoegl, *J. Chem. Phys.*, **44,** 2331 (1966).
6. R. S. Marvin and H. Oser, *J. Res. Nat. Bur. Stand.*, **66B,** 171 (1962).
7. R. B. Blizard, *J. Appl. Phys.*, **22,** 730 (1951).
8. B. Gross and R. M. Fuoss, *J. Polym. Sci.*, **19,** 39 (1956).
9. R. S. Marvin, in *Viscoelasticity—Phenomenological Aspects,* J. T. Bergen, editor, Academic Press, New York, 1960, p. 27.
10. H. Oser and R. S. Marvin, *J. Res. Nat. Bur. Stand.*, **67B,** 87 (1963).
11. K. Ninomiya, *J. Colloid Sci.*, **14,** 49 (1959).
12. K. Ninomiya, *J. Colloid Sci.*, **17,** 759 (1962).
13. K. Ninomiya and J. D. Ferry, *J. Colloid Sci.*, **18,** 421 (1963).
14. K. Ninomiya, J. D. Ferry, and Y. Ōyanagi, *J. Phys. Chem.*, **67,** 2297 (1963).
15. H. Leaderman, R. G. Smith, and L. C. Williams, *J. Polym. Sci.*, **36,** 233 (1959).
16. E. Menefee and W. L. Peticolas, *J. Chem. Phys.*, **35,** 946 (1961).
17. W. L. Peticolas and E. Menefee, *J. Chem. Phys.*, **35,** 951 (1961).
18. W. L. Peticolas, *Rubber Chem. Technol.*, **36,** 1422 (1963).
19. J. D. Ferry, M. L. Williams, and D. M. Stern, *J. Phys. Chem.*, **58,** 987 (1954).
20. B. H. Zimm and R. W. Kilb, *J. Polym. Sci.*, **37,** 19 (1959).
21. J. S. Ham, *J. Chem. Phys.*, **26,** 625 (1957).
22. L. R. G. Treloar, *The Physics of Rubber Elasticity,* 3rd ed., Oxford, 1975.
23. T. L. Smith, in *Treatise on Materials Science and Technology,* Volume 10, Part A, Academic Press, 1977, p. 369.
24. P. J. Flory, C. A. J. Hoeve, and A. Ciferri, *J. Polym. Sci.*, **34,** 337 (1959).
25. A. V. Tobolsky, D. W. Carlson, and N. Indictor, *J. Polym. Sci.*, **54,** 175 (1961).
26. A. J. Chompff and J. A. Duiser, *J. Chem. Phys.*, **45,** 1505 (1966).
27. P. J. Flory, *J. Chem. Phys.*, **66,** 5270 (1977).
28. W. W. Graessley, *Macromolecules,* **8,** 186 (1975); D. S. Pearson and W. W. Graessley, *Macromolecules,* **11,** 528 (1978).
29. M. Morton and D. C. Rubio, presented at U. S.–Japan Joint Seminar on Elastomers, Akron, Ohio, 1977.
30. E. M. Valles and C. W. Macosko, presented at U. S.–Japan Joint Seminar on Elastomers, Akron, Ohio, 1977.
31. M. Mooney, *J. Polym. Sci.*, **34,** 599 (1959).
32. A. Ziabicki, *Macromolecules,* **7,** 501 (1974).
33. R. A. Dickie and J. D. Ferry, *J. Phys. Chem.*; **70,** 2594 (1966).
34. F. Bueche, *J. Chem. Phys.*, **22,** 603 (1954).
35. O. Nakada, *J. Phys. Soc. Jpn.*, **10,** 804 (1955).

36. O. Kramer and J. D. Ferry, in *Science and Technology of Rubber*, edited by F. R. Eirich, Academic Press, New York, 1978, p. 180.
37. R. A. Stratton and J. D. Ferry, *J. Phys. Chem.*, **67**, 2781 (1963); S. E. Lovell, J. E. Frederick, and J. D. Ferry, unpublished calculations.
38. N. R. Langley, *Macromolecules*, **1**, 348 (1968).
39. N. R. Langley and K. E. Polmanteer, *J. Polym. Sci., Polym. Phys. Ed.*, **12**, 925 (1974).
40. L. R. G. Treloar, *Trans. Faraday Soc.*, **36**, 538 (1940).
41. L. E. Nielsen and R. Buchdahl, *J. Colloid Sci.*, **5**, 282 (1950).
42. H. Mark and A. V. Tobolsky, *Physical Chemistry of High Polymeric Systems*, Interscience, New York, 1950, Chapter X and p. 344.
43. R. D. Andrews and A. V. Tobolsky, *J. Polym. Sci.*, **7**, 224 (1951).
44. F. Bueche, *Physical Properties of Polymers*, Interscience, New York, 1962.
45. T. G. Fox, S. Gratch, and S. Loshaek, in *Rheology*, F. R. Eirich, editor, Volume I, p. 446, Academic Press, New York, 1956.
46. M. S. Green and A. V. Tobolsky, *J. Chem. Phys.*, **14**, 80 (1946).
47. A. S. Lodge, *Elastic Liquids*, Academic Press, New York, 1964.
48. M. Yamamoto, *J. Phys. Soc. Jpn.*, **11**, 413 (1956); **12**, 1148 (1957); **13**, 1200 (1958).
49. R. Longworth and H. Morawetz, *J. Polym. Sci.*, **29**, 307 (1958).
50. Yu. N. Panov, K. Ye. Nordbeck, and S. Ya. Frenkel, *Vysokomol. Soed.*, **6**, 47 (1964).
51. T. G. Fox and others, *J. Am. Chem. Soc.*, **80**, 1768 (1958).
52. W. Philippoff and F. H. Gaskins, *Trans. Soc. Rheol.*, **2**, 263 (1958).
53. J. D. Huppler, E. Ashare, and L. A. Holmes, *Trans. Soc. Rheol.*, **11**, 159 (1967).
54. R. F. Landel, J. W. Berge, and J. D. Ferry, *J. Colloid Sci.*, **12**, 400 (1957).
55. F. E. Helders, J. D. Ferry, H. Markovitz, and L. J. Zapas, *J. Phys. Chem.*, **60**, 1575 (1956).
56. H. H. Meyer, W. F. Pfeiffer, Jr., and J. D. Ferry, *Biopolymers*, **5**, 123 (1967).
57. N. W. Tschoegl and J. D. Ferry, *J. Am. Chem. Soc.*, **86**, 1474 (1964).
58. G. C. Berry and S. M. Liwak, *J. Polym. Sci., Polym. Phys. Ed.*, **14**, 1717 (1976).
59. P. R. Saunders, D. M. Stern, S. F. Kurath, C. Sakoonkim, and J. D. Ferry, *J. Colloid Sci.*, **14**, 222 (1959).
60. W. W. Graessley, *Adv. Polym. Sci.*, **16**, 1 (1974).
61. S. F. Edwards, *Proc. Phys. Soc.*, **91**, 513 (1967).
62. M. Hoffmann, *Rheol. Acta*, **6**, 92 (1967).
63. M. Hoffmann, *Rheol. Acta*, **6**, 377 (1967).
64. S. F. Edwards and J. W. V. Grant, *J. Phys.*, **A6**, 1169 (1973).
65. S. F. Edwards and J. W. V. Grant, *J. Phys.*, **A6**, 1186 (1973).
66. A. Ziabicki and R. Takserman-Krozer, *J. Polym. Sci.*, A-2, **7**, 2005 (1969).
66a. R. Takserman-Krozer and A. Ziabicki, *J. Polym. Sci.*, A-2, **8**, 321 (1970).
67. A. Ziabicki and W. Klonowski, *Rheol. Acta*, **14**, 113 (1975).
67a. A. Ziabicki, *J. Chem. Phys.*, **64**, 4100 (1976).
68. O. Kramer, R. L. Carpenter, V. Ty, and J. D. Ferry, *Macromolecules*, **7**, 79 (1974); R. L. Carpenter, H.-C. Kan, and J. D. Ferry, *Polym. Eng. Sci.*, **19**, 267 (1979).
69. P. J. Flory, *Trans. Faraday Soc.*, **56**, 722 (1960).
69a. H.-C. Kan and J. D. Ferry, *Macromolecules*, **13**, 1313 (1980).
70. S. F. Edwards, *Proc. Phys. Soc.*, **92**, 9 (1967).
71. P. G. de Gennes, *J. Chem. Phys.*, **55**, 572 (1971).
72. M. Doi and S. F. Edwards, *J. Chem. Soc. Faraday Trans. II*, **74**, 1789, 1802, 1818 (1978); **75**, 38 (1979).
73. M. Doi, *J. Polym. Sci., Polym, Phys. Ed.*, **18**, 1005 (1980).
74. M. Doi and S. F. Edwards, *The Theory of Polymer Dynamics*, Clarendon Press, Oxford, 1986.
75. J. Klein, *Macromolecules*, **11**, 852 (1978).
76. P. G. de Gennes, *Macromolecules*, **9**, 587, 594 (1976).
77. W. W. Graessley, *J. Polym. Sci., Polym. Phys. Ed.*, **18**, 27 (1980).
78. F. Bueche, *J. Appl. Phys.*, **26**, 738 (1955).
79. A. J. Chompff and W. Prins, *J. Chem. Phys.*, **48**, 235 (1968).

80. R. S. Marvin and H. Oser, *J. Res. Nat. Bur. Stand.*, **66B**, 171 (1962).
81. A. V. Tobolsky, R. Schaffhauser, and R. Böhme, *Polym. Lett.*, **2**, 103 (1964).
82. D. J. Plazek, *Relaxation in Complex Systems*, K. L. Ngai and G. B. Wright. Eds, Office of Naval Research, Arlington, Va (1985).
83. S. Onogi, T. Masuda, and K. Kitagawa, *Macromolecules*, **3**, 109 (1970).
84. W. W. Graessley, *J. Chem. Phys.*, **54**, 5143 (1971).
85. D. R. Hansen, M. C. Williams, and M. Shen, *Macromolecules*, **9**, 345 (1976).
86. S. D. Hong, D. R. Hansen, M. C. Williams, and M. Shen, *J. Polym. Sci., Polym. Phys. Ed.*, **15**, 1869 (1977).
87. S. Hayashi, *J. Phys. Soc. Jpn.*, **18**, 131, 249 (1963); **19**, 101, 2306 (1964).
88. P. G. de Gennes, *J. Phys.*, **36**, 1199 (1975).
89. G. Akovali, *J. Polym. Sci.*, A-2, **5**, 875 (1967).
90. T. Masuda, K. Kitagawa, T. Inoue, and S. Onogi, *Macromolecules*, **3**, 116 (1970).
91. N. J. Mills and A. Nevin, *J. Polym. Sci.*, A-2, **9**, 267 (1971).
92. K. Ninomiya, *J. Colloid Sci.*, **14**, 49 (1959); **17**, 759 (1962).
93. D. C. Bogue, T. Masuda, Y. Einaga, and S. Onogi, *Polym. J.*, **1**, 563 (1970).
94. W. M. Prest, *Polym. J.*, **4**, 163 (1973).
95. M. Kurata, K. Osaki, Y. Einaga, and T. Sugie, *J. Polym. Sci., Polym. Phys. Ed.*, **12**, 849 (1974).
96. A. S. Lodge, *Rheol. Acta*, **7**, 379 (1968).
97. A. S. Lodge, *Body Tensor Fields in Continuum Mechanics*, Academic Press, New York, 1974.
98. G. C. Berry, B. L. Hager, and C.-P. Wong, *Macromolecules*, **10**, 361 (1977).
99. J. L. White and N. Tokita, *J. Appl. Polym. Sci.*, **11**, 321 (1967).
100. P. Thirion, *J. Polym. Sci., Polym. Lett., Ed.*, **11**, 673 (1973).
101. K. Shibayama, H. Morimoto, and F. Ishiguro, *Mitsubishi Denki Lab. Rep.*, **5**, 91 (1964).
102. W. W. Graessley, *J. Chem. Phys.*, **47**, 1942 (1967).
103. M. C. Williams, *AIChE J.*, **12**, 1064 (1966).
104. T. Ree and H. Eyring, *J. Appl. Phys.*, **26**, 793 (1955).
105. R. A. Stratton, *J. Colloid Interface Sci.*, **9**, 2911 (1965).
106. C. L. Lee, K. E. Polmanteer, and E. G. King, *J. Polym. Sci.*, A-2, **8**, 1909 (1970).
107. M. C. Williams, *AIChE J.*, **12**, 1064 (1966).
108. R. C. Penwell, W. W. Graessley, and A. J. Kovacs, *J. Polym. Sci., Polym. Phys. Ed.*, **12**, 1771 (1974).
109. W. W. Graessley and L. Segal, *Macromolecules*, **2**, 49 (1969).
110. G. Kraus and J. T. Gruver, *J. Polym. Sci.*, **A2**, 797 (1964).
111. R. B. Bird, R. C. Armstrong, O. Hassager, and C. F. Curtiss, *Dynamics of Polymeric Liquids*, Wiley, New York, 1977.
112. C. R. Taylor, R. Greco, O. Kramer, and J. D. Ferry, *Trans. Soc. Rheol.*, **20**, 141 (1976).
113. Y. Einaga, K. Osaki, M. Kurata, S. Kimura, and M. Tamura, *Polym. J.*, **2**, 550 (1971).
114. L. J. Zapas and T. Craft, *J. Res. Nat. Bur. Stand.*, **69A**, 541 (1965).
115. B. Bernstein, E. A. Kearsley, and L. J. Zapas, *Trans. Soc. Rheol.*, **8**, 391 (1963).
116. W. V. Chang, R. Bloch, and N. W. Tschoegl, *Rheol. Acta*, **15**, 367 (1976).
117. M. C. Phillips, *J. Non-Newt. Fluid Mech.*, **2**, 109, 123, 139 (1977).
118. M. H. Wagner, *J. Non-Newt. Fluid Mech.*, **4**, 39 (1978).
119. M. H. Wagner and S. E. Stephenson, *J. Rheol.*, **23**, 489 (1979).
120. H. Kajiura, M. Sakai, and M. Nagasawa, *Trans. Soc. Rheol.*, **20**, 575 (1976).
121. C. F. Curtiss and R. B. Bird, R. C. Armstrong, O. Hassagen and C. F. Curtiss, *Dynamics of Polymeric Liquids*, 2nd Ed., Wiley, New York, 1987.

CHAPTER 11

Dependence of Viscoelastic Behavior on Temperature and Pressure

Until now, there has been no explicit discussion of the effect of temperature or pressure on any of the viscoelastic functions, although it has been mentioned that below the glass transition temperature the configurations of polymer chain backbones are largely immobilized and the tremendous changes in viscoelastic properties with time or frequency which characterize polymeric systems do not appear (curves V in the figures in Chapter 2).

It is in the transition zone between glasslike and rubberlike consistency that the dependence of viscoelastic functions on temperature is most spectacular, just as is the dependence on time or frequency. An example is given in Fig. 11-1 for the real part of the complex compliance of poly(*n*-octyl methacrylate).[1] Below −5°C, the experimental frequency range appears to correspond to the glassy zone; the compliance is quite low, around $10^{-9.5}$ cm^2/dyne ($10^{-8.5}$ Pa^{-1}), and does not change much with frequency. Above 120°C, the behavior appears to correspond to the plateau zone; the compliance is characteristic of a very soft rubberlike solid ($10^{-5.5}$ cm^2/dyne or $10^{-4.5}$ Pa^{-1}), and again changes only slowly with frequency. At intermediate temperatures, the transition zone makes its appearance.

This behavior can be understood qualitatively on the basis that the retardation and relaxation times which constitute the viscoelastic spectra decrease rapidly with increasing temperature. At low temperatures, where all $\omega\tau_i \gg 1$, practically no configurational changes occur within the period of deformation; in equation 26 of Chapter 3, the integral over L makes very little contribution, and J' is close to J_g. But at high temperatures, where all $\omega\tau_i$ corresponding to mechanisms in the transition zone are much less than 1, all configurational modes of motion within entanglement coupling points (or within the confines of a virtual tube) can freely

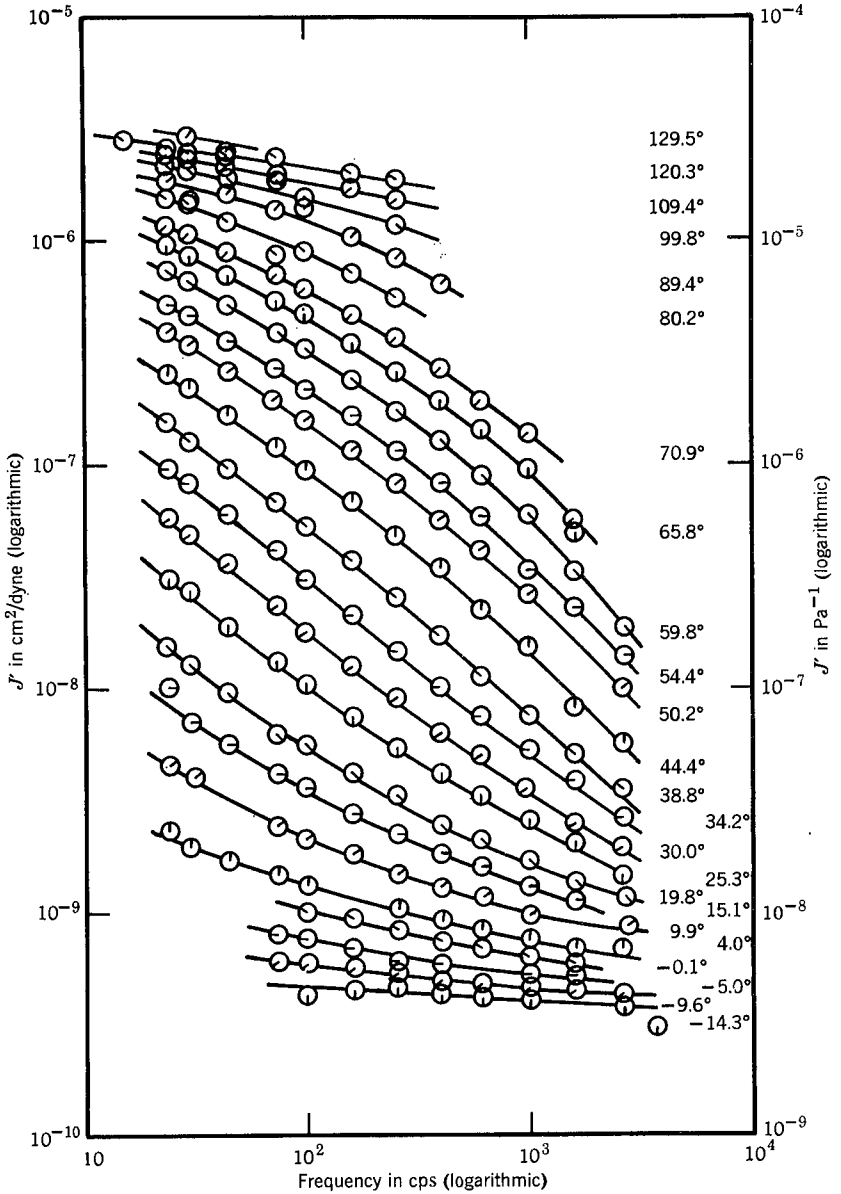


FIG. 11-1. Storage compliance of poly(*n*-octyl methacrylate) in the transition zone between glasslike and rubberlike consistency, plotted logarithmically against frequency at 24 temperatures as indicated.

occur. The integral over L then makes a large contribution, and J' is in the region corresponding to the compliance of the entanglement network.

Any attempt to analyze the temperature dependence by seeking an analytical

form for $J'(T)$ at constant frequency (or, in a corresponding family of creep curves, for example, $J(t)$ as a function of T at constant time) would lead to very complicated results. Instead, we take recourse in a method of reduced variables or viscoelastic corresponding states. This has already been mentioned as a device for enlarging the effective time or frequency scale available for experimental measurements, and in one form it has been used in Chapter 9 for presenting the data in Fig. 9-21. It affords a valuable simplification in separating the two principal variables of time and temperature on which the viscoelastic properties depend, and expressing the properties in terms of a single function of each, whose form can be determined experimentally whether or not it can be conveniently represented by an analytical expression. We are now prepared to examine this method in detail and to see how the parameters which describe temperature dependence are related to molecular constitution and structure.

It turns out that the effects of static confining pressure on the viscoelastic properties can be described by reduced variables and interpreted on a molecular basis in a similar manner.

A. ORIGIN OF THE METHOD OF REDUCED VARIABLES

1. Deduction from the Dilute-Solution Theories for Flexible Random Coils

Although the use of reduced variables developed empirically in advance of the theories which support it, we shall introduce it as a logical consequence of some of the relations in the preceding chapters.

In the theories for dilute solutions of flexible molecules based on the bead-spring model, the contribution of the solute to the storage shear modulus, loss modulus, or relaxation modulus is given by a series of terms the magnitude of each of which is proportional to nkT, *i.e.*, to cRT/M, as in equation 18 of Chapter 9; alternatively, the definition of $[G']_R$ as the zero-concentration limit of $G'M/cRT$ (equations 1 and 6 of Chapter 9) implies that all contributions are proportional to nkT. Each contribution is associated with a relaxation time which is proportional to $[\eta]\eta_s M/RT$; the proportionality constant ($= S_1^{-1}$ for τ_1) depends on which theory applies (Rouse, Zimm, etc.) but is independent of temperature, as is evident, for example, in equation 27 of Chapter 9. Thus the temperature dependence of viscoelastic properties enters in four variables: $[\eta]$, η_s, T explicitly, and c (which decreases slightly with increasing temperature because of thermal expansion).

It is implicit in equation 27 of Chapter 9, and the corresponding general equation for any degree of hydrodynamic interaction in which the factor $6/\pi^2$ is replaced by S_1^{-1}, that all the relaxation times have the same temperature dependence. This can be conveniently represented by the ratio of any specific relaxation time τ_p, such as τ_1, at temperature T to its value at an arbitrary reference temperature T_0:

$$[\tau_p]_T/[\tau_p]_{T_0} = a_T = ([\eta]\eta_s)_T T_0/([\eta]\eta_s)_{T_0} T \tag{1}$$

The value of the ratio a_T (< 1 if $T > T_0$, > 1 if $T < T_0$) is determined primarily

by the temperature dependence of η_s, since $[\eta]$, c, and T itself change more slowly. (This discussion implies that the spacings between the relaxation times will not be significantly affected by a change in hydrodynamic interaction with temperature. In the immediate vicinity of the Θ-temperature, there will be a significant temperature dependence and more complicated behavior will be observed.)

In equation 18 of Chapter 9, which may be written

$$G'(\omega) = (cRT/M) \sum \omega^2\tau_p^2/(1 + \omega^2\tau_p^2) \tag{2}$$

the effect of a change of temperature from T_0 to T is to multiply the factor before the summation sign by cT/c_0T_0 and to multiply each τ_p by a_T. Because of the form of the equation, the latter result is the same as though ω were multiplied by a_T. In other words, G' measured at frequency ω and temperature T is, except for the relatively small difference of the factor in front, equivalent to G' measured at frequency ωa_T and temperature T_0. It follows that measurements at a variety of temperatures, if plotted as $G'c_0T_0/cT$ against ωa_T, will all correspond to measurements at T_0 and form a single composite curve. The shape of this curve represents the frequency dependence at constant temperature, which can cover a very extended frequency range; and the temperature dependence of a_T represents the basic effect of temperature on viscoelastic properties.

From the relations among the viscoelastic functions, it follows that multiplication of any modulus function—$G''(\omega)$, $G(t)$, $E(t)$, etc.—by c_0T_0/cT and plotting against ωa_T or t/a_T will combine measurements at various temperatures to give a single composite curve which represents reduction of the data to T_0. Correspondingly, any compliance function multiplied by cT/c_0T_0 can be reduced in a similar manner. Multiplication by the concentration-temperature ratio is often denoted by the subscript p. It should be emphasized that the ratio c_0/c differs from unity by only a very small amount associated with thermal expansion.

2. Deduction from Theory for Undiluted Polymers

From the modification of the Rouse theory for undiluted polymers in Chapter 10, Section A, it is evident also that all contributions to G' (equation 1 of Chapter 10) should be proportional to ρT and all relaxation times should have the same temperature dependence. In this case the factor a_T is expressed from equation 4 of Chapter 10 by

$$a_T = [a^2\zeta_0]_T T_0/[a^2\zeta_0]_{T_0} T \tag{3}$$

Here the temperature dependence is very largely due to the change in ζ_0, although T enters again explicitly as a factor and the mean-square end-to-end distance per monomer unit, a, may change slightly.[2] Thus the effect of a change from T to T_0 is to multiply G' by $T_0\rho_0/T\rho$ and multiply the frequency scale by a_T; for J', to multiply by $T\rho/T_0\rho_0$ with the same frequency adjustment. The density ratio is again due merely to thermal expansion. This is illustrated in Fig. 11-2 by shifting, on logarithmic scales, the curve for 19.8° in Fig. 11-1 to $T_0 = 100°C$. When each curve in Fig. 11-1 is shifted in this manner, the result is shown in Fig. 11-3; except for

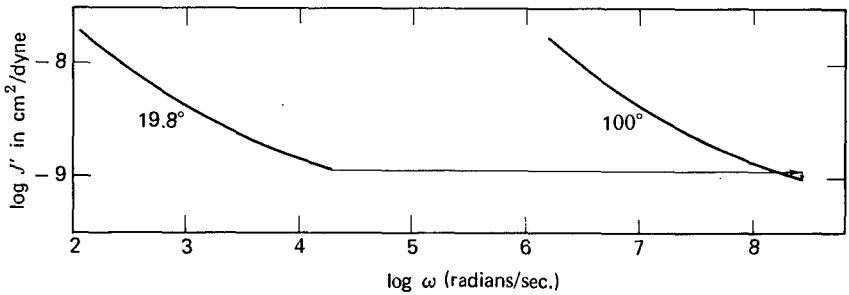


FIG. 11-2. Effect of change of temperature from T = 19.8° to T_0 = 100.0° for the J' curve at 19.8° in Fig. 11-1.

a few points, a single composite curve is obtained which represents the frequency dependence that would have been obtained over a much wider frequency range at a single temperature. It is actually this reduced plot which appeared as part of curve IV in Fig. 2-6. The temperature dependence of a_T, which in this case is determined empirically by making everything superpose on Fig. 11-3, is shown in Fig. 11-4. Thus, starting from a complicated dependence on both temperature and frequency, these two variables have been separated to give a function of frequency alone (Fig. 11-3) and one of temperature alone (Fig. 11-4). The choice of T_0 is, of course,

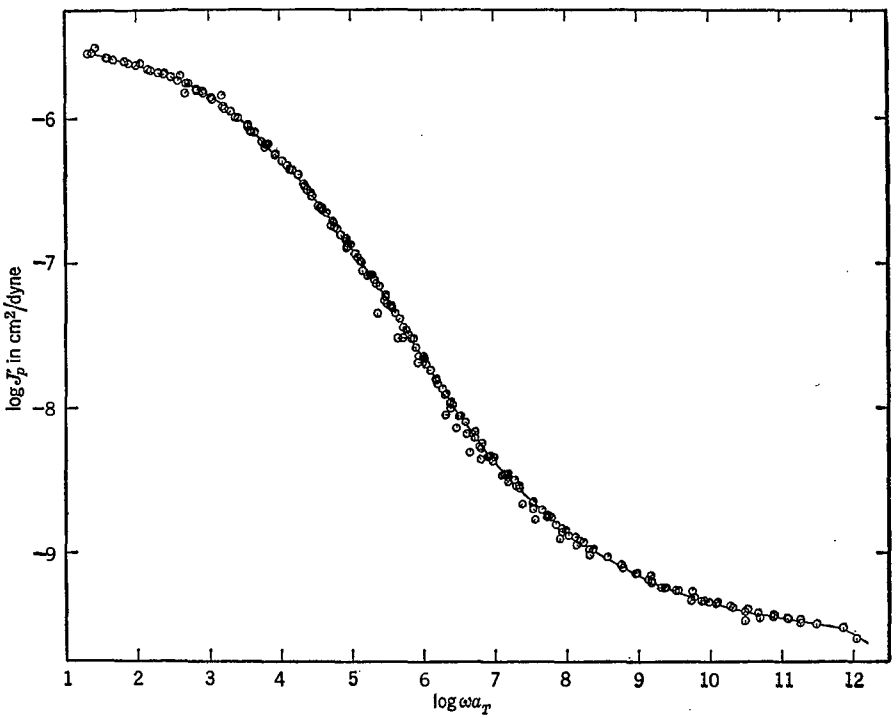


FIG. 11-3. Composite curve obtained by plotting the data of Fig. 11-1 with reduced variables, representing the behavior over an extended frequency scale at temperature T_0 = 100°C.

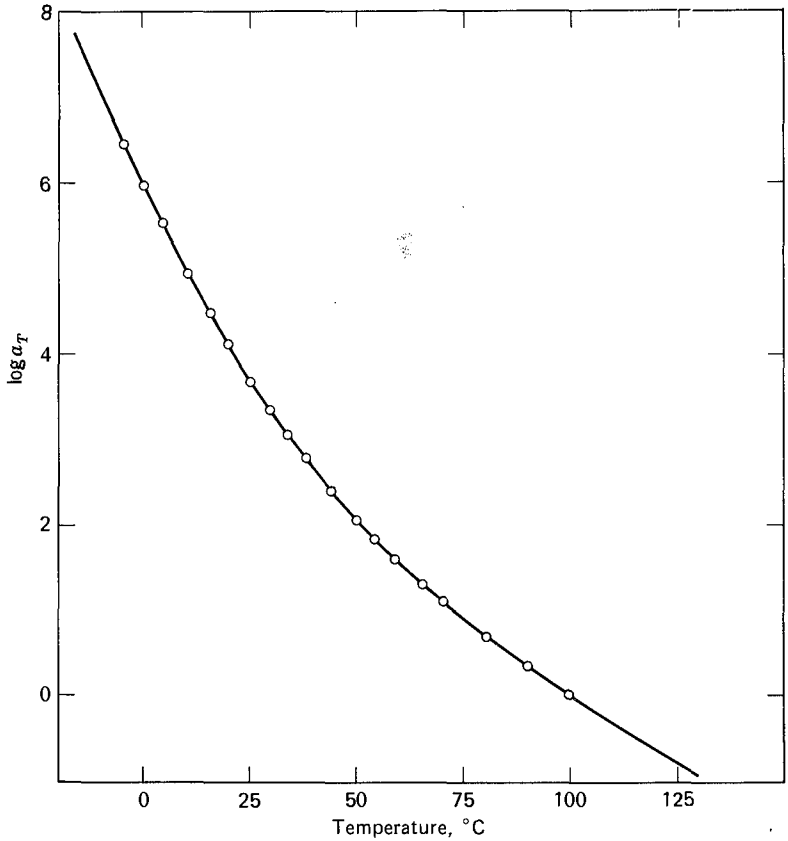


FIG. 11-4. Temperature dependence of the shift factor a_T used in plotting Fig. 11-3. Points, chosen empirically; curve, from equation 21.

arbitrary and a matter of convenience. From these two curves, J' can be obtained at any other desired temperature by reversing the reduction.

Although equation 3 was obtained from the Rouse theory, the application of reduced variables in Fig. 11-3 is based on a much more general hypothesis, namely, that the modulus contributions are proportional to ρT and the relaxation times to $a^2\zeta_0/T$ whether or not the specific spectrum of times predicted by the Rouse theory is applicable. (In fact, the shape of the curve in Fig. 11-3 deviates considerably from the Rouse theory predictions.) This hypothesis is widely fulfilled but must be carefully examined each time it is used. An important criterion is that the shapes of the original curves at different temperatures must match over a *substantial* range of frequencies; other criteria will be discussed in Section B.

Temperature reduction of the various viscoelastic functions can be obtained by plotting as follows:

$$H_p = HT_0\rho_0/T\rho, \qquad vs. \qquad \tau/a_T \tag{4}$$

$$L_p = LT\rho/T_0\rho_0, \qquad vs. \qquad \tau/a_T \tag{5}$$

$$G_p(t) = G(t)T_0\rho_0/T\rho, \quad vs. \quad t/a_T \tag{6}$$

$$G'_p = G'T_0\rho_0/T\rho, \quad vs. \quad \omega a_T \tag{7}$$

$$G''_p = G''T_0\rho_0/T\rho, \quad vs. \quad \omega a_T \tag{8}$$

$$\eta'_p = \eta'T_0\rho_0/a_TT\rho, \quad vs. \quad \omega a_T \tag{9}$$

$$J_p(t) = J(t)T\rho/T_0\rho_0, \quad vs. \quad t/a_T \tag{10}$$

$$J'_p = J'T\rho/T_0\rho_0, \quad vs. \quad \omega a_T \tag{11}$$

$$J''_p = J''T\rho/T_0\rho_0, \quad vs. \quad \omega a_T \tag{12}$$

3. Empirical Development of the Use of Reduced Variables

The scheme for construction of a composite curve like Fig. 11-3 by empirical shifts of data obtained at different temperatures along a logarithmic time or frequency axis was applied to dielectric measurements many decades ago.[3] Its application to mechanical, dielectric, and magnetic relaxation phenomena was discussed by Leaderman[4] and Müller.[5] These early treatments ignored the factor $T\rho/T_0\rho_0$, which enters the coordinate schemes 4 to 12 because of the entropy-spring nature of the stored elastic energy in the flexible chain theory; the need for such a factor would often go unnoticed in the empirical matching of curve shapes, as explained below. Andrews and Tobolsky[6] included the factor T_0/T in recognition of the rubberlike character of the elasticity for reduction of stress relaxation data. The factor $T_0\rho_0/T\rho$ was subsequently applied in reducing dynamic[7] and creep[8] data. The significance of the empirical shifting procedure in terms of molecular parameters, and the relation of the shift factor a_T to the temperature dependence of ζ_0 (equation 3), became evident with the appearance of Rouse's theory[9] in 1953, though it was also inherent in Kirkwood's theory for cross-linked networks[10] in 1946.

It should be noted again that the proportionality of moduli to $T\rho/T_0\rho_0$ (and of compliances to $T_0\rho_0/T\rho$) and the applicability of a single friction coefficient ζ_0 are more general principles than the detailed predictions of any specific theory, and these principles can be applied without assuming that the form of the time or frequency dependence follows any prescribed function. There have been some other schemes[11,8] for constructing composite curves in which it was assumed at the outset that log a_T was a linear function of reciprocal absolute temperature (by analogy with the theory of rate processes[12]), and it has sometimes been erroneously believed that the method of reduced variables implies a specific form such as this for the temperature dependence. On the contrary, the shape of the curve in Fig. 11-4 is determined empirically from the data, although it may be useful to fit it subsequently to a suitable analytical expression (Section **B** below).

In regions where the modulus or compliance is changing rapidly, as near 40° in Fig. 11-1, it would be possible to match adjacent curves empirically whether they were first shifted vertically in accordance with the factor $T\rho/T_0\rho_0$ or with T/T_0 or not shifted at all. Slightly

different values of a_T would be obtained in each case, of course. In regions where the viscoelastic function is flat, however, the influence of a vertical shift is much more apparent, and in several cases[13-15] it has been demonstrated that such a shift is necessary for satisfactory matching. It is impossible to distinguish empirically between the merits of $T\rho/T_0\rho_0$ and T/T_0, since their logarithms are both relatively small and usually differ by only about 20%. However, the former factor is clearly indicated by the flexible chain theory in equation 2 or any other of its various modifications.

The principle on which the use of reduced variables is based has been referred to by various names, such as thermorheological simplicity,[16] the time-temperature superposition principle[17] (not to be confused with the Boltzmann superposition principle!), and time-temperature reducibility;[18] the composite plots with reduced variables are often called master curves.[19]

4. Reduced Variables for Undiluted Polymers in Terms of Steady-Flow Viscosity

For uncross-linked polymers of low molecular weight, *i.e.*, for $M < M_C$, the relation between τ_p and η_0 as given by equation 7 of Chapter 10 leads to the following expression for a_T:

$$a_T = \eta_0 T_0 \rho_0 / \eta_{00} T \rho \tag{13}$$

where the second subscript 0 refers to the reference temperature T_0. Thus, if the temperature dependence of the Newtonian viscosity is known, a_T can be obtained without the empirical shifts used for Fig. 11-4 (as it is from the temperature dependence of $[\eta]\eta_s$ at infinite dilution in equation 1). The appropriate reduced coordinates for several of the viscoelastic functions are

$$G_p(t) = G(t)T_0\rho_0/T\rho, \quad vs. \quad t\eta_{00}T\rho/\eta_0 T_0 \rho_0 \tag{14}$$

$$G'_p = G'T_0\rho_0/T\rho, \quad vs. \quad \omega\eta_0 T_0\rho_0/\eta_{00}T\rho \tag{15}$$

$$G''_p = G''T_0\rho_0/T\rho, \quad vs. \quad \omega\eta_0 T_0\rho_0/\eta_{00}T\rho \tag{16}$$

$$\eta'_p = \eta'\eta_{00}/\eta_0 \quad vs. \quad \omega\eta_0 T_0\rho_0/\eta_{00}T\rho \tag{17}$$

$$\eta'_r = \eta'/\eta_0, \quad vs. \quad \omega\eta_0 T_0\rho_0/\eta_{00}T\rho \tag{18}$$

In the last, a dimensionless reduced variable has been chosen for the ordinate. Similar coordinates can be employed for $J(t)$, J', and J''.

5. Reduced Variables Applied to Polymers of High Molecular Weight

When the molecular weight of an uncross-linked polymer is sufficiently high for entanglement coupling to appear ($M > M_C$), the friction coefficient for short relaxation times is the same ζ_0 appearing in equation 3. For the longest relaxation times, other factors enter which may be temperature dependent, but there is still a factor of ζ_0 which contributes most of the temperature dependence (equations 46, 51, 53, 55, and 57 of Chapter 10). In applying reduced variables, several different cases must be distinguished.

If interest is restricted to the transition zone, the relevant motions are governed by ζ_0 and the reduction coordinates 5 through 12 are applicable; in fact, the data of Figs. 11-4 refer to such a polymer of high molecular weight which is examined here in the transition zone only.

If interest is restricted to the terminal zone, the relevant motions correspond to drag through entanglements or escape of a molecule from the effective tube which follows its contour. The terminal relaxation times are predicted to be proportional to the steady-flow viscosity η_0 (equations 53 and 57 of Chapter 10), and the reduction coordinates 14 through 18 are applicable, whether or not the parameter M_e is temperature dependent (but if it is they are applicable in the terminal zone *only*). Reduction thus on the basis of steady-flow viscosity has been rather successful in many cases, including polyisobutylene,[20] poly(vinyl acetate),[21] and very concentrated solutions of polystyrene,[22] poly(vinyl acetate),[23] and poly(*n*-butyl methacrylate).[24]

The question as to whether the same a_T reduction factors can be applicable in both the transition and terminal zones depends on whether parameters such as Q_e or M_e vary with temperature. On the basis of the entanglement concept or the tube model, such temperature dependence would be expected to be very slight. In a number of cases, the same reduction factors have been found to be applicable in both zones to a close approximation.[21-23] However, in polyisobutylene[20] and especially in very precise investigations of polystyrene[25,26] and poly(vinyl acetate)[27] the absolute values of log a_T in the transition zone were found to be somewhat greater than those calculated from equation 13. On the other hand, for certain methacrylate polymers and their concentrated solutions, the absolute values of log a_T are found to be smaller in the transition zone than in the terminal zone. This behavior, formally attributable to a temperature-dependent Q_e or M_e, does not prevent successful use of the method of reduced variables within a single zone of the time scale, but in the plateau zone a complicated transition takes place (Section F below).

6. Application of Reduced Variables near the Glassy Zone of Time or Frequency

At very short times or high frequencies where configurational rearrangements of the polymer chains do not take place within the experimental time scale, the predictions of the flexible chain theories can no longer be used as guides to a reduction scheme. The factor T/T_0 is not applicable, since the energy storage does not correspond to an entropy spring. Moreover, whatever local motions occur certainly cannot be described in terms of the friction coefficient ζ_0.

In the approach to the glassy zone, the existence of an approximately asymptotic limiting value of the compliance J_g can be taken into account by modifying reduction coordinates 10 and 11 as follows:

$$J_p(t) = J_{g0} + (J(t) - J_g)T\rho/T_0\rho_0 \qquad vs. \qquad t/a_T \tag{19}$$

$$J'_p = J_{g0} + (J' - J_g)T\rho/T_0\rho_0 \qquad vs. \qquad \omega a_T \tag{20}$$

The reduction of J'' remains unchanged, whereas those for the moduli cannot be

expressed in simple form. Here J_{g0} is the glasslike (high frequency) compliance at T_0 and J_g the corresponding value at T. These equations have been used[29] with the approximation that J_g is independent of temperature, but from the work of Lamb and collaborators[30,31] J_g may be expected to increase linearly with increasing T (the opposite direction to the temperature dependence of the rubberlike contributions to the compliance). This subject will be discussed more fully in Section F1 below and in Chapter 15. When J'/J_g or $J(t)/J_g > 10$, the simpler reduction coordinates 10 and 11 should be satisfactory.

When other viscoelastic mechanisms such as those attributed to motions of side groups make contributions comparable in magnitude to those of the backbone configurational motions, there are two types of temperature dependence superposed on each other, as described in Section F below.

B. PROCEDURE AND CRITERIA FOR APPLICABILITY OF THE METHOD OF REDUCED VARIABLES

Exact matching of the shapes of adjacent curves has already been cited as one criterion for the applicability of reduced variables. Two others which should be applied to any experimental example when possible are (a) the same values of a_T must superpose all the viscoelastic functions; (b) the temperature dependence of a_T must have a reasonable form consistent with experience.

The two components of the complex dynamic modulus (or of the complex compliance) are weighted quite differently with respect to the long-time and short-time contributions to H (or L). For example, as is evident from equations 26 and 27 of Chapter 3, J' at a particular frequency ω is determined primarily by the spectral contributions for which $\omega\tau < 1$, whereas J'' is determined by those for which $\omega\tau \simeq 1$. If for any reason a_T is not the same for long retardation times and short retardation times, not only will the curves for J' and J'' fail to match in shape, but any attempt at a forced fit will provide one set of apparent a_T values for J' and a different set for J''. Whenever this occurs, the method of reduced variables in its simple form as given above must be rejected; no master curves can be drawn without subjecting the data to a more complicated analysis.

An example of this sort of test, for the data of Fig. 11-1 and the corresponding values of J'' which were determined in the same series of measurements, is shown in Table 11-I. The procedure was as follows.[1] First, a reference temperature T_0 somewhere within the range of the experiments was arbitrarily chosen (in this case, 373.2°K). Then logarithmic plots of $J'T\rho/T_0\rho_0$ against ω (very similar in appearance to Fig. 11-1, but with slight vertical shifts produced by the $T\rho/T_0\rho_0$ factor) and of $J''T\rho/T_0\rho_0$ were prepared. The horizontal distance between each pair of adjacent curves was measured with a pair of dividers and recorded as $\Delta \log a_T$. (If the curves were not parallel, or if their slopes were such that no reliable measurement could be made, no value was recorded. Where the values of $\Delta \log a_T$ from J' and J'' were the same within reasonable error, the average was taken. (At low temperatures, the spacings from J'' are often preferred because the nature of the experimental method makes them somewhat more reliable; depending on

Table 11-I

DETERMINATION OF a_T VALUES FOR POLY(*n*-OCTYL METHACRYLATE) FROM FIG. 11-1 AND CORRESPONDING DATA FOR J''

T, °K	log[a] $T\rho/T_0\rho_0$	$\Delta \log a_T$ From J'	$\Delta \log a_T$ From J''	Chosen	log a_T Tent.[a]	$\frac{T - T_0}{\log a_T}$	log a_T Calc.[b]
268.2	−0.11				6.45	16.29	6.52
273.1	−0.11	0.58[c]	0.47	0.47	5.98	16.74	5.98
277.2	−0.10	0.43	0.42	0.42	5.56	17.27	5.57
283.1	−0.10	0.62	0.60	0.61	4.95	18.22	4.99
288.3	−0.09	0.45	0.47	0.46	4.49	18.90	4.53
293.0	−0.08	0.35	0.37	0.36	4.13	19.42	4.14
298.5	−0.08	0.41	0.44	0.43	3.70	20.20	3.72
303.2	−0.07	0.31	0.34	0.33	3.37	20.80	3.38
307.4	−0.07	0.29	0.30	0.30	3.07	21.45	3.10
312.0	−0.06	0.29	0.30	0.30	2.77	22.10	2.80
317.6	−0.05	0.35	0.35	0.35	2.42	22.98	2.46
323.4	−0.05	0.32	0.32	0.32	2.10	23.74	2.13
327.6	−0.04	0.22	0.24	0.23	1.87	24.40	1.91
333.0	−0.04	0.27	0.26	0.26	1.61	25.00	1.64
339.0	−0.03	0.27	0.27	0.27	1.34	25.55	1.35
344.1	−0.03	0.22	0.22	0.22	1.12	26.05	1.12
353.4	−0.02	0.37	0.40	0.38	0.74	*e*	0.73
362.6	−0.01	0.34	*d*	0.34	0.40	*e*	0.37
373.0	0	0.39	*d*	0.39	0.01	*e*	0.01
382.6	0.01	0.31	*d*	0.31			−0.30
393.5	0.02	*d*	*d*				−0.62
402.7	0.02	*d*	*d*				−0.87

[a] Choosing $T_0 = 373.2$°K.
[b] With $c_1^0 = 7.60$, $c_2^0 = 227.3$.
[c] Poor fit.
[d] Curves too flat to determine $\Delta \log a_T$.
[e] Dividend and divisor too small for precision.

the experiments, either J' or J'' may be the more reliable measurement in certain regions of frequency and consistency.) The selected values of $\Delta \log a_T$ were then added progressively from T_0 to obtain $\log a_T$ at each temperature.

The next criterion, the form of $\log a_T$ as a function of temperature, was applied first by noting that it was a smooth function with no gross fluctuations or irregularities and then by fitting the empirical values to an expression which has proved to be widely applicable (*cf.* Section C below):

$$\log a_T = -c_1^0(T - T_0)/(c_2^0 + T - T_0) \tag{21}$$

For this purpose, $(T - T_0)/\log a_T$ as listed in Table 11-I was plotted against $T - T_0$, and from the slope s and intercept i of the resulting straight line the two empirical constants were calculated:

$$c_1^0 = -1/s \tag{22}$$

$$c_2^0 = i/s \tag{23}$$

Finally, values of log a_T were calculated from equation 21 with the selected coefficients $c_1^0 = 7.60$, $c_2^0 = 227.3$; these are given in the last column of Table 11-I, and amount to a smoothing of the values in the first log a_T column. They agree quite closely with the initial tentative values. The calculated values were actually used in constructing Fig. 11-3, and also the corresponding reduced plot of the imaginary part of the compliance, which is shown in Fig. 11-5. The criterion that both components be reduced with the same a_T values is clearly satisfied, except for a slight anomaly at the highest reduced frequencies.

Still another criterion for satisfactory reduction is that the coefficients c_1^0 and c_2^0 should have magnitudes in accord with experience when they are transformed to the values appropriate to the glass transition temperature T_g as reference temperature. This subject is discussed in Section C below.

The form of equation 21 is independent of the choice of T_0. To check the determination of c_1^0 and c_2^0, it is frequently useful to choose a second reference temperature T_1 and repeat

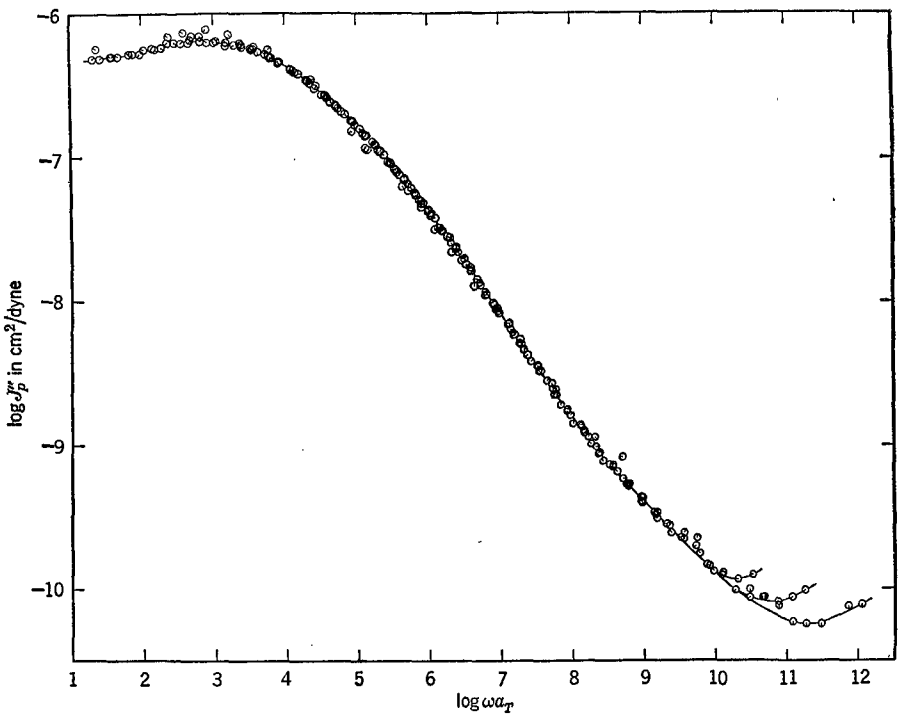


FIG. 11-5. Composite curve for the loss compliance of poly(*n*-octyl methacrylate) obtained from the same series of measurements as the data of Figs. 11-1 and 11-3 and reduced to $T_0 = 100°C$ with the same values of a_T.

the graphical evaluation, which provides coefficients c_1^1 and c_1^2 corresponding to T_1. These are then transformed to the values appropriate to T_0 by the relations

$$c_1^0 = c_1^1 c_2^1/(c_2^1 + T_0 - T_1) \tag{24}$$

$$c_2^0 = c_2^1 + T_0 - T_1 \tag{25}$$

If desired, several independent determinations of c_1^0 and c_2^0 can be made in this manner for better utilization of the data. For example, in Table 11-I the high-temperature data are wasted, but they could be used in a plot with $T_1 = 273.2°K$. A final choice of c_1^0 and c_2^0 from several such plots is rather subjective, however.

A somewhat more objective procedure[32,33] is based on the observation from equation 25 that

$$T_0 - c_2^0 = T_1 - c_2^1 \equiv T_\infty \tag{26}$$

where T_∞ is a fixed temperature at which, regardless of the arbitrary choice of T_0, $\log a_T$ becomes infinite in accordance with equation 21. The temperature T_∞ is often called the Vogel temperature because a similar characteristic temperature was used in an empirical equation for temperature dependence of viscosity by Vogel.[34] Equation 21 can then be rewritten as

$$\log a_T = c_1^0(T - T_0)/(T - T_\infty) \tag{27}$$

A plot of $\log a_T$ against $(T - T_0)/(T - T_\infty)$ is linear through the origin if T_∞ is chosen correctly; trials can be made with different values of T_∞ until curvature is eliminated, starting from the rule of thumb that T_∞ is usually about 50° below the glass transition temperature (Section C). Then the slope is c_1^0, and c_2^0 can be obtained from equation 26. To make a really precise determination of T_∞ for this purpose, a least-squares fit to equation 27 can be done with a computer program. Pierson and Kovacs[35,36] have shown with an analogous treatment of the temperature dependence of viscosity that T_∞ can be successfully determined within 0.5° or less by minimizing the standard deviation of both slope and intercept of the corresponding linear plot. In another method for determining c_1 and c_2, due to Taylor,[37] small adjustments are made to a preliminary arbitrarily chosen value of T_0 as well as to c_1 and c_2 by computer to minimize the differences between calculated and observed values of a_T.

There have been many examples where experimental viscoelastic data, both transient and dynamic, superpose with remarkable precision when reduced to a reference temperature in this manner. In other cases, the reduction is successful only in a restricted zone, and deviations occur in other regions of viscoelastic consistency or of temperature. Some examples of the latter and their interpretation are given in Section F below.

Since in a single investigation dynamic measurements usually do not extend over more than three decades of logarithmic frequency, nor transient measurements over more than six decades, specific numerical tests of the accuracy of the reduction procedure are usually limited to distances of this order, although the span of the reduced viscoelastic function may cover 12 decades as in Fig. 11-3 or even more.

Table 11-II

PARAMETERS CHARACTERIZING TEMPERATURE DEPENDENCE OF a_T FOR VARIOUS POLYMER SYSTEMS

Polymer	T_0, °K	c_1^0	c_2^0, deg	T_g, °K	f_∞/B	α_f/B, deg^{-1} x 10^{-4}	$\Delta\alpha$, deg^{-1} x 10^{-4}	T_∞, °K	Ref.
General									
Polyisobutylene[a]	298	8.61	200.4	205	0.026	2.5	4.9	101	191
Poly(vinyl acetate)	349	8.86	101.6	305	0.028	5.9	4.4	258	192,193
Poly(vinyl chloroacetate)[b]	346	8.86	101.6	296	0.025	6.2		256	133,192
Polystyrene	373	12.7	49.8	370	0.033	6.9		325	25
	373	13.7	50.0	373	0.032	6.3	3.7	323	31
Poly(α-methyl styrene)	445	13.7	49.3	445	0.032	6.4	3.8	396	194,195
	441	16.8	53.5	441	0.026	4.8			
Poly(methyl acrylate)	324	8.86	101.6	276	0.024	5.3	4	222	192,196
	326	8.86	101.6					224	197
Poly(hexene-1)	218	17.4	51.6	218	0.020	9.7		198	198
Poly(dimethyl siloxane)	303	1.90	222	150	0.071	10.3	10.9	81	199
Polyacetaldehyde[b]	243	14.5	24	243	0.030	12.5		219	200
Poly(propylene oxide)[b]	198	16.2	24	198	0.027	11.3		174	113
Zinc phosphinate polymer	373	6.94	66.6	324	0.017	9.4		306	201
Styrene-*n*-hexyl methacrylate copolymer[c]	373	7.11	192.6	277	0.030	3.2		180	202
Styrene-*n*-hexyl methacrylate copolymer[d]	373	6.56	156.4	287	0.030	4.2		217	202
Rubbers									
Hevea rubber	248	8.86	101.6	200	0.026	4.8		146	135
	298	5.94	151.6					146	203
Polybutadiene, cis-trans[e]	298	3.64	186.5	172	0.039	6.4		112	204
Polybutadiene, high cis[f]	298	3.44	196.6	161	0.039	6.4		112	205
Polybutadiene, cis-trans-vinyl[g]	263	5.97	123.2	205	0.038	5.9		149	206

Table 11–II (Continued)

Polymer	T_0, °K	c_1^0	c_2^0, deg	T_g, °K	f_g/B	α_f/B, deg^{-1} x 10^{-4}	$\Delta\alpha$, deg^{-1} x 10^{-4}	T_∞, °K	Ref.
Polybutadiene,[e] high vinyl[h]	298	6.23	72.5	261	0.034	9.6		226	207
Styrene-butadiene copolymer[i]	298	4.57	113.6	210	0.021	8.2		184	208
Butyl rubber[j]	298	9.03	201.6	205	0.026	2.4		96	209
Ethylene-propylene copolymer[k]	298	5.52	96.7	242	0.033	8.1		201	210
Ethylene-propylene copolymer[l]	298	4.35	122.7	216	0.033	8.1		175	210
Polyurethane[m]	283	8.86	101.6	238	0.028	8.5		205	211
Polyurethane[n]	231	16.7	68.0	221	0.022	3.8		163	212
Methacrylate Polymers									
Methyl (atactic)[o]	381	34.0	80	381	0.013	1.6	4.1	301	82
Methyl (isotactic)	323	8.90	23.0					300	214
Methyl (conventional)[o]	388	32.2	80	388	0.013	1.7	3.6	308	82
	493	7.00	173	378	0.021	3.6		320	219
Ethyl	373	11.18	103.5	335	0.025	3.7	3	270	171
n-Butyl	373	9.70	169.6	300	0.026	2.6	3	203	172
n-Hexyl	373	9.80	234.4	268	0.025	1.9	2–3	139	173
n-Octyl	373	7.60	227.3	253	0.027	2.5	2–3	146	1
2-Ethyl hexyl	373	11.58	208.9	284	0.021	1.8		164	215

Diluted Systems									
Polystyrene in Decalin 62%	291	8.86	101.6					189	216,192
Poly(vinyl acetate) in tricresyl phosphate 50%	293	8.86	101.6					191	217,192
Poly(*n*-butyl methacrylate) in diethyl phthalate 50%	273	9.98	153.1	206	0.024	2.8	3	120	167
Poly(*n*-butyl methacrylate) in diethyl phthalate 60%	273	12.80	157.3	227	0.024	2.2	1	116	167
Cellulose tributyrate in dimethyl phthalate 21%	247	8.86	101.6	188	0.021	4.8	5	145	177a,218
Cellulose tributyrate in dimethyl phthalate 43%	251	8.86	101.6	193	0.019	4.8	4	154	177a,218
Cellulose nitrate in diethyl phthalate 23%	298	8.48	165.5	166	0.016	3.1	4	113	218
Poly(methyl methacrylate) in diethyl phthalate 30%	298	7.11	130.1	211	0.020	4.7	2	168	168

[a] Another assignment ($f_g/B = 0.031$, $\alpha_f/B = 4.4 \times 10^{-4}$) also fits the data and provides a more reasonable value of α_f/B.
[b] From dielectric rather than mechanical data.
[c] Styrene:*n*-hexyl methacrylate = 0.26:0.74 (by mole).
[d] Styrene:*n*-hexyl methacrylate = 0.41:0.59 (by mole).
[e] Cis:trans:vinyl = 43:50:7.
[f] Cis:trans:vinyl = 96:2:2.
[g] Cis:trans:vinyl = 27:37:36.
[h] Cis:trans:vinyl = 7:1.5:91.5.
[i] Styrene:butadiene = 23.5:76.5, random (by weight).
[j] Lightly vulcanized with sulfur.
[k] Ethylene:propylene = 16:84 (by mole).
[l] Ethylene:propylene = 56:44 (by mole).
[m] Copolymer of adipic acid and ethylene and propylene glycols, cross-linked by naphthalene 1,4-diisocyanate and 1,4-butanediol.
[n] Poly(propylene ether) cross-linked by toluene diisocyanate and trimethylol propane.
[o] Two mechanisms with different temperature dependences identified in later study.[213]

In a few cases[38,39] satisfactory agreement has been obtained over a wider distance of time scale by comparing a very high frequency measurement at a high temperature with a transient at long times at a low temperature. However, caution should be exercised in using a reduced viscoelastic function to predict properties at frequencies or times many decades removed from the range of experimental measurements, since small errors in $\Delta \log a_T$ may be cumulative in the process illustrated in Table 11-I. Plazek[40] has shown how creep measurements over a range of three decades of time can be superposed with apparent success to give a composite curve that is nevertheless in error by an order of magnitude when compared with direct measurements extended to five decades.

To interpret a reduced curve such as Fig. 11-3 in terms of actual physical behavior at its extremes can become physically or operationally obscure. Thus, Fig. 11-3 could be used to predict the compliance of poly(*n*-octyl methacrylate) at 120°C at a frequency of 10^{13} Hz. Since this is of the order of molecular vibration frequencies, there is some question whether the calculation would be valid. At the other extreme, the reduced curves of this polymer (curves IV) in Chapter 2 could be used to predict its properties at T_g at a frequency of 5×10^{-9} rad/sec or a time of 2×10^8 sec. This is about six years, and other examples could be cited where the period would transcend historical time. Over long periods, chemical changes may occur. Such questions do not detract, however, from the usefulness of the reduced curve and the accompanying function $a_T(T)$ as an economical expression of data from which the properties can be predicted over wide ranges of temperature and time scale within reasonable limits.

Values of c_1^0 and c_2^0, referred to an arbitrary reference temperature T_0 which is usually somewhere within a temperature range of experimental interest, have been determined for many polymer systems and some are listed in Table 11-II. Values appropriate to any other reference temperature can be obtained from equations 24 and 25.

C. THE WLF EQUATION AND THE RELATION OF TEMPERATURE DEPENDENCE OF RELAXATION TIMES TO FREE VOLUME

Equation 21, sometimes called the WLF equation, was introduced[41,42] as an empirical expression for a general curve $a_T(T)$ in which many different polymers had been reduced to standard states in a manner which will be described below. Its utility has been illustrated in the preceding section; its physical significance will now be examined. First, a digression is necessary to consider the nature of the glass transition in amorphous polymers and supercooled liquids.

1. The Glass Transition and Free Volume

In Chapters 1 and 2, the glass transition was described as the point, or narrow region, on the temperature scale where the thermal expansion coefficient α

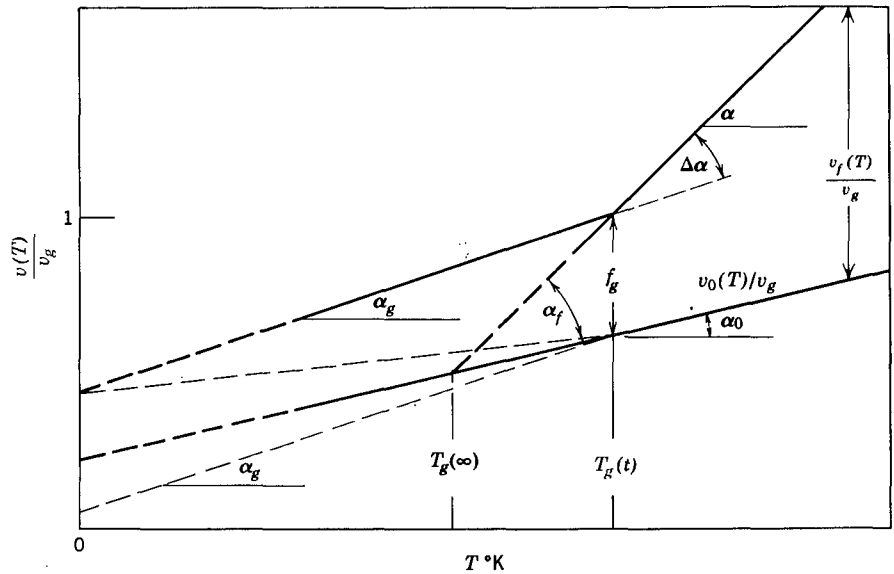


FIG. 11-6. Schematic variation of total specific volume, occupied volume, and free volume (relative to specific volume at T_g) with temperature for a supercooled liquid. (After Kovacs.)[45]

undergoes a discontinuity and below which configurational rearrangements of polymer chain backbones are extremely slow. The most unambiguous definition of it is in terms of the discontinuity in α (which is also accompanied by discontinuities in heat capacity and in compressibility[43,44]). It corresponds to a change in slope in a plot of specific volume against temperature, as illustrated schematically[45] in Fig. 11-6. This phenomenon is characteristic not only of amorphous polymers but of any liquid which can be supercooled to a sufficiently low temperature without crystallizing. Above temperature $T_g(t)$, α has the magnitude α_l characteristic of liquids, of the order of 10^{-3} deg^{-1}; below T_g, it is smaller by a factor of one-half to one-third (α_g). The behavior can be readily understood in terms of a rather vaguely defined concept, the free volume.

Many of the properties of liquids, whether polymeric or not, demonstrate the presence of a substantial proportion of free volume, which may be present as holes of the order of molecular (monomeric) dimensions or smaller voids associated with packing irregularities.[46-48] Although the free volume per gram, v_f, is poorly defined operationally,[49] it is a useful semiquantitative concept. In particular, the thermal expansion coefficient of liquids (whether polymeric or not) represents primarily the creation of additional free volume with rising temperature, whereas the much smaller magnitudes characteristic of crystalline solids and glasses arise from anharmonicity in the dependence of potential energy on interatomic or intermolecular distances.[50]

We picture the total volume per gram, v, as the sum of v_f and an "occupied volume" v_o, which includes not only the volume of the molecules as represented by their van der Waals radii but also the volume associated with vibrational motions.

The occupied volume also increases with temperature, but its magnitude and thermal expansion coefficient α_o, as drawn schematically in Fig. 11-6, remain a matter of conjecture and can be estimated only indirectly. It cannot be identified with the van der Waals covolume. In Fig. 11-6, the specific volumes are normalized by the volume v_g at the glass transition temperature. Thus the fractional free volume, f, a dimensionless number, is v_f/v_g. (Alternatively, f may be defined as v_f/v, which is nearly equivalent since v varies by only a few per cent in a temperature range of interest.)

At temperatures high enough so that Brownian motion is rapid in a polymeric liquid or soft solid, a lowering of temperature is accompanied by collapse of free volume as the molecular adjustments take place within a normal experimental time scale of cooling; this corresponds to Fig. 11-6 above $T_g(\tau)$. At lower temperatures, the adjustments are slower, and if crystallization does not occur first a temperature is reached where the collapse can no longer occur within the experimental cooling times. Then the only residual contraction is of a solidlike character, as in Fig. 11-6 below $T_g(\tau)$. Here, α_g is only a little or possibly no larger than α_o. It should be emphasized that the dimensional changes correspond to bulk compression with no shear, as mentioned in Chapter 8, so that no long-range contour changes of polymeric molecules are involved. The character of the phenomenon is therefore independent of molecular weight, though the magnitude of the free volume may depend somewhat on molecular weight as discussed in Section D. In fact, the same discontinuity in α has long been known in ordinary noncrystallizing the liquids of low molecular weight,[51,52] and the detailed interrelations among volume, temperature, and time for glucose (for example) and polystyrene or poly(vinyl acetate) are closely parallel.[45]

It is inherent in the above discussion that T_g must depend on the time scale of the volumetric measurement. It has in fact been demonstrated[53,54] that a slower measurement pattern leads to a lower value of T_g. The most extensive experiments have been performed by Kovacs.[45,54,55] A sample well equilibrated far above T_g is cooled to a temperature T_1 near T_g and its specific volume v is followed as a function of time. Representative results are shown in Fig. 11-7 for poly(vinyl acetate). Contraction occurs gradually over many hours, and if T_1 is not very far below T_g a stable equilibrium volume $v(\infty)$ is eventually reached. The results here are plotted as $v(t) - v(\infty)$. These data correspond qualitatively to bulk creep experiments; although they do not of course represent contraction under a constant confining pressure, the molecular adjustments responsible for collapse of free volume are similar in nature. The lower the temperature, the longer is the time required to reach voluminal equilibrium. Intercepts of these curves at $t = 0.02$ hr, when expressed as $v(t)$ instead of $v(t) - v(\infty)$, give the upper line at the left in Fig. 11-8; intercepts at $t = 100$ hr give the lower line at the left. The intersections of these two respective lines with the equilibrium volume-temperature line at high temperatures give values of $T_g = 32.5°$ and 24.5° at 0.02 hr and 100 hr respectively. In principle, one can picture a value $T_g(\infty)$ obtained from an experiment of infinite duration, as shown in Fig. 11-6.

Values of T_g of poly(vinyl acetate) quoted in the literature range from 25° to

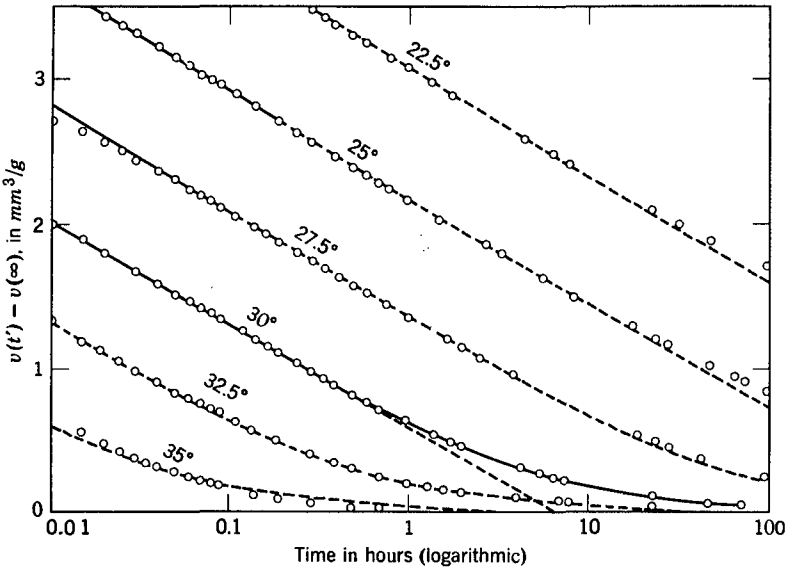


FIG. 11-7. Contraction of poly(vinyl acetate) plotted against logarithm of time after cooling from well above T_g to the temperature indicated. (Kovacs.[55]) Dashed curves represent translations of the curve at 30° along the abscissa axis.

33°. Actually, most T_g values in the literature are based on volumetric measurements with a different experimental pattern, in which the temperature is raised (or lowered) either continuously at a slow rate or intermittently with pauses of the order of an hour between, without strictly controlling the time sequence. Since T_g changes only about 3° with a change in time scale of a factor of 10 (as shown by the application of the WLF equation below), these values are significant within a degree or two, and with this reservation will be used for various derived calculations in the sections to follow. It would be preferable, however, to define T_g in terms of an experimental pattern like that on which Fig. 11-8 is based, with a conventional time interval; Kovacs[45] has recommended 3 min. Moreover, the previous thermal history and possible traces of diluents of low molecular weight—in some cases, moisture—can influence the experimental determination. As a result, values of T_g from different laboratories frequently fail to agree, and the proper value to use for correlation with the temperature dependence of viscoelastic properties is sometimes uncertain.

We now examine more closely the details of the volume contraction as portrayed in Fig. 11-7. The isotherms at different temperatures are closely superposable by horizontal translations just as are those for shear deformation in Fig. 11-1. Moreover, if one particular temperature in the transition region is arbitrarily designated as T_g, the translations of logarithmic time expressed as $\log a_T$ follow equation 21 closely. This result, obtained by Kovacs for several polymers, indicates that the temperature dependences of the molecular processes in bulk compression and in shear deformation are identical. Moreover, it permits calculation of the effect

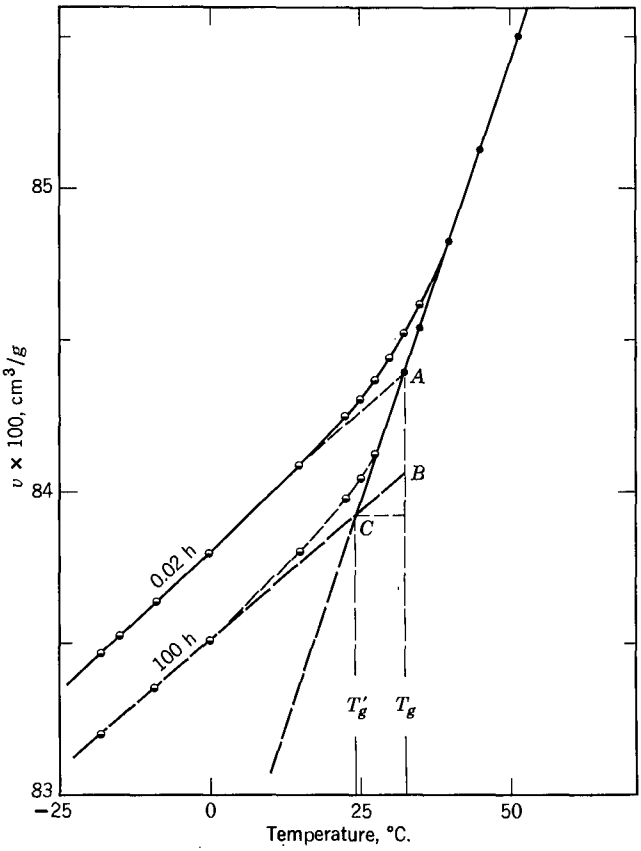


FIG.11-8. Specific volume vs. temperature for poly(vinyl acetate), measured after cooling quickly from well above T_g. Black points, equilibrium values; half black, values measured 0.02 hr and 100 hr, after quenching the sample is indicated. (Kovacs.[55])

of experimental time scale on the apparent glass transition temperature, by differentiating equation 21 at $T_0 = T_g$, and using appropriate values of the constants c_1^g and c_2^g from Section 3 below:

$$dT_g/d \log a_T \cong c_2^g/c_1^g \cong 3° \tag{28}$$

The shapes of the curves in Fig. 11-7 can yield information about the retardation spectrum in bulk deformation, as discussed in Chapter 18. From this analysis it follows, however, that their shapes should not be exactly the same, but that another somewhat more complicated function of volume when plotted against log t should be exactly superposable by horizontal shifts; this is in fact observed.[45]

The glass transition temperature is thus defined in terms of a kinetic process involving *volume contraction,* at an arbitrary but convenient (and not highly critical) time interval. Efforts have often been made to specify the glass transition in terms of a kinetic process involving shear deformation instead—corresponding

to the temperature at which the transition from rubberlike to glasslike consistency as portrayed in Fig. 11-1 reaches a certain stage at an arbitrary time interval; these are so-called softening temperatures, brittle temperatures, Vicat temperatures, etc. They are far more subject to ambiguity because of the more gradual nature of the phenomenon as compared with that of Fig. 11-8, and the difficulty of comparing magnitudes of moduli or compliances in different types of systems. They are not recommended as possessing any significance comparable with that of T_g; it cannot be expected that any kind of transition temperature based on time-dependent mechanical measurements in shear can be substituted for the T_g represented in Figs. 11-6 and 11-8. Only the volumetric transition reflects the temperature below which the collapse of the free volume is very slow, and it is the free volume which determines the rates of relaxation processes, as will become evident below.

It should be mentioned that there are alternative, slightly different free volume concepts, involving the assumption[48,56] that $\alpha_o = 0$, or an unrealistic linear extrapolation of the equilibrium volume below T_g in Fig. 11-6 to the absolute zero;[57] these may lead to larger values of f than are obtained by pursuing the concept of Fig. 11-6 in Section 2 below.

The nature of the glass transition has been extensively discussed from the standpoint of thermodynamics,[44,58] irreversible thermodynamics,[59-62] and statistical mechanics.[63-66] Just as the volume cannot go on decreasing with decreasing temperature at the rate observed above T_g without attaining unrealistically small values, so the entropy cannot go on decreasing at the rate specified by the heat capacity above T_g without becoming negative.[43] Gibbs and DiMarzio[64-66] have predicted on the basis of a lattice model of a polymeric system that the configurational entropy should become zero at a characteristic temperature. The relation of the hypothetical second-order transition temperature to time-dependent and rate phenomena was investigated by Adam and Gibbs,[67] who derived an equation equivalent to equation 21. The entropy[64-69] or enthalpy[70,71] is sometimes considered to be a more basic parameter in determining the features of the glass transition than is the volume. However, these three variables must be closely associated.[60,72,73] Since volume is much more easily measured experimentally than entropy or enthalpy, and is plausibly related to molecular mobility in a simple manner, the following discussion will be restricted to the free volume.

2. Relation of Molecular Mobility to Free Volume

The appearance of the glass transition results from the reduction of molecular mobility as the temperature falls, slowing the collapse of free volume. We now introduce the concept that the mobility at any temperature depends primarily on the free volume remaining, so that the rates of both bulk and shear deformations can be advantageously expressed in terms of v_f rather than T as the independent variable. This principle was applied long ago to the shear viscosity of simple liquids by Batchinski,[74] and more recently by Doolittle[75] with an empirical equation which was found to represent with high accuracy viscosities of ordinary liquids of low

molecular weight:

$$\ln \eta_0 = \ln A + B(v - v_f)/v_f \tag{29}$$

where A and B are empirical constants, the latter of the order of unity.

The physical basis of equation 29 can be understood from the theory of Cohen and Turnbull,[76,77] which treats the self-diffusion of spherical molecules with the assumption that motion of a molecule can occur only when a void exceeding some critical volume v_m^* is available for it to move into. If no energy is required for free volume redistribution at constant volume, a calculation of fluctuations gives a result which is equivalent to expressing the translational friction coefficient ζ as follows:

$$\ln \zeta/kT = \ln \zeta^0/kT + \gamma v_m^*/v_{fm} \tag{30}$$

Here ζ^0 should be proportional to $T^{-1/2}$; γ is a numerical factor between 0.5 and 1, and v_{fm} is the average free volume per molecule. From relations such as equations 44, 51, or 55 of Chapter 10, the viscosity η_0 should have essentially the same temperature dependence as ζ. Hence equations 29 and 30 are equivalent, provided (a) the slight temperature dependence of ζ^0 and the factor $1/T$ can be neglected; (b) $v_m^*/v_{fm} \cong (v - v_f)/v_f$, *i.e.*, the minimum void size is close to the occupied volume per molecule; (c) B and γ are negligibly different from unity, or equal; (d) in the case of polymers, v_m^* and v_{fm} refer to volumes per some kind of segmental unit instead of volumes per molecule. (Other derivations of equations similar in form to equation 29 have been given by Bueche.[78-80])

Equations 29 and 30 imply that free volume is the sole parameter in determining the rate of molecular rearrangements and transport phenomena such as diffusion and viscosity which depend on them. In older theories of liquids,[46,47] the temperature dependence of viscosity is determined by an energy barrier for hole formation. This leads to a viscosity proportional to $\exp(\Delta H_\eta/RT)$, where ΔH_η is the activation energy for flow, independent of temperature—an Arrhenius form. It will be shown in Section 6 that the latter type of temperature dependence is applicable at temperatures very far above T_g; whereas equation 29 is applicable for 100° or so above T_g, and hybrid expressions may also be useful over a more extended range.

To express equation 29 in terms of the shift factor a_T, we employ equation 13, together with the definition $f = v_f/v$, and obtain

$$\log a_T = \frac{B}{2.303}\left(\frac{1}{f} - \frac{1}{f_0}\right) + \log (T_0\rho_0/T\rho) \tag{31}$$

where f_0 is the fractional free volume at an arbitrary reference temperature T_0. In practice, this equation is almost always used without the last term:

$$\log a_T = \frac{B}{2.303}\left(\frac{1}{f} - \frac{1}{f_0}\right) \tag{32}$$

This procedure amounts to either neglecting the slow temperature variation of $T\rho$ or else expressing equation 29 in terms of $\ln \tau_i$ instead of $\ln \eta_0$ with the recognition

that the numerical value of the constant B may differ very slightly. Equation 32 is the basis of the WLF equation.

3. The WLF Equation

It may be assumed that f increases linearly with temperature in accordance with the relation

$$f = f_0 + \alpha_f(T - T_0) \tag{33}$$

(If $f = v_f/v_g$, this means a linear dependence of v on temperature, which is not quite the same as constant α because the latter ($\alpha = (1/v)(dv/dT)$) implies an exponential dependence of v. Because of the small magnitude of α, however, these discrepancies are usually ignored; they are discussed further in references 35 and 77. A modification in which f is taken as a linear function of $T^{3/2}$ instead of T has been introduced by Litt.[81]) Substitution of equation 33 in equation 32 gives

$$\log a_T = -\frac{(B/2.303f_0)(T - T_0)}{f_0/\alpha_f + T - T_0} \tag{34}$$

which is identical in form with the WLF equation, equation 21. Identification of the constants specifies that

$$c_1^0 = B/2.303f_0 \tag{35}$$

$$c_2^0 = f_0/\alpha_f \tag{36}$$

$$f_0 = B/2.303c_1^0 \tag{37}$$

$$\alpha_f = B/2.303c_1^0c_2^0 \tag{38}$$

The foregoing equations apply to any arbitrary reference temperature T_0. Of particular interest, however, is the use of T_g as the reference temperature, with the reservation of course that the latter depends somewhat on the experimental time scale. Equation 38 is unchanged since it is valid for any reference temperature, as may be shown by combining equations 24 and 25. Equation 37 becomes

$$f_g = B/2.303c_1^g \tag{39}$$

where c_1^g is obtained from c_1^0 by analogs of equations 24 and 25.

To obtain f_g and α_f from equations 38 and 39, some further assumption is necessary.[82-84] One possibility is to assume that $\alpha_f = \Delta\alpha$ (*i.e.*, that the lines for glass volume and occupied volume are parallel in Fig. 11-6); then the experimentally determined $\Delta\alpha$ is substituted into equation 38 to obtain the unknown numerical constant B. Another possibility is to assume that $\alpha_o = 0$ so that $\alpha_f = \alpha_l$ in Fig. 11-6 and to obtain B in the same manner. Calculations of this sort[82] yield values of B of the order of 0.9 ± 0.3 for different polymers from the first method and 1.6 ± 0.6 from the second. By combining temperature and pressure dependence (Section D1), Fillers and Tschoegl[106] deduced values of B of the order of 0.2 to 0.6 for several polymers. However, for the sake of simplicity, B has usually been set arbitrarily equal to unity. This implies that α_f is more nearly equal to $\Delta\alpha$ than to α_l.

Values of f_g/B and α_f/B, which on the latter basis may be identified simply with f_g and α_f, are included in Table 11-II, together with $\Delta\alpha$ and the characteristic temperature T_∞ of equation 26. Since the data are all for polymers with reasonably high molecular weight, the dependence of T_g on molecular weight when the latter is low (mentioned in Section D) is avoided. For the great majority of systems, $f_g = 0.025 \pm 0.005$. The view that the free volume at the glass transition temperature should be a constant was first introduced by Fox and Flory.[85] The magnitude is reasonable, but no precise significance can be attached to it because the concept of v_f as originally introduced remains operationally undefined. Nevertheless, fractional free volumes thus calculated from the dependence of relaxation times on temperature are consistent with those calculated independently from a free-volume analysis of dependence of relaxation times on pressure (Section D) and dilution with solvent (Chapter 17), and this consistency reinforces the utility of f in equation 32. It should be noted that f_g as calculated from equation 39 depends on the time scale of the experiment in which T_g was determined, and the values in the table refer to the usual scale—unspecified, but probably of the order of an hour. If the time scale were varied sufficiently to lower T_g by 8° (the extreme shown in Fig. 11-8), f_g would be reduced from 0.025 to 0.022. Other concepts of free volume may lead to somewhat larger numerical values[86] but these are irrelevant to the treatment here.

The values of α_f show considerably more variation. However, it is perhaps the most convincing success of the free-volume interpretation that α_f does turn out to be the correct magnitude for a thermal expansion coefficient. In fact, it is in most cases rather close to $\Delta\alpha$, which also varies somewhat depending on chemical structure. Certain polymers whose shear viscoelastic behavior reveals distinct contributions from chain backbone and side chain motions (Section F below) tend to have low values of both α_f and $\Delta\alpha$. Such polymers sometimes exhibit additional changes in slope of plots of volume against temperature below the primary glass transition. The variation in α_f, and especially the occasional unexpected appearance of $\alpha_f < \Delta\alpha$, may be attributed to values of B other than unity. The variation of B, in turn, may be associated through equation 30 with differences in the minimum hole size required for local segmental motions.

It should be remarked that α_f and f_g are quite sensitive to the graphical fitting of experimental a_T data as described in the preceding section, and some degree of uncertainty can be expected from this source. For practical purposes, this feature in reverse is an advantage: to predict the function a_T for a new polymer which has not been subjected to detailed experimental measurements, reasonable values of f_g and α_f can be assumed and the prediction will be relatively insensitive to the choice. Only T_g needs to be known for this purpose.

In the first application of the WLF equation,[42] average values of c_1^g and c_2^g were obtained by fitting data on a large number of polymers, and estimated to be 17.44 and 51.6 respectively. It is evident that the actual variation from one polymer to another is too great to permit use of these "universal" values except as a last resort in the absence of other specific data. In a somewhat better approximation,[42] fixed

values of $c_1^s = 8.86$ and $c_2^s = 101.6$ were used in conjunction with a reference temperature T_s, which was allowed to be an adjustable parameter but generally fell about 50° above T_g, as follows:

$$\log a_T = -8.86(T - T_s)/(101.6 + T - T_s) \tag{40}$$

This procedure has been widely used, and composite data for many different polymers[40,42] are described by equation 40 with the single adjustable parameter T_s. However, if possible, it is better to determine specific values of c_1^0 and c_2^0 or c_1^0 and T_∞. Conversion from one reference temperature to another can always be accomplished by equations 24 and 25.

The characteristic temperature T_∞ of equation 26 appears in an empirical equation for viscosity introduced by Fulcher[87] and Tammann and Hesse:[88]

$$\log \eta_0 = A' + B'/(T - T_\infty) \tag{41}$$

(This has sometimes erroneously been called the Vogel equation, but the relation introduced by Vogel,[34] which also includes a temperature T_∞ at which the viscosity becomes infinite, has a different form. The well-established designation of T_∞ as the Vogel temperature seems appropriate although the equation should be attributed to the other authors.[214]) If the slight differences between the temperature dependences of η_0 and τ_i are ignored (*cf.* equations 31 and 32), the WLF coefficients are related to the parameters of equation 41 as follows:[45]

$$c_1^0 = B'(T_0 - T_\infty) \tag{42}$$

$$c_2^0 = T_0 - T_\infty \tag{43}$$

The formal prediction of equation 41 that η_0 and τ_i become infinite at T_∞ is of no concern since, like the WLF equation, the Fulcher equation holds only above T_g. The relation of B' to internal stiffness of the polymer chain has been discussed by Miller.[89,90]

4. Modification of the WLF Equation with an Energy Term

In theories of the temperature dependence of viscosity which yield an Arrhenius form, with a linear dependence of ln η_0 on $\Delta H_\eta/RT$, the parameter ΔH_η is interpreted as an activation energy for an elementary flow process. From the WLF equation, an apparent activation energy for viscoelastic relaxation can be calculated formally as

$$\begin{aligned}\Delta H_a &= R\, d \ln a_T/d(1/T) \\ &= 2.303Rc_1^0c_2^0T^2/(c_2^0 + T - T_0)^2\end{aligned} \tag{44}$$

This quantity, instead of being temperature independent as reaction-rate theory would predict, increases rapidly with decreasing temperature and a T_g attains the value $2.303Rc_1^gT_g^2/c_2^g = BRT_g^2\alpha_f/f_g^2$. Thus it is independent of chemical structure except as reflected by T_g itself and minor variations in f_g and α_f. It is of the order

of 62 kcal if $T_g = 200°K$ and 250 kcal if $T_g = 400°K$. That the temperature dependence of relaxation processes is indeed independent of chemical structure is evident from the applicability of the WLF equation not only to a variety of polymers in Table 11-II but also to organic liquids of low molecular weight[42,73] and inorganic glasses.[73,91] (For the latter, the values of f_g are close to those obtained for polymeric and other organic glasses; the values of α_f are often rather small, of the order of 1×10^{-4} deg^{-1}, but agree rather well with $\Delta\alpha$ as measured macroscopically.)

On the other hand, at high temperatures equation 44 reduces to

$$\Delta H_a = 2.303 R c_1^0 c_2^0 \cong 4.1 \text{ kcal} \tag{45}$$

Thus the Arrhenius type of temperature dependence applies, but here the prediction that ΔH_a is the same for all systems irrespective of molecular constitution is certainly incorrect. Among liquids far above their freezing (or vitrification) points, where the proportion of free volume is far higher (perhaps 0.3 instead of 0.03) the apparent activation energies vary widely and can be correlated with chemical structure.[49] We must expect, then, the WLF equation to become inapplicable at high temperatures and the temperature dependence of relaxation processes to be governed by more specific features.

Extensions of the WLF equation to include a parameter with Arrheniuslike temperature dependence, characteristic of chemical structure, have been developed in several different ways.[82,92-94] All are essentially equivalent to the form

$$\ln \eta_0 = \text{const} + E^*/RT + B''/(T - T_\infty) \tag{46}$$

in which B'' is controlled by the expansion coefficient of free volume in the manner of the Cohen-Turnbull derivation and E^* is an activation energy which must be surmounted in addition to the requirement of a minimum hole size for molecular rearrangement. A better description of temperature dependence of viscosity (and, by implication, viscoelastic relaxation) can be obtained in this way over a wide temperature range. However, the addition of another adjustable parameter provides some latitude in the assignment of numerical values. Since the temperature dependence is partially attributed to the E^* term even at low temperatures, the result is that the role of free volume is less and larger values of the fractional free volume f are deduced. Specifically,[95,96] with T_g as a reference temperature, equation 34 becomes

$$c_1^g = (B + B_E)/2.303 f_g \tag{47}$$

where

$$B_E = (c_2^g/T_g)(E^* f/RT) \tag{48}$$

The contribution of B_E increases with increasing temperature, but over a range 100° above T_g, with typical values for the parameters, taking $E^* = 10$ kcal/mole, it does not exceed 10%. The values of f_g and α_f calculated from the experimentally determined c_1^g and c_2^g are increased by this amount. At higher temperatures, of course, the E^* term in equation 46 becomes dominant.

D. FREE-VOLUME INTERPRETATION OF THE DEPENDENCE OF RELAXATION TIMES ON PRESSURE AND OTHER VARIABLES

It is well known that under static confining pressure the viscosities of ordinary liquids are increased.[97] The same effect is observed for the steady flow viscosity of polymers[98,99] and for viscoelastic relaxation times,[100,101] though the latter have been usually studied in bulk deformation or bulk longitudinal deformation rather than in shear. Qualitatively this behavior can be understood in terms of the dependence of segmental mobility on the fractional free volume, since the free volume must decrease with increasing pressure just as it does with decreasing temperature. Quantitative relations analogous to equations 32 and 34 can be readily derived, not only for pressure dependence[102,103] but also for dependence on certain other variables that affect the free volume.

1. Pressure Dependence of Relaxation Times

Equation 31 can be generalized[102] to give the ratio a_{12} of a particular relaxation time τ_i in state 2 to that in state 1, in terms of the free volumes f_1 and f_2 in these states:

$$\log a_{12} = \frac{B}{2.303}\left(\frac{1}{f_2} - \frac{1}{f_1}\right) \tag{49}$$

If states 1 and 2 refer to atmospheric pressure P_0 and a higher pressure P respectively, we have (at constant temperature)

$$\log a_P = \frac{B}{2.303}\left(\frac{1}{f_P} - \frac{1}{f_0}\right) \tag{50}$$

With increasing pressure, only the total volume decrease can be measured experimentally; it is presumably the sum of the free volume collapse and a diminution of the occupied volume of the molecules. The presence of substantial free volume in ordinary liquids makes them more compressible than ordinary solids; for example, the compressibility coefficients β, or $-(1/v)(\partial v/\partial P)_T$, for liquid and solid benzene are about 9 and 3×10^{-11} cm^2/dyne respectively. Similarly, for polystyrene[104] 100° above T_g, β is about 9×10^{-11} cm^2/dyne and 80° below T_g it is 3×10^{-11}. These figures refer to low pressures, of the order of a few atmospheres. Unlike the change of volume with temperature, the change with pressure is markedly nonlinear, as illustrated[104] in Fig. 11-9. In the pressure range of thousands of atmospheres, the compressibility of polystyrene 100° above T_g falls to a value which is characteristic of the glassy state at low pressures. Qualitatively, it would indeed be expected that the compression of both the free volume and the occupied volume would become progressively more difficult. The compressibility of the free volume, defined as $\beta_f = -(1/v)(\partial v_f/\partial P)_T \cong -(\partial f/\partial P)_T$, is presumably, like the total compressibility β, a decreasing function of P.

Within the limited pressure range where β_f can be considered constant, the

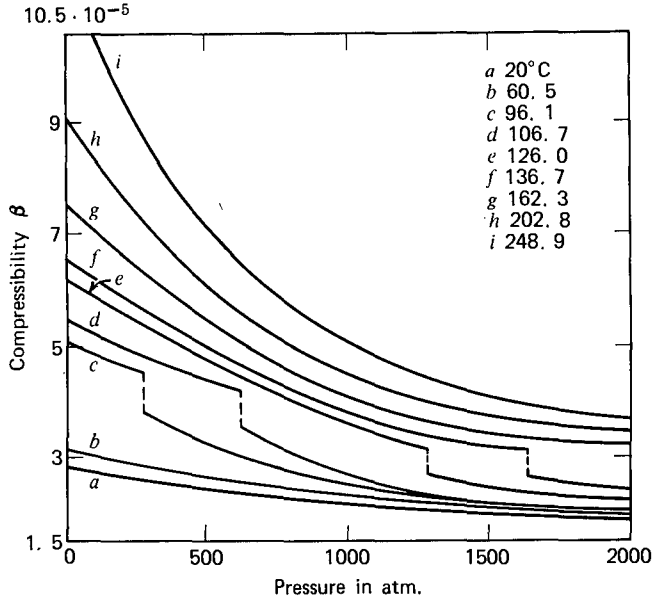


FIG. 11-9. Compressibility in atm^{-1} plotted against pressure in atm for polystyrene at several different temperatures as indicated. (Hellwege, Knappe, and Lehmann.)[104]

change in f with P can be written as

$$f_P = f_0 - \beta_f(P - P_0) \tag{51}$$

and substitution into equation 48 yields[102]

$$\log a_P = \frac{(B/2.303f_0)(P - P_0)}{f_0/\beta_f - (P - P_0)} \tag{52}$$

Analysis of data following procedures analogous to the use of equations 22, 23, 37, and 38 can provide values for f_0 and β_f (if B is set equal to unity). This has been done successfully for the pressure dependence of viscosities of some ordinary liquids[102] and of bulk relaxation times of polyvinyl acetate.[100] For the latter, the value of f_0 at a particular reference temperature found from pressure dependence is consistent with that found from temperature dependence. In all cases, β_f is less than half of β, so the major portion of the volume change in compression is due to reduction of the occupied volume—in contrast to thermal expansion, where the major portion (often about two-thirds) is due to increase in the free volume. The compressibility β_f is presumably closely similar to the difference $\Delta\beta$ between the total compressibilities just above and just below T_g. This identification is subject to an important reservation, however, as described in Section 2 below.

At vanishing pressure, equation 52 reduces to

$$(\partial \log a_P/dP)_T = B\beta_f/2.303f_0^2 \tag{53}$$

It is clear that the effect of confining pressure on relaxation times will diminish

rapidly with increasing temperature above T_g because of the factor f_0^2 in the denominator of equation 53. If the temperature is high enough so that $f_0 > 0.11$ or 0.12, it may be expected that equation 50 and others derived from it may become inapplicable, just as the WLF equation does far above T_g where other features than free volume affect the rates of molecular motions.

At higher pressures, the nonlinear dependence of free volume on pressure, inferred from the behavior of the total volume as illustrated in Fig. 11-9, can be taken into account in several ways.[103,105-107] If the pressure dependence of the free volume is represented by the following equation[96]

$$f_P = \Pi f_0/(P - P_0 + \Pi) \tag{54}$$

where Π is an empirical constant, a particularly simple result is obtained by substitution into equation 50:

$$\log a_P = (B/2.303)(P - P_0)\Pi f_0 \tag{55}$$

so the nonlinear dependence of f actually produces a linear dependence of $\log a_P$ on pressure, as has sometimes been observed experimentally.[99,108] A better agreement with experiment over a wide range of pressures and temperatures is obtained by expressing the nonlinear pressure dependence of f in a different way, introduced by Fillers and Tschoegl;[106] the bulk modulus $K(P, T)$ is taken as a linear function of pressure:

$$K(P, T) = K^0(T) + kP \tag{56}$$

and the bulk modulus of the occupied volume $K_\phi(P, T)$ has a pressure dependence of the same form. The compressibility $\beta_f(P, T)$ is obtained as $1/K - 1/K_\phi$, and is integrated from the reference pressure P_0 to P to obtain the decrease in f with increasing pressure. The final expression for the shift factor is

$$\log a_{T,P} = \frac{(B/2.303f_0)[T - T_0 - \Theta(P)]}{f_0/\alpha_f(P) + T - T_0 - \Theta(P)} \tag{57}$$

where $\Theta(P)$ is a rather complicated function of K^0, k, K_ϕ^0, and k_ϕ; all the parameters can be determined from experimental measurements.

The shift factor a_P can be used to combine time-dependent or frequency-dependent data measured at different pressures, exactly as a_T is used for different temperatures in Section A above, and with a shift factor $a_{T,P}$ data at different temperatures and pressures can be combined. It is necessary to take into account the pressure dependence of the limiting values of the specific viscoelastic function at high and low frequencies, of course, in an analogous manner to the use of a temperature-dependent J_g and the factor $T\rho/T_0\rho_0$ in equations 19 and 20. The pressure dependence of dynamic shear measurements has been analyzed in this way by Zosel[109] and Tokiura.[108] A very comprehensive study of stress relaxation in simple elongation, with the results converted to the shear relaxation modulus, of several polymers was made by Fillers and Tschoegl.[106] An example of measurements on Hypalon 40 (a chlorosulfonated polyethylene lightly filled with 4% carbon black) at pressures from 1 to 4600 bars and a constant temperature of 25°C

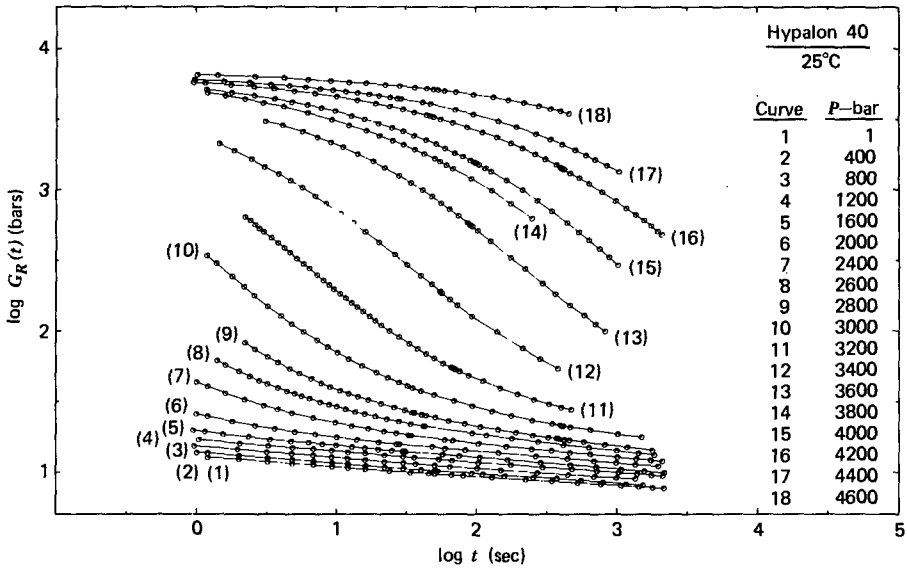


FIG.11-10. Logarithmic plot of shear relaxation modulus against time at 25°C and various pressures from 1 to 4600 bars as indicated, for a chlorosulfonated polyethylene. (Fillers and Tschoegl.[106]) Reproduced, by permission from The Transactions of The Society of Rheology.

is shown in Fig. 11-10. A pattern exactly analogous to that of Fig. 11-1 is seen; the polymer is rubbery at low pressures (shear modulus of the order of 10^7 dynes/cm^2 or 10^6 Pa) over the time scale covered, is a hard glass at high pressures (modulus about 6×10^9 dynes/cm^2), and at intermediate pressures $G(t)$ goes through the transition zone as a function of time. These data together with others at different temperatures are combined by reduced variables in Fig. 11-11, which shows also in a three-dimensional inset the forms of temperature and pressure dependence of the shift factor $a_{T,P}$. The treatment is very successful; the slight divergence of the isobaric and isothermal curves at short reduced times is expected because of the difference in specification of the glassy state.

The pressure dependence of viscoelastic relaxation times is of considerable practical importance because of the hydrostatic pressures encountered in various extrusion and molding processes.[109a]

2. Interrelation of Effects of Temperature and Pressure on Relaxation Times

Although the effect of combined temperature and pressure changes on the shift factor $a_{T,P}$ is complicated if the nonlinear pressure dependence of f is taken into account, as seen in equation 57, a simple formulation is obtained in the linear range where β_f is constant; the difference between f_2 and f_1 in equation 49 is given by

$$f_2 = f_1 + \alpha_f(T - T_0) - \beta_f(P - P_0) \tag{58}$$

If the free volume is maintained constant by appropriately increasing both T and

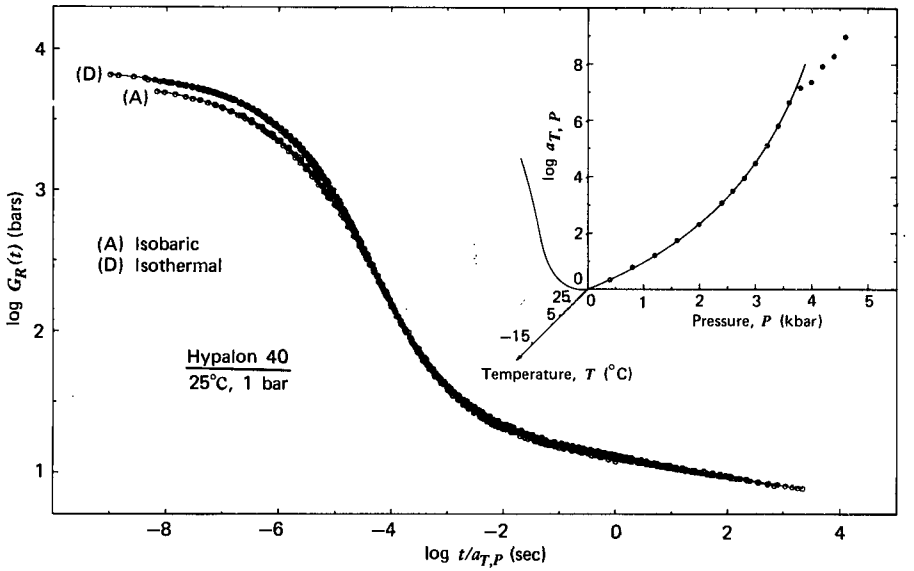


FIG. 11-11. Data of Fig. 11-10 (isothermal) and others at different temperatures down to −15°C (isobaric) reduced to 25°C and 1 bar by shift factors $a_{T,P}$ whose magnitudes are indicated in the three-dimensional insert. (Fillers and Tschoegl.[106]) Reproduced by permission from the Transactions of The Society of Rheology.

P, a_{12} should remain unity with no change in relaxation times; differentiation of equation 58 with $f_2 = f_1$ gives for this condition

$$(\partial T/\partial P)_\tau = (\partial T/\partial P)_f = \beta_f/\alpha_f \qquad (59)$$

Values of $(\partial T/\partial P)_\tau$ have been determined for a number of polymers[96-100] from bulk viscoelasticity measurements (Chapter 18) or dielectric or nuclear magnetic resonance measurements (Section E below). They are listed in Table 11-III. The magnitude of this derivative is generally 0.020 ± 0.005 deg/atm. From equation 59 and the observation in Table 11-II that α_f is generally near 5×10^{-4} deg^{-1} (within a factor of 2), it may be concluded that β_f is of the order of 1×10^{-5} atm^{-1} or 1×10^{-11} cm^2/dyne, though substantial differences from one polymer to another may be expected.

It is plausible to identify β_f with the difference between the compressibilities just above and just below T_g, namely, $\Delta\beta = \beta_l - \beta_g$. However, the definition of β_g for this purpose must be made with caution, because of the failure of voluminal equilibrium in the glassy state as illustrated in Figs. 11-7 and 11-8. The difficulty is demonstrated[96,114,115] in Fig. 11-10.

Here the volume-temperature lines of pressure P_0 intersect at the conventional glass transition T_g. If the liquid at v_1 is compressed, the volume decreases to v_2, lower by an amount equal to $v_0\beta_l(P - P_0)$, where β_l is the liquid compressibility. (The initial factor will be written as v_0 in all these expressions, representing the magnitude of v near T_g, since all these volumes differ only very slightly; and we

Table 11-III

TEMPERATURE-PRESSURE SHIFT RATIOS

Polymer	$(\partial T/\partial P)_\tau$, deg/atm	Method	Ref.
Poly(vinyl chloride)	0.017	Dynamic shear deformation	109
Poly(methyl methacrylate)	0.024	Dynamic shear deformation	109
Polyisobutylene	0.025	Longitudinal bulk wave propagation	101
Natural rubber[a]	0.024	Dynamic bulk deformation	110
Poly(vinyl acetate)	0.020	Dynamic bulk deformation	100
Poly(vinyl acetate)	0.022	Dielectric dispersion	105
Poly(vinyl chloride)	0.017	Dielectric dispersion[b]	111
Poly(methyl acrylate)	0.015–0.022[c]	Dielectric dispersion	112
Poly(propylene oxide)	0.014–0.017[c]	Dielectric dispersion	113
Hypalon 40[d]	0.019	Stress relaxation	106

[a] Lightly cross-linked with sulfur.
[b] Primary dispersion.
[c] Depends on frequency range.
[d] Chlorosulfonated polyethylene (*cf.* Fig. 11-11).

restrict the discussion to moderately low pressures where the compressibility is constant.) If the liquid is then cooled, the volume follows the lines to v_5; this is lower than the corresponding point v_3 at P_0 by an amount equal to $v_0\beta'_g(P - P_0)$ whereby β'_g is defined. On the other hand, if we start from v_3 and compress the glass, the volume decreases to a value v_4, lower by an amount $v_0\beta''_g(P - P_0)$, where β''_g is the actual compressibility of the glass obtained in a normal isothermal measurement. It has been observed[115,116] that $\beta''_g < \beta'_g$. When the sample is warmed at constant pressure, the volume must eventually reach v_2, but first it follows a line approximately parallel to the glass line through v_5.

In applying equation 59, data are used above the glass transition temperature, where voluminal equilibrium is maintained. Hence in identifying β_f with $\beta_l - \beta_g$, the glass compressibility must be taken as that defined by $\beta'_g = (1/v_0)(v_3 - v_5)/(P - P_0)$, and not that which would be measured by a conventional compression of the glass, $\beta''_g = (1/v_0)(v_3 - v_4)/(P - P_0)$.

It may be noted in Fig. 11-12 that determination of the glass transition temperature by the usual intersection of volume-temperature lines for glass and liquid can give two different values at pressure P, namely T'_g if the glass line through v_5 is followed, or T''_g if the glass line through v_4 is followed. Hence the elevation of T_g under pressure can have two alternative values. From the geometry of the figure (neglecting second-order effects arising from the fact that the lines at the two pressures are not exactly parallel either above or below T_g), it can be shown[96] that

$$\frac{T'_g - T_g}{P - P_0} = \frac{\beta_l - \beta'_g}{\alpha_l - \alpha_g} \tag{60}$$

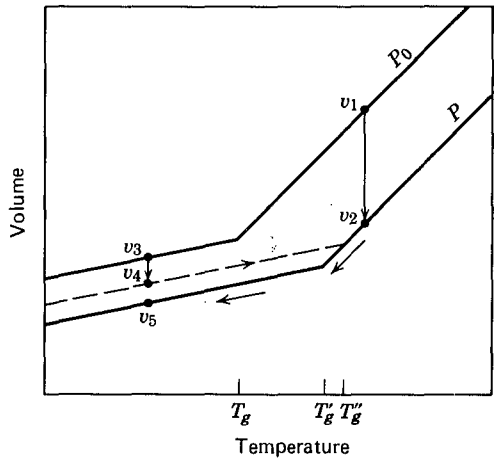


FIG. 11-12. Schematic representation of volume-temperature-pressure relations near the glass transition with different sequences of changes of temperature and pressure. (After Kovacs.)[114]

whereas

$$\frac{T_g'' - T_g}{P - P_0} = \frac{\beta_l - \beta_g''}{\alpha_l - \alpha_g} \tag{61}$$

where α_l and α_g are, as in Fig. 11-6, the normalized slopes of the volume-temperature lines above and below the transition. Thus for *either* type of experiment we have in the limit of small changes of T and P

$$dT_g/dP = \Delta\beta/\Delta\alpha \tag{62}$$

provided T_g and β_g are defined consistently. A T_g under pressure obtained by the route $v_1 \rightarrow v_2 \rightarrow v_5$ cannot be used in the same equation with a glass compressibility determined by the route $v_3 \rightarrow v_4$.

Equation 62 has been derived by irreversible thermodynamics[58,59] with certain assumptions about the number of parameters required to define the state. The reservations in its applicability have been discussed thoroughly by Gee[117] and Bianchi.[118] If the glass transition itself is regarded as controlled by relaxation processes whose rates are constant at constant f, then combination of equations 62 and 59 evidently specifies that $\beta_f/\alpha_f = \Delta\beta/\Delta\alpha$. However, a critical analysis shows that rates depend on both f (which is a function of both temperature and time) and T in a complicated manner.[60-62]

The derivation of equation 59 corresponds to the statement that the temperature (or pressure) dependence of relaxation times at constant free volume is zero; *i.e.*,

$$(\partial \log a_T/\partial T)_f = 0 \tag{63}$$

That is not true at constant *total* volume, however. If the pressure and temperature are increased to keep v constant, the fractional free volume increases, because β_f

is a smaller fraction of β than α_f is of α, as noted in Section D1. The same conclusion can be drawn[96] from the observed fact that the volume v_g at T_g decreases with increasing pressure.[100,111,116] The dependence of f on T at constant total volume is given by[96]

$$(\partial f(T, P)/\partial T)_v = \alpha_f - \alpha\beta_f/\beta \equiv \alpha_v > 0 \tag{64}$$

and the temperature dependence of relaxation times under this condition by an analog of equation 34:

$$\log (a_T)_v = -\frac{(B/2.303f_0)(T - T_0)}{f_0/\alpha_v + T - T_0} \tag{65}$$

Such a decrease in $\log a_T$ with increasing T at constant volume has been observed experimentally.[99,111]

3. Changes in Relaxation Times during Isothermal Contraction near the Glass Transition

Perhaps the most direct observation of the relation between relaxation times and free volume, as expressed in its most general form by equation 49, is obtained from viscoelastic[119-121] (or viscosity[122] or dielectric[95,123]) measurements repeated over a period of time during the spontaneous contraction of a glassy sample that occurs after quenching it to a temperature near or below T_g, as portrayed in Fig. 11-7. As the volume decreases, the relaxation times increase. Since the contraction takes place at constant temperature and pressure, the change in a_T can be entirely attributed to collapse of free volume as a function of elapsed time. Moreover, since the occupied volume should remain constant at constant T and P, experimental measurements of the decrease in v provide the decrease in v_f directly. Thus, during such an isothermal contraction at temperature T, the fractional free volume at time t is

$$f_2(T, t) = f_1(T_0, \infty) + \alpha_f(T - T_0) + [\{v(t) - v_\infty\}/v_\infty]_T \tag{66}$$

where f_1 is the equilibrium value of f at a reference temperature T_0, and $v(t)$ and v_∞ are the specific volumes, at temperature T, at time t and at equilibrium respectively. Substitution into equation 49 gives $\log a_{T,t}$ for various temperatures and elapsed times. Values calculated in this manner have been rather successful in reducing dynamic shear data from experiments of this sort on poly(vinyl acetate)[119] and poly(*n*-butyl methacrylate).[120] However, some change in shape of the relaxation spectrum with temperature was detected. Experiments of this type are discussed more fully in Chapter 18.

4. Effects of Molecular Weight and Other Variables on Free Volume and Relaxation Times

Although this chapter is concerned primarily with effects of temperature and pressure, it is convenient to mention here the effects of some other variables on

relaxation times which seem also to be controlled by the free volume—molecular weight, dilution with solvent (plasticizer), and static tensile strain.

It has already been mentioned in Chapter 10 that the friction coefficient ζ_0 governing the viscoelastic relaxation times increases with molecular weight but approaches a constant limiting value ζ_{00} at high molecular weight (where it must be taken as applying only to the shorter relaxation times corresponding to motions between entanglement points), as illustrated in Fig. 10–1. It was shown long ago by Fox and Flory[85] that the specific volume of a polymer is a linear function of $1/\overline{M}_n$, and they proposed that the free volume should follow the same relation, accounting for an additional free volume at low molecular weights associated with imperfect packing around the ends of the molecules. Thus, at constant temperature (equation 15 of Chapter 10)

$$f_M = f_0 + A/\overline{M}_n \tag{67}$$

where f_0 refers to the fractional free volume at infinite molecular weight and A/ρ is the additional molar free volume associated with a mole of pairs of molecular ends. For nonuniform molecular weight, $\overline{M}_n$ is the proper average because its reciprocal is proportional to the number of chain ends. The analog of equation 49 in this situation is equation 14 of Chapter 10,

$$\log \zeta_0 = \log \zeta_{00} + (B/2.303)(1/f_M - 1/f_0) \tag{68}$$

Since a_{12} is a ratio of relaxation times, the relaxation times are proportional to $a^2\zeta_0/T$ (equation 4 of Chapter 10), and in a comparison of different molecular weights a^2 and T are constant. Substitution of equation 67 into equation 68 gives the molecular weight dependence of ζ_0 at constant temperature.

It follows from this treatment that the magnitude of the temperature derivative of ζ_0 is smaller for very low molecular weights than for high (when compared at the same temperature), and that the molecular weight average which controls this effect is $\overline{M}_n$. Thus, for example, the apparent activation energy for viscoelastic relaxation at a temperature T_0 can be expressed by combining equations 35, 56, and 44:

$$\Delta H_a = BRT_0^2\alpha_f/f_M^2 \tag{69}$$

The increase in f_M with decreasing $\overline{M}_n$ according to equation 66 will diminish ΔH_a. These aspects were recognized at an early date by Fox and Flory.[85]

The application of equations 67 and 68 to blends of samples of the same polymer with widely different molecular weights or broad molecular weight distributions depends on the hypothesis that the free volumes of the different species are additive in their volume fractions. A rather good confirmation of these equations was obtained from shear creep measurements by Ninomiya, Ferry, and Ōyanagi on a series of poly(vinyl acetate) fractions and their blends.[21,124] First, f_0 was determined from the temperature dependence of a_T for a sample of very high molecular weight and equation 34 (with $B = 1$). Then f_M was evaluated for each sample and blend from equation 68 and experimental data in the transition zone which provided $\log \zeta_{00} - \log \zeta_0$; it was found to be always consistent with equation 34 and the temperature

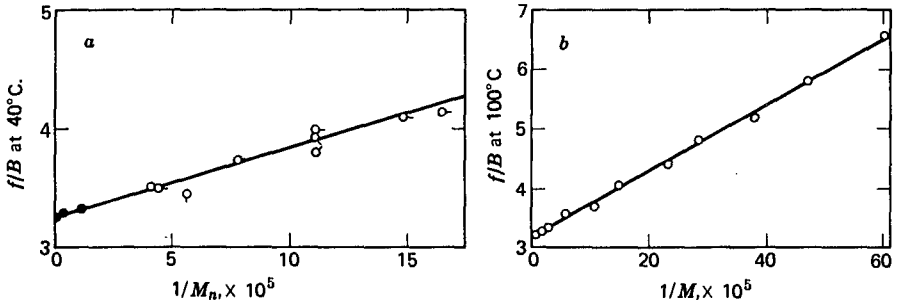


FIG.11-13. Fractional free volume plotted against $1/\overline{M}_n$ at constant temperature, (*a*) Polyvinyl acetate fractions (black circles) and blends (open circles), recalculated from data of Ninomiya, Ferry, and Ōyanagi.[21] (*b*) Polystyrenes with sharp molecular weight distribution, from Pierson and Kovacs.[36]

dependence of a_T for the individual sample. Finally, f_M so obtained was found for blends to be quite close to the values calculated from additivity of the free volumes of the blend components, and f_M was also a linear function of $1/\overline{M}_n$ as specified by equation 67. The latter plot is shown in Fig. 11-13 (corrected for an error in the original calculations). The constant A was about 52 g/mole at 40°C.

In connection with this study of poly(vinyl acetate), it should be pointed out that later work by D. J. Plazek (private communication) gives somewhat larger values of ζ_0, suggesting the presence of a trace of water in the samples studied by Ninomiya, Ferry, and Ōyanagi. However, the relative values of ζ_0 as a function of $\bar{M}_n$ are probably satisfactory.

In a similar analysis of the temperature dependence of viscosity for a series of polystyrenes of sharp molecular weight distribution and a wide range of molecular weights, Pierson and Kovacs[36] obtained f_0/B from equation 34 for each sample and found it to be a linear function of $1/M$ in accordance with equation 67. This plot is also included in Fig. 11-13. The constant A was about 54 g/mole at 0°C. Comparison of these constants with the molecular weight of a dimer (172 for poly(vinyl acetate), 208 for polystyrene) indicates that the additional free volume associated with a pair of molecular ends is about 30% of the total volume associated with two monomer units.

The molecular weight dependence of the viscosity for $M < M_C$ can also serve as a test of equations 67 and 68 after separating out the additional proportionality to M as given by equation 44 of Chapter 10 (*cf.* Fig. 10-11). Data of Allen and Fox[125] on polystyrenes of sharp molecular weight distribution and binary blends of such samples showed that the molecular weight dependence of η_0/M corresponded to free-volume differences as described by equations 67 and 68; specifically, in blends with constant $\overline{M}_n$ but varying $\overline{M}_w$, $\eta_0/\overline{M}_w$ was constant.

At very low molecular weights, f_g/B and α_f/B are found[36] to increase and decrease slightly, respectively, with increasing M. The total thermal expansion coefficient also decreases[126,172] with increasing M, and is a linear function of $1/M$. Although f_g/B is slightly dependent on molecular weight, as a first approximation

the glass transition temperature corresponds to a fixed value of f_g, and therefore T_g decreases substantially with decreasing M; it is also approximately a linear function[85,126] of $1/\overline{M}_n$. The effect of M on the friction coefficient can alternatively be discussed in terms of a depression of T_g at low molecular weights.[128,129] However, at very low molecular weights, T_g appears to correspond more nearly to a fixed viscosity than to a fixed fractional free volume when different molecular weights are compared.[36]

Free volume also plays an important role in the effects of two other variables on relaxation times. When diluent (*i.e.*, solvent or plastizer) is added to an undiluted polymer, the relaxation times decrease rapidly. The magnitude of the effect can be successfully interpreted in terms of additional free volume introduced with the diluent molecules, as will be discussed in Chapter 17. Finally, under static tensile strain, viscoelastic relaxation times in hard glasslike polymers are decreased. This effect can be attributed to a free-volume increase accompanying the total volume increase which occurs because Poisson's ratio is less than $\frac{1}{2}$ (Chapter 1, equation 50); it will be discussed in Chapter 18.

E. REDUCED VARIABLES AND FREE-VOLUME PARAMETERS FROM OTHER THAN VISCOELASTIC MEASUREMENTS

There are other physical measurements which reflect molecular mobility and can be related to relaxation times and friction coefficients similar to those which characterize the rates of viscoelastic relaxations. Although such phenomena are outside the scope of this book, they are mentioned here because in some cases their dependence on temperature and other variables can be described by reduced variables; and, by means of equation 49 or modifications of it, free volume parameters can be deduced which are closely related to those obtained from viscoelastic data. These include measurements of dispersion of the dielectric constant, nuclear magnetic resonance relaxation, diffusion of small molecules through polymers, and diffusion-controlled aspects of crystallization and polymerization.

1. Dielectric Dispersion

Some data related to free volume parameters, obtained from dielectric dispersion experiments rather than mechanical measurements, have already been quoted in Tables 11-II and 11-III. The complex dielectric constant bears certain formal analogies to the complex compliance, and the frequency dependence of its real and imaginary components is determined for some polymers by molecular motions similar to those which determine the rate of response to mechanical stresses. Depending on the location of the dipoles which respond to alternating electrical potential and their degree of coupling to the configurational motions of the polymer chain backbone, there will be varying degrees of correlation between dynamic electrical and mechanical properties.[130-132] In numerous cases, there are two or

more clearly separated regions on the frequency scale where the frequency dependence of the dielectric constant corresponds to different types of motions (backbone configurational changes and side group rotations, for example).

For some polymers and polymer solutions the temperature and frequency dependence of the components of the dielectric constant can be analyzed by reduced variables to determine a function b_T analogous to the shift factor a_T of Sections A and B.[41,112,113,131,133-136] When the temperature dependence of b_T follows equation 21, especially if the coefficients are the same or nearly so as those derived from mechanical measurements on the same polymer, it may be concluded that the dipole response involves backbone configurational changes controlled by the same ζ_0 which enters the theories of Chapter 10 and equation 3 of this chapter. In other cases b_T appears to follow the Arrhenius equation with a rather low activation energy, and in still others the form of the frequency dependence changes so rapidly with temperature that the method of reduced variables is inapplicable.[132,134,137,138]

The dispersion of the dielectric constant has been rather extensively used to study the pressure dependence of relaxation processes and the derivative $(\partial T/\partial P)_\tau$ as in Table 11-III, because it is so much easier to make dielectric measurements than mechanical measurements under high confining pressures.[111-113,139,140]

2. Nuclear Magnetic Resonance Relaxation

The spin-lattice relaxation time T_1 in nuclear magnetic resonance, measured for amorphous polymers as a function of temperature, typically passes through a minimum at a temperature well above T_g where the thermal motions most effectively transfer energy from oriented nuclear spins to the molecular environment. This transfer depends on components of molecular thermal motion in a frequency range corresponding to the resonant frequency imposed on the nuclei by the magnetic field employed. Ordinarily, the latter frequency is constant in a series of experiments; but in one study of natural rubber[141] it was varied from 2 to 60 MHz, and the temperature corresponding to the minimum in T_1 varied concomitantly from above $-7°$ to 30°C. Within experimental error, the relation between temperature and frequency followed the WLF equation with the "universal" values of c_1^g and c_2^g, indicating that even at these very high frequencies the rates of the relevant molecular motions are controlled by the temperature through the free volume as described in Section C above.

The combined effects of temperature and pressure on nuclear magnetic relaxation have been studied to obtain the derivative $(\partial T/\partial P)_{T_1}$ from spin-lattice relaxation time measurements as well as $\partial T/\partial P$ at constant line width in the region of line narrowing.[152] Even at a single frequency, the determination can be made at various temperatures. The spin-lattice measurement corresponds to frequencies of the order of 10^8 Hz; the spin-spin or line width measurement, of 10^4 Hz. The lower the temperature, the more short range is the character of the motions reflected at a given frequency; and the numerical values for $(\partial T/\partial P)_{T_1}$ appear to decrease with decreasing temperature for natural rubber, *cis*-polybutadiene, and other poly-

mers.[143] They are, however, all of similar magnitude to those appearing in Table 11-III from mechanical and dielectric relaxation measurements.

3. Diffusion of Small Molecules in Polymers

The translatory diffusion of a small molecule through an essentially undiluted polymer is opposed by a frictional resistance of force per unit velocity which has the same units as the monomeric friction coefficient of a polymer segment ζ_0 appearing in equation 3, and arises from similar molecular characteristics—*i.e.*, the time-dependent configurational changes of the polymer—especially if the small molecule has a molecular weight of 100 or more; these remarks might not apply to diffusion of a very small molecule such as hydrogen or argon. In the general case of a concentration gradient, the definition and calculation of the diffusion coefficient D may be rather complicated.[144,145] However, there are three situations in which the measurement corresponds closely to self-diffusion of the small molecule (penetrant) in the absence of a concentration gradient: measurements with a radioactive tracer at constant total penetrant concentration;[146,147] measurements with a radioactive tracer in trace amounts;[147,148] and spin-echo measurements of nuclear magnetic resonance.[149,150] Then the diffusion coefficient of the penetrant may be expressed as

$$D_1 = kT/\zeta_1 \tag{70}$$

where ζ_1 is the translational friction coefficient of a penetrant molecule moving through its average environment.

Whereas equations 3 and 32 together are essentially equivalent to writing

$$\log \zeta_0 = \text{const} + B/2.303f \tag{71}$$

Fujita[144,151] has proposed for diffusion a relation essentially equivalent to

$$\log \zeta_1 = \text{const} + B_d/2.303f \tag{72}$$

in which B_d may be different from B in recognition of the possibility that the minimal void size (in the sense of the Turnbull-Cohen theory) may not be the same in relation to the size of the moving unit for the types of motion represented by ζ_0 and ζ_1. The ratio B_d/B can be determined from temperature-dependence measurements of diffusion and mechanical properties in two ways. If the temperature range is sufficient to apply the WLF equation in the form of equation 21 and its counterpart for diffusion,[148]

$$\log (DT_0/D_0T) = c_1^D(T - T_0)/(c_2^D + T - T_0) \tag{73}$$

where D and D_0 are the diffusion coefficients at T and T_0, then $B_d/B = c_1^D/c_1^0$. Alternatively, if the temperature range is so narrow that only an apparent activation energy can be obtained as given by equation 44 and its analog ΔH_D for diffusion, then $B_d/B = \Delta H_D/\Delta H_a$.

From measurements of the diffusion of radioactively tagged n-hexadecane through various polymers (above T_g) and polymer solutions,[147,148,152] values of

B_d/B ranging from 0.6 to 1.0 have been obtained. From a more complicated analysis involving dependence on concentration as well as temperature, Fujita and Kishimoto[153] have found values of B_d/B for many systems to be generally somewhat less than unity; these studies will be described in Chapter 17. With this provision, the free-volume interpretation of temperature dependence of diffusion appears to be quite satisfactory and offers an alternative method for analyzing the rates of molecular motions.

A close analogy to the role of free volume in affecting diffusion of a small foreign molecule through its influence on the molecular mobility of a polymer is found in studies of ionic conductance in polymers.[154] A more indirect manifestation of the relation between molecular mobility and free volume is seen in the experiments of Gordon and Simpson[155] on the rate of three-dimensional polymerization in the preparation of densely cross-linked polymers, which appears to be diffusion controlled. The rate, as measured by the increase in T_g during the polymerization process, depends on the temperature of polymerization in a manner which can be described by the WLF equation. Also, the relation between molecular mobility and free volume is involved in the theory of rates of crystallization and spherulite growth in polymeric systems.[156–160]

F. EXAMPLES OF MORE LIMITED APPLICABILITY OF THE METHOD OF REDUCED VARIABLES

The method of reduced variables as outlined in Section B above, including fitting the function $a_T(T)$ to the WLF equation, is appropriate for data in the transition, plateau, and terminal zones of time scale, with the provision that all contributions to the measured viscoelastic properties involve the same friction coefficient ζ_0 and moreover that the internal structure of the system does not change with changing temperature. The latter restrictions are inherent in the development of Section A. In glassy and crystalline polymers, and in situations where two or more different classes of molecular motions with different temperature dependences are involved, some modifications in the treatment are necessary.

1. Glassy and Highly Crystalline Polymers

Below T_g, although long-range configurational changes take place exceedingly slowly, more rapid viscoelastic responses exist which are attributed to a variety of local backbone and side chain motions and cover a very wide spectrum of relaxation times, as illustrated by curves V of Chapter 2. Such motions can certainly not be described in terms of a monomeric friction coefficient. However, if it is assumed that all the relaxation times concerned with a particular type of motion have the same temperature dependence, reduced variables can be applied to the glassy zone in the region where the response is dominated by this motion as a separate calculation. The curves in Chapter 2 alluded to were in fact obtained in this way from data on poly(methyl methacrylate) by Iwayanagi,[161] who combined various viscoelastic measurements.

Because the time and frequency dependences in the glassy state are relatively small, the vertical shift on a logarithmic plot associated with the temperature dependence of the magnitudes of the viscoelastic mechanisms, as in Fig. 11-2, is a much more important feature of the reduction than in the transition zone where the horizontal shift associated with the time scale dominates. Whereas, in the transition zone, the vertical logarithmic shift of moduli by log $T_0\rho_0/T\rho$ can be inferred from theory as in Section A above, in the glassy state there is no *a priori* source of information. As mentioned in Section A6, the temperature dependence has the opposite sign—contributions to modulus decrease in magnitude with increasing temperature; it can be estimated from the temperature dependence of the storage modulus at very high frequencies where the frequency dependence is slight.[26,27,162] This problem has been discussed thoroughly by McCrum and Morris,[163] who showed that creep data for glassy poly(methyl methacrylate), in a range of time and temperature where the so-called β mechanism dominates, could be satisfactorily treated in this manner. The temperature dependence of a_T followed an equation of the Arrhenius form, with an apparent activation energy ΔH_a independent of temperature and relatively small in magnitude (17 kcal). If the vertical shift is not taken into account, a somewhat larger value of ΔH_a is obtained. In general, however, the same values of a_T would not be expected to apply to the entire relaxation spectrum in the glassy state, because of the variety of molecular motions. Those associated with rotations of side groups may have very low activation energies.[164]

In highly crystalline polymers, also, there are different mechanisms with different temperature dependences some of which can be attributed, for example, to uncoordinated motions within the crystal lattice and to deformation of amorphous regions between crystal lamellae.[165] The contributions to elastic modulus diminish with increasing temperature as in glasses, with the added complication that the temperature dependence is expected to be highly anisotropic for a single crystal and the macroscopic properties represent an average of a compound system. With extensive precise data,[166] it is possible to analyze separate contributions with different temperature dependences and determine their individual activation energies.

2. Multiple Viscoelastic Mechanisms with Different Temperature Dependences

It has already been noted in Section A5 that the temperature reduction factors in the transition and terminal zones may be somewhat different. An example of a very complete study by Plazek[25] on a polystyrene with almost uniform molecular weight 46,900 is shown in Fig. 11-14. The creep compliance $J_p(t)$ reduced to a reference temperature of 100° by shift factors a_T calculated from the viscosity—*i.e.*, from equation 13—provides satisfactory superposition of data in the terminal zone, but in the transition zone the reduced data diverge. Alternatively, the recoverable compliance $J_p(t) - t/\eta_0$ can be satisfactorily reduced in the transition zone with a slightly different set of reduction factors; these, however, appear to give a slight divergence in the terminal zone (Fig. 11-15). Both sets of shift factors follow the WLF equation, equation 21, but with slightly different coefficients: in Fig. 11-14,

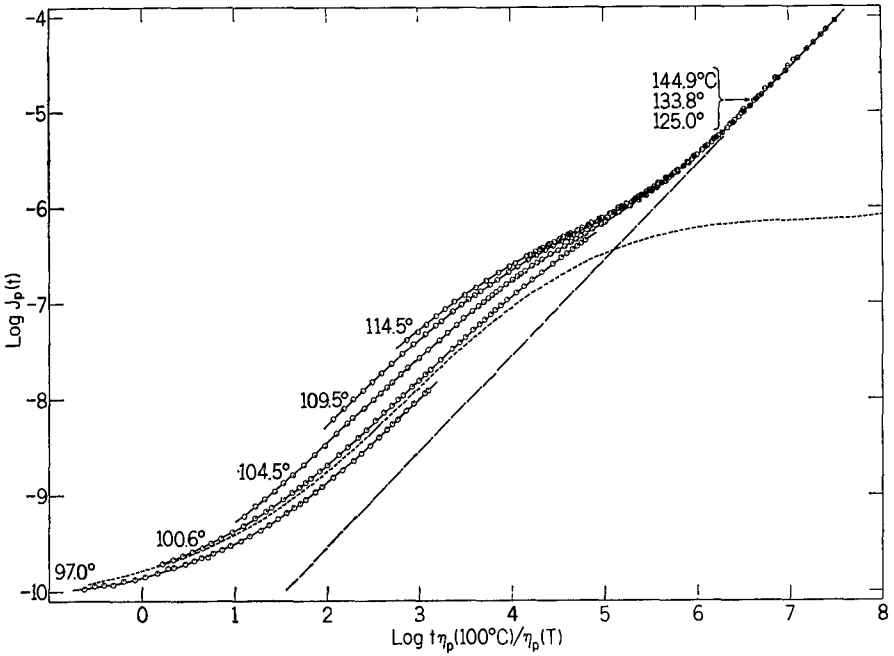


FIG. 11-14. Creep measurements on a polystyrene with molecular weight 46,900, reduced from different temperatures as indicated to 100°C with shift factors calculated from steady flow viscosity. (After Plazek.[25]) Subscript p denotes multiplication by $T\rho/T_0\rho_0$.

$c_1^0 = 12.7$ and $c_2^0 = 19.8$; in Fig. 11-15, $c_1^0 = 10.7$ and $c_2^0 = 29.9$. Near T_g, the differences in a_T are substantial and correspond to Vogel temperatures T_∞ which can differ as much as 30°, that for the viscosity being lower;[26] however, above T_g + 30°, or in the presence of small amounts of diluent, the differences disappear. The assignment in Table 11-II is based on viscosity. Similar behavior has been found for other polystyrenes[40] and poly(vinyl acetate).[27]

An exaggerated form of the deviations illustrated for polystyrene, but in the opposite direction, has been observed in some methacrylate polymers and their solutions.[24,28,167,168] When dynamic data are reduced with a_T values derived from the transition zone, they fail to superpose in the plateau and terminal zone, as exemplified for solutions of poly(*n*-butyl methacrylate)[167] by plots of J'' in Fig. 11-16. With increasing temperature, the maximum in J'' shifts upward and to the left.

This maximum is associated with the presence of a network (Fig. 10-7; also Fig. 2-7), which in this case is due to entanglement coupling (Chapter 10, Section C) rather than permanent cross-links. But since entanglement slippage should be slight in this zone, the behavior of permanently cross-linked networks can be used as a guide to the effect of the degree of coupling on J''_{max}. The Mooney theory and its modifications (Fig. 10-7 and associated discussion) predict that J''_{max} should be proportional to P_c and its location on the frequency scale inversely proportional to P_c^2, where P_c is the degree of polymerization between linkage points. The magnitudes and time constants associated with all individual contributions to the re-

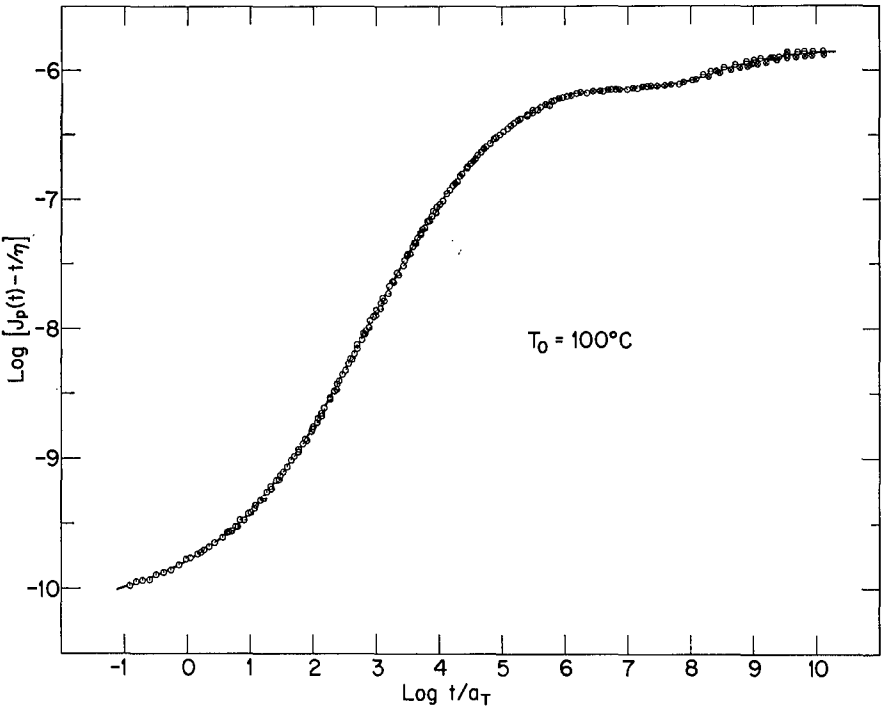


FIG. 11-15. Recoverable creep compliance from data of Fig. 11-14 reduced to 100° by shift factors chosen empirically in the transition zone and fitted to equation 21. (The small rise to the right of 8 on the abscissa scale is attributed to a very small proportion of species of much higher molecular weight.)

tardation spectrum are affected in the same manner, provided the distribution of strand lengths between linkage points remains unaltered in form. Hence if, with a change in temperature from T_0 to T, the number of network strands per cc n_c is changed by a factor $\mathfrak{f}$ (P_c correspondingly changing by $1/\mathfrak{f}$), the magnitude of the complex compliance J^* changes by $1/\mathfrak{f}$ and its position on the frequency scale by $\mathfrak{f}^2$.

It follows that an additional reduction of the data can be made to take into account the effect of temperature on network spacing as well as the local friction coefficient by plotting log $J_p''\mathfrak{f}$ against log $\omega a_T/\mathfrak{f}^2$. The data of Fig. 11-16 are shown reduced in this manner in Fig. 11-17, using $\mathfrak{f}$ values which fit an equation of the Arrhenius or van't Hoff form with $\Delta H = 2.1$ kcal/mole. The quantity ΔH is not an activation energy. It can be formally interpreted as a heat of dissociation of coupling points, but its molecular significance is not clear. The reduction is quite successful in providing single composite curves; similar results, with similar low values of ΔH, have been obtained for several undiluted methacrylate polymers.[28]

The $\mathfrak{f}$ shift is in the direction of a slope of $-\frac{1}{2}$ on a logarithmic plot of J' or J'' against frequency, and hence its effect disappears in the transition zone where the

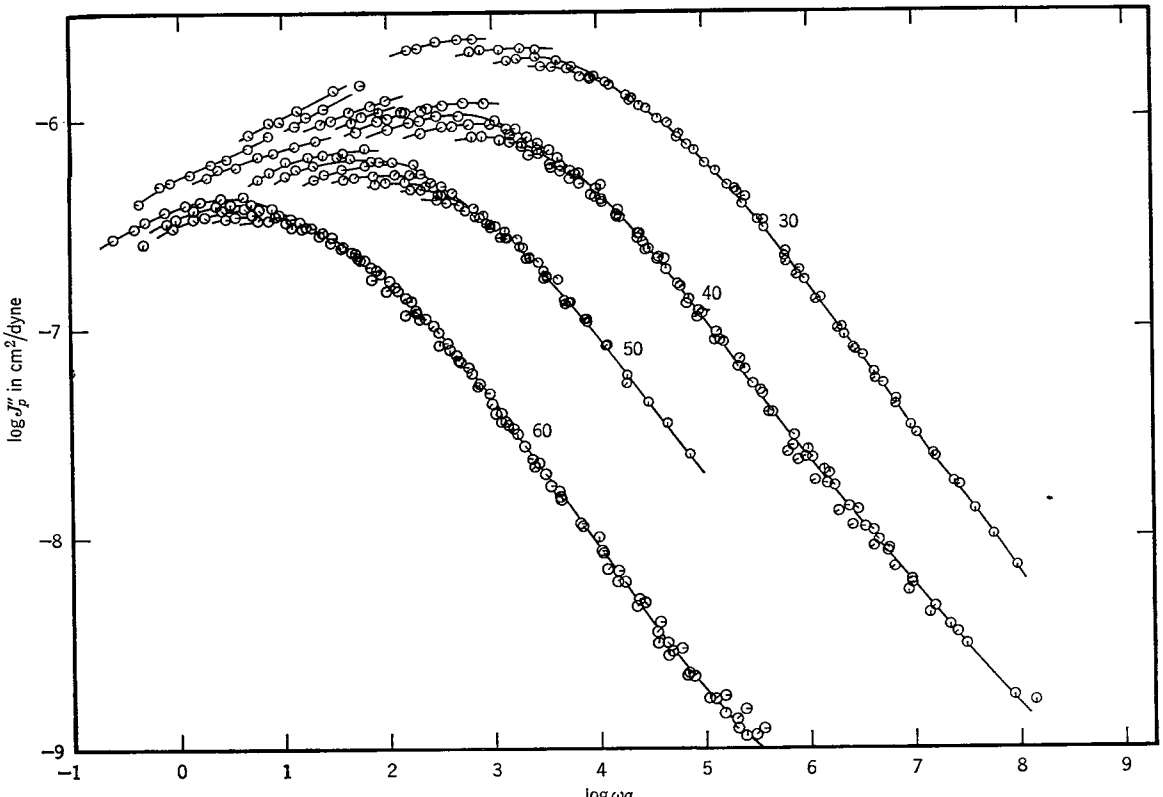


FIG. 11-16. Loss compliance of four solutions of poly(*n*-butyl methacrylate)[167] in the plateau zone, reduced to a reference temperature of 0°C by a_T factors derived from data in the transition zone and fitted to equation 21. Numbers denote concentrations in weight percent.

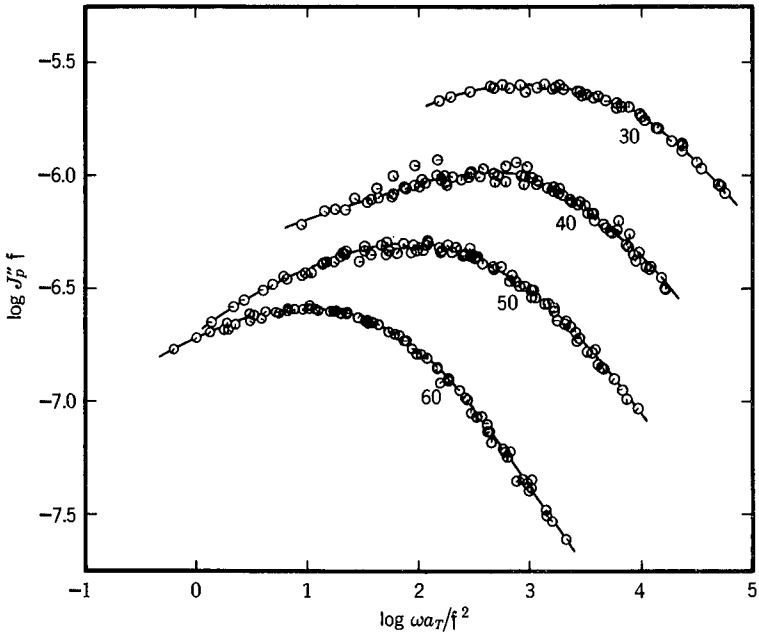


FIG.11-17. Data of Fig. 11-16 reduced for the effect of temperature on entanglement coupling spacing, as measured by $\mathfrak{f}$, in addition to its effect on the local friction coefficient, as measured by a_T.

slopes of these functions themselves approach the value of $-\frac{1}{2}$ predicted by the Rouse and Bueche theories. Indeed, at high frequencies the viscoelastic response is governed by short-range configurational motions which should be oblivious of the entanglement spacing. The storage modulus J' is never sharply affected by this entanglement anomaly because it never has a positive slope. The anomaly is most apparent on the left side of the maximum in J'' where the $\mathfrak{f}$ shift has a slope of opposite sign to that of the loss compliance.

If P_e, or M_e, or M_C increases with increasing temperature, the factor Q_e must decrease in accordance with equation 48 of Chapter 10, and it follows from equation 47 of Chapter 10 that the temperature dependence of the viscosity will be exaggerated, combining the effects of temperature on ζ_0 and Q_e; a similar conclusion would be reached from equations 51 or 55 of Chapter 10. Quantitative agreement has been obtained on this basis for temperature dependence of the viscosity.[24]

It is possible that such prominent effects of temperature on the apparent entanglement spacing appear only when the topological features of entanglement are supplemented by some local attraction associated, for example, with tactic ordering in methacrylate polymers.[169,170] Such restraints may be termed hyperentanglements.

Anomalies in the application of reduced variables have also been observed in the neighborhood of the glassy zone, especially for several methacrylate polymers,[171-173] and have been interpreted by assuming that the complex compliance

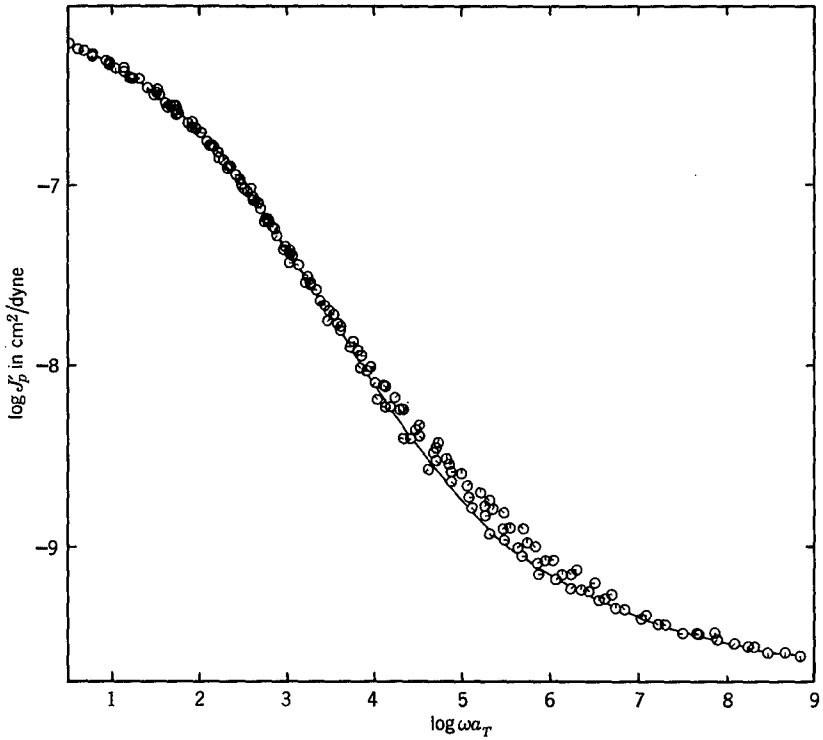


FIG. 11-18. Composite curve for the storage compliance of poly(*n*-butyl methacrylate),[172] with a_T factors derived from data in the transition zone.

is the sum of two contributions whose relaxation times have different temperature dependences: backbone motions which dominate in the transition zone, and side chain motions which dominate as the glassy zone is appraoched with increasing frequency.

For example, in data on poly(*n*-butyl methacrylate)[172] it was observed that the criteria for reduced variables as outlined in Section B were fulfilled over a temperature range from 45° to 135°C except for some deviations between 55° and 80°. The range of agreement was ample to specify the coefficients c_1^0 and c_2^0 of equation 21, and from the latter a_T was calculated for all temperatures. The resulting reduced plot of J' is shown in Fig. 11-18, revealing a marked anomaly in the points derived from temperatures between 55° and 80°. It was then assumed that the observed compliance is the sum of a contribution J'_α from backbone motions, whose relaxation times follow the WLF equation, and another J'_β from side chain motions (whose maximum value is far smaller than that of J_α, so it becomes obscured at low reduced frequencies where J'_α is large), and that J'_α could be approximated by the lower envelope of the observed points. By subtraction (not of the logarithms as plotted, of course, but of the actual values) point by point, J'_β was obtained at various temperatures and frequencies and subjected to a *separate* reduction treatment. The reduced plot of J'_β is shown in Fig. 11-19; the temperature dependence of log $a_{T\beta}$ follows the Arrhenius form with $\Delta H_a = 24$ kcal.

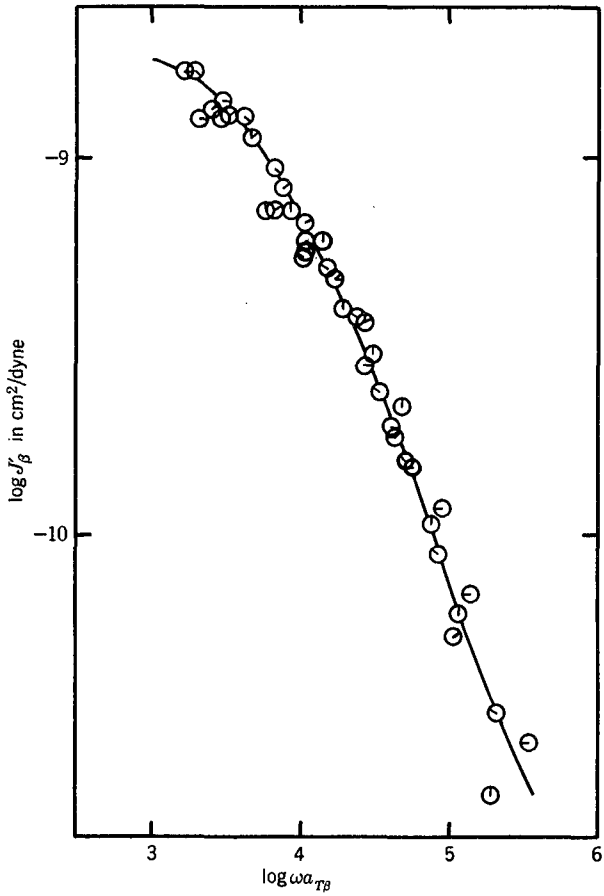


FIG. 11-19. Composite curve for the storage compliance of the β mechanism of poly(n-butyl methacrylate),[172] attributed to motions of the side chains.

This differential treatment pushes the accuracy of the data to its limits, but the results are supported by the conclusion of Hoff[174] from other mechanical and dielectric measurements that there are multiple classes of relaxation times in methacrylates, and that in the n-butyl polymer the mechanisms here denoted by α and β (following his terminology) are merged somewhat above T_g. Moreover, dielectric measurements by Strella,[134] which reflect dipole orientation due to side group motions, show the same temperature dependence of relaxation times with $\Delta H_a = 24$ kcal.

Contributions from the α mechanism shift much more rapidly along the frequency scale with temperature than do the contributions from the β mechanism. For the α mechanism, ΔH_a is of course a function of temperature in accordance with equation 44, but at 80°C it is 42 kcal and at 55° 52 kcal, in contrast with the considerably lower figure for the β mechanism. At high temperatures, therefore, the α mechanism overtakes the β and obscures it. Only where the two mechanisms make contributions of comparable magnitude to J' is the reduction anomaly evident.

The exact nature of the side chain motions which cause the viscoelastic response called the β mechanism is still somewhat obscure.

Multiple mechanisms also appear in polyphase systems such as block copolymers or physical blends of different polymers in which there are domains of different chemical composition with specific morphologies depending on the method of preparation. A general method for applying time-temperature superposition to such systems, involving additivity of the compliances of the phase and the existence of a phase interlayer with different mechanical properties, has been developed by Fesko and Tschoegl.[175] Master curves with reduced variables covering a wide range of time or frequency scale can be constructed, but the shape depends markedly on the reference temperature.

3. Changes in Internal Structure due to Crystallinity

In a polymer, such as polyethylene, that is capable of a high degree of crystallinity, the internal structure changes markedly with decreasing temperature from the melting point down to a temperature where the crystallinity approaches its maximum value. In this range the method of reduced variables is wholly inapplicable, as emphasized by Tobolsky.[176] Empirically, it may appear that horizontal shifts combined with rather large vertical shifts on logarithmic plots might achieve a single composite curve from a family of curves for a given viscoelastic function, but theoretical guides for performing such a manipulation are rather tenuous.

A similar situation may occur in a polymer with side groups long enough to crystallize, as in poly(*n*-dodecyl methacrylate)[177] where the method of reduced variables is applicable in its normal form down to $-28°$ but at lower temperatures large deviations appear. These have been attributed to crystallization of the side groups. In some polymer gels,[177a,178] also, the degree of cross-linking changes progressively with temperature, and the method of reduced variables cannot be employed without substantial modification.

The above examples illustrate how failures of the method of reduced variables, when applied in its simple form, serve as clues to additional information about the systems treated. They represent characteristic symptoms which may guide in the interpretation of other anomalies that may be observed in the future.

For practical purposes, temperature dependence in systems that for any reason do not conform to the simple treatment with reduced variables can be represented by two-dimensional contour (isotimic) plots of temperature against frequency or time with curves for constant G', G'', and so forth.[178a]

G. TREATMENT OF DATA AT FIXED FREQUENCY OR TIME AND VARYING TEMPERATURE

Critical application of the method of reduced variables requires a series of isotherms as in Fig. 11-1, each covering a wide enough range of frequency or time

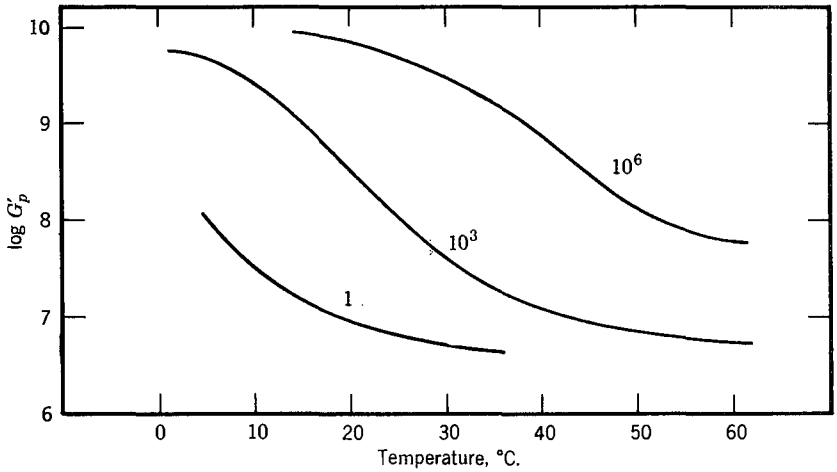


FIG. 11-20. Storage shear modulus of a 40% gel of polyvinyl chloride in dimethyl thianthrene plotted against temperature at three frequencies as indicated in radians/sec (data of Fitzgerald and Ferry.)[179]

to specify the shape of the experimental viscoelastic function. In some experimental methods, it is easier to vary the temperature than the frequency, so that data are available instead as isochrones plotted against the temperature at a few selected frequencies, as shown (calculated) for a poly(vinylchloride) gel[179] in Fig. 11-20. Such curves are *not* superposable by horizontal shifts along the temperature axis; their shapes are quite different, because of the nonlinear temperature dependence of a_T. For example, the slopes drawn at log $G' = 8$ in the figure are obviously different for the three isochrones. Such slopes depend on both the steepness of $G'(\omega)$ at the particular frequency and the steepness of $a_T(T)$ at the particular temperature, in accordance with the equation

$$(\partial \log G'/\partial T)_\omega = (\partial \log G'/\partial \log \omega a_T)_T (\partial \log \omega a_T/\partial T)_\omega \qquad (74)$$

Failure to recognize this feature has led to some erroneous conclusions about the applicability of the method of reduced variables.

From a single isochrone, neither the temperature dependence of a_T nor any of the basic viscoelastic functions can be determined. However, if $a_T(T)$ is known from another source (*e.g.*, dielectric measurements under circumstances where a judicious identification can be made) or if a reasonable assumption of its form can be made, the isochrone can be transformed to an effective isotherm[180] simply by plotting against ωa_T, and the other viscoelastic functions can be obtained by the methods of Chapter 4. In particular, in the transition zone, $a_T(T)$ can be estimated from the WLF equation in one or another of its forms provided T_g is known.

In certain other experimental methods, notably those involving resonance vi-

brations (Chapter 7), both temperature and frequency vary simultaneously in a sequence of measurements, and it is even more difficult to obtain basic information. However, such results are useful for exploratory studies, especially in identifying multiple viscoelastic mechanisms.[131]

An interesting treatment has been proposed by Hopkins[181] in which the temperature is changed according to a prescribed function of time *during* a transient viscoelastic experiment (creep or stress relaxation). By comparing the results, $J(t)$ or $G(t)$, with those obtained in a second experiment under conventional isothermal conditions, the factor a_T can be calculated over the temperature range concerned.[182] In another modification, termed "thermally stimulated creep," a strain is imposed, the temperature is suddenly lowered, and the stress is removed; with subsequent temperature increase at a constant rate, the creep recovery is followed.[183]

H. APPLICATION OF REDUCED VARIABLES TO BULK AND NONLINEAR VISCOELASTIC PROPERTIES

The preceding sections have dealt almost solely with linear viscoelastic behavior in shear or in simple extension which for soft materials is essentially determined by shear deformation characteristics. However, the use of reduced variables in describing temperature and pressure dependence of viscoelastic properties has considerably wider applicability.

1. Bulk (Volume) Viscoelasticity

The inclusion of values in Table 11-III derived from dynamic bulk viscoelastic measurements implies the concept that the relaxation times describing time-dependent volume changes also depend on the fractional free volume—consistent with the picture of the glass transition outlined in Section C. In fact, the measurements of dynamic storage and loss bulk compliance of poly(vinyl acetate)[100] shown in Fig. 2-9 are reduced from data at different temperatures and pressures using shift factors calculated from free volume parameters obtained from shear measurements, so it may be concluded that the local molecular motions needed to accomplish volume collapse depend on the magnitude of the free volume in the same manner as the motions which accomplish shear displacements. Moreover, it was pointed out in connection with Fig. 11-7 that the isothermal contraction following a quench to a temperature near or below T_g has a temperature dependence which can be described by reduced variables with shift factors a_T identical with those for shear viscoelastic behavior.[45] These features will be discussed more fully in Chapter 18.

2. Normal Stresses

In steady-state shear flow at very low rates of shear $\dot{\gamma}$, the primary normal stress difference $\sigma_{11} - \sigma_{22}$ is related to the dynamic storage modulus at very low

frequencies as follows:

$$(\sigma_{11} - \sigma_{22})/\dot{\gamma}^2 = \Psi_{1,0} = 2G'/\omega^2 \tag{75}$$

as cited in equation 75 of Chapter 3. It follows that the temperature dependence of normal stresses should be described with reduced variables by plotting (analogous to coordinates 14 of Section A4) $(\sigma_{11} - \sigma_{22})T_0\rho_0/T\rho$ against $\dot{\gamma}a_T$ or $\dot{\gamma}\eta_0 T_0\rho_0/\eta_{00}T\rho$. Experimental data at different temperatures, plotted in this manner,[184,185] superpose very well both at low $\dot{\gamma}$ and at higher $\dot{\gamma}$ where equation 75 is no longer applicable, showing that the time constants governing the normal stresses have the same temperature dependence as those involved in linear viscoelastic behavior.

3. Non-Newtonian Viscosity

In the nonlinear phenomenological theories,[186] the same time constants often enter the equations for non-Newtonian flow and linear viscoelastic properties. Also, in molecular theories of non-Newtonian flow, the product of $\dot{\gamma}$ and a characteristic time which is similar to the terminal viscoelastic relaxation time is the controlling parameter in specifying the magnitude of non-Newtonian effects (Chapter 10, Section E). Hence it may be expected that temperature dependence of non-Newtonian viscosity should be described with reduced variables by plotting (analogous to coordinates 18 of Section A4) η/η_0 against $\dot{\gamma}a_T$ or $\dot{\gamma}\eta_0 T_0\rho_0/\eta_{00}T\rho$. Such a plot, or a minor modification of it, has been used widely to combine data at different temperatures and predict non-Newtonian behavior outside limits of T or $\dot{\gamma}$ which can be conveniently achieved experimentally.[187-189] The effect of pressure can be described in an analogous manner.[190]

4. Ultimate Properties and Other Practical Aspects of Behavior

Certain other much more complicated aspects of mechanical behavior, such as tensile strength, ultimate elongation, tear propagation, friction, and wear have also been analyzed with reduced variables to describe and predict temperature dependence, using the same shift factors a_T which govern linear viscoelastic properties and are related to free volume as described in this chapter. In general, an experimental parameter containing a factor of reciprocal time is multiplied by a_T for this purpose. The success of this sort of analysis is presumably associated with a rate-determining step for the phenomenon observed which depends on the same molecular motions that determine viscoelastic relaxation times. These properties will be discussed in Chapter 19.

In this chapter, the discussion of temperature and pressure dependence has emphasized the shifts of the viscoelastic functions on the logarithmic scale of time or frequency. The actual change in magnitude of a viscoelastic property such as $G(t)$ or J' will depend on the shape of the function whose argument is shifted, as expressed in equation 74. The shapes of these functions are discussed in the next few chapters.

REFERENCES

1. W. Dannhauser, W. C. Child, Jr., and J. D. Ferry, *J. Colloid Sci.*, **13,** 103 (1958).
2. P. J. Flory, C. A. Hoeve, and A. Ciferri, *J. Polym. Sci.*, **34,** 337 (1959).
3. K. W. Wagner, *Elektrotech. Z.*, **36,** 135, 163 (1915).
4. H. Leaderman, *Elastic and Creep Properties of Filamentous Materials and Other High Polymers,* The Textile Foundation, Washington, 1943.
5. F. H. Müller, *Kolloid-Z.*, **114,** 2 (1949).
6. A. V. Tobolsky and R. D. Andrews, *J. Chem. Phys.*, **11,** 125 (1943).
7. J. D. Ferry, *J. Am. Chem. Soc.*, **72,** 3746 (1950).
8. C. A. Dahlquist and M. R. Hatfield, *J. Colloid. Sci.*, **7,** 253 (1952).
9. P. E. Rouse, Jr., *J. Chem. Phys.*, **21,** 1272 (1953).
10. J. G. Kirkwood, *J. Chem. Phys.*, **14,** 51 (1946).
11. R. C. Harper, H. Markovitz, and T. W. De Witt, *J. Polym. Sci.*, **8,** 435 (1952).
12. S. Glasstone, K. Laidler, and H. Eyring, *Theory of Rate Processes,* McGraw-Hill, New York, 1941.
13. I. L. Hopkins, *J. Appl. Phys.*, **24,** 1300 (1953).
14. W. Philippoff, *J. Appl. Phys.*, **25,** 1102 (1954).
15. D. J. Plazek, W. Dannhauser, and J. D. Ferry, *J. Colloid Sci.*, **16,** 101 (1961).
16. F. Schwarzl and A. J. Staverman, *J. Appl. Phys.*, **23,** 838 (1952).
17. A. V. Tobolsky, *J. Appl. Phys.*, **27,** 673 (1956).
18. O. Nakada, *J. Phys. Soc. Jpn.*, **12,** 1218 (1957).
19. J. Bischoff, E. Catsiff, and A. V. Tobolsky, *J. Am. Chem. Soc.*, **74,** 3378 (1952).
20. J. D. Ferry, L. D. Grandine, Jr., and E. R. Fitzgerald, *J. Appl. Phys.*, **24,** 911 (1953).
21. K. Ninomiya, J. D. Ferry, and Y. Ōyanagi, *J. Phys. Chem.*, **67,** 2297 (1963).
22. L. D. Grandine, Jr., and J. D. Ferry, *J. Appl. Phys.*, **24,** 679 (1953).
23. M. L. Williams and J. D. Ferry, *J. Colloid Sci.*, **10,** 1 (1955).
24. T. E. Newlin, S. E. Lovell, P. R. Saunders, and J. D. Ferry, *J. Colloid Sci.*, **17,** 10 (1962).
25. D. J. Plazek, *J. Phys. Chem.*, **69,** 3480 (1965).
26. D. J. Plazek and P. Agarwal, *J. Appl. Polym. Sci.*, **22,** 2127 (1978).
27. D. J. Plazek, *Polymer J.*, **12,** 43 (1980).
28. J. W. Berge, P. R. Saunders, and J. D. Ferry, *J. Colloid Sci.*, **14,** 135 (1959).
29. J. D. Ferry and E. R. Fitzgerald, *J. Colloid Sci.*, **8,** 224 (1953).
30. A. J. Barlow, J. Lamb, A. J. Matheson, P. R. K. L. Padmini, and J. Richter, *Proc. R. Soc.*, **A298,** 467 (1967).
31. A. J. Barlow, A. Erginsay, and J. Lamb, *Proc. R. Soc.*, **A298,** 481 (1967).
32. A. A. Miller, *J. Polym. Sci.*, **A2,** 1095 (1964).
33. P. J. Blatz, private communication.
34. H. Vogel, *Phys. Z.*, **22,** 645 (1921).
35. J. F. Pierson, thesis, University of Strasbourg, 1968.
36. J. F. Pierson and A. J. Kovacs, unpublished experiments.
37. C. R. Taylor, private communication.
38. R. S. Marvin, *Proc. 2nd Intern. Cong. Rheology,* Butterworths, London, 1953, p. 156.
39. A. V. Tobolsky and E. Catsiff, *J. Polym. Sci.*, **19,** 111 (1956).
40. D. J. Plazek, *J. Polym. Sci.*, A2, **6,** 621 (1968).
41. M. L. Williams, *J. Phys. Chem.*, **59,** 95 (1955).
42. M. L. Williams, R. F. Landel, and J. D. Ferry, *J. Am. Chem. Soc.*, **77,** 3701 (1955).
43. W. Kauzmann, *Chem. Rev.*, **43,** 219 (1948).
44. R. O. Davies and G. O. Jones, *Adv. Phys.*, **2,** 370 (1953).
45. A. Kovacs, *Adv. Polym. Sci.*, **3,** 394 (1964).
46. H. Eyring and J. O. Hirschfelder, *J. Phys. Chem.*, **41,** 249 (1937).
47. J. Frenkel, *Kinetic Theory of Liquids,* Oxford University Press, 1946.
48. A. K. Doolittle, *J. Appl. Phys.*, **22,** 1471 (1951).
49. A. Bondi, *Ann. N. Y. Acad. Sci.*, **53,** 870 (1951).

50. C. Kittel, *Introduction to Solid-State Physics,* Wiley, New York, 1956.
51. G. Tammann, *Aggregatzustände,* Leipzig, 1922; *Der Glaszustand,* Leipzig, 1933.
52. G. S. Parks and H. M. Huffman, *Science,* **64,** 363 (1926).
53. T. Alfrey, G. Goldfinger, and H. Mark, *J. Appl. Phys.,* **14,** 700 (1943).
54. A. Kovacs, Sc. D. thesis, University of Paris, 1955.
55. A. Kovacs, *J. Polym. Sci.,* **30,** 131 (1958).
56. M. L. Williams, *J. Appl. Phys.,* **29,** 1395 (1958).
57. R. Simha and R. F. Boyer, *J. Chem. Phys.,* **37,** 1003 (1962).
58. R. O. Davies and G. O. Jones, *Proc. R. Soc.,* **217A,** 27 (1953).
59. I. Prigogine and R. Defay, in *Thermodynamique Chimique,* edited by Desoer, Liège, 1950.
60. J. M. Hutchinson and A. J. Kovacs, *J. Polym. Sci., Polym. Phys. Ed.,* **14,** 1575 (1976).
61. A. J. Kovacs, J. M. Hutchinson, and J. J. Aklonis, in *The Structure of Non-Crystalline Materials,* edited by P. H. Gaskell, Taylor and Francis, London, 1977, p. 153.
62. A. J. Kovacs, J. J. Aklonis, J. M. Hutchinson, and A. R. Ramos, *J. Polym. Sci., Polym. Phys. Ed.,* **17,** 1097 (1979).
63. J. H. Gibbs and E. A. DiMarzio, *J. Chem. Phys.,* **28,** 373 (1958).
64. E. A. DiMarzio and J. H. Gibbs, *J. Polym. Sci.,* **40,** 121 (1959).
65. E. A. DiMarzio and J. H. Gibbs, *J. Polym. Sci.,* **A1,** 1417 (1963).
66. E. A. DiMarzio, *J. Res. Nat. Bur. Stand.,* **A68,** 611 (1964).
67. G. Adam and J. H. Gibbs, *J. Chem. Phys.,* **43,** 139 (1965).
68. B. Wunderlich, *J. Phys. Chem.,* **64,** 1052 (1960).
69. A. B. Bestul and S. S. Chang, *J. Chem. Phys.,* **40,** 3731 (1964).
70. M. Goldstein, *J. Chem. Phys.,* **39,** 3369 (1963).
71. S. E. B. Petrie, *J. Polym. Sci.,* A-2, **10,** 1255 (1972).
72. A. Eisenberg and S. Saito, *J. Chem. Phys.,* **45,** 1673 (1966).
73. M. C. Shen and A. Eisenberg, *Prog. Solid State Chem.,* **3,** 407 (1966).
74. A. J. Batchinski, *Z. Phys. Chem.,* **84,** 644 (1913).
75. A. K. Doolittle and D. B. Doolittle, *J. Appl. Phys.,* **28,** 901 (1957).
76. M. H. Cohen and D. Turnbull, *J. Chem. Phys.,* **31,** 1164 (1959).
77. D. Turnbull and M. H. Cohen, *J. Chem. Phys.,* **34,** 120 (1961).
78. F. Bueche, *J. Chem. Phys.,* **24,** 418 (1956).
79. F. Bueche, *J. Chem. Phys.,* **30,** 748 (1959).
80. F. Bueche, *J. Chem. Phys.,* **36,** 2940 (1962).
81. M. Litt, *Trans. Soc. Rheol.,* **20,** 47 (1976).
82. G. C. Berry and T. G. Fox, *Adv. Polym. Sci.,* **5,** 261 (1967).
83. A. J. Kovacs, *Rheol. Acta,* **5,** 262 (1966).
84. S. Kästner, *Kolloid-Z.,* **216–7,** 46 (1967).
85. T. G. Fox and P. J. Flory, *J. Appl. Phys.,* **21,** 581 (1950).
86. A. Bondi, *J. Polym. Sci.,* **A2,** 3159 (1964).
87. G. S. Fulcher, *J. Am. Chem. Soc.,* **8,** 339, 789 (1925).
88. G. Tammann and G. Hesse, *Z. Anorg. Allg. Chem.,* **156,** 245 (1926).
89. A. A. Miller, *J. Polym. Sci.,* A2, **6,** 249 (1968).
90. A. A. Miller, *Macromolecules,* **11,** 859 (1978).
91. A. B. Bestul, *Glastech. Ber.,* **32K,** 59 (1959).
92. G. J. Dienes, *J. Appl. Phys.,* **24,** 779 (1953).
93. P. B. Macedo and T. A. Litovitz, *J. Chem. Phys.,* **42,** 245 (1965).
94. H. S. Chung, *J. Chem. Phys.,* **44,** 1362 (1966).
95. S. Kästner, *J. Polym. Sci.,* **C16,** 4121 (1968).
96. A. J. Kovacs, personal communication.
97. P. W. Bridgman, *The Physics of High Pressure,* G. Bell and Sons, London, 1949.
98. B. Maxwell and A. Jung, *Mod. Plast.,* **35,** 3, 174 (1957).
99. K. H. Hellwege, W. Knappe, F. Paul, and V. Semjonow, *Rheol. Acta,* **6,** 165 (1967).
100. J. E. McKinney and H. V. Belcher, *J. Res. Nat. Bur. Stand.,* **67A,** 43 (1963).
101. H. Singh and A. W. Nolle, *J. Appl. Phys.,* **30,** 337 (1959).

102. J. D. Ferry and R. A. Stratton, *Kolloid-Z.*, **171,** 107 (1960).
103. A. J. Matheson, *J. Chem. Phys.*, **44,** 695 (1966).
104. K. Hellwege, W. Knappe, and P. Lehmann, *Kolloid-Z.*, **183,** 110 (1963).
105. J. M. O'Reilly, *J. Polym. Sci.*, **57,** 429 (1962).
106. R. W. Fillers and N. W. Tschoegl, *Trans. Soc. Rheol.*, **21,** 51 (1977).
107. F. Bueche, *J. Chem. Phys.*, **36,** 2940 (1962).
108. S. Tokiura, S. Ogihara, Y. Yamazaki, K. Tabata, and H. Sasaki, *Zairyo,* **17,** 365 (1968).
109. A. Zosel, *Kolloid-Z.*, **199,** 113 (1964).
109a. R. C. Penwell, R. S. Porter, and S. Middleman, *J. Polym. Sci.*, A-2, **9,** 463, 731 (1971).
110. J. E. McKinney, H. V. Belcher, and R. S. Marvin, *Trans. Soc. Rheol.*, **4,** 347 (1960).
111. J. Koppelmann and J. Gielessen, *Z. Elektrochem.*, **65,** 689 (1961); *Proc. 4th Intern. Congr. Rheology,* Part 3, Interscience, New York, 1965, p. 361.
112. G. Williams, *Trans. Faraday Soc.*, **60,** 1548, 1556 (1964).
113. G. Williams, *Trans. Faraday Soc.*, **61,** 1564 (1965).
114. G. Goldbach and G. Rehage, *Rheol. Acta,* **6,** 30 (1967).
115. H. Breuer and G. Rehage, *Kolloid-Z., Z. Polym.*, **216–217,** 159 (1967).
116. J. M. O'Reilly, in *Modern Aspects of the Vitreous State,* edited by J. D. MacKenzie, Butterworths, London, 1964.
117. G. Gee, *Polymer,* **7,** 177 (1966).
118. U. Bianchi, *J. Phys. Chem.*, **69,** 1497 (1965).
119. A. J. Kovacs, R. A. Stratton, and J. D. Ferry, *J. Phys. Chem.*, **67,** 152 (1963).
120. H. H. Meyer, P.-M. F. Mangin, and J. D. Ferry, *J. Polym. Sci.*, **A3,** 1785 (1965).
120a. D. J. Plazek and J. H. Magill, *J. Chem. Phys.*, **45,** 3038 (1966).
121. L. C. E. Struik, *Rheol. Acta,* **5,** 303 (1966).
122. A. L. Zijlstra, *Phys. Chem. Glasses,* **4,** 143 (1963).
123. G. Guiroy, thesis, Ecole Supérieure de Physique et Chimie, Paris 1968.
124. K. Ninomiya and J. D. Ferry, *J. Phys. Chem.*, **67,** 2292 (1963).
125. V. R. Allen and T. G. Fox, *J. Chem. Phys.*, **41,** 337 (1964).
126. T. G. Fox and S. Loshaek, *J. Polym. Sci.*, **15,** 371 (1955).
127. K. Ueberreiter and G. Kanig, *J. Colloid Sci.*, **7,** 569 (1952).
128. R. B. Beevers and E. F. T. White, *Trans. Faraday Soc.*, **56,** 744 (1960).
129. F. Bueche and F. N. Kelley, *J. Polym. Sci.*, **45,** 267 (1960).
130. W. H. Stockmayer, *Pure Appl. Chem.*, **15,** 539 (1967).
131. N. G. McCrum, B. E. Read, and G. Williams, *Anelastic and Dielectric Effects in Polymeric Solids,* Wiley, New York, 1967.
132. F. E. Karasz, editor, *Dielectric Properties of Polymers,* Plenum, New York, 1972.
133. J. D. Ferry, M. L. Williams, and E. R. Fitzgerald, *J. Phys. Chem.*, **59,** 403 (1955).
134. J. D. Ferry and S. Strella, *J. Colloid Sci.*, **13,** 459 (1958).
135. A. R. Payne, in *Rheology of Elastomers,* edited by P. Mason and N. Wookey, Pergamon, London, 1958.
136. A. Tsutsumi, M. Kaneko, et al., *J. Macromol. Sci.-Phys.*, **B8,** 413 (1973).
137. L. de Brouckère and G. Offergeld, *Bull. Soc. Chim. Belg.*, **67,** 96 (1958).
138. R. N. Work and S. Fujita, *J. Chem. Phys.*, **45,** 3779 (1966).
139. W. H. Stockmayer and M. Bauer, *J. Am. Chem. Soc.*, **86,** 3485 (1964).
140. H. Sasabe and S. Saito, *J. Polym. Sci., A2,* **6,** 1401 (1968).
141. W. P. Slichter and D. D. Davis, *J. Appl. Phys.*, **34,** 98 (1963).
142. A. W. Nolle and J. J. Billings, *J. Chem. Phys.*, **30,** 84 (1959).
143. W. P. Slichter and D. D. Davis, *Bull. Am. Phys. Soc., Ser.* II, **13,** 471 (1968).
144. H. Fujita, *Adv. Polym. Sci.*, **3,** 1 (1961).
145. R. J. Bearman, *J. Phys. Chem.*, **65,** 1961 (1961).
146. I. Auerbach, S. D. Gehman, W. R. Miller, and W. C. Kuryla, *J. Polym. Sci.*, **28,** 129 (1958).
147. R. S. Moore and J. D. Ferry, *J. Phys. Chem.*, **66,** 2699 (1962).
148. S. P. Chen and J. D. Ferry, *Macromolecules,* **1,** 270 (1968).

149. D. C. Douglass and D. W. McCall, *J. Phys. Chem.*, **62,** 1102 (1958).
150. B. D. Boss, E. O. Stejskal, and J. D. Ferry, *J. Phys. Chem.*, **71,** 1501 (1967).
151. H. Fujita, A. Kishimoto, and K. Matsumoto, *Trans. Faraday Soc.*, **56,** 424 (1960).
152. C.-P. Wong, J. L. Schrag, and J. D. Ferry, *J. Polym. Sci.*, A-2, **8,** 991 (1970).
153. A. Kishimoto, *J. Polym. Sci.*, **A2,** 1421 (1964).
154. H. Sasabe and S. Saito, *Polym. J.*, **3,** 624 (1972).
155. M. Gordon and W. Simpson, *Polymer*, **2,** 383 (1961).
156. J. D. Hoffman and J. I. Lauritzen, *J. Res. Nat. Bur. Stand.*, **65A,** 297 (1961).
157. J. D. Hoffman, *SPE Trans.*, **4,** 1 (1964).
158. J. H. Magill, *J. Polym. Sci.*, **A3,** 1195 (1965); *Polymer*, **6,** 367 (1965).
159. J. H. Magill and D. J. Plazek, *J. Chem. Phys.*, **46,** 3757 (1967).
160. J. Boon, G. Challa, and D. W. van Krevelen, *J. Polym. Sci.*, A2, **6,** 1835 (1968).
161. K. Sato, H. Nakane, T. Hideshima, and S. Iwayanagi, *J. Phys. Soc. Jpn.*, **9,** 413 (1954; S. Iwayanagi, *J. Sci. Res. Inst. Tokyo*, **49,** 4 (1955).
162. Y. Wada, H. Hirose, T. Asano, and S. Fukutomi, *J. Phys. Soc. Jpn.*, **14,** 1064 (1959).
163. N. G. McCrum and E. L. Morris, *Proc. R. Soc.*, **A281,** 258 (1964).
164. K. Shimizu, O. Yano, Y. Wada, and Y. Kawamura, *J. Polym. Sci., Polym. Phys. Ed.*, **11,** 1641 (1973).
165. R. Masui and Y. Wada, *J. Macromol. Sci. (Phys).*, **B10,** 71 (1974).
166. H. Nakayasu, H. Markovitz, and D. J. Plazek, *Trans. Soc. Rheol.*, **5,** 261 (1961).
167. P. R. Saunders, D. M. Stern, S. F. Kurath, C. Sakoonkim, and J. D. Ferry, *J. Colloid Sci.*, **14,** 222 (1959).
168. D. M. Stern, J. W. Berge, S. F. Kurath, C. Sakoonkim, and J. D. Ferry, *J. Colloid Sci.*, **17,** 409 (1962).
169. R. Chiang, J. J. Burke, J. O. Threlkeld, and T. A. Orofino, *J. Phys. Chem.*, **70,** 3591 (1966).
170. T. Miyamoto and H. Inagaki, *Macromolecules*, **2,** 554 (1969); *Polym. J.*, **1,** 46 (1970).
171. J. D. Ferry, W. C. Child, Jr., R. Zand, D. M. Stern, M. L. Williams, and R. F. Landel, *J. Colloid Sci.*, **12,** 53 (1957).
172. W. C. Child, Jr., and J. D. Ferry, *J. Colloid Sci.*, **12,** 327 (1957).
173. W. C. Childr, Jr., and J. D. Ferry, *J. Colloid Sci.*, **12,** 389 (1957).
174. E. A. W. Hoff, D. W. Robinson, and A. H. Wilbourn, *J. Polym. Sci.*, **18,** 161 (1955).
175. D. G. Fesko and N. W. Tschoegl, *J. Polym. Sci.*, **C35,** 51 (1971); *Int. J. Polym. Mater.*, **3,** 51 (1974).
176. A. V. Tobolsky and J. R. McLoughlin, *J. Phys. Chem.*, **59,** 989 (1955).
177. S. F. Kurath, T. P. Yin, J. W. Berge, and J. D. Ferry, *J. Colloid Sci.*, **14,** 147 (1959).
177a. R. F. Landel and J. D. Ferry, *J. Phys. Chem.*, **60,** 294 (1956).
178. P. R. Saunders and A. G. Ward, in *Rheology*, edited by F. R. Eirich, Volume II, Chapter 8, Academic Press, New York, 1958.
178a. R. E. Cohen and N. W. Tschoegl, *Trans. Soc. Rheol.*, **20,** 153 (1976).
179. J. D. Ferry and E. R. Fitzgerald, *Proc. 2nd Intern. Cong. Rheology*, Butterworths, London, 1953, p. 140.
180. S. Onogi and K. Ui, *J. Colloid Sci.*, **11,** 214 (1956); A. Naemura and M. Tsuchida, *Zairyo*, **16,** 501 (1967).
181. I. L. Hopkins, *J. Polym. Sci.*, **28,** 631 (1958).
182. P. Forgacs, *J. Polym. Sci., Polym. Lett. Ed.*, **16,** 1 (1978).
183. J. C. Monpagens, D. G. Chatain, C. Lacabanne, and P. G. Gautier, *J. Polym. Sci., Polym. Phys. Ed.*, **15,** 767 (1977).
184. T. Kotaka, M. Kurata, and M. Tamura, *Rheol. Acta*, **2,** 179 (1962).
185. T. Kotaka and K. Osaki, *J. Polym. Sci.*, **C15,** 453 (1966).
186. R. B. Bird, R. C. Armstrong, and O. Hassager, *Dynamics of Polymeric Liquids*, Volume I, Wiley, New York, 1977.
187. J. D. Ferry, M. L. Williams, and D. M. Stern, *J. Phys. Chem.*, **58,** 987 (1954).
188. G. Kraus and J. T. Gruver, *J. Appl. Polym. Sci.*, **9,** 739 (1965).

189. W. W. Graessley, *Adv. Polym. Sci.*, **16,** 1 (1974).
190. S. Y. Choi and N. Nakajima, *Bull. Am. Phys. Soc., Ser. II,* **13,** 371 (1968).
191. E. R. Fitzgerald. L. D. Grandine, Jr., and J. D. Ferry, *J. Appl. Phys.,* **24,** 650 (1953).
192. J. D. Ferry and R. F. Landel, *Kolloid-Z.*, **148,** 1 (1956).
193. M. L. Williams and J. D. Ferry, *J. Colloid Sci.*, **9,** 479 (1954).
194. H. Endo, T. Fujimoto, and M. Nagasawa, *J. Polym. Sci.*, **7,** 1669 (1969).
195. H. Odani, N. Nemoto, S. Kitamura, M. Kurata, and M. Tamura, *Polym. J.*, **1,** 356 (1970).
196. M. L. Williams and J. D. Ferry, *J. Colloid Sci.*, **10,** 474 (1955).
197. K. Fujino, K. Senshu, and H. Kawai, *J. Colloid Sci.*, **16,** 1 (1961).
198. S. F. Kurath, E. Passaglia, and R. Pariser, *J. Appl. Phys.*, **28,** 499 (1957).
199. A. J. Barlow, G. Harrison, and J. Lamb, *Proc. R. Soc.*, **A282,** 228 (1964).
200. G. Williams, *Trans. Faraday Soc.*, **59,** 1397 (1963).
201. D. J. Plazek, *Trans. Soc. Rheol.*, **9:1,** 119 (1965).
202. A. S. Nigmankhodjaev, L.-K. Bi, C.-P. Wong, J. L. Schrag, and J. D. Ferry, *J. Polym. Sci.*, A-2, **8,** 1927 (1970).
203. R. A. Dickie and J. D. Ferry, *J. Phys. Chem.*, **70,** 2594 (1966).
204. E. Maekawa, R. G. Mancke, and J. D. Ferry, *J. Phys. Chem.*, **69,** 2811 (1965).
205. J. F. Sanders, Ph. D. thesis, University of Wisconsin, 1968.
206. C. R. Taylor, personal communication.
207. J. F. Sanders, R. H. Valentine, and J. D. Ferry, *J. Polym. Sci.*, A2, **6,** 967 (1968).
208. R. G. Mancke and J. D. Ferry, *Trans. Soc. Rheol.*, **12,** 335 (1968).
209. J. F. Sanders and J. D. Ferry, *Macromolecules*, **7,** 681 (1974).
210. J. R. Richards, R. G. Mancke, and J. D. Ferry, *Polym. Lett.*, **2,** 197 (1964).
211. R. F. Landel, *J. Colloid Sci.*, **12,** 308 (1957).
212. F. R. Schwarzl, C. W. van der Wal, and H. W. Bree, *Chim. Ind.*, **54,** 51 (1972).
213. D. J. Plazek, V. Tan, and V. M. O'Rourke, *Rheol. Acta*, **13,** 367 (1974).
214. D. J. Plazek, personal communication.
215. T. P. Yin and J. D. Ferry, *J. Colloid Sci.*, **16,** 166 (1961).
216. L. D. Grandine, Jr., and J. D. Ferry, *J. Appl. Phys.*, **24,** 679 (1953).
217. M. L. Williams and J. D. Ferry, *J. Colloid Sci.*, **10,** 1 (1955).
218 D. J. Plazek, *J. Colloid Sci.*, **15,** 50 (1960); M. N. Vrancken and J. D. Ferry, *J. Polym. Sci.*, **24,** 27 (1957).
219. T. Masuda, N. Toda, Y Aoto, and S. Onogi, *Polym. J.*, **3,** 315 (1972).

CHAPTER 12

The Transition Zone from Rubberlike to Glasslike Consistency

Having examined the nature of the temperature and pressure dependence of the relaxation and retardation times, we now turn attention to the details of the time and frequency dependence of the basic viscoelastic functions and their correlation with chemical structure. Each zone of time scale represents a separate problem. The one most characteristic of polymers is the subject of this chapter, the transition from rubberlike to glasslike consistency, where the moduli increase and the compliances decrease by several powers of 10 as a function of time or frequency, as illustrated in Chapter 2.

The term "transition" to describe this zone is perhaps unfortunate (though probably too firmly established to change), since there is a tendency to confuse it with the glass transition as a function of temperature or pressure which was described in the preceding chapter. The two phenomena are distinct. As the time or frequency is varied, the magnitude of the shear modulus (for example) derived from the measurement changes from rubberlike to glasslike, but there is no change in the thermodynamic state of the material such as occurs when the glass transition temperature is traversed. In the latter case the system is in equilibrium above T_g with respect to temperature, pressure, and internal parameters of order; below T_g it is not in equilibrium with respect to all these variables,[1] though it may be in virtual equilibrium with respect to temperature and pressure at temperatures far below T_g. The distinction between the two phenomena is clear in the discussion of dielectric dispersion long ago by Thomas,[2] bulk viscoelasticity by Litovitz,[3] and shear viscoelasticity by Plazek.[4]

The shapes of the viscoelastic functions in the transition zone are grossly similar for all polymers, as illustrated by the curves in Chapter 2, being qualitatively in accord with the predictions of the flexible chain theories outlined in Chapter 10.

The most striking feature which varies among polymers is therefore the position of the transition zone on the time or frequency scale, when different systems are examined either all at the same temperature or at suitable corresponding temperatures. This comparison will first be undertaken, both in terms of directly measured quantities and in terms of the monomeric friction coefficient ζ_0 whose magnitude sets the time scale according to theory. Subsequently, detailed differences in the shapes of all the spectra will be scrutinized.

In practically all cases, composite functions are utilized, obtained by reduction of data from experiments at various temperatures as described in the preceding chapter. Most of the data refer to uncross-linked polymers of quite high molecular weight, but since moderate cross-linking affects the transition zone only to a minor degree, a few cross-linked systems are included. Polymers of low molecular weight are discussed in Section D.

A. THE LOCATION OF THE TRANSITION ZONE ON THE TIME OR FREQUENCY SCALE

As an example of the effect of chemical structure on the time scale of the transition zone, the storage modulus reduced to 100°C is plotted logarithmically against frequency in Fig. 12-1 for polymers of five *n*-alkyl methacrylates[5-9] whose ester groups contain respectively 2, 4, 6, 8, and 12 carbon atoms and one with a branched ester group.[10] With increasing side group length, the position of the transition shifts to higher frequencies, at first rapidly and then more slowly, traversing more than

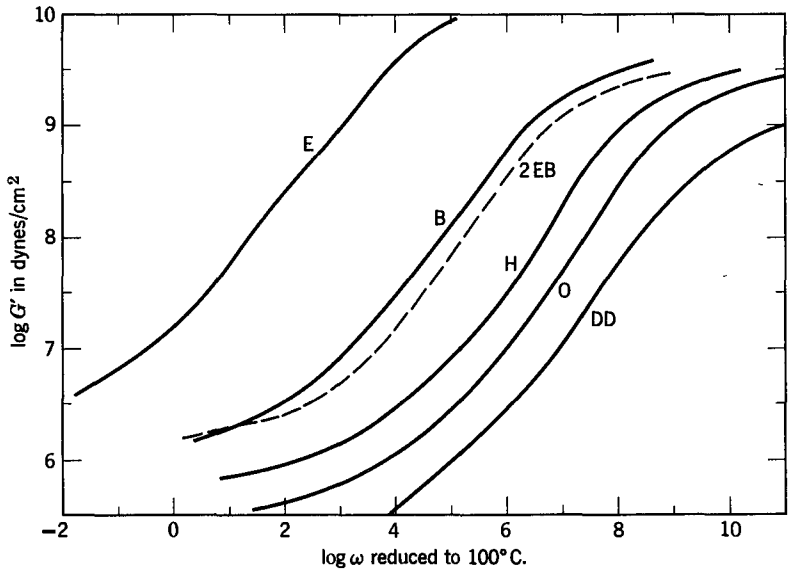


FIG. 12-1. Storage modulus plotted against frequency reduced to 100°C for six methacrylate polymers.[5-10] (E) Ethyl; (B) *n*-butyl; (H) *n*-hexyl; (O) *n*-octyl; (DD) *n*-dodecyl; (2-EB) 2-ethyl butyl.

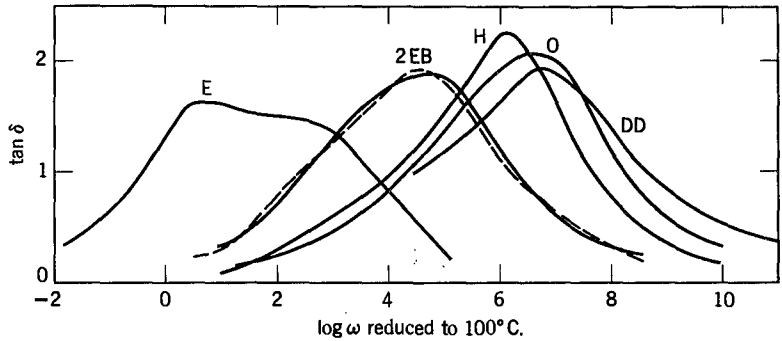


FIG. 12-2. Loss tangent plotted against frequency reduced to 100°C, for the same polymers as in Fig. 12-1, similarly identified.

six decades of the logarithmic frequency scale. The displacement reflects a decrease in all the relaxation times which is in turn caused by a decrease in the monomeric friction coefficient. At the same time, the level of G' approached at low frequencies (representing very roughly the pseudoequilibrium modulus of the entanglement network and therefore inversely proportional to the average molecular weight between coupling points) appears to fall with increasing side group length, and so does the level approached at high frequencies (representing roughly the modulus in the glassy state). It should be mentioned that for the first three members of the series the effect of a β mechanism has already been separated out as described in Section F of the preceding chapter. The properties of the 2-ethyl butyl methacrylate polymer are intermediate between those of the *n*-butyl (with the same side chain length) and those of the *n*-hexyl (with the same side chain mass) but are closer to the former.

The loss tangent, $G''/G' = J''/J'$, is plotted against frequency for the same series in Fig. 12-2. This quantity, whose maximum occurs roughly near the middle of the transition zone, shifts to higher frequencies in the same manner. It also experiences minor changes in shape, its sharpness first increasing slightly and then decreasing with increasing side group length. It will be recalled that the loss tangent is not susceptible of direct molecular interpretation, but it is important in determining various physical properties of practical interest. (The maxima in G'' and J'', which are equally valid as locations of "loss maxima," occur at quite different points, at higher and lower frequencies respectively than that of tan δ, as noted in Chapter 2.)

For a more extensive comparison of polymers, two quantities have been somewhat arbitrarily selected as gauges of the location of the transition zone: the frequency where $G' = 10^8$ dynes/cm^2, a value intermediate between those characteristic of the rubberlike and glasslike states (corresponding approximately to the reciprocal time where $G(t) = 0.8 \times 10^8$ dynes/cm^2, since tan $\delta \cong 1$ in this region—*cf.* equation 13 of Chapter 10), and the frequency where tan δ is a maximum. These are summarized for the polymers of Figs. 12-1 and 12-2 and a number of others from data taken from the literature[11-31] at several different temperatures in Table 12-I. For

Table 12-I

FREQUENCIES (HERTZ) CHARACTERIZING THE TRANSITION ZONE FOR VARIOUS POLYMERS

Polymer	T_g	log ν at which $G' = 10^8$ dyn/cm^2			log ν for max. tan δ			Ref.
		298°	373°	398°	298°	373°	398°	
Methacrylate Polymers								
Methyl	388	—	—	0.5	—	—	—	11
Ethyl	335	—	0.5	2.6	—	1.0	3.1	5
n-Butyl	300	—	4.0	5.2	—	3.7	4.9	6
2-Ethyl Butyl	284	−2.0	4.5	5.7	−2.8	3.7	4.9	10
n-Hexyl	268	1.4	5.9	6.8	0.8	5.3	6.2	7
n-Octyl	253	3.2	6.8	7.5	2.2	5.8	6.5	8
n-Dodecyl		5.6	7.5	—	4.1	6.0	—	9
Rubbers								
Hevea Rubber	200	7.0	9.0	—	7.1	9.1	—	12
	200	7.2	9.2	—	7.2	9.2	—	13
1,4-Polybutadiene[a]	172	6.1	7.1	7.4	—	—	—	14
1,2-Polybutadiene	261	3.9	7.1	7.5	4.3	7.5	7.9	15
Styrene-butadiene copolymer[b]	210	5.9	7.7	8.0	5.5	7.3	7.6	16
Butyl rubber[c]	205	4.2	6.6	7.2	4.0	6.4	7.0	17
Ethylene-propylene copolymer[d]	242	4.6	7.0	7.4	>5.7	—	—	18
Ethylene-propylene copolymer[e]	216	6.1	7.7	8.0	>7.2	—	—	18
Polyurethane[f]	238	4.9	—	—	5.7	—	—	19
General								
Polyisobutylene	205	4.4	6.7	7.2	3.9	6.2	6.7	20
Polystyrene	373	—	—	2.6	—	—	2.1	21
	373	—	−4.0	2.9	—	−4.4	—	22,31
Poly(vinyl acetate)	305	—	5.3	6.4	—	5.2	6.3	23
	305	—	5.3	6.4	—	5.0	6.1	24
Poly(methyl acrylate)	276	0.0	6.3	7.2	−0.3	6.0	6.9	25
Poly(vinyl chloride)	347	—	2.2	—	—	2.6	—	26
Polyhexene-1	218	5.4	—	—	4.4	—	—	27
Poly(1,1-dihydro-perfluorobutyl acrylate)	—	4.4	—	—	4.5	—	—	28
Polyacetaldehyde	243	5.5	7.7	8.0	5.0	7.2	7.5	29
Poly(dimethyl siloxane)	150	8.3	8.8	8.9	—	—	—	30

[a] cis:trans:vinyl = 43:50:7, lightly cross-linked by dicumyl peroxide.

[b] Random copolymer, 23.5% styrene.

[c] Lightly cross-linked with sulfur.

[d] Ethylene:propylene = 16:84 by mole.

[e] Ethylene:propylene = 56:44 by mole.

[f] Copolymer of adipic acid and ethylene and propylene glycols, cross-linked by naphthalene 1,4-diisocyanate and 1,4-butanediol.

practical orientation, the frequencies are given in Hz rather than the rad/sec (ω) used in Figs. 12–1 and 12–2. In several cases, values are available from more than one experimental source, usually obtained by entirely different methods of measurement, and the agreement is satisfactory. (The difference between the two frequency locations specified by G' and by tan δ, which can be in either direction, reflects in an indirect manner the level of entanglement coupling in the uncross-linked polymer.)

The values for the methacrylate series show the effect of side chain length already observed. The other polymers do not fit into any comparative series. They show that a low T_g is generally associated with a high frequency for the transition zone, but this is not the only controlling parameter as evidenced by a comparison of polyisobutylene and unvulcanized Hevea rubber at 298°K. Although T_g is nearly the same for these two, the transition lies at higher frequencies by nearly three logarithmic decades in the rubber. Such differences will be discussed in more detail in terms of the monomeric friction coefficient in Section B below.

An alternative means of comparing the locations of the transition zone in various polymers is to specify the temperature at which a characteristic feature of the transition is reached for a fixed time or frequency scale. For example, at fixed frequency G' drops rapidly with increasing temperature, and the lower the chosen frequency the steeper the drop (*cf.* Fig. 11–20). At approximately 1 Hz, most of the change from the glasslike to the rubberlike level is accomplished within 5° or 10°, and an inflection point can be chosen with relatively little ambiguity to represent the midpoint temperature, corresponding usually to G' somewhere between 10^8 and 10^9; near this point, tan δ as a function of temperature goes through a rather sharp maximum, as illustrated in Fig. 12–3 from data of Schmieder and Wolf[32] for three isomeric poly(butyl ether)s. (The logarithmic decrement Δ is approximately (tan δ)/π.) Data of this sort have been adduced by many investigators,[32–39] mostly from compound resonance devices, especially the torsion pendulum (Chapter 6). It is ordinarily impossible to obtain data at strictly constant frequency, but in those of Schmieder and Wolf the frequency at the transition midpoint has been kept within a narrow range for purposes of comparison.

Midpoint temperatures T_M determined in this way at about 1 Hz for a variety of polymers are listed in Table 12–II, together with the glass transition temperatures where available. In the homologous series of the acrylates and vinyl ethers, increasing the length of flexible side groups shifts T_M to lower temperatures, corresponding to the shifts to higher frequencies in the methacrylate series in Figs. 12–1 and 12–2 and Table 12–I. However, branched side groups are less effective (*cf.* the 2-ethyl butyl methacrylate in Table 12–I) and may even raise T_M. In the vulcanized rubbers with substantial amounts of sulfur, the changes of T_M are attributable primarily to the alteration in chemical composition and not to the cross-linking;[40] if cross-linking involves negligible change in composition, T_M is independent of the degree of cross-linking until the latter becomes very high. In general, T_M is from 1° to 25° higher than T_g, but since the difference between them is variable one cannot be predicted from the other.

If a higher frequency is chosen for comparing such data, the ambiguity in specifying T_M becomes more serious because the transition occurs at higher temperatures where log a_T

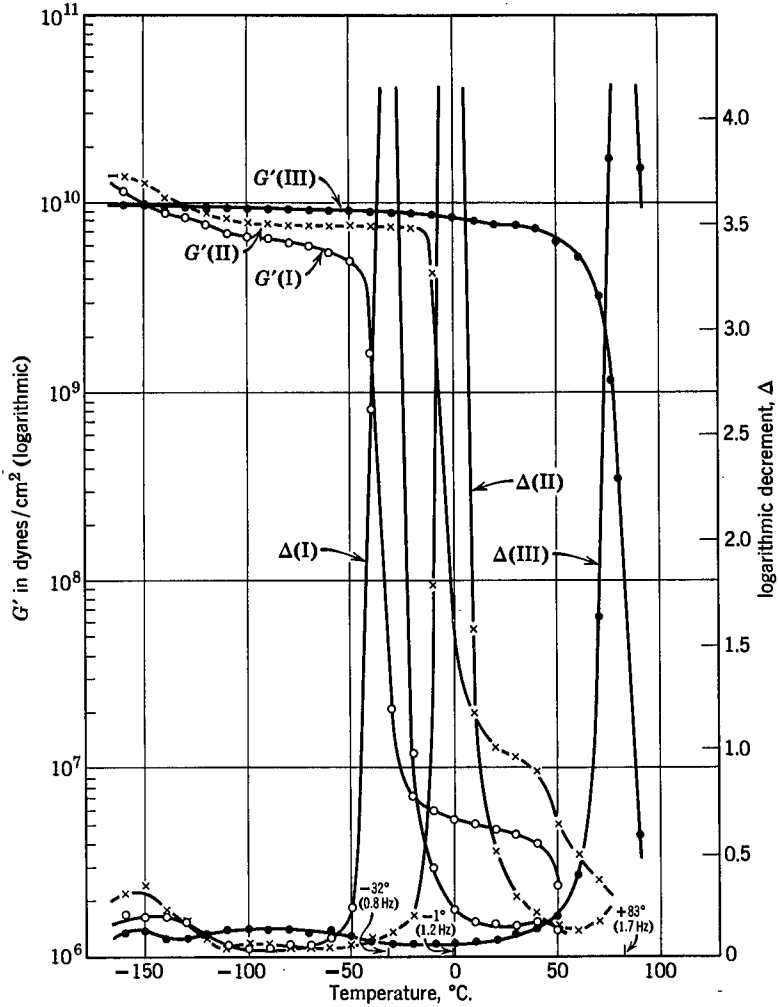


FIG. 12-3. Storage modulus G' and logarithmic decrement Δ (approximately proportional to loss tangent), plotted against temperature at frequencies near 1 Hz, for three poly(vinylbutyl ether)s.[32] (I) *n*-Butyl; (II) *i*-butyl; (III) *t*-butyl.

is less temperature dependent; as a result the transition is broader on the temperature scale (*cf.* Fig. 11-20).

As long as the molecular weight is sufficiently high that the friction coefficient is uninfluenced by molecular ends, *i.e.*, M of the order of 20,000 or more, the position of the transition zone on the time scale is quite independent of molecular weight. This expectation was embodied in the schematic plots of molecular weight dependence in Fig. 10-2; it has been demonstrated experimentally not only by determining T_M at constant frequency for polyisobutylenes,[32] but by showing the

Table 12-II

TEMPERATURES CORRESPONDING TO TRANSITION MID-POINTS FOR G' AT FREQUENCIES NEAR 1 HERTZ

Polymer		T_M, °K	Freq. of Measurement, Hz	T_g, °K	Ref.
Acrylate Polymers					
Methyl		298	1.2	276	32
Ethyl		268	1.6		32
n-Butyl		241	0.8		32
Vinyl Ether Polymers					
Methyl		263	2.7	260	32,33
Ethyl		256	1.1	254	32,33
Propyl		246	1.1		32
n-Butyl		241	0.8	217	32,33
i-Butyl		272	1.2	251	32,33
t-Butyl		356	1.7		32
General					
Polyisobutylene		225	1	202	32
Polystyrene		389	0.9	373	32
Poly(vinyl acetate)		306	1.9	305	32
Poly(vinyl chloride)		363	0.7	347	32
Poly(methyl methacrylate)		393	0.12		32
Poly(vinyl propionate)		285	1.5		32
Polyacetaldehyde		258[d]	1	243	29
Poly(propylene oxide)[a]		213[d]	1	198	29
Polycarbonate[b]		431[d]	1		37
Polycarbonate[c]		380[d]	1		37
Rubbers					
Hevea, unvulcanized		223	1.2	200	32
vulcanized with	0.5% S	223	1.9		32
	1.5	223	1.9		32
	2.0	224	5.4		32
	2.5	226	3.1		32
	3.0	228	2.1		32
	5.0	233	1.5		32
	10	253	2.8		32
	15	274	2.0		32
	20	296	1.7		32
	30	336	1.8		32

[a] Amorphous, copolymerized with 10% butadiene monoxide and vulcanized with 2% sulfur.

[b] Of 4,4′ dioxyphenyl 2,2′ propane.

[c] Of 1,5 naphthalene di-β-oxyethyl ether.

[d] Corresponding to $G' = 10^8$ dynes/cm^2.

virtual coincidence of entire viscoelastic functions throughout the transition zone for different molecular weights of polyisobutylene,[41] poly(methyl methacrylate),[11] poly(ethyl methacrylate),[5] poly(*n*-butyl methacrylate),[6] poly(vinyl acetate),[24,42] and poly(dimethyl siloxane),[30] covering wide ranges of molecular weight up to several million.

Extensive compilations of characteristic temperatures which are defined in a manner closely resembling the somewhat arbitrary definition of T_M given here have been made by Boyer[43] and McCrum, Read, and Williams.[38]

B. THE MONOMERIC FRICTION COEFFICIENT

The position of the transition zone on the time scale reflects the absolute magnitudes of the relaxation and retardation times, and therefore that of the monomeric friction coefficient upon which (according to the flexible chain theories of viscoelasticity) they all depend. It is therefore of interest to examine the friction coefficient ζ_0 as a basis for more quantitative considerations. It is a measure of the frictional resistance per monomer unit encountered by a chain segment in translatory motions. As discussed in this section, it refers to polymers of sufficiently high molecular weight that the effects of free molecular ends can be ignored, so it corresponds to the limiting value ζ_{00} of equations 14 of Chapter 10 and 68 of Chapter 11. Such a value could be adjusted to lower molecular weights by the latter equation with a reasonable guess for the parameter A in equation 67 of Chapter 11.

The friction coefficient has usually been calculated by applying equation 45 of Chapter 10 to the relaxation spectrum H, as follows:

$$\log \zeta_0 = 2 \log H + \log \tau + \log (6/kT) + 2 \log (2\pi M_0/a\rho N_0) \qquad (1)$$

At the long-time end of the transition zone, there is often a segment of H which conforms to the theoretical slope of $-\frac{1}{2}$ on a doubly logarithmic plot, between the steeper slope which prevails at short times and the flattening or minimum characteristic of the plateau region. This feature is illustrated in Fig. 12-4 for the six methacrylate polymers of Figs. 12-1 and 12-2. Sometimes, because of the very restricted applicability of the modified Rouse theory as discussed in Chapter 10, the experimental curve can be matched to the theoretical slope of $-\frac{1}{2}$ only by drawing a tangent. In any case, from the position of a tangent in this region, ζ_0 is calculated. It is necessary to know the density ρ and monomer molecular weight M_0, as well as a, the root-mean-square end-to-end length per square root of the number of monomer units. The latter is usually taken as the value determined in dilute solution in a Θ-solvent,[44] under the assumption that the molecular configuration in the undiluted polymer is unperturbed by long-range effects; in the absence of specific information, an estimate can usually be made from data on some other polymer of similar structure. (Because information on a may be uncertain, and also the value of M_0 may be somewhat arbitrary in the case of copolymers, the product $a^2\zeta_0/M_0^2$ has also been used as a measure of segmental frictional resistance.[16])

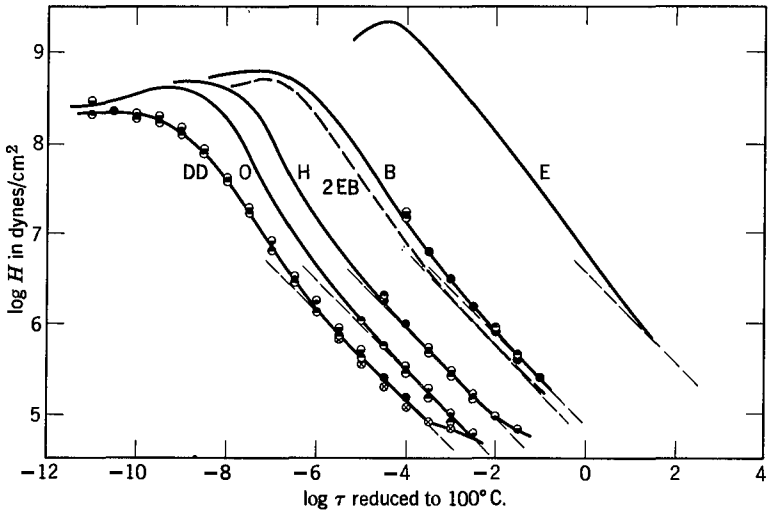


FIG. 12-4. Relaxation spectrum in the transition zone for the six methacrylate polymers of Fig. 12-1, similarly identified and reduced to 100°C, to illustrate calculation of ζ_0.

Since the retardation spectrum L provides in principle the same information as the relaxation spectrum H, it might be expected that ζ_0 could be calculated from L also, using the analog of equation 1, which (*cf.* equation 24 of Chapter 9) is

$$\log \zeta_0 = -2 \log L + \log \tau + \log (6/kT) + 2 \log (2M_0/\pi a \rho N_0) \qquad (2)$$

provided L is proportional to $\tau^{1/2}$ as specified by the modified Rouse theory. However, a substantial segment of L with a slope of $\frac{1}{2}$ on a logarithmic plot does not appear in polymers of high molecular weight; in the appropriate region of the time scale, L is changing slope rapidly, approaching the maximum which characterizes the entanglement network (Fig. 3-4).

The reason for this apparent paradox is the difference in weighting of H and L by mechanisms in different regions of the time scale. In L, the magnitudes of the contributions increase rapidly with increasing retardation time. For spectra conforming to the Rouse theory, this feature is evident in the discussion following equation 22 of Chapter 9, and in Fig. 9-9. And regardless of the precise form of the spectra, the long-time contributions to L will always be strongly weighted relative to their contributions to H, as shown by the general relations of the phenomenological theory.[45]

At the long-time end of the transition zone in a polymer of high molecular weight, the deviations from the simple flexible chain theory caused by entanglement coupling thus appear in L sooner and more strongly than in H. As a result, in this region where H is making its closest fit to the simple theory and permitting calculation of ζ_0, L is entering the maximum which provides information about the entanglement network as discussed in the following chapter.

1. Comparisons at Constant Temperature

Values of log ζ_0 for most of the polymers of Table 12-I, together with a few others,[46-51] are given in Table 12-III. The values of M_0 and a used for their cal-

Table 12–III

MONOMERIC FRICTION COEFFICIENTS OF VARIOUS POLYMERS

Polymer	T_g	M_0	$a \times 10^8$, cm	log ζ_0 (dynes-sec/cm) at 298°	373°	398°	T_g	$T_g + 100°$	Ref.
Methacrylate Polymers									
Methyl (conventional)	390	100	6.9			0.66			11
						2.17	4.97	−3.3	46,47
Methyl (isotactic)	323	100	6.9		0.45	−0.26	6.55	−0.68	47
Methyl (atactic)	379	100	6.9			−1.28	5.54	−3.8	46,47
Ethyl	335	114	5.9		−0.21	−2.35	6.22	−4.40	5
n-Butyl	300	142	6.4		−3.44	−4.66	3.81	−4.77	6
2-Ethyl butyl	284	170	6.5	2.80	−3.69	−4.93	4.79	−4.27	10
n-Hexyl	268	170	7.5	−0.75	−5.25	−6.16	2.59	−5.18	7
n-Octyl	253	198	7.0	−2.29	−5.93	−6.65	2.39	−5.37	8
n-Dodecyl		254	8.75	−4.69	−6.57				9
n-Docosyl		394							48
Oxymethacrylate Polymers									
Methyoxyethyl	293	144	7.0	4.35	−3.11	−4.25	5.39	−4.04	49
Propoxyethyl	253	172	7.0	−1.09	−5.39	−6.18	5.50	−4.60	49
Ethylene glycol monomethacrylate	366	130	7.0	—	3.79	−0.42	5.71	−4.37	49
Diethylene glycol monomethacrylate	284	174	7.0	3.28	−2.20	−2.92	6.09	−2.55	49
Rubbers									
Hevea Rubber[a]	200	68	6.8	−6.41	−8.38	−8.77	4.47	−6.49	50
Poly-1,4-butadiene[b]	172	54	6.0	−6.75	−7.79	−8.02	0.83	−6.16	14
Poly-1,2-butadiene	261	54	7.55	−4.11	−7.27	−7.72	2.38	−7.01	15

Styrene-butadiene copolymer[c]	210	65.5	6.7	−6.11	−7.93	−8.25	—	−6.55	16
Butyl rubber[d]	205	56	5.9	−4.16	−6.61	−7.15	3.57	−4.46	17
Ethylene-propylene copolymer[e]	242	39.9	5.5	−4.50	−6.91	−7.31	3.10	−6.23	18
Ethylene-propylene copolymer[f]	216	34.3	5.5	−6.36	−8.01	−8.31	2.40	−7.11	18
Polyurethane[g]	238	[h]	[h]	−4.33			5.77	−6.02	19
General									
Polyisobutylene	205	56	5.9	−4.35	−6.77	−7.30	3.47	−4.67	20
Polystyrene	373	104	7.4		2.06	−2.54	2.06	−6.95	21
Poly(vinyl acetate)	305	86	6.9		−4.87	−5.98	4.29	−6.32	23
Poly(methyl acrylate)	276	86	6.8	0.32	−5.99	−6.83	6.24	−6.24	25
Poly(vinyl chloride)	347	62.5	6			−4.57	4.05[j]	−7.46	26
Polyhexene-1	218	84	7	−4.72				−5.48	27
Poly(1,1-dihydroperfluorobutyl acrylate)		308	8	−4.7					28
Poly(dimethyl siloxane)	150	74	6.2	−8.05	−8.55	−8.66	−3.60	−7.50	30
Poly(ethylene oxide)		44			<−6.4				51

[a] Lightly vulcanized with dicumyl peroxide.
[b] Cis:trans:vinyl = 43:50:7, lightly vulcanized with dicumyl peroxide.
[c] Random copolymer, 23.5% styrene.
[d] Lightly cross-linked with sulfur.
[e] Ethylene:propylene = 16:84, by mole.
[f] Ethylene:propylene = 56:44, by mole.
[g] Copolymer of adipic acid and ethylene and propylene glycols, cross-linked by naphthalene 1,4-diisocyanate and 1,4-butanediol.
[h] M_0/a estimated to be 12×10^8.
[i] Estimated to be −7.2 at 335°K.
[j] Difficult to estimate reliably because c_1^g and c_2^g uncertain; based on "universal" values.

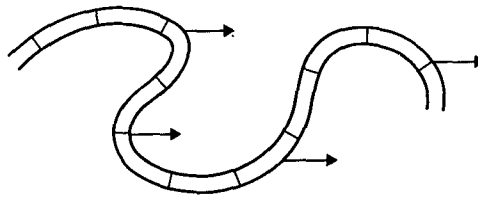


FIG. 12-5. Sketch to illustrate definition of monomeric friction coefficient ζ_0: a group of n monomer units moving together with translational velocity v encounter a frictional force of $n\zeta_0 v$. Reproduced, by permission, from *Science and Technology of Rubber*, edited by F. R. Eirich, Academic Press, 1978.

culation are also listed. It is impossible to compare all the systems at any one temperature, but at 398°K, where a majority are comparable, ζ_0 in dynes-sec/cm ranges from the order of 1 to 10^{-9}. The significance of the friction coefficient, measuring the average force per monomer unit required for a chain segment to push its way through its local surroundings at unit velocity, is recalled by the crude diagram of Fig. 12-5. Since the frictional force is due to other similar polymer segments, it must depend on the free volume and/or intermolecular forces and steric hindrances to rotations around free bonds. Comparison of log ζ_0 for the poly(methyl methacrylate)s with the far smaller value for poly(methyl acrylate) at 398°K shows the marked steric blocking of the extra methyl group in the former. The steric effects in the poly(methyl methacrylate)s depend greatly on the tacticity, the isotactic having a higher friction coefficient over most of the temperature range; this may be associated with a helical structure with strong coupling of the side group dipole to the chain backbone.[47] In the methacrylate series from methyl to *n*-docosyl, there is a progressive decrease in frictional resistance with increasing side chain length. In this series, with the steric blocking near the backbone and some degree of polarity in intermolecular forces, it is necessary to have an ester side group with 12 carbon atoms (log $\zeta_0 = -4.69$ at 298°) to achieve the same mobility as in polyhexene-1 with a hydrocarbon group of 4 atoms and no extra methyl substituent (log $\zeta_0 = -4.72$ at 298°K). A few other comparisons may be noted. In the ethylene-propylene copolymers, increasing the ethylene content from 16 to 56 mole percent lowers the friction coefficient by a factor of 10 at 373°K or 398°K. (At still higher ethylene contents, crystallinity develops and the viscoelastic properties become entirely different.) Of the polybutadiene isomers, the 1,2 configuration has a higher friction coefficient by a factor which at 298°K is over 400, though it diminishes with increasing temperature. This difference is probably primarily due to the double bonds in the chain backbone of the 1,4 configuration; although there is no rotation around the double bond itself, the adjacent single bonds have unusually low steric hindrance to rotation. Other polybutadiene microstructures with varying proportions of *cis*, *trans*, and vinyl will be discussed in Section B5 below. In general, friction coefficients of polymers with related structures approach each other with increasing temperature because the higher friction coefficient is usually associated with a higher glass transition temperature and therefore falls more rapidly for a given temperature increment.

2. Relation of Friction Coefficient to Free Volume in the Methacrylate Series

Since the dependence of the friction coefficient on temperature, pressure, molecular weight (at low molecular weights), and small amounts of diluent can be described in terms of the free volume, it is of interest to examine whether its variation with chemical composition in a homologous series such as that of the methacrylates can be explained in a similar manner. With increasing side group length, the local packing undoubtedly becomes less efficient, and of the rather large increase in specific volume v progressing from the ethyl to the dodecyl polymeric ester ($v = 0.917$ to $v = 1.127$ cc/g at 100°C) some can be attributed to an increase in empty space.[52]

The effect of increased free volume due to side group extension on the friction coefficient may be inferred from equation 49 of Chapter 11 (with $B = 1$) to be

$$\Delta_i \log a^2\zeta_0 \equiv \log (a^2\zeta_0)_i - \log (a^2\zeta_0)_R = (1/2.303)(1/f_i - 1/f_R) \qquad (3)$$

where $\Delta_i \log a^2\zeta_0$ is the analog of a_T or a_P, since all relaxation times are proportional to $a^2\zeta_0/T$ (equation 3 of Chapter 11) and we are now considering comparisons at constant temperature; f_i is the fractional free volume of the ith member of the series, and f_R that of a particular member chosen as a reference. On this basis, the data for the methacrylate series have been analyzed by Dannhauser, Child, and Ferry[8] and by Fujita and Kishimoto.[53] The two treatments differ somewhat; the latter, being more general, is employed here. If the reference polymer is chosen as that with the highest T_g and the latter temperature is chosen for the comparisons, it can be shown from equation 3 (provided f_g is the same for all members of the series) that

$$-1/\Delta_i \log a^2\zeta_0 = 2.303 f_g + 2.303 f_g^2/\Delta\alpha_i \Delta T_{gi} \qquad (4)$$

where $\Delta\alpha_i$ is the change in thermal expansion coefficient at T_g for the ith polymer, and $\Delta T_{gi} = T_{gR} - T_{gi}$. It follows that a plot of the left side of equation 4 against $1/\Delta\alpha_i \Delta T_{gi}$ should be linear and f_g should be calculable from both its intercept and its slope.

Data for this purpose[9] (not the same set originally used by Fujita and Kishimoto) are assembled in Table 12-IV. It may be remarked that the quantity $a^2\zeta_0$ is directly obtainable from the intercepts of the tangents in Fig. 12-4 without specification of the somewhat uncertain parameter a, and is therefore better determined experimentally than ζ_0 itself. The quantity $\Delta\alpha_i$ was taken as 2.4×10^{-4} for all the polymers. The results are plotted in Fig. 12-6, and a moderately good line is obtained; from its intercept, f_g is calculated to be 0.026, and from its slope 0.018. The reasonable agreement between these values and these of 0.025 to 0.027 obtained from the analysis of temperature dependence (Table 11-II) lends confidence to the view that the enhancement of mobility with increasing side group length is primarily due to the increase in free volume.

In the table, values for the increase in f and in v with side group length are also given, leading to the conclusion that of the order of 15% of the increase in v is attributable to f. This estimate had already been made by Rogers and Mandelkern[52]

Table 12–IV

DATA FOR FUJITA-KISHIMOTO PLOT FOR POLY(ALKYL METHACRYLATE)S

Polymer	Ethyl	Butyl	2-Ethyl Butyl	Hexyl	Octyl	Dodecyl
$\log a^2\zeta_0$ at T_g for ethyl	−8.24	−15.03	−15.50	−17.60	−18.71	−19.45
ΔT_{gi}	0	35	51	67	82	108
$f_i - f_R$ at T_g for ethyl	0	0.008	0.005	0.016	0.020	0.026
$v_i - v_R$ at T_g for ethyl	0	0.073		0.117	0.122	0.141
$(f_i - f_R)/(v_i - v_R)$		0.11		0.14	0.16	0.18

and formed the basis of the analysis of Dannhauser, Child, and Ferry,[8,9] in which the free volumes at 100° (far above T_g for all the polymers) were calculated both from equation 2 and from dilatometric measurements, with reasonable agreement.

It may be noted that the point for poly(2-ethyl butyl methacrylate) in Fig. 12–5 falls above the line; the friction coefficient for this polymer with branched side

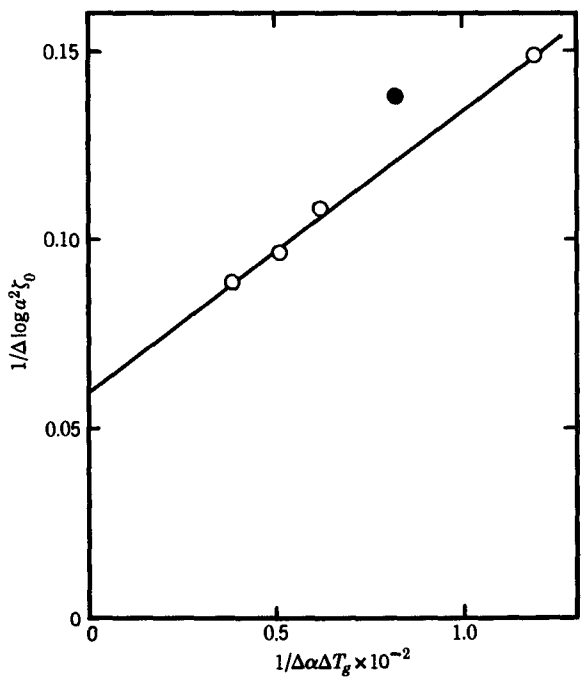


FIG. 12–6. Fujita-Kishimoto plot for the methacrylate series, with the ethyl polymer as reference. Black circle: 2-ethylbutyl polymer.

groups is thus somewhat larger than would be expected from free volume alone on the basis of the *n*-alkyl series. Also, the free volume appears to be abnormally small. Striking effects of side chain flexibility on friction coefficient can also be inferred from the isochronal data on isomeric poly(vinylbutyl ether)s shown in Fig. 12-3.

Attempts to correlate the friction coefficient at constant temperature with free volume for other polymers with widely different chemical structures are not particularly instructive, although for a group of hydrocarbon polymers a good correlation can be obtained.[54]

3. Comparisons at Corresponding Temperatures

If ζ_0 were a function of free volume alone, all polymers should have the same ζ_0 when compared each at its own T_g, since f_g is similar for all (Table 11-II).

This is not quite a fair statement since ζ_0 is the coefficient per monomer unit and a large monomer should encounter more frictional force, other things being equal, than a small one. However, by analogy with Stokes' law we should expect the effects of size to be proportional to the cube root of the molecular volume—a small variation among most of the systems in Table 12-III.

If T_g is chosen as a corresponding temperature at which different polymers are to be compared, the calculation of ζ_0 involves reduction of the time scale by extrapolation, since experimental measurements in the transition zone cannot easily be made at T_g directly. In most cases the extrapolation can be made by the WLF equation and the coefficients of Table 11-II. The results are included in Table 12-III, and show that even when compared each at its own T_g polymers can still have different monomeric friction coefficients. In particular, ζ_{0g} decreases with increasing side chain length in the polymethacrylate series, although it appears to be approaching a limiting value. (Recent work[138] casts doubt on some of the T_g values used in this Table, especially for poly(methyl acrylate) and poly(methyl methacrylate), and the values for ζ_0 at T_g will require future revision.

It is clear that the friction coefficient does not depend on free volume alone. It is doubtful whether a detailed interpretation of values reduced to T_g should be attempted, however, since the extrapolation of the time scale is somewhat uncertain and moreover the specification of T_g is sensitive to thermal history and especially to traces of diluents (Chapter 17), including water vapor in the case of polar polymers. These difficulties are avoided by choosing as a corresponding temperature T_g plus a constant, such as 100°. The choice of the increment is arbitrary, but 100° makes the corresponding temperature fall generally within the range where experiments were actually conducted so usually no extrapolated reduction is necessary. Comparisons at T_g + 100° are also included in Table 12-III and are ordered on a vertical scale in Fig. 12-7. Again, the values range over several orders of magnitude; most are between 10^{-7} and 10^{-4} dynes-sec/cm (10^{-10} and 10^{-7} N-sec/m).

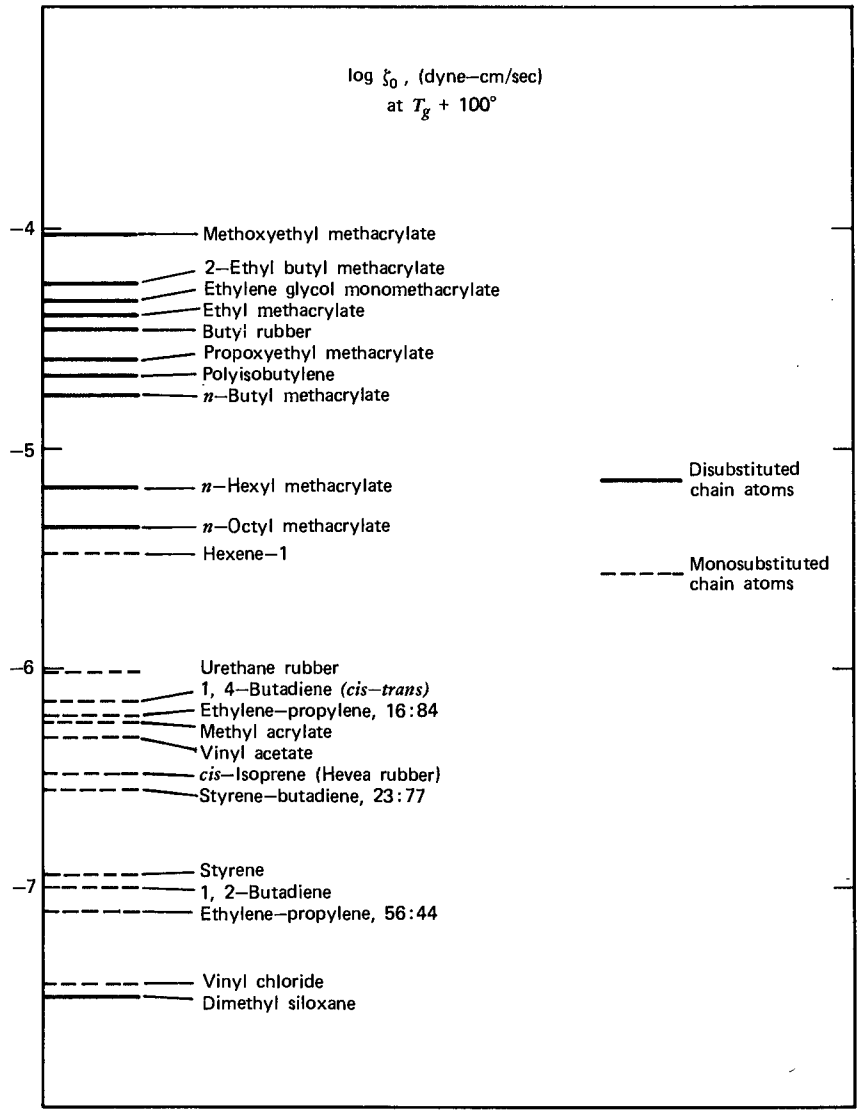


FIG. 12-7. Ordering of log ζ_0 to T_g + 100° on a vertical scale for various polymers. Solid lines, disubstituted chain atoms; dashed lines, monosubstituted chain atoms.

It is notable that, with two exceptions, 10^{-6} dynes-sec/cm is the dividing line between polymers with disubstituted backbone chain atoms (methacrylate polymers, polyisobutylene) and those with monosubstituted backbone atoms. The presence of two substituents on the same chain atom probably introduces substantial steric hindrances to internal rotation, as can be inferred from molecular models. (A striking exception is poly(dimethyl siloxane), which is in a class by itself at the bottom of the order.) There does not seem to be any particular correlation with the

strength of intermolecular forces as measured, for example, by the cohesive energy density. The latter property is reflected in the magnitude of T_g, of course, but is apparently eliminated by comparing friction coefficients at temperatures equally removed from T_g.

It is possible that a more detailed knowledge of local packing geometry could help interpret the range of values observed in Fig. 12–7. The average fractional free volume 100° above T_g, as calculated from f_g and α_f in Table 11–II, differs somewhat from one polymer to another, but the detailed disposition of the free volume may differ much more, in some cases facilitating certain configurational changes more than others.

It may be of interest to make a very crude calculation of the effective local viscosity η_e at the glass transition temperature based on Stokes' law for an isolated sphere of radius r: $\zeta_0 = 6\pi\eta_e r$. For a molar volume of 100 cc and $\log \zeta_0 = 6$, the effective viscosity is 1.6×10^{12} poises, which is not far from the level of 10^{13} often specified as the *macroscopic* viscosity characteristic of the glass transition.[55] This suggests that 10^6 dynes-sec/cm or 10^3 N-sec/m may be nearly an upper limit for ζ_0 at T_g. By contrast, Stokes' law estimates at temperatures well above T_g give local viscosities far smaller than the macroscopic viscosity, as will be seen in the comparisons with diffusion data in Section 5 below.

4. Estimation of ζ_0 from the Steady-Flow Viscosity

According to the modified Rouse theory of Section A1 of Chapter 10, for uncross-linked polymers of sufficiently low molecular weight to avoid entanglements, the monomeric friction coefficient is related to the steady-flow viscosity by the following equation, which can be obtained from equations 4 and 10 of Chapter 10 and was originally derived by Bueche.[56]

$$\zeta_0 = \frac{36M_0}{\rho r_0^2 N_0}\eta_0 = \frac{36M_0^2}{\rho a^2 M N_0}\eta_0 \tag{5}$$

where N_0 is Avogadro's number. To obtain the limiting value of ζ_0 for molecular weights sufficiently high to avoid the effects of free ends (ζ_{00} in equations 14 of Chapter 10 and 68 of Chapter 11), it is convenient to take the viscosity at a molecular weight just below the critical value M_C for onset of entanglement coupling, *i.e.*, just below the change in slope in Figs. 10–10 and 10–11. This calculation has been made for several polymers by Berry and Fox[57] (though expressed in somewhat different form; their ζ_0 is proportional to ours but defined differently).

Some results are compared in Table 12–V with values obtained from equation 1, and they agree within about a factor of 3, though the calculation from viscosity is consistently higher. Since the two sources of data involve entirely different experiments and polymers in very different molecular weight ranges, and the calculations involve two quite different applications of the modified Rouse theory, even this degree of conformity is reassuring. It suggests that, in the absence of viscoelastic data, the friction coefficient can be estimated simply from data on the steady-flow viscosity provided the molecular weight of the sample is chosen correctly. (The

Table 12-V

COMPARISON OF MONOMERIC FRICTION COEFFICIENTS FROM RELAXATION SPECTRUM IN TRANSITION ZONE AND FROM VISCOSITY AT LOW MOLECULAR WEIGHTS

Polymer	Temperature, °K	$\log \zeta_0$ at 373°K	
		From H (Table 12-II)	From Equation 5
Poly(methyl acrylate)	298	0.32	0.0
Poly(vinyl acetate)	373	−4.87	−4.1
Poly(*n*-butyl methacrylate)	373	−3.44	−2.9
Polyisobutylene	298	−4.35	−3.7
Poly(dimethyl siloxane)	298	−8.05	−7.6
			−7.83[a]

[a] Reported by Kataoka and Ueda.[58]

molecular weight distribution should be fairly sharp to avoid complications from free ends of low molecular weight species and entanglements of high molecular weight species respectively.) Such an estimation may be important for practical purposes because the friction coefficient sets the time scale of the transition zone for all viscoelastic properties. Another independent method for estimating the friction coefficient is described in the following section.

5. Correlation of ζ_0 with Data from Diffusion of Small Foreign Molecules

Though ζ_0 is normally determined by mechanical measurements, it is evident from its definition that it is related in a simple manner to translatory diffusion, and in principle it can be determined from self-diffusion measurements in a polymer with sufficiently low molecular weight to avoid entanglements. Some data of this sort have been obtained from diffusion of radioactively tagged molecules[59,60] and spin-echo nuclear magnetic resonance measurements,[61-63] as well as from diffusion of deuterated molecules whose concentration can be followed by infrared absorption.[64] They yield the product $P\zeta_0$, since the frictional resistance for the entire molecule is measured.

A much easier experiment involves measuring the diffusion coefficient of a small foreign molecule, similar in size to the monomer unit or an oligomeric unit of several chain atoms, through the polymer. If this penetrant is introduced in trace amounts (of the order of 1% or less), the molecules diffusing down a concentration gradient may be regarded as pushing their way individually past the polymer segments. The frictional resistance they encounter will be closely related to that experienced by the polymer segments themselves in their random thermal motions (*i.e.*, ζ_0). Under these conditions, the friction coefficient of the foreign molecule is simply given by

$$\zeta_s = kT/D_s \tag{6}$$

where D_0 is the diffusion coefficient at vanishing concentration of penetrant (which is free of complications arising from thermodynamic nonideality[65,66] or ambiguity of frames of reference[67]). Such conditions are fulfilled also when a radioactively tagged solvent is used in a solution of constant chemical composition[68-71] and in the application of spin-echo nuclear magnetic resonance.[61,63,72] On the other hand, when diffusion is measured by transpiration or absorption-desorption,[73-77] an extrapolation must be performed to obtain D_0 from data at finite concentrations.

Naturally ζ_1 depends on the size and shape of the foreign molecule, and for very large molecules the dependence can be quite marked.[78,79] However, for normal paraffin chains ζ_1 is approximately directly proportional to molecular length,[63,68,80] corresponding to the principle that the friction encountered by a polymer segment is proportional to its length, upon which the definition of ζ_0 is based. (For quite short chains the dependence appears to be somewhat less.[74]) Thus by choosing a foreign molecule similar in structure and length to the monomeric unit of the polymer, a comparison can be obtained between an isolated unit and one which is an integral part of the polymer backbone.

Some information collected from the literature for this purpose[66,69] is given in Table 12-VI. In some cases, the chemical similarity between foreign molecule and polymer is not very close because of the paucity of available data. However, it appears that for temperatures *far above* T_g, as in the polyisobutylene and rubber, the friction coefficients ζ_0 and ζ_1 for the chain unit and for a foreign molecule of like size are closely similar. This leads to the conclusion that the monomeric friction coefficient reflects almost wholly the force of pushing aside neighboring chains of the environment, and to a negligible extent the difficulty of articulating the chain in which the monomer unit is located.

When the temperature is closer to T_g, however, the friction coefficient for the smaller molecule is considerably smaller than that for the chain unit, to a degree which is substantial for $T - T_g \cong 50$ and quite large for $T - T_g < 40$. This effect is accompanied by a growing discrepancy between the apparent activation energies for diffusion and viscoelastic relaxation, the former usually being the smaller.[66,69] It has been tentatively attributed[66] to additional local free volume in the immediate vicinity of a foreign molecule due to inefficient packing.[81] For a vanishing concentration of the low molecular weight component, the extra space is too small to affect the overall average free volume perceptibly, but it occurs in just the right places to facilitate motion of the small molecules. Near T_g, where the average free volume is small, this is supposed to be a very important influence. Far above T_g, on the other hand, where f may be several times as large as its value near T_g, the small molecule has no significant advantage over the polymeric chain unit; the friction coefficient is determined by f alone.

Additional examples of ζ_1 for *n*-hexadecane in various rubbers,[54] most of them studied far above T_g, are given in Table 12-VII and compared with the corresponding values of ζ_0. Here the penetrant has 3 to 4 times the molecular weight of the chain unit, but ζ_0 and ζ_1 are quite similar over a range of nearly four powers of 10. Even the 1,2-polybutadiene, which is fairly near T_g, shows no great discrepancy. That they are so similar in magnitude is somewhat unexpected, but that

Table 12–VI

MOLECULAR FRICTION COEFFICIENTS FROM DIFFUSION IN POLYMERS COMPARED WITH MONOMERIC FRICTION COEFFICIENTS

Polymer	Temperature °K	$T - T_g$	Diffusing Unit	Mol. Wt.	$\log \zeta_1$	$\log \zeta_0$	Ref.
Polyisobutylene	298	96	*n*-Butane	58	−4.46		75
			i-Butane	58	−4.11		75
			n-Pentane	72	−4.42		75
			Chain unit	56		−4.35	*a*
Hevea rubber	303	103	*n*-Butane	58	−6.74		74
			i-Butane	58	−6.56		74
			n-Pentane	72	−6.74		74
			Chain unit	68		−6.90	*a*
Poly(methyl acrylate)	323	47	Ethyl alcohol	58	−3.69		76
			Chain unit	86		−3.15	*a*
Poly(vinyl acetate)	313	8	*n*-Propyl alcohol	60	−1.41		77
			n-Propyl chloride	79	−1.49		77
			Chain unit	86		1.75	*a*
Poly(vinyl acetate)	343	38	Ethyl chloride	65	−4.63		76
			Ethyl bromide	109	−4.37		76
			Chain unit	86		−2.63	*a*
Poly(*n*-hexyl methacrylate)	298	30	*n*-Hexadecane	226	−4.96		69
			Chain unit	170		−0.75	*a*
Poly(*n*-octyl methacrylate)	298	45	*n*-Hexadecane	226	−5.58		69
			Chain unit	198		−2.29	*a*
Poly(*n*-dodecyl methacrylate)	298	50	*n*-Hexadecane	226	−5.75		69
			Chain unit	254		−4.69	*a*

[a] From the values in Table 12–III, reduced where necessary to different temperatures by the data of Table 11–II.

they are roughly proportional over a wide range is a reassuring confirmation of the significance of the friction coefficient in governing the rates of molecular motions. The apparent activation energies for diffusion and viscoelastic relaxation were also found to be closely similar for all these polymers except Hevea rubber, for which the former was somewhat smaller.[54] According to the free-volume interpretation[82] (*cf.* equation 73 of Chapter 11 and associated discussion), the ratio of B_d/B is 0.64 for Hevea rubber, but close to unity for the others. A similar value of B_d/B for polyisoprene has been found from pulsed field-gradient spin-echo nuclear magnetic resonance measurements.[63]

Table 12–VII

MOLECULAR FRICTION COEFFICIENTS AT 298°K FROM DIFFUSION OF *n*-HEXADECANE IN RUBBERS COMPARED WITH MONOMERIC FRICTION COEFFICIENTS[54]

Polymer	$T - T_g$	$\log \zeta_1$	$\log \zeta_0$
Poly(dimethyl siloxane)[a]	148	−7.59	−8.05
1,4-Polybutadiene[b]	126	−6.73	−6.75
Hevea rubber[a]	98	−6.27	−6.41
Styrene-butadiene rubber[c]	88	−5.81	−6.11
1,2-Polybutadiene	37	−4.36	4.11
Polyisobutylene	93	−4.17	−4.35

[a] Extrapolated to zero cross-linking from measurements on lightly cross-linked samples for which the dependence on cross-linking was very slight.

[b] Cis:trans:vinyl = 43:50:7.

[c] Random copolymer, 23.5% styrene.

It is of particular interest to compare polyisobutylene and Hevea rubber, both hydrocarbons with almost identical glass transition temperatures. At 25°, the monomeric friction coefficient of the latter is smaller by more than 2 orders of magnitude. Exactly the same difference appears in the diffusion friction coefficients for butane and pentane (Table 12–VI) and hexadecane (Table 12–VII), as well as dodecane.[54] Thus the higher mobility of the rubber backbone appears as a decrease in the effective local viscosity surrounding a given chain segment rather than an "internal" viscosity of the chain segment itself. If crude Stokes' law estimates of the effective viscosity are made as described above, they provide values of 80 and 0.2 poises, respectively, for the polyisobutylene and the rubber. These clearly bear no relation to the macroscopic viscosity, which depending on the molecular weight might be as high as 10^{10} for the former, and for the latter (if cross-linked) essentially infinite.

If Stokes' law is applied to translational friction, in a polymer matrix, of spherical bodies with various sizes increasing from molecular up to macroscopic dimensions, the effective viscosity η_e must increase by many orders of magnitude and eventually attain the macroscopic value. This phenomenon has been observed in measurements of diffusion[78,83] as well as centrifugation.[79,84] Kuhn[85] has pointed out that the increase in η_e with the size of the moving unit is analogous to the increase in the (macroscopic) dynamic viscosity η' with decreasing frequency as it reflects configurational rearrangements coordinated over increasingly large distances.

Since diffusion measurements are far easier to make than the viscoelastic measurements which are needed to determine ζ_0, they may be useful for practical purposes to estimate ζ_0 under certain circumstances, for predicting the time scale of the transition zone of viscoelastic properties. For example, measurements on 34 polybutadienes and random styrene-butadiene copolymers with different bu-

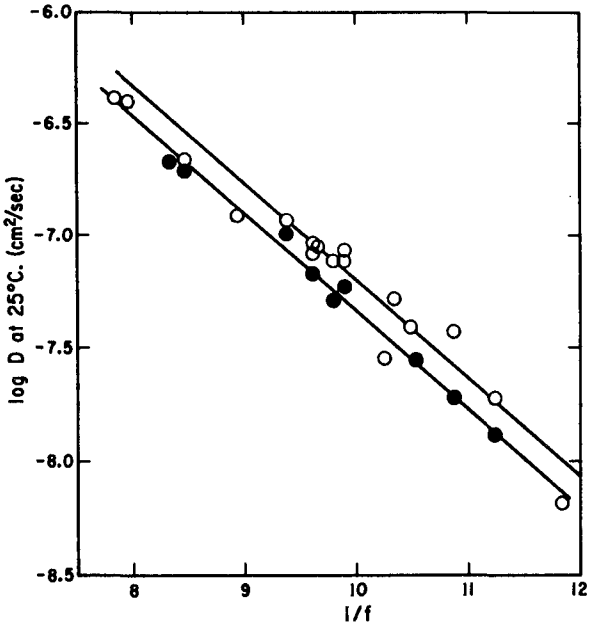


FIG. 12-8. Diffusion coefficient of *n*-hexadecane at 25°C through random styrene-butadiene copolymers plotted against reciprocal of fractional free volume calculated from equation 8. Open circles, uncross-linked samples; black circles, cross-linked. Lines drawn with slope of $-1/2.303$ as specified by equation 7. (Rhee and Ferry.[86]) Reproduced, by permission, from the Journal of Applied Polymer Science.

tadiene microstructures and styrene contents[54,86] established the relation (*cf.* equations 70 and 72 of Chapter 11)

$$\log D_0 = \log A_d - B_d/2.303f \qquad (7)$$

where f is calculated on the basis of additivity of the fractional free volumes of the structural components:

$$f = w_B(f_c c + f_t t + f_v v) + w_S f_S \qquad (8)$$

Here w_B and w_S are the weight fractions of butadiene and styrene and c, t, and v are the proportions of cis, trans, and vinyl microstructure in the butadiene moiety; the f's with subscripts correspond to the fractional free volumes of the pure species (hypothetical for styrene since the homopolymer would be below its T_g at the temperature of measurement). The values assigned are $f_c = 0.128$, $f_t = 0.122$, $f_v = 0.063$, and $f_S = 0.045$ at 25.0°C. A plot of log D_0 against $1/f$ establishes $B_d = 1$, as shown in Fig. 12-8. From this information, the dependence of ζ_0 on composition can be predicted for any random copolymer of known structure.

6. Relation of ζ_0 to the Onset of the Transition Zone

For practical purposes, it is often useful to locate the boundary on the frequency or time scale between the plateau and transition zone. An arbitrary specification

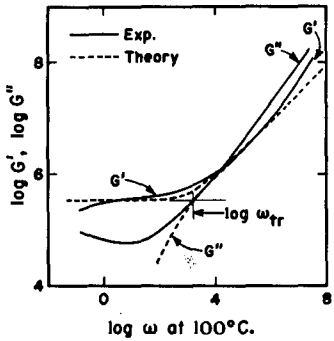


FIG. 12-9. Logarithmic plots of G' and G'' against frequency near the onset of the transition zone, enlarged from curves IV of Figs. 2-3 and 2-4, for poly(*n*-octyl methacrylate) at 100°C. Dashed curves drawn from Rouse-Mooney theory (Section B-1 of Chapter 10). Reproduced, by permission, from the same source as Fig. 12-5.

of this point can be designated as the intersection of two lines with slopes 0 and $\frac{1}{2}$ matched to a logarithmic plot of G' against frequency,[87] as illustrated in Fig. 12-9 for poly(n-octyl methacrylate) at 100°C (enlarged from curves IV of Figs. 2-3 and 2-4). If the Rouse-Mooney theory (Section B-1 of Chapter 10) applies, as represented by the dashed curves, the onset frequency ω_{tr} is equal to $8/\pi^2\tau_{tr}$, where τ_{tr} is the longest relaxation time in the transition zone. Combination with equation 37 of Chapter 10 gives

$$\omega_{tr} = 48kT/a^2P_c^2\zeta_0 \tag{9}$$

for a cross-linked polymer or, for an uncross-linked polymer of high molecular weight, the same with P_c replaced by P_e. At frequencies above ω_{tr}, viscoelastic losses will be prominent.

C. SHAPES OF THE SPECTRA AND VISCOELASTIC FUNCTIONS IN THE TRANSITION ZONE

We may now examine some detailed shapes of viscoelastic functions. For this purpose, it is convenient to reduce different polymers to corresponding states in which those portions of their relaxation spectra conforming to the flexible chain theories coincide.

1. Relaxation Spectra Reduced to Corresponding States

In equation 40 of Chapter 10, the time scale is set by the product $a^2\zeta_0/T$ (*cf.* also the discussion associated with equation 2 of the present chapter); in fact, $a^2\zeta_0/kT$ has the dimensions of time. The other quantities in equation 40 of Chapter 10 which may vary from one polymer to another appear as the ratio $T\rho/M_0$, *i.e.*, temperature times the moles of monomer units per cubic centimeter, which may be regarded as determining the magnitudes of contributions to H. Decreasing ρ/M_0 by having

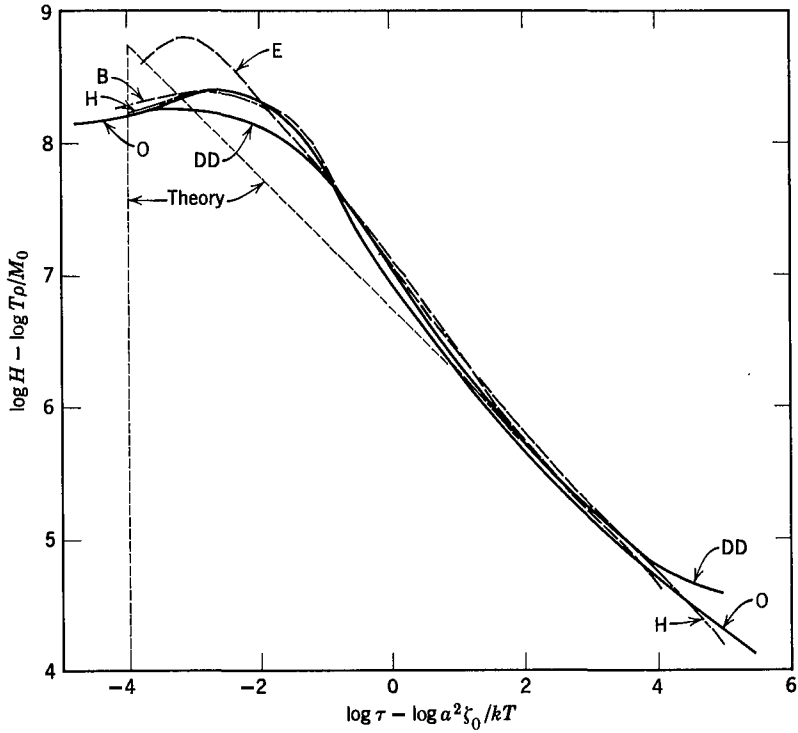


FIG. 12-10. Relaxation spectra of Fig. 12-4 reduced to corresponding states in which the portions at the long-time end of the transition zone coincide in accordance with the Rouse theory. Dotted line is the prediction of the modified Rouse theory with cutoff at minimum relaxation time of Marvin model.[88] Curve for 2-ethyl butyl polymer is indistinguishable from that for butyl to the right of maximum, and from that for octyl to the left.

a smaller density or larger monomeric molecular weight is equivalent to diluting the concentration of polymer chains and decreasing the magnitudes of all contributions to H proportionally; decreasing T also decreases H in proportion because of the entropy character of the elastic contributions.

Accordingly, the equation can be rearranged as follows:

$$[\log H - \log T\rho/M_0] = \log (R/2\pi)(\tfrac{1}{6})^{1/2} - \tfrac{1}{2}[\log \tau - \log a^2\zeta_0/kT] \quad (10)$$

a universal function of the variables expressed in brackets. Although this theoretical equation is valid only for the linear segment of the relaxation spectrum which conforms to the Rouse slope of $-\frac{1}{2}$ on a doubly logarithmic plot, where data for all polymers will coincide if plotted with the above reduced variables, it is of interest to examine how far coincidence will occur over wider ranges where deviations from the Rouse slope appear.

The relaxation spectra of the six methacrylate polymers of Fig. 12-4 are plotted in this manner[8-10] in Fig. 12-10. Their shapes coincide rather closely throughout the transition zone, though the maxima for the ethyl (experimentally uncertain)

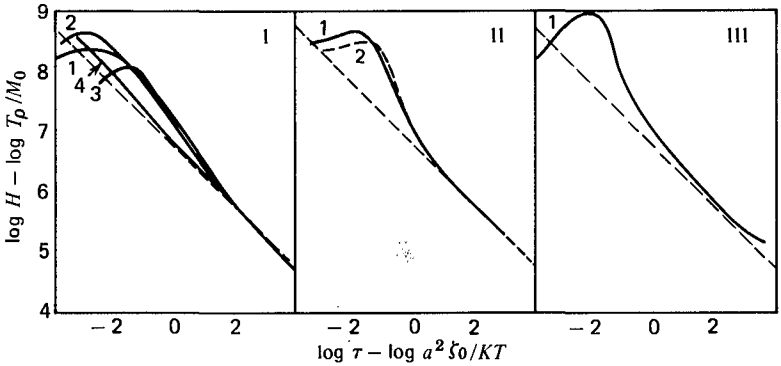


FIG. 12-11. Relaxation spectra of various polymers reduced to corresponding states. Panel I: (1) composite methacrylate polymers; (2) polyisobutylene; (3) polyhexene-1; (4) polyurethane rubber. Panel II: (1) poly(vinyl acetate); (2) poly(methyl acrylate). Panel III: (1) Hevea rubber.

and for the dodecyl are somewhat higher and lower, respectively, than the others. The straight line predicted by the Rouse theory up to the minimum relaxation time specified by the modified model of Marvin[88] (Chapter 10, Section D) is drawn in for comparison. For the latter purpose, log $G_g M_0/\rho$ was taken as 11.80, an approximation based on inspection of Fig. 12-1. It is evident that the deviations from the simple theoretical shape are of much the same character for all the methacrylates. The important conclusion may be drawn that these deviations are characteristic primarily of the polymer chain backbone rather than side group packing or cohesive energy density, both of which vary greatly in progressing from the ethyl to the dodecyl ester.

A wider variety of such comparisons is shown in Fig. 12-11, where the deviations from the simple linear spectrum appear to fall into three classes. The smallest upward curvature is exhibited by the group consisting of a polyurethane rubber,[19] polyisobutylene,[20] polyhexene-1,[27] and the methacrylate series (from Fig. 12-10). Sharper deviations are shown by poly(vinyl acetate)[23] and poly(methyl acrylate);[25] whereas Hevea rubber[12] shows very marked deviations with a steep slope far removed from the theoretical value of $\frac{1}{2}$. The first group (except for polyhexene-1, which appears anomalous because the maximum is abnormally low) is characterized by doubly substituted carbon atoms in the backbone (polyisobutylene, polymethacrylates) or essentially no substitution at all (polyesters composing the polyurethane). The second is characterized by monosubstituted backbone atoms (with presumably less hindrance to rotation than the disubstituted), whereas the third is characterized by the unusual rotation freedom of the unsaturated polybutadiene chain which has already been emphasized. Thus the shapes of the spectra appear again to be determined primarily by the nature of the chain backbone. It is still impossible, however, to go very far in making generalizations, and there is no theoretical guide to the magnitudes of the divergences.

It may be noted that the shape of the relaxation spectrum in the transition zone is also modified by the presence of diluent (Chapter 17) and also by cross-linking if the latter is made sufficiently dense.

2. Relation of the Shape of H to Those of Other Viscoelastic Functions

It is unnecessary to reproduce the general forms of the viscoelastic functions $G(t)$, $J(t)$, G', G'', etc. in the transition zone, since these have already been seen in Chapter 2; also, J' and J'' have been portrayed in detail in Figs. 11-3 and 11-5.

Even without an analytical expression to describe the shape of H, it is clear that increasing steepness of H in the transition zone as portrayed in Fig. 12-11 will be accompanied by a compression of the transition from rubberlike to glasslike consistency into a narrower region of logarithmic time scale. Plots of both transient and dynamic moduli and compliances, as exemplified in Chapter 2, rise and fall with steeper slopes. Perhaps the most sensitive index of the sharpness of the transition is the loss tangent, which is plotted in Fig. 12-12 for several prototypes: the polyurethane rubber, poly(*n*-octyl methacrylate), poly(vinyl acetate), and Hevea rubber. Here the frequency scale has been arbitrarily selected to make the maxima coincide. The sharpness in the loss maximum correlates with the slope of H in the transition zone. The shape emphasizes the failure of the modified Rouse theory to provide a detailed description of the properties in the transition zone, since it predicts $\tan \delta = 1$ independent of frequency in this region. The drop in $\tan \delta$ at high

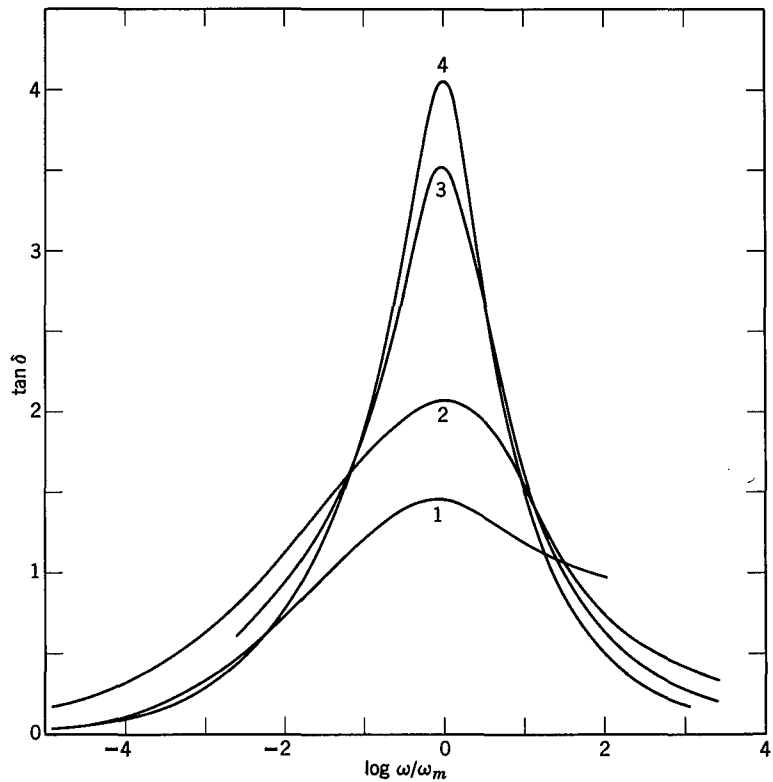


FIG. 12-12. Loss tangent in the transition zone plotted against frequency for (1) polyurethane rubber, (2) poly(*n*-octyl methacrylate), (3) poly(vinyl acetate), (4) Hevea rubber.

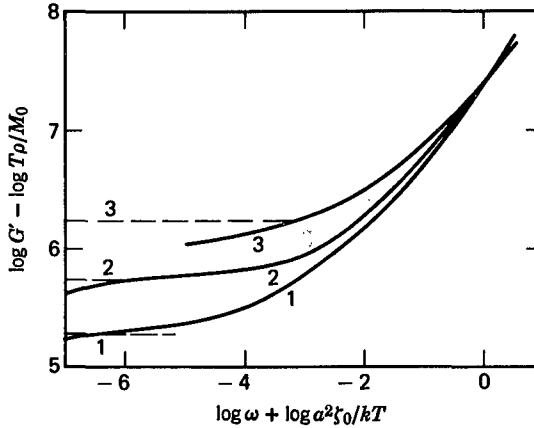


FIG. 12-13. Storage modulus plotted logarithmically against frequency after reduction to corresponding states as in Figs. 12-10 and 12-11. (1) Poly(*n*-octyl methacrylate); (2) polyisobutylene; (3) ethylene-propylene copolymer with 56% ethylene. Dashed lines represent $-\log J_N^0 - \log T\rho/M_0$ (*cf.* Table 13-1).

frequencies is associated with entrance into the glassy zone; the drop at low frequencies is associated with the entanglement network in uncross-linked polymers of high molecular weight, without which the loss tangent would increase monotonically with decreasing frequency.

From the latter statement it is evident that the behavior of the viscoelastic functions of an uncross-linked polymer in the long-time or low-frequency end of the transition zone will depend not only on the shape of H but also to some degree on the density of the entanglement network, as reflected for example in the effective modulus $G_N^0 = 1/J_N^0$, where J_N^0 is the plateau level of the compliance which has been mentioned in Chapters 2 and 10 will be discussed in detail in Chapter 13. This feature is illustrated in Fig. 12-13 by plots of G' for three polymers with quite different values of J_N^0 (derived as described in Chapter 13). The frequency scales are reduced by the factor $a^2\zeta_0/kT$ and the modulus by $T\rho/M_0$ as in Figs. 12-7 and 12-8, to provide corresponding states. Without such reduction, the vertical differences would be even greater. Whereas increasing steepness of H compresses the transition zone into a narrower region of time or frequency scale, increasing entanglement density (decreasing J_N^0) compresses it into a narrower range of magnitudes. For cross-linked polymers, the corresponding statement is that with increasing cross-link density the range of magnitudes of compliance or modulus encompassed by the transition zone becomes narrower. In an extreme case of high cross-linking,[89,90] the magnitude of the modulus may be as high as 10^9 dynes/cm^2 in the "rubbery" zone, so the transition zone involves a change only from 10^9 to 10^{10}. Here the network strands are so short that their rearrangements could not possibly be described by the Rouse theory, but the qualitative features of viscoelastic behavior are similar to those described above.

If the sharpness of the transition from rubberlike to glasslike behavior is examined

by mechanical measurements expressed as a function of *temperature* at constant time or frequency, as in Fig. 12–3, it must be remembered that this depends both on the steepness with respect to time as illustrated in Fig. 12–11 or Fig. 12–12 and on the rate of change of a_T in the particular temperature range concerned.

Empirical analytical expressions have sometimes been used to represent viscoelastic functions in the transition zone, especially the relaxation modulus $G(t)$.

The error function representation of Tobolsky,[91] which reproduces rather closely the observed curvature in the transition region, gives for $G(t)$

$$\log G(t) = (\log G_g + \log G_e)/2 - [(\log G_g - \log G_e)/2] \operatorname{erf} h \log (t/K) \quad (11)$$

where G_g is the glassy modulus and G_e is the equilibrium modulus if cross-linked; if uncross-linked, G_e should be replaced by $1/J_N^0$, the reciprocal of the entanglement compliance. There are two adjustable parameters, h and K, and erf is the error function.

Other empirical formulations applied by Smith[92] are

$$G(t) = G_e + (G_g - G_e)/[1 + (t/t_0)^b] \quad (12)$$

and, alternatively,

$$G(t) = G_e + (G_g - G_e)/(1 + t/t_0)^\beta \quad (13)$$

where G_g and G_e have the same significance as in equation 11, and t_0, b, and β are empirical constants. The relaxation spectrum corresponding to equation 13 has the analytical form

$$H = (G_g - G_e)(\tau/t_0)^{-\beta} e^{-t_0/\tau} \Gamma(\beta) \quad (14)$$

where Γ is the gamma function. Equations 11 to 13 have been used to fit experimental data quite closely. Analogous equations can be written for the creep compliance and the dynamic modulus and compliance.[92,93]

The steepness of the viscoelastic functions in the transition zone is governed primarily by the parameter b or β in these formulations. Another index of steepness, used by Aklonis,[94] is simply the absolute value of maximum slope of a logarithmic plot of $G(t)$ or $J(t)$ in the transition zone.

3. Behavior of Copolymers and Polymer Mixtures

Data on several copolymers have already been included in some of the preceding tables. Insofar as the chemical heterogeneity is on a sufficiently local basis that regions with the dimensions of a Rouse submolecule have the same average chemical composition, the effect of varying the monomer ratio is primarily to change the local friction coefficient. This is illustrated by dynamic data on the two ethylene-propylene copolymers[18] quoted in Tables 12–I and 12–III, whose storage and loss compliances and moduli are very similar in shape though widely separated on the frequency scale. Similar results were obtained by Nigmankhodjaev and coauthors[95] for two copolymers of styrene and *n*-hexyl methacrylate with 0.26 and 0.41 mole fraction of styrene, in which the ratio $a^2\zeta_0/M_0^2$ (a simpler index of comparison for

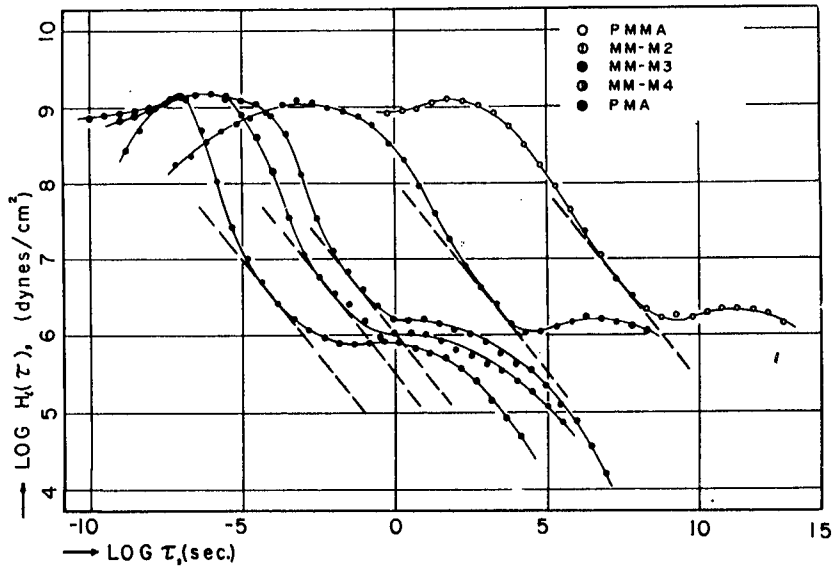


FIG. 12-14. Relaxation spectra in extension ($\overline{H}$) of poly(methyl acrylate), poly(methyl methacrylate), and three copolymers with compositions indicated, reduced to 100°C. Lines drawn with slope of $-\frac{1}{2}$. Mole percent methacrylate, left to right: 0, 42, 61, 75, 100. (Fujino, Senshu, and Kawai.[100])

copolymers, since it avoids the need for averaging over a and M_0 in equation 1) was shifted slightly to higher values than that of poly(n-hexyl methacrylate) with retention of the same shapes for $J'(\omega)$ and $H(\tau)$. More extensive data have been reported for stress relaxation of random styrene-butadiene copolymers by Kraus and Rollmann,[98] and creep of butylmethacrylate-ethylene glycol monomethacrylate copolymers by Ilavský and Kolařík.[99] In the latter system, the entire composition range involved shifts of up to eight decades of logarithmic time scale with very little change in the shape of the creep compliance in the transition zone.

On the other hand, if the two comonomers in their respective pure polymeric states have relaxation spectra somewhat different in shape, such as poly(methyl methacrylate) and poly(methyl acrylate) (panels I and II respectively of Fig. 12-11), then the spectra of their random copolymers show a progressive change with composition of both the shape and the position on the time or frequency scale. This is illustrated by the relaxation spectra (in extention, $\overline{H}$) of methyl methacrylate-methyl acrylate polymers in Fig. 12-14, from stress-relaxation measurements of Fujino, Senshu, and Kawai.[100] The location of the lower end of the transition zone, and the value of the monomeric friction coefficient, change by about 12 logarithmic decades of time scale with changing composition (although the location for poly(methyl methacrylate) homopolymer, which is close to its T_g, is somewhat uncertain because of a sensitive temperature shift). Moreover, the shape of $\overline{H}$ changes gradually from that characteristic of the one homopolymer to that characteristic of the other (*cf.* Fig. 12-10).

Examination of the relaxation modulus in extension, $E(t)$, for this same series

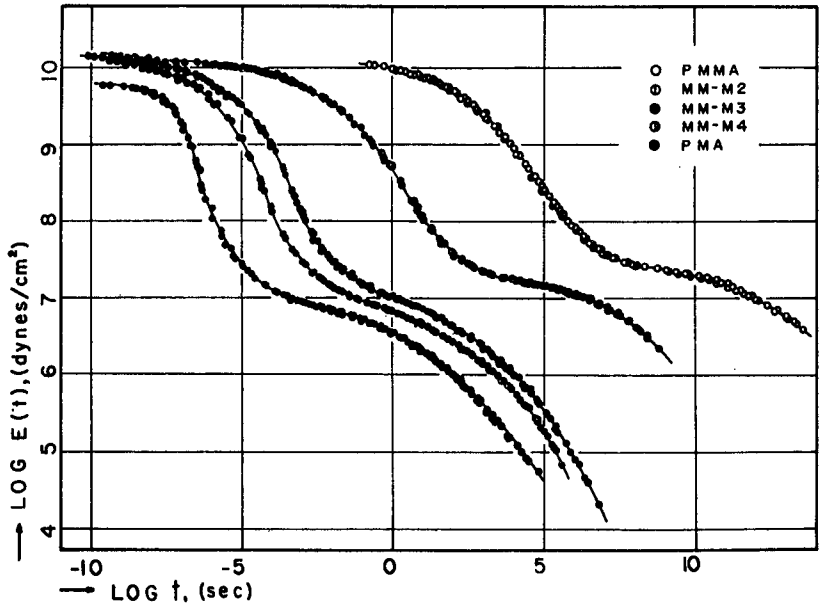


FIG. 12-15. Composite curves for the relaxation modulus in extension, $E(t)$, for the polymers and copolymers of Fig. 12-14, reduced to 100°C. Mole percent methacrylate, left to right, as in Fig. 12-14.

of copolymers (Fig. 12-15) reveals a third feature, not apparent in the relaxation spectrum, which changes gradually with copolymer composition. This is the plateau level of the modulus associated with the entanglement network, approximately reflected by the value of $E(t)$ near its minimum slope—in the neighborhood of 10^7 dynes/cm^2. This quantity, similar to $1/J_N^0$ in Fig. 12-13, is higher by about a factor of three for poly(methyl methacrylate) than for poly(methyl acrylate), and for the copolymers it changes progressively with composition. Closely similar results were obtained by Murakami and Shiina.[101] In copolymers of 1,3-butadiene and 1,4-diphenyl-1,3-butadiene, also, there is a change in shape of the viscoelastic functions with composition.[102]

The effect of such a change in J_N^0 with composition on the mechanical properties is particularly striking when one homopolymer is crystalline, as in the studies of Kawai and associates[103-105] on stress relaxation and dynamic viscoelastic properties of copolymers of polyvinyl alcohol. These materials were obtained not by a copolymerization process but by partial chemical reaction of polyvinyl alcohol to produce random comonomer units of vinyl acetate[103] or vinyl acetals[104] or vinyl formate.[105] Sequences of vinyl alcohol units are able to crystallize, but with increasing removal of hydroxyl groups by esterification or acetal formation the degree of crystallinity diminishes and eventually vanishes as judged by examination of X-ray diffraction patterns. An example is shown in Fig. 12-16 for the relaxation modulus in extension of poly(vinyl alcohol), poly(vinyl formate), and samples with five intermediate degrees of esterification. For esterification of 70% or greater, the

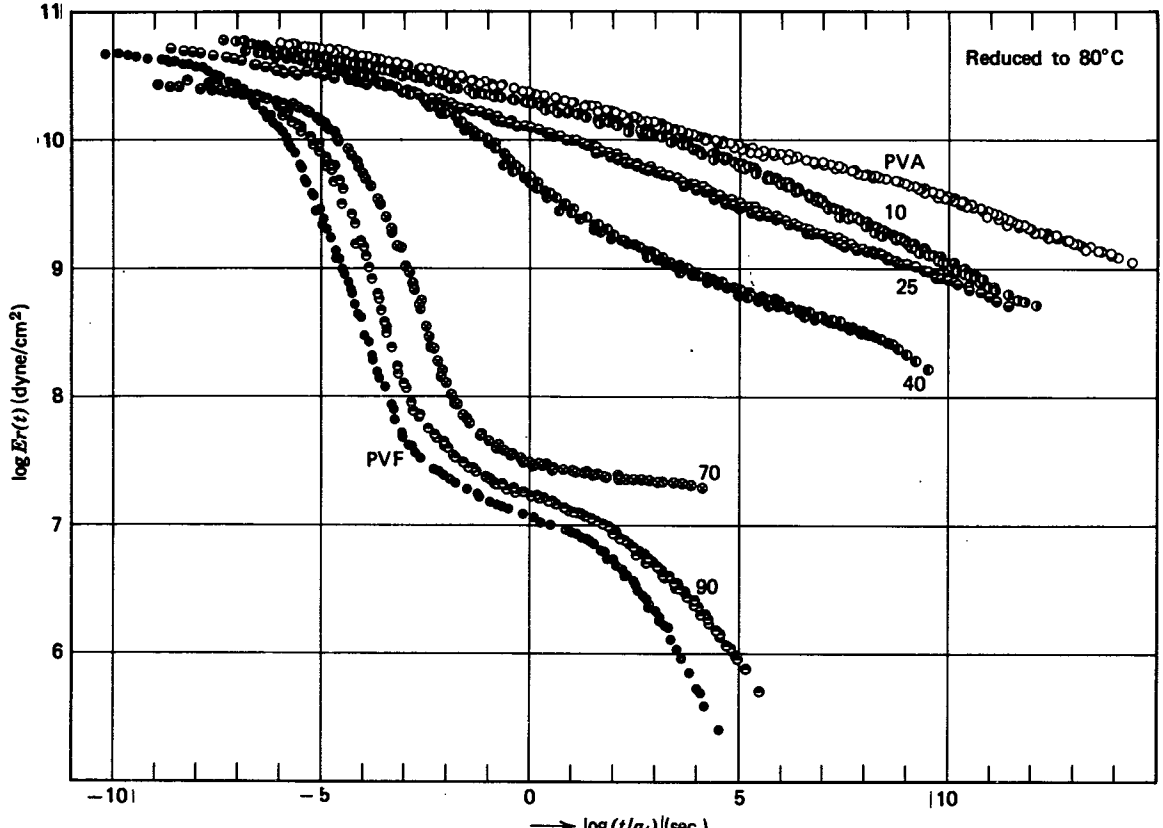


FIG. 12–16. Relaxation modulus of poly(vinyl alcohol) (PVA) poly(vinyl formate) (PVF) and partially formylated poly(vinyl alcohol)s with mole percentages of esterification as indicated, reduced to 80°C. (Nakatani, Iijima, Suganuma, and Kawai.[105])

behavior resembles that of Fig. 12–15; with increasing proportion of ester groups the transition zone moves to shorter times and the plateau level of the modulus diminishes. For esterification of 40% or less, the transition zone does not appear at all in the usual form chracteristic of amorphous polymers; the relaxation modulus changes very slowly with time, with the behavior characteristic of partly crystalline systems as discussed in Chapter 16, and no friction coefficient can be calculated from the corresponding relaxation spectrum.

The effects of varying composition in random copolymers can also be seen in isochronal or pseudoisochronal studies such as those in Fig. 12–3. Thus, Jenckel and Herwig[106] found in copolymers of styrene and methyl acrylate that the maximum in tan δ (measured in torsion at a frequency of 0.14 sec^{-1}) on the temperature scale shifted from about 20° to 110° with increasing proportions of styrene; the sharpness of the maximum was not much affected. Similar progressive changes with composition have been described for random copolymers of styrene and α-methyl styrene[107] and of methyl methacrylate and tri-*n*-propyl tin methacrylate.[108]

If the copolymerization is not random, quite different behavior is encountered. Varying degrees of nonrandomness can be distinguished, as pointed out by Kraus.[109] In *uniform* random copolymers, all the molecules have the same statistical composition, and the preceding paragraphs apply in principle to such systems. If, however, the polymerization reaction is carried to high conversion, the average compositions of polymer molecules formed at the beginning and at the end of the reaction may be quite different, depending on the relative rates at which the monomer units add to the growing chain.[110] Although such a product is random in the sense that there are no long blocks of identical units, it is molecularly heterogeneous. Nielsen,[111] in pseudoisochronal measurements on copolymers of vinyl chloride and methyl acrylate, found that increasing degrees of this kind of molecular heterogeneity caused a broadening of the transition zone on the temperature scale; G' decreased less steeply near its inflection, and the maximum in tan δ was lower.

A much greater degree of nonrandomness is represented by block copolymers, which contain long sequences of identical units. When all molecules contain the same pattern of blocks (often three, ABA, or two, AB) and all blocks are homogeneous, the product is termed an "ideal" block copolymer.[109] Since different polymers are almost always incompatible (insoluble in each other) the A and B blocks tend to aggregate separately in domains which can be distinguished in the electron microscope[112] and by small-angle X-ray scattering[113] and whose morphology depends somewhat on thermal history and/or the manner of deposition from a solvent. Each of the two phases then exhibits its own transition zone of viscoelastic properties.

If in a copolymer of the ABA pattern the glass transition temperature of B is below that of A, the mechanical properties in the temperature range between the two values of T_g resemble those of a filled rubbery polymer as described in Section 4 below; the A domains are hard and glasslike and bind the B blocks as though the ends were cross-linked. At temperatures above both T_g values, two transition zones

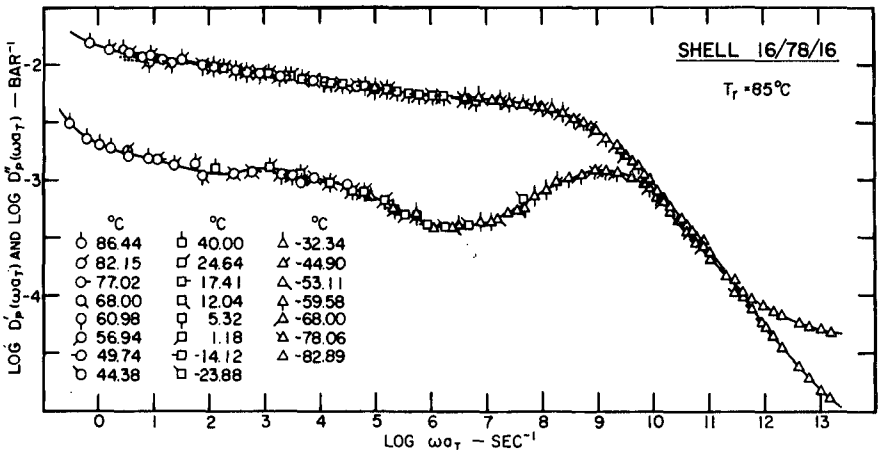


FIG. 12–17. Logarithmic plots of the storage (D') and loss (D'') tensile compliance against frequency for a triblock styrene-butadiene copolymer reduced to T_0 = 85°C. The block lengths S/B/S have molecular weights 16,000/78,000/16,000 and the morphology corresponds to spherical polystyrene domains in a polybutadiene matrix. Temperatures of measurement from −82.89° to 86.44°C are identified. (Fesko and Tschoegl.[116]) Reproduced, by permission, from the International Journal of Polymeric Materials.

can be inferred from isochronal measurements.[109,114,115] Even at temperatures between the two T_g's, the temperature dependences of the two phases must be treated separately, as mentioned in Section F2 of Chapter 11.[116] In a very thorough study of styrene-butadiene copolymers (triblock, SBS) by both forced and free oscillation dynamic measurements, Fesko and Tschoegl[116] provided master curves of storage and loss tensile compliance reduced to different temperatures. Examples are shown in Figs. 12–17 and 12–18; an enormous range is covered and the shapes are different because of the different temperature dependences of the phases (a correction for a phase interlayer has also been applied). The transition zone of the polybutadiene appears at high reduced frequency. A second dispersion region at lower frequencies is attributed to slippage of trapped entanglements on the polybutadiene segments. Relaxation occurs in the polystyrene domains at reduced frequencies which are exceedingly low, especially at 25°C, which is far below the polystyrene glass transition temperature. Further studies of blends of triblock and diblock styrene-butadiene copolymers have been reported by Cohen and Tschoegl.[117,117a]

In isochronal measurements where the temperature is varied, the two transition zones are clearly distinguished, as illustrated in Fig. 12–19 for a styrene-butadiene triblock copolymer.[118]

The average sequence lengths in a copolymer can be varied in the course of synthesis to produce varying degrees of "blockiness" from random to long blocks.[119] Unless the blocks are quite long, a single transition zone is observed in isochronal experiments.[98] (However, even slight blockiness can affect the steady flow viscosity and its shear rate dependence.)

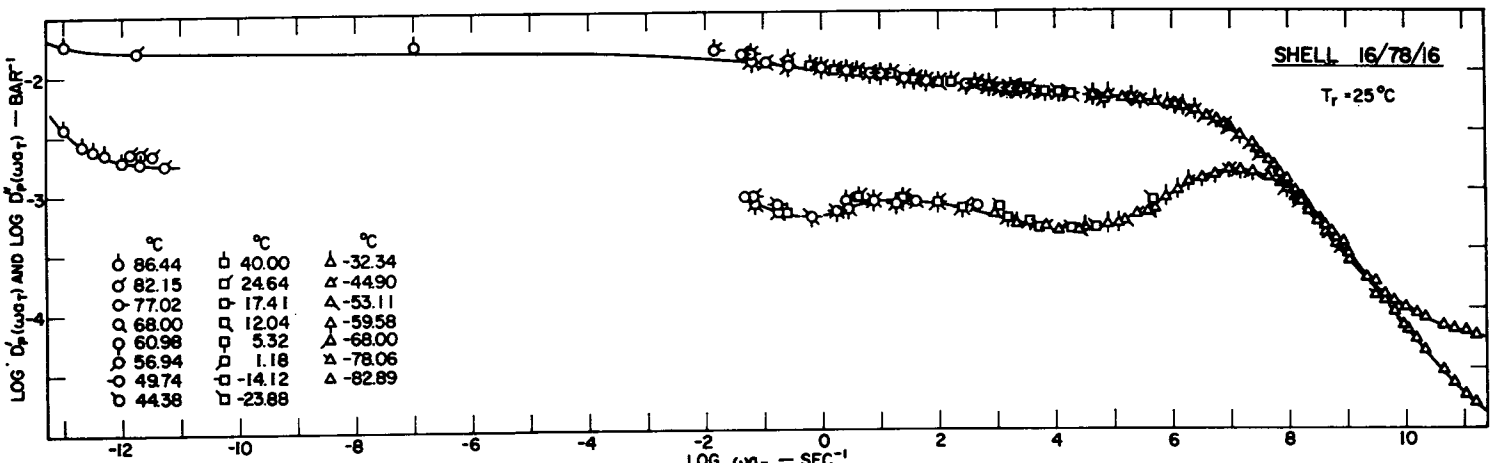


FIG. 12–18. Logarithmic plots of the data of Fig. 12–17 reduced to 25°C after an interlayer correction.
Reproduced, by permission, from the International Journal of Polymeric Materials.

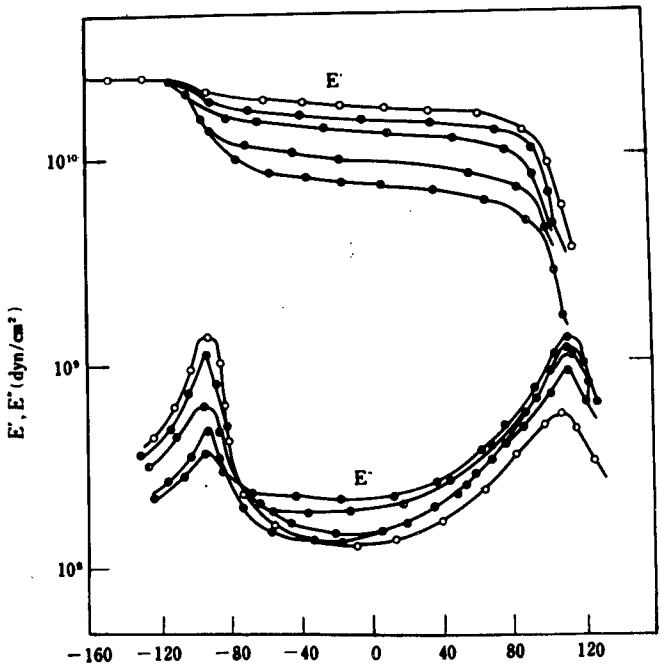


FIG. 12–19. Isochronal plots of storage and loss Young's modulus (with a logarithmic scale) at a frequency of 110 Hz against temperature for styrene-butadiene triblock copolymers. Decreasing values of E' correspond to decreasing styrene/butadiene ratio (West and Cooper, after Matsuo; reproduced by permission of the publishers, IPC Business Press Ltd.[118])

Copolymers of polyelectrolytes with ionized groups also form domain structures in which the charged groups and their counterions are clustered. These exhibit more than one transition zone.[120]

The extreme case of the molecular heterogeneity resulting from combinations of different monomer units is simply a mixture of two pure homopolymers. Such mixtures, with few exceptions, are incompatible, representing physical blending rather than solution. For the exceptional case (*e.g.*, poly(vinyl chloride) and butadiene-acrylonitrile rubber,[111] where the severe thermodynamic requirements[121] for compatibility appear to be met) a single broad transition is noted. For the more common case of incompatibility, however, physical blending leaves moderately large regions of homogeneous composition (which often show their presence by opacity), and each type of region experiences its own transition. This is illustrated in isochronal plots of G' and tan δ for mixtures of poly(methyl methacrylate) and poly(vinyl acetate) in Fig. 12–20, from data of Jenckel and Herwig.[106] Similar behavior has been found for mixtures of polystyrene with butadiene-styrene copolymer[111] and others.[121–124] The application of reduced variables to superpose time-dependent data at different temperatures to obtain isothermal plots has been discussed by Kaplan and Tschoegl.[125] The behavior of such composite systems is further discussed in Chapter 14.

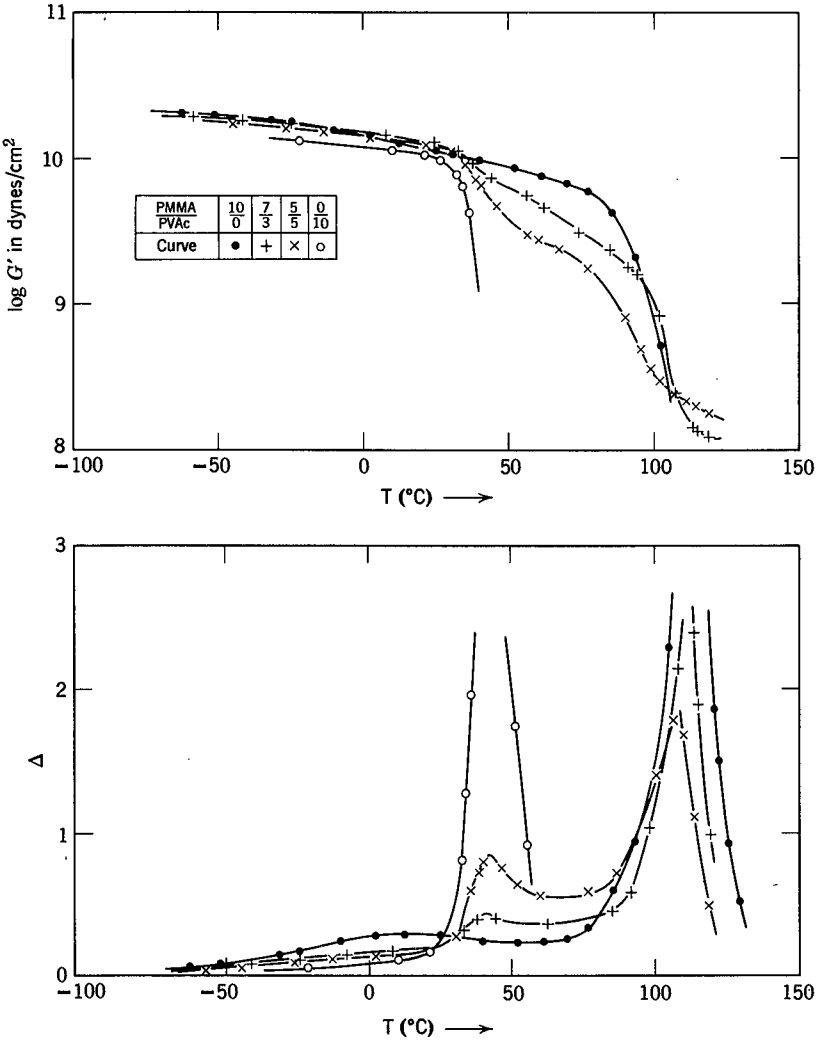


FIG. 12-20. Storage modulus and logarithmic decrement (approximately proportional to loss tangent) plotted against temperature, for physical mixtures of poly(methyl methacrylate) and poly(vinyl acetate), with compositions as indicated. (Jenckel and Herwig.[106])

4. Behavior of Filled Systems

When a polymer is mixed ("loaded") with a particulate filler which does not interact strongly with the polymer, the principal effects on viscoelastic properties in the transition zone arise from the partial occupancy of volume by rigid and immobile masses. Extensive studies by Landel[126,127] on polyisobutylene loaded with glass beads of the order of 0.004 cm in diameter show the changes in the isothermal viscoelastic functions. In this case the particles are large enough so that the average distances between them even at the highest loading considered are large compared

with the root-mean-square end-to-end separation of the polymer molecules; the latter maintain their Gaussian distributions. Moreover, the particles are too far apart to be bridged by single molecules.

The temperature dependence of relaxation and retardation times in these loaded systems could be described by the WLF equation in the form of equation 40 of Chapter 11 with an adjustable reference temperature T_s and $c_1^s = 8.86$, $c_2^s = 101.6$. The value of T_s increased roughly linearly with the volume fraction (ϕ) occupied by filler; for $\phi = 0.37$, T_s was 7° higher than for the unloaded polymer. For each individual filled sample, the method of reduced variables could be applied to obtain single composite curves for the viscoelastic functions plotted against reduced frequency or time. The applicability of reduced variables was also apparent in earlier work on filled rubberlike polymers by Becker and Oberst[128] and Blatz.[129] (It must be noted that in thermal expansion studies by van der Wal, Bree, and Schwarzl[130] on elastomers filled with finely divided sodium chloride, no dependence of the glass transition temperature on filler content up to 50% by volume was found, although $\Delta\alpha$, the change in thermal expansion coefficient at T_g, decreased linearly with increasing filler content. It is not certain, therefore, whether the small increase in T_s for polyisobutylene with glass beads reflects a parallel increase in T_g.)

When samples of polyisobutylene with different proportions of glass beads are compared in corresponding temperature states (*i.e.*, 298°K for the unloaded polymer, 298° + ΔT_s for each of the loaded samples), the retardation and relaxation spectra fall rather closely together at short times up to a filler volume fraction of 0.2, as illustrated in Fig. 12–21. At higher loadings, H is elevated and L is depressed throughout; and at longer times the maximum in L is depressed progressively with increasing volume fraction of filler. The plateau level of the modulus, which will be discussed in Chapter 14, increases progressively with filler content.

Without the small temperature correction, the spectra in Fig. 12–21 would show a slight progressive shift to longer times with increasing filler content. An analogous effect in isochronal measurements is seen in the experiments of Schwarzl[131] on rubbers filled with sodium chloride, where the characteristic temperature T_M shifts upward a few degrees with increasing proportion of filler up to 50% by volume. At a given filler concentration, however, the mechanical properties are almost independent of the particle size between 35 and 400 microns.

In a rubber loaded with finely divided carbon black, the behavior is somewhat different. There is good evidence that the polymer molecules are attached to the filler particles by chemical bonds.[132] Moreover, in a compound containing 50% by weight of particles of the order of 300 Å in diameter, the interparticle separations are of the order of 100 Å, which is similar to the average vector distance between cross-links in a lightly cross-linked rubber vulcanizate. Hence each filler particle may be bridged to others by many polymer chains, and it acts as a multiple cross-link as well as a rigid occupier of space. (Agglomeration of the particles may also complicate the picture.) The effect on the transition from rubberlike to glasslike consistency is illustrated by storage and loss modulus data of Ecker[133] on a styrene-butadiene rubber with two levels of loading by carbon black (Fig. 12–22). Both moduli, especially the loss, are substantially increased in the rubbery zone and the

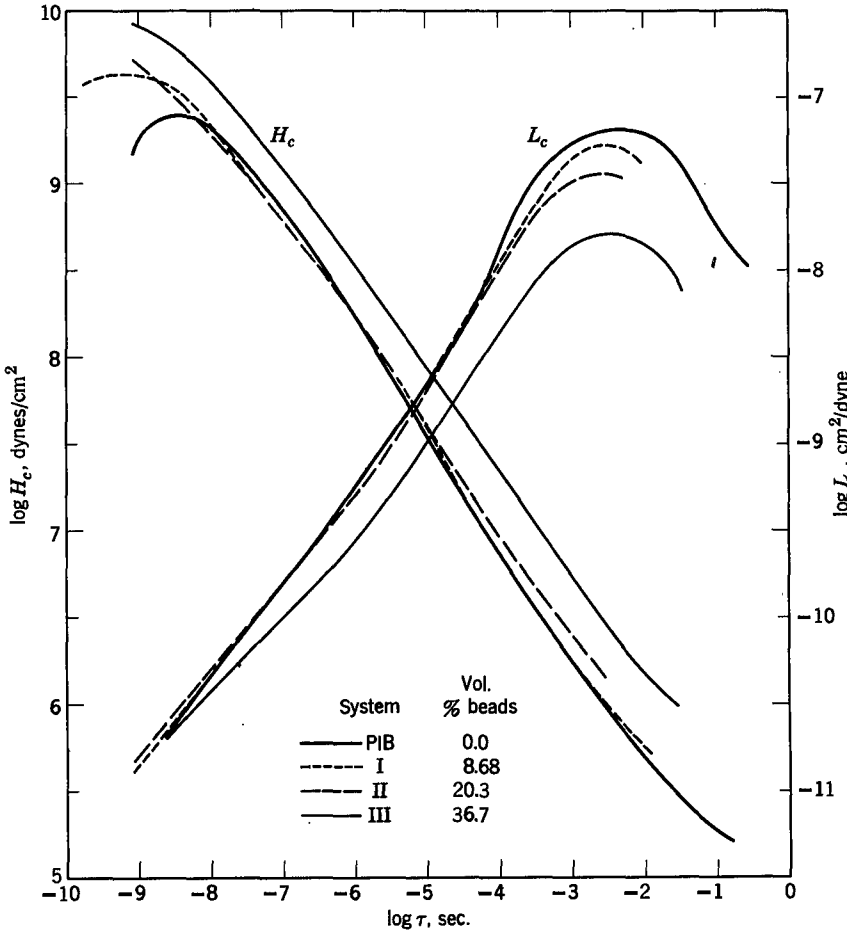


FIG. 12-21. Relaxation and retardation spectra plotted logarithmically for polyisobutylene and three compositions loaded with glass beads, with volume fractions as indicated, reduced to corresponding temperature states (equal values of $T - T_s$). (Landel.[123])

transition zone is broadened, while the losses persist to much lower frequencies than in the unfilled rubber. Relaxation and retardation spectra calculated from such data are flattened and the former does not attain a slope of $-\frac{1}{2}$ on the doubly logarithmic plot in the lower region of the transition zone where friction coefficients are usually estimated. These effects of carbon black depend not only on the extent of loading but also on the structure of the black and can be correlated with its specific surface area as measured by adsorption.[134] At very short times, however, the dynamic moduli and spectra are essentially unaffected by the filler.

If the midpoint of the transition is roughly characterized by the inflection in G' or the maximum in tan δ (the latter corresponding to the characterizations in Table 12-I), the effect of 50 parts by weight of furnace-type carbon black in natural rubber appears in similar data of Payne[12,135] as a shift to lower frequencies by about

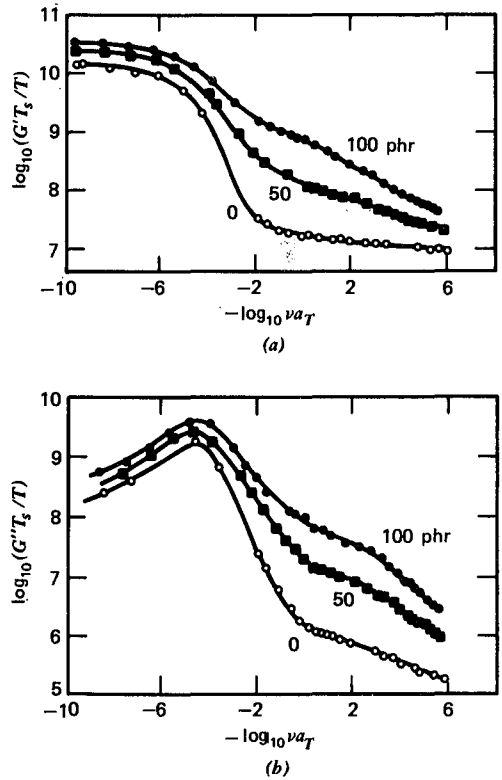


FIG. 12–22. Logarithmic plots of storage and loss shear modulus against frequency reduced to 263°K for styrene-butadiene rubber unfilled (open circles) and with two loadings of carbon black. Numbers (*phr*) denote parts black per hundred parts rubber by weight. (After Ecker[132,133].) Reproduced, by permission, from Advances in Polymer Science.

1.2 logarithmic units. For an isochronal description as in Table 12–II, this would correspond to elevating T_M by about 25°. The effect of the filler on the temperature dependence of relaxation and retardation times could be described in terms of an increase in T_s of 3° to 5°C. This change, very mild in comparison with the other effects of the filler, is comparable with that produced by the glass beads in polyisobutylene as discussed above. If T_g is also increased by only 5°, the separation between T_g and T_M is enhanced by the filler.

Other aspects of the behavior of filled systems will be mentioned in Chapter 14.

D. THE TRANSITION ZONE IN POLYMERS OF LOW MOLECULAR WEIGHT

The preceding sections have dealt with polymers of high molecular weight, well above the critical value for entanglement coupling, because only in such substances

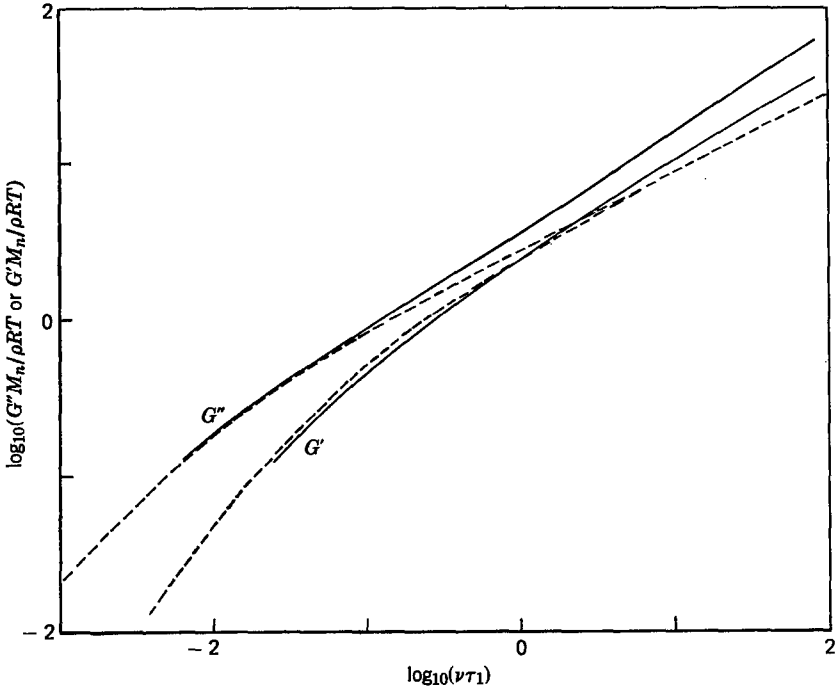


FIG. 12-23. Storage and loss shear moduli of a poly(dimethyl siloxane) with number-average molecular weight $\overline{M}_n$ = 16,000, plotted logarithmically against frequency ν with reduced scales. τ_1 is the terminal relaxation time calculated as $3\eta_0\overline{M}_n/\pi^2\rho RT$. Solid curves, experimental; dashed curves, from modified Rouse theory for most probable distribution of molecular weights. (Barlow, Harrison, and Lamb.[30])

(or in lightly cross-linked networks) is there a zone of rubberlike behavior; otherwise there cannot be a transition from rubberlike to glasslike consistency. In polymers of lower molecular weight, the transition goes directly from the terminal zone (of steady flow with elastic energy storage) to the glassy zone, with no intermediate rubbery range. This was illustrated by curves II in the figures in Chapter 2.

For molecular weights below or near the minimum for entanglement coupling, the storage and loss shear moduli in the low frequency or long-time end of the transition zone conform rather well to the Rouse theory as modified for undiluted polymer in Section A of Chapter 10, as long as the temperature is well above T_g (*e.g.*, 40° or more). An example is shown in Fig. 12-23 for the storage and loss shear moduli of a poly(dimethyl siloxane) of number-average molecular weight 16,000, with data of Lamb and collaborators,[30] compared with the Rouse theory calculated for a most probable molecular weight distribution as outlined in Chapter 10, Section A3. At higher frequencies, the data deviate in the direction expected for hydrodynamic interaction (Chapter 9). However, the behavior over a much wider frequency range can be represented by combining a small number of Rouse modes with a model for behavior of a low molecular weight liquid in the glassy state which will be introduced in Chapter 15. This is illustrated in Fig. 12-24 for a polystyrene of molecular weight 3500, where the number of Rouse submolecules is taken as 7. (The behavior in the glassy zone is discussed in Chapter 15.)

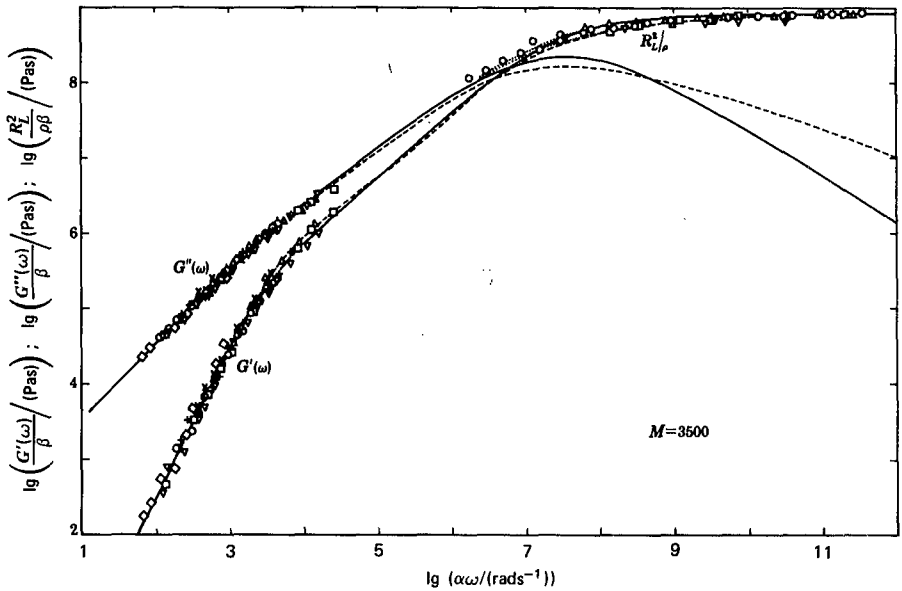


FIG. 12–24. Logarithmic plots of storage and loss shear modulus against frequency reduced to 123°C. ($T_g + 60°$) for a polystyrene with molecular weight 3500. (R_L^2/ρ is an experimentally measured function which approaches G'/ω at high frequencies; $\beta = (J_\infty)_{T0}/(J_\infty)_T$, where J_∞ is the high-frequency limiting value of J'.) Dashed curves calculated for a summation of seven Rouse modes with the low molecular weight liquid behavior described by equations 5 and 6 of Chapter 15; solid curves calculated from Davidson-Cole equations, equation 7 of Chapter 15. (Gray, Harrison, and Lamb.[136]) Reproduced, by permission, from the Proceedings of The Royal Society.

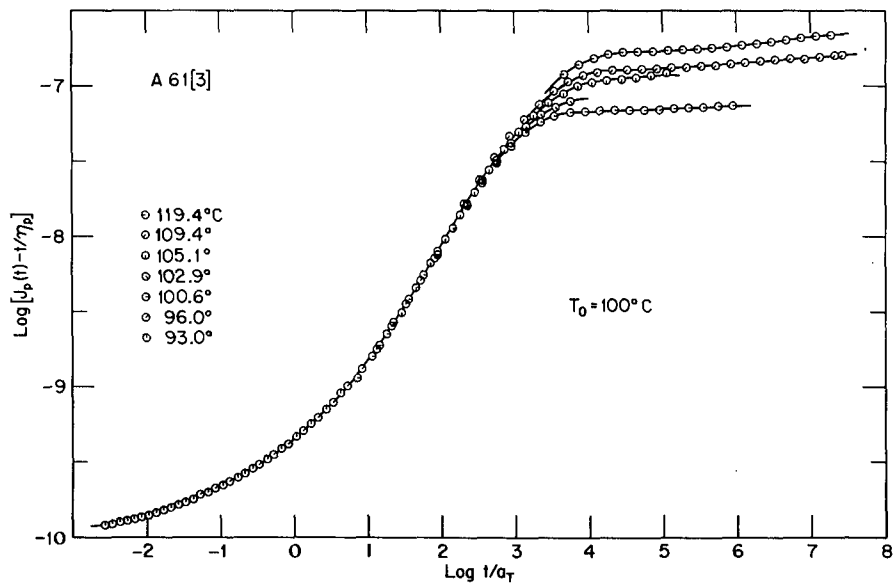


FIG. 12–25. Recoverable creep compliance of narrow-distribution polystyrene with molecular weight 16,400, measured at various temperatures as indicated and reduced to 100°C with reduction factors appropriate in the transition zone. (Plazek and O'Rourke.[137])

Extensive creep measurements on polystyrenes of molecular weights in the range from 1100 to 16,000 by Plazek and O'Rourke[137] show similar behavior, with terminal, transition, and glassy zones but no plateau, as illustrated in Fig. 12–25 for a molecular weight of 16,400. The anomaly in temperature reduction (*cf.* Fig. 11–14) becomes exacerbated with decreasing molecular weight and is associated with large deviations from the Rouse theory. For example, far above T_g the steady-state compliance J_e^0 agrees rather well with the Rouse prediction of equation 11 of Chapter 10 (*cf.* Fig. 10–14), but with decreasing temperature as T_g is approached it drops sharply, for $M \leq 3400$ by at least an order of magnitude.[137] (This phenomenon appears also for higher molecular weights but only very near T_g.)

REFERENCES

1. R. O. Davies and G. O. Jones, *Proc. R. Soc.*, **217A,** 27 (1953).
2. S. B. Thomas, *J. Phys. Chem.*, **35,** 2103 (1931).
3. T. A. Litovitz, in *Non-Crystalline Solids,* edited by V. D. Frechette, Wiley, New York, 1960, p. 252.
4. D. J. Plazek, *Proc. Conference on Polymer Structure and Mechanical Properties,* U. S. Army Natick Laboratories, 1967.
5. J. D. Ferry, W. C. Child, Jr., R. Zand, D. M. Stern, M. L. Williams, and R. F. Landel, *J. Colloid Sci.*, **12,** 53 (1957).
6. W. C. Child, Jr., and J. D. Ferry, *J. Colloid Sci.*, **12,** 327 (1957).
7. W. C. Child, Jr., and J. D. Ferry, *J. Colloid Sci.*, **12,** 389 (1957).
8. W. Dannhauser, W. C. Child, Jr., and J. D. Ferry, *J. Colloid Sci.*, **13,** 103 (1958).
9. S. F. Kurath, T. P. Yin, J. W. Berge, and J. D. Ferry, *J. Colloid Sci.*, **14,** 147 (1959).
10. T. P. Yin and J. D. Ferry, *J. Colloid Sci.*, **16,** 166 (1961).
11. J. R. McLoughlin and A. V. Tobolsky, *J. Colloid Sci.*, **7,** 555 (1952).
12. A. R. Payne, in *Rheology of Elastomers,* edited by P. Mason and N. Wookey, Pergamon, London, 1958, p. 86.
13. L. J. Zapas, S. L. Shufler, and T. W. De Witt, *J. Polym. Sci.*, **18,** 245 (1955).
14. E. Maekawa, R. G. Mancke, and J. D. Ferry, *J. Phys. Chem.*, **69,** 2811 (1965).
15. J. F. Sanders, R. H. Valentine, and J. D. Ferry, *J. Polym. Sci.*, A-2, **6,** 967 (1968).
16. R. G. Mancke and J. D. Ferry, *Trans. Soc. Rheol.*, **12,** 335 (1968).
17. J. F. Sanders, Ph. D. thesis, University of Wisconsin, 1968.
18. J. R. Richards, R. G. Mancke, and J. D. Ferry, *J. Polym. Sci.*, **B-2,** 197 (1964).
19. R. F. Landel, *J. Colloid Sci.*, **12,** 308 (1957).
20. J. D. Ferry, L. D. Grandine, Jr., and E. R. Fitzgerald, *J. Appl. Phys.*, **24,** 911 (1953).
21. L. D. Grandine and J. D. Ferry, *J. Appl. Phys.*, **24,** 679 (1953).
22. H. Fujita and K. Ninomiya, *J. Polym. Sci.*, **24,** 233 (1957).
23. M. L. Williams and J. D. Ferry, *J. Colloid Sci.*, **9,** 479 (1954).
24. K. Ninomiya and H. Fujita, *J. Colloid Sci.*, **12,** 204 (1957).
25. M. L. Williams and J. D. Ferry, *J. Colloid Sci.*, **10,** 474 (1955).
26. G. W. Becker, *Kolloid-Z.*, **140,** 1 (1955).
27. S. F. Kurath, E. Passaglia, and R. Pariser, *J. Appl. Phys.*, **28,** 499 (1957).
28. K. E. Owens and C. F. Dahlquist, *Trans. Soc. Rheol.*, **2,** 23 (1958).
29. B. E. Read, *Polymer,* **3,** 529 (1962).
30. A. J. Barlow, G. Harrison, and J. Lamb, *Proc. R. Soc.*, **A282,** 228 (1964).
31. D. J. Plazek and V. M. O'Rourke, personal communication.
32. K. Schmeider and K. Wolf, *Kolloid-Z.*, **127,** 65 (1952); **134,** 149 (1953).
33. R. A. Haldon, W. J. Schell, and R. Simha, in *Cryogenic Properties of Polymers,* edited by T. T. Serafini and J. L. Koenig, Dekker, New York, 1968, pp. 137–153.

34. L. E. Nielsen, R. Buchdahl, and G. C. Claver, *Ind. Eng. Chem.*, **43**, 341 (1951).
35. E. Jenckel, *Kolloid-Z.*, **136**, 142 (1954).
36. A. B. Thompson and D. W. Woods, *Trans. Faraday Soc.*, **52**, 1383 (1956).
37. K. H. Illers and H. Breuer, *Kolloid-Z.*, **176**, 110 (1961).
38. N. G. McCrum, B. E. Read, and G. Williams, *Anelastic and Dielectric Effects in Polymeric Solids*, Wiley, New York, 1967.
39. L. E. Nielsen, *Mechanical Properties of Polymers and Composites*, Volume 1, Dekker, New York, 1974.
40. H. D. Heinze, K. Schmieder, G. Schnell, and K. A. Wolf, *Kautsch. Gummi*, **14**, 208 (1961).
41. A. W. Tobolsky and J. R. McLoughlin, *J. Polym. Sci.*, **8**, 543 (1952).
42. K. Ninomiya and J. D. Ferry, *J. Phys. Chem.*, **67**, 2292 (1963); K. Ninomiya, J. D. Ferry, and F. Ōyanagi, *J. Phys. Chem.*, **67**, 2297 (1963).
43. R. F. Boyer, *Rubber Chem. Techn.*, **36**, 1303 (1963).
44. P. J. Flory, *Principles of Polymer Chemistry*, Cornell University Press, Ithaca, 1953, Chapter XIV.
45. B. Gross, *Mathematical Structure of the Theories of Viscoelasticity*, Hermann et Cie., Paris, 1953.
46. D. J. Plazek, V. Tan, and V. M. O'Rourke, *Rheol. Acta*, **13**, 367 (1974).
47. D. J. Plazek, personal communication.
48. P. R. Saunders and J. D. Ferry, *J. Colloid Sci.*, **14**, 239 (1959).
49. M. Ilavský, J. Hasa, and J. Janáček, *Collect. Czech. Chem. Commun.*, **33**, 3197 (1968).
50. R. A. Dickie and J. D. Ferry, *J. Phys. Chem.*, **70**, 2594 (1966).
51. T. P. Yin and J. D. Ferry, *J. Phys. Chem.*, **65**, 534 (1961).
52. S. S. Rogers and L. Mandelkern, *J. Phys. Chem.*, **61**, 985 (1957).
53. H. Fujita and A. Kishimoto, *J. Colloid Sci.*, **13**, 418 (1958).
54. S. P. Chen and J. D. Ferry *Macromolecules*, **1**, 270 (1968).
55. E. Jenckel, in H. A. Stuart *Die Physik der Hochpolymeren*, Volume III, Springer-Verlag, Berlin, 1955, p. 615.
56. F. Bueche, *J. Chem. Phys.*, **20**, 1959 (1952).
57. G. C. Berry and T. G. Fox, *Adv. Polym. Sci.*, **5**, 261 (1967).
58. T. Kataoka and S. Ueda, *J. Polym. Sci.*, A2, **5**, 973 (1967).
59. F. Bueche, W. M. Cashin, and P. Debye, *J. Chem. Phys.*, **20**, 1956 (1952).
60. J. D. Skewis, *Rubber Chem. Technol.*, **39**, 217 (1966).
61. B. D. Boss, E. O. Stejskal, and J. D. Ferry, *J. Phys. Chem.*, **71**, 1501 (1967).
62. J. E. Tanner, *Macromolecules*, **4**, 748 (1971).
63. E. von Meerwall, *Adv. Polym. Sci.*, **54**, 1 (1983)
64. J. Klein and B. J. Briscoe, *Polymer*, **17**, 481 (1976).
65. A. T. Hutcheon, R. J. Kokes, J. L. Hoard, and F. A. Long, *J. Chem. Phys.*, **20**, 1232 (1952).
66. J. D. Ferry and R. F. Landel, *Kolloid-Z.*, **148**, 1 (1956).
67. A. W. Adamson and R. Irani, *J. Chim. Phys.*, **55**, 102 (1958).
68. I. Auerbach, S. D. Gehman, W. R. Miller, and W. C. Kuryla, *J. Polym. Sci.*, **28**, 129 (1958).
69. R. S. Moore and J. D. Ferry, *J. Phys. Chem.*, **66**, 2699 (1962).
70. R. E. Pattle, P. J. A. Smith, and R. W. Hill, *Trans. Faraday Soc.*, **63**, 2389 (1967).
71. C. P. Wong, J. L. Schrag, and J. D. Ferry, *Polym. J.*, **2**, 274 (1971).
72. D. W. McCall, D. C. Douglass, and E. W. Anderson, *J. Polym. Sci.*, **A1**, 1709 (1963).
73. G. S. Park, *Proc. 2nd Radioisotope Cong.*, Butterworths, London, 1954, p. 11.
74. A. Aitken and R. M. Barrer, *Trans. Faraday Soc.*, **51**, 116 (1955).
75. S. Prager, E. Bagley, and F. A. Long, *J. Am. Chem. Soc.*, **75**, 1255 (1953).
76. S. N. Zhurkov and G. Ya. Ryskin, *Zh. Tekh. Fiz.*, **24**, 797 (1954).
77. R. J. Kokes and F. A. Long, *J. Am. Chem. Soc.*, **75**, 6142 (1953).
78. F. Grün, *Experientia*, **3**, 490 (1947).

79. S. D. Morton and J. D. Ferry, *J. Phys. Chem.*, **63,** 1335 (1959).
80. C. K. Rhee, J. D. Ferry, and L. J. Fetters, *J. Appl. Polym. Sci.*, **21,** 783 (1977).
81. J. B. Wilkens and F. A. Long, *Trans. Faraday Soc.*, **53,** 1146 (1957).
82. H. Fujita, *Adv. Polym. Sci.*, **3,** 1 (1961).
83. Y. Nishijima and G. Oster, *J. Polym. Sci.*, **19,** 337 (1956).
84. H. K. Schachman and W. F. Harrington, *J. Am. Chem. Soc.*, **74,** 3965 (1952).
85. W. Kuhn, *Makromol. Chem.*, **6,** 224 (1951).
86. C. K. Rhee and J. D. Ferry, *J. Appl. Polym. Sci.*, **21,** 467 (1977).
87. O. Kramer and J. D. Ferry, in *Science and Technology of Rubber,* edited by F. R. Eirich, Academic Press, New York, 1978, Chapter 5.
88. R. S. Marvin, in *Viscoelasticity—Phenomenological Aspects,* edited by J. T. Bergen, Academic Press, New York, 1960, p. 27.
89. A. V. Tobolsky, D. Katz, R. Thach, and R. Schaffhauser, *J. Polym. Sci.*, **62,** 5176 (1962).
90. R. F. Landel, in *Polymer Networks—Structure and Mechanical Properties,* edited by A. J. Chompff and S. Newman, Plenum Press, New York, 1971, p. 219.
91. A. V. Tobolsky, *J. Appl. Phys.*, **27,** 673 (1956).
92. T. L. Smith, *J. Polym. Sci.*, **C35,** 39 (1971).
93. A. V. Tobolsky and E. Catsiff, *J. Polym. Sci.*, **19,** 111 (1956).
94. J. J. Aklonis and V. B. Rele, *J. Polym. Sci.*, **C46,** 127 (1974).
95. A. S. Nigmankhodjaev, L.-K. Bi, C.-P. Wong, J. L. Schrag, and J. D. Ferry, *J. Polym. Sci.*, A-2, **8,** 1927 (1970).
96. E. Catsiff and A. V. Tobolsky, *J. Appl. Phys.*, **25,** 1092 (1954).
97. A. V. Tobolsky, *J. Appl. Phys.*, **27,** 673 (1956).
98. G. Kraus and K. W. Rollman, *Angew. Makromol. Chem.*, **16/17,** 271 (1971).
99. M. Ilavský and J. Kolařik, *Collect. Czech. Chem. Commun.*, **34,** 2473 (1969).
100. K. Fujino, K. Senshu, and H. Kawai, *J. Colloid Sci.*, **16,** 411 (1961).
101. K. Murakami and K. Shiina, *Zairyo,* **17,** 349 (1968).
102. H. L. Hsieh and G. Kraus, *J. Polym. Sci., Polym. Chem. Ed.*, **11,** 453 (1973).
103. K. Fujino, T. Horino, K. Miyamoto, and H. Kawai, *J. Colloid Sci.*, **16,** 411 (1961).
104. K. Fujino, K. Senshu, T. Horino, and H. Kawai, *J. Colloid Sci.*, **17,** 726 (1962).
105. M. Nakatani, K. Iijima, A. Suganuma, and H. Kawai, *J. Macromol. Sci. (Phys.)*, **B2,** 55 (1968).
106. E. Jenckel and H. U. Herwig, *Kolloid-Z.*, **148,** 57 (1956).
107. D. Heinze, *Makromol. Chem.*, **101,** 166 (1966).
108. G. Rehage and E. E. Schäfer, *Z. Anal. Chem.*, **235,** 137 (1967).
109. G. Kraus, C. W. Childers, and J. T. Gruver, *J. Appl. Polym. Sci.*, **11,** 1581 (1967).
110. P. J. Flory, *Principles of Polymer Chemistry,* Cornell University Press, Ithaca, 1953, Chapter V.
111. L. E. Nielsen, *J. Am. Chem. Soc.*, **75,** 1435 (1953).
112. T. Hashimoto, K. Nagatoshi, A. Todo, H. Hasegawa, and H. Kawai, *Macromolecules,* **7,** 364 (1974).
113. J. Burke and V. Weiss, editors, *Block and Graft Copolymers,* Syracuse University Press, Syracuse, New York, 1973.
114. D. Heinze, *Makromol. Chem.*, **101,** 166 (1967).
115. D. S. Huh and S. L. Cooper, *Polym. Eng. Sci.*, **11,** 369 (1971).
116. D. G. Fesko and N. W. Tschoegl, *J. Polym. Sci.*, **C35,** 51 (1971); *Int. J. Polym. Mater.*, **3,** 51 (1974).
117. R. E. Cohen and N. W. Tschoegl, *Int. J. Polym. Mater.*, **2,** 49, 205 (1972); **3,** 3 (1974).
117a. R. E. Cohen and N. W. Tschoegl, *Trans. Soc. Rheol.*, **20,** 153 (1976).
118. M. Matsuo, *Jpn. Plast.*, **2,** 6 (1968), *Polymer,* **9,** 425 (1968); J. C. West and S. L. Cooper, in *Science and Technology of Rubber,* edited by F. R. Eirich, Academic Press, New York, 1978, p. 546.
119. T. Kotani and Y. Kuwabara, *Kogyo Kagaku Zasshi,* **74,** 287 (1971).
120. A. Eisenberg, *Pure Appl. Chem.*, **46,** 171 (1976).

121. R. Buchdahl and L. E. Nielsen, *J. Polym. Sci.*, **15**, 1 (1955).
122. E. B. Atkinson and R. F. Eagling, in *The Physical Properties of Polymers*, Soc. Chem. Ind. Monograph, No. 5, 1959, p. 197.
123. R. F. Landel, *Trans. Soc. Rheol.*, **2**, 53 (1958).
124. T. Horino, Y. Ogawa, T. Soen, and H. Kawai, *J. Appl. Polym. Sci.*, **9**, 2261 (1965).
125. D. Kaplan and N. W. Tschoegl, *Polym. Eng. Sci.*, **14**, 43 (1974).
126. R. F. Landel, *Trans. Soc. Rheol.*, **2**, 53 (1958).
127. R. F. Landel and T. L. Smith, *J. Am. Rocket Soc.*, **31**, 599 (1961).
128. G. W. Becker and H. Oberst, *Kolloid-Z.*, **148**, 6 (1956).
129. P. J. Blatz, *Ind. Eng. Chem.*, **48**, 727 (1956).
130. C. W. van der Wal, H. W. Bree, and F. R. Schwarzl, *J. Appl. Polym. Sci.*, **9**, 2143 (1965).
131. F. R. Schwarzl, H. W. Bree, and C. J. Nederveen, *Proc. 4th Intern. Cong. Rheology*, edited by E. H. Lee, Interscience, New York, Part 3, 1965, p. 241; *Rheol. Acta*, **5**, 270 (1966).
132. G. Kraus, *Adv. Polym. Sci.*, **8**, 155 (1971).
133. R. Ecker, *Kautsch. Gummi, Kunstst.*, **21**, 304 (1968), quoted in reference 132.
134. G. Kraus, in *Science and Technology of Rubber*, edited by F. R. Eirich, Academic Press, New York, 1978.
135. A. R. Payne, in *Physical Properties of Polymers*, Macmillan, New York, 1959, p. 273.
136. R. W. Gray, G. Harrison, and J. Lamb, *Proc. R. Soc.*, **A356**, 77 (1977).
137. D. J. Plazek and V. M. O'Rourke, *J. Polym. Sci.*, A-2, **9**, 209 (1971).
138. D. J. Plazek, M. J. Rosner, and D. L. Plazek, *J. Polym. Sci., Polym. Phys. Ed.*, in press (1987).

CHAPTER 13

The Plateau and Terminal Zones in Uncross-linked Polymers

In the transition zone treated in the preceding chapter, viscoelastic properties are dominated by configurational rearrangements of molecular segments which are sufficiently short so that entanglements or even cross-links (unless very closely spaced) play a minor role. As a result, the behavior is not much affected by differences in molecular weight or molecular weight distribution, except when the molecular weight is quite low. In the plateau and terminal zones now to be discussed, the properties are dominated by a quite different feature: the presence of an entanglement network or equivalent topological restraints, which strongly inhibit long-range configurational motions. For the slower relaxation processes, the influence of the molecular environment can no longer be described solely in terms of an average friction coefficient. Molecular weight and molecular weight distribution strongly influence the viscoelastic behavior. Some theoretical expectations of the effects of entanglements have been discussed in Chapter 10, and their manifestation in viscoelastic properties was seen in Chapter 2 in Examples III and IV portrayed there. These features will now be examined in more detail.

A. MANIFESTATIONS OF ENTANGLEMENT NETWORKS

1. Maxima in the Loss Compliance and Retardation Spectrum

Probably the most striking manifestation of a network structure in uncross-linked polymers of high molecular weight, well above the critical value for entanglement coupling, is the maximum in J'' and the corresponding maximum in L which appear in curves III and IV of Figs. 2-7 and 3-4, roughly at the boundary between the

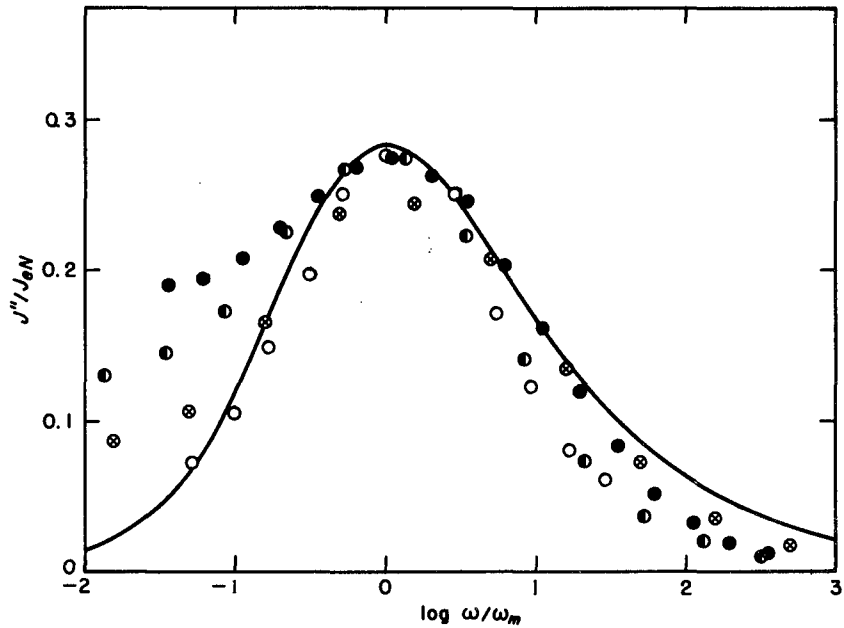


FIG. 13-1. Plots of J''/J_N^0 against ω/ω_m for four polymers:[1] black circles, 1,2-polybutadiene; open circles, 1,4-polybutadiene, cis:trans = 43:50; half black, styrene-butadiene copolymer; crossed circles, polyisobutylene. J_N^0 from equation 4, except for 1,4-polybutadiene (chosen to match the other curves); ω_m from position of maximum on frequency scale. Solid curve is curve D of Fig. 10-7, with linear ordinate (Mooney modification of Rouse theory with most probable distribution of strand lengths). (Sanders, Valentine, and Ferry.[1])

transition and plateau zones of the time or frequency scale. The molecular weight must be sufficiently high so that there are many entanglements per molecule to have these maxima clearly defined.

The Rouse theory modified for *permanently* cross-linked networks predicts such a maximum in J'' as discussed in Section B of Chapter 10, and it is portrayed in Fig. 10-7 with several alternative refinements. In the latter figure, J'' was normalized by dividing by the equilibrium compliance J_e. To examine the shape of J'' for entanglement networks, it is convenient to normalize by the analogous entanglement compliance, J_N^0, which can be obtained by a procedure to be described in the following section. Such a plot is shown in Fig. 13-1, with a linear ordinate scale, for four uncross-linked polymers of high molecular weight;[1,2] the abscissa scale has been arbitrarily adjusted to make the maxima coincide. The shape of the maximum is closely similar for all the polymers and it is rather close to the theoretical prediction of curve *D* of Fig. 10-7, which is shown as a solid curve. At low frequencies, of course, the curves diverge because of entanglement slippage (or, in more general terms, escape from topological restraints); the lower the molecular weight, the more prominently this divergence appears. But the behavior near the maximum and at higher frequencies indicates that the entanglements are acting very similarly to cross-links in this frequency range.

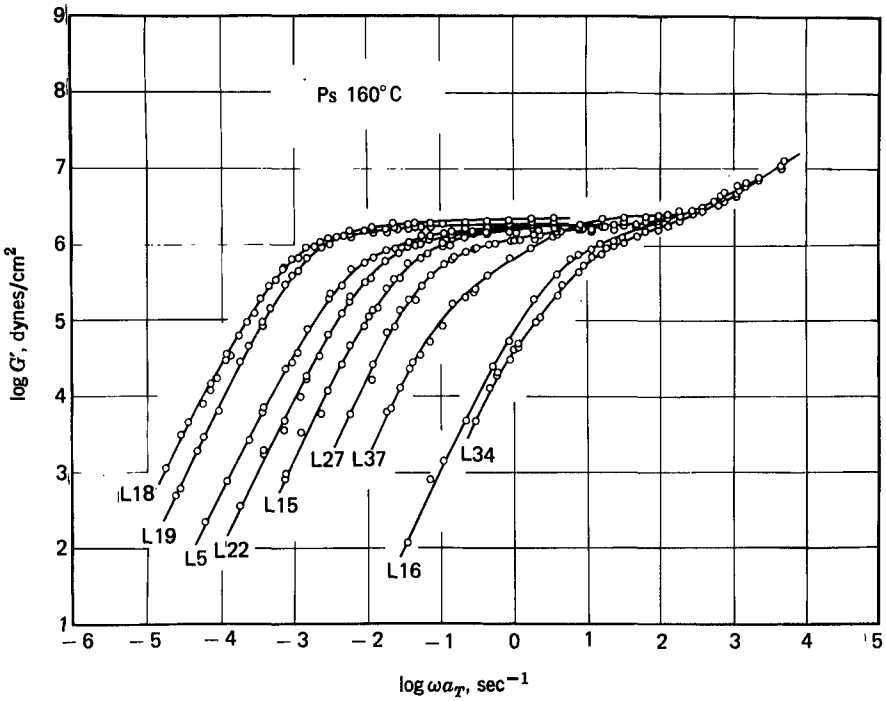


FIG. 13-2. Storage modulus of narrow-distribution polystyrenes,[3] plotted logarithmically against frequency reduced to 160°C. Viscosity-average molecular weights from left to right, $\times 10^{-4}$: 58, 51, 35, 27.5, 21.5, 16.7, 11.3, 5.9, 4.7. (Onogi, Masuda, and Kitagawa.[3])

2. Storage Modulus and Loss Tangent

As pointed out in Section C of Chapter 10, the concept of an entanglement network (or the restraint of each molecule in an effective tube) is associated with a terminal relaxation time which is much longer than it would be in the absence of such topological restraints and increases rapidly with molecular weight. By contrast, the shorter relaxation times are governed by the same monomeric friction coefficient that characterizes rates of translatory motion of short segments in the absence of entanglements. As a result, the terminal zone of the storage modulus (for example) is displaced toward lower frequencies to an extent which increases with increasing molecular weight, while between the terminal zone and the transition zone there appears a plateau region where G' changes only slightly with frequency. This behavior was seen in Fig. 2-3 and is illustrated in more detail in Fig. 13-2. Here, for polystyrenes with sharp molecular weight distribution,[3] the terminal zone shifts progressively to lower frequencies with increasing molecular weight and the plateau zone becomes longer and flatter, while all curves converge in the transition zone. Logarithmic plots of the relaxation modulus against time would have a very similar aspect with the direction of the abscissa scale reversed. A characteristic feature of the plateau zone is that the magnitude of G'' is smaller

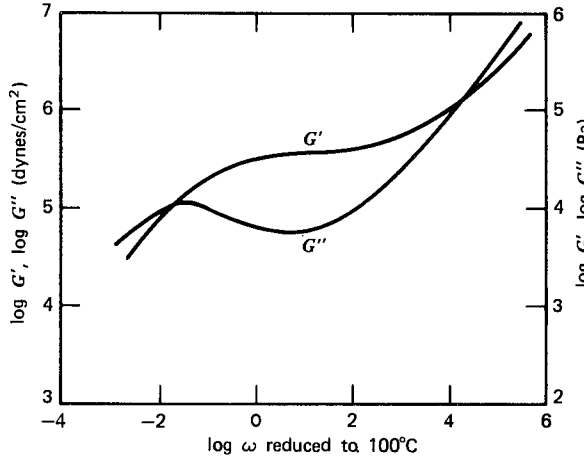


FIG. 13-3. Logarithmic plots of G' and G'' against frequency reduced to 100°C encompassing the plateau zone, from curves IV of Figs. 2-3 and 2-4 (*cf.* also Fig. 12-9), for poly(*n*-octyl methacrylate).

than that of G', as illustrated in Fig. 13-3. In the absence of entanglement coupling, this behavior is never seen in uncross-linked polymers; G'' is always at least as large as G'.

In the plateau zone, the loss tangent thus passes through a minimum as was seen in Fig. 2-8; qualitatively, the losses are small here because the period of oscillation is long compared with the longest relaxation time of an entanglement network strand but short compared with any relaxation times for motions involving entanglement slippage. The minimum in tan δ is illustrated in Fig. 13-4 for several poly(vinyl acetate) fractions.[4] With increasing molecular weight, the minimum deepens (corresponding to decreasing slope of G' in Fig. 13-2) and its location shifts somewhat to lower frequencies.

3. Relaxation and Retardation Spectra

The relaxation spectrum should pass through a minimum in the region where the storage modulus or relaxation modulus is flat, separating the two sets of relaxation times corresponding to motions within entanglement strands and motions across entanglement loci. In practice, the minimum is often blurred, probably in part because of distributions of entanglement spacings and some inhomogeneity of molecular weight even in relatively sharp polymer fractions. Examples illustrated in Fig. 13-5 vary in shape from an extended level region which has been approximated by a rectangular box[5,6] to an undulating form with broad minimum and maximum. A still sharper minimum and maximum are seen in Example III of Fig. 3-3. The box approximation corresponds to rather simple analytical expressions for the viscoelastic functions. For example, the relaxation modulus is given by

$$G(t) = H_b[\mathrm{Ei}\,(-t/\tau_e) - \mathrm{Ei}\,(-t/\tau_m)] \qquad (1)$$

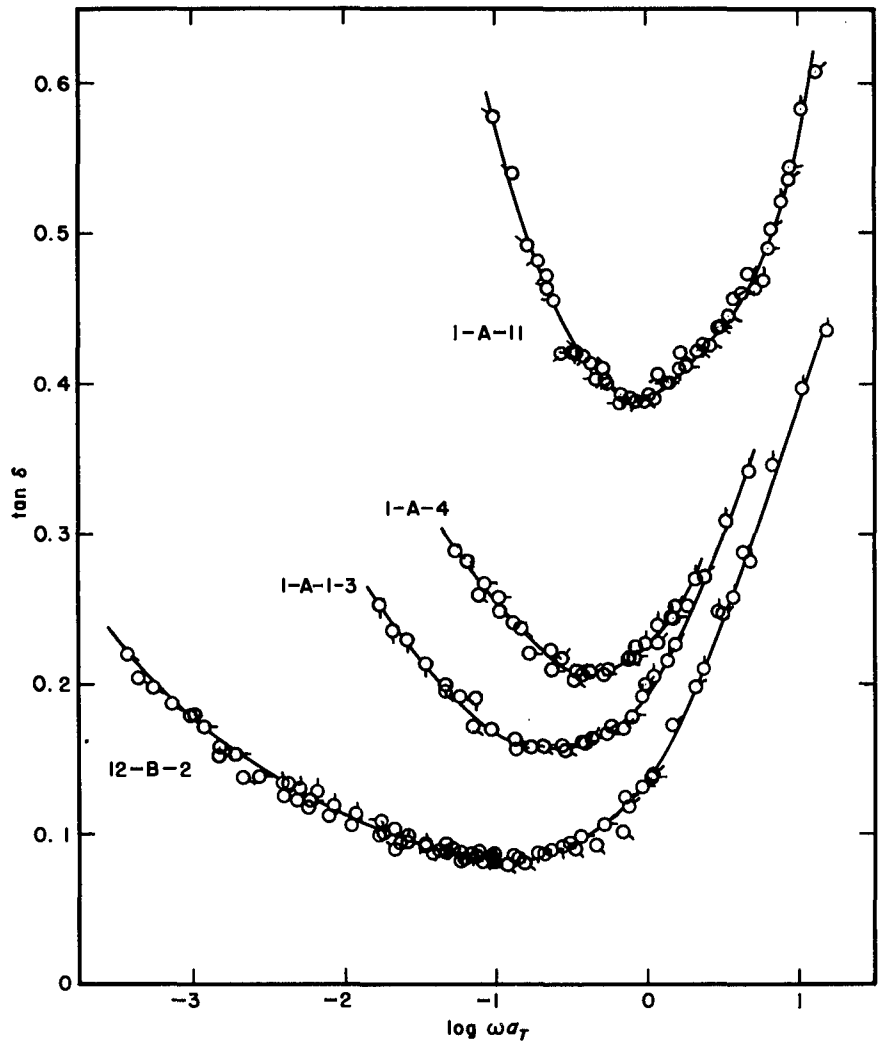


FIG. 13-4. Loss tangent of sharp poly(vinyl acetate) fractions, plotted logarithmically against frequency reduced to 75°C. Viscosity-average molecular weights from top to bottom, $\times 10^{-4}$: 11.2, 26.2, 35.0, 78.0. Points with different pip directions refer to different temperatures of measurement. (Ōyanagi and Ferry.[4])

where Ei is the exponential integral function and the τ's represent the boundaries of the box as shown in Fig. 13-5. In some cases, moderately good agreement with experimental data has been achieved,[5-8] but only for polymers with broad molecular weight distributions. For uniform molecular weight distribution, the theories of Graessley[9] and Doi and Edwards[10] would predict that the relaxation spectrum essentially vanishes in the plateau zone, whereas the intermediate behavior that

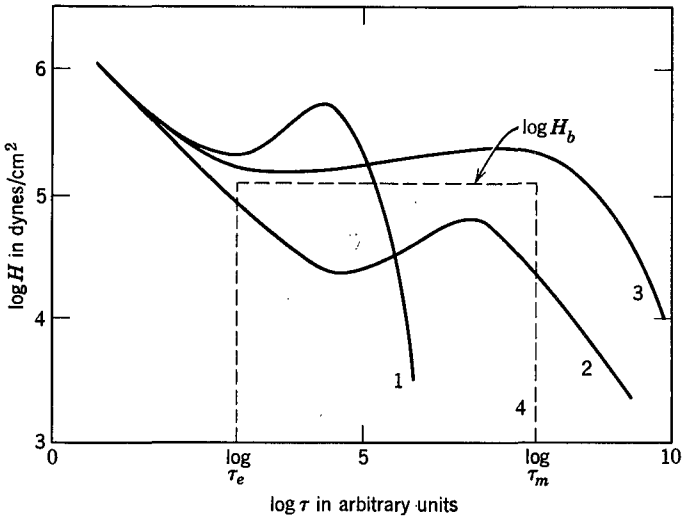


FIG. 13-5. Examples of shapes of the relaxation spectrum in the plateau zone. (1) Polystyrene, very narrow distribution;[3] (2) poly(*n*-octyl methyacrylate), moderately sharp fraction (curve IV, Fig. 3-3); (3) polyisobutylene, broad distribution; (4) box idealization.

is actually observed can be described by the models of Hansen, Williams, and Shen[11] or Thirion[12] with several empirical parameters.

The retardation spectrum is also bimodal as illustrated by Example III of Fig. 3-4 and additional examples[12a] in Fig. 13-6. The separation between the maxima provides a measure of the width of the plateau zone on the logarithmic time scale.[12b,12c]

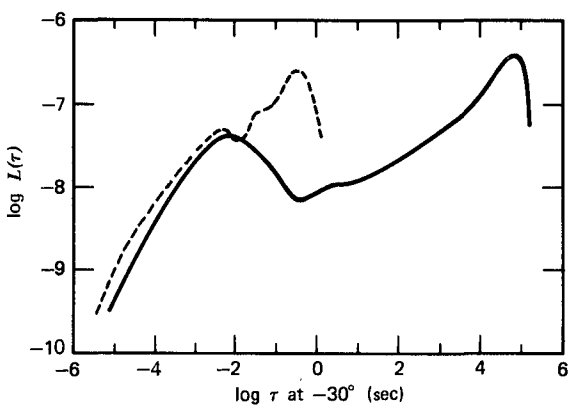


FIG. 13-6. Logarithmic plot of retardation spectrum reduced to −30°C for poly(cis-isoprene) with molecular weight 1.75×10^4 (dotted curve) and 3.95×10^5 (solid curve). (Nemoto, Odani, and Kurata.[12a]) Reproduced with permission from Macromolecules, **5**, 531 (1972). Copyright by The American Chemical Society.

B. ESTIMATIONS OF ENTANGLEMENT SPACINGS

In the conceptual scheme of entanglement coupling, the most important parameter is the average molecular weight between coupling loci, M_e, or the average number of chain atoms, $jP_e \equiv jM_e/M_0$, where j is the number of chain atoms per monomer unit and M_0 the monomer molecular weight; this spacing, or its equivalent in the tube model which corresponds to the tube diameter, is an essential parameter in the theories discussed in Section C of Chapter 10. It should be considered as a measure of the spacing between topological restraints which may not have a clear physical definition but nevertheless can be assigned a numerical value from which various viscoelastic properties can be calculated. There are several methods for estimating this value.

If G' were absolutely independent of frequency in the plateau zone—corresponding to a horizontal segment in the curves of Fig. 13-2—its value here, which may be called G_N^0, the pseudoequilibrium modulus of the entanglement network, could be related by analogy with equation 33 of Chapter 10 to the density of entanglement network strands ν_e:

$$G_N^0 = g_N \nu_e RT = g_N \rho RT/M_e = 1/J_N^0 \tag{2}$$

where g_N is a numerical factor (not necessarily the same as g in the earlier equation but assumed to be unity) and ρ is the density. The factor $\overline{r_E^2}/\overline{r_0^2}$ would be unity because there are no permanent constraints on the strands. (Previously G_N^0 and J_N^0 have often been written G_{eN}^0 and J_{eN}^0.) The value of G_N^0 could similarly be obtained from the plateau zone of the relaxation modulus; or its reciprocal, J_N^0 (*cf.* the discussion in Chapter 2, Section A2), from the plateau of the creep compliance or the dynamic storage compliance. Many values estimated in this manner have been given in the literature. However, unless the molecular weight is exceedingly high, these curves have sufficient slope to make the selection of J_N^0 or G_N^0 quite uncertain. Other methods will now be reviewed.

1. Integration of Retardation Spectrum or Loss Compliance

In Chapter 3, it was pointed out that the contribution of a certain class of retardation mechanisms to the equilibrium compliance can be obtained by integrating over the appropriate portion of the retardation spectrum if a maximum appears there which can be separated from neighboring contributions; the integration is performed in accordance with equation 33 of Chapter 3, and it is illustrated in Fig. 3-7. Alternatively, an integration can be performed over the corresponding maximum in J'' by equation 53 of Chapter 3 with finite limits, as illustrated in Fig. 3-8.

The same procedure can be used for an uncross-linked polymer with sufficiently high molecular weight so that the maximum in L or J'' associated with the entanglement network can be reasonably separated from the contributions at longer times or lower frequencies. The appropriate equations are

$$J_N^0 = \int_a^b L \, d \ln \tau \tag{3}$$

$$J_N^0 = \frac{2}{\pi} \int_a^b J'' \, d \ln \omega \tag{4}$$

Here, the terms J_g and $1/\omega\eta_0$ in equation 53 of Chapter 3 have been omitted because they are negligible. The limits a and b are chosen to encompass the maximum. A similar integration can be performed over the appropriate maximum in G'' (which can be seen in curves III and IV of Fig. 2–4, also Fig. 13–3 and is related to the maximum in H at long times seen in Fig. 13–5), by the following equation (*cf.* equation 55 of Chapter 3 and associated discussion):

$$1/J_N^0 = G_N^0 = \frac{2}{\pi} \int_{-\infty}^{a} G'' \, d \ln \omega \tag{5}$$

There is convergence at the lower limit but the upper must be adjusted to terminate before the transition zone is entered. Corresponding to equation 3, it is also possible

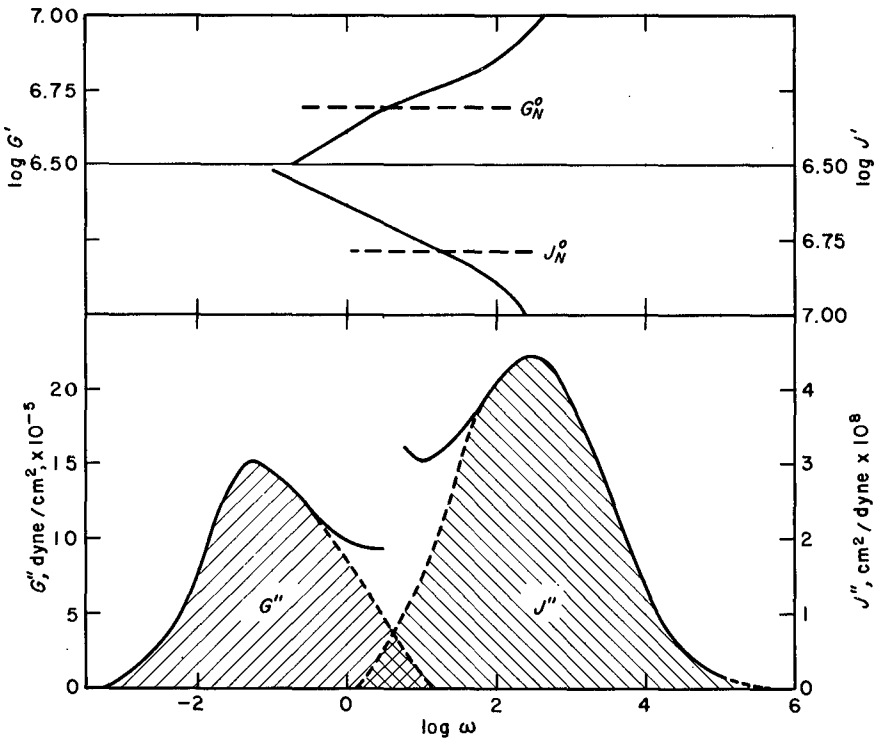


FIG. 13–7. Plateau "levels" in G' and J', and plots of G'' and J'' for integration according to equations 4 and 5, for 1,2-polybutadiene with number-average molecular weight 99,000. Dashed horizontal lines correspond to values of G_N^0 and J_N^0 from these integrations.[1]

Table 13-I

ENTANGLEMENT SPACINGS FROM INTEGRATION OF LOSS COMPLIANCE OR SIMILAR CALCULATIONS

Polymer	Temperature, °C	$\log J_N^0$ (cm^2/dyne)	M_e	j	M_0	jP_e	Ref.
Methacrylate Polymers							
Methyl (conventional)	170	−6.94	4,700	2	100	94	15
Methyl (atactic)[a]	220	−6.59	10,000	2	100	200	16
Methyl (atactic)	131	−6.90	4,800	2	100	96	15
2-Ethyl Butyl	100	−6.16	21,400	2	170	250	17
n-Hexyl	100	−5.94	33,900	2	170	400	18
n-Octyl	100	−5.52	87,000	2	198	880	19
Rubbers							
Hevea rubber	25	−6.76	6,100	4	68	360	1
Hevea rubber	−30	−6.85	3,500	4	68	210	20
1,4-Polybutadiene[c]	25	−7.06	1,900	4	54	140	2
1,4-Polybutadiene[d]	25	−7.12	1,700	4	54	130	21
1,4-Polybutadiene, cis[e]	25	−6.88	2,900	4	54	220	22
Polybutadiene[f]	−10	−6.94	2,500	—	—	—	14
1,2-Polybutadiene[g]	25	−6.79	3,550	2	54	130	1
Styrene-butadiene copolymer[h]	25	−6.89	3,000	4	65.5	180	23
Butyl rubber[b]	25	−6.46	8,500	2	56	300	24
Ethylene-propylene copolymer[i]	25	−7.10	1,660	2	34.3	100	25
General							
Polyethylene	190	−7.36	1,250	2	28	90	25a
Polyisobutylene	25	−6.40	8,900	2	56	320	26
Polyisobutylene	25	−6.46	7,600	2	56	270	30
Poly(dimethyl siloxane)[j]	25	−6.47	8,100	2	74	220	27
Poly(dimethyl siloxane)	25	−6.30	12,000	2	74	330	27a
Poly(dimethyl siloxane)[k]	23	—	8,800	2	74	230	28
Poly(dimethyl siloxane)	25	−6.33	11,300	2	74	300	29
Polystyrene[l]	160	−6.30	18,100	2	104	350	3
Polystyrene	140	−6.31	17,300	2	104	333	30a
Poly(α-methyl styrene)	186	−7.00	13,500	2	118	230	31,32
Poly(vinyl acetate)	60	−6.55	9,100	2	86	210	30

to integrate over the relaxation spectrum H from $-\ln \tau = -\infty$ to a'; this procedure has been used by Chompff and Prins,[13] with a' defined by the location of the minimum in the spectrum.

Numerical integrations for equations 4 and 5 are illustrated in Fig. 13-7 for a 1,2-polybutadiene of number-average molecular weight 99,000. Some guesswork is necessary to decompose the low-frequency end of J'' and the high-frequency end of G'' as measured experimentally and separate the portion attributed to the entanglement network contributions, but the major part of each integral is specified. The higher the molecular weight, the easier it is to define the maximum. In Fig. 13-7, the fact that experimental data from quite different parts of the frequency scale give rather consistent results ($\log J_N^0 = -6.79$, $-\log G_N^0 = -6.69$) is reassuring. These values are drawn as horizontal lines in the upper part of the figure through the measured curves for J' and G' respectively, to illustrate the difficulty of obtaining the entanglement levels from the storage components (although the level at the inflection point is often a good approximation[30]). The integrations can also be performed by computer after fitting the data to an analytical formulation.[14,14a]

Data for equation 4 are more commonly available than for equation 5, which generally requires accurate measurements at very low frequencies or conversion from equivalent transient measurements. Values of J_N^0 calculated from equation 4 for several polymers are summarized in Table 13-I. The data are taken from various sources.[1-3,15-30] In two cases (footnotes h and j), J_N^0 was taken as negligibly different from the corresponding value for J_N for a very lightly cross-linked network, obtained by integrating over the maximum in J'' at *low* frequencies and subtracting this from the equilibrium compliance J_e:

$$J_N = J_e - \frac{2}{\pi} \int_{-\infty}^{a} J'' \, d \ln \omega \tag{6}$$

An analytical extrapolation is necessary to attain the lower limit in this case.[23,27]

The values of J_N^0 range from about 0.8 to 7×10^{-7} cm^2/dyne (except for very large values associated with bulky side groups); to obtain $\log J_N^0$ for units of Pa^{-1},

---

[a] Appears to depend somewhat on molecular weight.

[b] Estimated from very lightly cross-linked sample.

[c] Cis:trans:vinyl = 43:50:7; J_N^0 chosen to normalize data in Fig. 13-1.

[d] Cis:trans:vinyl ≅ 40:50:10.

[e] Cis:trans:vinyl = 96.5:1.9:1.6.

[f] Cis:trans:vinyl = 27:37:36.

[g] Cis:trans:vinyl = 7:1.5:91.5.

[h] Random copolymer, 23.5% styrene by weight; calculated from both equation 4 and equation 6.

[i] Ethylene:propylene = 56:44 by mole.

[j] Calculated from equation 6.

[k] Calculated from analyses of data on cross-linked samples.

[l] Calculated from equation 5.

add 1 to the numbers in column 3. To calculate M_e, it is necessary to make some assumption about g_N in equation 2; it has been simply taken as unity, and this leaves some uncertainty about the absolute values although they should be reliable on a relative basis. Also, it should be mentioned that the use of equation 2 to calculate M_e implies that the compliance of the entanglement network is inversely proportional to T, as it would be for a cross-linked network if the strain energy is entirely entropic. This may not be the case, since the steady-state compliance J_e^0 is inversely proportional to T only far above T_g, and at temperatures in the range from $1.2T_g$ to $2T_g$ may be almost independent of temperature[33] (Section C3 below). Whether the temperature dependence of J_N^0 is similar to that of J_e^0 is not clear; if so, many of the values of M_e in Table 13–I may be too high by as much as 25%, but this does not affect their usefulness for comparative purposes, and for practical application J_N^0 itself rather than M_e is the more important parameter.

To obtain the number of backbone chain atoms between entanglements, jP_e, there is some latitude in deciding how many bonds to count per monomer unit.[34] The values of j chosen and the corresponding values of M_0, suitably averaged in the case of copolymers, are included in the table. The quantity jP_e ranges from 120 to 350, again omitting poly(*n*-octyl methacrylate) in which a much larger value is associated with long side groups. There have been several attempts to correlate jP_e, or simply G_N^0, with molecular structure.[34-38] Qualitatively, it appears to increase with the mean square end-to-end length per monomer unit a and to decrease with increasing M_0. An increase in M_0 (e.g., by larger side groups) is equvalent to diluting the main chain and its effect should be analogous to that of dilution with solvent; increasing a expands each polymer molecule to pervade a larger volume. On the basis of dimensional arguments, Graessley and Edwards[38] deduced that G_N^0 should be proportional to $kT(\nu L)^b l^{2b-3}$, where νL is the total molecular contour length per unit volume (sum of lengths of all main chain bonds), b is the exponent describing the concentration dependence of G_N^0 in concentrated solutions (2 to 2.3, *cf.* pp. 503, 509) and l is the Kuhn step length (related to a). This agrees quite well with data on many different polymers.

2. Other Methods for Estimating M_e

Instead of integrating over the entire maximum of J'' or G'', one can obtain the value of J_N^0 or G_N^0 simply from the peak value of the respective loss component if the shape of the maximum is specified. For example, a phenomenological theory of Marvin and Oser[39,40] predicts the relations

$$J''_m = 0.417 J_N^0 \tag{7}$$

$$G''_m = 0.207 G_N^0 \tag{8}$$

where the subscript m refers to the maximum value at the center of the region which is integrated over in equations 4 and 5 respectively. The Marvin-Oser model corresponds to a uniform entanglement spacing. Actually, from Fig. 13–1 it is evident that the ratio J''_m/J_N^0 corresponds more nearly to the prediction for a cross-linked network with a most probable distribution of strand lengths, for which[41] as por-

trayed in Fig. 10–7

$$J''_m = 0.286 J^0_N \tag{9}$$

The ratio J''_m/J^0_N for other polymers in Table 13–I varies from 0.24 to 0.32. Equation 9 could be used to obtain a rough estimate of J^0_N and from it M_e and jP_e by equation 2; for example, for poly(vinyl acetate), poly(methyl acrylate), and poly(*n*-docosyl methacrylate), values for jP_e of 280, 220, and 2800 respectively are calculated in this manner. An important aspect of this method is that, although the distribution of entanglement strand lengths influences the calculation, neither the distribution of molecular weight nor the magnitude of the average molecular weight affects the result as long as all molecular species are large enough to participate in entanglements. Thus it is unnecessary to have data on a sharply fractionated sample.

3. The Critical Molecular Weight M_C from Viscosity or Viscoelastic Time Scale

Another parameter which characterizes the spacing between entanglements is M_C, the critical molecular weight for influencing steady-flow viscosity by entanglement coupling. As discussed in Section C1 of Chapter 10, M_e and M_C are related, though not in a simple manner; approximately, $M_C \cong 2M_e$. The theory of Graessley[9,32,42] described in Chapter 10 predicts $M_C/M_e \cong 2.5$.

A simple procedure for estimating M_C is from the intersection on the log M scale of two lines drawn through data of steady-flow viscosity plotted logarithmically against molecular weight as in Fig. 10–11. To achieve a slope of unity for $M < M_C$, the data should be corrected for the limiting high molecular weight value of the friction coefficient as explained in connection with that figure. This procedure has been performed for many polymers;[34,43] values are summarized in Table 13–II. Comparisons with M_e values from Table 13–I and in other compilations[32] give ratios for M_C/M_e ranging from 1.7 to 3.0.

The minimum in tan δ as portrayed in Fig. 13–4 is closely related to M_C. According to the Marvin-Oser theory, the depth of this minimum for a polymer with sharp molecular weight distribution is given by[40,46]

$$\tan \delta_m = 1.04(M/M_C)^{-0.80} \tag{10}$$

so that with increasing molecular weight the minimum becomes deeper as observed in Fig. 13–4. Measurements on a series of poly(vinyl acetate) blends[4] showed that, if the molecular weight is not uniform, M in equation 10 can be replaced by $\overline{M}_n$ provided no species with $M < M_C$ are present; otherwise, the observed tan δ_m is smaller than that calculated. The exponent of −0.8 was confirmed, but the value of M_C obtained was 32,500, as compared with 24,500 from the dependence of viscosity on molecular weight.[34] The difference may be due to a distribution of entanglement strand lengths; it suggests that an estimate of M_C may be obtained by equation 10 from measurements on a single sample of known $\overline{M}_n$, with an empirical correction factor of 0.75.

Table 13–II

CRITICAL MOLECULAR WEIGHT M_C FOR ENTANGLEMENT COUPLING FROM DEPENDENCE OF VISCOSITY ON MOLECULAR WEIGHT[32,34]

Polymer	Temperature, °C	M_C	j	M_0	jP_C
Poly(vinyl acetate)	155	24,500	2	86	570
Poly(methyl methacrylate)[a]	217	27,500	2	100	550
Poly(methyl methacrylate)[b]	217	31,500	2	100	630
Polystyrene	217	31,200	2	104	600
	70–230	38,000[d]	2	104	730[d]
	183	33,000[e]	2	104	640[e]
Poly(α-methyl styrene)	186	28,000	2	118	470
Polyisobutylene	217	15,200	2	56	540
Poly(ethylene glycol)	80	4,400	3	44	300
Poly(dimethyl siloxane)	25	24,500	2	74	660
1,4-Polybutadiene[c]	27	5,900	4	54	440
Polyethylene	150	3,800	2	28	270
Poly(decamethylene adipate)	110	5,000	18	284	320

[a] Conventional tacticity.
[b] Atactic.
[c] About 50% cis.
[d] Reference 44.
[e] Reference 45.

From the Marvin-Oser theory, the location of the maximum in J'' on the frequency scale can also be related to entanglement parameters. However, both M_e and M_C are involved; the frequency at the maximum is independent of M (if sufficiently high) but is inversely proportional to M_eM_C. The maximum in G'' occurs at a frequency which is proportional to M_C/M_e and hence is essentially independent of the entanglement spacing, though it is inversely proportional to M^2.

Even though the nature of the entanglement coupling mechanism is described somewhat differently in different theoretical models, as discussed in Section C of Chapter 10, the numerical values in Tables 13–I and 13–II are valuable as quantitative measures of the magnitude of the effect. Pending better understanding of the relation between M_e and M_C, it is probably desirable to use M_e or jP_e in calculations involving magnitudes of moduli or compliances, and M_C or jP_C in calculations involving viscosities or time or frequency scales.

4. The Critical Molecular Weight M'_C from Steady-State Compliance

Still another parameter which is related to the spacing between entanglements is M'_C, the critical molecular weight above which the steady-state compliance J_e^0 becomes independent of molecular weight instead of directly proportional to it.

Table 13–III

CRITICAL MOLECULAR WEIGHT M'_C FOR ENTANGLEMENT COUPLING FROM DEPENDENCE OF STEADY-STATE COMPLIANCE ON MOLECULAR WEIGHT[32]

Polymer	M'_C	M'_C/M_C
Polystyrene	130,000	4.2
Poly(α-methyl styrene)	104,000	3.7
Polybutadiene (about 50% cis)	13,800	2.3
Poly(vinyl acetate)	86,000	3.5
Poly(dimethyl siloxane)	61,000	2.5
cis-Polyisoprene	60,000	6.0

This can be specified in a manner analogous to that which defines M_C, by the intersection of two lines drawn on a logarithmic plot of J_e^0 against M as illustrated in Fig. 10–14. Some values are summarized in Table 13–III. As mentioned in Chapter 10, M'_C is at least twice as large as M_C; the theory of Graessley[32,42] predicts a ratio of 1.8. In view of the extreme sensitivity of J_e^0 to molecular weight distribution (Section C3 of Chapter 10, and Section C below), the higher values in Table 13–III may be associated with residual molecular weight distribution in the polymer fraction studied.[32]

C. BEHAVIOR IN THE TERMINAL ZONE

The viscoelastic properties in the terminal zone are dominated by the characteristic constants η_0, J_e^0, A_G, and $\Psi_{1,0}$ (equation 74 of Chapter 3); and if the molecular weight distribution is sharp, additional constants are the terminal relaxation time τ_1 (or τ_w or τ_d) and a related characteristic time constant τ_η which sets the scale for the shear dependence of non-Newtonian viscosity. Here the entanglements have their maximum effect in influencing the properties which reflect the longest-range molecular motions.

1. Viscosity at Vanishing Shear Rate

A complete discussion of the dependence of the steady-flow viscosity at very small shear rates, η_0, on temperature, molecular weight, and molecular weight distribution is outside the scope of this book; it is available in other sources.[32,34] The theoretical basis has been given in Chapters 10 and 11, and the relation to chemical structure through the monomeric friction coefficient has been pointed out in Section B4 of Chapter 12. A few additional comments are pertinent.

In Figure 10–11, it is evident that η_0 is proportional to $M^{3.4}$ over a considerable range of molecular weights for many polymers. Some investigations[3,44,45,47] have obtained exponents ranging from 3.3 to 3.7. It is doubtful whether these differences are significant departures, in view of the uncertainties of measuring very high molecular weights and the difficulty of making sure that steady-state flow is at-

tained in creep experiments on such materials. A small amount of branched material could result in a higher exponent for very high molecular weights (Section C5 below).

2. Dependence of Non-Newtonian Shear Viscosity on Shear Rate

The dependence of the non-Newtonian viscosity η on shear rate at relatively low shear rates is a property which can be classed with viscoelastic behavior in the terminal zone, since it reflects long-range configurational motions which are influenced by entanglements to the maximum degree. As pointed out in Chapter 10, the characteristic time τ_η which specifies the onset of non-Newtonian behavior with increasing shear rate is closely related to the terminal viscoelastic relaxation time. (In this discussion of shear viscosity, the subscript 21 will be omitted from stress σ and strain γ.)

Values of η measured at different temperatures can be reduced by a procedure exactly analogous to the coordinates numbered 18 in Chapter 11 (*cf.* Section H3 of Chapter 11):

$$\eta_r = \eta/\eta_0 \qquad vs. \qquad \dot{\gamma}\eta_0 T_0\rho_0/\eta_{00}T\rho \tag{11}$$

With logarithmic coordinates this will provide a single composite curve.[3,44,45,48] (Equally good reduction can be obtained by substituting η for η_0 in the abscissa coordinate;[44] this is equivalent to plotting against $\sigma T_0\rho_0/T\rho$, or, almost, simply to plotting against σ, since $\sigma = \dot{\gamma}\eta$ and η_0 is a constant.) Thus the time constants involved in the non-Newtonian mechanism have the same temperature dependence, just as do the relaxation times which specify linear viscoelastic behavior.

Logarithmic plots of η/η_0 reduced to a constant temperature in this manner have very similar shapes in the region of moderate deviations from Newtonian behavior, as already seen in Fig. 10–20 and further illustrated in Fig. 13–8, if samples of sharp molecular weight distribution and different molecular weights are compared; they can be superposed by horizontal shifts along the abscissa axis. The shifts are often found to be linear functions of log M, corresponding to

$$-(\partial \log \dot{\gamma}/\partial \log M)_{\eta/\eta_0} = m_{\dot{\gamma}} \tag{12}$$

$$-(\partial \log \sigma/\partial \log M)_{\eta/\eta_0} = m_\sigma \tag{13}$$

for reduced plots against $\dot{\gamma}$ and against σ respectively. It can be readily shown[45] that $m_\sigma = m_{\dot{\gamma}} + \alpha$, where $\alpha = d \log \eta_0/d \log M$, the exponent discussed in the preceding section. For polystyrenes of sharp molecular weight distribution, two investigations[44,45] have given 4.15 and 4.10 respectively for $m_{\dot{\gamma}}$, with 3.45 for α, so that m_σ is 0.75 or 0.70.

In molecular theories for non-Newtonian viscosity (Section E1 of Chapter 10), the reciprocal of a characteristic time τ_η is a measure of the shear rate above which non-Newtonian viscosity is observed (for example, where η/η_0 falls to about 0.8). It follows from equation 12 that $d \log \tau_\eta/d \log M = m_{\dot{\gamma}}$, and in the above investigations τ_η appears to be proportional to $\eta_0 M^{0.7}$. Studies over wide ranges of molecular weight (many of which include polymer concentration as an additional

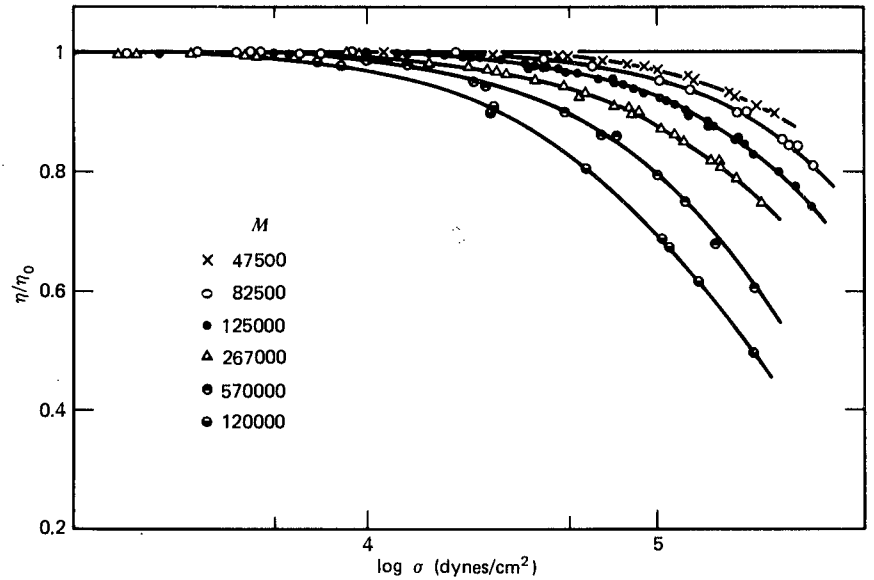


FIG. 13-8. Ratio η/η_0 plotted against logarithm of shear stress, for narrow-distribution polystyrenes[44] with molecular weights as shown.

variable[32]) indicate that, for low M, τ_η is proportional to $\eta_0 M$; whereas, for high M, τ_η is proportional to η_0 only. These correspond, of course, to the molecular weight dependences of the terminal viscoelastic relaxation time τ_1 at low M (equation 7 of Chapter 10) and at high M where entanglements dominate the terminal zone (equation 53 or 57 of Chapter 10). This correspondence confirms the close relation between the two characteristic times τ_1 and τ_η, similar in magnitude and both reflecting the time required for a molecule to escape from its topological restraints (or enter new ones).

At rather high shear rates, plots of log η (not η/η_0) against log $\dot{\gamma}$ for samples of different molecular weights often converge to a single curve[45,49,50] which is practically linear, as illustrated by the data of Stratton[45] in Fig. 13-9. This behavior is reminiscent of the fact that linear viscoelastic properties (including the dynamic viscosity, η') become independent of molecular weight in the transition zone as pointed out in Chapter 12, but it must have a somewhat different molecular origin since long-range molecular motions are certainly involved in steady-state flow even at high shear rates. If the converged curve in Fig. 13-9 is linear (as is provided by the Graessley theory[32] and certain nonlinear constitutive equations[51]) with a slope β, it can be shown that $m_{\dot{\gamma}}$ in equation 13 is equal to $-\alpha/\beta$. For the polystyrene data quoted,[44,45] this makes $\beta = -0.82$, which is the observed slope in Fig. 13-9, and also agrees with the predicted slope of $-9/11$ in the theory of Graessley.[42] This slope has also been observed for poly(dimethyl siloxane)s[52]; it may be a general limiting value for high M. In concentrated polymer solutions, the slope β is often less negative but appears to approach -0.82 as the product cM (where c is concentration in g/cc) increases.[32]

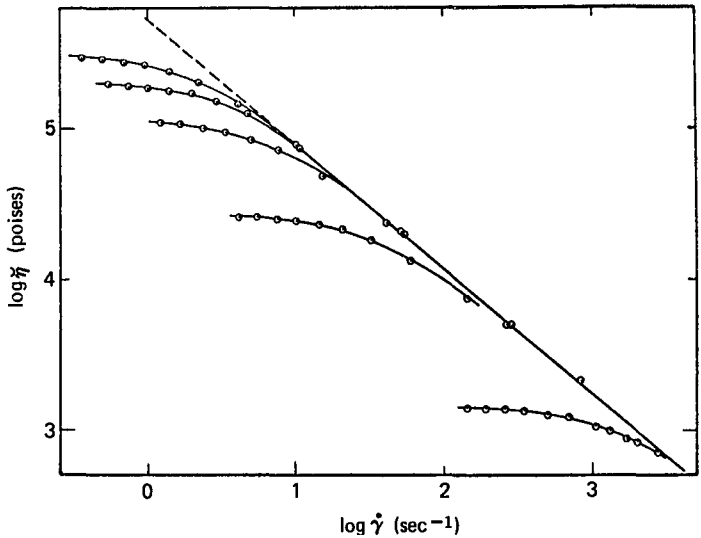


FIG. 13-9. Non-Newtonian viscosity η plotted against shear rate, for narrow-distribution polystyrenes.[45] Molecular weights from top to bottom, $\times 10^{-4}$: 24.2, 21.7, 17.9, 11.7, 4.85.

Although at low shear rates and low frequencies, respectively, the non-Newtonian viscosity η and the dynamic viscosity η' reflect similar characteristic times, it would not be expected that $\eta'(\omega)$ and $\eta(\dot{\gamma})$ should be similar functions at large values of their respective arguments, since steady flow at a high shear rate involves very different molecular motions from oscillating flow at low amplitudes where escape from topological restraints is not required. However, it has been frequently observed that $|\eta^*|(\omega)$ closely resembles $\eta(\dot{\gamma})$. Here $|\eta^*|(\omega) = (\eta'^2 + \eta''^2)^{1/2} = |G^*|/\omega$, with G^* defined by equation 25 of Chapter 1. This correspondence, known as the Cox-Merz rule,[53] has been confirmed experimentally[53-55] and is predicted by certain nonlinear constitutive equations.[56]

3. Terminal Relaxation Time and Steady-State Compliance

For polymers with sharp molecular weight distribution, a terminal relaxation time τ_1 can usually be determined experimentally from the final stages of stress relaxation either after sudden strain[57] or after cessation of steady-state flow;[44] the latter kind of experiment weights the desired parameter more strongly as can be shown by equations 19 and 64 of Chapter 3, when expressed in terms of a discontinuous set of relaxation times rather than a continuous spectrum. Alternatively, it can be obtained from the constant A_G (the ratio of G'/ω^2 at very low frequencies). Since the very narrow distribution of relaxation times in the terminal zone is close to a *single* terminal time τ_1, which may be approximately identified with τ_w of the Graessley theory or τ_d of the Doi-Edwards theory (Section C3 of Chapter 10), equation 3 of Chapter 3 applies approximately and

$$\tau_1 \cong (A_G/G_N^0)^{1/2} \tag{14}$$

Measurements of stress relaxation of polystyrenes[44,58] and poly(α-methylstyrene)s[47] as well as dynamic moduli of polystyrenes[59] have shown that τ_1 is proportional to $M^{3.4}$ as predicted for τ_w by equation 53 or for τ_d by 57 of Chapter 10 together with the empirically established dependence of η_0 on M.

The steady-state compliance J_e^0 can be determined from careful measurements of creep recovery,[60] or from the constant A_G from dynamic measurements at low frequencies[3] by equation 34 of Chapter 3; or, much less directly, from integration over stress relaxation data following sudden strain[58] by equation 54 of Chapter 3 or following cessation of steady-state flow[61] by equation 67 of Chapter 3. Still other sources for this important quantity are from normal stress measurements (equation 74 of Chapter 3)[62] and measurements of the extinction angle in flow birefringence at low shear rates.[63] Data must be regarded with caution not only because of the necessity of carrying experiments to long times or low frequencies but also because traces of species with higher molecular weight (amounts too small to detect by usual molecular weight distribution methods) can cause large errors[60] (*cf.* Section 5 below).

According to the modified Rouse theory of Section A of Chapter 10 for polymers of *low* molecular weight, J_e^0 should be given by equation 11 of Chapter 10:

$$J_e^0 = 0.40M/\rho RT \tag{15}$$

and this agrees rather well with experiment as long as the molecular weight distribution is very narrow (especially free of any high molecular weight tail[60]), M is less than M_C', and the temperature is well above T_g. Data have been reviewed by Graessley,[32] expressed in terms of the dimensionless ratio $J_e^0\rho RT/M$, which varies from 0.3 to 0.5.

For $M \gg M_C'$, if there were really a single terminal relaxation time as implied by equation 14, combination of that equation with equation 34 of Chapter 3 would make the steady-state compliance the same as the plateau compliance: $J_e^0 = J_N^0 = 1/G_N^0$, with J_N^0 given by equation 2. Actually, as shown by Graessley,[32] the ratio J_e^0/J_N^0 is the ratio of what may be termed the weight- and number-average relaxation times in the terminal zone:

$$J_e^0/J_N^0 = \tau_w/\tau_n \tag{16}$$

$$\tau_w = \int_a^\infty \tau^2 H \, d\ln\tau \Big/ \int_a^\infty \tau H \, d\ln\tau \tag{17}$$

$$\tau_n = \int_a^\infty \tau H \, d\ln\tau \Big/ \int_a^\infty H \, d\ln\tau \tag{18}$$

where the lower limit of integration is understood to be set to include the terminal zone only. For uniform molecular weight distribution, the Graessley theory[9] predicts $J_e^0/J_N^0 = 1.798$; the Doi-Edwards theory[10] predicts 1.20.[64] Observed values are somewhat larger than either of these figures, as shown in Table 13-IV. At least part of the difference is probably due to residual molecular weight distribution, since it has been demonstrated[60] that an extremely small amount of material of higher molecular weight can increase J_e^0 substantially. In any case, J_e^0 is essentially

Table 13-IV

STEADY-STATE COMPLIANCES AND RATIOS TO PLATEAU COMPLIANCES, NARROW DISTRIBUTION POLYMERS, $M \gg M'_C$[32]

Polymer	T, °C	J_e^0 cm²/dyne × 10^6	J_e^0/J_N^0
Polyethylene	190	0.22	—
1,4-polybutadiene[a]	25	0.25	2.9
Poly(α-methylstyrene)	200	1.0	3.2
Poly(dimethyl siloxane)	20	1.0	3.0
Poly(vinyl acetate)	30	1.25	3.3
cis-1,4 Polyisoprene	−30	1.4	5.5
Polystyrene	200	1.75	3.5
	160	1.4[30]	2.2

[a] Cis:trans:vinyl = 43:50:7.

independent of M, for very narrow molecular weight distribution and $M \gg M'_C$.

In a molecular weight range near M'_C, the molecular weight dependence of J_e^0 can be described by an empirical equation[32]

$$J_e^0 = \frac{0.40M/\rho RT}{[1 + (M/M'_C)^2]^{1/2}} \tag{19}$$

which for $M \ll M'_C$ reduces to equation 15 and, for $M \gg M'_C$, to the Graessley or Doi-Edwards prediction if M'_C/M_e is 7 or 5 respectively (*cf.* Tables 13-II and 13-III).

In Chapter 12, Section D, it was noted that J_e^0 for polymers of low molecular weight falls sharply with decreasing temperature as T_g is approached, as illustrated in Fig. 12-24. For high molecular weights, incipient behavior of this sort appears to balance the inverse proportionality of J_e^0 to T which is implied in the Graessley or Doi-Edwards theories (equations 52 and 56 of Chapter 10), so that there is a temperature range where J_e^0 goes through a broad maximum and is almost independent of temperature. This is illustrated[33] in Fig. 13-10, where the ratio $(J_e^0/J_{e,\max}^0)^{-1}$ is plotted against T/T_g for several polymers. For this series, a single composite curve is obtained, although it is not expected to apply universally.[33]

It may be noted by combining equations 52 and 53 or 56 and 57 of Chapter 10 that from the Graessley or Doi-Edwards theories

$$\tau_1 = \eta_0 J_e^0 \tag{20}$$

where τ_1 is identified with τ_w or τ_d respectively; and the same is true even for the Rouse theory except for a factor of 1.5. This is convenient for interrelating the effects of different variables on these three terminal zone constants. It has also been noted by Graessley[32,65] that the characteristic time τ_η for onset of non-Newtonian flow is similarly related:

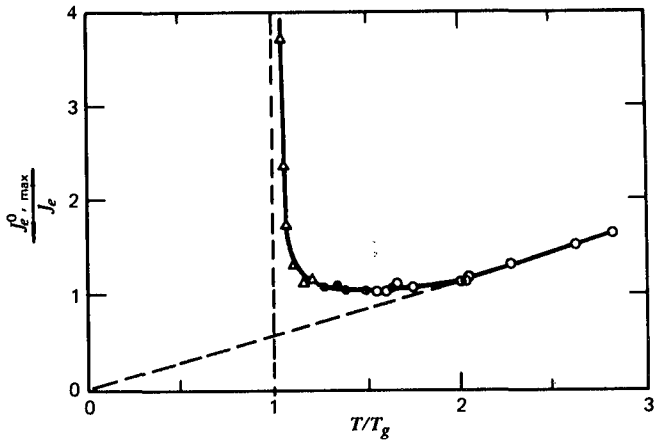


FIG. 13-10. Plot of $J^0_{e,\max}/J^0_e$ against T/T_g for several polymers: open circles, poly(dimethyl siloxane); black circles, polyisobutylene; triangles, polystyrene. (Plazek and Chelko;[33].) Reproduced by permission of the publishers, © IPC Business Press Ltd.

$$\tau_\eta \cong 1.6\ \eta_0 J^0_e \tag{21}$$

again confirming the similarity between τ_1 and τ_η.

4. Effects of Branching

The effect of long-chain branching on the steady-flow viscosity has been extensively studied with branched molecules of various topologies.[34,65] The shape for which results can be most easily interpreted is that of a star with arms of equal length. In the absence of entanglements, the theory of Ham,[66] applicable to this case, gives for the ratio η_{0B}/η_{0L} (where the subscripts B and L refer to branched and linear polymers of the same molecular weight) a value less than unity, as illustrated in Table 10-1; it is equal to g, the ratio of the squares of the respective radii of gyration, and $g = (3f - 2)/f^2$, where f is the number of star arms.[67] When the molecular weight is not too large (approximately, for $M/f < M_C$), this relation agrees reasonably with experiment.[65,34] At higher molecular weights, η_{0B} increases more rapidly and becomes very much larger than η_{0L}, as illustrated by the data of Kraus and Gruver[68] in Fig. 13-11 for polybutadiene stars with three and four arms. Similar results have been obtained for other polymers,[65] especially in concentrated solutions[69] where the highest viscosities are less excessive (as will be described in Chapter 17). The molecular weight dependence of η_0 then corresponds to exponents considerably higher than 3.4, although a logarithmic plot of η_0 against M is generally curved.

This behavior can be understood qualitatively in terms of the tube model for topological constraints, as pointed out by de Gennes;[70] the presence of a branch strongly inhibits the reptation of a molecule along its contour, and motions must be accomplished by "tube reorganization."[71] The critical molecular weight for onset of this behavior would be expected to depend on the branch length; *i.e.*,

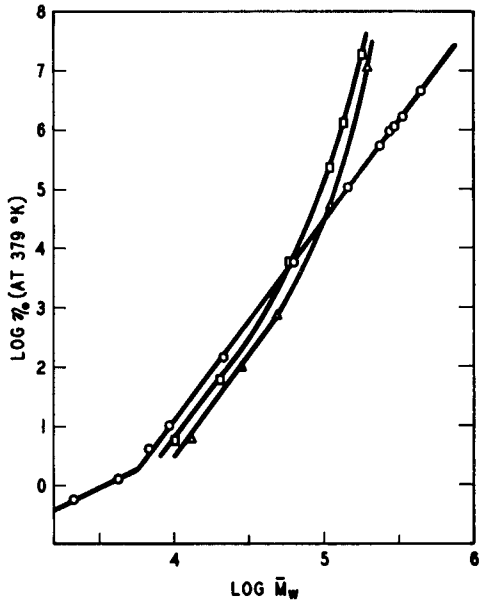


FIG. 13-11. Logarithmic plot of steady-flow viscosity at 379°K against weight-average molecular weight for polybutadienes: circles, linear; squares, three-arm star; triangles, four-arm star. (Kraus and Gruver.[68]) Reproduced, by permission, from the Journal of Polymer Science.

$M/f > M_C$. An approximate theory for the viscosity enhancement due to branching has been presented by Graessley.[65] In some cases, the viscosity of a polymer of very high molecular weight has been observed to be infinite (at small stresses),[27a] despite the absence of a cross-linked network as evidenced by complete solubility; this behavior is probably due to extensive branching which completely inhibits the ability of a molecule to escape from its constraints.

The onset of non-Newtonian flow occurs at a lower shear rate for branched than for linear polymers of the same molecular weight,[68,69] so that at high shear rates the apparent viscosity η may be lower for a branched polymer even when $M > fM_C$. This corresponds to a relatively large value for the characteristic time τ_η.

The effect of long-chain branching on the steady-state compliance in the absence of entanglements would be expected to be a decrease, as for η_0; this is also apparent in Table 10-I, and the ratio $J^0_{eB}/J^0_{eL} = g_2$ can be calculated[73] for stars with f arms of equal length as $g_2 = (15f - 14)/(3f - 2)^2$. (The diminution of J^0_e by branching is seen in dilute solution where entanglements are absent even at high molecular weights, as mentioned in Section B8 of Chapter 9.) When the branches are long enough to entangle, however, J^0_{eB} is larger than J^0_{eL} and often enormously so, as much as a factor of 10 for four-arm stars even when the molecular weight distribution is very narrow.[21,74] For comb-shaped branched polymers, with multiple branched points, a factor of 50 has been observed.[75] In randomly branched polymers, the branching is usually accompanied by a broad molecular weight distri-

bution, and in this case an enormous enhancement of J_e^0 is found.[76] The physical significance of this effect of branching is not clear at present.

It has been observed by Graessley[21,65] that equation 21, and presumably also equation 20, holds also for branched polymers. Since both η_0 and J_e^0 are enhanced by branching when the branches are long enough to entangle, it follows that the terminal relaxation time τ_1 is greatly increased, corresponding to the increase in τ_η which is apparent in the onset of non-Newtonian viscosity.

In branched polymers, the plateau compliance J_N^0 is often not well defined; even for narrow molecular weight distribution, there is no obvious plateau.[21,76a] This is probably related to the suppression of reptation, which forces each molecule to relax by different mechanisms with a broad spectrum of relaxation times.

5. Effects of Molecular Weight Distribution

The effects of molecular weight distribution can be studied by measurements on polymer samples with known continuous distributions or, more instructively, on binary blends, preferably by combining samples with sharp distributions. In the latter case, different results may be expected depending[77] on whether both, only one, or neither of the components has a molecular weight exceeding M_C and can participate in entanglements.

If at least one component has such a low molecular weight that the fractional free volume is affected by molecular ends, the friction coefficient ζ_0 for short-range molecular motions will depend on the blend composition and this influences all time-dependent properties even in the terminal zone. However, the fractional free volume is a linear function of $1/\overline{M}_n$ (equation 67 of Chapter 11) and the time or frequency scale for time-dependent properties (or viscosity) can be corrected[78] to correspond to the limiting value ζ_{00} at high molecular weights by equation 68 of Chapter 11. The necessary information for the correction to constant friction coefficient can be obtained from a variety of sources: time-dependent measurements in the transition zone where differences in ζ_0 can be measured directly;[78] analysis of temperature dependence, giving values of the WLF coefficients which reflect differences in free volume; measurements of the glass transition temperature; and in principle, measurements of the diffusion coefficients of small foreign molecules or of fluorescence depolarization of added dyes (Chapter 12, Section B5). Unless the correction is made, some quite confusing effects can be observed.[78]

The different aspects of behavior in the terminal zone will be reviewed in the same order as the preceding sections: η_0, η, τ_1, and J_e^0.

The steady-flow viscosity η_0 has repeatedly been found to be determined by $\overline{M}_w$ in blends and distributions of widely varying composition,[34,78–80] provided the free volume correction mentioned above is made when necessary, to eliminate the complication that the friction coefficient depends on $\overline{M}_n$ whereas the effects of chain length depend on $\overline{M}_w$.

The decrease in η with increasing $\dot{\gamma}$ is more gradual when there is a broad distribution of molecular weights than for a sharply fractionated polymer. Not many examples have been reported for undiluted polymers[50,81] though there are many

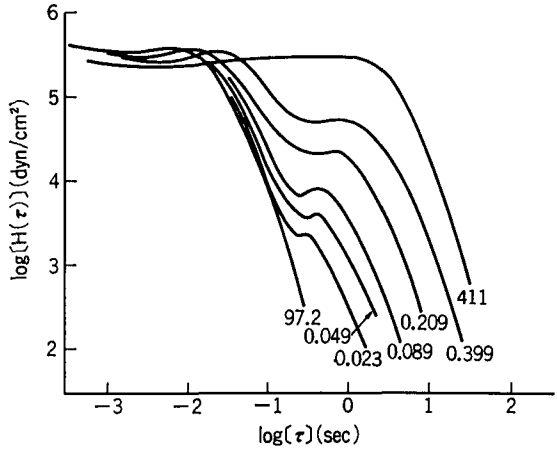


FIG. 13-12. Relaxation spectra reduced to 192°C of blends of two narrow-distribution polystyrenes with molecular weights 97.2 and 411 × 10^3. The outermost curves are for the individual components; numbers on the others denote w_2, the weight fraction of the component with higher molecular weight. (Prest.[85]) Reproduced, by permission, from *Polymer Journal*.

for concentrated solutions (Chapter 17). The shape of a curve of η against $\dot{\gamma}$ can be calculated from the theory of Graessley[42] for any arbitrary molecular weight distribution. A characteristic time constant τ_η can still be identified by matching experiment to theory.[82]

The terminal relaxation time τ_1 is probably impossible to define for a polymer with continuous molecular weight distribution, but for a binary blend in which the molecular weights differ by a substantial factor the final relaxation processes will involve only the component of higher molecular weight. The separation of the contributions of the two components is sharper in transient than in dynamic measurements. In general, the longest relaxation time for component 2, with the higher molecular weight, τ_{1b}, will be smaller than the corresponding value τ_{12} for this component in the pure state by a factor λ_2, as formalized in equation 26 of Chapter 10 and associated discussion.[83,84] Similarly, the longest relaxation time for component 1 is expected to be larger in the blend than in the pure state by a factor λ_1. These effects can be seen qualitatively in Fig. 13-12, where the relaxation spectrum H is plotted in the terminal zone for blends of two narrow-distribution polystyrenes[85] with molecular weights M_1 = 97,000 and M_2 = 411,000. The portion of the spectrum attributable to component 2 shifts to shorter times with increasing proportions of component 1 and vice versa.

The simple blending law of Ninomiya[83] for the relaxation modulus, equation 26 of Chapter 10,

$$G_b(t) = v_1 G_1(t/\lambda_1) + v_2 G_2(t/\lambda_2) \tag{22}$$

where the v's are volume fractions, appears to be satisfactory for low molecular weights.[78] However, it must be modified when entanglements are present. One

modification[85] is to use empirical weighting factors V_i which are not necessarily the volume fractions v_i. In terms of the relaxation spectrum,

$$H_b(\tau) = V_1 H_1(\tau/\lambda_1) + V_2 H_2(\tau/\lambda_2) \tag{23}$$

Application of this formulation by Prest[85] to the data of Fig. 13–12 indicated that $V_1 = v_1$ but $V_2 \cong v_2^2$, at least for $V_2 > 0.4$. The corresponding time shift factors λ_1 and λ_2 were functions of $\overline{M}_w$ and $\overline{M}_z$ respectively. It is of interest that, if the relaxation spectrum is to be independent of molecular weight in the transition zone where H is proportional to $\tau^{-1/2}$ (Section C2 of Chapter 10), the following equation must be fulfilled:

$$V_1\lambda_1^{1/2} + V_2\lambda_2^{1/2} = 1 \tag{24}$$

This was found to be the case for the data of Fig. 13–12.

Alternatively, the volume fractions can be retained as weighting factors, and the viscoelastic functions can be described by higher order blending laws. A quadratic form[85–87] is

$$H_b(\tau) = v_1^2 H_{11}(\tau/\lambda_{11}) + 2v_1v_2H_{12}(\tau/\lambda_{12}) + v_2^2H_{22}(\tau/\lambda_{22}) \tag{25}$$

where the cross-relaxation function H_{12} and shift factor λ_{12} are chosen empirically. An alternative quadratic form derived by Graessley[9] includes two cross terms, H_{12} and H_{21}, which are not necessarily equal. Further extension to a cubic form has been introduced by Kurata and collaborators,[87] with rather good agreement with experimental data on concentrated solutions.

The viscoelastic properties of blends of narrow-distribution polystyrenes[80] and poly(methyl methacrylate)s[88] have also been studied in detail by Onogi and collaborators.

The dependence of the steady-state compliance J_e^0 on molecular weight distribution has received much attention because of its importance in polymer processing. Since, above M_C, J_e^0 is independent of molecular weight, for binary blends it is the same for both components but higher in all mixtures, as illustrated in Fig. 13–13 from data of Akovali[89] and Mills.[90]

The blend compliance J_{eb}^0 cannot be expected to be given by equation 32 of Chapter 10, which was derived from the Rouse theory and applies only in the absence of entanglements. If the compliances of the two components are equal, as in Fig. 13–13, and designated J_e^0, the simple blending law of Ninomiya[5] (equation 22) leads to (*cf.* equation 29 of Chapter 10)

$$J_{eb}^0 = J_{e0}^0[v_1(\lambda_1\eta_{01}/\eta_{0b})^2 + v_2(\lambda_2\eta_{02}/\eta_{0b})^2] \tag{26}$$

where the η_0's are the respective steady-flow viscosities. Combination with equation 28 of Chapter 10 shows that, for $v_2 \gg v_1$, $J_{eb}^0 = J_{e0}^0 v_2^{-1}$. On the other hand, the quadratic blending law, equation 25, or the modified simple blending law of equation 23 with $V_2 = v_2^2$, leads to $J_{eb}^0 = J_{e0}^0 v_2^{-2}$ when $v_2 \gg v_1$.[85] Similarly, a cubic blending law[87] predicts $J_e^0 v_2^{-3}$. Thus the behavior for small additions of a component of lower molecular weight provides an experimental test. Proportionality to v_2^{-2} has often been observed.[3,80]

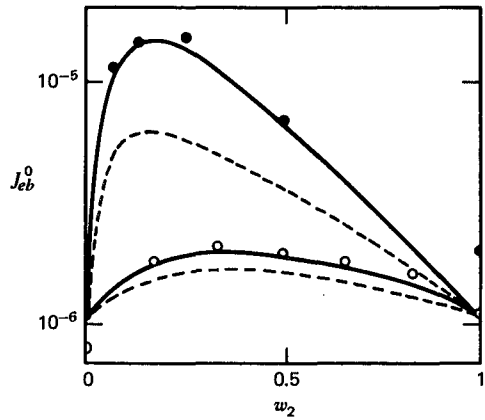


FIG. 13–13. Steady-state compliance J^0_{eb} plotted against weight fraction of high molecular weight component w_2 for binary blends of undiluted polystyrenes: open circles, results of Akovali et al.[89] with $M_1 = 1.25 \times 10^5$ and $M_2 = 2.67 \times 10^5$; black circles results of Mills et al.[90] with $M_1 = 8.68 \times 10^4$ and $M_2 = 5.00 \times 10^5$; solid curves theoretical results from cubic blending law; dotted curves theoretical from quadratic blending law. (Kurata and collaborators.[87]) Reproduced, by permission, from the Journal of Polymer Science.

In terms of molecular weight averages, the simple blending law predicts that J^0_{eb} should be proportional to $\overline{M}_z/\overline{M}_w$, and the quadratic and cubic laws, with the empirical proportionality of η_0 to $M_w^{3.4}$ and certain assumptions about the cross terms, predict proportionality to $(\overline{M}_z/\overline{M}_w)^2$ and $(\overline{M}_z/\overline{M}_w)^3$ respectively.[87] The theoretical curves in Fig. 13–13 indicate that the cubic law is somewhat better for the data shown there. Proportionality of J^0_{eb} to a somewhat higher power of $\overline{M}_z/\overline{M}_w$ (3.4 to 3.7) has also been reported empirically.[90–92] Experimental data must be interpreted with caution, because of possible traces of molecular weight distribution in blend components, which can cause large effects if there are species which have very high molecular weight.

In binary blends composed of component 1 with $M < M_C$ and component 2 with $M > M_C$, different behavior is observed.[93] With increasing proportion of component 1, the short time maximum in the retardation spectrum L is shifted to longer times and the long-time (terminal) maximum is shifted somewhat to shorter times. This behavior is also seen when a diluent is added to a polymer of high molecular weight (Chapter 17).

For a continuous molecular weight distribution, as in most commercial polymers, the terminal zone is broadened enormously and extended to much longer times or lower frequencies than for a uniform molecular weight with the same number-average or even weight-average. This is illustrated by data of Onogi and collaborators with comparison of G' and G'' for two polystyrene samples[80] in Fig. 13–14. The narrow-distribution sample shows the characteristic slopes of 2 for G' and 1 for G'' on the logarithmic plot in the terminal zone. The broad distribution sample, with $\overline{M}_w/\overline{M}_n = 1.57$, has a G' curve extending to lower frequencies without attaining

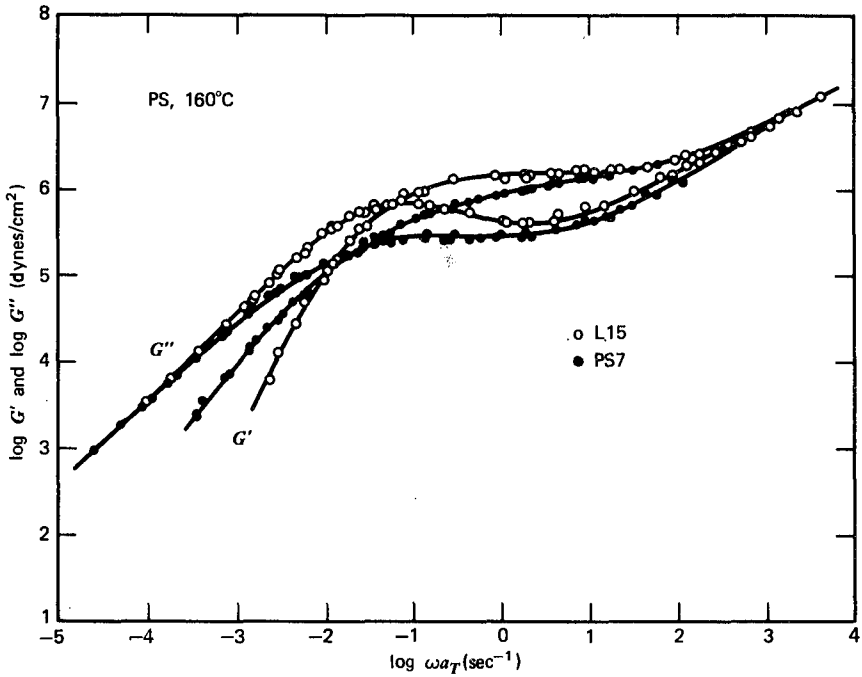


FIG. 13-14. Logarithmic plots of storage and loss shear moduli against frequency reduced to 160°C for narrow-distribution polystyrene with $\overline{M}_w$ = 215,000 (open circles) and broad-distribution with $\overline{M}_w$ = 303,000 and $\overline{M}_w/\overline{M}_n$ = 1.57 (black circles). (Masuda, Kitagawa, Inoue, and Onogi.[80]). Reprinted with permission from Macromolecules, **3**, 116 (1970). Copyright by the American Chemical Society.

the limiting slope of 2, and the G'' curve has much more gradual curvature. In a study of several commercial polystyrenes with $\overline{M}_w/\overline{M}_n$ between 2 and 3, Plazek[94] found retardation mechanisms extending to 10^3 longer times than in a narrow-distribution sample of the same $\overline{M}_n$, and J_e^0 was 20 to 40 × 10^{-6} cm²/dyne as compared with 1.4 or 1.75 × 10^{-6} in Table 13-IV.

From J_e^0, the coefficient $A_G = \lim_{\omega \to 0} G'/\omega^2$ and the limiting primary normal stress coefficient $\Psi_{1,0}$ can be calculated from equations 34 and 74 of Chapter 3 respectively. It is clear that both these coefficients are strongly increased by molecular weight distribution.

D. BEHAVIOR IN THE PLATEAU ZONE

The general features of the plateau zone of linear viscoelastic behavior are already apparent in Figs. 13-2, 13-3, 13-5 and 13-6; it is a region of the time or frequency scale where $G(t)$, $J(t)$, G', and J' change relatively slowly and G'', J'', H, and L exhibit shallow maxima and minima.

1. Width of Plateau Zone on Time Scale

The width of the plateau zone on the logarithmic time or frequency scale involves an arbitrary definition; it could be taken as $\log \tau_1/\tau_{tr}$, where τ_1 is the terminal relaxation time (identifiable with τ_w or τ_d in equations 53 or 57 of Chapter 10) and τ_{tr} is the longest Rouse-mode relaxation time in the transition zone, which can be estimated from equation 37 of Chapter 10 with $p = 1$ and substitution of P_e for P_c (*cf.* Section B6 of Chapter 12). If for τ_1 we choose τ_w of the Graessley theory, the result is from equations 51 and 53 of Chapter

$$\log \tau_1/\tau_{tr} = \log 0.3 + 3.5 \log (M/M_e) \tag{27}$$

This would mean disappearance of the plateau zone with $M/M_e \leq 1.4$, a reasonable point since the effect of entanglements on viscosity disappears at $M \leq M_C$ or approximately $M/M_e \leq 2$.

Experimentally the width of the plateau zone can probably be most clearly defined by the separation between the two peaks in the retardation spectrum as seen in Fig. 13–6. From data on polystyrenes,[30] this appears to be equal to $3.4 \log M/M_C$ when the molecular weight distribution is narrow.

2. Andrade Creep

In creep experiments at the long-time end of the plateau zone where the terminal zone is being entered, it has been shown by Plazek[72,95–97] that the creep compliance can be described with high accuracy by the relation

$$J(t) = J_A + \beta t^{1/3} + t/\eta_0 \tag{28}$$

for poly(dimethyl siloxane)s, polyisoprene, polystyrene, poly(methyl methacrylate), and a solution of cellulose nitrate. The fit is made by plotting $J(t) - t/\eta_0$, after η_0 has been determined from steady-state flow, against $t^{1/3}$ as in Fig. 13–15. An equation similar to this (but without the t/η_0 term) was originally introduced by Andrade[98] to describe the creep of metals. The coefficient β has a temperature dependence corresponding to that for configurational rearrangements characterizing the transition zone; when referred to a standard reference temperature T_0, the ratio $\beta_0 T_0 \rho_0/\beta T \rho$ is found to be identical with $a_T^{1/3}$ as determined from dynamic measurements in the transition zone. Thus, whatever molecular processes are responsible for this slow creep appear to be governed in rate by the monomeric friction coefficient which governs short-range configurational rearrangements.

Equation 28 would imply that the creep compliance in excess of the steady-flow term increases without limit instead of approaching the customary limit J_e^0, and cannot be valid at extremely long times. However, in a range where the last two terms are of similar magnitude, it can provide a useful simplification in calculating η_0 from creep measurements.[95] It is not necessary to wait until $J(t)$ is a strictly linear function of time. A plot of $J(t)$ against $t^{1/3}$ is made, and J_A and β are determined from its linear portion at intermediate times; then $J(t) - J_A - \beta t^{1/3}$ is found to be strictly proportional to t, thus providing a determination of $1/\eta_0$.

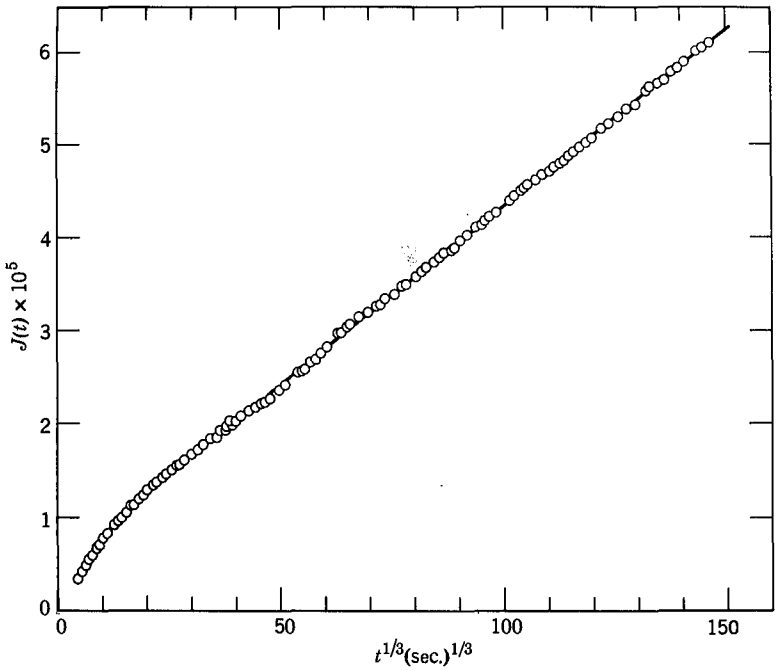


FIG. 13–15. Andrade plot of the creep of poly(dimethyl siloxane), weight-average molecular weight 2.7×10^6, at 25°C for 36 days.[72] The term t/η_0 is negligible.

The retardation spectrum corresponding to equation 28 is[95]

$$L = 0.246\,\beta\,\tau^{1/3} \tag{29}$$

and logarithmic plots of L frequently show a segment over several decades with a slope of $\frac{1}{3}$, as illustrated for conventional poly(methyl methacrylate)[97] in Fig. 13–16. There is an additional segment with the same slope at much shorter times where the glassy zone is entered; between the two is the maximum that is associated with the entanglement network (Section A1).

3. Effects of Molecular Weight Distribution

The presence of molecular weight distribution affects the plateau zone, as would be expected, by making transient and storage functions less flat and smoothing out the maxima and minima in the loss functions and the spectra. In binary (or ternary) blends, multiple plateaus are sometimes discernible, as illustrated for blends of narrow-distribution polystyrenes[80] in Figs. 13–17 and 13–18. It is quite likely that these are related to different species of entanglements, those of component A with component A (highest molecular weight) being effective at lower frequencies than those of A with B or B with B, while component C, having a very low molecular weight, does not participate in entanglements at all.

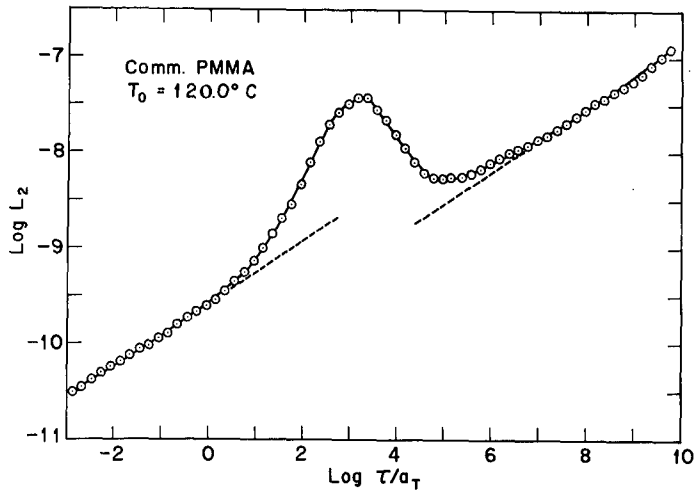


FIG. 13-16. Retardation spectrum of conventional poly(methyl methacrylate) with $\overline{M}_v = 7.6 \times 10^5$, reduced to 120°C. (Plazek, Tan, and O'Rourke.[97]) Reproduced, by permission, from Plazek/Rourke, *Rheol. Acta*, **13**, 367 (1974), Steinkopff Verlag, Darmstadt.

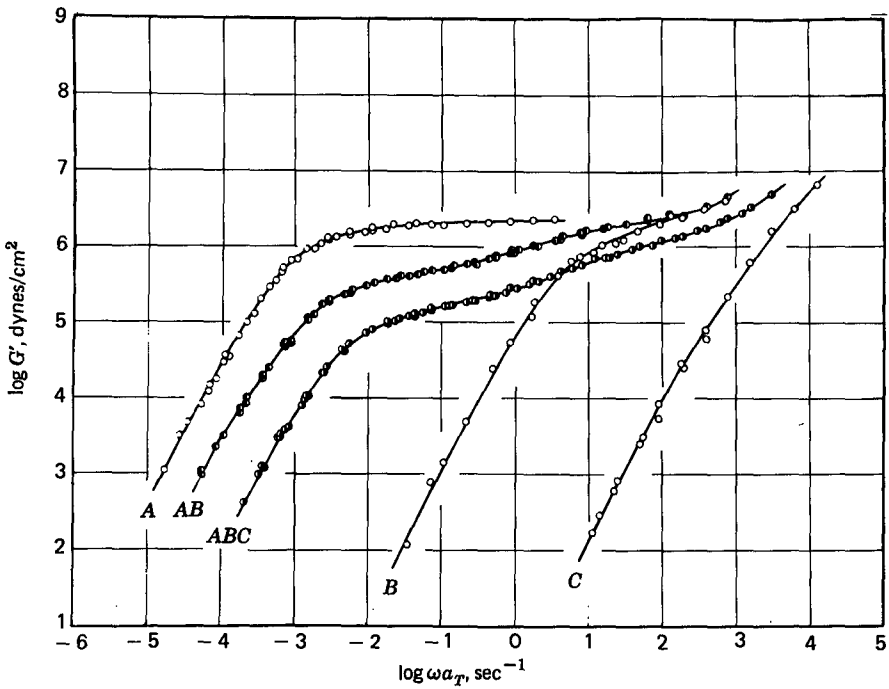


FIG. 13-17. Storage shear modulus reduced to 160°C, for three narrow-distribution polystyrenes and one binary and one ternary blend.[3] Viscosity-average molecular weights, $\times 10^{-4}$: (*A*) 58; (*B*) 5.9; (*C*) 0.89. (*AB*) $v_A = v_B = 0.50$; (*ABC*) $v_A = v_B = v_C = 0.33$.

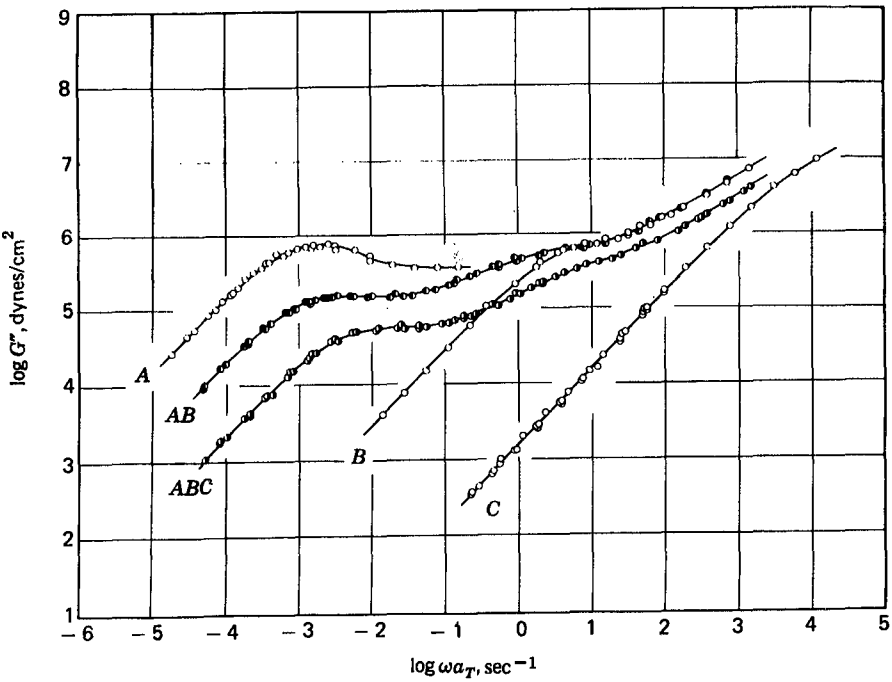


FIG. 13-18. Loss shear modulus reduced to 160°C, for three polystyrenes and two blends as in Fig. 13-17.

The inflections in G' would be expected to correspond to maxima in G'' if the contributions are sufficiently separated; this feature is apparent in Fig. 13-18. In the terminal zone, the curves for G'' and G' are separated substantially corresponding to values of η_0 and A_G respectively which depend on composition as described in Section C above. In the transition zone, the curves all converge except that those for component C and blend ABC lie somewhat to the right on account of the excess free volume caused by the large concentration of molecular ends contributed by the C molecules.

In the terminal and lower plateau regions, component C of blend ABC is acting essentially as a solvent of low molecular weight, in a manner which will be analyzed in Chapter 17. There are many recent studies of binary and ternary blends.[123-126]

E. NONLINEAR BEHAVIOR IN UNIAXIAL EXTENSION

In addition to non-Newtonian shear viscosity, which has been mentioned in Sections C2 and C5, there are a wide variety of nonlinear phenomena observed in various types of deformation, especially shear and simple (uniaxial) extension for deformations with large strains and large strain rates. Some of these have been mentioned in Chapters 1 and 3. Nonlinear behavior in shear has been studied mostly

in concentrated polymer solutions and will be described in Chapter 17. Some aspects of nonlinear behavior in simple extension are discussed here.

1. Stress Relaxation

The time-dependent stress observed in relaxation experiments with large uniaxial extensions is often expressed in terms of a "reduced force" [99] or apparent Young's modulus,[100] as defined in equation 10 of Chapter 6, by analogy with the statistical theory of rubberlike elasticity:

$$E_a(t, \lambda) = 3\sigma_T(t)/(\lambda^2 - \lambda^{-1}) = (3f(t)/A_0)/(\lambda - \lambda^{-2}) \qquad (30)$$

where σ_T is the true tensile stress, f the tensile force, A_0 the initial cross-section area, and λ the stretch ratio (the subscript 1 has been omitted for simplicity). The Gaussian theory of rubberlike elasticity[101] (neo-Hookean elasticity) for a *cross-linked* rubbery polymer at equilibrium predicts that the quantity defined by equation 30 is a constant, equal to Young's modulus E measured in small deformations. Observations at equilibrium show that it is actually a function of λ which has been described by various empirical and theoretical formulations.

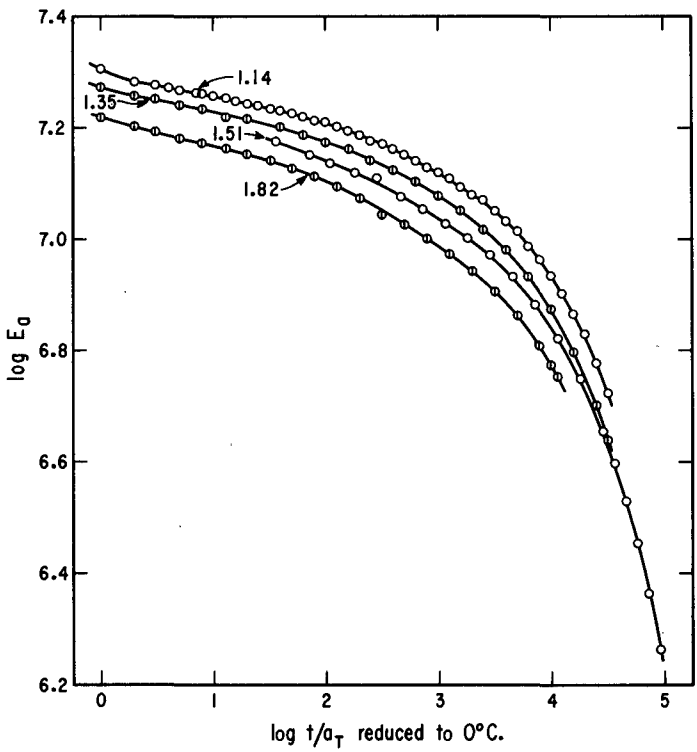


FIG. 13-19. Logarithmic plot of $E_a(t, \lambda)$ as defined by equation 30 against t reduced to 0°C, for a 1,2-polybutadiene at various stretch ratios λ as indicated. (Noordermeer and Ferry.[102]) Reproduced, by permission, from the Journal of Polymer Science.

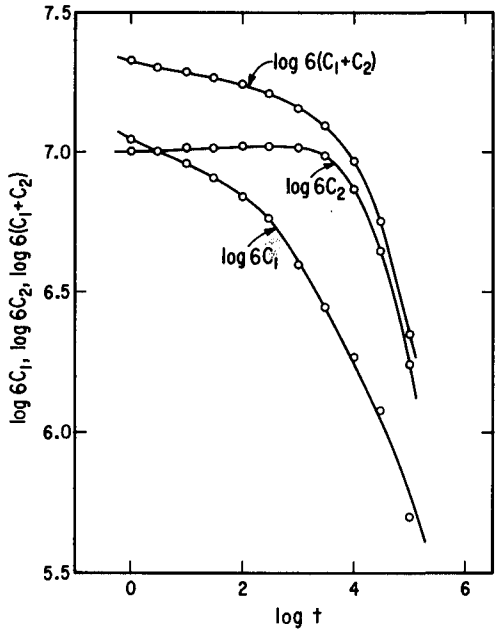


FIG. 13–20. Time-dependent Mooney-Rivlin coefficients C_1 and C_2 calculated from the data of Fig. 13–19. (Noordermeer and Ferry.[102]) Reproduced, by permission, from the Journal of Polymer Science.

The course of stress relaxation in an uncross-linked polymer is illustrated in Fig. 13–19 for a 1,2-polybutadiene[102] by plotting $E_a(t, \lambda)$ logarithmically against t for various λ. If $E_a(t)$ were independent of λ, the curves should coincide. If the stress could be factored into a function of time and a function of strain, as in equation 8 of Chapter 6, the curves should be parallel. Such "factorization" has been observed over more limited time scale for stress relaxation[103] and other time-dependent experiments,[104] but when both plateau and terminal zones are included the curves such as in Fig. 13–19 are not parallel,[100,102,105] as first noted by Arai and Ninomi.[105]

Again by analogy with the treatment of cross-linked polymers, the dependence of E_a on λ at constant time can be fitted to the Mooney-Rivlin equation:[101]

$$E_a(t, \lambda) = 6C_1(t) + 6C_2(t)/\lambda \tag{31}$$

For cross-linked polymers at equilibrium (Chapter 14, Section C1), an equation of this form provides a good empirical fit to stress-strain relations up to moderate extensions,[99] although it is not a proper constitutive equation and is inconsistent with behavior in other types of deformation.[101,106] The data of Fig. 13–19 and many other examples[100,104,105,107] are quite well described by equation 31 with time-dependent C_1 and C_2 as illustrated in Fig. 13–20. The sum, $6(C_1 + C_2)$, corresponds to the relaxation modulus $E(t)$ of linear viscoelasticity. The term with C_1 (which corresponds to neo-Hookean strain dependence) relaxes first and the term with C_2 relaxes about two decades later.

Although the Mooney-Rivlin formulation gives a useful, simple description, and may be convenient for certain derived calculations,[108] the behavior in Fig. 13-19 is preferably described by the theory of Doi,[109] which provides a proper constitutive equation applicable to different types of deformation as well as a molecular basis for the two stages of relaxation. As outlined in Chapter 10, in the framework of the tube model for topological restraints, at times longer than τ_{1r} each segment between restraints has regained a random distribution of configurations but there are two stages of subsequent relaxation if the strain is large: first the different segments equalize their deformations inside the tube with a characteristic time τ_{eq}, resulting in a contraction in the contour defined by the tube, and later the molecule escapes from the tube with a characteristic time τ_d. The predictions of this model describe the data of Fig. 13-19 very well and can also be simulated approximately by the form of equation 31, confirming the utility of the latter for limited purposes. The theory also predicts two stages of stress relaxation in large shear deformations, and agrees well with extensive experiments on concentrated solutions of linear polymers by Osaki and collaborators[123,124] and Ball and Pearson.[125] The stress can be factored into a function of time and a function of strain in the terminal zone, but not if both terminal and plateau zones are included. For extremely high molecular weights, however, deviations from the Doi theory are observed.[123,125]

2. Uniaxial Extension at Constant Strain Rate

The time dependence of stress under conditions of constant strain rate has been discussed for the case of linear viscoelasticity in Section F1 of Chapter 3. For uniaxial extension at constant strain rate $\dot{\epsilon}_1 = (1/\lambda)(d\lambda/dt)$, the time-dependent tensile stress $\sigma_T(t)$ is often expressed in terms of a time-dependent viscosity $\bar{\eta}^+(t) = \sigma_T(t)/\dot{\epsilon}_1$. An example of the stress growth in such elongational flow[110,111] from measurements of Meissner is shown in Fig. 13-21. At low strain rates, $\bar{\eta}^+(t)$ rises at a steadily decreasing rate to approach its steady-state value, as would be expected from equation 58 of Chapter 3, and the steady-state value is $\bar{\eta}_0 = 3\eta_0$ as expected from equation 57 of Chapter 1 when Poisson's ratio is close to $\frac{1}{2}$. At higher strain rates, $\bar{\eta}^+(t)$ departs from the low-shear-rate curve at a time which is approximately inversely proportional to the strain rate and corresponds to a strain of approximately 0.3. It then rises steeply and does not reach a steady state under the conditions of these experiments.

It is evident that the steady-state elongational viscosity, unlike the shear viscosity, increases with strain rate, at least at first. From other experiments by Laun and Münstedt[112] in which the steady state was reached, a comparison of $\bar{\eta}(\dot{\epsilon}_1)$ and $\eta(\dot{\gamma})$ can be made, as in Fig. 13-22. With increasing strain rate, $\bar{\eta}$ rises by nearly an order of magnitude and subsequently falls, while η decreases monotonically with in-

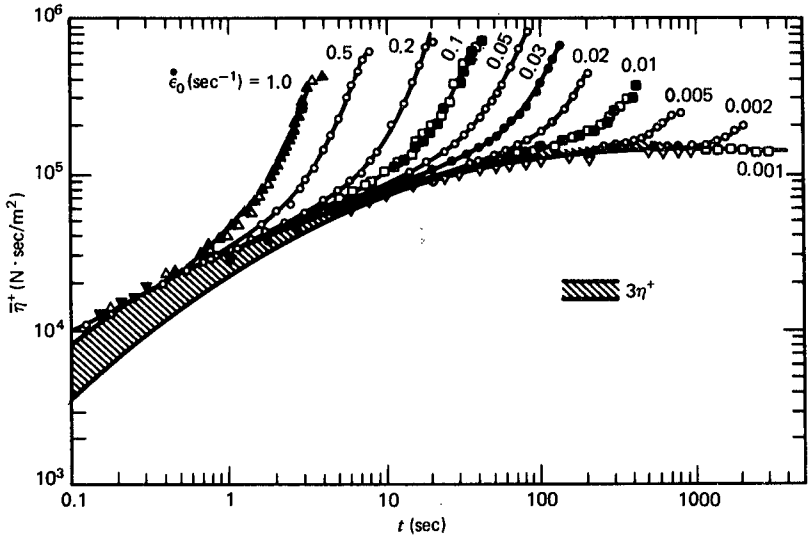


FIG. 13-21. Logarithmic plots of elongational growth viscosity against time for a polyethylene at 150°C at various rates of elongation as indicated. The shaded area is $3\eta^+(t)$ where $\eta^+(t)$ is obtained from shear flow experiments. (Bird,[111] after Meissner.[110]) Reproduced, by permission, from Meissner, *Rheol. Acta,* **10,** 230 (1971). Steinkopff Verlag, Darmstadt.

creasing $\dot{\gamma}$. During the approach to steady state, $\bar{\eta}^+(t)$ sometimes rises monotonically[111,113] but a maximum (stress overshoot) has been observed.[114] Many experiments of this kind have been reported,[115-117] but many of them are on polymers with extremely broad molecular weight distribution and possible branching so that

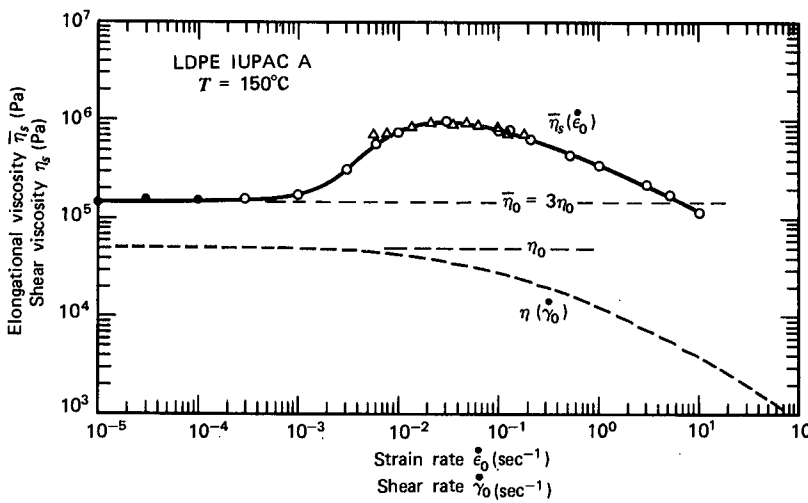


FIG. 13-22. Comparison of shear viscosity $\eta(\dot{\gamma})$ and elongational viscosity $\bar{\eta}\dot{\epsilon}_1$ plotted logarithmically against the respective strain rates, for a polyethylene at 150°C. (Laun and Münstedt.[112]) Reproduced, by permission, from Laun/Münstedt, *Rheol. Acta.,* **17,** 415 (1978), Steinkopff Verlag, Darmstadt.

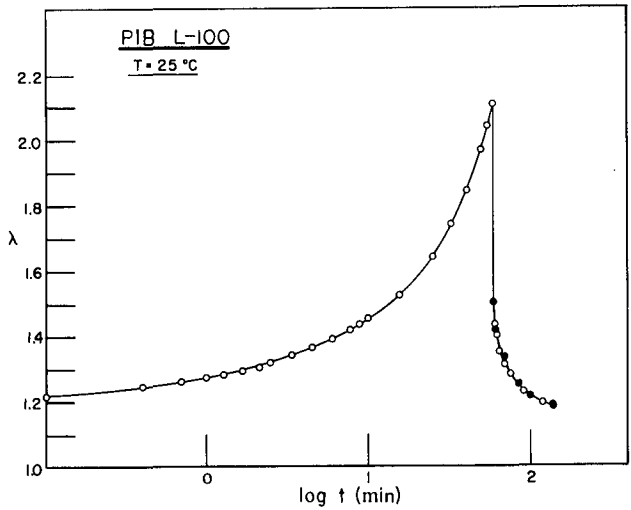


FIG. 13-23. Tensile creep and creep recovery of polyisobutylene of high molecular weight, under large tensile stress; $\lambda = 1 + \epsilon$.[120]

molecular interpretation is difficult. A comprehensive and critical review by Petrie of experimental results and theory has recently appeared.[118]

3. Creep and Creep Recovery

In the course of tensile creep, the form of the time dependence of strain (as expressed by the stretch ratio λ, for example) depends on the magnitude of tensile stress at high stresses.[116,119] Recovery is considerably more rapid than would be predicted from the Boltzmann superposition principle, as illustrated in Fig. 13-23 for polyisobutylene of high molecular weight.[120] The course of recovery is predicted successfully by the theory of Bernstein, Kearsley, and Zapas.[121,122] The stress-dependent recoverable steady-state compliance $D_\sigma = \epsilon_r/\sigma_T$, which is equal to D_e^0 at low stresses, decreases with increasing σ_T.[119] This effect, moderate when the tensile strain ϵ is defined as $\lambda - 1$, is more pronounced when it is replaced by the Hencky strain, defined as $\ln \lambda$.[119] The stress dependence of steady-state compliance in shear will be discussed in Chapter 17. The reader is referred to the review by Petrie[118] for more details.

Various other aspects of nonlinear viscoelastic behavior observed in concentrated solutions, mostly in shear deformations, will be discussed in Chapter 17.

REFERENCES

1. J. F. Sanders, J. D. Ferry, and R. H. Valentine, *J. Polym. Sci.*, A-2, **6**, 967 (1968).
2. R. G. Mancke, R. A. Dickie, and J. D. Ferry, *J. Polym. Sci.*, A-2, **6**, 1783 (1968).
3. S. Onogi, T. Masuda, and K. Kitagawa, *Macromolecules*, **3**, 109 (1970).

4. Y. Ōyanagi and J. D. Ferry, *Proc. 4th Intern. Cong. Rheology,* Part 2, Interscience, New York, 1965, p. 491.
5. W. Kuhn, O. Künzle, and A. Preissmann, *Helv. Chim. Acta,* **30,** 307, 464 (1947).
6. R. D. Andrews, N. Hofman-Bang, and A. V. Tobolsky, *J. Polym. Sci.,* **3,** 669 (1948).
7. R. D. Andrews and A. V. Tobolsky, *J. Polym. Sci.,* **6,** 221 (1951).
8. A. V. Tobolsky, *J. Am. Chem. Soc.,* **74,** 3786 (1952).
9. W. W. Graessley, *J. Chem. Phys.,* **54,** 5143 (1971).
10. M. Doi and S. F. Edwards, *J. Chem. Soc., Faraday Trans. II,* **74,** 1818 (1978).
11. D. R. Hansen, M. C. Williams, and M. Shen, *J. Polym. Sci., Polym. Phys. Ed.,* **9,** 345 (1976).
12. P. Thirion, *J. Polymer Sci., Polym. Lett. Ed.,* **11,** 673 (1973).

12a. N. Nemoto, H. Odani, and M. Kurata, *Macromolecules,* **5,** 531 (1973).

12b. N. Ragupathi, Ph. D. thesis, University of Pittsburgh, 1975.

12c. D. J. Plazek, *Am. Chem. Soc. Div. Org. Coat. Plast. Paper,* **35,** 389 (1975).

13. A. J. Chompff and W. Prins, *J. Chem. Phys.,* **48,** 235 (1968).
14. S. J. Orbon, Ph. D. thesis, University of Pittsburgh, 1978.

14a. C. R. Taylor, personal communication.

15. D. J. Plazek, V. Tan, and V. M. O'Rourke, *Rheol. Acta,* **13,** 367 (1974).
16. T. Masuda, K. Kitagawa, and S. Onogi, *Polym. J.,* **1,** 418 (1970).
17. T. P. Yin and J. D. Ferry, *J. Colloid. Sci.,* **16,** 166 (1961).
18. W. C. Child, Jr., and J. D. Ferry, *J. Colloid Sci.,* **12,** 389 (1957).
19. W. Dannhauser, W. C. Child, Jr., and J. D. Ferry, *J. Colloid Sci.,* **13,** 103 (1958).
20. N. Nemoto, M. Moriwaki, H. Odani, and M. Kurata, *Macromolecules,* **4,** 215 (1971).
21. W. E. Rochefort, G. G. Smith, H. Rachapudy, V. R. Raju, and W. W. Graessley, *J. Polym. Sci., Polym. Phys. Ed.,* **17,** 1197 (1979).
22. J. F. Sanders, Ph. D. thesis, University of Wisconsin, 1968.
23. R. G. Mancke and J. D. Ferry, *Trans. Soc. Rheol.,* **12,** 335 (1968).
24. J. F. Sanders and J. D. Ferry, *Macromolecules,* **7,** 681 (1974).
25. J. R. Richards, R. G. Mancke, and J. D. Ferry, *J. Polym. Sci.,* **B2,** 197 (1964).

25a. V. R. Raju, H. Rachapudy, and W. W. Graessley, *J. Polym. Sci., Polym. Phys. Ed.,* **17,** 1223 (1979).

26. J. D. Ferry, L. D. Grandine, Jr., and E. R. Fitzgerald, *J. Appl. Phys.,* **24,** 911 (1953).
27. N. R. Langley and J. D. Ferry, *Macromolecules,* **1,** 353 (1968).

27a. D. J. Plazek, W. Dannhauser, and J. D. Ferry, *J. Colloid Sci.,* **16,** 101 (1961).

28. N. R. Langley and K. E. Polmanteer, *J. Polym. Sci.,* **12,** 1023 (1974).
29. M. Gottlieb and C. W. Macosko, personal communication.
30. D. J. Plazek, personal communication.

30a. D. J. Plazek, E. Riande, H. Markovitz, and N. Ragupathi, *J. Polym. Sci., Polym. Phys. Ed.,* **17,** 2189 (1979).

31. T. Fujimoto, N. Ozaki, and M. Nagawawa, *J. Polym. Sci.,* A-2, **6,** 129 (1968).
32. W. W. Graessley, *Adv. Polym. Sci.,* **16,** 1 (1974).
33. D. J. Plazek and A. J. Chelko, Jr., *Polymer,* **18,** 15 (1977).
34. G. C. Berry and T. G. Fox, *Adv. Polym. Sci.,* **5,** 261 (1967).
35. D. W. van Krevelen, *Properties of Polymers,* Elsevier, Amsterdam, 1976, p. 338.
36. R. F. Boyer and R. L. Miller, *Rubber Chem. Technol.,* **51,** 718 (1978).
37. S. M. Aharoni, *Polym. Lett.,* **12,** 549 (1974).
38. D. J. Plazek and N. Ragupathi, *Polym. Prepr. Am. Chem. Soc.,* **15(1),** 53 (1974).
39. R. S. Marvin and H. Oser, *J. Res. Nat. Bur. Stand.,* **66B,** 171 (1962).
40. H. Oser and R. S. Marvin, *J. Res. Nat. Bur. Stand.,* **67B,** 87 (1963).
41. R. A. Stratton and J. D. Ferry, *J. Phys. Chem.,* **67,** 2781 (1963).
42. W. W. Graessley, *J. Chem. Phys.,* **47,** 1942 (1967).
43. R. S. Porter and J. F. Johnson, *Rheol. Acta,* **7,** 332 (1968).
44. A. J. Pierson and A. J. Kovacs, personal communication.
45. R. A. Stratton, *J. Colloid Interface Sci.,* **22,** 517 (1966).

46. H. Högberg, S. E. Lovell, and J. D. Ferry, *Acta Chem. Scand.*, **14,** 1424 (1960).
47. T. Fujimoto, N. Ozaki, and M. Nagasawa, *J. Polym. Sci.*, A-2, **6,** 129 (1968).
48. S. Onogi, T. Fujii, H. Kato, and S. Ogihara, *J. Phys. Chem.*, **68,** 1598 (1964).
49. T. Kataoka and S. Ueda, *J. Polym. Sci.*, **A3,** 2947 (1965).
50. D. P. Wyman, L. J. Elyash, and W. J. Frazer, *J. Polym. Sci.*, **A3,** 681 (1965).
51. R. B. Bird, R. C. Armstrong, and O. Hassager, *Dynamics of Polymeric Liquids*, Volume I, Wiley, New York, 1977.
52. C. L. Lee, K. E. Polmanteer, and E. G. King, *J. Polym. Sci.*, A-2, **8,** 1909 (1970).
53. W. P. Cox and E. H. Merz, *J. Polym. Sci.*, **28,** 619 (1958).
54. S. Onogi, H. Kato, S. Ueki, and T. Ibaragi, *J. Polym. Sci.*, **C15,** 481 (1966).
55. E. K. Harris, Jr., Ph. D. thesis, University of Wisconsin, 1968.
56. Reference 51, p. 379.
57. A. V. Tobolsky, J. J. Aklonis, and G. Akovali, *J. Chem. Phys.*, **42,** 723 (1965).
58. A. V. Tobolsky, R. Schaffhauser, and R. Böhme, *Polym. Lett.*, **2,** 103 (1964).
59. J. M. O'Reilly and W. M. Prest, Jr., presented at 5th Intern. Congr. Rheology, Kyoto, 1968.
60. D. J. Plazek and M. O'Rourke, *J. Polym. Sci.*, A-2, **9,** 209 (1971).
61. R. A. Stratton and A. F. Butcher, *J. Polym. Sci., Polym. Phys. Ed.*, **11,** 1747 (1973).
62. W. M. Prest, Jr., *J. Polym. Sci.*, A-2, **8,** 1897 (1970).
63. H. Janeschitz-Kriegl, *Adv. Polym. Sci.*, **6,** 170 (1969).
64. W. W. Graessley, *J. Polym. Sci., Polym. Phys. Ed.*, **18,** 27 (1980).
65. W. W. Graessley, *Acc. Chem. Res.*, **10,** 332 (1977).
66. J. S. Ham, *J. Chem. Phys.*, **26,** 625 (1957).
67. B. H. Zimm and W. H. Stockmayer, *J. Chem. Phys.*, **17,** 1301 (1949).
68. G. Kraus and J. R. Gruver, *J. Polym. Sci.*, **A3,** 105 (1965); *J. Appl. Polym. Sci.*, **9,** 739 (1965).
69. W. W. Graessley, T. Masuda, J. E. L. Roovers, and N. Hadjichristidis, *Macromolecules*, **9,** 127 (1976).
70. P. G. de Gennes, *J. Phys.*, **36,** 1199 (1975).
71. J. Klein, personal communication.
72. J. Klein, *Macromolecules*, **11,** 852 (1978).
73. J. S. Ham, *J. Chem. Phys.*, **26,** 625 (1957).
74. T. Masuda, Y. Ohta, and S. Onogi, *Macromolecules*, **4,** 763 (1971).
75. T. Fujimoto, H. Narukawa, and M. Nagasawa, *Macromolecules*, **3,** 57 (1970).
76. R. H. Valentine, J. D. Ferry, T. Homma, and K. Ninomiya, *J. Polym. Sci.*, A-2, **6,** 479 (1968).

76a. S. Onogi, T. Masuda, and Y. Ohta, reported at Society of Rheology, October, 1979.

77. S. Onogi, T. Masuda, and T. Ibaragi, *Kolloid-Z., Z. Polym.*, **222,** 110 (1968).
78. K. Ninomiya, J. D. Ferry, and Y. Ōyanagi, *J. Phys. Chem.*, **67,** 2297 (1963).
79. T. Kataoka and S. Ueda, *J. Polym. Sci.*, A-1, **5,** 3071 (1967).
80. T. Masuda, K. Kitagawa, T. Inoue, and S. Onogi, *Macromolecules*, **3,** 116 (1970).
81. T. Kataoka, *J. Polym. Sci.*, **B5,** 1063 (1967).
82. W. W. Graessley and L. Segal, *AIChE J.*, **16,** 261 (1970).
83. K. Ninomiya, *J. Colloid Sci.*, **14,** 49 (1959).
84. K. Ninomiya and J. D. Ferry, *J. Colloid Sci.*, **18,** 421 (1963).
85. W. M. Prest, Jr., *Polym. J.*, **4,** 163 (1973).
86. D. C. Bogue, T. Masuda, Y. Einaga, and S. Onogi, *Polym. J.*, **1,** 563 (1970).
87. M. Kurata, K. Osaki, Y. Einaga, and T. Sugie, *J. Polym. Sci., Polym. Phys. Ed.*, **12,** 849 (1974).
88. S. Onogi, T. Masuda, N. Toda, and K. Koga, *Polym. J.*, **1,** 542 (1970).
89. G. Akovali, *J. Polym. Sci.*, A-2, **5,** 875 (1967).
90. N. J. Mills and A. Nevin, *J. Polym. Sci.*, A-2, **9,** 267 (1971).
91. H. J. M. A. Mieras and C. F. H. vanPijn, *Nature*, **218,** 865 (1968).
92. N. J. Mills, *Nature*, **219,** 1249 (1968).

93. S. J. Orbon and D. J. Plazek, *J. Polym. Sci., Polym. Phys. Ed.*, **17**, 1871 (1979).
94. D. J. Plazek and P. K. Agarwal, *Proc. 7th Intern. Cong. Rheology*, Chalmers Univ. Gothenburg, Sweden, 1977, p. 488.
95. D. J. Plazek, *J. Colloid Sci.*, **15**, 50 (1960).
96. D. J. Plazek, *J. Polymer Sci.*, A-2, **4**, 745 (1966).
97. D. J. Plazek, V. Tan, and V. M. O'Rourke, *Rheol. Acta*, **13**, 367 (1964).
98. E. N. da C. Andrade, *Proc. R. Soc.*, **A84**, 1 (1910).
99. J. E. Mark, *Rubber Chem. Technol.*, **48**, 495 (1975).
100. C. R. Taylor, R. Greco, O. Kramer, and J. D. Ferry, *Trans. Soc. Rheol.*, **20**, 141 (1976).
101. L. R. G. Treloar, *The Physics of Rubber Elasticity*, 3rd ed., Oxford, 1975.
102. J. W. M. Noordermeer and J. D. Ferry, *J. Polym. Sci., Poly. Phys. Ed.*, **14**, 509 (1976).
103. R. Bloch, W. V. Chang, and N. W. Tschoegl, *J. Rheol.*, **22**, 1 (1978).
104. M. H. Wagner, *Rheol. Acta*, **15**, 136 (1976); **16**, 43 (1977); M. H. Wagner and H. M. Laun, *Rheol. Acta*, **17**, 138 (1978).
105. K. Arai and M. Niinomi, *Kogyo Kagaku Zasshi*, **74**, 2525 (1971).
106. W. V. Chang, R. Bloch, and N. W. Tschoegl, *Rheol. Acta*, **15**, 367 (1976).
107. C. A. Berglund, *J. Polym. Sci., Polym. Phys. Ed.*, **15**, 2037 (1977).
108. R. L. Carpenter, O. Kramer, and J. D. Ferry, *Macromolecules*, **10**, 117 (1977).
109. M. Doi, and S. F. Edwards, *The Theory of Polymer Dynamics* Claredon Press, Oxford, 1986.
110. J. Meissner, *Rheol. Acta*, **10**, 230 (1971).
111. R. B. Bird, R. C. Armstrong, and O. Hassager, *Dynamics of Polymeric Liquids*, Volume I, Wiley, New York, 1977, p. 188.
112. H. M. Laun and H. Münstedt, *Rheol. Acta*, **17**, 415 (1978).
113. A. S. Lodge and J. Meissner, *Rheol. Acta*, **12**, 41 (1973).
114. M. H. Wagner, T. Raible, and J. Meissner, *Rheol. Acta*, **18**, 427 (1979).
115. J. Meissner, *Pure Appl. Chem.*, **42**, 553 (1975).
116. H. M. Laun and H. Münstedt, *Rheol. Acta*, **15**, 517 (1976).
117. H. Harima and Y. Ōyanagi, *Kōbunshi Kagaku*, **29**, 240, 245 (1972).
118. C. J. S. Petrie, *Elongational Flows*, Pitman, London, 1979.
119. H. Münstedt, *J. Rheol.*, **23**, 421 (1979).
120. L. J. Zapas and T. Craft, *J. Res. Nat. Bur. Stand.*, **69A**, 541 (1965).
121. B. Bernstein, E. A. Kearsley, and L. J. Zapas, *Trans. Soc. Rheol.*, **7**, 391 (1963).
122. A. Kaye, College of Aeronautics, Cranfield, U. K., Note No. 134, 1962.
123. M. Kurata, *Macromolecules*, **17**, 895 (1984).
124. J. P. Montfort, G. Marin, and P. Monge, *Macromolecules*, **17**, 1551 (1984).
125. H. Watanabe and T. Kotaka, *Macromolecules*, **17**, 2316 (1984).
126. H. Watanabe and T. Kotaka, *Macromolecules*, **20**, 535 (1987).

CHAPTER 14

Cross-Linked Polymers and Composite Systems

The introduction of chemical cross-links into an uncross-linked polymer converts it from a viscoelastic liquid to a viscoelastic solid in the sense of the definitions of Chapter 1 and the classification of Chapter 2; the viscosity becomes infinite and the material acquires an equilibrium modulus and compliance, so the properties in the plateau and terminal zones change profoundly. However, the properties in the transition zone may change very little. The effects of cross-linking are discussed in this chapter, as well as the effects in the plateau and terminal zones of incorporating fillers (finely divided particles, usually of high modulus) or other combinations of more than one phase.

A. EFFECTS OF CROSS-LINKING IN THE TRANSITION ZONE

The onset of the transition zone on the frequency scale can be defined as in Fig. 12–9 except that for a cross-linked polymer the left side of the curve for G' goes into the equilibrium modulus G_e instead of the plateau G_N^0 (except for the very lightly cross-linked systems discussed in Section B4 below). The boundary frequency ω_{tr} is given by equation 9 of Chapter 12 according to the Rouse-Mooney theory. Various cross-linked rubbery polymers show similar frequency dependences of G' as the transition zone is entered, as shown in Fig. 14–1; if the logarithmic scales are arbitrarily shifted to make G_e and ω_{tr} coincide for all four polymers shown, the curves nearly coincide.[1]

From the low-frequency region of the transition zone where the corresponding relaxation spectrum has a slope of $-\frac{1}{2}$ on the logarithmic scales, as in Fig. 12–4, the monomeric friction coefficient ζ_0 can be calculated by equation 1 of Chapter 12. If the cross-linking process is not accompanied by side reactions which significantly alter the chemical nature of the polymer, the effects on ζ_0 and the position

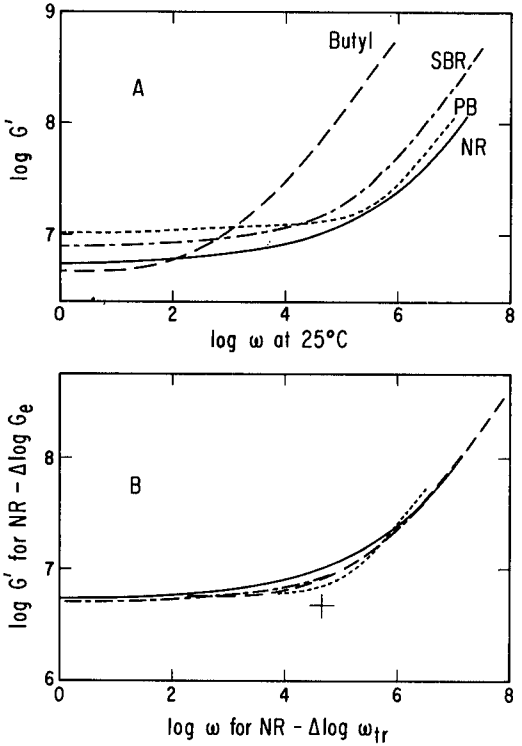


FIG. 14–1. Logarithmic plots of G' against radian frequency at 25°C for four cross-linked polymers showing the onset of the transition zone. (NR) natural rubber; (PB) 1,4-polybutadiene, about 50% trans; (SBR) styrene-butadiene rubber with 23.5% styrene; (Butyl) butyl rubber. All cross-linked with sulfur except SBR by dicumyl peroxide. (A) Plotted directly; (B) with scales shifted to make G_e and ω_{tr} coincide with the values for natural rubber (indicated by cross). Reproduced by permission, from *Science and Technology of Rubber*, edited by F. R. Eirich, Academic Press, New York, 1978.

of the viscoelastic functions on the time or frequency scale are extremely slight as already mentioned in Chapter 12. There appears to be a small shift to longer times or lower frequencies when 1,4-polybutadiene[2] or styrene-butadiene copolymer[3] is cross-linked by dicumyl peroxide, but it is difficult to determine it precisely from viscoelastic measurements. It is probably more accurate to estimate the effect on the monomeric friction coefficient by studying the diffusion of a small foreign molecule and applying the analogy which is evident in Table 12–VII, with the expectation that for a given polymer small differences in ζ_1 will closely reflect small differences in ζ_0. In Fig. 14–2, the diffusion coefficient D_0 of *n*-hexadecane is shown as a function of cross-linking density for three rubbery polymers far above their glass transition temperatures, cross-linked by small amounts of dicumyl peroxide, as measured by Chen.[4] For values of network strand density up to about 2.5×10^{-4} moles/cc, D_0 decreases (and ζ_1 increases) by about 20%.

The origin of the change is not certain, but it may be associated with a decrease in average fractional free volume associated with the formation of a cross-link[5] (in the case of dicumyl peroxide, believed to be a carbon-carbon bond between two

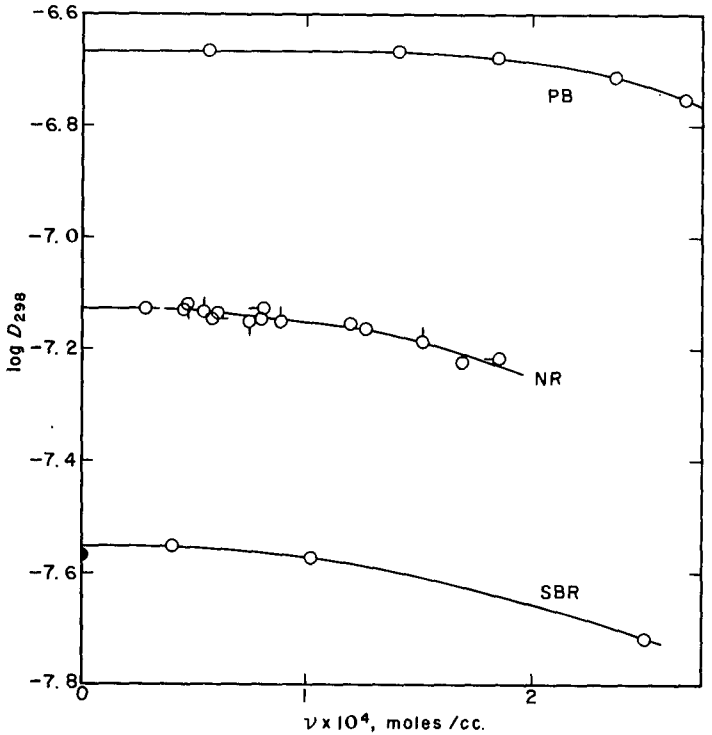


FIG. 14-2. Dependence of diffusion coefficient of *n*-hexadecane on the degree of cross-linking in three polymers in the rubberlike state at 25°C. (PB) 1,4-Polybutadiene, cis:trans:vinyl = 40:53:7; (NR) natural rubber (pips denote four different initial molecular weights before cross-linking, from 2.3 to 7.7 × 10^5); (SBR) styrene-butadiene random copolymer, 23.5% styrene. Abscissa is moles effective network strands per cubic centimeter estimated from swelling measurements. (Chen.[4])

chain atoms[6,7]). Account should also be taken, however, of the slight increase in free volume caused by dilution of the polymer by the cross-linking agent and/or its decomposition products.[3]

If side reactions with the cross-linking agent modify the chemical nature of the polymer, the monomeric friction coefficient can change substantially, as in vulcanization of natural rubber by sulfur, where combined sulfur increases the cohesive energy density of the polymer. The increase in the monomeric friction coefficient[2,8,9] may be attributed to a decrease in free volume in accordance with equations 3 and 49 of Chapter 11; this is associated with an increase in the glass transition temperature with increasing combined sulfur. Such a change is clearly evident in Payne's analysis of dielectric dispersion measurements[10] by the WLF equation in the form with universal constants and an adjustable reference temperature T_s (equation 40, Chapter 11, Section C3); T_s is found to increase progressively with sulfur content. Similarly, in isochronal measurements[11] by Schmieder and Wolf of the characteristic temperature T_M listed in Table 12-II, this temperature was found to increase with content of bound sulfur. By contrast, in parallel studies on natural rubber cross-linked by high energy radiation,[11] no change in T_M was noted. Similar conclusions can be drawn from dielectric dispersion measurements.[12]

B. EFFECTS OF CROSS-LINKING IN THE PLATEAU AND TERMINAL ZONES

1. Maxima in the Loss Compliance and Retardation Spectrum

It has already been pointed out in Chapter 13, Section A1, that maxima in the loss compliance and the retardation spectrum are characteristic of network structures as predicted from the Rouse theory, suitably modified, in Fig. 10–7. Such maxima appear in moderately cross-linked polymers as well as in uncross-linked polymers of high molecular weight, and their shapes are remarkably similar. In Fig. 14–3, J'' is compared for styrene-butadiene copolymer without cross-links[13] and cross-linked[3] to a value of $G_e = 7.3 \times 10^6$ dynes/cm^2, characteristic of a well-vulcanized soft rubber (*e.g.*, curve VI of Figs. 2–1 to 2–8). The curves are both close in shape to that predicted by the Rouse-Mooney theory for a most probable distribution of network strands, *i.e.*, curve *D* of Fig. 10–7, as already evident from Fig. 13–1.

The similarity is not so surprising when it is noted that the *equilibrium compliance* of the cross-linked sample ($\log J_e = -6.865$) is close to the *entanglement network compliance* of the uncross-linked sample ($\log J_N^0 = -6.89$), though the latter has no equilibrium compliance. Generally, in soft vulcanized rubbers, the equilibrium modulus is similar in magnitude to the entanglement network modulus before vulcanization, though it may be higher by as much as a factor of 2; this implies that the entanglements trapped by the cross-linking make a substantial contribution to the elastic properties even at equilibrium, as discussed in the following section. Typically, the ratio of trapped entanglements to cross-links may

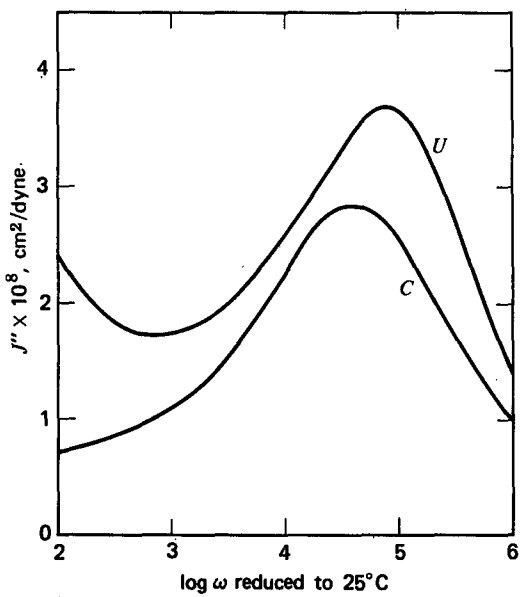


FIG. 14–3. Loss shear compliance (reduced to 25°C) of styrene-butadiene rubber, uncross-linked (*U*)[13] and cross-linked[2] with $\log J_e = -6.86_5$ (*C*).

be from 1 to 9.[14] Thus, the cross-links may not add much to the behavior at the high-frequency end of the plateau zone, although they make an enormous difference at longer times or lower frequencies. The interactions between entanglements and cross-links which determine this behavior are discussed in the sections to follow.

2. Additivity of Contributions of Cross-Links and Trapped Entanglements to the Equilibrium Modulus

According to equation 33 of Chapter 10, the equilibrium shear modulus should be related to the moles of elastically effective network strands per cubic centimeter, ν, as follows:

$$G_e = g(\overline{r_E^2}/\overline{r_0^2})\nu RT \tag{1}$$

where the ratio in parentheses is often taken as unity if the volume has not been changed subsequent to cross-linking. In the absence of trapped entanglements, ν would be interpreted as ν_X, the density of strands terminated by cross-links. It is generally difficult to test this equation by an independent determination of ν_X; careful control of stoichiometry in the introduction of chemical cross-links may give a close estimate in certain cases when the chemistry of the process is clearly understood.[15] However, the proper value of g may remain in doubt; in particular, if the cross-links experience fluctuations instead of being displaced affinely, an additional factor of $(f-2)/f$ should be introduced, or else ν_X should be replaced by $\nu_X - \mu$, where μ is the density of junction points, as discussed in connection with equation 33 of Chapter 10.[16] For present purposes, affine motion of junction points (both cross-links and entanglements) is assumed.

If the initial molecular weight before cross-linking, M, is much higher than the average molecular weight between cross-links, M_c, so that the average number of cross-linked points γ per original molecule is large, the free ends can be neglected and if the cross-linking is tetrafunctional (a bond joining two chains becoming a tetrafunctional branch point), the moles of elastically effective strands between cross-links ν_X should be twice the moles of cross-links ν_c per cubic centimeter. For other functionalities and for lower degrees of cross-linking (only a few cross-linked points per original molecule), the relation between ν_X and ν_c is more complicated.[16,17] The effect of free ends can be approximately taken into account by an additional factor in equation 1 of $1 - b/2\nu_c M$, where b is near 2ρ.[18,19]

Some early studies in which ν_c was estimated stoichiometrically (Bueche,[20] Mullins,[21] and van der Hoff[22]) or by combining data on systems cross-linked to different extents (Kraus[23]) led to the conclusion that ν calculated from equation 1 is not proportional to ν_c, even when corrected for the effect of free ends, and hence that it includes a contribution which is independent of ν_c and is attributed to elastically effective strands terminated by entanglements that were present in the polymer before cross-linking and became permanently trapped by the cross-links, as mentioned in Section B4 of Chapter 10. It is assumed that the total concentration of effective strands (reticulation density[23a]) is

$$\nu = \nu_X + \nu_N \tag{2}$$

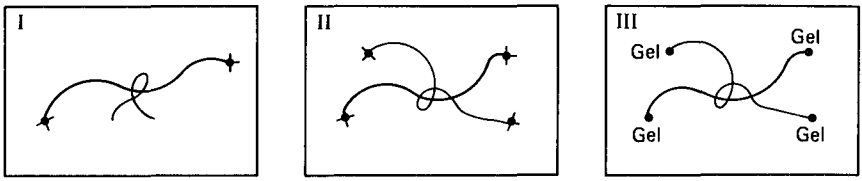


FIG. 14–4. Schematic drawings of criteria for entanglement trapping. (I) Bueche,[20] Mullins,[21] and Kraus;[23] (II) Mancke, Dickie, and Ferry;[24] (III) Langley.[26] Black circles are chemical cross-links.

where ν_N is the concentration of strands terminated by trapped entanglements. (It is evident that the sum of strands terminated by trapped entanglements regardless of whether cross-links intervene and strands terminated by cross-links regardless of whether trapped entanglements intervene is the total number of strands terminated by either type of junction.)

The early treatments of trapped entanglements were based on the criterion that any entanglement on a strand running between two chemical cross-links is trapped, as in Fig. 14–4–I; this led to the relation (for tetrafunctional cross-linking)

$$\nu = 2(\nu_c + \varepsilon)(1 - b/2\nu_c\overline{M}_n) \tag{3}$$

where ε is the moles of entanglement loci per cubic centimeter, *i.e.*, $\varepsilon = \rho/2M_e$; M_e is the average molecular weight between entanglement coupling points. The criterion of Fig. 14–4–I is not sufficiently restrictive; moreover, to apply equation 3 it is necessary to obtain ν from equation 1 assuming $g = 1$ and to trust stoichiometric data for ν_c. Nevertheless, this treatment led to some values of ε and M_e which were similar in magnitude to those derived from viscoelasticity of uncross-linked polymers as reviewed in Section B of Chapter 13.

For quantitative treatment, a more realistic criterion for entanglement trapping is necessary. As an improvement,[24] it can be assumed that all four strands radiating from an entanglement locus must be terminated by chemical cross-links, as in Fig. 14–4–II. In this case, equation 3 must be replaced by

$$\nu = 2\nu_c(1 - b/2\nu_c\overline{M}_n) + 2\varepsilon(1 - b/2\nu_c\overline{M}_n)^2 \tag{4}$$

(An alternative but almost equivalent expression was introduced by Scott.[25])

A more rigorous criterion for entanglement entrapment is that all four strands radiating from an entanglement locus must lead to the permanent three-dimensional network or gel structure, as in Fig. 14–4–III. The probability T_e that an entanglement is trapped in this manner has been calculated by Langley,[26] who treated the more general case where the cross-linking process may be accompanied by simultaneous chain scission, and the gel fraction w_g may not necessarily be unity, as follows:

$$T_e = x^4[1 - 2(1 - e^{-yP})/yP + e^{-yP}]^2 \tag{5}$$

where $x = qw_g/(p + qw_g)$, $y = p + qw_g$, p is the probability that a randomly chosen monomer unit of the original polymer has undergone scission in the cross-linking process, and q is the probability that such a unit is cross-linked (*i.e.*, $\nu_c = q\rho/2M_0$,

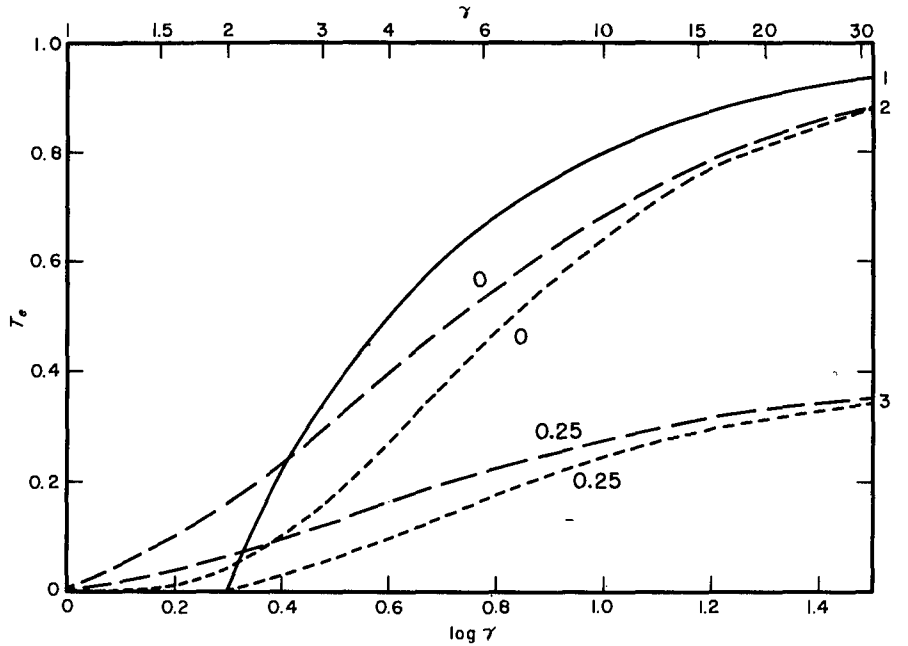


FIG. 14–5. Proportion of trapped entanglements T_e plotted against logarithm of average number of cross-linked points per original polymer molecule. Solid curve, Bueche-Mullins criterion (Fig. 14-4-I); dashed curves, Langley criterion (Fig. 14-4-III). Short dashes, equation 5, for uniform initial molecular weight; long dashes, for initial most probable molecular weight distribution. Numbers denote values of p/q.

where M_0 is the monomer molecular weight); P is the degree of polymerization of the original polymer. Equation 5 holds for uniform molecular weight, but the case for molecular weight distribution has also been treated.[26] In Fig. 14–5, T_e is plotted against the logarithm of the cross-linking index γ (defined as $q\overline{P}_n$), as given by equation 5 with no scission and also with $p/q = 0.25$; the curve corresponding to equation 3, which corresponds to $T_e = 1 - b/2\nu_e\overline{M}_n$, with $b = 2\rho$, is given for comparison. It is notable that substantial fractions of untrapped entanglements remain even for relatively high degrees of cross-linking ($\gamma = 10$, for example); the untrapped entanglements have profound effects on the viscoelastic properties at long times or low frequencies as will be shown below. The total concentration of effective strands is found to be

$$\nu = \nu_X + \nu_N = (q\rho/M_0)w_g T_e^{1/2} + 2\varepsilon T_e \tag{6}$$

as stated in equation 43 of Chapter 10. An example of the increases in ν_X and ν_N with progressive cross-linking is shown in Fig. 14–6. Eventually T_e approaches unity, the entanglements become all trapped, and ν_N approaches 2ε.

Additivity of the contributions to modulus from cross-links and from trapped entanglements with T_e calculated from the Langley theory has been confirmed in several investigations in which ν_X has been obtained from analysis of sol-gel

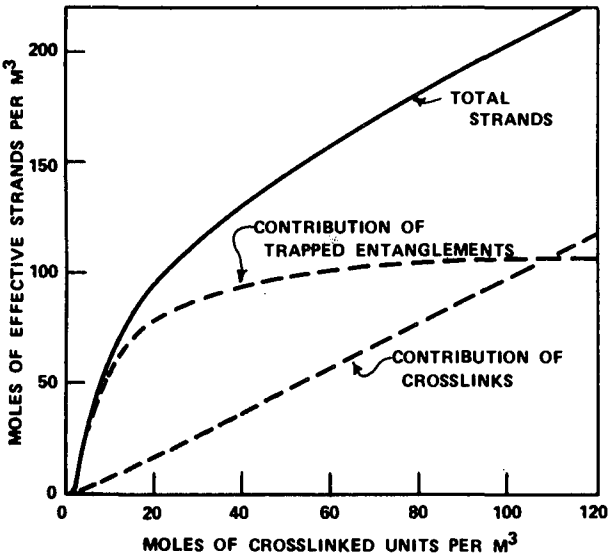


FIG. 14-6. Calculated contributions of cross-link strands and trapped entanglement strands to total number of effective strands in moles/m^3, plotted against concentration of cross-linked units, for poly-(dimethyl siloxane) with $\overline{M}_n = 0.5 \times 10^6$ and $\overline{M}_w = 1.0 \times 10^6$ from equation 6. (Langley and Polmanteer.[27]) Reproduced by permission, from The Journal of Polymer Science.

relations[27-29] or from stoichiometry where bifunctionally terminated oligomers are joined by trifunctional or tetrafunctional cross-linking agents to form end-linked networks.[30] In the latter case, a slight departure from completeness of the reaction can sharply diminish both ν_X and ν_N.[30a] Also, studies of networks cross-linked in strained states permit confirmation of this additivity with agreement with the Langley calculation for T_e from mechanical measurements alone.[31,32] There is, however, some uncertainty about the proper value of the front factor g in equation 1 (*cf.* Section B1 of Chapter 10).

It should be added that alternative interpretations of the relation of modulus to degree of cross-linking have been presented,[33-35] and in particular that the above discussion of additivity has ignored the fact that there is an important contribution to modulus from the strain enthalpy[35] in addition to the contribution from strain entropy which is proportional to T in equation 1. However, the additivity expressed in equation 2 is consistent with many aspects of viscoelastic behavior and will be taken as the basis of much of the discussion in this chapter.

3. Changes in the Retardation Spectrum during Early Stages of Cross-Linking

Focusing attention on permanent linkages between molecules only, and ignoring entanglements for the moment, we can cite well-known statistical theories[16,36-40] to show what happens in branching and network formation during progressive random cross-linking of an initially linear polymer. At first there is branching with progressively increasing complexity, and the weight-average molecular weight rises

at an increasing rate to become infinity at the gel point where the three-dimensional network first appears. For an initially uniform molecular weight, the gel point corresponds to a value of γ, the average number of cross-linked units on each molecule, of unity. With further cross-linking, an increasing proportion of the total mass is bound to the permanent network or gel; this proportion, w_g, is related to γ by the equation[37]

$$\gamma = -[\ln(1 - w_g)]/w_g \tag{7}$$

Eventually, at high γ, w_g becomes unity. In the neighborhood of the gel point, the molecular weight distribution is extremely broad, and the smallest species are the last, on the average, to become attached to the network as $w_g \to 1$. When there is an initial molecular weight distribution or if the cross-linking process is accompanied by simultaneous scission of molecules, the treatment is more complicated.

Because of the high molecular weight, broad molecular weight distribution, and extensive branching, a polymer approaching the gel point can be expected to have not only a very high viscosity (approaching infinity) but also a very high steady-state compliance, on the basis of the discussion in Sections C4 and C5 of Chapter 13; and also some viscoelastic mechanisms with extremely long relaxation or retardation times. This was found to be the case in a study by Valentine[41] on 1,4-polybutadiene, which can be combined with other data on more highly cross-linked samples[2] to show the progressive changes in viscoelastic properties, as illustrated by the retardation spectra in Fig. 14–7.

Here curve 0 is for the initial uncross-linked polymer, with molecular weight 180,000 (fairly sharp distribution) and in accordance with Table 13–I about 95 entangled loci on each molecule. It shows the classic retardation spectrum of this type of system (*cf.* curves III and IV of Fig. 3–4); there is a maximum at the left associated with the entanglement network and a maximum at the right associated with mechanisms involving entanglement slippage. The longest retardation time is of the order of 10 sec. Curve 1 is for $\gamma = 0.3$, *i.e.*, moderate branching well short of the gel point. The contributions to compliance from mechanisms with long retardation times are enormously increased, and in fact neither η_0 nor J_e^0 could be measured within the experimental time scale. Curve 2 is for $\gamma = 1.2$, just past the gel point ($\gamma = 0.9$ for this molecular weight distribution), with $w_g = 0.32$. The magnitudes of the long-time contributions are now diminished, but they extend to enormously long times, in excess of one day (10^5 sec). Progressively increasing extents of cross-linking (curve 3: $\gamma = 3.7$, $w_g = 0.97$; curve 4: $\gamma = 13$; curve 5: $\gamma = 25$) cause progressive decreases in these mechanisms at long times, until at 25 cross-link points per molecule they have nearly disappeared, although some contributions remain with retardation times as long as 1 sec.

It is notable that with increasing cross-linking the first maximum in the spectrum, in the neighborhood of -6 on the logarithmic time scale, changes very little though it shifts slightly downward and to the right. The change downward is consistent with the fact that up to 25 cross-links per molecule have been added to the 95 entanglements per molecule in the network which this maximum represents. The longest relaxation time of a single network strand would be calculated by the modified Rouse theory and equation 37 of Chapter 10, if the strands were of uniform

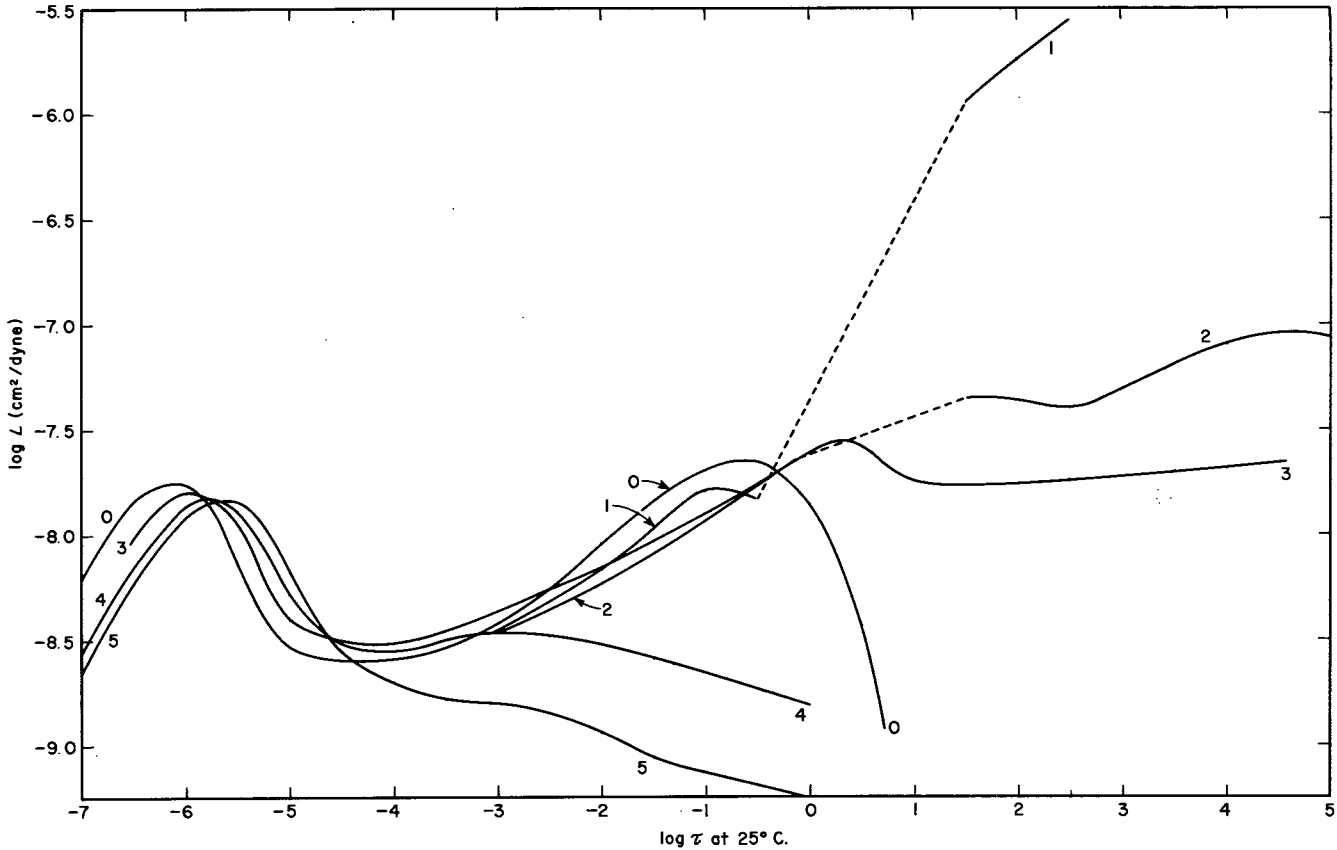


FIG. 14-7. Retardation spectra of 1,4-polybutadiene (cis:trans:vinyl = 40:53:7, $\overline{M}_w$ = 180,000) at various stages of cross-linking, reduced to 25°C. Values of γ, cross-linked units per molecule: (0) none; (1) 0.28; (2) 1.2; (3) 3.7; (4) 13; (5) 25. 1 and 2 cross-linked by sulfur (0.35 and 0.52%, respectively); 3, 4, and 5 by dicumyl peroxide. Dashes join curves in regions where data are missing.[41]

length, to be 0.3×10^{-6} sec, in agreement with the location of this maximum on the abscissa scale.

This investigation is subject to some reservations because of gaps in the time scale covered and the fact that some of the samples were cross-linked with sulfur (in very small amounts) and others with dicumyl peroxide. However, it presents a qualitative view of the profound changes in viscoelastic properties in the early stages of cross-linking. The very slow retardation processes evident in curve 1, short of the gel point, may be attributed to the combined effects of branching and entanglements. The slow processes evident in curves 2 and 3 may be attributed primarily to the motions of dangling or floating branched structures which are attached to the network but pass through untrapped entanglements which eventually permit relaxation to random configurations as discussed in Section 4 below. It is striking that the times required for such motions are longer than the longest relaxation time of a single network strand by a factor of at least 10^{11}.

4. Approach to Elastic Equilibrium in Lightly Cross-Linked Systems

Curve 3 of Fig. 14–7 shows that, in a polymer sufficiently cross-linked to bind 97% of the mass to the gel structure, there are time-dependent processes extending to at least the length of one day at 25°C. This means that attainment of elastic equilibrium is difficult, and measurement of the equilibrium modulus G_e (or J_e, E_e, or D_e) must be performed with caution. Actually, even when the degree of cross-linking is considerably greater, precise measurements of stress and strain can detect progressive changes over long periods. This behavior was observed by Martin, Roth, and Stiehler[42] and Wood and Roth[43]; it has been extensively studied in stress relaxation experiments by Thirion and Chasset[44-47] and in creep by Ferry, Dickie, Mancke and Sanders[2,47-49] and by Plazek[50] on natural rubber, styrene-butadiene rubber, and polybutadienes; and by Sperling and Tobolsky[52] on cross-linked poly(dimethyl siloxane) and poly(ethyl methacrylate).

An example of stress relaxation experiments[45] in extension is shown in Fig. 14–8, for five samples of natural rubber cross-linked by dicumyl peroxide. Values of M_c, the number-average molecular weight between cross-links, are given, though these must be considered as having only relative significance since they are derived from swelling measurements and based on uncertain assumptions. The stress at 50% extension reaches an equilibrium value within experimental error for $M_c = 5400$, but for larger values of M_c (less cross-linking) the stress is still relaxing after one day. In such experiments, indeed, it is necessary to distinguish carefully between viscoelastic stress relaxation and loss of stress due to chemical degradation,[44] since the latter may set in before the former is finished. Since the measurements of Fig. 14–8 and others in extension are made at substantial finite deformation, the linear relaxation modulus $E(t)$ cannot be obtained from them directly. However, measurements at different elongations show that equation 8 of Chapter 6,

$$\sigma_T(t, \lambda_1) = \mathcal{J}(\lambda_1)E(t) \tag{8}$$

where $\lambda_1 = 1 + \epsilon$, is followed very closely; *i.e.*, logarithmic plots of σ_T against time at different tensile strains are closely parallel. Empirical determination of the

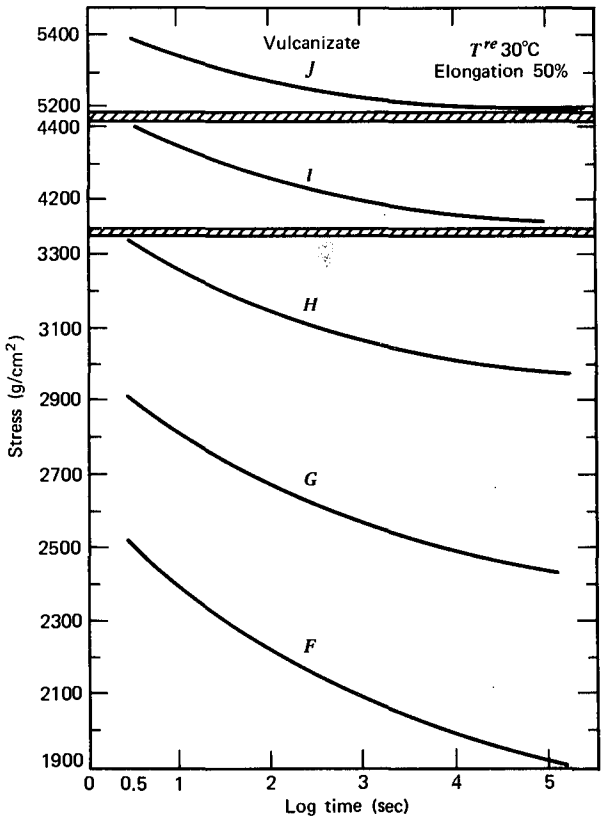


FIG. 14-8. Stress relaxation in natural rubber in extension at $\lambda_1 = 1.5$, for samples cross-linked to values of log G_e as follows: (F) 6.29; (G) 6.41; (H) 6.51; (I) 6.65; (J) 6.75. M_c from 5400 (J) to 20,000 (F). (Chasset and Thirion.[45])

function $\mathcal{F}(\lambda_1)$ permits extrapolation to $\lambda_1 \to 1$ (or $\epsilon \to 0$) to obtain the linear modulus $E(t)$.

While the equilibrium Young's modulus cannot be obtained directly from such measurements, it can be estimated from an empirical equation which is found to fit many such data extremely well,[45] including relaxation measurements of other lightly cross-linked polymers:

$$E(t) = E_e[1 + (t/t_m)^{-m}] \tag{9}$$

where t_m and m are adjustable parameters. Several graphical procedures are available[2,44-46,48] for choosing $E(t)$, t_m, and m for the best fit to data.

Creep data[51] in shear, in small deformations, are shown for four of the above five samples in Fig. 14-9, after reduction to 30° from various temperatures of measurement. When $J(t)$ is converted to $G(t)$ by equation 47 of Chapter 4, and the latter is multiplied by 3 to give $E(t)$, Poisson's ratio being of course negligibly different from $\frac{1}{2}$, these data are in excellent agreement with the stress relaxation results extrapolated by equation 8. The very large ordinate scale and high precision of the data should be noted.

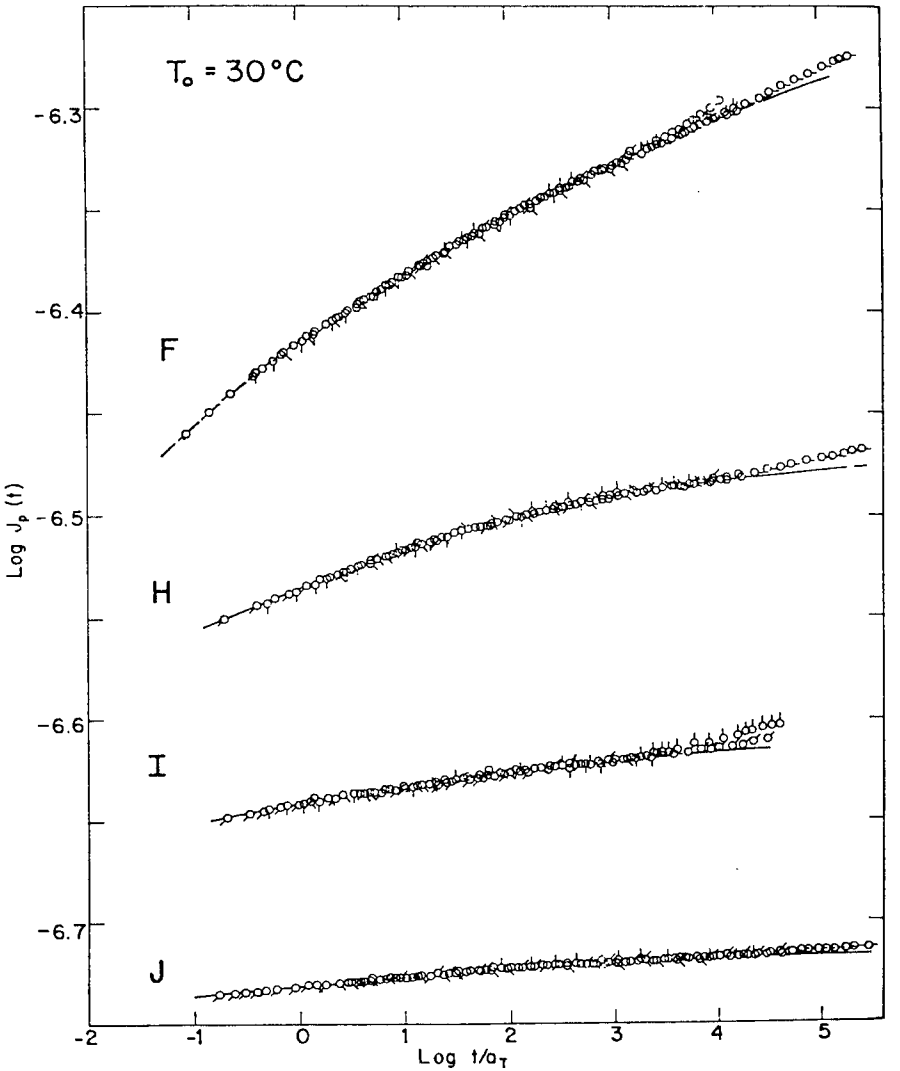


FIG. 14-9. Creep compliance of samples F, H, I, and J of Fig. 14-4 in shear with small deformations, reduced to 30°C. Pips refer to measurements at different temperatures from −50° to 90°C. (Plazek.[51])

Other creep data[48] on the same samples have been extrapolated to infinite time to obtain J_e by the analog of equation 3:

$$J(t) = J_e[1 + (t/t_m)^{-m}]^{-1} \tag{10}$$

which is equivalent to equation 9 since m in equation 47 of Chapter 4 (not exactly the same as m in equation 10 here) is always very small in the region of interest. Values of J_e from creep and $3/E_e$ from stress relaxation (equation 9) have been found to agree closely for both natural rubber[48] and styrene-butadiene copolymer.[2]

A rather surprising concurrence of the shapes of the curves in Fig. 14–8 or Fig. 14–9 is found by plotting $E(t)/E_e$, or $J(t)/J_e$, logarithmically against t/a_x, where a_x is an empirical shift factor which depends on the degree of cross-linking.[46,51] This procedure can alternatively be used to determine J_e by matching the shapes of logarithmic plots with horizontal and vertical adjustments. The factor a_x varies enormously with the extent of cross-linking, being proportional to the 15.4 power of M_c for both natural rubber and styrene-butadiene copolymer.[51] The significance of this relation is not clear.

Though the time-dependent processes are very slow, they are affected by temperature in the same manner as the friction coefficient which controls short-range molecular motions many decades removed in the time scale, since temperature reduction can be made with the same WLF coefficients as in the transition zone. Moreover, they are affected in the same manner by the introduction of diluent,[45] which reduces the friction coefficient in a manner attributable to an increase in fractional free volume (Chapter 17).

Similar very slow molecular processes are revealed in the approach to a state of ease of networks which have been very lightly cross-linked in strained states.[31,32,53,54]

5. Slow Relaxation Mechanisms and the Plateau Modulus G_N

In very lightly cross-linked systems, the slow relaxation processes described in the preceding section occur in a region of time scale separated by several logarithmic decades from the transition zone, and in between there is a plateau characterized by a shear modulus G_N or compliance J_N as pointed out in curves VII in the figures in Chapter 2. This is analogous in some respects to the plateau G_N^0 or J_N^0 in uncross-linked polymers. An example is portrayed in Fig. 14–10, for the storage compliance of three samples of styrene-butadiene copolymer lightly cross-linked with dicumyl peroxide. In the neighborhood of 3 on the abscissa scale, there is a region of low slope reminiscent of that in uncross-linked polymers. (One of the curves in Fig. 14–10 has already been seen as curve VII of Fig. 2–6.) The persistence of such a plateau after moderate cross-linking would indeed be expected from the retardation spectra in Fig. 14–7, where the minimum in L changes very little in the early stages of vulcanization. It can be plausibly attributed to a network of all the entanglement points (whether trapped or not) plus the chemical cross-links introduced.

The values of J_N can be obtained by an integration[48,49] like equation 4 of Chapter 13 or by equation 6 of Chapter 13 or by certain comparisons[24] with J_N^0. By analogy with equation 1, it may be expected to be related to the total concentration of strands terminated by cross-links or entanglements whether trapped or not, ν':

$$G_N = 1/J_N = g'\nu'RT \tag{11}$$

so if g and g' can be considered as equal,

$$G_N/G_e = \nu'/\nu \tag{12}$$

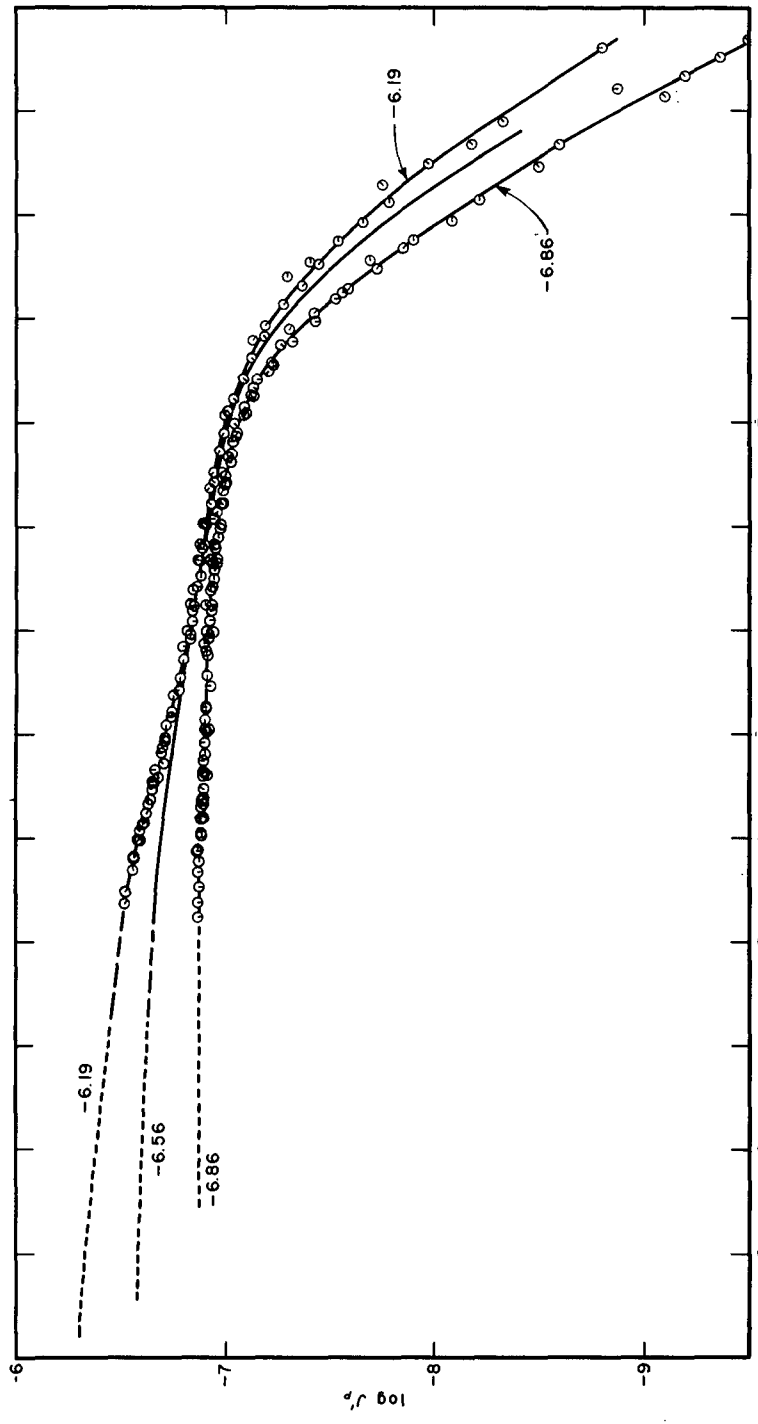


FIG. 14–10. Storage compliance, reduced to 25°C, plotted logarithmically for styrene-butadiene copolymer cross-linked to three different extents as gauged by the values of log J_e shown. (Mancke and Ferry.[2])

where ν' includes strands terminated by all entanglements, and ν only those that are trapped (equation 2). From the theory of Langley,[26] ν'/ν can be calculated in terms of the degree of cross-linking. Equation 12 has been tested by some experimental data on lightly cross-linked poly(dimethyl siloxane)[47] with rather good agreement.

With this interpretation, the slow relaxation mechanisms seen in Figs. 14-8, 14-9, and 14-10 are attributed to rearrangements of configurations by slippage of untrapped entanglements, *i.e.*, those from which not all the four radiating strands are anchored to the network. A dangling chain anchored at one end to the network and passing through several entanglements cannot rearrange its configurations by reptation, as pointed out by de Gennes,[55] but can rearrange by a much slower process similar to that postulated for star polymers (Chapter 13, Section C4), retraction of the chain within its effective tube. Theories developed by Curro and collaborators[51] predict both equation 9 and the dependence of the shift factor a_x on degree of cross-linking as observed by Plazek.[50]

6. Relaxation of Unattached Macromolecules in Networks

If a mixture of two polymeric species which are almost identical chemically except that only one of them carries cross-linkable reactive groups is subjected to cross-linking, a network is formed through which are threaded unattached macromolecules. From viscoelastic measurements, the motions of these molecules through the network can be deduced, as illustrated in Fig. 14-11 for stress relaxation of ethylene-propylene terpolymer networks containing 25% of unattached linear copolymer with essentially the same chemical composition.[56] A network containing no unattached species undergoes very little relaxation in the time scale covered,

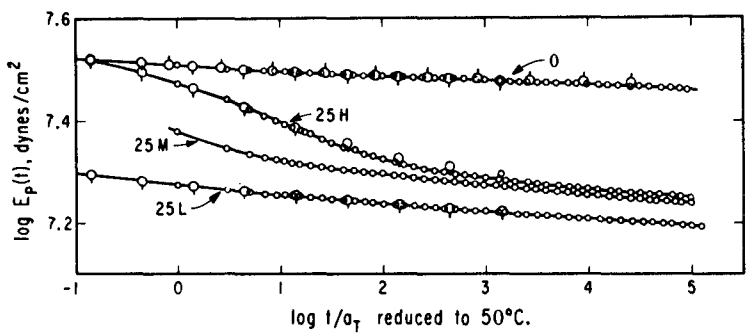


FIG. 14-11. Logarithmic plots of relaxation modulus in extension against time in seconds reduced to 50°C for ethylene-propylene terpolymer networks. (Subscript p denotes multiplication by $T_0\rho_0/T\rho$). Small circles, directly measured at 50°; large circles, interpolated from measurements at 10° (pip down) and 30° (pip up). Sample 0, with no unattached species; others, containing 25% of unattached linear ethylene-propylene copolymer with the following weight-average molecular weights: 25L, 3.6×10^4; 25M, 17×10^4, 25H, 45×10^4. (Kramer, Greco, Ferry, and McDonel.[56]) Reproduced by permission, from The Journal of Polymer Science.

having nearly reached its equilibrium modulus. In the others, relaxation of the unattached species occurs in a time scale which depends strongly on its molecular weight. Approximately, the characteristic time is proportional to the 3 to 3.5 power of M,[56-59] as is the terminal relaxation time in uncross-linked polymers of high molecular weight (Section C3 of Chapter 13). For reptation through a tube, the exponent should be 3 (Chapter , equations 55 and 57). The time scale for the relaxation in the cross-linked network appears to be similar to that for the unattached species in its own environment (*i.e.*, the corresponding uncross-linked polymer alone), but displaced to slightly longer times.[58,60] Experiments thus far have not determined the dependence on the spacing between the restraints (equivalent to the tube diameter).

7. Densely Cross-Linked Polymers

At high degrees of cross-linking, equilibrium shear moduli greater than 10^8 dynes/cm^2 (10^7 Pa) are obtained. If equation 1 is applied to such values of G_e, the density of network strands corresponds to very low values of M_e with fewer than 10 chain atoms between cross-links. Surprisingly, approximate proportionality to absolute temperature as predicted by the statistical theory of rubberlike elasticity is observed for polyethylene cross-linked by high-energy radiation,[61] epoxy polymers cross-linked by polyamines,[62] and networks formed from various monomers copolymerized with a dimethacrylate in substantial proportions.[63] Thus the elastic energy storage appears to be based largely on an entropy effect even though the statistical theory based on Gaussian distributions must be modified for such short strands; the modulus increases rapidly with network strand density.[63a]

Measurements of viscoelastic properties of such tight network structures are largely limited to isochronal studies of a modulus at fixed time or frequency as a function of temperature.[61-65] It can be concluded indirectly, however, that the relaxation and retardation spectra broaden with increasing cross-link density[64] or decreasing length of the molecule serving as the cross-linking agent.[65] Some creep and stress relaxation data have been reported.[67] It is probable that molecular interpretation of viscoelasticity in such systems will require consideration of rotations around individual chain bonds.[68]

C. NONLINEAR BEHAVIOR IN CROSS-LINKED POLYMERS

1. Nonlinear Behavior at Equilibrium

A full discussion of stress-strain relations at equilibrium for large deformations in rubbery cross-linked polymers is beyond the scope of this chapter; there have been many investigations of uniaxial deformations (simple extension, compression,) torsion, and biaxial deformations, which have been critically reviewed elsewhere.[69-71] A few comments will introduce the discussion of nonlinear viscoelastic behavior.

The state of strain in large deformations is commonly described either by the principal extension ratios, $\lambda_1, \lambda_2, \lambda_3$, defined in the notation of Chapter 1 as $\lambda_i = 1 + u_i/x_i$, with the coordinate axes suitably oriented, or by three strain invariants[70] whose values are independent of the coordinate system. In simple extension, $\lambda_1 = 1 + \epsilon$, where ϵ is the (practical) tensile strain u_1/x_1 (*cf.* equation 8 above), not to be confused with the ε in equations 3, 4 and 6. Most of this section is concerned with simple extension.

The statistical theory of rubberlike elasticity predicts the following stress-strain relation in simple extension, often designated as neo-Hookean:

$$\sigma_T = (\lambda_1 E_e/3)(\lambda_1 - \lambda_1^{-2}) \tag{13}$$

Thus the strain function $\mathcal{F}(\lambda_1)$ in equation 8 is $(\lambda_1^2 - 1/\lambda_1)/3$, which correctly reduces to ϵ as λ_1 approaches unity, to give the correct definition of Young's modulus E_e in small strains. (Here σ_T is the stress calculated on the actual cross-section area; sometimes in the literature the "nominal" or "engineering" stress is expressed on the basis of the initial cross-section, and is lower by a factor of $1/\lambda_1$).

Equation 13 does not hold closely above extensions of about 20%. For larger deformations the following formulation, known as the Mooney-Rivlin equation,[72,73] is commonly used:

$$\sigma_T = 2\lambda_1(C_1 + C_2/\lambda_1)(\lambda_1 - \lambda_1^{-2}) \tag{14}$$

which has been mentioned in slightly different form as equation 31 of Chapter 13. For $C_2 = 0$, it reduces to equation 13. At low elongations, it corresponds to $E_e = 6(C_1 + C_2)$. This equation often describes data for extension up to $\lambda_1 \cong 2$, but is seriously deficient because it is not a proper constitutive equation, shows deviations at very small deformations, and is inconsistent with behavior in other types of deformation especially uniaxial compression.[69,74,75] Many data for C_1 and C_2 of various cross-linked rubbers are reported in the literature.[33]

Because of the limited usefulness of the Mooney-Rivlin equation, it is probably not worthwhile to seek a molecular interpretation of the coefficients C_1 and C_2; the deviations from neo-Hookean behavior should be examined in some other framework. However, if the deviations are expressed in terms of the ratio $\psi = C_2/(C_1 + C_2)$, this quantity can be correlated rather successfully with the relative numbers of trapped entanglements and cross-links in the network.[14] It may be inferred from this and other studies[29] that both trapped entanglements and cross-links contribute to C_1, but that C_2 is associated with trapped entanglements only.

The deviations from neo-Hookean elasticity which are approximately described by equation 14 can be represented by several alternative formulations, derived from either molecular[34,76,77] or continuum mechanics[75,75a,78,79] considerations which avoid the defects of the Mooney-Rivlin equation and introduce one or more parameters with at least a qualitative molecular significance. One with wide applicability is obtained from the theory of Blatz, Sharda, and Tschoegl,[78] which provides for uniaxial extension

$$\sigma_T = (2G_e/n)(\lambda_1^n - \lambda_1^{-n/2}) \tag{15}$$

where n is a dimensionless material parameter. For $n = 2$, this reduces to equation 13. This formulation can also be applied with additivity of strands terminated by cross-links and by trapped entanglements, with $n = 2$ for the former and a smaller value of n for the latter.[79a]

At higher extensions, as well as in compression, the relation between σ_T and λ_1 can be described very well by an empirical equation of Martin, Roth, and Stiehler:[42,80]

$$\sigma_T = E_e(1 - \lambda_1^{-1}) \exp K(\lambda_1 - \lambda_1^{-1}) \tag{15a}$$

where K is an empirical constant.

At still higher extensions, the finite extensibility of the network strands causes the stress to rise rapidly.[70] This behavior can be approximately described in terms of a maximum extensibility λ_m^e at which the stress (hypothetically) becomes infinite. Here, the superscript e refers to equilibrium. For this purpose, an equation of the following form has been proposed by Smith:[71,81,82]

$$\sigma_T = (E_e/3)(\lambda_m^e/3)[\lambda_1 \mathcal{L}^{-1}(\lambda_1/\lambda_m^e) - \lambda_1^{-1/2}\mathcal{L}^{-1}(1/\lambda_1^{1/2}\lambda_m^e)] \tag{16}$$

where $\mathcal{L}^{-1}$ is the inverse Langevin function.

In view of the comments in Section B4 above about the difficulty of attaining elastic equilibrium, it is evident that experimental tests of such stress-strain relations must be carried out with great care. In examining the approach to equilibrium at different values of λ_1, it has been observed that the time dependence of the stress $\sigma_T(t)$ in a stress-relaxation experiment resides largely in the C_2 term when expressed in the form of equation 14.[83-85] Here, again, C_2 appears to be associated with entanglements, in this case with a contribution from untrapped entanglements.

2. Stress Relaxation and Creep

Nonlinear time-dependent behavior of cross-linked polymers in stress relaxation and creep has been extensively studied for the case of simple extension. To a close approximation, equation 8 has usually been found to apply to stress-relaxation data and to permit factorization of the tensile stress into a strain-dependent function $\mathcal{F}(\lambda_1)$ and the ordinary relaxation modulus $E(t)$,[45,46,86-89] although this appears to be inconsistent with the statement in the preceding paragraph. This separation of variables is successful over wide ranges of time scale and up to elongations corresponding to $\lambda_1 = 2$ or 3, and applies for many different rubbery polymers of different chemical structure. The function $\mathcal{F}(\lambda_1)$ can be taken from equation 15 or 15a. (For uncross-linked polymers, it will be recalled that the strain and time dependences over a wide range of time scale cannot be factored, as discussed in Section E1 of Chapter 13.) In application to experimental data measured at various temperatures, it is found that the temperature shift factors a_T are the same at high extensions as in the range of linear viscoelastic behavior.[87-90] Moreover, it can be concluded[91-93] that the monomeric friction coefficient ζ_0 changes very little with extension up to $\lambda_1 = 2$ or 3. Data for creep[94] and deformation at constant rate of

elongation[91,92] can be analyzed in a similar manner. By introducing the formulation of Blatz, Sharda, and Tschoegl into the superposition integral (analogous to equation 7 of Chapter 1), Chang, Bloch, and Tschoegl[75] were able to describe various types of time-dependent nonlinear viscoelastic behavior in uniaxial extension.

At higher extensions ($\lambda_1 > 3$), it is necessary to take into account the finite extensibility of the network strands in a manner analogous to equation 16, but with a maximum extensibility λ_m which is a monotonically increasing function of time[89,92] and approaches λ_m^e at long times, changing perhaps by a factor of 2 in the plateau region. This corresponds to a slow rearrangement of network topology to permit strands to assume configurations most appropriate for high extension. Then the stress contains an additional factor which is a function of $(\lambda_1 - 1)\lambda_m^e/\lambda_m$. Analysis of extensive data for simple extension of a cross-linked styrene-butadiene copolymer at constant rates of strain[95] in this manner describes very successfully the dependence of stress on time, temperature, strain, and strain rate. The maximum extensibility λ_m attains its equilibrium value in somewhat less than 1 sec at 25°C and hence involves some rather slow motions as indicated by the time scale for the storage compliance of this polymer in Fig. 14–10. This time-dependent feature is apparent *only* at large strains.

Behavior in simple extension is, of course, a relatively elementary aspect of nonlinear viscoelasticity. Other types of deformation, and combinations of deformations, can provide additional information which must be described by appropriate constitutive equations and eventually interpreted on a molecular basis. Some investigations of time-dependent properties in pure shear[95,96] and biaxial extension of thin, flat specimens[95,97–99] of soft rubbery polymers have been reported.

3. Stress-Strain Behavior at Constant Rate of Deformation

As mentioned in the preceding section, stress data for simple extension at a constant rate of elongation can be analyzed to obtain information about nonlinear viscoelasticity. However, it should be emphasized that even under conditions when the viscoelasticity is linear, or nearly so, extension at a constant rate of tensile strain $\dot{\epsilon}$ will give a plot of stress σ_T against ϵ (= $\dot{\epsilon}t$, where t is the elapsed time) which is strongly nonlinear owing to the viscoelasticity alone. For linear viscoelastic behavior, the tensile stress σ_T is given by the analog of equation 56 of Chapter 3 for simple extension:

$$\sigma_T = E_e \dot{\epsilon} t + \dot{\epsilon} \int_{-\infty}^{\infty} \tau \overline{H}(1 - e^{-\epsilon/\dot{\epsilon}\tau}) d \ln \tau \tag{17}$$

and such a curve can be differentiated to obtain the relaxation modulus $E(t)$ in accordance with equation 59 of Chapter 3. Actually, expansion of equation 13 in series shows that for extensions up to 50% the departure from direct proportionality of σ_T to ϵ at equilibrium is relatively small, so that equation 17 describes approximately the shape of σ_T as a function of time and of strain up to such moderate extensions. The method of reduced variables can be applied by plotting log $\sigma_T T_0/$

$\dot{\epsilon}\, Ta_T$ against log $\epsilon/\dot{\epsilon}a_T$ to combine data measured at different temperatures and strain rates to obtain a composite curve extending over many decades of time scale. For larger deformations, a much more elaborate analysis is necessary to identify the time-dependent and strain-dependent features of the behavior.[95]

Examination of the stress as a function of time during retraction at constant strain rate following extension, and in particular for several successive cycles of elongation and retraction, reveals some further complications.[100,101] The stresses during retraction are smaller than would be calculated on the basis of equation 8, and are smaller during extension in the second cycle than in the first. (This phenomenon, known as the Mullins effect,[102] is particularly evident in filled rubbers, but appears also in the absence of filler.[101,103])

4. Small Dynamic Strains Superimposed on Large Static Strains

A cross-linked polymer in a state of large static strain, at equilibrium, may be considered as a new anisotropic material whose linear viscoelastic properties could be studied.[104] A relatively simple example is a strip stretched in simple elongation which is further deformed by small oscillating elongations in the same direction. This type of experiment was performed by Mason[105] by propagation of longitudinal waves as described in Section D of Chapter 6, and by Voet and Morawski[106] and Meinecke[107] by direct measurements of stress and strain. For conventional cross-linked rubbers at room temperature and frequencies 10 Hz or less, the differential storage and loss Young's moduli, E' and E'', appear to be independent of stretch ratio λ_1 up to $\lambda_1 = 2$. At higher frequencies[105] or higher stress ratios,[105,107] both moduli increase with λ_1. For filled polymers, very large increases are observed.[106]

Differential dynamic measurements have also been made with other kinds of oscillating deformations. In studies by Painter[108] of small dynamic shear deformations superimposed on large static shear strains in the same direction, the dynamic storage modulus G' of cross-linked natural rubber and poly(dimethyl siloxane) at 24 Hz was found to increase with increasing static strains in excess of $\gamma_{21} = 0.2$. Here γ_{21} is defined as u_1/x_2 in the notation of Chapter 1. After a history of large static strain, however, the change in G' with static strain in a second (and subsequent) sequence of experiments was much smaller. These history-dependent effects are no doubt related to the behavior in repeated stress-strain cycles in extension mentioned in Section 3 above. Some experiments on torsional deformations of stretched rubber strips have been reported.[109,110]

5. Oscillating Deformations with Large Amplitudes

Repeated cycles of extension and retraction at constant rate of strain as described in Section 3 above may be regarded as oscillating deformations with a zigzag strain function. Sinusoidally oscillating deformations with large amplitudes can also be employed to study nonlinear behavior, though in general if the strain is a simple sinusoidal function of time the stress cannot be expected to be so, and vice versa;

the corresponding time dependence of the stress can be analyzed in terms of contributions from odd harmonics.[111] Studies of cross-linked natural rubber and poly(dimethyl siloxane) by Painter showed G' and G'' decreasing somewhat with increasing amplitude of sinusoidal shear deformation up to $\gamma_{21}^0 = 0.1$. Somewhat surprisingly, no deviations from the sinusoidal form of either stress or strain were detected. Later measurements by Warnaka[113] revealed changes with successive cycles of deformation similar to those described above for zigzag cycles. Similar studies have been made by Prevorsek.[114]

D. TIME-DEPENDENT MECHANICAL PHENOMENA DUE TO CHEMICAL CHANGES

If the chemical structure of a polymer is altered during a viscoelastic experiment—in particular, if a cross-linked network is subjected to a reaction which increases or decreases the number of network strands while it is being investigated in the rubbery zone of viscoelastic behavior—the apparent mechanical properties will be profoundly influenced. For example, scission of the network strands will cause stress relaxation at constant strain[115,116] (Fig. 14–12) or creep under constant stress. Formally, if a single first-order chemical reaction is responsible, the relaxation may be described by a single relaxation time which is the reciprocal of the chemical rate constant, instead of the broad spectra which are characteristic of the usual mechanical processes.

The effects of chemical stress relaxation (sometimes referred to as chemorheology) depend on whether the network scissions occur at the original cross-links or are randomly disposed at all points along the network strands.[117,118] They also depend on whether the broken bonds join again to leave the same number of network

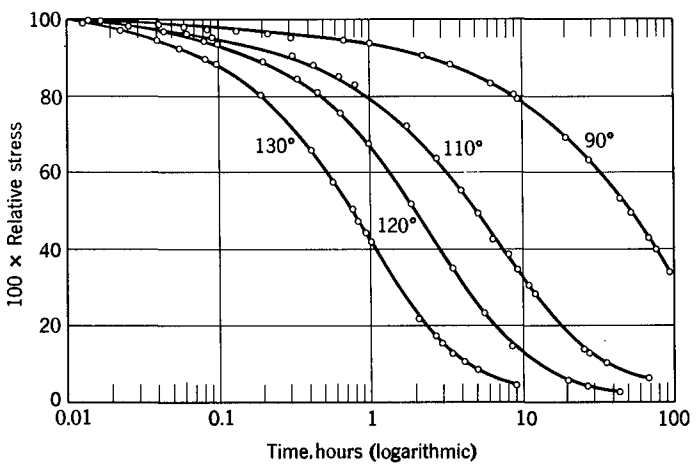


FIG. 14–12. Stress relaxation of a polyester rubber (Vulcollan A) due to chemical scission of network strands, at four temperatures as shown. (Offenbach and Tobolsky.[116])

strands but with an undistorted distribution of configurations, or remain permanently cut.[119,120] In some cases the reaction may be a bond interchange.[121,122]

This subject is beyond the scope of the present discussion, but is mentioned here to refer the reader to other sources of information.[123–126a]

E. EFFECTS OF RIGID-PARTICLE FILLERS

The influence of particulate fillers mixed with a polymer on the linear viscoelastic properties in the transition zone have been discussed briefly in Section C4 of Chapter 12. We now discuss briefly their effects in the plateau and terminal zones and at equilibrium, including nonlinear behavior.

1. Equilibrium Elastic Properties

The reservations about determining equilibrium moduli and compliances for unloaded polymers, occasioned by slow approaches to elastic equilibrium, apply also to filled materials, but by making measurements at rather long times (or even dynamic measurements at low frequency, at elevated temperatures) the modulus or compliance can be obtained with sufficient accuracy to study its dependence on filler content and size. For noninteracting rigid fillers, the shear modulus appears to be independent of the particle size and increases with volume fraction of filler in accordance with an empirical equation of Eilers and van Dijk:[127,128]

$$G_e/G_{e0} = [1 + 1.25\phi/(1 - \phi/\phi_m)]^2 \tag{18}$$

Here G_{e0} is the equilibrium modulus of the unfilled polymer, ϕ is the volume fraction of filler, and ϕ_m is a maximum volume fraction corresponding to close packing, which may be between 0.74 and 0.80. For $\phi < 0.70$, this equation is equivalent[129] to the result of a theoretical formulation by van der Poel[130] (which can be evaluated only numerically) relating the shear and bulk moduli of a composite with spherical particles to the shear and bulk moduli and Poisson's ratios of the two component materials. The derivation of van der Poel has been corrected and simplified by Smith.[130a] For a hard solid in a rubbery polymer, the ratio of the shear moduli is so large that the result is insensitive to its magnitude. An example is shown in Fig. 14-13 for data of Schwarzl, Bree, and Nederveen[129] for nearly monodisperse sodium chloride particles of several different sizes embedded in a cross-linked polypropylene ether. Extensive comparisons of data with equation 18 have been made by Landel,[131,132] who has also employed an alternative relation[133]

$$G_e/G_{e0} = (1 - \phi/\phi_m)^{-2.5} \tag{19}$$

In Fig. 14-13, shear moduli measured at low temperature where the polymer is essentially in the glassy state are also plotted, and are observed to increase linearly with ϕ. In this case, also, agreement is obtained with the theory of van der Poel with a ratio of shear moduli of 8.4 (filler/polymer) and Poisson's ratio of 0.25 and 0.5 respectively for the two phases. Measurements of the bulk modulus K_e for a poly-

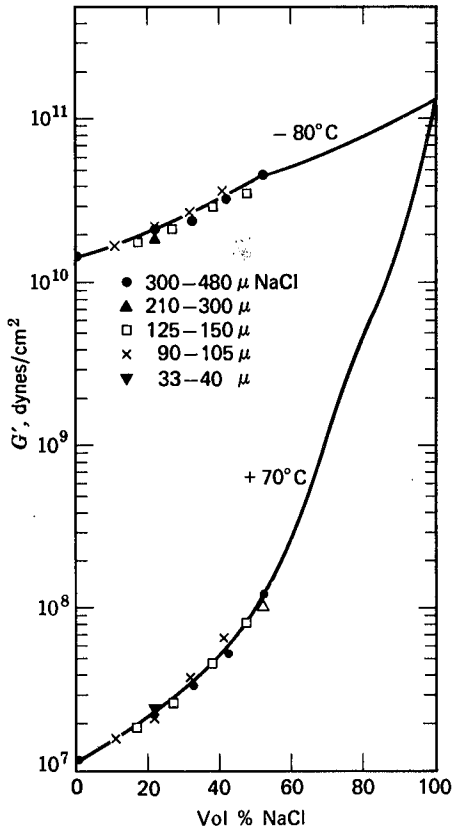


FIG. 14–13. Shear storage modulus G' at 1 Hz for a cross-linked polypropylene ether containing sodium chloride particles with sharp size distributions in the ranges shown, plotted against volume fraction of particles at two temperatures where G' should be close to G_e and G_g respectively.[129] Curves calculated from theory of van der Poel.[130]

urethane rubber filled with sodium chloride particles are plotted[134] against ϕ in Fig. 14–14; these also agree with the van der Poel theory with a suitable choice for the ratio of the bulk moduli of the two phases at each temperature. There are several alternative formulations for the dependence of shear modulus on volume fraction of the disperse phase, which have been reviewed in detail elsewhere.[135,136]

Nonlinear behavior in simple extension with large strains for such composite materials is illustrated in Fig. 14–15 for a styrene-butadiene rubber containing various proportions of glass beads.[132] With increasing volume fraction of filler, the initial modulus increases, but the nonlinearity becomes much more prominent so that at high extensions the curves actually cross. This behavior can be described in part by a combination[132] of the relation represented by equation 19 and a nonlinear stress-strain relation involving finite extensibility similar in character to equation 16. At high extensions, however, deviations appear which can be attributed to "dewetting" or loss of contact between particles and polymer, with the creation

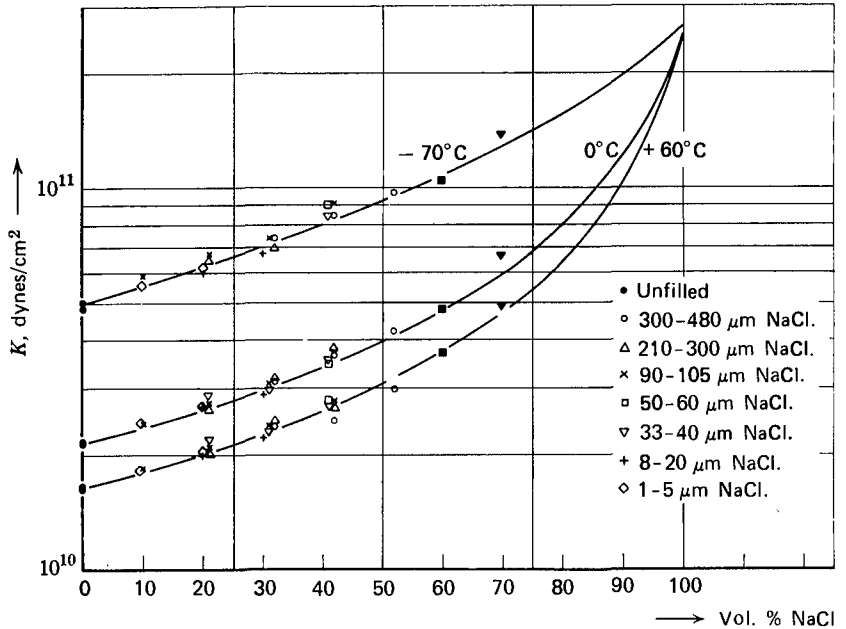


FIG. 14-14. Bulk moduli at three temperatures as indicated for a polyurethane rubber containing sodium chloride particles with sharp size distributions in the ranges shown, plotted against volume fraction of particles.[134] Curves calculated from the theory of van der Poel.[130]

of voids.[137,138] The presence of the latter is shown by an increase in total volume with tensile strain;[132] the magnitude of the volume increase can be predicted by a theoretical treatment which relates it to ϕ_m and one adjustable parameter concerned with the strength of the particle-polymer interface.[137]

Nonlinear equilibrium behavior of systems with strongly interacting particles such as natural rubber with carbon black is beyond the scope of this discussion.[139,140]

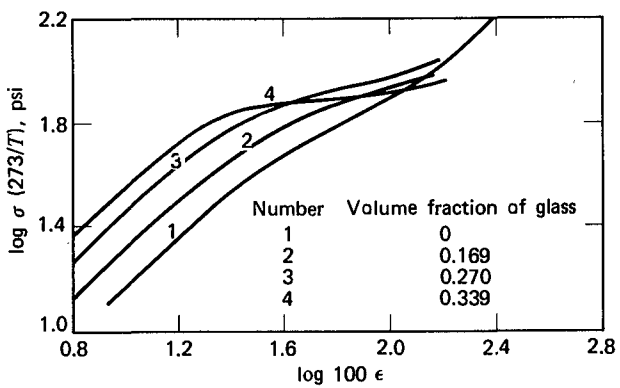


FIG. 14-15. Stress-strain curves at 60°C for styrene-butadiene rubber containing small glass beads at several volume fractions as shown. (Fedors and Landel.)[132]

2. Viscoelastic Properties

Time-dependent properties of filled rubbery systems, both uncross-linked and cross-linked, have been studied by both transient[137] and dynamic experiments.[9,111,135,141,142]

For an uncross-linked system in the terminal and plateau zones (polystyrene containing 30% by weight of carbon black, at elevated temperatures), the dynamic shear experiments of Onogi, Masuda, and Matsumoto[111] show several striking effects. (*a*) At relatively low strain amplitudes (maximum 3.5%) there is distinct nonlinearity, so that a sinusoidally varying strain is associated with a nonsinusoidal stress which can be decomposed by Fourier analysis to separate a substantial third harmonic contribution to both the in-phase and the out-of-phase components. The first harmonic contribution is used to calculate G_1' and G_1''. (*b*) The temperature shift factors a_T are smaller than in the pure polymer, especially at higher temperatures. (*c*) The magnitudes of G_1' and G_1'' in the plateau region are increased over those of the pure polymer by about a factor of 3 (roughly what would be expected from Equation 18 or 19). (*d*) The terminal zone of the pure polymer is replaced by a plateau zone in which G_1' has a level of about 10^5 dynes/cm^2 with relaxation times extending out to extremely low frequencies. The latter feature is also apparent in measurements of Kambe[141] on suspensions of various inactive fillers in polyethylene at elevated temperatures. It suggests the presence of an effective network of filler particles.[142,143]

In the plateau zone at higher frequencies, with oscillating deformations of sufficiently small amplitude to maintain linear behavior, the presence of calcium carbonate as a filler in styrene butadiene rubber and *cis*-polybutadiene[144] up to a weight fraction of 50% was found to increase the magnitudes of the storage and loss moduli to approximately the same degree without changing the relaxation times significantly. As a result, logarithmic curves for the loss tangent as a function of frequency have similar shapes and can be superimposed as illustrated in Fig. 14-16.

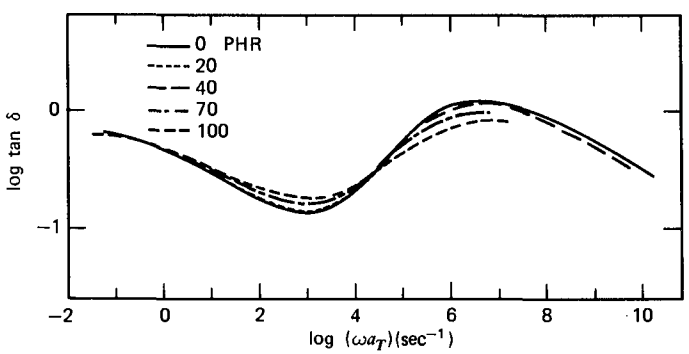


FIG. 14-16. Loss tangents reduced to 28°C for styrene-butadiene copolymer containing various proportions of calcium carbonate particles as indicated (parts filler per 100 parts polymer). (Maekawa, Nakao, and Ninomiya.[144])

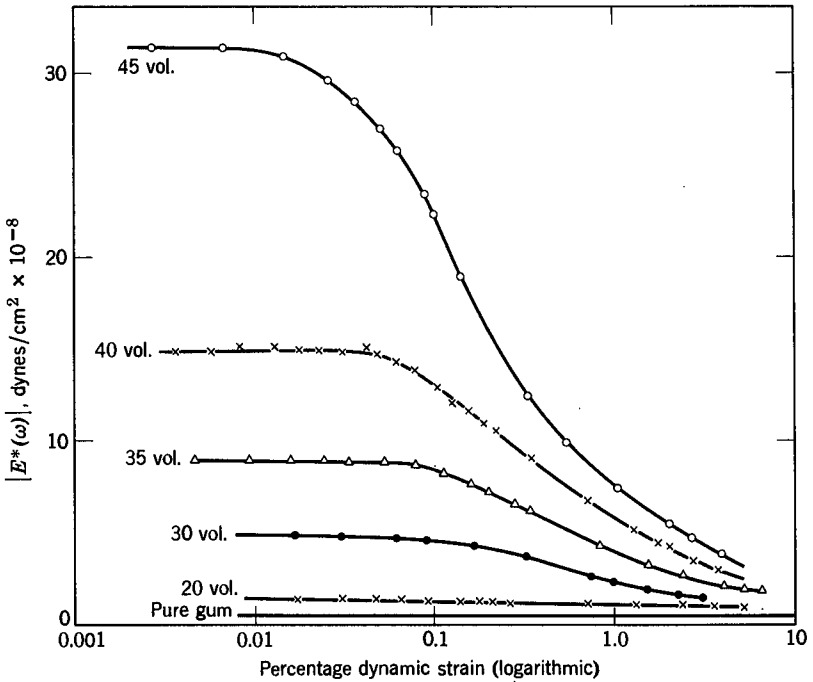


FIG. 14-17. Absolute Young's modulus $|E^*|$ plotted against amplitude of sinusoidal strain (with logarithmic scale) at 0.5 Hz, for natural rubber loaded with carbon black at various volumes (per 100 volumes of rubber) as indicated. (Payne.[148])

In oscillating deformations of vulcanized rubbers filled with carbon black, very marked nonlinear effects are observed.[145] Even at low strains,[146,147] G' falls substantially with increasing amplitude, while G'' may pass through a slight minimum at very low amplitudes and then rise slightly; as a result, tan δ increases markedly with amplitude.

The results of an investigation carried to extremely low strain,[148] though with measurement only of the absolute Young's modulus $|E^*|$ rather than its individual components, is shown in Fig. 14-17. Linear viscoelastic behavior is achieved below a strain of 0.1%, and the modulus falls off with increasing amplitude beyond a sort of yield-point strain whose magnitude decreases with increasing proportion of filler. At high strains, the drop in modulus is enormous, and all the compounds appear to approach the unfilled (pure gum) vulcanizate whose modulus is low throughout the amplitude scale.

Investigations of the effect of strain history in the systems of Fig. 14-17 showed[148] that the decrease in modulus was of the nature of a thixotropic change; immediately after measurements at high amplitude, low amplitude measurements gave abnormally small values which gradually recovered over a period of time and eventually regained their initial magnitude. This behavior implies the breaking of certain linkages, strained beyond their elastic limits, which can however form again if

sufficient time elapses (*cf.* Section C3 above). Contacts between polymer and filler are probably involved.[102,140]

F. BEHAVIOR OF BLENDS OF INCOMPATIBLE POLYMERS

In a composite system consisting of two phases both of which are viscoelastic, the properties depend in a complicated manner on the viscoelastic properties of the individual components, their volume fractions, and the morphology of the mixture. Some illustrations of these complications in the transition zone[149,150] have been mentioned in Chapter 12, Section C3.

Examples of such systems are particulate dispersions of a glassy polymer in a rubbery matrix, dispersions of rubbery polymer in a glassy matrix, block copolymers, and partially crystalline polymers in which amorphous and crystalline phases coexist (Chapter 16). As alternatives to a single continuous phase (matrix), the cases of two interpenetrating phases and compound dispersions (phase 1 within particles of phase 2 dispersed in phase 1) are also frequently encountered. Also, if the two phases are not completely incompatible, a boundary layer of varying composition may exist between them. Various classification schemes have been presented.[135,136,149]

In a region of temperature and time or frequency where the viscoelastic functions of both phases are slowly varying (*e.g.*, one phase glassy and the other in the rubbery plateau), the additivity of the two phases can be described in terms of a pseudoequilibrium modulus. Many mixing rules have been proposed for this purpose.[135,136,150,151] In general, neither the moduli nor the compliances will be exactly additive,[152,153] but a compromise can be formulated in terms of the mechanical model introduced by Takayanagi,[151,153] illustrated in Fig. 14–18 for the case of a partially crystalline polymer. Approximate agreement with experimental data can be obtained by adding moduli (for dynamic properties, G^*) where the elements appear in parallel and compliances (J^*) where they appear in series, with suitable choice of parameters such as φ and λ illustrated in Fig. 14–18.[151–154] However,

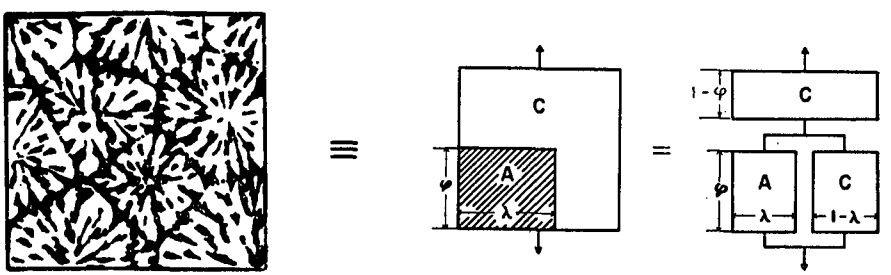


FIG. 14–18. Schematic representation of a partially crystalline polymer system (crystalline white, amorphous black) by a mechanical model with blocks whose viscoelastic properties correspond to those of the individual phases, arranged partly in series and partly in parallel in accordance with two empirical ratios φ and λ. (Takayanagi.[151])

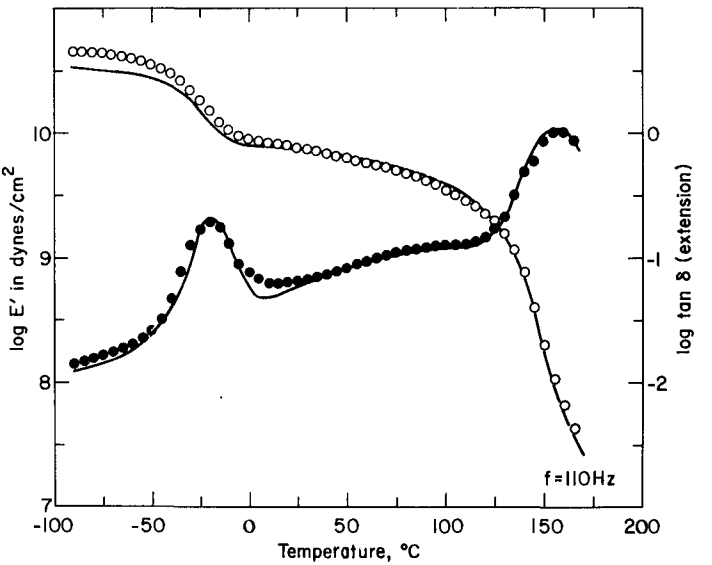


FIG. 14–19. Plots of log E' and log tan δ against temperature at a frequency of 110 Hz for a two-phase blend of equal weight fractions of poly(methyl methacrylate) and slightly cross-linked poly(butyl acrylate). Curves calculated from modified Kerner equation for a poly(methyl methacrylate) matrix with inclusions of poly(butyl acrylate) containing 14.4% poly(methyl methacrylate) by volume. (Dickie and Cheung.[158]) Reproduced, by permission, from the Journal of Polymer Science.

the properties of the blend are described in terms of those of the components with no identification of features characteristic of the blend itself.[155]

The morphology pictured on the left of Fig. 14–18 is supposed to portray a complex interpenetration of crystalline and amorphous phases. Often in two-phase systems the geometry is much less random; block copolymers for example sometimes form spherical domains of one phase arrayed almost in a regular lattice in a matrix of the other phase. Depending on the mechanism of formation of the composite system, the disperse phase may also exist in rodlike or lamellar shapes.[156,157]

Alternative formulations, which may be equivalent to the Takayanagi model in certain special cases, have been reviewed in detail by Nielsen[150] and Dickie.[136] Dickie[136,158,159] has used with considerable success a modification of an equation derived by Kerner[160] which predicts E^* of a two-phase system in terms of the complex moduli of the two components, their Poisson's ratios, and their volume fractions. An example is shown in Fig. 14–19 with an isochronal plot of E' and tan δ against temperature at 110 Hz for a physical blend of poly(methyl methacrylate) and slightly cross-linked poly(butyl acrylate) in equal parts by weight. The blend was prepared by coagulation of a latex of mixed particles. In other studies, blends were prepared by latex polymerization of one polymer on seed particles of the other, to control which polymer becomes the continuous phase. In many cases the dynamic properties are satisfactorily described by the modified Kerner equation; the details are beyond the scope of this Chapter.

Viscoelastic properties of three-component blends of two polymers together with a block copolymer of the two species have also been investigated.[162]

The properties of composite systems in which the disperse phase consists of fibers or other anisotropic particles are of great technological importance.[161]

REFERENCES

1. O. Kramer and J. D. Ferry, in *Science and Technology of Rubber,* edited by F. R. Eirich, Academic Press, New York, 1978, Chapter 5.
2. E. Maekawa, R. G. Mancke, and J. D. Ferry, *J. Phys. Chem.*, **69,** 2811 (1965).
3. R. G. Mancke and J. D. Ferry, *Trans. Soc. Rheol.*, **12,** 335 (1968).
4. S. P. Chen and J. D. Ferry, *Macromolecules,* **1,** 270 (1968).
5. P. Mason, *J. Chem. Phys.*, **35,** 1523 (1961); *Polymer,* **5,** 625 (1964).
6. M. Braden and W. P. Fletcher, *Trans. Inst. Rubber Ind.*, **31,** 155 (1955).
7. C. G. Moore and W. F. Watson, *J. Polym. Sci.*, **19,** 237 (1956).
8. R. A. Stratton and J. D. Ferry, *J. Phys. Chem.*, **67,** 2781 (1963).
9. J. D. Ferry, R. G. Mancke, E. Mackawa, Y. Ōyanagi, and R. A. Dickie, *J. Phys. Chem.*, **68,** 3414 (1964).
10. A. R. Payne, in *Rheology of Elastomers,* edited by P. Mason and N. Wookey, Pergamon, London, 1958, p. 86.
11. K. Schmieder and K. Wolf, *Kolloid-Z.*, **134,** 149 (1953); H. D. Heinze, K. Schmieder, G. Schnell, and K. A. Wolf, *Kautsch. Gummi,* **14,** 208 WT (1961).
12. R. Bakule and A. Havránek, *J. Polym. Sci.*, **C53,** 347 (1975).
13. E. Maekawa, I. Furuta, M. Nakao, and G. Yasuda, *Gomukyōkaishi,* **40,** 26 (1967).
14. J. D. Ferry and H.-C. Kan, *Rubber Chem. Technol.*, **51,** 731 (1978).
15. A. R. Shultz, in *Characterization of Macromolecular Structure,* National Academy of Sciences Publ. No. 1573, Washington, 1968.
16. D. S. Pearson and W. W. Graessley, *Macromolecules,* **11,** 528 (1978).
17. M. Gordon and S. B. Ross-Murphy, *Pure Appl. Chem.*, **43,** 1 (1975).
18. P. J. Flory, *Chem. Rev.*, **35,** 51 (1944).
19. L. Mullins and A. G. Thomas, *J. Polym. Sci.*, **43,** 13 (1960).
20. A. M. Bueche, *J. Polym. Sci.*, **19,** 297 (1956).
21. L. Mullins, *J. Appl. Polym. Sci.*, **2,** 1 (1959).
22. B. M. E. van der Hoff, *J. Macromol. Sci. (Chem.)*, **A1,** 747 (1967).
23. G. Kraus, *J. Appl. Polym. Sci.*, **7,** 1257 (1963).

23a. N. W. Tschoegl, personal communication.

24. R. G. Mancke, R. A. Dickie, and J. D. Ferry, *J. Polym. Sci.*, A-2, **6,** 1783 (1968).
25. K. W. Scott, V. R. Allen, and M. Morton, *Proc. 6th JANAF Conf. on Elastomers,* 1960, p. 78.
26. N. R. Langley, *Macromolecules,* **1,** 348 (1968).
27. N. R. Langley and K. E. Polmanteer, *J. Polym. Sci., Polym. Phys. Ed.*, **12,** 1023 (1974).
28. D. S. Pearson, B. J. Skutnik, and G. G. A. Böhm, *J. Polym. Sci., Polym. Phys. Ed.*, **12,** 925 (1974).
29. L. Dossin and W. W. Graessley, *Macromolecules,* **12,** 123 (1979).
30. E. M. Valles and C. W. Macosko, *Macromolecules,* **12,** 673 (1979).

30a. M. Gottlieb, C. W. Macosko, G. S. Benjamin, K. O. Meyers, and E. W. Merrill, *Macromolecules,* **14,** 1039 (1981).

31. R. L. Carpenter, H.-C. Kan, and J. D. Ferry, *Polym. Eng. Sci.*, **19,** 267 (1979).
32. H.-C. Kan and J. D. Ferry, *Macromolecules,* **12,** 494 (1979).
33. J. E. Mark, *Rubber Chem. Technol.*, **48,** 495 (1975).
34. P. J. Flory, *J. Chem. Phys.*, **66,** 5720 (1977).
35. L. A. Wood, *J. Res. Nat. Bur. Stand.*, **80A,** 451 (1976).

36. W. H. Stockmayer, *J. Chem. Phys.*, **12,** 125 (1944).
37. P. J. Flory, *Principles of Polymer Chemistry,* Cornell University Press, Ithaca, N. Y., 1953.
38. A. Charlesby, *Proc. R. Soc.*, **A222,** 542 (1954); **A224,** 120 (1954).
39. M. Inokuti, *J. Chem. Phys.*, **38,** 2999 (1963).
40. C. W. Macosko and D. R. Miller, *Macromolecules,* **9,** 199 (1976).
41. R. H. Valentine, J. D. Ferry, T. Homma, and K. Ninomiya, *J. Polym. Sci.*, A-2, **6,** 479 (1968).
42. G. M. Martin, F. L. Roth, and R. D. Stiehler, *Trans. Inst. Rubber Ind.*, **32,** 189 (1956).
43. L. A. Wood and F. L. Roth, *Proc. 4th Rubber Technology Conf.*, London, 1962; *Rubber Chem. Technol.*, **36,** 611 (1963).
44. P. Thirion and R. Chasset, *Rev. Gen. Caoutch.*, **41,** 271 (1964); **44,** 1041 (1967).
45. R. Chasset and P. Thirion, *Proc. Conf. on Physics of Non-Crystalline Solids,* edited by J. A. Prins, North Holland Publishing, Amsterdam, 1965, p. 345.
46. P. Thirion and R. Chasset, *Chim. Ind. (Paris),* **97,** 618 (1967).
47. N. R. Langley and J. D. Ferry, *Macromolecules,* **1,** 353 (1968).
48. R. A. Dickie and J. D. Ferry, *J. Phys., Chem.*, **70,** 2594 (1966).
49. J. F. Sanders and J. D. Ferry, *Macromolecules,* **7,** 681 (1974).
50. D. J. Plazek, *J. Polym. Sci.*, A-2, **4,** 745 (1966).
51. J. G. Curro *et al., Macromolecules,* **16,** 559 (1983); Ibid., **18,** 1157 (1985).
52. L. H. Sperling and A. V. Tobolsky, *J. Polym. Sci.*, A-2, **6,** 259.
53. H.-C. Kan and J. D. Ferry, *Macromolecules,* **11,** 1049 (1978).
54. R. L. Carpenter, O. Kramer, and J. D. Ferry, *J. Appl. Polym. Sci.*, **22,** 335 (1978).
55. P. G. de Gennes, *J. Phys. Chem. Solids,* **36,** 1199 (1975).
56. O. Kramer, R. Greco, J. D. Ferry, and E. T. McDonel, *J. Polym. Sci., Polym. Phys. Ed.*, **13,** 1675 (1975).
57. O. Kramer, R. Greco, R. A. Neira, and J. D. Ferry, *J. Polym. Sci., Polym. Phys. Ed.*, **12,** 2361 (1974).
58. R. Greco, C. R. Taylor, O. Kramer, and J. D. Ferry, *J. Polym. Sci., Polym. Phys. Ed.*, **13,** 1687 (1975).
59. G. Kraus and K. W. Rollman, *J. Polym. Sci., Polym. Phys. Ed.*, **15,** 385 (1977).
60. G. W. Nelb, S. Pedersen, C. R. Taylor, and J. D. Ferry, *J. Polym. Sci., Polym. Phys. Ed.*, **18,** 645 (1980).
61. C. W. Deeley, D. E. Kline, J. A. Sauer, and A. E. Woodward, *J. Polym. Sci.*, **28,** 109 (1958).
62. D. Katz and A. V. Tobolsky, *Polymer,* **4,** 417 (1963).
63. A. V. Tobolsky, D. Katz, R. Thach, and R. Schaffhauser, *J. Polym. Sci.*, **62,** S176 (1962); A. V. Tobolsky, M. Takahashi, D. Katz, and R. Schaffhauser, *J. Polym. Sci.*, **A2,** 2749 (1964).

63a. T. L. Smith, *J. Polym. Sci., Polym. Symp.*, **46,** 97 (1974).

64. K. Shibayama and Y. Suzuki, *J. Polym. Sci.*, **A3,** 2637 (1965).
65. T. K. Kwei, *J. Polym. Sci.*, A-2, **4,** 943 (1966).
66. L. E. Nielsen, *Mechanical Properties of Polymers and Composites,* Dekker, New York, 1974, Volume 1, p. 177 *ff.*
67. P. Theocaris, *J. Appl. Polym. Sci.*, **8,** 399 (1964).
68. A. V. Tobolsky and D. B. DuPré, *Adv. Polym. Sci.*, **6,** 103 (1969).
69. L. R. G. Treloar, *Rep. Prog. Phys.*, **36,** 755 (1973).
70. L. R. G. Treloar, *The Physics of Rubber Elasticity,* 3rd ed., Clarendon Press, Oxford, 1975.
71. T. L. Smith, in *Treatise on Materials Science and Technology,* Academic Press, New York, 1977.
72. R. S. Rivlin, in *Rheology,* edited by F. R. Eirich, Volume I, Academic Press, New York, 1956, Chapter 10.
73. M. Mooney, *J. Appl. Phys.*, **11,** 582 (1940).
74. L. A. Wood, *J. Res. Nat. Bur. Stand.*, **82,** 57 (1977).

75. W. V. Chang, R. Bloch, and N. W. Tschoegl, *Rheol. Acta,* **15,** 367 (1976).
75a. K. C. Valanis and R. F. Landel, *J. Appl. Phys.,* **38,** 2997 (1967).
76. W. W. Graessley and D. S. Pearson, *J. Chem. Phys.,* **66,** 3363 (1977).
77. A. H. Crossland and B. M. E. van der Hoff, *J. Macromol. Sci.-Chem.,* **A-10,** 825 (1976).
78. P. J. Blatz, S. C. Sharda, and N. W. Tschoegl, *Trans. Soc. Rheol.,* **18,** 145 (1974).
79. R. Bloch, W. V. Chang, and N. W. Tschoegl, *J. Rheol.,* **22,** 1 (1978).
79a. W. V. Chang, R. Bloch, and N. W. Tschoegl, in *Chemistry and Properties of Cross-Linked Polymers,* edited by S. Labana, Academic Press, New York, 1977, p. 431.
80. L. A. Wood, *Rubber Chem. Technol.,* **51,** 840 (1978).
81. F. Bueche, *Physical Properties of Polymers,* Interscience, New York, 1962, p. 57.
82. T. L. Smith and J. E. Frederick, *J. Appl. Phys.,* **36,** 2996 (1965).
83. G. Kraus and G. A. Moczygemba, *J. Polym. Sci.,* **A2,** 277 (1964).
84. A. Ciferri and P. J. Flory, *J. Appl. Phys.,* **30,** 1498 (1959).
85. T. L. Smith, *J. Polym. Sci.,* **C16,** 841 (1967).
86. E. Guth, P. E. Wack, and R. L. Anthony, *J. Appl. Phys.,* **17,** 347 (1946).
87. R. F. Landel and P. J. Stedry, *J. Appl. Phys.,* **17,** 1885 (1960).
88. J. C. Halpin, *J. Polym. Sci.,* **B2,** 959 (1964).
89. J. C. Halpin, *J. Appl. Phys.,* **36,** 2975 (1965).
90. K. A. Grosch, *Proc. R. Soc.,* **A274,** 21 (1963).
91. T. L. Smith, *Trans. Soc. Rheol.,* **6,** 61 (1962).
92. T. L. Smith and R. A. Dickie, *J. Polym. Sci.,* A-2, **7,** 635 (1969).
93. C.-P. Wong and J. L. Schrag, *Macromolecules,* **3,** 468 (1970).
94. H. Leaderman, *Trans. Soc. Rheol.,* **6,** 361 (1962).
95. R. A. Dickie and T. L. Smith, *Trans. Soc. Rheol.,* **15,** 91 (1971).
96. T. L. Smith and J. E. Frederick, *Trans. Soc. Rheol.,* **12,** 363 (1968).
97. L. J. Zapas, *J. Res. Nat. Bur. Stand.,* **70A,** 525 (1966).
98. K. C. Valanis and R. F. Landel, *Trans. Soc. Rheol.,* **11,** 243 (1967).
99. G. W. Becker and O. Krüger, in *Deformation and Fracture of High Polymers,* edited by H. H. Kausch, J. A. Hassell, and R. I. Jaffee, Plenum Press, New York, 1973, p. 115.
100. J. A. C. Harwood and A. R. Payne, *J. Appl. Polym. Sci.,* **10,** 1203 (1966).
101. J. A. C. Harwood and A. Schallamach, *J. Appl. Polym. Sci.,* **11,** 1835 (1967).
102. L. Mullins, *J. Rubber Res.,* **16,** 275 (1947); *J. Phys. Colloid Chem.,* **54,** 239 (1950).
103. J. A. C. Harwood, L. Mullins, and A. R. Payne, *J. Appl. Polym. Sci.,* **9,** 3011 (1965).
104. I. M. Ward, *Mechanical Properties of Solid Polymers,* Wiley-Interscience, London, 1971, Chapter 10.
105. P. Mason, *J. Appl. Polym. Sci.,* **1,** 63 (1959); **5,** 428 (1961).
106. A. Voet and C. Morawski, *Rubber Chem. Technol.,* **47,** 765 (1974).
107. E. A. Meinecke, *Rheol. Acta,* **10,** 302 (1971).
108. G. W. Painter, *Trans. ASME,* **76,** 1131 (1954).
109. W. Kuhn and O. Künzle, *Helv. Chim. Acta,* **30,** 839 (1947).
110. P. Mason, *Trans. Faraday Soc.,* **55,** 1461 (1959).
111. S. Onogi, T. Masuda, and T. Matsumoto, *Trans. Soc. Rheol.,* **14,** 275 (1970).
112. G. W. Painter, *Soc. Autom. Eng. J.,* **67,** 53 (1959).
113. G. E. Warnaka, *Rubber Chem. Technol.,* **39,** 1421 (1966).
114. Y. D. Kwon, R. K. Sharma, and D. C. Prevorsek, *Polym. Prepr. Am. Chem. Soc.,* **18(2),** 99 (1977).
115. A. V. Tobolsky, I. B. Prettyman, and J. H. Dillon, *J. Appl. Phys.,* **15,** 380 (1944).
116. J. A. Offenbach and A. V. Tobolsky, *J. Colloid Sci.,* **11,** 39 (1956).
117. A. M. Bueche, *J. Chem. Phys.,* **21,** 614 (1953).
118. J. P. Berry and W. F. Watson, *J. Polym. Sci.,* **18,** 201 (1955).
119. R. S. Stein and A. V. Tobolsky, *Text. Res. J.,* **18,** 302 (1948).
120. R. D. Andrews, A. V. Tobolsky, and E. E. Hanson, *J. Appl. Phys.,* **17,** 352 (1948).
121. M. D. Stern and A. V. Tobolsky, *J. Chem. Phys.,* **14,** 93 (1946).
122. M. Mochulsky and A. V. Tobolsky, *Ind. Eng. Chem.,* **40,** 2155 (1948).
123. A. V. Tobolsky, *J. Appl. Phys.,* **27,** 673 (1956).

124. H. Yu and L. A. Wall, *J. Phys. Chem.*, **69**, 2072 (1965).
125. K. Murakami, *Rubber Chem. Technol.*, **48**, 913 (1975).
126. J. Moacanin, *J. Chem. Phys.*, **64**, 430 (1976).
127. H. Eilers, *Kolloid-Z.*, **97**, 313 (1941).
128. P. J. Blatz, *Ind. Eng. Chem.*, **48**, 727 (1956).
129. F. R. Schwarzl, H. W. Bree, and C. J. Nederveen, *Proc. 4th Intern. Cong. Rheol.*, edited by E. H. Lee, Interscience, New York, Part 3, 1965, p. 241.
130. C. van der Poel, *Rheol. Acta*, **1**, 198 (1958).
130a. J. C. Smith, *J. Res. Nat. Bur. Stand.*, **A78**, 355 (1974); *ibid.*, **A79**, 419 (1975); *Polym. Eng. Sci.*, **16**, 394 (1976).
131. R. F. Landel, *Trans. Soc. Rheol.*, **2**, 53 (1958).
132. R. F. Fedors and R. F. Landel, *AIAA Paper 67–491*, Amer. Inst. Aeron. Astron., 1967.
133. R. F. Landel, B. G. Moser, and A. Bauman, *Proc. 4th Intern. Cong. Rheol.*, edited by E. H. Lee, Interscience, New York, Part 2, 1965, p. 663.
134. C. W. van der Wal, H. W. Bree, and F. R. Schwarzl, *J. Appl. Polym. Sci.*, **9**, 2143 (1965).
135. L. E. Nielsen, *Mechanical Properties of Polymers, and Composites*, Volume 2, Dekker, New York, 1974, Chapter 7.
136. R. A. Dickie, in *Polymer Blends*, edited by D. R. Paul and S. Newman, Volume I, Academic Press, New York, 1978, Chapter 8.
137. R. F. Fedors and R. F. Landel, SPS 37-41, Volume IV, Jet Propulsion Laboratory.
138. F. Schwarzl, H. W. Bree, G. A. Schwippert, L. C. E. Struik, and C. W. van der Wal, *Proc. 5th Intern. Cong. Rheology*, Volume 3, University of Tokyo Press, 1970, p. 3.
139. A. E. Oberth, *Rubber Chem. Technol.*, **40**, 1337 (1967).
140. G. Kraus, in *Science and Technology of Rubber*, edited by F. R. Eirich, Academic Press, New York, 1978, Chapter 8.
141. H. Kambe and M. Takano, *Proc. 4th Intern. Cong. Rheology*, edited by E. H. Lee, Part 3, Interscience, New York, 1965, p. 557.
142. S. Onogi, T. Masuda, and T. Matsumoto, *Trans. Soc. Rheol.*, **14**, 275 (1970).
143. G. V. Vinogradov, A. Ya. Malkin, E. P. Plotnikova, O. Yu. Sabsai, and N. E. Nikolayeva, *Int. J. Polym. Mater.*, **2**, 1 (1972).
144. E. Maekawa, M. Nakao, and K. Ninomiya, *Nippon Gomu Kyokaishi*, **40**, 549 (1967).
145. A. R. Payne, *Rubber Plast. Age*, **42**, 963 (1961).
146. W. P. Fletcher and A. N. Gent, *Trans. Inst. Rubber Ind.*, **29**, 266 (1953).
147. A. R. Payne, R. E. Whittaker, and J. F. Smith, *J. Appl. Polym. Sci.*, **16**, 1191 (1972).
148. A. R. Payne, *J. Appl. Polym. Sci.*, **3**, 127 (1960).
149. J. A. Manson and L. H. Sperling, *Polymer Blends and Composites*, Plenum Press, New York, 1976.
150. L. E. Nielsen, *Predicting the Properties of Mixtures*, Dekker, New York, 1978.
151. M. Takayanagi, *Proc. 4th Intern. Cong. Rheology*, Part 1, Interscience, New York, 1965, p. 161.
152. K. Fujino, Y. Ogawa, and H. Kawai, *J. Appl. Polym. Sci.*, **8**, 2147 (1964).
153. M. Takayanagi, S. Uemura, and S. Minami, *J. Polym. Sci.*, **C5**, 113 (1964).
154. R. E. Cohen and A. R. Ramos, *J. Macromol. Sci.—Phys.*, in press.
155. R. A. Dickie, *Polym. Eng. Sci.*, **19**, 1042 (1979).
156. H. Kawai, T. Soen, T. Inoue, T. Ono, and T. Uchida, *Prog. Polym. Sci., Jpn.*, **4**, 145 (1972).
157. H. Kawai, *Kobunshi*, **25**, 302 (1976).
158. R. A. Dickie and M.-F. Cheung, *J. Appl. Polym. Sci.*, **17**, 79 (1973).
159. R. A. Dickie, *J. Polym. Sci., Polym. Phys. Ed.*, **14**, 2073 (1976).
160. E. H. Kerner, *Proc. Phys. Soc.*, **69B**, 808 (1956).
161. L. E. Nielsen, *Mechanical Properties of Polymers and Composites*, Volume 2, Dekker, New York, 1978, Chapter 8.
162. R. E. Cohen and A. R. Ramos, *Macromolecules*, **12**, 131 (1979).

CHAPTER 15

The Glassy State

It has been mentioned in several previous chapters that below the glass transition temperature the convolutions of polymer chain backbones are largely immobilized. Thus, most viscoelastic properties in the glassy state must reflect limited local molecular motions. There are several possible types of these: torsional oscillations, rotations around chain backbone bonds with short-range coordination, various configurational rearrangements of side chains, and rotations of terminal groups of side chains such as methyl which require very little cooperation from the environment.

Molecular motions very similar to some of these may also occur in vitrifying liquids of low molecular weight near and below T_g. Indeed, the bulk viscoelastic properties, as evidenced by the course of volume contraction near T_g illustrated in Fig. 11-7 and discussed further in Chapter 18, seem to be very similar for both polymers and small molecules (Section B1 of Chapter 18). In shear viscoelastic properties, however, there are some characteristic differences, and it is instructive to examine the behavior of small molecules first.

In many investigations on both polymers and substances of low molecular weight, local motions are studied by high-frequency viscoelastic measurements above T_g rather than low-frequency or transient measurements below T_g. These two types of studies probably give closely related but not quite identical information. Above T_g, the local structure changes with temperature far more than below T_g, as reflected by a larger thermal expansion coefficient. As a result the temperature dependence of the magnitudes of relaxation and retardation spectra (both shear and bulk), which are important in applying the method of reduced variables, for example (Section A6 of Chapter 11), may be different above and below T_g.[1,2] Nevertheless, some high-frequency measurements above T_g are included in the present discussion.

A. AMORPHOUS SOLIDS AND SUPERCOOLED LIQUIDS OF LOW MOLECULAR WEIGHT

In an early investigation of Benbow,[3] the dynamic mechanical properties of a glass of low molecular weight, 2′-hydroxy-2:4:4:6:5′-pentamethyl flavan, were measured over a wide frequency range. Over a range of at least three logarithmic decades, from 10^{-3} to 1 Hz, the storage and loss shear moduli followed the frequency dependence prescribed for a single Maxwell element, equations 3 and 4 of Chapter 3. This behavior corresponds to a retardation spectrum with a single line; the retardation time was $\tau_1 = 0.15$ sec at 16°C, and over the range from 10° to 20° it varied in accordance with the Arrhenius form with an apparent activation energy of 75 kcal/mole. At frequencies well below $1/\tau_1$, G'' was directly proportional to frequency, and η' was essentially a constant (approximately equal to the steady flow viscosity,[4] indicating that no other viscoelastic mechanisms enter at lower frequencies); the magnitude of η' was in the range from 10^8 to 10^{10} poises in the temperature range from 10° to 18°C. Other organic glasses formed from bulky-shaped molecules of low molecular weight were found by Benbow and Wood[4] to behave similarly, as shown in Fig. 15–1, where tan δ is plotted against frequency. For a Maxwell element, tan δ is inversely proportional to frequency (equation 8 of Chapter 3), and this is followed as evidenced by a slope of -1 on a logarithmic plot at low frequencies for the hydroxypentamethylflavan as well as 2-phenyl-3-*p*-tolylindanone and glycerol sextol phthalate.

At high frequencies, however, there is a transition (abrupt in the hydroxypen-

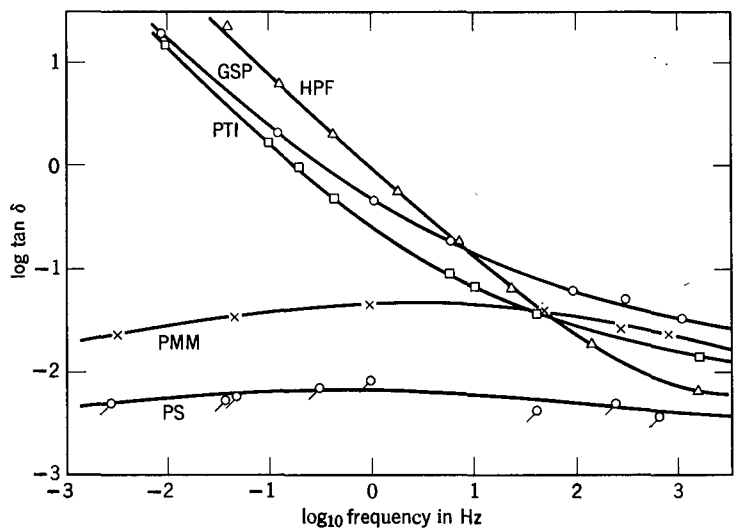


FIG. 15–1. Loss tangent plotted against frequency for three glasses of low molecular weight and two polymeric glasses. (HPF) Hydroxypentamethyl flavan; (GSP) glycerol sextol phthalate; (I) 2-phenyl-3-*p*-tolylindanone; (PMM) polymethyl methacrylate (calculated from data of Lethersich[25]); (PS) polystyrene. (After Benbow and Wood.[4])

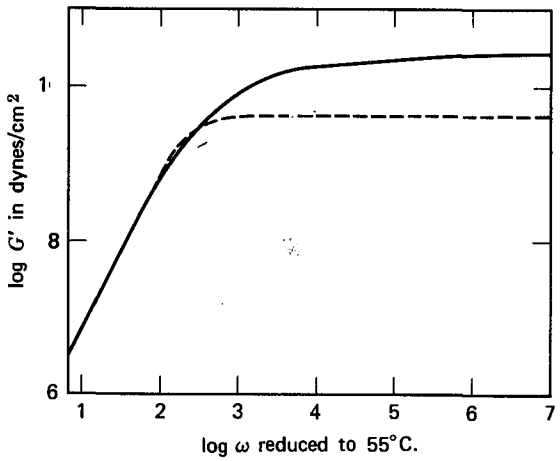


FIG. 15-2. Storage shear modulus of supercooled glucose, from data of Philippoff[6,7] and Meyer and Ferry[8] reduced to 55°C. Dashed curve represents behavior of a single Maxwell element with parameters given in the text.

tamethylflavan at about $\omega\tau_1 = 10$, more gradual in the others) to a region where tan δ becomes nearly independent of frequency. Here, G'' is approximately constant (instead of directly proportional to ω) and η' is approximately inversely proportional to ω (instead of constant); the retardation spectrum is a flat plateau instead of a single line. The limiting high-frequency value of tan δ for these and a number of other glasses of low molecular weight[4] ranges from 0.03 to 0.11 when they are compared at temperatures of equal steady-flow viscosity (4×10^9 poises). Its magnitude apparently increases with the degree of internal flexibility of the molecule,[4] suggesting that the broad retardation spectrum in this region of short times is associated with internal molecular motions.

Rather similar results are seen for glucose glass by combining the data of Philippoff[5-7] and Meyer and Ferry,[8] represented as G' in Fig. 15-2. Here the data are reduced from several different temperatures and there is some uncertainty, associated perhaps with ignoring the temperature dependence of the limiting high-frequency value of G' (see below). However, it is clear that a large part of the viscoelastic dispersion can be described by a single Maxwell element with $G_1 = 0.44 \times 10^{10}$ dynes/cm^2 and $\tau_1 = 4.15 \times 10^{-3}$ sec (dotted curve), which gives the correct steady-flow viscosity of 1.8×10^7 poises. At high frequencies, there are additional contributions with much shorter retardation times spread over a broad range, corresponding to the flattening of log tan δ at high frequencies in Fig. 15-1. These give rise to a steady-state compliance J_e^0 of 2.2×10^{-10} cm^2/dyne. Measurements on dehydroabietic acid by Tobolsky and Taylor[9] similarly revealed a single retardation time in a region corresponding to lower frequencies.

From very precise measurements of shear creep and creep recovery, over a range of temperatures near T_g, Plazek and Magill[10] found for 1:3:5-tri-α-naphthyl benzene a retardation spectrum peaking sharply at long times with a broad tail at

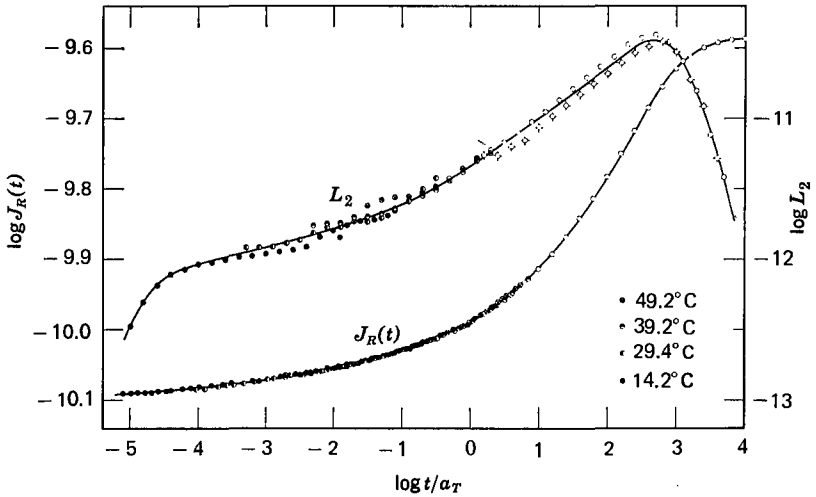


FIG. 15-3. Recoverable shear creep compliance and retardation spectrum of 1:3:5-tri-α-naphthyl benzene, reduced to 64.2°C from measurements at that temperature and above (open circles) and at four other temperatures as indicated. (Points for spectrum calculated in several different ways.) (Plazek and Magill.[10])

short times, thus qualitatively resembling the behavior seen in Figs. 15-1 and 15-2. In Fig. 15-3, both the recoverable creep compliance and the retardation spectrum are plotted. The limiting modulus is of the order of 1.3×10^{10} dynes/cm^2 (though not attained); the steady-state compliance J_e^0 is 2.6×10^{-10} cm^2/dyne, and log η_0 is 12.35 at 64.2°, about 5° below T_g. In the region from -1 to 2 on the abscissa scale, the compliance conforms to the Andrade equation (equation 28 of Chapter 13).

The studies described in the preceding paragraphs were made in a temperature range from slightly below T_g to 20° or 30° above. In very extensive measurements by Lamb, Barlow, and collaborators,[11-15] shear viscoelastic properties of many supercooled liquids have been studied at very high frequencies, from T_g to about 50° above. For $T < T_g + 20°$, generally, $1/G'$ was found to be a linear function of temperature at 30 to 500 MHz and this was taken as the limting high-frequency value, G'_∞; from the relation

$$1/G'_\infty = 1/G_0 + C(T - T_\infty) \tag{1}$$

where T_∞ is the Vogel temperature chosen as reference (equation 41 of Chapter 11), G'_∞ could be calculated at each temperature of measurement. The product CG_0 was of the order of 1 to 4×10^{-2}; *i.e.*, the limiting high-frequency compliance increased a few percent per degree. This change may be attributed primarily to reduction of intermolecular forces by thermal expansion. Equation 1 makes it possible to account for the temperature dependence of the magnitude of elastic mechanisms in reducing data for G' and G'' at different temperatures; these were accordingly plotted as G/G'_∞ and G''/G'_∞ against $\omega\eta_0/G'_\infty$, where η_0 is the

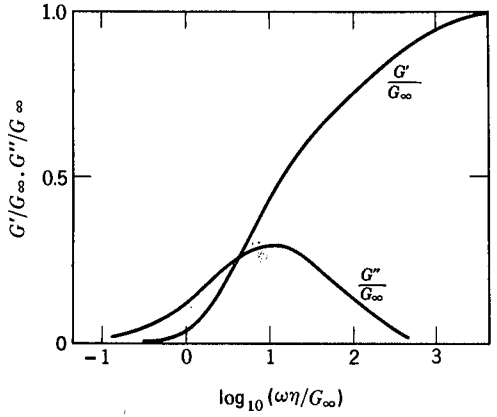


FIG. 15–4. Normalized components of the complex shear modulus of di-(2-ethyl hexyl) phthalate measured over a wide range of temperatures and plotted against log $\omega\eta_0/G'_\infty$ (Lamb and collaborators.[11])

steady-flow viscosity measured separately, providing single composite curves. An example is shown in Fig. 15–4 for di-2-ethylhexyl phthalate.[11] Qualitatively, it corresponds to a relaxation spectrum peaking at low frequencies (approaching a single relaxation time with a large contribution) with a broad high-frequency tail, and thus resembles somewhat the behavior seen in Figs. 15–1 to 15–3. However, the dispersion over the entire frequency range can be described by a single empirical equation.

The quantities directly measured in these dynamic experiments are the components of the characteristic mechanical impedance $\mathcal{R}_M$ and $\mathcal{X}_M$, related to G' and G'' by equations 28–32 of Chapter 5. From those relations it is evident that $\mathcal{R}_M$ and $\mathcal{X}_M$ can be reduced by the factor $(1/\rho G'_\infty)^{1/2}$ for plotting with reduced variables. An example is given in Fig. 15–5 for 11 liquids of moderately complex but widely differing structures.[16] Surprisingly, the character of the frequency dependence is the same for all. Moreover, it corresponds closely to a relatively simple formulation:

$$\frac{\mathcal{R}_M}{(\rho G_\infty)^{1/2}} = \frac{(\omega\eta_0/2G'_\infty)^{1/2}[1 + (2\omega\eta_0/G'_\infty)^{1/2}]}{[1 + (\omega\eta_0/2G'_\infty)^{1/2}]^2 + (\omega\eta_0/2G'_\infty)} \tag{2}$$

$$\frac{\mathcal{X}_M}{(\rho G_\infty)^{1/2}} = \frac{(\omega\eta_0/2G'_\infty)^{1/2}}{[1 + (\omega\eta_0/2G'_\infty)^{1/2}]^2 + (\omega\eta_0/2G'_\infty)} \tag{3}$$

Equations 2 and 3 are represented by the solid curves in Fig. 15–5 (with no adjustable parameters).

In terms of the complex compliance, equations 2 and 3 correspond to a very simple formulation, the equations of Barlow, Erginsav, and Lamb (BEL):[16]

$$J^* = J'_\infty + 1/i\omega\eta_0 + 2J'_\infty\,(i\omega\eta_0 J'_\infty)^{-1/2} \tag{4}$$

$$J' = J'_\infty + J'_\infty/(\omega\eta_0 J'_\infty/2)^{1/2} \tag{5}$$

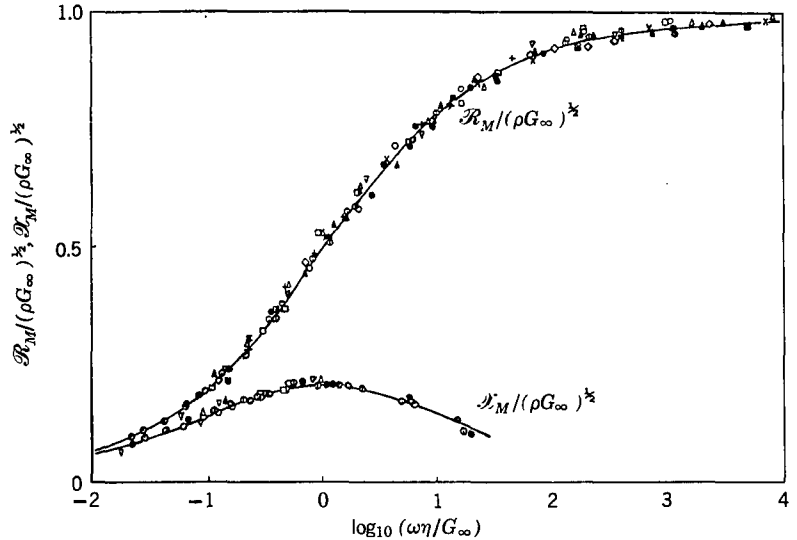


FIG. 15–5. Normalized components of the complex characteristic impedance plotted against log $\omega\eta_0/G'_\infty$ and compared with curves drawn from equations 2 and 3, for 11 liquids: squalane, trichloroethyl phosphate, tri-(*m*-tolyl) phosphate, tris(2-ethyl hexyl) phosphate, tetra(2-ethyl hexyl) silicate, bis(*m*-phenoxyphenoxy) phenyl ether, diisobutyl phthalate, di-*n*-butyl phthalate, isopropyl benzene, *n*-propyl benzene, and *s*-butyl benzene. (Barlow and Lamb.[16])

$$J'' = 1/\omega\eta_0 + J'_\infty/(\omega\eta_0 J'_\infty/2)^{1/2} \tag{6}$$

with $J'_\infty = 1/G'_\infty$. The first term of each equation again corresponds to the behavior of a single Maxwell element with a retardation time $\eta_0 J'_\infty$. These equations have been derived by Phillips, Barlow, and Lamb[17] on the basis of a one-dimensional defect diffusion model, in which relaxation occurs by a diffusion of defect holes which are of the order of molecular dimensions. It is remarkable that the viscoelastic behavior can be predicted from the two constants J'_∞ and η_0 alone. However, the model is not expected to be applicable to polymeric liquids. An alternative model was proposed by Montrose and Litovitz.[18]

Although these equations give very close agreement with experiment over a wide frequency range, they do not provide for a finite value of steady-state compliance J_e^0 at low frequencies or long times as observed for example in the data of Fig. 13–3. The most precise data[12] show small deviations from the BEL equations and are better fitted by an empirical equation[12] which is reminiscent of the equation used by Davidson and Cole[19] to represent dielectric relaxation:

$$J^* = J'_\infty + 1/i\omega\eta_0 + (J_e^0 - J'_\infty)/(1 + i\omega\tau_r)^\beta \tag{7}$$

Here an additional characteristic time τ_r and an empirical exponent β have been introduced. For $\beta = \frac{1}{2}$, $\omega\tau_r \gg 1$, and $J'_\infty \ll J_e^0$, this reduces to the BEL form, but at lower frequencies it correctly provides a finite value of J_e^0. Values of β from 0.3 to 0.6 are found empirically.[12–15] The creep data of Fig. 15–3 can also be represented by equation 7 with $J'_\infty = 0.81 \times 10^{-10}$ cm^2/dyne, $\beta = 0.3$, and $\tau_r = 7.8\ \eta_0 J'_\infty$,

i.e., about an order of magnitude larger than the retardation time corresponding to the first two terms of the equation. The frequency dependence described by equation 7 is very similar to that for dielectric relaxation in several liquids for which the comparison has been made.[20]

The viscoelastic behavior at high pressures can also be described very well by the BEL equations with the pressure dependence of J_∞' and η_0 taken into account; $G_\infty' = 1/J_\infty'$ is found to increase linearly with pressure.[14,21,22]

Data on mixtures of two liquids can be fitted closely by modifying equations 4 to 6 with a single parameter.[23,24] It corresponds to sharpening the distribution over most of the composition range where the mole fraction of the component of lower molecular weight is less than $\frac{1}{2}$, and broadening the distribution over most of the other side of the composition range. The behavior appears to be independent of the identity of the liquids mixed (though all are fairly large molecules as in Fig. 15-4).

The similarities in the behavior of liquids with widely different chemical structures are remarkable. Possibly more extended measurements over wide ranges of frequency and temperatures below T_g, as will be described for polymeric glasses below, would reveal differences associated with specific structures and motions.

For polymers of very low molecular weight, the viscoelastic properties are intermediate between those described for ordinary liquids and those characteristic of high polymers.[25,26] For example, the frequency dependence of viscoelastic properties for a poly-1-butene oligomer[25] with eight monomer units conformed to equations 2 to 5, but oligomers of somewhat higher molecular weights, up to 2700, showed increasing contributions from processes with longer relaxation times and the character of the frequency dependence was intermediate between that of Figs. 15-4 and 15-5 and that predicted by the Rouse theory. Similar data on oligomers of poly(butyl acrylate), and poly(ethyl acrylate), and polystyrene[26] could be described very well by a combination of Rouse modes at lower frequencies and a higher frequency dependence of the form of equations 4 and 5 (*cf.* Section D of Chapter 12).

B. POLYMERS IN THE GLASSY ZONE

The characteristic retardation spectrum of a polymeric glass has already been portrayed as curve V in Fig. 3-4 as a relatively flat plateau. The loss tangent in Fig. 2-8 is correspondingly relatively independent of frequency. In Fig. 15-1, loss tangents for two polymers in the glassy state are included; their magnitudes are similar to those of the simple glasses at high frequencies, and presumably they reflect similar motions. The macromolecular structure evidently prevents any motion of the type characterizing the simple glasses at low frequencies. Thus the most important difference is the absence of the dominant relaxation which is prominent in the glasses and supercooled liquids of low molecular weight, represented in equations 4-7 by the initial terms and the Maxwell retardation time $\eta_0 J_\infty'$.

The loss tangent curves for the polymers show shallow maxima, often designated

as secondary viscoelastic mechanisms to distinguish them from the much larger maximum in tan δ which occurs above T_g when the transition from rubberlike to glasslike consistency is traversed (Figs. 12-3 and 12-11)—the so-called primary of α mechanism. The existence of such maxima, which of course change their positions on the frequency scale with temperature, makes it difficult to draw any significant comparisons among the general magnitudes of the losses in different polymers. However, tan δ in glassy polymers rarely falls below the level indicated in Fig. 15-1 for polystyrene, of the order of 3×10^{-3}.

1. Viscoelastic Functions at Constant Temperature

Only in a few cases have measurements been made at enough frequencies or over a sufficient range of time scale to define isothermal viscoelastic functions. The small magnitude of tan δ is of course associated with a small frequency dependence of the relaxation or storage modulus and the creep or storage compliance, so that high precision is required to determine it; and, as pointed out in Chapter 7, measurements on hard solids are more difficult because compliance of the apparatus can cause large errors. Moreover, such measurements require careful control of certain variables which are not so critical in the transition and rubbery zones treated in previous chapters. The absorption of a trace of diluent—in some cases, moisture[27]—can shift the time scale to shorter values or even introduce a new maximum in the loss tangent.[28] The thermal history is obviously important in determining the properties in the glassy state, since relaxation times change with isothermal contraction (Section D3 of Chapter 11). In particular, rapid quenching from above T_g may leave a larger proportion of uncollapsed free volume and consequently shift the viscoelastic dispersion to shorter times.[29] This effect, and time-dependent changes in viscoelastic properties during aging of quenched samples, will be discussed in Chapter 18. Also, mechanical deformation itself can affect the free volume and the time scale for relaxation processes.[30] These difficulties may be responsible for some lack of agreement among investigations in different laboratories.

An unusually extensive study of the viscoelastic functions through a secondary mechanism in poly(methyl methacrylate) by Koppelmann[31] is shown in Fig. 15-6. Dynamic measurements of G', E', G''/G', and E''/E' are plotted against frequency over seven logarithmic decades. The results illustrate, in the first place, that for glassy polymers shear and elongation do not give equivalent information, as emphasized in Chapter 7; unlike the situation for the softer systems described in the preceding two chapters, elongation includes a perceptible volume change. With increasing frequency both G' and E' undergo gradual increases of the order of 50%, but the inflection in the former lies at a lower frequency by about one power of 10. However, the loss tangents appear within experimental error to be identical. This behavior indicates that the imaginary component of Poisson's ratio, μ'', is small, perhaps zero.[31a] The maximum in tan δ is of the order of 0.1, somewhat higher than that appearing in Fig. 15-1 for the same polymer; the discrepancy probably represents a difference between the two samples investigated. The location of the maximum on the frequency scale (about 1 Hz near room temperature) is in ap-

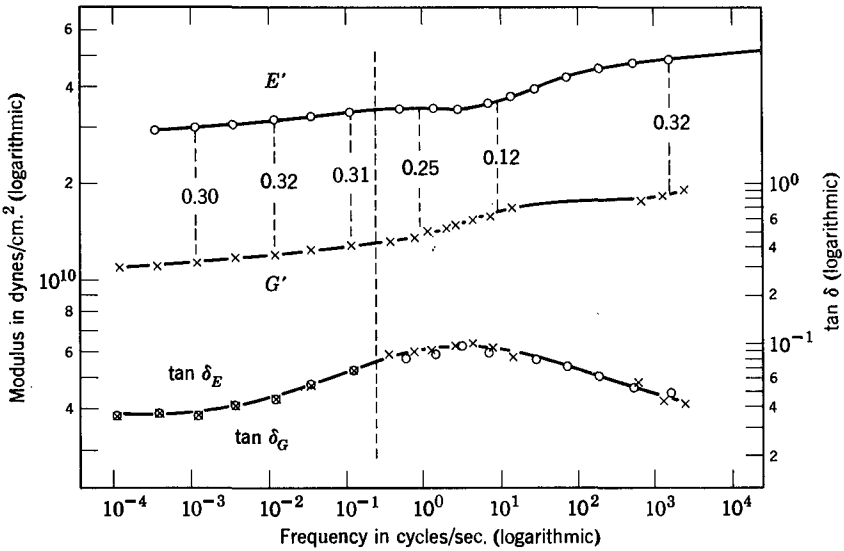


FIG. 15-6. Storage moduli in shear and extension, and loss tangents, of poly(methyl methacrylate) near 25°C, plotted logarithmically against frequency. The numbers between E' and G' denote values of Poisson's ratio. (After Koppelmann.[31])

proximate agreement, however, and has been confirmed by various other investigators.[32-35] This mechanism, being the first secondary maximum in tan δ (as the temperature is decreased below T_g, or the frequency is increased at a given temperature near T_g), is often designated the β mechanism following the terminology of Hoff.[32]

In principle, the frequency dependence of the complex bulk modulus could be obtained from the data for E', E'', G', and G''. In Fig. 15-6, the shear and extension data have been combined to calculate Poisson's ratio μ as a function of frequency. The values indicated show that μ passes through a minimum between the inflections in the dispersion of G' and of E'.

Although the data of Fig. 15-6 have not been used to calculate relaxation and retardation spectra, it is clear from the very gradual frequency dependence of the moduli and tan δ that the spectra are relatively flat over a wide range of frequency scale, as already illustrated as curves V in Figs. 3-3 and 3-4 for this same polymer in the glassy state. The latter were derived from shear creep data of Iwayanagi,[36] confirmed by comparison with similar data of Lethersich.[37]

The loss tangent for the β mechanism in poly(methyl methacrylate)[36,37] can now be compared with those of other homologs, the ethyl, tertiary butyl, and cyclohexyl methacrylates, in Fig. 15-7, cited by Heijboer.[38] The maximum for ethyl occurs at about the same frequency, but with greater magnitude. From other (isochronal) measurements by Heijboer,[39] it is evident that the magnitude of tan δ_{max} increases in the order methyl, ethyl, *n*-propyl, and *n*-butyl, while the frequency remains about the same. This is also evident in the maximum in the retardation spectrum as derived from shear creep measurements by Hideshima[40] when the methyl, *n*-propyl, and

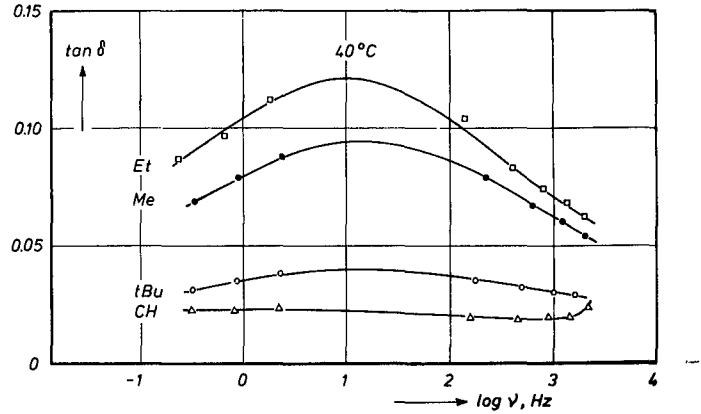


FIG. 15-7. Plots of loss tangent against log ν for four poly(methacrylate)s at 40°C. (Et) Ethyl; (Me) methyl; (t-Bu) t-butyl; (CH) cyclohexyl. (Heijboer.[38]) Reproduced by permission from The International Journal of Polymeric Materials.

n-butyl methacrylate polymers are compared. However, when the side group is relatively rigid as in the t-butyl and cyclohexyl methacrylates, there is very little mechanical loss in this region, as seen in Fig. 15-7. (The retardation spectra of the β mechanism for ethyl and n-butyl methacrylate polymers have also been estimated[41,42] *above* T_g by resolving the overlapping α and β mechanisms in accordance with their temperature dependences as described in Section F2 of Chapter 11. They appear to be sharper and higher, but this method is less reliable.)

Another comparison of interest is shown in Fig. 15-8, where the loss tangent corresponding to the frequency region of the β mechanism is plotted for poly(methyl methacrylate) and two plasticized compositions containing 9.1 and 16.7% by weight

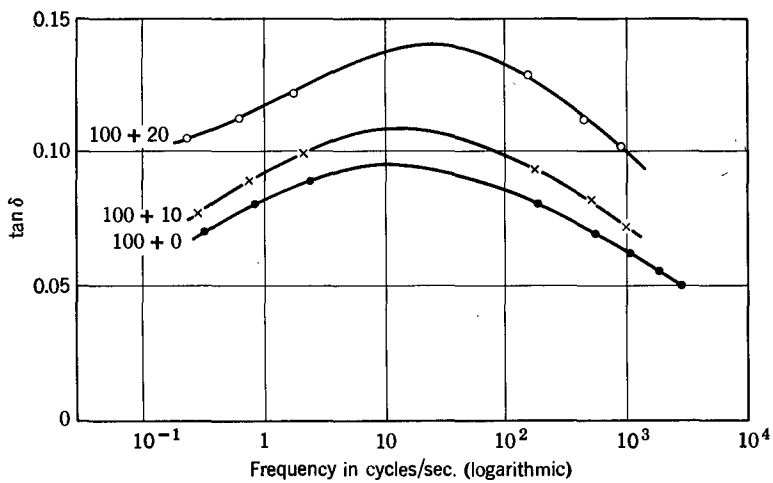


FIG. 15-8. Loss tangent plotted against logarithm of frequency at 40°C for poly(methyl methacrylate) and two solutions containing dibutyl phthalate with weight compositions as indicated. (Heijboer.[35])

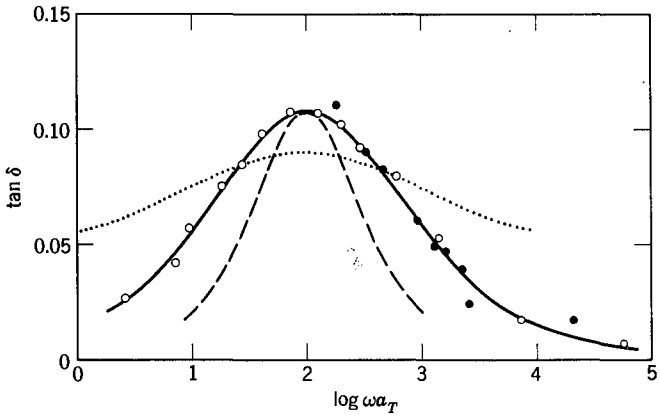


FIG. 15-9. Loss tangent for secondary relaxation mechanism in poly(cyclohexyl methacrylate), reduced to −60°C from data of Heijboer[35] measured from −90° to −42°C. Open circles, from torsion (G''/G'); closed circles, from flexure (E''/E'). Dashed line is prediction from a single-line retardation spectrum with constants adjusted to make the maximum coincide; dotted line, loss tangent of poly(methyl methacrylate) from Fig. 15-6 adjusted to same location of maximum on frequency scale.

of dibutyl phthalate. In these results of Heijboer,[35] the shape of the maximum (*cf.* Fig. 15-7) is not much changed by the addition of diluent, but its height is increased; and the position of the maximum on the frequency scale is shifted slightly to higher frequencies. The latter displacement is much more moderate than that observed for the α mechanism (the primary transition between glasslike and rubberlike consistency) for small amounts of diluent as will be discussed in Chapter 17. It probably represents a slight loosening of the local structure, facilitating the side group motions to which the β mechanism is attributed.

A much sharper viscoelastic mechanism is evidenced in dynamic measurements on poly(cyclohexylmethacrylate) by Hoff[32] and Heijboer.[35,43] In Fig. 15-9, tan δ as measured by Heijboer at several different frequencies and temperatures has been reduced to a reference temperature of −60° by values of a_T calculated from the Arrhenius relation with ΔH_a = 11.3 kcal, and plotted against the logarithm of the reduced frequency. Here measurements in both shear (torsion) and extension (flexure) are combined in the same graph; where the reduced values overlap, they coincide as does tan δ in shear and extension in Fig. 15-6. A reduced curve for G'' looks very similar with a maximum of about 1.5×10^8 Pa (1.5×10^9 dynes/cm^2).[38] The experimental curve for tan δ can be compared with one predicted on the basis of a single retardation time (one Voigt element in series with a spring, the constants adjusted to give the same maximum value of tan δ and the corresponding frequency). The single-valued spectrum gives a peak only moderately sharper than that observed, in contrast to the very broad maximum in poly(methyl methacrylate), also drawn in Fig. 15-9 for comparison. This has been designated as a γ mechanism because of its location on the frequency scale, the β mechanism being scarcely evident as seen in Fig. 15-7.[38]

For the cyclohexyl methacrylate, a very specific internal molecular motion has

been postulated[35,43] to account for this secondary viscoelastic mechanism: the flipping of the cyclohexane ring between two isomeric chair forms, differing in their orientation with respect to attachment to the polymer chain, and separated by an intermediate configuration representing an energy barrier. This interpretation is consistent with the magnitude of the apparent activation energy as well as the fact that the position on the frequency scale is the same for other polymers and copolymers containing the cyclohexyl group and even for a plasticized polymer in which the cyclohexyl is in the plasticizer—except when the plasticizer is 1,1-dichlorocyclohexane, for which the two chair forms are identical. It is also supported by dielectric measurements.[43]

Many other secondary viscoelastic mehcanisms observed in the glassy state have been tentatively identified with various types of local molecular motions with less specific descriptions than in the case of the cyclohexyl group. Most of these identifications are based on isochronal rather than isothermal measurements.

2. Isochronal or Quasi-Isochronal Viscoelastic Measurements

Because of the greater ease of experimental measurements, there have been far more studies of dynamic viscoelastic properties of glassy polymers where the temperature has been varied at approximately constant frequency, as discussed for polymers in the transition zone in Chapter 12, Section A. For example, Fig. 12-3 with data of Schmieder and Wolf[34] on certain poly(vinyl ether)s includes measurements of G' and tan δ in shear below the glass transition temperature, and secondary mechanisms are apparent in the small maxima in tan δ near $-150°$ as well as the corresponding negative slopes of G' in this region.

Another example is shown in Fig. 15-10 for G' and tan δ plotted logarithmically against temperature, at 1 Hz for four methacrylate polymers.[44] The loss tangents show different maxima in characteristic temperature regions. The sharp peak at the right is the α mechanism associated with the transition from glasslike to rubberlike consistency; it shifts to lower temperatures with increasing side chain length because of the change in monomeric friction coefficient at constant temperature, as discussed in detail in Chapter 12. In the neighborhood of 20°C, the β mechanism appears (*cf.* the isothermal plots against frequency in Fig. 15-7); it is very clear in the methyl polymer, but is overtaken by the α mechanism with increasing side chain length and is almost concealed by the latter in the *n*-butyl polymer. A third mechanism near $-180°$C, designated γ, appears in the *n*-propyl and *n*-butyl polymers. Inflections in G' correspond in general to maxima in tan δ.

An enormous volume of information on such loss mechanisms is available in the literature; it has been summarized in various reviews[38,39,45-47] and the identification of mechanisms with molecular processes has been critically discussed.[38,47] Some measurements have been made at extremely low temperatures.[48] A full discussion is beyond the scope of this book.

In many studies, isochronal measurements have been made at two or more different frequencies and the loci of maxima in the loss tangent mapped against temperature and frequency, often supplemented by dielectric and nuclear magnetic resonance data, as illustrated for polystyrene[49] in Fig. 15-11. Here, five mechanisms

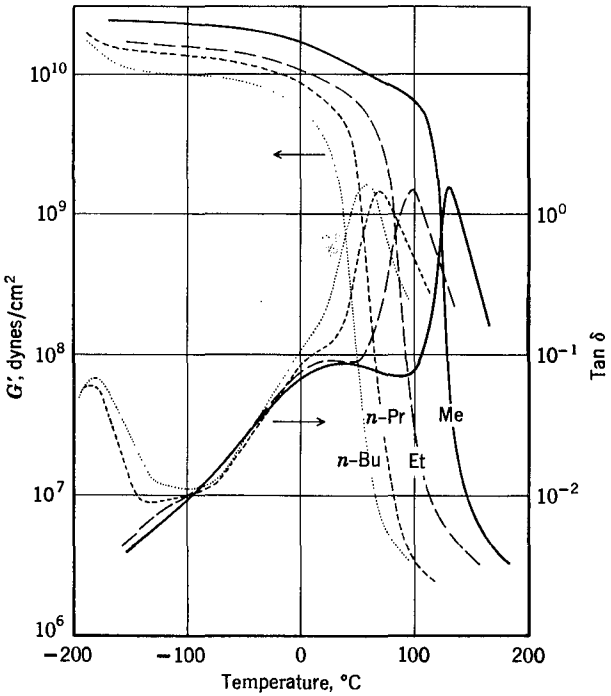


FIG. 15–10. Logarithms of storage shear modulus and loss tangent at 1 Hz plotted against temperature for four methacylate polymers. (Me) methyl; (Et) ethyl; (*n*-Pr) *n*-propyl; (*n*-Bu) *n*-butyl. (Heijboer.[44])

are distinguished (one of them apparent only in dielectric dispersion). To the extent that the locus lines are straight, when log ν is plotted against $1/T$, apparent activation energies can be calculated from their slopes. This must be considered a somewhat arbitrary and approximate procedure, since the form of the frequency dependence may change somewhat with temperature; the maximum in tan δ has a different locus from the maximum in G'' or the maximum in J'', for example, and their slopes may not be the same. However, such maps are useful for identifying different mechanisms which often appear in fragmentary form in individual experiments. A close correspondence among mechanical, dielectric, and nuclear magnetic resonance relaxations cannot be expected. The latter depend on orientation of electrical dipoles and nuclear spins, respectively; although similar molecular motions may be involved, the quantities measured (electrical polarization, energy absorption in a magnetic field) corresponding to various molecular processes may have very different relative magnitudes from those observed mechanically or may be completely absent.

3. Local Molecular Motions

Many types of short-range molecular motions have been proposed to account for the various viscoelastic dispersions observed in the glassy state. These will be

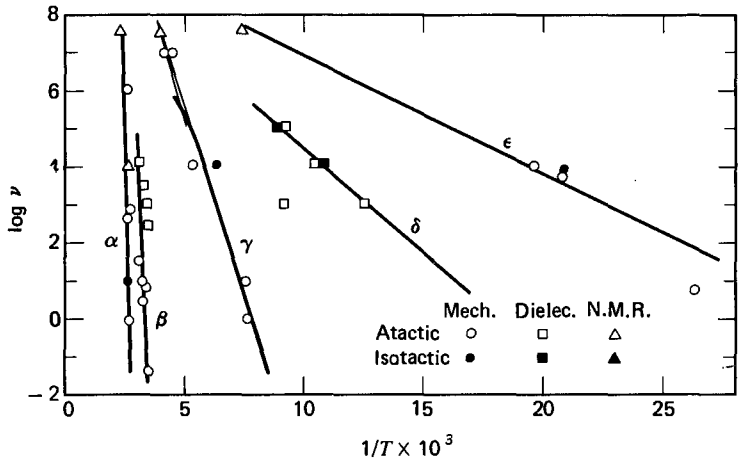


FIG. 15-11. Loci of mechanical and dielectric loss maxima and of nuclear magnetic resonance T_1 minimum (4×10^7 Hz) and line narrowing (10^4 Hz): logarithm of frequency in Hertz plotted against reciprocal absolute temperature, for polystyrene. Points refer to different types of measurements as indicated. (Wada.[49])

summarized without attempting to review the evidence for assigning them to specific mechanisms observed experimentally.[38,47]

Local Mode Relaxation. Loss maxima are observed in some amorphous glasses of polymers such as poly(vinyl chloride), poly(ethylene terephthalate), and poly(trifluoromonochloroethylene), which do not have flexible side groups. They have been attributed to uncoordinated torsional oscillations of chain segments associated with rotations of moderately small amplitude around chemical bonds without crossing the energy barrier separating the favored trans and gauche positions, as well as other vibrational modes.[50,51] An equilibrium distribution of torsional displacements of motional units of the main chain is perturbed by mechanical (or electrical) excitation and energy is dissipated in the establishment of a new distribution. The theory of energy dissipation has been elaborated in detail for crystalline polymers, in which a known regular structure is present, and has been extended to amorphous glassy polymers.[53]

Crankshaft and Kink Motions. If rotation around a chemical bond from one isomeric equilibrium position (trans or gauche) occurs in a medium where the mobility is very small, it must be accompanied by a coordinated motion around a neighboring collinear bond to produce a minimum of disturbance. The two collinear bonds may be separated by three[46] or five[54] chain bonds, which move together as a crankshaft. This process has been proposed to explain relaxation mechanisms which appear only when several CH_2 groups occur in sequence, either in the chain backbone or in side chains (*cf.* the β maxima in Fig. 15-10). In a much more general concept, Pechhold[55,56] has treated motions in which kinks progress along a chain by coordinated rotations between gauche and trans positions.

Rotations of Terminal Groups, Especially Methyl. A methyl group, either directly attached to the backbone (as in methacrylate polymers or polypropylene)

or on the end of a side group can rotate among three equilibrium positions.[57] If on the backbone, the methyl group presumably requires some cooperation from the main chain to rotate through a large angle, and this can result in mechanical relaxation. If on the end of a side group, rotation is probably ineffective in mechanical relaxation[57] although prominently observed in nuclear magnetic resonance relaxation.[58] The rotation of such a terminal, roughly spherical symmetrical group may be the only case where motion in an undiluted polymer is governed primarily by intrachain potential barriers rather than by such environmental features as local packing and cooperation of neighboring segments. A terminal methyl group attached to an oxygen hinge can be identified with a different temperature-frequency locus from that characteristic of a terminal methyl attached to methylene;[57,59] their apparent activation energies have been estimated as 0.3 and 1.8 kcal/mole respectively. The rotation of a methyl group may involve quantum mechanical tunneling.[60,61]

Other Side Chain Motions. The motion of an entire side group around the bond joining it to the chain backbone is usually considered to be the origin of the β mechanism in methacrylate polymers (Figs. 15–7 and 15–10). The presence of the opposite methyl group makes some cooperation of the main chain necessary, as evidenced by experiments with copolymers (see below), but it must be of a very short-range nature distinct from the motions which are reflected in the transition zone (the α mechanism).[44,62,63] Motion of a rigid side group, such a phenyl in polystyrene, around the bond joining it to the main chain (rotation, restricted rotation, and/or wagging) is also postulated as the origin of a viscoelastic mechanism,[47,63] although such motions must be severely inhibited by steric restrictions.[63a] Other mechanisms are attributed to rotational motions within flexible side groups such as those in poly(*n*-alkyl methacrylates)[44,63] as mentioned above.

It has been suggested by Andrews and Hammack[46] that short-range motions such as these can be associated with various types of loosening of intermolecular attractions.

Vibrational Relaxations. The transfer of energy from a vibrational degree of freedom to other modes due to anharmonic coupling has also been proposed as a loss mechanism.[64]

Local Intermolecular Rearrangements. Whereas most of the preceding mechanisms have emphasized motions of a single molecule, it is evident that such motions even on a local scale must, in the glassy state, require the cooperation of neighboring molecules. It has been proposed that relaxations associated with local cooperative rearrangements are an inherent property of the glassy state and need not be attributed to specific intramolecular motions.[64a]

As an example of assignments of mechanisms for a specific polymer, the temperature-frequency loci shown in Fig. 15–11 for polystyrene have been attributed to the following motions:[49] α, segmental motions of the main chain governed by the monomeric friction coefficient (*i.e.*, the transition zone of viscoelastic behavior); β, local mode torsional oscillations of the main chain;[52] γ, rotation of the phenyl group around the bond joining it to the main chain; δ (observed in dielectric measurements only, and nearly absent in isotactic polymer), relaxations of resultant

dipoles from head-to-head pairs of phenyl groups; ε, unknown. Many such assignments have been proposed for various polymers, based on deductions from the behavior of copolymers of progressively varying composition,[44,62,65] chemical substitution,[66-69] polymers with different tacticities,[44,70] and systems with added diluent,[71] effects of thermal history,[72] and comparison of mechanical, dielectric and nuclear magnetic resonance relaxations.[45,58,73-78]

The absorption of mechanical energy by relaxation mechanisms in the glassy state is important in providing toughness and resistance to fracture, and the relations to these properties have been discussed by several authors.[79-82]

C. NONLINEAR BEHAVIOR OF GLASSY POLYMERS

The preceding sections have of course dealt with deformations under small stresses, where the viscoelastic behavior is linear. For glassy polymers, which with their high moduli can support substantial stresses, nonlinear phenomena can be encountered even when the strains are relatively small (of the order of 1% strain for 5% nonlinearity[85,86]). The nature of the nonlinearity is quite different, therefore, from that in the rubbery zone (Chapter 14, Section C), which is associated with high strains rather than high stresses. Experimental measurements are rather sparse.

1. Stress and Strain Dependence of Viscoelastic Properties

In tensile creep of glassy polystyrene under high stresses, of the order of 10^8 dynes/cm^2, the rate of deformation at a given time after loading increases with something like the fourth power of the applied stress, instead of being directly proportional.[83] Similar nonlinear stress dependence for shear creep of poly(methyl methacrylate) below T_g was found by Lethersich,[84] and the creep and creep recovery functions were very different in shape, even though the total deformation (of the order of 5%) was fully recoverable.

In stress relaxation of glassy polycarbonate at tensile strains ϵ up to 4%, Yannas and Haskell[87] found that the time-dependent tensile stress σ_T could be expressed by a power series:

$$\sigma_T(t) = E_1(t)\epsilon + E_2(t)\epsilon^2 + E_3(t)\epsilon^3 \tag{8}$$

in which $E_1(t)$ is the linear tensile relaxation modulus; $E_2(t)$ and $E_3(t)$ are negative. Equation 8 can be derived from an integral expansion which represents an extension of the Boltzmann superposition principle.[85,86,88] However, no physical significance was assigned to the higher terms, since they appeared to vary erratically with temperature.

Nonlinear oscillatory viscoelastic behavior of glassy polycarbonate and polymethyl methacrylate has been investigated in a thorough study by Davis and Macosko[86] with very nearly homogeneous shear strains up to 4%. The analog of equation 8, derived in the same manner from the extension of the Boltzmann su-

perposition principle,[86] corresponding to the linear equation 19 of Chapter 1 for a sinusoidally varying shear strain $\gamma = \gamma_0 \sin \omega t$, is:

$$\sigma = G_1' \gamma_0 \sin \omega t + G_1'' \gamma_0 \cos \omega t + G_3' \gamma_0^3 \sin \omega t + G_3'' \gamma_0^3 \cos \omega t + H_3' \gamma_0^3 \sin 3\omega t + H_3'' \gamma_0^3 \cos 3\omega t + \text{higher odd terms} \quad (9)$$

Here G_1' and G_1'' are the ordinary storage and loss shear moduli. Nonlinearity may appear in the fundamental frequency terms with G_3' and G_3'', and also in the first odd harmonic with a frequency of 3ω in the terms with H_3' and H_3''. (The same equation was derived earlier by Onogi, Masuda, and Matsumoto[89] and applied to suspensions of particles in viscoelastic liquids.) In the strain range covered, H_3' and H_3'' were found to be small enough to be ignored; G_3' was negative and of the order of $-0.01\ G_1'$; G_3'' was positive and of the order of $-0.1\ G_1'$. The isochronal temperature dependence at a frequency of 1 Hz showed an increase in $-G_3'$ and G_3'' as the glass transition temperature was approached, and in addition, for the polycarbonate, large maxima at about the same temperature that secondary loss mechanisms were observed in G_1' and G_1''.

In dynamic longitudinal deformations at low audio frequencies, polystyrene was found by Sauer and collaborators[83] to exhibit an energy dissipation per cycle which increased rapidly with the amplitude of vibration.

Nonlinear phenomena such as these have been discussed in terms of transition-state kinetics by Schwarzl.[90] A substantial asymmetry of a potential barrier to molecular motions, imposed by high external stress, leads to a shift of the viscoelastic time scale to shorter times as well as a broadening of the retardation spectrum. The nonlinear behavior of fibers in transient loading experiments has been interpreted in this way by Eyring and collaborators.[91]

An additional nonlinear effect which appears in extension under high stresses, attributable to the volume expansion associated with the fact that Poisson's ratio is less than $\frac{1}{2}$, will be discussed in Chapter 18; it is manifested by a decrease in all the relaxation and retardation times.[92-95] This effect is especially prominent in more complicated stress patterns such as combined tension and torsion, as studied by Sternstein.[30,96] Nonlinear creep behavior under combined tension and torsion with the additional complication of changing temperature during the experiment has been studied by Mark and Findley.[97]

Under very high stresses, especially if combined with bulk stress (confining pressure), glassy polymers can exhibit yield phenomena with quite large deformations. This behavior is also associated with volume changes.[30,98-99]

2. Anisotropic Systems

Time-dependent mechanical deformations at small amplitudes can easily be superimposed on large static deformations in glassy polymers without maintaining static stresses, since the static deformations are frozen in after orienting or drawing. However, there appear to be very few direct measurements of time-dependent mechanical properties of highly oriented amorphous polymers in the glassy state.[100] Högberg[101] has studied periodic flexual deformations of polymers oriented by in-

jection molding, and found somewhat higher moduli when the orientation was in the longitudinal direction (parallel to the bar length). That secondary loss mechanisms are affected by orientation is indicated by dielectric loss measurements on polystyrene and poly(vinyl chloride).[102]

REFERENCES

1. T. A. Litovitz and T. Lyon, *J. Acoust. Soc. Am.*, **30,** 856 (1958).
2. T. A. Litovitz, in *Non-Crystalline Solids,* edited by V. D. Frechette, Wiley, New York, 1960, p. 252.
3. J. J. Benbow, *Proc. Phys. Soc.*, **B67,** 120 (1954).
4. J. J. Benbow and D. J. C. Wood, *Trans. Faraday Soc.*, **54,** 1581 (1958).
5. W. Philippoff, unpublished data.
6. W. Philippoff and J. Brodnyan, *Bull. Am. Phys. Soc.*, **30,** No. 2, 26 (1955).
7. W. Philippoff, in *Physical Acoustics,* edited by W. P. Mason, Volume IIB, Academic Press, New York, 1965, p. 1.
8. H. H. Meyer and J. D. Ferry, *Trans. Soc. Rheol.*, **9:2,** 343 (1965).
9. A. V. Tobolsky and R. B. Taylor, *J. Phys. Chem.*, **67,** 2439 (1963).
10. D. J. Plazek and J. H. Magill, *J. Chem. Phys.*, **45,** 3038 (1966).
11. A. J. Barlow, J. Lamb, A. J. Matheson, P. R. K. L. Padmini, and J. Richter, *Proc. R. Soc.*, **A298,** 467 (1967).
12. A. J. Barlow and A. Erginsav, *Proc. R. Soc.*, **A327,** 175 (1972).
13. A. J. Barlow, A. Erginsav, R. J. McLachlan, and R. P. Singh, *J. Chem. Soc., Faraday Trans. II,* **70,** 1288 (1974).
14. M. G. Kim, *J. Chem. Soc., Faraday Trans. II,* **71,** 415 (1975).
15. J. Lamb, in *Molecular Motions in Liquids,* edited by J. Lascombe, Reidel Publishing Company, Dordrecht, 1974, p. 29; *J. Rheol.*, **22,** 317 (1978).
16. A. J. Barlow, A. Erginsav, and J. Lamb, *Proc. R. Soc.*, **A298,** 481 (1967).
17. M. C. Phillips, A. J. Barlow, and J. Lamb, *Proc. R. Soc.*, **A329,** 193 (1972).
18. C. J. Montrose and T. A. Litovitz, *J. Acoust. Soc. Am.*, **47,** 1250 (1970).
19. D. W. Davidson and R. H. Cole, *J. Chem. Phys.*, **19,** 1484 (1951).
20. M. F. Shears, G. Williams, A. J. Barlow, and J. Lamb, *J. Chem. Soc., Faraday Trans. II,* **70,** 1783 (1974).
21. A. J. Barlow, G. Harrison, J. B. Irving, M. G. Kim, J. Lamb, and W. C. Pursley, *Proc. R. Soc.*, **A327,** 403 (1972).
22. A. J. Barlow, G. Harrison, M. G. Kim, and J. Lamb, *J. Chem. Soc., Faraday Trans. II,* **69,** 1446 (1973).
23. A. J. Barlow, A. Erginsav, and J. Lamb, *Proc. R. Soc.*, **A309,** 473 (1969).
24. A. J. Barlow and A. Erginsav, *J. Chem. Soc., Faraday Trans. II,* **69,** 1200 (1973).
25. A. J. Barlow, R. A. Dickie, and J. Lamb, *Proc. R. Soc.*, **A300,** 356 (1967).
26. R. W. Gray, G. Harrison, and J. Lamb, *Proc. R. Soc.*, **356,** 77 (1977).
27. J. R. McLoughlin and A. V. Tobolsky, *J. Colloid Sci.*, **7,** 658 (1951).
28. K. H. Illers, *Makromol. Chem.*, **38,** 168 (1960).
29. L. C. E. Struik, Thesis, Delft Technical University, 1977.
30. S. S. Sternstein, in *Treatise on Materials Science and Technology,* Volume 10, Part B, Academic Press, New York, 1977, p. 541.
31. J. Koppelmann, *Rheol. Acta.*, **1,** 20 (1958).

31a. D. J. Massa, Personal communication.

32. E. A. W. Hoff, D. W. Robinson, and A. H. Willbourn, *J. Polym. Sci.*, **18,** 161 (1955).
33. S. Iwayanagi and T. Hideshima, *J. Phys. Soc. Jpn.*, **8,** 368 (1953).
34. K. Schmieder and K. Wolf, *Kolloid-Z.*, **134,** 149 (1953).

35. J. Heijboer, *Kolloid-Z.*, **148,** 36 (1956).
36. K. Sato, H. Nakane, T. Hideshima, and S. Iwayanagi, *J. Phys. Soc. Jpn.*, **9,** 413 (1954).
37. W. Lethersich, *Br. J. Appl. Phys.*, **1,** 294 (1950).
38. J. Heijboer, *Int. J. Polym. Mater.*, **6,** 11 (1977).
39. J. Heijboer, *Ann. N. Y. Acad. Sci.*, **279,** 104 (1976).
40. T. Hideshima, *Rep. Prog. Polym. Phys. Jpn.*, **2,** 53 (1959); *6,* 143 (1963).
41. J. D. Ferry, W. C. Child, Jr., R. Zand, D. M. Stern, M. L. Williams, and R. F. Landel, *J. Colloid Sci.*, **12,** 53 (1957).
42. W. C. Child, Jr., and J. D. Ferry, *J. Colloid Sci.*, **12,** 327 (1957).
43. J. Heijboer, *Kolloid-Z.*, **171,** 7 (1960).
44. J. Heijboer, *Proc. Intern. Conf. on Physics of Non-Crystalline Solids,* edited by J. A. Prins, North Holland Publishing, Amsterdam, 1965, p. 231.
45. N. G. McCrum, B. E. Read, and G. Williams, *Anelastic and Dielectric Effects in Polymeric Solids,* Wiley, New York, 1967.
46. R. F. Boyer, *Rubber Chem. Technol.*, **36,** 1303 (1963).
47. G. E. Roberts and E. F. T. White, in *The Physics of Glassy Polymers,* edited by R. N. Haward, Wiley, New York, 1973.
48. K. M. Sinnott, *J. Polym. Sci.*, **35,** 273 (1959); *Soc. Plast. Eng. Trans.*, **2,** 65 (1962).
49. O. Yano and Y. Wada, *J. Polym. Sci.*, A-2, **9,** 669 (1971).
50. K. Okano, *Rep. Prog. Polym. Phys. Jpn.*, **3,** 71 (1960).
51. K. Yamafuji, *J. Phys. Soc. Jpn.*, **15,** 2295 (1960).
52. N. Saito, K. Okano, S. Iwayanagi, and T. Hideshima, in *Solid State Physics,* edited by F. Seitz and D. Turnbull, Volume 14, Academic Press, New York, 1963, pp. 387, 419.
53. R. Hayakawa and Y. Wada, *J. Polym. Sci.*, **12,** 2119 (1974).
54. T. F. Schatzki, *J. Polym. Sci.*, **57,** 496 (1962).
55. W. Pechhold, *Kolloid-Z. Z. Polym.*, **228,** 1 (1968).
56. W. Pechhold, *Kolloid-Z. Z. Polym.*, **216:7,** 235 (1967).
57. Y. Tanabe, J. Hirose, K. Okano, and Y. Wada, *Rep. Prog. Polym. Phys. Jpn.*, **11,** 257 (1968).
58. W. P. Slichter, *Adv. Polym. Sci.*, **1,** 1 (1958).
59. Y. Wada, *Kobunshi no Busseikogaku,* Busseikogaku Volume 7, Ohm, Tokyo, 1967, p. 303.
60. E. O. Stejskal and H. S. Gutowsky, *J. Chem. Phys.*, **28,** 388 (1958).
61. J. Williams and A. Eisenberg, *Macromolecules,* **11,** 700 (1978).
62. Y. Kawamura, S. Nagai, and Y. Wada, *Rep. Prog. Polym. Phys. Jpn.*, **11,** 365 (1968).
63. O. Yano and Y. Wada, *Rep. Prog. Polym. Phys. Jpn.*, **9,** 287 (1966).

63a. A. E. Tonelli, *Macromolecules,* **6,** 682 (1973).

64. K. Shimizu, O. Yano, Y. Wada, and Y. Kawamura, *Polym. J.*, **5,** 107 (1973).

64a. G. P. Johari and M. Goldstein, *J. Chem. Phys.*, **53,** 2372 (1970); **55,** 4245 (1971).

65. J. Hirose and Y. Wada, *Rep. Prog. Polym. Phys. Jpn.*, **10,** 439 (1967).
66. K. H. Illers, *Z. Elektrochem.*, **65,** 679 (1961).
67. M. Baccaredda, E. Butta, V. Frosini, and P. L. Magagnini, *J. Polym. Sci.*, A-2, **4,** 789 (1966).
68. V. Frosini, P. Magagnini, E. Butta, and M. Baccaredda, *Kolloid-Z., Z. Polymere,* **213,** 115 (1966).
69. M. C. Shen, J. D. Strong, and F. J. Matusik, *J. Macromol. Sci.*, **B1,** 15 (1967).
70. M. Baccaredda, E. Butta, and V. Frosini, *J. Polym. Sci.*, **B3,** 185 (1965).
71. K. H. Illers and E. Jenckel, *Rheol. Acta,* **1,** 322 (1958); *J. Polym. Sci.*, **41,** 528 (1959).
72. G. Goldbach and G. Rehage, *Kolloid-Z., Z. Polymere,* **216,** 56 (1967).
73. G. S. Fielding-Russell and R. E. Wetton, *Spec. Publ. Chem. Soc.*, **20,** 95 (1966).
74. H. Thurn and K. Wolf, *Kolloid-Z.*, **156,** 21 (1958).
75. J. D. Ferry and S. Strella, *J. Colloid Sci.*, **13,** 459 (1958).
76. K. Shimizu, O. Yano, and Y. Wada, *J. Polym. Sci., Polym. Phys. Ed.*, **13,** 1959 (1975).
77. K. Shimizu, O. Yano, and Y. Wada, *J. Polym. Sci., Polym. Phys. Ed.*, **13,** 2357 (1975).
78. D. J. Massa and P. P. Rusanowsky, *Polym. Prepr. Am. Chem. Soc.*, **17(2),** 184 (1976).

79. Y. Wada and T. Kasahara, *J. Appl. Polym. Sci.*, **11,** 1661 (1967).
80. J. Heijboer, *J. Polym. Sci.*, **C16,** 3755 (1968).
81. J. R. Kastelic and E. Baer, *J. Macromol. Sci. Phys.*, **B7,** 679 (1973).
82. W. W. Gerberich and G. C. Martin, *J. Polym. Sci., Polym. Phys. Ed.*, **14,** 897 (1976).
83. J. A. Sauer, J. Marin, and C. C. Hsiao, *J. Appl. Phys.*, **20,** 507 (1949).
84. W. Lethersich, *Proc. XI Cong. Pure and Applied Chem.*, London, Volume 5, 1947, p. 591.
85. I. V. Yannas, *Macromol. Rev.*, **9,** 163 (1974).
86. W. M. Davis and C. W. Macosko, *J. Rheol.*, **22,** 53 (1978).
87. I. V. Yannas and V. C. Haskell, *J. Appl. Phys.*, **42,** 610 (1971).
88. I. M. Ward, *Mechanical Properties of Solid Polymers,* Wiley-Interscience, London, 1971, p. 218.
89. S. Onogi, T. Masuda, and T. Matsumoto, *Trans. Soc. Rheol.*, **14,** 275 (1970).
90. F. Schwarzl, *Kolloid-Z.*, **165,** 88 (1959).
91. G. Halsey, H. J. White, Jr., and H. Eyring, *Text. Res. J.*, **15,** 295 (1945); C. H. Reichardt and H. Eyring, *ibid.*, **16,** 635 (1946).
92. D. H. Ender, *Bull. Am. Phys. Soc.*, Ser. II, **13,** 396 (1968).
93. G. M. Bryant, *Text. Res. J.*, **31,** 399 (1961).
94. S. Matsuoka, Advances in Chemistry Series No. 154, 1976, p. 3.
95. S. Matsuoka, H. E. Bair, S. S. Bearder, H. E. Kern, and J. T. Ryan, *Polym. Eng. Sci.*, **18,** 1073 (1978).
96. S. S. Sternstein and T. C. Ho, *J. Appl. Phys.*, **43,** 4370 (1972).
97. R. Mark and W. N. Findley, *Trans. Soc. Rheol.*, **19,** 201 (1975).
98. D. H. Ender and R. D. Andrews, *J. Appl. Phys.*, **36,** 3057 (1965).
99. W. Whitney and R. D. Andrews, *J. Polym. Sci.*, **C16,** 2981 (1967).
100. H. Thurn, *Kolloid-Z.*, **165,** 57 (1959).
101. H. Högberg, *Symposium on Plastics Testing and Standardization,* Am. Soc. Testing Matls. Special Technical Publications, No. 247, 1958, p. 95.
102. K. Huff and F. H. Müller, *Kolloid-Z.*, **153,** 5 (1957).

CHAPTER 16

Crystalline Polymers

When the local structure along a polymer chain has enough regularity and symmetry to permit ordering in a crystal lattice, a decrease in temperature results in a partially crystallized system instead of an amorphous glass such as those described in the preceding chapter. The extent of order and the morphology depend on the circumstances of crystallization and subsequent thermal and mechanical treatment in a very complicated manner.[1-4]

When crystallized from dilute solution, the polymer molecules form thin lamellar single crystals in which the chains run parallel to the thin direction (of the order of 100 Å) and are folded back and forth many times. On the surfaces of the lamellae, there is some disorder where the chains loop to reverse direction. The lamellar thickness depends on the degree of supercooling at the temperature where crystallization takes place. Certain viscoelastic properties of such single crystals can be observed by propagation of longitudinal waves through suspensions,[5] which provides a determination of the complex bulk modulus as mentioned in Chapter 8. Stress-strain relations have been successfully measured[6] on single crystals by a specially designed "nanotensilometer," but this is extremely difficult. Most information on single crystals has been obtained with thin mats in which the crystals have been deposited in oriented layers to build up a thickness of the order of 0.2 mm. Both transient and dynamic viscoelastic properties in extension can be measured on strips cut from such mats.[7-9]

When polymers with a high degree of molecular symmetry such as linear polyethylene, isotactic polypropylene, or polyoxymethylene are crystallized from the melt, similar lamellar structures are formed, organized into larger morphological units such as spherulites. Some molecules may run as ties from one lamella into another. If the molecular weight is not uniform, fractionation occurs with species of lower molecular weight remaining uncrystallized between the lamellae and sometimes subsequently crystallizing in an extended rather than folded form.[10,11] Various kinds of defects and features of disorder may be present; they are enhanced by the presence of side groups (especially if irregular as in polyethylene with short

branches), atacticity, comonomers, or other features which diminish molecular symmetry. Melt-crystallized polymers can be much more easily investigated than single crystal mats, but interpretation of their viscoelastic properties is more complicated. Throughout the range of viscoelastic time scale, the shear and Young's moduli are quite high, and as in glassy polymers there is nothing corresponding to the primary transition zone of viscoelastic behavior. Highly crystalline polymer samples can also be prepared from evaporation of concentrated solutions; these presumably resemble melt-crystallized samples much more than single crystal mats.

When crystallization is severely inhibited by lack of molecular symmetry, as in certain copolymers,[12,13] the density is substantially less than that corresponding to the crystalline state, and amorphous regions may exist. If they are large enough, the polymer in these regions may undergo a glass transition corresponding to the ordinary transition of the bulk amorphous polymer in the quenched, supercooled state. As a function of time or frequency, the shear and Young's moduli may undergo a transition from the order of 10^8 to 10^{10} dynes/cm^2 (10^7 to 10^9 Pa), sometimes described as a transition from leathery to glasslike consistency. In such polymers with low degrees of crystallinity, individual molecules may thread in and out of crystalline regions which act as multiple cross-links.

Investigations of viscoelastic properties of crystalline polymers, like those of polymers in the glassy state, have been characterized by identification of various loss or relaxation mechanisms and attempts to identify these with various types of molecular motion.[14–17a]

A. VISCOELASTIC FUNCTIONS AT CONSTANT TEMPERATURE

It has already been noted in curves VIII of Figs. 2–1 to 2–8 and 3–3 and 3–4 that for a highly crystalline polymer the viscoelastic functions have a comparatively slight time or frequency dependence. The three types of crystalline systems distinguished above will be discussed separatively.

1. Oriented Single Crystal Mats

In a very extensive study of both stress relaxation and dynamic mechanical properties in simple extension, on single crystal mats of fractions of linear polyethylene, Takayanagi and collaborators[9] were able to combine data at different temperatures by reduced variables over most of the range from 16°C up to the temperature of crystallization and also to show that the dynamic and transient data corresponded fairly closely, provided the latter were corrected for nonlinear behavior by an extrapolation procedure to zero strain. It is characteristic of crystalline polymers that departures from linear viscoelastic behavior appear at very small strains, and are sometimes significant in stress relaxation even at a tensile strain of $\epsilon = 0.001$. In dynamic measurements, the strains are usually small enough to fall within the linear range.

The relaxation spectrum $\overline{H}$, reduced to 16°C, is plotted with a linear ordinate

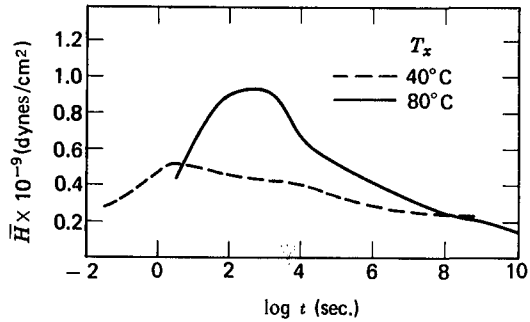


Fig. 16-1. Relaxation spectrum in extension for single crystal mat of linear polyethylene fraction, $\overline{M}_v$ = 15,000, reduced to 16°C, for samples crystallized at two different temperatures T_x as shown. (Manabe, Sakoda, Katada, and Takayanagi.[9])

scale in Fig. 16-1 for two samples of molecular weight 15,000 crystallized at 40° and 80°C respectively. With the large scale, features are apparent which would scarcely be perceptible in a plot such as curve VIII of Fig. 3-3. A maximum sharpens and shifts to longer relaxation times with increasing temperature of crystallization, corresponding to a change in the lamellar thickness (determined from small-angle X-ray scattering) from 87 Å to 129 Å. Over this range of time scale, the relaxation modulus $E(t)$ and the storage modulus E' change only from about $10^{10.3}$ to $10^{9.4}$ dynes/cm^2 ($10^{9.3}$ to $10^{8.4}$ Pa).

In such studies, measurements are made over a range of temperatures but never higher than the original temperature of crystallization, T_x. If the crystal mat is annealed at a temperature T_a higher than T_x, the lamellar thickness increases to a value characteristic of both T_x and T_a. The relaxation spectrum also changes, but in a manner opposite to that which would be expected from Fig. 16-1 if the sample had been originally crystallized at the higher temperature; the maximum broadens and develops complicated fine structure, as illustrated in Fig. 16-2. From electron microscope observations, as well as a change in the interchain lattice spacing,[18] it can be inferred that the extensive chain rearrangements necessary to

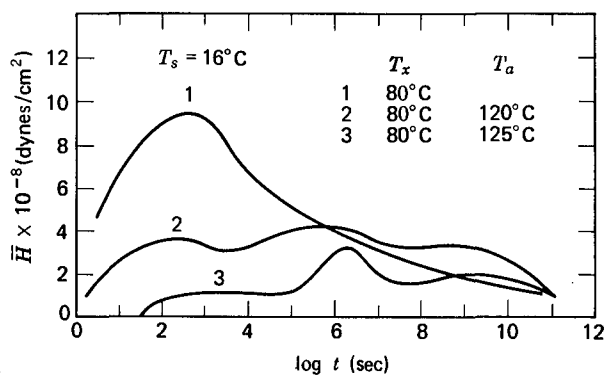


Fig. 16-2. Relaxation spectrum in extension for single crystal mat of linear polyethylene, crystallized at 80°C as in Fig. 16-1, and subsequently annealed at two different temperatures T_a as shown.[9]

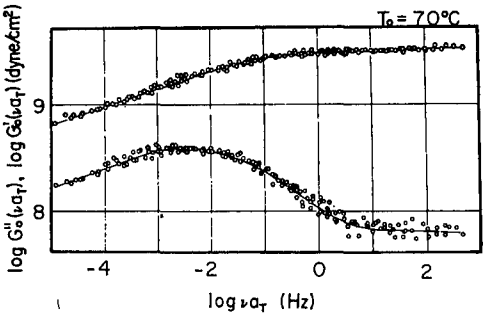


Fig. 16–3. Logarithmic plots of storage and loss shear moduli against frequency in Hz reduced to 70°C for single crystal blocks of polyoxymethylene, from measurements at different temperatures from 23° to 115°C. (Miki.[16]) Reproduced, by permission, from *Polymer Journal.*

accomplish an increase in the distance between lamellar folds create defects in the crystal lattice, and that these are responsible for the changes in viscoelastic properties.

A decrease in molecular weight, with consequent increase in molecular ends and hence lattice irregularities, causes the maximum in $\overline{H}$ to broaden and shift to shorter times.[9]

The shift factors a_T used for temperature reduction here followed a temperature dependence of the Arrhenius form with an apparent activation energy of 46 kcal/mole independent of the temperature of crystallization or annealing and of molecular weight. In this reduction, no vertical shift was made for temperature dependence of the magnitudes of modulus contributions. The latter is expected to be positive for rubberlike polymers and negative for glasses, as discussed in Chapter 11; for crystals it is small and negative, and its magnitude depends on the direction of the deformation in oriented samples.[19]

Mats of single crystals have also been built up to greater thicknesses to form blocks from which specimens can be cut for sinusoidal measurements in torsion at various orientations.[16,19] From data on polyoxymethylene single crystal blocks over a temperature range from 23° to 125°C and frequency range from 2×10^{-3} to 1 Hz, Miki[16] constructed composite curves for G' and G'' as illustrated in Fig. 16–3. The corresponding loss tangent is shown in Fig. 16–4. Superposition of the loss tangent data requires no vertical shift, of course; for the G' and G'' data, a very small vertical shift was applied for temperatures above 100°C. The range of G' is from about $10^{8.8}$ to $10^{9.5}$ dyn/cm² ($10^{7.8}$ to $10^{8.5}$ Pa). The shift factors a_T used for reduction of the frequency scale, plotted logarithmically against reciprocal absolute temperature, showed regions of different slopes corresponding to activation energies from 25 to 38 kcal/mole.

2. Highly Crystalline Polymers from Melts

An example of the viscoelastic behavior of a polymer with a high degree of crystallinity prepared by crystallization from the melt is shown in Figs. 16–5 and

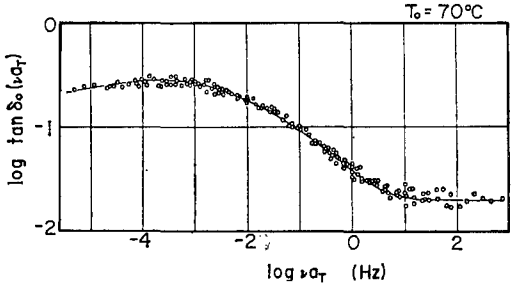


Fig. 16-4. Logarithmic plot of loss tangent against frequency reduced to 70°C from data of Fig. 16-3. (Miki.[16]) Reproduced, by permission, from *Polymer Journal.*

16-6, where the shear storage and loss compliances J' and J'' are plotted logarithmically against frequency over a wide range of temperatures (well below the crystallization temperature), from measurements by Nakayasu, Markovitz, and Plazek[20] on linear polyethylene (not a sharp fraction). The ordinate scales are again very large to show details of behavior in a material whose viscoelastic functions change very slowly with time or frequency.

Whereas reduced variables could be applied to the data of Figs. 16-1 and 16-2 to combine measurements at different temperatures over a considerable range to a close approximation, there were deviations at higher temperatures and/or longer times. A similar effect is found in the data of Fig. 16-6; if the data at higher frequencies are superposed as shown in Fig. 16-7, using empirical a_T factors, the data at lower frequencies do not coincide. However, if J'' is postulated to be the sum of two contributions, J''_I and J''_{II}, with different temperature dependences, and the logarithmic frequency dependence of the former is assumed to be symmetrical as represented by the dashed line in Fig. 16-7, it is found that the second

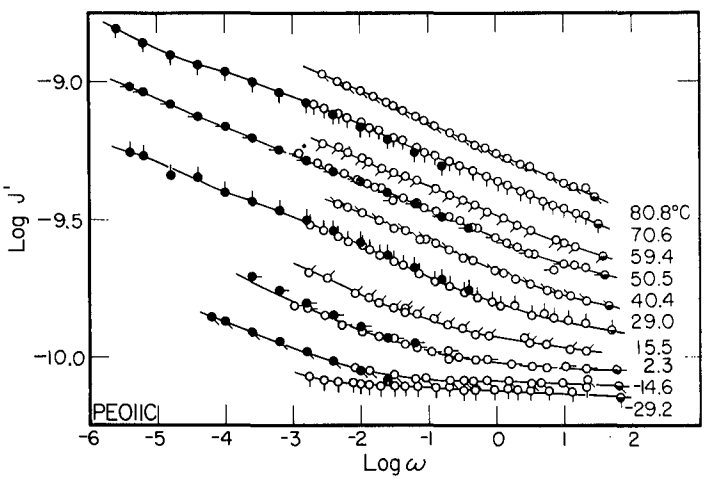


Fig. 16-5. Storage compliance of linear polyethylene crystallized from the melt, measured at 10 different temperatures as shown. Open circles, from forced oscillation; half black, from free vibration; black, calculated indirectly from creep measurements. (Nakayasu, Markovitz, and Plazek.[20])

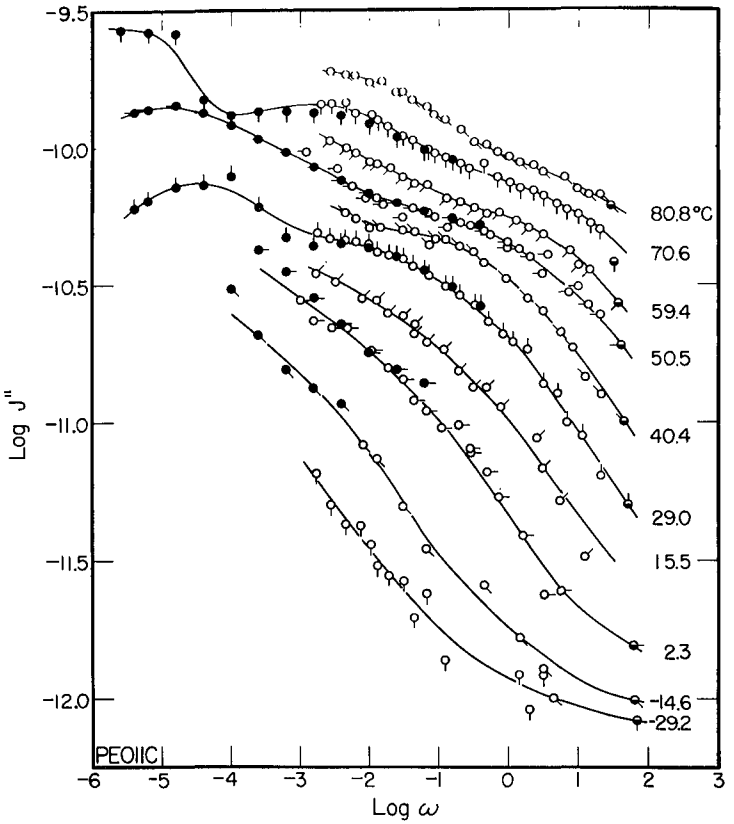


Fig. 16-6. Loss compliance of linear polyethylene crystallized from the melt, corresponding to Fig. 16-5, with same identifications.[20]

contribution, J''_{II} can be superposed with reduced variables over the temperature range from 29° to 81° with only slight deviations at the lowest reduced frequencies. Both sets of a_T factors followed the Arrhenius form of temperature dependence with apparent activation energies of 28 and 46 kcal respectively. The latter, corresponding to the mechanism which dominates between 29° and 81°, agrees exactly with the value from the data of Figs. 16-1 and 16-2 between 16° and 80°, indicating that this mechanism has a similar molecular origin in both single crystal mats and bulk crystalline polymer.

The storage compliance J' in Fig. 16-5 could be decomposed into two contributions J'_I and J'_{II} in the same manner, each of which could be combined to give a single composite reduced frequency dependence with the same a_T factors as for the corresponding contribution to J''; and the corresponding values of J' and J'' were consistent with the interrelations of linear viscoelasticity theory as given in Chapters 3 and 4. This agreement gives some confidence to the procedure of decomposition, which has already been illustrated for other cases of multiple mechanisms in Section F2 of Chapter 11. A similar analysis was made for data on partly

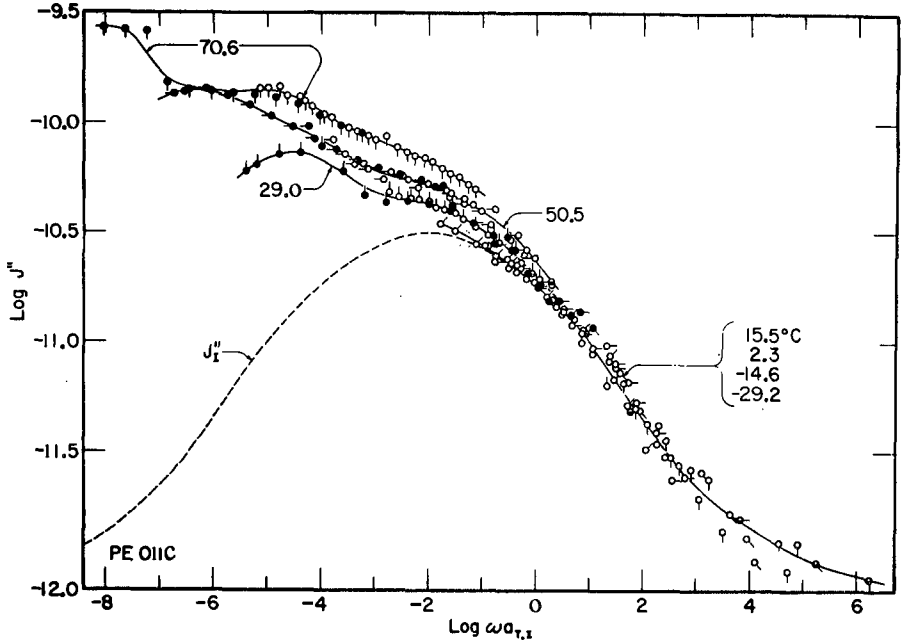


Fig. 16-7. Data of Fig. 16-6 reduced to 29°C with shift factors applicable to the data at higher frequencies and corresponding to an apparent activation energy of 28 kcal.[20]

crystalline poly(tetramethyl-*p*-silphenylene siloxane) by Murray and Markovitz.[21]

It is somewhat arbitrary to select the compliances rather than the moduli for decomposition, without more knowledge of the origin of the viscoelasticity. In fact, a similar analysis on the basis of the moduli E' and E'' has been performed on data for crystalline polyethylene terephthalate by Kawai and associates.[22,23] The two procedures correspond to assuming that the stress or the strain, respectively, is homogeneous throughout the sample. Actually, depending on the structure and microscopic features of the viscoelastic response, neither may be strictly homogeneous (*cf.* Chapter 14, Section F).

It is difficult to compare the shapes of the viscoelastic functions for single crystal mats and bulk crystalline polymer from the data of Figs. 16-1, 16-2, 16-5, and 16-6 without extensive recalculation under circumstances where approximation methods give poor precision because the functions vary so slowly with time or frequency (*cf.* equation 40 of Chapter 4). Comparisons of the two types of samples will be shown for isochronal viscoelastic functions in Section B below.

Other isothermal viscoelastic functions, in most cases either stress relaxation or creep, have been reported for other highly crystalline polymers including polychlorotrifluoroethylene,[24] polytetrafluoroethylene,[25,26] and polyethylenes with varying degrees of crystallinity.[27-30] In general, the relaxation modulus or creep compliance changes within a rather narrow range of one logarithmic decade, like

the storage compliance in Fig. 16–5, unless the experiments include higher temperatures where there is a loss of crystalline structure. The data can usually be combined by reduced variables at least approximately to give composite functions which correspond to very broad relaxation or retardation spectra (though in some cases a small temperature dependence of the magnitude of modulus or compliance is taken into account as in Fig. 16–3). The kind of fine structure illustrated in Figs. 16–2 and 16–6 can be detected only by very accurate measurements of changes of slope in relaxation or creep data. It is more easily perceived in dynamic measurements.

3. Polymers with Low Degree of Crystallinity

If the crystallization is restricted by lack of molecular symmetry, as in low-density polyethylene with short-chain branching[31] or polyvinyl alcohol partially esterified[22] or subjected to acetal formation,[13] the polymer remains partly amorphous, although the morphology of the crystalline and amorphous domains is uncertain. Crystallization can also be inhibited by rapid quenching from the melt. With decreasing degree of crystallinity, the magnitude of the relaxation modulus is diminished, as illustrated for polyethylene[30] with different degrees of short-chain branching and hence different degrees of crystallinity (as estimated from the density) in Fig. 16–8. However, the time dependence of the relaxation modulus remains very gradual.

With decreasing crystallinity, the viscoelastic properties begin to resemble to some degree those of highly cross-linked networks described in Section B7 of Chapter 14 or of filled systems described in Section C4 of Chapter 12 and Section E of Chapter 14. A region resembling a transition zone may appear, and the properties above and below the glass transition temperature of the amorphous regions show discernible differences.

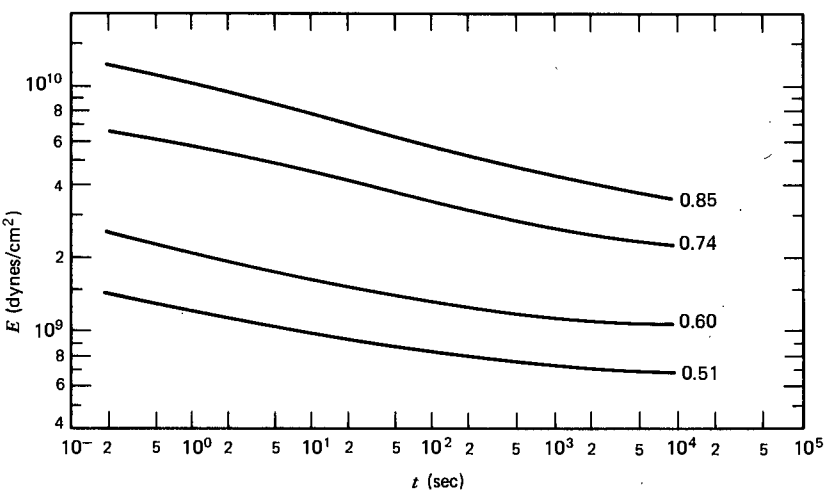


Fig. 16–8. Tensile relaxation modulus at 40.7°C for four polyethylene samples with different degrees of crystallinity indicated by numbers at right, plotted logarithmically. (Becker.[30])

Above T_g, the properties of such partly crystalline systems have already been illustrated in Fig. 12–15. Here the relaxation modulus for poly(vinyl alcohol) resembles those of the polyethylenes in Fig. 16–8, although the slope is steeper; probably the lack of tacticity leads to substantial imperfections of crystallinity even without esterification. With increasing esterification, the curves become steeper, and at 40% esterification the relaxation modulus falls by two and a half logarithmic decades in the range of reduced time investigated.

Below T_g, loss mechanisms identifiable with secondary processes in the glassy state of the amorphous regions may be observed.[32]

B. ISOCHRONAL VISCOELASTIC MEASUREMENTS

As for the glassy polymers discussed in Chapter 15, there have been far more studies of viscoelastic properties of crystalline polymers as a function of temperature at constant or nearly constant frequency.

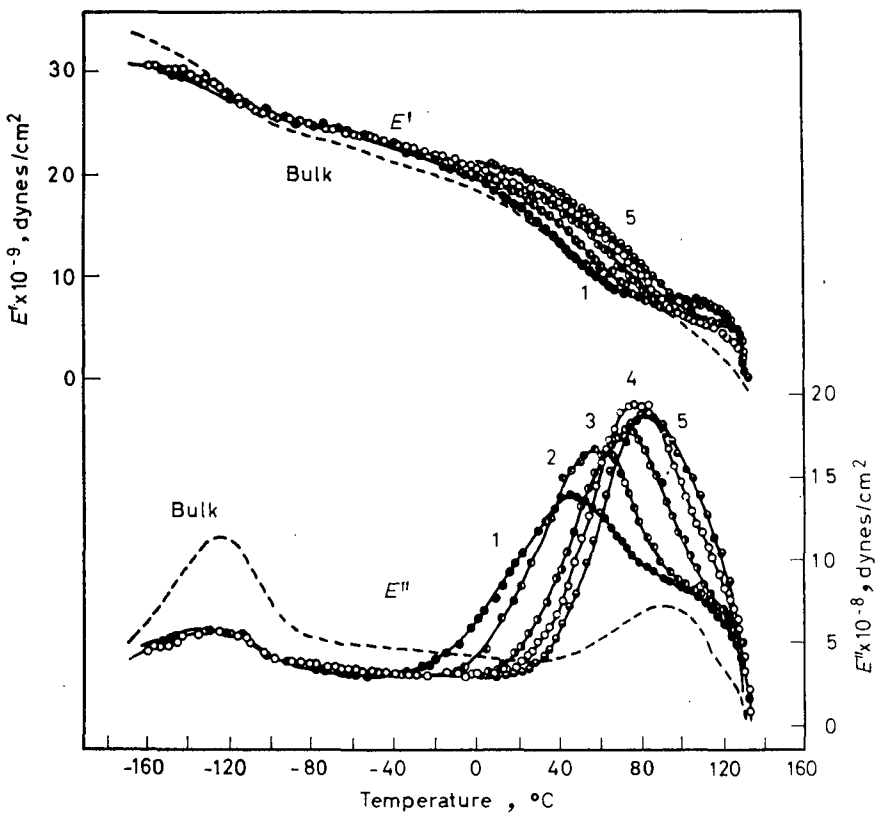


Fig. 16–9. Storage and loss moduli in extension at 110 Hz, plotted against temperature, for single crystal mats of linear polyethylene crystallized at five different temperatures with the following lamellar thicknesses in Å: 1, 94; 2, 104; 3, 114; 4, 137; 5, 167. Dashed curves are for the polymer crystallized from the melt in bulk. (Takayanagi.[8])

1. Oriented Single Crystal Mats

An example of the temperature dependence of the storage and loss moduli E' and E'' at 110 Hz for single crystal mats of polyethylene is shown in Fig. 16-9. By crystallization at different temperatures, samples and lamella thicknesses from 94 Å to 167 Å were prepared. Curves for the polymer crystallized from the melt in bulk are also shown.[8,33,34]

Two zones of dispersion are apparent. The one at low temperatures is independent of lamella thickness, and is much more prominent in the melt-crystallized sample. The one at high temperatures shifts to higher temperatures and sharpens with increasing lamella thickness (increasing temperature of crystallization). This behavior is, of course, exactly consistent with the relaxation spectra from isothermal viscoelastic functions shown in Fig. 16-1. The effect of annealing also corresponds; with increasing annealing temperature, and hence increasing lamella thickness introduced by annealing, the maximum in E'' broadens, diminishes, and shifts to higher temperatures, as illustrated in Fig. 16-10. Close study of fine structure reveals the appearance of additional maxima under certain conditions of crystallization and annealing.[34]

Similar investigations have been made on single crystal mats of *trans*-1,4-

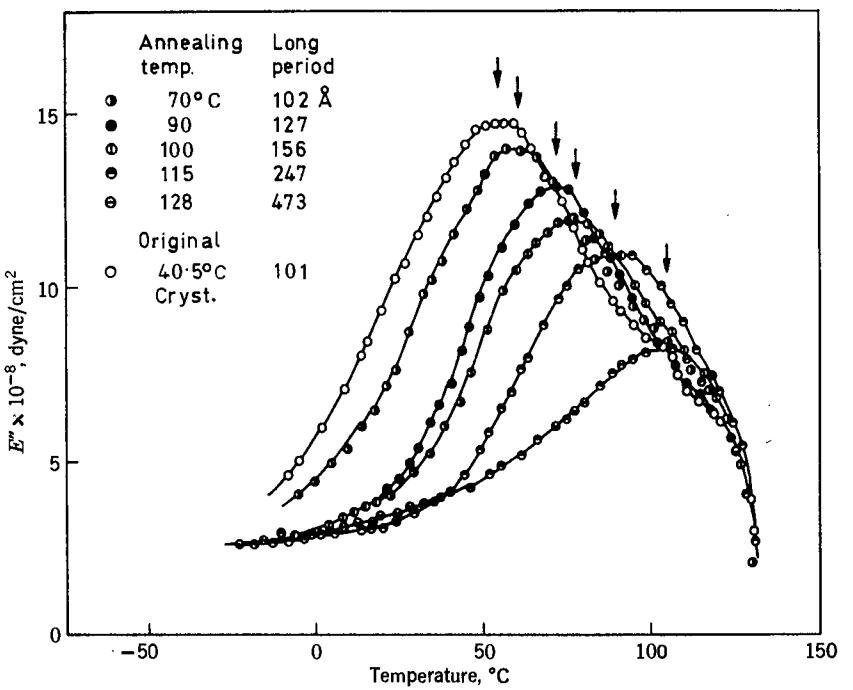


Fig. 16-10. Loss modulus in extension at 110 Hz for single crystal mat of linear polyethylene with initial lamellar thickness of 101 Å (corresponding approximately to curve 2 of Fig. 16-9) and after annealing at five different higher temperatures as shown.[8]

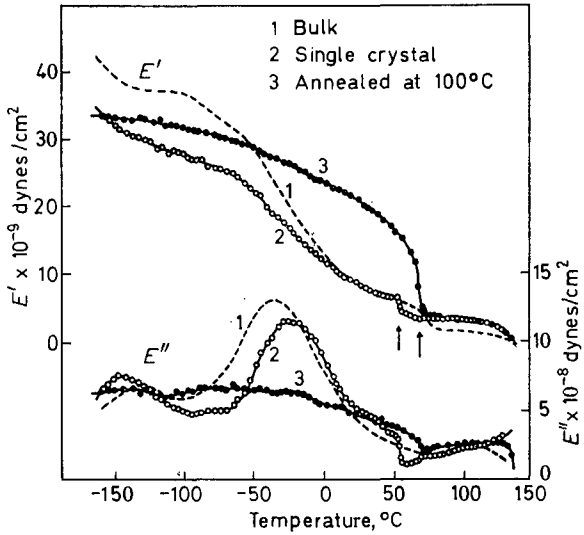


Fig. 16-11. Storage and loss moduli in extension at 110 Hz for *trans*-1,4-polybutadiene. 1, sample crystallized from the melt in bulk; 2, single crystal mat, crystallized at 18°C; 3, mat after annealing at 100°C. (Takayanagi.[8])

polybutadiene,[35] poly(4-methyl pentene-1),[36] isotactic polybutene-1,[37] various polyamides,[38] isotactic polypropylene,[8] and other polymers. Again, several dispersion mechanisms are evident, and there are marked effects of annealing, as well as differences between single crystal mats and melt-crystallized samples, as illustrated for *trans*-1,4-polybutadiene in Fig. 16-11. A detailed discussion of these phenomena and their interpretation is beyond the scope of this chapter.

2. Highly Crystalline Polymers from Melts or Cast from Solvents

Examples of isochronal functions for polymers crystallized in bulk from the melt have already been shown in Figs. 16-9 and 16-11 for comparison with the corresponding data for single crystal mats. Others have been reported for many different highly crystalline polymers, including polyethylene,[39] poly(vinyl alcohol),[40] isotactic polypropylene,[41] poly(ethylene terephthalate),[42] polyoxymethylene,[43,44] polyoxyethylene,[43] poly(propylene oxide),[43] poly(tetramethylene oxide),[43] poly(ethyl vinyl ether),[43] *trans*-1,4-polybutadiene,[45] polycarbonates,[46] isotactic polystyrene,[40] and poly(glutamic acid) esters.[17,47] Many results have been reviewed by Takayanagi[8] and by McCrum, Read, and Williams.[48] Some examples are illustrated in Fig. 16-12. Characteristically, several loss mechanisms are observed. In some of these investigations, the effects of other variables such as presence of traces of diluent or effects of high-energy radiation have been investigated. In others,[40,42,43] samples have been used which appear not to have had very high degrees of crystallinity so that the properties approach those described in the following section.

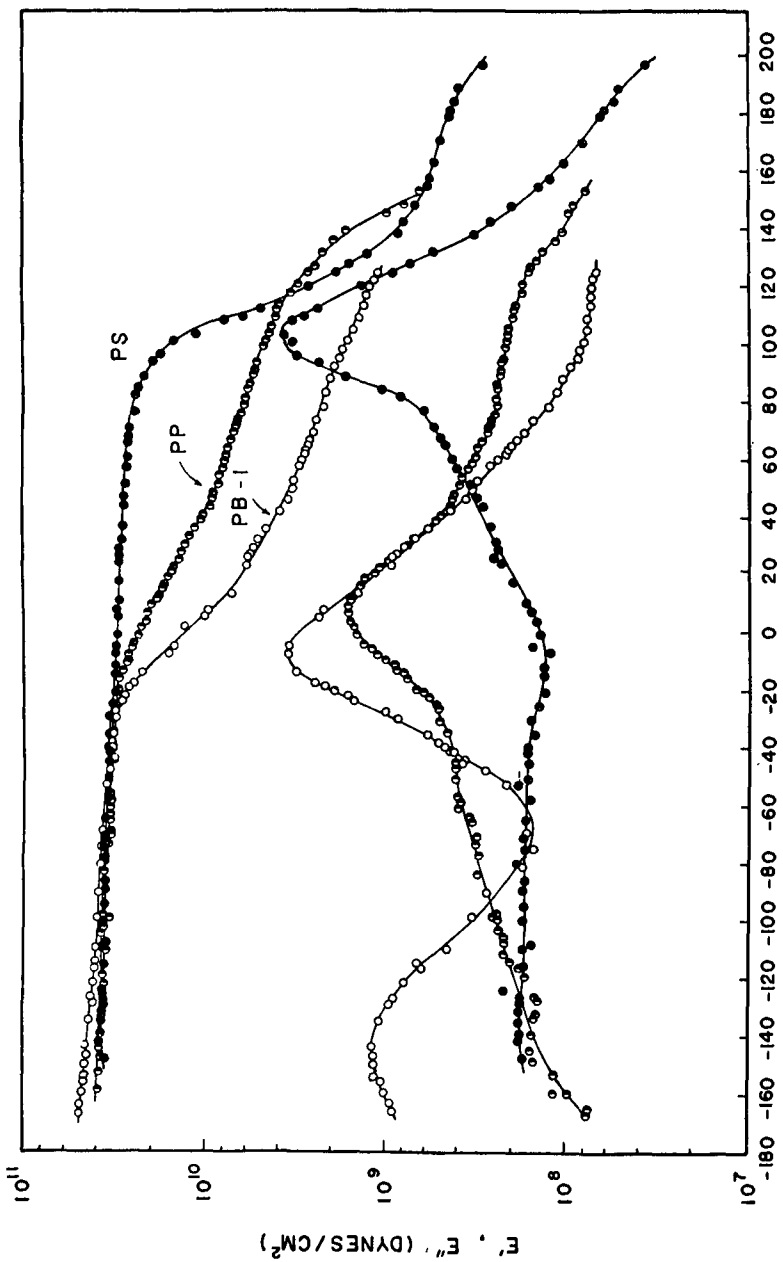


Fig. 16-12. Storage and loss moduli in extension at 100 Hz, plotted with logarithmic scale against temperature for isotactic polystyrene (PS), isotactic polypropylene (PP), and isotactic polybutene-1 (PB-1), crystallized from the melt. Degrees of crystallinity estimated as 43%, 65%, and 45% respectively. (Takayanagi.[40])

3. Polymers with Low Degree of Crystallinity

If the degree of crystallinity is low enough, the isochronal modulus can fall more steeply with increasing temperature, reflecting changes in molecular mobility in the amorphous domains. In a temperature range which is well below the melting point of the crystalline polymer but above the glass transition temperature of the amorphous domains, the storage modulus drops by perhaps 2 orders of magnitude and the loss (either loss modulus or loss tangent) goes through a maximum. The behavior resembles that illustrated for completely amorphous polymers in Fig. 12–3, except that the modulus level corresponding to the rubberlike state is higher (leathery rather than rubberlike) and the change is much less abrupt. An example is shown in Fig. 16–13 with data of Schmieder and Wolf[49] for samples of polychlorotrifluoroethylene and poly(vinyl fluoride) in which the degree of crystallinity was evidently comparatively low. Here, as in Fig. 12–3, the logarithmic decrement Δ, approximately proportional to tan δ, is used as a measure of loss.

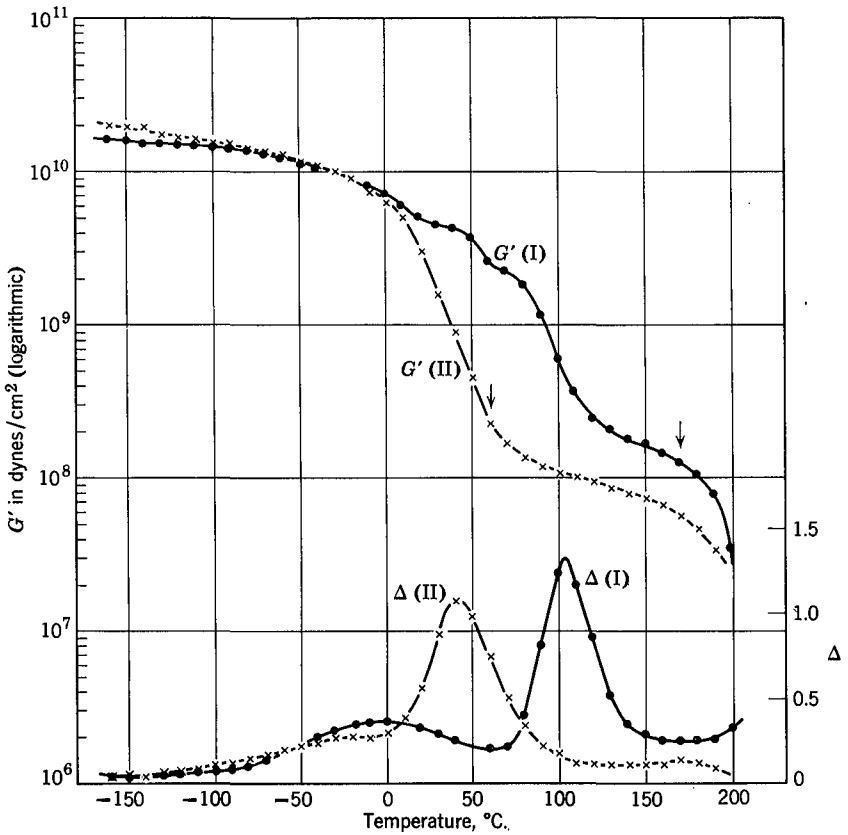


Fig. 16–13. Storage shear modulus and logarithmic decrement (approximately proportional to loss tangent) of polychlorotrifluoroethylene (I) and poly(vinyl fluoride) (II), plotted against temperature at approximately 3 and 2 Hz respectively. (Schmieder and Wolf.[49])

This viscoelastic mechanism corresponding to the transition zone (the primary or α mechanism in the language applied to classification of mechanisms in amorphous polymers as discussed in Chapter 15) can be identified only at low degrees of crystallinity. For example, Fig. 16–14 show isochronal curves for modulus and

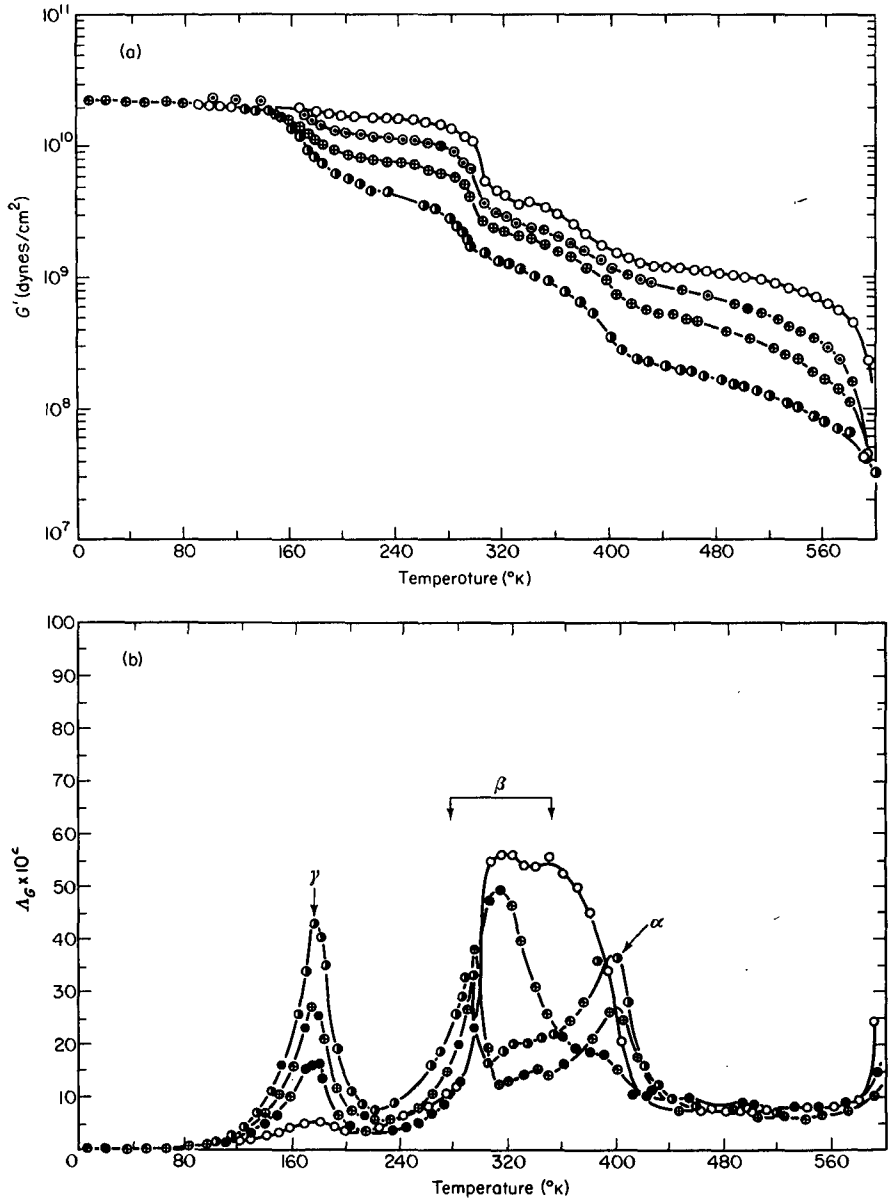


Fig. 16–14. Storage shear modulus (*a*) and logarithmic decrement (*b*) plotted against temperature at approximately 1 Hz for polytetrafluoroethylene with the following degrees of crystallinity: open circles, 92%; black, 76%; crossed, 64%; half black, 48%.[50]

logarithmic decrement for four samples of polytetrafluoroethylene with different degrees of crystallinity (estimated by infrared absorption measurements), from data of McCrum.[50] Only for 64% crystallinity or less is this α mechanism clearly distinguished.

The temperature of the midpoint of the primary transition can be roughly specified by the inflection in G' (not the point where $G' = 10^8$ dynes/cm^2 as in Chapter 12) or the maximum in tan δ or Δ. Such transition midpoint temperatures have been determined for numerous crystalline polymers,[17,21,42,43,46,48-55] and some are summarized in Table 16-I. (The midpoint temperature T_M should not be confused with the melting point.) Comparison with Table 12-II indicates that these midpoint temperatures are slightly higher for partially crystalline polymers than for amorphous polymers of the same or similar chemical composition. There is in some cases a perceptible increase in T_M with degree of crystallinity. It will be recalled that in loaded rubbers, also, the filler increases T_M slightly[56] (Section C4 of Chapter 12).

Of course, there is a further drop in the isochronal modulus with increasing temperature in the vicinity of the crystal melting point. As the crystalline regions melt (over a finite temperature range), the material becomes completely amorphous. This phenomenon appears in Fig. 16-14 near 600°K which is the melting point for polytetrafluoroethylene.

Polytetrafluoroethylene is unusual in possessing a transition in crystal form near 20°C and another transition near 30° attributed to random chain motions. These structural modifications are accompanied by marked changes in viscoelastic

Table 16-I

TEMPERATURES IDENTIFIED WITH MIDPOINTS OF TRANSITION FROM FLEXIBLE TO GLASSLIKE CONSISTENCY IN CRYSTALLINE POLYMERS

Polymer	T_M, °K	Frequency of Measurement, Hz	Ref.
Polyethylene	268-273[a]	1	51
Polytetrafluoroethylene	393-403[a]	1	48,51,52
Polychlorotrifluoroethylene	397	3	49,51
Poly(vinyl fluoride)	314	2	49
Poly(vinylidene chloride)	353	5	49
Polyacrylonitrile	413	4	49
Poly(ethylene terephthalate)	355-370[a]	1-6	42,49,53
Polyamides[b]	~330	1	51,54
Polypropylene	253		55
Poly(propylene oxide)	220	1	43
Polystyrene, isotactic	395	100	40

[a] Depends on degree of crystallinity.

[b] Approximately the same for various polyamides with different CH_2-group spacings between the amide linkages.

properties.[24,45,51] A transition in crystal form also appears in *trans*-1,4-polybutadiene.[35]

The additional viscoelastic mechanisms which are observed in isochronal measurements at temperatures below the primary or α mechanism, both in samples with low crystallinity as in Figs. 16–13 and 16–14 and also in samples with high crystallinity where the ordinary amorphous mechanism is absent such as in Figs. 16–9 to 16–10, have been labeled in various ways by Greek letters with subscripts and primes. The one at the highest temperature is usually designated as α even in highly crystalline systems where it cannot be attributed to amorphous domains and may be ascribed instead to some kind of motion in the crystal lamellae. Because of the unsettled state of this subject, no attempt is made here either to systematize the labeling of the mechanisms or to review the evidence for attributing them to various kinds of molecular motion. However, as in the discussion of secondary viscoelastic mechanisms in Chapter 15, a number of types of molecular motion which have been proposed will be summarized in the following Section.

C. RELATION OF VISCOELASTICITY TO MOLECULAR MOTIONS

The assignment of observed viscoelastic mechanisms to specific types of postulated molecular motion is facilitated by examining the effects of different degrees of crystallinity,[30] different lamellar thicknesses achieved by crystallization at various temperatures,[8] defects introduced by annealing,[8,16] irradiation with consequent cross-linking,[36,40,57] introduction of diluent,[58] and solvent extraction of components of lower molecular weight or tacticity;[40,59] as well as comparison of viscoelastic properties with dielectric and nuclear magnetic resonance data[48,60] and with dynamic birefringence and X-ray diffraction measurements,[61] and direct observations by electron microscopy.[62] In most cases, the assignment is qualitative, though theories have been introduced to relate molecular motion to macroscopic behavior.

1. Motions within the Crystal Lattice

Because of the weak lateral attractive forces between a polymer chain and its parallel neighbors in the crystal lattice, the chain may be expected to undergo torsional oscillations with rather large amplitudes, and the oscillations of neighboring chains are incoherent. Under mechanical deformation, a different distribution of torsional fluctuations is achieved, and this takes time, corresponding to a viscoelastic relaxation or dissipation of energy in dynamic deformations. This concept evolved from the views of several authors[63–66] and is the basis of theoretical calculations[60,65–58] of the temperature dependence of lattice constants and the instantaneous and equilibrium moduli in the *a* and *b* axis directions of the crystal unit cell, by Okano, Hayakawa, and Wada. At least part of the viscoelastic behavior at higher temperatures in polymers with a high degree of crystallinity has been attributed to this mechanism.[60] The application of this concept to the temperature dependence of the magnitudes of modulus contributions in the procedure of reduced

variables has been discussed by Miki and Kaneko,[69] and the restrictive role of the loops at the ends of chain segments traversing a lamella has been emphasized by Takayanagi and Matsuo.[34]

In crystals of polyglutamic acid esters, motions of the α-helical regions such as torsion, coaxial vibration, and bending can contribute to mechanical loss, as discussed by Kajiyama, Kuroishi, and Takayanagi.[70]

The motions of a crystal lamella were treated quite differently on a macroscopic basis by Kawai and collaborators,[71] who represented it as an elastic membrane in a viscous medium, and calculated the normal modes of motion. The result corresponded to a boxlike distribution for the relaxation and retardation spectra; this agrees with the general very broad shape of all the spectra such as in Figs. 16–1 and 16–2 (considering the very magnified vertical scale of these plots), but provides no prediction for the locations or heights of maxima. The role of bending and twisting motions in the lamellae has been discussed by Stein.[71a]

The possible role of crystal dislocations within the crystal lattice has been discussed by Williams.[72]

2. Motions outside the Lattice

If there is substantial disorder at the surface of a lamella where the polymer chains are folded and reverse their directions, two additional types of motions can be expected: short-range configurational rearrangements such as are detected at high frequencies in amorphous polymers, and sliding of the lamellae with respect to each other with a frictional resistance related to some kind of local viscosity of the disordered interface layers. The former may include some of the motions discussed for glasses in Section B3 of Chapter 15; the latter has been described as a grain boundary relaxation[17,20,34] and its relaxation times have been related to the interstitial viscosity. If fractionation during crystallization has left a preponderance of low molecular weight species outside the lamellae, this type of motion should be significantly affected. The defects introduced by annealing,[8,9] which perhaps lead to a mosaic structure of fragments within a lamella, provide the opportunity for additional relaxation processes.[34] On a larger scale, viscoelasticity associated with deformation of spherulites has been discussed.[71a,73]

With decreasing extent of crystallinity, and appearance of amorphous domains large enough to permit configurational rearrangements of longer chain segments such as occur in amorphous polymers, these motions presumably gradually approach in character those which are familiar in the amorphous state in the transition zone of viscoelastic behavior. When separate crystalline and amorphous phases can be identified, the macroscopic properties can be related to those of the individual phases by mixing rules as discussed in Section F of Chapter 14.

D. RESONANCE DISPERSION

Crystalline polymers,[74–79] as well as other crystalline solids,[81,82] have been found by Fitzgerald and Bodner to exhibit unusual responses to periodic mechanical stress

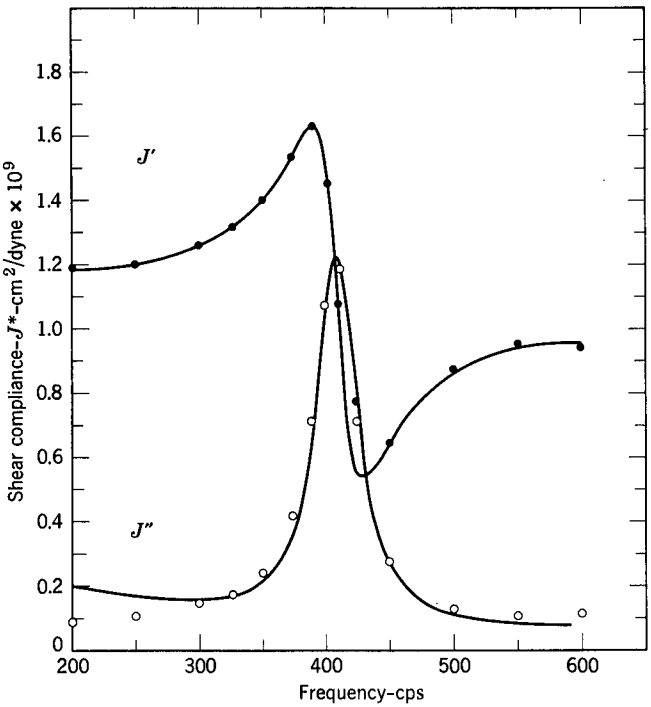


Fig. 16-15. Frequency dependence of the components of the complex compliance of polytetrafluoroethylene at 22.6° near 400 Hz. (Fitzgerald.[74]) The curves are calculated in accordance with the model of Fig. 16-16.

under certain conditions. The frequency dependence of the components of the complex compliance has the characteristic of a resonance dispersion, formally equivalent to resonance absorption in optics.[82] Mechanically, the sample behaves as though the molecular elements possessed inertia as well as elasticity and viscous resistance; its response resembles that of the entire apparatus of a resonance system such as Fig. 6-5. The loss compliance goes through a very sharp maximum on the frequency scale which is much narrower than would be given even by a single retardation time in ordinary viscoelastic behavior. At the same time, the storage compliance goes through a maximum and minimum and may even become negative.

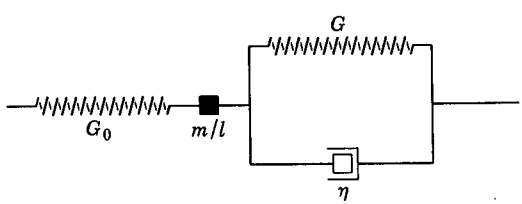


Fig. 16-16. Mechanical model corresponding to resonance dispersion; m/l is an effective mass per unit length.

An example for polytetrafluoroethylene[74] is shown in Fig. 16–15. The experimental points are rather well matched by curves calculated from the simple mechanical model of Fig. 16–16 with suitable values of the four parameters and an added constant background loss of 0.1×10^{-9} cm^2/dyne for J''. This model differs from those usually associated with linear viscoelasticity by the inclusion of the inertial unit m/l, with dimensions of mass per unit length. The values of G_0 and G are determined by the limiting levels of J' on the two sides of the dispersion, m/l by the resonance frequency; and η by the breadth of the dispersion. The magnitude of η is reasonable, 10^6 poises. However, that of m/l is too large to be identifiable physically as a real mass per unit length. This result corresponds to the elementary calculation that to produce an audio-frequency resonance with an elastic member of the shape and modulus of the sample, an inertial member with mass considerably greater than that of the sample would be required.

Several resonances of this type have been found in polytetrafluoroethylene, as well as in polyethylene (of both low and high degrees of short-chain branching), and polyvinyl stearate,[75] and natural rubber stretched to an elongation where crystallinity appears.[77] They require measurements at very closely spaced frequencies for recognition. Their locations and magnitudes depend somewhat on temperature and thermal history but much more on stress history, being apparently most prominent after static compression perpendicular to the direction of shear and subsequent release of stress. Similar resonances have been observed in bone[83] and intervertebral discs.[84] They have been attributed to a quantum mechanical effect associated with structural inhomogeneities of the order of 10^{-4} cm in dimensions.[81,85,86]

E. NONLINEAR VISCOELASTIC BEHAVIOR

It has already been emphasized in Section A1 above that marked departures from linear viscoelasticity appear in crystalline polymers at small strains. For tensile stress relaxation of single crystal mats of polyethylene, the ratio of stress to strain decreases more rapidly with time at higher extensions, in the range from $\epsilon = 0.0003$ to 0.003; the degree of nonlinearity increases markedly with decreasing temperature in the range from 40° to 10°C.[9] For polyethylene crystallized in bulk, the temperature dependence of the nonlinearity is in the same direction,[87] but for polyethylene terephthalate it is the opposite.[88,89] Extensive studies of tensile creep of polypropylene have been made by Turner.[90]

An example of nonlinear stress relaxation is shown in Fig. 16–17, where the ratio of time-dependent tensile stress to tensile strain is plotted logarithmically against time for different strains for cellulose monofilaments.[91] (In this case the structure is no doubt preoriented.) The differences can be interpreted as due to a decrease in relaxation times with increasing stress, and the curves can be combined approximately into a composite curve by plotting with reduced variables, with a shift factor a_s which decreases very rapidly with increasing strain. It is doubtful, however,[92] whether the latter can be entirely related to fractional free volume in crystalline polymers as it is for amorphous polymers (Section C1 of Chapter 15).

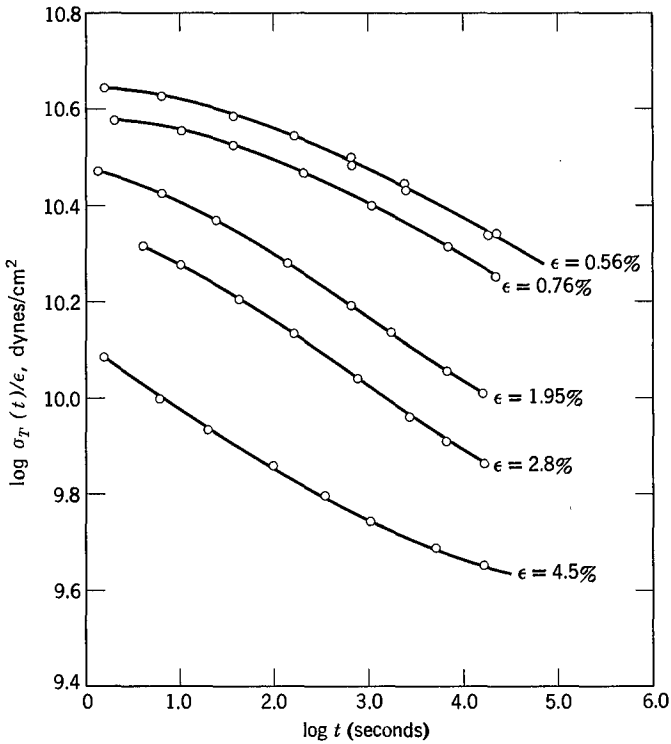


Fig. 16-17. Extensional stress relaxation in isotropic cellulose monofilaments at 50% relative humidity and 25°C, for various constant strains as indicated. (Passaglia and Koppehele.[91])

Nonlinearity in creep is associated with severe deviations from the Boltzmann superposition principle in creep recovery. An example of extreme effects in a crystalline polymer is shown in Fig. 16-18 for recovery of polyethylene[93] following partial stress relaxation at constant strain for various times and strain magnitudes. It is clear that recovery is much slower at large strains but is somewhat faster for shorter durations of the initial straining. In general, strains less than 0.01% appear to be required for conformity to the Boltzmann superposition principle in this system.[93]

If the viscoelastic behavior is nonlinear, stress-strain curves at constant rate of loading or deformation will be so *a fortiori,* since they can depart from linearity even without this complication. Calculations by Van Holde[94] show that the nonlinearity of tensile creep in nitrocellulose implies a stress-strain curve at constant rate of loading with a sharp change in slope at strains of about 5% which resembles the apparent yield points observed in such experiments on many textile fibers.[95,96]

Another consequence of nonlinearity is that the relaxation modulus can no longer be calculated by differentiation of a stess-strain curve at constant rate of strain; the tensile analog of equation 59 of Chapter 3 is not applicable. Examples of the

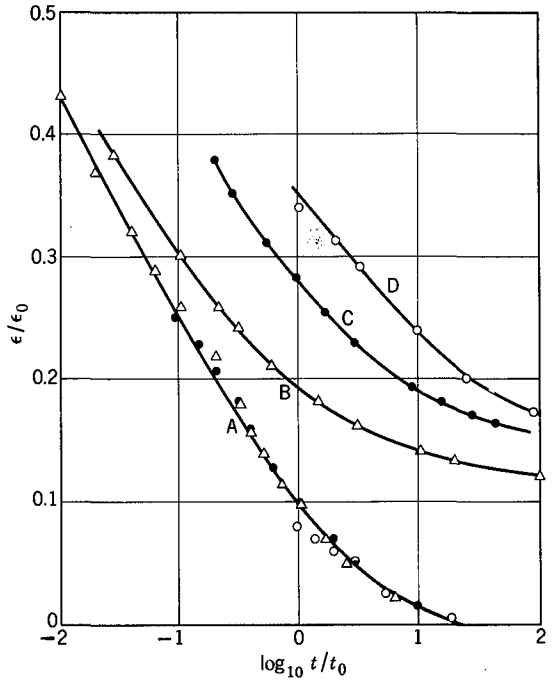


Fig. 16–18. Recovery of polyethylene at 30°C after having been held at strain ϵ_0 for a time t_0. A, ϵ_0 = 0.0012; B, C, D, ϵ_0 = 1.03. A, t_0 = 10, 10^2, and 10^3 sec; B, 10^3 sec; C, 10^2 sec; D, 10 sec. (Benbow.[93])

discrepancies between $E(t)$ so calculated and directly measured for polyethylene have been given by Sandiford.[97] Nonlinear behavior is sinusoidal deformations with large amplitudes has also been investigated.[98]

F. EFFECTS OF ORIENTATION AND DRAWING

Interpretation of viscoelastic properties of crystalline polymers is always complicated by the anisotropic character of the crystalline regions, which certainly have very different mechanical properties in different directions. In a suitably prepared sample, the average properties may be nearly isotropic. Alternatively, various kinds of orientation maybe introduced, giving much more complicated behavior but also additional information. If the orientation is produced by substantial stretching or drawing, there is usually a complete reorganization of the crystal structure,[99–101] with replacement of lamellar by fibrous elements and a large increase in Young's modulus in the draw direction. In any case, a full description of the anisotropy requires separate specification of the orientations of crystallites and amorphous regions.[102,103]

The viscoelastic properties of an oriented, anisotropic sample are of course different in different directions. The usual shape chosen for study is a thin strip or fiber oriented by elongation and then subjected to deformations of small amplitude, either by extension (strain in the same direction as the original elongation), cross-extension (elongation at right angles or in other directions), or torsion (shear at right angles to the original elongation). Complete specification of even the equilibrium elastic properties involves in general nine elastic constants.[104] Determination of certain of these constants by measurements on oriented films or fibers is explained in a treatise by Ward.[104] Sometimes, the moduli corresponding to extension or torsion are denoted by E and G respectively, but it must be remembered that these do not have the unique character of the corresponding symbols for isotropic bodies.

Drawing in uniaxial elongation often increases the level of the pseudoequilibrium Young's modulus in extension in the stretch direction without greatly affecting the Young's modulus for extension at right angles or the shear modulus measured in torsion around the axis of elongation. The first comparison is shown in Fig. 16–19 for cold-drawn sheets of low-density polyethylene at −125°C.[105] The second is illustrated in Fig. 16–20 by dynamic measurements on fibers of poly(ethylene terephthalate) at frequencies in the general range from 100 to 1000 Hz at 21°C, by Wakelin and associates.[106] For the undrawn fiber, $E'/G' = 2.5$, corresponding to a reasonable value of Poisson's ratio. At high draw ratio, E' increases by a factor of 7, and E'/G' becomes very large. Similar increases of E' with orientation have been found in polyamides (*e.g.*,[106] Nylon 6–6), polyethylene,[107] and other crystalline polymers.[104] They may be due in part to the reorganization of the crystal structure and in part to the stretching of many of the intercrystalline strands or tie molecules nearly taut in the direction of elongation.[99] In certain systems, such as low-density polyethylene sheets at room temperature, considerably more complicated behavior is observed.[108]

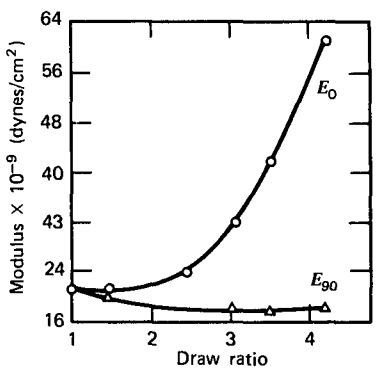


Fig. 16–19. Pseudoequilibrium Young's modulus parallel (E_0) and perpendicular (E_{90}) to draw direction for cold-drawn sheets of low-density polyethylene, at −125°C. (Gupta and Ward.[105]) Reproduced by permission, from Reference 105, p. 382, by courtesy of Marcel Dekker, Inc.

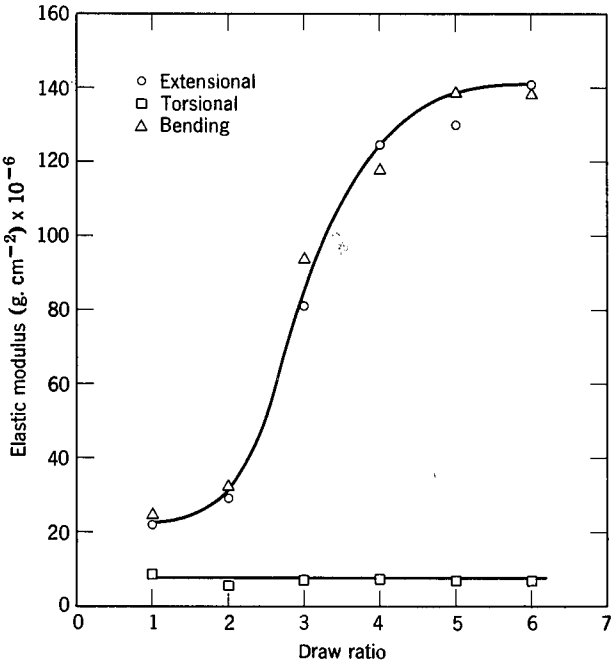


Fig. 16–20. Storage components of Young's modulus in direction of stretch (extensional and bending) and shear modulus perpendicular to that direction (torsional), for poly(ethylene terephthalate) fibers at 21° and frequencies in the range from 100 to 1000 Hz, plotted against draw ratio. (Wakelin.[106])

In Fig. 16–20, the frequency dependence of E', which within a decade of logarithmic time scale is relatively slight, has been ignored. To obtain the effect of orientation on the viscoelastic functions, measurements over a wide range of frequencies are required. An example is provided by the experiments of Tokita[109] on the polyamide Nylon-6 with about 25% crystallinity. Here, by combining a variety of dynamic methods (Chapter 8), E' and E'' were obtained over six logarithmic decades of frequency at a single temperature, 20°C. The relaxation spectra obtained from these measurements on undrawn fibers and after drawing to 100% elongation are shown in Fig. 16–21. The level of the spectrum is raised somewhat by the orientation, and it is shifted considerably toward longer times. The latter change seems reasonable for rearrangements to give stress release in a direction in which many strands may be already stretched approaching their maximum extensions. Stress relaxation measurements on drawn polyethylene films by Onogi and collaborators[110] show a more complicated dependence of the relaxation spectrum on draw ratio, and reveal nonlinear effects at strain levels up to 12%.

An isochronal plot which shows the same type of influence as the isothermal plot of Fig. 16–21 is shown by plotting tan δ as determined for extension by Thompson and Woods[53] for poly(ethylene terephthalate), undrawn and stretched by drawing (Fig. 16–22). The drawing broadens the maximum and displaces it to higher temperatures, corresponding to the shift to longer times in the preceding figure. Similar results have been obtained for highly crystalline polyethylene at very high

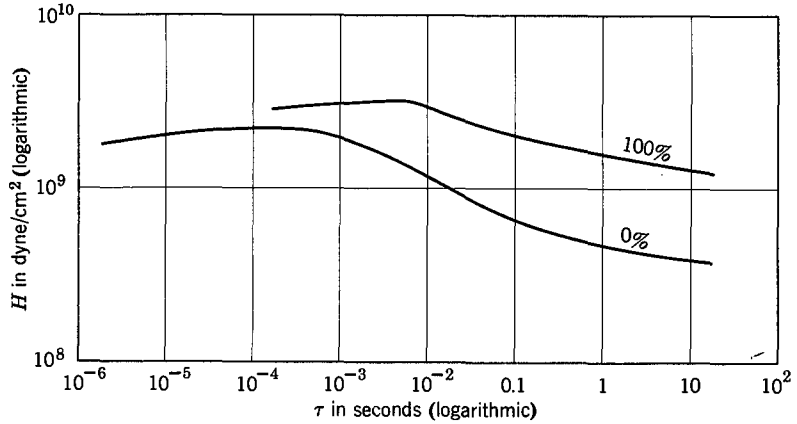


Fig. 16-21. Relaxation spectra in extension for Nylon-6 with about 25% crystallinity at 20°C, undrawn (0%) and drawn (100%). (Data of Tokita.[109])

draw ratios.[111] Extensive measurements of isochronal storage and loss moduli in extension have been made by Takayanagi and collaborators[8,40,112] on oriented polyethylene, polypropylene, polyoxymethylene, poly(ethylene oxide), and polytetrahydrofuran, both with and without subsequent annealing. If orientation is followed by annealing, the tensile moduli show the behavior illustrated in Fig. 16-23; both components are higher in the direction parallel to stretch at low temperatures but higher in the direction perpendicular to stretch at high temperatures. This result can be interpreted in terms of the disposition of amorphous and crystalline regions as postulated by Hosemann[113] and supported by X-ray scattering evidence.[8] On the other hand, if the annealing treatment is omitted, the parallel moduli are higher than the perpendicular moduli over almost all the temperature range, as illustrated by Fig. 16-24.

Propagation of shear and longitudinal waves through oriented polymers in various directions with respect to the direction of stretch also yields important information

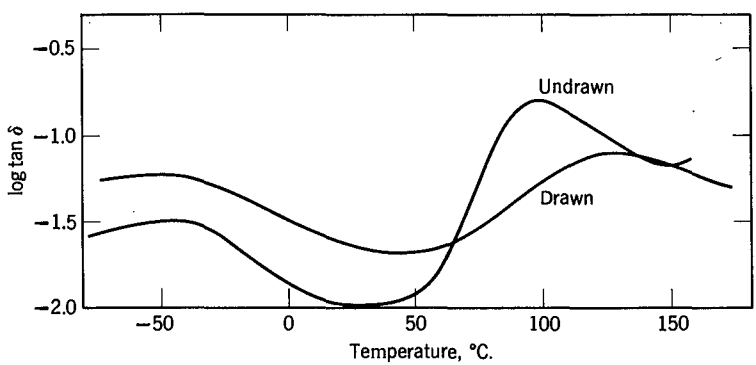


Fig. 16-22. Loss tangent in extension plotted against temperature at about 0.7 Hz for poly(ethylene terephthalate), undrawn and drawn (conditions of draw not specified). (Thompson and Woods.[53])

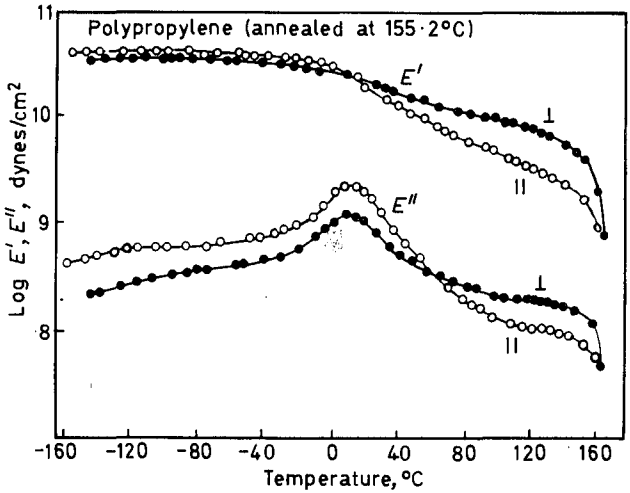


Fig. 16-23. Storage and loss tensile moduli at 110 Hz plotted against temperature, parallel and perpendicular to the draw direction, for polypropylene drawn eightfold at 30°C and subsequently annealed at 155°C. (Takayanagi.[112])

concerning molecular mechanisms corresponding to responses at very high frequencies.[114]

Effects of orientation are observed in various other physical properties,[115] and can aid in identification and interpretation of the time-dependent mechanical

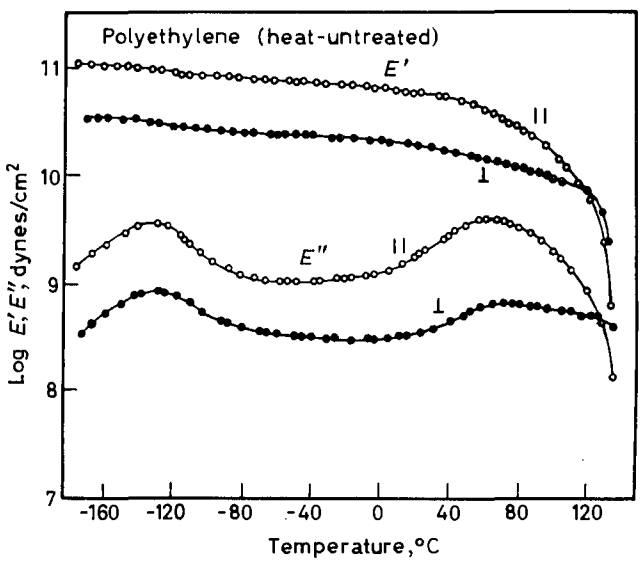


Fig. 16-24. Storage and loss tensile moduli at 110 Hz plotted against temperature, parallel and perpendicular to the draw direction, for linear polyethylene drawn fivefold at 38°C with no subsequent annealing. (Takayanagi.[112])

properties, especially where the available information concerning the latter is limited.[116]

A quite different phenomenon is sometimes observed in partly crystallized systems at substantial strains if the degree of crystallinity increases during a transient experiment. Deformation favors increasing crystallization, as can be shown by thermodynamics,[117] because the prolongation of the crystallites provides the remaining amorphous strands with a wider assortment of configurations and diminishes the forces on their ends. As a result, growth of crystallites during a stress relaxation experiment causes an abnormal decrease of stress whose rate is governed by the crystallization kinetics rather than by viscoelastic properties and can be quite rapid. In fact, after stress relaxation in extension, the sample may elongate spontaneously beyond its initial unstretched length. This process has been investigated in both unvulcanized[118] and vulcanized[119–121] rubbers. The melting point of the crystallites is strongly influenced by tensile stress.[3,122]

REFERENCES

1. P. H. Geil, *Polymer Single Crystals,* Interscience, New York, 1963.
2. P. H. Lindenmeyer, *Science,* **147,** 1256 (1965).
3. L. Mandelkern, *Crystallization of Polymers,* McGraw-Hill, New York, 1964.
4. K. Kobayashi and T. Nagasawa, *J. Polym. Sci.,* **C15,** 163 (1966).
5. K. Arai, O. Yano, and Y. Wada, *Rep. Prog. Polymer Phys. Jpn.* **11,** 267 (1968).
6. C. G. Andeen and R. W. Hoffman, *Polym. Prep. Am. Chem. Soc.,* **18(2),** 97 (1977).
7. M. Takayanagi, *Proc. 4th Intern. Cong. Rheology,* Part 1, Interscience, New York, 1965, p. 161.
8. M. Takayanagi, *Pure Appl. Chem.,* **15,** 555 (1967).
9. S. Manabe, A. Sakoda, A. Katada, and M. Takayanagi, *Mem. Fac. Eng. Kyushu Univ.,* **28,** 277 (1969).
10. L. Mandelkern, *J. Polym. Sci.,* **C15,** 129 (1966).
11. H. D. Keith and F. J. Padden, *J. Appl. Phys.,* **35,** 1270, 1286 (1964).
12. J. B. Jackson, P. J. Flory, R. Chiang, and M. J. Richardson, *Polymer,* **4,** 237 (1963).
13. K. Fujino, K. Senshu, T. Horino, and H. Kawai, *J. Colloid Sci.,* **18,** 119 (1963).
14. N. G. McCrum and E. L. Morris, *Jpn. J. Appl. Phys.,* **4,** 542 (1965).
15. R. P. Kambour and R. E. Robertson, in *Polymer Science—a Materials Science Handbook,* edited by A. D. Jenkins, North Holland Publishing Co., Amsterdam, 1972, Vol. I, p. 687.
16. K. Miki, *Polym. J.,* **1,** 432 (1970).
17. T. Kajiyama, M. Kuroishi, and M. Takayanagi, *J. Macromol. Sci.—Phys.,* **B11,** 195 (1975).

17a. K. Miyasaki and K. Ishikawa, *Prog. Polym. Sci. Jpn.,* **6,** 153 (1973).

18. K. Iohara, K. Imada, and M. Takayanagi, *Polym. J.,* **3,** 357 (1972).
19. K. Miki, J. Yasukawa, and M. Kaneko, *Jpn. J. Appl. Phys.,* **8,** 159 (1969).
20. H. Nakayasu, H. Markovitz, and D. J. Plazek, *Trans. Soc. Rheol.,* **5,** 261 (1961).
21. A. D. Murray and H. Markovitz, *J. Polym. Sci., Polym. Phys. Ed.,* **12,** 587 (1974).
22. M. Nakatani, K. Iijima, A. Suganuma, and H. Kawai, *J. Macromol. Sci.—Phys.,* **B2,** 55 (1968).
23. K. Tajiri, Y. Fujii, M. Aida, and H. Kawai, *J. Macromol. Sci.—Phys.,* **B4,** 1 (1970).
24. K. Nagamatsu and T. Yoshitomo, *J. Colloid Sci.,* **14,** 377 (1959).
25. K. Nagamatsu, T. Yoshitomi, and T. Takemoto, *J. Colloid Sci.,* **13,** 257 (1958).
26. Y. Ohzawa and Y. Wada, *Jpn. J. Appl. Phys.,* **3,** 436 (1964).
27. E. Catsiff, J. Offenbach, and A. V. Tobolsky, *J. Colloid Sci.,* **11,** 48 (1956).
28. J. A. Faucher, *Trans. Soc. Rheology,* **3,** 81 (1959).

29. K. Nagamatsu, *Kolloid-Z.*, **172,** 141 (1960).
30. G. W. Becker, *Kolloid-Z.*, **175,** 99 (1961).
31. C. W. Bunn, in *Polythene,* edited by A. Renfrew and P. Morgan, Iliffe, London, 1960, Chapter.
32. K. H. Illers, *Makromol. Chem.*, **38,** 168 (1960).
33. M. Takayanagi, *Zairyo,* **14,** 343 (1965).
34. M. Takayanagi and T. Matsuo, *J. Macromol. Sci.—Phys.*, **B1,** 407 (1967).
35. T. Tatsumi, T. Fukushima, K. Imada, and M. Takayanagi, *J. Macromol. Sci.—Phys.*, **B1,** 459 (1967).
36. M. Takayanagi and N. Kawasaki, *J. Macromol. Sci.—Phys.*, **B1,** 741 (1967).
37. H. Yasuda, Y. Tanda, and M. Takayanagi, *J. Chem. Soc. Jpn., Ind. Chem. Sect.*, **69,** 304 (1966).
38. K. Neki and M. Takayanagi, *Rep. Prog. Polym. Phys. Jpn,* **8,** 28 (1965).
39. M. Takayanagi, *J. Macromol. Sci.—Phys.*, **B9,** 391 (1974).
40. M. Takayanagi, *Mem. Fac. Eng. Kyushu Univ.*, **23,** No. 1, p. 41.
41. E. Passaglia and G. M. Martin, *J. Res. Nat. Bur. Stand.*, **68A,** 519 (1964).
42. K. H. Illers and H. Breuer, *J. Colloid Sci.*, **18,** 1 (1963).
43. R. E. Wetton and G. Allen, *Polymer,* **7,** 331 (1966).
44. K. Miki, K. Hikichi, and M. Kaneko, *Jpn. J. Appl. Phys.*, **6,** 931 (1967).
45. S. Iwayanagi and H. Nakane, *Proc. 5th Intern. Cong. Rheology,* edited by S. Onogi, Volume 3, University of Tokyo Press, 1970, p. 203.
46. K. H. Illers and H. Breuer, *Kolloid-Z.*, **176,** 110 (1961).
47. T. Kajiyama, M. Kuroishi, and M. Takayanagi, *J. Macromol. Sci.—Phys.*, **B11,** 121 (1975).
48. N. G. McCrum, B. E. Read, and G. Williams, *Anelastic and Dielectric Effects in Polymeric Solids,* Wiley, New York, 1967.
49. K. Schmieder and K. Wolf, *Kolloid Z.*, **134,** 149 (1953).
50. N. G. McCrum, *J. Polym. Sci.*, **34,** 355 (1959).
51. A. E. Woodward and J. A. Sauer, *Fortschr. Hochpolym. Forsch.*, **1,** 114 (1958).
52. K. H. Illers and E. Jenckel, *Kolloid-Z.*, **160,** 97 (1958).
53. A. B. Thompson and D. W. Woods, *Trans. Faraday Soc.*, **52,** 1383 (1956).
54. K. H. Illers, *Makromol. Chem.*, **38,** 168 (1960).
55. A. E. Woodward, *J. Appl. Phys.*, **25,** 1209 (1954).
56. F. R. Schwarzl, H. W. Bree, and C. J. Nederveen, *Proc. 4th Intern. Cong. Rheology,* edited by E. H. Lee, Part 3, Interscience, New York, 1965, p. 241.
57. C. W. Deeley, D. E. Kline, J. A. Sauer, and A. E. Woodward, *J. Polym. Sci.*, **28,** 109 (1958).
58. T. Hideshima, *Rep. Prog. Polym. Phys. Jpn.*, **9,** 279 (1966).
59. J. M. Crissman, *J. Polym. Sci., Polym. Phys. Ed.*, **13,** 1407 (1975).
60. R. Hayakawa and Y. Wada, *J. Polym. Sci., Polym. Phys. Ed.*, **10,** 2119 (1974).
61. R. S. Stein, E. P. Chang, A. Tanaka, and B. Delf, *Am. Chem. Soc. Polym. Prepr.*, **10,** 117 (1969).
62. C. Nakafuku, K. Minato, and T. Takemura, *Jpn. J. Appl. Phys.*, **7,** 1155 (1968).
63. R. C. Rempel, H. E. Weaver, H. H. Sands, and R. L. Miller, *J. Appl. Phys.*, **28,** 1082 (1957).
64. A. Peterlin, *J. Appl. Phys.* **31,** 1934 (1960).
65. K. Okano, *Rep. Prog. Polym. Phys. Jpn.*, **3,** 71 (1960).
66. K. Yamafuji, *J. Phys. Soc. Jpn.*, **15,** 2295 (1960).
67. Y. Wada, *J. Phys. Soc. Jpn.*, **16,** 1226 (1961).
68. K. Yamafuji and Y. Ishida, *Kolloid-Z.*, **183,** 15 (1962).
69. K. Miki, K. Hikicho, and M. Kaneko, *Jpn. J. Appl. Phys.*, **6,** 931 (1967).
70. T. Kajiyama, M. Kuroishi, and M. Takayanagi, *J. Macromol. Sci.—Phys.*, **B11,** 195 (1975).
71. N. Yoshioka, Y. Obata, and H. Kawai, *J. Macromol. Sci.—Phys.*, **B1,** 567 (1967).

71a. R. S. Stein, reported at Society of Rheology, October, 1979.
72. M. L. Williams, *Ann. N. Y. Acad., Sci.,* **155,** 539 (1969).
73. M. Matsuo, *Rep. Prog. Polym. Phys. Jpn.,* **20,** 285, 289, 293, 297 (1977).
74. E. R. Fitzgerald, *J. Chem. Phys.,* **27,** 1180 (1957).
75. E. R. Fitzgerald, *J. Appl. Phys.,* **29,** 1442 (1958).
76. E. R. Fitzgerald and A. E. Woodward, *Kolloid-Z.,* **172,** 177 (1960).
77. E. R. Fitzgerald, *J. Acoust. Soc. Am.,* **33,** 1305 (1961).
78. S. R. Bodner, *Trans. Soc. Rheol.,* **4,** 141 (1960).
79. E. R. Fitzgerald, *J. Acoust. Soc. Am.,* **39,** 870 (1966).
80. E. R. Fitzgerald, *J. Chem. Phys.,* **32,** 771 (1960).
81. E. R. Fitzgerald, *Particle Waves and Deformation in Crystalline Solids,* Wiley, New York, 1966.
82. G. Joos, *Theoretical Physics,* 3rd ed., Hafner, New York, p. 452.
83. J. W. Pugh, R. M. Rose, I. L. Paul, and E. L. Radin, *Science,* **181,** 271 (1973).
84. E. R. Fitzgerald and A. E. Freeland, *Med. Biol. Eng.,* **9,** 459 (1970).
85. E. R. Fitzgerald, *J. Acoust. Soc. Am.,* **39,** 856 (1966).
86. J. Black, *Science,* **181,** 273 (1973).
87. T. Takemura and M. Kuroki, *Rep. Prog. Polym. Phys. Jpn.,* **4,** 55 (1961).
88. M. Kuroki and T. Takemura, *Rep. Prog. Polym. Phys. Jpn.,* **4,** 59 (1961).
89. T. Takemura and M. Kuroki, *Rep. Prog. Polym. Phys. Jpn.,* **6,** 65 (1963).
90. S. Turner, *Polym. Eng. Sci.,* **6,** 306 (1966).
91. E. Passaglia and H. P. Koppehele, *J. Polym. Sci.,* **33,** 281 (1958).
92. T. Takemura and M. Kuroki, *Rep. Prog. Polym. Phys. Jpn.,* **6,** 63 (1963).
93. J. J. Benbow, in *Rheology of Elastomers,* edited by P. Mason and N. Wookey, Pergamon, London, 1958, p. 164.
94. K. E. Van Hold, *J. Polym. Sci.,* **24,** 417 (1957).
95. *Mechanical Properties of Textile Fibers,* edited by R. Meredith, North Holland, Amsterdam, 1956.
96. A. K. Van der Vegt, in *Die Physik der Hochpolymeren,* edited by H. A. Stuart, Volume IV, Springer-Verlag, Berlin, 1956, p. 460.
97. D. J. H. Sandiford, in *Physical Properties of Polymers,* Macmillan, New York, 1959, p. 213.
98. A. Tanaka, M. Fukuda, and S. Onogi, *Rep. Prog. Polym. Phys. Jpn.,* **21,** 269 (1978).
99. A. Peterlin, in *Ultra-High Modulus Polymers,* edited by A. Ciferri and I. M. Ward, Applied Science Publishers, Barking, 1979, p. 279.
100. H. Horio, *Proc. 4th Intern. Cong. Rheology,* Part 1, Interscience, New York, 1965, p. 29.
101. M. Takayanagi, *J. Macromol. Sci.—Phys.,* **B9,** 391 (1974).
102. R. S. Stein, *J. Polym. Sci.,* **34,** 709 (1959).
103. K. Yamada and M. Takayanagi, *Rep. Prog. Polym. Phys. Jpn.,* **20,** 329 (1977).
104. I. M. Ward, *Mechanical Properties of Solid Polymers,* Wiley-Interscience, London, 1971, Chapter 10.
105. V. B. Gupta and I. M. Ward, *J. Macromol. Sci.—Phys.,* **B2,** 373 (1967).
106. J. H. Wakelin, E. T. L. Voong, D. J. Montgomery, and J. H. Dusenbury, *J. Appl. Phys.,* **26,** 786 (1955).
107. K. W. Hillier and H. Kolsky, *Proc. Phys. Soc.,* **B62,** 111 (1949).
108. G. Raumann and D. W. Saunders, *Proc. Phys. Soc.,* **77,** 1028 (1961).
109. N. Tokita, *J. Polym. Sci.,* **20,** 515 (1956).
110. S. Onogi, A. Tanaka, Y. Ishikawa, and T. Igarashi, *Polym. J.,* **7,** 467 (1975).
111. J. B. Smith, G. R. Davies, G. Capaccio, and I. M. Ward, *J. Polym. Sci., Polym. Phys. Ed.,* **13,** 2331 (1975).
112. M. Takayanagi, K. Imada, and T. Kajiyama, *J. Polym. Sci.,* **C15,** 263 (1966).

113. R. Hosemann, *J. Appl. Phys.*, **34,** 25 (1963).
114. Y. Kawamura and Y. Wada, *Jpn. Appl. Phys.*, **6,** 100 (1967).
115. I. M. Ward, *Polym. Symposia,* **58,** 1 (1977).
116. K. Huff and F. H. Müller, *Kolloid-Z.*, **153,** 5 (1957).
117. H. Thurn, *Kolloid-Z.*, **165,** 57 (1959).
118. P. J. Flory, *Principles of Polymer Chemistry,* Cornell University Press, Ithaca, 1953, p. 453.
119. A. V. Tobolsky and G. M. Brown, *J. Polym. Sci.*, **17,** 547 (1955).
120. R. D. Andrews, Ph. D. thesis, Princeton University, 1948.
121. M. Mooney and W. E. Wolstenhome, *Ind. Eng. Chem.*, **44,** 335 (1952).
122. J. F. M. Oth and P. J. Flory, *J. Am. Chem. Soc.*, **80,** 1297 (1958).

CHAPTER 17

Concentrated Solutions, Plasticized Polymers, and Gels

When a polymer is diluted with a solvent of low molecular weight, with which it forms a true solution in the sense that the solvent is molecularly dispersed, the local friction coefficient is usually sharply reduced. Each polymeric chain unit has in its vicinity diluent molecules as well as other polymeric segments, and the former can be displaced in translatory motion much more easily, thus lowering the effective local viscosity. The resulting reduction in all relaxation times is the most striking effect on viscoelastic properties. However, the detailed shapes of the viscoelastic spectra may also be altered in the transition zone. Furthermore, when the molecular weight is high enough for entanglement coupling to be present, the effective spacing between coupling points is increased by the introduction of diluent, and the mechanism of escape from the topological restraints may be somewhat modified. The viscoelastic properties in the plateau zone are strongly affected. The effect of diluent on the terminal zone of time scale in uncross-linked polymers is closely associated with its effect on the steady-flow viscosity. Even in the glassy state far below T_g, viscoelastic properties are affected to some extent by the presence of small molecules, as was illustrated in Fig. 15-8.

The present chapter deals only with concentrated solutions, which might be defined for convenience, in accordance with Section D of Chapter 9, as those with the product $c[\eta]$ of at least 10. Such a solution usually has a relative viscosity of the order of at least 100, though it depends on the polymer, the solvent, and the temperature. The viscoelastic properties of more dilute solutions have already been reviewed in Chapter 9. The upper limit of the concentration range in the present chapter is the undiluted polymer. There is considerable interest in the properties of systems containing only small amounts of diluents or plasticizers. Gels, or diluted cross-linked systems, are also considered in this chapter.

A. THE TRANSITION ZONE

The effects of a diluent or plasticizer on viscoelastic properties in the transition zone can be analyzed in terms of its influence on the temperature dependence function, $a_T(t)$, and, separately, on the absolute values of friction coefficients and the shapes of viscoelastic spectra.

1. The Temperature Dependence of Relaxation and Retardation Times

The function a_T follows the WLF equation for diluted as for undiluted systems, and several concentrated solutions were included in the summary of Table 11-II. In terms of T_g as the reference temperature, the WLF equation is

$$\log a_T = -c_1^g(T - T_g)/(c_2^g + T - T_g) \tag{1}$$

in which c_1^g and c_2^g do not vary widely, so a diluent influences the temperature dependence of relaxation times primarily through its effect on T_g.

Addition of a diluent of low molecular weight depresses T_g sharply, linearly at first in accordance with the equation[1]

$$T_g = T_{g2} - kw_1 \tag{2}$$

where w_1 is the weight fraction of diluent and the coefficient k ranges from 200° to 500° for various solvents in polystyrene, for example (Fig. 17-1). At higher dilution, the curves in this figure are somewhat concave upwards as found also in other studies on various polymers.[2-6] The depression of T_g can be attributed to the introduction of additional free volume with the diluent, as would be expected if the fractional free volume of the diluent (f_1) exceeds that of the polymer (f_2) and the free volumes are additive or approximately so. Almost always, $f_1 > f_2$, corresponding to $T_{g1} < T_{g2}$; sometimes T_{g1} is hypothetical (if the diluent crystallizes without supercooling) but for many commonly used diluents it can be measured.[1,5]

The relation of T_g to fractional free volume has been treated by several authors.[4-9] In the linear range where equation 2 holds, a linear dependence of f on w_1 is expected:[8]

$$f(T, w_1) = f_2(T) + \beta w_1 \tag{3}$$

or

$$f(T, v_1) = f_2(T) + \beta' v_1 \tag{4}$$

where v_1 is the volume fraction of solvent and (since in this range $v_1 \ll 1$) $\beta' = \beta\rho_1/\rho_2$. If the glass transition is a state of iso-free-volume, it follows that in equation 2, $k = \beta/\alpha_f$, or $\beta' = k\alpha_f\rho_1/\rho_2$. An alternative expression[5] for β' is

$$\beta' = \alpha_{f1}(T - T_{g1}) - \alpha_{f2}(T - T_{g2}) \tag{5}$$

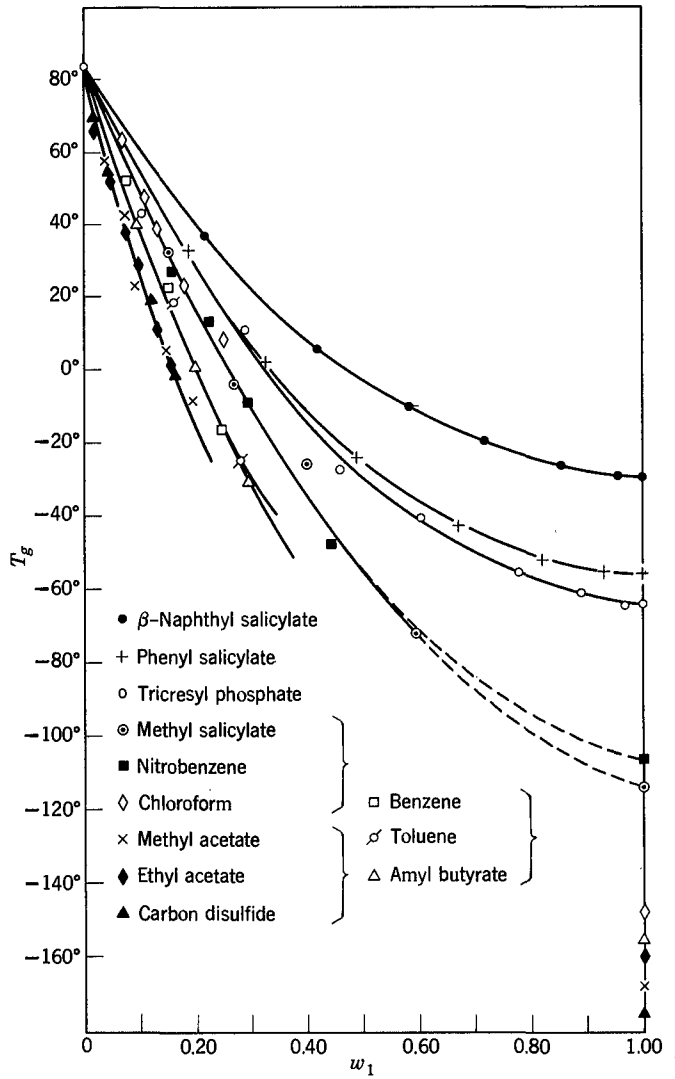


FIG. 17-1. Glass transition temperatures of polystyrene solutions with various diluents of low molecular weight, plotted against weight fraction of diluent. The T_g for the undiluted polymer is somewhat lower than that usually accepted (Table 11-II). (Jenckel and Heusch.[1])

where the α_f coefficients are the fractional free volume expansion coefficients as in equation 33 of Chapter 11.

The curvature in Fig. 17-1 can be explained by assuming that the fractional free volumes are not quite additive,[6] so the total fractional free volume depends on (volume) composition as follows:

$$f = v_1 f_1 + v_2 f_2 + k_v' v_1 v_2 \tag{6}$$

in which the interaction constant k_v' is negative and of the order of 10^{-2}. This fits in well with the experimental evidence[1] that the total specific volume, $1/\rho$, depends on (weight) composition in a similar manner:

$$1/\rho = w_1/\rho_1 + w_2/\rho_2 + k_v w_1 w_2 \tag{7}$$

and implies that the occupied volumes are strictly additive. Equation 6 leads to the following dependence on T_g on composition:[6]

$$T_g = \frac{v_1\alpha_{f1}T_{g1} + v_2\alpha_{f2}T_{g2} - k_v' v_1 v_2}{v_1\alpha_{f1} + v_2\alpha_{f2}} \tag{8}$$

(An interesting consequence of this relation is the possibility of a critical value of v_1 above which T_g decreases much more rapidly with increasing v_1; this discontinuity has been observed for polystyrene diluted with toluene,[6] and also in solutions of polystyrene in tricresyl phosphate, which exhibit two glass transitions in a certain concentration range.[10])

In the range of small amounts of diluent ($v_1 \ll 1$), equation 6 corresponds to[11]

$$\beta' = f_1 - f_2 + k_v' \tag{9}$$

and, since the last two terms are relatively small, β' can be qualitatively identified with f_1. In fact, values of β' calculated as $k\alpha_f\rho_1/\rho_2$ fall in the range[8] from 0.1 to 0.3, the correct order of magnitude for the fractional free volume of a liquid far above its glass transition temperature.

With increasing dilution, the temperature dependence of relaxation times referred to a fixed reference temperature T_0 becomes less pronounced as T_g is depressed more and more below T_0 and, in equation 21 of Chapter 11, c_2^0 increases while c_1^0 decreases. It is possible to analyze the temperature dependence of the shift factor a_T at several different diluent concentrations and thus to obtain the dependence of α_f and f_0 (at T_0) on composition without comparing the *magnitudes* of relaxation times at different concentrations. More commonly, however, the magnitudes are compared through a shift factor a_c and the latter is related directly to differences in free volume as explained in the following section.

2. Concentration Dependence of the Monomeric Friction Coefficient

With increasing proportion of diluent, the monomeric friction coefficient ζ_0 is normally diminished, as evidenced by displacement of logarithmic plots of viscoelastic functions in the transition zone to higher frequencies or shorter times with relatively little change in shape. Examples are shown in Fig. 17-2 for the relaxation spectrum of poly(*n*-butyl methacrylate),[12] and in Fig. 17-3 for the creep compliance of poly(vinyl acetate),[13] both diluted to varying extents with diethyl phthalate. (In the latter figure, we focus attention now on the transition zone, where $\log J(t) < -6.5$; the other zones will be discussed later.) Introduction of diluent displaces the time scale by many orders of magnitude. Similar results were obtained in an ex-

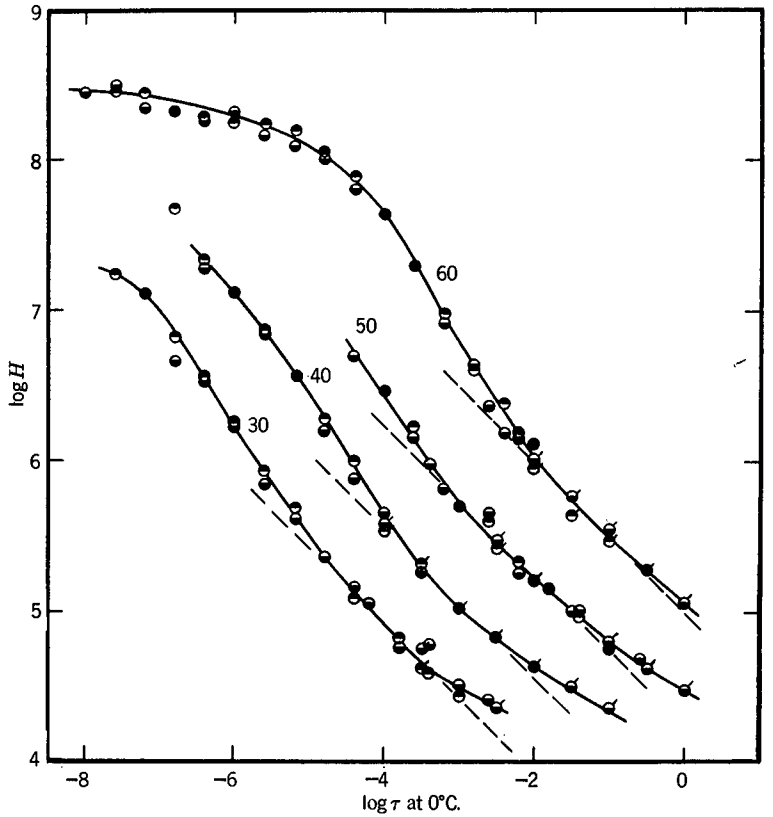


FIG. 17-2. Relaxation spectra of four solutions of poly(*n*-butyl methacrylate) in diethyl phthalate,[12] reduced to 0°C. Dashed lines are tangents drawn with theoretical slope of $-\frac{1}{2}$. Points with top black, calculated from G'; bottom black, from G''. Numbers denote polymer concentration in weight %.

tensive study of polystyrene diluted with tricresyl phosphate by Plazek and collaborators.[14]

By analogy with equations 1 and 3 of Chapter 11, we can define a factor a_c with the relation

$$[\tau_p]_c/[\tau_p]_\rho = [\zeta_0]_c/[\zeta_0]_\rho = a_c \tag{10}$$

representing the factor by which the monomeric friction coefficient and the relaxation times change as the polymer concentration in grams per cubic centimeter is reduced from ρ_2 (corresponding to pure polymer) to c; $c = \rho_2 v_2$. (In this chapter, we express polymer concentration variously as v_2, c, w_2, or weight percent; alternatively, the composition is specified by v_1 or w_1. No attempt is made to use a single measure of composition, since the choice depends on the circumstances and interconversions are trivial.) If data for the undiluted polymer are inaccessible, another concentration can be chosen as a reference.

To calculate ζ_0 from the relaxation spectrum as in Fig. 17-2, equation 1 of Chapter 12 must be modified by substituting c for ρ_2:

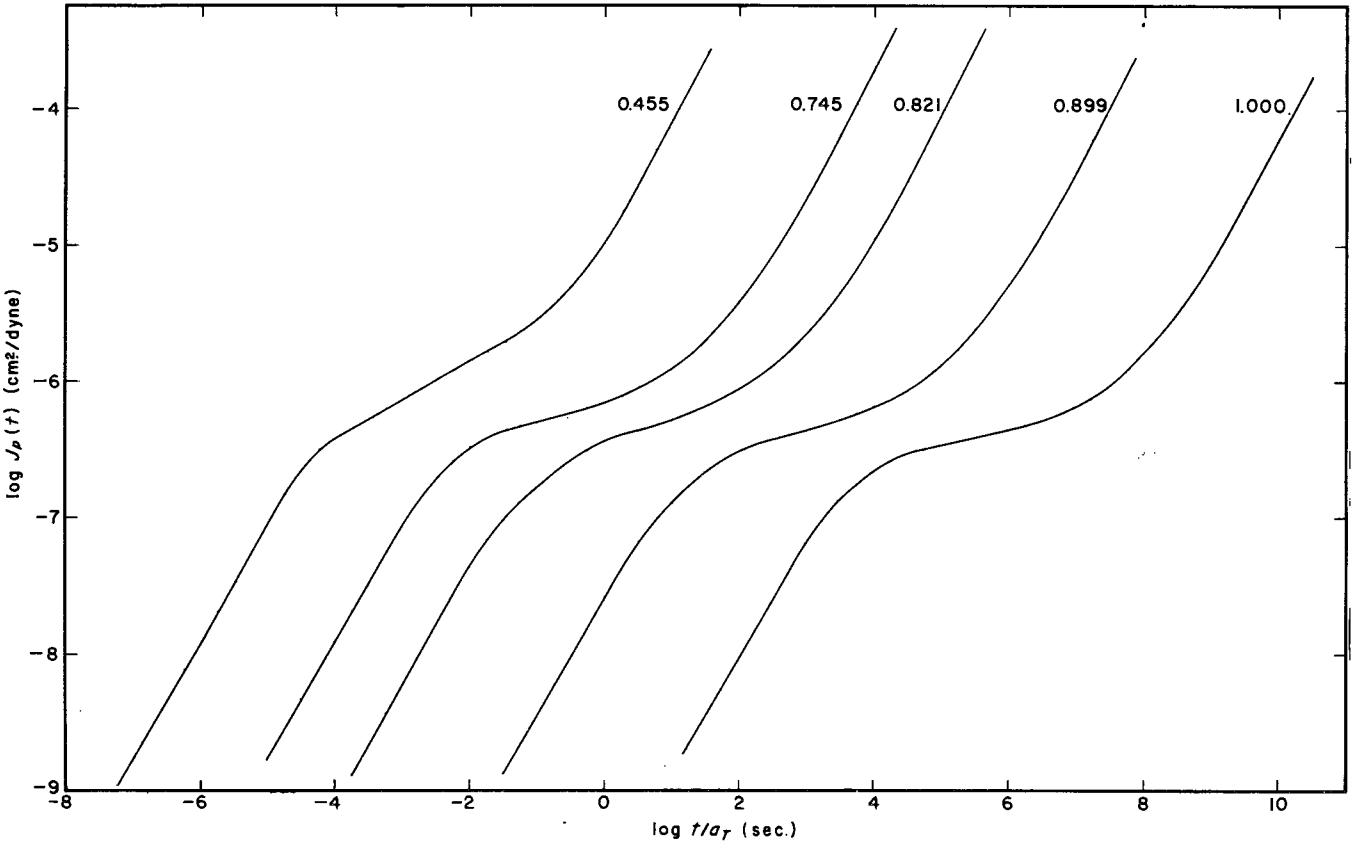


FIG. 17-3. Shear creep compliance of poly(vinyl acetate), M = 240,000, and four solutions in diethyl phthalate with indicated values of v_2 reduced to 40°C. (Ōyanagi and Ferry.[13])

$$\log \zeta_0 = 2 \log H + \log \tau + \log (6/kT) + 2 \log (2\pi M_0/acN_0) \qquad (11)$$

Correspondingly, if a_c is to be determined from displacements along the logarithmic time or frequency axis, moduli or relaxation spectra must first be divided by v_2, or compliances or retardation spectra multiplied by v_2, to take into account the change in the number of polymer molecules per cc. with dilution. This is analogous to the factor $T\rho/T_0\rho_0$ in temperature reduction or the factor $T\rho/M_0$ used in equation 10 of Chapter 12 to reduce relaxation spectra to corresponding states.

The marked reduction in ζ_0 apparent in Figs. 17-2 and 17-3, like the drop in T_g in Fig. 17-1, can be attributed to an increase in free volume caused by the diluent, and the generalized Doolittle relation, equation 49 of Chapter 11, can be applied to this case as follows:[8,11,15]

$$\log a_c = \frac{B}{2.303}\left(\frac{1}{f_c} - \frac{1}{f_2}\right) \qquad (12)$$

where f_c is the fractional free volume at concentration c and f_2 that of the undiluted polymer. Equation 12 can be combined with either equation 4 or equation 6 to predict the dependence of a_c on composition, expressed now in terms of v_1; in practice, the linear equation 4 is generally used,[8,11] with B taken as unity, to give

$$\log a_c = -v_1/2.303 f_2(f_2/\beta' + v_1) \qquad (13)$$

or, in terms of a reference concentration v_1^0 other than the undiluted polymer,[15]

$$\log a_c = -(v_1 - v_1^0)/2.303 f_2^0(f_2^0/\beta' + v_1 - v_1^0) \qquad (14)$$

As pointed out by Fujita,[8-15] equation 13 can be rearranged to provide for two alternative linear plots to test its applicability to experimental data and to determine the parameters f_2 and β from slopes and intercepts:

$$-1/\ln a_c = f_2 + f_2^2/v_1\beta' \qquad (15)$$

$$-v_1/\ln a_c = f_2^2/\beta' + v_1 f_2 \qquad (16)$$

Linearity of both the left side of equation 15 against $1/v_1$ and the left side of equation 16 against v_1 constitutes a rather severe test. If f_2 is obtained in this manner it should be identical with the f_0 of equation 37 of Chapter 11, derived from analysis of the *temperature* dependence of relaxation times; and if f_2 is obtained at several different temperatures, its temperature coefficient should correspond to the α_f of equation 38 of Chapter 11.

An example of the application of equation 13 to the data in the transition zone of Fig. 17-3 is shown in Fig. 17-4. The curve for a_c calculated from equation 13 with $f_2 = 0.036$, $\beta' = 0.128$ agrees very well with the measured values over the enormous range of nearly eight logarithmic decades. From the temperature dependence of a_T for pure poly(vinyl acetate) as given by f_g and α_f in Table 11-II, f_2 at 40°C is calculated to be 0.033, in reasonable agreement; and the empirical value of β' is also reasonable.

This analysis can be applied equally well to the concentration dependence of the

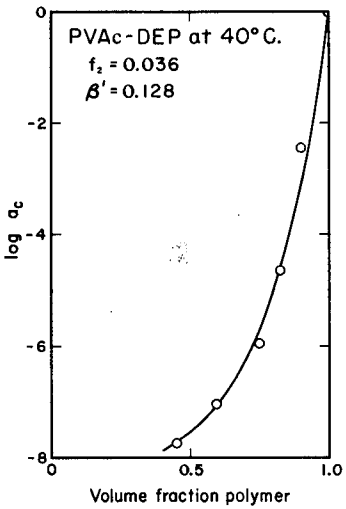


FIG. 17-4. Plot of log a_c against volume fraction of polymer, for data of Fig. 17-3 in the transition zone. Curve drawn from equation 13 with parameters as shown. Reproduced, by permission, from *Molecular Fluids,* edited by R. Balian and G. Weill, Gordon and Breach, London, copyright 1976.

friction coefficient ζ_1 of a small foreign molecule as derived from diffusion measurements, which as shown in Tables 12-VI and 12-VII is closely correlated with ζ_0. The only reservation is that the coefficient B in equation 12, taken as unity above, may be somewhat different.[16] The experiment is simplest if the diffusing molecule is chemically identical with the diluent but is radioactively tagged so that the

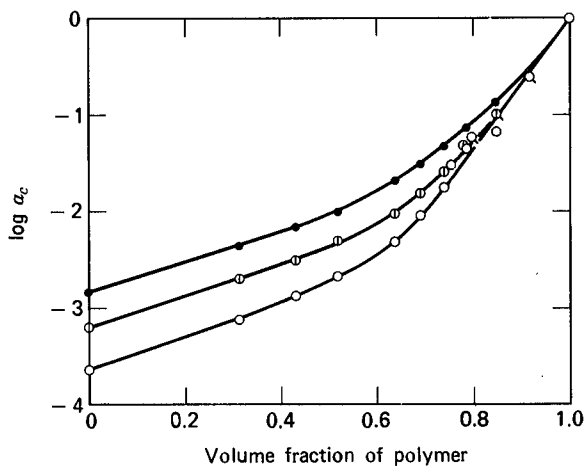


FIG. 17-5. Log a_c plotted against v_2 for solutions of polyisobutylene in *n*-hexadecane.[17,18] Data from diffusion: open circles 24.0°C; slotted circles, 40.0°C; black circles, 48.4°C. Data from viscoelastic measurements in the transition zone: circles with tags, 25.0°C.

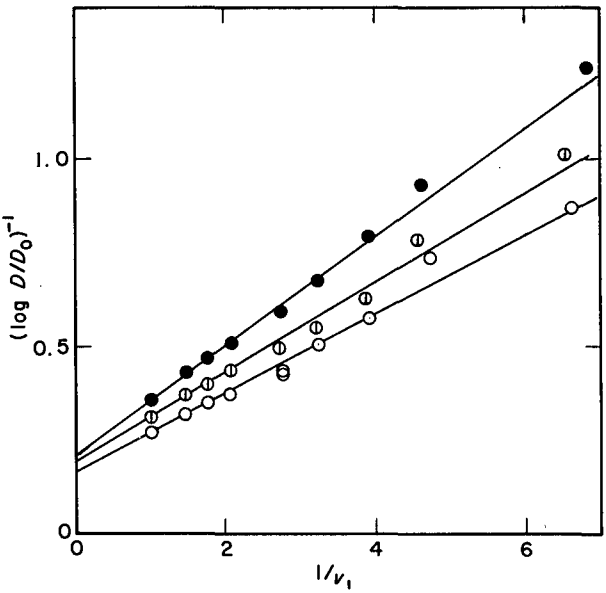


FIG. 17-6. Test plot of equation 15 with data of Fig. 17-5 and parameters of Table 17-I. (Moore and Ferry.[17])

chemical composition remains uniform during the diffusion process. This case is chosen here to illustrate equations 15 and 16 because data are available over the entire concentration range for solutions of polyisobutylene in *n*-hexadecane from the experiments of Moore,[17] as well as some less extensive data on mechanical measurements for the same system by Richards, Ninomiya, and Ferry;[18] the values of a_c from the latter are essentially the same as those from diffusion where they overlap, thus supporting the conclusion in Chapter 12 that the two types of experiment measure molecular mobility in a similar manner. In Fig. 17-5, $\log a_c$ is plotted against v_2 at three different temperatures, including points from viscoelastic measurements at 25°. The test plots corresponding to equations 15 and 16 are shown in Figs. 17-6 and 17-7 respectively. Both yield the same values of the parameters f_2 and β', which are listed in Table 17-I.

Table 17-I

FREE VOLUME PARAMETERS FROM CONCENTRATION DEPENDENCE OF FRICTION COEFFICIENT ζ_1 IN POLYISOBUTYLENE-*n*-HEXADECANE SYSTEM

T, °C	β'	f_2
24.0	0.120	0.074
40.0	0.141	0.085
48.4	0.134	0.092

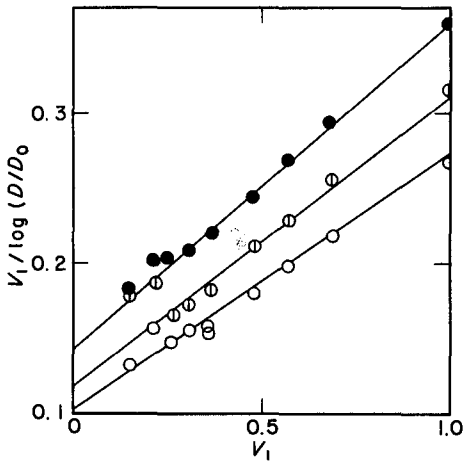


FIG. 17-7. Test plot of equation 16 with data of Fig. 17—5 and parameters of Table 17-I. (Moore and Ferry.[17])

The values of f_2 are somewhat higher than those calculated from temperature dependence of viscoelastic properties using the parameters α_f/B and f_g/B (with $B = 1$) in Table 11-II, which give $f_2 \cong 0.05$, but agree very well with those calculated from the alternative assignment of α_f/B and f_g/B given in footnote *a* of that table. The temperature coefficient of f_2 is too high, but cannot be expected to be very accurate. The values of β' correspond (according to equation 9, neglecting k'_v) to $f_1 \cong 0.22$, which is certainly reasonable for a liquid of low molecular weight. (It agrees almost exactly[17] with an estimate based on an analysis by Doolittle[19] of the temperature dependence of the viscosity of normal paraffins, but the latter is not quite consistent with the free-volume analysis employed here.)

Similar analyses have been made on many systems by Fujita and collaborators to determine free-volume parameters from viscosity data. In this case, f_0 and α_f have been calculated independently from the temperature dependence of a_T at various concentrations[20,21] and from the concentration dependence of a_c at various temperatures[15,22] (as in Figs. 17-5 to 17-7). From the temperature dependence of viscosity, a_T can be obtained directly provided the parameters M_e and Q_e used to describe entanglement coupling or tube restraint are temperature independent as mentioned in Section A5 of Chapter 11; *cf.* equations 27 of 55 of Chapter 10. From the concentration dependence of viscosity, a_c cannot be obtained directly if the molecular weight is higher than M_C, since M_e, M_C, and Q_e will certainly be concentration dependent as discussed in Section C1 below; direct comparison of viscosity data yields rather the factor λ_2 (*cf.* equation 26 of Chapter 10 and the discussion in Section C5 of Chapter 13). However, if the temperature is not too far above T_g, the concentration dependence of ζ_0 in equation 47 of Chapter 10 far outweighs that of M_e or Q_e. The frequent success of the analysis without correcting for Q_e is undoubtedly due to this feature; values of f_2 and α_f are obtained which have the correct magnitude and are generally consistent with results from the temperature dependence of viscoelastic properties of the undiluted polymer and also from diffusion measurements.

Equivalent free-volume parameters have also been obtained by Fujita, Kishimoto, and collaborators from the concentration dependence of the diffusion coefficient in polymer-diluent mixtures.[16,23-25] In these experiments without radioactive tagging, there is a chemical concentration gradient which requires a more complicated treatment of the data. However, values of f_2 and α_f are obtained which are consistent in magnitude with those obtained from other sources. For example, f_2 as a function of T for undiluted poly(methyl acrylate), derived from concentration dependence of diffusion measurements in concentrated benzene solutions,[23] agrees almost exactly with the results from concentration dependence of viscosity measurements in concentrated diethyl phthalate solutions[22] and fairly well with the values from temperature dependence of viscoelastic properties of the pure polymer[26] (Table 11-II). Also, the values of β', interpreted as approximately equal to f_1, and their increase with temperature are reasonable. The consistency of free-volume parameters obtained from entirely different sources gives confidence that these figures have physical significance even though an operational definition of the fractional free volume is lacking.

If the undiluted polymer is near T_g, addition of small amounts of diluent can cause rather large changes in a_c with a consequent rapid shift of the viscoelastic functions in the transition zone to shorter times or higher frequencies. This can be shown[11] by taking the derivative of equation 13 for small v_1:

$$(d \log a_c/dv_1)_{v_1 \to 0} = -\beta'/2.303f_2^2 \tag{17}$$

The appearance of f_2^2 in the denominator shows that the "plasticizing effectiveness" represented by the left side of this equation increases rapidly as the temperature is lowered and T_g is approached. Also, β' in the numerator indicates that the most important characteristic of the diluent in plasticizing effectiveness is its own free volume.

Examples of large changes in a_c with a few percent of diluent are shown in Fig.

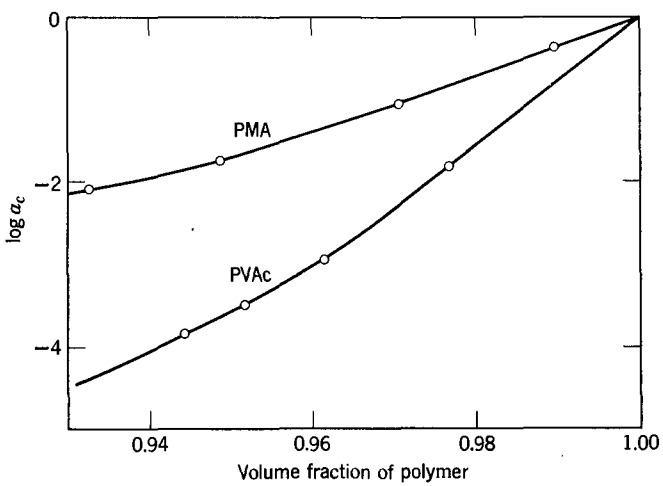


FIG. 17-8. Log a_c plotted against v_2, from stress relaxation measurements (Fujita and Kishimoto[8]) on poly(vinyl acetate) (PVAc) and poly(methyl acrylate) (PMA) at 40°C.

17–8 for poly(methyl acrylate) and poly(vinyl acetate) containing small amounts of methyl alcohol, derived from stress relaxation measurements by Fujita and Kishimoto[8] at 40°C. The slope at $v_2 = 1$ ($v_1 = 0$) is steeper for poly(vinyl acetate) because its T_g (32°) is closer to 40° than is that of poly(methyl acrylate) (3°). In fact, the ratio of f_2^2 for the two polymers, from the data of Table 11–II, is 1.8, as compared with the ratio of 2.1 for the two slopes in the figure.

A dependence of relaxation times on free volume per molecule close to that described by equation 12 has been found by computer simulation of molecular motions in a polymer–solvent system modeled with a three-dimensional lattice, by Kranbuehl and Schardt.[27]

Empirically, a_c has often been found to be an exponential function of c or v_2, both from viscoelastic[12,28] and from diffusion[29,30] measurements. This relation may be useful for interpolation purposes, but does not appear to provide any insight into molecular mechanisms. There have been many empirical correlations of plasticizing effectiveness with various physical properties of diluents.[29,31] An analysis of the concentration dependence of a_c based on changes in configurational entropy has been presented by Havlíček and collaborators,[32] and provides good agreement with experiment.

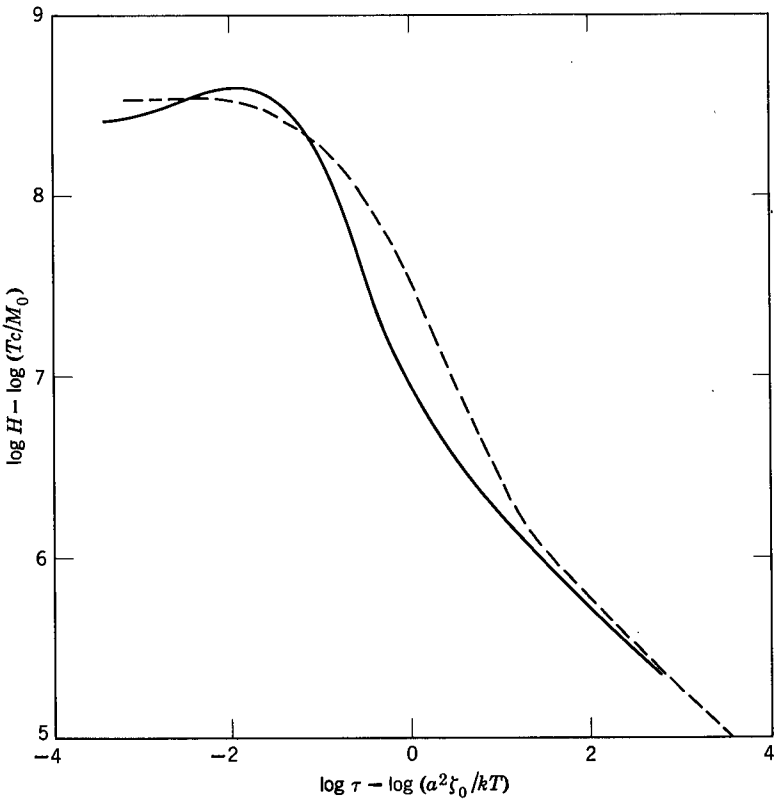


FIG. 17-9. Corresponding-state plots of the relaxation spectra of poly(vinyl acetate) (solid line) and a 50% solution by weight (dashed line) in tri-*m*-cresyl phosphate. (Williams and Ferry.[33,34])

3. Shapes of the Viscoelastic Functions

To show the effect of diluent on the detailed shapes of viscoelastic functions, it is convenient to employ corresponding-state plots as in Section C of Chapter 12. For the relaxation spectrum, we plot $\log H - \log Tc/M_0$ against $\log \tau - \log (a^2\zeta_0/kT)$. Of course, for a single polymer and its solutions the only variables are ζ_0 and c (which in the pure polymer becomes ρ). In Fig. 17-9, poly(vinyl acetate)[33] is compared in this manner with its 50% solution[34] in tri-*m*-cresyl phosphate. The values of $\log \zeta_0$ at 40°C for these two systems are 1.75 and −5.25, respectively—the diluent reduces the local friction coefficient by a factor of 10^7. The curves after reduction coincide at the bottom of the transition zone because this is fixed by the corresponding-state conditions, and are rather similar in shape throughout. However, the diluent causes the spectrum to rise somewhat more sharply from the theoretical slope of $-\frac{1}{2}$ at short times; but at still shorter times it crosses the spectrum of the pure polymer, and its entrance into the glassy zone involves a broader maximum than the latter.

In Fig. 17-10, poly(*n*-butyl methacrylate)[35] is similarly compared with two of the solutions in diethyl phthalate[12] whose relaxation spectra appear in Fig. 17-2. The other two solutions with intermediate concentrations would fall very near the curves drawn. The differences in shape between the spectra of the pure polymer

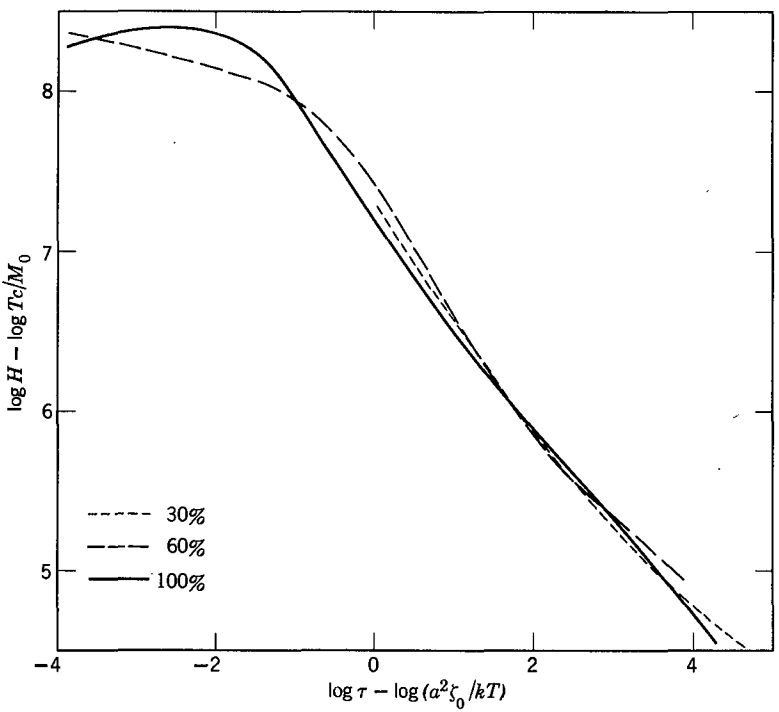


FIG. 17-10. Corresponding-state plots of the relaxation spectra of poly(*n*-butyl methacrylate) and two solutions in diethyl phthalate, with indicated polymer concentration in weight percent.[35,12]

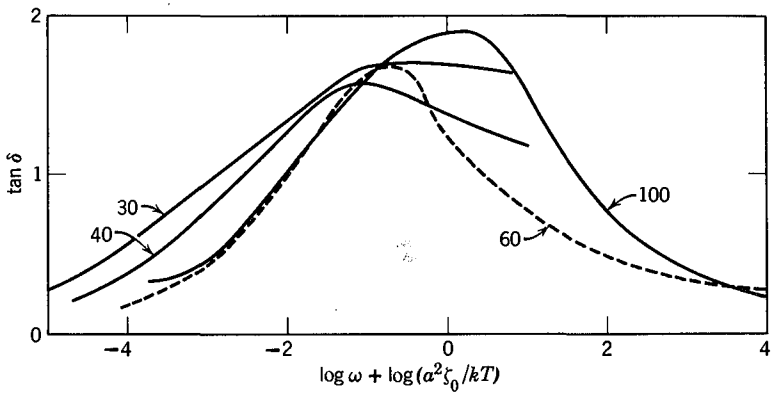


FIG. 17-11. Loss tangents of poly(*n*-butyl methacrylate) and three solutions in diethyl phthalate, plotted against the logarithm of the frequency reduced as in the abscissa of Fig. 17-10. Numbers denote polymer concentration in weight percent.

and its solutions are similar in nature to those for the poly(vinyl acetate), but less prominent. Some shape differences are also observed for logarithmic plots of creep compliances and retardation spectra of concentrated solutions of polystyrene in tricresyl phosphate.[14] In Fig. 17-3, it is evident that the shapes of the creep compliance in the transition zone are quite similar but not identical.

It has been pointed out by Aklonis and Rele[36] that the steepness of the transition zone in polystyrene is diminished by diluent and that the magnitude of the change depends on the thermodynamic interaction of solvent with polymer, being least when the cohesive energy densities of the two components are closely matched. Molecular interpretation is uncertain since the molecular basis for shape of the relaxation spectrum at short times is poorly understood (Chapter 10, Section D).

The differences in spectral shape are of course reflected in the other viscoelastic functions, especially the loss tangent, which is always the most sensitive. The loss tangents for poly(*n*-butyl methacrylate) and three of its solutions are plotted in Fig. 17-11 with the frequency scale reduced in the same way as the abscissa in Fig. 17-10. They show some degree of broadening with increasing dilution, but their maxima remain considerably above the theoretical value of 1.0 which would be predicted throughout the transition zone by the flexible chain theory in its simple form. Similar behavior has been reported for concentrated solutions of polystyrene in tricresyl phosphate, by Wasser and Kurath.[37]

4. Isochronal or Quasi-Isochronal Viscoelastic Measurements

When measurements are made at approximately constant frequency on plasticized polymers over a range of temperatures, the location of the transition zone naturally shifts to lower temperatures with increasing dilution. It is difficult to find examples for uncross-linked polymers, because most experimental methods are not adapted to the fluid systems obtained at higher dilutions. However, the pattern

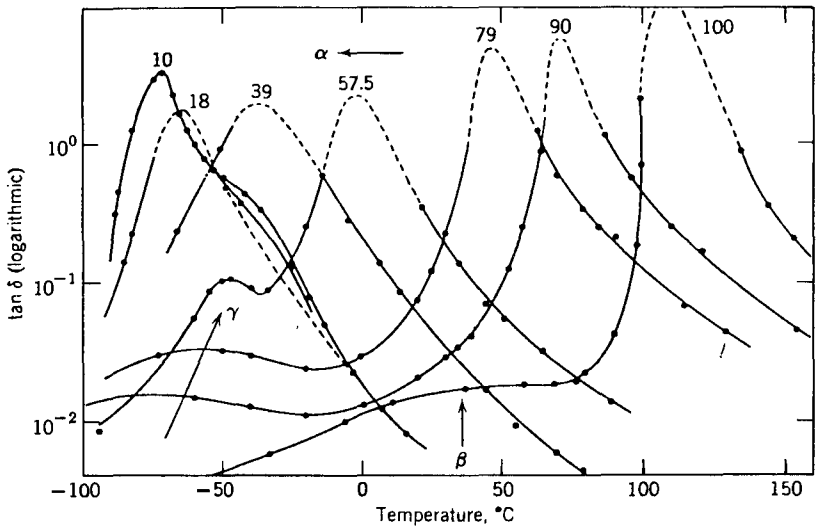


FIG. 17-12. Loss tangents of lightly cross-linked polystyrene swollen to various extents in dibutyl phthalate, plotted against temperature at a frequency of 1 Hz. Numbers denote polymer concentration in weight percent. (Illers and Jenckel.[38])

can be illustrated by lightly cross-linked polystyrene swollen in dibutyl phthalate to various extents, as shown in Fig. 17-12, where measurements of tan δ at 1 Hz by Illers and Jenckel[38] are plotted against temperature at various polymer concentrations. (As mentioned in Section F below, swelling after cross-linking distorts the polymer chains from their most probable configuration distributions, but this probably does not greatly change the behavior illustrated, and the cross-linked systems have of course the advantage of maintaining rigidity so that they can be studied with equipment designed for solid samples.) The shift to lower temperatures is accompanied by minor changes in the height of the maximum and the peak breadth. Such changes reflect a combination of the effect of diluent on the a_T function *and* its effect on the shapes of the isothermal viscoelastic functions.

5. Reduced Variables for Concentration Dependence

The corresponding-state plot of Fig. 17-10 implies, insofar as the curves coincide in the transition region, that all relaxation times are proportional to ζ_0 and that the magnitudes of contributions to H are all proportional to c as well as to T. This is, of course, exactly what the bead-spring chain theories predict, as in equations 18 and 20 of Chapter 9, for example (recalling that n is proportional to c). On this basis, a scheme of reduced variables can be devised to combine measurements at different concentrations as well as temperatures, without actually calculating ζ_0 and without requiring that the detailed shapes of the viscoelastic functions conform to the simple theories.

Any composition may be chosen as a reference state. If the undiluted polymer is selected, and a_c denotes as above the ratio of relaxation times at concentration

c to those in the pure polymer at concentration ρ_2, the analogs of the coordinates numbered 6, 7, 10, and 11 in Chapter 11 are:[39]

$$G_c(t) = (\rho_2/c)G(t), \quad vs. \quad t/a_c \tag{18}$$

$$G'_c = (\rho_2/c)G', \quad vs. \quad \omega a_c \tag{19}$$

$$J_c(t) = (c/\rho_2)J(t), \quad vs. \quad t/a_c \tag{20}$$

$$J'_c = (c/\rho_2)J', \quad vs. \quad \omega a_c \tag{21}$$

in which the subscript c denotes reduction by concentration to the pure polymer. Extension to the other viscoelastic functions is obvious. This method has been applied to obtain composite functions for a number of polymers in the range of small amounts of added diluent,[8,40–42] with a_c determined empirically. It cannot in general be expected, however, that the values of a_c applicable in the transition zone will also be successful in the plateau and terminal zones for polymers of high molecular weight, because of the effects of dilution on entanglement coupling.

B. THE PLATEAU ZONE

The effects of a diluent on viscoelastic properties of an uncross-linked polymer in the plateau zone are dominated by its influence on the entanglement network, and especially the average entanglement spacing. They are apparent in several characteristic aspects.

1. Manifestations of Changes in Entanglement Spacing with Concentration

In Fig. 17-3, it is evident that the level of the plateau near $\log J(t) = -6.5$, reflecting the compliance of the entanglement network, rises somewhat and becomes less flat with increasing dilution. This would be expected if the concentration of entanglement loci diminishes, and the molecular weight between entanglements, M_e, increases correspondingly. A quantitative calculation of M_e cannot be made from these curves, however, as explained in Section B of Chapter 13. The same effect is observed in the storage compliance for concentrated solutions of polyisobutylene in n-hexadecane[16] in Fig. 17-13. In both cases, the effect is exaggerated somewhat if the curves are compared at the same time or frequency because of the simultaneous effect of dilution in changing the time scale by the factor a_c as described in the preceding section. If the creep compliance is plotted against $\log t/a_c$, or the storage compliance against ωa_c, however, the vertical separations in the plateau zone are related to entanglement spacing differences.

The plateau compliance J_N^0 or its reciprocal, the modulus G_N^0, can be obtained from stress relaxation, creep, or dynamic data by integrations such as equations 3 to 5 of Chapter 13 in order to determine its concentration dependence without complication of time scale shifts. Examples are shown[43] in Fig. 17-14 for concentrated solutions of poly(methyl methacrylate)[44] and *cis*-polyisoprene.[45] The

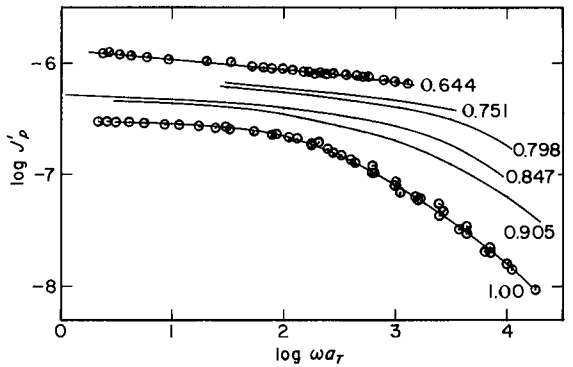


FIG. 17-13. Storage compliance of polyisobutylene ($\bar{M}_v = 1.5 \times 10^6$) and five solutions in *n*-hexadecane with indicated values of v_2 reduced to 25.0°C. Pips in circles denote individual temperatures of measurement, from 15° to 60°. Points omitted from intermediate curves to avoid confusion. (Richards, Ninomiya, and Ferry.[18])

modulus G_N^0 is closely proportional to c^2. This dependence is also consistent, approximately, with the data of Figs. 17-3 and 17-13, as well as data of binary blends of poly(vinyl acetate)s[46] in which one component has a molecular weight low enough to be essentially a diluent while the other has a high enough molecular weight to participate in entanglements.

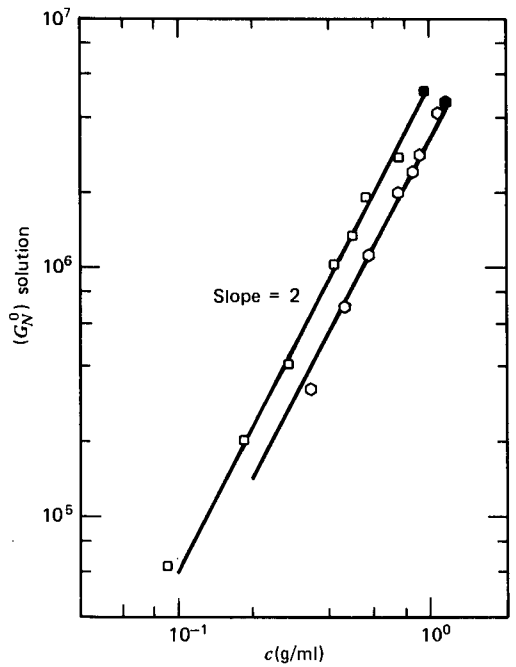


FIG. 17-14. Logarithmic plot of plateau modulus (in dynes/cm^2) against concentration for solutions of poly(methyl methacrylate) (hexagons) and *cis*-polyisoprene (squares). The black points are for the undiluted polymers. (After Graessley.[43]) Reproduced, by permission, from *Advances in Polymer Science*.

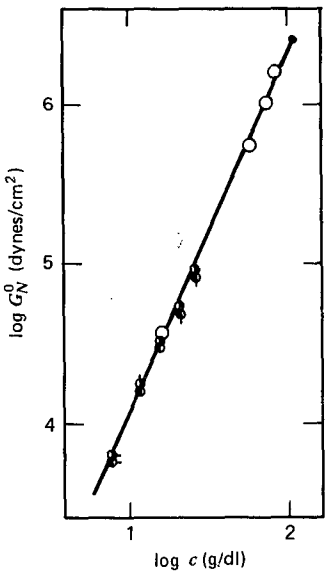


FIG. 17–15. Logarithmic plot of plateau modulus against concentration for solutions of polystyrene in benzyl *n*-butyl phthalate at 100°C. Different symbols correspond to calculations from various integration procedures and different molecular weights from 1.4×10^6 to 1.2×10^7. Line drawn with slope between 2.2 and 2.3. (Nagasawa and collaborators.[47]) Reprinted with permission from *Macromolecules*, **11**, 888 (1978). Copyright by The American Chemical Society.

In other studies of creep of solutions of polystyrene in tricresyl phosphate[10] and creep and dynamic properties of polystyrene in benzyl *n*-butyl phthalate,[47] a slightly higher concentration dependence has been observed. An example is shown in Fig. 17–15, where points are plotted from various integration procedures like equations 3 to 5 of Chapter 13. The slope of the logarithmic plot is 2.2 to 2.3. In these studies, data at different temperatures must be reduced to a reference temperature, and it is uncertain whether G_N^0 should be directly proportional to cT (*cf.* Fig. 13–10 and associated discussion); if it is, an exponent near 2 is obtained.[48] In recent measurements on solutions of polybutadiene, which do not require temperature reduction for comparison, an exponent between 2.2 and 2.3 has also been obtained.[49]

If every contact between two polymer molecules has a constant probability of entanglement, as has often been assumed *a priori*,[9,50] M_e should be proportional to v_2^{-1}, *i.e.*, to $(c/\rho_2)^{-1}$. In equation 2 of Chapter 13, $\nu_e = c/M_e$ (neglecting loose end corrections), and is therefore proportional to c^2; the latter equation becomes

$$G_N^0 = g_N c^2 RT/M_e^0 \rho_2 = v_2^2 G_N^{00} \tag{22}$$

where M_e^0 and G_N^{00} are the molecular weight between entanglements and the plateau modulus, respectively, of the undiluted polymer. This agrees with Fig. 17–14. However, de Gennes has concluded[51,52] from scaling laws applied to the conditions for overlap of random coils that a characteristic modulus identifiable with G_N^0 should be proportional to $c^{9/4}$ as observed in Fig. 17–15. Further work is needed to resolve

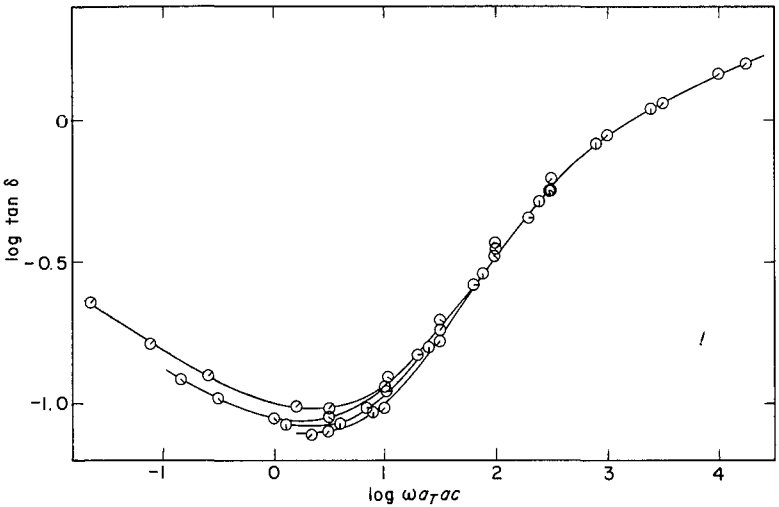


FIG. 17-16. Loss tangents of solutions of Fig. 17-13 plotted logarithmically against frequency reduced for both temperature and concentration dependence, using a_c factors from Fig. 17-5. Minima from top to bottom correspond to $v_2 = 0.751, 0.847, 0.905$, and 1.000.

these differences, although for practical purposes they are slight; proportionality of M_e to v_2^{-1} and G_N^0 to v_2^2 is at least a close approximation.

Another measure of entanglement spacing is, of course, M_C, the critical value for the influence of entanglements on steady flow viscosity. It also varies with dilution in a manner that can be determined from careful analysis of the dependence of viscosity on molecular weight and concentration, though data of high accuracy are required. Studies of poly(vinyl acetate)[53] in diethyl phthalate and cetyl alcohol and polystyrene in dibenzyl ether,[54] as well as other systems reviewed by Berry and Fox,[50] support the expectation that M_C, like M_e, is proportional to v_2^{-1}; $M_C = M_C^0 v_2^{-1}$, where M_C^0 is the value for the undiluted polymer. (A slight difference in the concentration dependences of M_e and M_C, probably too small to detect experimentally,[50] has been predicted by Kelley and Bueche.[9])

The depth of the minimum in the loss tangent from dynamic viscoelastic measurements is an alternative source of information on M_C, as expressed by equation 10 of Chapter 13. In Fig. 17-16, tan δ is plotted logarithmically against $\omega a_T a_c$ for the polyisobutylene solutions whose storage compliance appears in Fig. 17-13. With increasing dilution, the minimum rises progressively. Equation 10 of Chapter 13 can thus be used to obtain relative entanglement spacings, and M_C is again found to be approximately proportional to v_2^{-1}, though the precision is not great. Also, in studies of poly(vinyl acetate) blends[55] with one component of very low molecular weight ($M_1 = 5500$), the minimum value of tan δ is found to be proportional to $v_2^{-0.8}$ and this in conjunction with equation 10 of Chapter 13 means that M_C is proportional to v_2^{-1}.

Still another way of estimating the dependence of M_C on dilution is the com-

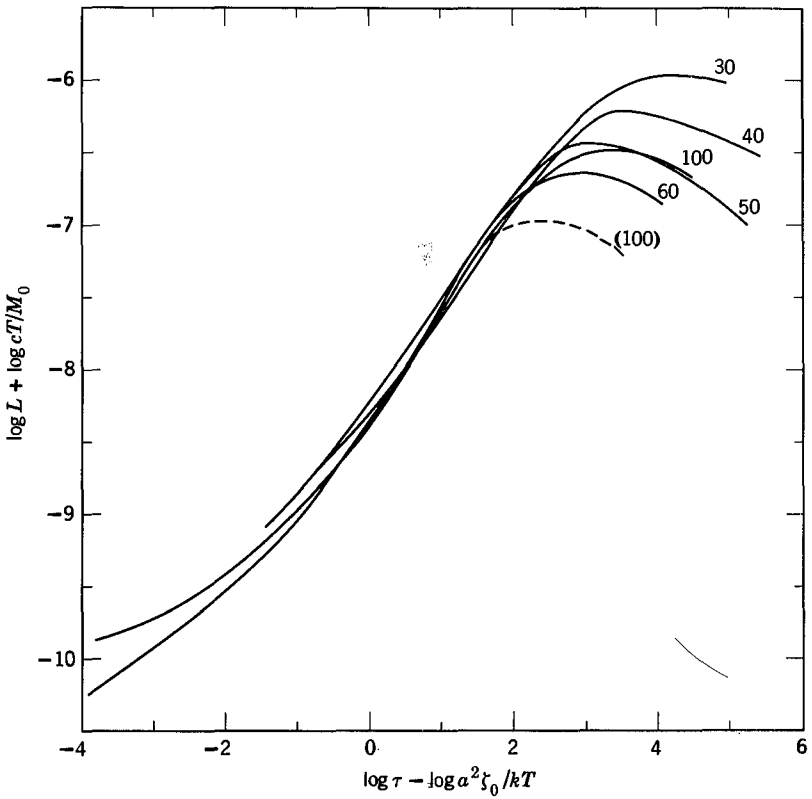


FIG. 17-17. Corresponding-state plots of the retardation spectra of four solutions[12,35] of poly(*n*-butyl methacrylate) in diethyl phthalate and the undiluted polymer,[35] identified by polymer concentrations in weight percent. Dashed line is reduced for temperature dependence of f factor (Section F2 of Chapter 11).

parison of data in the transition and terminal zones as discussed in Section C3 below.

Another qualitative manifestation of the change in entanglement coupling with concentration is the width on the logarithmic frequency scale of the region where $\tan \delta < 1$, *i.e.*, $G'' < G'$. For an undiluted polymer of high molecular weight, as illustrated in Fig. 13-3, this extends over many decades. With increasing dilution, it shrinks and finally disappears, as seen in Fig. 9-22.

The above examples have been polymers with relatively weak intermolecular forces and no heterogeneity in composition or structure along the chain. There are other cases in which the entanglement spacing appears to depend more strongly on dilution—*e.g.*, solutions of poly(*n*-butyl methacrylate) and poly(methyl methacrylate). To illustrate this behavior, still another experimental source of information is cited—the maximum in the retardation spectrum, which, with the corresponding maximum in the loss compliance, is the most characteristic symptom of the entanglement network. In Fig. 17-17, the retardation spectra[12,56] are plotted

for the same solutions whose relaxation spectra appear in Fig. 17–2, together with that for undiluted poly(*n*-butyl methacrylate)[57] (after reduction to the same temperature with the f factor discussed in Section F2 of Chapter 11). The maximum in L differs from that in J'' only by a factor of $2/\pi$ (equation 34 of Chapter 4, where $B = 2/\pi$ when $m = 0$) and relative entanglement spacings M_e can therefore be obtained from equations 2 and 7 of Chapter 13 even if the absolute values are subject to correction. In this way, M_e is found to be proportional to $v_2^{-2.6}$. More fragmentary data on poly(methyl methacrylate) solutions[58] in diethyl phthalate indicate a similar large negative exponent, different from that seen in Fig. 17–14. It follows from equation 2 of Chapter 13 with ρ replaced by c that the density of entanglement loci is proportional to $v_2^{3.6}$ and J_N^0 to $v_2^{-3.6}$ instead of to v_2^{-2} as in simple entanglement systems. Thus there is a very exaggerated concentration dependence of the plateau level of the compliance, and it is in fact observed to correspond approximately to this exponent.[56]

This behavior is probably related to the anomalous temperature dependence discussed in Section F2 of Chapter 11 and may be attributed to hyperentanglements with some kind of attraction between tactic regions in imperfectly atactic polymers. Such attractions can occur as evidenced by gel formation in solutions of mixed isotactic and syndiotactic poly(methyl methacrylate).[59–62] Similar effects might be expected in copolymer systems where hydrogen bonding can occur at widely separated points.[63]

2. Reduced Variables for Concentration Dependence

It is evident from the foregoing discussion that the concentration reduction scheme for the transition zone described in Section A5 above cannot be applied in the plateau zone, and indeed that no simple method for combining data at different concentrations can exist; Figs. 17–3 and 17–16 show that the shapes of the viscoelastic functions change significantly with dilution. In particular, the appropriate reduction factor for the magnitude of $G(t)$ or G' in the transition zone is c^{-1} or v_2^{-1}, and for $J(t)$ or J' it is c or v_2 (coordinates 18 to 21 above); whereas in the plateau zone, for simple entanglement systems, the appropriate factors are c^{-2} or v_2^{-2} and c^2 or v_2^2 respectively. Several investigators[64–66] have found the latter factors to be applicable to data in the plateau zone provided $M \gg M_C$ (bearing in mind that M_C increases with dilution). The appropriate time or frequency reduction can be deduced by analogy with the f-shift discussed in Section F2 of Chapter 11; the appropriate coordinates are:

$$(\rho_2/c)^2 G(t) \quad vs. \quad (\rho_2/c)^{-2} t/a_c \tag{23}$$

$$(\rho_2/c)^2 G' \quad vs. \quad (\rho_2/c)^2 \omega a_c \tag{24}$$

$$(c/\rho_2)^2 J(t) \quad vs. \quad (\rho_2/c)^{-2} t/a_c \tag{25}$$

$$(c/\rho_2)^2 J' \quad vs. \quad (\rho_2/c)^2 \omega a_c \tag{26}$$

For anomalous entanglements such as those in solutions of methacrylate polymers, higher exponents are required[56] in accordance with the dependence of M_e on

$v_2(= c/\rho_2)$. The applicability of these reduction coordinates is, however, quite restricted.

3. Elongated Rigid or Semirigid Macromolecules

The dilute solution properties of elongated rigid macromolecules whose shapes can be approximated by cylinders or elongated ellipsoids, such as tobacco mosaic virus, or elongated rodlike molecules with partial flexibility such as helical poly(γ-benzyl-L-glutamate), were treated in Chapter 9, and it was mentioned that interactions between such molecules appear at very low concentrations. Above a critical concentration, symptoms very similar to those of entanglement coupling in concentrated solutions of flexible polymers appear. The onset of such behavior is illustrated in Fig. 17-18 by measurements of Tschoegl[67] on a 2% solution of helical poly(γ-benzyl-L-glutamate); there is a short region where $G' > G'' - \omega\eta_s$, as in entangled flexible polymers and their concentrated solutions (*cf.* Fig. 13-3). At 2% the solution is already "concentrated" because of the large domain of the elongated macromolecule. Similar behavior was observed in solutions of shear-degraded helical calf thymus deoxyribonucleic acid[68] at concentrations up to 0.0013 g/cc; the width of the "crossover" region was a linear function of log cM and it reached zero at $cM = 3600$, implying a very low critical molecular weight for the interaction. An even more dramatic effect is seen in the data of Berry[69] on viscosities of solutions of BBB (a condensation polymer of naphthalene-1,4,5,8-tetracarboxylic

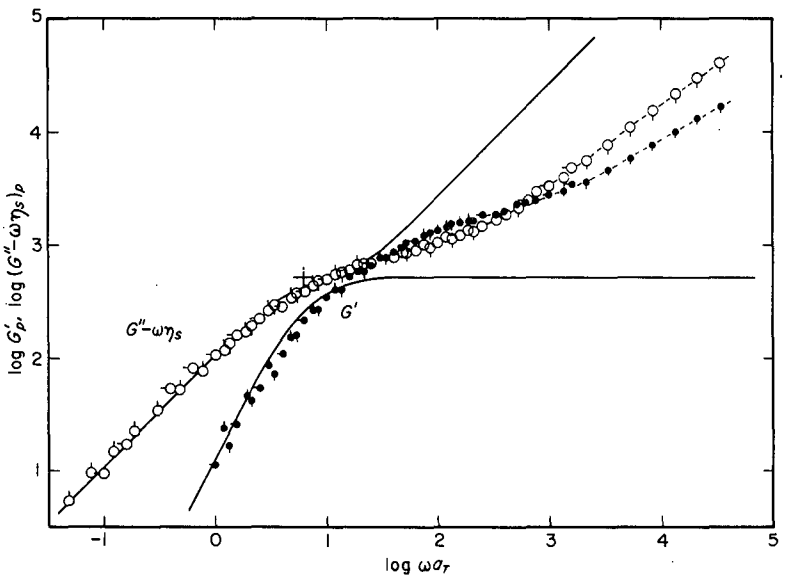


FIG. 17-18. Storage and loss moduli of a 2% solution of poly(γ-benzyl-L-glutamate) (molecular weight 345,000) in *m*-methoxyphenol (a helicogenic solvent) reduced to 25°C. Pips denote individual temperatures of measurement (−0.1°, 25.0°, 49.9°). Solid curves represent Kirkwood-Auer theory (*cf.* equations 8 and 9 of Chapter 9). (Tschoegl and Ferry.[67])

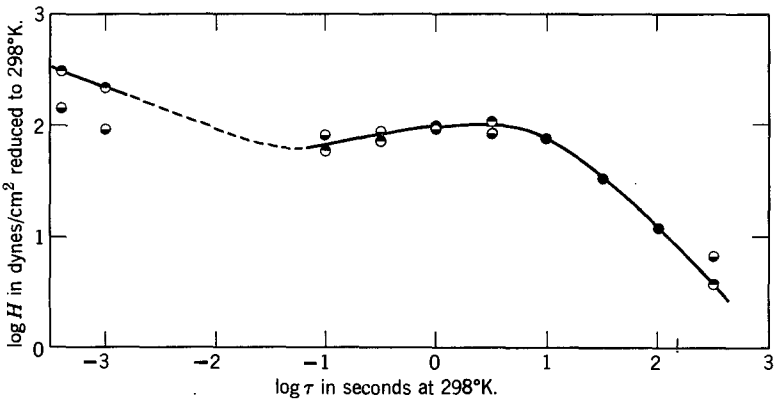


FIG. 17-19. Relaxation spectrum of aqueous deoxyribonucleic acid (sodium salt), concentration 0.012 g/ml reduced to 25°C. Points top black, calculated from G'; bottom black, from η'. (Helders, Ferry, Markovitz, and Zapas.[76])

acid and 3,3-diaminobenzidine) in methane sulfonic acid; the critical value M_C is proportional to v_2^{-1} and the product $(v_2M)_c$ is only 230. This molecule is not highly elongated but its stiff backbone provides far more limited opportunities for configurational changes than in ordinary flexible polymers. Similar behavior has been seen for other macromolecules with stiff backbones.[70]

Isotropic solutions of rodlike molecules are thermodynamically stable only at very low concentrations; at higher concentrations, they separate into two phases, the more concentrated of which is anisotropic.[71-73] The critical concentration for phase separation is increased somewhat by partial flexibility.[72,73] In the solutions described above, the concentration is high enough to provide substantial interpenetration of domains but is below the phase separation point. The finite viscosities of these solutions imply some degree of molecular flexibility; a structure of highly interpenetrating completely rigid rods (possibly thermodynamically metastable if phase separation is sterically impeded) should be elastic with no flow.[74] Although the interactions of these very stiff molecules mimic the symptoms of entanglement coupling, they must be quite different in view of the much smaller values of M_C^0, as low as 230 compared with the order of 30,000 for several of the flexible polymers in Table 13-II. The motions of interpenetrating rodlike molecules have been discussed theoretically by Doi and Edwards.[75]

As an extreme example of the symptoms of intermolecular coupling in a stiff molecule of very high molecular weight, the relaxation spectrum of deoxyribonucleic acid with weight-average molecular weight 5.8×10^6 at a concentration of 0.012 g/ml is shown in Fig. 17-19.[76] Even at this very low concentration, there is a plateau zone which extends over many decades, and its shape is similar to that exhibited by entangled flexible molecules of very high molecular weight. However, an attempt to estimate the entanglement spacing from the relations applicable to flexible polymers leads again to a meaninglessly small value.

C. LINEAR VISCOELASTIC BEHAVIOR IN THE TERMINAL ZONE

In discussing the effects of dilution in the terminal zone, we review first the viscosity at vanishing shear rate, the terminal relaxation time, and the steady-state compliance.

1. Viscosity at Vanishing Shear Rate

Either equation 50 or equation 51 of Chapter 10, with the density ρ_2 of the undiluted polymer replaced by concentration c, can be used to predict the viscosity of a concentrated solution when the molecular weight and/or concentration is sufficiently high that $Mc/\rho_2 > M_C^0$, where M_C^0 is the critical value for onset of the 3.4 proportionality in the undiluted polymer. The empirical molecular weight dependence is given most closely by equation 50, which provides

$$\eta_0 = 0.028cN_0 a^2 \zeta_0 M^{3.4}/M_C^{2.4}M_0^2 \tag{27}$$

In any case the effect of diluent on viscosity can be expected[50,77] to depend on, besides the factor of c, (a) the change in ζ_0 as expressed by the shift factor a_c which has already been discussed in Section A above; (b) the change in the entanglement spacing as measured by M_C or M_e; and (c) possible change in the root-mean-square end-to-end distance as measured by a, which is usually small in comparison to the others. Depending on the proximity to T_g, either (a) or (b) may be dominant. In the work of Fujita[15,21,22] quoted in Section A, the concentration dependence of viscosity was determined primarily by that of a_c, and could be very satisfactorily described over the whole concentration range by free-volume parameters. On the other hand, in measurements of Kraus and Gruver[77] on plasticized hydrocarbon polymers far above T_g, the concentration dependence of viscosity was determined almost solely by the concentration dependence of M_C.

For normal entanglement networks (excluding polymers such as methacrylates), where M_C and M_e appear to be proportional to v_2^{-1}, if the exponent of M_C in equation 27 is denoted by b, the dependence of viscosity on concentration should be (since $c = v_2\rho_2$)

$$\eta_0/\eta_{2,0} = a_c v_2^{b+1} \tag{28}$$

where $\eta_{2,0}$ is the viscosity of the undiluted polymer. The factor a_c can be determined independently from measurements in the transition zone[13,78] or from equation 12 with fractional free volumes estimated from temperature dependence or glass transition temperature measurements.[44] From the theories of Graessley or Doi and Edwards (equations 51 and 55 of Chapter 10) the exponent b should be 2.5 or 2 respectively if M_C/M_e is independent of molecular weight, rather than 2.4 as in equation 27. Experimental tests from equation 28 are generally consistent with any of these, since the precision is not very good.[13,78]

With increasing dilution, M_C increases and eventually is no longer small compared with M so the effects of entanglements disappear. At low concentrations,

therefore, the exponent b should be smaller. The critical value of concentration for this change in behavior might in principle serve as another measure of the spacing between entanglements, but the transition is gradual on account of the concomitant change in a_c; and even special plotting methods designed to make it more prominent[79] are not very satisfactory unless correction is made for the change in a_c. The boundary between the two concentration regimes has been described by Klein, in the framework of the tube model for entanglement effects, as the concentration below which reorganization of the entire tube contributes to configurational rearrangements. The remaining discussion refers only to higher molecular weights and/or concentrations where $v_2M > M_C^0$.

According to the theories of Graessley and Doi and Edwards, as expressed by equations 51 and 55 of Chapter 10 with the polymer density ρ replaced by concentration c, together with inverse proportionality of M_C or M_e to v_2 or c, the dependence of η_0/ζ_0 or η_0/a_c on both M and c can be combined with the same exponent:

$$\eta_0/\zeta_0 \propto (cM)^{3.5} \qquad \text{(Graessley)} \tag{29}$$

$$\eta_0/\zeta_0 \propto (cM)^{3} \qquad \text{(Doi-Edwards)} \tag{30}$$

Detailed studies of poly(vinyl acetate) in diethyl phthalate and cetyl alcohol[81] and polystyrene in dibenzyl ether[82] by Fox, Berry, and collaborators, in which the concentration dependence of ζ_0 was determined from temperature-dependence data, showed that η_0/ζ_0 was proportional to $(cM)^{3.4}$ over wide concentration ranges as would be specified by equation 27 with $M_C = M_C^0 v_2^{-1}$. At lower concentrations in good solvents, however, an additional small dependence of the characteristic length a in all the equations cited must be taken into account; the coil dimensions decrease with increasing c and become constant corresponding to Θ-solvent dimensions above $v_2 = 0.25$.[81]

If the viscosity is not "corrected" for the concentration dependence of ζ_0 or a_c as in equations 29 and 30, it is found empirically that η_0 can be represented as a single function of cM^γ over wide ranges of c and M. The exponent γ is 0.68 for polyisobutylene in several different solvents[83] and cellulose tributyrate in 1,2,3-trichloropropane;[79] for various solutions of polystyrene, poly(vinyl acetate), polyisobutylene, and other polymers it was found to range from 0.50 to 0.74.[84,85] When η_0 is proportional to $M^{3.4}$, as frequently observed[50,83,86] at sufficiently high values of M and c, and $\gamma = 0.68$, η_0 is then proportional[79,83] to c^5. Fifth-power dependence on c has been observed over limited concentration ranges, but must be considered as an empirical approximation because it includes a concentration dependence of ζ_0 or a_c which should preferably be described by a relation of the form of equation 12.

In systems such as the poly(*n*-butyl methacrylate) solutions of Fig. 17-17, where the entanglement coupling appears to be intensified by some kind of specific attractive forces (hyperentanglements) and M_e is proportional to v_2 to a higher negative power than unity, *e.g.*, -2.6, it follows from the preceding discussion than η_0 should be proportional to a very high power of concentration. This is in fact found to be the case;[56] the viscosity for these poly(*n*-butyl methacrylate) solutions is

proportional to $c^{14.4}$ in the concentration range from 30 to 50% polymer. (A very strong concentration dependence can also be observed in the absence of hyperentanglements when the solution is near its glass transition temperature, but this is due to a rapid variation of a_c in equation 28 rather than to the v_2 factor.)

When viscosities of solutions in different solvents are compared at the same values of c and M, the most important parameter is the solvent viscosity η_s, to which η_0 of the solution is proportional at moderate concentrations.[83] This cannot hold as the concentration approaches undiluted polymer, of course, because all systems must then approach η_0 of the polymer regardless of η_s. The nature of the thermodynamic interaction between polymer and solvent appears to be of minor importance,[81,83] although higher viscosities in poor than in good solvents have been reported.[88]

An alternative correlation of the dependence of viscosity on concentration and molecular weight is to treat the dimensionless product of concentration and intrinsic viscosity as the significant independent variable.[89–91] Many other empirical relations have been proposed.[92]

The above comparisons are all isothermal. The temperature dependence of viscosity in concentrated polymer solutions can be explained very well in terms of free-volume parameters as discussed in Section A.[20,21,50] Over limited temperature ranges, it can be expressed alternatively by an Arrhenius form of equation with an apparent activation energy ΔH_η. The latter quantity increases with concentration; it has been observed in several cases to increase linearly[83,93,94] over a moderate range. This relation is useful for empirical purposes.

2. Terminal Relaxation Time and Steady-State Compliance

The Graessley and Doi-Edwards theories can also be applied to predict the dependence of the terminal relaxation time (identified as τ_w or τ_d respectively) on concentration when Mc/ρ_2 is substantially greater than M_C^0 (or, approximately, $2M_e^0$). Replacement of ρ_2 by c in equations 53 and 57 respectively gives

$$\tau_w = 1.798\, M_e \eta_0 / cRT \tag{31}$$

$$\tau_d = (10/\pi^2) M_e \eta_0 / cRT \tag{32}$$

and combination with equations 29 and 30, together with the relation $M_e = M_e^0 v_2^{-1}$ (excluding hyperentanglements), provides

$$\tau_w \propto \zeta_0 v_2^{1.5} M^{3.5} \tag{33}$$

$$\tau_d \propto \zeta_0 v_2 M^3 \tag{34}$$

or, following the formulation of equation 28, at constant M,

$$\tau_1 / \tau_{1,0} = a_c v_2^{b-1} \tag{35}$$

where $\tau_{1,0}$ is the terminal relaxation time of the undiluted polymer. Thus, the effect of dilution in the terminal zone is greater than that in the transition zone (specified by a_c) by an additional factor of v_2 or $v_2^{1.5}$ depending on the theory or $v_2^{1.4}$ based on

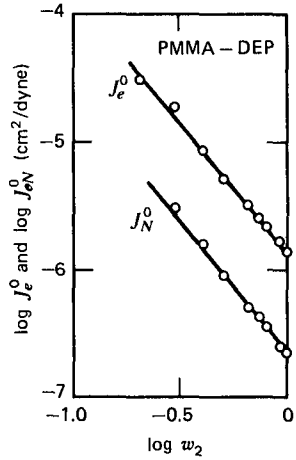


FIG. 17-20. Logarithmic plots of J_e^0 and J_N^0 against weight fraction of polymer for solutions of poly(methyl methacrylate), $\overline{M}_w = 1.91 \times 10^5$, in diethyl phthalate. Lines drawn with slope of −2. (Masuda, Toda, Aoto, and Onogi.[44]) Reproduced, by permission, from *Polymer Journal*.

empirical results. The difference can be seen qualitatively in Fig. 17-3, where the terminal zone of creep is shifted to shorter times by dilution to a greater extent in the terminal than in the transition zone. Alternatively, it is evident from equation 31 or 32 that τ_1 is proportional to $\eta_0 v_2^{-2}$.

[In a formal manner, a concentrated solution can be described as a blend in which the solvent does not contribute to the relaxation spectrum. A quadratic blending law such as equation 25 of Chapter 13 would then reduce, in terms of the relaxation modulus, to

$$G(t) = v_2^2 G_2(t/\lambda_2) \tag{36}$$

in which the magnitudes of the modulus contributions are reduced by v_2^2 in agreement with equation 22 and the terminal relaxation time (or times) is reduced by a factor $\lambda_2 = a_c v_2^{b-1}$ in accordance with equation 35. Thus the behavior as described is consistent with a quadratic blending law. Earlier attempts to represent the concentration dependence of viscoelastic properties in the terminal zone by a linear blending law,[13] although apparently successful, are not applicable because they imply an erroneous dependence of G_N^0 on v_2 rather than v_2^2.]

The steady-state compliance, as expressed by the theories of Graessley or Doi and Edwards for undiluted polymers (equations 52 and 56 of Chapter 10), is proportional to M_e/ρ and independent of M when $M \gg M_c'$. For concentrated solutions, ρ must be replaced by $c = \rho v_2$, and, if $M_e = M_e^0 v_2^{-1}$ as discussed in Section B1 above, the concentration dependence of J_e^0 under conditions of high entanglement becomes

$$J_e^0 = (J_e^0)^0 v_2^{-2} \tag{37}$$

where $(J_e^0)^0$ is the value for the undiluted polymer. Inverse proportionality to v_2^2 has been repeatedly observed;[43,95] an example is shown in Fig. 17-20 for solutions

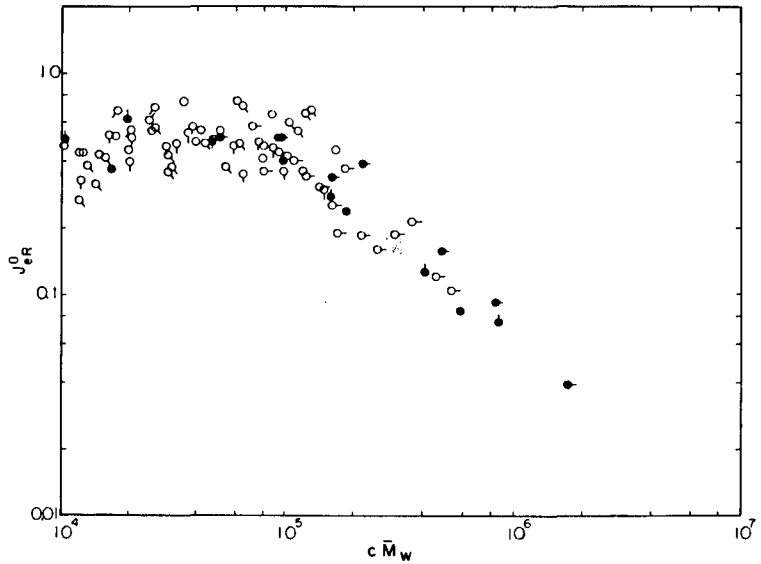


FIG. 17-21. Reduced steady-state compliance J^0_{eR} plotted against $c\overline{M}_w$ with logarithmic scales for solutions (open circles) and undiluted samples (black circles) of narrow-distribution polystyrenes. Data from various measurements and various sources. (Graessley.[43]) Reproduced, by permission, from *Advances in Polymer Science*.

of poly(methyl methacrylate) in diethyl phthalate[44] (plotted against weight fraction w_2, which differs only slightly from v_2). The plateau compliance $J^0_N = 1/G^0_N$ is also shown; the ratio J^0_e/J^0_N is about 5 independent of concentration (compare Table 13-IV and associated discussion for undiluted polymers). More complicated dependence of J^0_e on v_2 or c, including an exponent in equation 37 approaching -3 as v_2 approaches 1, has also been observed.[95-97]

In some analyses, a dimensionless reduced steady-state compliance $J^0_{eR} = [J^0_e cRT/M][\eta_0/(\eta_0 - \eta_s)]^2$ has been used; this is the same quantity that was defined by equation 51 of Chapter 9. Under conditions of high entanglement, the last factor in brackets is indistinguishable from unity and equation 37 implies that J^0_{eR} is proportional to v_2^{-1} and M^{-1}.

It may be noted that under conditions of high entanglement the dependence of η_0 on c and M should be the ratio of the dependences of τ_1 and J^0_e on these variables, in accordance with equations 53 and 57 of Chapter 10.

At lower concentrations, where Mv_2 is no longer much larger than $(M'_c)^0$ and the effects of entanglement on steady-state compliance are incomplete, J^0_e decreases less rapidly with decreasing concentration and becomes proportional to v_2^{-1}; it also becomes directly proportional to the molecular weight instead of independent of it. Thus J^0_{eR} becomes independent of both concentration and molecular weight. An example is shown in Fig. 17-21 for both concentrated solutions of and undiluted polystyrenes of different molecular weights,[43] with J^0_{eR} derived from a variety of experimental measurements[98-101] (hence perhaps the scatter). The boundary between the two regimes (J^0_e proportional to v_2^{-2} and independent of M; J^0_e propor-

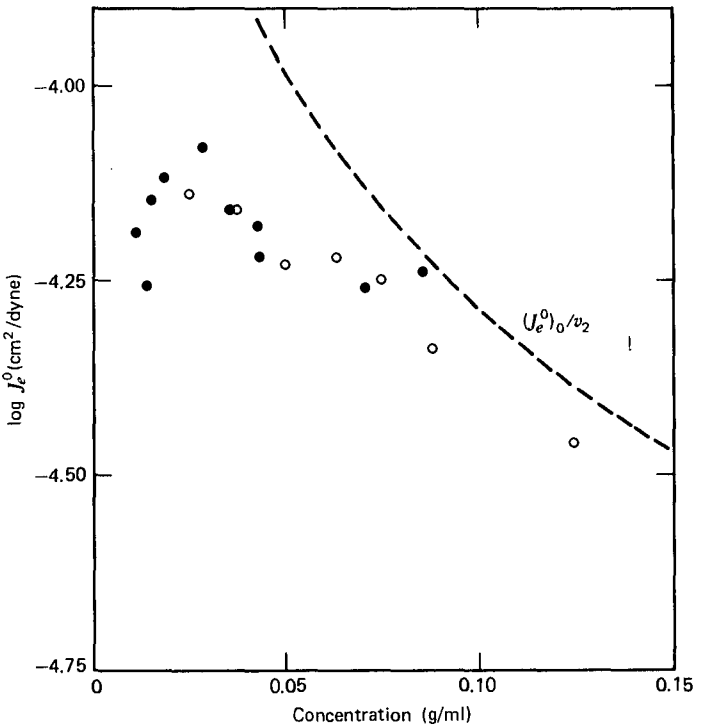


FIG. 17-22. Plot of log J_e^0 against concentration for solutions of polystyrene, M_w = 267,000, in chlorinated diphenyl, in the lower concentration range where J_e^0 passes through a maximum. (Holmes, Ninomiya, and Ferry.[102]) Open and black circles refer to solutions in solvents of different viscosities.

tional to $v_2^{-1}M$) appears at a value of $c\overline{M}_w$ of about 1.3×10^5, in agreement with M'_C in Table 13-III. The constant value of J_{eR}^0 at $c\overline{M}_w < 1.3 \times 10^5$ is roughly 0.4, which would be specified by the Rouse theory in the absence of entanglements (equation 15 of Chapter 13 with ρ replaced by c). This value of J_{eR}^0 has been found in numerous studies in the appropriate range of cM, where J_e^0 has been determined from low-frequency measurements of G' and the constant A_G, from flow birefringence, or from the primary normal stress difference; many data are reviewed in reference 43.

At still lower concentrations, J_e^0 passes through a maximum, since at vanishing concentration it must be directly instead of inversely proportional to v_2 or c; in the context of the bead-spring theories of Section B of Chapter 9, at sufficiently low concentrations,

$$J_e^0 = (S_2/S_1^2)cM[\eta]^2/RT \tag{38}$$

where $[\eta]$ is the intrinsic viscosity (*cf.* equation 13 of Chapter 9), and in a Θ-solvent S_2/S_1^2 should have the Zimm value of 0.206. An example[102] of the maximum is shown in Fig. 17-22. It is analogous to the maximum in blends of two undiluted

polymers of different low molecular weights without entanglements, as illustrated in Fig. 10–4, the solvent representing the component of lower molecular weight. The linear blending law of Ninomiya[103] (equation 26 of Chapter 10) can be applied; it predicts[102,103] that the maximum will appear at $c \cong \sqrt{2}/[\eta]$. The magnitude of the maximum is predicted to be $J_e^0(\max) = (J_e^0)^0[\eta]\rho_2/4\sqrt{2}$ if $M < M_C'$; if $M > M_C'$, there is an additional factor of M/M_C'.[49]

3. Effects of Branching and Molecular Weight Distribution

The influence of branching and molecular weight distribution on η_0, J_e^0, and relaxation times in the terminal zone for concentrated solutions is qualitatively similar to that observed in undiluted polymers as described in Sections C4 and C5 of Chapter 13 but with some additional complications.

The ratio η_{0B}/η_{0L}, when B and L refer to star-branched and linear polymers of the same molecular weight, remains less than unity in concentrated solutions of polystyrenes[104] and polyisoprenes[104a] up to rather high molecular weights, but is greater than unity when the molecular weight is extremely high.[104a] Similarly, for randomly branched polystyrenes, η_{0B} is less than η_{0L} and the difference can be explained by the factor g defined in Chapter 13.[105] With increasing concentration, J_e^0 for four-arm star polystyrenes[106] is at first proportional to $c^{-1}M$ and then to c^{-2} and independent of M as described for linear polymers, but at still higher concentrations J_e^0 falls more sharply with increasing c and passes through a minimum. A complicated dependence of J_e^0 on c and M has been studied in solutions of four-arm and six-arm star polyisoprenes.[104a] The critical molecular weight M_C' above which J_e^0 becomes independent of M is much higher for the branched than for linear polymers at the same concentration. The concentration dependence of J_e^0 shows some curious inflections. In randomly branched polystyrenes,[105] J_e^0 was found to be proportional to $M^{0.84}$ and nearly independent of concentration in a region of c and M where J_e^0 for linear polymers is proportional to c^{-2} and independent of M. The effects of branching on these and other properties have been reviewed by Graessley.[106a]

In concentrated solution blends of two polymer components of different molecular weight at a constant total polymer concentration, η_0 is determined by $\overline{M}_w$ of the polymer blend, while J_e^0 is in general higher than that of either of the components. The dependence of J_e^0 on blend proportions, and to some extent the time or frequency dependence of viscoelastic functions, can be described by a cubic blending law[107] (*cf.* Section C5 of Chapter 13). At considerably lower concentrations, however, a linear blending law is fairly satisfactory.[108]

D. NONLINEAR VISCOELASTIC BEHAVIOR IN THE TERMINAL ZONE

A wider variety of nonlinear behavior has been investigated in concentrated solutions than in undiluted polymers because stresses are smaller and more con-

veniently measured, introduction of samples into apparatus is easier, and elevated temperatures are not required. Most of the examples cited refer to deformation in shear.

1. Dependence of Non-Newtonian Shear Viscosity on Shear Rate

The character of non-Newtonian viscosity in concentrated polymer solutions is very similar to that of undiluted polymers as discussed in Section C2 of Chapter 13. An example is shown in Fig. 17-23 for narrow-distribution polystyrene. With decreasing concentration, the onset of non-Newtonian behavior shifts to higher shear rates. At high shear rates, the logarithmic plot becomes linear, as seen in Fig. 10-20, but the slope β becomes less negative with decreasing concentration; it appears to be determined by the product $c[\eta]$, which is a measure of the degree of coil overlap, as shown in Fig. 17-24, and at high concentrations it approaches the value of about -0.8 observed in several undiluted polymers.

Values of η measured at different temperatures can be reduced to a single curve as described for undiluted polymers with concentration c substituted for polymer density ρ; η/η_0 is plotted logarithmically against $\dot{\gamma}\eta_0 T_0 c_0/\eta_{00} Tc$. Moreover, at concentrations sufficiently high that β approaches its maximum negative value ($c[\eta] > 30$), the shapes of the curves at different concentrations are similar[43] and all can be combined by plotting η/η_0 logarithmically against $\dot{\gamma}\tau_\eta$, as shown in Fig. 17-25 for narrow distribution polystyrene solutions studied by Graessley and collaborators.[109,110] Here τ_η is (*cf.* Section E1 of Chapter 10) a characteristic time that is the reciprocal of $\dot{\gamma}$ corresponding to $\eta/\eta_0 \cong 0.8$. Under conditions of high entanglement, τ_η is found to be proportional to $\eta_0 v_2^{-2}$, as is the terminal relaxation time τ_1 (Section C2 above).[110-112] However, at lower concentrations τ_η is proportional to $\eta_0 M v_2^{-1}$, as is the terminal relaxation time in the absence of entan-

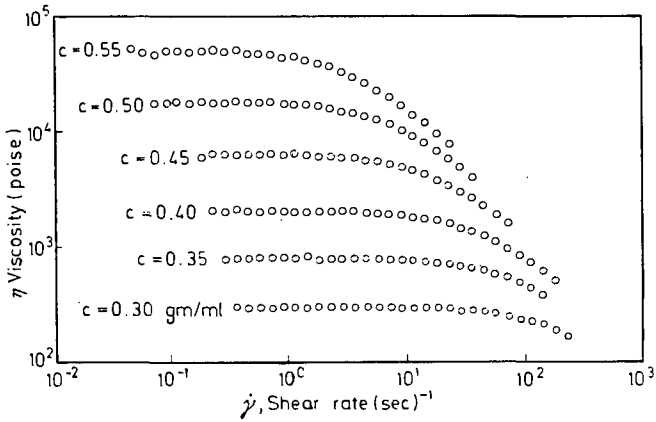


FIG. 17-23. Logarithmic plots of non-Newtonian viscosity against shear rate for solutions of polystyrene, M_w = 411,000, in *n*-butyl benzene at 30°, with various concentrations as shown. (Graessley, Hazleton, and Lindeman.[110]) Reproduced, by permission, from *Advances in Polymer Science*.

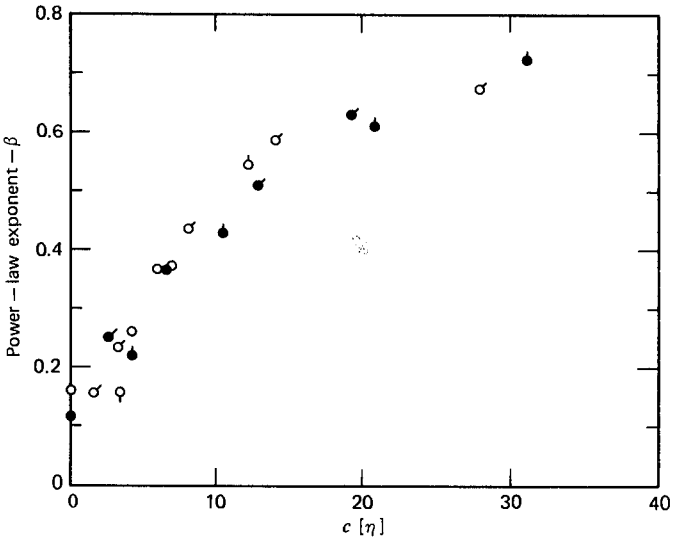


FIG. 17-24. Power law exponent β as a function of the coil overlap parameter $c[\eta]$, for solutions of polystyrene (black circles) and poly(α-methyl styrene) (open circles), mostly in chlorinated diphenyls. Molecular weights range from 0.86 to 13.6 × 10^6 for polystyrene; from 0.44 to 7.5 × 10^6 for poly(α-methyl styrene). (Graessley.[43]) Reproduced, by permission, from *Advances in Polymer Science*.

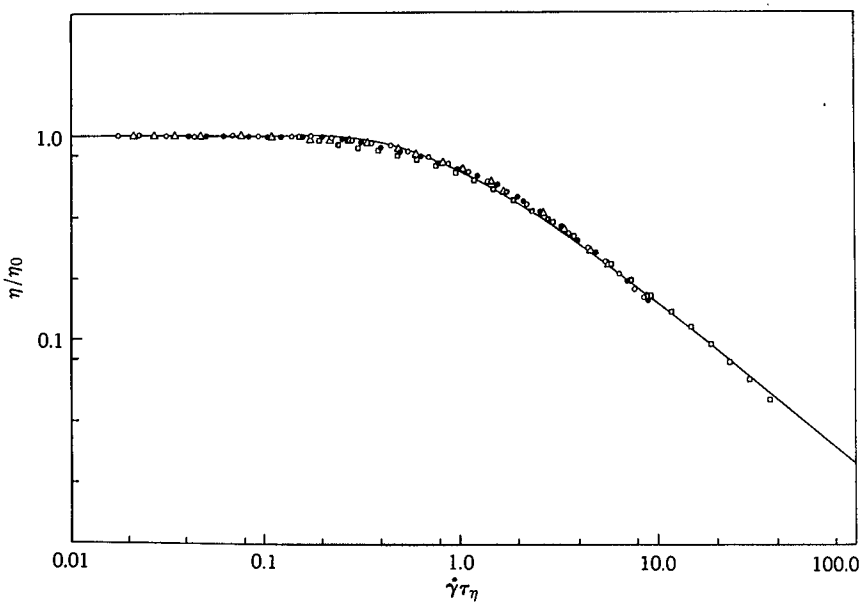


FIG. 17-25. Non-Newtonian viscosity ratio η/η_0 for solutions of narrow-distribution polystyrenes in *n*-butyl benzene, plotted logarithmically against log $\dot{\gamma}\tau_\eta$ with characteristic time constant τ_η chosen empirically for each solution. Molecular weights from 0.16 to 2.4 × 10^6, concentrations from 0.20 to 0 55 g/cc. Solid curve from Graessley theory.[109,110]

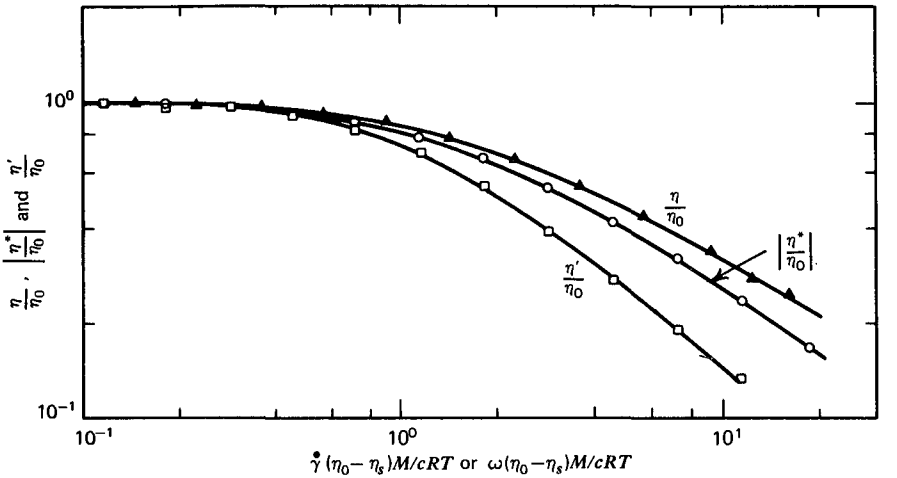


FIG. 17-26. Comparison of $\eta(\dot{\gamma})$, $\eta'(\omega)$, and $|\eta^*|(\omega)$ normalized by η_0 and plotted against $\dot{\gamma}$ and ω respectively multiplied by $(\eta_0 - \eta_s)M/cRT$, for a solution of polystyrene in chlorinated diphenyl at 25°C; M_w = 860,000, c = 0.071 g/ml. (Harris.[113]) Reproduced, by permission, from *Advances in Polymer Science*.

glements as given by the Rouse theory (equation 7 of Chapter 10 with ρ replaced by c).[43] Again τ_1 and τ_η are very similar in behavior (*cf.* Section C2 of Chapter 13). Over a considerable range of the product cM, the ratio $J_e^0\eta_0^2/\tau_\eta(\eta_0 - \eta_s)$ is found to vary within relatively narrow limits for a variety of polymers.[43]

The characteristic times τ_1 and τ_η are also similar in magnitude, as noted in Section C3 of Chapter 13, so the drop in η'/η_0 with increasing radian frequency ω resembles that in η/η_0 with increasing $\dot{\gamma}$; an example is shown in Fig. 17-26, for a moderately concentrated solution of polystyrene.[113,43] A plot of $|\eta^*|/\eta_0$ is also shown, which according to the Cox-Merz rule should resemble η/η_0 more closely[114]; *cf.* Section C2 of Chapter 13. At higher values of ω, the dynamic and steady flow deformations must involve entirely different molecular motions. Even at relatively low $\dot{\gamma}$ and ω, there is deviation from the Cox-Merz rule in polystyrene solutions when the product cM is very high ($> 10^6$).[115] The decrease in η with increasing $\dot{\gamma}$ can be understood qualitatively as due to a decrease in the density of entanglements during flow, as described by the Graessley theory[43] and discussed in Chapter 10.

In solutions of star-branched polyisoprenes, the characteristic time τ_η is greater than for linear polymers of the same molecular weight when c and M are sufficiently high that both η_0 and J_e^0 are enhanced by the branching. However, the ratio $\eta_0 J_e^0/\tau_\eta$ (*cf.* equation 21 of Chapter 13) is not only nearly independent of c and M but also nearly the same for linear, four-arm, and six-arm branched polymers.[104a]

2. Creep and Creep Recovery

When stresses are large enough to cause deviations from linear viscoelasticity, not only the steady-flow viscosity but also the entire creep and creep recovery be-

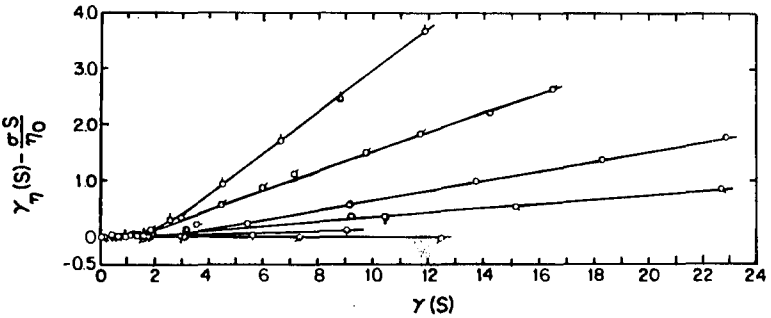


FIG. 17-27. Plot of $\Delta\gamma(t)$ defined by equation 41 against strain for solution of poly(α-methyl styrene) in α-chloronaphthalene at 0.25° C; $M_w = 1.8 \times 10^6$, $c = 0.192$ g/ml. Curves from bottom to top correspond to stresses of 980, 2340, 3370, 6050, and 8910 dynes/cm^2. (Berry, Hager, and Wong.[116]) Reproduced with permission from *Macromolecules*, **10**, 363 (1977). Copyright by The American Chemical Society.

havior requires a more complicated description than the simple creep compliance $J(t)$ that is defined for linear conditions. In a thorough study by Berry, Hager, and Wong,[116] the following functions are defined:

$$J_\sigma(t) = \gamma(t)/\sigma \tag{39}$$

This describes creep after imposition of stress σ under nonlinear conditions; it becomes $J(t)$ for small σ. Also,

$$\gamma_\eta(t) = \sigma J_\sigma(t) - \gamma_{R,\sigma}(t, \infty) \tag{40}$$

Here $\gamma_{R,\sigma}(t, \infty)$ is the total recovered strain after cessation of creep for time t under stress σ. The quantity $\gamma_\eta(t)$ is a measure of the viscous deformation in a time interval t and for the linear case would be $\sigma t/\eta_0$. Finally,

$$\Delta\gamma(t) = \gamma_\eta(t) - \sigma t/\eta_0 \tag{41}$$

is a measure of the effect of nonlinearity on the viscous deformation.

In Fig. 17-27, $\Delta\gamma(t)$ is plotted against the total strain achieved in the time interval t, for several stresses.[116] It is evident that it remains zero for γ less than a critical value γ^* which in this case is about 1.7 independent of the stress. Thus exceeding a critical strain rate $\dot{\gamma}$ (as measured by τ_η^{-1}) is a necessary but not a sufficient condition for onset of nonlinear flow behavior; it is also necessary that the total strain exceed a critical value γ^*. The factors influencing the magnitude of γ^* are not yet clearly determined, but it generally appears to be of the order of unity. At higher γ, the deviation from linear behavior increases with the magnitude of stress applied. In steady-state shear flow, the criterion $\gamma > \gamma^*$ is automatically satisfied. This behavior can be understood qualitatively in terms of a finite deformation required to diminish the density of entanglements, and it is related to the phenomenon of stress overshoot to be discussed in Section 5 below.

The steady-state shear compliance as determined by recovery after cessation of steady-state non-Newtonian flow may be defined by analogy with equations 40

and 41 of Chapter 1 as

$$R_{\dot{\gamma}} = [\gamma(t_2) - \gamma(\infty)]/\sigma \tag{42}$$

where $\gamma(t_2)$ is the shear strain at the time t_2 (long enough so steady-state flow has been achieved) when the stress σ is removed, and $\gamma(\infty)$ is the residual strain after recovery is complete. The limit of $R_{\dot{\gamma}}$ as σ approaches zero is J_e^0. With increasing stress, $R_{\dot{\gamma}}$ appears at first to decrease but subsequently depends on stress in a complicated manner.[116]

3. Normal Stress Differences

The primary normal stress coefficient at low shear rates, $\Psi_{1,0}$, gives the same information as J_e^0, as specified by equation 74 of Chapter 3:

$$\Psi_{1,0} = 2\eta_0^2 J_e^0 \tag{43}$$

and some of the information on J_e^0 discussed in Section C2 above was derived from this source. In a few cases, equation 43 has been tested by combining normal stress data with creep recovery.[43] At higher shear rates, there is not a simple relation between Ψ_1 and $R_{\dot{\gamma}}$. However, Ψ_1 does decrease with increasing $\dot{\gamma}$ as was seen in Fig. 2-10, where $\sigma_{11} - \sigma_{22}$ increases less rapidly than proportional to $\dot{\gamma}^2$. Another example is shown in Fig. 17-28, where Ψ_1 falls by several orders of magnitude with increasing $\dot{\gamma}$.

The ratio $\Psi_1/2\eta^2$, where both numerator and denominator depend on shear rate, is another function which approaches J_e^0 as $\dot{\gamma}$ approaches zero; this is denoted $S_{\dot{\gamma}}$ by Berry and collaborators.[116] The ratio $S_{\dot{\gamma}}/J_e^0$ is plotted together with η/η_0 in Fig. 17-29 for solutions of poly(α-methyl styrene) in α-chloronaphthalene in ranges of c and M where $cM > (M'_C)^0$ (the value of M'_C for the undiluted polymer—*cf.* Table 13-III) from data of Nagasawa and collaborators.[97] The shear rate is reduced by a characteristic time τ_0, which is proportional to η_0/c^2RT in conformity to the discussion in Section C2 above for highly entangled systems, and all data at different c and M superpose. The shear rate dependence of $S_{\dot{\gamma}}$ is positive but less marked than that of η.

4. Stress Relaxation after Large Sudden Strains

After imposition of a large sudden shear strain, stress relaxation can be described by the apparent modulus $G_\gamma(t) = \sigma(t)/\gamma$, defined by analogy with equation 39 above. This may decrease dramatically with increasing γ as already seen in Fig. 2-12. Another example[117] is shown in Fig. 17-30. Here data at two different temperatures for a polystyrene solution with concentration 0.221 g/cm^3 have been combined by reduced variables.[117] It is evident that with increasing strain the magnitude of the apparent modulus in the terminal zone is greatly diminished but the time scale of the relaxation is not much affected. This behavior can be analyzed quantitatively by expressing $G_\gamma(t)$ as a series of exponential terms (*cf.* equation 17 of Chapter 3 for the corresponding case for linear viscoelasticity):

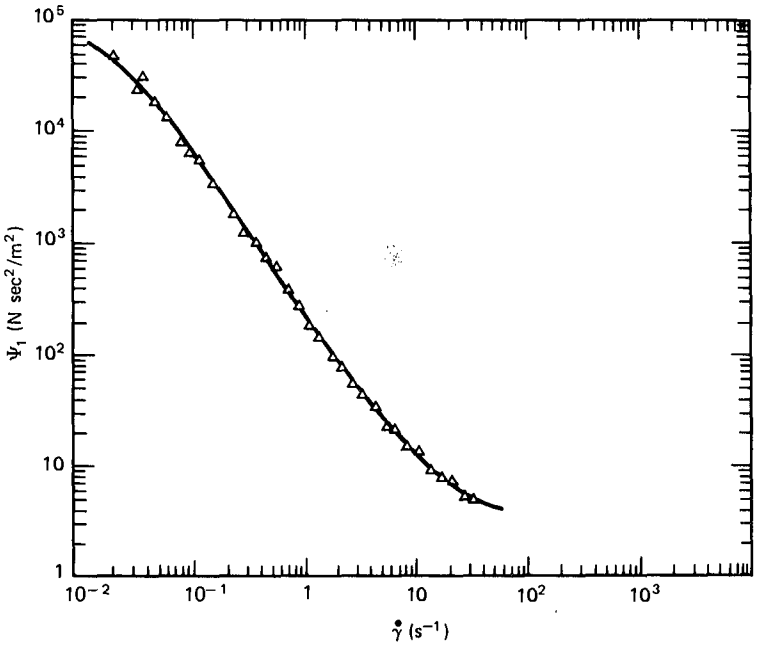


FIG. 17-28. Plot of primary normal stress coefficient against shear rate with logarithmic scales for 20% solution of polyisobutylene in Primol D oil at 25°C. (Data of Huppler, Ashare, and Holmes.[123]) Reproduced, by permission, from *Dynamics of Polymeric Liquids,* by R. B. Bird, R. C. Armstrong, and O. Hassager, John Wiley and Sons, New York, 1977.

$$G_\gamma(t) = \sum_{i=1}^{\infty} G_i(\gamma) e^{-t/\tau_i(\gamma)} \tag{44}$$

and estimating the two longest relaxation times τ_1 and τ_2, with their modulus contributions G_1 and G_2, by suitable plotting methods.[118] The results are shown in Fig. 17-31. The relaxation times are independent of the imposed strain over a

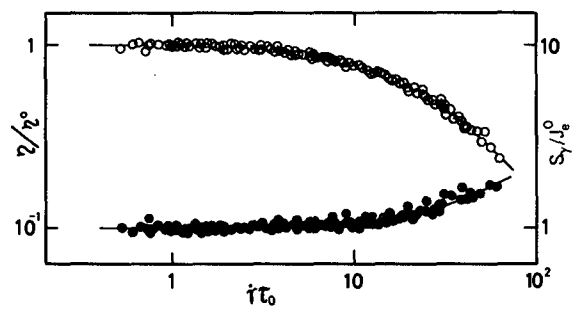


FIG. 17-29. Plots with logarithmic scales of S_γ/J_e^0 (black circles) and η/η_0 (open circles) against $\dot{\gamma}\tau_0$ for concentrated solutions of poly(α-methyl styrene) in α-chlonaphthalene. The characteristic time τ_0 is proportional to η_0/c^2RT. (Sakai, Fujimoto, and Nagasawa;[97] after Graessley.[43]) Reproduced, by permission, from *Advances in Polymer Science.*

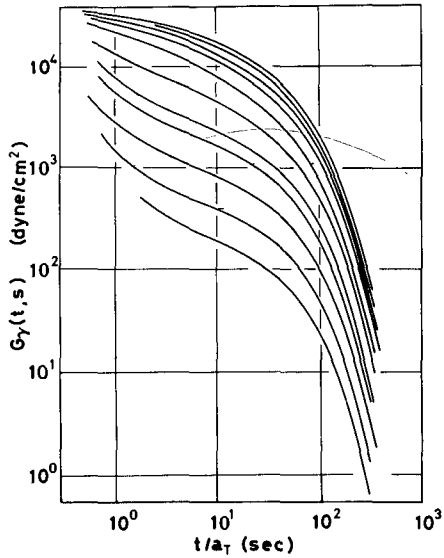


FIG. 17-30. Plots with logarithmic scales of nonlinear relaxation modulus $G_\gamma(t)$ against time reduced to 30°C for a solution of polystyrene ($M = 3.10 \times 10^6$, $c = 0.221$ g/ml) in diethyl phthalate. Temperatures of measurement 10.5 and 30°C. Magnitude of shear, from top to bottom: 0.166 and 0.222 (these coincide), 0.44, 1.11, 1.88, 3.34, 5.22, 6.68, 10.0, 15.3, and 20.5. (Fukuda, Osaki, and Kurata.[117]) Reproduced, by permission, from *The Journal of Polymer Science*.

large range but the modulus contributions drop by two orders of magnitude. Similar behavior has been found for numerous concentrated solutions.[119,120] However, for extremely high values of the product cM ($>10^6$), the curve for decreasing G_1 with increasing γ has a more complicated shape with a hint of a plateau at intermediate strains. Qualitative agreement with these phenomena is predicted by the relaxation theory of Doi.[121]

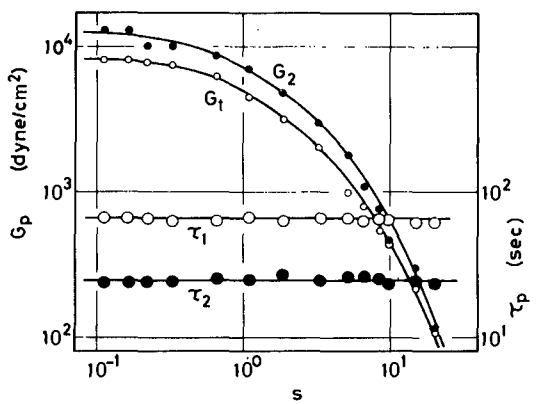


FIG. 17-31. Plots with logarithmic scales of G_1, G_2, τ_1, *and* τ_2 (*cf.* equation 44) against magnitude of shear from the data of Fig. 17-30. (Fukuda, Osaki, and Kurata.[117]) Reproduced, by permission, from *The Journal of Polymer Science*.

5. Stress Growth and Relaxation following Initiation and Cessation of a Constant Shear Rate

If a constant shear rate $\dot{\gamma}$ is imposed on a viscoelastic liquid, the stress rises as described by $\sigma(t)$ or the time-dependent viscosity function $\eta^+(t) = \sigma(t)/\dot{\gamma}$, and these quantities approach their steady-state values as steady flow is reached. If the steady-state flow is terminated, the subsequent stress relaxation is described by $\sigma^{ss}(t)$ or the time-dependent viscosity function $\eta^-(t)\dot{\gamma}$, discussed in Sections C2 and C3 of Chapter 1. If the viscoelastic behavior is linear, these functions are monotonic and related to the relaxation modulus $G(t)$ by equations 13 and 14 of Chapter 1. The functions $\eta^+(t)$ and $\eta^-(t)$ are independent of $\dot{\gamma}$ and their sum is simply η_0. At large strain rates, however, both $\eta^+(t)$ and $\eta^-(t)$ become strongly dependent on $\dot{\gamma}$.

An example of stress growth is shown in Fig. 17-32 for a concentrated solution of polystyrene in chlorinated biphenyl.[122] The steady-state value of $\eta^+(t)$ is the ordinary non-Newtonian viscosity $\eta(\dot{\gamma})$ which decreases with increasing $\dot{\gamma}$. At high $\dot{\gamma}$, $\eta^+(t)$ does not increase monotonically but passes through a maximum. This phenomenon of stress overshoot has been observed repeatedly.[123-127] Another example for a solution of poly(α-methyl styrene) is shown in Fig. 17-33, where the shear stresses are normalized by their maximum values and combined with data on normal stress differences to be mentioned below. Qualitatively, the phenomenon can be understood in terms of a finite time and finite magnitude of shear required to accomplish the reduction in the density of entanglements to which the non-Newtonian viscosity is attributed; in Fig. 17-32, at high $\dot{\gamma}$, the viscosity first starts as though heading for the low-shear-rate value, but only later "decides" to drop down to the steady-state value characteristic of the high-shear-rate condition. The

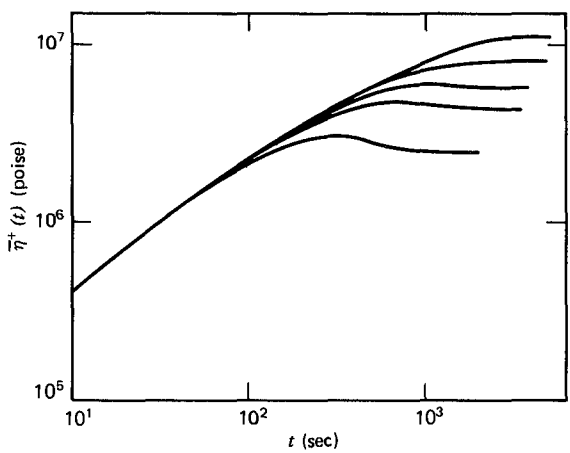


FIG. 17-32. Plots with logarithmic scales of stress growth viscosity $\eta^+(t)$ against time for a solution of polystyrene in chlorinated diphenyl ($M = 1.80 \times 10^6$, $w_2 = 0.20$) at 30°C. Rates of shear from top to bottom, $\times 10^3$: 0.170, 0.865, 2.30, 3.61, and 8.86 sec^{-1}. (Osaki, Einaga, Yamada, and Kurata.[122]) Reproduced by permission, from *Polymer Journal*.

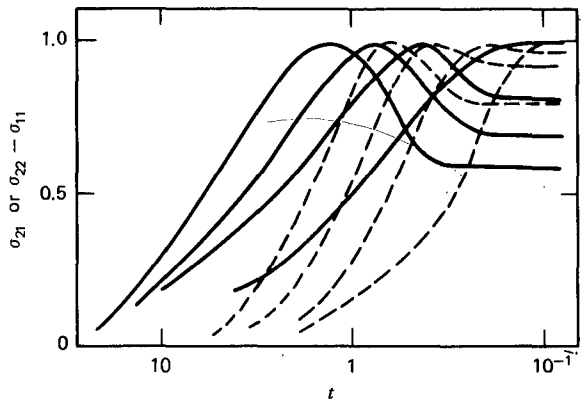


FIG. 17-33. Plots of ratios of σ_{21} (solid curves) and $\sigma_{22} - \sigma_{11}$ (dashed curves) to their respective maximum values during stress growth at constant shear rate for a solution of poly(α-methyl styrene) in chlorinated diphenyl, $M = 1.25 \times 10^6$, $w_2 = 0.101$. Rates of shear, left to right: 4.29, 2.15, 1.08, and 0.27 sec^{-1}. (Sakai, Fukaya, and Nagasawa.[124]) Reproduced, by permission, from the *Transactions of the Society of Rheology*.

phenomenon is qualitatively related to the strain magnitude criterion for nonlinear creep behavior as discussed in Section D3 above.

An example of stress decay after cessation of steady flow is shown in Fig. 17-34 for the same solution as in Fig. 17-32. The time-dependent viscosity $\eta^-(t)$ is smaller for higher $\dot{\gamma}$ throughout the relaxation process but the time scale of the relaxation

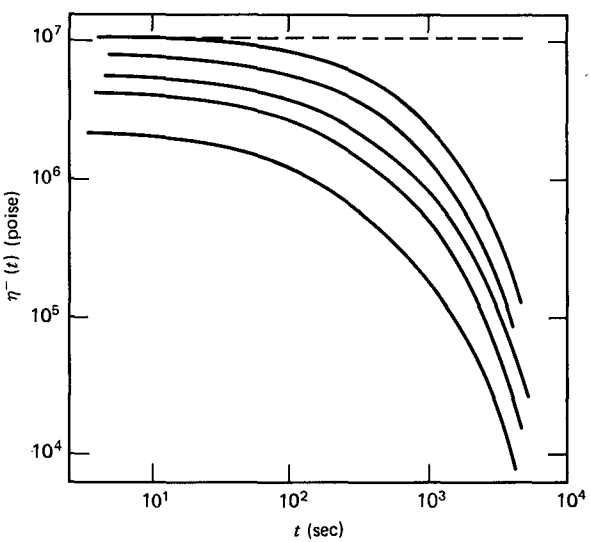


FIG. 17-34. Plots with logarithmic scales of the stress relaxation viscosity $\eta^-(t)$ after cessation of flow for the solution of Fig. 17-32. Shear rates from top to bottom same as in Fig. 17-32. Dashed line is $\eta^+(t) + \eta^-(t)$ for $\dot{\gamma} = 0.170 \times 10^{-3}\ s^{-1}$. (Osaki, Einaga, Yamada, and Kurata.[122]) Reproduced, by permission, from *Polymer Journal*.

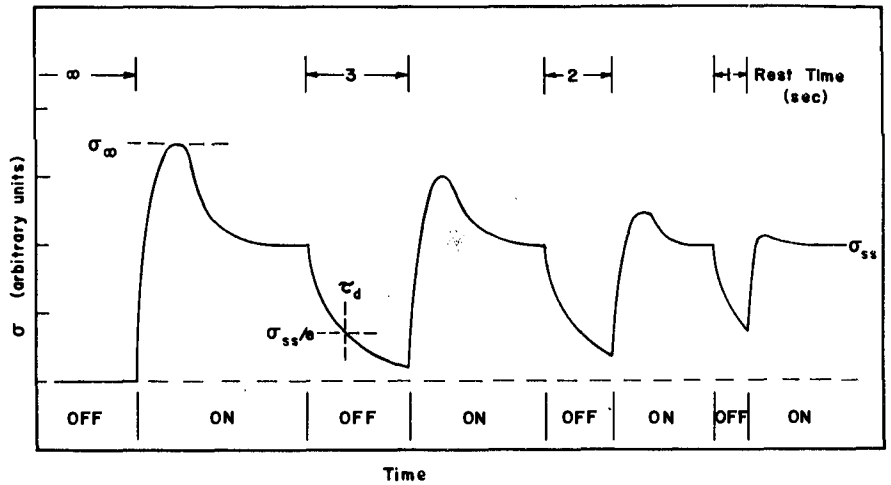


FIG. 17-35. Shear stress growth and relaxation for successive impositions of a constant shear rate with intervening rest periods of different lengths, for a 3% polyisobutylene solution ($\overline{M}_w = 2.8 \times 10^6$) at 25°C. (Stratton and Butcher.[128]) Reproduced, by permission, from the *Journal of Polymer Science*.

is not much affected. In fact, if $\eta^-(t)$ in such an experiment is represented by a series of exponential terms analogous to equation 44, the longest relaxation time is found to be independent of the magnitude of $\dot{\gamma}$ preceding the relaxation,[115] as in Fig. 17-31. The contributions associated with the longest relaxation times are greatly reduced in magnitude, however. Such results have often been described in terms of a relaxation spectrum which is dependent on the shear rate preceding cessation of flow, and the long-time part of the spectrum is truncated. In a previous example of this nonlinear relaxation shown in Fig. 2-13, the stress $\sigma^{ss}(t)$ normalized by its steady-state value appears to relax faster for a high shear rate preceding cessation of flow; this difference may be associated with a lower concentration in the latter case, corresponding to a different entanglement regime.

During the relaxation, the density of entanglements is presumably increasing toward the value characteristic of the rest state, but the new entanglements of course do not contribute to the stress. The course of this process can be followed by the ingenious "stop-start" experiments of Stratton and Butcher,[128] as illustrated schematically in Fig. 17-35. If the shear rate is resumed after a brief interval of relaxation, the overshoot is smaller because the rest-state entanglement density has not been fully established. A plot of the stress at the overshoot maximum against the logarithm of the rest time interval, shown in Fig. 17-36, shows the time course of entanglement reestablishment. Estimates of the characteristic time τ_d for entanglement rearrangement during the relaxation phase and a time τ_e for entanglement reestablishment from Fig. 17-37, made roughly on the basis of a single exponential relation, indicated that τ_e was larger by about a factor of 10 and both times decreased with increasing $\dot{\gamma}$. The product cM in the solution studied here was smaller than in the polystyrene solution of Figs. 17-32 and 17-33; the apparent

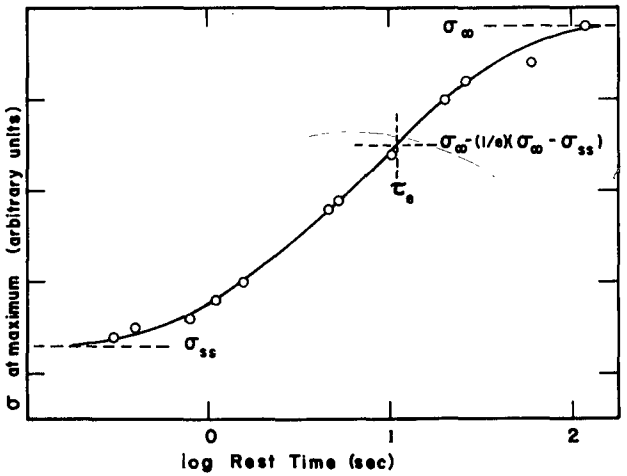


FIG. 17-36. Plot of stress overshoot maximum against logarithm of preceding rest time, from data similar to those of Fig. 17-35. (Stratton and Butcher.[128]) Reproduced, by permission, from the *Journal of Polymer Science*.

difference in dependence of time scale on $\dot{\gamma}$ may be related to this or to the presence of molecular weight distribution in the polymer of Fig. 17-37.

The observation that τ_e is greater than τ_d is reminiscent of the classical phenomenon of thixotropy as described by the colloid chemist, in which a structure

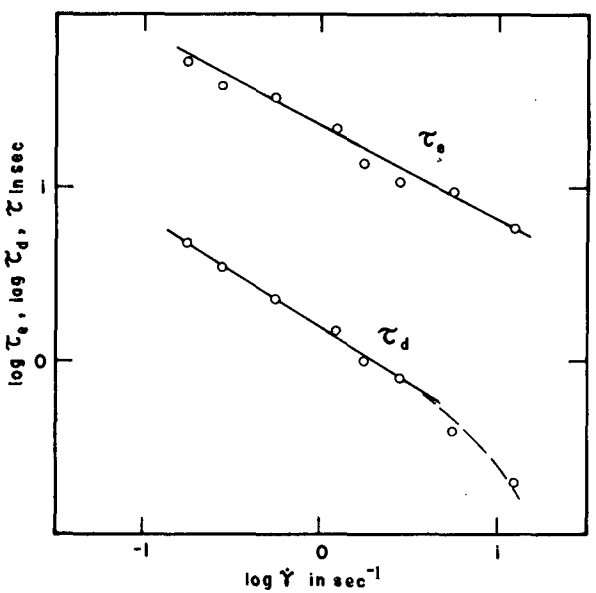


FIG. 17-37. Logarithmic plots of estimated entanglement disengagement time (τ_d) and entanglement reestablishment time (τ_e) for the solution of Fig. 17-35. Reproduced, by permission, from the *Journal of Polymer Science*.

of dispersed particles[129] or ordered arrays[130] is broken down by shearing and subsequently at rest reestablishes itself slowly. However, the molecular mechanisms in the latter examples are quite different, and it would be dangerous to reason by analogy from one system to another.

Examples have also been observed in which an entanglement network of flexible macromolecules appears to be enhanced, rather than diminished, by shearing.[131]

The qualitative interpretation of these phenomena has been given here in the vocabulary of entanglements; with the alternative tube model of topological restraint, the theory of Doi and Edwards[131a] also predicts this phenomenon and is in qualitative agreement with experiment.

The primary normal stress difference also experiences an overshoot during the establishment of steady flow following onset of a constant shear rate. An example is included in Fig. 17–33; the normal stress maximum appears considerably later than the shear stress maximum, as found also in earlier measurements on a solution of polyisobutylene by Huppler and collaborators.[123] In relaxation following cessation of steady-state flow, the primary normal stress difference falls more slowly than the shear stress, as seen in Fig. 2–13 and also the measurements on poly(α-methyl styrene) by Nagasawa and collaborators;[124] when normalized by the steady-flow value, the primary normal stress difference appears to fall somewhat more rapidly with increasing $\dot{\gamma}$.

6. Combined Oscillatory and Steady-State Shear

If a viscoelastic liquid is subjected to steady-state shear at a constant rate $\dot{\gamma}_{21}$ and superimposed on this is an oscillatory shear of small maximum amplitude γ_{21} (in the parallel direction) or γ_{23} (in the transverse direction), the dynamic storage and loss moduli are found to be dependent on $\dot{\gamma}_{21}$. The geometry is illustrated in Fig. 17–38; a systematic discussion of these phenomena has been given by Markovitz[132] and Walters.[133]

An example of this effect observed in the parallel direction is shown in Fig. 17–39 from measurements of Osaki and collaborators[134] on a concentrated solution of polystyrene in toluene subjected to steady shear rates up to 5 sec^{-1} superimposed on small oscillating deformations in the range from 0.06 to 40 rad/sec. In the absence of steady shear, G' and G'' show the usual behavior of the terminal zone with slopes of 2 and 1 respectively when plotted logarithmically against frequency. With increasing shear rate, the terminal zone is shifted progressively to higher frequencies (especially as manifested in G'), though the curves converge as they enter the plateau zone. The effect appears more strikingly in Fig. 17–40 for a concentrated solution of ethylene-propylene copolymer studied by Booij.[135] Here the data are plotted logarithmically as G'/ω^2 against ω; they do not extend to low enough frequencies to reach the limiting value of this ratio, A_G. Not only is the terminal zone shifted to higher frequencies, but G'/ω^2 passes through a maximum. At very low frequencies, G' may actually be negative. This sort of behavior can be described qualitatively by a relatively simple nonlinear constitutive equation[136] and rather

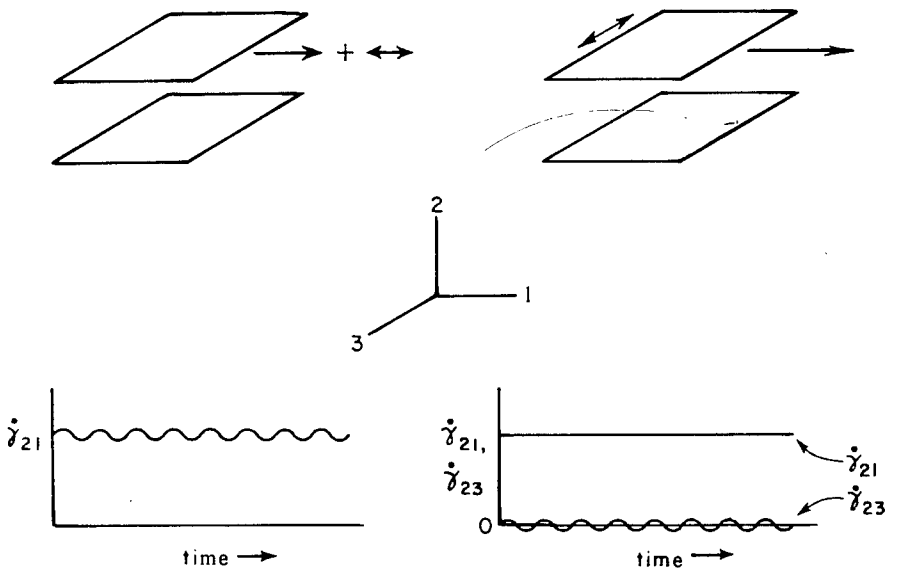


FIG. 17-38. Geometry for combined steady state shear with oscillating shear in parallel and transverse directions.

well quantitatively by the nonlinear model of Spriggs, Huppler, and Bird.[137-138] It corresponds to a sharp loss in contributions associated with the longest relaxation times under conditions of high $\dot{\gamma}$, as seen in the phenomena of the preceding section, and can again be interpreted qualitatively in terms of a reduction of entanglement density.

The effect of steady-state shear on the oscillating *normal* stresses produced by parallel oscillating shear deformations has also been studied by Booij.[139] Whereas, in the absence of steady shear, the oscillatory component of the normal stress has twice the frequency of the shear strain in accordance with equation 76 of Chapter 3, with increasing steady shear a component with the same frequency develops and eventually dominates. The storage and loss components of the complex normal stress depend on frequency in a complicated manner.

Small oscillating deformations transverse to steady-state shear have been studied by Simmons,[140] with results which also correspond qualitatively to the progressive disappearance of mechanisms with the longest relaxation times as the steady shear rate is increased.

7. Nonlinear Constitutive Equations

It is evident in the foregoing examples that deviations from linear viscoelastic behavior are evoked by both large strains and large strain rates. Phenomenological constitutive equations have been developed in which one or the other has a dominant role, as described for example by memory functions which depend either on strain invariants or on strain rate invariants.[120,141-143] In critical comparisons of pre-

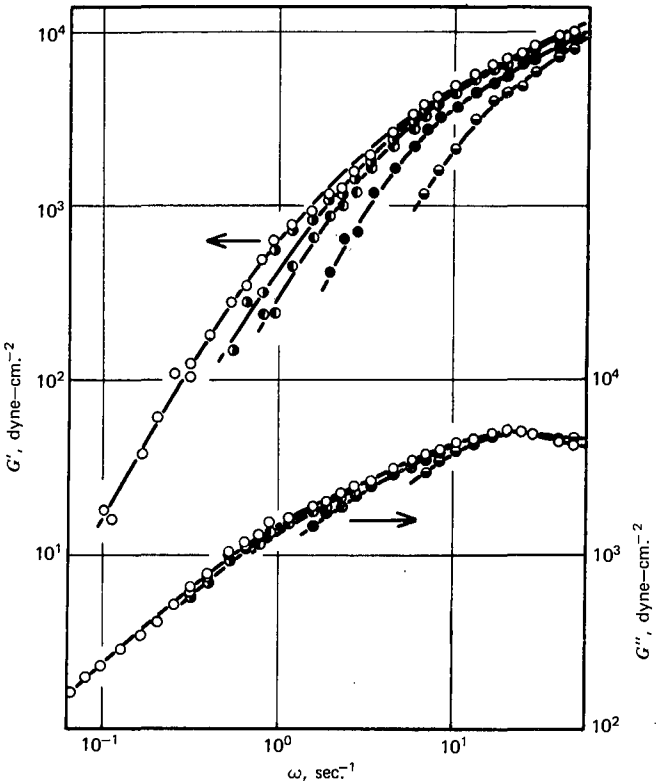


FIG. 17-39. Storage and loss moduli of a 15% solution of polystyrene ($\overline{M}_v = 2.5 \times 10^6$) in toluene at 30°C, plotted logarithmically against radian frequency; superimposed rates of shear in parallel direction, from left to right: 0, 0.162, 0.505, 1.62, and 5.13 sec^{-1}. (Osaki, Tamura, Kurata, and Kotaka.[134])

dictions for the various nonlinear phenomena described in the preceding experiments,[120,143,144] strain-dependent memory functions as in the BKZ model[145] have sometimes been found to be more successful, but a critical strain may also be taken into account[142] as implied in the experiments cited in Sections D3 and D5. Stress-dependent memory functions have also been proposed.[143] The subject is currently in a state of rapid development, with the advent of constitutive equations based on molecular models as in the theory of Doi and Edwards.[131a]

E. GELS CROSS-LINKED IN SOLUTION

Although the term "gel" has been used with varied and imprecise implications in the literature, we shall adopt the definition that it is a substantially diluted system which exhibits no steady-state flow. A polymer gel is then a cross-linked solution, whether linked by chemical bonds or crystallites or some other kind of junction.

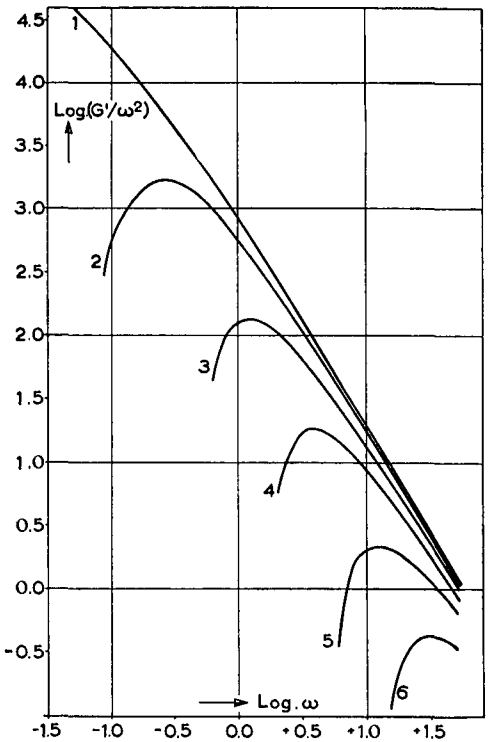


FIG. 17-40. Ratio G'/ω^2 plotted logarithmically against radian frequency for a 5% solution of ethylene-propylene copolymer ($\overline{M}_w = 6.6 \times 10^6$, broad molecular weight distribution) in Decalin at 27°C; superimposed rates of shear in parallel direction, from top to bottom; 0, 0.2, 1, 3.2, 10, and 25 sec^{-1}. (Booij.[135])

A distinction must be drawn between gels which are diluted first and then cross-linked and those which are cross-linked first and then swollen (Section F below). In the former, the network strands have their average random configurations in a more or less unstrained state (except perhaps for gels linked at quite high dilution, where the polymer coils overlap each others' domains only to a limited extent). In the latter, however, the strands are all extended beyond their normal root-mean-square lengths, in proportion to the cube root of the swelling factor $\rho/c = v_2^{-1}$.

This section deals with gels cross-linked in the presence of diluent. The simplest kind is formed by the introduction of chemical cross-links which are permanent and under favorable conditions have known stoichiometry.[146-148] Study of such systems has been mostly limited to their equilibrium elastic properties. In other gels, the linkages are formed by spontaneous association of widely separated loci, usually attributed to incipient crystallization as in poly(vinyl chloride),[149,150] polyacrylonitrile,[151] or cellulose nitrate.[152] The crystalline regions may be extremely small. In other cases such as gelatin[153] and pectin[154] the nature of the linkage is obscure. Partial helical configuration may contribute in gelatin and other protein gels. Most viscoelastic measurements have been made on gels such as these.

1. Pseudo-Equilibrium Mechanical Properties

In gels with permanent chemical tetrafunctional cross-links, the equilibrium shear elasticity would be expected to be given by equation 33 of Chapter 10,

$$G_e = g\nu RT \tag{45}$$

but the concentration of effective network strands ν may be strongly influenced by a large proportion of strands with loose ends and a possible nonzero sol fraction, *i.e.*, the proportion of the polymeric solute which does not participate in the network structure. The relation of ν to the molecular weight M and the average molecular weight between cross-links M_c can be derived from rather complicated statistical calculations of Pearson and Graessley.[155] In fact, measurements[146,148] of G_e, as well as estimation of network strand densities from swelling measurements,[147] indicate that the number of elastically effective strands can be much smaller than that calculated from the stoichiometry of cross-linking.

When the network is formed by spontaneous association, additional complications appear. The fact that crystallites melt or secondary bonds dissociate with rising temperature implies an equilibrium, or quasi-equilibrium, with the consequence that the number of linkages also changes with changing polymer concentration. This feature complicates the effects of concentration on all the viscoelastic properties, and has the disadvantage that the degree of cross-linking cannot be varied independently of the temperature or concentration. Moreover, the equilibrium structure may be very slowly established. Thus the term "pseudo-equilibrium" in the title of this section refers not only to the difficulty of obtaining a strict stress-strain equilibrium in a network polymer as discussed at the end of Section B4 of Chapter 14, but also to the frequent failure to obtain thermodynamic equilibrium with respect to the unstressed state of a gel network following a change in temperature. A gel system is usually mixed at a temperature well above the melting points of crystallites, or so high that no links due to secondary bonds are present, and then cooled to a temperature at which the cross-links will form. The pseudo-equilibrium modulus increases rapidly with time as the network is built up, but it does not approach a limiting value; it goes on increasing for long periods of time. An extreme example is shown in Fig. 17–41 for gels of polyacrylonitrile in dimethyl formamide containing 20% polymer, studied by Bisschops.[151] The pseudo-equilibrium modulus increases linearly with time at a rate which increases rapidly with decreasing temperature. The rate is also very strongly dependent on concentration, being proportional to something like c^{22} in a narrow range between 18 and 23% concentration by weight. The temperature and concentration dependence can be interpreted in terms of the rate of nucleation of the crystallites which act as cross-linking points in the network whose elasticity is being measured. Detailed studies of changes in viscoelastic properties with time in gels of poly(vinyl chloride) in several solvents have been reported by te Nijenhuis.[151a]

In other cases, the changes with time are slower, as for polyacrylonitrile in dimethyl acetamide,[151] cellulose trinitrate in isophorone,[156] and poly(vinyl chloride) in di-2-ethylhexyl phthalate.[149] In the latter, and in other polymers with structural irregularity due to lack of tactic order or copolymerization, the degree of crystallinity is presumably limited[157–159] and the increase in G_e with time eventually be-

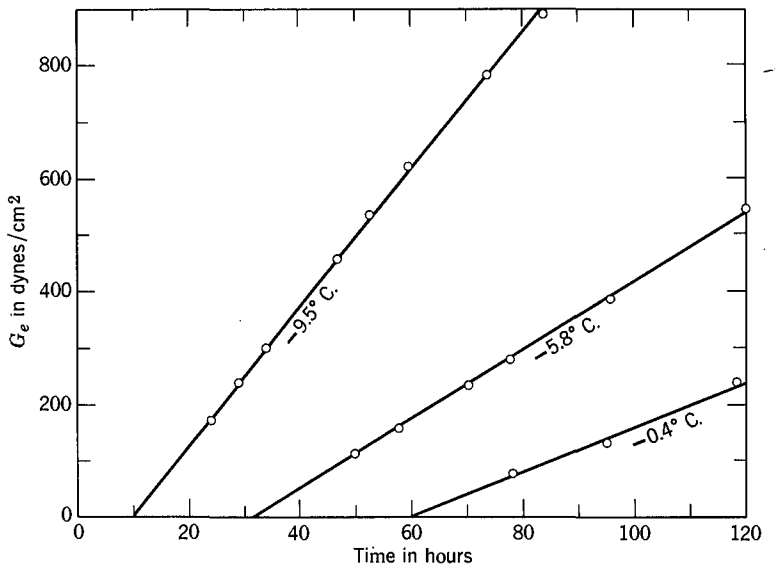


FIG. 17-41. Pseudoequilibrium shear modulus plotted against time for 20% gels of polyacrylonitrile in dimethyl formamide, aged at the three temperatures indicated. (Bisschops.[151]).

comes sufficiently slow to permit viscoelastic measurements on a reasonably stable sample. In some cases, it is desirable to age a gel for many weeks prior to viscoelastic measurements.

Changes in temperature after the network is established lead to complicated hysteretic effects[149,151] which can be interpreted qualitatively in terms of the relative stabilities of crystallites formed at different temperatures. Those formed at the highest temperatures are most resistant to melting,[160,161] and the resistance to melting also increases with aging.[149] Similar phenomena are evident in gelatin gels[162] although it is not certain just how the linkages are formed.[153] The network (as measured relatively by the magnitude of G_e) is somewhat more stable with respect to time when a gel is aged at a low temperature and then brought to a somewhat higher temperature and kept there until the weaker linkages are dissociated.

If a stable network is attained, its pseudo-equilibrium rigidity should be proportional to the absolute temperature in accordance with equation 45. In some gels with permanent chemical cross-linkages, this proportionality has been confirmed.[163,164] In those with dissociable or fusible cross-links, it can hold only in a temperature range where the network density has attained its maximum value. This is fulfilled,[149] for example, for a 10% gel of poly(vinyl chloride) in di-2-ethylhexyl phthalate between −30° and 25°C, and for gels of poly(vinyl alcohol) with Congo red in water, from measurements of Hirai,[165] from 0° to about 40°. At higher temperatures the modulus drops rapidly as the crystallites melt or the secondary associations dissociate. In many gels, such as aqueous gelatin, the latter phenomenon dominates over the entire experimentally accessible temperature range, and the

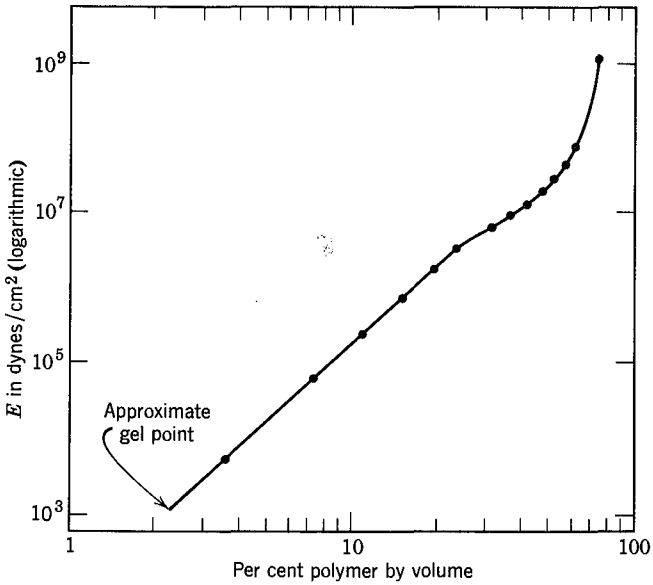


FIG. 17–42. Pseudoequilibrium Young's modulus plotted logarithmically against polymer concentration by volume for gels of poly(vinyl chloride) in di-2-ethylhexyl phthalate near room temperature, after aging 30 days. (Walter.[149])

modulus is a monotomically decreasing function with increasing temperature; it vanishes above a melting point which represents the melting or dissociation temperature of the strongest linkages present.

The concentration dependence of the pseudoequilibrium modulus can be expressed by a power relation over a moderate range of concentration, as illustrated for gels of poly(vinyl chloride) in Fig. 17–42. The slope of the linear portion of this doubly logarithmic plot is 3.47. Slopes between 3 and 4 are obtained for poly(vinyl chloride) gels in many other solvents. For gelatin gels in water, on the other hand, the slope of this plot is usually[162,166] close to 2.

At very high polymer concentrations the modulus veers sharply upward from the linear power relation, in a range where its magnitude is approaching that of hard solid. The network is so dense here that the strands are not long enough to execute the configurational changes required for rubberlike elasticity. The viscoelastic properties of such solutions, like those of the densely netted systems briefly referred to in Section B7 of Chapter 14, could not be described in terms of flexible chain theories. At the other end of the concentration scale, the modulus drops sharply as the concentration decreases toward the minimum value needed for establishment of a network. In accordance with the statistical theory of gel formation,[167] a minimum of two linked units (weight average) per molecule is required for the latter. The minimum concentration for gelation increases of course with increasing temperature and decreasing molecular weight. Below this minimum concentration, there is no pseudoequilibrium modulus, and the viscoelastic properties are those of an uncross-linked solution as described earlier in this chapter

(containing, however, a substantial proportion of branched aggregates if the concentration is only slightly below the gel point[152,168]). The extreme imperfection of gel networks, together with the probable feature that in crystallite networks the junctions are multiple with many strands radiating from a linkage, make the concentration dependence of G_e difficult to formulate theoretically.

There are also gels in which G_e decreases rapidly with decreasing temperature (much more rapidly than proportional to T) and vanishes below a sort of inverted melting point.[152,169] This phenomenon arises from an unusual thermodynamic interaction between polymer and solvent, causing crystallites (or association linkages) to be stable at higher temperatures.[152]

2. Viscoelastic Properties in the Transition Zone

The principles outlined in Section A above for the behavior of uncross-linked solutions in the transition zone are applicable to gels with very little change. For temperature dependence, for example, the primary effect of the diluent is to depress T_g and increase the fractional free volume. However, the usual reduced variables cannot be used for gels with dissociating linkages unless the degree of cross-linking changes negligibly within the temperature range covered or else the frequency or time scale is such that the measurements reflect rearrangements of chain segments short enough to be oblivious of the cross-links. In a number of cases, these qualifications have been fulfilled, permitting the construction of composite viscoelastic functions over a wide range of temperatures.[170-172] In others,[173,176] where the cross-linking is attributable to partial crystallization, decreasing temperature may cause increasing crystallization which amounts to introduction of a rigid phase with concomitant dilution of the amorphous phase. These effects can be taken into account[176] with a more complicated reduction method based on a blending law for a composite system with a rigid and a viscoelastic phase.[177]

The frequency dependence of G' and G'' at the low-frequency end of the transition zone, and the time dependence of the relaxation spectrum H, frequently correspond to the Rouse theory slopes as in undiluted cross-linked networks (Fig. 10-5) or the uncross-linked concentrated solutions of Fig. 17-2, and permit calculation of the monomeric friction coefficient by equation 11. Such calculations have been made for gels of poly(vinyl chloride),[170,172,174,175] cellulose tributyrate,[171] cellulose nitrate,[173,176,177] and gelatin.[178] The monomeric friction coefficient changes rapidly with concentration in gels of poly(vinyl chloride)[170,172,175] and cellulose tributyrate,[171] and its concentration dependence is qualitatively similar to that in uncross-linked solutions, though there are insufficient data for an analysis in terms of free volume as described in Section A. The relaxation spectra of several poly(vinyl chloride) gels in two different solvents, with concentrations ranging from 1.6 to 40%, are shown in Fig. 17-43; their relative displacements on the logarithmic time axis reflect differences in $\log \zeta_0 c^2$ according to equation 11. Their slopes are close to the value of $-\frac{1}{2}$ specified by that equation, as is the case for gelatin,[178] over several logarithmic decades of time. Comparison of the two 10% gels in different solvents is not instructive because their viscosities do not differ greatly.

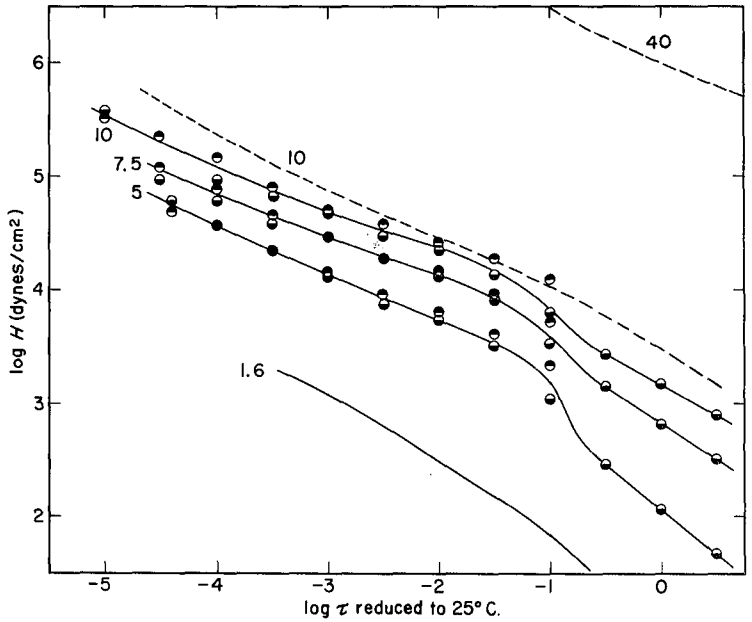


FIG. 17-43. Relaxation spectra, reduced to 25°C, of four poly(vinyl chloride) gels in di-2-ethylhexyl phthalate (solid curves) and two gels im dimethyl thianthrene (dashed curves). Points top black, calculated from G'; bottom black, from G''. Numbers denote polymer concentration in volume percent.[170,172-175]

At higher concentrations, such as in cellulose tributyrate gels[171] at concentrations above 40%, the rigidity at the long-time end of the transition zone corresponds to a densely cross-linked network as described in Section B7 of Chapter 14, and the relaxation spectrum does not exhibit a region with slope $-\frac{1}{2}$ from which a monomeric friction coefficient can be calculated; the storage modulus changes more gradually with frequency and the maximum in the loss modulus is less sharp.

Isochronal viscoelastic measurements in the transition zone have also been made on gels, and show the characteristic inflection in storage modulus and maximum in loss tangent at approximately constant frequency. Examples are shown in Fig. 17-44, where log G' and tan δ derived from dynamic measurements at about 1 Hz are plotted against temperature for plasticized compositions of poly(vinyl chloride) in diethylhexyl succinate ranging from 41% to 100% polymer.[179] (The lower concentrations, at least, could be described as gels.) The effect of changing concentration must include its effects on ζ_0 and the shapes of the viscoelastic functions as well as on the temperature dependence of a_T. The location of the maximum shifts rapidly to higher temperatures with increasing concentration as in Fig. 17-12. With increasing c, the transition first becomes more gradual, evidenced by the decrease in steepness at the inflection of G' and the flattening in tan δ; this corresponds to the same trend in the isothermal viscoelastic functions. As the composition approaches pure polymer, however, the transition on the temperature scale sharpens again. It is difficult to interpret the latter phenomenon without knowledge of the

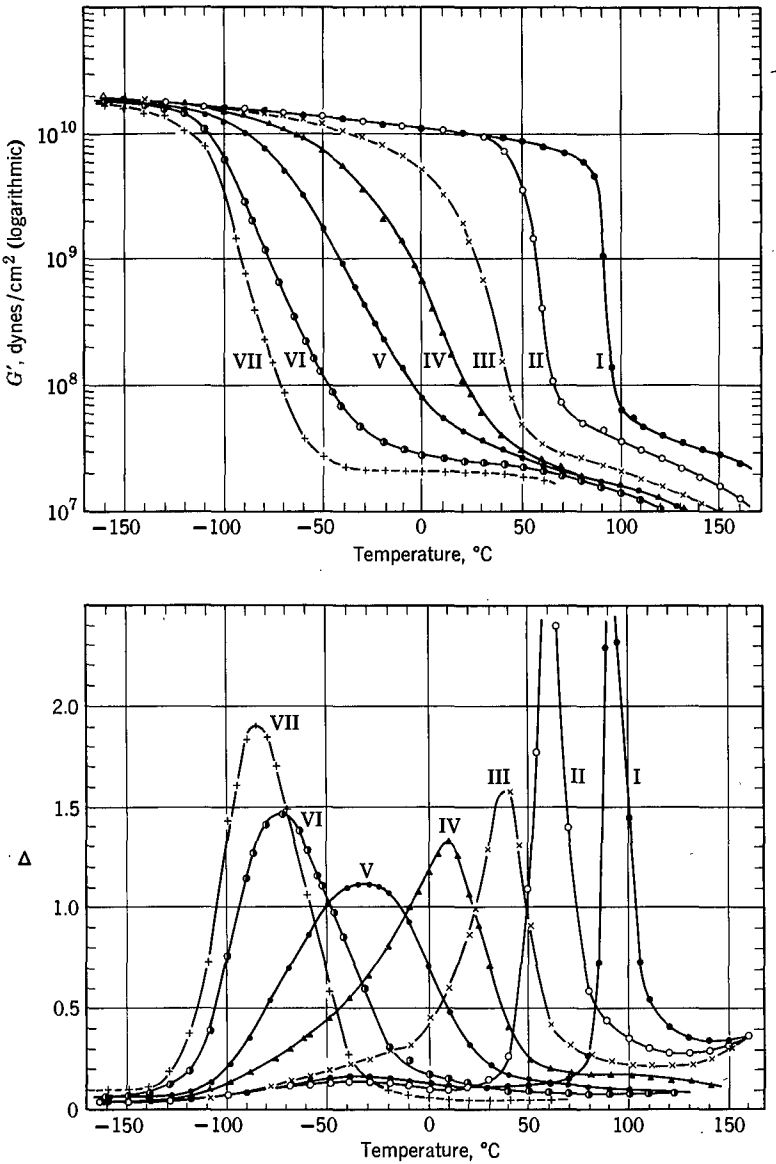


FIG. 17-44. Log G' and Δ plotted against temperature at approximately 1 Hz for poly(vinyl chloride) plasticized with diethylhexyl succinate, with compositions as indicated: (I) 100% polymer; (II) 91%; (III) 79%; (IV) 70.5%; (V) 60.7% (VI) 51.8%; (VII) 40.8%. (Schmieder and Wolf.[179])

individual functions $a_T(T)$ and $G'(\omega)$. It may, however, be associated with the melting of some crystallites and consequent loosening of the network in the high-temperature range where the high-concentration data fall. Similar isochronal measurements have been reported by other investigators.[180]

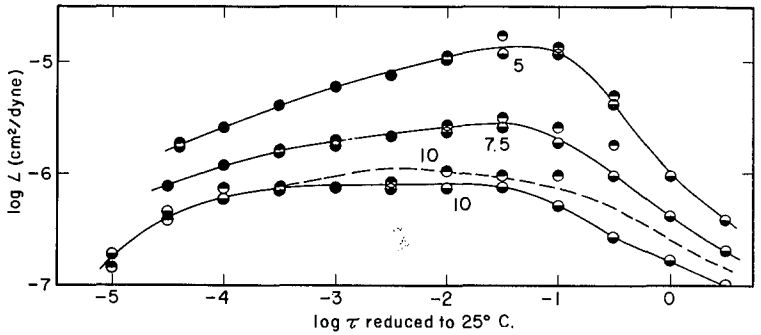


FIG. 17-45. Retardation spectra of poly(vinyl chloride) gels in di-2-ethylhexyl phthalate (solid curves) and dimethyl thianthrene (dashed curve) identified as in Fig. 17-43. Points top black, calculated from J'; bottom black, from J''.

3. Viscoelastic Properties in the Plateau Zone

The plateau zone is characterized by the maxima in J'' and L that are always symptomatic of networks (Section B1 of Chapter 14). However, these maxima are considerably broader than for entanglement networks or lightly cross-linked undiluted polymers (Figs. 13-1 and 14-2). Examples are shown for poly(vinyl chloride) gels in Fig. 17-45. The maxima in L are lower than for lightly cross-linked undiluted polymers, being of the order of $0.1J_e$ instead of about $0.18J_e$. The origin of this difference is obscure; it may be related to the multiple functionality of the cross-links in the gels.

At long times, unusual inflections are observed in the relaxation spectra in Fig. 17-43. These have been tentatively attributed to the effects of substantial proportions of sol fraction (loose molecules) and dangling branched structures in these gels.[172]

4. Behavior at Very Long Times

In describing the mechanical response of gel networks at long times, it is necessary to distinguish between conditions where the cross-links are stable and where they may be forming and dissociating during the period of the experiment. In the former case, the behavior may resemble that of permanently cross-linked networks as discussed in Section B4 of Chapter 14. The relaxation of stress beyond the pseudoequilibrium value, or the additional creep beyond the pseudoequilibrium compliance, is very slight, however. Some creep measurements have been fitted[181,182] to an equation of the Andrade form, equation 28 of Chapter 13 (with infinite viscosity).

If, on the other hand, cross-links are forming and dissociating while the measurements are in progress, phenomena similar to chemical stress relaxation (Section D of Chapter 14) may be encountered. The stress may drop nearly to zero in a stress relaxation process, whereas the shear modulus as measured in a moderately rapid

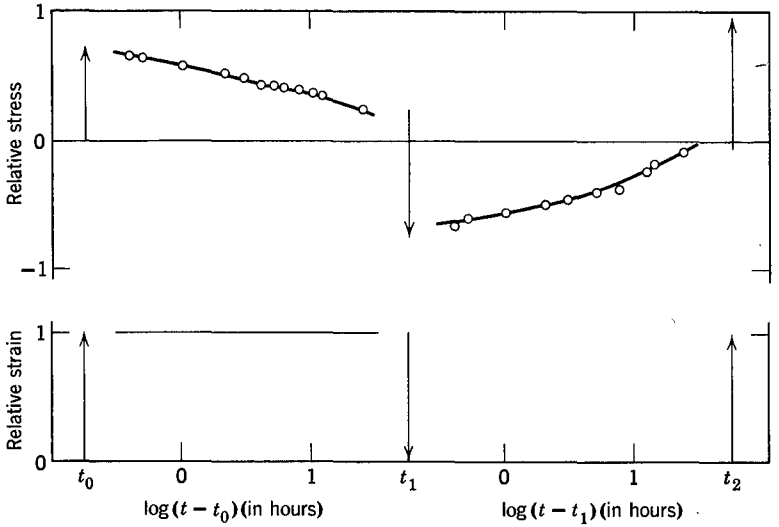


FIG. 17-46. Stress relaxation and reverse relaxation in a 5.9% aqueous gelatin gel at 20.2°. (For explanation see text.)[183]

deformation (corresponding to the pseudoequilibrium zone of time scale) remains nearly unchanged.[183] Such behavior, observed in gelatin gels at temperatures not far below the gel melting point, has been attributed to the dissociation of cross-links and the formation of new ones with the network strands in unstressed configurations.[183] The dissociation of the linkages cannot be described by a single rate constant, however, as in the chemical scission of networks. The relaxation is gradual, corresponding to a broad spectrum. It is slower at lower temperatures and slower in gels which have been aged longer.

Useful information about this complicated phenomenon can be obtained by reverse relaxation experiments, as illustrated in Fig. 17-46. Here[183] a 5.9% aqueous gelatin gel was aged for 12.3 hr at 20.2°C. A small shearing strain was suddenly imposed, and the instantaneous stress corresponded to a shear modulus of 0.73×10^4 dynes/cm^2. After 24 hr, the stress had relaxed to 0.35 of its initial value. The strain was then returned to zero. The change in stress corresponded to a shear modulus of 0.99×10^4; *i.e.*, the rigidity had increased slightly while the stress was relaxing, indicating that while some links were breaking a somewhat greater number were forming. During the next 24 hr, the new stress, opposite in direction to the original, relaxed to 0.31 of its initial value. Then the strain was imposed again as in the original deformation, and the change in stress corresponded to a shear modulus of 0.91×10^4.

In such experiments, for a constant period of aging before the initial relaxation, the longer the period of the initial relaxation the slower is the reverse relaxation; the new bonds formed in the strained state have more time to anneal and develop resistance to dissociation. But when the period of initial relaxation is kept constant and the period of aging preceding it is varied, a long aging period is followed by a rapid reverse relaxation. This is the result of

the slow initial relaxation in a well-aged gel, which does not allow the new bonds to form until toward the end of the initial relaxation period, leaving them relatively weak.

In general, these results can be interpreted in terms of a complicated steady state of making and breaking of linkages, in which the longer a given linkage lasts without dissociation, the smaller its probability of dissociation becomes.

Extensive dynamic viscoelastic measurements on polyvinyl chloride gels with well-defined tacticities and thermal histories have revealed changes in aging which affect the plateau zone as some crystallites melt and others are formed.[151a,184] The appearance of secondary loss mechanisms is attributed to the formation of entanglements during the aging process.

F. GELS SWOLLEN AFTER CROSS-LINKING

As an alternative to cross-linking in solution, a network polymer formed in the undiluted state may be swollen in diluent to any desired degree of dilution within the limit of the equilibrium degree of swelling specified by the thermodynamic interaction and the free energy of distention of the network.[185] The result is a gel which differs from one cross-linked in solution at the same concentration; the network strands are more extended in their average configurations, and the topology is different with respect to proportion of loose ends, entanglement entrapment, and presence of small cyclic structures. Actually, the sequence of cross-linking and swelling can be modified in various ways with formation of the network at one concentration and investigation of its properties at another concentration, either higher or lower. For example, a gel cross-linked in solution can be freed of diluent to give an undiluted cross-linked polymer with a different topology.[186–189] There have been numerous studies of the equilibrium modulus of polymer networks formed at one concentration and measured at another.[185,186–192]

An extensive study of viscoelastic properties has been made on gels of poly(β-hydroxyethyl methacrylate) swollen in diethylene glycol.[27,193–197] These gels were cross-linked by copolymerization with ethylene glycol dimethacrylate. The monomeric friction coefficient could be calculated from measurements in the transition zone by equation 11. Its dependence on concentration was similar to that observed in concentrated solutions as described in Section A above, and the free-volume parameters calculated from equation 13 agreed with those derived from the temperature dependence of ζ_0 at individual concentrations by application of the WLF equation (Section C3 of Chapter 11).[27] In the plateau and pseudoequilibrium zones, however, contributions to modulus were not proportional to v_2 as in equation 11, but to a lower power of v_2, especially for high degrees of cross-linking and high degrees of swelling.[194] According to the statistical theory of rubberlike elasticity, the equilibrium modulus of a swollen network should be proportional to $v_2^{1/3}$;[198] the observed behavior is probably associated with the extension of network strands. Secondary loss mechanisms, such as described for lightly cross-linked undiluted networks (Section B5 of Chapter 14), were also observed.[27,195]

G. GELS OF SEMIRIGID MACROMOLECULES

In the gels described in the preceding Sections E and F, the network strands are flexible and the energy storage in deformation is associated with entropy changes as described by the statistical theory of rubber elasticity for equilibrium elasticity and the bead-spring theories of Chapters 9 and 10 for viscoelasticity. Other gels can be formed from elongated macromolecules with helical or other reinforced structures which impart considerable rigidity. Examples are poly(γ-benzyl-L-glutamate)[199] and fibrin formed by the polymerization of fibrinogen.[200] The network strands appear to be bundles of macromolecules and the three-dimensional structure is sometimes formed by anastomosis of these bundles, although a rigid structure could be accomplished simply by interpenetration of long rigid rods.[74] The mechanism of energy storage in such gels has not been established but may be associated with a combination of bending and stretching of the semirigid structural units.[201]

REFERENCES

1. E. Jenckel and R. Heusch, *Kolloid-Z.*, **130,** 89 (1953).
2. R. B. Beevers and E. F. T. White, *Trans. Farday Soc.*, **56,** 1529 (1960).
3. R. B. Beevers and E. F. T. White, *J. Polym. Sci.*, **B1,** 171 (1963).
4. K. H. Illers, *Kolloid-Z.*, **190,** 16 (1963).
5. L. J. Garfield and S. E. Petrie, *J. Phys. Chem.*, **68,** 1750 (1964).
6. G. Braun and A. J. Kovacs, *Proc. Conf. on Physics of Non-Crystalline Solids,* edited by J. A. Prins, North Holland, Amsterdam, 1965, p. 303.
7. M. Gordon and J. S. Taylor, *J. Appl. Chem.*, **2,** 493 (1952).
8. H. Fujita and A. Kishimoto, *J. Polym. Sci.*, **28,** 547 (1958).
9. F. N. Kelley and F. Bueche, *J. Polym. Sci.*, **50,** 549 (1961).
10. E. Riande, H. Markovitz, D. J. Plazek, and N. Ragupathi, *J. Polym. Sci., Polym. Symp.*, **50,** 405 (1975).
11. J. D. Ferry and R. A. Stratton, *Kolloid-Z.*, **171,** 107 (1960).
12. P. R. Saunders, D. M. Stern, S. F. Kurath, C. Sakoonkim, and J. D. Ferry, *J. Colloid Sci.*, **14,** 222 (1959).
13. Y. Oyanagi and J. D. Ferry, *J. Colloid Sci.*, **21,** 547 (1966).
14. D. J. Plazek, E. Riandi, H. Markovitz, and N. Raghupathi, *J. Polym. Sci.*,
15. H. Fujita and A. Kishimoto, *J. Chem. Phys.*, **34,** 393 (1961).
16. H. Fujita, *Adv. Polym. Sci.*, **3,** 1 (1961).
17. R. S. Moore and J. D. Ferry, *J. Phys. Chem.*, **66,** 2699 (1962).
18. J. R. Richards, K. Ninomiya, and J. D. Ferry, *J. Phys. Chem.*, **67,** 323 (1963).
19. A. K. Doolittle, *J. Appl. Phys.*, **23,** 236 (1952).
20. A. Teramoto, R. Okada, and H. Fujita, *J. Phys. Chem.*, **67,** 1228 (1963).
21. A Teramoto, S. Kusamizu, H. Tanaka, Y. Murakami, and H. Fujita, *Makromol. Chem.*, **90,** 78 (1966).
22. H. Fujita and E. Maekawa, *J. Phys. Chem.*, **66,** 1053 (1962).
23. A. Kishimoto and Y. Enda, *J. Polym. Sci.*, **A1,** 1799 (1963).
24. H. Fujita, A. Kishimoto, and K. Matsumoto, *Trans. Faraday Soc.*, **56,** 424 (1960).
25. A. Kishimoto, *J. Polym. Sci.*, **A2,** 1421 (1964).
26. M. L. Williams and J. D. Ferry, *J. Colloid Sci.*, **10,** 474 (1955).
27. D. E. Kranbuehl and B. Schardt, in *Computer Simulation of Bulk Matter from a Molecular Perspective,* edited by P. Lykos, A. C. S. Symposium Series, 1979.

28. J. Janáček and J. D. Ferry, *Macromolecules,* **2,** 370 (1969).
29. E. Jenckel, in *Die Physik der Hochpolymeren,* edited by H. A. Stuart, Volume IV, Springer-Verlag, Berlin, 1956, p. 566.
30. S. Prager and F. A. Long, *J. Am. Chem. Soc.,* **73,** 4072 (1951).
31. *Plasticization and Plasticizer Processes,* Advances in Chemistry Series No. 48, American Chemical Society, Washington, 1965.
32. I. Havlíček, M. Ilavsky, and J. Hrouz, *J. Polym. Sci., Polym. Phys. Ed.,* **16,** 653 (1978).
33. M. L. Williams and J. D. Ferry, *J. Colloid Sci.,* **9,** 479 (1954).
34. M. L. Williams and J. D. Ferry, *J. Colloid Sci.,* **10,** 1 (1955).
35. W. C. Child, Jr., and J. D. Ferry, *J. Colloid Sci.,* **12,** 327 (1957).
36. J. J. Aklonis and V. B. Rele, *J. Polym. Sci., Polym. Symp.,* **46,** 127 (1974).
37. R. B. Wasser and S. F. Kurath, *J. Colloid Interface Sci.,* **21,** 183 (1966).
38. K. H. Illers and E. Jenckel, *Rheol. Acta,* **1,** 322 (1958).
39. J. D. Ferry, *J. Am. Chem. Soc.,* **72,** 3746 (1950).
40. A. W. Nolle and J. F. Mifsud, *J. Appl. Phys.,* **24,** 5 (1953).
41. E. Catsiff, T. Alfrey , Jr., and M. T. O'Shaugnessy, *Text. Res. J.,* **23,** 808 (1953).
42. T. Yoshitomi, K. Nagamatsu, and K. Kosiyama, *J. Polym. Sci.,* **27,** 335 (1958).
43. W. W. Graessley, *Adv. Polym. Sci.,* **16,** 1 (1974).
44. T. Masuda, N. Toda, Y. Aoto, and S. Onogi, *Polym. J.,* **3,** 315 (1972).
45. N. Nemoto, T. Ogawa, H. Odani, and M. Kurata, *Macromolecules,* **5,** 641 (1942).
46. K. Ninomiya, J. D. Ferry, and Y. Ōyanagi, *J. Phys. Chem.,* **67,** 2297 (1963).
47. Y. Isono, T. Fujimoto, N. Takeno, H. Kajiura, and M. Nagasawa, *Macromolecules,* **11,** 888 (1978).
48. Reference 10, footnote p. 416.
49. W. W. Graessley, private communication.
50. G. C. Berry and T. G. Fox, *Adv. Polym. Sci.,* **5,** 261 (1967).
51. P. G. de Gennes, *Macromolecules,* **9,** 587 (1976).
52. P. G. de Gennes, *Macromolecules,* **9,** 594 (1976).
53. H. Nakayasu and T. G. Fox, *Abstracts 137th Meeting,* Am. Chem. Soc., p. 11-I (1960).
54. A. R. Shultz, W. B. Shultz, and T. G. Fox, unpublished experiments.
55. Y. Ōyanagi and J. D. Ferry, *Proc. 4th Intern. Cong. Rheology,* Part 2, Interscience, New York, 1965, p. 491.
56. T. E. Newlin, S. E. Lovell, P. R. Saunders, and J. D. Ferry, *J. Colloid Sci.,* **17,** 10 (1962).
57. J. W. Berge, P. R. Saunders, and J. D. Ferry, *J. Colloid Sci.,* **14,** 135 (1959).
58. D. M. Stern, J. W. Berge, S. F. Kurath, C. Sakoonkim, and J. D. Ferry, *J. Colloid Sci.,* **17,** 409 (1962).
59. T. G. Fox, B. S. Garrett, W. E. Goode, S. Gratch, and J. F. Kincaid, *J. Am. Chem. Soc.,* **80,** 1768 (1950).
60. C. F. Ryan and P. C. Fleischer, Jr., *J. Phys. Chem.,* **69,** 3384 (1965).
61. M. Pyrlik and G. Rehage, *Rheol. Acta,* **14,** 303 (1975).
62. M. Pyrlik, W. Borchard, G. Rehage, and E. P. Uerpmann, *Angew. Makromol. Chem.,* **36,** 133 (1974).
63. Yu. N. Panov, K. Ye. Nordbek, and S. Ya. Frenkel, *Vysokomol. Soed.,* **6,** 47 (1964).
64. T. W. De Witt, H. Markovitz, F. J. Padden, Jr., and L. J. Zapas, *J. Colloid Sci.,* **10,** 174 (1955).
65. J. D. Ferry, I. Jordan, W. W. Evans, and M. F. Johnson, *J. Polym. Sci.,* **14,** 261 (1954).
66. M. R. Hatfield and G. B. Rathmann, *J. Appl. Phys.,* **25,** 1082 (1954).
67. N. W. Tschoegl and J. D. Ferry, *J. Phys. Chem.,* **86,** 1474 (1964).
68. H. H. Meyer, W. F. Pfeiffer, Jr., and J. D. Ferry, *Biopolymers,* **5,** 123, (1967).
69. G. C. Berry, *Disc. Faraday Soc.,* **49,** 121 (1970).
70. C.-P. Wong, H. Ohnuma, and G. C. Berry, *J. Polym. Sci., Polym. Symp.,* **69,** 173 (1979).
71. L. Onsager, *Ann. N. Y. Acad. Sci.,* **51,** 627 (1949).
72. P. J. Flory, *Proc.R. Soc.,* **A234,** 73 (1956).
73. P. J. Flory, *Macromolecules,* **11,** 1141 (1978).
74. M. Doi and N. Y. Kuzuu, *J. Polym. Sci., Polym. Phys. Ed.,* **18,** 409 (1980).

75. M. Doi and S. F. Edwards, *J. Chem. Soc., Faraday Trans. II*, **74**, 560, 918 (1978).
76. F. E. Helders, J. D. Ferry, H. Markovitz, and L. J. Zapas, *J. Phys. Chem.*, **60**, 1575 (1956).
77. G. Kraus and J. T. Gruver, *Trans. Soc. Rheol.*, **9:2**, 17 (1965).
78. K. Ninomiya, J. R. Richards, and J. D. Ferry, *J. Phys. Chem.*, **67**, 327 (1963).
79. R. F. Landel, J. W. Berge, and J. D. Ferry, *J. Colloid Sci.*, **12**, 400 (1957).
80. J. Klein, *Macromolecules*, **11**, 852 (1978).
81. G. C. Berry, H. Nakayasu, and T. G. Fox, *J. Polym. Sci., Polym. Phys. Ed.*, **17**, 1825 (1979).
82. A. R. Shultz, W. B. Shultz, and T. G. Fox, quoted in reference 50.
83. M. F. Johnson, W. W. Evans, I. Jordan, and J. D. Ferry, *J. Colloid Sci.*, **7**, 498. (1982).
84. S. Onogi, S. Kimura, T. Kato, T. Masuda, and N. Miyanaga, *J. Polym. Sci.*, **C15**, 381 (1966).
85. S. Onogi, T. Masuda, N. Miyanaga, and Y. Kimura, *J. Polym. Sci.*, A-2, **5**, 899 (1967).
86. S. Onogi, I. Hamana, and H. Hirai, *J. Appl. Phys.*, **29**, 1503 (1958).
87. A. A. Tager, *Rheol. Acta*, **13**, 323 (1974).
88. R. Simha and J. L. Zakin, *J. Colloid Sci.*, **17**, 270 (1962).
89. L. Utracki and R. Simha, *J. Polym. Sci.*, **A1**, 1089 (1963); *J. Phys. Chem.*, **67**, 1052 (1963).
90. G. Pezzin and N. Gligo, *J. Appl. Polym. Sci.*, **10**, 1 (1966).
91. G. Pezzin, *J. Appl. Polym. Sci.*, **10**, 21 (1966).
92. A. K. Doolittle, in *Colloid Chemistry*, edited by J. Alexander, Volume VII, Chapter 8, Reinhold, 1950.
93. J. D. Ferry, E. L. Foster, G. V. Browning, and W. M. Sawyer, *J. Colloid Sci.*, **6**, 367.
94. J. D. Ferry, L. D. Grandine, Jr., and D. C. Udy, *J. Colloid Sci.*, **8**, 529 (1953).
95. K. Osaki and Y. Einaga, *Adv. Polym. Sci. Jpn.*, **1**, 321 (1970).
96. N. Nemoto, T. Ogawa, H. Odani, and M. Kurata, *Macromolecules*, **5**, 641 (1972).
97. M. Sakai, T. Fujimoto, and M. Nagasawa, *Macromolecules*, **5**, 786 (1972).
98. R. A. Stratton and A. F. Butcher, *J. Polym. Sci.*, A2, **9**, 170 3 (1971).
99. W. W. Graessley and L. Segal, *Macromolecules*, **2**, 49 (1969).
100. L. A. Holmes and J. D. Ferry, *J. Polym. Sci.*, **23**, 291 (1968).
101. S. Kusamizu, L. A. Holmes, A. A. Moore, and J. D. Ferry, *Trans. Soc. Rheol.*, **12**, 559 (1968).
102. L. A. Holmes, K. Ninomiya, and J. D. Ferry, *J. Phys. Chem.*, **70**, 2714 (1966).
103. K. Ninomiya and J. D. Ferry, *J. Colloid Sci.*, **18**, 421 (1963).
104. L. A. Utracki and J. E. L. Roovers, *Macromolecules*, **6**, 366 (1973).
104a. W. W. Graessley, T. Masuda, J. E. L. Roovers, and N. Hadjichristidis, *Macromolecules*, **9**, 127 (1976).
105. T. Masuda, Y. Nakagawa, Y. Ohta, and S. Onogi, *Polym. J.*, **3**, 92 (1972).
106. T. Masuda, Y. Ohta, M. Minamide, and S. Onogi, *Zairyo*, **21**, 436 (1972).
106a. W. W. Graessley, *Acc. Chem. Res.*, **10**, 332 (1977).
107. M. Kurata, K. Osaki, Y. Einaga, and T. Sugie, *J. Polym. Sci., Polym. Phys. Ed.*, **12**, 849 (1974).
108. H. Endo, T. Fujimoto, and M. Nagasawa, *J. Polym. Sci.*, A-2, **9**, 345 (1971).
109. W. W. Graessley, *J. Chem. Phys.*, **47**, 1942 (1967).
110. W. W. Graessley, R. L. Hazleton, and L. R. Lindeman, *Trans. Soc. Rheol.*, **11:3**, 267 (1967).
111. W. W. Graessley and L. Segal, *Macromolecules*, **2**, 49 (1969).
112. E. Ashare, Ph. D. thesis, University of Wisconsin, 1968.
113. E. K. Harris, Jr., Ph. D. thesis, University of Wisconsin, 1970.
114. R. B. Bird, R. C. Armstrong, and O. Hassager, *Dynamics of Polymeric Liquids*, Volume I, Wiley, New York, 1977, p. 379.
115. K. Osaki, M. Fukuda, S. Ohta, B. S. Kim, and M. Kurata, *J. Polym. Sci., Polym. Phys. Ed.*, **13**, 1577 (1975).

116. G. C. Berry, B. L. Hager, and C. P. Wong, *Macromolecules,* **10,** 361 (1977).
117. M. Fukuda, K. Osaki, and M. Kurata, *J. Polym. Sci., Polym. Phys. Ed.,* **13,** 1563 (1975).
118. A. V. Tobolsky and K. Murakami, *J. Polym. Sci.,* **40,** 443 (1959).
119. L. J. Zapas and J. C. Phillips, *J. Res. Nat. Bur. Stand.,* **75A,** 33 (1971).
120. K. Osaki, *Proc. VIIth Intern. Cong. Rheology,* edited by C. Klason and J. Kubat, Swedish Society of Rheology, Gothenburg, 1976, p. 104.
121. M. Doi, *J. Polym. Sci., Polym. Phys. Ed.,* in press.
122. K. Osaki, Y. Einaga, N. Yamada, and M. Kurata, *Polym. J.,* **6,** 72 (1974).
123. J. D. Huppler, I. F. Macdonald, E. Ashare, T. W. Spriggs, R. B. Bird, and L. A. Holmes, *Trans. Soc. Rheol.,* **11,** 181 (1967).
124. M. Sakai, H. Fukaya, and M. Nagasawa, *Trans. Soc. Rheol.,* **16,** 635 (1972).
125. Reference 114, p. 154.
126. A. A. Trapeznikov and A. T. Pylaeva, *Vysokomol. Soed.,* **A10,** 1539 (1968).
127. J. Schurz, *Kolloid-Z., Z. Polym.,* **227,** 72 (1968).
128. R. A. Stratton and A. F. Butcher, *J. Polym. Sci., Polym. Phys. Ed.,* **11,** 1747 (1973).
129. W. H. Bauer and E. A. Collins, in *Rheology,* edited by F. R. Eirich, Volume IV, Academic Press, 1967.
130. T. Alfrey, Jr., and C. W. Rodewald, *J. Colloid Sci.,* **4,** 283 (1949).
131. T. Matsuo, A. Pavan, A. Peterlin, and D. T. Turner, *J. Colloid Interference, Sci.,* **24,** 241 (1967).
131a. M. Doi and S. F. Edwards, *J. Chem. Soc. Faraday Trans. II,* **74,** 1818 (1978); **75,** 38 (1979).
132. H. Markovitz, *Proc. 5th Intern. Cong. Rheology,* edited by S. Onogi, Volume 1, University of Tokyo Press, 1969, p. 499.
133. K. Walters, *Rheometry,* Wiley, New York, 1975.
134. K. Osaki, M. Tamura, M. Kurata, and T. Kotaka, *J. Phys. Chem.,* **69,** 4183 (1965).
135. H. C. Booij, *Rheol. Acta,* **5,** 215 (1966).
136. H. C. Booij, *Rheol. Acta,* **5,** 222 (1966).
137. I. F. Macdonald and R. B. Bird, *J. Phys. Chem.,* **70,** 2068 (1966).
138. T. W. Spriggs, J. D. Huppler, and R. B. Bird, *Trans. Soc. Rheol.,* **10,** 191 (1966).
139. H. C. Booij, *Rheol. Acta,* **7,** 202 (1968); Ph. D. thesis, University of Leiden, 1970.
140. J. M. Simmons, *Rheol. Acta,* **7,** 184 (1968).
141. Reference 114, pp. 383, 444.
142. H. Kajiura, M. Sakai, and M. Nagasawa, *Trans. Soc. Rheol.,* **20,** 575 (1976).
143. M. Takahashi, T. Masuda, and S. Onogi, *Trans. Soc. Rheol.,* **21,** 337 (1977).
144. K. Osaki, S. Ohta, M. Fukuda, and M. Kurata, *J. Polym. Sci., Polym. Phys. Ed.,* **14,** 1701 (1976).
145. B. Bernstein, E. A. Kearsley, and L. J. Zapas, *Trans. Soc. Rheol.,* **7,** 391 (1963); **9,** 27 (1965).
146. M. C. Shen and A. V. Tobolsky, *J. Polym. Sci.,* **A2,** 2513 (1964).
147. B. Mukherji and W. Prins. *J. Polym. Sci.,* **A2,** 4367 (1964).
148. J. F. Jackson and S. J. Gill, *J. Polym. Sci.,* A-2, **5,** 663 (1967).
149. A. T. Walter, *J. Polym. Sci.,* **13,** 207 (1954).
150. P. J. Lemstra, A. Keller, and M. Cudby, *J. Polym. Sci., Polym. Phys. Ed.,* **16,** 1507 (1978).
151. J. Bisschops. *J. Polym. Sci.,* **17,** 89 (1955).
151a. K. te Nijenhuis, Thesis, Delft Technical University, 1979.
152. S. Newman, W. R. Krigbaum, and D. K. Carpenter, *J. Phys. Chem.,* **60,** 648 (1956).
153. A. Veis, *Macromolecular Chemistry of Gelatin,* Academic Press, New York, 1964.
154. H. Deuel, J. Solms, and H. Altermatt, *Vierteljahrsschr. Naturforsch. Ges. Zürich,* **98,** 49 (1953).
155. D. S. Pearson and W. W. Graessley, *Macromolecules,* **11,** 528 (1978).
156. D. J. Plazek and J. D. Ferry, *J. Phys. Chem.,* **60,** 289 (1956).
157. B. D. Coleman, *J. Polym. Sci.,* **31,** 155 (1958).

158. F. E. Bailey, Jr., and R. D. Lundberg, *Abstr. American Chemical Society,* Chicago, 1958, p. 2T.
159. H. C. Haas and R. L. MacDonald, *J. Polym. Sci., Polym. Chem. Ed.,* **11,** 1133 (1973).
160. L. A. Wood. *Adv. Colloid Sci.,* **2,** 57 (1946).
161. L. Mandelkern, *Chem. Rev.,* **56,** 903 (1956).
162. J. D. Ferry, *Adv. Protein Chem.,* **4,** 1 (1948).
163. P. R. Saunders and A. G. Ward, in *Rheology of Elastomers,* edited by P. Mason and N. Wookey, Pergamon, London, 1958, p. 45.
164. K. L. Dorrington, N. G. McCrum, and W. R. Watson, *J. Polym. Sci., Polym. Lett. Ed.,* **15,** 733 (1977).
165. N. Hirai, *Bull. Inst. Chem. Res. Kyoto Univ.,* **33,** 21 (1955).
166. J. D. Ferry, *J. Amer. Chem. Soc.,* **70,** 2244 (1948).
167. P. J. Flory, *Principles of Polymer Chemistry,* Cornell University Press, Ithaca, 1953, Chapter IX.
168. H. Boedtker and P. Doty, *J. J. Phys. Chem.,* **58,** 968 (1954).
169. A. K. Doolittle, *Ind. Eng. Chem.,* **38,** 535 (1946).
170. J. D. Ferry and E. R. Fitzgerald, *J. Colloid Sci.,* **8,** 224 (1953).
171. R. F. Landel and J. D. Ferry, *J. Phys. Chem.,* **60,** 294 (1956).
172. S. D. Morton and J. D. Ferry, *J. Phys. Chem.,* **66,** 1639 (1962).
173. D. J. Plazek, *J. Colloid Sci.,* **15,** 50 (1960).
174. M. H. Birnboim and J. D. Ferry, *J. Appl. Phys.,* **32,** 2305 (1961).
175. J. D. Ferry, D. J. Plazek, and G. E. Heckler, *J. Chim. Phys.,* **55,** 152 (1958).
176. K. Ninomiya and J. D. Ferry, *J. Polym. Sci.,* A-2, **5,** 195 (1967).
177. K. Ninomiya and E. Maekawa, *Nippon Gomu Kyokaishi,* **39,** 601 (1966).
178. J.-L. Laurent, P. A. Janmey, and J. D. Ferry, *J. Rheol.,* **24,** 87 (1980).
179. K. Schmieder and K. Wolf, *Kolloid-Z.,* **127,** 65 (1952).
180. L. E. Nielsen, R. Buchdahl, and R. Levreault, *J. Appl. Phys.,* **21,** 607 (1950).
181. L. N. G. Filon and H. T. Jessop, *Phil. Trans. R. Soc.,* **A223,** 89 (1928).
182. D. J. Plazek, *J. Colloid Sci.,* **15,** 50 (1960).
183. M. Miller, J. D. Ferry, F. W. Schremp, and J. E. Eldridge, *J. Phys. Colloid Chem.,* **55,** 1387 (1951).
184. K. te Nijenhuis and H. Dijkstra, *Rheol. Acta,* **14,** 71 (1975).
185. P. J. Flory, *Principles of Polymer Chemistry,* Cornell University Press, Ithaca, 1953.
186. B. Meissner, *J. Polym. Sci.,* **C16,** 781, 793 (1967).
187. N. R. Langley, R. A. Dickie, C. P. Wong, J. D. Ferry, R. Chasset, and P. Thirion, *J. Polym. Soc.,* A-2, **6,** 1371 (1968).
188. J. E. Mark, *Rubber Chem. Technol.,* **48,** 495 (1975).
189. R. E. Cohen, S. D. Severson, C. U. Yu, and J. E. Mark, *Macromolecules,* **10,** 663 (1977).
190. G. Gee, *Trans. Faraday Soc.,* **42,** 585 (1946).
191. P. J. Flory, A. Ciferri, and C. A. J. Hoeve, *J. Polym. Sci.,* **34,** 357 (1959).
192. G. Rehage and J. Schwarz, *Z. Anal. Chem.,* **235,** 143 (1967).
193. J. Janáček and J. D. Ferry, *Rheol. Acta,* **9,** 208 (1970).
194. J. Janáček and J. D. Ferry, *J. Polym. Sci.,* A-2, **7,** 1681 (1969).
195. J. Janáček and J. D. Ferry, *Macromolecules,* **2,** 379 (1969).
196. J. Janáček and J. D. Ferry, *J. Macromol. Sci.—Phys.,* **B5,** 219 (1971).
197. J. Janáček and J. D. Ferry, *J. Polym. Sci.,* A-2, **10,** 345 (1972).
198. L. R. G. Treloar, *The Physics of Rubber Elasticity,* 3rd ed., Clarendon Press, Oxford, 1975.
199. W. G. Miller, L. Kou, K. Tohyama, and V. Voltaggio, *J. Polym. Sci., Polym. Symp.,* **65,** 91 (1978).
200. G. W. Nelb, C. Gerth, and J. D. Ferry, *Biophys. Chem.,* **5,** 377 (1976).
201. S. S. Sternstein, in *Cellulose and Cellulose Derivatives,* edited by N. Bikales and L. Segal, Volume 5, Part 4, Wiley, New York, 1971, p. 649.

CHAPTER 18

Viscoelastic Behavior in Bulk (Volume) Deformation

Bulk viscoelastic behavior differs from that in shear in several respects which have been mentioned in previous chapters. The modulus or compliance has comparatively a very narrow range of magnitudes when measured over a wide range of time or frequency. From a molecular standpoint, the viscoelastic properties depend only on very local motions of the polymer molecules; entanglements and cross-links have no role. Finally, there is an inherent nonlinearity in the time-dependent relations between pressure and volume, arising from the fact that the magnitudes of relaxation and retardation times depend on the volume through its connection with the fractional free volume. For a general treatment of volume viscoelasticity, the reader is referred to a review by Marvin and McKinney.[1]

Transient experiments have been made both following a sudden pressure change (analogous to creep in shear or simple extension viscoelasticity) and following a sudden temperature change (the isothermal contraction experiment portrayed in Fig. 11-7, if the temperature change is negative). Dynamic experiments have been made both by bulk compression where the deformation corresponds exactly to that specified in the definition of the bulk modulus K^*, and by propagation of longitudinal waves where the deformation corresponds to that specified by the modulus M^*, which is not exactly the same although it is often dominated by K^* (*cf.* equation 58 of Chapter 1 and equations 1-3 of Chapter 8).

A. VOLUME CREEP

Transient experiments of bulk viscoelasticity are generally of interest only at temperatures below about $T_g + 20°$, since otherwise the volume changes are too rapid for convenient observation. At higher temperatures, the equilibrium bulk modulus K_e and thermodynamic compressibility $\beta = B_e$ have been determined for numerous polymers.[2,3]

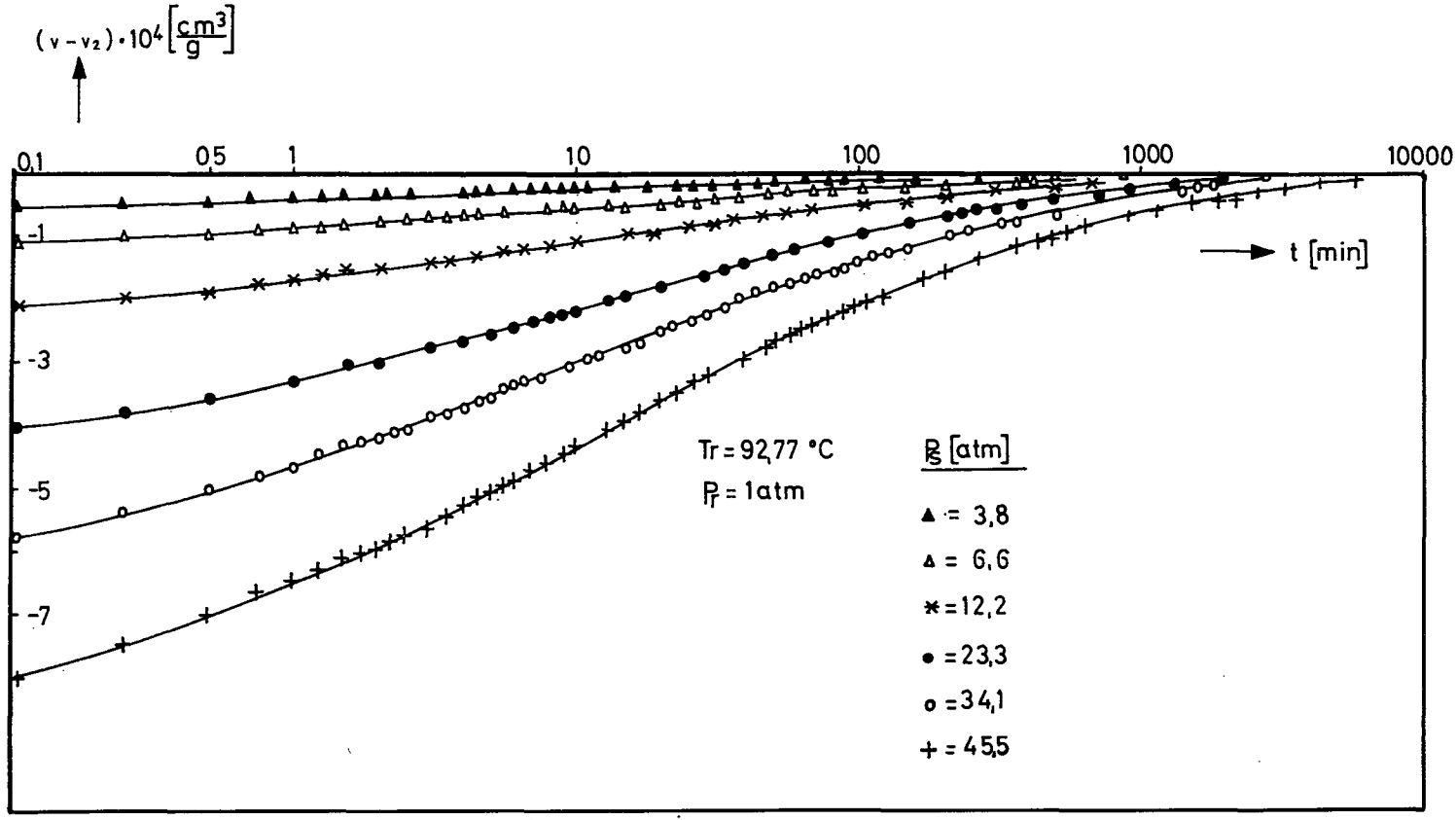


FIG. 18-1. Volume change of polystyrene following sudden pressure reduction from values of P_1 indicated to $P_2 = 1$ atm, at 92.77°C, plotted against elapsed time in minutes (logarithmic scale). (Data of Goldbach and Rehage.[4])

1. Criteria of Linearity and Relation of Nonlinearity to Free Volume

The volume change following a sudden pressure change $\Delta P = P_2 - P_1$ can be described in the range of linear bulk viscoelastic behavior by the relation

$$v = v_1 - \Delta P B(t) \tag{1}$$

and the volume v approaches an equilibrium value $v_2 = v_1 - \Delta P\beta$, where β is the thermodynamic compressibility. As a test of linearity, it is convenient to examine the normalized volume change $(v - v_2)/(v_1 - v_2) = B(t)/\beta$ as a function of time; in the linear range, it should be independent of ΔP. An example of volume creep in expansion (following release of pressure or negative ΔP) is shown in Fig. 18-1 for a polystyrene with $\overline{M}_n = 500{,}000$, studied by Goldbach and Rehage,[4] at 92.77°C. Extremely precise measurements are needed to follow the small volume changes associated with ΔP of only a few atmospheres; at 6 atm, the maximum relative change is 10^{-4}. When the data are plotted as $(v - v_2)/(v_1 - v_2)$, the points for several values of $-\Delta P$ up to 22 atm fall on a single curve as shown in Fig. 18-2, so the behavior is linear within experimental error in this range. This is to be expected since only a very small proportion of the free volume is collapsed in the experiment; near T_g, f is about 0.025, and the volume change is only of the order of 0.0001. The time-dependent volume change extends over several decades of logarithmic time, implying a rather broad distribution of voluminal retardation times. A formulation of this distribution in terms of free volume fluctuations has been proposed by Kästner.[5]

For much higher pressure changes, a marked departure from linearity may be expected because of the diminution of free volume under pressure. The effects of such volume reduction on shear relaxation times (and dielectric and nuclear magnetic relaxation times) have been described in Sections D and E of Chapter 11; the bulk relaxation and retardation times are presumably similarly affected. The origin of this kind of nonlinearity can be understood qualitatively on the basis of a theory developed by Kovacs[6] for a single retardation time.

The theory of Kovacs can be visualized by a mechanical model as shown in Fig.

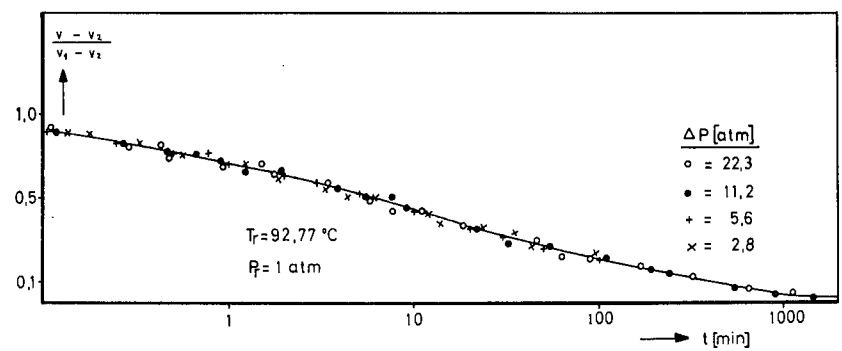


FIG. 18-2. Data of Fig. 18-1 plotted as $(v - v_2)/(v_1 - v_2)$. Points refer to different values of $\Delta P = P_2 - P_1$ as indicated.

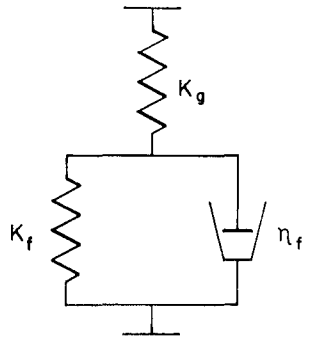


FIG. 18-3. Mechanical model for volume creep with a single retardation time whose value depends on displacement through the changing viscosity η_f. (Kovacs[6]).

18-3. The spring K_g is analogous to a bulk modulus associated with compression of the occupied volume, and K_f to a modulus associated with collapse of the free volume. The dashpot η_f is not an ordinary one, but corresponds to a viscosity which increases with downward displacement of the piston, so that the retardation time $\tau_f = \eta_f/K_f$ progressively increases with the decrease in volume under pressure.

If a small pressure change ΔP from P_1 to P_2 is suddenly imposed there will be an immediate change in specific volume from an initial value v_1 to a value $v_i = v_1 (1 - \Delta P/K_g)$ followed by a time-dependent change whose rate is governed by the differential equation corresponding to the model:[7]

$$dv/dt = -K_f(v - v_2)/\eta_f = -(v - v_2)/\tau_f \tag{2}$$

where v_2 is the equilibrium volume at pressure P_2, *viz.*, $v_1[1 - \Delta P(1/K_g + 1/K_f)]$. If τ_f were independent of v, equation 2 would integrate to an expression analogous to that for creep of a single Voigt element, equation 9 of Chapter 3:

$$v(t) = v_i + (v_2 - v_i)(1 - e^{-t/\tau_f}) \tag{3}$$

However, as v decreases the fractional free volume decreases, and τ may be expected to increase by a factor a_P which is assumed to be the same as that for shear relaxation processes expressed by equation 50 of Chapter 11:

$$\tau_f = \tau_1 \exp B(1/f(t) - 1/f_1) \tag{4}$$

where f_1 $(= f_i)$ is the fractional free volume at the beginning of the experiment. Since all the time-dependent volume change is attributed to free-volume collapse, we have to a close approximation $f(t) = f_1 + [v(t) - v_1]/v_1$. Combining these equations, the course of the time-dependent volume change is given approximately as

$$\mathrm{Ei}(-s_i) - \mathrm{Ei}(-s) + f_2(e^{-s} - e^{-s_i}) = (t - t_i)/a_P\tau_1 \tag{5}$$

where $a_P = \exp B(1/f_2 - 1/f_1)$, $s = B[1/f_2 - 1/f(t)]$ and Ei is the exponential integral function. Equation 5 describes the course of contraction when ΔP is positive. For the opposite experiment, negative ΔP (release of pressure), the sign of s in

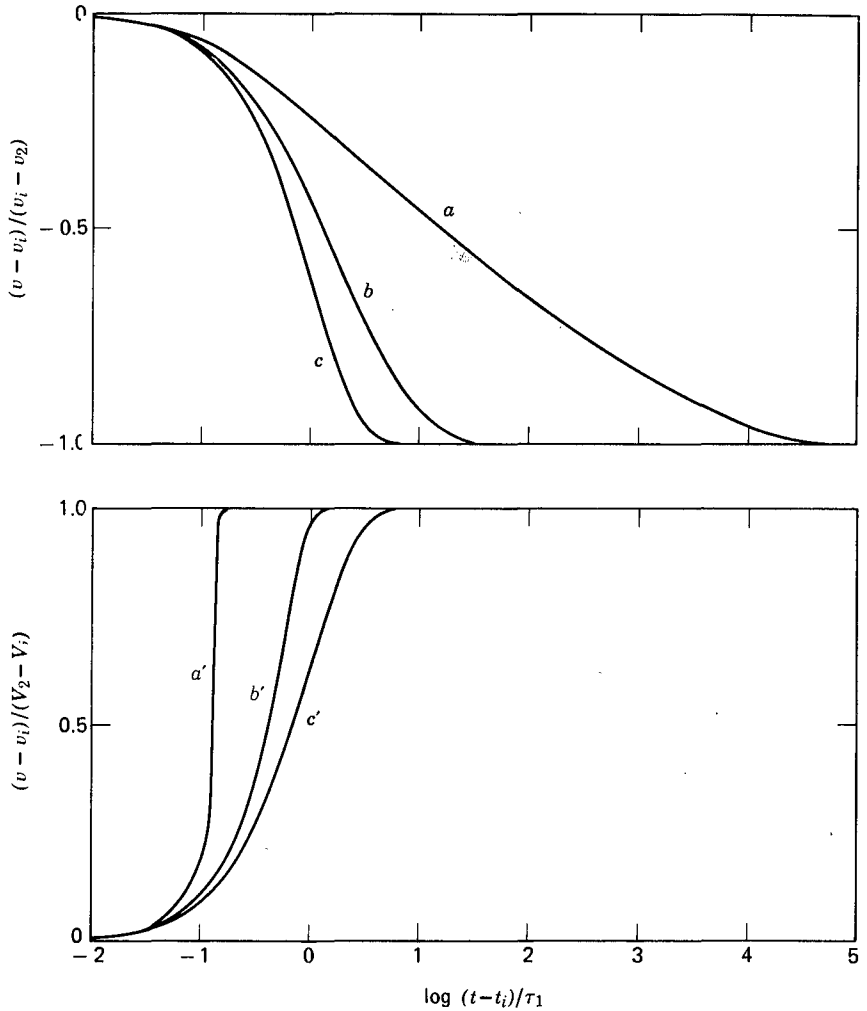


FIG. 18–4. Asymmetric, nonlinear volume creep and creep recovery, calculated from equation 5, with parameters given in text,[4] plotted as $(v - v_i)/(v_2 - v_i)$. (a, a') $\Delta P = \pm 5 \times 10^8$ dynes/cm^2; (b, b') $\Delta P = \pm 1.2 \times 10^8$; ($c$, c') ΔP sufficiently small so that equation 5 reduces to equation 3 (linear behavior with single retardation time).

equation 5 must be changed. In this case, the volume change goes progressively faster instead of progressively slower than the simple exponential course given by equation 3. The two functions are illustrated in Fig. 18–4 for an appropriate choice of parameters: $\Delta P = 5 \times 10^8$ dynes/cm^2 (about 500 atm) or 1.2×10^8, $f_i = 0.025$, $K_f = 10^{11}$ dynes/cm^2. (This plot differs slightly from Fig. 18–2 in that the instantaneous volume change $v_i - v_1$ has been omitted.) The highly unsymmetrical nature of the nonlinear behavior is evident. For very small ΔP, equation 5 reduces to equation 3, which is also shown in Fig. 18–4 for comparison; this is of course

symmetrical for ΔP positive or negative. If ΔP is not small, obviously the shape of the curves for both contraction and expansion will depend greatly on its magnitude.

This formulation is clearly oversimplified because it involves only one retardation time, whereas it is clear from Fig. 18–2 that there is a broad distribution. The nonlinear phenomenon in volume contraction (curve *a* in Fig. 18–4) causes an extension of the time scale which superficially resembles the effect of a distribution of retardation times for the *linear* case in Fig. 18–2. However, from temperature-jump experiments as described in Section B below, the two effects can be distinguished and the distribution of retardation times can be evaluated, extending over several decades of logarithmic time scale.[8,9]

2. Experimental Measurements

Although there have been several studies of compression of polymers at equilibrium,[2,3,10–12] measurements of volume creep are rather sparse. In the most extensive study on polystyrene by Goldbach and Rehage,[4] normalized curves like Fig. 18–2 were obtained at 91.84°, 92.77°, and 95.46°; they were very similar in shape and their positions on the logarithmic time axis corresponded to a shift with temperature of $d \log t/dT = 0.38 \text{ deg}^{-1}$. (The reciprocal, $dT/d \log t = 2.6$ deg, agrees well with the expectation from the WLF equation near T_g as expressed by equation 28 of Chapter 11.) The form of the distribution function of bulk retardation times,[13] calculable from Fig. 18–2 by the methods of Chapter 4, is thus independent of temperature within this range and the method of reduced variables is applicable.

Other investigations primarily in the linear range have been made by Robinet and Buvet[14] and, extending to pressures where nonlinear effects would be expected, by Martynyuk[15] and Findley.[16] However, there appear to have been no comparisons of volume creep data with the Kovacs nonlinear theory.

B. ISOTHERMAL VOLUME CHANGE AFTER TEMPERATURE JUMP

The time-dependent volume contraction which follows a sudden quench to a temperature near T_g has been illustrated in Fig. 11–7, and the prolongation of shear relaxation times which occurs during the course of such a contraction has been described in Section D3 of Chapter 11. The reverse experiment of a sudden positive change in temperature is characterized by an autoaccelerating volume change[17] which is accompanied by corresponding shortening of shear relaxation times.[18,19]

The approach to voluminal equilibrium after a sudden temperature change ("temperature jump") is closely analogous to that described in the preceding section after sudden pressure change ("pressure jump"), though it has been pointed out by Meixner[20] that the relaxation times describing the approach to equilibrium may

not necessarily be the same in both cases. The temperature-jump experiment is much easier to perform than the pressure jump, since it requires no complicated apparatus (although high precision is necessary).

1. Kinetics of Volume Changes

The criteria for linearity are similar to those described in Section A1 above for pressure-jump experiments. In a series of measurements, samples may be brought to the same final temperature T_2 from different initial temperatures T_1. If the course of the volume contraction, which takes place always at a fixed temperature T_2 after different temperature changes $\Delta T = T_2 - T_1$, is described again by the ratio $(v - v_2)/(v_1 - v_2)$, then points for different ΔT should lie on the same curve plotted against $\log t$. Such data are illustrated in Fig. 18–5 from experiments of Goldbach and Rehage[4] on the same polystyrene used in the pressure-jump experiments of Figs. 18–1 and 18–2; ΔT ranged from -10.79 to $+1.04°$. For $-1.8° < \Delta T < 0.6°$, the behavior appears to be linear, but outside this range the shape of the curve depends on ΔT. Moreover, the deviations are asymmetric with respect to the sign of ΔT; for a quench ($\Delta T < 0$) equilibrium is approached sooner than for sudden warming ($\Delta T > 0$).

This essential asymmetry was noted long ago for volume changes of inorganic glasses[21] and has been studied in detail for several polymers (as well as glucose[22]) near their glass transition temperatures by Kovacs.[17,22] An example is shown in Fig. 18–6 for a poly(vinyl acetate) subjected to temperature changes of $+5°$ and $-5°$ to a final temperature of 35°. For quench ($\Delta T < 0$), the volume change is prolonged over many decades; for $\Delta T > 0$, the volume change occurs very slowly at first but with increasing speed toward the end of the process. The last decade of the time scale reflects the same kind of difference as seen in Fig. 18–5 for the two extremes of ΔT. This behavior is attributable to the effect of free volume on retardation times exactly as in the nonlinear analysis of bulk creep in Section A. In contraction ($\Delta T < 0$), the retardation times become progressively longer as the free volume collapses; but in dilatation ($\Delta T > 0$), they become progressively

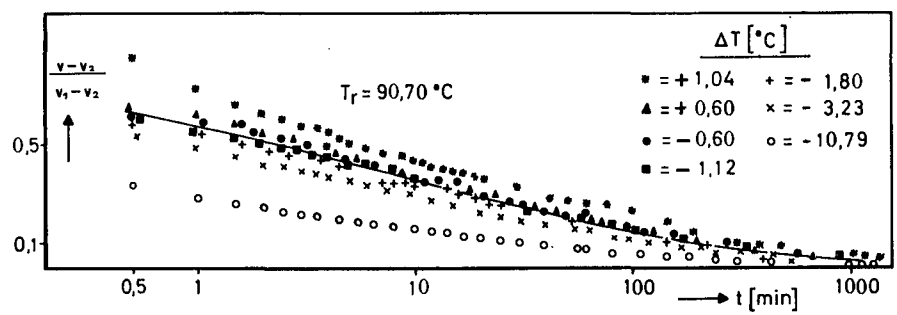


FIG. 18–5. Volume changes of polystyrene following sudden temperature changes to final temperature $T_2 = 90.70°C$ at 1 atm with different positive and negative values of $\Delta T = T_2 - T_1$ as indicated, plotted as $(v - v_2)/(v_1 - v_2)$. (Data of Goldbach and Rehage.[4])

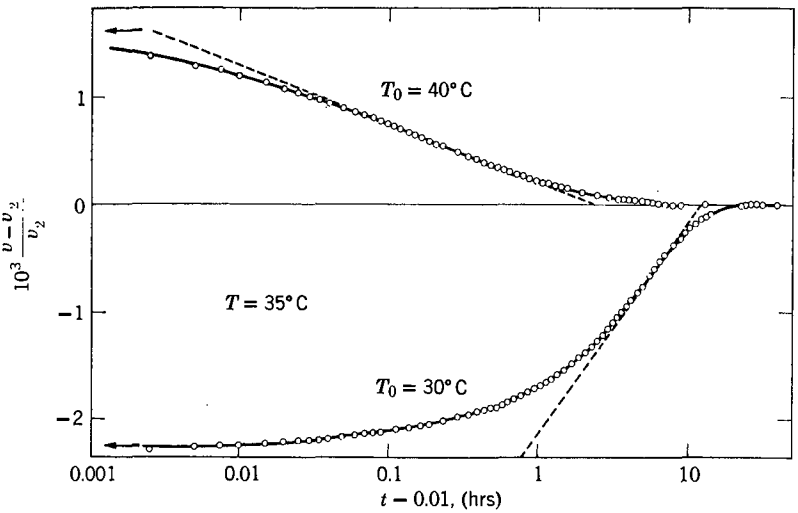


FIG. 18-6. Asymmetric isothermal volume changes of poly(vinyl acetate) at 35° following sudden ΔT of −5° and +5° respectively, plotted as $(v - v_2)/v_2$ against $t - 0.01$ in hours with logarithmic scale. (Kovacs.[17])

shorter as the free volume expands, in accordance with equation 4. (At the beginning of the experiment, the difference in behavior is associated with the fact that the experimental temperature jump approximates more nearly an instantaneous step on the time scale of the material at 30° than it does at 40°.)

With this concept, equation 5 can be applied to isothermal volume contraction following $\Delta T < 0$, if a_P is replaced by $a_T = \exp B(1/f_2 - 1/f_1)$, where f_1 and f_2 are the equilibrium volumes at the initial and final temperatures. Even with the unrealistic approximation of a single retardation time, quite good agreement with experimentally observed isothermal contraction curves can be obtained with equation 5 if suitable values of f_1 and α_f are chosen to obtain f_2 at a series of final temperatures. For example,[17] Fig. 18-7 shows a set of contraction curves for poly(vinyl acetate) quenched from 40° to several different temperatures ranging from 25° to 37.5°. (Here 0.01 hr has been subtracted from the measured time to allow for coming to thermal equilibrium.) Fig. 18-8 shows the curves calculated from equation 5 with $f_{40} = 0.0216$, $\alpha_f = 4.2 \times 10^{-4}$, $B = 1$. The shapes of the isotherms, and their positions along the time axis, are almost coincident with the experimental data, since Figs. 18-8 and 18-7 can be superposed *en bloc*. However, both f_{40} and α_f as used here are smaller than would be expected from temperature dependence of shear viscoelasticity (Table 11-II). The discrepancy arises in part from a distribution of retardation times, the effect of which can be imitated by exaggerating the role of free volume with parameters that are a little too small. For volume expansion following $\Delta T > 0$, qualitative agreement can also be obtained but it is less satisfactory, probably because the exaggeration of the free-volume effect now works in the wrong direction to imitate a distribution of retardation times. A more detailed differential analysis[17] of the curves of Figs. 18-7 and 18-8 reveals

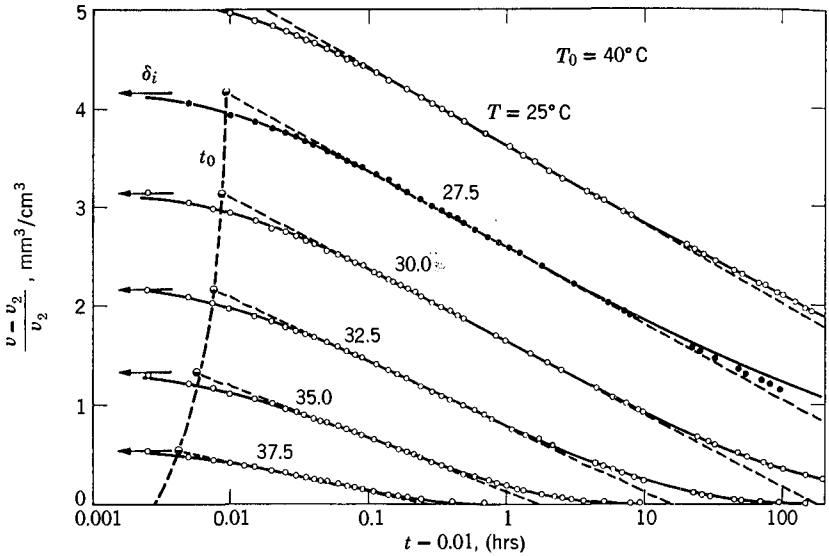


FIG. 18-7. Isothermal volume changes of poly(vinyl acetate) after sudden quench from 40°C to temperatures indicated, plotted as $(v - v_2)/v_2$ against $t - 0.01$ in hours with logarithmic scale. (Kovacs.[17]).

other discrepancies which may be attributed to a distribution of retardation times and fluctuations in free volume; these cannot be described without more parameters. Recently, more extended theoretical treatments by Narayanaswamy,[23a] Moynihan,[23b] and Kovacs and collaborators[8,9,23,23c] have introduced additional parameters. Use of a spectrum of retardation times with a time scale which depends not only on temperature and pressure but also on the instantaneous state of the system

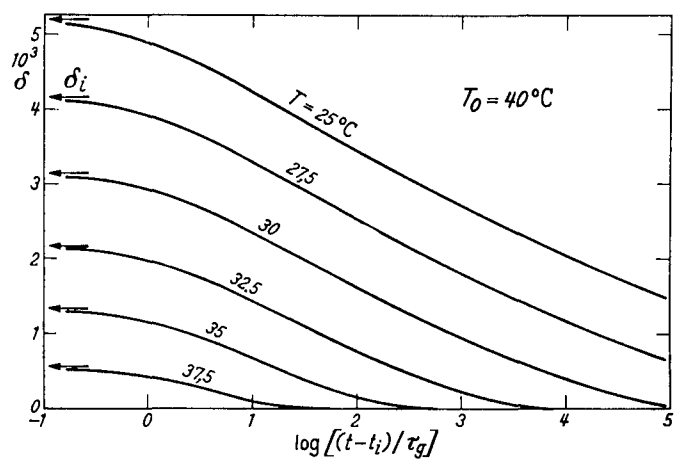


FIG. 18-8. Theoretical curves corresponding to Fig. 18-8, calculated from equation 5 with parameters given in text. (Kovacs.[17])

as characterized by its overall departure from equilibrium reduces the problem to a linear analysis and gives satisfactory agreement with experiment including behavior in more complicated thermal histories such as successive temperature jumps.[8,9,23,23c] There are parallel effects in the time dependence of enthalpy.[9]

2. Effects of Isothermal Volume Changes on Shear and Elongational Relaxation Processes

Changes in shear relaxation times during volume contraction after a quench to a temperature near T_g were implicit in viscosity measurements of inorganic glasses long ago by Lillie,[21] and more recently by Prod'homme[24] and Zijlstra,[25] who found the steady-flow viscosity (naturally extremely high, of the order of 10^{13} poises) to increase progressively with time. The simple theory for $a_{T,t}$, the shift factor for relaxation times which provides for differences in both temperature and elapsed time, has been given in Chapter 11 (Section D3, equation 66.) The progressive change in state of a polymer near or below T_g at constant temperature and pressure has been described as "physical aging." [26-28]

In an extensive series of measurements on poly(vinyl acetate), Kovacs, Stratton, and Ferry[18] studied the dynamic storage and loss shear moduli over a range of frequencies as a function of elapsed time after quenches from a temperature well above T_g to several selected temperatures near T_g. Examples for the storage modulus are shown in Fig. 18-9. The heavy curves represent measurements at voluminal equilibrium at the temperatures indicated; the points and light curves represent the data measured repeatedly during approach to voluminal equilibrium. At 30°, for example, measurements 50 min after quench lie close to the equilibrium curve at 33.8°. With elapsed time, the curve for G' as a function of ω shifts to the left; at 1360 min it lies close to the equilibrium curve at 31.25°; and it eventually reaches its own equilibrium position. These shifts correspond to progressive increases in the relaxation times. Parallel dilatometric measurements of volume contraction were made and from them the shift factor $a_{T,t}$ was calculated by equations 66 and 49 of Chapter 11 (taking $\alpha_f = 5.3 \times 10^{-4}$ and $f_{35,\infty} = 0.0225$, where the subscript 35, ∞ refers to voluminal equilibrium at 35°C; these values differ slightly from the data in Table 11-II but give a better representation of the temperature dependence of dynamic data at voluminal equilibrium in the immediate vicinity of T_g). When plotted against log $\omega a_{T,t}$, all the data of Fig. 18-9, as well as other data for a quench to 25°, fall on a single composite curve. Later measurements by Lamandé and Kovacs[29] with different apparatus gave identical results, and additional data for quenches to 2°, 10°, and 16° fell on the same composite curve when plotted against log $\omega a_{T,t}$.

Data for G'' measured at various temperatures and elapsed times did not reduce satisfactorily in this manner, however; for $f < 0.022$, deviations appeared indicating a slight change in the shape of the relaxation spectrum, to which G'' is more sensitive in this region then G'. The magnitude of the deviation appeared to be a single-valued function of f, for all temperatures and elapsed times.[18,26]

Measurement of viscoelastic properties as a function of elapsed time following

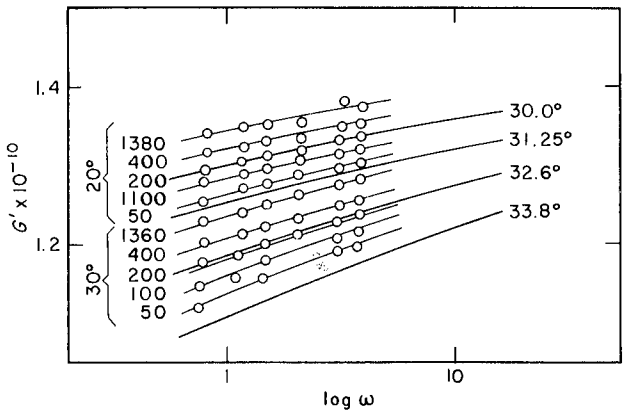


FIG. 18-9. Storage shear modulus plotted against logarithm of radian frequency for poly(vinyl acetate) after sudden quench from 45° to 20° or 30°, at different elapsed times in minutes as indicated by numbers at left. Heavy curves refer to measurements at voluminal equilibrium (after completion of isothermal contraction) at the temperatures indicated at right.[18]

a positive ΔT show the autoaccelerating character[18] expected from the course of the volume change observed in such an experiment (Fig. 18-6).

Similar results have been observed in oscillatory measurements on poly(*n*-butyl methacrylate).[30]

Viscoelastic properties in shear can also be studied by transient measurements during isothermal volume changes. An example is shown in Fig. 18-10 for torsional creep of polystyrene after quench from 100° to 50°C measured by Struik.[19,27] The time scale shifts progressively to longer times with aging at 50°C with no change in the form of the creep compliance function as shown by the superposition of points (although a small shift in the magnitude of the compliance is empirically imposed). The shift factor a_t changed with elapsed time in the manner expected from parallel dilatometric measurements. If the time period of the creep experiment is comparable with the aging period, the dependence on elapsed time is not quite so clear-cut as in dynamic measurements, but by interpolation the creep compliance $J(t)$ can be obtained as a function of time after application of stress at constant values of elapsed time since temperature quench—an isoaeonal creep curve. From similar measurements on poly(vinyl acetate) by Lamandé,[27] composite curves of $J(t)$ against $t/a_{T,t}$ were obtained, in which the shift factor $a_{T,t}$ for different temperatures and elapsed times was related to free-volume parameters that agreed fairly closely with those derived from the dependence of mechanical properties on temperature alone.

It is of interest that very similar results are obtained for torsional creep measurements on amorphous glucose quenched from above T_g ($\cong$ 40°C) to 22°C and aged for up to 12 hr.[27] As mentioned in Chapter 15, shear relaxation processes in glasses of low molecular weight are quite similar in some respects to those in polymeric glasses.

Creep in uniaxial extension also shows the effect of progressive isothermal pro-

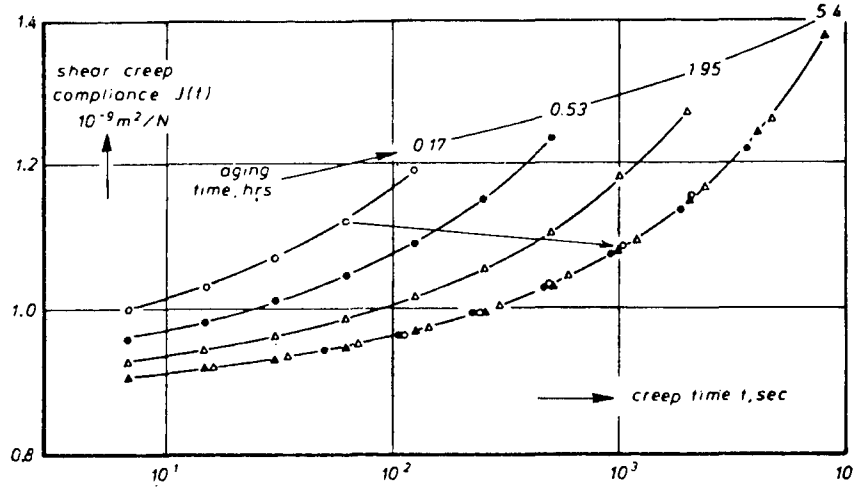


FIG. 18-10. Shear creep compliance plotted against time with a logarithmic scale for polystyrene quenched from 100°C to 50°C and aged for varying periods as shown. Curve at right contains all the points after shift of each individual curve with large horizontal and small vertical shifts. (Struik.[27]) Reproduced, by permission, from *Physical Aging in Amorphous Polymers and Other Materials*, by L. C. E. Struik, Elsevier/North Holland Biomedical Press, 1978.

longation of relaxation times, as illustrated in Fig. 18-11 by measurements of Struik on poly(vinyl chloride) quenched from 90°C (about 10° above T_g) to 40° and kept for varying periods up to 4 years. The shifts in time scale provide excellent superposition with almost no adjustment in the magnitude of the tensile compliance $D(t)$. In this case, $D(t)$ reflects both bulk and shear deformations (equation 55 of Chapter 1) since near the glass transition temperature Poisson's ratio is not near $\frac{1}{2}$.[31] However, since both bulk and shear relaxation times depend on free volume in a similar manner, it is not surprising that this experiment also gives very similar results.

Measurements of stress relaxation of polystyrene and polycarbonate below T_g also show the effects of increasing all the relaxation times with elapsed time following a temperature quench, associated with contraction of free volume.[32]

The above examples refer to linear viscoelastic behavior under small stresses. At higher shear stresses, the shear relaxation times also increase with elapsed time but to a lesser extent.[27] Other aspects of the changes in viscoelastic properties with elapsed time, including prediction of properties after long time periods, have been discussed in detail by Struik.[27]

A closely related phenomenon appears when application of a tensile strain increases the volume under circumstances where Poisson's ratio μ is substantially less than $\frac{1}{2}$—*i.e.*, near or below the glass transition temperature. In accordance with the definition of μ in connection with equation 50 of Chapter 1, the volume increase accompanying longitudinal extension is given by

$$\partial v/\partial \epsilon = v(1 - 2\mu) \tag{6}$$

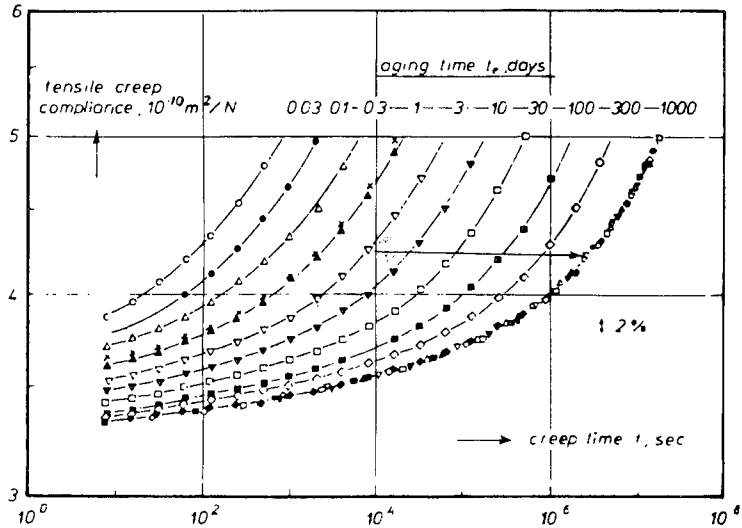


FIG. 18-11. Tensile creep compliance plotted against time with a logarithmic scale for poly(vinyl chloride) quenched from 90°C to 40° and aged for varying periods as shown up to 1000 days. Curve at right contains all points after shifts as in Fig. 18-10 (almost no vertical shift). (Struik.[27]) Reproduced, by permission, from *Physical Aging in Amorphous Polymers and Other Materials*, by L. C. E. Struik, Elsevier/North Holland Biomedical Press, 1978.

A portion of this volume increase may be attributed to expansion of free volume, and since it is caused by the dilatational component of the applied stress, the proportion can be estimated[33] to be the same as the ratio of the compressibilities β_f and β (Chapter 11, Section D1); then $\partial f/\partial \epsilon = (\beta_f/\beta)(1/v)(\partial v/\partial \epsilon)$. Substitution into equation 49 of Chapter 11, for small tensile strains where $\partial f/\partial \epsilon$ can be approximated by $(f_2 - f_1)/\epsilon$, predicts that all relaxation times will be modified by a shift factor a_ϵ whose value is given by[33]

$$\log a_\epsilon = -\frac{(B/2.303f_0)\epsilon}{f_0/(\beta_f/\beta)(1-2\mu)+\epsilon} \tag{7}$$

Here f_0 ($= f_1$ of equation 49 of Chapter 11) is the fractional free volume at zero strain. For reasonable values of parameters near T_g, it can be estimated that a tensile strain of 1% would shift the time scale by about one logarithmic decade. In a simpler formulation, the ratio β_f/β may be taken as unity.[34] Experiments of this sort have been reported for poly(methyl methacrylate),[35,36] copolymers consisting largely of polyacrylonitrile,[37] polycarbonate,[32,34] and an acrylonitrile-butadiene-styrene copolymer blend;[32] the effects of strain dilatation on tensile stress relaxation, torsional stress relaxation, and combined tensile and torsional stress relaxation have been compared.[28,36]

Still another related effect can be observed when a quenched glassy polymer is subjected to varying mechanical history by successive stress relaxation experiments in uniaxial extension.[28,36] The relaxation times of poly(methyl methacrylate) appear to increase with this progressive stress history more rapidly than with the lapse of

time at rest as in Figs. 18–9 to 18–11; the phenomenon is termed "mechanical aging."

C. DYNAMIC PROPERTIES IN BULK COMPRESSION

In dynamic bulk viscoelastic measurements, the deformations are ordinarily exceedingly small and therefore in the linear range of behavior; the change in free volume during a cycle of deformation is a very small proportion of the total free volume. However, a large constant hydrostatic pressure can be imposed if desired on the small periodic pressure changes, thereby altering the free volume and hence the relaxation times and the frequency scale of the viscoelastic dispersion.

The most extensive measurements of dynamic bulk compression have been those of McKinney and Belcher[38] on poly(vinyl acetate), covering ranges of frequency from 50 to 1000 Hz, temperature from 0° to 100°C, and superposed hydrostatic pressure from 1 to about 1000 atm. Both storage and loss bulk compliances, B' and B'', were obtained. All data were successfully combined by the method of reduced variables taking into account the substantial dependence of both B_e and B_g (the equilibrium and glasslike bulk compliances) on both T and P, as follows:

$$B^*(T_0, P_0, \omega_0) = B_g(T_0, P_0) + [\Delta B(T_0, P_0)/\Delta B(T, P)][B^*(T, P, \omega) - B_g(T, P)] \quad (8)$$

where the subscripts 0 refer to reference conditions, chosen two at a time (see below) as 50°C, 1 atm, and 1000 Hz, and

$$\Delta B(T, P) = B_e(T, P) - B_g(T, P) \quad (9)$$

The equilibrium compliance B_e may be attributed to compression of the occupied volume plus collapse of free volume; and the glasslike compliance B_g, which B' approaches at high frequencies and low temperatures, is attributed to compression of the occupied volume only. The dependences of these quantities on T and P were evaluated from the data to be

$$B_e(T, P) \times 10^5 = 2.919 + 1.905 \times 10^{-2}\, T - 0.950 \times 10^{-3}\, P - 1.011 \times {}^{-5}\, TP \quad (10)$$

$$B_g(T, P) \times 10^5 = 1.865 + 0.836 \times 10^{-2}\, T - 0.433 \times 10^{-3}\, P - 0.685 \times 10^{-5}\, TP \quad (11)$$

(Here the units of compliance are bars^{-1}, or 10^{-6} cm^2/dyne.)

The conventional reduced curves plotted against reduced frequency are obtained by choosing ω as the independent variable in equation 6 and reducing B' and B'' to T_0 and P_0 by equations 8–11, then plotting against $\omega a_{T,P}$ where $a_{T,P} = a_{12}$ is given in terms of free volume by equations 49 and 58 of Chapter 11. For this purpose, α_f was taken as 4.8×10^{-4} deg^{-1}, β_f as 0.96×10^{-11} cm^2/dyne, and $f = 0.025$ at 17°C and 1 atm. The results have already been seen in Fig. 2–9 as the classical example of bulk viscoelastic behavior.

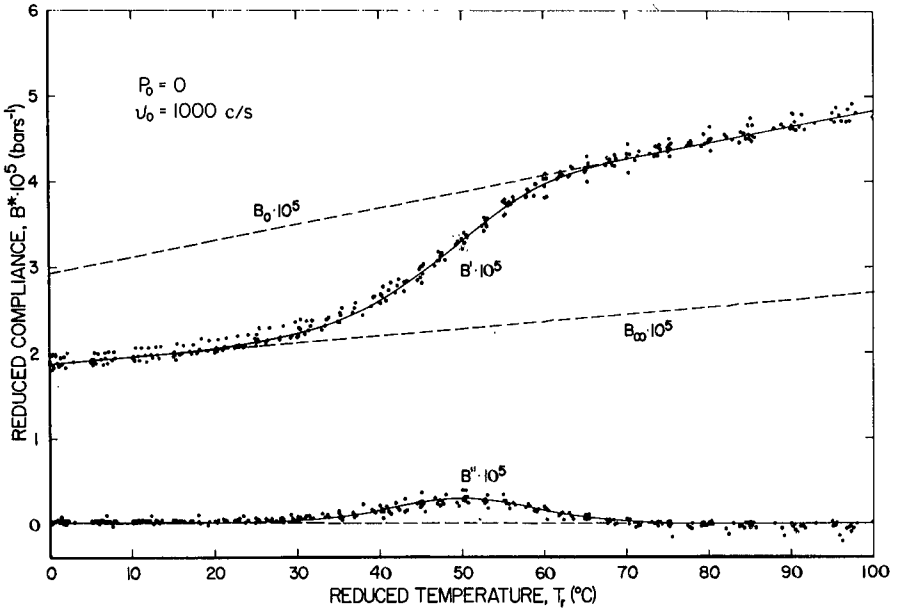


FIG. 18-12. Dynamic bulk storage and loss compliances of poly(vinyl acetate) reduced to 1 atm and 1000 Hz by equation 6 and plotted against reduced temperature defined by equation 12. B_0 and B_∞ correspond to B_e and B_g in the text. (McKinney and Belcher.[38])

Alternatively, T may be chosen as the independent variable and the data reduced to ω_0 and P_0 for plotting against a reduced temperature. The latter must be defined by the rather complicated relation

$$T_r = T - \frac{\beta_f}{\alpha_f} P + \frac{1}{\alpha_f} \cdot \frac{[f_g + \alpha_f(T - T_{g0}) - \beta_f P]^2 \ln(\omega_0/\omega)}{1 - [f_g + \alpha_f(T - T_{g0}) - \beta_f P] \ln(\omega_0/\omega)} \tag{12}$$

where T_{g0} is the glass transition temperature at 1 atm. The data are plotted in this manner in Fig. 18-12, representing the behavior over an extended temperature range at 1 atm and 1000 Hz. The importance of the positive temperature dependence of B_e and B_g is apparent. (For shear measurements of a cross-linked network, the J_e line in such a plot would have a negative slope, but would lie so far above the J_g line that the two could scarcely be portrayed in the same figure.)

Finally, the data can be reduced to ω_0 and T_0 and plotted against a reduced pressure defined by a relation analogous to equation 12. This plot is shown in Fig. 18-13; it emphasizes the strong pressure dependence of B_e and B_g.

A similar investigation of a soft vulcanized rubber containing 12% sulfur, by McKinney, Belcher, and Marvin,[39] gave results very similar to those portrayed in Figs. 2-9, 18-12, and 18-13; the plot against reduced frequency, analogous to Fig. 2-9, is shown in Fig. 18-14. In early calculations by Marvin, Aldrich, and Sack[40] on polyisobutylene, data on the dynamic bulk longitudinal modulus M^* were combined with G^* data to give the storage and loss components of the dynamic

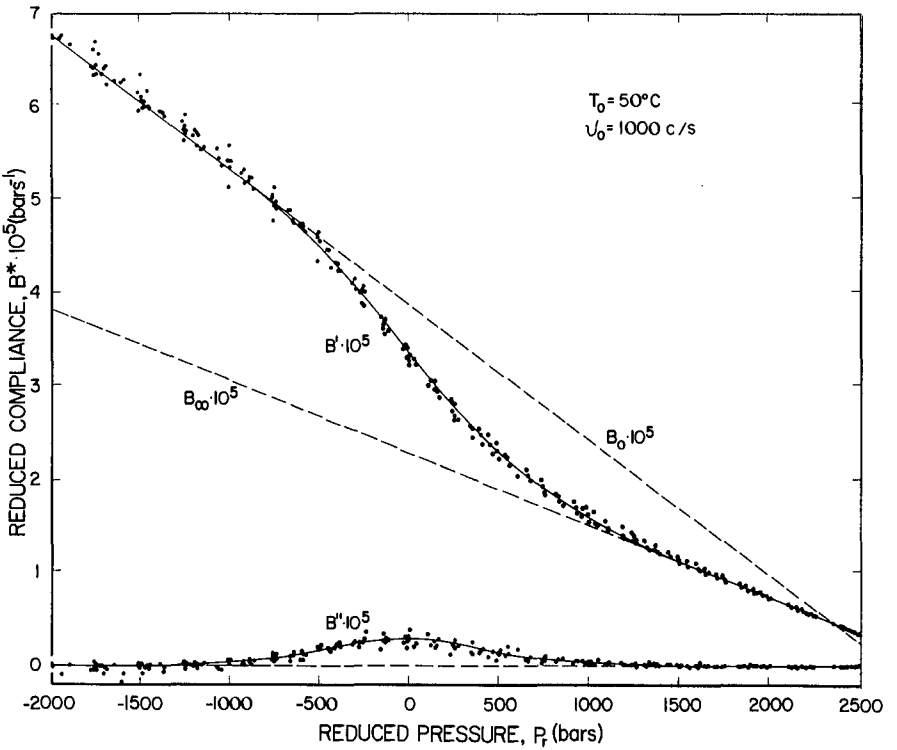


FIG. 18–13. Data of Fig. 18–12 reduced to 50°C and 1000 Hz by equation 6 and plotted against reduced pressure (McKinney and Belcher[38]). B_0 and B_∞ correspond to B_e and B_g in the text.

bulk modulus K^* by the relations derived from equation 58 of Chapter 1:

$$K' = M' - \tfrac{4}{3}G' \tag{13}$$

$$K'' = M'' - \tfrac{4}{3}G'' \tag{14}$$

and these data can in turn be converted to B' and B'', though with less precision.

Some features of these measurements are summarized in Table 18–I. (It must be remembered that all these dynamic compliances are adiabatic (Chapter 5, Section I) and are subject to significant corrections before they can be compared with the results of isothermal transient measurements.)

The quantity $\Delta B/B_e$ represents the proportion of the total compressibility which can be attributed to time-dependent configurational readjustments and decrease of free volume. It ranges from 0.25 to 0.68 for the three polymers listed. However, for a given polymer this ratio depends on the temperature so that comparisons have only qualitative significance unless made at temperatures equally removed from T_g, as is the case for the first two entries in the table.

The quantity $B''_{max}/\Delta B$ is an indication of the breadth of the retardation spectrum;

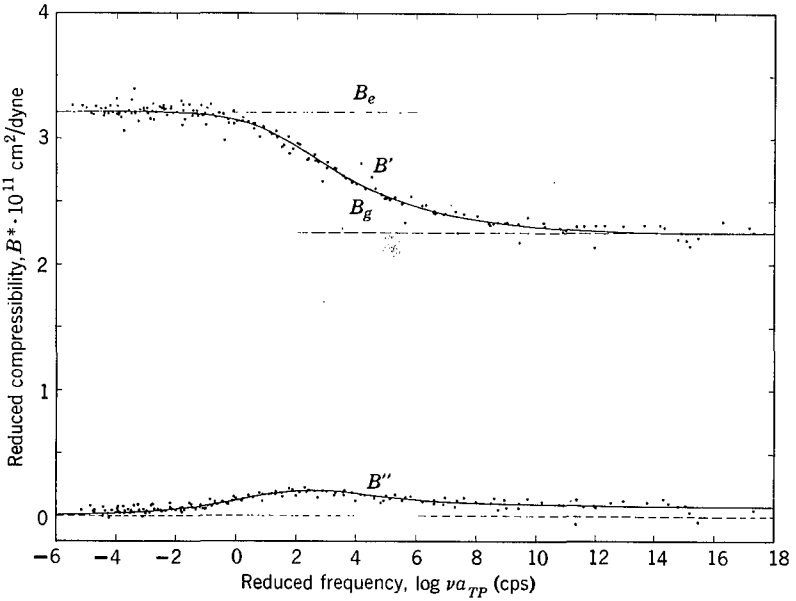


FIG. 18-14. Dynamic bulk storage and loss compliances of natural rubber vulcanized by sulfur, reduced to 0°C and 1 atm pressure by equation 6 and plotted against logarithm of reduced frequency, $\nu a_{T,p}$ (McKinney, Belcher, and Marvin.[39])

it would be 0.50 for a single relaxation time (such as represented by the mechanical model of Fig. 18-3 for the limit of linear behavior). Here it varies from 0.12 to 0.28, indicating a rather broad distribution. The analog of this quantity for shear deformations is $J''_{\max}/J_e$, since for shear the difference between $J_e - J_g$ and J_e is negligible; this ratio is of the order of 0.3 for lightly cross-linked networks and (replacing J_e by J_N^0) for entanglement networks, as discussed in Chapters 13 and 14, so the spectrum is if anything broader for bulk deformation. The results are

Table 18-I

CHARACTERISTIC DATA FOR DYNAMIC BULK COMPLIANCE AND MODULUS

Polymer	Temperature, °C	ΔB^a, cm²/dyne × 10^{11}	$\Delta B/B_e$	$B''_{\max}$, cm²/dyne × 10^{11}	$\frac{B''_{\max}}{\Delta B}$	Ref.
Poly(vinyl acetate)	50° [b]	1.59	0.41	0.30	0.19	38
Natural rubber vulcanized with 12% sulfur	0° [b]	0.71	0.25	0.20	0.28	39
Polyisobutylene	25°	4.2	0.68	0.50	0.12	40

[a] At the temperature and frequency corresponding to the maximum in B'' or K'' respectively.

[b] Approximately 25° above T_g.

qualitatively consistent with the course of linear bulk creep as depicted in Fig. 18–2, though the time scales of the two types of experiments are enormously different.

If the quantity ΔB can be interpreted as the compressibility of the free volume, it should be the same (after applying a correction to isothermal conditions) as $\beta_f = \alpha_f(\partial T/\partial P)_\tau$, the free volume compressibility appearing in equation 59 of Chapter 11. In the investigations of Marvin and collaborators,[38,39] this was found to be the case for natural rubber vulcanized with sulfur; but not for poly(vinyl acetate), where β_f was smaller than the isothermally corrected ΔB by nearly a factor of 2. The difference may be associated with the presence of side groups which are considerably bigger than the methyl group of natural rubber.

Other investigations by Kono[41–43] and Wada[44–46] have provided less complete information on a variety of polymers including styrene-butadiene rubber, polystyrene, poly(vinyl chloride), and polyethylene; and poly(methyl, poly(ethyl, poly(*n*-butyl, and poly(*i*-butyl methacrylate)s. These measurements were made at much higher frequencies and in most cases were based on combining data for M^* and G^* by equations 13 and 14. With frequency and temperature as variables, reduced curves for K' and K'' against reduced frequency were obtained for styrene-butadiene rubber; converted to B' and B'', these resemble qualitatively those of Figs. 2–9 and 18–14. In other investigations, temperature was the only variable, leading to plots similar to Fig. 18–12 but covering a narrower temperature range. The method of wave propagation in a dilute suspension[45,56] has also been used to obtain dynamic bulk properties of several polymers. The results all resemble the features described above, but generally do not provide enough information to estimate B_e and B_g at the same temperature in order to calculate ΔB and thence the ratios in Table 18–I.

There has been considerable interest[1,41–43] in comparing the dependence of K'' and G'' on temperature or frequency to see whether the two loss maxima appear at the same point on the abscissa scale. This is easily done when the bulk properties are derived from simultaneous bulk longitudinal and shear wave propagation at the same frequency. It appears that for polymers with no large side groups the two maxima often occur at about the same temperature, but the presence of side groups causes G''_{max} to appear at a lower temperature than K''_{max}, to a degree which increases with increasing length of the side group. This comparison is somewhat arbitrary, however. If it were made in terms of J''_{max} and B''_{max}, the former would appear at lower temperatures than G''_{max} and the latter would be at almost the same location as K''_{max}, because of the differences in the magnitudes of the two dispersions; hence the discrepancies would be magnified. Secondary dispersions attributable to side groups have been found[41,42] in the bulk modulus as well as the shear modulus below T_g, and these may play an important role in comparing the two types of deformation.[1]

D. BULK LONGITUDINAL VISCOELASTIC BEHAVIOR

The components B' and B'' of the complex dynamic bulk compliance, or th components K' and K'' of the dynamic bulk modulus, were obtained in experiment

such as those of Wada and Kono described above by combining shear and bulk longitudinal wave propagation measurements. In many investigations, however, only the bulk longitudinal modulus $M' + iM''$ is measured. Often the velocity of propagation and absorption coefficient for bulk longitudinal waves are called simply "velocity of sound" and "sound absorption" (or, depending on the frequency, ultrasonic velocity and absorption) respectively.

In simple liquids, $G' = 0$ and so measuring M' is equivalent to measuring K'. Also, for dilute polymer solutions and soft polymers, *i.e.*, those for which $G' \ll K'$ at the frequency of measurements, the term in G' can obviously be neglected. However, the two terms in equation 14 may be of similar magnitude, so if G'' is not known the only recourse is to examine the behavior of M'' without attempting to interpret its shear and bulk contributions separately.

The loss component M'' is frequently expressed in terms of the absorption coefficient for wave propagation, α (*cf.* Chapter 5, equation 35 and associated discussion). Often the acoustic attenuation is given in decibels/cm ($= 8.686\alpha$). When $\alpha\lambda/2\pi \ll 1$, the analog of equation 40 of Chapter 5 for bulk longitudinal waves is

$$M'' = 2\rho v^3 \alpha/\omega$$

or

$$M''/\omega = 2\rho v^3 \alpha/\omega^2 = \eta_v' + \tfrac{4}{3}\eta' \tag{15}$$

where v is the velocity of propagation. Thus at low frequencies α is proportional to ω^2, and from their ratio the low-frequency limiting value of the right side of equation 15, *viz.*, $\eta_v + \frac{4}{3}\eta_0$, can be calculated. Since η_0 is known from shear measurements, η_v can be obtained by difference.[47,48]

For many simple polyatomic liquids, the energy absorption (loss) is far greater than given by the $\frac{4}{3}\eta_0$ term in equation 15, and M^* undergoes a dispersion which can be attributed to a lag in the transfer from translational to vibrational energy.[48–52] In such circumstances equation 15 would be inapplicable. This phenomenon is much less apparent in associated and highly viscous liquids, however, and is presumably absent in polymers. For associated liquids, η_v obtained from equation 15 is of the same order as or smaller than η_0, and their temperature dependences are the same.[52,53] Here the additional absorption besides that represented by the $\frac{4}{3}\eta_0$ term is attributed to structural rearrangement as in the case of polymers.

1. Dilute Polymer Solutions

Extensive measurements of ultrasonic velocity and absorption have been made on many polymer solutions at concentrations of the order of 0.01 to 0.1 g/cc.[54–61] Results for acoustic absorption are usually expressed as α/ν^2, where ν is the frequency in Hz ($= \omega/2\pi$), which from equation 15 is given by

$$\alpha/\nu^2 = (2\pi^2/\rho v^3)[\eta_v' + \tfrac{4}{3}\eta'] \tag{16}$$

For dilute solutions, the difference in acoustic absorption between solution and

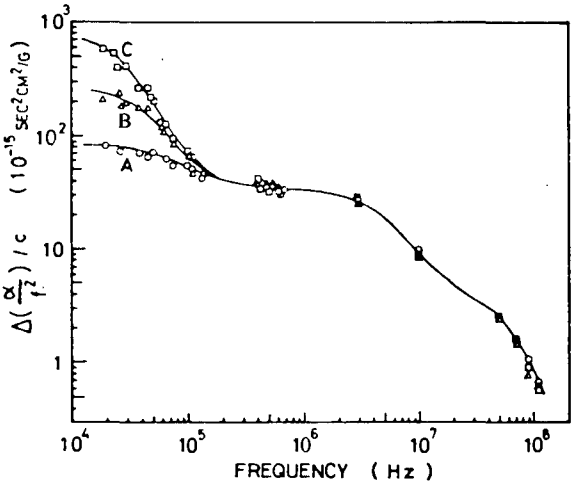


FIG. 18-15. Plot with logarithmic scales of $\Delta(\alpha/\nu^2)/c$ against frequency for solutions of three polystyrenes in xylene. Molecular weights $\times 10^{-5}$: (A) 2.1; (B) 3.7; (C) 10.0. (Ono, Shintani, Yano, and Wada.[57]) Reproduced, by permission, from *Polymer Journal*.

solvent, $\Delta(\alpha/\nu^2)$, is found to be proportional to concentration c at the high frequencies usually employed.[57-60]

An example of the frequency dependence of $\Delta(\alpha/\nu^2)/c$ for solutions of polystyrenes of different molecular weights in xylene in the concentration range 0.01 to 0.02 g/cc is shown from data of Wada and collaborators[57] in Fig. 18-15. There is evidently a low-frequency absorption which increases with molecular weight and a high-frequency absorption (above 10^5 Hz) which is independent of molecular weight. Qualitatively, this resembles the behavior in shearing deformations as discussed in Chapter 9, but a quantitative comparison is complicated.[57] For samples in a lower molecular weight range, a molecular weight dependence is observed even at higher frequencies, as shown in Fig. 18-16 from data of North and collaborators,[56] and has been attributed to a different relaxation process for the ends of the molecules.

It has been concluded that the term $\frac{4}{3}\eta'$ in equation 16 is relatively small in these experiments,[57] so the energy dissipation is largely due to the volume viscosity η_v'. The molecular mechanism has been discussed from different points of view,[56,57,62] but is beyond the scope of this chapter.

Such measurements on polyamino acids such as poly(L-glutamic acid) and poly(benzyl-L-glutamate) are of particular interest because the character of the absorption is different for the helical and random coil configurations which are found in different solvents.[63,64]

2. Undiluted Polymers and Concentrated Solutions

The longitudinal bulk wave velocity has often been measured in polymers as a function of temperature at constant frequency. Because M' and M'' are relatively

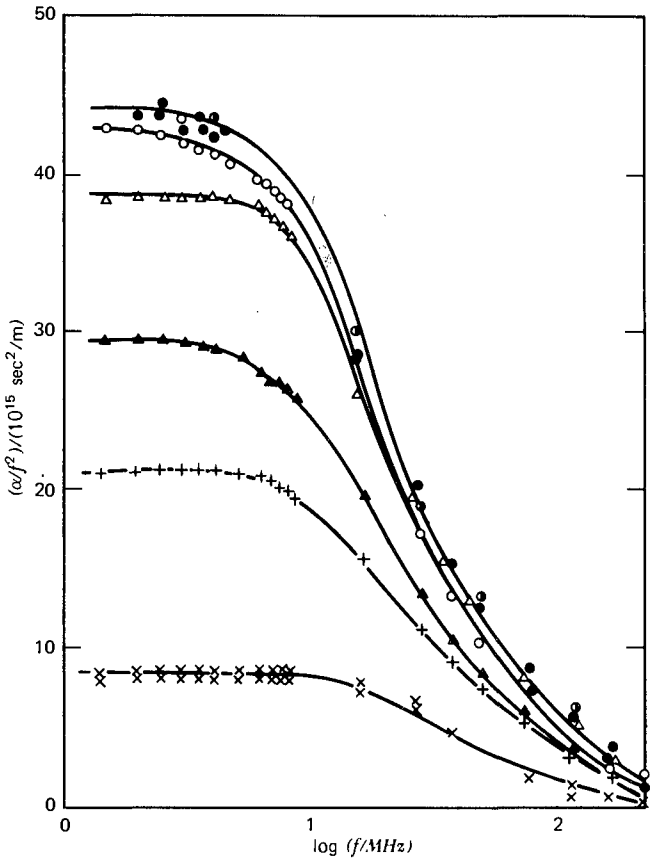


FIG. 18-16. Plot of α/ν^2 against the logarithm of frequency in megahertz for solutions of seven polystyrenes in toluene at 30°C, $c = 0.025$ g/ml. Molecular weights, bottom to top: 600, 2000, 4000, 10,000, 20,400, 51,000, 97,000. (Cochran, Dunbar, North, and Pethrick.[56]) Reproduced, by permission, from *Journal of the Chemical Society Faraday Transactions II.*

unfamiliar quantities, experimental data are often left in the form of the propagation velocity v and attenuation or absorption coefficient α, rather than converted to M' and M'' by the analogs of equations 39 and 40 of Chapter 5. For the sake of orientation, it may be noted that v is roughly proportional to $\sqrt{M'}$, while α is related to tan δ by the following equation:

$$\tan \delta = \alpha\lambda/\pi[1 - (\alpha\lambda/2\pi)^2]$$

An example is shown in Fig. 18-17, where v and attenuation ($= 8.686\alpha$) at 2×10^6 Hz are plotted against temperature for poly(vinyl acetate), as reported by Thurn and Wolf.[65] Three zones of dispersion are apparent. The one at 93°C undoubtedly represents the primary transition from glasslike to rubberlike consistency, in which v drops by about 50% because of the virtual disappearance of the $\frac{4}{3}G'$ term in equation 13 as it becomes smaller than K' by several orders of magnitude. But

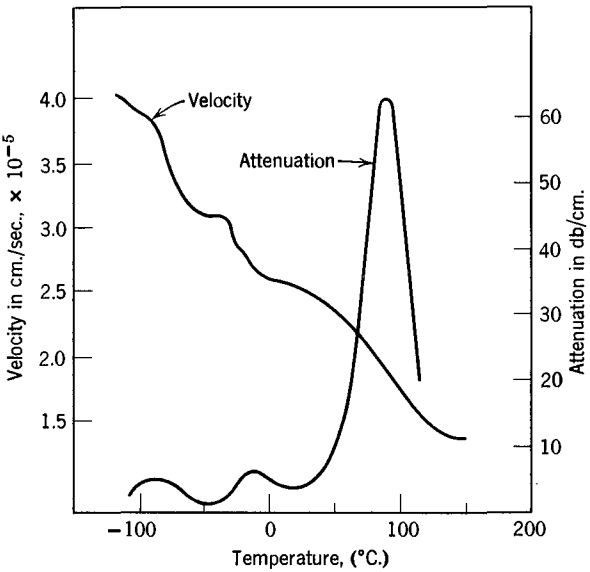


FIG. 18-17. Bulk longitudinal wave velocity (v) and attenuation (α) at 2×10^6 Hz plotted against temperature for poly(vinyl acetate). (Thurn and Wolf.[65])

a dispersion in K' itself like those of Fig. 18-14 may well be included here also. A retardation time of the Kovacs type of 10 min at T_g would at 93°C be reduced (with the data of Table 11-II) to about 3×10^{-8} sec, corresponding to a critical frequency of 5×10^6 Hz, rather near the experimental frequency.

The secondary dispersions, at −10° and −85°, presumably can be attributed to side group rearrangements as are the β mechanisms and other secondary effects discussed in Chapter 15. But it is difficult to guess the relative roles of volume and shear deformations in these motions. In shear (torsion) measurements at about 10 Hz, Schmieder and Wolf[66] found secondary maxima in tan δ at −30° and −100°C. No certain identification of these respective mechanisms can be made, since maxima in α and tan δ are not really equivalent, and the respective frequency ranges are very different. If the secondary maxima in Fig. 18-17 do correspond to the secondary shear maxima, the temperature dependence of the associated relaxation times must be quite high.

The temperature locations of attenuation maxima such as those in Fig. 18-17 have been determined for many polymers by Thurn and Wolf,[65] and these and other results have been discussed by Woodward and Sauer.[67] They can tentatively be identified as corresponding to the shear maxima discussed in Chapter 15; at 2×10^6 Hz, the bulk longitudinal maxima in attenuation occur at temperatures 20° to 70° higher than the respective shear maxima in tan δ at much lower frequencies. In measurements of acoustic attenuation in the megahertz range in a series of poly(methacrylate)s, North and collaborators[68] observed one relaxation in the methyl and ethyl polymers and two in the *n*-butyl and *i*-butyl; the one at lower temperatures was identified as the γ-mechanism.

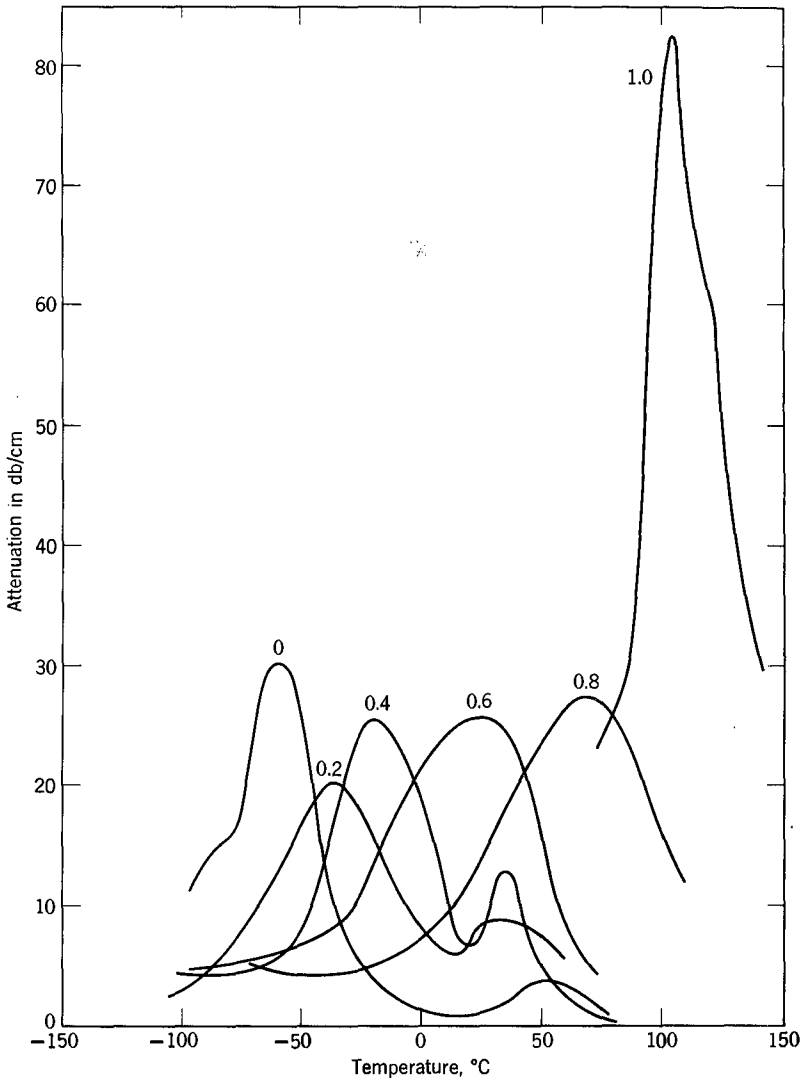


FIG. 18–18. Isochronal plots of bulk longitudinal wave attenuation at 2×10^6 Hz against temperature for mixtures of poly(vinyl chloride) and di-*n*-butyl phthalate. Figures denote weight fraction of polymer. (Thurn and Würstlin.[68])

Further investigations of plasticized systems[69] have outlined some complex changes in isochronal plots of attenuation against temperature with varying composition. Some examples for the system poly(vinyl chloride)–di-*n*-butyl phthalate are given in Fig. 18–18. The pure plasticizer has its own glass transition, reflected in a peak near −50°, and another at much higher temperatures which must represent compressional phenomena only. The pure polymer has a peak at about 100° which reflects the transition from glasslike to rubberlike consistency (possibly plus

a bulk dispersion). At intermediate compositions, there are in some cases single and in others multiple maxima, whose positions on the temperature scale generally (but not always) shift upwards with increasing polymer concentration.

It should be noted that the temperature coefficient of longitudinal wave velocity may change abruptly at the glass transition temperature owing purely to the change in thermal expansion coefficient (since it depends on the density as well as the viscoelastic properties); this does not represent any discontinuity in the viscoelastic properties measured at high frequency.[48]

REFERENCES

1. R. S. Marvin and J. E. McKinney, in *Physical Acoustics,* edited by W. P. Mason, Volume IIB, Academic Press, New York, 1965.
2. S. Beret and J. M. Prausnitz, *Macromolecules,* **8,** 536 (1975).
3. H. Shih and P. J. Flory, *Macromolecules,* **5,** 758 (1972).
4. G. Goldbach and G. Rehage, *Rheol. Acta,* **6,** 30 (1967); *J. Polym. Sci.,* **C16,** 2289 (1967).
5. S. Kästner, *Kolloid-Z.,* **206,** 143 (1966).
6. A. J. Kovacs, *Trans. Soc. Rheol.,* **5,** 285 (1961).
7. S. Matsuoka and B. Maxwell, *J. Polym. Sci.,* **32,** 131 (1958).
8. A. J. Kovacs, J. M. Hutchinson, and J. J. Aklonis, in *The Structure of Non-Crystalline Materials,* edited by P. H. Gaskell, Taylor and Francis, London, 1977, p. 153.
9. A. J. Kovacs, J. J. Aklonis, J. M. Hutchinson, and A. R. Ramos, *J. Polym. Sci., Polym. Phys. Ed.,* **17,** 1097 (1979).
10. L. A. Wood, *J. Polym. Sci.,* **B2,** 703 (1964); L. A. Wood and G. M. Martin, *J. Res. Nat. Bur. Stand.,* **68A,** 259 (1964).
11. K. H. Hellwege, W. Knappe, and P. Lehmann, *Kolloid-Z.,* **183,** 110 (1962).
12. G. Allen, G. Gee, D. Mangaraj, D. Sims, and G. J. Wilson, *Polymer,* **1,** 467 (1960).
13. G. Goldbach, thesis, Aachen, 1966.
14. J. C. Robinet and R. Buvet, *Cah. Groups Fr. Rheol.,* **3,** 131 (1966).
15. M. M. Martynyuk, *Vysokomol. Soed.,* **7,** 1978 (1965); *Kolloid Zh.,* **26,** 83 (1964).
16. W. H. Findley, R. M. Reed, and P. Stern, *J. Appl. Mech.,* **34,** 895 (1967).
17. A. J. Kovacs, *Adv. Polym. Sci.,* **3,** 394 (1964).
18. A. J. Kovacs, R. A. Stratton and J. D. Ferry, *J. Phys. Chem.,* **67,** 152 (1963).
19. L. C. E. Struik, *Rheol. Acta,* **5,** 303 (1966).
20. J. Meixner, *Kolloid-Z.,* **134,** 3 (1953); *Z. Naturforsch,* **9a,** 654 (1954).
21. H. R. Lillie, *J. Am. Ceram. Soc.,* **16,** 619 (1933).
22. A. J. Kovacs, thesis, Paris, 1954; A. J. Kovacs, *J. Polym. Sci.,* **30,** 131 (1958).
23. J. M. Hutchinson and A. J. Kovacs, *J. Polym. Sci., Polym. Phys. Ed.,* **14,** 1575 (1976).

23a. O. S. Narayanaswamy, *J. Am. Ceram. Soc.,* **54,** 491 (1971).

23b. M. A. DeBolt, A. J. Easteal, P. B. Macedo, and C. T. Moynihan, *J. Am. Ceram. Soc.,* **59,** 16 (1976).

23c. J. J. Aklonis and A. J. Kovacs, *Contemp. Topics Polym. Sci.,* **3,** 267 (1979).

24. M. Prod'homme, thesis, Paris, 1960.
25. A. L. Zijlstra, *Phys. Chem. Glasses,* **4,** 143 (1963).
26. L. C. E. Struik, *Ann. N. Y. Acad. Sci.,* **279,** 78 (1976).
27. L. C. E. Struik, thesis, Delft, Netherlands, 1977.
28. S. S. Sternstein, in *Treatise on Materials Science and Technology,* edited by J. M. Schultz, Volume 10, Part B, Academic Press, New York, 1977, p. 541.
29. A. Lamandé, thesis 3e cycle, University of Strasbourg, 1968; A. Lamandé and A. J. Kovacs, private communication.

30. H. H. Meyer, P.-M. F. Mangin, and J. D. Ferry, *J. Polym. Sci.,* **A3,** 1785 (1965).
31. H. Markovitz, *J. Polym. Sci., Polym. Phys. Ed.,* **11,** 1769 (1973).
32. S. Matsuoka, H. E. Bair, S. S. Bearder, H. E. Kern, and J. R. Ryan, *Polym. Eng. Sci.,* **18,** 1073 (1978).
33. J. D. Ferry and R. A. Stratton, *Kolloid-Z.,* **171,** 107 (1960).
34. S. Matsuoka, C. J. Aloisio, and H. E. Bair, *J. Appl. Phys.,* **44,** 4265 (1973).
35. D. H. Ender, *Bull. Am. Phys. Soc., Ser. II,* **13,** 396 (1968).
36. S. S. Sternstein and T. C. Ho, *J. Appl. Phys.,* **43,** 4370 (1972).
37. G. M. Bryant, *Text. Res. J.,* **31,** 399 (1961).
38. J. E. McKinney and H. V. Belcher, *J. Res. Nat. Bur. Stand.,* **A67,** 43 (1963).
39. J. E. McKinney, H. V. Belcher, and R. S. Marvin, *Trans. Soc. Rheol.,* **4,** 346 (1960).
40. R. S. Marvin, R. Aldrich, and H. S. Sack, *J. Appl. Phys.,* **25,** 1213 (1954).
41. R. Kono, *J. Phys. Soc. Jpn.,* **15,** 718 (1960).
42. R. Kono, *J. Phys. Soc. Jpn.,* **16,** 1580, 1793 (1961).
43. R. Kono, *Rep. Prog. Polym. Phys. Jpn.,* **6,** 141 (1963).
44. Y. Wada, R. Ito, and H. Ochiai, *J. Phys. Soc. Jpn.,* **17,** 213 (1962).
45. Y. Wada, H. Hirose, T. Asano, and S. Fukutomi, *J. Phys. Soc. Jpn.,* **14,** 1064 (1959).
46. Y. Wada, H. Hirose, H. Umebayashi, and M. Otomo, *J. Phys. Soc. Jpn.,* **15,** 2324 (1960).
47. T. F. Hueter and R. H. Bolt, *Sonics,* Wiley, New York, 1955, Appendix.
48. T. A. Litovitz and T. Lyon, *J. Acoust. Soc. Am.,* **30,** 856 (1958).
49. T. A. Litovitz, in *Non-Crystalline Solids,* edited by V. D. Frechette, Wiley, New York, 1960.
50. R. Meister, C. J. Marhoeffer, R. Sciamanda, L. Cotter, and T. Litovitz, *J. Appl. Phys.,* **31,** 854 (1960).
51. R. Bass and J. Lamb, *Proc. R. Soc.,* **A247,** 168 (1958).
52. T. A. Litovitz, *J. Acoust. Soc. Am.,* **31,** 681 (1959).
53. T. A. Litovitz and G. E. McDuffie, Jr., *J. Chem. Phys.,* **39,** 729 (1963).
54. R. A. Pethrick, *J. Macromol. Sci., Rev. Macromol. Chem.,* **C9,** 91 (1973).
55. M. A. Cochran, P. B. Jones, A. M. North, and R. A. Pethrick, *J. Chem. Soc., Faraday Trans. II,* **68,** 1719 (1972).
56. M. A. Cochran, J. H. Dunbar, A. M. North, and R. A. Pethrick, *J. Chem. Soc., Faraday Trans. II,* **70,** 215 (1974).
57. K. Ono, H. Shintani, O. Yano, and Y. Wada, *Polym. J.,* **5,** 164 (1973).
58. Y. Masuda and Y. Miyahara, *Nippon Kagaku Zasshi,* **83,** 878 (1962); **84,** 119 (1963).
59. H. Nomura and Y. Miyahara, *J. Appl. Polym. Sci.,* **8,** 1643 (1964).
60. Y. Miyahara and H. Nomura, *J. Polym. Sci.,* **C23,** (1968).
61. G. G. Hammes and T. B. Lewis, *J. Phys. Chem.,* **70,** 1610 (1966).
62. J. I. Dunbar, A. M. North, R. A. Pethrick, and D. B. Steinhauer, *J. Polym. Sci., Polym. Phys. Ed.,* **15,** 263 (1977).
63. R. Zana, S. Candau, and R. Cerf, *J. Chim. Phys.,* **60,** 869 (1963).
64. J. J. Burke, G. G. Hammes, and T. B. Lewis, *J. Chem. Phys.,* **42,** 3520 (1965).
65. H. Thurn and K. Wolf, *Kolloid-Z.,* **148,** 16 (1956).
66. K. Schmieder and K. W. Wolf, *Kolloid-Z.,* **134,** 149 (1953).
67. A. E. Woodward and J. A. Sauer, *Adv. Polym. Sci.,* **1,** 114 (1958).
68. A. M. North, R. A. Pethrick, and D. W. Phillips, *Polymer,* **18,** 324 (1977).
69. H. Thurn and F. Würstlin, *Kolloid-Z.,* **156,** 21 (1958).

CHAPTER 19

Applications to Practical Problems

The stress patterns prescribed in experimental measurements of the basic viscoelastic functions—creep, stress relaxation, and sinusoidally oscillating deformations—are sufficiently close to those occurring in certain conditions of processing and use of polymeric materials so that those functions are useful directly for prediction and interpretation of technological information. Often reduced variables can be used to make rough estimates of predicted behavior under widely different conditions of temperature, plasticization, and other variables.

There are other situations of processing and use, as well as empirical test procedures employed in technology, which correspond to more complicated experimental patterns of varying deformation and load. Insofar as the viscoelastic behavior is linear, such properties can often still be expressed in terms of the basic viscoelastic functions. When large deformations or large rates of deformation are involved, various nonlinear constitutive equations are available to describe the behavior; knowledge of the molecular origin of the viscoelasticity involved in the particular range of time and temperature concerned may aid in choosing an appropriate equation and also in estimating the magnitudes of the empirical parameters in it. Finally, the so-called ultimate properties of polymers, which describe the conditions for mechanical rupture, have underlying molecular mechanisms which are closely related to those involved in viscoelastic behavior, so that the dependence of ultimate strength and deformation on temperature, rate of loading, and other variables can be clarified to a considerable extent in terms of viscoelastic functions. Of course, in problems of processing and use, the geometry is often much more complicated than in the simple arrangements used for experimental measurements of basic functions. Various applied calculations of this sort are briefly illustrated here in the final chapter.

A. VISCOELASTIC BEHAVIOR UNDER MORE COMPLICATED TIME PATTERNS

Mechanical testing procedures in common use involve other patterns of stress history than the simple creep and relaxation experiments on which the definitions of the transient viscoelastic functions are based, and the sinusoidally varying stress which is inherent in the definitions of the so-called dynamic properties. Certain relations between the behavior under complicated conditions and the basic viscoelastic functions are presented here together with some related problems. They are limited to linear viscoelastic systems and hence small strains, but in some cases could be extended to describe larger deformations, especially for simple extension.

1. Tensile Stress Relaxation following Deformation at Constant Strain Rate

If a sample is stretched at constant strain rate to a strain ϵ at time t_1, and then the stress is allowed to relax at constant strain, the course of stress relaxation is given by linear viscoelasticity as

$$\sigma_T = (\epsilon/t_1) \int_{-\infty}^{\infty} \overline{H}\tau [e^{-(t-t_1)/\tau} - e^{-t/\tau}] \, d \ln \tau \tag{1}$$

where t is the total elapsed time, instead of the simple course followed after instantaneous strain,

$$\sigma_T = \epsilon \int_{-\infty}^{\infty} \overline{H} e^{-t/\tau} \, d \ln \tau = \epsilon E(t) \tag{2}$$

However, for $t \gg t_1$, equation 1 reduces to equation 2, thus justifying the assumption implicit in experimental procedures that rapid loading is equivalent to instantaneous for practical purposes. Equation 1 has been discussed by Meissner[1] and Smith[1a] in connection with combining deformation at constant strain rate with subsequent relaxation to obtain viscoelastic information, as mentioned in Section F1 of Chapter 3.

2. Energy Stored, Energy Dissipated, and Work of Deformation in Transient Loading

The total work of deformation in tests such as those described above has two contributions, corresponding to the stored elastic energy and the energy dissipated as heat (assuming isothermal conditions).[2] These can be formulated as allows for deformation in simple extension, the usual geometry for practical test procedures.

For deformation at constant rate of tensile strain, $\dot{\epsilon}$, the total work of deformation per unit volume is

$$W = \int_0^{\epsilon} \sigma_T \, d\epsilon = \dot{\epsilon}^2 t^2 E_e/2 + \dot{\epsilon}^2 \int_{-\infty}^{\infty} \overline{H}\tau [t - \tau(1 - e^{-t/\tau})] \, d \ln \tau \tag{3}$$

while the stored energy is

$$\mathscr{E}_{st} = \dot{\epsilon}^2 t^2 E_e/2 + (\dot{\epsilon}^2/2) \int_{-\infty}^{\infty} \overline{H} \tau^2 (1 - e^{-t/\tau})^2 \, d \ln \tau \tag{4}$$

where E_e is the equilibrium Young's modulus (cross-linked systems only) and t is the time elapsed since the beginning of the deformation. The difference between these two expressions is the energy dissipated. It is evident that the latter depends on $\overline{H}$ but not on E_e. It would be expected that the greater the proportion dissipated, the greater the work that can be put into deformation without occurrence of rupture. However, rupture depends on several different features as briefly discussed in Section E.

3. Energy Stored and Dissipated in Periodic (Sinusoidal) Loading

Qualitatively, it is evident that the ratio of energy dissipated to energy stored per cycle in a sinusoidal deformation is proportional to tan δ, and this statement has appeared many times in the literature. A thorough treatment of energy storage and dissipation for periodic and other time-dependent deformations has been presented by Tschoegl,[2] taking into account the fact that the energy storing and dissipating mechanisms are not in phase, the phases being regulated by the respective relaxation times. For sinusoidal deformations, the average energy per unit volume stored in a cycle is (for shear strain)

$$\mathscr{E}_{st} = \int_0^{\gamma_0} G' \gamma \, d\gamma = G' \gamma_0^2/4 \tag{5}$$

where $\gamma = \gamma_0 \sin \omega t$. The dissipated energy continuously increases; the dissipation in a complete cycle is

$$\mathscr{E}_d = \pi G'' \gamma_0^2 \tag{6}$$

One-half of the ratio of energy dissipated to average energy stored per cycle, which has been termed the specific loss, is

$$\mathscr{E}_d/\mathscr{E}_{st} = 2\pi \tan \delta \tag{7}$$

A related problem of interest is the ratio of energy dissipated per second to energy stored during steady-state flow of a viscoelastic liquid. This is readily calculated to be $2/J_e^0 \eta_0$, where J_e^0 is the steady-state compliance and η_0 the viscosity. It is close in magnitude to the reciprocal of the terminal relaxation time of the system. Thus, for a single Maxwell element, the above ratio is $2/\tau_1$; this should be a close approximation for an entangled system with narrow molecular weight distribution which can be almost described by a single terminal relaxation time. For an undiluted polymer or a concentrated solution with $\eta_0 \gg \eta_s$, but with cM too small to be in the entanglement regime, the modified Rouse theory gives $30/\pi^2 \tau_1$, or $3/\tau_1$.

4. Cycling Deformations at Constant Strain Rate

When a sample in an extension tester is stretched at a constant rate of elongation

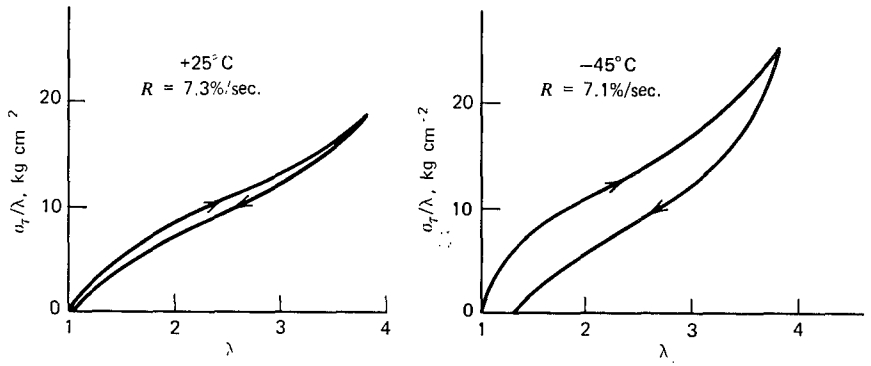


FIG. 19-1. Stress-strain hysteresis loop for uniaxial extension at constant strain rate R with reversal of direction at upper right, for cross-linked natural rubber at two temperatures as shown; σ_T/λ is the "engineering" stress. After Harwood and Schallamach.[3] Reproduced, by permission, from the *Journal of Applied Polymer Science.*

($\dot{\epsilon}$) to an elongation ϵ_1 at time $t_1 = \epsilon_1/\dot{\epsilon}$ and then the direction of travel is reversed to return it to its original length at a rate $-\dot{\epsilon}$, the strain is a periodic function of time with a zigzag form, as mentioned in Section C5 of Chapter 14. (For the difference between practical tensile strain rate and elongational strain rate, see Section E1 of Chapter 6.) The stress-strain curves trace a hysteresis loop as illustrated in Fig. 19-1.[3] The ratio of the hysteresis area to the work of deformation has sometimes been used as a measure of the loss characteristics of a viscoelastic material.[3,3a] However, for a single cycle, terminated at zero stress, the area of the loop cannot be equated to dissipated energy. The point of zero stress at the end of the cycle does not necessarily correspond to zero stored energy, since (in model language) some spring elements may be stretched and others compressed to balance the stress at zero. The apparent permanent set immediately after removal of the sample from the instrument would then undergo some modification with further creep recovery. Only in the steady state after repeated cycles, when the loop is closed, in the steady state, the area within it represents the energy dissipated as heat per cycle.[2,4]

If the linear viscoelasticity theory can be applied, the initial forward stress-strain curve is given by equation 56 of Chapter 3 written for extension:

$$\sigma_F = \dot{\epsilon} \int_{-\infty}^{\infty} \overline{H}\tau(1 - e^{-t_1/\tau})\, d \ln \tau + E_e \dot{\epsilon} t \tag{8}$$

whereas that for the initial reverse segment can be shown to be

$$\sigma_R = \dot{\epsilon} \int_{-\infty}^{\infty} \overline{H}\tau[(2 - e^{-t_1/\tau})e^{-(t-t_1)\tau} - 1]\, d \ln \tau + E_e \dot{\epsilon}(2t_1 - t) \tag{9}$$

The work of forward deformation is given by equation 3, while the work recovered on the reverse deformation cannot be readily calculated because zero stress on this segment corresponds to a finite strain which depends on the form of $\overline{H}$ in a complicated manner according to equation 9.

The stress response in cycling zigzag strain deformation, the strain response to cycling zigzag stress imposition, and other types of stepwise mechanical histories have been discussed by Tschoegl.[2,4]

5. Rebound of Rigid Spheres from Viscoelastic Surfaces

When a sphere of an essentially perfectly elastic material rebounds from a plane surface of a viscoelastic solid, its velocity is diminished by a factor called the coefficient of restitution,[5] $\mathfrak{Re}$. The impact can be provided either by dropping a ball vertically or by swinging it horizontally suspended from a string. If the viscoelastic plate is thick enough so that the time required for an elastic wave to be reflected from its other side and return is longer than the time of contact, then $\mathfrak{Re}$ is essentially independent of the thickness and in practice also of the velocity of impact. Otherwise, a correction for finite thickness can be made.[6,7] The experiment is similar physically to an oscillating free vibration measurement (as in a torsion pendulum) at an equivalent frequency which is nearly equal to the reciprocal of twice the time of contact.[5,8] The time of contact is proportional to m^2/E^2rv, where m and r are the mass and radius of the sphere respectively, E is Young's modulus of the rubber, and v is the velocity of impact.[7] This is the basis of the method of Vinh[9] for obtaining basic viscoelastic properties by measuring acceleration as a function of displacement, which of course provides far more information than does a determination of a single parameter $\mathfrak{Re}$. The relation of $\mathfrak{Re}$ to viscoelastic properties has been treated by Pao[10] and Hunter.[11] It is approximately determined by the logarithmic decrement Δ (equation 17 of Chapter 6), which can be estimated from the relation $\Delta = 1 - \mathfrak{Re}^2$. The deformation for a hard viscoelastic solid is of course a combination of shear and compression, but for the usual range of Poisson's ratio the majority of the stored energy is attributable to the shear.[5] Such measurements have been made on a variety of polymer systems,[12] and they are convenient for rapid scanning of changes in viscoelastic properties during a chemical reaction, for example.

6. Rolling Friction on a Viscoelastic Surface

When a rigid sphere is pressed against a plane viscoelastic surface with a normal force and is rolled along with a small force parallel to the surface, the viscoelastic material undergoes deformation (combination of shear and compression, but mostly shear) followed by recovery. The parallel force required to maintain a constant velocity is related to the energy loss in the viscoelastic substratum.[13]

The coefficient of rolling friction, λ, defined as the ratio of the vertical load (W) to the parallel rolling force, depends on the load, the sphere radius, and the viscoelastic properties of the substratum. The rather complicated relationships have been worked out by Atack and Tabor[14] and Flom and Bueche.[13,15] A measurement of λ is roughly equivalent to a measurement of $\tan \delta$ at a radian frequency of the order of the angular velocity of the rolling sphere; it passes through a maximum as a function of the velocity. The method has been applied to determinations of relative losses in a variety of rubbery and glassy polymers.[14,15]

Similarly, the coefficient of friction of a rolling cylinder on a viscoelastic surface has been treated by May, Morris, and Atack[16] and Hunter.[17] It also passes through a maximum as a function of the velocity. A more complete treatment by Minato and Takemura,[18] together with experimental data over a wide range of temperature

and velocity, has shown that $\tan \delta$ can be calculated from λ and vice versa with quite satisfactory agreement with direct measurements.

B. MISCELLANEOUS APPLICATIONS OF VISCOELASTIC PROPERTIES

Some practical aspects of viscoelastic behavior in dilute solutions (Chapter 9, Section G) and in the terminal zone (Chapter 10, Section C5) have already been mentioned; others are inherent in Chapters 16 and 17. We now call attention to some additional applications.

1. Generation of Heat in Rapid Oscillating Deformations

From equation 6 above, the energy dissipated *per second* in small oscillating deformations is (per unit volume of material)

$$\dot{\mathscr{E}} = \omega G'' \gamma_0^2/2 = \omega J'' \sigma_0^2/2 \tag{10}$$

where γ_0 and σ_0 are the peak shear strain and peak shear stress respectively. Thus for deformation with a specified strain the important function is G'', while for a specified stress it is J''.

The dissipated energy causes a rise in temperature, whose magnitude of course depends on the heat capacity of the system. The temperature may reach a steady-state value for continuous sinusoidal deformation, depending on the rate of heat loss to the surroundings. Equation 10 can be used to estimate heat production in various experimental procedures, where the strains are often purposely kept very small at high frequencies to prevent temperature rise as well as to insure linear viscoelastic behavior. It can also be used to estimate heat production in practical situations of cyclic deformations, such as the performance of automobile tires. Values can be compared on a relative basis even though the stress distribution in a loaded tire is complicated and the strains exceed the limitations of linear viscoelasticity; and the cyclic deformation does not follow a simple sinusoidal pattern.

Since in a tire under operating conditions the peak stress is specified, J'' is the relevant function in equation 10. It has been pointed out[19] that, although minimum heat dissipation at the frequency of wheel rotation is desired, higher losses at low frequencies may be beneficial in providing a smoother riding vehicle. Thus it would be desirable to operate on the left side of the maximum in Fig. 14–16. The losses should be compared not at the ambient temperature but at the steady-state temperature during operation.

As an example of a numerical calculation, a lightly cross-linked natural rubber with $J'' = 1.0 \times 10^{-8}$ cm^2/dyne under a sinusoidal deformation at 10 Hz and a peak shear stress of 10^6 dynes/cm^2 would dissipate 0.0038 calorie/cc/sec. Since the heat capacity is about 0.5 calorie/deg/g, the temperature would rise about 0.008 deg/sec if no heat were lost by conduction. Other examples are given by Kramer and Ferry.[20]

For deformation in flexure, the relevant loss functions are E'' and D''. The relation of E'' to the steady-state temperature rise ΔT in continuous cyclic deformation as measured in a Goodrich flexometer, taking into account nonlinearity of response and the effect of added filler in a rubbery polymer, has been studied extensively by Maekawa, Ninomiya, and collaborators.[21] A simplified equation which satisfactorily represented many experimental results is

$$\Delta T = c(1 - bv_1)[\omega\gamma_0^2 E''(\omega, T_1)/2] \tag{11}$$

where ω is the radian frequency of deformation, T_1 the steady-state temperature, and v_1 the volume fraction of filler; the coefficients c and b were found to be 1.1×10^{-6} deg cm^3 sec/erg and 2.4, respectively.

2. Vibration Damping and Noise Abatement

In contrast to the situation described above where minimum loss is desired, when polymeric materials are used to suppress vibrations the loss should be maximal. The frequency range of interest depends on the characteristic frequencies of the vibrating system, which involve the storage modulus of the polymer as well as masses and elastic stiffnesses of other components of the mechanical system. No attempt will be made to refer to the very large literature on damping of vibrations, which has been reviewed thoroughly by Payne[22,23] and Snowdon.[24] Knowledge of the form of the viscoelastic functions and use of the WLF equation can aid in designing devices for specific ranges of frequency and temperature.

Suppression of flexural vibrations in metal plates and bars by application of a thin layer of polymeric material, either spread directly or applied in the form of a tape, has become of great importance both for elimination of noise (especially in vehicles and airplanes) and for improving fatigue characteristics. It was mentioned in Chapter 7 that measurements of resonance frequencies and damping in such compound layered systems can be used for obtaining the viscoelastic properties of the polymeric stratum. Conversely, knowledge of the viscoelastic properties and their dependence on frequency and temperature (and plasticization, incorporation of fillers, etc.) aids in the selection of antidamping materials for specific applications.[25]

The theory for complex bending stiffness of composite plates has been developed by Oberst[26,27] for double layers (metal and polymer) and by Kerwin[28] for triple layers (polymer sandwiched between comparatively heavy substratum and thin outer constraining layer). The loss tangent for the composite system depends critically on the relative thicknesses of the layers as well as the properties of the respective materials. In practice, polymeric materials with loss tangents near or slightly greater than unity (probably the maximum achievable,[29] unless one is willing to limit the damping to a narrow frequency range) can provide loss tangents in the neighborhood of 0.1 for compound systems. Applications have been extensively discussed by Oberst and collaborators.[30-33]

Viscoelastic liquids have also been used to damp vibrations and absorb acoustic energy.[34,35] Networks with unattached linear molecules may be useful.[20]

It may be noted that in the acoustic literature the symbol η is often used not for viscosity but for the loss tangent (equal to the relative response width $(\Delta\omega)'/\omega_0$ as defined in Chapter 6, Section E).

3. Sliding Friction

The frictional force involved in sliding a layer of polymeric material along a hard surface (*e.g.*, of metal, glass, or a rough abrasive such as silicon carbide) is also related in part to the viscoelastic properties of the former. The coefficient of friction μ, defined as the ratio of tangential force at constant velocity to normal force, is almost independent of the normal force at moderate values of the latter but may vary somewhat in a manner depending on the nature of the underlying surface.[36-38] At constant normal force, the friction coefficient of a rubbery polymer on a fairly smooth surface as a function of either velocity (v) or temperature goes through a characteristic maximum. Moreover, data at different temperatures can be combined by reduced variables[39-41] with a plot against log va_T as illustrated in Fig. 19-2, where the shift factors a_T conform to the WLF equation.[40] The shift factors are essentially the same whether the underlying surface is smooth, rough, or lubricated

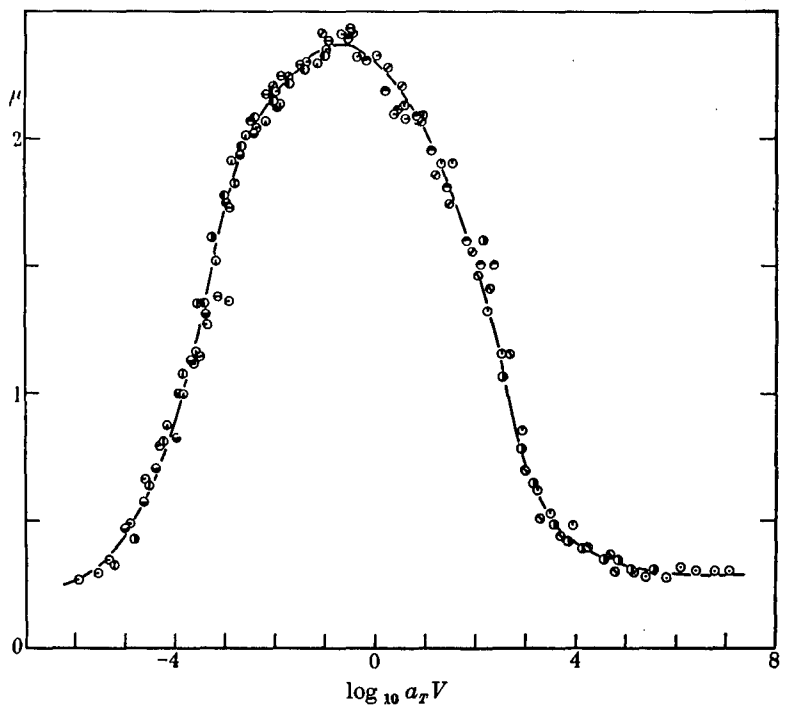


FIG. 19-2. Coefficient of friction for acrylonitrile-butadiene rubber sliding on wavy glass, plotted against logarithm of velocity times shift factor a_T reduced to 20°C. Temperature dependence of a_T corresponds to equation 40 of Chapter 11 with T_s = 30°C. Points identify 13 different temperatures from −15° (at right) to 85°C (at left). (Grosch.[40])

with fine powder, and also agree with those obtained from conventional viscoelastic measurements. (The shape of the composite curve depends on the nature of the underlying surface, however.) Similar results with good superposition except sometimes in the immediate vicinity of the maximum have been obtained for a variety of polymers in the rubbery state by Grosch;[40] the height of the maximum is generally between 2 and 3.

Extensive studies in which the nature of the surface has been varied as well as the velocity and temperature[40-42] have distinguished two sources of frictional work—dissipation of energy by periodic deformation of the polymer on a macroscopic scale associated with surface asperities, and adhesion on a molecular scale with periodic formation and rupture of contacts between the polymer and the underlying surface. The former, which is related to the energy losses in rolling friction described in Section A6 above, is obviously controlled by viscoelastic properties and can be predicted from them provided the asperities do not cause tearing of the polymer.[43] The latter presumably has the same kind of temperature dependence because the making and breaking of contacts are governed by molecular motions which involve the same characteristic times as those involved in viscoelastic properties (*cf.* Section 4 below). The adhesive mechanism dominates for rubbery polymers except when it is destroyed by lubrication with a dry powder. Detailed theories have been presented by Schallamach[44] and Bartenev and El'kin,[41] and Ludema and Tabor.[45] The subject has been thoroughly reviewed by Thirion and Chasset[38] and Tabor.[43]

For a polymer in the glassy or crystalline state, sliding on either another surface of the same polymer[46] or a metal surface,[41] the coefficient of friction passes through another maximum as a function of either velocity[46] or temperature[41] whose magnitude is lower (of the order of 0.4) than those of rubbery polymers. This has been attributed to energy losses associated with a secondary viscoelastic mechanism.

4. Tack and Adhesion

Tack refers to the adhesion of two surfaces of the same rubbery polymer. When two such surfaces are pressed together and subsequently pulled apart, the maximum force necessary to break the junction depends on the initial time of contact and the normal force applied, as well as the rate of separation and the temperature and other variables.[48-51] From the dependence on temperature and polymer molecular weight, it can be inferred that the effectiveness of the bond depends partly on the interdiffusion of molecules across the interface and hence on molecular motions which are reflected in viscoelastic properties in the terminal zone.[50,51] However, the effectiveness depends also on the ultimate properties of the polymer itself as discussed in Section E below, and the phenomenon is still not fully understood.

The more general phenomenon of adhesion between a rubbery polymer and a different surface is frequently studied by tests of the force required to peel a thin layer of polymer from a rigid substrate.[52,53] Data at different peel rates and different temperatures can be combined by reduced variables with shift factors given by the WLF equation, indicating that here as in friction the process is controlled by rates

of molecular motion. The extensive literature on this subject[53,54] is beyond the scope of this chapter.

5. Abrasion

In a sliding friction experiment as described in Section 3 above, if the hard surface is rough (silicon carbide, emery, etc.) the polymer is abraded away at a rate which is proportional to the normal force (if not too high) and therefore to the friction coefficient.[55-57] The abradibility (defined as the volume abraded away per unit normal force and unit sliding distance) decreases generally with increasing velocity or decreasing temperature, and results at different temperatures can be again combined by reduced variables with shift factors calculated from the WLF equation, using the same parameters that apply to viscoelastic properties.[57] This observation indicates that the abrasion is closely related to viscoelastic behavior; it is attributed to rupture of the type described in Section E below on a small scale, of the order of the size of the abrasive particles. In fact, the abradibility is approximately proportional to the work of deformation at break (*cf.* equation 3 above) measured at a high rate of extension (of the order of a tensile strain rate of 10^2 sec^{-1}).[57] For a rubbery polymer which crystallizes at high extensions (natural rubber, for example), or one filled with carbon black, however, the behavior is more complicated and reduced variables with the WLF equation cannot be applied.[57] There is a very extensive literature on this subject also,[54] but the mechanism of abrasion is still not well understood.

6. Processability

The behavior of uncross-linked rubbery polymers in processing machinery such as mixers, mills, calenders, extruders, and blow molding is obviously closely related to viscoelastic properties.[58-60] The most commonly used laboratory instrument for simulating processing conditions is the Mooney viscometer,[61] which measures a quantity proportional to an average non-Newtonian viscosity at shear rates of the order of 1 sec^{-1}, which is relatively high.[58,62,63] This "Mooney viscosity" and a terminal relaxation time τ_m estimated from a stress relaxation experiment (Section C5 of Chapter 10) are considered by White and Tokita[58] to be the most important parameters related to behavior in processing. However, these obviously represent a very small portion of the total viscoelastic characterization of a polymeric mixture. A measure of energy storage in flow, from the steady-state compliance J_e^0 or the primary normal stress coefficient Ψ_1, is an important additional parameter,[64,65] although $\Psi_{1,0}$ corresponding to low strain rates will be inadequate to correlate with processing at high strain rates. The relation of behavior in various processing operations to basic viscoelastic information has been discussed in detail by Meissner[64] and White.[66]

7. Technological Characteristics of Cross-Linked Rubbers

In addition to the properties of heat generation, vibration damping, friction, tack,

and abrasion which have been mentioned in the sections above, other characteristics of cross-linked rubbers that are important in technological applications include resilience (related to rebound described in Section A5), hardness, strain at break, stress at break, and wet skid resistance, as measured by practical tests. These can be correlated with rheological data to varying degrees, as discussed in detail by Ninomiya and collaborators.[59]

8. Tire Flatspotting

When an automobile starts after having stood for some time, the flat portions of the tires which were in contact with the road at rest may persist until the tire temperature rises from the ambient value to that of steady-state operation (*cf.* Section 1 above). This phenomenon is attributed to viscoelasticity of the tire cord, as follows. The cord fibers are strained by tire inflation, but in the flat spot the strain is less than elsewhere. In steady-state operation, the temperature is high enough so that some of the retardation times in the cord are shorter than the period of rotation and the strain associated with processes with longer retardation times is averaged. But when the tire cools at rest, the strain differential persists for a while after operation is resumed.[67-69] The process evidently depends on the elasticity of the rubber and the viscoelasticity of the cord, the most important features being the dependence of the latter on temperature, though moisture also has an effect. The severity of flatspotting can be correlated quantitatively with the creep compliance of the cord fibers.[69]

9. Lubrication

Many lubricating oils contain polymeric additives. Lubricant films are subjected not only to shear but to extremely high pressures, and in rotating systems the pressure changes are periodic. Thus both shear and bulk viscoelasticity are important in the performance of the lubricant, and the high confining pressures cause very large periodic changes in the relaxation times involved as well as the steady-flow viscosity. This subject has been reviewed by several authors.[70-74] However, many aspects of the role of polymeric additives, especially diminishing wear in bearings,[75] remain imperfectly understood.

C. NUMERICAL EXAMPLES OF APPROXIMATE PREDICTIONS OF VISCOELASTIC BEHAVIOR

Even though the molecular theory of viscoelasticity is far from complete, certain specific aspects of viscoelastic behavior can sometimes be predicted from knowledge of the molecular weight, temperature, and other variables together with basic information some of which is tabulated in preceding chapters. A few fragmentary examples are given here in the form of problem questions.

1. Minimum in Loss Tangent for Uncross-Linked Polymer

How high must the molecular weight of polyisobutylene be in order to be sufficiently "rubbery" to have a loss tangent as low as 0.05 in the frequency region of the loss tangent minimum?

The appropriate relation is equation 10 of Chapter 13 with a correction factor of 0.75 on $\overline{M}_n$ as explained in the associated discussion. If M_C is taken as 15,200 from Table 13–II, this equation gives $\overline{M}_n = 9 \times 10^5$. The result gives the number-average molecular weight if there are no species with $M < M_C$. Experimentally, a minimum loss tangent of 0.1 was observed for a sample with $\overline{M}_w = 15 \times 10^5$ which may have had a moderately broad molecular weight distribution.[76]

2. Onset of Transition Zone on Frequency Scale

Butyl rubber is cross-linked to give an equilibrium shear modulus of 4.0×10^6 dynes/cm^2. What is the longest relaxation time in the transition zone, τ_{tr}, and at what frequency will the onset of the transition zone be encountered as defined by Fig. 14–1, at 25°C?

The relaxation time τ_{tr} can be calculated from equation 37 of Chapter 10 with $p = 1$. The average degree of polymerization of a strand, $P_c = M_c/M_0$, is obtained from equation 33 of Chapter 10 with $g = 1$, noting that $M_c = \rho/\nu$, as 100. The friction coefficient ζ_0 and characteristic length a are obtained from Table 12–III. The result is $\log \tau_{tr} = -3.0$. The onset frequency for the beginning of the transition zone is approximately the reciprocal; in accordance with equation 9 of Chapter 12, $\log \omega_{tr} = 2.9$ or $\nu_{tr} = 130$ Hz. The experimental value from Fig. 14–1 is $\log \omega_{tr} = 2.4$.

3. Terminal Relaxation Time (Low Molecular Weight) and Its Dependence on Temperature and Pressure

For a sample of poly(vinyl acetate) with uniform molecular weight 1.1×10^5, whose viscosity at 76°C is 6.1×10^7 poises, what is the terminal relaxation time (controlling stress relaxation in a mold, approach to steady-state flow, etc.)? What increase of temperature is needed to decrease it by a factor of 10? At what confining pressure would it be increased by a factor of 10?

The terminal relaxation time τ_1 can be roughly estimated from equation 7 of Chapter 10, derived from the Rouse theory; it may be expected to be nearly correct since the molecular weight is only moderately greater than that for onset of entanglement coupling effects. The result is $\tau_1 = 1.2 \times 10^2$ sec, which happens to be very close to the observed value[77] of 1.3×10^2 sec.

The temperature dependence can be calculated from the WLF equation, equation 21 of Chapter 11, with 76°C as reference temperature and the coefficients c_1^0 and c_2^0 from Table 11–II. For a 10-fold decrease, $\log a_T = -1.00$; solving for T gives $T = 361$°K, or an increase of 13°.

The effect of pressure can be roughly estimated from the coefficient $(\partial T/\partial P)_\tau = 0.020$ in Table 11-III; a temperature change of 13° is equivalent to a pressure change of 650 atm.

4. Terminal Relaxation Time (High Molecular Weight)

What is the terminal relaxation time of a linear polybutadiene with cis:trans:vinyl = 55:38:7 and nearly uniform molecular weight 347,000, at 25°C?

Equation 57a of Chapter 10 can be used to estimate the disengagement time τ_d of the Doi-Edwards theory. The microstructure is sufficiently close to that of the polybutadiene identified with footnote *b* in Table 12-III and footnote *c* in Table 13-I to use the values of ζ_0 and J_N^0 $(= 1/G_N^0)$ from those sources. The result is 11 sec at 25°C. From experiments of Graessley and collaborators,[78] the product $\eta_0 J_e^0$, which should be approximately equal to τ_d, is 7 sec. However, over wide molecular weight ranges, an estimate as close as this may not be expected, since the molecular weight dependence is slightly different from that expressed in equation 57a of Chapter 10.

5. Effect of Plasticizer on Mechanical Loss

How much butyl acetate must be added to poly(methyl acrylate) to produce maximum damping (loss tangent or logarithmic decrement of free vibrations) at 60 Hz at 25°C?

From Table 12-I, the maximum in tan δ occurs at 0.5 Hz at 298°K in the pure polymer; the molecular weight does not enter, if sufficiently high. Enough diluent must be added to give $\log a_c = -2.1$, shifting the frequency from 0.5 to 60. In equation 13 of Chapter 17, β' for butyl acetate may be taken as 0.23; Fujita[79] lists values of 0.22 and 0.24 for this diluent in polystyrene and poly(methyl methacrylate) respectively. The fractional free volume of the polymer, f_2, is $f_g + \alpha_f(T - T_g)$; taking the values of the coefficients from Table 11-II, we obtain $f_2 = 0.037$. Equation 13 of Chapter 17 then takes the form

$$2.1 = \frac{v_1}{2.303 \times 0.037(0.037/0.23 + v_1)}$$

from which $v_1 = 0.035$. Thus addition of butyl acetate to a concentration of 3.5% by volume should produce the desired result.

6. Terminal Relaxation Time in Dilute Solution

A macromolecule of unknown structure but believed to be of uniform molecular weight and unbranched has an intrinsic viscosity of 2500 ml/g in water at 25°C and the molecular weight determined by light scattering is 1.0×10^6. What is the terminal relaxation time in this solvent?

An estimate can be made from equation 10 of Chapter 9 by taking $m = 1$. For rigid and semirigid rods, m is near unity; for linear flexible coils, $m = S_1^{-1}$ is not

smaller than 0.4. The calculation gives $\tau_1 = 0.9 \times 10^{-3}$ sec. The intrinsic viscosity, molecular weight, and terminal relaxation time could correspond to a highly charged flexible polyelectrolyte.[80]

D. ULTIMATE MECHANICAL PROPERTIES

When a polymeric material is subjected to tensile or shear stress of sufficiently high magnitude, it ruptures, as do all solids and under certain circumstances liquids.[81,82] In cross-linked polymers above T_g, crystalline polymers, and in general for polymers below T_g, rupture is usually associated with breaking of primary chemical bonds, as can be demonstrated directly by measurements of electron spin resonance[83,84] or the initiation of free radical polymerization.[85] Even uncross-linked polymers far above T_g and their concentrated solutions probably rupture with bond breakage unless the deformation is sufficiently slow to permit escape of the molecules from their topological restraints; the process of rupture depends enormously on the rate of deformation.[86-89] In fact, bond breakage can occur even in dilute polymer solutions under conditions of shear at high velocity gradients,[90,91] or at low velocity gradients for macromolecules of extremely high molecular weight.[92] However, as with other solids, the breaking strength cannot be calculated in terms of chemical bond energies or intermolecular attractive forces, which predict strengths too high by several orders of magnitude.[93-96] The initiation of fracture involves structural inhomogeneities, either microscopic or molecular, that lead to cavitation, and thereafter, the formation of microcracks, caused by the excess triaxial tensile stress near an inhomogeneity. If the stress is sufficient to cause propagation of a crack through the specimen, rupture results.[84]

The voluminous literature on correlation of ultimate properties with polymer structure cannot be adequately treated here; there are many excellent reviews.[83,84,97-102] However, certain aspects of the ultimate properties and their dependence on the time scale of measurement and on temperature are closely allied to viscoelastic properties in small deformations, and these will be briefly discussed.

There is a basic difference between rupture above the glass transition temperature where the polymer chain backbones have an opportunity to change their configurations before the sample fails, and below T_g (or somewhat above T_g with very rapid stressing) where the backbone configurations are essentially immobilized within the period of the experiment.

1. Rupture above the Glass Transition Temperature

Above the glass transition temperature, the crack propagation which culminates in rupture can be strongly influenced by relief of stress through viscoelastic relaxation, by crystallization at large extensions (as in natural rubber), by the presence of filler particles, and by mechanical hisotry in periodic stressing.[98,103]

The values of stress and strain at the moment of rupture—the so-called ultimate

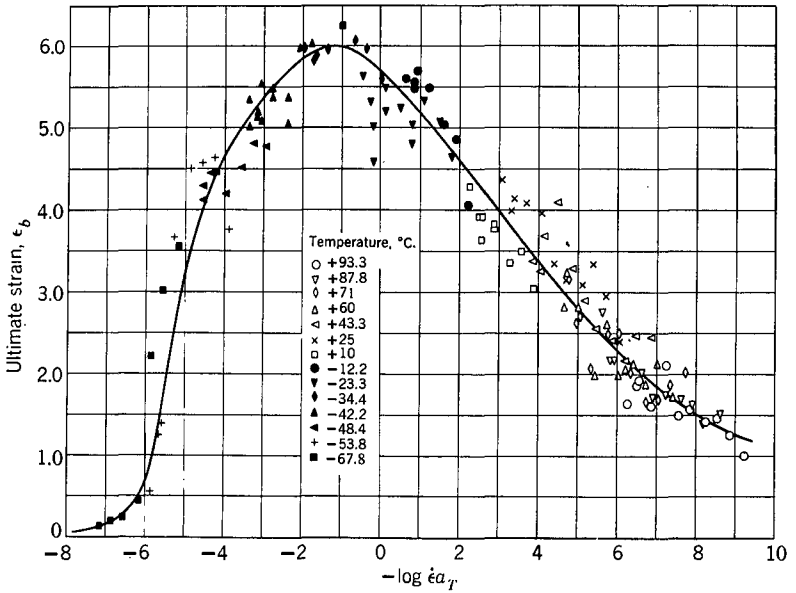


FIG. 19–3. Tensile strain at break plotted against logarithm of strain rate (in sec^{-1}) reduced to 263°K for a cross-linked styrene-butadiene rubber at 14 temperatures as indicated (Smith.[106])

properties—are far less reproducible than the relation between the stress and strain up to the breaking point, since the mechanical failure depends on quantities which are subject to statistical fluctuations; experimentally, the ultimate properties should more appropriately be expressed by distribution functions.[93,104,105] Despite this complication, and regardless of the detailed mechanism of the molecular breaking process, various experiments have shown that the dependence of ultimate properties on temperature and rate of deformation is closely related to that of viscoelastic properties and therefore reflects the rates of configurational rearrangements.

Most such experimental data refer to uniaxial extension, in which the rupture is characterized by an ultimate tensile strain ϵ_b $(= \lambda_b - 1)$ and breaking stress (tensile strength) $\sigma_T(b)$. If the extension is performed at constant strain rate $\dot{\epsilon}$, ϵ_b and $\sigma_T(b)$ can be plotted with reduced variables as illustrated in Figs. 19–3 and 19–4, where the abscissa is $-\log \dot{\epsilon} a_T$. In these examples from Smith,[106] data for a cross-linked styrene-butadiene rubber covering a temperature range from −68° to 93° are combined with shift factors a_T which agreed with those determined by reduction of stress-strain curves at lower elongations as discussed in connection with equation 17 of Chapter 14; the temperature dependence of a_T followed the WLF equation in the form of equation 40 of Chapter 11 with $T_s = 263°K$. Within the expected large scatter of individual break-point measurements, composite curves are obtained, representing the ultimate properties at temperature T_s over a very wide range of strain rates. (The deviations at the lowest temperatures are associated with cold drawing, where temperature gradients exist at the neck and the process is nonisothermal.) The elongation at break goes through a substantial maximum,

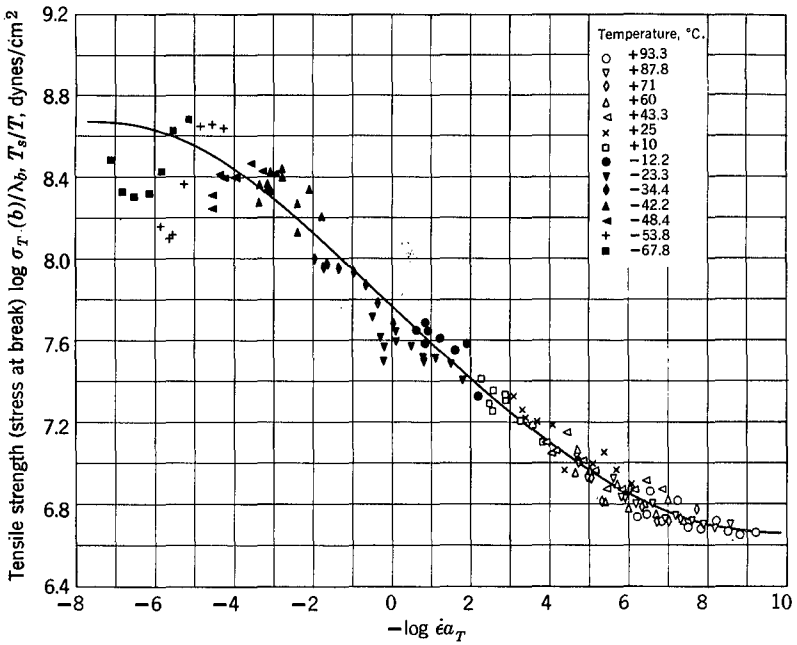


FIG. 19–4. Tensile strength in force per unit initial cross-section area, $\sigma_T(b)/\lambda_b$, plotted against logarithm of strain rate, both reduced to $T_s = 263°K$ for the material of Fig. 19–3 at the same 14 temperatures. (Smith.[106])

whereas the tensile stress (plotted here as $\sigma_T(b)/\lambda_b$, the force per unit cross-section area of the *unstrained* sample, denoted by σ_b in many publications) increases monotonically with increasing strain rate, but $\sigma_T(b)$ goes through a maximum.[102] This behavior can be interpreted by the concept[103] that the probability of rupture depends on the stored elastic energy per network strand. Reduced variables have been used in a similar manner for very densely cross-linked networks.[107]

If the breaking strength (reduced, as in Fig. 19–4, like a modulus by the factor T_s/T) is plotted logarithmically against the strain at break, the resulting failure envelope, introduced by Smith,[108] has several important properties (Fig. 19–5). The experimental scatter is reduced because the fluctuations in ϵ_b and $\sigma_T(b)/\lambda_b$ move around the curve while staying on its locus.[104] As the strain rate is increased or the temperature is decreased, the rupture point moves counterclockwise around the envelope. Moreover, the envelope describes failure properties in creep or stress relaxation as well as in constant rate of strain. For example, a sample with stress and strain denoted by point P in Fig. 19–5 could be maintained at constant strain; the stress would relax following a vertical line and the sample ruptures at the intersection of this line with the failure envelope. Alternatively, if a sample corresponding to point P is maintained under constant stress, it will creep with the strain following a horizontal line and again the sample ruptures at the intersection of this line with the failure envelope.[108] A failure envelope with points from the three different types of experiments is illustrated in Fig. 19–6.

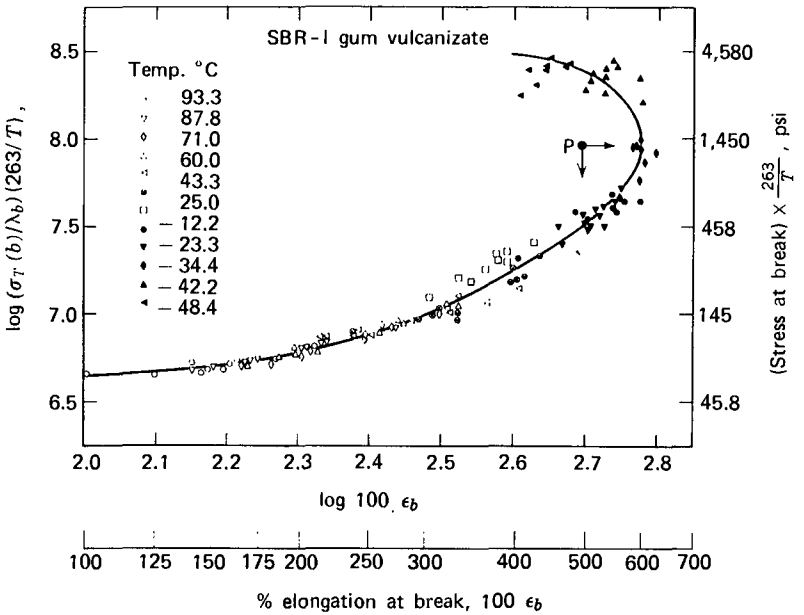


FIG. 19-5. Failure envelope from data of Figs. 19-3 and 19-4. (Smith.[108])

With increasing density of cross-linking, the failure envelope shifts to the left, but envelopes at different values of ν_e (moles effective network strands per cubic centimeter) can be superposed by plotting $\sigma_T(b)/\lambda_b$ logarithmically against $(\lambda_g - 1)/(\lambda_b - 1)_{max}$, as shown in Fig. 19-7 for data of Smith on a hydrofluorocarbon elastomer.[110] The maximum corresponding to the right edge of the envelope,

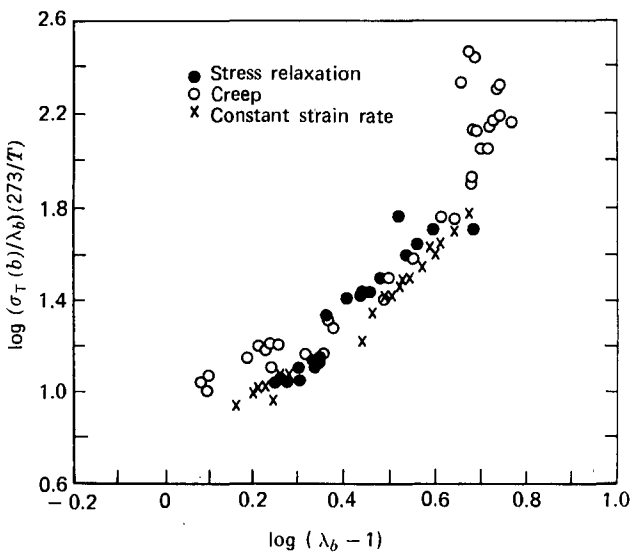


FIG. 19-6. Failure envelope for a styrene-butadiene rubber with points from three different types of experiment as indicated, reduced to 273°K. (Halpin.[109])

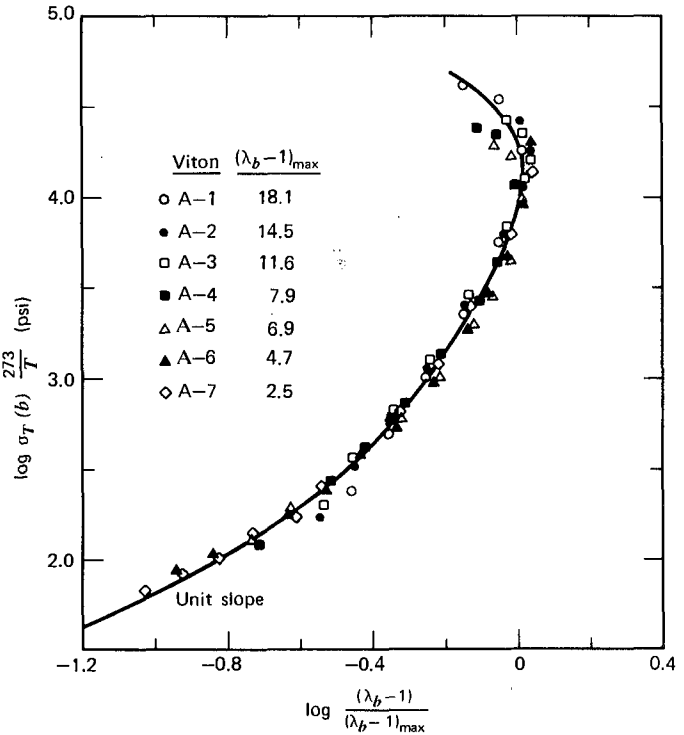


FIG. 19-7. Logarithmic plot of $\sigma_T(b)$ reduced to 273°K against $(\lambda_b - 1)/(\lambda_b - 1)_{max}$ for a hydrofluorocarbon elastomer cross-linked to various extents; ν_e increases from A-1 to A-7 in the approximate range 0.4 to 3.2 × 10^{-4} moles/cc. (Smith.[110]) Reproduced, by permission, from *Rheology*, edited by F. R. Eirich, Vol. V, Academic Press, New York, 1969.

$(\lambda_b)_{max}$, is approximately proportional to $\nu_e^{-1/2}$.[110,111] By introducing the maximum network extensibility parameter λ_m^e discussed in connection with equation 16 of Chapter 14, the dependence of the failure envelope on ν_e can be more accurately described;[112] it is found that λ_m^e is similar in magnitude to $\lambda_b(m)$ but may be somewhat larger. Failure envelopes have been studied for a variety of cross-linked rubbery polymers.[104-111]

Although most theoretical and experimental studies of rupture are concerned with behavior in uniaxial extension, failure in other types of deformation is also important. Behavior in compression, shear, biaxial extension, and triaxial extension has also been investigated.[98]

2. Rupture below the Glass Transition Temperature

When the chain backbone configurations are immobilized during the time of the experiment, ultimate properties do not involve long-range rearrangements. Nevertheless, dissipation of energy by local relaxation processes appears to be important in determining the degree of stress concentration at the tip of a crack,[100,113] and the breaking strength under impact.[114,115] The latter can be

correlated with the β mechanism of viscoelastic loss (Section B2 of Chapter 15) provided the latter is associated with motion of the chain backbone rather than only that of a side group;[115] it may be more closely correlated with nonlinear viscoelastic properties observed at high stresses.[116]

Experiments with biaxial stresses in varying ratio and combined tension and torsion have been used to distinguish between yielding by shear or normal stress failure.[117-119]

REFERENCES

1. J. Meissner, *J. Polym. Sci., Polym. Phys. Ed.*, **16,** 915 (1978).
1a. T. L. Smith, *J. Polym. Sci., Polym. Phys. Ed.*, **17,** 2181 (1979).
2. N. W. Tschoegl, *The Theory of Linear Viscoelastic Behavior,* Academic Press, 1980, Chapter 9.
2a. J. D. Ferry, *Rev. Mod. Phys.*, **31,** 130 (1959).
3. J. A. C. Harwood and A. Schallamach, *J. Appl. Polym. Sci.*, **11,** 1835 (1967).
3a. K. A. Grosch, J. A. C. Harwood, and A. R. Payne, in *Physical Basis of Yield and Fracture,* edited by A. C. Strickland, Institute of Physics and Physical Society, London, 1966, p. 144.
4. K. Yagii and N. W. Tschoegl, *Trans. Soc. Rheol.*, **14,** 1 (1970).
5. J. P. A. Tillet, *Proc. Phys. Soc.*, **B67,** 677 (1954).
6. N. E. Waters, *Br. J. Appl. Phys.*, **16,** 557 (1965).
7. E. Southern and A. G. Thomas, *J. Appl. Polym. Sci.*, **16,** 1641 (1972).
8. E. Jenckel and E. Klein, *Z. Naturforsch.*, **7a,** 619 (1952).
9. N. P. Vinh Tuong, *Mem. Artillerie Fr.*, 1965, p. 67.
10. Y. H. Pao, *J. Appl. Phys.*, **26,** 1082 (1955).
11. S. C. Hunter, *J. Mech. Phys. Solids,* **8,** 219 (1960).
12. M. Gordon and M. B. Grieveson, *J. Polym. Sci.*, **29,** 9 (1958).
13. D. G. Flom and A. M. Bueche, *J. Appl. Phys.*, **30,** 1725 (1959).
14. D. Atack and D. Tabor, *Proc. R. Soc.*, **A246,** 539 (1958).
15. D. G. Flom, *J. Appl. Phys.*, **31,** 306 (1960); *ibid.*, **32,** 1426 (1961).
16. W. D. May, E. L. Morris, and D. Atack, *J. Appl. Phys.*, **30,** 1713 (1959).
17. S. C. Hunter, *J. Appl. Mech.*, **28,** 611 (1961).
18. K. Minato and T. Takemura, *Jap. J. Appl. Phys.*, **6,** 719 (1967).
19. E. R. Fitzgerald, private communication.
20. O. Kramer and J. D. Ferry, in *Science and Technology of Rubber,* edited by F. R. Eirich, Academic Press, New York, 1978, Chapter 5.
21. E. Maekawa, I. Furuta, M. Nakao, and K. Ninomiya, *Nippon Gomu Kyokaishi,* **40,** 542 (1967).
22. A. R. Payne, *Rubber Chem. Technol.*, **34,** 1190 (1964).
23. A. R. Payne and R. E. Whittaker, *Rubber Chem. Technol.*, **44,** 340 (1971).
24. J. C. Snowdon, *Vibration and Shock in Damped Mechanical Systems,* Wiley, New York, 1968.
25. H. Thurn, *Kunstoffe,* **11,** 606 (1960).
26. H. Oberst, *Acustica,* **2,** Beih. 4, AB 181 (1952); **4,** Beih. 1, 433 (1954).
27. H. Oberst, *Ber. Ver. Deuts. Ing.*, **8,** 100 (1956).
28. E. M. Kerwin, Jr., *J. Acoust. Soc. Am.*, **31,** 952 (1959).
29. G. W. Becker and H. Oberst, *Kolloid-Z.*, **148,** 6 (1956).
30. F. Linhardt and H. Oberst, *Akust. Beih.*, **11,** 255 (1961).
31. H. Oberst, *Proc. 3rd Intern. Cong. Acoustics,* edited by L. Cremer, Elsevier, Amsterdam, 1962, p. 352.
32. H. Oberst, L. Bohn, and F. Linhardt, *Kunstoffe,* **51,** 495 (1961).
33. H. Oberst, in *Kunststoffe,* edited by R. Nitsche and K. A. Wolf, Springer-Verlag, Berlin, Volume

6, 1962, p. 404; Vol. 7, 1961, p. 280.
34. J. L. Hunter and P. R. Derdul, *J. Acoust. Soc. Am.*, **42,** 1041 (1967).
35. S. O. Williamson, U.S. Patent 3,234,817 (1966).
36. A. Schallamach, *Wear,* **1,** 384 (1958).
37. P. Thirion, *Rev. Gen. Caoutch.*, **23,** 101 (1946).
38. P. Thirion and R. Chasset, *Rev. Gen. Caoutch.*, **43,** 211 (1966).
39. D. Bulgin, G. Hubbard, and M. Walters, *Proc. 4th Rubber Tech. Conf.,* London, 1962, p. 173.
40. K. A. Grosch, *Nature,* **197,** 858 (1963); *Proc. R. Soc.,* **A274,** 21 (1963).
41. G. M. Bartenev and A. I. El'kin, *Wear,* **8,** 8 (1965).
42. J. A. Greenwood and D. Tabor, *Proc. Phys. Soc.*, **71,** 989 (1958).
43. D. Tabor, in *Advances in Polymer Friction and Wear,* edited by L.-H. Lee, Plenum Press, New York, 1974, p. 5.
44. A. Schallamach, *Wear,* **6,** 375 (1963).
45. K. C. Ludema and D. Tabor, *Wear,* **9,** 329 (1966).
46. K. G. McLaren and D. Tabor, *Nature,* **197,** 856 (1963).
47. J. R. Beatty, *Rubber Chem. Technol.*, **42,** 1040 (1969).
48. R. R. Myers, *Trans. Soc. Rheol.*, **4,** 43 (1960).
49. D. H. Kaelble, *Trans. Soc. Rheol.*, **4,** 45 (1960).
50. G. Yasuda, K. Ninomiya, and S. Ido, *Nippon Gomu Kyokaishi,* **36,** 1001 (1963).
51. G. Yasuda and S. Ido, *Nippon Gomu Kyokaishi,* **36,** 1089 (1963).
52. A. N. Gent and R. P. Petrich, *Proc. R. Soc.*, **A310,** 433 (1969).
53. D. H. Kaelble, *Physical Chemistry of Adhesion,* Wiley-Interscience, New York, 1971.
54. L.-H. Lee, editor, *Advances in Polymer Friction and Wear,* Plenum Press, New York, 1974.
55. K. A. Grosch and A. Schallamach, *Wear,* **4,** 356 (1961).
56. A. Schallamach, in *The Chemistry and Physics of Rubberlike Substances,* edited by L. R. Bateman, MacLaren and Sons, London, 1963, Chapter 13.
57. K. A. Grosch and A. Schallamach, *Trans. Inst. Rubber Ind.*, **41,** T80 (1965).
58. J. L. White and N. Tokita, *J. Appl. Polym. Sci.*, **9,** 1929 (1965); **11,** 321 (1967).
59. K. Ninomiya, S. Kusamizu, E. Maekawa, and G. Yasuda, *Prog. Polym. Sci. Jpn.*, **1,** 377 (1971).
60. N. Tokita and I. Pliskin, *Proc. Intern. Inst. Synthetic Rubber Producers,* 1973.
61. M. Mooney, *J. Appl. Phys.*, **7,** 73 (1936).
62. K. Ninomiya, *Nippon Gomu Kyokaishi,* **34,** 900 (1961).
63. G. Yasuda and K. Ninomiya, *Rubber Chem. Technol.*, **42,** 714 (1969).
64. J. Meissner, *Pure Appl. Chem.*, **42,** 553 (1975).
65. A. S. Lodge, *Body Tensor Fields in Continuum Mechanics,* Academic Press, New York, 1974, p. 212.
66. J. L. White, in *Science and Technology of Rubber,* edited by F. R. Eirich, Academic Press, New York, 1978, p. 224.
67. D. V. Papero, R. C. Wincklhofer, and H. J. Oswald, *Rubber Chem. Technol.*, **38,** 999 (1965).
68. W. E. Claxton, M. J. Forster, J. J. Robertson, and G. R. Thurman, *Text. Res. J.*, **36,** 903 (1966).
69. W. H. Howard and M. L. Williams, *Rubber Chem. Technol.*, **40,** 1139 (1967).
70. A. Dyson, *Phil. Trans. R. Soc.*, **A266,** 1 (1970).
71. W. Hirst and M. G. Lewis, *Proc. R. Soc.*, **A334,** 1 (1973).
72. G. Harrison and E. G. Trachman, *J. Lubr. Technol.*, **F94,** 306 (1972).
73. T. C. Davenport, editor, *The Rheology of Lubricants,* Halsted Press, London, 1973.
74. J. Lamb, *J. Rheol.*, **22,** 317 (1978).
75. M. J. Davies and K. Walters, in T. C. Davenport, editor, *The Rheology of Lubricants,* Halsted Press, London, 1973, p. 65.
76. J. R. Richards, K. Ninomiya, and J. D. Ferry, *J. Phys. Chem.*, **67,** 323 (1963).
77. K. Ninomiya and J. D. Ferry, *J. Phys. Chem.*, **67,** 2292 (1963).
78. W. E. Rochefort, G. G. Smith, H. Rachapudy, V. R. Raju, and W. W. Graessley, *J. Polym. Sci.,*

Polym. Phys. Ed., **17**, 1197 (1979).
79. H. Fujita and A. Kishimoto, *J. Polym. Sci.*, **28**, 547 (1958).
80. R. W. Rosser, N. Nemoto, J. L. Schrag, and J. D. Ferry, *J. Polym. Sci., Polym. Phys. Ed.*, **16**, 1031 (1978).
81. H. N. V. Temperley and L. G. Chambers, *Proc. Phys. Soc.*, **58**, 420 (1946).
82. T. H. Bull, *Phil. Mag.*, [8], **1**, 153 (1956); *Br. J. Appl. Phys.*, **7**, 416 (1956).
83. H. H. Kausch, *J. Macromol. Sci.—Rev. Macromol. Chem.*, **C4**, 243 (1970).
84. E. H. Andrews and P. E. Reed, *Adv. Polym. Sci.*, **27**, 1 (1978).
85. J. Becht and H. Fischer, *Kolloid Z., Z. Polym.*, **229**, 167 (1969).
86. S. Onogi, T. Matsumoto, and E. Kamei, *Polym. J.*, **3**, 531 (1972).
87. E. Kamei and S. Onogi, *Polym. J.*, **8**, 347 (1976).
88. G. V. Vinogradov, Polymer, **18**, 1275 (1977).
89. G. V. Vinogradov, *Pure Appl. Chem.*, **42**, 527 (1975); G. V. Vinogradov, B. V. Radushkevich, V. P. Napasnikov, and V. D. Fikhman, *Rheol. Acta*, **17**, 231 (1978).
90. R. S. Porter and J. F. Johnson, *J. Appl. Phys.*, **35**, 3149 (1964).
91. R. E. Harrington and B. H. Zimm, *J. Phys. Chem.*, **69**, 161 (1965).
92. D. McIntyre, L. J. Fetters, and E. Slagowski, *Science*, **176**, 1041 (1972).
93. F. Schwarzl and A. J. Staverman, in H. A. Stuart, *Die Physik der Hochpolymeren*, Volume IV, Springer-Verlag, Berlin, 1956, Chapter III.
94. R. Houwink, *Elasticity, Plasticity, and the Structure of Matter*, 2nd ed., Harren, Washington, 1953.
95. R. F. Landel, in *Mechanics and Chemistry of Solid Propellants*, Pergamon, Oxford, 1966, p. 575.
96. R. N. Haward, *Strength of Plastics and Glasses*, Interscience, New York, 1949.
97. E. H. Andrews, *Fracture in Polymers*, American Elsevier, New York, 1968.
98. A. N. Gent, in *Science and Technology of Rubber*, edited by F. R. Eirich, Academic Press, New York, 1978, p. 419.
99. F. R. Eirich and T. L. Smith, in *Fracture of Non-Metals and Composites*, edited by H. Liebowitz, Volume 7, Academic Press, New York, Chapter 7, p. 351.
99a. H. H. Kausch, *Polymer Fracture*, Springer-Verlag, New York, 1979.
100. J. G. Williams, *Adv. Polym. Sci.*, **27**, 67 (1978).
101. C. B. Bucknall, *Adv. Polym. Sci.*, **27**, 121 (1978).
102. T. L. Smith, *Rubber Chem. Technol.*, **51**, 225 (1978).
103. E. M. Dannenberg, *Rubber Chem. Technol.*, **48**, 419 (1975).
104. R. F. Fedors and R. F. Landel, *Trans. Soc. Rheol.*, **9:1**, 195 (1965).
105. J. C. Halpin and H. W. Polley, *J. Compos. Mater.*, **1**, 64 (1967).
106. T. L. Smith, *J. Polym. Sci.*, **32**, 99 (1958).
107. D. H. Kaelble, *J. Appl. Polym. Sci.*, **9**, 1213 (1965).
108. T. L. Smith, *J. Polym. Sci.*, **A1**, 3597 (1963); *J. Appl. Phys.*, **35**, 27 (1964).
109. J. C. Halpin, *J. Appl. Phys.*, **35**, 3133 (1964).
110. T. L. Smith, in *Rheology*, edited by F. R. Eirich, Vol. V, Academic Press, New York, 1969, p. 127.
111. T. L. Smith and W. H. Chu, *J. Polym. Sci.*, A-2, **10**, 133 (1972).
112. T. L. Smith and J. E. Frederick, *J. Appl. Phys.*, **36**, 2996 (1965).
113. W. W. Gerberich and G. C. Martin, *J. Polym. Sci.*, **14**, 897 (1976).
114. Y. Wada and T. Kasahara, *J. Appl. Polym. Sci.*, **11**, 1661 (1967).
115. J. Heijboer, *J. Polym. Sci.*, **C16**, 3755 (1968).
116. W. M. Davis and C. W. Macosko, *J. Rheol.*, **22**, 53 (1978).
117. G. M. Bartenev and Yu. S. Zuyev, *Strength and Failure of Viscoelastic Materials*, Pergamon, 1968.
118. S. S. Sternstein and F. A. Myers, *J. Macromol. Sci.—Phys.*, **B8**, 539 (1973).
119. S. S. Sternstein, in *Treatise on Materials Science and Technology*, edited by J. M. Schultz, Volume 10, Part B, Academic Press, New York, 1977, p. 541.

APPENDIX A

List of Symbols

To avoid introducing unfamiliar and exotic symbols, it has sometimes been necessary to use the same symbol with two or more different meanings. However, the context should always make the identification clear. The following list does not include all the various subscripts which are used in certain special applications. Numbers identify chapter and equation where, or near where in the accompanying text, each symbol is introduced. (If not introduced in an equation, the location is identified by a section number, like D3.)

	Ch.	Eq.	
a	9	B	root-mean-square end-to-end distance per square root of number of monomer units
a_T	11	1	ratio of relaxation times at two different temperatures
a_c	17	10	ratio of relaxation times at two different concentrations
a_P	11	50	ratio of relaxation times at two different pressures
a_t	18	B2	ratio of relaxation times at two different elapsed times
a_ϵ	18	7	ratio of relaxation times at two different tensile strains
a_{12}	11	49	ratio of relaxation times in states 2 and 1
b	5	2	sample coefficient or form factor, *or*
	9	A1	spacing in Kirkwood-Auer model, *or*
	17	28	exponent
c	9	1	concentration (g polymer per cc solution), *or*
	6	6	width (sample)
c^*	9	D1	critical concentration for coil overlap
c_1^0, c_2^0	11	21	coefficients in WLF equation referred to T_0 as reference
c_1^g, c_2^g	11	C2	coefficients in WLF equation referred to T_g as reference
d	6	6	thickness (sample)
e	5	D3	electromotive force, *or* base of natural logarithms
f	5	1	force, *or*
	11	31	fractional free volume, *or*
	10	B1	cross-linking functionality

f_g	11	39	fractional free volume at the glass transition temperature
f_0	9	B1	translational friction coefficient of a submolecule, *or*
	11	50	fractional free volume in a reference state
g	13	C4	ratio of squares of radii of gyration of branched and linear polymers, *or*
	10	33	front factor
g'	9	B8	ratio of intrinsic viscosities of branched and linear polymers
g_2	13	C4	ratio of steady-state compliances of branched and linear polymers
h	5	2	height, *or*
	9	29	hydrodynamic interaction parameter
h^*	9	29	alternative hydrodynamic interaction parameter
i	5	D3	current, *or* $\sqrt{-1}$, *or* intercept of linear plot
j	9	B	number of chain backbone atoms in a monomer unit
j^0_{eR}	9	13	reduced intrinsic steady-state compliance
k	9	14	Boltzmann's constant, *or* arbitrary constant in various equations
l	9	B	length
m	6	A	mass (sample), *or*
	4	4	slope of logarithmic plot, *or*
	9	10	coefficient in dilute solution theories
n	9	18	number of molecules per cubic centimeter
p	9	15	summation index, *or*
	14	5	scission probability
q	9	B	number of monomer units in a submolecule, *or*
	10	43	cross-linking probability, *or*
	5	5	numerical factor
r	9	39	radius, *or*
	5	39	wave damping parameter, *or* other dimensionless ratios
$(\overline{r_0^2})^{1/2}$	9	B	root-mean-square end-to-end distance of a macromolecule (unperturbed)
s			running time variable, *or* slope of linear plot
t			time
u			running time variable, *or*
	1	3	displacement
v	5	24	velocity, *or*
	11	29	specific volume
v_f	11	29	free volume per gram
v_i	10	25	volume fraction of component i
v_o	11	C2	occupied volume per gram
v_1	17	4	volume fraction of solvent

v_2	17	6	volume fraction of polymer
w_g	10	43	gel fraction
w_i	10	18	weight fraction of component i
x	5	1	linear displacement
x_0	5	35	critical damping distance
A	5	2	area, *or*
	4	12	numerical factor in approximation calculations, *or*
	5	36	real component of complex propagation constant, *or* empirical constant in various equations
A_G	3	34	limiting ratio of G'/ω^2 at low ω
B	1	46	bulk compliance, *or*
	4	26	numerical factor in approximation calculations, *or*
	5	25	magnetic flux density, *or*
	5	36	imaginary component of complex propagation constant, *or*
	11	29	constant in Doolittle equation, *or* empirical constant
$B(t)$	1	46	bulk creep compliance
B^*	1	46	complex dynamic bulk compliance
B'	1	46	bulk storage compliance
B''	1	46	bulk loss compliance
B_e	18	9	equilibrium bulk compliance
B_g	18	8	glasslike bulk compliance
B_n	7	10	numerical coefficient (vibrations of bars)
C_1, C_2			characteristic constants in various equations
C_v	5	41	heat capacity at constant volume
D	1	54	tensile compliance, *or*
	11	70	diffusion coefficient
$D(t)$	1	54	tensile creep compliance
D^*	1	54	complex dynamic tensile compliance
D'	1	54	tensile storage compliance
D''	1	54	tensile loss compliance
D_e	1	51	equilibrium tensile compliance
D_g	1	S1	glasslike tensile compliance
$E(t)$	1	52	tensile (Young's) relaxation modulus
E^*	11	46	activation energy in modified free volume theory, *or*
	1	54	complex dynamic tensile modulus
E'	1	54	tensile storage modulus
E''	1	54	tensile loss modulus
E_e	1	53	equilibrium or pseudo-equilibrium tensile modulus
E_g	1	S1	glasslike Young's modulus
F	5	14	thrust force
$F(t)$	3	60	constant strain rate elongational modulus
$G(t)$	1	7	shear relaxation modulus
G^*	1	24	complex dynamic shear modulus
G'	1	19	shear storage modulus

G''	1	19	shear loss modulus
G_e	1	53	equilibrium shear modulus
G_N	2	A3	shear modulus associated with entanglement network (in cross-linked systems)
G_N^0	12	C2	shear modulus associated with entanglement network (in uncross-linked systems)
G_g	2	A3	glasslike shear modulus
G_i	1	33	modulus contribution of model element
$\tilde{G}$	5	F	shear wave rigidity modulus
$[G']$	9	1	intrinsic storage shear modulus
$[G'']$	9	2	intrinsic loss shear modulus
H	3	19	relaxation spectrum (shear)
$\overline{H}$	3	B2	relaxation spectrum in extension
I	6	C4	moment of inertia
$J(t)$	1	9	shear creep compliance
J^*	1	26	complex dynamic shear compliance
J'	1	26	shear storage compliance
J''	1	26	shear loss compliance
J_e	1	38	equilibrium shear compliance
J_N	2	A2	shear compliance associated with entanglement network (in cross-linked systems)
J_e^0	1	40	steady-state shear compliance
J_N^0	2	A2	shear compliance associated with entanglement network (in uncross-linked systems)
J_g	2	A2	glasslike shear compliance
J_i	3	18	compliance contribution of model element
K	1	43	bulk modulus, *or*
	6	9	transducer constant, *or* characteristic constant
$K(t)$	1	43	bulk relaxation modulus
K^*	1	46	complex dynamic bulk modulus
K'	1	46	bulk storage modulus
K''	1	46	bulk loss modulus
K_e	1	53	equilibrium bulk modulus
K_{ad}	5	41	adiabatic bulk modulus
K_{is}	5	41	isothermal bulk modulus
L	3	20	retardation spectrum (shear), *or*
	5	4	depth
$\overline{L}$	3	B2	retardation spectrum in extension
M	1	58	modulus for one-dimensional extension in infinite medium, *or*
	4	4	numerical factor in approximation calculations, *or*
	5	33	mass, *or*
	9	6	molecular weight
M^*	1	58	complex dynamic longitudinal bulk modulus

M'	1	58	bulk longitudinal storage modulus
M''	1	58	bulk longitudinal loss modulus
$\overline{M}_n$			number-average molecular weight
$\overline{M}_w$			weight-average molecular weight
$\overline{M}_z$			z-average molecular weight
M_0	10	5	molecular weight per monomer unit
M_e	10	C1	average molecular weight between entanglement coupling points
M_c	10	B3	average molecular weight of a network strand
M_C	10	C1	critical molecular weight for effect of entanglement coupling on viscosity
M'_C	10	C3	critical molecular weight for effect of entanglement coupling on steady-state compliance
N	4	60	numerical factor in approximation calculations, *or*
	9	B	number of submolecules in a macromolecule
N_b	9	42	number of submolecules in a branch
N_0			Avogadro's number
P	1	6	pressure, *or*
	9	B	degree of polymerization
P_a	1	45	ambient pressure
P_c	10	37	average degree of polymerization of a network strand
P_e	10	C2	average degree of polymerization between entanglement coupling points
Q_e	10	46	entanglement coupling factor
R	5	7	radius, *or*
	5	26	electrical resistance, *or*
	9	6	gas constant
R_M	5	21	mechanical resistance
$R_{\dot{\gamma}}$	10	65	nonlinear steady-state compliance
S_1	9	26	sum of relaxation time ratios
S_2	9	36	sum of squares of relaxation time ratios
S_M	5	21	mechanical elastance
T	9	6	absolute temperature
T_0	11	1	reference temperature for reduced variables
T_∞	11	26	Vogel temperature
T_e	10	43	probability that an entanglement is trapped
T_s	11	40	adjustable standard reference temperature for WLF equation
T_g	2	A1	glass transition temperature
T_M	12	A	temperature of midpoint of transition from rubberlike to glasslike consistency (under arbitrary conditions of time or frequency)
W	19	3	work of deformation, *or*
	19	A6	load
X	5	26	electrical reactance

X_M	5	21	mechanical reactance
Y_M	6	10	mechanical admittance
Z	5	25	electrical impedance
Z'	9	46	real part of complex Zimm function
Z''	9	47	imaginary part of complex Zimm function
Z_M	5	21	mechanical impedance
f	11	F2	ratio of the numbers of entanglement network strands per cubic centimeter at two different temperatures
$\mathscr{E}_{st}$	19	4	stored energy per cubic centimeter
$\mathscr{E}_d$	19	6	dissipated energy per cubic centimeter (in a quarter cycle)
$\dot{\mathscr{E}}$	19	10	rate of dissipation of energy per second
$\mathscr{F}$	6	8	strain dependence function
$\mathscr{R}_M$	5	28	characteristic mechanical resistance
$\mathscr{S}$	5	6	torque
$\mathscr{X}_M$	5	29	characteristic mechanical reactance
α	5	8	angle of deformation, *or*
	11	C1	thermal expansion coefficient, *or*
	5	35	attenuation of propagated wave
α_f	11	33	thermal expansion of free volume relative to total volume
α_l	11	C1	thermal expansion coefficient above T_g
α_g	11	C1	thermal expansion coefficient below T_g
α_0	11	C1	thermal expansion coefficient of occupied volume relative to total volume
β	1	46	coefficient of compressibility, *or*
	13	28	parameter in Andrade creep equation, *or*
	9	52	parameter for onset of shear dependence of $[\eta]$, *or*
	17	3	parameter relating free volume to weight concentration of diluent
β'	17	4	parameter relating free volume to volume concentration of diluent
β_f	11	51	compressibility of fractional free volume
γ	1	3	strain, *or*
	14	B2	average number of cross-linked points on a polymer molecule
γ_{11}	1	3	tensile strain (twice the practical tensile strain ϵ)
γ_{21}	1	3	shear strain
γ_{ij}	1	3	component of strain tensor
$\dot{\gamma}$	1	16	rate of strain
δ	1	20	phase angle between stress and strain, *or* small increment, *or*
	1	42	Kronecker delta
ϵ	1	52	practical tensile strain ($\frac{1}{2}\gamma_{11}$), *or*
	9	34	Peterlin-Ptitsyn-Eizner parameter
$\dot{\epsilon}$	6	E1	practical tensile strain rate
$\dot{\epsilon}_1$	6	E1	elongational strain rate

ε	10	43	moles entanglement loci per cubic centimeter
ζ	11	30	translational friction coefficient
ζ_0	9	B1	translational friction coefficient per monomer unit
ζ_E	10	E1	monomeric translational elastic coefficient
ζ_1	11	70	translational friction coefficient for small foreign molecule
η	1	G2	non-Newtonian viscosity
η_0	1	31	steady-state shear viscosity at vanishing shear rate
η^*	1	31	complex dynamic shear viscosity
η'	1	31	real part of complex viscosity
η'_∞	9	E	high-frequency limiting value of η'
η''	1	32	imaginary part of complex viscosity
$\eta^-(t)$	1	13	stress relaxation viscosity
$\eta^+(t)$	1	14	stress growth viscosity
$\bar{\eta}$	2	C3	tensile viscosity
η_n	5	E	nominal viscosity from surface-loading instrument
η_v	8	A	bulk (volume) viscosity
η_i	1	33	viscosity contribution of model element
η_s	9	2	viscosity of solvent
$[\eta']$	9	3	real part of complex intrinsic viscosity
$[\eta'']$	9	4	imaginary part of complex intrinsic viscosity
θ	5	9	angle
κ	5	43	thermal conductivity
λ	5	35	wavelength, *or*
	6	9	relative length (in large deformations), *or*
	10	26	blending factor, *or*
	19	A6	coefficient of rolling friction
μ	1	50	Poisson's ratio, *or*
	19	B3	coefficient of sliding friction
ν	1	16	frequency in Hz, *or*
	10	33	moles network strands per cubic centimeter
ν_c	14	B2	moles chemical cross-links per cubic centimeter
ν_e	13	2	moles entanglement network strands per cubic centimeter (in uncross-linked systems)
ν_N	14	2	moles network strands per cubic centimeter terminated by trapped entanglements
ν_X	14	2	moles strands terminated by cross-links, per cubic centimeter
ξ	1	10	time variable
ρ	1	1	density
σ	1	4	stress, *or*
	9	B	root-mean-square end-to-end distance of a submolecule
σ_{ij}	1	4	component of stress tensor
σ^{ss}	1	13	stress following cessation of steady-state flow
σ_T	1	F2	practical tensile stress
τ	1	33	relaxation or retardation time; argument of H or L

τ_m	10	C5	empirical terminal relaxation time (White-Tokita)
τ_1	9	28	terminal relaxation time
τ_{tr}	10	B1	longest relaxation time in transition zone
τ_d	10	57	terminal relaxation (disengagement) time, Doi-Edwards theory
τ_w	10	53	weight-average terminal relaxation time, Graessley theory
τ_i	1	33	relaxation or retardation time of element of mechanical model
ϕ	12	C4	volume fraction (of filler)
ψ	4	50	numerical factor in approximation calculations
ψ'	4	51	numerical factor in approximation calculations
ω	1	16	frequency in rad/sec
ω_0	6	13	resonance frequency (forced oscillations)
ω_c	6	16	characteristic frequency (free oscillations)
ω_{tr}	10	B1	frequency boundary between transition and equilibrium or plateau zone
Γ	4	4	gamma function, *or*
	5	36	complex propagation constant
Δ			differencing symbol, *or*
	6	16	logarithmic decrement
Δ_v	1	45	dilation
ΔH_η	17	C1	apparent activation energy in viscous flow
ΔH_a	11	44	apparent activation energy for relaxation or retardation processes
Ψ_1	1	62	primary normal stress coefficient
$\Psi_{1,0}$	1	64	primary normal stress coefficient at vanishing shear rate
Ψ_2	1	63	secondary normal stress coefficient
Θ	19	A5	coefficient of restitution

APPENDIX B

Applicability of Various Dynamic Methods for Viscoelastic Measurements

The methods are classified here according to the loss characteristics and magnitude of the impedance (in the acoustic sense—a measure of $|G^*|$ or $|E^*|$) of the materials to be studied. Examples of the six classes are given in the footnotes for illustration. For the transient methods, X denotes applicability; for the dynamic methods, letters are used to denote approximate frequency ranges, as follows: VLF, <1 Hz; LF, 1 to 10^2 Hz; MF, 10^2 to 10^4 Hz; HF, 10^4 to 10^6 Hz; VHF, $>10^6$ Hz.

Method	Chapter	Ref.	High Loss ($\tan\delta \gg 1$) High Impedance[a]	High Loss ($\tan\delta \gg 1$) Low Impedance[b]	Medium Loss ($\tan\delta \simeq 1$) Med. Impedance[c]	Low Loss ($\tan\delta \ll 1$) High Impedance[d]	Low Loss ($\tan\delta \ll 1$) Med. Impedance[e]	Low Loss ($\tan\delta \ll 1$) Low Impedance[f]
Creep	5	5,8–12	X		X			X
	6	1	X		X			
	6	14,15	X		X			
	6	16,17	X		X		X	X
	7	2–6				X		
Stress relaxation	5	17,26–31	X					
	6	1						X
	6	24–36			X	X	X	
	7	7–11				X		
Direct measurement of stress and strain	5	4,22,128	LF-MF	LF-MF				LF-MF
		17	VLF					VLF
		55	LF-MF		LF-MF		LF-MF	LF-MF
	6	42			VLF		VLF	
		46			MF		MF	
		47,48			LF		LF	
		49–51			LF	LF	LF	
		56			VLF-MF		VLF-MF	
	7	13				VLF		
		17,18				VLF,LF		
Measurements with mechanical impedance of moving element	5	64,65		VLF-MF				VLF-MF
		68	VLF					
		70–77	LF					
	6	57,58					LF	
Transducer measurements by electrical impedance	5	64		MF				
		83	MF					

	6	12,59	MF			MF		MF	MF
		61	LF			LF		LF	LF
Compound resonance	6	65–67	LF					LF	
measurements (forced)		68–70						LF	
		71,72							LF
		75,76	MF					MF	
	7	40					MF		
		41,42	MF				MF	MF	
Compound resonance	6	17						VLF-LF	VLF-LF
measurements (free)	6	81–85					LF	LF	
	6	86						LF	
Shear, extensional, and	5	118,119							MF
flexural wave propagation	6	82,86–88					MF-HF	MF-HF	
	6	89–93					VHF	VHF	
	7	43–47					VHF		
Longitudinal bulk wave	8	28–38	VHF			VHF	VHF	VHF	
propagation	8	39–41		VHF					
Characteristic impedance	5	85		LF					
measurements (surface	5	86–89,103		MF					
loading)	5	84,91–95	HF	HF					
	5	93,96–100	VHF	VHF					
Resonance vibration	7	23–39					MF		
measurements									

[a] *E.g.*, uncross-linked polymers of high molecular weight and their concentrated solutions in the terminal zone.

[b] *E.g.*, dilute polymer solutions.

[c] *E.g.*, most systems in the transition zone between glasslike and rubberlike consistency.

[d] *E.g.*, glassy and highly crystalline polymers, or soft polymers at such high frequencies that the moduli approach glasslike magnitudes.

[e] *E.g.*, soft cross-linked polymers in the pseudo-equilibrium zone, or uncross-linked polymers of high molecular weight in the plateau zone.

[f] *E.g.*, soft gels in the pseudo-equilibrium zone.

APPENDIX C

Form Factors and Maximum Stresses and Strains for Various Deformation Geometries

Type of Geometry	Fig. No.	Form Factor (b) and Units	Equation No. and Chapter	Maximum Stress	Maximum Strain
Simple shear	5-1a	A/h (cm) or $m/h^2\rho$	2, Ch. 5	$\sigma_{21} = f/A$	$\gamma_{21} = x/h$
Simple shear sandwich	6-1a	$A_1/h_1 + A_2/h_2$ (cm) or $(m_1/h_1^2 + m_2/h_2^2)/\rho$	2, Ch. 6	$\sigma_{21} = f/(A_1 + A_2)$	$\gamma_{21} = x/h$
Segel-Pochettino	5-1f	$2\pi L/\ln (R_2/R_1)$ (cm)	13, Ch. 5	$\sigma_{21} = f/2\pi R_1 L$	$\gamma_{21} = x/R_1 \ln (R_2/R_1)$
Annular pumping	5-1b	$\dfrac{2\pi L(R_2^2 + R_1^2)/R_2^2 - R_1^2)}{(R_2^2 + R_1^2)\ln (R_2/R_1)/(R_2^2 - R_1^2) - 1}$ (cm)	4, 5, Ch. 5	$\sigma_{21} = \dfrac{f(R_2^2 - R_1^2)}{2\pi L R_1 (R_2^2 + R_1^2)}$	$\gamma_{21} = \dfrac{x/R_1}{(R_2^2 + R_1^2)\ln (R_2/R_1)/(R_2^2 - R_1^2) - 1}$
Torsion between coaxial cylinders	5-1c	$\dfrac{4\pi L}{1/R_1^2 - 1/R_2^2}$ (cm^3)	7, Ch. 5	$\sigma_{21} = \mathcal{S}/2\pi L R_1^2$	$\gamma_{21} = 2R_2^2\alpha/(R_2^2 - R_1^2)$
Torsion between cone and plate	5-1d	$2\pi R^3/3\theta$ (cm^3)	9, Ch. 5	$\sigma_{21} = 3\mathcal{S}/2\pi R^3$	$\gamma_{21} = \alpha/\theta$
Torsion of circular cylindrical rod	5-1e	$\pi R^4/2h$ (cm^3) or $m^2/2\pi h^3\rho^2$	11, Ch. 5	$\sigma_{21} = 2\mathcal{S}/\pi R^3$	$\gamma_{21} = \alpha R/h$
Simple extension	6-1b	A/L (cm)	4, Ch. 6	$\sigma_T = f/A$	$\epsilon = x/L$
Flexure (cantilever, one end clamped, rectangular cross-section)	7-1a	$cd^3/4L^3$ (cm)	2, Ch. 7	$\sigma_T = 6fL/cd^2$	$\epsilon = 3\,dx/2L^2$
Flexure (cantilever, one end clamped, circular cross-section)	7-1b	$3\pi R^4/4L^3$ (cm)	3, Ch. 7	$\sigma_T = 4fL/\pi R^3$	$\epsilon = 3Rx/L^2$
Flexure (two ends clamped)	7-1c	$16cd^3/L^3$ (cm)	4, Ch. 7	$\sigma_T = 3fL/4cd^2$	$\epsilon = 12\,dx/L^2$
Flexure (knife edge loading)	7-1d	$4cd^3/L^3$ (cm)	5, Ch. 7	$\sigma_T = 3fL/2cd^2$	$\epsilon = 6\,dx/L^2$

c	width	A	area	γ_{21}	shear strain
d	thickness	L	length	ϵ	practical tensile strain
f	force	R	radius	θ	angle (between cone and plate)
h	height	$\mathcal{S}$	torque	ρ	density
m	mass	α	angular displacement	σ_T	practical tensile stress
x	linear displacement			σ_{21}	shear stress

APPENDIX D

Examples of Numerical Data for Dynamic and Relaxation Moduli and Creep Compliance

The shapes of the various viscoelastic functions have been abundantly illustrated graphically, specially in Chapters 2, 12, 13, and 14. However, no numerical data have been cited. Indeed, such data are very rarely given in the literature, where space restrictions usually limit the presentation to graphical form. Thus the material for derived calculations such as those in Chapter 19 is difficult to obtain. A compendium of numerical data would be of considerable value. A few examples are given here reduced to standard reference temperatures as described in Chapter 11. The units are dynes/cm^2 for moduli, cm^2/dyne for compliances, sec for time (unless otherwise noted), and radians/sec for frequency.

1. Shear Creep Compliance of Polystyrene

Data of Plazek and O'Rourke[1] on atactic polystyrene of narrow molecular weight distribution, molecular weight 600,000, reduced to 100°C, have been presented as curves III in Figs. 2-1 to 2-8. Numerical data corresponding to the creep compliance $J(t)$ and recoverable compliance $J(t) - t/\eta_0$ in Fig. 2-1 are tabulated below.

log t	log $J(t)$	log $[J(t) - t/\eta_0]$	log t	log $J(t)$	log $[J(t) - t/\eta_0]$	log t	log $J(t)$	log $[J(t) - t/\eta_0]$
−3.0	−10.03	−10.03	3.8	−8.07	−8.07	9.4	−5.79	−6.15
−2.0	−10.02	−10.02	4.2	−7.73	−7.73	9.8	−5.51	−6.10
−1.5	−10.00	−10.00	4.6	−7.40	−7.40	10.2	−5.18	−6.04
−1.0	−9.99	−9.99	5.0	−7.11	−7.11	10.6	−4.81	−5.99
−0.6	−9.97	−9.97	5.4	−6.86	−6.86	11.0	−4.43	−5.95
−0.2	−9.95	−9.95	5.8	−6.65	−6.65	11.4	−4.04	−5.91
0.2	−9.91	−9.91	6.2	−6.50	−6.50	11.8	−3.64	−5.87
0.6	−9.86	−9.86	6.6	−6.41	−6.41	12.2	−3.24	−5.84
1.0	−9.77	−9.77	7.0	−6.37	−6.37	12.6	−2.84	−5.82
1.4	−9.65	−9.65	7.4	−6.33	−6.33	13.0	−2.44	−5.80
1.8	−9.50	−9.50	7.8	−6.28	−6.30	13.4	−2.05	−5.80
2.2	−9.30	−9.30	8.2	−6.24	−6.28	13.8	−1.64	−5.80
2.6	−9.05	−9.05	8.6	−6.15	−6.24	14.2	−1.24	−5.80
3.0	−8.76	−8.76	9.0	−6.00	−6.20	14.6	−0.84	−5.80
3.4	−8.43	−8.43						

2. Shear Creep Compliance of cis-Polyisoprene

Data of Nemoto, Moriwaki, Odani, and Kurata[2] on *cis*-polyisoprene of narrow molecular weight distribution, molecular weight 620,000, reduced to −30°C, are tabulated below.

log t	log $J(t)$	log $[J(t) - t/\eta_0]$	log t	log $J(t)$	log $[J(t) - t/\eta_0]$	log t	log $J(t)$	log $[J(t) - t/\eta_0]$
−5.5	−9.32	−9.32	−1.0	−6.84	−6.84	3.5	−6.57	−6.59
−5.0	−8.91	−8.91	−0.5	−6.81	−6.81	4.0	−6.46	−6.51
−4.5	−8.52	−8.52	0	−6.79	−6.79	4.5	−6.29	−6.41
−4.0	−8.15	−8.15	0.5	−6.78	−6.78	5.0	−6.06	−6.29
−3.5	−7.81	−7.81	1.0	−6.76	−6.76	5.5	−5.74	−6.19
−3.0	−7.50	−7.50	1.5	−6.74	−6.74	6.0	−5.35	−6.11
−2.5	−7.22	−7.22	2.0	−6.71	−6.71	6.5	−4.89	−5.96
−2.0	−7.02	−7.02	2.5	−6.68	−6.68	7.0	−4.42	−5.87
−1.5	−6.90	−6.90	3.0	−6.64	−6.65	7.35	−4.08	−5.85

3. Storage and Loss Shear Moduli of Polyisobutylene

The data for polyisobutylene refer to a sample with weight-average molecular weight 1.56×10^6 and a broad molecular weight distribution, distributed by Dr. R. S. Marvin of the National Bureau of Standards.[3] They are based primarily on dynamic measurements by Fitzgerald, Grandine, and Ferry,[4] Plazek, Vrancken, and Berge,[5] and Philippoff.[6] The reduction temperature is 25°C. The best coefficients for the WLF equation with $T_0 = 298.2$°K based on the data of references 4 and 5 are $c_1 = 9.08$ and $c_2 = 209$. The a_T factors calculated from these cofficients are negligibly different from those used earlier[4] before the introduction of the WLF equation.

$\log \omega$	$\log G'$	$\log G''$	$\log \omega$	$\log G'$	$\log G''$
−3.5	6.02	5.67	3.0	6.76	6.71
−3.0	6.12	5.66	3.5	6.96	7.03
−2.5	6.21	5.64	4.0	7.20	7.37
−2.0	6.25	5.60	4.5	7.49	7.69
−1.5	6.30	5.48	5.0	7.83	8.02
−1.0	6.35	5.45	5.5	8.16	8.34
−0.5	6.38	5.44	6.0	8.49	8.64
0	6.42	5.40	6.5	8.81	8.92
0.5	6.44	5.42	7.0	9.11	9.16
1.0	6.47	5.49	7.5	9.40	9.36
1.5	6.48	5.75	8.0	9.64	9.50
2.0	6.51	6.05	8.5	9.82	9.51
2.5	6.61	6.38	9.0	9.93	9.39

4. Storage and Loss Shear Moduli of Poly(*n*-octyl methacrylate)

The data for poly(*n*-octyl methacrylate)[7,8] are those presented in Figs. 2–3 and 2–4 as curves IV. The reduction temperature is 100°C. The data have been reduced for the f-shift described in Chapter 11, Section F2, as well as with the usual a_T factor.

log ω	log G'	log G''	log ω	log G'	log G''
−3.5[a]	3.98	4.01	4.5	6.20	6.22
−3.0[a]	4.30	4.30	5.0	6.45	6.58
−2.5[a]	4.61	4.64	5.5	6.67	6.90
−2.0[a]	4.89	4.76	6.0	6.98	7.26
−1.5[a]	5.16	5.01	6.5	7.31	7.63
−1.0[a]	5.38	5.14	7.0	7.68	7.98
−0.5	5.42	4.93	7.5	8.06	8.28
0	5.49	4.87	8.0	8.49	8.55
0.5	5.53	4.79	8.5	8.82	8.71
1.0	5.57	4.76	9.0	9.03	8.81
1.5	5.56	4.82	9.5	9.20	8.83
2.0	5.61	4.97	10.0	9.31	8.77
2.5	5.68	5.19	10.5	9.39	8.73
3.0	5.77	5.42	11.0	9.44	8.67
3.5	5.89	5.68	11.5	9.48	8.74
4.0	6.05	5.98	12.0	9.44	8.87

[a] Calculated indirectly from creep measurements by the methods of Chapter 4.

5. Storage and Loss Shear Moduli of Very Lightly Cross-Linked Styrene-Butadiene Rubber

The data for very lightly cross-linked styrene-butadiene rubber[9] are those presented in Figs. 2–3 and 2–4 as curves VII. The reduction temperature is 25°C.

log ω	log G'	log G''	log ω	log G'	log G''
−5.0[a]	6.29	5.02	1.5	6.76_5	5.98
−4.6[a]	6.31	5.09	2.0	6.82	5.98_5
−4.2[a]	6.32_5	5.14_5	2.5	6.86_5	5.98
−3.8[a]	6.34	5.20	3.0	6.91_5	6.01_5
−3.4[a]	6.35_5	5.25_5	3.5	6.95_5	6.10
−3.0[a]	6.37_5	5.31	4.0	7.01	6.29
−2.6[a]	6.39_5	5.37	4.5	7.07_5	6.56_5
−0.7	6.52	5.69	5.0	7.15_5	6.84_5
−0.5	6.53_5	5.72_5	5.5	7.27	7.12_5
0	6.58_5	5.81	6.0	7.41	7.42_5
0.5	6.64_5	5.89_5	6.5	7.60	7.73
1.0	6.70_5	5.95	7.0	7.84	8.07

[a] Calculated indirectly from creep measurements by the methods of Chapter 4.

6. Elongational Relaxation Modulus of Polyisobutylene

The data for polyisobutylene refer to the same sample as in Section 3 above, and are quoted from stress relaxation measurements by Tobolsky and collaborators.[10] The reduction temperature is again 25°C. The modulus is *Young's* modulus, and the units of time are *hours*.

log t	log $E(t)$	log t	log $E(t)$	log t	log $E(t)$
−14.4	10.48_5	−8.4	8.05_5	−2.4	6.79_5
−14.0	10.46_5	−8.0	7.80_5	−2.0	6.75_5
−13.6	10.44_5	−7.6	7.58_5	−1.6	6.71
−13.2	10.41	−7.2	7.38_5	−1.2	6.65_5
−12.8	10.37	−6.8	7.21	−0.8	6.59
−12.4	10.30	−6.4	7.08_5	−0.4	6.50_5
−12.0	10.20_5	−6.0	7.00_5	0	6.39_5
−11.6	10.07_5	−5.6	6.96	0.4	6.26
−11.2	9.88_5	−5.2	6.92_5	0.8	6.08
−10.8	9.65_5	−4.8	6.90_5	1.2	5.85
−10.4	9.39_5	−4.4	6.89_5	1.6	5.54
−10.0	9.12_5	−4.0	6.88_5	2.0	5.18
−9.6	8.86_5	−3.6	6.87_5	2.4	4.5
−9.2	8.60_5	−3.2	6.85_5	2.8	$-\infty$
−8.8	8.33	−2.8	6.82_5		

7. Elongational Relaxation Modulus of Polystyrene

The data for polystyrene refer to a sample with weight-average molecular weight 0.20×10^6, investigated by Fujita and Ninomiya.[11] The reduction temperature is 135°C, the modulus is Young's modulus, and the units of time are seconds.

log t	log $E(t)$	log t	log $E(t)$
−8.0	10.22	−1.5	6.91
−7.5	10.17	−1.0	6.84
−7.0	10.05	−0.5	6.65
−6.5	9.89	0	6.54
−6.0	9.64	0.5	6.45
−5.5	9.26	1.0	6.34
−5.0	8.82	1.5	6.20
−4.5	8.43	2.0	6.01
−4.0	8.12	2.5	5.77
−3.5	7.85	3.0	5.49
−3.0	7.59	3.5	5.11
−2.5	7.33	4.0	4.62
−2.0	7.10	4.5	3.95

An unusually complete tabulation of numerical data for both transient and dynamic viscoelastic functions for a cross-linked polyurethane rubber has been presented by Schwarzl, van der Wal, and Bree.[12]

It will be recalled from Chapters 12 and 14 that in the transition zone the values quoted in tables such as these for uncross-linked polymers are essentially independent of molecular weight and molecular weight distribution, and only slightly dependent on degree of cross-linking in networks, so they are characteristic of the chemical structure of each polymer. In the plateau and terminal zones, however, the viscoelastic properties reflect the molecular weight, molecular weight distribution, and possible branching in the particular sample investigated as well as its chemical structure.

REFERENCES

1. D. J. Plazek and V. M. O'Rourke, personal communication.
2. N. Nemoto, M. Moriwaki, H. Odani, and M. Kurata, *Macromolecules,* **4,** 215 (1971).
3. R. S. Marvin, *Proc. Second Intern. Congr. Rheology,* 1954, p. 156.
4. E. R. Fitzgerald, L. D. Grandine, Jr., and J. D. Ferry, *J. Appl. Phys.,* **24,** 650 (1953); **24,** 911 (1953).
5. D. J. Plazek, M. N. Vrancken, and J. W. Berge, *Trans. Soc. Rheol.,* **2,** 39 (1958).
6. W. Philippoff, *J. Appl. Phys.,* **24,** 685 (1953).
7. W. Dannhauser, W. C. Child, Jr., and J. D. Ferry, *J. Colloid Sci.,* **13,** 103 (1958).
8. J. W. Berge, P. R. Saunders, and J. D. Ferry, *J. Colloid Sci.,* **14,** 135 (1959).
9. R. G. Mancke and J. D. Ferry, *Trans. Soc. Rheol.,* **12,** 335 (1968).
10. A. V. Tobolsky and E. Catsiff, *J. Polym. Sci.,* **19,** 111 (1956).
11. H. Fujita and K. Ninomiya, *J. Polym. Sci.,* **24,** 233 (1957).
12. F. R. Schwarzl, C. W. van der Wal, and H. W. Bree, *Chim. Ind.,* **54,** 51 (1972).

APPENDIX E

Theoretical Viscoelastic Functions Reduced in Dimensionless Form

1. Rouse Theory for Infinite Dilution

Numerical evaluations of $[G']_R$, $[G'']_R$, and $[\eta']/[\eta]$ from equations 15, 16, 21, and 27 of Chapter 9 with large N are given below.[1]

$\log \omega\tau_1$	$\log [G']_R$	$\log [G'']_R$	$\log [\eta']/[\eta]$
−2.0	−3.97	−1.78	0
−1.8	−3.57	−1.58	0
−1.6	−3.17	−1.38	0
−1.4	−2.77	−1.18	0
−1.2	−2.37	−0.98	0
−1.0	−1.97	−0.79	0
−0.8	−1.58	−0.59	−0.01
−0.6	−1.19	−0.40	−0.02
−0.4	−0.83	−0.22	−0.04
−0.2	−0.50	−0.07	−0.08
0	−0.24	0.05	−0.16
0.2	−0.05	0.15	−0.26
0.4	0.10	0.24	−0.37
0.6	0.23	0.34	−0.47
0.8	0.36	0.44	−0.57
1.0	0.48	0.54	−0.67
1.2	0.59	0.64	−0.77
1.4	0.40	0.74	−0.87
1.6	0.81	0.84	−0.97
1.8	0.92	0.94	−1.07
2.0	1.02	1.04	−1.17

2. Zimm Theory (Dominant Hydrodynamic Interaction) for Infinite Dilution

Numerical evaluations of $[G']_R$, $[G'']_R$, and $[\eta']/[\eta]$ from equations 15, 16, and 21 of Chapter 9 with relaxation times corresponding to large h, or to $h^* = 0.25$ and large N, in equation 29, are given below.[1]

$\log \omega\tau_1$	$\log [G']_R$	$\log [G'']_R$	$\log [\eta']/[\eta]$
−2.0	−3.94	−1.63	0
−1.8	−3.54	−1.43	0
−1.6	−3.14	−1.23	0
−1.4	−2.74	−1.03	0
−1.2	−2.34	−0.83	0
−1.0	−1.94	−0.63	0
−0.8	−1.55	−0.43	0
−0.6	−1.16	−0.24	−0.01
−0.4	−0.79	−0.05	−0.03
−0.2	−0.46	0.11	−0.06
0	−0.19	0.26	−0.11
0.2	0.02	0.40	−0.18
0.4	0.20	0.53	−0.25
0.6	0.36	0.66	−0.31
0.8	0.51	0.79	−0.38
1.0	0.65	0.93	−0.45
1.2	0.80	1.06	−0.51
1.4	0.94	1.20	−0.58
1.6	1.08	1.33	−0.65
1.8	1.21	1.46	−0.71
2.0	1.35	1.60	−0.78

Evaluations based on exact eigenvalues calculated by Lodge and Wu[2] for $h^* = 0.25$ and $N = 300$ give values for $[G']_R$ that are negligibly different and for $[G'']_R$ somewhat smaller at the highest frequencies.

3. Rouse Theory for Undiluted Polymer of Low Molecular Weight

Values of dynamic and transient functions from equations 1 to 4 of Chapter 10 are reduced here according to the following definitions:

$$\omega_R = \omega\tau_1;\ t_R = t/\tau_1 \qquad J'_R = J'\rho RT/M$$

$$G'_R = G'M/\rho RT \qquad G_R(t) = G(t)M/\rho RT$$

$$G''_R = G''\,M/\rho RT \qquad J_R(t) = J(t)\rho RT/M$$

The quantities G'_R and G''_R are numerically identical to $[G']_R$ and $[G'']_R$ in Section 1.[1,3]

$\log \omega_R$ or $-\log t_R$	$\log G'_R$	$\log G''_R$	$\log J'_R$	$\log \eta'/\eta_0$	$\log G_R(t)$	$\log J_R(t)$
−2.0	−3.97	−1.78	−0.40	0		1.79
−1.8	−3.57	−1.58	−0.40	0		1.59
−1.6	−3.17	−1.38	−0.40	0		1.39
−1.4	−2.77	−1.18	−0.40	0		1.20
−1.2	−2.37	−0.98	−0.40	0		1.00
−1.0	−1.97	−0.79	−0.40	0	−4.34	0.81
−0.8	−1.58	−0.59	−0.40	−0.01	−2.74	0.62
−0.6	−1.19	−0.40	−0.40	−0.02	−1.73	0.45
−0.4	−0.83	−0.22	−0.40	−0.04	−1.09	0.28
−0.2	−0.50	−0.07	−0.41	−0.08	−0.68	0.13
0	−0.24	0.05	−0.45	−0.16	−0.41	−0.01
0.2	−0.05	0.15	−0.50	−0.26	−0.21	−0.14
0.4	0.10	0.24	−0.57	−0.37	−0.04	−0.26
0.6	0.23	0.34	−0.66	−0.47	0.10	−0.38
0.8	0.36	0.44	−0.75	−0.57	0.24	−0.49
1.0	0.48	0.54	−0.85	−0.67	0.36	−0.60
1.2	0.59	0.64	−0.95	−0.77	0.48	−0.71
1.4	0.70	0.74	−1.05	−0.87	0.60	−0.82
1.6	0.81	0.84	−1.15	−0.97	0.71	−0.92
1.8	0.92	0.94	−1.25	−1.07	0.82	−1.03
2.0	1.02	1.04	−1.35	−1.17	0.92	−1.13

4. Rouse Theory for Most Probable Molecular Weight Distribution, Undiluted Polymer of Low Molecular Weight

The definitions are the same as in Section 3 above except that the extra subscript n means $\overline{M}_n$ substituted for M, and $\overline{P}_n$ for P in equation 4 of Chapter 10.[1]

$\log \omega_{Rn}$	$\log G'_{Rn}$	$\log G''_{Rn}$	$\log \eta'/\eta$
−2.0	−2.63	−1.49	−0.01
−1.8	−2.27	−1.30	−0.02
−1.6	−1.93	−1.11	−0.03
−1.4	−1.62	−0.94	−0.05
−1.2	−1.34	−0.77	−0.09
−1.0	−1.09	−0.61	−0.13
−0.8	−0.86	−0.47	−0.19
−0.6	−0.66	−0.34	−0.26
−0.4	−0.47	−0.21	−0.33
−0.2	−0.31	−0.09	−0.41
0	−0.16	0.02	−0.50
0.2	−0.01	0.13	−0.59
0.4	0.12	0.23	−0.68
0.6	0.25	0.34	−0.78
0.8	0.37	0.44	−0.88
1.0	0.48	0.54	−0.97
1.2	0.60	0.64	−1.07
1.4	0.71	0.74	−1.17
1.6	0.82	0.84	−1.27
1.8	0.92	0.94	−1.37
2.0	1.03	1.04	−1.47

5. Rouse-Mooney Theory for Networks with Uniform Strand Length

Numerical evaluations from equations 34 to 37 of Chapter 10 are given below with the following definitions of reduced variables:[1]

$$\omega_R = \omega\tau_1; \quad G'_R = G'/\nu RT; \quad G''_R = G''/\nu RT; \quad J''_R = J''\nu RT.$$

$\log \omega_R$	$\log G'_R$	$\log G''_R$	$\log J''_R$
−2.0	0.000	−1.784	−1.784
−1.8	0.000	−1.584	−1.584
−1.6	0.000	−1.384	−1.385
−1.4	0.001	−1.184	−1.188
−1.2	0.002	−0.985	−0.994
−1.0	0.005	−0.787	−0.808
−0.8	0.011	−0.591	−0.639
−0.6	0.027	−0.401	−0.512
−0.4	0.061	−0.223	−0.449
−0.2	0.119	−0.069	−0.459
0	0.198	0.052	−0.523
0.2	0.279	0.150	−0.599
0.4	0.355	0.245	−0.670
0.6	0.434	0.345	−0.744
0.8	0.517	0.445	−0.824
1.0	0.603	0.545	−0.907
1.2	0.692	0.645	−0.996
1.4	0.776	0.745	−1.078
1.6	0.875	0.845	−1.177
1.8	0.969	0.945	−1.271
2.0	1.064	1.045	−1.365

6. Rouse-Mooney Theory for Networks with Most Probable Distribution of Strand Lengths

The reduced variables are defined as in Section 5 above with number-average value of P_c in equation 36 of Chapter 10 and $\nu = \rho/M_{cn}$ (M_{cn} = number-average value of M_c).[1]

$\log \omega_R$	$\log G'_R$	$\log G''_R$	$\log J''_R$
−2.0	0.001	−1.491	−1.493
−1.8	0.002	−1.299	−1.304
−1.6	0.005	−1.113	−1.126
−1.4	0.010	−0.936	−0.962
−1.2	0.019	−0.770	−0.819
−1.0	0.034	−0.615	−0.704
−0.8	0.056	−0.471	−0.620
−0.6	0.086	−0.338	−0.568
−0.4	0.126	−0.212	−0.547
−0.2	0.174	−0.094	−0.553
0	0.230	0.019	−0.580
0.2	0.294	0.128	−0.626
0.4	0.365	0.234	−0.686
0.6	0.441	0.338	−0.754
0.8	0.521	0.440	−0.830
1.0	0.606	0.542	−0.912
1.2	0.694	0.643	−0.998
1.4	0.784	0.744	−1.087
1.6	0.877	0.845	−1.179
1.8	0.970	0.945	−1.272
2.0	1.065	1.045	−1.366

REFERENCES

1. S. E. Lovell and J. E. Frederick, unpublished calculations.
2. A. S. Lodge and Y.-J. Wu, Mathematics Research Center Technical Summary Report No. 1250, University of Wisconsin, October 1972.
3. N. W. Tschoegl, *J. Chem. Phys.*, **44**, 2331 (1966).

Author Index

Adam, G., 285, 317
Adam, M., 212, 222
Adams, N., 127
Adamson, A. W., 363
Adelman, S. A., 222
Adler, F. T., 129
Adler, T. S., 222
Agarwal, P. K., 316, 403
Aharoni, S. M., 401
Aida, M., 483
Aitken, A., 363
Aklonis, J. J., 78, 79, 89, 95, 317, 348, 364, 402, 499, 541, 568
Akovali, G., 263, 389, 390, 402
Aldrich, R., 175, 176, 559, 569
Alekseyeva, V. M., 152
Alfrey, T., Jr., 3, 31, 78, 81, 94, 317, 541, 543
Allen, G., 136, 152, 483, 568
Allen, V. R., 300, 318, 433
Aloisio, C. J., 569
Altermatt, H., 543
Amari, T., 207, 221
Ament, W. S., 175
Andeen, C. G., 156, 166, 482
Anderson, E. W., 363
Anderson, R. L., 128, 166
Andrade, E. N. da C., 151, 392, 393, 403, 440
Andreatch, P., Jr., 129, 222
Andrews, E. H., 590
Andrews, R. D., 94, 151, 262, 270, 316, 401, 435, 451, 456, 485
Anthony, R. L., 151, 435
Aoto, Y., 320, 512, 541
Arai, K., 151, 175, 403, 482
Armstrong, R. C., 27, 31, 55, 76, 78, 79, 220, 222, 263, 319, 402, 403, 542
Asada, T., 153
Asano, T., 176, 319, 569
Ashare, E., 52, 55, 127, 222, 262, 521, 542, 543
Ashcroft, N., 31
Ashworth, J. N., 78, 129
Atack, D., 574, 588
Atkinson, E. B., 365
Auer, P. L., 180-182, 220
Auerbach, I., 318, 363

Baccaredda, M., 455
Baer, E., 456
Bagley, E., 363
Bailey, E. D., 117, 128
Bailey, F. E., Jr., 544
Bair, H. E., 456, 569
Baird, D. G., 128
Baker, W. O., 129, 152, 174, 176
Bakule, R., 433
Balakrishnan, C., 223
Ballman, R. T., 152
Ballou, J. W., 162, 167
Bancroft, D., 167
Barlow, A. J., 128, 129, 316, 320, 360, 362, 440-442, 454
Barlow, C. A., Jr., 78
Barrer, R. M., 363
Bartenev, G. M., 578, 589, 590
Bass, R., 569
Batchinski, A. J., 285, 317
Bauer, H.-J., 176
Bauer, M., 318
Bauer, W. H., 543
Bauman, A., 436
Bearder, S. S., 456, 569
Bearman, R. J., 318
Beatty, J. R., 589
Becht, J., 590
Becker, G. W., 151, 152, 166, 357, 362, 365, 435, 464, 483, 588
Beevers, R. B., 318, 540

Belcher, H. V., 48, 55, 175, 317, 318, 558-561, 569
Benbow, J. J., 92, 95, 166, 438, 454, 477, 484
Bennewitz, K., 78
Beret, S., 568
Berge, J. W., 35, 55, 127, 142-144, 151, 262, 316, 318, 362, 541, 542, 606, 609
Bergen, R. L., Jr., 78, 134, 151
Berglund, C. A., 403
Bernstein, B., 263, 400, 403, 543
Berry, G. C., 101, 127, 151, 187, 220, 221, 242, 244, 261-263, 317, 337, 363, 401, 504, 507, 510, 519, 520, 541-543
Berry, J. P., 435
Bestul, A. B., 317
Bi, L.-K., 320
Bianchi, U., 297, 318
Billings, J. J., 318
Birch, F., 166, 167
Bird, R. B., 5, 27, 29, 31, 55, 76-79, 128, 178, 180, 181, 187, 220, 223, 261, 263, 319, 399, 402, 403, 528, 542, 543
Birnboim, M. H., 110, 117, 128, 139, 152, 166, 195, 222, 544
Bischoff, J., 316
Bisschops, J., 531, 532, 543
Bixon, M., 205, 221
Black, J., 484
Blanchard, B. E., 171, 175
Bland, D. R., 78, 159, 166
Blatz, P. J., 316, 357, 365, 421, 423, 435, 436
Blizard, R. B., 229, 235, 237, 238, 240, 261
Bloch, R., 32, 151, 263, 403, 423, 435
Bodner, S. R., 473, 484
Boedtker, H., 544
Bogie, K., 110, 128
Bogue, D. C., 263, 402
Böhm, G. G. A., 433
Böhme, R., 263, 402
Bohn, L., 588
Bolt, R. H., 569
Boltzmann, L., 31
Bondi, A., 316, 317
Booij, H. C., 128, 527, 528, 530, 543
Boon, J., 319
Borchard, W., 541
Boss, B. D., 319, 363
Boyer, R. F., 317, 328, 363, 401, 455
Brachman, M. K., 78
Braden, M., 433
Bradfield, G., 172, 176
Bradley, R. S., 175
Braun, G., 540
Breazeale, F., 167
Bree, H. W., 357, 365, 426, 436, 483, 609
Breuer, H., 152, 318, 363, 483
Bridgman, P. W., 175, 317
Briscoe, B. J., 363
Broadbent, J. M., 127
Brodnyan, J., 169, 175, 454
Broersma, S., 182, 220
Brown, D. R., 127
Brown, G. M., 485
Browning, G. V., 542
Brueggeman, B. G., 222
Bryant, G. M., 456, 569
Buchdahl, R., 241, 262, 363, 365, 544
Bucknall, C. B., 590
Bueche, A. M., 408-410, 433, 435, 574, 588
Bueche, F., 185, 220, 224, 236, 242, 261, 262, 286, 317, 318, 337, 363, 435, 504, 540
Bulgin, D., 589
Bull, T. H., 590
Bunn, C. W., 483
Burke, J. J., 319, 364, 569
Burke, J. S., 128, 166
Burr, G. S., 152, 166
Butcher, A. F., 79, 402, 525, 526, 542, 543
Butta, E., 455
Buvet, R., 550, 568

Candau, S., 569
Capaccio, G., 485
Carlson, D. W., 261
Carpenter, D. K., 543
Carpenter, R. L., 262, 403, 433, 434
Carreau, P. J., 77, 79
Casassa, E. F., 187, 200, 221
Cashin, W. M., 363
Catsiff, E., 90, 95, 316, 364, 483, 541, 609
Cayrol, B., 158, 166
Cerf, R., 175, 176, 180-182, 220, 222, 569
Chaikin, M., 167
Challa, G., 319
Chamberlain, N. H., 167
Chambers, L. G., 590
Chang, E. P., 483
Chang, S. S., 317
Chang, W. V., 32, 151, 263, 403, 423, 435
Charlesby, A., 434
Chasset, R., 151, 152, 414, 415, 434, 544, 578, 589
Chatain, D. G., 319
Chelko, A. J., Jr., 385, 401
Chen, S. P., 318, 363, 405, 406, 433

Cheung, M.-F., 432, 436
Chiang, R., 319, 482
Child, W. C., Jr., 35, 55, 316, 319, 333, 334, 362, 401, 455, 541, 609
Childers, C. W., 364
Choi, S. Y., 320
Chompff, A. J., 110, 127, 237-239, 261, 262, 375, 401
Christiansen, E. B., 128
Christiansen, R. L., 223
Chu, W. H., 590
Chung, H. S., 317
Ciferri, A., 261, 316, 435, 544
Claver, G. C., 363
Claxton, W. E., 589
Cochran, M. A., 565, 569
Cohen, M. H., 286, 290, 303, 317
Cohen, R. E., 152, 319, 353, 364, 436, 544
Cole, R. H., 442, 454
Coleman, B. D., 31, 32, 79, 543
Collins, E. A., 543
Colwell, R. E., 127
Cooke, B. J., 222
Cooper, S. L., 355, 364
Cotter, L., 569
Cox, W. P., 382, 402, 518
Craft, T., 263, 403
Cramer, W. S., 175
Crissman, J. M., 483
Crossland, A. H., 435
Cudby, M., 543
Cunningham, J. R., 36, 55, 147, 148, 152
Curie, M., 78
Curtiss, C. F., 79, 220, 261, 263

Dahlquist, C. A., 151, 316, 362
Dannenberg, E. M., 590
Dannhauser, W., 35, 55, 316, 333, 334, 362, 401, 609
Date, M., 128
Davenport, T. C., 589
Davidson, D. W., 442, 454
Davies, G. R., 485
Davies, M. J., 589
Davies, R. O., 175, 316, 317, 362
Davis, D. D., 318
Davis, W. M., 129, 166, 452, 456, 590
Debye, P., 220, 363
de Cindio, B., 79
Deeley, C. W., 434, 483
Defay, R., 317
de Gennes, P. G., 55, 212, 222, 246, 251, 262, 263, 385, 402, 419, 434, 503, 541
Dekking, P., 166
Delf, B., 483
Delsanti, M., 212, 222
De Bolt, M. A., 568
de Brouckère, L., 318
DeMallie, R. B., Jr., 222
den Otter, J. L., 114, 128
Derdul, P. R., 589
Deuel, H., 543
DeWitt, T. W., 113, 114, 128, 136, 152, 316, 362, 541
Dick, W., 165, 167
Dickie, R. A., 152, 236, 261, 320, 363, 400, 409, 414, 432-436, 454, 544
Dienes, G. J., 317
Dijkstra, H., 544
Dillon, J. H., 140, 152, 167, 435
DiMarzio, E. A., 285, 317
Doi, M., 55, 207, 213, 221, 222, 246, 250, 259, 261, 262, 370, 382-384, 398, 401, 403, 508-512, 522, 527, 529, 541-543, 582
Doolittle, A. K., 285, 316, 317, 492, 495, 540, 542, 544
Doolittle, D. B., 317
Doolittle, L. R., 220
Doolittle, R. F., 220
Dorrington, K. L., 544
Dossin, L., 433
Doty, P., 78, 95, 544
Douglass, D. C., 319, 363
Drent, R. H. J. W. A., 151
Duiser, J. A., 114, 128, 237-239, 261
Dunbar, J. H., 565, 569
Dunell, B. A., 167
Du Pré, D. B., 434
Dusenbury, J. H., 166, 484
Dyson, A., 223, 589

Eagling, R. F., 365
Easteal, A. J., 568
Ecker, R., 357, 359, 365
Edelman, S., 170, 175
Edwards, S. F., 55, 209, 213, 222, 245, 246, 250, 259, 261, 262, 370, 382-384, 401, 508-512, 527, 529, 542, 543, 582
Eilers, H., 426, 436
Einaga, Y., 52, 53, 55, 79, 127, 222, 263, 402, 523, 524, 542, 543
Eirich, F. R., 590
Eisenberg, A., 317, 364, 455
Eisenberg, H., 221
Eizner, Yu. E., 193, 195, 221
Eldridge, J. E., 150, 544
El'kin, A. I., 578, 589

Elyash, L. J., 128, 402
Enabnit, R. S., 152
Enda, Y., 540
Ender, D. H., 456, 569
Endo, H., 320, 542
Erginsav, A., 316, 440, 454
Erhardt, P. F., 153
Evans, G. T., 222
Evans, W. W., 79, 95, 127, 150, 541, 542
Eyring, H., 263, 316, 453, 456

Faucher, J. A., 36, 55, 129, 483
Fedors, R. F., 151, 428, 436, 590
Ferguson, R. D., 363
Fesko, D. G., 312, 319, 353, 364
Fetters, L. J., 364, 590
Fielding-Russell, G. S., 455
Fikhman, V. D., 152, 590
Fillers, R. W., 287, 293-295, 318
Filon, L. N. G., 544
Findley, W. N., 167, 169, 175, 453, 456, 550, 568
Fischer, H., 590
Fitzgerald, E. R., 136-139, 150-153, 316, 318-320, 362, 401, 473, 474, 484, 544, 588, 606, 609
Fitzgerald, J. V., 129
Fixman, M., 219, 221-223
Fleischer, P. C., Jr., 541
Fletcher, W. P., 151, 433, 436
Flom, D. G., 574, 588
Flory, P. J., 151, 220, 222, 227, 237, 261, 262, 288, 299, 316, 317, 363, 364, 433-435, 482, 485, 541, 544, 568
Fong, J. T., 222
Forgacs, P., 319
Förster, F., 166
Forster, M. J., 589
Foster, E. L., 542
Fox, T. G., 151, 227, 242-244, 261, 262, 288, 299, 300, 317, 318, 337, 363, 401, 504, 510, 541, 542
Frazer, W. J., 402
Frederick, J. E., 222, 262, 435, 590, 615
Fredrickson, A. G., 26, 31, 32, 79
Freed, K. F., 209, 211, 222
Freeland, A. E., 484
Frenkel, J., 316
Frenkel, S. Ya., 262, 541
Fronsini, V., 455
Fujii, M., 221
Fujii, T., 128, 402
Fujii, Y., 483
Fujimori, S., 221
Fujimoto, T., 320, 401, 402, 521, 541, 542
Fujino, K., 151, 163, 164, 167, 320, 349, 364, 436, 482
Fujisawa, T., 153
Fujita, H., 78, 94, 303, 304, 318, 319, 333, 334, 362-364, 492, 495-497, 509, 540, 590, 608, 609
Fujita, S., 318
Fukada, E., 153
Fukawa, H., 524, 543
Fukuda, M., 484, 522, 542, 543
Fukui, Y., 153
Fukushima, T., 483
Fukutomi, S., 176, 319, 569
Fulcher, G. S., 289, 317
Fulton, R. W., 128, 220
Fung, Y. C., 31
Fuoss, R. M., 67, 78, 220, 261
Furuichi, J., 129, 195, 221
Furuta, I., 151, 433, 588

Garfield, L. J., 540
Garrett, B. S., 541
Garritano, R. G., 127, 152
Gaskins, F. H., 262
Gautier, P. G., 319
Gee, G., 297, 318, 544, 568
Gehman, S. D., 152, 318, 363
Geil, P. H., 482
Gemant, A., 167
Gent, A. N., 151, 436, 589, 590
Gerberich, W. W., 456, 590
Gerth, C., 544
Gibbs, J. H., 285, 317
Gielessen, J., 318
Gieniewski, C., 129, 222
Giesekus, H., 127, 220
Gill, S. J., 543
Gillham, J. K., 129
Glasstone, S., 316
Gligo, N., 542
Goddard, J. D., 26, 31, 77
Goldbach, G., 169, 175, 318, 455, 546, 547, 550, 551, 568
Goldbaum, D. M., 220
Goldberg, H., 127, 152
Goldfinger, G., 317
Goldman, S., 78
Goldstein, M., 317, 455
Goode, W. E., 541
Gordon, M., 304, 319, 433, 540, 588
Gordon, R. J., 223
Gortemaker, F. H., 79
Gotoh, R., 153

Gottlieb, M., 401
Graessley, W. W., 55, 222, 237, 249-252, 257-259, 261-263, 320, 370, 377, 379, 381-384, 386-389, 392, 401, 402, 419, 433, 435, 502, 509-513, 515-518, 521, 531, 541-543, 582, 589
Grandine, L. D., Jr., 316, 320, 362, 401, 542, 606, 609
Grant, J. W. V., 262
Gratch, S., 243, 262, 541
Gray, R. W., 361, 365, 454
Greaser, M., 221
Greco, R., 151, 263, 403, 419, 434
Green, M. S., 262
Greensmith, H. W., 127
Greenwood, J. A., 589
Grieco, A., 141, 152
Grieveson, B. M., 588
Grosch, K. A., 435, 577, 578, 588, 589
Gross, B., 64, 78, 189, 220, 261, 363
Grün, F., 363
Gruver, J. T., 263, 319, 364, 385, 386, 402, 509, 542
Guiroy, G., 318
Guofang, G., 129
Gupta, V. B., 478, 484
Guth, E., 151, 435
Guthrie, J. C., 167
Gutowsky, H. S., 455

Haas, H. C., 544
Hadjichristidis, N., 402, 542
Hager, B. L., 127, 263, 519, 543
Haldon, R. A., 362
Hall, G. L., 140, 152
Halpin, J. C., 435, 586, 590
Halsey, G., 456
Ham, J. S., 232, 233, 236, 261, 285, 402
Hamana, I., 542
Hammack, T. J., 451
Hammerle, W. G., 167
Hammes, G. G., 569
Hamming, T. W., 68, 78
Han, C. D., 221
Hansen, D. R., 249, 254, 263, 371, 401
Hansen, M. G., 79
Hanson, E. E., 435
Hargens, C. W., 152
Harima, H., 403
Harper, R. C., Jr., 128, 152, 316
Harrington, R. E., 590
Harrington, W. F., 364
Harris, E. K., Jr., 402, 518, 542
Harris, J., 110, 128
Harrison, G., 114, 128, 320, 360-363, 365, 454, 589
Harwood, J. A. C., 435, 573, 588
Hasa, J., 363
Hasegawa, H., 364
Hashimoto, T., 364
Haskell, V. C., 452, 456
Hassager, O., 27, 31, 55, 76, 78, 79, 183, 220, 263, 319, 402, 403, 542
Hässler, H., 175, 176
Hatfield, M. R., 316, 541
Havlíček, I., 497, 541
Havránek, A., 433
Haward, R. N., 590
Hayakawa, R., 455, 472, 483
Hayama, N., 153
Hayashi, S., 153, 249, 263
Hazleton, R. L., 516, 542
Heckler, G. E., 544
Heijboer, J., 166, 445-447, 449, 455, 456, 590
Heinze, H. D., 363, 364, 433
Heiss, J. H., 129, 152, 174, 176
Helders, F. E., 129, 262, 508, 542
Hellwege, K. H., 292, 317, 318, 568
Hendricks, J. O., 151
Hermans, J. J., 221
Herwig, H. U., 352, 355, 356, 364
Herzfeld, K. F., 171, 175
Hesse, G., 289, 317
Heusch, R., 488, 540
Heydemann, P., 152, 158, 166
Hideshima, T., 55, 166, 319, 445, 454, 455, 483
Higashitani, K., 107, 128
Hikichi, K., 483, 484
Hill, R. W., 363
Hillier, K. W., 167, 485
Hindman, H., 152, 166
Hirai, H., 542
Hirai, N., 532, 544
Hirose, H., 175, 176, 319, 569
Hirose, J., 455
Hirschfelder, J. O., 316
Hirst, W., 223, 589
Hlaváček, B., 82, 84, 87, 94
Ho, T. C., 456, 569
Hoard, J. L., 363
Hoeve, C. A. J., 261, 316, 544
Hoff, E. A. W., 311, 319, 445, 447, 454
Hoffman, J. D., 319
Hoffman, R. W., 156, 166, 482
Hoffmann, M., 245, 262
Hofman-Bang, N., 151, 401

Högberg, H., 165, 402, 453, 456
Holmes, L. A., 127, 222, 262, 514, 521, 542, 543
Holt, W. L., 151
Homma, T., 402, 434
Hong, S. D., 263
Hopkins, I. L., 68, 78, 142, 152, 314, 316, 319
Hopkinson, B., 149, 153
Hoppmann, W. H., II, 127
Horino, T., 163, 164, 167, 364, 365, 482
Horio, M., 104, 114, 127, 128, 166, 484
Hosemann, R., 480, 485
Hou, T. H., 127
Houwink, R., 590
Howard, W. H., 167, 589
Hrouz, J., 541
Hsiao, C. C., 166, 456
Hsieh, H. L., 364
Hubbard, G., 589
Hueter, T. F., 171, 175, 569
Huff, K., 456, 485
Huffman, H. M., 317
Huh, D. S., 364
Hunston, D. L., 129, 223
Hunter, J. L., 574, 589
Hunter, S. C., 574, 588
Huppler, J. D., 127, 128, 262, 521, 527, 528, 543
Hutcheon, A. T., 363
Hutchinson, J. M., 317, 568

Ibaragi, T., 402
Ido, S., 589
Igarashi, T., 485
Iijima, K., 151, 351, 364, 482
Ilavský, M., 349, 363, 364, 541
Illers, K. H., 124, 129, 152, 363, 454, 455, 483, 500, 540, 541
Imada, K., 482, 483, 485
Inagaki, H., 51, 55, 153, 222, 319
Indictor, N., 261
Inman, R. B., 221
Inokuti, M., 434
Inoue, T., 263, 391, 402, 436
Iohara, K., 482
Irani, R., 363
Irving, J. B., 454
Ishida, Y., 484
Ishiguro, F., 263
Ishikawa, K., 482
Ishikawa, Y., 485
Isono, Y., 541
Ito, R., 569
Ito, T., 153
Ito, Y., 222
Ivey, D. G., 36, 55, 147, 148, 152
Iwayanagi, S., 35, 55, 166, 319, 445, 454, 455, 483

Jackson, J. B., 482
Jackson, J. F., 543
Janáček, J., 363, 541, 544
Janeschitz-Kriegl, H., 79, 222, 402
Janmey, P. A., 129, 544
Jeffery, G. B., 222
Jenckel, E., 166, 175, 352, 355, 356, 363, 364, 455, 483, 488, 500, 540, 541, 588
Jessop, H. T., 544
Johari, G. P., 455
Johnson, J. F., 104, 127, 401, 590
Johnson, M. F., 541, 542
Johnson, M. W., 29
Johnson, R. M., 128, 152, 221
Jones, G. O., 175, 316, 317, 362
Jones, P. B., 569
Joos, G., 484
Jordan, I., 541, 542
Jung, A., 317

Kaelble, D. H., 158, 166, 589, 590
Kajiura, H., 263, 541, 543
Kajiyama, T., 153, 473, 482-485
Kambe, H., 113, 128, 429, 436
Kambour, R. P., 482
Kamei, E., 590
Kan, H.-C., 262, 433, 434
Kaneko, M., 116, 117, 128, 195, 221, 318, 473, 482-484
Kanig, G., 318
Kaplan, D., 355, 365
Karasz, F. E., 318
Kasahara, T., 456, 590
Kastelic, J. R., 456
Kästner, S., 78, 317, 547, 568
Katada, A., 459, 482
Kataoka, T., 338, 363, 402
Kato, H., 402
Kato, S., 129, 176
Kato, T., 542
Katz, D., 364, 434
Kausch, H. H., 590
Kauzmann, W., 316
Kawabata, S., 151
Kawaguchi, T., 153
Kawai, H., 136, 150, 151, 153, 163, 164, 167, 320, 349-351, 364, 365, 436, 463, 473, 482-484

awamura, Y., 319, 455, 485
awasaki, N., 483
aye, A., 127, 403
ê, T. S., 167
earsley, E. A., 263, 400, 403, 543
eedy, D. A., 153
egel, G., 78
eiper, D. A., 139, 152
eith, H. D., 482
elchner, R. E., 79
eller, A., 543
elley, F. N., 318, 504, 540
épès, A., 104, 125, 127
ern, H. E., 456, 569
erner, E. H., 432, 436
erwin, E. M., Jr., 576, 588
ilb, R. W., 200-204, 221, 232, 261
im, B. S., 542
im, K. Y., 127
im, M. G., 454
imball, A. L., 166
imura, S., 55, 127, 263, 542
incaid, J. F., 541
ing, E. G., 263, 402
irkwood, J. G., 31, 67, 78, 180-182, 191, 193, 220, 270, 316
ishimoto, A., 304, 319, 333, 334, 363, 496, 497, 540, 590
itagawa, K., 263, 368, 391, 400-402
itamura, S., 320
ittel, C., 31, 317
lein, E., 588
lein, J., 246, 262, 363, 402, 510, 542
line, D. E., 159, 166, 434, 483
lonowski, W., 262
nappe, W., 292, 317, 318, 568
nauss, C. J., 129
night, D. G., 129
noff, W. F., 78
nollman, G. C., 128
nox, E. O., 151
obayashi, K., 482
oga, K., 153, 402
ohler, O. C., 128
ohlrausch, R., 31
okes, R. J., 363
olařík, J., 349, 364
oleske, J. V., 129
olsky, H., 166, 167, 175, 485
omatsubara, M., 221
onaka, T., 129
ondo, T., 159, 166
önig, H., 78
onno, A., 116, 117, 128
Kono, R., 147, 152, 161, 166, 172, 176, 562, 563, 569
Koppehele, H. P., 476, 484
Koppelmann, J., 136, 145, 147, 151, 152, 157, 166, 173, 176, 318, 444, 445, 454
Kosiyama, K., 167, 541
Kosten, C. W., 152
Kotaka, T., 51, 55, 128, 222, 319, 529, 543
Kotani, T., 364
Kotrba, V., 84, 94
Kou, L., 544
Kovacs, A. J., 104, 105, 175, 259, 263, 276, 281-284, 297, 300, 316-318, 401, 540, 547, 548, 551-554, 566, 568
Kramer, O., 134, 151, 222, 262, 263, 364, 403, 419, 433, 434, 575, 588
Kramers, H. A., 69, 78
Kranbuehl, D. E., 497, 540
Kratky, O., 221
Kraus, G., 263, 319, 349, 352, 364, 365, 385, 386, 402, 408, 409, 433-436, 509, 542
Krigbaum, W. R., 543
Kronig, R. de L., 69, 78
Krüger, O., 435
Kubu, E. T., 166
Kuhn, W., 17, 31, 78, 152, 341, 363, 401, 435
Künzle, O., 152, 401, 435
Kurata, M., 55, 79, 127, 128, 220, 263, 319, 320, 371, 389, 390, 401, 402, 522-524, 529, 541-543, 605, 609
Kurath, S. F., 262, 319, 320, 362, 499, 540, 541
Kuroishi, M., 473, 482-484
Kuroki, M., 484
Kuryla, W. C., 318, 363
Kusamizu, S., 222, 540, 542, 589
Kutz, D., 129
Kuwabara, Y., 364
Kuzuu, N. Y., 541
Kwei, T. K., 434
Kwon, Y. D., 153, 435

Lacabanne, C., 319
Laidler, K., 316
Lamandé, A., 554, 555, 568
Lamb, J., 115, 120, 121, 128, 129, 218, 222, 273, 316, 320, 360-362, 365, 440-442, 454, 569, 589
Landau, L. D., 31
Landel, R. F., 151, 261, 262, 316, 319, 320, 356, 358, 362-365, 426, 428, 435, 436, 455, 542, 544, 590

Langley, N. R., 55, 240, 262, 401, 409-411, 419, 433, 434, 544
Laun, H. M., 79, 398, 399, 403
Laurent, J.-L., 544
Lauritzen, J. I., 319
Laville, G., 176
Leaderman, H., 19, 31, 94, 99, 127, 167, 231, 261, 270, 316, 435
Lee, C. L., 263, 402
Lee, E. H., 159, 166
Lee, L.-H., 589
LeGrand, D. G., 153
Lehmann, P., 292, 318, 568
Lemstra, P. J., 543
Leppard, W. R., 128
Lethersich, W., 166, 445, 452, 455, 456
Levreault, R., 544
Lewis, A. F., 129
Lewis, M. G., 223, 589
Lewis, T. B., 569
Lifschitz, E. M., 31
Lightfoot, E. N., 31
Lillie, H. R., 554, 568
Lindeman, L. R., 516, 542
Lindenmeyer, P. H., 482
Lindon, P., 115, 128
Linhardt, F., 588
Litovitz, T. A., 175, 317, 321, 362, 442, 454, 569
Litt, M., 287, 317
Liwak, S. M., 262
Lochner, J. P. A., 167
Lodge, A. S., 5, 26, 31, 77-79, 106, 107, 127, 128, 192, 197, 201, 204, 220, 252, 253, 262, 263, 403, 589, 611, 615
Long, F. A., 363, 364, 540
Longworth, R., 262
Loshaek, S., 243, 262, 318
Love, A. E. H., 31
Lovell, D. E., 166
Lovell, S. E., 221, 262, 316, 402, 541, 615
Ludema, K. C., 578, 589
Lumley, J. L., 223
Lundberg, R. D., 544
Lyon, T., 454, 569
Lyons, J. W., 127

McCall, D. W., 319, 363
McCrum, N. G., 305, 318, 319, 328, 363, 455, 467, 471, 482, 483, 544
Macdonald, I. F., 53, 55, 543
Macdonald, J. R., 78
MacDonald, R. L., 544
McDonel, E. T., 419, 434
McDuffie, G. E., Jr., 569
Macedo, P. B., 317, 568
MacInnes, D. A., 222
McIntyre, D., 590
McKannan, E. C., 127
McKinney, J. E., 48, 55, 168, 170, 175, 317, 318, 545, 558-561, 568, 569
MacKnight, W. J., 78, 129
McLachlan, R. J., 454
McLaren, K. G., 589
McLoughlin, J. R., 166, 319, 362, 363, 454
McMaster, L. P., 222
Macosko, C. W., 127, 129, 152, 166, 261, 401, 433, 434, 452, 456, 590
McSkimin, H. J., 120, 121, 129, 152, 174, 176, 222
Maekawa, E., 91, 95, 320, 362, 429, 433, 436, 540, 544, 576, 588, 589
Magagnini, P. L., 455
Magill, J. H., 318, 319, 439, 440, 454
Makino, S., 116, 117, 128
Malkin, A. Ya., 152, 436
Manabe, S., 459, 482
Mancke, R. G., 36, 55, 320, 362, 400, 401, 409, 414, 418, 433, 609
Mandelkern, L., 169, 175, 333, 363, 482, 544
Mangaraj, D., 568
Mangin, P.-M. F., 318, 569
Manson, J. A., 436
Marhoeffer, C. J., 569
Marin, J., 166, 456
Mark, H., 262, 317
Mark, J. E., 151, 403, 433, 544
Mark, R., 453, 456
Markovitz, H., 32, 79, 94, 95, 107, 108, 114, 127, 128, 152, 262, 316, 319, 401, 461, 463, 482, 508, 527, 540-543, 569
Martin, G. C., 456, 590
Martin, G. M., 36, 55, 175, 414, 422, 434, 483, 568
Martynyuk, M. M., 550, 568
Marvin, R. S., 69, 78, 136, 151, 152, 168, 170, 174, 175, 229, 255, 261, 262, 316, 318, 344, 345, 364, 376-378, 401, 545, 559, 561, 562, 568, 569, 606, 609
Mason, P., 150, 152, 153, 424, 433, 435
Mason, W., 166
Mason, W. P., 119, 120, 128, 129, 152, 174-176
Massa, D. J., 34, 55, 110, 128, 151, 222, 454, 455
Masuda, T., 263, 320, 368, 391, 400-402, 429, 435, 436, 453, 456, 512, 541, 542

Masuda, Y., 569
Masui, R., 319
Matheson, A. J., 129, 218, 220, 316, 318, 454
Matsumoto, K., 319, 540
Matsumoto, T., 429, 435, 436, 453, 456, 590
Matsuo, M., 355, 364, 484
Matsuo, T., 473, 483, 543
Matsuoka, S., 168, 175, 456, 568, 569
Matusik, F. J., 129, 166, 455
Maxwell, B., 157, 166, 168, 175, 317, 568
May, W. D., 574, 588
Meinecke, E. A., 150, 153, 424, 435
Meissner, B., 544
Meissner, J., 72, 79, 104, 127, 149, 153, 398, 399, 403, 571, 579, 588, 589
Meister, R., 569
Meixner, J., 74, 78, 79, 129, 550, 568
Menefee, E., 221, 261
Meredith, R., 167, 484
Merz, E. H., 382, 402, 518
Meskat, W., 167
Meyer, E., 175
Meyer, H. H., 262, 318, 439, 454, 541, 569
Middleman, S., 318
Mieras, H. J. M. A., 402
Mifsud, J. F., 541
Miki, K., 460, 461, 473, 482-484
Miles, D. O., 109, 128
Miller, A. A., 289, 316, 317
Miller, C., 26, 31, 77, 127
Miller, D. R., 434
Miller, M., 150, 544
Miller, R. L., 401, 483
Miller, W. G., 544
Miller, W. R., 318, 363
Milloway, W. T., 167
Mills, N. J., 263, 389, 390, 402
Minami, S., 436
Minamide, M., 542
Minato, K., 483, 574, 588
Minnick, M. G., 222
Mitsuda, Y., 221
Miyahara, Y., 129, 175, 176, 569
Miyamoto, K., 364
Miyamoto, T., 319
Miyanaga, N., 542
Miyasaki, K., 482
Moacanin, J., 436
Mochulsky, M., 435
Moczygemba, G. A., 435
Monpagens, J. C., 319
Montgomery, D. J., 166, 484
Montrose, C. J., 442, 454
Mooney, M., 234, 235, 237-240, 247, 261, 343, 397, 398, 404, 407, 421, 434, 485, 579, 589, 614, 615
Moore, A. A., 542
Moore, C. G., 433
Moore, R. S., 129, 222, 318, 363, 494, 495, 540
Morawetz, H., 262
Morawski, J. C., 153, 424, 435
Morgan, H. M., 167
Morimoto, H., 263
Moriwaki, M., 401, 605, 609
Morris, E. L., 305, 319, 482, 574, 588
Morrison, T. E., 113, 128, 152
Morton, D. H., 167
Morton, M., 261, 433
Morton, S. D., 364, 544
Moser, B. G., 436
Motz, J., 166
Mowry, S. C., 173, 175
Moynihan, C. T., 553, 568
Mukherji, B., 543
Müller, F. H., 165, 167, 270, 316, 456, 485
Mullins, L., 151, 408-410, 424, 433, 435
Münstedt, H., 149, 153, 398, 399, 403
Murakami, K., 350, 364, 436, 543
Murakami, Y., 540
Murray, A. D., 463, 482
Muthukumar, M., 209, 211, 222
Myers, F. A., 590
Myers, R. R., 129, 589

Nagai, S., 455
Nagamatsu, K., 166, 167, 483, 541
Nagasawa, M., 222, 263, 320, 401, 402, 503, 520, 521, 524, 527, 541-543
Nagasawa, T., 482
Nagatoshi, K., 364
Nakada, O., 236, 261, 316
Nakafuku, C., 483
Nakagawa, Y., 542
Nakajima, H., 129, 221, 222
Nakajima, N., 320
Nakamura, M., 221
Nakane, H., 55, 166, 319, 455, 483
Nakao, M., 429, 433, 436, 588
Nakatani, M., 151, 364, 482
Nakayasu, H., 319, 461, 482, 541, 542
Nally, M. C., 110, 128
Napasnikov, V. P., 590
Narayanaswamy, O. S., 553, 568
Narukawa, H., 402
Naunton, W. J. S., 152

Nederveen, C. J., 151, 166, 365, 426, 436, 483
Neira, R. A., 434
Neki, K., 483
Nelb, G. W., 434, 544
Nemoto, N., 128, 220-222, 320, 371, 401, 541, 542, 590, 605, 609
Nestler, F. H. M., 129, 220, 222
Neumann, R. M., 129
Nevin, A., 263, 402
Newlin, T. E., 316, 541
Newman, S., 543
Nielsen, L. E., 151, 152, 241, 262, 352, 363-365, 432, 434, 436, 544
Nigmankhodjaev, A. S., 320, 348, 364
Niinomi, M., 151, 403
Nikolayeva, N. E., 436
Ninomiya, K., 34, 55, 63, 65, 82, 84-87, 90, 94, 103, 127, 261, 263, 299, 300, 316, 318, 362, 363, 388, 389, 402, 429, 434, 436, 494, 502, 514, 515, 540-542, 544, 576, 580, 588, 589, 608, 609
Nishijima, Y., 364
Noda, I., 222
Noll, W., 31, 79
Nolle, A. W., 129, 145-147, 150, 152, 166, 172, 173, 175, 317, 318, 541
Nomura, H., 129, 176, 569
Noordermeer, J. W. M., 151, 222, 396, 397, 403
Nordbeck, K. Ye., 262, 541
North, A. M., 564, 565, 569

Obata, Y., 484
Oberst, H., 150, 160, 166, 357, 365, 576, 588
Oberth, A. E., 436
Ochiai, H., 569
Odani, H., 320, 371, 401, 541, 542, 605, 609
Offenbach, J. A., 425, 435, 483
Offergeld, G., 318
Ogawa, T., 541, 542
Ogawa, Y., 365, 436
Ogihara, S., 104, 127, 318, 402
Ohnuma, H., 541
Ohsawa, T., 176
Ohta, S., 79, 127, 542, 543
Ohta, Y., 402, 542
Ohzawa, Y., 483
Oka, S., 108, 127, 128
Okada, R., 540
Okamoto, H., 222
Okano, K., 129, 455, 472, 484
Okano, M., 94
Oldroyd, J. G., 26, 31
Oliver, P. H., 167
Olson, H. F., 78
Ono, K., 176, 564, 569
Ono, T., 436
Onogi, S., 104, 114, 127, 128, 153, 159, 166, 263, 319, 320, 368, 389-391, 394, 395, 400-402, 429, 435, 436, 453, 456, 479, 484, 485, 512, 541, 542, 590
Onsager, L., 541
Ookubo, N., 221
Oppliger, H. R., 129
Orbon, S. J., 35, 55, 67, 78, 94, 95, 401, 403
O'Reilly, J. M., 110, 128, 318, 402
Orofino, T. A., 319
O'Rourke, V. M., 35, 55, 249, 263, 320, 361-363, 365, 394, 401-403, 605, 609
Osaki, K., 55, 79, 127, 128, 187, 201, 202, 204, 220-222, 263, 319, 402, 522-524, 527, 529, 542, 543
Oser, H., 229, 261, 262, 376-378, 401
O'Shaugnessy, M. T., 541
Oster, G., 364
Oswald, H. J., 589
Oth, J. F. M., 485
Otomo, M., 175, 569
Overberg, R. J., 99, 127
Owens, K. E., 362
Ōyanagi, Y., 261, 289, 299, 300, 316, 328, 329, 347, 363, 370, 394, 400, 401, 402, 428, 429, 433, 462, 491, 523, 540, 541, 547, 570
Ozaki, N., 401, 402

Padden, F. J., Jr., 482, 541
Padmini, P. R. K. L., 129, 316, 454
Painter, G. W., 136, 150, 151, 424, 425, 435
Palmer, M. B., 129
Pals, D. T. F., 221
Panov, Yu. N., 262, 541
Pao, Y. H., 574, 588
Papero, D. V., 589
Pariser, R., 320, 362
Park, G. S., 363
Parks, G. S., 317
Passaglia, E., 320, 362, 476, 483, 484
Pattle, R. E., 363
Paul, F., 317
Paul, I. L., 484
Pavan, A., 543

Payne, A. R., 36, 55, 150, 318, 358, 362, 365, 406, 430, 433, 435, 436, 576, 588
Pearson, D. S., 55, 419, 433, 435, 531, 543
Pearson, J. R. A., 86, 94
Pechhold, W., 450, 455
Pedersen, S., 434
Peng, T. J., 152
Penwell, R. C., 259, 263, 318
Peterlin, A., 220, 222, 483, 484, 543
Pethrick, R. A., 565, 569
Peticolas, W. L., 221, 261
Petrich, R. P., 589
Petrie, C. J. S., 400, 403
Petrie, S. E. B., 317, 540
Pezzin, G., 542
Pfeiffer, W. F., Jr., 262, 541
Philippoff, W., 98, 112, 126, 128, 136, 150-153, 157, 166, 169, 175, 262, 316, 439, 454, 606, 609
Phillips, D. W., 569
Phillips, J. C., 543
Phillips, M. C., 263, 442, 454
Pierson, J. F., 104, 105, 127, 276, 300, 316, 401
Pinnock, P. R., 164, 167
Plazek, D. J., 35, 55, 67, 78, 83, 91, 94, 95, 101, 102, 127, 129, 133, 142-144, 151, 249, 263, 280, 305, 316, 318-321, 361-363, 365, 385, 392, 394, 401-403, 414, 416, 434, 439, 440, 454, 461, 482, 490, 540, 543, 544, 605, 606, 609
Pliskin, I., 589
Plotnikova, E. P., 436
Pochettino, A., 98, 127
Poincaré, H., 31
Polley, H. W., 590
Polmanteer, K. E., 262, 263, 401, 402, 411, 433
Porod, G., 221
Poeter, R. S., 104, 127, 128, 318, 401, 590
Prager, S., 363, 541
Prausnitz, J. M., 568
Preissmann, A., 401
Prest, W. M., Jr., 110, 128, 263, 388, 389, 402
Prettyman, I. B., 140, 152, 435
Prevorsek, D. C., 153, 425, 435
Prigogine, I., 317
Prins, W., 262, 375, 401, 543
Pritchard, W. G., 107, 128
Prod'homme, M., 554, 568
Ptitsyn, O. B., 193, 195, 221
Pugh, J. W., 484
Pursley, W. C., 454
Pylaeva, A. T., 543
Pyrlik, M., 541

Rachapudy, H., 401, 589
Radin, E. L., 484
Radushkevich, B. V., 152, 590
Ragupathi, N., 91, 94, 95, 401, 540
Raible, T., 403
Raju, V. R., 401, 589
Ram, A., 127
Ramos, A. R., 152, 317, 436, 568
Rathmann, G. B., 541
Raub, H. L., 166
Raumann, G., 485
Read, B. E., 153, 318, 328, 362, 363, 455, 467, 483
Read, W. T., 151
Record, M. T., Jr., 221
Ree, T., 263
Reed, P. E., 590
Reed, R. M., 175, 568
Rehage, G., 169, 175, 318, 364, 455, 541, 544, 546, 547, 550, 551, 568
Reichardt, C. H., 456
Rele, V. B., 364, 499, 541
Rempel, R. C., 483
Rhee, C. K., 342, 364
Riande, E., 94, 95, 401, 540
Rice, S. A., 31
Rich, S. R., 129
Richards, J. R., 320, 362, 401, 494, 502, 540, 542, 589
Richardson, M. J., 482
Richter, J., 128, 129, 316, 454
Riseman, J., 191, 193, 220
Rivlin, R. S., 32, 55, 127, 397, 398, 421, 434
Roberts, G. E., 455
Robertson, J. J., 589
Robertson, R. E., 482
Robinet, J. C., 550, 568
Robinson, D. W., 166, 319, 454
Rochefort, W. E., 401, 589
Rodewald, C. W., 543
Roelig, H., 151, 163, 167
Roesler, F. C., 84, 86, 94
Rogers, S. S., 333, 363
Rollmann, K. W., 349, 364, 434
Roovers, J. E. L., 402, 542
Rorden, H. C., 141, 152
Roscoe, R., 142, 152
Rose, R. M., 484
Rosenberg, O., 167
Rosser, R. W., 129, 221, 590

Ross-Murphy, S. B., 433
Rötger, H., 78
Roth, F. L., 36, 55, 414, 422, 434
Roth, J. L., 151
Roth, W., 129
Rouse, P. E., Jr., 117, 128, 185-192, 195, 198-200, 209, 218, 220, 225, 228, 230, 232-235, 237-240, 242, 247-250, 253-255, 266, 269, 270, 316, 328, 329, 337, 343-348, 360, 362, 367, 383, 389, 392, 404, 407, 443, 514, 518, 534, 572, 581, 610, 612-615
Rubio, D. C., 261
Rusanowsky, P. P., 455
Ryan, C. F., 541
Ryan, J. R., 569
Ryan, J. T., 456
Ryskin, G. Ya., 363

Sabsai, O. Yu., 436
Sack, H. S., 166, 175, 176, 559, 569
Saito, N., 222, 455
Saito, S., 317-319
Sakai, M., 263, 521, 524, 542, 543
Sakanishi, A., 119, 129, 195, 221
Sakoda, A., 459, 482
Sakoonkim, C., 262, 319, 540, 541
Sanders, J. F., 55, 320, 362, 367, 400, 401, 434
Sandiford, D. J. H., 477, 484
Sandler, C. S., 175
Sands, H. H., 483
Sandvik, O., 127, 152
Sasabe, H., 318, 319
Sasaki, H., 318
Sato, K., 55, 166, 319, 455
Sato, T., 153
Sauer, J. A., 166, 434, 453, 456, 483, 566, 569
Saunders, D. W., 55, 485
Saunders, P. R., 35, 55, 150, 262, 316, 319, 363, 540, 541, 544, 609
Sawyer, W. M., 78, 129, 542
Schachman, H. K., 364
Schaevitz, H., 151
Schäfer, E. E., 152, 364
Schaffhauser, R., 263, 364, 402, 434
Schallamach, A., 435, 573, 578, 588, 589
Schapery, R. A., 94
Schardt, B., 497, 540
Schatzki, T. F., 455
Schell, W. J., 362
Schlein, H., 166
Schlosser, E., 78
Schmieder, K., 166, 325, 362, 363, 406, 433, 448, 454, 469, 483, 536, 544, 566, 569
Schnell, G., 363, 433
Schowalter, W. R., 32
Schrag, J. L., 34, 55, 108, 110, 117, 118, 128, 129, 152, 195, 201, 204, 218, 220-222, 319, 320, 363, 435, 590
Schrama, J., 78
Schremp, F. W., 79, 95, 115, 127, 128, 139, 150, 152, 544
Schurz, J., 543
Schuster, N. A., 129
Schwarz, J., 544
Schwarzl, F. R., 78, 81-86, 90-92, 94, 95, 316, 320, 357, 365, 426, 436, 453, 456, 483, 590, 609
Schwippert, G. A., 151, 436
Sciamanda, R., 569
Scott, K. W., 409, 433
Segal, L., 55, 222, 263, 402, 542
Segel, M., 98, 127
Seguin, H., 120, 128, 129
Semjonow, V., 317
Senich, G. A., 129
Senshu, K., 320, 349, 364, 482
Severson, S. D., 544
Sharda, S. C., 421, 423, 435
Sharma, R. K., 153, 435
Shears, M. F., 454
Shen, M., 78, 159, 166, 249, 254, 263, 317, 371, 401, 455, 543
Shibayama, K., 256, 263, 434
Shih, H., 568
Shiina, K., 350, 364
Shimizu, K., 129, 319, 455
Shintani, H., 176, 564, 569
Shishido, S., 222
Shoulberg, R. H., 128
Shufler, S. L., 362
Shultz, A. R., 433, 541, 542
Shultz, W. B., 541, 542
Sieck, P. W., 129, 147, 152, 172, 175
Sieglaff, C. L., 32
Silva, H., 64, 78
Silver, I., 175
Simha, R., 222, 317, 362, 542
Simmons, J. M., 128, 528, 543
Simpson, W., 304, 319
Sims, D., 568
Singh, H., 317
Singh, R. P., 454
Sinnott, K. M., 166, 455
Sips, R., 79

Sittel, K., 117, 128
Skewis, J. D., 363
Skutnik, B. J., 433
Slagowski, E., 590
Slichter, W. P., 318, 455
Smith, G. G., 401, 589
Smith, J. B., 485
Smith, J. C., 162, 167, 426, 436
Smith, J. F., 436
Smith, P. J. A., 363
Smith, R. G., 231, 261
Smith, T. L., 67, 72, 78, 79, 87, 89, 92, 95, 115, 128, 139, 152, 261, 348, 364, 365, 434, 435, 571, 584-588, 590
Snowdon, J. C., 576, 588
Soen, T., 365, 436
Soli, A. L., 128
Solms, J., 543
Sommer, W., 79, 166
Sorin, P., 166
Southern, E., 588
Spangler, R. D., 127
Sperling, L. H., 414, 434, 436
Spriggs, T. W., 528, 543
Stambaugh, R. B., 152
Stanislav, J., 87, 94
Starita, J. M., 127, 152
Staverman, A. J., 78, 79, 82-86, 92, 94, 95, 166, 237, 316, 590
Stedry, P. J., 435
Stein, R. S., 151, 153, 435, 473, 483, 484
Steinhauer, D. B., 569
Stejskal, E. O., 319, 363, 455
Stephenson, S. E., 263
Stern, D. M., 82, 94, 151, 261, 262, 319, 362, 455, 540, 541
Stern, M. D., 435
Stern, P., 175, 568
Sternstein, S. S., 166, 453, 454, 456, 544, 568, 569, 590
Stevenson, J. F., 55
Stewart, W. E., 31
Stiehler, R. D., 36, 55, 414, 422, 434
Stockmayer, W. H., 205, 220, 221, 318, 402, 434
Stratton, R. A., 52, 55, 79, 262, 263, 318, 381, 401, 402, 433, 525, 526, 540, 541, 543, 554, 568, 569
Strella, S., 318, 455
Strong, J. D., 166, 455
Struik, J., 152
Struik, L. C. E., 81, 90, 94, 142, 151, 318, 436, 454, 555-557, 568
Stuart, H. A., 220
Suehiro, S., 153
Suganuma, A., 151, 351, 364, 482
Sugie, T., 263, 402, 542
Suzuki, H., 51, 55, 222
Suzuki, Y., 434

Tabata, K., 318
Tabata, Y., 159, 166
Tabor, D., 574, 578, 588, 589
Tager, A. A., 542
Tajiri, K., 483
Takahashi, M., 434, 543
Takami, A., 128
Takano, M., 113, 128, 436
Takayanagi, M., 136, 151, 153, 163, 167, 431, 436, 458, 459, 465, 467, 468, 473, 480-485
Takemori, M. T., 151
Takemoto, T., 166, 483
Takemura, T., 483, 484, 574, 588
Takenaka, T., 153
Takeno, N., 541
Takserman-Krozer, R., 262
Tamm, K., 175
Tammann, G., 289, 317
Tamura, M., 55, 127, 128, 263, 319, 320, 529, 543
Tan, V., 320, 363, 394, 401, 402
Tanabe, Y., 455
Tanaka, A., 483-485
Tanaka, H., 119, 129, 195, 221, 540
Tanda, Y., 483
Tanner, J. E., 363
Tanner, R. I., 128
Tatsumi, T., 483
Taylor, C. R., 151, 263, 276, 316, 320, 401, 403, 434
Taylor, J. S., 540
Taylor, N. W., 151
Taylor, R. B., 439, 454
Temperley, H. N. V., 590
te Nijenhuis, K., 531, 543, 544
Teramoto, A., 540
Thach, R., 364, 434
Theocaris, P., 434
Thirion, P., 151, 152, 254, 263, 371, 401, 414, 415, 434, 544, 578, 589
Thomas, A. G., 433, 588
Thomas, S. B., 321, 362
Thompson, A. B., 363, 479, 480, 483
Thorsen, W. J., 166
Threlkeld, J. O., 319
Thurman, G. R., 589
Thurn, H., 455, 456, 485, 565-567, 569, 588

Thurston, G. B., 121, 129
Tillett, J. P. A., 588
Tillmann, W., 127
Ting, R. Y., 223
Tobin, M. C., 129
Tobolsky, A. V., 78, 89, 90, 95, 151, 241, 248, 261-263, 270, 312, 316, 319, 348, 362-364, 401, 402, 414, 425, 434, 435, 439, 454, 483, 485, 543, 608, 609
Toda, N., 320, 402, 512, 541
Todo, A., 364
Tohyama, K., 544
Tokita, N., 164, 167, 263, 479, 480, 485, 579, 589
Tokiura, S., 293, 318
Toms, B. A., 223
Tonelli, A. E., 455
Trachman, E. G., 589
Trapeznikov, A. A., 543
Treloar, L. R. G., 55, 151, 220, 241, 261, 262, 403, 434, 544
Tschoegl, N. W., 24, 27, 29, 31, 32, 56, 59, 78, 79, 81-87, 92, 94, 111, 128, 151, 192, 193, 195, 198, 220-222, 228, 261-263, 287, 293-295, 312, 318, 319, 353, 355, 364, 365, 403, 421, 423, 433, 435, 507, 541, 572, 573, 588, 615
Tsutsumi, A., 318
Turnbull, D., 286, 290, 303, 317
Turner, D. T., 543
Turner, S., 475, 484
Twyman, W. A., 84, 86, 94
Ty, V., 262

Uchida, T., 436
Udy, D. C., 542
Ueberreiter, K., 318
Ueda, S., 338, 363, 402
Ueki, S., 402
Uemura, J., 153
Uemura, S., 436
Uerpmann, E. P., 541
Ui, K., 319
Ullman, R., 180, 220
Umebayashi, H., 175, 569
Urick, R. J., 171, 175
Utracki, L., 542

Valanis, K. C., 435
Vale, D. G., 127
Valentine, R. H., 55, 320, 362, 367, 400, 402, 412, 434
Valles, E. M., 261, 433
van der Hoff, B. M. E., 408, 433, 435
van der Poel, C., 426-428, 436
van der Vegt, A. K., 484
van der Wal, C. W., 151, 320, 357, 365, 436, 609
Van Holde, K. E., 151, 166, 476, 484
van Krevelen, D. W., 319, 401
Van Oort, W. P., 160, 166
van Pijn, C. F. H., 402
Van Vleck, J. H., 78
Van Wazer, J. R., 127, 152
Veis, A., 543
Verdier, P. H., 221
Veysseyre, R., 94
Vinh Tuong, N. P., 92, 94, 149, 153, 159, 166, 574, 588
Vinogradov, G. V., 152, 436, 590
Voet, A., 153, 424, 435
Vogel, H., 276, 289, 316, 440
Vogel, K., 151
Vol'kenshtein, M. V., 220
Voltaggio, V., 544
von Meerwall, E., 363
Voong, E. T. L., 166, 484
Vrancken, M. N., 127, 142-144, 151, 320, 606, 609

Wack, P. E., 151, 435
Wada, Y., 129, 171, 172, 175, 176, 207, 208, 221, 222, 319, 450, 455, 456, 472, 482-485, 562-564, 569, 590
Wagner, K. W., 316
Wagner, M. H., 263, 403
Wakelin, J. H., 165, 166, 478, 479, 484
Wall, L. A., 436
Walter, A. T., 533, 543
Walters, K., 26, 32, 55, 106, 110, 125, 127, 129, 151, 527, 543
Walters, M., 589
Walther, H., 166
Wang, F. W., 211, 222
Ward, A. G., 150, 319, 544
Ward, I. M., 151, 164, 166, 167, 435, 456, 478, 484, 485
Waring, J. R. S., 152
Warnaka, G. E., 425, 435
Warren, T. C., 220, 221
Wasser, R. B., 499, 541
Watanabe, K., 221
Waterman, H. A., 147, 152, 161, 166, 172, 176
Waters, N. E., 588
Watkins, J. M., 127
Watson, W. F., 433, 435
Watson, W. R., 544

Weaver, H. E., 483
Weber, W., 31
Wegel, R. L., 166
Wegener, W., 167
Weiss, V., 364
Weissenberg, K., 104, 110
Weissert, F. C., 127
West, J. C., 355, 364
Wetton, R. E., 136, 152, 455, 483
Whisnant, J., 167
White, E. F. T., 318, 455, 540
White, J. H., Jr., 456
White, J. L., 263, 579, 589
Whitney, W., 456
Whittaker, R. E., 436, 588
Wilkens, J. B., 364
Willbourn, A. H., 319, 454
Williams, G., 318, 320, 328, 363, 454, 455, 467, 483
Williams, J., 455
Williams, J. G., 590
Williams, J. W., 151
Williams, L. C., 231, 261
Williams, M. C., 127, 128, 221, 222, 249, 254, 258, 263, 371, 401
Williams, M. L., 81-85, 87, 94, 166, 228, 261, 316-320, 362, 455, 497, 540, 541, 589
Williams, M. L., 473, 484
Williamson, S. O., 589
Wilson, G. J., 568
Winckllhofer, R. C., 589
Wolf, K. A., 166, 325, 362, 363, 406, 433, 448, 454, 455, 469, 483, 536, 544, 565, 566, 569
Wolstenholme, W. E., 78, 485
Wong, C.-P., 101, 127, 151, 263, 319, 320, 363, 435, 519, 541, 543, 544
Wood, D. J. C., 438, 454
Wood, L. A., 414, 433-435, 544, 568
Woodbury, C. P., 221
Woodford, D. E., 152
Woods, D. W., 363, 479, 480, 483
Woodward, A. E., 434, 483, 484, 566, 569
Work, R. N., 166, 318
Worley, W. J., 167
Wu, Y.-J., 192, 197, 201, 204, 220, 611, 615
Wunderlich, B., 317
Würstlin, F., 567, 569
Wyman, D. P., 402

Yagii, K., 91, 95, 588
Yamada, K., 484
Yamada, N., 523, 524, 543
Yamada, T., 153
Yamada, Y., 222
Yamafuji, K., 455, 484
Yamakawa, H., 180, 181, 187, 220, 221
Yamamoto, K., 144, 463
Yamamoto, M., 262
Yamazaki, Y., 318
Yannas, I. V., 452, 456
Yano, O., 175, 176, 319, 455, 482, 564, 569
Yasuda, G., 94, 433, 589
Yasuda, H., 483
Yasukawa, J., 482
Yavorsky, P. M., 128, 152
Yee, A. F., 151
Yin, T. P., 319, 320, 362, 363, 401
Yoshino, M., 136, 151
Yoshioka, M., 484
Yoshitomi, T., 166, 167, 483, 541
Yu, C. U., 544
Yu, H., 221, 436

Zakin, J. L., 222, 542
Zana, R., 569
Zand, R., 319, 362, 455
Zapas, L. J., 113, 128, 152, 262, 263, 362, 400, 403, 435, 508, 541-543
Zemansky, M., 129
Zener, C., 166
Zhurkov, S. N., 363
Ziabicki, A., 245, 261, 262
Zijlstra, A. L., 318, 554, 568
Zimm, B. H., 120, 129, 185, 187, 190-193, 195, 197, 198, 200-204, 206, 208, 209, 211, 220, 222, 232, 261, 266, 402, 514, 590, 611
Zimmerli, F. H., 128
Zosel, A., 293, 318
Zuyev, Yu. S., 590
Zwanzig, R., 205, 221
Zwikker, C., 152

Subject Index

Abrasion, 579
Adhesion, 578
Adiabatic measurements, relation to isothermal, 125
Alfrey's rule, 81
Alpha mechanism, 311
Andrade creep, 392
Anisotropic systems, 477
Annular pumping geometry, 98
Apparatus form factors, 98, 132, 156, 602
Apparent activation energy:
  diffusion, 339
  viscoelastic mechanisms, 289
  viscous flow, 511
Applications to practical problems, 570-590
Attenuation, 121
Axial shearing between coaxial cylinders (Segel-Pochettino geometry), 98

Barlow-Erginsav-Lamb equation, 441
Bars, reeds, and rods, resonance vibrations, 158
Bead-spring models, 183
  characteristic parameters of theories, 194
Beta mechanisms, 311, 445, 448
Blatz-Sharda-Tschoegl equation, 421
Blending laws:
  different chemical compositions, 432
  different molecular weights, 229, 252, 388-391
Blends:
  different chemical compositions, 431-433
  different molecular weights, 229-231, 388-390
Boltzmann superposition principle, 17, 27
Branching, effect of:
  in concentrated solutions, 515
  on dilute solution properties, 200
  in undiluted polymers, high molecular weight, 385
  in undiluted polymers, low molecular weight, 232
Bulk compression, 21
Bulk longitudinal deformation, 25, 562-568
  in dilute solutions, 563
  in undiluted polymers and concentrated solutions, 564
  viscoelastic behavior, 562
  wave propagation, 124, 171
Bulk (volume) viscoelasticity, 21, 545-569
  in dynamic (sinusoidal) deformations, 169, 558
  experimental methods, 168-176
  illustrations, 48
  relation of nonlinearity to free volume, 547
  transient behavior, 545

Cerf ellipsoid model, 180, 181
Characteristic frequency, 117, 142, 158
Characteristic mechanical impedance measurements, 116
  experimental methods, 116
Characteristic mechanical reactance, 116, 117
Characteristic ratio (for coil dimensions), 185
Chemical stress relaxation, 425
Coaxial cylinder geometry, 97
Coil domain overlap, effects of, 209
Comb-shaped branched molecules, 202
Complex compliance, 13
  tensile, 24
Complex modulus, 12, 30
  tensile, 24
Complex viscosity, 14

Compliance:
bulk creep, 22
equilibrium, 18
loss, 13
maximum related to network structure, 366
plateau related to entanglement network, 39, 241, 372
shear creep, 10
steady-state, 19
blends of different molecular weights, 231
calculation from creep, 19, 103
change at onset of coil overlap, 211
dependence on concentration, 512
following cessation of flow at high shear rates, 259
intrinsic, at infinite dilution, 180, 194
undiluted polymers of high molecular weight, 248-252, 382-385
summary, 30
Composite systems, 426-433
Compound metal-polymer systems, vibrations, 160
Compressibility, 22, 291, 547
of fractional free volume, 291, 294
Concentrated solutions, 486-529
molecular theory, 224-263
Cone and plate geometry, 97
Constitutive equations, 2, 16, 260, 528
linear viscoelasticity in simple shear, 3, 6
relations from non-linear, 76
Copolymers, 348-355
Correction factors for viscoelastic spectra and functions, 93
Creep, 10
experimental methods, 99, 132, 156, 161, 168
thermally stimulated, 314
Creep compliance, 7, 10
bulk, 21
illustrations, 37
numerical data, 605
Creep recovery, 18, 73
Cross-linked polymers, 404-426
densely linked, 420
early stages of cross-linking, 411
molecular theory, 233-240
slow relaxation mechanisms, 414, 417
technological characteristics of rubbers, 579
transition zone, 404
with unattached macromolecules, 419
Crystalline polymers, 457-485
effects of orientation and drawing, 477
highly crystalline polymers from melts, 460, 467
oriented single crystal mats, 458, 466
polymers with low degrees of crystallinity, 464, 469
relation of behavior to molecular motions, 472
Curtiss-Bird theory, 261

Davidson-Cole equation, 442
Deformation:
at constant stress loading rate, 72
at constant strain rate, 71, 148, 423
cycling, 572
inhomogeneous, 25
Diffusion of small molecules, 338
dependence on concentration, 493, 495
relation to fractional free volume, 303, 338
in styrene-butadiene copolymers, 342
Dilation, 21
Dilute solutions, 177-223
bulk longitudinal behavior at high frequencies, 563
effect of branching, 200
effect of molecular weight distribution, 198
experimental results for linear flexible molecules, 194
extrapolation of shear data to infinite dilution, 195
in non-Θ-solvents, 193
practical aspects of viscoelasticity, 219
shear behavior at high frequencies and in high-viscosity solvents, 214
theory for linear flexible random coils, 183
in Θ-solvents, 192
transition from Zimmlike to Rouselike behavior at finite concentrations, 209, 211
Doi-Edwards theory for terminal zone, 250, 383, 398, 509, 511, 527, 529
Doolittle equation, 286
Dynamic (oscillatory) experiments, 11, 107, 135, 157, 163, 169, 424
Dynamic (oscillatory) mechanical measurements, 150

Elastic recovery, 17, 73
Electrical impedance, transducer measurements by, 114, 136
Elongated molecules, partially flexible, 204

in concentrated solution, 507
flexural modes, 207
Young's modulus, 207
Elongated rigid molecules, dilute-solution theory, 179
Elongation at break, 584
Elongational strain rate, 149
Energy storage and dissipation:
in nonsinusoidal cycling deformations, 572
in periodic (sinusoidal) loading, 572
in transient loading, 571
Entanglement coupling, 35, 241, 366-379
effect of diluent, 502
effect of temperature, 305
effect on relaxation times in terminal zone, 248-251
estimates of spacings, 372-379
manifestations, 366-371
in networks, 240, 408, 417
Entanglement spacings:
dependence on concentration, 502
estimations of, 372-379
from integration of retardation spectrum or loss compliance, 372
from other methods, 376
tabulation, 374, 375
Entanglements:
contributions to equilibrium modulus, 240, 408
trapped, 240, 408
Entanglement trapping probability, 240, 409
Equations of change, 4
Experimental data, tabulations, 604-609
Experimental methods:
bulk (voluminal) measurements, 168-176
for dynamic viscoelastic functions, 124
fibers, 161
hard viscoelastic solids, 154-167
soft viscoelastic solids, 130-153
viscoelastic liquids, 96-129
viscoelastic liquids in solid matrices, 124
Experimental methods for dynamic (sinusoidal) measurements, 107-124, 135-148, 157-161, 163-165
classification, 599

Factorization of strain and time dependence, 135, 260, 397, 414
Failure envelope, 585
Falling cylinder (Segel-Pochettino) geometry, 97
Fibers, experimental methods adapted to, 161-165
Filled (loaded) polymers, 426-431
Finite strains, 26
Flexural geometry, 155, 158
form factors, 156
Forced oscillation measurements (resonance), 139
Form factors (sample coefficients), 98, 132, 156, 602
Fractional free volume, 281
changes during aging, 298, 555
changes following temperature jump, 298, 555
dependence on concentration, 487
dependence on diluent, 301
dependence on molecular weight, 227, 299
dependence on pressure, 292
dependence on temperature, 287
dependence on tensile strain, 301, 556
influence of side-group length, 333
relation to composition in styrene-butadiene copolymers, 342
relation to molecular mobility and friction coefficient, 285, 333
relation to shift factors for relaxation times, 286, 291
in transient bulk (volume) viscoelasticity, 547
Free-draining, 185
Free oscillation measurements (resonance), 142
Friction coefficient:
for diffusion of small molecules, 338
submolecules, 185
see also Monomeric friction coefficient

Gamma mechanism, 448
"Gap loading" experimental methods, 107
compound resonance devices with forced oscillations, 139
compound resonance devices with free oscillations, 142
direct sinusoidal stress-strain measurements, 108, 135
measurements involving mechanical impedance, 110
transducer measurements by electrical impedance, 114, 136
Gels, 529-540
behavior at very long times, 537
effects of aging, 531, 537

pseudo-equilibrium mechanical properties, 531
plateau zone, 537
of semirigid macromolecules, 540
swollen after cross-linking, 539
viscoelastic properties in transition zone, 534
Glass transition temperature, 3, 36, 280
in concentrated solutions, 487
dependence on diluent, 487
dependence on pressure, 297
dependence on time scale of experiment, 284
relation to free volume, 281
Glassy zone, 437-456
in diluted systems, 446
effect of temperature on viscoelastic properties, 448
molecular theory, 254
multiple relaxation mechanisms, 448
relation of behavior to molecular motions, 449
supercooled liquids of low molecular weight, 438
Graessley theory, 249, 257, 381, 383, 386, 511, 517

Heat generation in oscillating deformations, 575
Helical macromolecules, 205
Hydrodynamic interaction parameter, 191, 197
Hydrodynamic interaction, partial, 192
Hyperentanglements, 309, 510

Imaginary component of complex modulus or compliance, 31
Impact measurements, experimental methods, 149
Incomplete flexibility, role in molecular theories, 214-219
"Incompressible" material, 24
Inhomogeneous deformations, 25
Intrinsic loss shear modulus, 177
reduced dimensionless, 178
Intrinsic storage shear modulus, 177
reduced dimensionless, 178
Intrinsic viscosity, 178
limiting value at high frequencies, 215
Isochronal viscoelastic functions, 313, 325, 448, 465, 499
Isothermal volume contraction, 282, 298, 550
effects on shear and elongational relaxation processes, 554
kinetics of volume changes, 551
Isothermal *vs.* adiabatic measurements, 125, 170

Jointed bead-rod model, 183

Ladder network, Blizard, 229
Marvin, 229, 255
trifurcate branching, 237
Langley theory, 240
Linear viscoelastic behavior, 2, 20
in bulk compression or dilatation, 21
in bulk longitudinal deformation, 25
definition, 2
finite, 27
in shear, 8-20
in simple (uniaxial) extension, 22
Lodge theory of elastic liquids, 252
Logarithmic decrement in free oscillations, 142, 158, 160
Loss compliance, 13
bulk, 21, 48
illustrations, 45
Loss modulus, 12
illustrations, 42
numerical data, 606
Loss tangent, 12
illustrations, 46
minimum associated with entanglement network, 368, 370, 581
Lubrication, 219, 580

Martin-Roth-Stiehler equation, 422
Master curves, 271
Maximum stresses and strains for various sample geometries, 602
Maxwell element, 15, 57
Maxwell model, 15, 188
Mechanical impedance, 110, 138
Mechanical loss, 47, 582
Mechanical models, analogies for linear viscoelastic behavior, 15, 57
of apparatus for sinusoidal measurements, 110
Memory function, 7
Moderately dilute solutions, 209
onset of coil overlap, 209
onset of entanglement coupling, 212
Modes, cooperative, for configurational changes, 186
Modulus:
bulk, 21
bulk longitudinal, 25

equilibrium, in networks, 234
loss, 12
shear, 9
storage, 12
summary, 30
Young's, 23
Molecular theory, dilute solutions, 177-223
Molecular theory, amorphous polymers, 224-263
cross-linked networks, 233-240
high molecular weight, 241-263
low molecular weight, 224-233
Molecular weight, effect of entanglements on viscosity (M_C), 212, 243, 248, 377 378
dependence on concentration, 212, 509
Molecular weight, characteristic for effect of entanglements on steady-state compliance (M'_C), 248, 378
Molecular weight, average spacing between entanglements (M_e), 243, 372-376
dependence on concentration, 503
Molecular weight distribution, effect of:
in concentrated solutions, 515
on dilute solution properties, 198
in undiluted polymers of high molecular weight:
plateau zone, 393
terminal zone, 387
in undiluted polymers of low molecular weight, 229
Monomeric friction coefficient, 185, 225, 247
calculation from relaxation spectrum in transition zone, 247, 328, 492
comparisons of data from different sources, 337, 338
at corresponding temperatures, 335
dependence on concentration, 489-497, 534
dependence on cross-linking, 404-406
dependence on molecular weight, 227
in gels, 534
relation to side-group length, 333
tabulation, 330, 331
Mooney-Rivlin equation, 397, 421
Multiple lumped resonator, 117

Networks cross-linked in strained states, 245
Noise abatement, 576
Non-linear viscoelastic behavior:
bulk (volume) deformation, 547-550
in concentrated solutions, 515-529
cross-linked polymers, 420
crystalline polymers, 475
glassy polymers, 452
illustrations, 49
intermittent shear rate experiments, 525
shear creep and creep recovery, 518
stress relaxation after sudden shear strain, 520
uncross-linked polymers of high molecular weight, 257, 260
in uniaxial extension, 260, 395
see also Non-Newtonian flow; Normal stress differences; Oscillatory measurements combined with steady-state shear; Stress growth
Non-Newtonian flow, 29
concentrated solutions, 516
dilute solutions, 219
illustrations, 51
undiluted polymers of high molecular weight, 257
Non-Newtonian viscosity, 29
in concentrated solutions, 516
dependence on shear rate in undiluted polymers, 380
Normal stress coefficient:
limiting primary, 28, 76
primary, 28, 76
oscillatory, 77
relaxation after cessation of steady-state flow, 53, 77
secondary, 28
Normal stress differences, 27
in concentrated solutions, 520
experimental methods, 105
growth and relaxation, 53, 527
illustrations, 49
in steady-state shear flow, 27
oscillatory, 77
Numerical data for viscoelastic functions, examples, 604-609

Oscillatory measurements:
combined with static simple extension, 150
combined with steady-state shear, 527
with large amplitudes, 149, 424

Periodic experiments, 11
Plasticized polymers, 486-529
Plasticizing effectiveness, 496
Plateau compliance, 39, 372-375, 417
dependence on concentration, 501-504
Plateau modulus, 41

Plateau zone, 33, 391-395
in concentrated solutions, 501-506
effect of cross-linking, 407
effect of diluent, 502
in lightly cross-linked systems, 417
macromolecules with internal rigidity, 507
molecular theory, 254
relaxation spectrum, 369
Poisson's ratio, 22
"Poker chip" geometry, 25
Polyelectrolytes, 207
Poly(dimethyl siloxane), 360, 414
Polyethylene, 36, 458, 461, 466
Polyisobutylene, 345, 357, 494, 501, 525, 606, 608
Poly(methyl methacrylate), 35, 445-449, 501, 506
Poly(*n*-octyl methacrylate), 35, 265, 273, 345, 607
Polystyrene, 34, 50, 51, 195, 209, 300, 362, 429, 499, 503, 520, 527, 605, 608
Poly(vinyl acetate), 34, 48, 298, 299, 345, 489, 496, 504, 510, 558
Poly(γ-benzyl-L-glutamate), 206, 507
Predictions of viscoelastic behavior, numerical examples, 580
Pressure, effect on relaxation times, 291-294
Pressure dependence of viscoelastic properties, 291-294
Pressure-temperature coefficient for relaxation times, 295
Processability, 579
Pseudo-equilibrium modulus in gels, 531
Pulse propagation:
longitudinal bulk, 172
shear, 119, 147, 161

Rate of strain tensor, 5
codeformational, 26
corotational, 26
Real part of complex modulus or compliance, 31
Rebound of spheres from viscoelastic surfaces, 574
Recovery after partial stress relaxation, 74
see also Creep recovery
Reduced variables:
for bulk viscoelastic properties, 314
for concentration dependence, 500, 506
criteria for applicability, 273
limitations, 304
multiple mechanisms with different temperature dependences, 305
for non-Newtonian viscosity, 315, 380
for normal stress differences, 314
other than viscoelastic properties, 301
for pressure dependence, 291
for temperature dependence, 266
for ultimate properties, 315, 584-586
theoretical basis, 266, 267
Relaxation modulus, 7, 9
bulk, 21
bulk longitudinal, 25
illustrations, 40
numerical data, 608
tensile, 23
Relaxation spectrum, 60
in blends of different molecular weights, 388
in concentrated solutions, 492
in corresponding states, 343
in crystalline polymers, 459
in diluted systems, 492
in filled polymers, 358
in gels, 534
hybrid, 205
illustrations, 60
in plateau zone, 369
in transition zone, 236
Rouse theory, 189
Relaxation time, 16, 179
dependence on concentration:
in terminal zone, 511
in transition zone, 492
dependence on molecular weight:
in terminal zone, 249-252, 383
in transition zone, 227, 299
dependence on pressure, 291
dependence on temperature, 266
longest in transition zone, 343
rotational, 179, 181
shift factors, 266, 291, 298, 417, 492, 557
terminal, 225, 249, 250
Reptation, 245
Resonance dispersion, 473
Resonance frequency, 116, 139, 158
Resonance measurements (compound):
forced oscillations, 139, 160
free oscillations, 142, 160
Resonance vibration methods:
associated with apparatus inertia, 139
associated with sample inertia, 158, 165, 173
Response curve, forced oscillations, 140, 158, 160

Response half-width in forced oscillations, 140
Retardation spectrum, 61
  changes during cross-linking, 412
  in concentrated solutions, 505, 508
  in corresponding states, 505
  in filled polymers, 358
  in gels, 537
  illustrations, 61
  maximum related to network structure, 366, 407
  in plateau zone, 369
  Rouse theory, 189
Rigid rodlike molecules:
  in concentrated solutions, 507
  experimental results, 182
  at finite concentrations, 213
  theory, 179
Rigid solute molecules in dilute solution, 179
Rolling friction, 574
Rotation between coaxial cylinders, 98, 99
Rotatory diffusion coefficient, 179
Rouse theory, 185
  in closed form, 228, 235
  concentrated solutions, 492
  cross-linked networks, 234
  dilute solutions, 185
  numerical values, 610, 612, 613
  undiluted:
    high molecular weight (transition zone), 247
    low molecular weight, 225
Rouse-Mooney theory, 234, 237, 247
  numerical values, 614, 615
Rubber, Hevea or polyisoprene, 36, 345, 414, 501, 559, 605
Rubber, styrene-butadiene, 36, 342, 414, 427, 429, 607
Rubber processability, 579
Rubberlike elasticity, classical theory, 234

Semidilute solutions, 212
Shift factors for relaxation times:
  concentration, 490-492
  elapsed time, after temperature jump, 298, 554
  pressure, 291
  temperature, 266
  tensile strain, 557
Simple extension, 22
  form factor, 132
Simple shear, 6
  form factor, 98
Simple extension at constant strain rate, 148, 423
  experimental methods, 148
Simple shear geometry, 98
Simple shear sandwich geometry, 132
Sinusoidal deformations, 11, 30
Sliding friction, 577
Sol fraction, 240
Solutions, *see* Concentrated solutions; Dilute solutions
Spacing between entanglement coupling loci, 243, 372-377
  dependence on diluent, 501-504
  dependence on temperature, 305
  methods for estimating, 372-377
  tabulations, 374-375
Spring-dashpot models, 15
Standing waves, 158, 173
Star-shaped branched molecules, 200, 232
State of ease, 245
Storage compliance, 13
  bulk, 21, 48
  illustrations, 44
Storage modulus, 12
  illustrations, 41
  numerical data, 606
Strain tensor, 4
  infinitesimal, 4
Stress growth, 9, 104
  in concentrated solutions, 523
Stress relaxation:
  after cessation of non-Newtonian steady-state flow, 52, 524
  after cessation of steady-state flow, 9, 73, 92, 104, 523
  due to chemical changes, 425
  after deformation at constant strain rate, 571
  experimental methods, 133, 156, 168
  non-linear, 52, 259, 520
  recovery after partial, 74
  after sudden (step) strain, 8, 259, 396, 520
Stress tensor, 5, 20, 26, 28
Submolecules:
  in bead-spring theories, 185
  friction coefficient, 185
  root-mean-square end-to-end distance, 185
"Surface loading" experimental measurements, 116
Symbols, 591-598

Tack, 578

Temperature dependence of viscoelastic properties, 264-290
Temperature, mid-point, of transition zone, 325-328
Tensile compliance, 133
Tensile (elongational) viscosity, 20
Tensile strain, practical, 23, 149
Tensile strain rate, practical, 149
Tensile strength, 584
Tensile stress, 22
Terminal relaxation time:
  dependence on concentration, 511
  in dilute solution, 194, 582
  examples of prediction, 581, 582
  in undiluted polymers of high molecular weight, 249, 250, 382
Terminal zone, 33, 225, 379-391
  in concentrated solutions, 509-529
  effect of diluent, 509
  effect of molecular weight, 248-250
  practical aspects, 253
  theory, high molecular weight, 247-253
Theoretical viscoelastic functions, reduced in dimensionless form, 610
Thermal expansion coefficient, 280
  of fractional free volume, 287
Thermally stimulated creep, 314
Theta solvent, 184, 191, 195
Time-temperature superposition, 271
Tire flatspotting, 580
Torsion of bar, 132
Torsion geometry (between parallel plates or cone and plate), 98, 101
Torsion pendulum:
  for free oscillations, 146
  hollow, 117
Transient network theories, 252
Transition zone (between glasslike and rubberlike consistency), 33, 321-365
  analytical expressions for viscoelastic functions, 348
  in block copolymers, 352-355
  in concentrated solutions, 487
  in copolymers and polymer mixtures, 348
  in cross-linked polymers, 404
  in filled systems, 356
  forms of viscoelastic functions, 346, 498
  in gels, 534
  location on temperature scale, 325
  location on time or frequency scale, 322
  onset frequency, 343, 404, 581
  in partially crystalline polymers, 350
  in polymers of low molecular weight, 226, 359
  theory:
    cross-linked networks, 234
    high molecular weight, 247
    low molecular weight, 226
Tube model for topological restraint, 246

Ultimate mechanical properties, 583-588
  rupture above glass transition temperature, 583
  rupture below glass transition temperature, 587
Ultrasonic absorption, 563
Ultrasonic velocity, 563
Uniaxial extension, 22

Vibration damping, 160, 576
Vibrating reed, 158
Viscoelastic behavior, illustrations, 33-55
Viscoelastic constants, calculations from experimental functions, 70, 76
  calculations from spectra, 76
Viscoelastic functions:
  calculations from spectra:
    approximate, 88
    exact, 64
  formulation with analytical expressions, 348
  interrelations among:
    approximate, 80-95
      between components of complex dynamic function, 92
      correction factors, table of, 93
      between creep and stress relaxation, 89
      criteria of applicability, 86, 92
      between relaxation and retardation spectra, 87
      spectra from viscoelastic functions, 81
      between transient and dynamic functions, 90
      viscoelastic functions from spectra, 88
    exact, 56-79
      between components of a complex dynamic function, 69
      between creep and stress relaxation, 68
      between relaxation and retardation spectra, 63
      spectra from viscoelastic functions, 67
      summary, 75
      between transient and dynamic functions, 68
      viscoelastic functions from spectra, 64

numerical data, 604-609
numerical evaluations from theories, 610
Viscoelastic liquid, 7, 16, 96
experimental methods, 96-129
Viscoelastic solid, 7, 16
experimental methods, hard solids, 154-167
experimental methods, soft solids, 130-153
Viscoelastic spectra:
calculations from experimental functions:
approximate, 81
exact, 67
continuous, 60-64
discrete, 58
interrelations, 60
Viscosity:
absolute, 44
dynamic, 14
dynamic intrinsic, 179, 188
effective local, 341
illustrations, 43
limiting value at high frequencies, 215
steady-flow:
calculation from creep, 19, 103
dependence on concentration, 509
dependence on molecular weight, 248-250, 379
dependence on temperature, 271, 309, 511
high molecular weight, theory, 248, 249
low molecular weight, theory, 242
Newtonian, 19
use in reduced variables, 271
at vanishing shear rate ("zero-shear"), 29, 379, 509
see also Non-Newtonian viscosity; Tensile (elongational) viscosity
Vogel temperature, 276
Voigt element, 16, 58
Voigt model, 16
Voluminal deformation, 21

Wavelength:
flexural, 146
longitudinal, 144
shear, 121
Wave propagation measurements, 121
bulk longitudinal, 124, 171
flexural, 146
longitudinal, 144
pulses, 147, 161, 172
shear, 121
"Wave rigidity modulus," 122
WLF equation, 274, 280, 287
with adjustable reference temperature, 289
modification by energy term, 289
tabulation of coefficients, 277-279
with reference T_g, 287

Yamakawa cylinder model, 180, 181
Young's modulus, 23
apparent (in finite extension), 135

Zimm theory, 185, 191
numerical values, 611